

Ahmed F. El-Sayed

Fundamentals of Aircraft and Rocket Propulsion



Fundamentals of Aircraft and Rocket Propulsion

Ahmed F. El-Sayed

Fundamentals of Aircraft and Rocket Propulsion



Springer

Ahmed F. El-Sayed
Department of Mechanical Engineering
Zagazig University
Zagazig, Egypt

ISBN 978-1-4471-6794-5 ISBN 978-1-4471-6796-9 (eBook)
DOI 10.1007/978-1-4471-6796-9

Library of Congress Control Number: 2016940096

© Springer-Verlag London 2016

The author(s) has/have asserted their right(s) to be identified as the author(s) of this work in accordance with the Copyright, Design and Patents Act 1988.

This work is subject to copyright. All rights are reserved by the Publisher, whether the whole or part of the material is concerned, specifically the rights of translation, reprinting, reuse of illustrations, recitation, broadcasting, reproduction on microfilms or in any other physical way, and transmission or information storage and retrieval, electronic adaptation, computer software, or by similar or dissimilar methodology now known or hereafter developed.

The use of general descriptive names, registered names, trademarks, service marks, etc. in this publication does not imply, even in the absence of a specific statement, that such names are exempt from the relevant protective laws and regulations and therefore free for general use.

The publisher, the authors and the editors are safe to assume that the advice and information in this book are believed to be true and accurate at the date of publication. Neither the publisher nor the authors or the editors give a warranty, express or implied, with respect to the material contained herein or for any errors or omissions that may have been made.

Printed on acid-free paper

This Springer imprint is published by Springer Nature
The registered company is Springer-Verlag London Ltd.

*To my parents whose endless love, support,
and encouragement were a constant source
for my inspiration*

Preface

Pedagogically, the fundamental principles are the foundation for lifelong learning. Thus, this book through a simple treatment can provide students of aerospace/aeronautical and mechanical engineering with a deep understanding of both aircraft and spacecraft propulsions. The development of aircrafts in only one century is far beyond expectations.

December 1903 was the dawn of human-engineered flight when the Wright Brothers flew their first flights that lasted for a few seconds in Ohio, USA. This first aircraft was powered by a single piston engine and had no passengers, neither did it have a fuselage nor landing gears. It is extremely amazing that in 2011 over 2.8 billion passengers were carried by the world's commercial airlines via more than 222,500 aircrafts powered by more than 260,000 different types of aero engines. Some of these aircrafts can carry as many as 800 passengers for more than 15 h of flying time, while others can fly at supersonic speeds. In 2015, the number of passengers exceeded 3.3 billion. Now, piston engines are no longer the single actor in propulsion theater, though they are still dominant! Turbojet engines were the first jet engines invented in the late 1930s and took a reasonable share in military and civil-powered flights for nearly two decades. In the late 1950s and early 1960s, turbofan engines (or bypass turbojet engines) were invented. These are the present prevailing engines which power faster, quieter, cleaner, and heavier aircrafts. In the 1950s also two other engine types, namely, turboprop and turboshaft, were invented to power commercial airliners and military transport aircrafts and rotorcrafts.

Due to the rapid advance in air transportation as well as military and intelligence missions, aircraft and rocket propulsion has become an essential part of engineering education. Propulsion is the combined aero-thermal science for aircrafts and rockets. Propulsion has both macro- and microscales. Macroscale handles the performance and operation of aircrafts and rockets during different missions, while microscale is concerned with component design including both rotary modules (i.e., compressor, fan, pump, and turbine) and stationary modules (i.e., intake, combustor, afterburner, and nozzle).

The primary aim of this text is to give students a thorough grounding in both the theory and practice of propulsion. It discusses the design, operation, installation and several inspections, repair, and maintenance aspects of aircraft and rocket engines.

This book serves as a text for undergraduate and first year graduate students in mechanical, aeronautical, aerospace, avionics, and aviation engineering departments. Moreover, it can be used by practicing engineers in aviation and gas turbine industries. Background in fluid mechanics and thermodynamics at fundamental levels is assumed. The book also provides educators with comprehensive solved examples, practical engine case studies, intelligent unsolved problems, and design projects. The material of this book is the outcome of industrial, research, and educational experience for more than 40 years in numerous civil, military institutions, and companies of 9 countries including the USA, Russia, Austria, UK, Belgium, China, and Japan as well as Egypt.

The book is composed of 11 chapters and 4 appendices. The first ten chapters handle air-breathing engines, while non-air-breathing (or rocket) engines are analyzed in Chap. 11.

Chapter 1 is rather a unique one! It provides a rigorous classification of all types of aircrafts and its sources of power. The first part classifies aircrafts as aerostats/aerodynes, fixed wing/rotary wing (or rotorcrafts), and hybrid fixed/rotary wings as well as all other lift aircrafts (flapping wing or ornithopter, lifting body, and fan wing). The second part handles power plant types. Power plants belong to two main groups, namely, external and internal combustion engines. External combustion engines are steam, Stirling, and nuclear engines. Internal combustion engines are further classified as shaft and reaction engines. Shaft engine group is either of the intermittent combustion types (Wankel and piston) or continuous combustion types (turboprop, turboshaft, and propfan). Reaction engines are either of the athodyd or turbine engines. Athodyd engines include ramjet, scramjet, and pulsejet (valved, valveless, and pulse detonation types). Finally, turbine-based engines include turbojet, turbofan, and turbo-ramjet engines.

Chapters 2 and 3 emphasize that a few fundamental physical principles, rightly applied, can provide a deep understanding of operation and performance of aircrafts and space vehicles.

Chapter 2 provides a review of basic laws of compressible flow with heat and friction. Conservation of mass, momentum, moment of momentum, and energy equations applied to open control volume are reviewed. A review for aspects of normal and oblique shock waves and Fanno and Rayleigh flows follows. Flow in diffusers in aircrafts as well as flow in nozzles in both aircrafts and rockets are discussed. Standard atmosphere is highlighted to emphasize variations of air properties at different altitudes.

Chapter 3 relies upon governing formulae reviewed in Chap. 2 in driving the different performance parameters of jet propulsion, namely, thrust force, operation efficiencies (propulsive, thermal, and overall), specific impulse, and fuel consumption. Other parameters that couple aircraft and engine performance like aircraft

range and endurance are presented. Analysis of aircraft mission, route planning, and non-return point are next highlighted.

Chapter 4 provides the necessary analyses of piston engines and propellers. Though piston engine was the first in-flight air-breathing engine employed by the Wright brothers in 1903, it maintains its strong existence until now. It represents more than 70 % of present-day air-breathing engines. They are extensively used in small fixed wing, sport aircrafts, UAVs, and lighter than air flying vehicles, as well as many rotorcrafts. Unfortunately, it is overlooked in most available propulsion books. A concise analysis of power cycles for two- and four-stroke engines, compression or spark ignition (CI and SI), and Wankel engines as well as turbo- and superchargers is reviewed for power and thermal efficiency optimization. Piston engines cannot generate the necessary propulsive force for a flying vehicle on its own. Thus, it should be coupled to propellers. Classifications of propellers based on various aspects are defined. Propeller's power and thrust force coefficients are defined using simple aerodynamic theories (momentum, modified momentum, and blade-element).

Chapter 5 is devoted to athodyd (nonrotating modules) engines, namely, pulsejet, ramjet, and scramjet engines. All cannot produce thrust force at zero flight speed, so other propulsive methods are used for takeoff operation. Each engine is composed of intake, combustion chamber, and nozzle. An analysis of ideal and real cycles as well as performance parameters of all engines is identified. Pulsejet engine is an internal combustion engine that produces thrust intermittently and is either of the valved or valveless type. Pulse detonation engine (PDE) is evolved in the last decade. PDE promises higher fuel efficiency (even compared with [turbofan](#) jet engines). Ramjet engine represents the first invented continuous combustion engine. It is used in both aircrafts and rockets. The third engine analyzed in this chapter is *scramjet* (*supersonic combustion ramjet*). Combustion takes place in [supersonic](#) airflow. Thus it can fly at extremely high speeds ([NASA X-43A](#) reached Mach 9.6). Finally, dual-mode (Ram-Scram) combustion engine is analyzed.

Chapters 6 and 7 treat air-breathing engines incorporating rotating modules. Chapter 6 handles turbine-based engines (turbojet, turbofan, and turbo-ramjet), while Chap. 7 treats shaft-based engines (turboprop, turboshaft, and propfan). One of the objectives of both chapters is to exercise students to practice realistic engines, build confidence, and a sense of professionalism. Both chapters start with a historical prospective and a classification of each engine. Next, thermodynamic and performance analyses for ideal and real cycles are introduced and further explained via solved examples. Chapter 6 starts by the first flown jet engine, namely, turbojet engine, which was coinvented in the 1930s by British and German activities. Analyses of single and double spools in the presence and absence of afterburner are described. Though rarely used in airliners or military planes in present days, it is still used in micro turbojets and turbojets powering rockets during sustained flight.

Turbofan engines are continuing its superiority for most present commercial airliners and military planes as well as some rockets for sustained flight. A unique classification of the numerous types of this engine based on fan location

(forward/aft), bypass ratio (low/high), number of spools (single/double/triple), number of nozzles (single/double), fan/turbine coupling (geared/ungeared), and finally afterburner (present/absent) is given. After detailed analyses for some (not all) types of turbofan, the third engine, namely, turbo-ramjet, is presented. It is found in two configurations: wraparound or above/under types. An analysis of its single mode or combined mode is precisely defined.

Chapter 7 is confined to shaft-based engines in which performance is controlled by shaft power rather than thrust force. Also, its economy is governed by brake-specific fuel consumption rather than thrust-specific fuel consumption. Turboprop engines power manned and unmanned aircrafts. It may be of the puller (tractor) or pusher types. It may be also either a single or double spool. This section is ended by an analogy between turboprop and turbofan engines. Next, turboshaft engines which mainly power helicopters are classified and analyzed. Exhaust speeds are no longer important in this type of engines as all available energy is converted into shaft power. Finally, propfan or unducted fan (UDF) engines, normally described as ultrahigh bypass (UHP) ratio engine, are classified based on fan location (forward/aft) and numbers of fan stages (single/double). A thermodynamic analysis of this engine is presented for the first time in this book. It combines features from both turbofan and turboprop engines.

Chapter 8 presents aero/thermodynamic analyses of stationary modules of jet engines, namely, intakes, combustion chamber, afterburner, and nozzle. At first, different methods for power plant installation (wing/fuselage/tail, or combinations) are discussed as it has a direct influence on air flow rates into intakes and ingestion of foreign objects into the engines. Also, intakes for fixed and rotary wing aircrafts as well as rockets are described. Moreover, subsonic and supersonic intakes are reviewed for optimum jet engine performance. Intake geometry and its performance are also presented. A review of combustion chambers including types, chemistry of combustion, aerodynamics, and thermodynamics of flow in its different elements is presented. Afterburners in turbojets/turbofans in supersonic aircrafts are analyzed. Different types of aviation fuels and biofuels as a future jet fuel for green aviation are examined. The exhaust system is treated here in a general scope. Convergent and convergent divergent (de Laval) nozzles are analyzed. Moreover, thrust reverse and thrust vectoring are reviewed. Noise control for nozzles is given.

Turbomachinery (i.e., fans, compressors, and turbines) are treated in Chaps. 9 and 10. The objective of both chapters is to provide a simplified understanding of its aerodynamics, thermal, and stresses in both compressors and turbines. In Chap. 9, different types of compressors are first identified, but only centrifugal and axial flow types are analyzed. The three main components of centrifugal compressor, namely, impeller, stator, and volute/scroll, are first analyzed taking into consideration their different types. Positive/negative prewhirl is also presented. Concerning axial compressor, the aerodynamics of single and multistages is reviewed. A performance map for both compressors is employed in identifying design and off-design operation. Lastly, different mechanisms for avoiding surge and rotating stall are discussed.

Chapter 10 treats radial and axial flow turbines. Radial turbine is to a great extent similar to centrifugal compressor. The aerodynamics and thermodynamics of its components (i.e., inlet, nozzle, rotor, and outlet duct) are presented. Next, single and multistage axial flow turbines are treated with either impulse or reaction blading. Mechanical design and cooling techniques are reviewed. Finally, turbine map and off-design performance of both turbines are discussed. Matching between compressors and turbines in both gas generators and jet engines ends this chapter.

Rocket propulsion is discussed in Chap. 11. It starts with a brief history of rocketry followed by classifications of rockets based on type, launching mode, range, engine, warhead, and guidance systems. Rocket performance parameters (i.e., thrust force, effective exhaust velocity, specific impulse, thrust coefficient, and combustion chamber pressure drop) are derived in closed forms similar to those in Chap. 3 for air-breathing engines. A comprehensive section for multistaging is presented. Finally, an analysis of exhaust system (i.e., nozzle geometry, exhaust velocity, and structural coefficient) is given. Both chemical and nonchemical rocket engines are reviewed. Chemical rockets are further divided into liquid, solid, and hybrid rockets. Solid propellant types, combustion chamber, and nozzles are defined. In liquid propellant rockets, a turbopump is added. A hybrid rocket combines liquid and solid propellant systems. Nonchemical rockets including nuclear heating and electrically powered and electrothermal, electromagnetic, and electrostatic thrusters are reviewed.

The book ends with 4 appendices. These lists chronicle details of piston, turbojet, and turbofan engines, as well as milestones for rockets.

Finally, I would like to express my sincere appreciation and gratitude to Airbus Industries and Rolls-Royce plc for their permission to use illustrations and photographs within this text.

I would like to express my sincere thanks to my editor, Charlotte Cross, who was a great help since day one and continued her support during the tough time of manuscript writing.

I'm deeply honored by the support of the dean and staff of Moscow Institute for Physics and Technology (MIPT), Moscow University, and for granting me their medal of 50th anniversary

Particular thanks for the continuous help and technical support of:

- Professor Darrell Pepper, Director, NCACM, University of Nevada Las Vegas, USA
- Mr. Joseph Veres, Compressor Section, NASA Glenn Research Center, Cleveland, USA
- Professor Louis Chow, University of Central Florida, Orlando, USA
- Dr. Dennis Barbeau, AIAA Phoenix Section, USA

I would like to express my sincere thanks and utmost gratitude to my students: Ahmed Z. Almeldein, Aerospace Department, Korea Advanced Institute of Science and Technology, South Korea; Mohamed Aziz and Eslam Said Ahmed, Institute of Aviation Engineering and Technology (IAET); Amr Kamel, Egyptian Air Force; Mohamed Emera and Ibrahim Roufael, Mechanical Power Engineering

Department, Zagazig University; and Ahmed Hamed, Senior Production Engineer, Engine Overhaul Directorate, EgyptAir Maintenance and Engineering Company.

At last, I extend my heartfelt gratitude to my wife, Amany, and sons Mohamed, Abdallah, and Khalid who were the real inspiration and motivation behind this work.

Zagazig, Egypt

Ahmed F. El-Sayed

Contents

1	Classifications of Aircrafts and Propulsion Systems	1
1.1	Introduction	1
1.2	Classifications of Aircrafts	3
1.2.1	General	3
1.2.2	Aerostats	3
1.2.3	Aerodynes	4
1.2.4	Fixed Wing Aircrafts	5
1.2.5	Rotorcrafts (Rotor-Wing Aircrafts)	31
1.2.6	Hybrid Fixed/Rotary Wings	44
1.2.7	Other Methods of Lift Aircrafts	47
1.3	Classifications of Propulsion Systems	51
1.3.1	External Combustion	51
1.3.2	Internal Combustion	55
1.3.3	Other Power Sources	78
	References	89
2	A Review of Basic Laws for a Compressible Flow	91
2.1	Introduction	91
2.2	System and Control Volume	92
2.3	Fundamental Equations	92
2.3.1	Conservation of Mass (Continuity Equation)	94
2.3.2	Linear Momentum (Newton's Second Law)	96
2.3.3	Angular Momentum Equation (Moment of Momentum)	103
2.3.4	Energy Equation (First Law of Thermodynamics)	106
2.3.5	The Second Law of Thermodynamics and the Entropy Equation	110
2.3.6	Equation of State	111

2.4	Steady One-Dimensional Compressible Flow	114
2.4.1	Isentropic Relations	114
2.4.2	Sonic Conditions	116
2.4.3	Classification of Mach Regimes	119
2.4.4	Diffusers and Nozzles	120
2.4.5	Shocks	125
2.5	Rayleigh Flow Equations	146
2.6	The Standard Atmosphere	151
	References	160
3	Performance Parameters of Jet Engines	161
3.1	Introduction	161
3.2	Thrust Force	162
3.3	Factors Affecting Thrust	174
3.3.1	Jet Nozzle	175
3.3.2	Air Speed	175
3.3.3	Mass Air Flow	175
3.3.4	Altitude	176
3.3.5	Ram Effect	177
3.4	Engine Performance Parameters	178
3.4.1	Propulsive Efficiency	179
3.4.2	Thermal Efficiency	186
3.4.3	Propeller Efficiency	189
3.4.4	Overall Efficiency	189
3.4.5	Takeoff Thrust	192
3.4.6	Specific Fuel Consumption	193
3.4.7	Aircraft Range	200
3.4.8	Range Factor	205
3.4.9	Endurance and Endurance Factor	205
3.4.10	Mission Segment Weight Fraction	206
3.4.11	Head- and Tail-Wind	206
3.4.12	Route Planning	209
3.4.13	Specific Impulse	213
	References	218
4	Piston Engines and Propellers	219
4.1	Introduction	219
4.2	Intermittent (or Piston) Engines	221
4.2.1	Milestones	223
4.2.2	Types of Aero Piston Engines	223
4.3	Aerodynamics and Thermodynamics of Reciprocating ICE	232
4.3.1	Terminology for Four-Stroke Engine	232
4.3.2	Air-Standard Analysis	233
4.3.3	Engine Cycles	235

4.4	Aircraft Propellers	261
4.4.1	Introduction	261
4.4.2	Nomenclature	264
4.5	Classifications	265
4.5.1	Source of Power	265
4.5.2	Material	265
4.5.3	Coupling to the Output Shaft	267
4.5.4	Control	267
4.5.5	Number of Propellers Coupled to Each Engine	269
4.5.6	Direction of Rotation	269
4.5.7	Propulsion Method	271
4.5.8	Number of Blades	271
4.6	Aerodynamic Design	273
4.6.1	Axial Momentum, (or Actuator Disk) Theory	274
4.6.2	Modified Momentum or Simple Vortex Model	281
4.6.3	Blade Element Considerations	282
4.7	Dimensionless Parameters	287
4.8	Typical Propeller Performance	293
4.9	Conclusion	304
	References	313
5	Pulsejet, Ramjet, and Scramjet Engines	315
5.1	Introduction to Athodyd Engines	315
5.2	Pulsejet	315
5.2.1	Introduction	315
5.2.2	Brief History	316
5.2.3	Valved Pulsejet	318
5.2.4	Thermodynamic Cycle	319
5.2.5	Valveless Pulsejet	327
5.2.6	Pulsating Nature of Flow Parameters in Pulsejet Engines	329
5.2.7	Pulse Detonation Engine (PDE)	330
5.3	Ramjet	337
5.3.1	Introduction	337
5.3.2	Applications	338
5.3.3	Aero-Thermodynamic Analysis of Modules	341
5.3.4	Aero-thermodynamic Analysis of Ramjet Cycle	348
5.3.5	Nuclear Ramjet	360
5.3.6	Double Throat Ramjet Engine	362
5.4	Scramjet	364
5.4.1	Introduction	364
5.4.2	Evolution of Scramjets	365
5.4.3	Advantages and Disadvantages of Scramjets	367
5.4.4	Aero-Thermodynamic Analysis of Scramjets	367

5.4.5	Performance Analysis	371
5.4.6	Dual-Mode Combustion Engine (Dual Ram-Scramjet)	376
5.5	Conclusion	386
	References	400
6	Turbine-Based Engines: Turbojet, Turbofan, and Turboramjet Engines	403
6.1	Introduction	403
6.2	Turbojet	404
6.2.1	Introduction	404
6.2.2	Milestones of Turbojet Engines	407
6.2.3	Thermodynamic Cycle Analysis of a Single Spool	407
6.2.4	Performance Parameters of a Single Spool	416
6.2.5	Important Definitions	417
6.2.6	Double-Spool Turbojet	430
6.2.7	Thermodynamic Analysis of Double-Spool Turbojet	430
6.2.8	Performance Parameters of Double-Spool Turbojet Engine	435
6.2.9	Micro-turbojet	441
6.3	Turbofan	445
6.3.1	Introduction	445
6.3.2	Milestones	446
6.3.3	Classifications of Turbofan Engines	446
6.3.4	Forward Fan Unmixed Double-Spool Configuration	448
6.3.5	Forward Fan Mixed-Flow Engine	461
6.3.6	Forward Fan Unmixed Three-Spool Engine	471
6.4	Turbine-Based Combined-Cycle (TBCC) Engines	479
6.4.1	Introduction	479
6.4.2	Historical Review of Supersonic and Hypersonic Aircrafts	481
6.4.3	Technology Challenges of the Future Flight	486
6.4.4	Propulsion System Configurations	486
6.4.5	Performance of TBCC (or Hybrid Engine)	490
6.4.6	Cycle Analysis of Turboramjet (or TBCC) Engine	492
6.4.7	General Analysis for a Turboramjet Engine	498
6.4.8	Design Procedure	508
6.4.9	Future TBCC Engine	509
6.5	Conclusion	509
	References	528

7 Shaft Engines Turboprop, Turboshaft, and Propfan	531
7.1 Introduction	531
7.2 Turboprop Engines	532
7.2.1 Introduction	532
7.2.2 Milestones	534
7.2.3 Thermodynamics Analysis of Turboprop Engines	538
7.2.4 Equivalent Engine Power	545
7.2.5 Fuel Consumption	546
7.2.6 Analogy with Turbofan Engines	552
7.3 Turboshaft	553
7.3.1 Introduction	553
7.3.2 Examples for Turboshaft Manufacturers and Engines	553
7.3.3 Thermodynamic Analysis of Turboshaft Engines . .	556
7.3.4 Power Generated by Turboshaft Engines	557
7.4 Propfan	564
7.4.1 Introduction	564
7.4.2 Historical Hints	565
7.4.3 Classifications of Propfans	567
7.4.4 Comparisons Between Turboprop, Propfan, and Turbofan	569
References	587
8 Stationary Modules Intakes, Combustors, and Nozzles	589
8.1 Intake	589
8.1.1 Introduction	589
8.1.2 Power Plant Installation	590
8.1.3 Inlet Performance Parameters	619
8.1.4 Subsonic Intakes	621
8.1.5 Supersonic Intakes	637
8.1.6 Hypersonic Inlets	645
8.1.7 Performance Parameters	646
8.2 Combustion Systems	653
8.2.1 Introduction	653
8.2.2 Types of Combustion Chamber	653
8.2.3 Components of Combustion Chamber	658
8.2.4 Aerodynamics of Combustion Chamber	661
8.2.5 The Chemistry of Combustion	665
8.2.6 The First Law Analysis of Combustion	668
8.2.7 Combustion Chamber Performance	669
8.2.8 Material	672
8.2.9 Aircraft Fuels	672
8.2.10 Emissions and Pollutants	674
8.2.11 Afterburner	675

8.3	Exhaust Nozzle	677
8.3.1	Introduction	677
8.3.2	Operation of Nozzles	680
8.3.3	Performance Parameters of Nozzles	681
8.3.4	High-Speed Vehicles	689
	References	700
9	Centrifugal and Axial Compressors	703
9.1	Introduction	703
9.2	Centrifugal Compressor	703
9.2.1	Introduction	703
9.2.2	Layout of Compressor	706
9.2.3	Classification of Centrifugal Compressors	708
9.2.4	Governing Equations	711
9.2.5	Slip Factor (σ)	718
9.2.6	Types of Impeller	724
9.2.7	Impeller Isentropic Efficiency	728
9.2.8	Radial Impeller	733
9.2.9	Diffuser	735
9.2.10	Prewirl	737
9.2.11	Discharge System	742
9.2.12	Compressor Map	742
9.2.13	Surge	746
9.3	Axial Flow Compressor	747
9.3.1	Introduction	747
9.3.2	Comparison Between Axial and Centrifugal Compressors	750
9.3.3	Mean Flow (Two-Dimensional Approach)	752
9.3.4	Basic Design Parameters	763
9.3.5	Design Parameters	770
9.3.6	Real Flow in Axial Compressor	773
9.3.7	Simplified Radial Equilibrium Equation (SRE)	775
9.3.8	Conceptual Design Procedure for Axial Compressor	794
9.3.9	Blade Design	808
9.3.10	Choice of Airfoil Type	812
9.3.11	Compressor Map	813
9.4	Centrifugal and Axial Compressors Material	818
9.5	Closure	819
	References	837
10	Turbines	839
10.1	Introduction	839
10.2	Axial Flow Turbines	840
10.2.1	Flow Features	840
10.2.2	Euler Equation	841

10.2.3	Efficiency and Pressure Ratio	843
10.2.4	Loss Coefficients in Nozzle and Rotor	845
10.2.5	Performance Parameters	846
10.2.6	Free Vortex Design	858
10.2.7	Turbine Cooling Techniques	867
10.2.8	Guide Lines for Axial Turbine Design	870
10.2.9	Turbine Map	872
10.3	Radial Flow Turbine	873
10.3.1	Introduction	873
10.3.2	Aero-Thermodynamics of Radial Inflow Turbine	873
10.3.3	Recommended Design Values for Radial Inflow Turbines	879
10.3.4	Radial Versus Axial Turbines	880
10.4	Gas Turbine Engine Matching	885
10.4.1	Introduction	885
10.4.2	Compatibility Conditions	885
10.4.3	Single Shaft Gas Turbine Engine	886
10.4.4	Off-Design of Free Turbine Engine	888
	References	905
11	Rocket Propulsion	907
11.1	Introduction	907
11.2	History	908
11.2.1	Important Events	908
11.2.2	Future Plans of Rocket and Space Flights (2014 and Beyond)	912
11.3	Classifications of Rockets	912
11.3.1	Method of Propulsion	912
11.3.2	Types of Missiles	912
11.3.3	Launch Mode	913
11.3.4	Range	914
11.3.5	Number of Stages	914
11.3.6	Applications	914
11.4	Rocket Performance Parameters	914
11.4.1	Thrust Force	915
11.4.2	Effective Exhaust Velocity (V_{eff})	915
11.4.3	Exhaust Velocity (u_e)	919
11.4.4	Important Nozzle Relations	920
11.4.5	Characteristic Velocity (C^*)	922
11.4.6	Thrust Coefficient (C_F)	922
11.4.7	Total Impulse (I_t)	924
11.4.8	Specific Impulse (I_{sp})	924
11.4.9	Specific Propellant Consumption	929
11.4.10	Mass Ratio (MR)	929

11.4.11	Propellant Mass Fraction (ζ)	929
11.4.12	Impulse-to-Weight Ratio	930
11.4.13	Efficiencies	930
11.5	The Rocket Equation	933
11.5.1	Single-Stage Rocket	933
11.5.2	Multistage Rockets	937
11.5.3	Rocket Equation for a Series Multistage Rocket	938
11.5.4	Rocket Equation for a Parallel Multistage Rocket	940
11.5.5	Advantages of Staging	940
11.5.6	Disadvantages of Staging	941
11.6	Chemical Rocket Engines	945
11.6.1	Introduction	945
11.6.2	Performance Characteristics	945
11.7	Solid Propellant	946
11.7.1	Introduction	946
11.7.2	Composition of a Solid Propellant	948
11.7.3	Basic Definitions	949
11.7.4	Burning Rate	950
11.7.5	Characteristics of Some Solid Propellants	958
11.8	Liquid-Propellant Rocket Engines (LREs)	959
11.8.1	Introduction	959
11.8.2	Applications	960
11.8.3	Propellant Feed System of LREs	961
11.8.4	Liquid Propellants	962
11.8.5	Fundamental Relations	965
11.8.6	Pump-Fed System	968
11.8.7	Rocket Pumps	972
11.8.8	Pump Materials and Fabrication Processes	973
11.8.9	Axial Turbine	974
11.9	Hybrid Propulsion	976
11.9.1	Introduction	976
11.9.2	Mathematical Modeling	978
11.9.3	Advantages and Disadvantages of Hybrid Engines	980
11.10	Nuclear Rocket Propulsion	981
11.11	Electric Rocket Propulsion	982
11.11.1	Introduction	982
11.11.2	Electrostatic Rockets	983
11.11.3	Electrothermal Rockets	983
11.11.4	Electromagnetic Rockets	984
	References	990

Contents	xxi
Appendices	993
Appendix A	993
Appendix B	994
Appendix C	996
Appendix D	999
Index	1003

Chapter 1

Classifications of Aircrafts and Propulsion Systems

1.1 Introduction

Aircraft engine is also denoted as aero engine, airbreathing engines, or aircraft power plant. It acts as the heart of aircraft (being the only source of power in aircrafts) similar to human's heart. The desire to fly is as old as the known history of man. Winged gods were plenty among all kinds of societies the man started to form in the early ages. These winged figures or figurines are shown on many temples of Egyptian civilization some 5000 B.C., Sumerian Civilization 3500–2500 B.C and Hittite civilization 3000–1000 B.C. Many of these idols of early civilization carried certain common features, namely the powerful body of a lion (representing leadership on land), head of a noble man (putting these idols on a more humane perspective), and wings of an eagle for mastering air.

There are also some interesting artifacts found among ancient ruins. A 6 inch wooden model of an aircraft featuring fuselage, wing, and tail (exactly similar to twentieth century civil transports) was found in one of the tombs in Saqqara, Egypt, that dates back to 200 BC (Fig. 1.1).

An ornament for a golden delta wing aircraft model dates back to 500–800 A.D. that is typical to F 102 jet fighter of the 1950s was found in Columbia (Fig. 1.2).

Also a golden model found in Central and South America that is identical to Grumman Aircraft X-29 (Fig. 1.3).

The axiom saying that “man cannot dream or imagine something that is not a part of his real life experience” makes us puzzled how such early civilizations that knew nothing about flight principals could produce such models that carry present features of aircrafts and same fuselage, wing, and tail construction?!

Flight story is long dated to several 100 years B.C. It started by mankind's dream of flight by imitating birds. History recorded some distinct cases. The first was due to Daedalus (a famous architect) and his son Icarus who were imprisoned in eighteenth century B.C in Crete. Daedalus built wings for himself and Icarus, fashioned with feathers held together with wax. Myth states that Icarus flying too



Fig. 1.1 Egyptian wooden model (200 BC)



Fig. 1.2 Columbian golden delta wing model (500–800 AD)

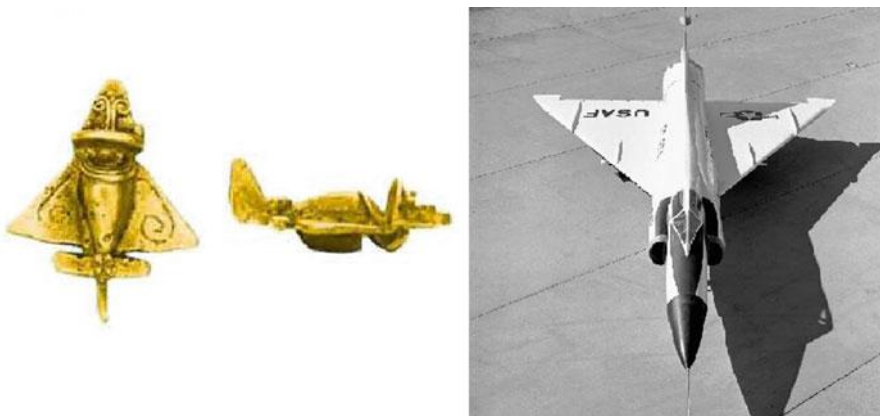


Fig. 1.3 Golden model from South America similar to Grumman aircraft X-29

close to the sun god Helios, the wax melted from the heat and he fell to his death. Another described case also is due to Abbas Ibn Farnas, an Arabic Mathematician and scientist who lived in Cordoba (810–887 AC) and could fly after jumping from a tower. However, ignoring the contribution of the tails of birds in flight control, he fell down and was hurt (but did not die) as he tried to return to ground. Several Turkish unsuccessful trials were recorded in the last centuries. The author of this book, in his previous book [1], chronicled flight story in terms of milestones

for both aircraft and engine inventions beginning with Leonardo da Vinci up through the twenty-first century. This book integrated with the previous one [1] provides a thorough understanding of engine propulsion concepts, including the performance of aero engines. Author of the present book introduces propulsion systems in a rather new flavor to both aviation and aerospace industries. Integrated with aircrafts, appropriate propulsion systems will be identified. An innovative classification for both military and civil aircrafts will be given. Next, classifications for aero engines will be followed. Appropriate power plants for each category of airplanes will be also highlighted.

1.2 Classifications of Aircrafts

1.2.1 General

An *aircraft* may be defined as a **vehicle** which is able to **fly** by being supported by the **air**, or in general, the **atmosphere** of a planet [2]. An aircraft counters the force of gravity by using either **static lift** or **dynamic lift** [3]. Although **rockets** and **missiles** also travel through the atmosphere, most are not considered aircraft because they use rocket thrust instead of aerodynamics as the primary means of lift. However, a **cruise missile** has to be considered as an aircraft because it relies on a lifting wing or fuselage/body. Based on method of lift, aircrafts may be classified as either lighter than air (AEROSTATS) or heavier than air (AERODYNES) (Fig. 1.4).

1.2.2 Aerostats

Aerostats use **buoyancy** to float in the air in much the same way that ships float on the water. They are characterized by one or more large gasbags or canopies, filled with a relatively low density gas such as **helium**, **hydrogen** or **hot air**, which is less dense than the surrounding air. Aerostats may be further subdivided into powered and unpowered types. Unpowered types are kite which was invented in China 500 B.C., **sky lanterns** (small hot air balloons; second type of aircraft to fly as invented 300 B.C.), balloons, and blimps.

A powered aerostat mostly denoted as *airship* or *dirigible* can be steered and propelled through the air using **rudders** and **propellers** or other **thrust**. The main types of airship are non-rigid, **semi-rigid**, and **rigid**. **Non-rigid** (sometimes denoted **blimps**) are small airships without internal skeletons. Semi-rigid airships are slightly larger and have some form of internal support such as a fixed keel. An example for rigid airship with full skeletons is **Zeppelin**. Although airships are no longer used for passenger transport, they are still used for other purposes such as **advertising**, **sightseeing**, surveillance, and research [4]. As demonstrated in Fig. 1.4,

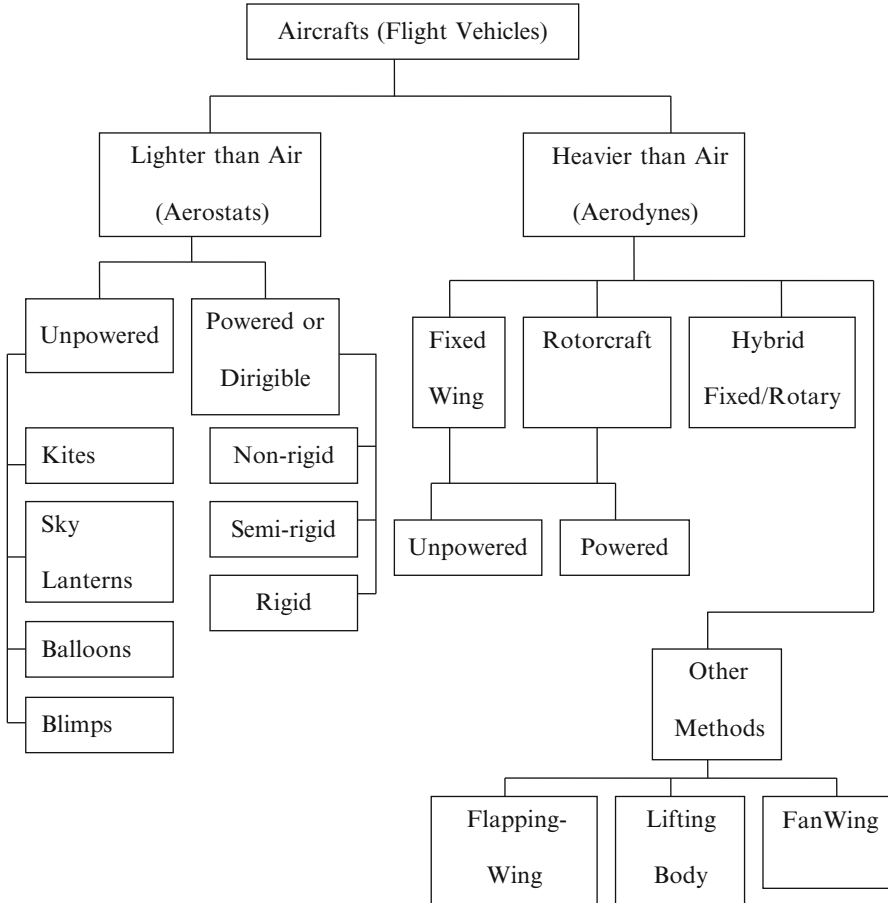


Fig. 1.4 Classifications of aircrafts

a blimp may be unpowered as well as powered. Figure 1.5 illustrates both unpowered (balloon) and powered ([Zeppelin](#)) aerostats.

1.2.3 Aerodynes

Aerodynes, or heavier than air vehicles, resemble almost all types of aircrafts. It pushes air or gas in one direction, so that a reaction occurs (by Newton's laws of motion) that pushes the aircraft in the other direction. There are four groups of aerodynes, namely, fixed wing aircrafts, rotorcrafts, hybrid fixed/rotary wing, and a fourth group relying upon other methods for generating lift. For fixed wing aircraft (generally denoted as airplane or aeroplane), aerodynamic lift is generated by

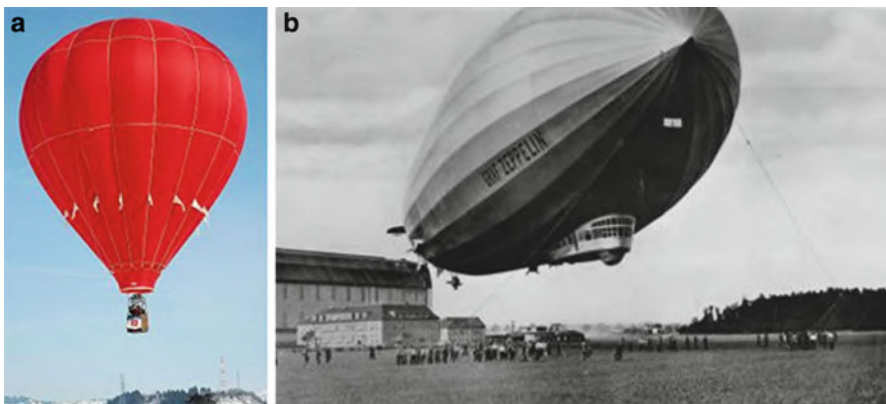


Fig. 1.5 Two types of aerostats (a) Balloon (b) Zeppelin

forward movement of wings, while for **rotorcraft** lift is generated by spinning wing-shaped rotors (sometimes called rotary wings). Fixed wing and rotorcraft types may be further divided into powered and unpowered (gliders) types, as will be described in details below. Rotorcrafts may also be divided into same categories of powered and unpowered types, e.g. helicopters and autogyro, respectively. The third group, namely, hybrid fixed/rotary wing aircrafts, is sometimes identified as compound rotorcraft and may include additional thrust engines or propellers and static lifting surfaces. This group has several types, namely, tilt-wing, tiltrotor, mono tiltrotor, mono-tilt-rotor rotary-ring, and coleopter.

The fourth group may be subdivided into three groups, namely: **lifting body**, flapping-Wing (Ornithopter), and **FanWing**. Lifting body configuration has an aircraft body shape to produce lift, e.g. **Martin-Marietta X-24**. **Powered lift** types rely on engine-derived lift for vertical operation either in takeoff, landing, or both. An ornithopter (from Greek ornithos “bird” and pteron “wing”) is an aircraft that **flies** by flapping its wings. The **FanWing** is a recent innovation (starting 2005 in United Kingdom) and represents a completely new class of aircraft. It uses a fixed wing with a cylindrical fan mounted spanwise just above the wing. As the fan spins, it creates airflow backwards over the upper surface of the wing creating lift.

In the succeeding sections heavier than air vehicles or aerodynes will be discussed in details.

1.2.4 *Fixed Wing Aircrafts*

1.2.4.1 General Classifications

Fixed wing aircrafts are further classified as either powered or unpowered vehicles (Fig. 1.6). Unpowered types may be next subdivided into six types, namely

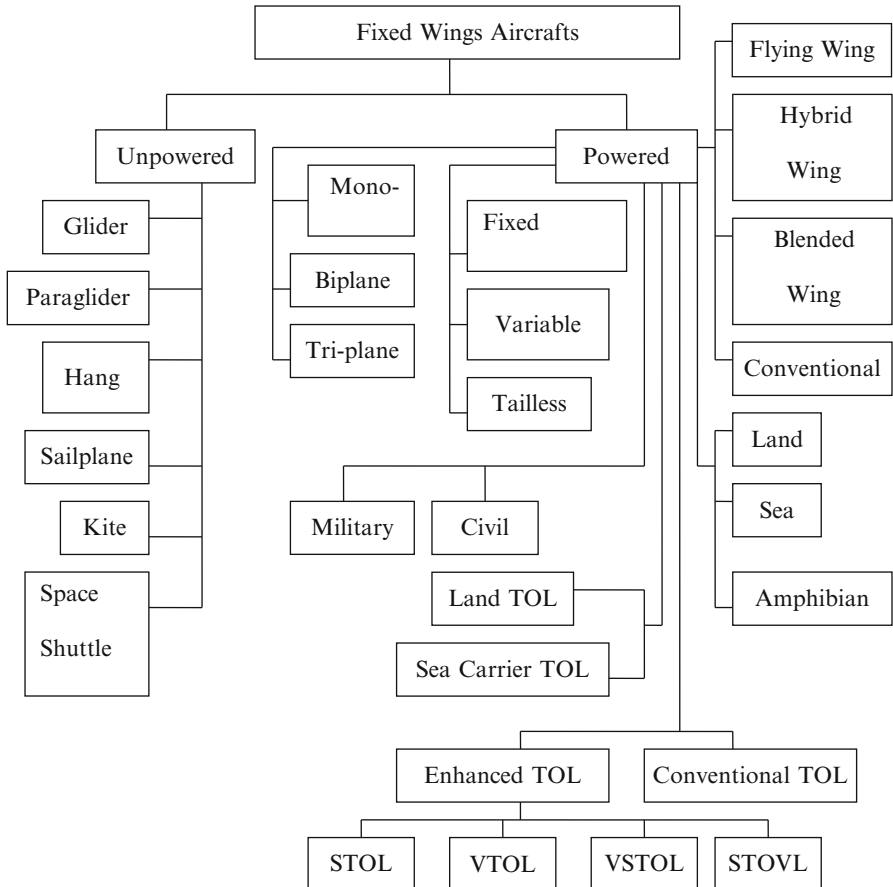


Fig. 1.6 Classifications of fixed wing aircrafts

gliders, hang gliders, paragliders, sailplanes, kites, and space shuttle in its return mission. Powered aircrafts are next classified based on several aspects. Based on the number of wings, it is mono-plane, biplane, or tri-plane. Based on geometry, it is fixed, variable (swept-back wings), or tailless as illustrated in Fig. 1.7. Swept back wings are adopted in some military aircrafts. Wings are swept back when aircraft flies in supersonic speeds. By tailless aircraft, it is meant an aircraft without horizontal tail.

Finally based on wing type, fixed wing aircrafts may be classified as conventional, flying wing, blended wing body (BWB), and hybrid wing body (HWB). Figure 1.8 illustrates blended wing body (BWB), while Fig. 1.9 illustrates a flying wing.

Based on takeoff and landing (TOL), they may be classified as either conventional or enhanced. Enhanced TOL types may be further divided into four categories, namely: Vertical Take Off and Landing (VTOL), Short Take Off and

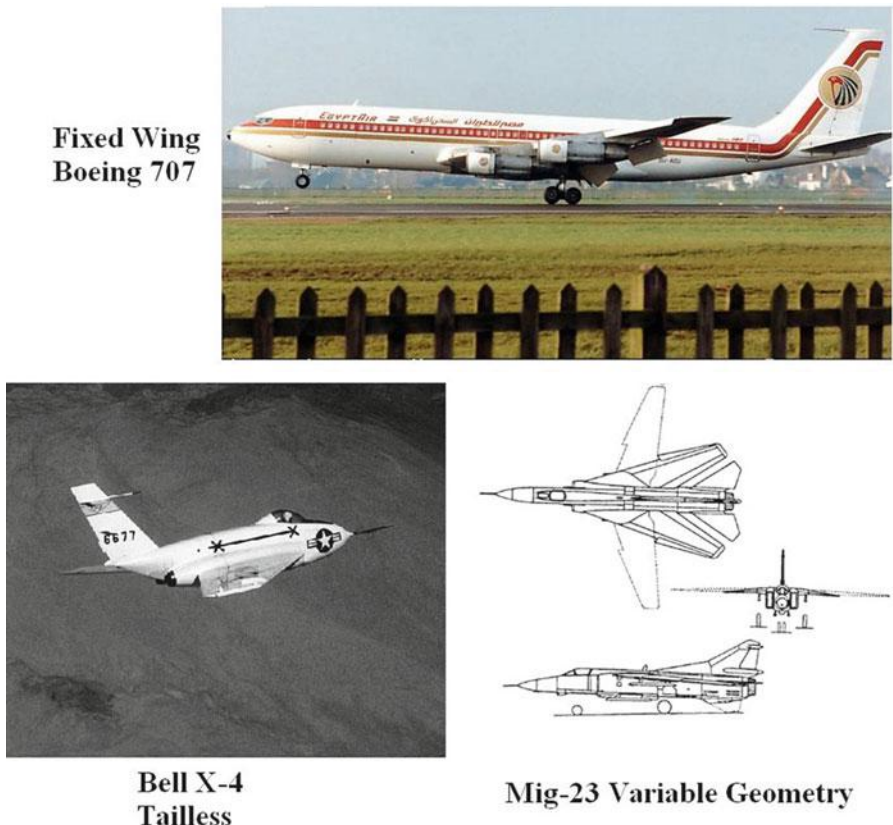


Fig. 1.7 Classification based on geometry

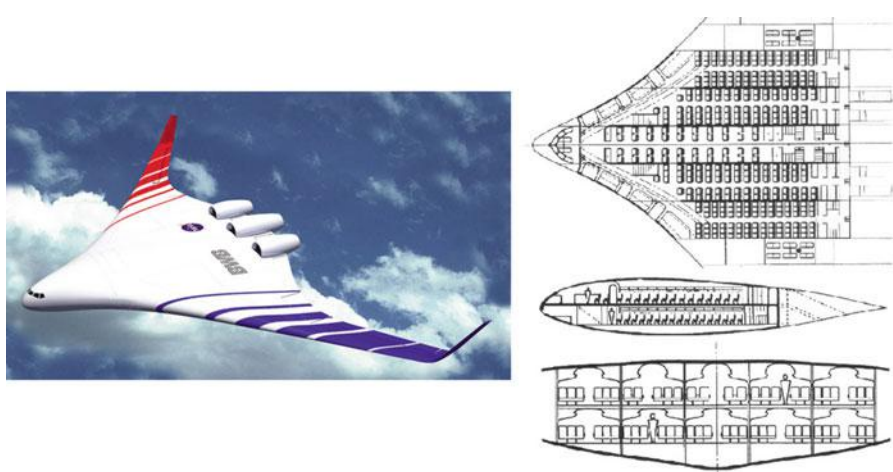


Fig. 1.8 Blended wing body (BWB)

Fig. 1.9 Flying wing (B-2 Spirit)



B-2 Spirit Flying Wing

Landing (STOL), Vertical and/or Short Take-Off and Landing (VSTOL), and Short Take Off and Vertical Landing (STOVL). A *tailsitter* is a type of [VTOL](#) aircraft that launches and lands on its tail, something akin to a [Buck Rogers](#) type rocket, such as the [McDonnell Douglas DC-X](#) Delta Clipper. One of the most famous examples of this type of aircraft is the Ryan [X-13 Vertijet](#). Among the [propeller](#)-driven versions were the [Lockheed XFV](#) and the [Convair XFY Pogo](#). It is important here to state some aircraft types may belong to more than one category of this group of enhanced TOL. As an example Harrier aircraft belongs to both VTOL and V/STOL types. This is not a unique case, but it is severally repeated in other classifications hereafter. Figure 1.10 illustrates four types of enhanced TOL aircrafts.

Furthermore, based also on takeoff and landing, fixed wing aircrafts may operate from land or sea carriers. A third classification based on takeoff and landing defines land, sea, and amphibious planes. A seaplane is a [fixed-wing](#) aircraft capable of [taking off](#) and [landing](#) (alighting) on water, while seaplanes which can also take-off and land on airfields are a small subclass called [Amphibian aircraft](#) (Fig. 1.11). Seaplanes and amphibians are usually divided into two categories based on their technological characteristics: [floatplanes](#) and [flying boats](#), which are generally far larger and can carry far more. These aircrafts were sometimes called hydroplanes.

Finally, fixed wings are seen in both civilian and military aircrafts.



Fig. 1.10 Enhanced TOL aircrafts

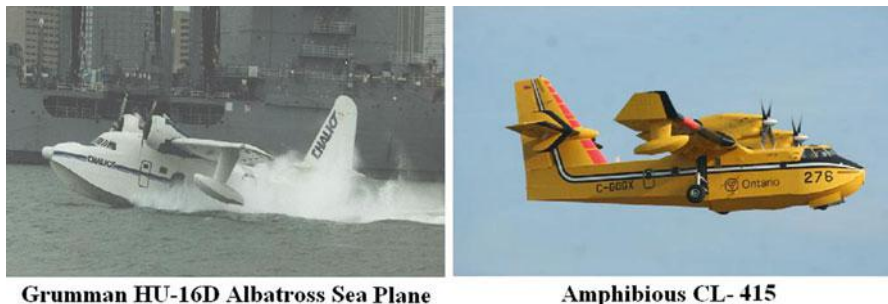


Fig. 1.11 Sea and amphibian aircrafts

1.2.4.2 Civil Aircrafts

As outlined above, fixed wings aircrafts may be either classified as civil or military types. Here civil aircrafts will be further discussed. It is decomposed into different groups, namely, commercial transport, agriculture, trainer, firefighting, experimental, research, search and rescue as well as sea/amphibious planes (Fig. 1.12).

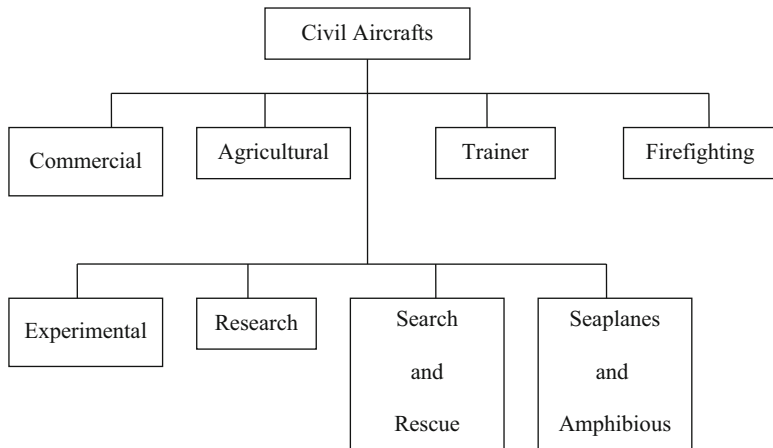


Fig. 1.12 Classification of civil aircrafts



Fig. 1.13 Agricultural aircraft

1.2.4.2.1 Agricultural Aircrafts

Agricultural aircrafts (Fig. 1.13) are aircrafts that have been built or converted for agricultural use – usually **aerial application of pesticides (crop dusting)** or **fertilizer (aerial topdressing)**; in these roles, they are referred to as “crop dusters” or “top dressers” [5].



Side by side (Pilot and Instructor)



Tandem (Pilot in front and Instructor Behind)

Fig. 1.14 Side-by-side and tandem trainer aircrafts

1.2.4.2.2 Trainer

A *trainer* is an [aircraft](#) used to develop piloting or navigational skills in flight crew. Civilian pilots are normally trained in a light aircraft, with two or more seats to allow for student and instructor. The two seating configurations for trainer aircraft are pilot and instructor side by side or in tandem, usually with the pilot in front and the instructor behind [6]. Training has two phases, namely, basic and advanced. Fig. 1.14 illustrates two configurations of trainer aircrafts.

1.2.4.2.3 Firefighting Aircraft

Firefighting aircraft is used in aerial firefighting and normally employed for steep, rocky, high, and unsafe areas. *Airtankers* or *water bombers* are fixed-

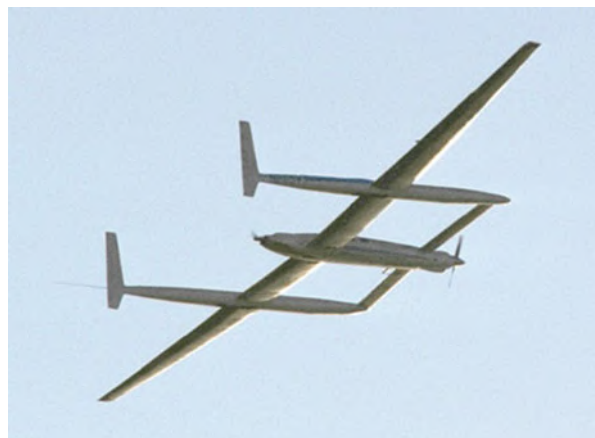


Fig. 1.15 Firefighting CL-215 aircraft dropping water

wing aircraft fitted with tanks that can be filled on the ground at an air tanker base (like C-130 and Grumman S-2 T) or, in the case of [flying boats](#) (CL 215 and Martin Mars Bomber) and [amphibious aircraft](#), by skimming water from lakes, reservoirs, or large rivers. Figure 1.15 illustrates CL 215 aircraft dropping water. Air-tankers may also use non-toxic retardants like [ammonium sulfate](#), which will then act as [fertilizers](#) to help the re-growth of plants after the fire.

1.2.4.2.4 Experimental Aircraft

An *experimental aircraft* is an [aircraft](#) that has not yet been fully proven in [flight](#) [7]. Often, this implies that new [aerospace](#) technologies are being tested on the aircraft. Experimental aircraft is also a specific term referring to an aircraft flown with an experimental category [Airworthiness Certificate](#). A notable example of an experimental aircraft is the [Rutan Voyager](#) (Fig. 1.16). It is the first aircraft to fly around the world without stopping or refueling. Model 76 Voyager powered by a piston engine.

Fig. 1.16 Rutan Voyager

1.2.4.2.5 Research

Research aircrafts can be identified as two main types, already manufactured aircraft or new designed ones. The first may be employed either as an airborne laboratory (DC-8) or in new projects for testing some operating conditions (transonic, sonic boom, and supersonic researches), flight procedure, and so on. The second is a newly designed aircrafts that incorporate developments in aerodynamic characteristics, material, equipments, systems (stall speed warning), and engine. [Centurion](#), Helios, and pathfinder are three types for solar-powered aircrafts.

1.2.4.2.6 Search and Rescue Aircrafts (SAR)

Search and rescue aircrafts (SAR) is the search for and provision of aid to people who are in distress or imminent danger like survivors of aircraft downed at sea as well as sailors and passengers of sea vessels in distress. An example for such aircrafts is de Havilland Canada

DHC-5 Buffalo. *Air ambulance* may be included to this category. It is used for [emergency medical assistance](#) in situations where either a traditional [ambulance](#) cannot reach the scene easily or quickly enough, or the patient needs to be transported over a distance or terrain that makes air transportation the most practical transport. King Air, King Air 200, and Pilatus PC 12/45 are examples for air ambulance aircrafts.

1.2.4.2.7 Seaplanes

Seaplanes are aircrafts capable for operating from sea only while *amphibious* ones can operate from both sea and land as described above. Examples of early Grumman's amphibian family are single-engine biplane G-22, twin-engine G-21, G-44, and G-73.

1.2.4.2.8 Commercial Transport

Commercial transport is an airplane used by airliner to deliver passengers or cargo (freight) for a fare or fee. Passenger aircrafts are now one of the mostly used methods of human transportation and includes numerous types as well be discussed later.

Cargo Aircrafts

A *cargo aircraft* (also known as *freight aircraft* or *freighter*) is designed or converted for the carriage of goods or mail rather than passengers [8]. Cargo airlines are a special category of air service that has grown rapidly in the last three decades to offer express delivery of priority freight. They are usually devoid of passenger amenities, and generally feature one or more large doors for the loading and unloading of cargo. Aircraft designed for cargo flight use have a number of features, refer to Fig. 1.17, that distinguish them from conventional passenger aircraft: a “fat” looking fuselage as displayed in Airbus A300 Beluga Supertransporter, a high-wing to allow the cargo area to sit near the ground like



Fig. 1.17 Cargo Aircrafts (Freighters) Top: An-225 and Bottom A300-600ST, Reproduced by permission from AIRBUS

Antonov An 225, a large number of wheels to allow it to land at unprepared locations, and a high-mounted tail to allow cargo to be driven directly into and off the aircraft and most important additional strengthening on key structural areas. Moreover, there is a wide range of aircraft suitable for all kinds of cargo flights, short-, medium-, and long-haul. Based on its capacity, it ranges from smaller aircraft performing short notice flights carrying vital spare parts up to large cargo aircraft able to transport any voluminous goods

Transports Aircrafts

Transport aircrafts are also called *airliners* or *airplanes*. The first scheduled airline commenced operation in 1914 between Tampa and St. Petersburg in Florida, USA. Passengers travelled the 35 km distance in a flying boat.

Transport aircrafts may be classified – based on flight speed – to supersonic transport (SST) and subsonic/transonic types (Fig. 1.18). Airplanes that are powered by jet engines are also called *jetliners*. Thus Airliners combine both piston engines aircrafts as well as jet engines ones. A supersonic transport (SST) is designed to transport passengers at speeds greater than the [speed of sound](#). The only SSTs to see regular service were [Concorde](#) and the [Tupolev Tu-144](#) (Fig. 1.19). Both are powered by afterburning turbojet engines. The first passenger flight of the Tu-144 was in June [1978](#), and the last flight Concorde's was on November 26, 2003.

Extensive research work by NASA staff is performed to introduce hypersonic transports (will fly in Mach number equal or greater than 5) in the coming decade. Subsonic/transonic aircrafts are described in details in [9]. Their different classes

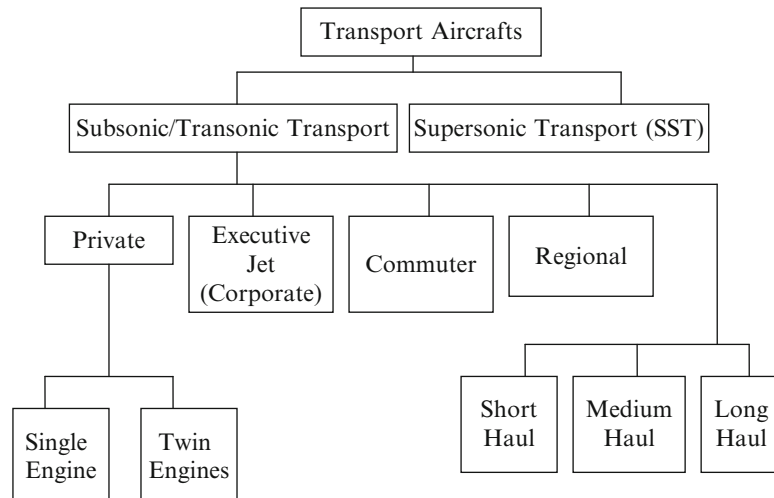


Fig. 1.18 Classification of transport aircrafts

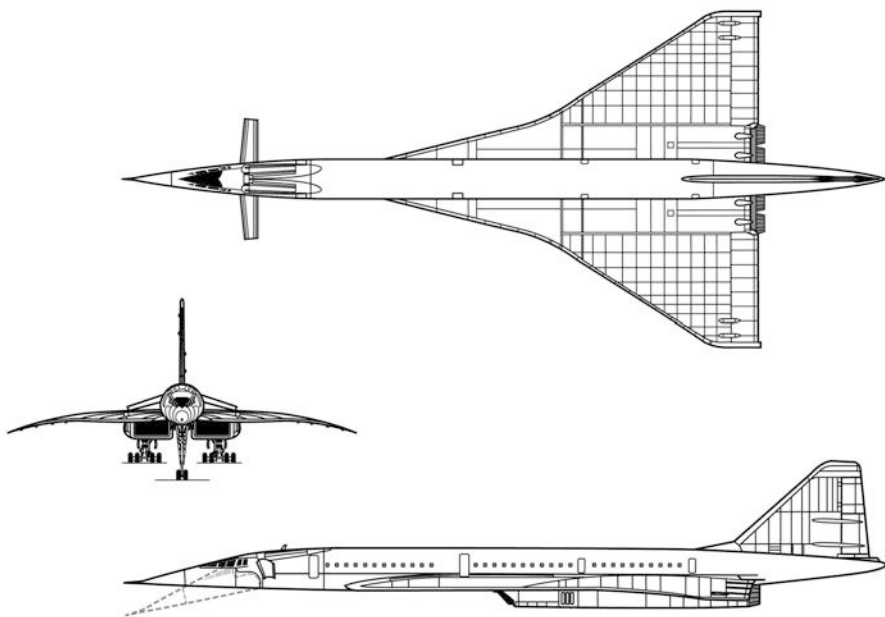


Fig. 1.19 Tu-144

are private (small), executive jet (corporate), commuter, regional, short haul, medium haul, and long haul.

Small Transport

Small transports (sometimes identified as private or air taxi) are either single-engine or twin-engine aircrafts. Examples for them are Cessna 172 and Beechcraft 58 TC Baron respectively, and both are powered by piston engines. Number of passengers for both types is three and six, respectively. *Executive* or corporate jet is private or charter aircraft. It is either powered by turboprop or jet engines. Examples are Raytheon-Beechcraft King Air B300, Cessna Citation II, and Gulfstream. Figure 1.20 illustrates Gulfstream G650 T2 which first flight was on February 25, 2010.

Commuter

A *Commuter* aircraft carry 19 or fewer passenger seats also sometimes called *feederliners*, depending on their size, engines, and seating configurations. Depending on local and national regulations, a commuter aircraft may not qualify as an airliner and may not be subject to the regulations applied to larger aircraft. Members of this class of aircraft normally lack such amenities as **lavatories** and **galley**s and typically do not carry a **flight attendant** as an **aircrew member**. The



Fig. 1.20 Gulfstream G650 T2 executive aircraft



Fig. 1.21 Beechcraft 1900 commuter aircraft

Beechcraft 1900, for example, has only 19 seats and powered by twin turboprop engines (Fig. 1.21). Other aircraft in this category are the Fairchild Metro, **Jetstream 31/41**, **IPTN CN-235**, and **Embraer EMB 110 Bandeirante**, which are all powered by twin turboprop engines.

Regional Airliner

A *regional airliner* is a small [airliner](#) designed to fly up to 100 passengers, and usually feeding larger carriers' hubs from small markets. This class of airliners is typically flown by the regional airlines that are either contracted by or subsidiaries of the larger airlines. It may be powered by [turbofans](#) or [turboprops](#). These airliners, though smaller than aircraft operated by major airlines, are equipped with [lavatories](#) and have a [flight attendant](#) to look after the in-flight needs of the passengers. Typical aircraft in this category are the Embraer ERJ 145 powered by two turbofan engines (Fig. 1.22). Other aircrafts of this category are [Bombardier CRJ](#) series and "Q" ([DASH-8](#)) series powered by turbofan engine, [ATR 42/72](#) and [Saab 340/2000](#). The last two aircrafts are powered by turboprop engines. Airlines and their partners sometimes use these for short flights between small hubs or for bringing passengers to hub cities where they may board larger aircraft.

In [aviation](#), the *flight length* is defined as the time airborne during a flight. Short haul flight is defined as a flight less than 3 h in length, while a medium haul is defined as a flight between 3 and 6 h. A long haul flight is a journey typically made by [wide-body aircraft](#) that involve long distances, typically beyond six and a half hours in length, and often are [non-stop flights](#).

Short Haul

Typical *short haul* airliners in the 1960s and 1970s are [Aerospatiale Caravelle](#), [Aérospatiale Corvette](#), [Hawker Siddeley Trident 1C/1E](#), [BAC One-Eleven](#),



Fig. 1.22 Embraer ERJ145 regional aircraft



Fig. 1.23 Aeroflot Yakovlev Yak-40 series Short Haul Aircraft

Douglas DC-9, Tupolev Tu-124, Tupolev Tu-134, Fokker F28, Yakovlev Yak-40 (Fig. 1.23), Boeing 737-100, Boeing 737-200, Dassault Mercure, and VFW-614. Concerning 1980s and 1990s short hauls, they are Airbus A320, Boeing 737-300, Boeing 737-400, Boeing 737-500, BAe 146, Fokker 70, Fokker 100, and Yakovlev Yak-42 (Fig. 1.22). Finally for 2005 and onward, they are Embraer E-190, Embraer E-195, and Bombardier Aerospace C-Series. All aircrafts are powered by turbofan engines.

Medium Haul

Medium haul aircrafts are more common class of airliners (normally narrow-body or single aisle aircraft). These airliners are generally used with fewer passengers than their wide-body counterparts. Examples include the Boeing 727, 757, MD-80/MD-90 series, Airbus A320 family, Tupolev Tu-204, Tu-214, Embraer E-Jets 190 & 195, and Tu-334. Older airliners like the Boeing 707, 727, McDonnell Douglas DC-8, Fokker F70/F100, VC10, Tupolev, and Yakovlev jets also fit into this category. All these airplanes are powered by turbofan engines. Figure 1.24 illustrates Airbus A320 aircraft floating in Hudson River in 15 January 2009. Due to a collision with a flock of birds, both engines were disabled several minutes after takeoff. Pilot made a successful landing in Hudson River, saving the lives of all 150 passengers and five crew.



Fig. 1.24 Medium Haul Airbus A320 aircraft (Reproduced by permission from AIRBUS)

Long Haul

Long haul aircrafts are the largest airliners, which are [wide-body](#) jets and many passengers. These aircraft are frequently twin-aisle aircraft. Aircraft in this category are the [Boeing 747](#), [Boeing 767](#), [Boeing 777](#), [Boeing 787](#), [Airbus A300/A310](#), [Airbus A330](#), [Airbus A340](#), [Airbus A380](#), [Airbus A350](#), [Lockheed L-1011 TriStar](#), [McDonnell Douglas DC-10](#), [McDonnell Douglas MD-11](#) (Fig. 1.25), [Tupolev Tu-214](#), [Ilyushin Il-86](#), and [Ilyushin Il-96](#). All aircrafts are powered by turbofan engines.

It is worth mentioning here that several aircrafts are manufactured in two versions, one as a transport and the second as a cargo. Moreover, many transports may be easily converted into cargo aircrafts. However, a few types are designed as a cargo type from cold start.

1.2.4.3 Military Aircrafts

Military aircrafts are either fixed wing or helicopters (Fig. 1.26). Both can be further subdivided into combat and non-combat aircrafts.



Fig. 1.25 Long Haul Airbus 380 (Reproduced by permission from AIRBUS)

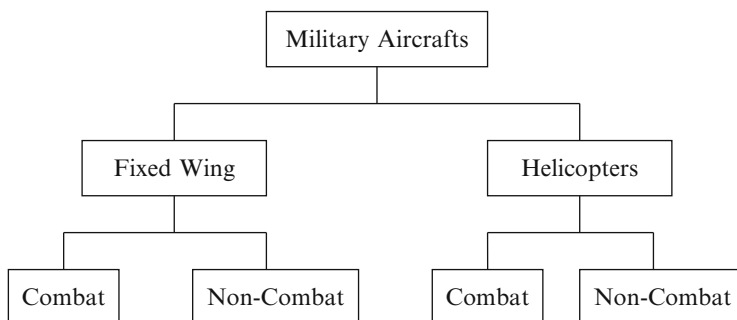


Fig. 1.26 Classification of military aircrafts

1.2.4.3.1 Combat Fixed Wing Military Aircrafts

Fixed wing combat aircrafts may be classified into seven categories, namely, fighter, bomber, fighter-bomber, maritime patrol, ground attack, and powered lift as illustrated in Fig. 1.27.

Bomber

A *bomber* is designed to attack ground and sea targets, primarily by dropping bombs on them [10]. It is worthy mentioning that the first non-stop transatlantic

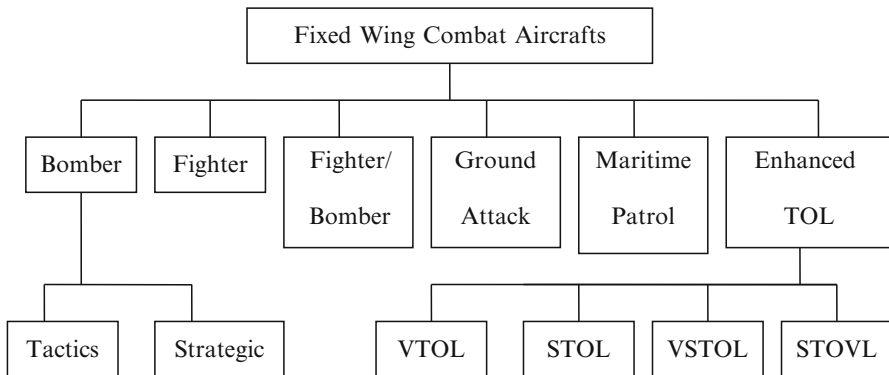


Fig. 1.27 Classification of fixed wing combat aircrafts



Fig. 1.28 Stealth strategic bomber B-2 and strategic bomber Tu-95 bear

flight in 1919 was made by two British aviators on their heavy twin engine Vickers Vimy Bomber in 16 h trip.

Bomber aircrafts are further divided into tactics and strategic types.

Strategic bombers are primarily designed for long-range strike missions into the enemy's heartland to destroy strategic targets such as supply bases, bridges, factories, shipyards, and cities. Examples include the: Avro Lancaster, Heinkel He-111, Junkers Ju 88, B-17 Flying Fortress, B-24 Liberator, B-29 Superfortress, B-36 Peacemaker, B-47 Stratojet, B-52 Stratofortress, General Dynamics F-111, Tupolev Tu-16 'Badger', Tupolev Tu-160 'Blackjack', and Tupolev Tu-95 'Bear'. Most – if not all – recent strategic bombers are *stealth*, while older ones are not. Figure 1.28 illustrates B-2 strategic stealth bomber (powered by turbofan engines) releasing bombs and Russian strategic bomber Tu-95 Bear (powered by turboprop engines).

Tactical bombers are smaller aircraft that operate in shorter range in the battle zone to attack troops, tanks, and military equipments. Examples for old ones are [Junkers Ju 87 Stuka](#) and [Ilyushin Il-2 Shturmovik](#), where both are powered by piston engines. More recent ones are [A-10 Thunderbolt II](#), [F-16 Fighting Falcon](#), [Panavia Tornado](#), [Lockheed F-117](#), [Mikoyan MiG-29](#), and [Sukhoi Su-25 ‘Frogfoot’](#), where all are powered by turbofan engines. Some strategic bombers are also stealth like B-2.

Fighter

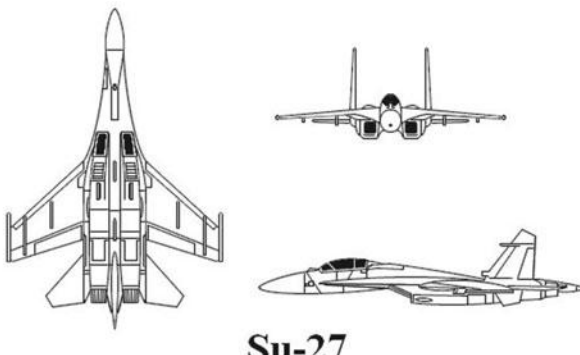
A *fighter aircraft* is a [military aircraft](#) designed primarily for air-to-air combat with other [aircraft](#). Fighters are small, fast, and maneuverable. The term “fighter” is also sometimes used colloquially for dedicated [ground-attack aircraft](#) [11]. Early fighters were very small and lightly armed by later standards and were mostly [biplanes](#). By [World War II](#), fighters were predominantly all-metal [monoplanes](#) with wing-mounted batteries of [cannons](#) or [machine guns](#).

Grumman F7F-3 Tigercat and Lavochkin La-9 were some of the last Grumman piston engine fighters. By the end of the war, [turbojet](#) engines were already beginning to replace piston engines as the means of propulsion, and increasingly sophisticated refinements to armament were already appearing. Modern jet fighters are predominantly powered by one or two [turbofan](#) engines and are equipped with [radar](#) as the primary method of [target acquisition](#). Armament consists primarily of [air-to-air missiles](#) (from as few as two on some lightweight [day fighters](#) to as many as eight or twelve on air superiority fighters like the Sukhoi Su-27 or [Boeing F-15 Eagle](#); Fig. 1.29), with a cannon as backup armament (typically between 20 and 30 mm); however, they can also often employ [air-to-surface missiles](#), as well as guided and unguided bombs.

In brief, any fighter aircraft belongs to one of six groups. First generation group subsonic jet fighters from mid-1940s to mid-1950s, second generation include jet fighters from mid-1950s to early 1960s, third-generation jet fighters resembles the period from early 1960s to circa 1970, fourth generation outline jet fighters of circa 1970 to mid-1990s, 4.5th generation jet fighters available from 1990s to 2005, and lastly, the fifth generation includes jet fighters from 2005 up to present.

Fighter-Bomber

Many fighters have secondary ground-attack capabilities, and some are dual-role as [fighter-bombers](#). A strike fighter is an American designation for a [fighter-bomber](#), examples are Su-7, Su-24, Su-34, F-111, and F-15 Eagle, [12]. A multi-role capable combat aircraft set up to operate primarily in the [tactical bombing](#) role. All are powered by afterburning turbofan engines.



F-15 Eagle

Fig. 1.29 Fighter aircrafts: Sukhoi Su-27 and [Boeing F-15 Eagle](#)

Ground-Attack

Ground-attack aircraft is also identified as *attack aircraft*, *fighter-bomber*, *tactical fighter*, *tank-buster*, [tactical bomber](#), *strafer*, and *strike aircraft*. It is designed to attack targets on the ground and is often deployed as [close air support](#). Examples include the American [A-10 Thunderbolt II](#) (powered by turbofan engine) and the Russian [Sukhoi Su-25](#) Frogfoot (powered by turbojet engine). Their role is tactical rather than strategic.

Maritime Patrol

A *maritime patrol aircraft*, also simply *patrol aircraft*, or by the older term *patrol bomber*, is a [fixed-wing aircraft](#) designed to operate for long durations over water in



Fig. 1.30 Maritime patrol aircraft Atlantique ATL3, France

maritime patrol, anti-shipping, anti-submarine (ASW), and search and rescue roles. Examples for this group during Cold War and Modern eras are Beriev Be-12 (Russia), Ilyushin Il-38 (Russia), Boeing P-8 Poseidon (USA), Lockheed P-2 Neptune (USA), Atlantique ATL3 – Maritime (France), CASA CN-235, C-295 Persuader (Spain), Canadair CP-107 Argus (Canada), Fokker F-27 Maritime (Netherlands), Hawker-Siddeley Nimrod (UK), and PZL M28B Bryza 1R (Poland). Some of these aircrafts are powered by turbofan engines, while others are powered by turboprop engines as seen in Fig. 1.30.

Enhanced Takeoff and Landing (TOL)

Enhanced Takeoff and Landing (TOL) types refer to aircrafts that can take off and land vertically and function differently from a rotorcraft in horizontal flight. It is subdivided into four main categories; VTOL, STOL, V/STOL, and STOVL. They stand for vertical takeoff and landing, short takeoff and landing, short and/or vertical takeoff, and lastly short takeoff and vertical landing, respectively. A list of all VTOL aircraft is listed in [13]. The two famous examples for vectored thrust aircrafts are F 35 (Fig. 1.10) and Harrier II (Fig. 1.31) aircrafts.

F-35 is powered by a single F135 turbofan engine with a lift fan, roll posts, and rear vectoring nozzle.

Harrier aircrafts has four famous versions and powered by turbofan engines with four swiveling nozzles.

There were also some experimental/prototypes for VTOL aircraft which are tailless. Examples include the Ryan X-13A-RY Vertijet, Ryan Model 69, Lockheed XFY, and Convair XFY Pogo. Ryan X-13A-RY Vertijet powered by a single RR Avon Turbojet engine (1950s), Lockheed XFY (tailsitter prototype), and Convair XFY Pogo tailsitter powered by a 5500 hp Allison YT40-A-16 turboprop engine.



Fig. 1.31 Harrier II enhanced TOL aircraft

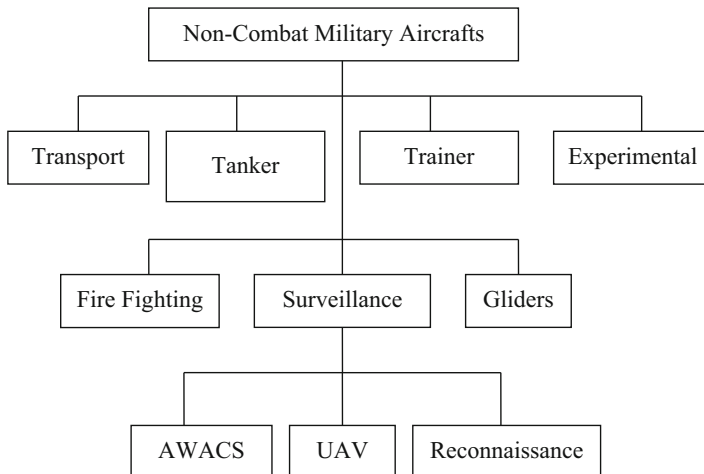


Fig. 1.32 Classification of fixed wing non-combat military aircrafts

1.2.4.3.2 Non-combat Fixed Wing Military Aircrafts

As shown in Fig. 1.32, non-combat military aircrafts may be assembled into the following groups, namely, transport, tanker (refueler), trainer, experimental,

gliders, firefighting, and surveillance. Moreover, surveillance aircrafts may be further subdivided into three subgroups: reconnaissance, UAV, and AWACS.

Transport

Military transport aircraft are typically fixed wing cargo aircraft, which are used to deliver troops, weapons, and other military equipment by a variety of methods to any area of military operations outside of the commercial flight routes in **uncontrolled airspace**. Some military transport aircraft are tasked to perform multi-role duties such as **aerial refueling** and tactical, operational and strategic **airlifts** onto unprepared runways, or those constructed by engineers. Examples for these aircrafts are An-24, Il-112, C-130, and Airbus A400 M, which are powered by turboprop engines. Others are An -124, Il -76, Galaxy C-5, C-17, C-141B, Kawasaki C-1, and C-X, which are powered by turbofan engines.

Aerial Refueling

Aerial refueling, also called *air refueling*, *in-flight refueling (IFR)*, *air-to-air refueling (AAR)*, or *tanking*, is the process of transferring **fuel** from one **aircraft** (the tanker) to another (the receiver) during flight. Figure 1.33 illustrates USAF KC-135R is refueling US Navy F-16. Other refuelers are **Airbus A400M**, **Boeing C-135**, **KC-10 Extender**, **KC-135 Stratotanker**, **Vickers VC-10**, and **Il-78**. All these



Fig. 1.33 Airbus A400M refueling a Spanish Air Force F/A-18 Hornet (Reproduced by permission from AIRBUS)

aircrafts are powered by turbofan engines, except Airbus A400M which is powered by turboprop engines.

Trainer

A military *trainer* is an [aircraft](#) used to develop piloting, navigational, or war-fighting skills in flight crew. Several training phases are followed which starts usually with [turboprop](#) trainers like the [Pilatus PC-9](#) and [Embraer Tucano](#). The final phase includes training for fast jet flying. Examples of such jet trainer aircraft include the [T-38 Talon](#) (actually capable of supersonic speeds), the [BAE Hawk](#), the [Dassault/Dornier Alpha Jet](#), and the [Aero L-39](#). All are powered by turbofan engines except for T-38, which is powered by afterburning turbojet engine.

Surveillance

A *surveillance aircraft* are used for monitoring enemy activity, usually carrying no armament. A surveillance aircraft does not necessarily require high-performance capability or [stealth](#) characteristics. Technically, anything which can fly and make observations (dynamically or via recording equipment/sensors) of visual information or electronic emissions qualifies as a surveillance aircraft. Surveillance aircraft are either reconnaissance, unmanned aerial vehicle (UAV), or Airborne Warning and Control System (AWACS).

Airborne Reconnaissance

An *airborne reconnaissance* goes back to the early era of [ballooning](#). The first reconnaissance flights took place during the [Balkan wars](#) in October 1912 by (Albatros) aircraft. One of the first aircrafts used for surveillance was the [Rumpler Taube](#) during [World War I](#). Japanese built [Mitsubishi Ki-46](#) twin-engine reconnaissance aircraft in 1939. Fighters such as the British [Spitfire](#), [Mosquito](#), the American [P-38 Lightning](#), and [P-51 Mustang](#) were adapted for photo-reconnaissance during [World War II](#). After World War II, long range aerial reconnaissance was taken up by adapted bombers like the [English Electric Canberra](#) and the American [Martin B-57](#). The first purpose-built jet covert surveillance aircraft, namely, the [Lockheed U-2](#) was constructed secretly for the United States. Modified versions of the U-2 remain in service in 2007. In the 1960s the [SR-71 Blackbird](#), the fastest manned jet-propelled aircraft ever built, was constructed as strategic reconnaissance aircraft.

There are claims that the USA constructed a new, secret, [hypersonic](#) surveillance aircraft – dubbed the [Aurora](#) – in the late 1980s, but no confirmation of this has ever emerged. Another category of surveillance aircraft that has been in vogue since World War II is the [maritime patrol aircraft](#). These are typically large, slow machines capable of flying continuously for many hours, with a wide range of sensors and electronic equipments on board. Such aircraft include the [Avro Shackleton](#) (powered by piston engines), the [Hawker-Siddeley Nimrod](#) (powered by

turbofan), the [Breguet Atlantique](#), the P-3 [Orion](#) and the [Tupolev Tu-95](#) (all powered by turboprop), and the P-2 [Neptune](#) (powered by radial engines). Moreover, finally, every fighter plane and ground attack plane can be used to perform surveillance (recent example is [F-35 Joint Strike Fighter](#)).

The second group of surveillance aircrafts is *unmanned aerial vehicle (UAV)*.

UAV

Remotely piloted vehicle (RPV), or *unmanned aircraft system (UAS)*, is an aircraft that flies without a human crew on board the aircraft. Their largest uses are in reconnaissance as well as attack missions. UAV is defined as a reusable, uncrewed vehicle capable of controlled, sustained, level flight and powered by a [jet](#) or [reciprocating engine](#). There are a wide variety of UAV shapes, sizes, configurations, and characteristics [14]. UAVs come in two varieties: some are controlled from a remote location, and others fly autonomously based on pre-programmed flight plans using more complex dynamic automation systems. Figure 1.34 illustrates A [MQ-9 Reaper](#), a [hunter-killer](#) surveillance UAV used by the USAF and [British Armed Forces](#) and powered by a 950-[shaft-horsepower](#) (712 kW) [turboprop](#) engine.

Airborne Warning and Control System (AWACS)

An *Airborne Warning and Control System (AWACS)* aircraft is designed to carry out [surveillance](#) and C2BM (command and control, battle management) functions.



Fig. 1.34 [MQ-9 Reaper](#), [Hunter-Killer](#) Surveillance UAV

AWACS aircraft are in service with the [USAF](#), [NATO](#), Russian Air Force, the [RAF](#), French Air Force, [Saudi Arabia](#), Pakistan Air Force, and the Japan Air Self-Defense Force.

Modern AWACS systems can detect aircraft from up to 400 km (250 miles) away. In air-to-air combat, AWACS systems can communicate with friendly aircraft, extend their sensor range, and give them added stealth, since they no longer need their own active radar to detect threats.

Examples are [Boeing E-3 Sentry](#) (Fig. 1.35; based on the Boeing 707) and Boeing 767 AWACS. Both are powered by turbofan engines.

Experimental

An *experimental aircraft* is an [aircraft](#) that has not yet been fully proven in [flight](#). Often this implies that new [aerospace](#) technologies are being tested on the aircraft. The *X-planes* (X-1 through X-55) are a series of experimental [United States aircraft](#) (and some [rockets](#)) [15].

The first of these, the [Bell X-1](#), became well-known as the first plane to break the [sound barrier](#), which it did in 1947. Later X-planes yielded



Fig. 1.35 Boeing E-3-D Sentry AWACS aircraft

important research results, but only the [North American X-15](#) rocket plane of the early 1960s achieved comparable fame. X-7 through X-12 were actually [missiles](#), and some other vehicles were unpiloted. Most X-planes are not expected to ever go into full-scale production except the [Lockheed Martin X-35](#), which competed against the [Boeing X-32](#) to become the [Joint Strike Fighter](#).

Glider

Military gliders have been used by the military of various countries for carrying troops and heavy equipment to a combat zone, mainly during [World War II](#). These engineless aircraft were towed into the air and most of the way to their target by military transport planes (e.g. [C-47 Skytrain or Dakota](#)) or bombers relegated to secondary activities (e.g. [Short Stirling](#)). Once released from the tow craft near the front, they were to land on any convenient open terrain close to target. These are one-way (disposable aircrafts), thus constructed from common and inexpensive materials such as wood, though a few were retrieved and re-used. Examples are German Junkers Ju 322, Japanese Ku-13, Soviet Antonov A-40, and American Waco CG-3.

Fire Fighting

Fire fighting aircraft is an *airtankers* or *water bombers* fitted with tanks that can be filled on the ground at an air tanker base. Examples are Grumman S-2 T and C-130 (Fig. [1.36](#)). Both are powered by turboprop engines.

1.2.5 Rotorcrafts (Rotor-Wing Aircrafts)

Rotorcraft, or rotary-wing aircraft, uses a spinning rotor with [aerofoil](#) section blades (a rotary wing) to provide lift. Types as depicted in Fig. [1.37](#) include powered and unpowered groups.

Unpowered are mainly rotor kites. Powered group includes three main sub-groups, namely, [helicopters](#), autogyro, and gyrodyne.

1.2.5.1 Powered Rotorcrafts

1.2.5.1.1 Gyrodyne

A *gyrodyne* is a rotorcraft with a rotor system that is normally driven by its engine for takeoff and landing – hovering like a helicopter and its forward thrust is obtained from a separate propulsion device (usually two propellers mounted in tips of short or stub wings) rather than from tilting the rotor. Being able to fly in



Fig. 1.36 Firefighting C-130 aircraft dropping water

autorotation gives the gyrodyne all of the advantages and simplicity of a gyroplane. Figure 1.38 illustrates the famous UK gyrodyne Rotodyne powered by turboprop engines and having a capacity of 44 passengers and speed of 200 mph.

1.2.5.1.2 Autogyro

An *autogyro* (sometimes called gyrocopter, gyroplane, or rotaplane) utilizes an unpowered rotor driven by aerodynamic forces in a state of **autorotation** to develop lift, and an engine-powered **propeller** (mostly piston), similar to that of a **fixed-wing aircraft**, to provide thrust (Fig. 1.39).

1.2.5.1.3 Helicopter

Helicopters have powered rotors (single or dual). The rotors are driven (directly or indirectly) by engine(s) that push air downwards to create lift. Rotors are driven by the engine(s) throughout the flight, to allow the helicopter to take off vertically, hover, fly forwards, backwards and laterally, as well as to land vertically. The first “helicopter” flight dates back to 1907. The Frenchman Paul Cornu took off with a

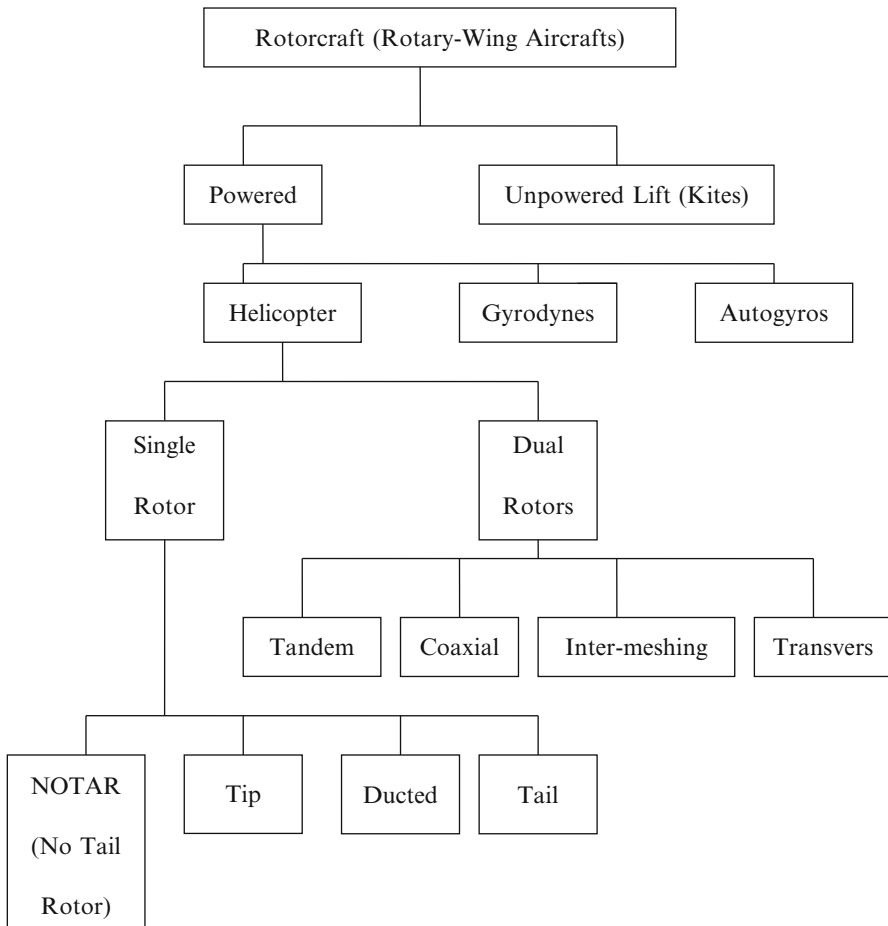


Fig. 1.37 Classification of rotorcrafts

helicopter and hovered at a height of 30 cm for approximately 20 s. Continuous developments in helicopter industry lead to the extended list of helicopters. Helicopters have several different configurations of one or more main rotors. Each main rotor has a number of blades between two and six.

Classifications Based on Rotor

Single Main Rotor

Helicopters with one driven main rotor require some sort of anti-torque device such as a **tail rotor**, **fantail**, or **NOTAR**, except some rare examples of helicopters using tip jet propulsion which generates almost no torque. Twin rotor has two rotor discs which usually rotate in opposite directions, so that no tail rotor or other yaw



Fig. 1.38 Gyrodyne rotorcraft



Fig. 1.39 Autogyro rotorcraft

stabilizer is needed. The two rotors are arranged in *tandem* (one in front of the other), *transverse* (side by side), *coaxial* (one rotor disc above the other), with concentric drive shafts or *intermeshing* (where the rotor discs may be arranged to pass through each other).

Tandem Rotor

Tandem rotor helicopters have two large horizontal rotor assemblies mounted one in front of the other [16]. Tandem rotor helicopters use counter-rotating rotors. This configuration is used for large cargo helicopters like CH-46 Sea Knight, CH-47 Chinook, Boeing Model 234, and Boeing Model 360.

Transverse Rotors

Transverse rotors are mounted on the end of wings or outriggers, perpendicular to the body of the aircraft and uses differential collective pitch. This configuration is found on the Focke-Wulf Fw 61 (powered by radial engine) and Focke-Achgelis Fa 223 (powered by radial engines), as well as the world's largest helicopter ever built, the Mil Mi-12 (powered by turboshaft engines). Figure 1.40 illustrates both tandem rotor (CH-47 Chinook) and transverse rotor (Focke-Achgelis Fa 223) helicopters.

Coaxial Rotors

Coaxial rotors (Fig. 1.41) are a pair of helicopter rotors mounted one above the other on concentric shafts, with the same axis of rotation, but that turn in opposite directions. This configuration is produced by the Russian Kamov helicopter design bureau.

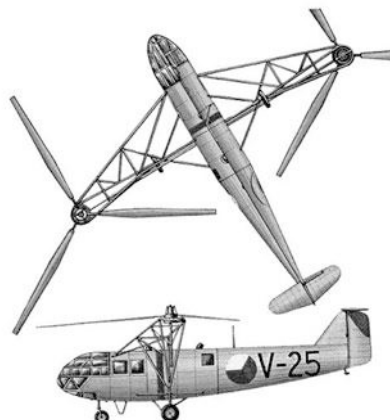


Fig. 1.40 Tandem rotor (CH-47 Chinook) and transverse rotor (Focke-Achgelis Fa 223)



Fig. 1.41 Kamov KA32 Coaxial rotor helicopter



Fig. 1.42 HH-43 Huskie with intermeshing rotors

Intermeshing Rotors

Intermeshing rotors (sometimes referred to as a *synchropter*) are a set of two rotors turning in opposite directions, with each rotor mast mounted on the helicopter with a slight angle to the other so that the blades intermesh without colliding. The

arrangement allows the helicopter to function without the need for a tail rotor. Figure 1.42 illustrates HH-43 Huskie helicopter with Intermeshing Rotors.

Early helicopter designs utilized rotary engines, but these were soon replaced by more powerful automobile engines and radial engines. Next, during the first half of the twentieth century, helicopters used the compact flat engine. Later on, turbine engines revolutionized helicopter industry, where turboshaft engine gave helicopters an engine with a large amount of power and a low weight penalty.

Civil Helicopters

Helicopters activities are daily increasing both in civilian and military disciplines. In civil world, helicopters are used in transportation, training, construction, remote sensing, search and rescue as well as firefighting (Fig. 1.43).

Transport

Helicopters are used as transport vehicles for commercial purposes. It includes commercial transport, tourism, and aerial photography. Thus it may transport employees say for oil search companies, isolated locations, or offshore sites. Moreover, many tourism companies use helicopters for sightseeing like those in Pyramids' area in Giza, Egypt, and Las Vegas, USA. Moreover, equipped helicopters are used in aerial photography. It is used also for transporting cargo and

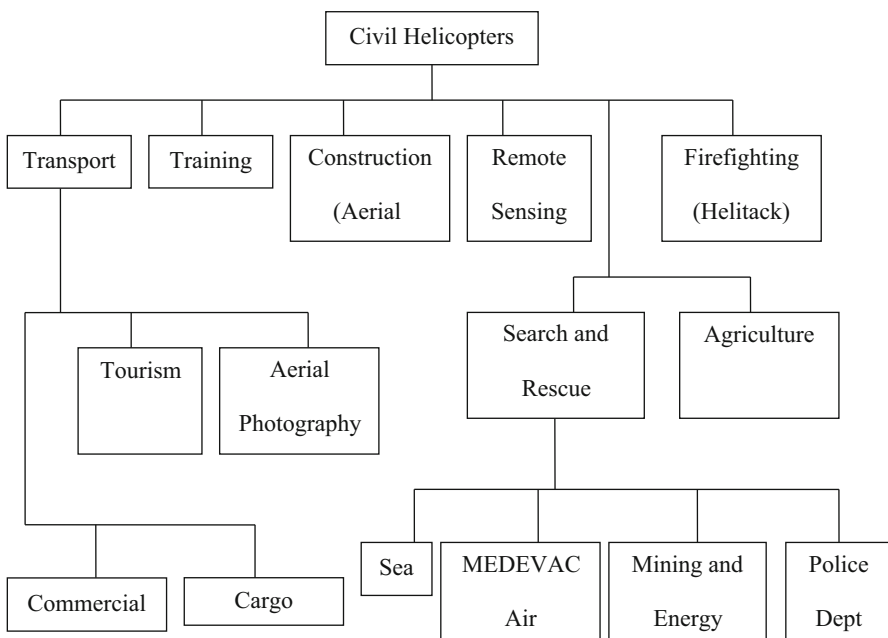


Fig. 1.43 Classification of civilian helicopters

equipments. All helicopters are powered by turboshaft engines, except small types which are powered by piston engines.

Training

Training helicopters are mostly single engine including MD500E, MD600, Bell 206 JetRanger, and Robinson R22 BetaII. All are powered by turboshaft engines except for the last one.

Aerial Cranes

Aerial cranes or skycranes are used to lift heavy loads. Figure 1.44 illustrates Sikorsky Skycrane S-64 (powered by turboshaft engine) carrying a house. Helicopters were first used as aerial cranes in the 1950s, but attained its popularity in the **construction** field in the 1960s.

The most consistent use of helicopters as aerial cranes is in the **logging** industry to lift large trees out of rugged terrain. Other lift services to the construction industry cover: HVAC removal and/or installation, steel tower construction, powerline construction, marine salvage, remote area operations/high-rise buildings, and congested areas and erect, remove, and replace all types of antennas and antenna towers.



Fig. 1.44 Sikorsky Skycrane S-64 carrying a house

Remote Sensing

Helicopters employed in aerial *remote sensing* for several reasons including: time flexibility in measurement, high maneuverability, surface sampling, fills gap between satellites and ground station, and satellite sensor calibration with helicopter sensors. Typical helicopter for remote sensing are Hughes/MD 500 and BK 117, both are powered by turboshaft engines.

Search and Rescue

Search and rescue helicopters have many duties as sea or coast guard, aerial ambulance, mining, and energy as well as police departments. Typical helicopters are Sikorsky series H-19, HH-52A Sea Guard, S-70, HSS-2, and CH-53. All are powered by turboshaft engines except for Sikorsky H-19, which is powered by radial engines.

Figure 1.45 illustrates Sikorsky HH-52A Sea Guard, which has the ability to land on the water.

Agriculture

Agriculture helicopters are used in crop spraying and dusting, seeding and spreading fertilizer, frost patrol, and insect eradication. These helicopters are equipped with special removable gear for spraying, fertilization, and generation of aerosols. Examples are Ka-15 M and Mi-1.



Fig. 1.45 Sikorsky HH-52A sea guard

Aerial Firefighting

Aerial firefighting is the use of [aircraft](#) and other aerial resources to combat [wildfires](#). Aircraft may be fixed-wing or helicopters. Helicopters may be fitted with tanks or carry buckets. Buckets are usually filled by submerging in lakes, rivers, reservoirs, or portable tanks. Popular firefighting helicopters include variants of the [Bell 205](#) (Fig. 1.46) and the [Erickson S-64 Aircrane](#) helitanker, which features a sea snorkel for filling while in flight. Both are powered by turboshaft engines.

Military Helicopters

A military helicopter is a helicopter that is either specifically built or converted for use by military forces. A military helicopter's mission is a function of its design or conversion. The most common types of military helicopters are transport, attack, training, experimental, search and rescue, UAV, maritime, tactics and operation, and finally observation (Fig. 1.47).

Attack

Attack helicopters are armed helicopters used in the [antitank](#) and [close air support](#) roles.



Fig. 1.46 Firefighting Bell 205 dropping water

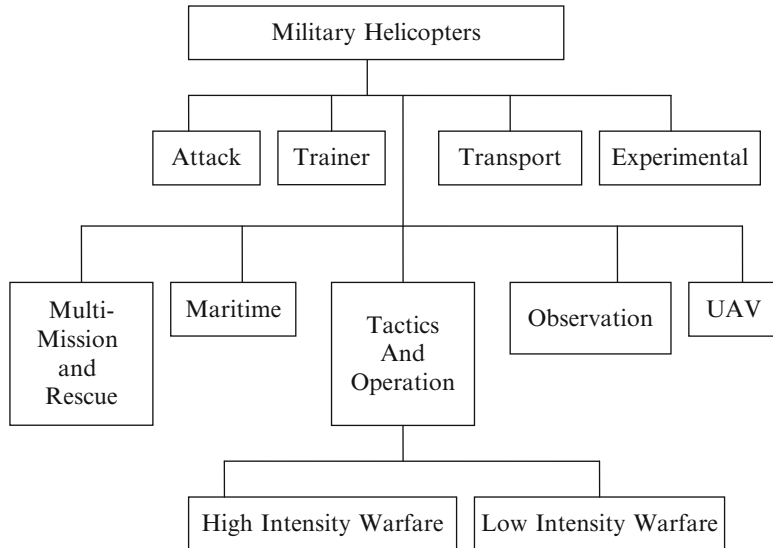


Fig. 1.47 Military helicopters

Weapons used on attack helicopters can include [autocannons](#), [machine-guns](#), [rockets](#), and guided [missiles](#) such as the [Hellfire](#). Today's attack helicopter has two main roles: first, to provide direct and accurate [close air support](#) for ground troops, and the second, in the [anti tank](#) role to destroy enemy armor concentrations. Examples are Mi -24P and Kamov Ka-50, Westland WAH-64 Apache, Boeing AH-64A Apache, Bell 209/AH-1 HueyCobra, Boeing/Sikorsky RAH-66 Comanche, Z-10, Eurocopter Tiger, Augusta A 129 Mangusta, and Denel AH-2 Rooivalk. All are powered by turboshaft engines (Fig. 1.48).

Trainer

Trainer helicopter is used for air education. An example for this category is HH-60G Pave Hawk helicopter, which is powered by turboshaft engine.

Transport

Transport helicopters are used in places where the use of conventional aircraft is impossible. It lands easily in any area. Transport helicopters are operated in assault, medium, and heavy classes. Examples for this category are [Aerospatiale SA 231 Super Frelon](#), [Eurocopter Puma/Cougar](#), [Eurocopter Dolphin/Panther](#), [NH Industries NH 90](#), [HAL Dhruv](#), [PZL Swidnik W-3 Sokol](#), [Mil Mi-8 Hip](#), [Mil Mi-26 Halo](#), [Westland Lynx](#), [Sikorsky S-70A/UH-60 Black Hawk](#), and [Boeing Helicopters CH-47 Chinook](#). All are powered by turboshaft engines.



Fig. 1.48 Attack helicopter Mi -24P

Experimental

Experimental helicopter as mentioned earlier is an [aircraft](#) that has not yet been fully proven in [flight](#). As an example, X-49A “Speedhawk”, Eurocopter X3, [Kamov Ka-50](#), [Mil Mi-X1](#), and [Sikorsky S-97](#). All are powered by turboshaft engines.

Search and Rescue (SAR)

Multi-mission and rescue, or Search and Rescue (SAR) which is sometimes identified as *Combat Search and Rescue (CSAR)* are helicopters that perform search and rescue missions in land and sea. The main objective is to use of available resources (personnel and facilities) to assist persons, ships, or crafts in potential or actual distress and provide for their initial medical or other needs, and deliver them to a place of safety. Examples are CH-118 Iroquois, CH-149 Cormorant, CH-146 Griffon, CH 53GS, HH 60/Pave Hawk, and HH-52A. A sub-group of this category is *Medical evacuation (MEDEVAC)*. The [US military](#) has recently employed [UH-60 Black Hawk](#) helicopters to provide air ambulance service. Also coast-guard helicopters like HH-65A Dolphin – which used in saving hundreds of lives since introduction in 1987 – belongs to this sub-category. All are powered by turboshaft engines.

Maritime Helicopters

Maritime helicopters operate from ships, destroyers, cruisers, and battleships. It may act as anti-submarine warfare (ASW), anti-shipping, transport, SAR, and reconnaissance roles. It must have enhanced protection against salt water corrosion and protection against ingestion of water. Examples are Royal Navy AgustaWestland EH101 Merlin anti-submarine warfare & medium-lift transport/utility helicopter, LAMPS SH-60B Seahawk, and Kamov Ka-27 (Fig. 1.49).

Tactics and Operations Helicopters

This category of helicopters gives a force multiplier that maximizes their impact in a combined arms approach. It is employed both as *high- and low-intensity warfare*. *High-intensity warfare* is characterized by large arrays of conventional armed forces, like Cobra helicopters, which armament included [anti-tank missiles](#), such as the [Nord SS.11](#), and [3M11 Falanga](#) missiles. Concerning *low-intensity warfare*, helicopters are used in counter-insurgency (COIN) warfare. It is powered by turboshaft engines.



Fig. 1.49 Maritime helicopter LAMPS SH-60B Seahawk

Observation

Observation helicopters were initially limited to visual observation thus featured rounded, well-glazed cockpits for maximum visibility. Today, they include low light level television and forward looking infrared cameras. Often, these are mounted in a stabilized mount along with multi-function lasers capable of rangefinder and targeting designators for weapons systems.

Examples are Gazelle, OH-58 Kiowa, Kawasaki OH-1, and Tiger ARH. All are powered by turboshaft engines

UAV

UAV rotorcraft also flies without a human crew on board similar to fixed wing UAV. They are powered by a jet or reciprocating engine. In addition to conducting intelligence, surveillance, and reconnaissance, it successfully could achieve new goals. Boeing's A160T Hummingbird UAV has the ability to resupply frontline troops in rough terrain (Fig. 1.50). Northrop Grumman Corporation's RQ-8 Fire Scout unmanned air vehicle (UAV) can successfully fire two rockets and has the ability of vertical landings on a moving ship without a pilot controlling the aircraft.

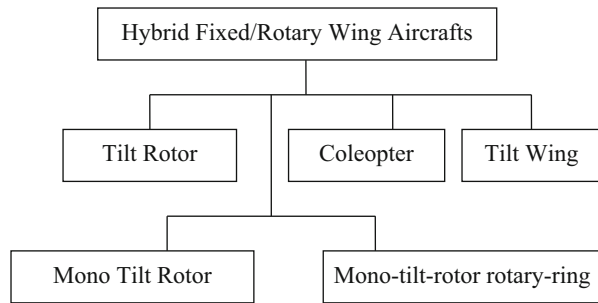
1.2.6 *Hybrid Fixed/Rotary Wings*

Hybrid fixed/rotary wing aircrafts are a group of aircraft that combines features of both fixed wing and aircrafts and rotorcrafts. Figure 1.2.38 illustrates that this group



Fig. 1.50 Boeing's A160T Hummingbird UAV

Fig. 1.51 Classification of hybrid fixed/rotary wing aircraft



includes five sub-groups, namely: tiltrotor, tiltwing, coleopter, mono tiltrotor, and Mono-tilt-rotor rotary-ring. The first two sub-groups are the most famous types (Fig. 1.51).

1.2.6.1 Tiltrotor

Tiltrotor represents a compound rotorcraft and vectored thrust [17]. Examples for tiltrotor are Osprey V-22, Bell XV-3, Doak VZ-4, Bell X-22, Aérospatiale N 500, Bell XV-15, Bell Eagle Eye, and Bell/Agusta BA609. Figure 1.52 illustrates V-22 Osprey with US marines jumping from. The Osprey V-22 can be armed with several types of machine guns pointing rearward that can be fired when the loading ramp is lowered.

1.2.6.2 Tiltwing

Tiltwing aircraft features a wing that is horizontal for conventional forward flight and rotates up for vertical takeoff and landing. Tiltwing aircraft are typically fully capable of [VTOL](#) operations. The tiltwing design offers certain advantages in vertical flight relative to a tiltrotor. Figure 1.53 illustrates Hiller X-18 tiltwing aircraft.

1.2.6.3 Coleopter

A *coleopter* is a type of [vertical take-off and landing](#) aircraft design where the fuselage is surrounded by an [annular](#) wing. The aircraft is intended to [take off and land on its tail](#).

[SNECMA Coléoptère](#) machine may have been the first of this type of aircraft to actually be constructed; the approach itself was first put forward in Germany late in World War II.

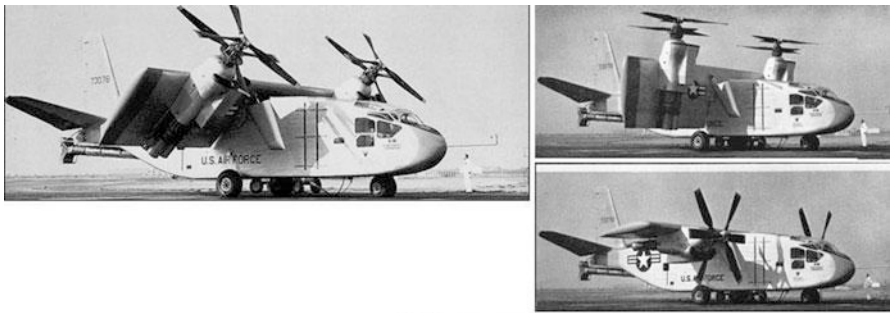


Fig. 1.52 Tilt Rotor Osprey V-22

SNECMA's experiences demonstrated formidable control problems, both with balancing the aircraft during vertical flight, and in transitioning between vertical and horizontal flight and back. An American design, the [Hiller VXT-8](#), was abandoned before a prototype was ever built.

1.2.6.4 Mono Tiltrotor

A *mono tiltrotor* aircraft combines the vertical lift capability and structural efficiency of a helicopter with the speed and range of an airplane [18].



X-18 Tilt Wing

Fig. 1.53 Hiller X-18 tilt wing aircrafts

1.2.6.5 Mono-Tilt-Rotor Rotary Wing

A *mono-tilt-rotor rotary-ring* VTOL aircraft is currently under development. It differs from previous tiltrotors in that instead of each rotor consisting of long blades attached to a central rotary ring; it has a single rotary ring which has a diameter equal to the entire wingspan of the aircraft, with the ring being attached to the tips of the wings [19].

1.2.7 Other Methods of Lift Aircrafts

It includes the following sub-groups: *Flapping Wing, Lifting Body, and FanWing*.

1.2.7.1 Flapping Wing or Ornithopter

Flapping wing or ornithopter is an [aircraft](#) that [flies](#) by flapping its wings similar to the flight of [birds](#), [bats](#), and [insects](#). Though machines may differ in form, they are usually built on the same [scale](#) as these flying creatures. Successful manned ornithopters have been built and flew in 1942 at Munich-Laim and more recently in 2006 at Canada. German *ornithopter* was driven by small flapping wings mounted at the sides of the [fuselage](#), behind a larger fixed wing. Fitted with a 3 [hp](#) Sachs motorcycle engine, it made flights up to 15 [min](#) in duration. Canadian [UTIAS Ornithopter No.1](#) designed by [Professor James DeLaurier](#) and his team made a jet-assisted takeoff and 14-second flight (Fig. 1.54).



Fig. 1.54 UTIAS Ornithopter No.1

1.2.7.2 Lifting Body

A *lifting body* is an aircraft configuration in which the body itself produces lift. A lifting body is a fuselage that generates lift without the shape of a typical thin and flat wing structure. Lifting bodies generally minimize the drag and structure of a wing for very high supersonic or hypersonic flight or spacecraft re-entry. In the period 1963 to 1975, Dryden Flight Research Center built the following lifting body vehicles M2-F1, M2-F2, M2-F3, HL-10, X-24A, and X-24B. The X-24 (Fig. 1.55) was one of a group of lifting bodies flown by the NASA to demonstrate the ability of pilots to maneuver and safely land wingless vehicles designed to fly back to Earth from space and be landed like an airplane at a predetermined site.

1.2.7.3 FanWing

FanWing or *fan wing* is a concept for a type of aircraft. It uses a fixed wing with a forced airflow produced by cylindrical fans mounted above the wing. Its makers claim it is the first horizontal-rotored integral lift and propulsion wing in history to sustain flight. A prototype was tested in 2007. It was airborne after a ground roll of just 1 m and had a flight speed of 29 km/h and endurance of 80 min. Its maximum take-off weight was 12 kg and powered by a 1.2 kW electric motor.



Fig. 1.55 X-24 lifting body

Example 1.1 Complete the following table

Aircraft	STOVL	Agricultural aircraft	Bomber	Skycrane	Tiltwing	Long haul transport	Balloon
<i>Aircraft type</i>							
<i>Aero-engine</i>							
<i>Vehicle example</i>							

Solution

First of all, some questions have to be answered:

- Does this vehicle belong to aerostat or aerodyne?
- Whether this vehicle is a fixed wing or a rotorcraft type?
- Is it of civilian or military nature?
- If civilian to which group does it belong?
- If military, whether it is a combat or non-combat military?

Let us proceed,

1. The first vehicle is STOVL, which stands for a short takeoff and vertical landing. It is an *aerodyne, fixed wing, military and combat aircraft*. Next, it is normally powered by an afterburning turbofan engine. An example for this aircraft is F35 aircraft.
2. Agricultural aircraft is also an *aerodyne, fixed wing, civilian aircraft*. It is normally powered by a piston engine. An example is HAL HA-31 powered by single Avco Lycoming IO-720-C1B flat-eight piston engine, 400 hp (298 kW).
3. *Bomber is also an aerodyne, fixed wing, military, and combat aircraft*. It is either powered by a turbofan or turboprop engine. Examples may be strategic B 52, B-2 strategic stealth, and Russian strategic bomber Tu-95 Bear.
4. *Skycrane is an aerodyne, rotorcraft, civilian helicopter*. It is powered by turboshaft engine. An example is S-64 helicopter.
5. *Tiltwing an aerodyne, hybrid fixed/rotary wing vehicle, research non-combat military aircraft*. It is powered by a jet engine. Example is Hiller X-18 aircraft powered by single turbojet and two turboprop engines.
6. *Long haul transport is an aerodyne, fixed wing, civilian transport aircraft. It is powered by a high bypass turbofan engine*. Examples are Boeing 747, 777, and Airbus A380 aircrafts.
7. Balloon is an *aerostat unpowered vehicle*. No aero engines are needed for its propulsion/motion. First balloon was flown by Montgolfier Brothers on October 1783. The highest altitude achieved by a balloon was 21,067 m by Chinese Vijaypat Singhania on November 26, 2005.

Aircraft	STOVL	Agricultural aircraft	Bomber	Skycrane	Tiltwing	Long haul transport	Balloon
Aircraft type	Fixed wing combat military	Fixed wing civil	Fixed wing combat military	Civil helicopter	Hybrid fixed/rotary wing Research non-combat military	Fixed wing, civilian transport aircraft	Aerostat unpowered vehicle
Example	F35	HAL HA-31	B-2	S-64	Hiller X-18	Boeing 777	First balloon (Montgolfier Brother, October 1783) and highest altitude (21,067 m) by Chinese Vijaypat Singhania November 26, 2005
Aero-engine	Turbofan	Piston engine	Turbofan	Turboshaft	One J34 Westinghouse turbojet engine + Two Allison T40-A-14 Turboprop engine	Turbofan	No engine

1.3 Classifications of Propulsion Systems

An *aircraft engine* (or aero engine) is a **propulsion** system for an **aircraft**. Aircraft engines are the key module or the heart in aviation progress. Since the early days of successful flight, the developments of both aero engines and aircraft structure are concurrent. Aero engines must be:

- Reliable, as losing power in an airplane, is a substantially greater problem than in road vehicles
- Operate at extreme temperature, pressure, and speed
- Light weight as a heavy engine increases the empty weight of the aircraft and reduces its payload
- Powerful, to overcome the weight and drag of the aircraft
- Small and easily streamlined to minimize the created drag
- Field repairable to keep the cost of replacement down. Minor repairs should be relatively inexpensive and possible outside of specialized shops
- Fuel efficient to give the aircraft the range and maneuverability the design requires
- Capable of operating at sufficient altitude for the aircraft
- Generate the least noise
- Generates the least emission

Aero engines may be classified based on input power into three main categories, namely, internal combustion engines, external combustion engines, and other power sources (Fig. 1.56).

1.3.1 External Combustion

External combustion engines are steam, stirling, or nuclear engines. In these types, all heat transfer takes place through the engine wall. This is in contrast to an **internal combustion engine** where the heat input is by combustion of a **fuel** within the body of the working fluid. Detailed description of the three types will be given hereafter.

1.3.1.1 Steam Engines

Steam aircraft are **aircraft** that are propelled by **steam engines**. They were unusual devices because of the difficulty in producing a **power plant** with a high enough **power to weight ratio** to be practical.

In 1899, **Gustave Whitehead** built and flew a steam powered airplane in Pittsburgh, Pennsylvania, and later on in Hartford, Connecticut. However, this flight has never been verified satisfactorily; there are no photographs, news, stories, or other media from 1899 to confirm it.

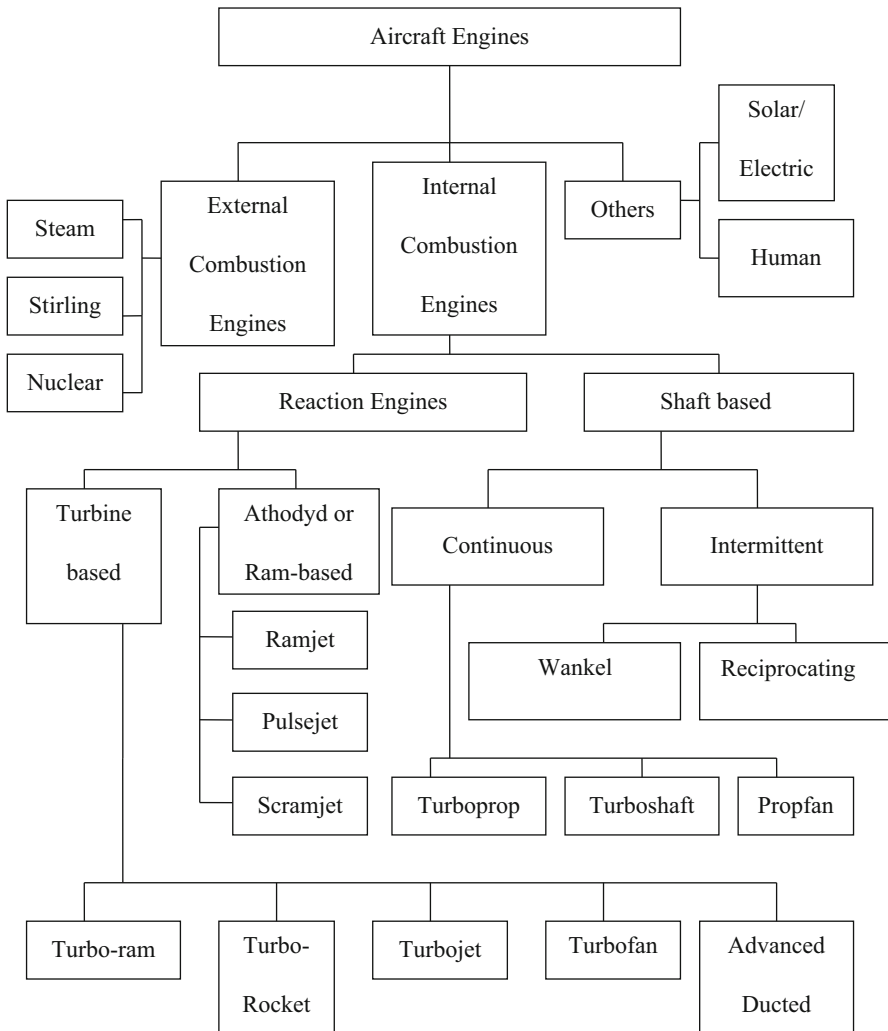


Fig. 1.56 Classification of propulsion systems

In 1902, Louis Gagnon flew a steam helicopter in [Rossland, British Columbia](#), called the “Flying Steam Shovel”. Control problems caused a crash.

On 12 April 1933, a Travel Air 2000 biplane made the world’s first piloted flight under steam power over Oakland, California. Brothers Besler (George and William) flew a prototype steam powered biplane, based on a [Travel Air 2000](#), several times (*taking off, circling about, and landing, to show the ease of control*) at [Oakland](#) airport. Airplane remained aloft for 5 min at each time. It was powered by a two-cylinder, double-acting reciprocating, 90° V engine, 150 hp (110 kW) weighing about 500 lbs.

Steam is generated from water by burning cheap crude oil. Sealed condensers return the steam from the cylinders to the boiler with only 1 % loss. Constant pressure in the boilers is maintained by electric gauges, which automatically ignite the burners when pressure begins to fall. Take-off pressure can be generated in 1 min. It was capable of **STOL** operation due to the ease of reversing thrust.

The strangest feature of the flight was its relative silence. The advantages of this engine were the elimination of audible noise and destructive vibration; greater efficiency at low engine speeds and also at high altitudes where lower air temperatures assisted condensation; reduced likelihood of engine failure; reduced maintenance and fuel costs. However, steam reciprocating engine turned out to be unsuitable for scaling up to the needs of large aircraft. Thus at present days no single aircraft is powered by steam engine.

1.3.1.2 Stirling Engines

A *stirling engine* is a **heat engine** having either air or other gas as a working fluid. It operates by cyclic compression and expansion of the working fluid, at different temperature levels such that there is a net conversion of **heat** energy to mechanical **work**. Stirling engines have many advantages like high power density and low cost, quieter, less polluting, gain efficiency with altitude due to lower ambient temperatures; more reliable due to fewer parts and the absence of an ignition system, produce much less vibration (airframes last longer), and safer, less explosive fuels may be used. However, they have low power density compared to the commonly used piston engines and gas turbine. This issue made them critical for use as aircraft engines.

1.3.1.3 Nuclear Engines

A *nuclear aircraft* is an aircraft powered by nuclear energy. Research into them was pursued during the Cold War by the United States and the Soviet Union as they would presumably allow a country to keep nuclear bombers in the air for extremely long periods of time, a useful tactic for nuclear deterrence. Neither country created any nuclear aircraft in production numbers. One design problem, never adequately solved, was the need for heavy shielding to protect the crew from radiation sickness. Also, in consideration, was the ecological impact of a crash during operations. Should one of these aircrafts were to crash in a populated area, the radiation fallout could have been disastrous.

1.3.1.3.1 U.S. Programs

In May 1946, the Nuclear Energy for the Propulsion of Aircraft (NEPA) project was started by the United States Air Force. Studies under this program were

done until May 1951, when NEPA was replaced by the Aircraft Nuclear Propulsion (ANP) program. The ANP program included provisions for studying two different types of nuclear-powered jet engines, General Electric's Direct Air Cycle and Pratt & Whitney's Indirect Air Cycle. ANP also contained plans for two B-36 s to be modified by Convair under the *MX-1589* project; one of the B-36 s was to be used to study shielding requirements for an airborne reactor while the other was to be the X-6. However, the program was cancelled before the X-6 was built.

The Oak Ridge National Laboratory conducted research (Aircraft Reactor Experiment) to produce a nuclear powered aircraft. GE produced the X-39 engine, which was a modified version of its J47s turbojet engine. The USA designed these engines to be used in a new specially designed nuclear bomber, the X-6. The X-6 was eventually terminated by Eisenhower.

The General Electric program in Evendale, Ohio, relied upon direct air cycle program because of its advantages in simplicity, reliability, suitability, and quick start ability. Conventional jet engine compressor and turbine sections were used, with the compressed air run through the reactor itself to heat it before being exhausted through the turbine.

The Indirect Air Cycle program was assigned to Pratt & Whitney, at a facility near Middletown, Connecticut. This concept would have produced far less radioactive pollution. One or two loops of liquid metal would carry the heat from the reactor to the engine. The Indirect Cycle program never approached anywhere near producing flight-ready hardware.

On September 5, 1951, the USAF awarded Consolidated-Vultee a contract to fly a nuclear reactor onboard a modified Convair B-36 under the *MX-1589* project of the ANP program. The NB-36H Nuclear Test Aircraft (NTA) was to study shielding requirements for an airborne reactor, to determine whether a nuclear aircraft was feasible. This was the only known airborne reactor experiment by the U.S. with an operational nuclear reactor on board. The NTA flew a total of 47 times testing the reactor over West Texas and Southern New Mexico. The reactor, named the Aircraft Shield Test Reactor (ASTR), was operational but did not power the plane, rather the primary purpose of the flight program was shield testing. Based on the results of the NTA, the X-6 and the entire nuclear aircraft program were abandoned in 1961.

1.3.1.3.2 Soviet Programs

The Soviet program of developing nuclear aircraft resulted in the experimental Tupolev 119 (Tu-95 LAL), which was based on a Tupolev Tu-95M bomber. It had 2 conventional turboprop engines and 2 experimental 'inboard' direct cycle jet engines powered by a minimally shielded nuclear reactor in the main fuselage. The Tu-119 completed 34 research flights. Most of these were made with the reactor shut down. The main purpose of the flight phase was examining the effectiveness of the radiation shielding which was one of the main concerns for the engineers.

Massive amounts of protection used resulted in radiation levels low enough to consider continuing development. But, as in the US, development never continued past this point. Budgetary constraints and the development of new conventional aircrafts designs were cited as the main reason for the cancellation of the program in August 1966. Several other projects reached only design phase.

1.3.1.4 Final Comment

As described above, the three external combustion engines are not appropriate for employment in aviation field for different reasons. Steam engines are only appropriate for small aircrafts while large ones need heavy boilers, piping and other accessories. Stirling engines generate also low power which is also improper for present aircrafts. Nuclear engines have two drawbacks regarding shielding of flight crew and passengers versus radiation, as well as the risk of crash in residence areas leading to catastrophic situation.

1.3.2 Internal Combustion

Internal combustion engines have two broad categories; namely, *shaft* and *reaction* engines. *Shaft* engines are either of the intermittent or continuous types. Moreover, intermittent combustion engines may be either of the reciprocating or the Wankel (rotary design) types. Continuous combustion engines, which may also be identified as turbine shaft engines, are next categorized as turboprop, turboshaft and propfan engines. The other main group of internal combustion is the reaction engines. This engine group is either of the *athodyd* (where *athodyd* stands for Aero T_HermODY-namic Duct) or *turbine* types. Athodyd group includes ramjet, pulsejet and scramjet engines, while turbine engines includes turbojet, turbofan, turbo ramjet, turbo rocket and advanced ducted fan engines.

1.3.2.1 Shaft Engines

Shaft engines as previously defined are classified, based on type of combustion, into two subgroups; namely, intermittent combustion and continuous combustion.

1.3.2.1.1 Intermittent Combustion

Intermittent combustion engines are either Wankel or reciprocating engines.

Wankel Engine

The *Wankel engine* invented by German engineer **Felix Wankel** in 1950, is a type of **internal combustion engine** which uses a **rotary design** to convert pressure into a rotating motion. Figure 1.57 illustrates *Diamond DA20 aircraft powered by Wankel engine*. Its four-stroke cycle takes place in a space between the inside of an oval-like epitrochoid-shaped housing and a rotor that is similar in shape to a Reuleaux triangle but with sides that are somewhat flatter [20]. This design delivers smooth high-rpm power from a compact size. The first Wankel rotary-engine aircraft was the experimental **Lockheed Q-Star** in 1968/1969. It was powered by a 185 hp **Curtiss-Wright RC2-60** Wankel rotary engine. The compact size and quiet operation of Wankel engine encouraged its usage in **UAVs**. Wankel engines are also becoming increasingly popular in homebuilt experimental aircraft being very cheap compared with certified aircraft engines, providing engines ranging from 100 to 300 horsepower (220 kW) at a fraction of the cost of traditional engines. Wankel engines operate at a relatively high **rotational speed** with relatively low torque, thus, propeller aircraft must use a **Propeller Speed Reduction Unit (PSRU)** to keep conventional propellers within the proper speed range.

Piston Engine

A *Piston engine*, also often known as a *reciprocating engine*, is a **heat engine** that uses one or more **reciprocating pistons** to convert **pressure** into a **rotating motion**. It



Wankel Engine

**Diamond
DA20
Aircraft**

Fig. 1.57 Wankel engine

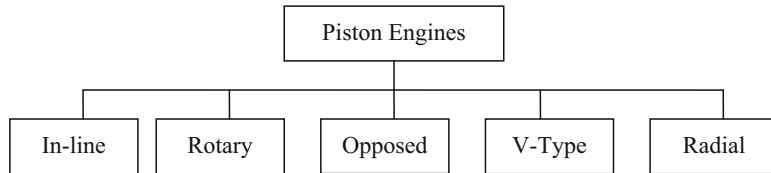


Fig. 1.58 Classification of piston engines

is well known that *piston engine* powered the first ever piloted motorized flight made by Orville and Wilbur Wright on 17th December 1903 in Kitty Hawk, North Carolina, USA. Since then, continuous developments were enhanced. Piston engines may be classified into five groups as shown in Fig. 1.58. These are in-line, rotary, V-type, radial, and opposed. These engines are coupled to a propeller to furnish the forward flight of airplanes.

In-Line

An *in-line* engine has cylinders lined up in one row. It typically has an even number of cylinders, but there are instances of three- and five- cylinder engines. Inline engines were common in early aircraft, including the Wright Flyer (12 horsepower), the aircraft that made the first controlled powered flight. An in-line engine may be air cooled but mostly liquid cooled.

The biggest advantage of an inline engine is that it allows the aircraft to be designed with a narrow frontal area for low drag. If the engine crankshaft is located above the cylinders, it is called an inverted inline engine, which allows the propeller to be mounted up high for ground clearance even with short landing gear. The disadvantages of an inline engine include a poor power-to-weight ratio, because the crankcase and crankshaft are long and thus heavy. Thus inline design was abandoned, becoming a rarity in modern aviation.

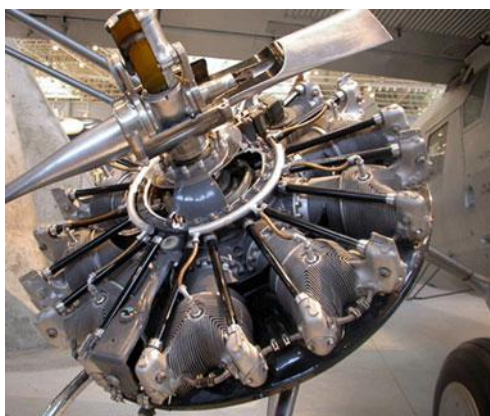
Rotary Engine

Rotary engine was extensively used in World War I as it is lightweight, powerful, cheap, and easy to manufacture in large quantities. Rotary engines have all the cylinders in a circle around the crankcase like a radial engine, but the difference is that the crankshaft is bolted to the airframe, and the propeller is bolted to the engine case. The entire engine rotates with the propeller, providing plenty of airflow for cooling regardless of the aircraft's forward speed. Some of these engines were a two-stroke design, giving them a high specific power and power-to-weight ratio. Unfortunately, the severe gyroscopic effects from the heavy rotating engine made the aircraft very difficult to fly. The engines also consumed large amounts of castor oil, spreading it all over the airframe and creating fumes which were nauseating to the pilots.

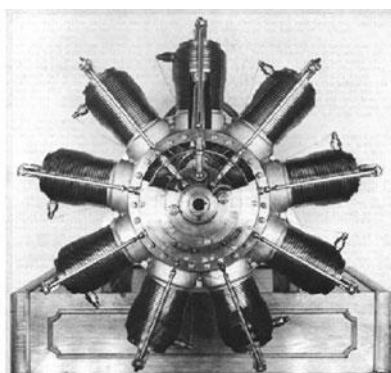
Radial Engine

Radial engine has one or more rows of cylinders arranged in a circle around a centrally located crankcase. Each row must have an odd number of cylinders in order to produce smooth operation. A radial engine has only one crank throw per row and a relatively small crankcase, resulting in a favorable power to weight ratio. Because the cylinder arrangement exposes a large amount of the engine's heat radiating surfaces to the air and tends to cancel reciprocating forces, radials tend to cool evenly and run smoothly. Wasp engine, completed in the Christmas eve of 1925, was a radial piston engine with a 1340 cubic inches displacement and manufactured by Pratt & Whitney company (P&W). Wasp engines dominated Navy and Army Air Force fighter planes as well as commercial transports. It powered approximately 100 different experimental and production airplanes including Boeing 40A, Boeing F2B-1 shipboard fighters, and Ford Tri-Motor. By the early 1930s, P&W worked on twin-row radial engines. Its twin Wasp (1830 cubic inches and 1350 horsepower) performed magnificently. A total of 173,618 engines were produced that powered a large number of fighters, bombers (which participated later in WWII), and transports. The twin Wasp was followed by Double Wasp, which is an 18-cylinder twin-row radial with 2800 cubic inches of displacement. P&W engines from the wasp to the Double Wasp produced, licensed, and affiliated over 363,000 engines. Wasp major was the last P&W piston engine. It was 28-cylinder, 4360 cubic inch displacement and rated power up to 4300 horsepower. The cylinders were four in rows, arranged for a spiral for better cooling. Its primary application was in heavy transport and bombers. Examples are Boeing's giant double-decked Strato-cruiser, the 377 and Air Force B-50; both were powered by four Wasp Majors.

BMW 801 was the first German double-row radial engine manufactured in 1940/1941. Figure 1.59 illustrates both rotary and radial piston engines.



P& W R-985 Wasp Jr
Radial Engine



100 hp Gnome Rotary
Engine

Fig. 1.59 Rotary and radial piston engines

V-Type

Cylinders in *V-type engine* are arranged in two in-line banks, tilted 30-60° apart from each other. The vast majority of V engines are water-cooled. Perhaps the most famous example of this design is the legendary Rolls Royce Merlin engine, a 27-l (1649 in³) 60° V12 engine used in, among others, the Spitfires that played a major role in the Battle of Britain (Fig. 1.60).

Opposed-Type

An *opposed-type engine* has two banks of cylinders on opposite sides of a centrally located crankcase; ULPower UL260i as an example. The engine is either air cooled or liquid cooled, but air cooled versions predominate. Opposed engines are mounted with the crankshaft horizontal in airplanes, but may be mounted with the crankshaft vertical in helicopters. Due to the cylinder layout, reciprocating forces tend to cancel, resulting in a smooth running engine. Opposed, air-cooled four and six cylinder piston engines are by far the most common engines used in small general aviation aircraft requiring up to 400 horsepower (300 kW) per engine. Aircraft which require more than 400 horsepower (300 kW) per engine tend to be powered by turbine engines.

1.3.2.1.2 Continuous Combustion Engines

Continuous combustion engines are mainly turbine shaft engines. It includes turboprop turboshaft and propfan engines. They are featured with rotating elements

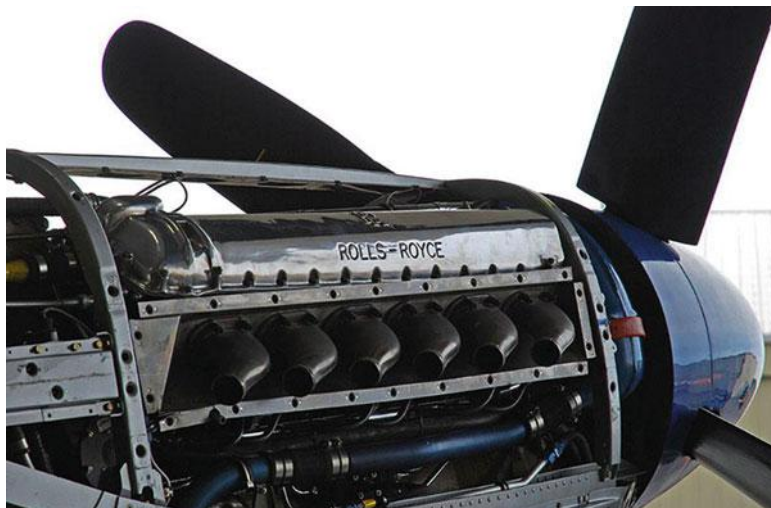


Fig. 1.60 The Rolls-Royce Merlin V-12 piston aero engine

known as turbomachines, as sub-modules. These modules may be fan, compressor(s), and turbine(s) as well as propellers/propfans.

Turboprop

Turboprop engines power both civil and military transport aircrafts with a cruise speed less than 450 mph (700 km). It is composed of a gas generator (compressor, combustion chamber and turbine) as well as a propeller. The turbine drives both compressor and propeller. Because gas turbines optimally spin at high speed, a turboprop features a gearbox to lower the speed of the shaft so that the propeller tips do not reach supersonic speeds. An alternative to the above turboprop engines, a second turbine is added which drives only the propeller either directly or via a gearbox. The first turbine in this case drives the compressor only. Thus it is free to rotate at its own best speed (referred to as a free- or power-turbine). The other turbine is identified as compressor-turbine. Recent turboprop engines generate thrust force from both propeller and exhaust jet stream. A fraction of 10–20 % of thrust is generated from jet stream. Consequently, some people classify turboprop as jet engine or reaction engine. Figure 1.61 illustrates two turboprop engines, the left is a single-shafted one with propeller coupled to compressor-turbine shaft and the right one is of the free turbine type.

Examples for turboprop engines are Rolls-Royce T56 (3460 shaft horsepower installed to P-3 Orion, C-130, C-2A aircrafts), Rolls-Royce AE2100 engine (3600–6000 shp installed to C-27 J Spartan, ShinMaywa US-1A Kai aircrafts), and Rolls-Royce TP400-D6 engine (11,000+ shp installed to Airbus Military A400M aircraft). The T34 is one of the earliest turboprop engines manufactured by Pratt & Whitney, which powered B-17 flying testbed, KC-97 J, and Douglas C-133A Cargomaster. PT6 turboprop engine (Pratt & Whitney of Canada) is the most popular power plant in its class (475–1650 hp). It has been selected for more than 130 different business, commuter, trainer, and utility aircraft applications. Example for GE turboprop engines is CT7, which powers Saab 340 and CASA- IPTN CN235.

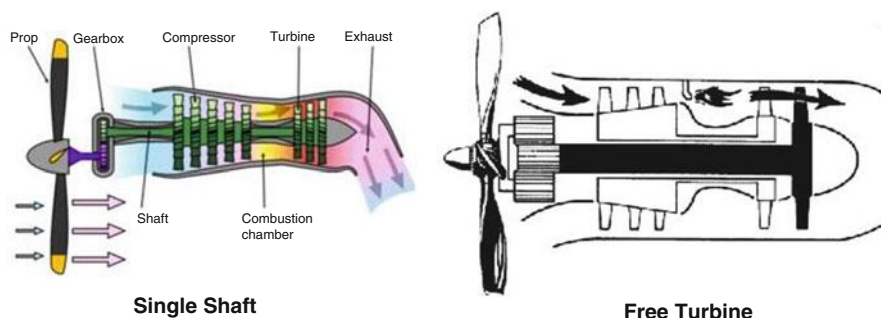


Fig. 1.61 Two types of turboprop engine

Turboshaft

Turboshaft engines are used primarily for helicopters and auxiliary power units. A turboshaft engine is very similar to a turboprop, with a key difference: In a turboprop the propeller is supported by the engine, and the engine is bolted to the airframe. In a turboshaft, the engine does not provide any direct physical support to the helicopter's rotors. The rotor is connected to a transmission, which itself is bolted to the airframe, and the turboshaft engine simply feeds the transmission via a rotating shaft. The distinction is seen by some as a slim one, as in some cases aircraft companies make both turboprop and turboshaft engines based on the same design. An example for turboshaft engine is GE T700, which powers Seahawk helicopter (Fig. 1.62).

Other examples for turboshaft engines are Rolls-Royce RTM322 (2100–2550 shp, which powers AgustaWestland WAH-64 Apache), Rolls-Royce Gnome (1175–1660 shp, which powers AgustaWestland Sea King and Kawasaki/Boeing Vertol 107), and T800 (1360–1680 shp, which powers AgustaWestland Super Lynx 300/3 CTS800) manufactured by LHTEC, a joint venture between Rolls-Royce and Honeywell. GE T700 is one of the historical turboshaft engines that powers the Marine Corps "SuperCobra" built by Bell, military Sikorsky H-60 and international versions of the Sikorsky S-70. The commercial version of T700, namely, CT7, powers Bell 214ST, Sikorsky S-70C, and Westland WS-70.

Propfan

A *propfan* or an *unducted fan* (sometimes denoted in former Soviet Union as turbopropfan) is a modified turbofan engine, with the fan placed outside of the engine nacelle on the same axis as the compressor blades. Propfans are also known as ultra-high bypass (*UHB*) engines and, most recently, *open rotor* jet engines. The design is intended to offer the speed and performance of a turbofan, with the fuel economy of a turboprop.

The propfan concept was developed to deliver better fuel efficiency than contemporary turbofans. However, this achievement has noise penalty. Most propfans

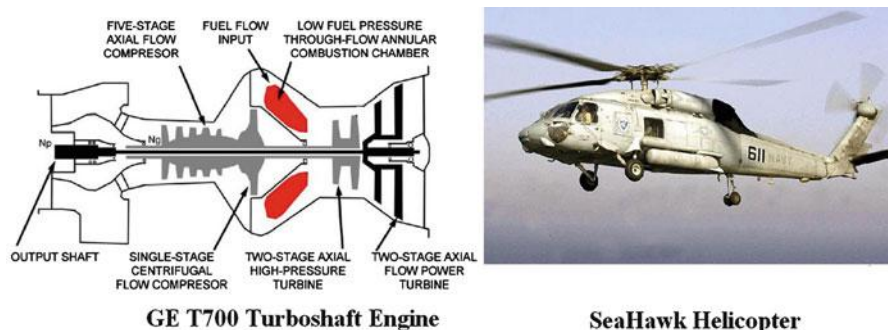


Fig. 1.62 GE T700 turboshaft engine powering Seahawk helicopter



Fig. 1.63 General electric GE-36 unducted fan (propfan) engine

are experimental engines. Examples are General Electric's GE36 Unducted Fan and Pratt & Whitney/Allison 578-DX. General Electric's GE36 Unducted Fan (Fig. 1.63) was a variation on NASA's original propfan concept and appears similar to a pusher configuration for piston or turboprop engines.

McDonnell Douglas developed a proof-of-concept aircraft by modifying its MD-80. They removed the JT8D turbofan engine from the left side of the fuselage and replaced it with the GE36. The test flights conducted in Mojave, CA, USA, and ended in 1988 demonstrated a 30 % reduction in fuel burn over turbo-fan powered MD-80 and low-levels of exterior and interior noise/vibration. However, due to jet-fuel price drops and shifting marketing priorities, Douglas shelved the program the following year.

In the 1980s, Allison collaborated with Pratt & Whitney on demonstrating the 578-DX propfan. The 578-DX was successfully flight tested on a McDonnell Douglas MD-80. However, none of the above projects came to fruition, mainly because of excessive cabin noise (compared to turbofans) and low fuel prices.

The Ivchenko-Progress D-27 propfan developed in the USSR with the propfan blades at the front of the engine in a tractor configuration (Fig. 1.64). D-27's propfans propelled the Antonov An-70. D-27 propfan engine is a three-shaft propfan engine with a propeller diameter of 4.5 m and dry weight of 1650 kg (3638 lb). Its gas generator is made up of an axial low-pressure compressor, a mixed-flow high-pressure compressor, an annular combustion chamber, a single-stage high-pressure turbine, and a single-stage low-pressure turbine. The SV-27 contra-rotating propfan is driven by a four-stage turbine via a shaft connected to a planetary reduction gear.

With the current high price for jet fuel and the emphasis on engine/airframe efficiency to reduce emissions, there is renewed interest in the propfan concept for



Fig. 1.64 The Ivchenko-progress D-27 powering an An-70 aircraft

jetliners that might come into service beyond the Boeing 787 and Airbus A350XWB. For instance, Airbus has patented aircraft designs with twin rear-mounted counter-rotating propfans.

1.3.2.2 Reaction Engines

The other main group of internal combustion engines, namely, the reaction engines is next subdivided into the athodyd (where athodyd stands for Aero *T*hermODY-namic *D*uct) or turbine types. Athodyd group includes ramjet, pulsejet, and scramjet engines. Turbine engines include engines that have turbomachinery modules, which combine all types of turbojet, turbofan, turbo ramjet, turbo rocket, and advanced ducted fan engines. In short, all *reaction engines* develop its propulsive force as a reaction to the jet exhaust gases. Three essential modules are seen in all reaction types, namely, an entry duct (sometimes identified as inlet duct or intake), a combustion chamber or burner, and an exhaust nozzle. The exhaust nozzle (s) accelerate air/gases to greater speeds than flight speed, thus create thrust that pushes the aircraft forward.

1.3.2.2.1 Athodyd Types

Athodyd group includes ramjet, pulsejet, and scramjet engines, which do not have any major rotating elements or turbomachinery. The pulsejet operates intermittently and has found limited applications [21]. In ramjet engines, ram compression of the air becomes sufficient to overcome the need for mechanical compression. Ramjet engine is also appropriate for supersonic flight speeds [22]. If the flight speed is so high, fuel combustion must occur supersonically, and then this ramjet is called a scramjet [23].

Ramjet Engine

A *ramjet*, sometimes referred to as a *stovepipe jet*, is a form of jet engine using the engine's forward motion to admit and compress incoming air, without a rotary compressor. Ramjets cannot produce thrust at zero airspeed and thus cannot move an aircraft from a standstill. It is composed of three modules: inlet duct, burner or combustor, and nozzle. It has two types: namely liquid- and solid-fuel ramjets. Ramjet engines may be subsonic or supersonic (Fig. 1.65). Subsonic ramjets do not need a sophisticated inlet since the airflow is already subsonic and a simple hole is usually used. For supersonic ramjets, supersonic flow is decelerated to subsonic speeds at the inlet through one or more oblique shock wave(s), terminated by a strong normal shock.

Thus air attains subsonic speeds at the entrance of combustion chamber. The combustor adds heat and mass to the compressed air by burning a fuel. The combustion chamber includes flame holders that stop the flames from blowing out. A ramjet combustor can safely operate at stoichiometric fuel to air ratios, which implies a combustor exit stagnation temperature of the order of 2400 K for kerosene. Products of combustion leaving the combustion chamber are reaccelerated through a nozzle, to supersonic speeds via a convergent-divergent nozzle to produce thrust. For a ramjet operating at a subsonic flight Mach number, exhaust flow is accelerated through a converging nozzle. Supersonic ramjet engines work most efficiently at speeds around Mach 3 and can operate up to speeds of at least Mach 5.

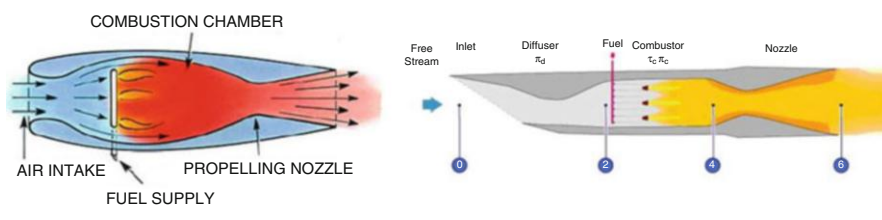


Fig. 1.65 Lorin's and supersonic ramjet engines



Fig. 1.66 Leduc 010

Historically, ramjet was invented in 1913 by the *French* inventor *René Lorin*, who was granted a patent for his device illustrated in Fig. 1.65. Attempts to build a prototype failed due to inadequate materials [24]. However, in 1949, the works of *René Leduc* led to design of Leduc 010, which was one of the first ramjet-powered aircrafts that flew in 1949 and displayed in Fig. 1.66. Later on, the French *Nord 1500 Griffon* reached Mach 2.19 in 1958.

In 1915, the *Hungarian* inventor *Albert Fonó* devised a solution for increasing the range of artillery, comprising a gun-launched projectile by adding a ramjet propulsion unit. He submitted a German patent describing an “air-jet engine” suitable for high-altitude supersonic aircraft. In an additional patent application, he adapted the engine for subsonic speed. The patent was finally granted in 1932 after 4 years of examination.

In the *Soviet Union*, a theory of supersonic ramjet engines was presented in 1928 by Boris S. Stechkin. The first successful ramjet engine, namely, GIRD-04, was designed by I.A. Merkulov and tested in April 1933. The GIRD-08 phosphorus-fueled ramjet was tested by firing it from artillery cannon. These shells may have been the first jet powered projectiles to break the speed of sound. In August 1939, Merkulov developed the first ramjet engine for use as an auxiliary motor of DM-1 aircraft. The world’s *first ramjet powered airplane* flight took place in December 1939, using two DM-2 engines on a modified Polikarpov I-15. Merkulov designed a ramjet fighter “Samolet D” in 1941. Two of his DM-4 engines were installed on the YaK-7PVRD fighter, during World War II. In 1940, the Kostikov-302 experimental plane was designed, powered by liquid fuel rocket for take-off and ramjet engines for flight. In 1947, Mstislav Keldysh proposed a long-range antipodal bomber powered by ramjet instead of rocket.

Pulsejet Engine

A *pulse jet engine* (or *pulsejet*) is a very simple type of jet engine in which combustion occurs in pulses. Pulsejets use an intermittent combustion while ramjets employ a continuous combustion process. Pulsejet engines are a *unique type of jet engine, able to operate statically with few* [25] or no moving parts [26]. They are very simple and cheap to construct. They feature an excellent balance of cost and

function, as could run on any grade of petroleum and the ignition shutter system. Their accompanying noise is unacceptable by modern standards. They have both a higher efficiency and very high thrust-to-weight ratio compared to other jet engines. Pulsejet engines may be produced in many sizes with different outputs ranging from a few pounds to thousands of pounds of thrust. There are *two main types* of pulsejet engines: *valved* (Fig. 1.67) and *valveless* (Fig. 1.68). Both types use resonant combustion and harness the expanding combustion products to form a pulsating exhaust jet, which produces thrust intermittently.

Valved

Valved engines use a mechanical one-way valve, which is a simple leaf-spring type of shutter. With the valve open, a fresh charge of air is admitted. The air mixes with the fuel and then an explosion takes place, which shuts the valve and forces the hot gas to go out the back of the engine through the tailpipe only, and allow fresh air and more fuel to enter through the intake (Fig. 1.67). The superheated exhaust gases exit through an acoustically resonant exhaust pipe.

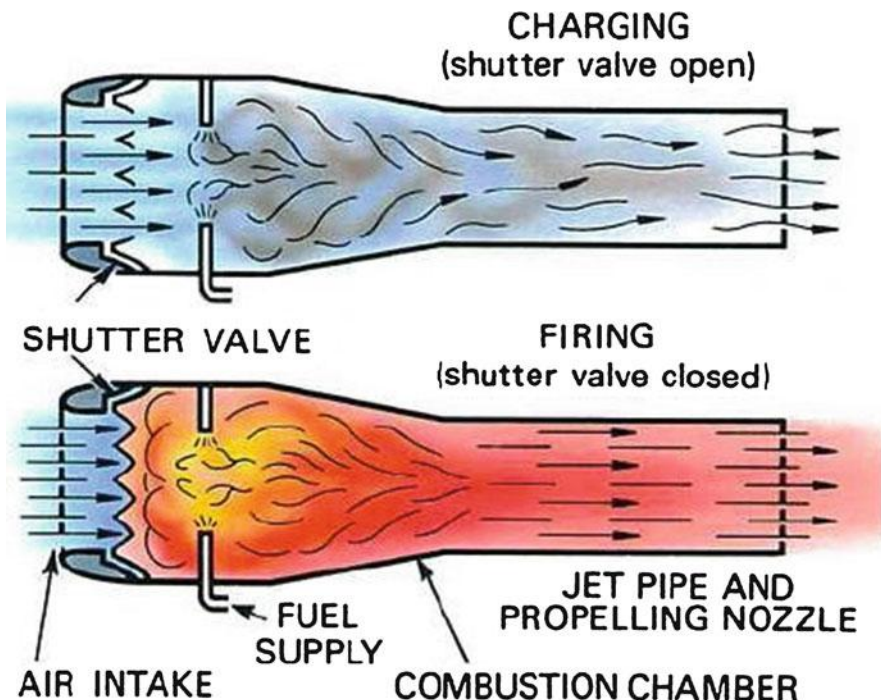


Fig. 1.67 Valved pulsejet operation, reproduced with the permission of Rolls-Royce plc, copyright © Rolls-Royce plc [28]

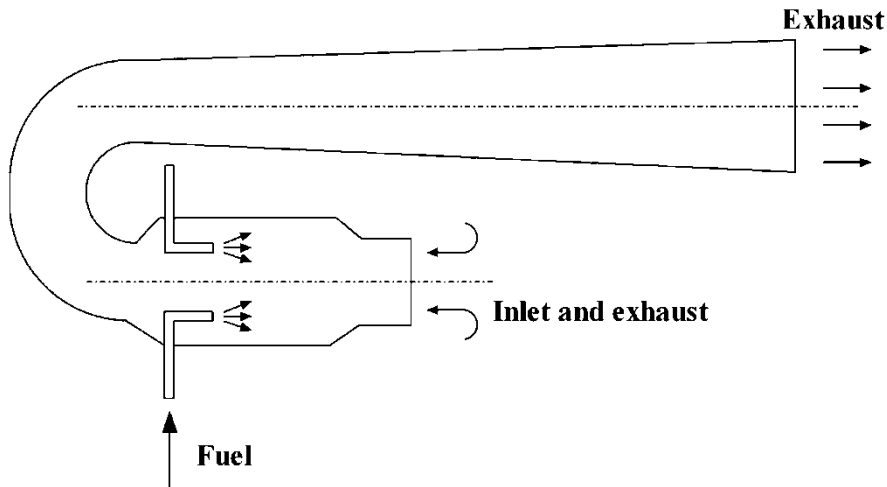


Fig. 1.68 Valveless pulsejet, Courtesy El-Sayed [1]

Valveless

Valveless pulsejets have no moving parts and use only their geometry to control the flow of exhaust out of the engine (Fig. 1.68). Valveless engines expel exhaust out of both the intakes and the exhaust, most try to have the majority of exhaust go out the longer tail pipe, for more efficient propulsion. The valveless pulse jet engine operates on the same principle as valved type. Combustion process creates two shock wave fronts, one travelling down the upper long pipe (tube) and the other down the short lower tube. By properly “tuning” of the system, a resonating combustion process can be achieved, which yields considerable thrust. Fuel consumption is very high and noise level is also unacceptable. The French engine manufacturer SNECMA developed these pulsejets in late forties for use on drones. One application was the Dutch AT-21 target drone built by Aviolanda Aircraft from 1954–1958 [27].

Historically, the first working pulsejet was patented in 1906 by Russian engineer V.V. Karavodin, completing a working model in 1907. The French inventor Georges Marconnet patented his valveless pulsejet engine in 1908. A German designer and inventor Schmidt designed the V-1 flying bomb in 1933. The original Schmidt design had the pulsejet placed in a fuselage like a modern jet fighter, unlike the eventual V-1 which had the engine placed above the warhead and fuselage (Fig. 1.69). Schmidt working for Argus Company, the pulsejet was modified and identified as the Argus As 109-014. The first unpowered drop occurred at Peenemünde on 28 October 1942 and the first powered flight occurred on 10 December 1942. Later on it was used in the bombing of London in 1944. Its static thrust was 500 lbf (2200 N), while in flight thrust reached approximately 750 lbf (3300 N).

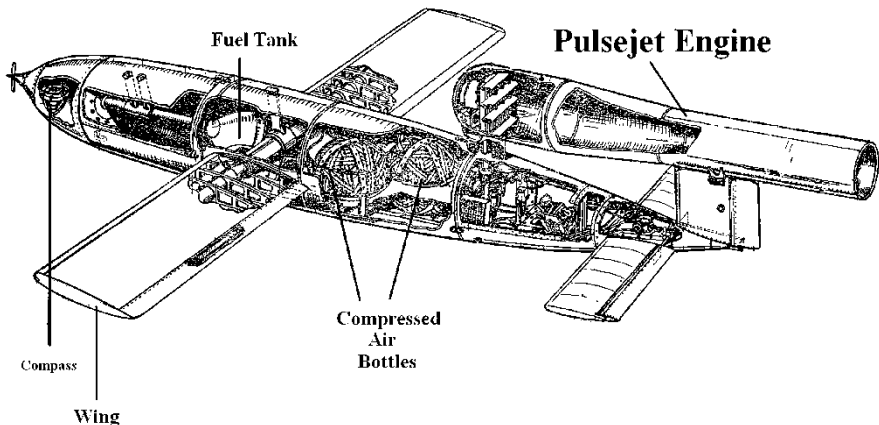


Fig. 1.69 V1 buzz bomb

The high noise levels of pulsejets made them impractical for other than military and other similarly restricted applications. They have been used to power experimental helicopters, the engines being attached to the extreme ends of the rotor blades. Pulsejets have the distinct advantage over conventional turbine engines of not producing the usual reaction torque upon the fuselage.

Pulse Detonation Engine (PDE)

The *pulse detonation engine (PDE)* marks a new approach towards non-continuous jet engines and promises higher fuel efficiency compared even to turbofan jet engines, at least at very high speeds. Pratt & Whitney and General Electric now have active PDE research programs. Most PDE research programs use pulsejet engines for testing ideas early in the design phase.

Scramjet Engine

Scramjet is an evolution of the ramjets that are able to operate at much higher speeds than ramjets or any other kind of airbreathing engines. It is an acronym for *Supersonic Combustion Ramjet*, or in other words combustion of fuel and air occurs in a supersonic flow relative to engine. Scramjets start working at speeds of at least Mach 4 and have a theoretical maximum speed of Mach 17.

In the 1950s and 1960s, a variety of experimental scramjets engines were built and ground tested in USA and the UK. In 1981, tests were made in Australia. Presently, Brazil, China, France, Germany, India, Italy, Japan, Russia, South Korea, and Sweden have also hypersonic propulsion programs. No scramjet powered vehicle has yet been produced outside an experimental program. Scramjet engines find its applications in many recent hypersonic speed vehicles like rockets, future

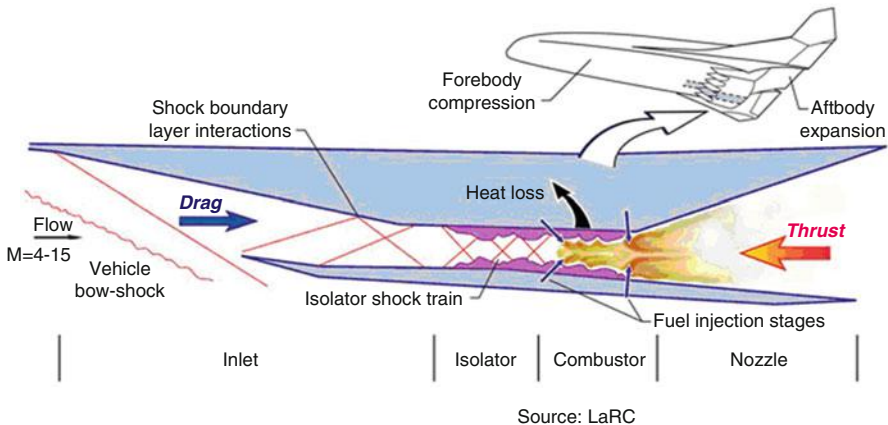


Fig. 1.70 Scramjet engine

commercial transports in the twenty-first century as well as single stage to orbit (SSTO) launchers.

It provides the most integrated engine–vehicle design for aircraft and missiles. The engine occupies the entire lower surface of the vehicle body (Fig. 1.70). The propulsion system consists of five major engine-components and two vehicle-components: the internal inlet, isolator, combustor, internal nozzle, and fuel supply subsystem, and the craft’s forebody, essential for air induction, and aft-body, which is a critical part of the nozzle component.

Both hydrocarbon and hydrogen are used as fuels for scramjets. Scramjets are mechanically simple but aerodynamically more complex than a jet engine. It uses the speed of the aircraft to compress the air, so very few moving parts are needed to operate it. The minimum functional speed, however, requires acceleration by other jet engine to hypersonic speed before the scramjet can become active. [Boeing or NASA X-43](#) is an example for experimental scramjet with a world speed record for a jet-powered aircraft – Mach 9.7, nearly 12,000 km/h (\approx 7000 mph) at an altitude of about 36,000 m (\approx 110,000 ft). The X-43A set the flight speed record on 16 November 2004.

Moreover, [Boeing X-51 \(also known as X-51 WaveRider\)](#) is an unmanned scramjet demonstration aircraft. It completed its first powered hypersonic flight on 26 May 2010 for over 6 min and reached speeds of over Mach 5 for 210 s on 1st May 2013 for the longest duration hypersonic flight.

Turbine Engine

Turbine engine category includes five types, namely, turbojet, turbofan, turbo-ramjet, turbo-rocket, and advanced ducted fan engines.

Turbojet

A *turbojet* is a type of gas turbine engine that was co-invented by Frank Whittle (in UK) and von Ohain (in Germany) in the thirties. It is the simplest of all aircraft gas turbines. It features one or more compressors to draw air in and compress it, a combustion section which adds fuel and ignites it, one or more turbines that extract power from the expanding exhaust gases to drive the compressor(s) and provide power to aircraft systems, as well as an exhaust nozzle which accelerates the exhaust out the back of the engine to create thrust. Each compressor is connected by a *shaft* to a turbine.

The compressor is either of the axial or centrifugal type (Fig. 1.71). The first turbojet engines of Frank Whittle and von Ohain were of the centrifugal compressor type. All the turbines used are of the axial type. Axial compressors and the turbines are composed of many blade rows: some are rotating called rotor and others are stationary identified as stator. When turbojets were introduced, the top speed of fighter aircraft equipped with them was at least 100 miles per hour faster than competing piston-driven aircraft.

Many subsequent turbojet engines were designed and manufactured in Europe by Rolls Royce, like Viper engine which powered MB339 and HAL HJT Kiran. General Electric (GE) produced America's first jet engine based on Whittle's design. It was GE-I-A where two of which powered the first United States first jet aircraft, the Bell XP-59A in October 1942. In USA also, Pratt & Whitney designed and produced its first gas turbine engine of its design, namely, J42 Turbo-Wasp engine, which was delivered to the Navy in November 1948 for installation in the Grumman F9F-2 Panther. In order for fighter planes to fly faster than sound (supersonically), an afterburner is added to a core turbojet (Fig. 1.72). When the afterburner is turned on, additional fuel is injected, which burns and produces additional thrust. Thus additional thrust is gained but much more fuel is burnt. When the afterburner is turned off, the engine performs like a basic turbojet. Afterburners are only used on fighter planes and the supersonic airliner, Concorde.

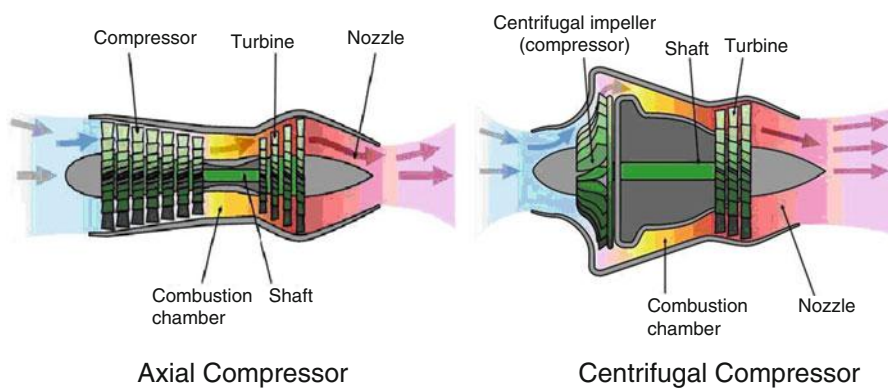


Fig. 1.71 Turbojet engines

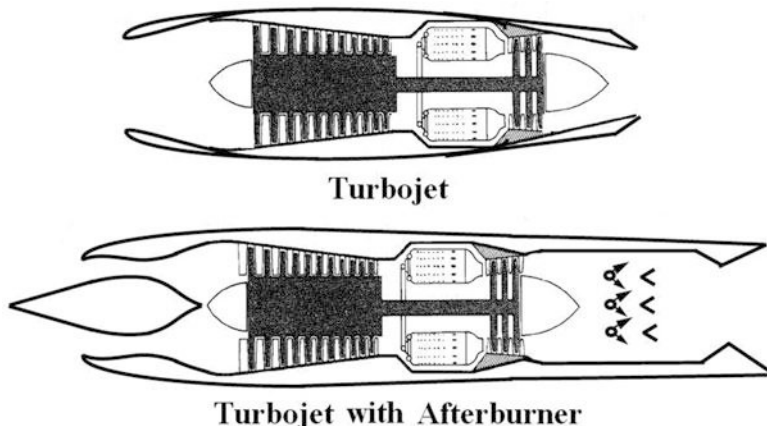


Fig. 1.72 Subsonic and supersonic turbojet engines

It was clear that below about Mach 2, turbojets are very fuel inefficient and create tremendous amounts of noise. These drawbacks eventually led to the downfall of the pure turbojet, and only a handful of types are still in production. Thus, turbojet engines were replaced by turbofan engines. The last airliner that used turbojets was the Concorde, whose Mach-2 flight crossed the threshold into efficient turbojet operation.

Examples for turbojet engines are General Electric GE J33 (powered the jet fighter – the Lockheed P-80) and GE J35 (powered the first Boeing XB-47, the Northrop YB-49A flying wing and the Douglas D-558-1). GE J47 turbojet engine set a record of over 35,000 produced engines that powered various military aircrafts in the mid 1950s. Moreover, one of the most famous turbojet engines is GE J79, which enabled some US fighters to reach twice speed of sound. These include the Convair B-58 “Hustler”, the Lockheed F-104 “Starfighter”, and the McDonnell F-4 “Phantom II”. Pratt & Whitney produced many turbojet engines like J48 (which powered F9F-6 Cougar and Lockheed F-94C Starfire) and J57 which is a twin spool (powered North American F-100 Sabre, McDonnell F-101 Voodoo, and Lockheed U-2 Air Force reconnaissance plane). A commercial version of J57 is the JT3 which powered Boeing 707 and Douglas DC-8. A distinguished turbojet engine was also P&W J58 that was selected to power the Air Force SR-71 Blackbird surveillance/reconnaissance aircraft. It may be concluded here that turbojet engine is outdated now and seldom seen either in military or civil aircrafts.

Turbofan

Most modern airliners, troop, and cargo transports as well as military aircrafts use *turbofan* engines because of their high thrust and good fuel efficiency. As with other gas turbines, there is a core engine similar to a turbojet engine, which is surrounded

by a fan in the front (or rear for aft turbofan engines) and an additional turbine at the rear. The fan and fan turbine are composed of many blade rows and are connected to an additional shaft. As with the core compressor and turbine, some of the fan blades turn with the shaft and some blades remain stationary. The fan shaft passes through the core shaft for mechanical reasons. This type of arrangement is called a *two spool* engine (one “spool” for the fan, one “spool” for the core). Some advanced engines have additional spools for even higher efficiency. The incoming air is captured by the engine inlet. Some of the incoming air passes through the fan and continues on into the core compressor and then the burner, where it is mixed with fuel and combustion occurs. The hot exhaust passes through the core and fan turbines and then out the nozzle, as in a basic turbojet. The rest of the incoming air passes through the fan and *bypasses*, or goes around the engine, just like the air through a propeller. The air that goes through the fan has a velocity that is slightly increased from free stream. So a turbofan gets some of its thrust from the core and some of its thrust from the fan. The ratio of the air that goes around the engine to the air that goes through the core is called the *bypass ratio*. Engines with bypass ratios of 1–2 are generally termed *low bypass ratio turbofans*. High bypass turbofans found on most current transport aircraft, where bypass ratio is continuously increasing and reached 10 or more in some turbofan engines. Figure 1.73 illustrates high and low bypass ratio turbofan Engines

Because the fuel flow rate for the core is changed only a small amount by the addition of the fan, a turbofan generates more thrust for nearly the same amount of fuel used by the core. This means that a turbofan is very fuel efficient. In fact, high bypass ratio turbofans are nearly as fuel efficient as turboprops. Since the fan is enclosed by the inlet and is composed of many blades, it can operate efficiently at higher speeds than a simple propeller. That is why turbofans are found on high speed transports and propellers are used on low speed transports. Low bypass ratio turbofans are still more fuel efficient than basic turbojets.

Many modern fighter planes actually use low bypass ratio turbofans equipped with afterburners. They can then cruise efficiently but still have high thrust when

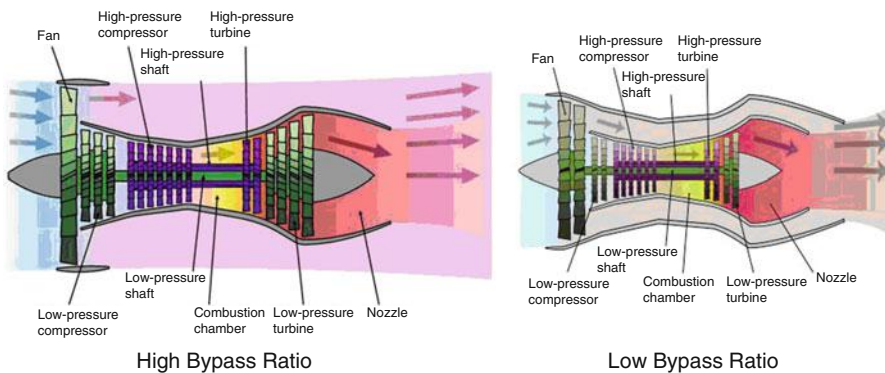


Fig. 1.73 High and low bypass ratio turbofan engines

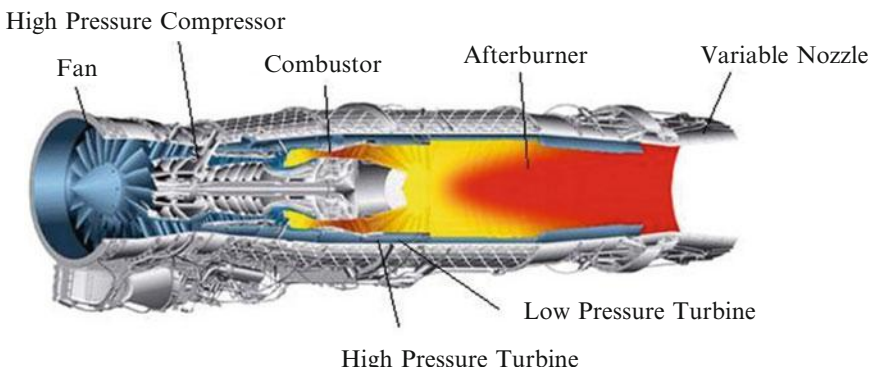
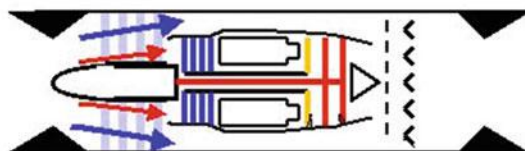
a**b**

Fig. 1.74 Low bypass ratio afterburning turbofan engines

dog fighting. Even though the fighter plane can fly much faster than the speed of sound, the air going into the engine must travel less than the speed of sound for high efficiency. Therefore, the airplane inlet slows the air down from supersonic speeds. Figure 1.74 illustrates a layout (A) and a schematic diagram (B) for an afterburning low bypass ratio turbofan engine.

A few examples for turbofan engines are listed in the following table arranged by manufacturer's products (Table 1.1).

Example 1.2 Write down the following data (sea level static thrust SLS, maximum diameter, length, weight, bypass ratio, and application) for the following turbofan engines: ALF502R-6, CFM56-2-C1, GE90-90B, Trent 1000-A1, V2500-A1, RB211-524H, Tay 620, Trent 800, JT8D-217, PW2037, PW4098

Solution

The requested data is arranged in Table 1.2.

Figure 1.75 illustrates an *aft fan turbofan* engine. It is featured an integrated aft fan/low pressure (LP) turbine unit located in a turbojet exhaust jet pipe. Hot gases from the turbojet turbine exhaust expand through the LP turbine, the fan blades being a radial extension of the turbine blades. The difference between aft fan turbofan engine and propfan or unducted fan (UDF) is that aft fan is a/an ducted/enclosed turbomachine (or surrounded by a casing), while propfan/UDF configuration is not surrounded by any casing. One of the problems with the aft fan configuration is hot gas leakage from the LP turbine to the fan.

Table 1.1 Turbofan engines

Company	Engine	Thrust range	Aircraft
		lbf	
Rolls-Royce (RR)	FJ44	1900–2400	Saab SK-6
RR	RB211-535	37,400–43,100	1. Tupolev Tu 204-120 2. Boeing 757-200, -300
RR	Trent 800	75,000–95,000	Boeing 777-300, -200, -200ER
RR, MTU, Avio, ITP	EJ200	13,500 lbf (Non-Reheated) 20,000 lbf (Reheated)	Eurofighter Typhoon
GE	F101	30,000 lbf thrust class	B-1
GE & SNECMA	CFM56	22,000–24,000 LBF	Super 70 DC-8, Boeing 737-300,-400 and -500, Airbus a340
GE	CF6-80	48,000–61,500	Boeing 767, 747-400, Airbus A300,A310, A330, MD-11
GE	GE90	76,000–115,540	Boeing 747, Boeing 777-300ER
GE	GEnx	53,000–75,000	Boeing 747-8, Boeing 787-8, -9
Pratt & Whitney (P&W)	JT8D	14,000–17,400	Boeing 727, Boeing 737, DC-9, C-1 Transport
P&W	JT9D	45,800–53,000	Boeing 747, 767, Airbus A300, A310, McDonnell Douglas DC-10
P&W	F100	25,000	F-15, F-16
P&W	PW2000	37,000–43,000	Boeing 757, Ilyushin Il-96 M, C-17 Globemaster III
P&W	PW4000	52,000–99,040 lbf	Airbus A300, A310, A330, Boeing 747-400, 767, 777, McDonnell Douglas MD-11
P&W	F119	35,000 lbf class	F-22 Raptor
International Aero Engines	V2500	23,500–28,000	Airbus A319, Airbus A320, MD-90-30
IAE			
General Electric, Pratt & Whitney	GP7000	76,500–81,500 lbf	Airbus A380

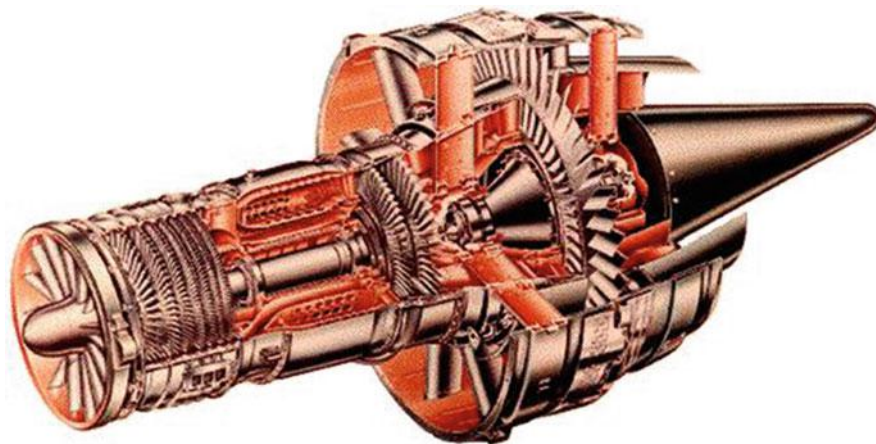
An example for aft-turbofan engine is a modified version of the turbojet engine CJ805, which powered the Convair CV- 990 aircraft.

Turbo Ramjet Engine

Turbo ramjet is a combination engine that can operate as a turbojet or ramjet engine. It is a type of jet engine intended for high speed flight. The turbo ramjet

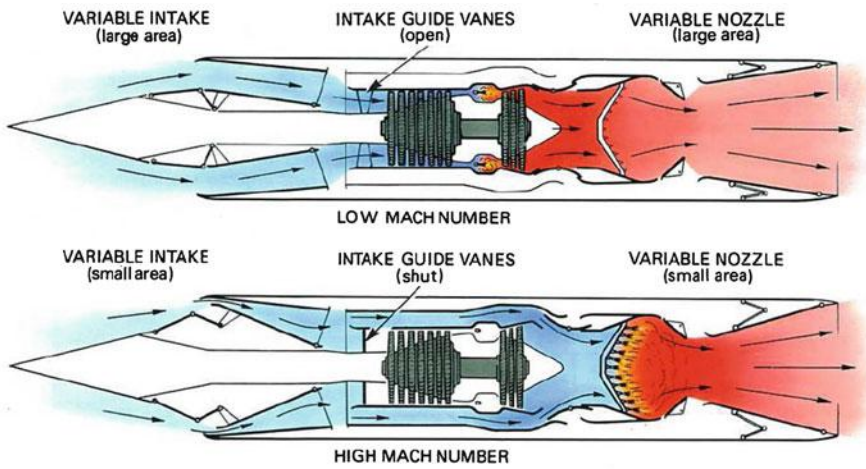
Table 1.2 Some basic data for high bypass ratio turbofan engines

Engine	SLS Thrust (lb)	Max Dia.	Length	Weight (lb)	BPR	Applications
ALF502R-6	7500	50	65.6	1375	5.6	BAE-146
CFM56-2-C1	22,200	72	95.7	4635	6	A340
GE90-90B	90,000	134	204	16,644	9	B777-200/300
Trent 1000-A1	63,800	112	153	11,924	10	B787-8
V2500-A1	25,000	67.5	126	5210	5.4	A319-321
RB211-524H	60,600	86.3	125	9499	4.1	747-400/767-300
Tay 620	13,850	60	102	3185	3.04	Fokker 70/100
Trent 800	92,000	110	172	14,400	6.5	777
JT8D-217	20,850	56.3	154	4430	1.74	MD-80
PW2037	38,250	84.8	146.8	7160	5.8	757, C-17
PW4098	98,000	112	191.7	16,165	5.8	777

**Fig. 1.75** Aft fan turbofan engine

engine (Fig. 1.76) combines the turbojet engine for speeds up to Mach 3 with the ramjet engine, which has good performance at high Mach numbers [28].

The engine is surrounded by a duct that has a variable intake at the front and an afterburning jet pipe with a variable nozzle at the rear. During takeoff and acceleration, the engine functions as a conventional turbojet with the afterburner lit while at other flight conditions up to Mach 3, the afterburner is inoperative. As the aircraft accelerates through Mach 3, the turbojet is shut down and the intake air is diverted from the compressor, by guide vanes, and ducted straight into the afterburning jet pipe, which becomes a ramjet combustion chamber. This engine is suitable for an



A turbo/ram jet engine.

Fig. 1.76 Turbo ramjet engine, reproduced with the permission of Rolls-Royce plc, copyright © Rolls-Royce plc

aircraft requiring high speed and sustained high Mach number cruise conditions where the engine operates in the ram jet mode.

Figure 1.77 shows Pratt & Whitney J58 engines powering the SR-71 aircrafts. P&W J58 is an example for turbo-ramjet engine [29]. It could be converted during flight from being largely a turbojet to being largely a compressor-assisted ramjet. At high speeds (above Mach 2.4), the engine used variable geometry vanes to direct excess air through six bypass pipes from downstream of the fourth compressor stage into the afterburner. Thus, 80 % of the SR-71's thrust at high speed was generated in this way, giving much higher thrust, improving specific impulse by 10–15 %, and permitting continuous operation at Mach 3.2.

Turborocket Engine

The turborocket (or air turborocket) engine (Fig. 1.78) is a type of airbreathing engine combining elements of a jet engine and a rocket, which is also known by its acronym as the ATR. The ATR belongs to a general class of propulsion engines known as Turbine-Based Combined-Cycle, or TBCC, engines. It could be considered as an alternative engine to the turbo ramjet. However, it has one major difference in that it carries its own oxygen to provide combustion at high speed [28]. The engine has a low pressure compressor driven by a multi-stage turbine; the power to drive the turbine is derived from combustion of kerosene and liquid oxygen in a rocket-type combustion chamber. Since the gas temperature will be in the order of 3500° C, additional fuel is sprayed into the combustion chamber for cooling purposes before the gas enters the turbine. This fuel-rich mixture (gas) is



Fig. 1.77 Pratt & Whitney J58 Turbo ramjet Engine (upper) powering SR-71 aircraft (lower)

then diluted with air from the compressor and the surplus fuel burnt in a conventional afterburning system. It is finally exhausting through a convergent-divergent propelling nozzle. In some ATRs, the hot gas can be produced by burning of a solid propellant.

Although the engine is smaller and lighter than the turbo ramjet, it has higher fuel consumption. This tends to make it more suitable for an interceptor or space-launcher type of aircraft that requires high speed and high altitude performance and normally has a flight plan that is entirely accelerative and of short duration.

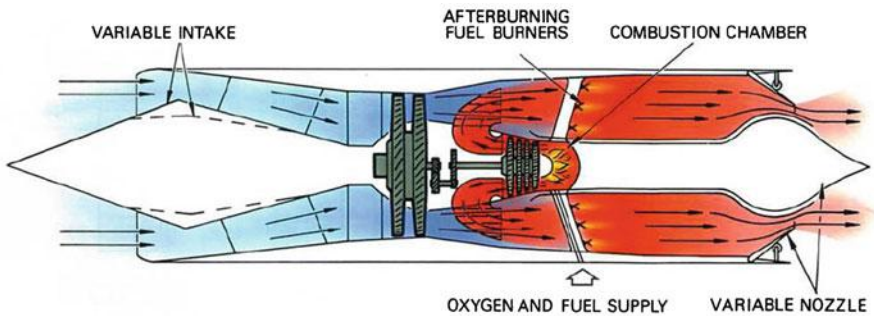


Fig. 1.78 Turborocket engine, reproduced with the permission of Rolls-Royce plc, copyright © Rolls-Royce plc

Advanced Ducted Fan

Advanced ducted fan are essentially turbofans with large swept fan blades that have pitch control and reduction gearing similar to propfans, but the fans are enclosed in ducts like turbofan engines [1]. Bypass ratio for advanced ducted fan is from 15:1 to 25:1 [30]. There are two basic types: one with geared, variable pitch, single propeller fan, and the other with counter-rotating blades. Extensive work has been done in some aero engine manufacturing companies like Pratt & Whitney, MTU, and Fiat Avio for the design of this type of engines. A thin-lip, slim-line nacelle is required to give such a high bypass ratio.

1.3.3 Other Power Sources

This third and last group of aircraft engines (identified as others) is subdivided into human- and electric-powered engines.

1.3.3.1 Electric-Powered Aircraft

An *electric aircraft* is an aircraft that runs on electric motors rather than internal combustion engines, with electricity coming from fuel cells, solar cells, ultra capacitors, power beaming, and/or batteries. The advantages of electric aircraft include increased safety due to decreased chance of mechanical failure, such as from volcanic ash, less risk of explosion or fire in the event of a collision, less noise, and no emissions and pollution. The main disadvantage of electric aircraft is decreased range. The range can be increased by adding solar cells to the aircraft's body to create a *solar airplane*. However, the plane's surface area must be large compared to its weight to have a significant impact on range. Electric powered model aircraft have been flown since the 1970s including manned and unmanned

aerial vehicles. About 60 electrically powered aircrafts have been designed since the 1960s, some are used as military drones.

The 27 lb (12 kg) unmanned AstroFlight Sunrise was the world's first *solar-powered flight* flew on 4 November 1974. The improved Sunrise II flew on 27 September 1975 at Nellis AFB.

The world's first official flight in a manned solar-powered aircraft took place on 29 April 1979 [30]. The aircraft used photovoltaic cells that produced 350 W at 30 V.

The aircraft was capable of powering the motor for 3–5 min, following a 1.5 h charge, enabling it to reach a gliding altitude. The Solar Challenger set an altitude record of 14,300 f. on 7 July 1981 and flew 163 miles from Cormeilles-en-Vexin Airport near Paris across the English Channel to RAF Manston near London. The German Solair 1 employed 2500 wing-mounted solar cells giving an output of 2.2 kW (3 hp) with an aircraft weight of 180 kg (397 lb). The aircraft first flew was on 21 August 1983, while the first flight of Solair II took place 2 years later in Mai 1998 [31].

NASA Pathfinder (Fig. 1.79) and Helios were a series of solar and fuel cell system-powered unmanned aircraft.

In 1990, the solar powered airplane Sunseeker successfully flew across the USA. It used a small battery charged by solar cells on the wing to drive a propeller for takeoff, and then flew on direct solar power and took advantage of soaring conditions when possible.

The Sunseeker II, built in 2002, was updated in 2005–2006 with a more powerful motor, larger wing, lithium battery packs, and updated control electronics. As of December 2008, it was the only manned solar-powered airplane in flying condition and is operated regularly by Solar Flight (Fig. 1.80). In 2009, it became the first solar-powered aircraft to cross the Alps.

China's first solar-powered aircraft "Soaring" was designed and built in 1992. The body and wings are hand-built predominantly of carbon fiber, Kevlar, and wood.

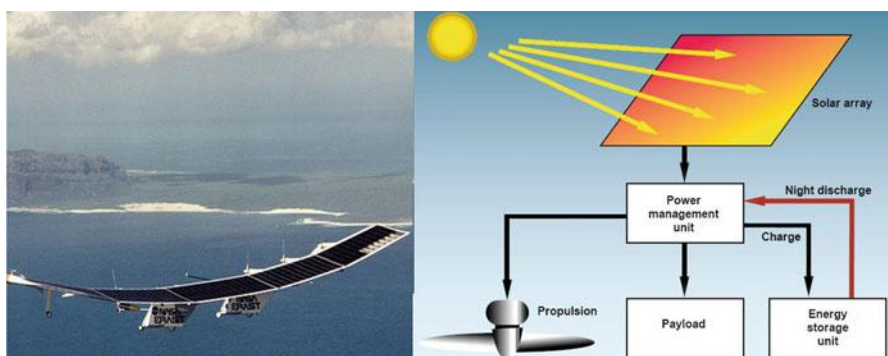


Fig. 1.79 NASA Pathfinder



Fig. 1.80 Sunseeker II solar airplane

Solar Impulse prototype had its first short-hop (350 m) test flight on 3 December 2009 (Fig. 1.81). In its present configuration, it has a wingspan of 64 m, weighs 1588 kg and powered by four 10-horsepower (7 kW) electric motors each turning a propeller. Solar Impulse will capture sunlight using 12,000 photovoltaic cells on its wings and horizontal stabilizer. Power from the solar cells is stored in lithium polymer batteries and used to drive 3.5-m (11 ft) propellers turning at speed of 200–400 rpm. Take-off speed is 19 knots (35 km/h) and cruising speed is 60 knots (111 km/h). The aircraft had its first high flight on 7 April 2010, when it flew to an altitude of 1200 m (3937 ft) in a 1.5 h flight on battery power alone. In July 2010, Solar impulse's HB-SIA prototype airplane made its first successful night flight attempt at Payerne airport. The aircraft took off July 7 at 06:51 am and reached an altitude of 8700 m (28,543 ft) by the end of the day. It then slowly descent to 1500 m (4921 ft) and flew during the night on the batteries, charged during the day by 12,000 solar cells, which powered the four electric motors. It landed July 8 at 09.00 am (GMT 2) for a flight time of 26 h 9 min setting the longest and highest flight ever made by a solar plane. Later on, it completed successful solar-powered flights from Switzerland to Spain and then Morocco in 2012, and conducted a multi-stage flight across the United States in 2013.

In 2014, *Solar Impulse 2* was manufactured with more solar cells and powerful motors. In March 2015, it began an attempt to circumnavigate the globe with *Solar Impulse 2*, departing from Abu Dhabi in the United Arab Emirates. By 1 June 2015, the plane had traversed Asia. On 3 July 2015, the plane completed the longest leg of its journey, from Japan to Hawaii, but the aircraft's batteries experienced thermal damage that is expected to take months to repair.

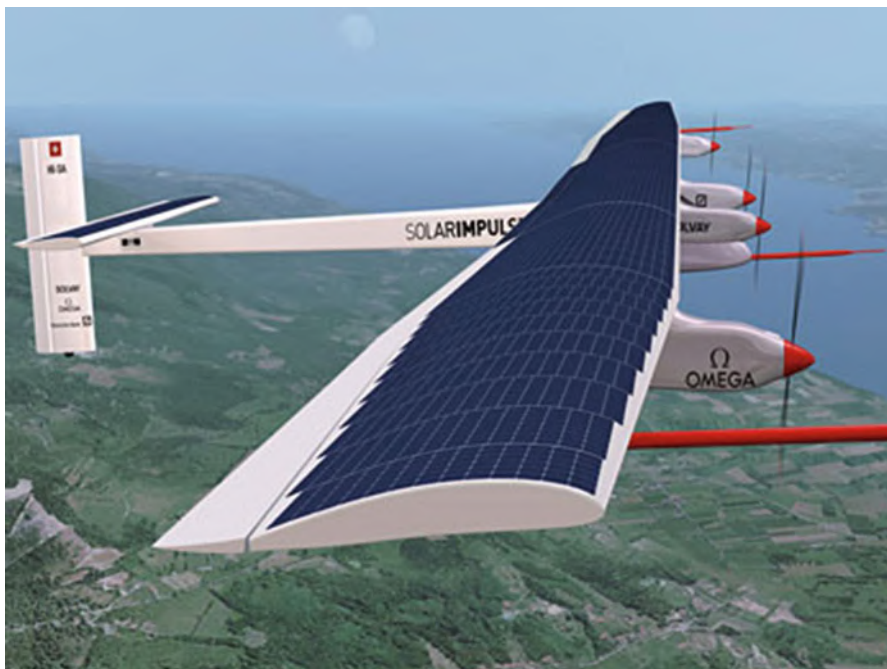


Fig. 1.81 Solar Impulse airplane

1.3.3.2 Human-Powered Aircraft (HPA)

A *human-powered aircraft (HPA)* is an aircraft capable of sustained, controlled flight by human power alone through an act of pedaling, which activates a mechanism for turning a propeller for thrust (Fig. 1.82). HPA inevitably experience assist from thermals or rising air currents. Pure HPA do not use hybrid flows of energy (solar energy, wound rubber band, fuel cell, etc.) for thrust. The first recorded successful HPA flight happened in 1936 through the “Pedaliante”, an aircraft built and designed in Italy. As of 2008, human-powered aircraft have been successfully flown over considerable distances. However, they are primarily constructed as an engineering challenge rather than for any kind of recreational or utilitarian purpose.

1.3.3.2.1 Closure

It is evident from this chapter how mankind’s life is now increasingly dependent on aircrafts. In both civil and war, airplanes have its essential role. Detailed description of commercial jetliners, helicopters, and defense systems are given. Thus fixed and rotary wing aircrafts utilized in both civil and military fields are fully classified.



Fig. 1.82 Human-powered airplane

Civilian fixed wing aircrafts are employed both in passengers and freight transportation, search and rescue, agricultural, research, fire fighting, and training activities. Fixed wing military aircrafts display itself in battle fields as fighter, ground attack, bombers, and rescue, while transport, search and rescue, training as well as firefighting. Reconnaissance and refueling aircrafts fly between conflict areas and air force bases. Rotary wing aircrafts are also extensively seen both in civil and military disciplines. It has the capability to take off/land in unpaved areas. Tourism, search and rescue, firefighting, and police works are some of its civilian activities. Transport, fighting, bombing, and rescue are some important military applications.

Moreover, various propulsion systems are thoroughly described. Both shaft and reaction engines are classified. Internal combustion engines are one class of shaft engines that has three main groups, namely: Wankel, piston, and turbine types. Turbine group is again subdivided into turboprop, turboshaft, and propfan engines. Other shaft engines are either solar- or human-powered type. Reaction engines are the most dominant power plants including ramjet, pulsejet, turbojet, turbofan, turbo ramjet, and turbo rocket engines. Turbofan engines are the mostly employed airbreathing engines in both civil and military fixed wing applications. Turboshaft engines are the present unique power plants used in helicopters. Turboprop engines power most of the heavy transport civil and military aircrafts.

Detailed analyses for all of the above power plants will be given in this book. It is categorized as ram-based engines, turbine-based engines and shaft-based engines. A complete chapter is devoted for each group.

Problems

1.1 Complete the following table for aircraft classifications:

Aircraft	Mono-plane transport	Mono-plane military	Bi-plane transport	Bi-plane military	Tri-plane transport	Tri-plane military	Tri-plane military
<i>Aircraft type</i>							
<i>Aero engine</i>							
<i>Example</i>							

1.2 Complete the following table for aircraft classifications:

Aircraft	Blended wing body (BWB)	Hybrid wing body (HWB)	Sea	Amphibian	STOL	VTOL	V/STOL
<i>Aircraft type</i>							
<i>Aero engine</i>							
<i>Example</i>							

1.3 Complete the following table for aircraft classifications based on its utility:

Aircraft	STOVL	Agricultural	Civilian trainer	Civilian search and rescue	Civilian firefighting	Civilian experimental	Single engine private transport
<i>Aircraft type</i>							
<i>Aero engine</i>							
<i>Example</i>							

1.4 Complete the following table for civil transport aircrafts:

Aircraft	Twin engine private transport	Executive jet (corporate)	Commuter	Regional	Short haul	Medium haul	Long haul
<i>Aircraft type</i>							
<i>Aero engine</i>							
<i>Example</i>							

1.5 Complete the following table:

Aircraft	Tactics bomber	Strategic bomber	Fighter bomber	Ground attack	Maritime patrol	Interceptor	Enhanced TOL
<i>Aircraft type</i>							
<i>Aero engine</i>							
<i>Example</i>							

1.6 Complete the following table for non-combat military aircrafts:

<i>Aircraft</i>	Military transport	Tanker (refueling)	Military trainer	Military experimental	Military fire-fighting	AWACS	Reconnaissance
<i>Aircraft type</i>							
<i>Aero engine</i>							
<i>Example</i>							

1.7 Complete the following table for fixed/rotary wing aircrafts:

<i>Aircraft</i>	Military UAV	Military glider	NOTAR helicopter	Tip jet helicopter	Ducted fan helicopter	Tail rotor helicopter	Tandem helicopter
<i>Aircraft type</i>							
<i>Aero-engine</i>							
<i>Example</i>							

1.8 Complete the following table for rotorcrafts:

<i>Aircraft</i>	Coaxial helicopter	Inter-meshing helicopter	Transverse helicopter	Gyrodynes	Autogyros	Transport helicopter	Training helicopter
<i>Aircraft type</i>							
<i>Aero-engine</i>							
<i>Example</i>							

1.9 Complete the following table for helicopters

<i>Aircraft</i>	Construction (aerial cranes)	Inter-meshing helicopter	Search and rescue helicopter	Remote sensing helicopter	Firefighting (helitack)	MEDEVAC air ambulance	Sea helicopter
<i>Aircraft type</i>							
<i>Aero engine</i>							
<i>Example</i>							

1.10 Complete the following table for helicopters:

<i>Aircraft</i>	Attack helicopter	Trainer helicopter	Transport helicopter	Experimental helicopter	Multi-mission and rescue helicopter	Maritime helicopter	Tactics and operation helicopter
<i>Aero engine</i>							
<i>Example</i>							

1.11 Complete the following table:

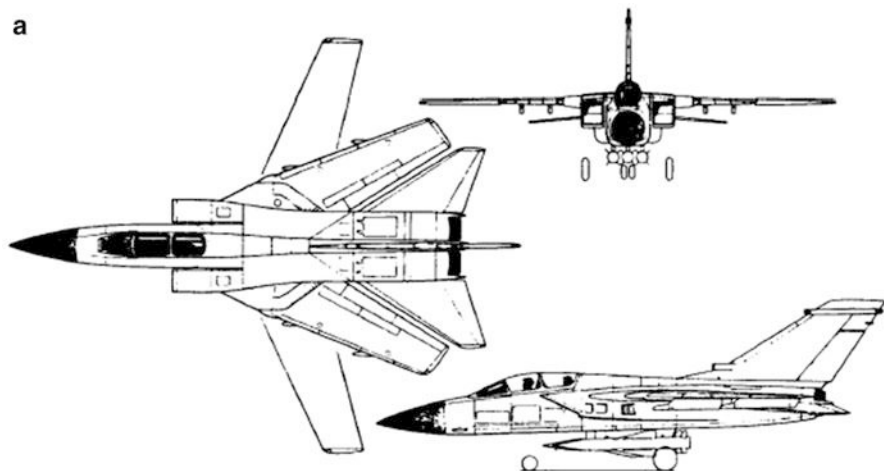
<i>Aircraft</i>	Observation helicopter	UAV helicopter	Tiltrotor	Coleopter	Tiltwing	Mono tiltrotor	Mono-tilt-rotor rotary-ring
<i>Aero engine</i>							
<i>Example</i>							

1.12 *Classify the following aircrafts giving the name of a possible installed power plant:*

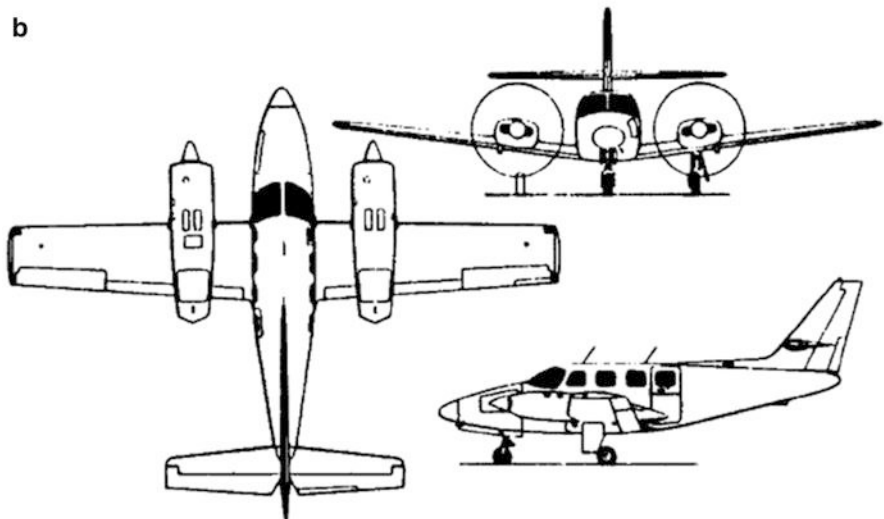
Airbus A300, Antonov An 2 M, AVRO Vulcan B-2, B-52, B 767, B737, B777, BAE 146 Model Series 200, BEECH STARSHIP I, Beriev Be-42, C-17, C-130, Cessna Model 402 C, Dassault Breguet Alpha Jet CH 53, DC-3, DC-10, DeHavilland Canada Dash-8, Embraer EMB-120, Embraer EMB-312 Tucano, F15, F35, Fokker F-27 Friendship MK 200, Gates LEARJET 35A, Lockheed Jetstar, McDonnell Douglas MD-80, Mig-29, Mirag-2000, Prion P-3, Piper Tomahawk II, Saab 340, SIAI Marchetti S-211, SR-71, Su-27, U-2, X-15

1.13 *Classify the shown aircrafts*

a



b

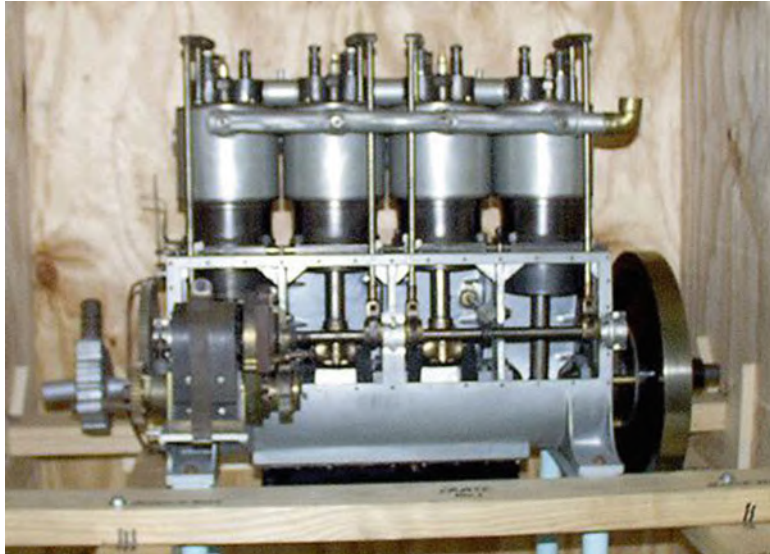


1.14 Mark *right* or *wrong*, then correct wrong statement(s):

- The world's first certified commercial transport helicopter was S-55 Chick-asaw (H-19) ()
- The world's first turbine gas-powered engine was Kaman K-225 ()
- MD 902 is one of the highest cruise speed helicopter; 258 km/h ()
- Dhruv helicopter records one of the highest ceiling namely 27,500 ft ()
- PZL SW-4 helicopter has one of the largest ranges namely 990 km ()
- Eurocopter AS 532 is a military transport having a capacity of 20 troops ()
- Agusta AZ 101 G being one of the largest capacity transport helicopters has a capacity of 45 passengers ()
- Small helicopter-type unmanned aerial vehicles use electric motors as power sources ()

1.15 The shown figure illustrates a model for the engine-powered Wright Brothers flyer.

Write down its type and specifications



1.16 *Classify the following engines* giving the name of a possible powered aircraft:

CF6-50C, CF34-GE-400A, CFM56-3C, F100-PW-100, F101-GE-102, F135, F404-GE-400,

J57-P-10, J60-P-3, J75-P-13B, JT8D-17, JT9D-7 F, Pegasus 11-21, PT6 Twin Pac, PW100, PW2040, PW4090, RB211-524H, RB211-TRENT 768, R-985 WASP JR, R-1340, Spey 506-14 W, Tay 650, TF30-P-6, TF33-PW-102, V2500-A1

- 1.17 Identify the type of the shown engine, giving three examples for engines and the installed aircrafts



- 1.18 Give a detailed description of the shown Helios aircraft



- 1.19 The shown figure illustrates
Kuznetsov NK-12 M Turboprop, powering
Tu-95 aircraft. Give details of the engine; number of shafts, power, propeller type, possible installations to other aircrafts.



1.20 Compare between the following propfan engines:

- Pratt & Whitney/Allison 578-DX
- *General Electric GE36*
- Ivchenko-Progress D-27

1.21 Complete the missing data in the following table:

Engine	SLS Thrust (lbs)	Max diameter	Length (in)	Weight (lbs)	BPR	Applications
TFE731-2	3500	39.4	51	725	2.67	??
TFE731-20	3650	39.4	51	885	??	??
BR710	20,000	52.9	87	3520	??	??
AE3007	7580	43.5	106.5	1581	??	??
FJ44-1	1900	20.9	41.9	445	??	??
FJ44-2	2300	23.7	40.2	448	3.28	??
JT3-D-7	19,000	52.9	134.4	4300	??	??
JT8D-11	15,000	43	120	3310	??	??
JT9D-3A	43,500	95.6	128.2	8608	??	??
GE4	69,000	90	296.04	13,243	??	B2707 SST design Mach 2.7
GE21J11B14	65,000	74.16	282	??	??	SCAR study Mach 2.6
Olympus 593	38,000	49	150	6780	??	Concorde
TBE-M1.6	70,600	??	??	9252	??	NASA Mach 1.6 study

(continued)

TBE-M2.0	69,000	??	??	9278	??	NASA Mach 2.0 study
TBE-2.4	65,500	??	??	9587	??	NASA Mach 2.4 study
Rolls VCE	49,460	??	??	??	??	HSCT design study
Rolls Tandem	49,460	??	??	??	??	HSCT design study

References

1. El-Sayed AF (2008) Aircraft propulsion and gas turbine engines. Taylor & Francis, Boca Raton
2. <http://dictionary.reference.com/browse/aircraft>
3. Gunston B (1986) Jane's aerospace dictionary. Jane's Publishing Company Limited, London
4. <http://www.myairship.com/database/index.html>
5. Timothy RG (2001) Amazing agricultural aircraft. Enslow Publishers, Berkeley Heights
6. Brian W (1999) Trainer Aircraft Markets (Jane's Information Group, Special Report)
7. Jim Winchester J (2005) Concept aircraft: prototypes, X-planes, and experimental aircraft (aviation factfile). Thunder Bay Press, San Diego
8. Morton JK (2001) Flying freighters. Zenith Press, Minneapolis
9. Trani A, Aircraft Classification, Virginia Tech (http://128.173.204.63/courses/cee5614/cee5614_pub/acft_classifications.pdf)
10. Deighton L (2006) Bomber. HarperCollins, London
11. March PR (2006) Fighter aircraft (top trumps). J H Haynes & Co Ltd, Newbury Park
12. <http://www.airforce-technology.com/projects/su34/>
13. http://en.wikipedia.org/wiki/List_of_VTOL_aircraft
14. Musial M (2008) System architecture of small autonomous UAVs. VDM Verlag, Saarbrücken
15. Miller J (2001) The X-planes: X-1 to X-45: 3rd edition. Midland Publishing, Milbank
16. Helicopter Flying Handbook (2010) CHAPTER 4 FAA, USA
17. Albert JA, Zuk J (1987) Civil applications of high-speed rotorcraft and powered-lift aircraft configurations, SAE Paper No. 872372
18. Leishman JG (2006) Principles of helicopter aerodynamics. Cambridge University Press, Cambridge, England
19. http://en.wikipedia.org/wiki/Aerocopter_Sarus
20. Hege JB (2006) Wankel rotary engine: a history. McFarland Pub. Co., Jefferson
21. Foa JV (1960) Element of flight propulsion. Wiley, New York
22. Archer RD, Saarlas M (1996) An introduction to aerospace propulsion. Prentice-Hall, Upper Saddle River
23. Billing FS (1993) Research on supersonic combustion. AIAA J Propulsion Power 9 (4):499–514
24. Zucker RD, Biblarz O (2002) Fundamentals of gas dynamics. Wiley, Hoboken
25. <http://gofurther.utsi.edu/Projects/PulseDE.htm>
26. <http://news.google.com/patents/about?id=vOZsAAAAEBAJ>
27. Roskam J, Lan C-TE (1997) Airplane aerodynamics and performance DARcorporation
28. The Jet Engine (1996) Rolls-Royce plc, 5th ed. Reprinted with revisions
29. The Aircraft Gas Turbine Engine and Its Operation (1988) Pratt & Whitney Operating Instructions 200
30. <http://www.alternative-energy-news.info/10-best-solar-airplane-concepts/>
31. Noth A (2008) History of solar flight. In: Autonomous systems lab. Swiss Federal Institute of Technology, Zürich

Chapter 2

A Review of Basic Laws for a Compressible Flow

2.1 Introduction

The operation of aero engines and rockets is governed by the laws of fluid mechanics (or more specifically aerodynamics and gas dynamics) as well as thermodynamics. Understanding and analyzing the performance of aero engines and rocket motors requires a closed set of governing equations (conservation of mass and energy, linear and angular momentums, entropy) as well as several compressible flow relations that govern the isentropic flow, normal and oblique shock waves, expansion waves, and finally Fanno and Rayleigh flow. For understanding the basic physical phenomena, gas will be modeled as a *perfect gas*, and apart from the rotating elements (fans, compressors, and turbines), the flow will be assumed *one dimensional*, where its properties are assumed constant across the flow and vary only in the flow direction (axial direction). It is assumed that the students have studied a first course in both fluid mechanics and thermodynamics. A review of thermo-fluid physics and one-dimensional gas dynamics will be given in this chapter. For more details, students are asked to refer to the following set of textbooks: Shames and White [1, 2] for fluid mechanics and Shapiro, Zucrow and Hoffman, and Zucker [3–5] for gas dynamics together with Keenan, Sonntag, et al. as well as Cengel and Boles [6–8] for thermodynamics.

Macroscopic approach rather than microscopic one will be followed here. The concepts of system and control volume are followed in specifying a definite collection of material and a region in space that will be analyzed.

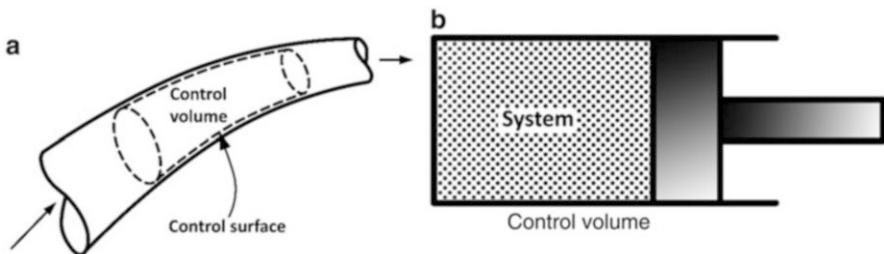


Fig. 2.1 System and control volume. (a) System. (b) Control volume

2.2 System and Control Volume

A *system* is a collection of matter of fixed identity. It may be considered enclosed by an invisible, massless, flexible surface through which may change shape, and position, but must always entail the same matter. For example, one may choose the steam in an engine cylinder (Fig. 2.1) as a system. As the piston moves, the volume of the system changes, but there is no change in the quantity and identity of mass. The terms system and control mass have identical meaning.

A *control volume* is a region of constant shape and size that is fixed in space relative to the observer. The boundary of this volume is known as the control surface. This control surface may be imagined as massless, invisible, and rigid envelope which offers no resistance to the passage of mass. The amount and identity of the matter in the control volume may change with the time, but the shape of the control volume is fixed. For instance, to study flow through a variable geometry duct, one could choose, as a control volume, the interior of the duct as shown in Fig. 2.1. We note that the control volume and the system can be infinitesimal.

2.3 Fundamental Equations

Four basic laws must be satisfied for the continuous medium (or continuum) inside aero engines and rocket motors, namely:

1. Conservation of matter (continuity equation)
2. Newton's second law (momentum and moment-of-momentum equations)
3. Conservation of energy (first law of thermodynamics)
4. Second law of thermodynamics

In addition to these general laws, there are numerous subsidiary laws, sometimes called constitutive relations, that apply to specific types of media, like the equation of state for the perfect gas and Newton's viscosity law for certain viscous fluids. Furthermore, for high-speed flows additional compressible flow features have to be

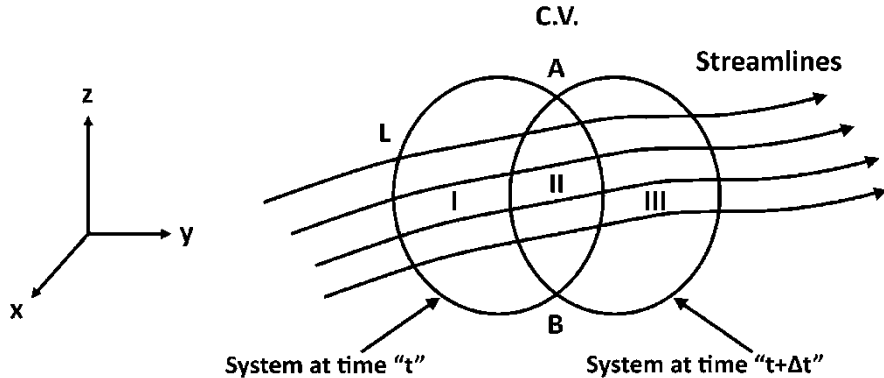


Fig. 2.2 Simplified view of moving system

governed by *isentropic, Rayleigh and Fanno flow relations together with normal and oblique shock relations* if encountered. In thermodynamics we have two kinds of properties of a substance. Those whose measure depends on the amount of mass of the substance are called *extensive* properties, and those whose measure is independent of the amount of mass of the substance present are called *intensive* properties. Temperature and pressure are two famous examples for intensive properties. Examples of extensive properties are weight, momentum, volume, and energy. Each extensive variable such as enthalpy (H) and energy (E), we have $H = \iiint hpdv$ and $E = \iiint epdv$, has its intensive properties: (h) and (e).

Consider next an arbitrary flow field $V(x,y,z,t)$ as seen from some frame of reference xyz wherein we observe a system of fluid of finite mass at times " t " and " $t + \Delta t$ " as shown in Fig. 2.2. The streamlines correspond to those at time " t ." In addition to this system, we will consider that the volume in space occupied by the system at time " t " is the control volume fixed in position and shape in xyz . Hence, at time " t " our system is identical to the fluid inside our control volume. Let us now consider some arbitrary extensive property "N" of the fluid. The distribution of "N" per unit mass will be given as " η " such that $N = \iiint \eta pdv$ with dv representing an element of volume.

We have divided up the overlapping systems at time " $t + \Delta t$ " and at time " t " into three regions, as shown in Fig. 2.2. The region II is common to the system at both times " t " and " $t + \Delta t$." Let us compute the rate of change of N with respect to time for the system by the following limiting process:

$$\left(\frac{dN}{dt} \right)_{\text{system}} = \frac{DN}{Dt}$$

$$\frac{DN}{Dt} = \lim_{\Delta t \rightarrow 0} \left[\frac{\left(\iiint_{III} \eta \rho dv + \iiint_{II} \eta \rho dv \right)_{t+\Delta t} - \left(\iiint_I \eta \rho dv + \iiint_{II} \eta \rho dv \right)_t}{\Delta t} \right] \quad (2.1)$$

Equation (2.1) can be rearranged to the form

$$\begin{aligned} \frac{DN}{Dt} &= \lim_{\Delta t \rightarrow 0} \left[\frac{1}{\Delta t} \left\{ \left(\iiint_{II} \eta \rho dv \right)_{t+\Delta t} - \left(\iiint_{II} \eta \rho dv \right)_t \right\} \right] \\ &\quad + \lim_{\Delta t \rightarrow 0} \left[\frac{1}{\Delta t} \left\{ \left(\iiint_{III} \eta \rho dv \right)_{t+\Delta t} - \left(\iiint_I \eta \rho dv \right)_t \right\} \right] \end{aligned} \quad (2.2)$$

After some manipulation, with the net efflux rate equal to the outlet rates efflux minus the rate influx through the control surface, we arrive at the relation

$$\frac{DN}{Dt} = \frac{\partial}{\partial t} \iiint_{C.V.} \eta \rho dv + \oint_{C.S.} \eta (\rho V \bullet dA) \quad (2.3)$$

Equation (2.3) is called *Reynolds transport equation*. This equation permits us to change from a system approach to a control-volume approach.

2.3.1 Conservation of Mass (Continuity Equation)

Now, let us apply Reynolds transport Eq. (2.3) to reach the continuity equation. In this case:

1. The extensive property “N” is the mass of a fluid system “M.”
2. The quantity “ η ” is unity, since $M = \iiint_{C.V.} \rho dv$.

Then Reynolds transport equation will have the form

$$\frac{DM}{Dt} = \frac{\partial}{\partial t} \iiint_{C.V.} \rho dv + \oint_{C.S.} (\rho \bar{V} \cdot \bar{dA}) = 0 \quad (2.4a)$$

Since we can choose a system of any shape at time “t,” the relation above is then valid for any control volume at time “t” as follows:

$$\iint_{C.S.} \rho (\bar{V} \cdot \bar{dA}) = - \frac{\partial}{\partial t} \iiint_{C.V.} \rho dv \quad (2.4b)$$

That is, the net efflux rate of mass through the control surface equals the rate of decrease of mass inside the control volume. Equation (2.4) and its simplified forms are called equation of continuity.

If the flow is steady relative to a reference fixed to the control volume, all fluid properties, including the density at any fixed position in the reference, must remain invariant with time. The right side of Eq. (2.4) can be written in the form $\iiint (\partial \rho / \partial t) dv$, and this integral is zero. Hence, we can state that any steady flow

$$\iint_{C.S.} \rho (\bar{V} \cdot \bar{dA}) = 0 \quad (2.5a)$$

Next, consider the case of incompressible flow, in this case, ρ is constant at all positions in the domain and for all even if the velocity field is unsteady. The right side of Eq. (2.4) vanishes then, and on the left side of this equation, we can extract ρ from under the integral sign. We then arrive at the relation:

$$\iint_{C.S.} (\bar{V} \cdot \bar{dA}) = 0 \quad (2.5b)$$

Thus, for any incompressible flow, conservation of mass reduces to conservation of volume. Let us consider the very common situation in which fluid enters some device through a pipe and leaves the device through a second pipe, as shown diagrammatically in Fig. 2.3. A dashed line indicates the chosen control surface. We assume that the flow is steady relative to the control volume and that the inlet and outlet flows are one dimensional. Applying Eq. (2.5a) for this case, we get

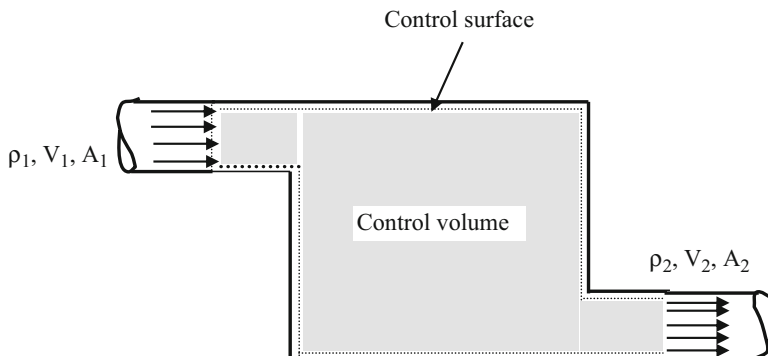


Fig. 2.3 Control volume for device with 1-D inlet and outlet

$$\iint_{CS} (\rho \bar{V} \bullet d\bar{A}) = \iint_{A_1} (\rho \bar{V} \bullet d\bar{A}) + \iint_{A_2} (\rho \bar{V} \bullet d\bar{A})$$

where A_1 and A_2 are, respectively, the entrance and exit areas

$$\iint_{CS} (\rho \bar{V} \bullet d\bar{A}) = - \iint_{A_1} \rho V dA + \iint_{A_2} \rho V dA$$

With ρ and V constant at inlet and outlet sections, we obtain the following equation:

$$-\rho_1 V_1 \iint_{A_1} dA + \rho_2 V_2 \iint_{A_2} dA = 0$$

Integrating, we get

$$\rho_1 V_1 A_1 = \rho_2 V_2 A_2 \quad (2.6)$$

2.3.2 Linear Momentum (Newton's Second Law)

Newton's second law states that

$$\overline{F}_R = \left(\frac{d}{dt} \right)_{\text{system}} \left[\iiint_M \bar{V} dm \right] = \left(\frac{d\bar{P}}{dt} \right)_{\text{system}} \quad (2.7)$$

where

\overline{F}_R is the resultant external force and \bar{P} is the linear momentum vector.

\overline{F}_R is classified as the surface force and body force distributions. The surface force is denoted as $\bar{T}(x, y, z, t)$ and given as force per unit area on the boundary surfaces. The body force distribution is denoted as $\bar{B}(x, y, z, t)$ and given as force per unit mass. For example, gravity is the most common body force distribution, and thus, $\bar{B} = -g \bar{K}$. We can rewrite Eq. (2.7) as follows:

$$\iint_{CS} \bar{T} dA + \iiint_{CV} \bar{B} \rho dv = \frac{D\bar{P}}{Dt} \quad (2.8a)$$

The linear momentum \bar{P} is the extensive property to be considered in the Reynolds transport Eq. (2.3). The quantity η becomes momentum per unit mass, which is " \bar{V} ."

Thus

$$\frac{D\bar{P}}{Dt} = \oint_{C.S.} \bar{V}\rho(\bar{V} \cdot d\bar{A}) + \frac{\partial}{\partial t} \iiint_{C.V.} \bar{V}\rho dv \quad (2.8b)$$

We then have from Eq. (2.8) the linear momentum equation expressed as

$$\oint_{C.S.} \bar{T}dA + \iiint_{C.V.} \bar{B}\rho dv = \oint_{C.S.} \bar{V}\rho(\bar{V} \cdot d\bar{A}) + \frac{\partial}{\partial t} \iiint_{C.V.} \bar{V}\rho dv \quad (2.9)$$

This equation then equates the sum of these force distributions with the rate of efflux of linear momentum across the control surface plus the rate of increase of linear momentum inside the control volume. For steady flow and negligible body forces, as is often the case in *propulsion applications*, the equation above becomes

$$\oint_{C.S.} \bar{T}dA = \oint_{C.S.} \bar{V}\rho (\bar{V} \cdot d\bar{A}) \quad (2.10)$$

Since the momentum Eq. (2.9) is a vector equation, then the scalar component equations in the orthogonal x , y , and z directions may then be written as

$$\begin{aligned} \oint_{C.S.} T_x dA + \iiint_{C.V.} B_x \rho dv &= \oint_{C.S.} V_x \rho (\bar{V} \cdot d\bar{A}) + \frac{\partial}{\partial t} \iiint_{C.V.} V_x \rho dv \oint_{C.S.} T_y dA + \iiint_{C.V.} B_y \rho dv \\ &= \oint_{C.S.} V_y \rho (\bar{V} \cdot d\bar{A}) + \frac{\partial}{\partial t} \iiint_{C.V.} V_y \rho dv \oint_{C.S.} T_z dA + \iiint_{C.V.} B_z \rho dv \\ &= \oint_{C.S.} V_z \rho (\bar{V} \cdot d\bar{A}) + \frac{\partial}{\partial t} \iiint_{C.V.} V_z \rho dv \end{aligned} \quad (2.11)$$

In using Eq. (2.11), one selects directions for the positive directions of the inertial reference axes x , y , and z . Then the positive directions of the velocities V_x , V_y , and V_z , as well as the surface and body force T_x and B_x , and so on, are established.

Example 2.1 A turbojet engine is powering an aircraft flying at a speed of (u) as shown in Fig. 2.4. Air flows into the engine at the rate of (\dot{m}_a) through the inlet area (A_i). Fuel is injected into the combustors at the rate of (\dot{m}_f). The exhaust gases are leaving the propelling nozzle at the rate of (\dot{m}_e) and speed of (u_e) via an exit area (A_e). The ambient and exit pressures are (P_a and P_e). Prove that the generated thrust force is expressed as

$$\tau = \dot{m}_a[(1+f)u_e - u] + (P_e - P_a)A_e$$

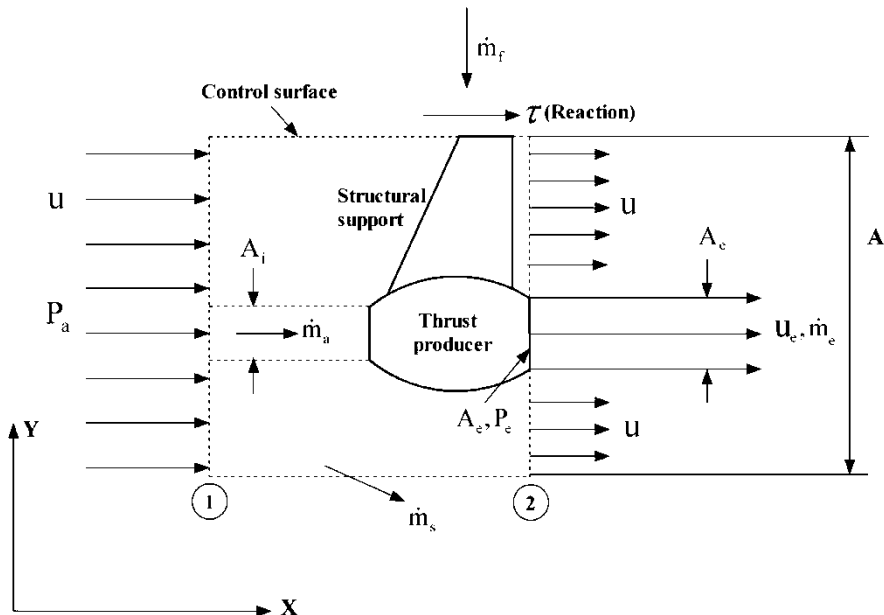


Fig. 2.4 Control volume around a turbojet engine

Figure 2.4, illustrates a turbojet engine with a part of its pod installation (which is a structural support for hanging the engine to the wing). It also defines a control volume which control surface passes through the engine outlet (exhaust) plane (2) and extends far upstream at (1). The two side faces of the control volume are parallel to the flight velocity u . The upper surface cuts the structural support, while the lower one is far below the engine. The surface area at planes (1) and (2) is equal and denoted A . The stream tube of air entering the engine has an area A_i at plane (1), while the exhaust area for gases leaving the engine is A_e . Over plane (1), the velocity and pressure are u (which is the flight speed) and P_a (ambient pressure at this altitude). The velocity and pressure over plane (2) are still u and P_a except over the exhaust area of the engine A_e which values are u_e and P_e . The x - and y -directions employed here are chosen parallel and normal to the centerline of the engine.

The following assumptions are assumed:

1. The flow is steady within the control volume; thus, all the properties within the control do not change with time.
2. The external flow is reversible; thus, the pressures and velocities are constants over the control surface except over the exhaust area P_e of the engine.

Conservation of mass across the engine gives

$$\dot{m}_a + \dot{m}_f = \dot{m}_e$$

where \dot{m}_a and \dot{m}_e are expressed as

$$\dot{m}_a = \rho u A_i, \quad \dot{m}_e = \rho_e u_e P_e$$

The fuel flow rate is thus expressed as

$$\dot{m}_f = \rho_e u_e A_e - \rho u A_i \quad (\text{A})$$

The fuel-to-air ratio is defined here as

$$f = \frac{\dot{m}_f}{\dot{m}_a}$$

$$\dot{m}_e = \dot{m}_a(1+f) \quad (\text{B})$$

Apply the continuity equation over the control volume

$$\frac{\partial}{\partial t} \iiint_{CV} \rho dv + \oint_{CS} \rho \bar{u} \cdot d\bar{A} = 0$$

For a steady flow, $\frac{\partial}{\partial t} \iiint_{CV} \rho dv = 0$, then $\oint_{CS} \rho \bar{u} \cdot d\bar{A} = 0$

$$\text{or } \dot{m}_e + \dot{m}_s + \rho u(A - A_e) - \dot{m}_a - \dot{m}_f - \rho u(A - A_i) = 0$$

where (\dot{m}_s) is the side air leaving the control volume.

Rearranging and applying Eq. (A), we get the side mass flow rate as

$$\dot{m}_s = \rho u(A_e - A_i) \quad (\text{C})$$

According to the momentum equation

$$\sum \vec{F} = \frac{\partial}{\partial t} \iiint_{CV} \rho \bar{u} dv + \oint_{CS} \bar{u} (\rho \bar{u} \cdot d\bar{A}) = 0$$

where $\sum \vec{F}$ is the vector sum of all forces acting on the material within the control volume which are surface forces (pressure force as well as the reaction to thrust force through the structural support denoted by τ) and the body force (which is the gravitational force here).

For steady flow

$$\sum \vec{F} = \oint_{CS} \bar{u} (\rho \bar{u} \cdot d\bar{A})$$

The x -component of the momentum equation

$$\sum F_x = (P_a - P_e)A_e + \tau = \oint_{CS} u_x (\rho \bar{u} \cdot d\bar{A}) \quad (D)$$

If the sides of the control volume are assumed sufficient distant from the engine, then the side mass flow rate leaves the control volume nearly in the x -direction. Thus,

$$\begin{aligned} \oint_{CS} u_x (\rho \bar{u} \cdot d\bar{A}) &= \dot{m}_e u_e + u[\rho u(A - A_e)] + \dot{m}_s u - \dot{m}_a u - u[\rho u(A - A_i)] \\ \therefore \oint_{CS} u_x (\rho \bar{u} \cdot d\bar{A}) &= \dot{m}_e u_e - \dot{m}_a u - \rho u^2 (A_e - A_i) + \dot{m}_s u \end{aligned}$$

From Eq. (C)

$$\therefore \oint_{CS} u_x (\rho \bar{u} \cdot d\bar{A}) = \dot{m}_e u_e - \dot{m}_a u \quad (E)$$

From Eqs. (D) and (E) then

$$\tau - (P_e - P_a)A_e = \dot{m}_e u_e - \dot{m}_a u$$

From Eq. (B)

$$\therefore \tau = \dot{m}_a[(1+f)u_e - u] + (P_e - P_a)A_e$$

The following terminology is always used:

Net thrust = τ

Gross thrust = $\dot{m}_a[(1+f)u_e] + (P_e - P_a)A_e$

Momentum thrust = $\dot{m}_a[(1+f)u_e]$

Pressure thrust = $(P_e - P_a)A_e$

Momentum drag = $\dot{m}_a u$

Thus: Net thrust = Gross thrust – Momentum drag

Or in other words:

Net thrust = Momentum thrust + Pressure thrust – Momentum drag

Example 2.2 A fighter airplane is being refueled in flight using the hose-and-drogue system as shown in Fig. 2.5 at the rate of 300 gal/min of fuel having a specific gravity of 0.7. The inside diameter of hose is 0.12 m. The fluid pressure at the entrance of the fighter plane is 30 kPa gage. What additional thrust does the plane need to develop to maintain the constant velocity it had before the hookup?



Fig. 2.5 Aerial refueling using the hose-and-drogue system

Solution

At first, it is worthy defining *aerial refueling* (which is also identified as *air refueling*, *in-flight refueling (IFR)*, *air-to-air refueling (AAR)*, or *tanking*) as the process of transferring *fuel* from one *aircraft* (the tanker) to another (the receiver) during flight. When applied to *helicopters*, it is known as *HAR* for helicopter aerial refueling. A series of air refueling can give range limited only by crew fatigue and engineering factors such as engine oil consumption.

Now, back to our problem, consider a control volume starting from the probe to the fuel tank. This is an inertial control volume with the positive *x*-direction parallel to aircraft flight direction.

Thus the linear momentum equation in the *x*-direction is

$$F_x = \iint_{C.S.} V_x \rho (\bar{V} \cdot \bar{dA}) + \frac{\partial}{\partial t} \iiint_{C.V.} V_x \rho \, dv$$

where F_x is the force in the *x*-direction. Since a steady flow is assumed in refueling process, then

$$F_x = \iint_{C.S.} V_x \rho (\bar{V} \cdot \bar{dA})$$

which is rewritten as: $T_x - pA = -[V_x \times (-\rho V_x A)] = \rho V_x^2 A$

where T_x is the needed additional thrust and the velocity of fuel flow into the probe is V_x . Since

$$V_x = \frac{Q}{A} = \frac{(300 \times 3.785 \times 10^{-3} / 60)}{\left[\pi \times (0.12)^2 / 4 \right]} = \frac{0.018925}{0.01131} = 1.6733 \text{ m/s}$$

$$\rho = 0.7 \times 1000 = 700 \text{ kg/m}^3$$

The additional thrust is then

$$T_x = (p + \rho V_x^2)A = \left[30 \times 10^3 + 700 \times (1.6733)^2 \right] \times 0.01131 = 364 \text{ N}$$

Example 2.3 The idling turbojet engines of a landing airplane produce forward thrust when operating in a normal manner, but they can produce reverse thrust if the jet is properly deflected. Suppose that, while the aircraft rolls down the runway at 180 km/h, the idling engine consumes air at 40 kg/s and produces an exhaust velocity of 150 m/s.

- (a) What is the forward thrust of the engine?
- (b) What is the magnitude and direction (forward or reverse) if the exhaust is deflected 90° and the mass flow is kept constant?

Solution

Forward thrust has positive values and reverse thrust has negative values.

- (a) The flight speed is $U = 180/3.6 = 50 \text{ m/s}$.

The thrust force represents the horizontal or the x -component of the momentum equation.

$$T = \dot{m}_a(u_e - u)$$

$$T = 40 * (150 - 50) = 4000 \text{ N}$$

- (b) Since the exhaust velocity is now vertical due to thrust reverse application, then it has a zero horizontal component; thus, the thrust equation is

$$T = \dot{m}_a(u_e - u)$$

$$T = 40 * (0 - 50) = -2000 \text{ N}$$

$$T = -2000 \text{ N}(\text{reverse})$$

2.3.3 Angular Momentum Equation (Moment of Momentum)

Consider a finite system of fluid as shown in Fig. 2.6. An element dm of the system is acted on by a force $d\bar{F}$ and has a linear momentum $(md\bar{V})$. From Newton's law, we can write

$$d\bar{F} = \frac{D}{Dt} (\bar{V} dm) \quad (2.12)$$

Now take the cross product of each side using the position vector \bar{r} . Thus,

$$\bar{r} \otimes d\bar{F} = \bar{r} \otimes \frac{D}{Dt} (\bar{V} dm)$$

Consider next the following operation:

$$\frac{D}{Dt} (\bar{r} \otimes dm\bar{V}) = \frac{D\bar{r}}{Dt} \otimes dm\bar{V} + \bar{r} \otimes \frac{D}{Dt} (dm\bar{V})$$

Note that $D\bar{r}/Dt = \bar{V}$, so that the first expression on the right side is zero, since $\bar{V} \times \bar{V} = 0$.

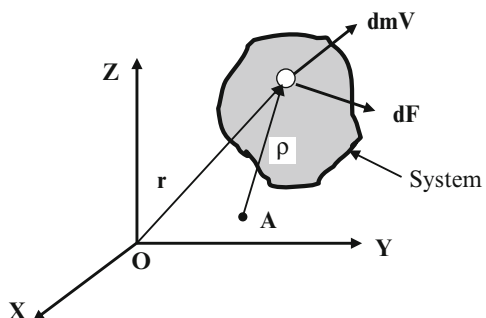
Thus, we arrive at the relation:

$$\bar{r} \otimes d\bar{F} = \frac{D}{Dt} (\bar{r} \otimes dm\bar{V}) \quad (2.13a)$$

Next, we integrate Eq. (2.13a) over the entire system to get

$$\int \bar{r} \otimes d\bar{F} = \iiint_M \frac{D}{Dt} (\bar{r} \otimes \bar{V}) dm \quad (2.13b)$$

Fig. 2.6 Mass (dm) in a finite system



Since the mass of the system is fixed so that the limits of the integration on the right side of Eq. (2.13b) are fixed, thus we can write

$$\int \bar{r} \otimes d\bar{F} = \frac{D}{Dt} \left(\iiint_M \bar{r} \otimes \bar{V} dm \right) = \frac{D\bar{H}}{Dt}$$

where \bar{H} is the moment about a fixed point (a) in inertial space of the linear momentum of the system. The integral on the left side of the equation represents the total moment about point (a) of the external forces acting on the system and may be given as

$$\int \bar{r} \otimes d\bar{F} = \iint_{C.S} \bar{r} \otimes \bar{T} dA + \iiint_{C.V} \bar{r} \otimes \bar{B} \rho dv \quad (2.14)$$

We may now give the moment-of-momentum equation for a finite system as follows:

$$\iint_{C.S} \bar{r} \otimes \bar{T} dA + \iiint_{C.V} \bar{r} \otimes \bar{B} \rho dv = \frac{D\bar{H}}{Dt}$$

Next, since $(\bar{H}) \equiv \iiint (\bar{r} \otimes \bar{V}) \rho dv$ is the extensive property, then its intensive property (η) is $(\bar{r} \otimes \bar{V})$. Thus applying Reynolds transport equation, one gets

$$\frac{D\bar{H}}{Dt} = \iint_{CS} (\bar{r} \otimes \bar{V}) (\rho \bar{V} \bullet \bar{dA}) + \frac{\partial}{\partial t} \iiint_{CV} (\bar{r} \otimes \bar{V}) (\rho dv)$$

We then have the desired moment-of-momentum equation for an inertial control volume:

$$\begin{aligned} \iint_{CS} \bar{r} \otimes \bar{T} dA + \iiint_{CV} \bar{r} \otimes \bar{B} \rho dv &= \iint_{CS} (\bar{r} \otimes \bar{V}) (\rho \bar{V} \bullet \bar{dA}) \\ &+ \frac{\partial}{\partial t} \iiint_{CV} (\bar{r} \otimes \bar{V}) (\rho dv) \end{aligned} \quad (2.15)$$

The terms on the right side represent the efflux of moment of momentum through the control surface plus the rate of increase of moment of momentum inside the control volume where both quantities are observed from the control volume.

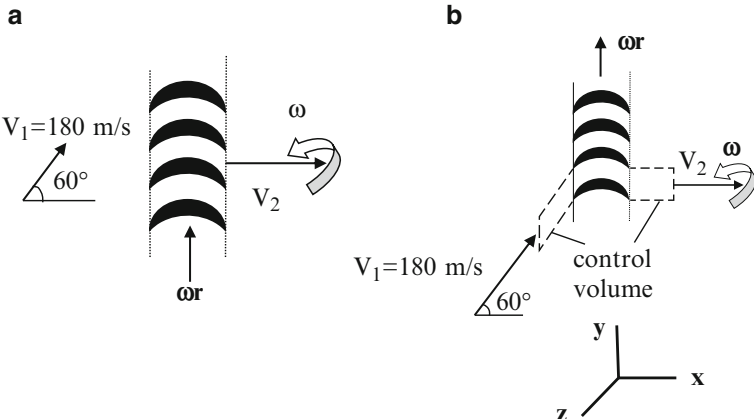


Fig. 2.7 Impulse turbine. (a) Layout. (b) Control volume

Example 2.4 An impulse turbine blade row is illustrated in Fig. 2.7a. The rotor has an average radius r of 0.6 m and rotates at a constant angular speed ω . What is the transverse torque on the turbine if the air mass flow rate is 100 kg/s?

Solution

Choosing the shown control volume described in Fig. 2.7a, and assuming the flow is steady, then Eq. (2.14) is reduced to

$$\iint_{CS} \bar{r} \otimes \bar{T} dA = \iint_{CS} (\bar{r} \otimes \bar{V}) (\rho \bar{V} \bullet \bar{dA})$$

Or the torque $\bar{\tau}$ is expressed by the relation

$$\bar{\tau} = \iint_{CS} (\bar{r} \otimes \bar{V}) (\rho \bar{V} \bullet \bar{dA})$$

The flow is fast enough to assume a constant density; thus, the x -component of the torque which is responsible for turbine rotation is expressed by the relation:

$$\begin{aligned} \tau_x &= \dot{m} \times r_z \times [(V_{out})_y - (V_{in})_y] \\ \tau_x &= 100 \times 0.6 \times [0 - (180 \times \sin 60)] = -9,353 \text{ N.m} \end{aligned}$$

The negative sign indicates that the turbine rotor rotates in a counterclockwise direction as shown in figure.

Another Solution

The above problem can also be solved using the linear momentum Eq. (2.11). The tangential force (T_y) is expressed by the relation:

$$\iint_{C.S.} T_y dA + \iiint_{C.V.} B_y \rho dv = \iint_{C.S.} V_y \rho (\bar{V} \cdot \bar{dA}) + \frac{\partial}{\partial t} \iiint_{C.V.} V_y \rho dv$$

Again for the same assumptions of steady constant density flow, then T_y is expressed as

$$T_y = \iint_{C.S.} V_y \rho (\bar{V} \cdot \bar{dA}) = \dot{m} \times \left[(V_{out})_y - (V_{in})_y \right]$$

$$T_y = 100 \times (0 - 180 \times \sin 60) = -15,588 \text{ N}$$

$$\tau_x = r_z \times T_y = 0.6 \times (-15,588) = -9,353 \text{ N.m} = -9.353 \text{ kN.m}$$

2.3.4 Energy Equation (First Law of Thermodynamics)

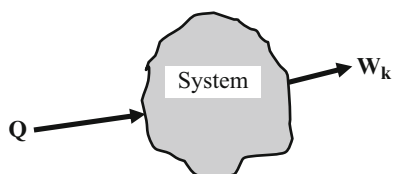
The first law of thermodynamics is a statement of macroscopic experience which states that energy must at all times be conserved. It will be convenient to classify energy under two main categories: stored energy and energy in transition. The types of *stored energy* of an element of mass are:

1. Kinetic energy E_k : energy associated with the motion of the mass
2. Potential energy E_P : energy associated with the position of the mass in conservative external fields
3. Internal energy U : molecular and atomic energy associated with the internal fields of the mass

The types of *energy in transition* are heat and work. Heat is the energy in transition from one mass to another as a result of a temperature difference. On the other hand, work, as learned in mechanics, is the energy in transition to or from a system which occurs when external forces, acting on the system, move through a distance.

For an arbitrary system (shown in Fig. 2.8), the net heat added to the system and the net work done by the system on the surroundings during the time interval Δt are designated as Q and W_k , respectively.

Fig. 2.8 Heat and work on system



If E represents the total stored energy of a system at any time t and its property as a point function is employed, conservation of energy demands that for a process occurring during a time interval between t_1 and t_2 , then

$$Q - W_k = \Delta E = E_2 - E_1 = (E_k + E_p + U)_2 - (E_k + E_p + U)_1 \quad (2.16)$$

The differential form of Eq. (2.16) may be written in the following manner:

$$dE = dQ - dW_k$$

Accordingly, we can employ the usual derivative notation dQ/dt and dW_k/dt for time derivative. However, E is a point function and expressible in terms of spatial variables and time. Thus, we have for the time variations of stored energy and energy in transition for a system.

$$\frac{DE}{Dt} = \frac{dQ}{dt} - \frac{dW_K}{dt} \quad (2.17)$$

To develop the control-volume approach, we will consider E being the extensive property to be used in the Reynolds transport equation. The term (e) will then represent stored energy per unit mass. We can then say using the Reynolds transport equation

$$\frac{DE}{Dt} = \oint_{C.S.} e (\rho \bar{V} \cdot \bar{dA}) + \frac{\partial}{\partial t} \iiint_{C.V.} e \rho dv \quad (2.18)$$

Using Eq. (2.17) in the left side of Eq. (2.18), we get

$$\frac{dQ}{dt} - \frac{dW_k}{dt} = \oint_{C.S.} e (\rho \bar{V} \cdot \bar{dA}) + \frac{\partial}{\partial t} \iiint_{C.V.} e \rho dv \quad (2.19)$$

Equation (2.19) then states that the net rate of energy transferred into the control volume by heat and work equals the rate of efflux of stored energy from control volume plus the rate of increase of stored energy inside the control volume.

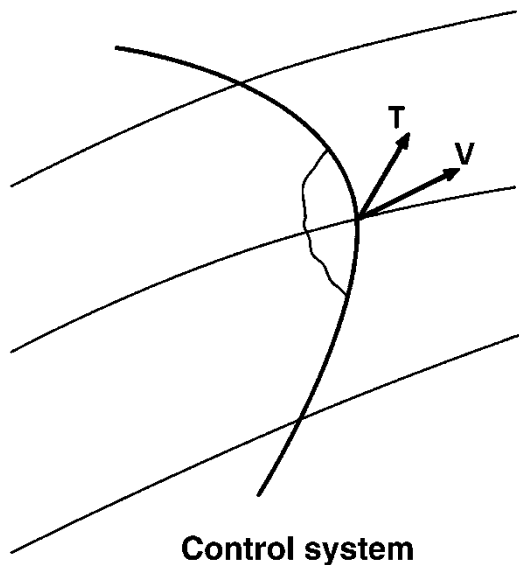
Where (e) is expressed as

$$e = \frac{V^2}{2} + gz + u \quad (2.20)$$

Next let us discuss the term dW_k/dt in Eq. (2.19) which is classified into three groups:

1. Net work done on the surroundings as a result of traction force \bar{T} .

Fig. 2.9 Flow work and control surface



2. Any other work transferred by direct contact between inside and outside non-fluid elements, like shafts or by electric currents. We call this work shaft work and denote it as W_S .
3. Work transferred by body forces. Since the effects of gravity have already been taken into account as the potential energy (in Eq. 2.20), so the body force \bar{B} must not include gravity; it may include, for instance, contributions from magnetic and electric force distributions.

Referring to Fig. 2.9, the time rate of the work leaving the control volume—the total rate of flow work—is given as

$$\text{Total rate of flow work} = - \oint_{CS} \bar{T} \cdot \bar{V} dA$$

Also, the total rate of body force work leaving the control volume is given by:

$$\text{Total rate of body force work} = - \iiint_{CV} \bar{B} \cdot \bar{V} \rho dv$$

A general form of the first law can now be given as

$$\begin{aligned} \frac{dQ}{dt} - \frac{dW_s}{dt} + \oint_{CS} \bar{T} \cdot \bar{V} dA + \iiint_{CV} \bar{B} \cdot \bar{V} \rho dv \\ = \oint_{CS} \left(\frac{V^2}{2} + gz + u \right) (\rho \bar{V} \cdot \bar{dA}) + \frac{\partial}{\partial t} \iiint_{CV} \left(\frac{V^2}{2} + gz + u \right) \rho dv \end{aligned} \quad (2.21)$$

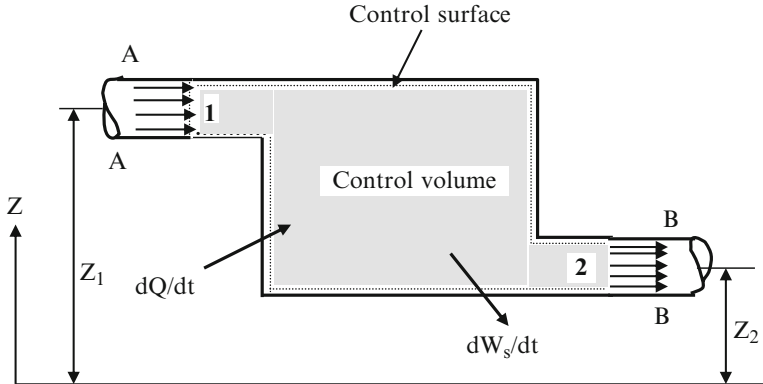


Fig. 2.10 Control volume for idealized machine

Figure 2.10 illustrates a simple example for a steady flow device having one-dimensional inlet and outlet flows. This may represent, for instance, a gas turbine having inlet and outlet at sections AA and BB. The traction force power occurs at sections AA and BB and is given as $+p_1 V_1 A_1$ and $-p_2 V_2 A_2$, respectively. Furthermore, $\rho \bar{V} \bullet d\bar{A}$ at these sections becomes $-\rho_1 V_1 A_1$ and $+\rho_2 V_2 A_2$, respectively. The equation becomes

$$\frac{dQ}{dt} - \frac{dW_s}{dt} + p_1 V_1 A_1 - p_2 V_2 A_2 = -\left(\frac{V_1^2}{2} + gz_1 + u_1\right) \rho_1 V_1 A_1 + \left(\frac{V_2^2}{2} + gz_2 + u_2\right) \rho_2 V_2 A_2 \quad (2.22)$$

Since the products $\rho_1 v_1$ and $\rho_2 v_2$ (where v_1 and v_2 are the specific volumes) equal unity, the following form of the first law:

$$\begin{aligned} \frac{dQ}{dt} + \left(\frac{V_1^2}{2} + gz_1 + u_1 + p_1 v_1\right) \rho_1 V_1 A_1 \\ = \frac{dW_s}{dt} + \left(\frac{V_2^2}{2} + gz_2 + u_2 + p_2 v_2\right) \rho_2 V_2 A_2 \end{aligned} \quad (2.23a)$$

Since the enthalpy h is defined as $h = u + pv$, and $\rho_1 V_1 A_1 = \rho_2 V_2 A_2 = dm/dt$, then Eq. (2.23a) can be written as:

$$\frac{dQ}{dt} + \left(\frac{V_1^2}{2} + gz_1 + h_1\right) \frac{dm}{dt} = \frac{dW_s}{dt} + \left(\frac{V_2^2}{2} + gz_2 + h_2\right) \frac{dm}{dt} \quad (2.23b)$$

If the following assumptions are satisfied:

1. The flow is steady.
2. Air is an ideal gas with constant specific heats.
3. Potential energy changes are negligible ($gz_1 = gz_2 = 0$).
4. There are no work interactions ($\frac{dW_s}{dt} = 0$).
5. The diffuser is adiabatic ($\frac{dQ}{dt} = 0$).

then Eq. (2.23b) is reduced to

$$\frac{V_1^2}{2} + h_1 = \frac{V_2^2}{2} + h_2 \quad (2.24)$$

Finally, if $V_1 = 0$, then the total or stagnation enthalpy (h_1) is defined as

$$h_1 = \frac{V_2^2}{2} + h_2 \quad (2.25)$$

Example 2.5 Air is decelerated in an adiabatic diffuser. The inlet conditions are pressure = 100 kPa, temperature = 50 °C, and velocity = 500 m/s. The outlet conditions are pressure = 150 kPa and temperature = 50 °C. The specific heat at constant pressure is 1.007 kJ/kg. K. Calculate the velocity at outlet to diffuser.

Solution

Since the above-listed assumptions hold (steady flow with negligible changes in height, no work or heat exchanges, and the fluid is an ideal gas with constant specific heats), then Eq. (2.25) may be applied. Thus,

$$V_2 = \sqrt{2(h_1 - h_2) + V_1^2} = \sqrt{2C_p(T_1 - T_2) + V_1^2}$$

$$V_2 = \sqrt{2 \times 1007 \times (20 - 50) + (500)^2} = 435.4 \text{ m/s}$$

2.3.5 The Second Law of Thermodynamics and the Entropy Equation

The second law of thermodynamics states that: *it is impossible for a system to perform a cyclic process that produces work (say raising of a weight) and exchanges heat with a single reservoir of uniform temperature.* The second law permits the definition of the property *entropy* (s). For a system,

$$ds = \left(\frac{dQ}{T} \right)_{\text{reversible}} \quad (2.26)$$

where ds is the change of entropy during a reversible heat exchange. Irreversible processes are processes which involve one of these features: friction, heat transfer with finite temperature gradient, mass transfer with finite concentration gradient, or unrestrained expansion. For any process,

$$ds \geq \frac{dQ}{T} \quad (2.27)$$

where equality holds only for reversible process. If the process is reversible and adiabatic ($dQ = 0$), it must be isentropic ($ds = 0$).

For a small system composed of pure substance in the absence of gravity motion, then if the properties are uniform throughout the system, then the first law for incremental changes is

$$dq = du + dw$$

where q and w are the heat and work per unit mass. If the system experiences a reversible process for which the incremental work $dw = pdv$, then from Eq. (2.28), we can write

$$Tds = du + pdv \quad (2.28)$$

2.3.6 Equation of State

In compressible gases, it is necessary to define the thermodynamic state of the gas with state variables, e. g., the static pressure p , the static density ρ , and the static temperature T . Their interdependence is described by the thermal equation of state. If the law given by Boyle, Mariotte, and Gay-Lussac is used, then

$$p = \rho RT \quad (2.29)$$

The gas is called thermally perfect. For thermally non-perfect gases, other relations must be used, as, for example, the Van der Waals law. The specific gas constant R depends on the molecular weight of the gas. For air it is $R = 287 \text{ J/kg.K}$. The gas constant is related to the *universal* gas constant (R_u) and the molecular weight of gas (M) by the relation

$$R = \frac{R_u}{M}$$

The value of universal gas constant is $R_u = 8.31434 \text{ kJ/(kmol.K)}$

Internal energy is a state variable, which is defined by two thermodynamic quantities, namely, the temperature T and the specific volume ($v = 1/\rho$):

$$u = u(v, T) \quad (2.30)$$

This relation is known as the caloric equation of state. The total derivative is

$$du = \left(\frac{\partial u}{\partial v} \right)_T dv + \left(\frac{\partial u}{\partial T} \right)_v dT \quad (2.31)$$

The internal energy of thermally perfect gases depends on the temperature only. It then follows that

$$du = \left(\frac{du}{dT} \right)_v dT$$

where

$$C_v = \left(\frac{du}{dT} \right)_v \quad (2.32)$$

The quantity $\left(\frac{du}{dT} \right)_v$ is called specific heat at constant volume (C_v). If C_v is constant, the gas is called calorically perfect, and the internal energy is given by

$$u = C_v T + u_r \quad (2.33)$$

The quantity u_r is a reference value.

The enthalpy h was defined earlier and repeated here is defined as

$$h = u + p v \quad (2.34)$$

Similar to the internal energy, the enthalpy of thermally perfect gases depends on the temperature only, or

$$dh = C_p dT \quad (2.35a)$$

The quantity C_p is the specific heat at constant pressure, or

$$C_p = \left(\frac{dh}{dT} \right)_p \quad (2.36a)$$

It follows from the relation for the specific heats C_v and C_p

$$C_p = C_v + R \quad (2.36b)$$

for calorically perfect gases, that C_p is constant. Hence,

$$h = C_p T + h_r \quad (2.35b)$$

where h_r is again a reference value.

The ratio of the specific heats $C_p/C_v = \gamma$, where γ , according to the gas kinetic theory, is given by the number n of degrees of freedom

$$\gamma = \frac{n+2}{n}$$

For monatomic gases ($n=3$) $\gamma=1.667$, and for diatomic gases ($n=5$) $\gamma=1.4$. At high temperatures additional degrees of freedom are excited, and the ratio C_p/C_v decreases. For air at a temperature of 300 K, then $\gamma=1.4$, while at temperature 3000 K, then $\gamma=1.292$.

From Eqs. (2.28) and (2.33) and since $\frac{P}{T} = \frac{R}{v}$ then

$$ds = C_v \frac{dT}{T} + R \frac{dv}{v} \quad (2.37)$$

Similarly, from Eqs. (2.28) and (2.34)

$$Tds = dh - v dP$$

From Eq. (2.34) and ideal gas relation, $\frac{v}{T} = \frac{R}{P}$, then

$$ds = C_p \frac{dT}{T} - R \frac{dP}{P} \quad (2.38)$$

Example 2.6 The constant volume-specific heat of an ideal gas varies according to the equation $C_v = aT^2$, where $a = 2.32 \times 10^{-5} \text{ kJ/kg.K}^3$. If the gas is heated from 50 to 80 °C at constant volume, find the change in entropy.

Solution

From Eq. (2.40), the change in entropy is expressed as

$$\Delta s = \int_{T_1}^{T_2} C_v \frac{dT}{T} = a \int_{T_1}^{T_2} T^2 \frac{dT}{T} = a \int_{T_1}^{T_2} T dT = a \frac{[T^2]}{2} \Big|_{T_1}^{T_2}$$

$$T_1 = 50 + 273 = 323 \text{ K}$$

$$T_2 = 80 + 273 = 353 \text{ K}$$

$$\Delta s = 2.32 \times 10^{-5} [353^2 - 323^2] / 2 = 0.235 \text{ kJ/kg.K}$$

2.4 Steady One-Dimensional Compressible Flow

One-dimensional flow refers to flow involving uniform distributions of fluid properties over any flow cross section area. It provides accurately the stream-wise variation of average fluid properties. The flow in diffusers, combustors, and nozzles exhibits the major characteristics of one-dimensional flow. Though one-dimensional analysis for the flow in rotating elements (fans, compressors, and turbines) provides also the mean flow features, it is more appropriate to extend the analysis of flow within them to either two dimensional (2-D) or three dimensional (3-D). This is attributed to the large variations normal to streamlines, which are no longer limited to the thin layer adjacent to the surface and known as boundary layer.

2.4.1 Isentropic Relations

It follows from the conservation equations for one-dimensional, steady, compressible flow that the sum of the kinetic energy ($u^2/2$) and the static enthalpy (h) remains constant. The value of this constant is given by the stagnation (or total) enthalpy, and Eq. (2.25) may be rewritten as

$$h_0 = h + u^2/2 \quad (2.25)$$

Generally, the stagnation state is a theoretical state in which the flow is brought into a complete motionless condition in isentropic process without other forces (e.g., gravity force).

Several properties can be represented by this theoretical process which includes temperature, pressure, density, etc. and denoted by the subscript “0.”

For calorically perfect gases, the enthalpy can be replaced by the product of static temperature and the specific heat at constant pressure ($C_p T$), thus,

$$C_p T_0 = C_p T + u^2/2$$

or

$$T_0 = T + \frac{u^2}{2C_p} \quad (2.39)$$

Introducing the thermal equation of state there in (2.39) results

$$\frac{\gamma}{\gamma - 1} \frac{p_0}{\rho_0} = \frac{\gamma}{\gamma - 1} \frac{p}{\rho} + \frac{u^2}{2} \quad (2.40)$$

and with the definition of the speed of sound (a) as

Table 2.1 Sonic speeds at different temperatures for air and helium

	Temperature (K)	200	300	1000
Air	Sonic speed [m/s]	284	347	634
Helium	Sonic speed [m/s]	832	1019	1861

$$a^2 = \frac{\gamma p}{\rho} = \gamma RT$$

Equation (2.40) will be reduced to

$$\frac{a_0^2}{\gamma - 1} = \frac{a^2}{\gamma - 1} + \frac{u^2}{2} \quad (2.41)$$

The speed of sound depends on the gas constant (R) and temperature (T); thus, the sonic speed for air and helium ($R_{\text{air}} = 287 \text{ J/kg.K}$, $R_{\text{Helium}} = 2077 \text{ J/kg.K}$) at different temperatures are given in the Table 2.1.

Rewriting Eq. (2.39), the following important set of equations can be derived:

$$T_0 = T + \frac{u^2}{2C_p} = T + \frac{(\gamma - 1)u^2}{2\gamma R} \quad (2.42)$$

$$\frac{T_0}{T} = 1 + \frac{\gamma - 1}{2} \frac{u^2}{\gamma RT}$$

Introducing the Mach number as the ratio of velocity to speed of sound

$$M = \frac{u}{a} \quad (2.43)$$

It very useful to convert Eq. (2.42) into a dimensionless form and denote

$$\frac{T_0}{T} = 1 + \frac{\gamma - 1}{2} M^2 \quad (2.44a)$$

$$M = \sqrt{\frac{2}{\gamma - 1} \left(\frac{T_0}{T} - 1 \right)} \quad (2.44b)$$

$$\frac{a_0}{a} = \sqrt{1 + \frac{\gamma - 1}{2} M^2} \quad (2.44c)$$

$$\frac{P_0}{P} = \left(1 + \frac{\gamma - 1}{2} M^2 \right)^{\frac{\gamma}{\gamma - 1}} \quad (2.44d)$$

$$\frac{\rho_0}{\rho} = \left(1 + \frac{\gamma - 1}{2} M^2 \right)^{\frac{1}{\gamma - 1}} \quad (2.44e)$$

The mass flow per unit area is

$$\frac{\dot{m}}{A} = \rho u$$

Using Eqs. (2.43) and (2.44), the velocity may be expressed as

$$u = M \sqrt{\frac{\gamma RT_0}{1 + \frac{\gamma-1}{2} M^2}}$$

From the density relation, the *mass flow rate* parameter is expressed as

$$\frac{\dot{m}}{A} = \frac{P_0 \sqrt{\gamma}}{\sqrt{RT_0}} M \left(\frac{1}{1 + \frac{\gamma-1}{2} M^2} \right)^{\frac{\gamma+1}{2(\gamma-1)}} \quad (2.45a)$$

For a given fluid (γ, R) and inlet state (P_0, T_0), it can be readily shown that the mass flow rate per unit area is maximum at $M = 1$. Denoting the properties of the flow at $M = 1$ with an asterisk, the maximum flow per unit area is

$$\frac{\dot{m}}{A^*} = \frac{P_0 \sqrt{\gamma}}{\sqrt{RT_0}} \left(\frac{2}{\gamma + 1} \right)^{\frac{\gamma+1}{2(\gamma-1)}} \quad (2.45b)$$

From the above two Eqs. (2.45a) and (2.45b), we get

$$\frac{A}{A^*} = \frac{1}{M} \left[\frac{2}{\gamma + 1} \left(1 + \frac{\gamma - 1}{2} M^2 \right) \right]^{\frac{\gamma+1}{2(\gamma-1)}} \quad (2.46)$$

Gas dynamics books ([4, 5] as examples) include in its appendices a set of tables for isentropic flow parameters defined by Eqs. (2.44) and (2.46) for specific heat ($\gamma = 1.4$). Table 2.2 illustrates few lines of such tables.

For a given isentropic flow and known ($\gamma, R, P_0, T_0, \dot{m}$), it is clear that A^* is a constant, so we can use these relations to plot the fluid properties versus Mach number (Fig. 2.11).

2.4.2 Sonic Conditions

If the local flow velocity is equal to the speed of sound ($M = 1$), then such sonic condition is referred to as the *critical state* and is designated by an asterisk (*). The temperature, pressure, and density attain the following values, which solely depend on the stagnation conditions of the gas. From Eq. (2.44), we get

Table 2.2 Isentropic flow parameters ($\gamma = 1.4$)

M	P/P_0	T/T_0	A/A^*	PA/P_0A^*
0	1.0	1.0	∞	∞
0.5	0.84302	0.95238	1.33984	1.12951
1.0	0.52828	0.83333	1.0	0.52828
5.0	0.00189	0.16667	25.0	0.04725

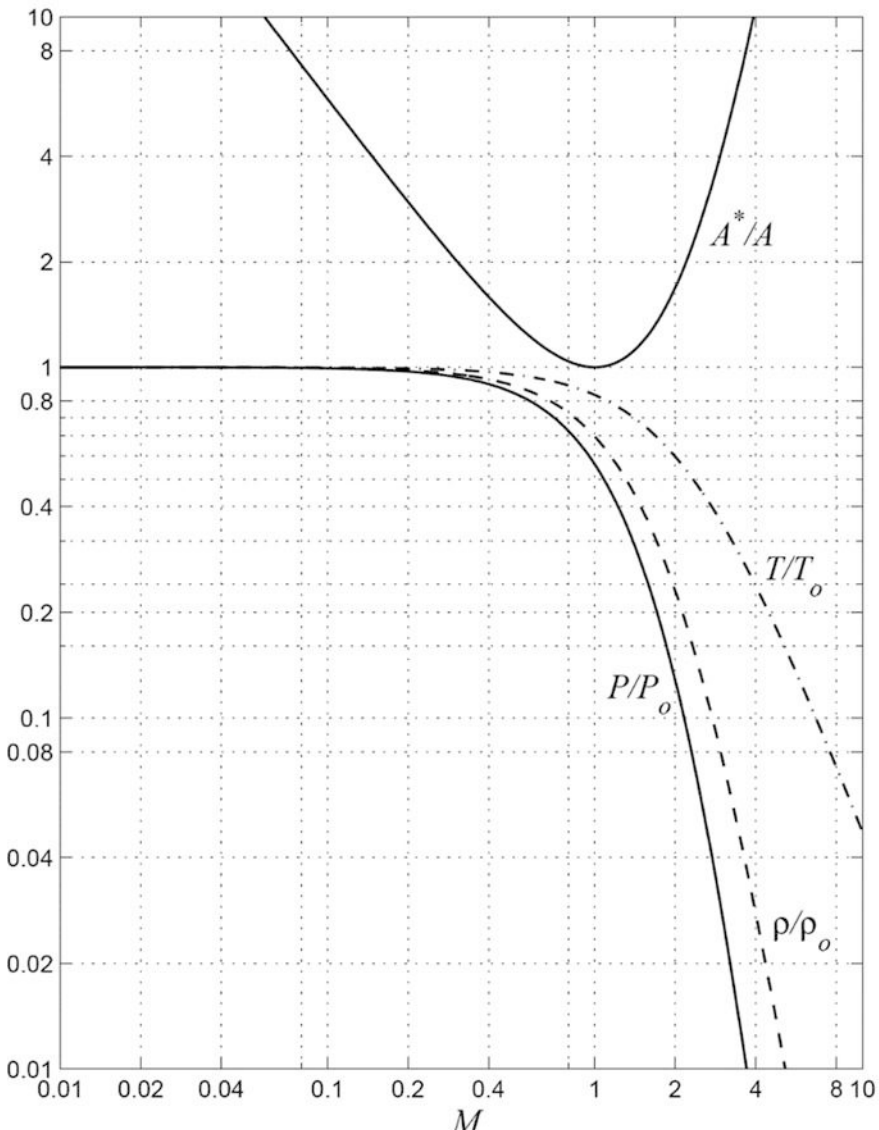
**Fig. 2.11** One-dimensional isentropic flow of a perfect gas

Table 2.3 Critical ratios for different values of (γ)

γ	$\frac{T_0}{T^*}$	$\frac{P_0}{P^*}$	$\frac{\rho_0}{\rho^*}$	$\frac{a_0}{a^*}$
1.135	1.0675	1.7318	1.6223	1.0332
1.3	1.15	1.8324	1.5934	1.0723
1.4	1.2	1.8929	1.5774	1.095
1.667	1.335	2.0534	1.5429	1.155

$$\begin{aligned} \frac{T_0}{T^*} &= \frac{\gamma + 1}{2} \\ \frac{a_0}{a^*} &= \sqrt{\frac{\gamma + 1}{2}} \\ \frac{P_0}{P^*} &= \left(\frac{\gamma + 1}{2}\right)^{\frac{1}{\gamma-1}} \\ \frac{\rho_0}{\rho} &= \left(\frac{\gamma + 1}{2}\right)^{\frac{1}{\gamma-1}} \end{aligned} \quad (2.47)$$

For air with $\gamma = 1.4$, the critical values are as follows (Table 2.3):

$$\frac{T_0}{T^*} = 1.2, \quad \frac{P_0}{P^*} = 1.8929, \quad \frac{\rho_0}{\rho^*} = 1.5774, \quad \frac{a_0}{a^*} = 1.095 \quad (2.48)$$

Instead of the local speed of sound (a), the critical speed of sound can be used to define a Mach number, which is called the critical Mach number:

$$M^* = u/a^* \quad (2.49)$$

The relation between the local Mach number ($M = u/a$) and the critical Mach number (M^*) is derived from the relations (2.47) and (2.49), as

$$M^{*2} = \frac{\gamma + 1}{\gamma - 1 + \frac{2}{M^2}} \quad (2.50)$$

For $M \rightarrow \infty$, the critical Mach number M^* approaches the following limiting value:

$$\lim_{M \rightarrow \infty} M^* = \sqrt{\frac{\gamma + 1}{\gamma - 1}} \quad (2.51)$$

With these relations the ratios of the temperature, pressure, density, and speed of sound, referred to their stagnation values, can be expressed by the critical Mach number:

$$\begin{aligned}
 \frac{T_0}{T} &= \left(1 - \frac{\gamma - 1}{\gamma + 1} M^{*2} \right)^{-1} \\
 \frac{a_0}{a} &= \left(1 - \frac{\gamma - 1}{\gamma + 1} M^{*2} \right)^{\frac{-1}{2}} \\
 \frac{P_0}{P} &= \left(1 - \frac{\gamma - 1}{\gamma + 1} M^{*2} \right)^{\frac{-\gamma}{\gamma-1}} \\
 \frac{\rho_0}{\rho} &= \left(1 - \frac{\gamma - 1}{\gamma + 1} M^{*2} \right)^{\frac{-1}{\gamma-1}}
 \end{aligned} \tag{2.52}$$

2.4.3 Classification of Mach Regimes

Aerodynamicists often classify airflow regimes using Mach number values. Six flight regimes may be identified, namely, subsonic, transonic, supersonic, hypersonic, high hypersonic, and re-entry ones. Subsonic and supersonic speeds are associated with values of Mach number less or greater than unity, respectively. An in-between region defined as “transonic regime” where Mach number is around unity (from say 0.8 to 1.2). Mach values associated with supersonic regime vary from 1.2 to 5. For hypersonic regime Mach number ranges from 5 to 10. [NASA](#) defines “high” hypersonic when Mach number ranges from 10 to 25 and re-entry speeds as anything greater than Mach 25 ([Space Shuttle](#) as an application). Table 2.4 illustrates such a classification.

Table 2.4 Classification of flow regimes

Regime	Mach	General plane characteristics
Subsonic	<0.8	Propeller-driven and commercial turbofan aircrafts
Transonic	0.8–1.3	All present airliners (B777, 767, 747 Airbus A320, A330, and A340) fly at the lowest transonic speeds (typical speeds are greater than 250 mph but less than 760 mph)
Supersonic	1.3–5.0	Modern combat aircrafts including Ilyushin IL-76TD, MIG31, F117 Night Hawk, F 22 Raptor
Hypersonic	5.0–10.0	Aircrafts have cooled nickel-titanium skin, highly integrated, small wings (X-51A WaveRider as an example)
High hypersonic	10.0–25.0	Vehicles are thermally controlled; its structure is protected by special silicate tiles or similar. They have blunt nose configurations to resist aerodynamic heating
Re-entry	>25.0	Vehicles have an ablative heat shield, no wings, blunt capsule shape

2.4.4 Diffusers and Nozzles

Diffusers and nozzles are commonly utilized in jet engines, rockets, and spacecrafts. A diffuser is a device that increases the pressure of a fluid by slowing it down, while a nozzle is a device that increases the velocity of a fluid at the expense of pressure. That is, diffusers and nozzles perform opposite tasks. Diffusers and nozzles involve no work ($\dot{W} \approx 0$) and negligible changes in potential energy ($\Delta P E \approx 0$). Moreover, the rate of heat transfer between the fluid flowing through a diffuser or a nozzle and the surroundings is usually very small ($\dot{Q} \approx 0$). This is due to the very short time air (or gas) spends in either duct (few or fraction of milliseconds) which is insufficient for a significant heat transfer to take place. However, fluid passing through diffusers and nozzles experiences large changes in velocity. Therefore, the kinetic energy changes must be accounted for ($\Delta K E \neq 0$). The shape of both diffuser and nozzle may be convergent or divergent depending on the velocity of flowing fluid. Rockets and military high supersonic aircrafts normally have *convergent-divergent* or *CD nozzles*. In a CD rocket nozzle, the hot exhaust leaves the combustion chamber and converges down to the minimum area, or *throat*, of the nozzle. The throat size is chosen to *choke* the flow and *set the mass flow rate* through the system. The flow in the throat is sonic which means the *Mach number* is equal to one in the throat. Downstream of the throat, the geometry diverges, and the flow is *isentropically* expanded to a supersonic Mach number that depends on the *area ratio* of the exit to the throat. The expansion of a supersonic flow causes the static pressure and temperature to decrease from the throat to the exit, so the amount of the expansion also determines the exit pressure and temperature. The exit temperature determines the exit *speed of sound*, which determines the exit velocity. The exit velocity, pressure, and mass flow through the nozzle *determine* the amount of thrust produced by the nozzle.

2.4.4.1 Variation of Fluid Velocity with Flow Area

We begin with the *conservation of mass equation*:

$$\dot{m} = \rho V A = \text{constant}$$

where \dot{m} is the mass flow rate, ρ is the gas *density*, V is the gas velocity, and A is the cross-sectional flow area. If we differentiate this equation, we obtain

$$V A d\rho + \rho A dV + \rho V dA = 0$$

Divide by $(\rho V A)$ to get

$$\frac{d\rho}{\rho} + \frac{dV}{V} + \frac{dA}{A} = 0$$

Now we use the **conservation of momentum equation**:

$$\rho V dV = -dP$$

and an **isentropic flow relation**: $Tds = dh - v dP$

$$\frac{dP}{P} = \gamma \frac{d\rho}{\rho}$$

where γ is the **ratio of specific heats**. Rewrite the above equation to obtain

$$dP = \gamma \frac{P}{\rho} d\rho$$

and use the **equation of state** ($\frac{P}{\rho} = RT$) to get

$$dP = \gamma R T d\rho$$

Since (γRT) is the square of the **speed of sound** (a), then

$$dP = a^2 d\rho$$

Combining this equation for the change in pressure with the momentum equation, we obtain

$$\begin{aligned} \rho V dV &= -a^2 d\rho \\ \frac{V}{a^2} dV &= -\frac{d\rho}{\rho} \end{aligned}$$

using the definition of the **Mach number** $M = V/a$, then

$$-M^2 \frac{dV}{V} = \frac{d\rho}{\rho} \quad (2.53)$$

Now we substitute this value of $(d\rho/\rho)$ into the mass flow equation to get

$$\begin{aligned} -M^2 \frac{dV}{V} + \frac{dV}{V} + \frac{dA}{A} &= 0 \\ (1 - M^2) \frac{dV}{V} &= -\frac{dA}{A} \end{aligned} \quad (2.54)$$

Equation (2.59) tells us how the velocity (V) changes when the area (A) changes and the results depend on the Mach number (M) of the flow.

If the flow is *subsonic* then ($M < 1.0$)—the term multiplying the velocity change is positive [$(1 - M^2) > 0$]—then an increase in the area ($dA > 0$) produces a decrease in the velocity ($dV < 0$), which is the case of a diffuser. On the contrary a decrease in the area produces an increase in velocity, which is the case of a nozzle.

For a *supersonic* flow ($M > 1.0$), the term multiplying velocity change is negative [$(1 - M^2) < 0$]. Then an increase in the area ($dA > 0$) produces an increase in the velocity ($dV > 0$) or a nozzle. The decrease in the area leads to a decrease in velocity or a diffuser.

Table 2.5 summarizes this behavior.

Figure 2.12 illustrates the geometry of diffusers and nozzles in subsonic and supersonic speeds.

For the case of CD nozzle, if the flow in the throat is subsonic, the flow downstream of the throat will decelerate and stay subsonic. So if the converging section is too large and does not choke the flow in the throat, the exit velocity is very slow and does not produce much thrust. On the other hand, if the converging section is small enough so that the flow chokes in the throat, then a slight increase in area causes the flow to go supersonic. This is exactly the opposite of what happens subsonically.

Table 2.5 Variation of duct area with inlet Mach number

	Accelerated flow (nozzle)	Decelerated flow (diffuser)	Constant velocity
	$dV > 0$	$dV < 0$	
$M < 1.0$	$dA < 0$	$dA > 0$	$dA = 0$
$M > 1.0$	$dA > 0$	$dA < 0$	$dA = 0$

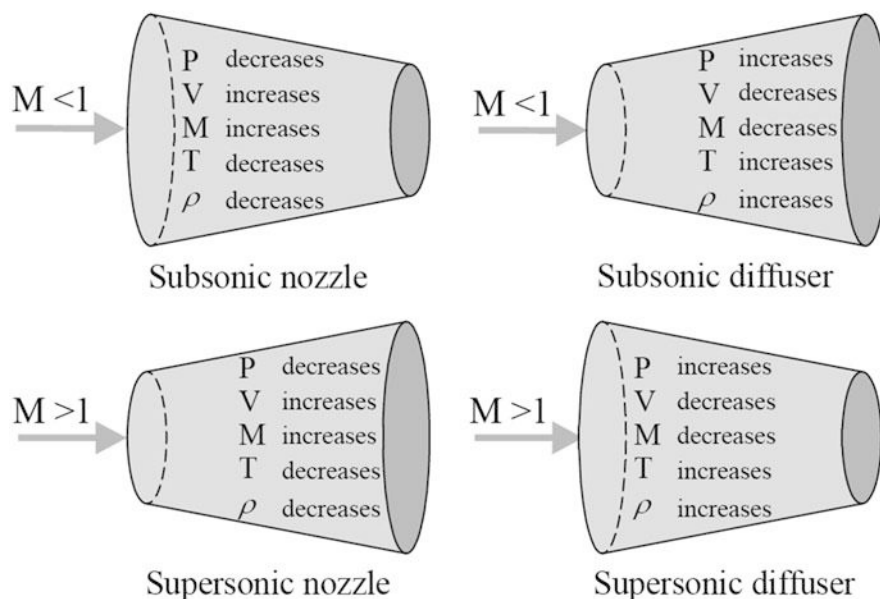
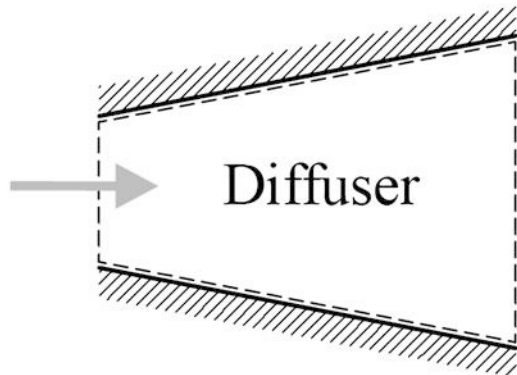


Fig. 2.12 Variation of flow properties in subsonic and supersonic nozzles and diffusers

Fig. 2.13 Diffuser and control volume



Example 2.7 Air at 5 °C and 80 kPa enters the diffuser of a jet engine steadily with a velocity of 200 m/s. The inlet area of the diffuser is 0.4 m². The air leaves the diffuser with a velocity that is very small compared with the inlet velocity. Determine (a) the mass flow rate of the air and (b) the temperature of the air leaving the diffuser.

Solution

We take the *diffuser* as the system (Fig. 2.13). This is a *control volume* since mass crosses the system boundary during the process. We observe that there is only one inlet and one exit and thus $\dot{m}_1 = \dot{m}_2 = \dot{m}$.

- (a) To determine the mass flow rate, we need to find the density of the air first. This is determined from the ideal gas relation at the inlet conditions:

$$\rho_1 = \frac{P_1}{RT_1} = \frac{80 \times 10^3}{287 \times (273 + 5)} = 1.0027 \text{ kg/m}^3$$

$$\dot{m} = \rho_1 V_1 A_1 = 1.0027 \times 200 \times 0.4 = 79.8 \text{ kg/s}$$

- (b) From the energy equation

$$\frac{dQ}{dt} + \left(\frac{V_1^2}{2} + gz_1 + h_1 \right) \dot{m} = \frac{dW_s}{dt} + \left(\frac{V_2^2}{2} + gz_2 + h_2 \right) \dot{m}$$

With small exit velocity ($V_2 \approx 0$), negligible potential energy variation as well as heat and work exchange ($z_1 \approx z_2$, $dQ/dt = dW_s/dt = 0$), then, energy equation is reduced to

$$h_2 = h_1 + \frac{V_1^2}{2}$$

$$T_2 = T_1 + \frac{V_1^2}{2Cp} = 278 + \frac{200^2}{2 \times 1005} = 297.9 \text{ K}$$

Example 2.8 Gas flows through a converging–diverging nozzle. Points G and H lie between the inlet and outlet of the nozzle. At a point “G,” the cross-sectional area is 500 cm^2 and the Mach number was measured to be 0.4. At point “H” in the nozzle, the cross-sectional area is 400 cm^2 . Find the Mach number at point H. Assume that the flow is isentropic and the gas-specific heat ratio is 1:3.

Solution

To obtain the Mach number at point G, apply Eq. (2.46) to find the ratio between the area (A_G) to the critical one (A^*)

$$\begin{aligned}\frac{A_G}{A^*} &= \frac{1}{M_G} \left[\frac{2}{\gamma+1} \left(1 + \frac{\gamma-1}{2} M_G^2 \right) \right]^{\frac{\gamma+1}{2(\gamma-1)}} \\ \frac{A_G}{A^*} &= \left(\frac{1}{0.4} \right) \left[\left(\frac{2}{1.3+1} \right) \left(1 + \frac{1.3-1}{2} (0.4)^2 \right) \right]^{\frac{2.3}{2(0.3)}} = 1.6023\end{aligned}$$

At point H, the area ratio is evaluated from the relation:

$$\frac{A_H}{A^*} = \frac{A_H}{A_G} \frac{A_G}{A^*} = \frac{400}{500} \times 1.6023 = 1.2818$$

Again from Eq. (2.46)

$$\frac{A_H}{A^*} = \frac{1}{M_H} \left[\frac{2}{\gamma+1} \left(1 + \frac{\gamma-1}{2} M_H^2 \right) \right]^{\frac{\gamma+1}{2(\gamma-1)}}$$

Rearranging to solve for the Mach number M_H ,

$$\begin{aligned}\left(M_H \frac{A_H}{A^*} \right)^{\frac{2(\gamma-1)}{\gamma+1}} - \frac{\gamma-1}{\gamma+1} M_H^2 &= \frac{2}{\gamma+1} \\ \left(M_H \frac{A_H}{A^*} \right)^{\frac{2(\gamma-1)}{\gamma+1}} - \frac{\gamma-1}{\gamma+1} M_H^2 &= \frac{2}{\gamma+1} \\ 1.0669 M_H^{0.2609} - 0.1304 M_H^2 &= 0.8696\end{aligned}$$

Solving the above equation by *trial and error*, we get either

$$M_H = 0.5374 \quad \text{or} \quad M_H = 1.612$$

Both solutions are possible, the first is still a subsonic Mach number which may be located in the convergent section, while the second one is supersonic which may be located in the divergent section if the speed at throat is sonic: $M_{\text{throat}} = 1.0$.

2.4.5 Shocks

A shock is an irreversible flow discontinuity in a (partly) supersonic flow fluid. It may be also defined as a pressure front which travels at speed through a gas. Upon crossing the shock waves, pressure, temperature, density, and entropy rise while the normal velocity decreases. There are two types of shocks, namely, normal and oblique.

2.4.5.1 Normal Shock Waves

Consider a plane supersonic flow with a normal compression shock in a channel with constant cross-sectional area (Fig. 2.14). The conditions upstream and downstream the shock are denoted by subscripts (1) and (2), respectively. Under the following assumptions—steady, one dimensional, adiabatic ($\delta q = 0$), no shaft work ($\delta w = 0$), negligible potential ($\delta z = 0$), constant area ($A_1 = A_2$) and negligible wall shear—then equations of state and integral forms of conservation equations will have the following forms:

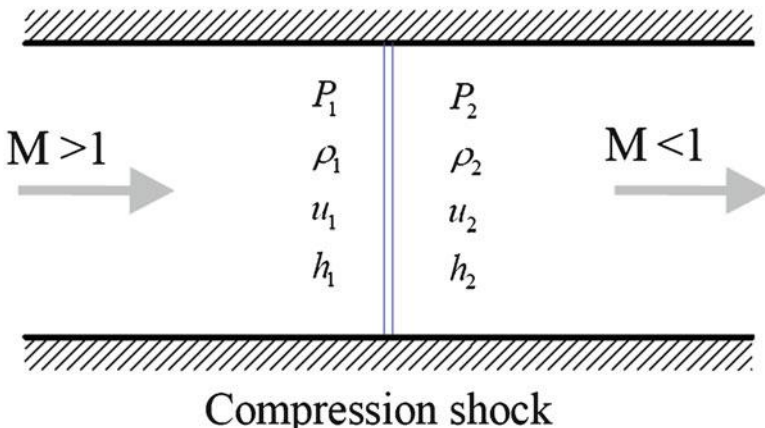


Fig. 2.14 One-dimensional shock waves

$$\begin{aligned}
 \text{Continuity equation} \quad & \frac{\dot{m}}{A} = \rho_1 u_1 = \rho_2 u_2 \\
 \text{Momentum equation} \quad & p_1 + \rho_1 u_1^2 = p_2 + \rho_2 u_2^2 \\
 \text{Energy equation} \quad & h_{01} \equiv h_1 + u_1^2/2 = h_2 + u_2^2/2 = h_{02} \\
 \text{Equation of state} \quad & \frac{p_1}{\rho_1 T_1} = \frac{p_2}{\rho_2 T_2}
 \end{aligned} \tag{2.55}$$

From the continuity equation, equation of state for perfect gas, and the velocity relation

$$u = M \sqrt{\gamma RT}$$

we arrive at the relation

$$\frac{p_1 M_1}{\sqrt{T_1}} = \frac{p_2 M_2}{\sqrt{T_2}}$$

Moreover, the energy equation together with the perfect gas relation (2.44a)

$$T_0 = T \left(1 + \frac{\gamma - 1}{2} M^2 \right)$$

yields the following relation:

$$T_1 \left(1 + \frac{\gamma - 1}{2} M_1^2 \right) = T_2 \left(1 + \frac{\gamma - 1}{2} M_2^2 \right)$$

The momentum equation together with the equation of state provides the following relation:

$$p_1 (1 + \gamma M_1^2) = p_2 (1 + \gamma M_2^2)$$

The following relations give the downstream Mach number, static temperature, pressure, and density ratios as well as the total pressure and temperature ratios across the shock:

$$M_2^2 = \frac{(\gamma - 1) M_1^2 + 2}{2\gamma M_1^2 - (\gamma - 1)} \tag{2.56}$$

$$\frac{T_2}{T_1} = \frac{[2\gamma M_1^2 - (\gamma - 1)][(\gamma - 1)M_1^2 + 2]}{(\gamma + 1)^2 M_1^2} \tag{2.57}$$

$$\frac{P_2}{P_1} = \left[\frac{2\gamma M_1^2 - (\gamma - 1)}{\gamma + 1} \right] \quad (2.58)$$

$$\frac{\rho_2}{\rho_1} = \left[\frac{(\gamma + 1)M_1^2}{2 + (\gamma - 1)M_1^2} \right] = \frac{u_1}{u_2} \quad (2.59)$$

$$\frac{P_{02}}{P_{01}} = \left[\frac{(\gamma + 1)M_1^2}{2 + (\gamma - 1)M_1^2} \right]^{\frac{\gamma}{\gamma-1}} \left[\frac{(\gamma + 1)}{2\gamma M_1^2 - (\gamma - 1)} \right]^{\frac{1}{\gamma-1}} \quad (2.60)$$

$$\frac{T_{02}}{T_{01}} = 1$$

$$u_1 u_2 = a^{*2}$$

This means that $u_1 > a^* > u_2$. The critical sonic speed is expressed as

$$a^{*2} = \frac{2\gamma R T_0}{(\gamma + 1)} = \frac{2(\gamma - 1)}{(\gamma + 1)} C_p T_0$$

From the entropy relation, the total pressure ratio can be also expressed as

$$\frac{P_{02}}{P_{01}} = e^{-\left(\frac{s_2 - s_1}{R}\right)}$$

Equations (2.56), (2.57), (2.58), (2.59), and (2.60) are plotted in Fig. 2.15.

We can state two simple rules of thumb:

1. A normal shock wave always forms between supersonic and subsonic flow.
2. The flow behind a normal shock wave is always subsonic.

Normal shock waves are encountered in the flow in intakes and nozzles as well as over aircraft wings. Figure 2.16 illustrates normal shock waves formed on the suction or both suction and pressure surfaces of wing sections.

It is obvious that a very useful table for fluid flow changes across a normal shock can be constructed using the above equations. This kind of table is available in all gas dynamics or compressible flow texts [4, 5]. Table 2.6 illustrates these relations. You are encouraged to complete missing data in Table 2.6.

Example 2.9 Air is flowing through normal shock. Flow conditions upstream of the shock are $u_1 = 600 \text{ m/s}$, $T_{01} = 500 \text{ K}$, $P_{01} = 700 \text{ kPa}$. It is required to calculate the downstream conditions M_2 , u_2 , T_2 , P_2 , P_{02} and $(s_2 - s_1)$. Assume: calorically perfect ideal gas.

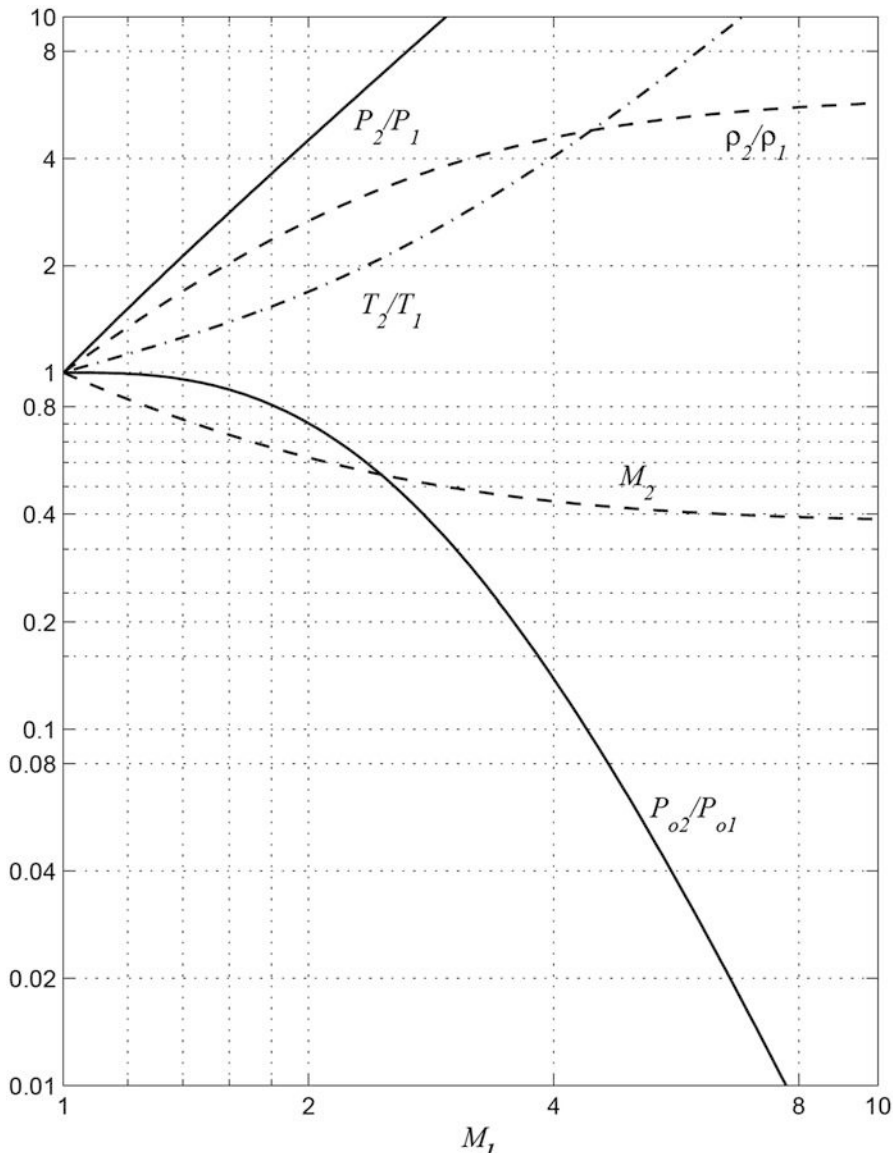


Fig. 2.15 Normal shock functions ($\gamma = 1.4$)

Solution

The upstream conditions (static temperature, pressure, and density as well as sonic speed and Mach numbers) can be calculated from the following relations:

$$T_1 = T_{01} - \frac{u_1^2}{2C_p} = 500 - \frac{(600)^2}{2 \times 1005} = 320.89 \text{ K}$$

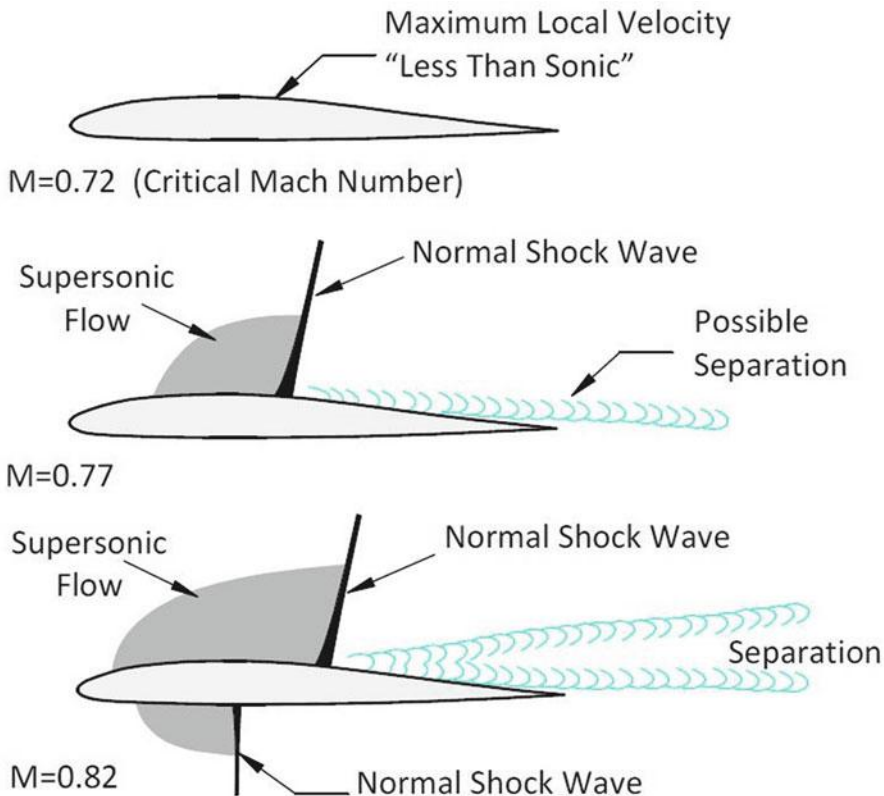


Fig. 2.16 Normal shock waves over either suction or suction/pressure sides of wing section

Table 2.6 Normal shock parameters ($\gamma = 1.4$)

M_1	M_2	P_2/P_1	T_2/T_1	P_{02}/P_{01}
3.0	0.47519	10.3333	2.6790	0.32834
2.5	?	?	?	?
2.0	0.57735	4.5000	1.6875	0.72089
1.5	?	?	?	?
1.00	1.00	1.00	1.00	1.00

$$P_1 = P_{01} / \left(1 + \frac{\gamma - 1}{2} M_1^2 \right)^{\frac{\gamma}{\gamma-1}} = 700 / 4.7249 = 148.15 \text{ kPa}$$

$$\rho_1 = P_1 / RT_1 = \frac{148.15}{0.287 \times 320.9} = 1.609 \text{ kg/m}^3$$

$$a_1 = \sqrt{\gamma RT_1} = \sqrt{1.4 \times 287 \times 320.89} = 359.0 \text{ m/s}$$

$$M_1 = u_1 / a_1 = 600 / 359 = 1.671$$

Mach number downstream the shock wave (M_2) is evaluated from the relation:

$$M_2^2 = \frac{(\gamma - 1)M_1^2 + 2}{2\gamma M_1^2 - (\gamma - 1)} = \frac{0.4 \times (1.671)^2 + 2}{2 \times 1.4 \times (1.671)^2 - 0.4} = \frac{3.1169}{7.418} = 0.34489$$

$$M_2 = 0.648$$

From known Mach number (M_2), the air properties downstream of the normal shock can be evaluated as follows:

$$\frac{T_2}{T_1} = \frac{[2\gamma M_1^2 - (\gamma - 1)][(\gamma - 1)M_1^2 + 2]}{(\gamma + 1)^2 M_1^2}$$

$$= \frac{[2 \times 1.4 \times (1.671)^2 - 0.4][0.4 \times (1.671)^2 + 2]}{(2.4 \times 1.671)^2}$$

$$\frac{T_2}{T_1} = \frac{7.4183 \times 3.1169}{16.0833} = 1.4376$$

$$T_2 = 461.34 \text{ K}$$

$$u_2 = M_2 \times c_2 = M_2 \times \sqrt{\gamma RT_2} = 0.648 \times \sqrt{1.4 \times 287 \times 461.34} = 278.9 \text{ m/s}$$

$$\rho_2 = \rho_1 u_1 / u_2 = 1.609 \times 600 / 278.9 = 3.4614 \text{ kg/m}^3$$

$$p_2 = p_1 + \rho_1 u_1^2 - \rho_2 u_2^2$$

$$P_2 = 148.15 \times 10^3 + 1.609 \times (600)^2 - 3.4614 \times (278.9)^2$$

$$P_2 = 458,144 \text{ Pa} = 458.14 \text{ kPa}$$

$$\text{Since } \frac{P_{02}}{P_{01}} = \left[\frac{(\gamma + 1)M_1^2}{2 + (\gamma - 1)M_1^2} \right]^{\frac{\gamma}{\gamma-1}} \left[\frac{(\gamma + 1)}{2\gamma M_1^2 - (\gamma - 1)} \right]^{\frac{1}{\gamma-1}}$$

$$\text{Then } \frac{P_{02}}{P_{01}} = \left[\frac{2.4 \times (1.671)^2}{2 + 0.4(1.671)^2} \right]^{3.5} \left[\frac{2.4}{2.8 \times (1.671)^2 - 0.4} \right]^{2.5} = 0.86759$$

$$P_{02} = 607.32 \text{ kPa}$$

As a check, calculate the value of (T_{02}):

$$T_{02} = T_2 \left(1 + \frac{\gamma - 1}{2} M_2^2 \right) = 461.34 \times [1 + 0.2 \times (0.648)^2] = 500 \text{ K}$$

This confirms the total temperature (or enthalpy) equality, $T_{02} = T_{01}$, as stated above.

$$\text{Since } \frac{P_{02}}{P_{01}} = e^{-\left(\frac{s_2-s_1}{R}\right)}$$

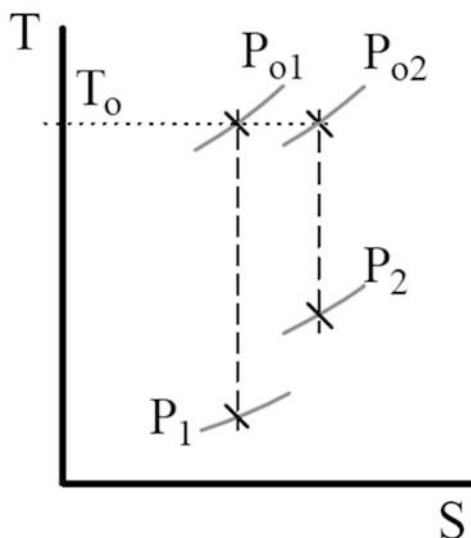
$$\text{Then } s_2 - s_1 = -R \ln \left(\frac{P_{02}}{P_{01}} \right) = 40.764 \text{ J/kg K}$$

The temperature–entropy diagram is illustrated by Fig. 2.17, which shows the static and total conditions upstream and downstream of the shock. Note the entropy increased despite not including any entropy-generating mechanisms in this model. Why? First, the differential equations themselves required the assumption of continuous differentiable functions. Our shock violates this.

When one returns to the more fundamental control volume forms, it can be shown that the entropy-generating mechanism returns. From a continuum point of view, one can also show that the neglected terms, that momentum and energy diffusion, actually give rise to a *smeared* shock. These mechanisms generate just enough entropy to satisfy the entropy jump which was just calculated.

Another interpretation may be also given as follows: the assumption that the compression shock represents a discontinuity is only an approximation. In reality the shock has a thickness (δ) of the order of magnitude of several free mean paths. If the gas flowing through the shock can be assumed to be a continuum, the Navier–Stokes equations can be employed for the description of the flow between the upstream and downstream edge of the compression shock. The flow quantities do not change discontinuously in the form of a jump but in a continuous transition from the free-stream conditions to the flow conditions downstream from the shock. The increase of the entropy can now be explained as an action of the frictional forces and the heat conduction within the shock region of finite thickness.

Fig. 2.17 Static and total conditions



2.4.5.2 Off Design and Normal Shock Waves in Nozzles

The objective of CD nozzle is to obtain supersonic flow. Thus, the design operating condition is to have a subsonic flow in the convergent section, a sonic condition at throat, and a supersonic flow in the divergent part. For off-design conditions, many possibilities for the speed at the nozzle exit may be encountered depending on the back pressure P_b . The fluid may find itself decelerating in the diverging section instead of accelerating. A detailed description is given with the aid of Fig. 2.18. When a fluid enters the nozzle with a low velocity at stagnation pressure P_0 , the state of the nozzle flow is determined by the overall pressure ratio P_b/P_0 . When the back pressure $P_b = P_0$ (case A), there will be no flow through the nozzle. This is expected since the flow in a nozzle is driven by the pressure difference between the nozzle inlet and the exit. Now let us examine what happens as the back pressure is lowered.

1. When $P_0 > P_b > P_C$ (critical pressure), the flow remains subsonic throughout the nozzle, and the mass flow is less than that for choked flow. The fluid velocity increases in the converging section and reaches a maximum at the throat (but still subsonic; $M < 1$). However, most of the gain in velocity is lost in the diverging section of the nozzle, which acts as a diffuser. The pressure decreases in the converging section, reaches a minimum at the throat, and increases at the expense of velocity in the diverging section.
2. When $P_b = P_C$, the throat pressure becomes P^* and the fluid achieves sonic velocity at the throat. But the diverging section of the nozzle still acts as a diffuser, slowing the fluid to subsonic velocities. The mass flow rate that was increasing with decreasing P_b also reaches its maximum value. Recall that P^* is the lowest pressure that can be obtained at the throat, and the sonic velocity is the highest velocity that can be achieved with a converging nozzle. Thus, lowering P_b further has no influence on the fluid flow in the converging part of the nozzle or the mass flow rate through the nozzle. However, it does influence the character of the flow in the diverging section. This mode of operation is frequently called the *first critical* [5].
3. When $P_C > P_b > P_E$, the fluid that achieved a sonic velocity at the throat continues accelerating to supersonic velocities in the diverging section as the pressure decreases. This acceleration comes to a sudden stop, however, as a *normal shock* develops at a section between the throat and the exit plane, which causes a sudden drop in velocity to subsonic levels and a sudden increase in pressure. This mode of operation is frequently called the *second critical* [5]. The fluid then continues to decelerate further in the remaining part of the converging–diverging nozzle. Flow through the shock is highly irreversible, and thus it cannot be approximated as isentropic. The normal shock moves downstream away from the throat as P_b is decreased, and it approaches the nozzle exit plane as P_b approaches P_E . When $P_b = P_E$, the normal shock forms at the exit plane of the nozzle. The flow is supersonic through the entire diverging section in this case, and it can be approximated as isentropic.

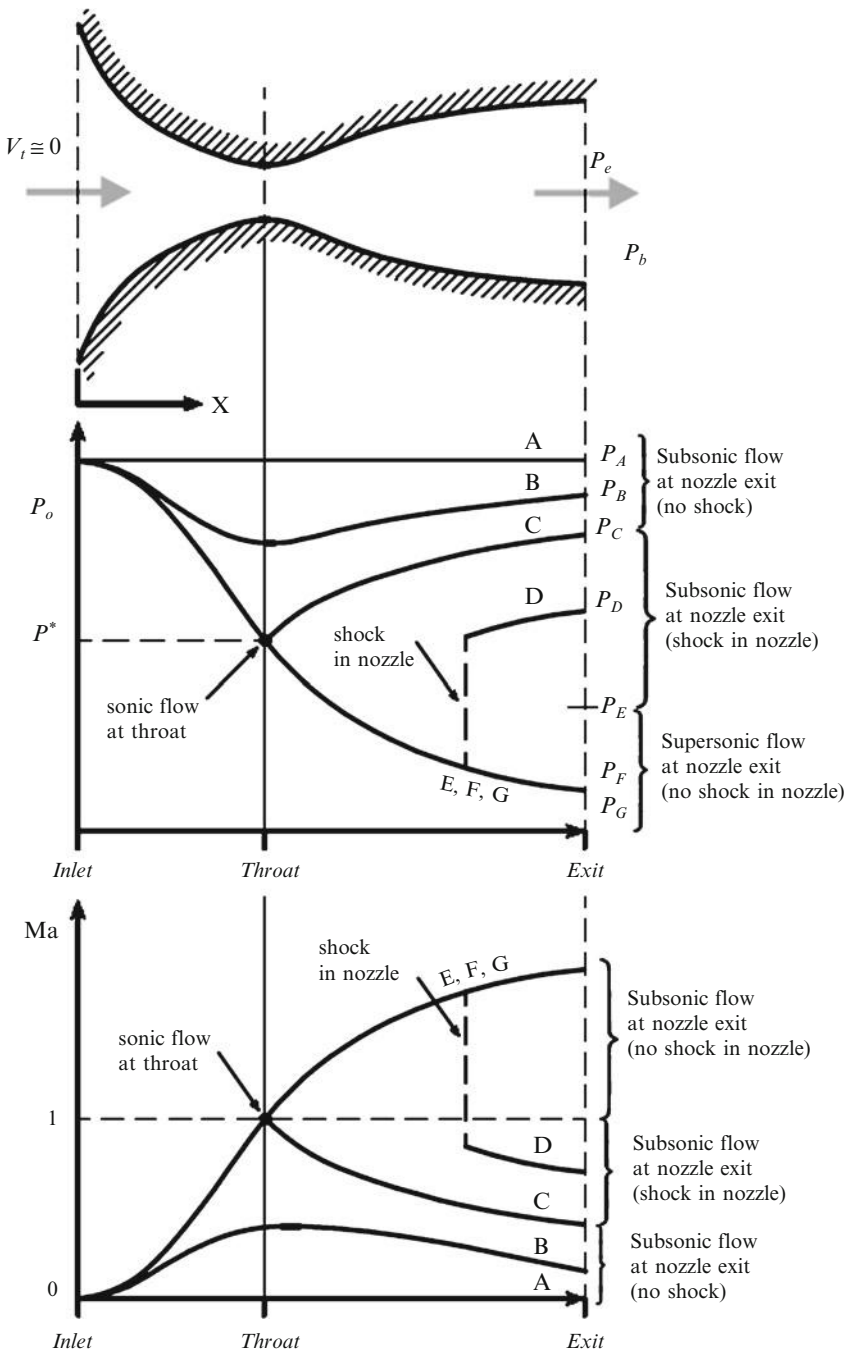


Fig. 2.18 The effects of back pressure on the flow through a converging–diverging nozzle

However, the fluid velocity drops to subsonic levels just before leaving the nozzle as it crosses the normal shock.

- When $P_E > P_b > 0$, the flow in the diverging section is supersonic, and the fluid expands to P_F at the nozzle exit with no normal shock forming within the nozzle. Thus, the flow through the nozzle can be approximated as isentropic. When $P_b = P_F$, no shocks occur within or outside the nozzle. This mode of operation is frequently called the *third critical* [5]. When $P_b < P_F$ (*underexpanded case*), irreversible mixing and expansion waves occur downstream of the exit plane of the nozzle. When $P_b > P_F$ (*overexpanded case*), however, the pressure of the fluid increases from P_F to P_b irreversibly in the wake of the nozzle exit, creating what are called *oblique shocks*.

Example 2.10 A large tank with compressed air is attached into a converging-diverging nozzle (Fig. 2.19) with pressure 8 bar and temperature of 327 °C. Nozzle throat area is 30 cm² and the exit area is 90 cm². The shock occurs in a location where the cross section area is 60 cm². Calculate the back pressure and the temperature of the flow. Also determine the critical subsonic and supersonic points for the back pressure (point “a” and point “b”).

Solution

The stagnation temperature and pressure at the nozzle inlet are equal to the specified values in the tank.

$$P_{01} = 8 \text{ bar}, \quad T_{01} = 327 + 273 = 600 \text{ K}$$

Since the star area (the throat area), A^* , and the area upstream of the shock are known, then this ratio is given as

$$\frac{A_x}{A^*} = \frac{60}{30} = 2$$

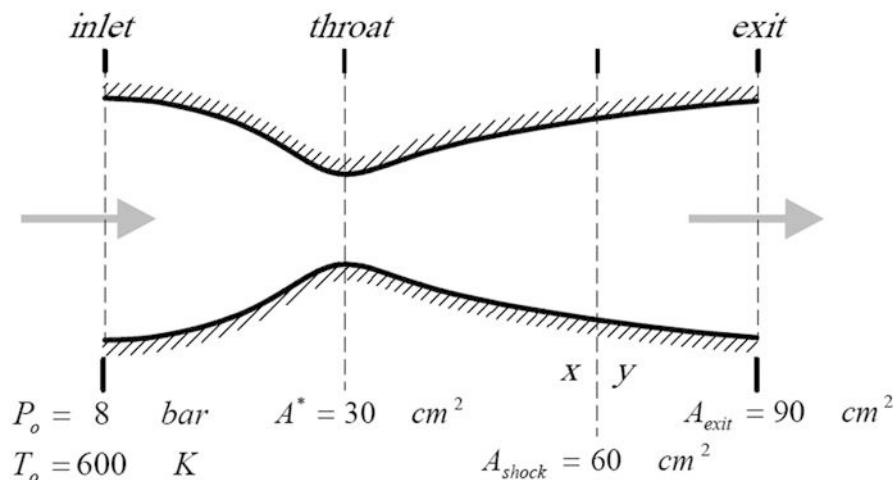


Fig. 2.19 Convergent-divergent nozzle

To evaluate the conditions upstream of the normal shock (state x), Eq. (2.46) is employed. It may be reduced to

$$\left(M_x \frac{A_x}{A^*}\right)^{\frac{2(\gamma-1)}{\gamma+1}} - \frac{\gamma-1}{\gamma+1} M_x^2 = \frac{2}{\gamma+1}$$

with $\gamma = 1.4$, then it is further simplified to

$$1.25992M_x^{0.3333} - 0.16667M_x^2 = 0.8333$$

Solve the above equation by trial and error to get $M_x = 2.1972$

From isentropic relations (2.44)

$$\frac{T_0}{T_x} = 1 + \frac{\gamma-1}{2} M_x^2 = 1.96554$$

$$T_x = 305.3 \text{ K}$$

$$\frac{P_{0x}}{P_x} = \left(1 + \frac{\gamma-1}{2} M_x^2\right)^{\frac{\gamma}{\gamma-1}} = 10.64596$$

$$P_x = 0.7515 \text{ bar}$$

From normal shock relations (2.56), (2.57), (2.58), (2.59), and (2.60)

$$M_y^2 = \frac{(\gamma-1)M_x^2 + 2}{2\gamma M_x^2 - (\gamma-1)} = \frac{3.931075}{13.11752}$$

$$M_y = 0.54743$$

$$\frac{T_y}{T_x} = \frac{[2\gamma M_x^2 - (\gamma-1)][(\gamma-1)M_x^2 + 2]}{(\gamma+1)^2 M_x^2} = \frac{13.117523 \times 3.931}{27.8074}$$

$$\frac{T_y}{T_x} = 1.8543$$

$$T_y = 566.1 \text{ K}$$

$$\frac{P_y}{P_x} = \frac{[2\gamma M_x^2 - (\gamma-1)]}{\gamma+1} = 5.46564$$

$$P_y = 4.1 \text{ bar}$$

$$\frac{P_{0y}}{P_{0x}} = \left[\frac{(\gamma + 1)M_x^2}{2 + (\gamma - 1)M_x^2} \right]^{\frac{\gamma}{\gamma-1}} \left[\frac{(\gamma + 1)}{2\gamma M_x^2 - (\gamma - 1)} \right]^{\frac{\gamma}{\gamma-1}}$$

$$\frac{P_{0y}}{P_{0x}} = \left[\frac{2.4 \times (2.1972)^2}{2 + 0.4 \times (2.1972)^2} \right]^{3.5} \left[\frac{2.4}{2.8 \times (2.1972)^2 - 0.4} \right]^{2.5}$$

$$\frac{P_{0y}}{P_{0x}} = 43.95788 \times 0.014318 = 0.62941$$

$$P_{0y} = 4.11 \text{ bar}$$

Again utilizing the isentropic relationship, the exit conditions can be evaluated. With known Mach number the new star area ratio (A_y/A^*) can be calculated from the relation:

$$\frac{A_y}{A^*} = \frac{1}{M_y} \left[\frac{2}{\gamma + 1} \left(1 + \frac{\gamma - 1}{2} M_y^2 \right) \right]^{\frac{\gamma+1}{2(\gamma-1)}}$$

$$\frac{A_y}{A^*} = \frac{1}{0.54743} \left[\frac{2}{2.4} \left(1 + 0.2(0.54743)^2 \right) \right]^3 = 1.25883$$

From known exit area, then

$$\frac{A_e}{A^*} = \frac{A_e}{A_y} \frac{A_y}{A^*} = \frac{90}{60} \times 1.25883 = 1.88824$$

From this area ratio, then (M_e) can be calculated by trial and error using the relation

$$\left(M_e \frac{A_e}{A^*} \right)^{\frac{2(\gamma-1)}{\gamma+1}} - \frac{\gamma - 1}{\gamma + 1} M_e^2 = \frac{2}{\gamma + 1}$$

$$1.236M_x^{0.3333} - 0.16667M_x^2 = 0.8333$$

$$M_e = 0.327$$

From isentropic relations (2.44)

$$\frac{T_0}{T_e} = 1 + \frac{\gamma - 1}{2} M_e^2 = 1.02138$$

$$\frac{P_{0e}}{P_e} = \frac{P_{0y}}{P_e} = \left(1 + \frac{\gamma - 1}{2} M_e^2 \right)^{\frac{\gamma}{\gamma-1}} = 1.07687$$

$$P_e = \frac{P_e}{P_{0y}} \frac{P_{0y}}{P_{0x}} P_{0x} = \frac{1}{1.07687} \times 0.62941 \times 8 = 4.6758 \text{ bar}$$

Table 2.7 Properties of air inside the nozzle

	Inlet	Upstream normal shock	Downstream normal shock	Exit
M	0	2.1972	0.54743	0.327
P_0 (bar)	8	8	4.11	4.11
P (bar)	–	0.7515	4.1	4.6758
T (K)	–	305.3	566.1	587.4

$$T_e = \frac{T_e}{T_0} T_0 = \frac{1}{1.02138} \times 600 = 587.4 \text{ K}$$

A summary of the above results is given here in Table 2.7.

The “critical” points “a” and “b” at nozzle exit resemble the subsonic and supersonic limits if no shock waves exist and the flow achieves a Mach equal of unity at the throat. The area ratio for both cases is calculated from the relation:

$$\frac{A_e}{A^*} = \frac{1}{M_e} \left[\frac{2}{\gamma + 1} \left(1 + \frac{\gamma - 1}{2} M_e^2 \right) \right]^{\frac{\gamma+1}{2(\gamma-1)}}$$

Since $\frac{A_e}{A^*} = \frac{90}{30} = 3.0$, then the exit Mach number may be calculated by trial and error from the relation:

$$\left(M_e \frac{A_e}{A^*} \right)^{\frac{2(\gamma-1)}{\gamma+1}} - \frac{\gamma-1}{\gamma+1} M_e^2 = \frac{2}{\gamma+1}$$

$$1.4422 M_e^{0.3333} - 0.16667 M_e^2 = 0.8333$$

Two solutions are obtained, namely, $M_e = 0.19745$ and $M_e = 2.6374$. Both solutions are illustrated by points (a) and (b) in Fig. 2.20.

For point “a,” $M_a = 0.19745$:

The exit pressure and temperature are determined as follows:

$$\frac{T_0}{T_a} = 1 + \frac{\gamma-1}{2} M_a^2 = 1.00779$$

$$T_a = 600 / 1.00779 = 595.3 \text{ K}$$

$$\frac{P_0}{P_a} = \left(1 + \frac{\gamma-1}{2} M_a^2 \right)^{\frac{\gamma}{\gamma-1}} = 1.027557$$

$$P_a = 8 / 1.027557 = 7.785 \text{ bar}$$

For point “b,” $M_b = 2.6374$.

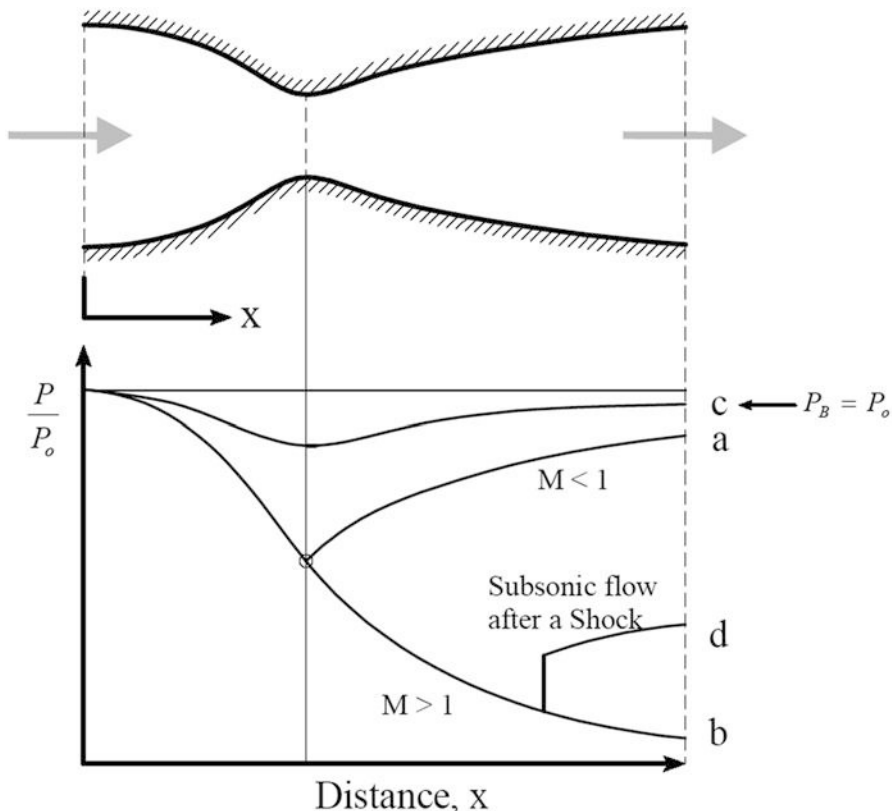


Fig. 2.20 Subsonic and supersonic solutions

Table 2.8 Subsonic and supersonic solutions

	Mach number	Static temperature (K)	Static pressure (bar)
Point (a) (subsonic solution)	0.19745	595.3	7.785
Point (b) (supersonic solution)	2.6374	250.92	0.3784

The exit pressure and temperature are determined as follows:

$$\frac{T_0}{T_b} = 1 + \frac{\gamma - 1}{2} M_b^2 = 2.39117$$

$$T_b = 600 / 2.39117 = 250.92 \text{ K}$$

$$\frac{P_0}{P_b} = \left(1 + \frac{\gamma - 1}{2} M_b^2 \right)^{\frac{\gamma}{\gamma-1}} = 21.14172$$

$$P_b = 0.3784 \text{ bar}$$

A summary of these results are given in Table 2.8.

2.4.5.3 Oblique Shock Wave Relations

Normal shock was examined in Sect. 2.4.4.2. Normal shock is a special case of the general inclined one. When shock is inclined to the flow direction, it is identified as an oblique shock. When a wedge-shaped object is placed in a two-dimensional supersonic flow, a plane-attached shock wave may emanate from the nose of the body at an angle (β) as long as shown in Fig. 2.21. The flow Mach number and the wedge angle (δ) together define the resulting attached or detached shock configuration. Similarly, when a supersonic flow encounters a concave corner with an angle (δ), two possibilities of attached or detached shock waves exist. Figure 2.22 illustrates the abovementioned four cases. There is a maximum deflection angle (δ_{max}) associated with any given Mach number. When the deflection angle exceeds δ_{max} , a detached shock forms which has a curved wave front. Behind this curved (or -bow-like) wave, we find all possible shock solutions associated with the initial Mach number M_1 . At the center a normal shock exists, with subsonic flow resulting. As the wave front curves around, the shock angle decreases continually, with a resultant decrease in shock strength. Eventually, we reach a point where supersonic flow exists after the shock front.

Oblique shock waves are preferred predominantly in engineering applications compared with normal shock waves. This can be attributed to the fact that using one or a combination of oblique shock waves results in more favorable post-shock conditions (lower post-shock temperature and pressure) when compared to utilizing a single normal shock. An example of this technique can be seen in the design of supersonic aircraft engine inlets, which are wedge shaped to compress airflow into the combustion chamber while minimizing thermodynamic losses. Early supersonic aircraft jet engine inlets were designed using compression from a single normal

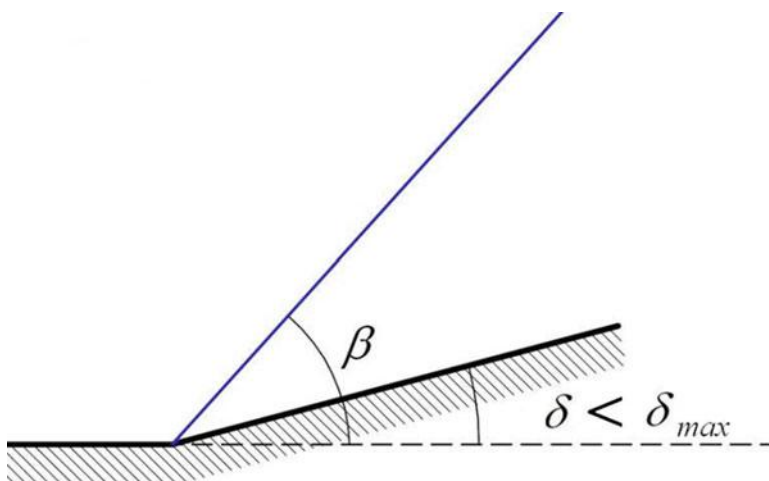


Fig. 2.21 Oblique shock wave applications

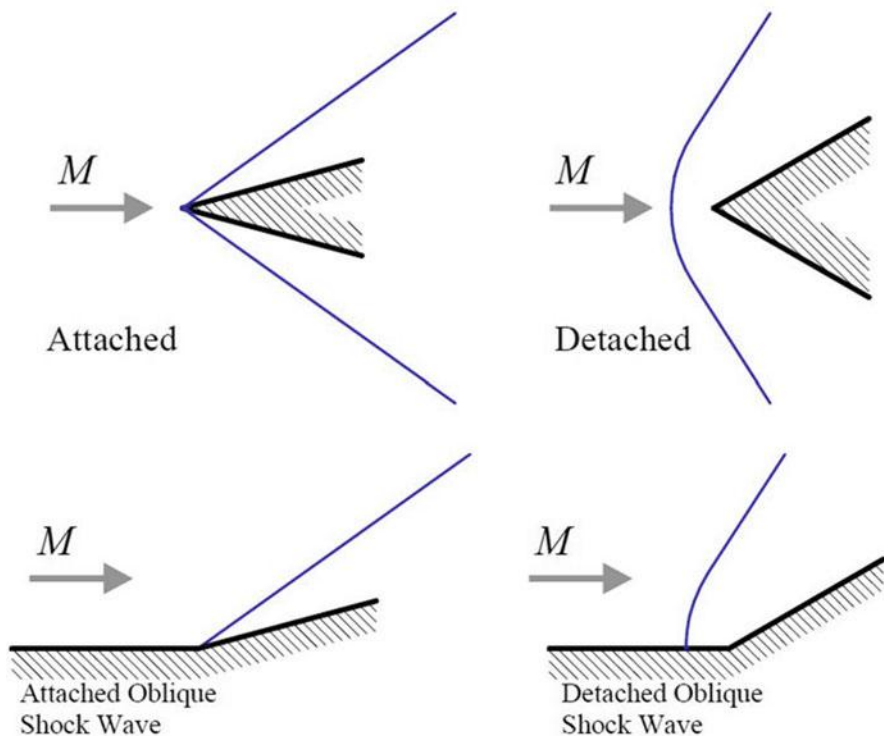


Fig. 2.22 Oblique shock wave applications

shock, but this approach caps the maximum achievable Mach number to roughly 1.6. The wedge-shaped inlets are clearly visible on the sides of the [F-14 Tomcat](#), which has a maximum speed of Mach 2.34.

For analyzing oblique shock, consider Fig. 2.23 where the flow is deflected angle δ , and a shock generated inclined an angle β to the flow direction. The flow approaches the shock wave with a velocity V_1 and Mach number M_1 at an angle β with respect to the shock. It is turned through an angle δ as it passes through the shock, leaving with a velocity V_2 and a Mach number M_2 at an angle $(\beta - \delta)$ with respect to the shock. The inlet and exit velocities can be separated into tangential and normal components. The tangential velocity components upstream and downstream the shocks are equal. The normal velocity component may be treated as flow through a normal shock. This means that V_{1n} is supersonic and V_{2n} is subsonic, but still the downstream velocity V_2 is supersonic. The following relations define the normal and tangential velocity components and Mach number for both upstream and downstream conditions:

$$V_{1t} = V_{2t}$$

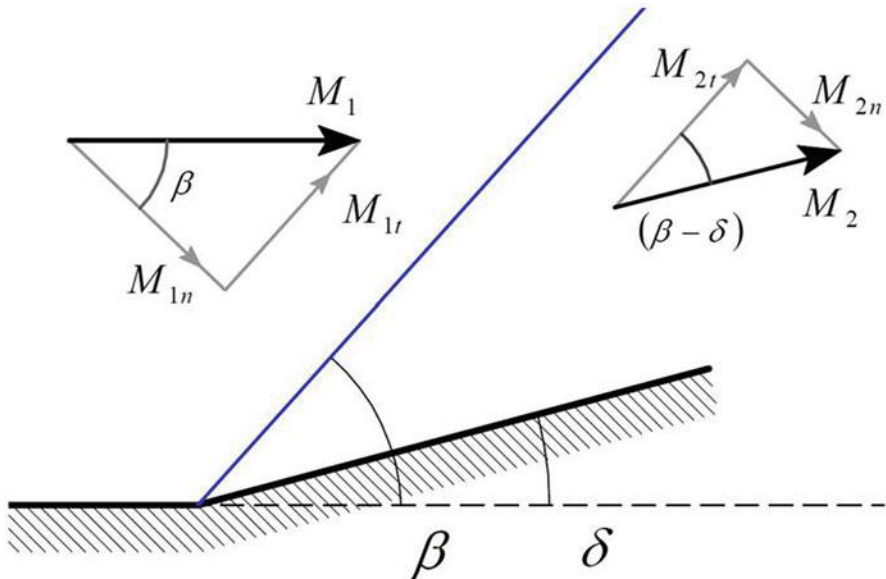


Fig. 2.23 Nomenclature of oblique shock wave

$$\begin{aligned}
 V_{1t} &= V_1 \cos \beta & V_{2t} &= V_2 \cos (\beta - \delta) \\
 V_{1n} &= V_1 \sin \beta & V_{2n} &= V_2 \sin (\beta - \delta) \\
 M_{1n} &= M_1 \sin \beta > 1.0 & M_{2n} &= M_2 \sin (\beta - \delta) < 1.0 \\
 M_{1t} &= M_1 \cos \beta & M_{2t} &= M_2 \cos (\beta - \delta) \\
 M_1 &> 1.0, & M_2 &> 1.0
 \end{aligned}$$

Since the oblique shock can be treated as a normal shock having an upstream Mach number $M_{1n} = M_1 \sin \beta$ and a tangential component $M_{1t} = M_1 \cos \beta$, then using Eqs. (2.56), (2.57), (2.58), (2.59), and (2.60), the relations (2.62–2.66) can be deduced; [9] and [10]. The relation between (δ, β, M_1) is given by Eq. (2.61).

$$\tan \delta = \frac{2 \cot \beta (M_1^2 \sin^2 \beta - 1)}{(\gamma + 1) M_1^2 - 2(M_1^2 \sin^2 \beta - 1)} \quad (2.61a)$$

For $\gamma = 7/4$, then

$$\tan \delta = 5 \frac{M_1^2 \sin 2\beta - 2 \cot \beta}{10 + M_1^2(7 + 5 \cos 2\beta)} \quad (2.61b)$$

$$M_{2n}^2 = \frac{(\gamma - 1)M_{1n}^2 + 2}{2\gamma M_{1n}^2 - (\gamma - 1)} \quad (2.62a)$$

$$M_2^2 \sin^2(\beta - \delta) = \frac{(\gamma - 1)M_1^2 \sin^2\beta + 2}{2\gamma M_1^2 \sin^2\beta - (\gamma - 1)} \quad (2.62b)$$

For $\gamma = 7/4$, then

$$M_2^2 = \frac{36M_1^4 \sin^2\beta - 5(M_1^2 \sin^2\beta - 1)(7M_1^2 \sin^2\beta + 5)}{(7M_1^2 \sin^2\beta - 1)(M_1^2 \sin^2\beta + 5)} \quad (2.62c)$$

$$\frac{P_2}{P_1} = \left[\frac{2\gamma M_1^2 \sin^2\beta - (\gamma - 1)}{\gamma + 1} \right] \quad (2.63a)$$

For $\gamma = 7/4$, then

$$\frac{P_2}{P_1} = \left(\frac{7M_1^2 \sin^2\beta - 1}{6} \right) \quad (2.63b)$$

$$\frac{T_2}{T_1} = \frac{[2\gamma M_1^2 \sin^2\beta - (\gamma - 1)][(\gamma - 1)M_1^2 \sin^2\beta + 2]}{(\gamma + 1)^2 M_1^2 \sin^2\beta} \quad (2.64a)$$

For $\gamma = 7/4$, then

$$\frac{T_2}{T_1} = \frac{(7M_1^2 \sin^2\beta - 1)(M_1^2 \sin^2\beta + 5)}{36M_1^2 \sin^2\beta} \quad (2.64b)$$

$$\frac{\rho_2}{\rho_1} = \left[\frac{(\gamma + 1)M_1^2 \sin^2\beta}{2 + (\gamma - 1)M_1^2 \sin^2\beta} \right] \quad (2.65a)$$

For $\gamma = 7/4$, then

$$\frac{\rho_2}{\rho_1} = \left[\frac{6M_1^2 \sin^2\beta}{M_1^2 \sin^2\beta + 5} \right] \quad (2.65b)$$

$$\frac{P_{02}}{P_{01}} = \left[\frac{(\gamma + 1)M_1^2 \sin^2\beta}{(\gamma - 1)M_1^2 \sin^2\beta + 2} \right]^{\frac{\gamma}{\gamma-1}} \left[\frac{\gamma + 1}{2\gamma M_1^2 \sin^2\beta - (\gamma - 1)} \right]^{\left(\frac{5}{\gamma-1}\right)} \quad (2.66a)$$

For $\gamma = 7/4$, then the relation for total pressure ratio will be

$$\frac{P_{02}}{P_{01}} = \left[\frac{6M_1^2 \sin^2\beta}{M_1^2 \sin^2\beta + 5} \right]^{\frac{7}{2}} \left[\frac{6}{7M_1^2 \sin^2\beta - 1} \right]^{\left(\frac{5}{2}\right)} \quad (2.66b)$$

Figure 2.24 illustrates the relation between M_1 , β and δ for oblique shock wave for the case of $\gamma = 1.4$. Figure 2.25 illustrates the downstream Mach number M_2 for oblique shock wave also for $\gamma = 1.4$.

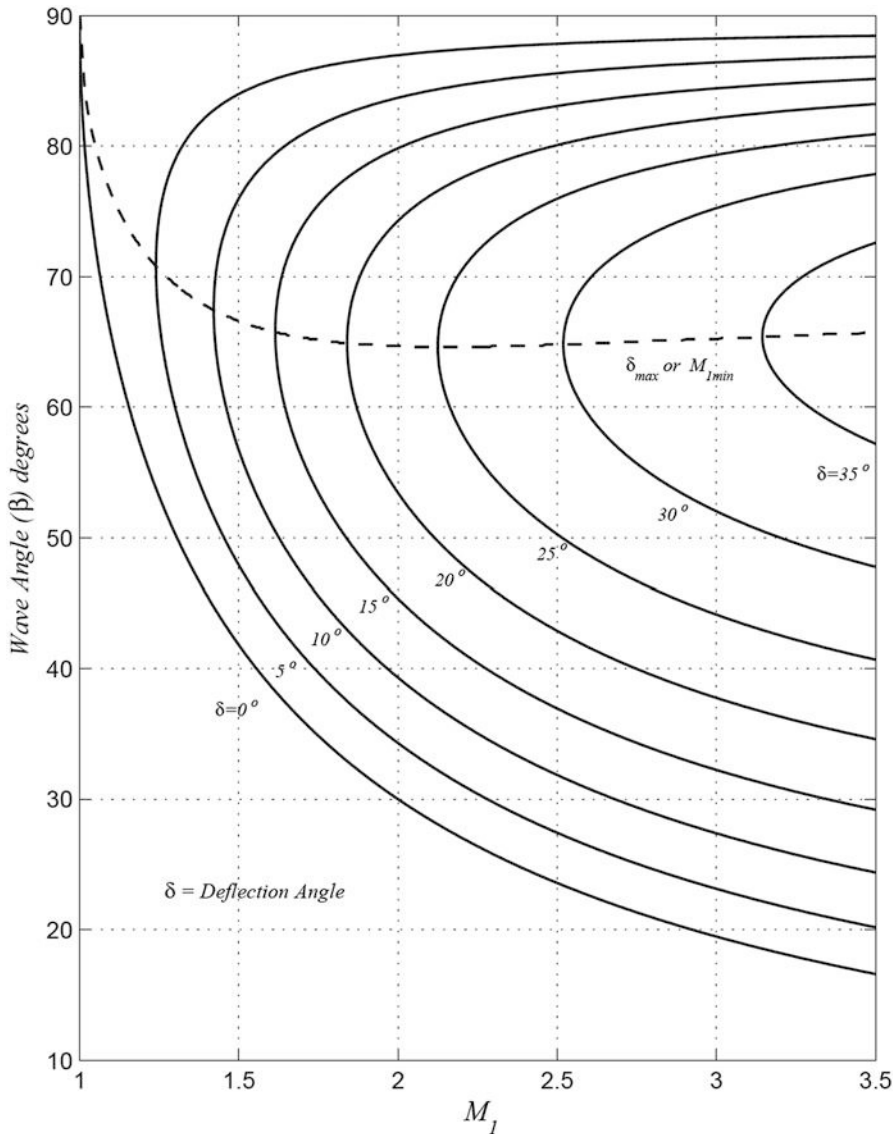


Fig. 2.24 Relation between M_1, β and δ for oblique shock wave $\gamma = 1.4$

Example 2.11 An oblique shock wave has the following upstream static conditions and Mach number: $P_1 = 150$ kPa, $T_1 = 500$ K, $M_1 = 1.605$ and a shock angle $\beta = 60^\circ$. It is required to calculate:

1. Upstream velocity (V_1), deflection angle (δ)
2. Downstream Mach number (M_2)

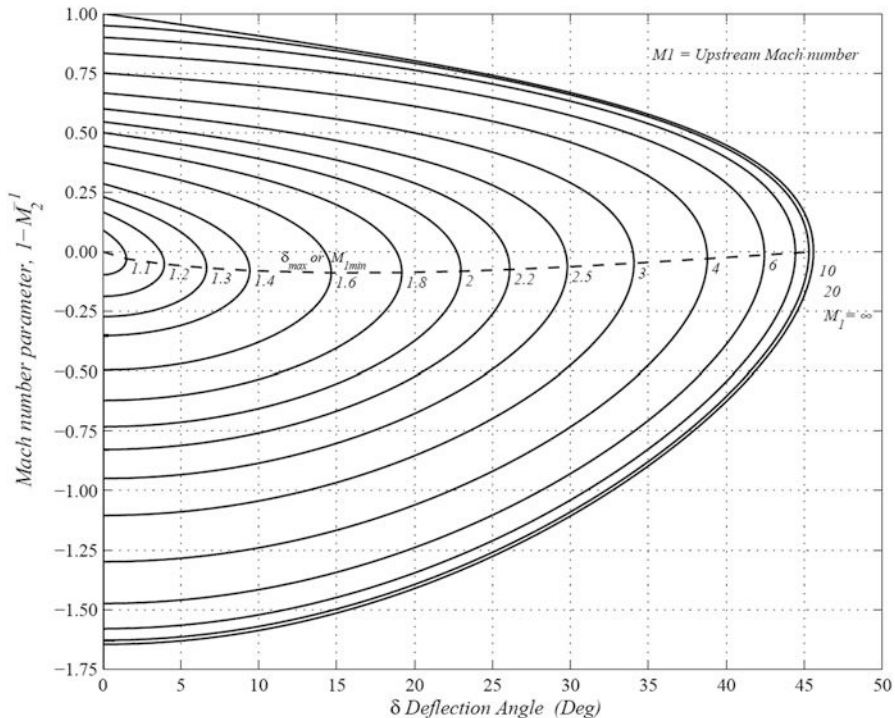


Fig. 2.25 Downstream Mach number M_2 for oblique shock wave $\gamma = 1.4$

3. Static and total temperatures (T_2, T_{01}, T_{02})
4. Normal and tangential velocity components upstream and downstream of the oblique shock ($V_{1n}, V_{1t}, V_{2n}, V_{2t}$)
5. Static and total pressures (P_2, P_{01}, P_{02})

Solution

$$V_1 = M_1 a_1 = M_1 \sqrt{\gamma R T_1} = 1.609 \times \sqrt{1.4 \times 287 \times 500}$$

$$V_1 = 719.4 \text{ m/s}$$

The deflection angle is calculated from Eq. (2.61a):

$$\tan \delta = \frac{2 \cot 60 \left[(1.605 \sin 60)^2 - 1 \right]}{(2.4)(1.605)^2 - 2 \left[(1.605 \sin 60)^2 - 1 \right]} = 0.24916$$

$$\delta = 14^\circ$$

From Eq. (2.62b)

$$M_2^2 \sin^2(60 - 14) = \frac{0.4 \times (1.604 \sin 60)^2 + 2}{2.8 \times (1.604 \sin 60)^2 - 0.4}$$

$$M_2^2 = 1.06968$$

$$M_2 = 1.042$$

From Eq. (2.64a)

$$\frac{T_2}{T_1} = \frac{[2.8 \times 1.932 - 0.4][0.4 \times 1.932 + 2]}{(2.4)^2 \times 1.932} = 1.2482$$

$$T_2 = 624.1 \text{ K}$$

Isentropic relation at inlet gives

$$T_{01} = T_1 \left(1 + \frac{\gamma - 1}{2} M_1^2 \right) = 500 \times 1.5152 = 757.6 \text{ K} = T_{02}$$

$$V_{1n} = V_1 \sin \beta = 719.4 \times \sin 60 = 623 \text{ m/s}$$

$$V_{1t} = V_1 \cos \beta = 359.7 \text{ m/s}$$

$$V_2 = M_2 a_2 = M_2 \sqrt{\gamma R T_2} = 1.034 \times \sqrt{1.4 \times 287 \times 624} = 517.8 \text{ m/s}$$

$$V_2 = 517.8 \text{ m/s}$$

$$V_{2n} = V_2 \sin (\beta - \delta) = 372.5 \text{ m/s}$$

$$V_{2t} = V_2 \cos (\beta - \delta) = 359.7 \equiv V_{1t}$$

From Eqs. (2.63a) and (2.63b),

$$\frac{P_2}{P_1} = \left[\frac{2\gamma M_1^2 \sin^2 \beta - (\gamma - 1)}{\gamma + 1} \right] = \left(\frac{7M_1^2 \sin^2 \beta - 1}{6} \right)$$

$$\frac{P_2}{P_1} = \frac{7 \times (1.605 \times \sin 60)^2 - 1}{6} = 2.0874$$

$$P_2 = 313.1 \text{ kPa}$$

$$P_{01} = P_1 \left(1 + \frac{\gamma - 1}{2} M_1^2 \right)^{\frac{\gamma}{\gamma-1}} = 150 \times \left[1 + 0.2 \times (1.605)^2 \right]^{3.5} = 642.3 \text{ kPa}$$

From Eqs. (2.66a) and (2.65b),

$$\frac{P_{02}}{P_{01}} = \left[\frac{6M_1^2 \sin^2 \beta}{M_1^2 \sin^2 \beta + 5} \right]^{\frac{7}{2}} \left[\frac{6}{7M_1^2 \sin^2 \beta - 1} \right]^{\left(\frac{5}{2}\right)}$$

$$\frac{P_{02}}{P_{01}} = \left[\frac{6 \times 1.932}{1.932 + 5} \right]^{\frac{7}{2}} \left[\frac{6}{7 \times 1.932 - 1} \right]^{\left(\frac{5}{2}\right)} = 0.96$$

$$P_{02} = 0.96 P_{01} = 616.6 \text{ kPa}$$

As a comment here, oblique shock wave has the following features:

- Downstream flow is maintained supersonic.
- Both downstream static pressure and temperature are increased.
- Total temperature is kept constant while downstream total pressure is slightly reduced.

2.5 Rayleigh Flow Equations

Rayleigh flow resembles the case of a steady one-dimensional flow with *heat transfer*. Thus, it is appropriate to treat the flow in combustion chambers as a Rayleigh flow case. Consider the fluid flow in Fig. 2.26. No work exchange while heat is added (${}_1Q_2$).

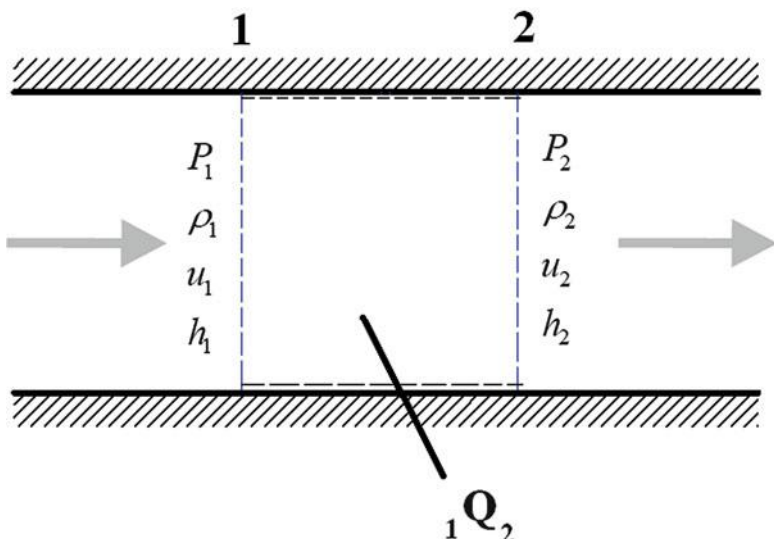


Fig. 2.26 Steady one-dimensional frictionless flow in a constant-area duct with heat transfer

The governing equations are

$$\begin{aligned} \text{Continuity equation} \quad & \frac{\dot{m}}{A} = \rho_1 u_1 = \rho_2 u_2 \\ \text{Momentum equation} \quad & p_1 + \rho_1 u_1^2 = p_2 + \rho_2 u_2^2 \\ \text{Energy equation} \quad & h_{02} \equiv h_2 + \frac{V_2^2}{2} = h_{01} + \frac{V_1^2}{2} + Q_2 = h_1 + \frac{V_1^2}{2} + Q_2 \\ \text{Equation of state} \quad & \frac{p_1}{\rho_1 T_1} = \frac{p_2}{\rho_2 T_2} \end{aligned}$$

For a perfect gas, the momentum equation can be rewritten as

$$p_1 \left(1 + \frac{\rho_1 u_1^2}{p_1} \right) = p_2 \left(1 + \frac{\rho_2 u_2^2}{p_2} \right)$$

or

$$\frac{P_2}{P_1} = \left[\frac{1 + \gamma M_1^2}{1 + \gamma M_2^2} \right] \quad (2.67)$$

From continuity equation

$$\begin{aligned} \rho_1 u_1 &= \rho_2 u_2 \\ \frac{P_1 M_1}{\sqrt{T_1}} &= \frac{P_2 M_2}{\sqrt{T_2}} \end{aligned}$$

Thus

$$\frac{T_2}{T_1} = \left(\frac{1 + \gamma M_1^2}{1 + \gamma M_2^2} \right)^2 \frac{M_2^2}{M_1^2} \quad (2.68)$$

Since the total and static temperatures are related by the relation:

$$\frac{T_0}{T} = 1 + \frac{\gamma - 1}{2} M^2$$

Then

$$\frac{T_{02}}{T_{01}} = \left(\frac{1 + \gamma M_1^2}{1 + \gamma M_2^2} \right)^2 \left(\frac{M_2}{M_1} \right)^2 \left(\frac{1 + \frac{\gamma - 1}{2} M_2^2}{1 + \frac{\gamma - 1}{2} M_1^2} \right) \quad (2.69)$$

Similarly, the total pressure and static density ratios may be expressed as

$$\frac{P_{02}}{P_{01}} = \frac{1 + \gamma M_1^2}{1 + \gamma M_2^2} \left(\frac{1 + \frac{\gamma-1}{2} M_2^2}{1 + \frac{\gamma-1}{2} M_1^2} \right)^{\frac{\gamma}{\gamma-1}} \quad (2.70)$$

$$\frac{\rho_2}{\rho_1} = \left(\frac{M_1}{M_2} \right)^2 \left(\frac{1 + \gamma M_2^2}{1 + \gamma M_1^2} \right) \quad (2.71)$$

The downstream Mach number is expressed by the relation:

$$M_2^2 = \frac{(\gamma - 1)M_1^2 + 2}{2\gamma M_1^2 - (\gamma - 1)} \quad (2.72)$$

At critical conditions, these relations will be reduced to

$$\frac{P}{P^*} = \left[\frac{\gamma + 1}{1 + \gamma M^2} \right] \quad (2.73)$$

$$\frac{T}{T^*} = \frac{M^2(\gamma + 1)^2}{(1 + \gamma M^2)^2} \quad (2.74)$$

$$\frac{T_0}{T_0^*} = \frac{2(1 + \gamma)M^2}{(1 + \gamma M^2)^2} \left(1 + \frac{\gamma - 1}{2} M^2 \right) \quad (2.75)$$

$$\frac{P_0}{P_0^*} = \frac{(1 + \gamma)}{(1 + \gamma M^2)} \left(\frac{1 + \frac{\gamma-1}{2} M^2}{\frac{\gamma+1}{2}} \right)^{\frac{\gamma}{\gamma-1}} \quad (2.76)$$

$$\frac{\rho}{\rho^*} = \frac{1 + \gamma M^2}{(1 + \gamma)M^2} \quad (2.77)$$

Example 2.12 The combustion chamber in a ramjet engine has the following characteristics:

$$T_{01} = 360 \text{ K}, \quad T_{02} = 1440 \text{ K}, \quad M_2 = 0.9.$$

It is required to calculate:

- The inlet Mach number M_1
- The amount of heat added

Assume that $\gamma = 1.3$ and $R = 287 \text{ J/kg.K}$

Solution

From Eq. (2.69)

$$M_1^2 \left(1 + \frac{\gamma - 1}{2} M_1^2 \right) = \frac{T_{01}}{T_{02}} \frac{M_2^2 (1 + \frac{\gamma - 1}{2} M_2^2)}{(1 + \gamma M_2^2)^2} (1 + \gamma M_1^2)^2$$

$$M_1^4 \left(\gamma^2 A - \frac{\gamma - 1}{2} \right) + M_1^2 (2\gamma A - 1) + A = 0$$

Where $A = \frac{T_{01}}{T_{02}} \frac{M_2^2 (1 + \frac{\gamma - 1}{2} M_2^2)}{(1 + \gamma M_2^2)^2} = \frac{360}{1440} \frac{(0.9)^2 [1 + 0.15 \times (0.9)^2]}{[1 + 1.3 \times (0.9)^2]^2} = 0.0538823$

$$M_1^4 (-0.0589389) + M_1^2 (-0.0859906) + 0.0538823 = 0$$

$$M_1^2 = 0.0623939$$

Thus $M_1 = 0.24979$

Since

$$Cp = \frac{\gamma R}{\gamma - 1} = \frac{1.3 \times 287}{0.3} = 1243.67 \text{ J/kg.K}$$

The heat added is then from energy equation:

$$Q = h_{02} - h_{01} = Cp(T_{02} - T_{01}) = 1243.67(1440 - 360) = 1,343,160 \text{ J/kg.K}$$

$$Q = 1343.16 \text{ kJ/kg.K}$$

Example 2.13 The combustion chamber in a turbojet engine has the following inlet conditions:

$T_{01} = 500 \text{ K}$, $P_{01} = 15 \text{ bar}$, $M_1 = 0.15$, $\dot{m}_1 = 200 \text{ kg/s}$, the exit temperature is $T_{02} = 1500 \text{ K}$, and fuel-to-air ratio is $f = 0.0273$. Calculate:

1. Inlet area of combustor (A_1)
2. The total pressure ratio across the combustor
3. Mach number and area at combustor outlet (M_2, A_2)

Assume that $\gamma = 1.4$ and $R = 287 \text{ J/kg.K}$

Solution

The static temperature and pressure at inlet are

$$T_1 = \frac{T_{01}}{1 + \frac{\gamma - 1}{2} M_1^2} = \frac{500}{1 + 0.2 \times (0.15)^2} = 497.8 \text{ K}$$

$$P_1 = \frac{P_{01}}{\left(1 + \frac{\gamma-1}{2} M^2\right)^{\frac{\gamma}{\gamma-1}}} = \frac{15}{\left(1 + 0.2 \times (0.15)^2\right)^{3.5}} = 14.766 \text{ bar}$$

$$V_1 = M_1 a_1 = M_1 \sqrt{\gamma R T_1} = 0.15 \times \sqrt{1.4 \times 287 \times 500} = 67.23 \text{ m/s}$$

$$\rho_1 = \frac{P_1}{R T_1} = 10.335 \text{ kg/m}^3$$

$$A_1 = \frac{\dot{m}_1}{\rho_1 V_1} = \frac{200}{10.335 \times 67.23} = 0.288 \text{ m}^2$$

To evaluate Mach number at combustor outlet, we can use Eq. (2.69):

$$\begin{aligned} \frac{T_{02}}{T_{01}} = 3 &= \left(\frac{1 + 1.4 \times [0.15]^2}{1 + 1.4 \times M_2^2} \right)^2 \left(\frac{M_2}{0.15} \right)^2 \left(\frac{1 + 0.2 M_2^2}{1 + 0.2 \times [0.15]^2} \right) \\ 3 &= 47.08 \times \frac{M_2^2 \times (1 + 0.2 M_2^2)}{(1 + 1.4 \times M_2^2)^2} \end{aligned}$$

The above equation is solved by trial and error to obtain $M_2 = 0.277$

Now the total pressure ratio across the combustor is obtained from Eq. (2.70); thus,

$$\begin{aligned} \frac{P_{02}}{P_{01}} &= \frac{1 + 1.4 \times (0.15)^2}{1 + 1.4 \times (0.277)^2} \left(\frac{1 + 0.2 \times (0.277)^2}{1 + 0.2 \times (0.15)^2} \right)^{3.5} = \frac{1.0315}{1.1074} \times 1.0383 \\ \frac{P_{02}}{P_{01}} &= 0.9671 \end{aligned}$$

The static properties at the outlet of combustion chamber are obtained from relations (2.67), (2.68), and (2.71).

$$\begin{aligned} \frac{P_2}{P_1} &= \left[\frac{1 + 1.4 \times 0.15^2}{1 + 1.4 \times 0.277^2} \right] = 0.93144 \\ \frac{T_2}{T_1} &= \left(\frac{1 + 1.4 \times 0.15^2}{1 + 1.4 \times 0.277^2} \times \frac{0.277}{0.15} \right)^2 = 2.9586 \\ \frac{\rho_2}{\rho_1} &= \left(\frac{0.15}{0.277} \right)^2 \left(\frac{1 + 1.4 \times 0.277^2}{1 + 1.4 \times 0.15^2} \right) = 0.3148 \\ \rho_2 &= 3.2535 \text{ kg/m}^3, \quad T_2 = 1472.8 \text{ K} \\ V_2 &= M_2 \sqrt{\gamma R T_2} = 213 \text{ m/s} \end{aligned}$$

The outlet mass flow rate is $\dot{m}_2 = \dot{m}_1 (1 + f) = 200(1 + 0.0273) = 205.46 \text{ kg/s}$

The outlet area of combustor is then

$$A_2 = \frac{\dot{m}_2}{\rho_2 V_2} = \frac{205.46}{3.2535 \times 213} = 0.2965 \text{ m}^2$$

2.6 The Standard Atmosphere

For a fluid in rest without shearing stresses, any elementary fluid element will be subjected to two types of forces, namely, *surface forces* due to the pressure and a *body force* equal to the weight of the element. Force balance will yield the following relation:

$$\nabla p = -\gamma \bar{k}$$

where γ is the specific weight of fluid and \bar{k} is the unit vector in the positive vertical direction (opposite to the gravitational force) and

$$\gamma = \rho g$$

Thus,

$$\frac{\partial p}{\partial x} = 0, \quad \frac{\partial p}{\partial y} = 0, \quad \frac{\partial p}{\partial z} = -\gamma = -\rho g \quad (2.78)$$

The first two derivatives in Eq. (2.78), show that the pressure does not depend on x or y . Thus, as we move from one point to another in a horizontal plane (any plane parallel to the x - y plane), the pressure does not change. Since p depends only on z , the last of Eq. (2.78) can be written as the ordinary differential equation

$$\frac{dp}{dz} = -\gamma = -\rho g \quad (2.79)$$

Equation (2.79) is the fundamental equation for fluids at rest and can be used to determine how pressure changes with elevation. This equation indicates that the pressure gradient in the vertical direction is negative; that is, the pressure decreases as we move upward in a fluid at rest. For the Earth's atmosphere where the variations in heights are large, on the order of thousands of feet, attention must be given to the variation in the specific weight (γ). Since air may be considered an ideal (or perfect) gas, its equation of state ($p = \rho RT$) is used.

This relationship can be combined with Eq. (2.79) to give

$$\frac{dp}{dz} = -\frac{gp}{RT}$$

and by separating variables

$$\int_{p_1}^{p_2} \frac{dp}{p} = \ln \frac{p_2}{p_1} = -\frac{g}{R} \int_{z_1}^{z_2} \frac{dz}{T} \quad (2.80)$$

where g and R are assumed to be constant over the range of elevation involved.

Equation (2.80) relates to the variation in pressure in the Earth's atmosphere.

Ideally, we would like to have measurements of pressure versus altitude over the specific range of altitude. However, this type of information is usually not available. Thus, a "standard atmosphere" has been determined that can be used in the design of aircraft and rockets. The concept of a standard atmosphere was first developed in the 1920s, and since that time many US and international committees and organizations have pursued the development of such a standard. The currently accepted standard atmosphere is based on a report published in 1962 and updated in 1976 [11, 12], defining the so-called *US standard atmosphere*, which is an idealized representation of middle-latitude, year-round mean conditions of the Earth's atmosphere. Figure 2.27 shows the temperature profile for the US standard atmosphere.

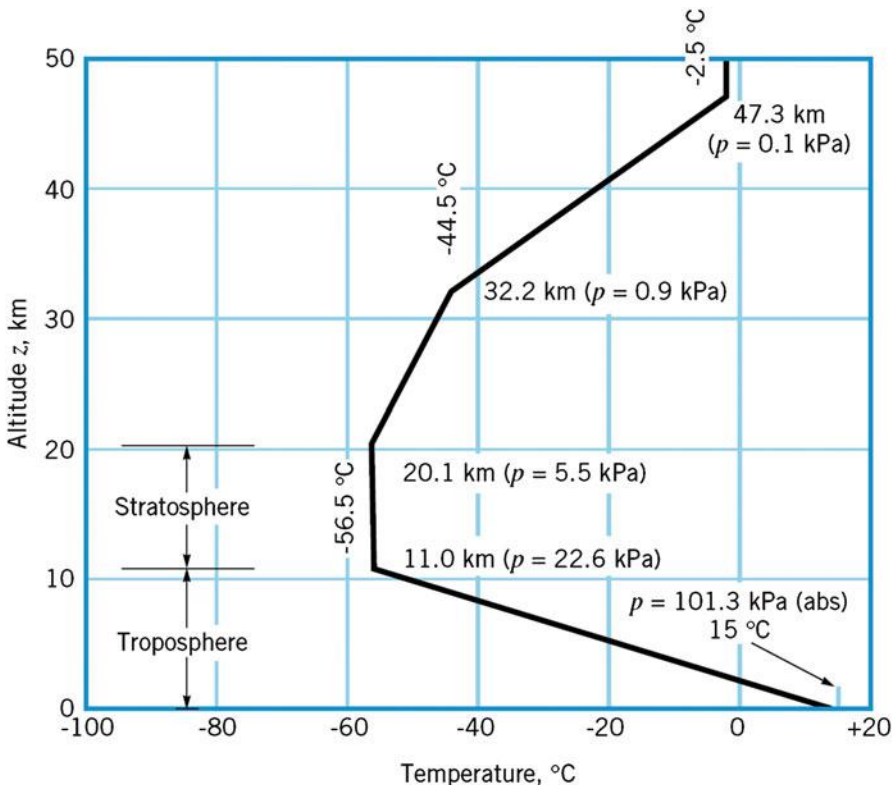


Fig. 2.27 Variation of temperature with altitude in the US Standard Atmosphere

As is shown in this figure, the temperature decreases with altitude in the region nearest the Earth's surface (*troposphere*), then becomes essentially constant in the next layer (*stratosphere*), and subsequently starts to increase in the next layer. Since the temperature variation is represented by a series of linear segments, it is possible to integrate Eq. (2.80) to obtain the corresponding pressure variation. For example, in the troposphere, which extends to an altitude of about 11 km ($\approx 36,000$ ft), the temperature variation is of the form

$$T = T_a - \beta z \quad (2.81a)$$

where T_a is the temperature at sea level ($z = 0$) and β is the *lapse rate* (the rate of change of temperature with elevation), $0.00356616^\circ\text{F}/\text{ft}$, or $0.0019812^\circ\text{C}/\text{ft}$. For the standard atmosphere in the troposphere, and if (z) represents altitude in feet, then Eq. (2.81a) may be further expressed as

$$T = 518.67 - 0.00356616 z^\circ\text{R} \quad (2.81b)$$

$$T = 288.15 - 0.0019812 z^\circ\text{K} \quad (2.81c)$$

$$t = 59 - 0.00356616 z^\circ\text{F} \quad (2.81d)$$

$$t = 15 - 0.0019812 z^\circ\text{C} \quad (2.81e)$$

Equation (2.81a) together with Eq. (2.80) yields

$$p = p_a \left(1 - \frac{\beta z}{T_a} \right)^{\frac{g}{\beta R}} \quad (2.82)$$

where (p_a) is the absolute pressure at $z = 0$. With $p_a = 101.33$ kPa, $T_a = 288.15$ K and $g = 9.807 \text{ m/s}^2$, and with the gas constant $R = 286.9 \text{ J/kg.K}$. The pressure variation throughout the troposphere can be determined from Eq. (2.82). This calculation shows that at the outer edge of the troposphere, where the temperature is -56.5°C , the absolute pressure is about 23 kPa. It is to be noted that modern jetliners cruise at approximately this altitude.

For the stratosphere atmospheric layer (between 11.0 and 20.1 km), the temperature has a constant value (*isothermal conditions*) which is -56.5°C (or -69.7°F , 389.97°R , 216.65°K).

It then follows from Eq. (2.80), the pressure-elevation relationship expressed as

$$p = p_0 \exp \left[-\frac{g(z - z_0)}{RT_0} \right] \quad (2.83)$$

where p_0 , T_0 , and z_0 are the pressure, temperature, and altitude of the lower edge of the stratosphere (23 kPa, -56.5°C , 36,000 ft).

Figure 2.28 illustrates the variation of temperature with altitude. Figure 2.29 illustrates flight altitudes appropriate to different aircrafts. Table 2.9 defines the properties of the Earth standard atmosphere [12].

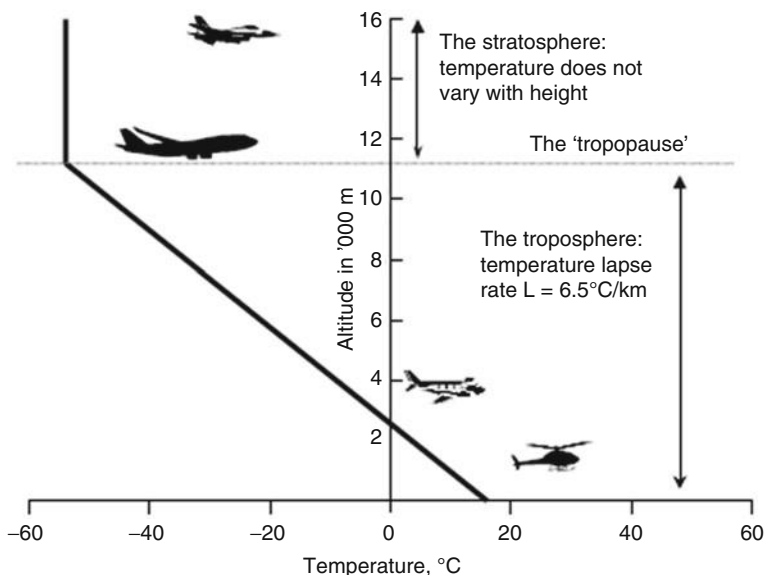


Fig. 2.28 The ISA: variation of temperature with altitude

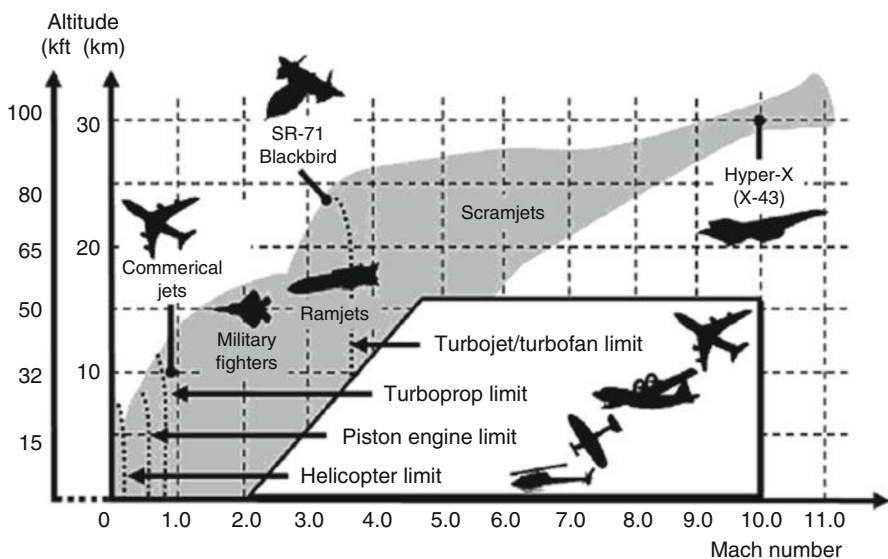


Fig. 2.29 Flight envelopes of aircraft with different engine types

Table 2.9 Properties of the Earth's standard atmosphere (Ref. [12])

Altitude (m)	Temperature (K)	Pressure ratio	Density
			(kg/m ³)
0 (sea level)	288.150	1.0000	1.2250
1000	281.651	8.87×10^{-1}	1.11117
3000	268.650	6.6919×10^{-1}	0.90912
5000	255.65	5.3313×10^{-1}	0.76312
10,000	223.252	2.6151×10^{-1}	4.1351×10^{-1}
25,000	221.552	2.5158×10^{-2}	4.0084×10^{-2}
50,000	270.650	7.8735×10^{-4}	1.0269×10^{-3}
75,000	206.650	2.0408×10^{-5}	3.4861×10^{-5}
100,000	195.08	3.1593×10^{-7}	5.604×10^{-7}
130,000	469.27	1.2341×10^{-8}	8.152×10^{-9}
160,000	696.29	2.9997×10^{-9}	1.233×10^{-9}
200,000	845.56	8.3628×10^{-10}	2.541×10^{-10}
300,000	976.01	8.6557×10^{-11}	1.916×10^{-11}
400,000	995.83	1.4328×10^{-11}	2.803×10^{-12}
600,000	999.85	8.1056×10^{-13}	2.137×10^{-13}
1,000,000	1000.00	7.4155×10^{-14}	3.561×10^{-15}

Problems

- 2.1 Calculate the Mach number for a flight vehicle flying at a speed of 10,000 km/h at the following altitudes:
 sea level – 10,000 m – 25,000 m – 50,000 m – 100,000 m – 200,000 m – 400,000 m – 1,000,000 m.
- 2.2 Describe probe-and-drogue air-to-air refueling system.
- 2.3 What are the advantages of refueling a military aircraft?
- 2.4 **Tornado GR4** refueling from the drogue of an RAF **VC10** tanker as shown in figure Problem 2.4 at the rate of 600 gal/min of fuel having a specific gravity of 0.75. The inside diameter of hose is 0.14 m. The fluid pressure at the entrance of the fighter plane is 40 kPa gage. What additional thrust does the plane need to develop to maintain the constant velocity it had before the hookup?



Figure (Problem 2.4)

2.5 Fighter airplane is *refueling from the DC-10 tanker* as shown in figure Problem 2.5 at the rate of 700 gal/min of fuel having a specific gravity of 0.72. The inside diameter of hose is 0.13 m. The fluid pressure at the entrance of the fighter plane is 45 kPa gage. What additional thrust does the plane need to develop to maintain the constant velocity it had before the hookup?



Figure (Problem 2.5)

- 2.6 A jet plane is on the runway after touching down. The pilot puts into play movable vanes to achieve a reverse thrust from his two engines. Each engine takes in 50 kg of air per second, The fuel-to-air ratio is 1–40. If the exit velocity of the combustion products is 800 m/s relative to the plane, what is the total reverse thrust of the airplane if it is moving at a speed of 180 km/h? The exit jets are close to atmospheric pressure.

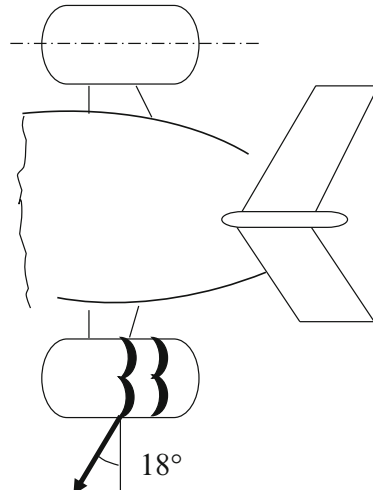


Figure (Problem 2.6)

- 2.7 A fighter plane is climbing at an angle θ of 60° at a constant speed of 900 Km/h. The plane takes in air at a rate of 450 kg/s. The fuel-to-air ratio is 2 %. The exit speed of the combustion products is 1800 m/s relative to the plane. If the plane changes to an inclination angle θ of 20° , what will be the speed of the plane when it reaches uniform speed? The new engine settings are such that the same amount of air taken in and the exhaust speed relative to the plane are the same. The plane weights 150 kN. The drag force is proportional to the speed squared of the plane.
- 2.8 If the fighter plane in problem (2.7) is climbing also at an angle $\theta = 60^\circ$ but at a constant acceleration (a). The weight, thrust, and drag forces are 150, 715, and 500 kN, respectively. Calculate the acceleration (a). Next, the plane changes its angle to 20° , while the air mass flow rate is 450 kg/s, exhaust speed of gases is 1800 m/s, and fuel-to-air ratio is 2 %. For the same value of acceleration calculated above and if the drag force is proportional to the speed squared of the plane, what will be the aircraft velocity.
- 2.9 Figure Problem (2.9) illustrates [supersonic jet fighter aircraft](#) Mikoyan-Gurevich MiG-21. One type of its armament is Nudelman-Rikhter NR-30, twin-barrel 23 mm GSh-23 cannon. It had a muzzle velocity of 800 m/s. Each bullet (cartridge) is 30×155 mm and has a mass of 400 [grams](#) and a rate of fire of 900 cycles per minute. What is the additional thrust needed to keep a constant aircraft speed of 600 km/h? (Neglect the change of mass of aircraft.)

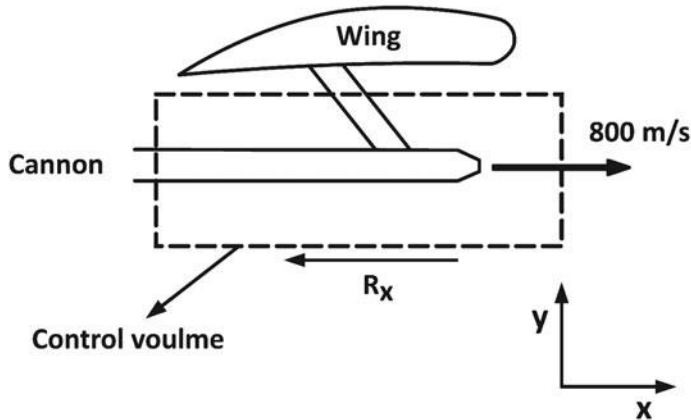


Figure (Problem 2.9)

2.10 If the specific heat at constant pressure is expressed by the relation

$$\frac{C_p}{R} = \frac{7}{2} + \left[\frac{T_R/(2T)}{\sinh\{T_R/(2T)\}} \right]^2$$

where the reference temperature $T_R = 3060\text{ K}$, plot C_p , C_v , γ and h of air as a function of T/T_R over the range 300 to 3800 K.

2.11 A rocket engine uses nitric acid as oxidizer. The oxidizer flow rate is 2.60 kg/s and a fuel flow of 0.945 kg/s. Thus, the propellant flow rate is 3.545 kg/s. If the flow leaves the nozzle at 1900 m/s through an area of 0.012 m² with a pressure of 110 kPa, what is the thrust of the rocket motor?

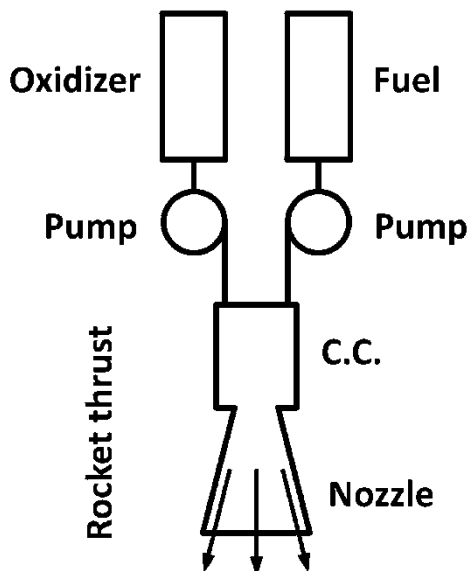


Figure (Problem 2.11)

- 2.12 A rocket is designed to have four nozzles, each canted at 30° with respect to the rocket's centerline. The gases exit at 2200 m/s through the exit area of 1.2 m^2 . The density of the exhaust gases is 0.3 kg/m^3 , and the exhaust pressure is 55 kPa . The atmospheric pressure is 12 kPa . Determine the thrust on the rocket.

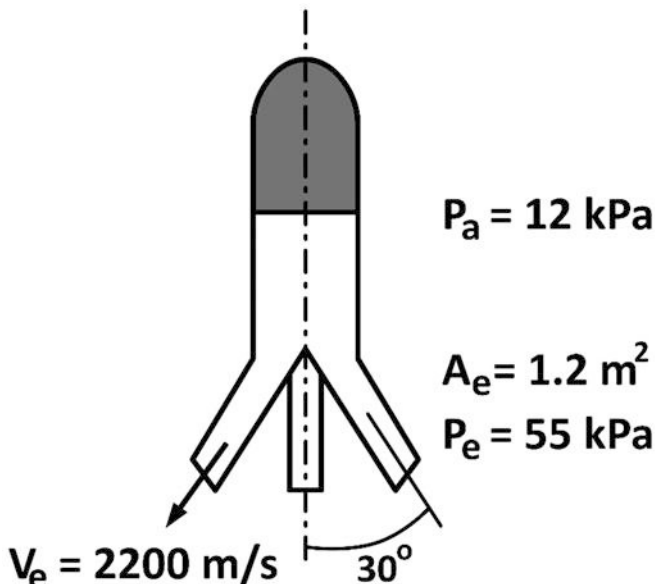


Figure (Problem 2.12)

- 2.13 A convergent nozzle has an exit area of 500 mm^2 . Air enters the nozzle with a stagnation pressure of 1000 kPa and a stagnation temperature of 360 K. Determine the mass rate of flow for back pressures of 850, 528, and 350 kPa, assuming isentropic flow.
- 2.14 A converging–diverging nozzle has an exit area to throat area ratio of 2. Air enters this nozzle with a stagnation pressure of 1000 kPa and a stagnation temperature of 460 K.
- The throat area is 500 mm^2 . Determine the mass rate of flow, exit pressure, exit temperature, exit Mach number, and exit velocity for the following conditions:
- Sonic velocity at the throat, diverging section acting as a nozzle (corresponds to point G in Fig. 2.18)
 - Sonic velocity at the throat, diverging section acting as a diffuser (corresponding to point C in Fig. 2.18)

- 2.15 An oblique shock wave has the following data

$$M_1 = 3.0, \quad P_1 = 1 \text{ atm}, \quad T_1 = 288 \text{ K}, \quad \gamma = 1.4, \quad \delta = 20^\circ$$

- Compute shock wave angle (weak)
- Compute P_{02} , T_{02} , P_2 , T_2 , M_2 behind shock

References

- Shames I (2002) Mechanics of fluids, 4th edn. McGraw-Hill, New York
- White FM (2010) Fluid mechanics, 7th edn. McGraw-Hill, New York
- Shapiro AH (1953) The dynamics and thermodynamics of compressible fluid flow, vol 1. Wiley, New York
- Zucrow MJ, Hoffman JD (1976) Gas dynamics, vol 1. Wiley, New York
- Zucker RD, Biblarz O (2002) Fundamentals of gas dynamics, 2nd edn. Wiley, Hoboken, New Jersey
- Keenan JH (1941) Thermodynamics. Wiley, New York
- Sonntag RE, Borgnakke C, Van Wylen GJ (2002) Fundamentals of thermodynamics, 6th edn. Wiley, New York
- Cengel's Y, Boles's M (2010) Thermodynamics: an engineering approach, 7th edn. McGraw-Hill, New York
- Compressible Flow Data Book for Engineering Tripos (2004) Cambridge University Engineering Department
- Equations, Tables and Charts for Compressible Flow (1953) NACA Report 1153, Ames Research Staff
- The U.S. Standard Atmosphere (1962) U.S. Government Printing Office, Washington, DC
- The U.S. Standard Atmosphere (1976) U.S. Government Printing Office, Washington, DC

Chapter 3

Performance Parameters of Jet Engines

3.1 Introduction

The designer of an aircraft engine must recognize the differing requirements for take-off, climb, cruise, and maneuvering. The relative importance of these being different for civil and military applications and for long- and short-haul aircrafts. In the early aircrafts, it was common practice to focus on the take-off thrust. This is no longer adequate for later and present day aircrafts. For long-range civil transports like Boeing 747, 777, 787 and Airbus A 340, A380 (the world's truly double-deck airliner), A350 XWB (extra wide body), the fuel consumption through some 10 or more flight hours is the dominant parameter. Military aircrafts have numerous criteria like the rate of climb, maneuverability for fighters, short take-off distance for aircrafts operating from air carriers, maximum ceilings for high altitude reconnaissance aircrafts like SR-71 Blackbird aircrafts. For civil and military freighter airplanes, the maximum payload is its main requirement.

In all types of aircrafts, the engines are requested to provide efficiently the thrust force necessary for their propelling during different flight phases and at different operating conditions including hottest/coldest ambient temperature and rainy/windy/snowing weather.

This chapter resembles a first window for air breathing engines. It starts by a derivation for the thrust force or the propelling force generated in the direction opposite to the flow of air entering the engine in accordance with Newton's laws of motion. Consequently, all jet engines including rocket motors belong to the class of power plants called *reaction engines*. It is the internal imbalance of forces within the gas turbine engines that give all reaction engines their names. The propulsive force developed by a jet engine is the result of a complex series of actions and reactions that occur within the engine. The thrust constituents and the different factors affecting the thrust are next explained. Some of these factors are related to the engine, others are related to the medium in which the engine operates.

The performance of jet engines is evaluated through the following efficiencies: propulsive, thermal, and overall. The propeller efficiency of turboprop engines is also evaluated. Fuel consumption is properly evaluated through a parameter identified as the thrust-specific fuel consumption, which is the ratio of fuel flow rate into the engine to the generated thrust. Thus different jet engines may be compared. The range of aircraft is a combined engine/aircraft parameter where the fuel consumption through the engine is coupled to the aircraft's lift and drag forces.

3.2 Thrust Force

Thrust force is the force responsible for propelling the aircraft in its different flight regimes.

It is in addition to the lift, drag, and weight represent the four forces that govern the aircraft motion. During the cruise phase of flight, where the aircraft is flying steadily at a constant speed and altitude, each parallel pair of the four forces are in equilibrium (lift and weight as well as thrust and drag). During landing, thrust force is either fully or partially used in braking of the aircraft through a thrust reversing mechanism. The basic conservation laws of mass and momentum are used in their integral forms to derive an expression for thrust force.

As described in example (2.1) and Fig. 2.4, the thrust generated by a turbojet is given by the relation:

$$T = \dot{m}_a[(1+f)u_e - u] + (P_e - P_a)A_e \quad (3.1)$$

where

$$\text{Net thrust} = T$$

The other types of thrusts are

$$\text{Gross thrust} = \dot{m}_a[(1+f)u_e] + (P_e - P_a)A_e$$

$$\text{Momentum thrust} = \dot{m}_a[(1+f)u_e]$$

$$\text{Pressure thrust} = (P_e - P_a)A_e$$

$$\text{Momentum drag} = \dot{m}_a u$$

$$\text{Thus: } \text{Net thrust} = \text{Gross thrust} - \text{Momentum drag}$$

$$\text{Or in other words, } \text{Net thrust} = \text{Momentum thrust} + \text{Pressure thrust} - \text{Momentum drag}$$

If the nozzle is unchoked, then $P_e = P_a$, the pressure thrust cancels in Eq. (3.1). The thrust is then expressed as

$$T = \dot{m}_a[(1+f)u_e - u] \quad (3.2)$$

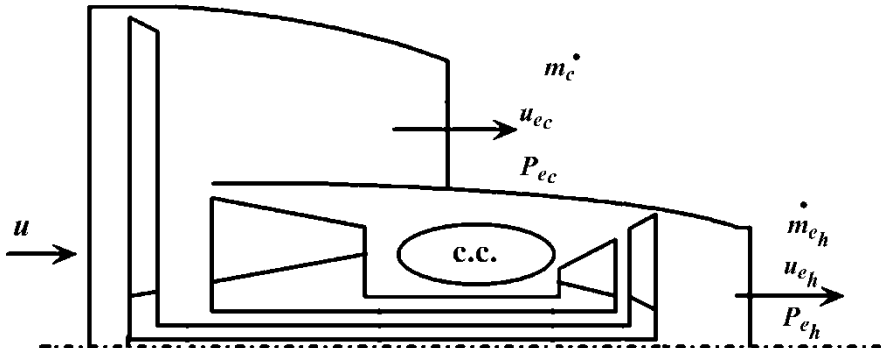


Fig. 3.1 An unmixed two-spool turbofan engine

In many cases the fuel to air ratio is negligible, thus the thrust force equation is reduced to the simple form:

$$T = \dot{m}_a(u_e - u) \quad (3.3)$$

The thrust force in turbojet engine attains high values as the exhaust speed is high and much greater than the flight speed, or: $u_e/u \gg 1$.

In a similar way, the thrust force for two stream engines like *turbofan* (Fig. 3.1) and *prop fan* engines can be derived. It will be expressed as

$$T = \dot{m}_h[(1+f)u_{eh} - u] + \dot{m}_c(u_{ec} - u) + A_{eh}(P_{eh} - P_a) + A_{ec}(P_{ec} - P_a) \quad (3.4)$$

where

$f = \frac{\dot{m}_f}{\dot{m}_h}$; fuel to air ratio

\dot{m}_h : Air mass flow passing through the hot section of engine; turbine(s)

$\dot{m}_{e_h} = \dot{m}_h(1+f)$: Mass of hot gases leaving the engine

\dot{m}_c : Air mass flow passing through the fan

u_{eh} : Velocity of hot gases leaving the turbine nozzle

u_{ec} : Velocity of cold air leaving the fan nozzle

P_{eh} : Exhaust pressure of the hot stream

P_{ec} : Exhaust pressure of the cold stream

A_{eh} : Exit area for the hot stream

A_{ec} : Exit area for the cold stream

The *specific thrust* is defined as the thrust per unit air mass flow rate (T/\dot{m}_a), which can be obtained from Eq. (3.4). It has the dimensions of a velocity (say m/s).

For turboprop engines (Fig. 3.2), the high value of thrust is achieved by the very large quantity of the airflow rate, though the exhaust and flight speeds are very close. An analogous formula to Eq. (3.4) may be employed as follows:

$$T = \dot{m}_c[(1+f)u_e - u_1] + \dot{m}_0(u_1 - u_0) \quad (3.5)$$

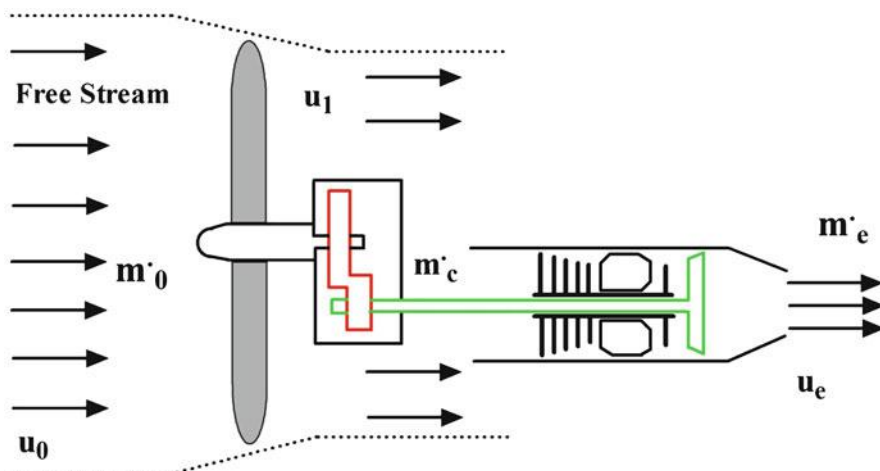


Fig. 3.2 Turboprop engine

where \dot{m}_0 is the air mass flow sucked by the propeller, while \dot{m}_c is a part of the air flow crossed the propeller and then entered the engine through its intake. Here, u_0 , u_1 , and u_e are air speed upstream and downstream the propeller and gases speed at the engine exhaust. The exhaust nozzle is normally unchoked.

Example 3.1 Air flows through a turbojet engine at the rate of 50.0 kg/s and the fuel flow rate is 1.0 kg/s. The exhaust gases leave the jet nozzle with a relative velocity of 600 m/s. Compute the velocity of the airplane, if the thrust power is 1.5 MW in the following two cases:

1. Pressure equilibrium exists over the exit plane
2. If the pressure thrust is 8 kN

Solution

1. When the nozzle is unchoked, pressure equilibrium exists over the exit plane. Then, thrust force is expressed as

$$T = (\dot{m}_a + \dot{m}_f)u_e - \dot{m}_a u$$

$$\text{Thrust power} = T \times u$$

$$\text{Thrust power} = (\dot{m}_a + \dot{m}_f)u_e u - \dot{m}_a u^2$$

$$1.5 \times 10^6 = (51)(600)u - 50u^2$$

$$50u^2 - 30,600u + 1.5 \times 10^6 = 0$$

$$\text{or } u = \frac{30,600 \pm 10^3 \sqrt{936.36 - 300}}{100}$$

Thus, either $u = 558.26$ m/s or $u = 53.74$ m/s

2. When the exit pressure is greater than the ambient pressure, a pressure thrust (T_p) is generated. The thrust equation with pressure thrust is then

$$T = (\dot{m}_a + \dot{m}_f)u_e - \dot{m}_a u + T_p$$

Thus, the thrust power is

$$\begin{aligned} T \times u &= (\dot{m}_a + \dot{m}_f)u_e u - \dot{m}_a u^2 + T_p \times u = [(\dot{m}_a + \dot{m}_f)u_e + T_p] \times u - \dot{m}_a u^2 \\ 1.5 \times 10^6 &= [51 \times 600 + 8000] \times u - 50u^2 = 38,600 u - 50 u^2 \\ 50 u^2 - 38,600 u + 1.5 \times 10^6 &= 0 \\ u &= \frac{38,600 \pm 10^3 \sqrt{1490 - 300}}{100} = \frac{38,600 \pm 34,495}{100} \end{aligned}$$

Thus either $u = 731$ m/s or 41 m/s

Example 3.2 A fighter airplane is powered by two turbojet engines. It has the following characteristics during cruise flight conditions:

Wing area (S) = 49.24 m^2

Engine inlet area $A_i = 0.06 \text{ m}^2$

Cruise speed $V_f = 243 \text{ m/s}$

Flight altitude = 35,000 ft

Drag and lift coefficients are $C_D = 0.045$, $C_L = 15 C_D$

Exhaust total temperature $T_0 = 1005 K$

Specific heat ratio and specific heat at exit are $\gamma = 1.3$, $C_p = 1100 \text{ J/(kgK)}$

It is required to calculate:

1. Net thrust
2. Gross thrust
3. Weight
4. Jet speed assuming exhaust pressure is equal to ambient pressure if $P_e = P_a$
5. Static temperature of exhaust T_e
6. Exhaust Mach number M_e

Solution

At 35,000 m altitude, the properties of ambient conditions are

Temperature $T = -54.3^\circ\text{C}$, pressure $P = 23.84 \text{ kPa}$, and density 0.3798 kg/m^3

The mass flow rate is $\dot{m} = \rho_a V_f A_i = 0.3798 \times 243 \times 0.6 = 55.375 \text{ kg/m}^3$

1. During cruise flight segment, the thrust and drag force (D) are equal. Thus for two engines and (T) is the net thrust of each engine, then

$$2T = D = \rho V^2 A C_D / 2$$

$$T = 0.3798 \times (243)^2 \times 49.24 \times 0.045 / 4 = 12,423 \text{ N} = 12.423 \text{ kN}$$

2. Gross thrust = Net thrust + Ram drag

$$T_{\text{gross}} = T + \dot{m} V_f = 12,423 + 55.3 \times 243 = 25,879 \text{ N} = 25.879 \text{ kN}$$

3. Since Weight = Lift, thus $L = W$.

Moreover, lift and drag are correlated by the relation:

$$C_L = 15 C_D = 0.675$$

$$L = W = 15D = 30T = 37,2690 \text{ N} = 372.69 \text{ kN}$$

4. Assuming negligible fuel flow ratio, and since $P_e = P_a$, then the net thrust is expressed by the relation:

$$T = \dot{m} (V_J - V_f)$$

$$V_J = V_f + \frac{T}{\dot{m}} = 243 + \frac{12,423}{55.375} = 467.3 \text{ m/s}$$

5. Exhaust static temperature is expressed by the relation:

$$T_e = T_{0e} - \frac{V_j^2}{2C_p} = 1005 - \frac{(467)^2}{2 \times 1100} = 905.9 \text{ K}$$

6. Sonic speed at exit $a_e = \sqrt{\gamma RT} = \sqrt{1.3 \times 287 \times 905.7} = 581.3 \text{ m/s}$

Exhaust Mach number is $M_e = \frac{V_j}{a_e} = 0.804$

Example 3.3 It is required to calculate and plot the momentum drag as well as momentum, pressure, gross, and net thrusts versus the flight speed for a turbojet engine powering an aircraft flying at 9 km (ambient temperature and pressure are 229.74 K and 30.8 kPa) and having the following characteristics, $A_i = 0.24 \text{ m}^2$, $A_e = 0.26 \text{ m}^2$, $f = 0.02$, $U_e = 600 \text{ m/s}$, $P_e = 87.50 \text{ kPa}$.

The flight speed varies from 500 to 4000 km/h. Consider the following cases:

The air mass flow rate is constant and equal to 40 kg/s irrespective of the variation of flight speed.

- A. Air mass flow rate varies with the flight speed
- B. Repeat the above procedure for altitudes 3, 6, and 12 km considering a variable air mass flow rate and a constant exhaust pressure of $P_e = 87.50 \text{ kPa}$
- C. Repeat the above procedure for altitudes 3, 6, 9, and 12 km considering a variable air mass and a variable exhaust pressure given by the relation: $P_e/P_{alt} = 1.25$

Solution

- A. The mass flow rate is constant and equal to 40 kg/s at altitude 9 km

The momentum thrust (T_{momentum}) is constant and given by the relation

$$T_{\text{momentum}} = \dot{m}_a(1+f)U_e = 40 \times 1.02 \times 600 = 24,480 \text{ N}$$

The pressure thrust (T_{pressure}) is also constant and calculated as

$$T_{\text{pressure}} = A_e \times (P_e - P_a) = 0.26 \times (87.5 - 30.8) \times 10^3 = 14,742 \text{ N}$$

The gross thrust (T_{gross}) is constant and equal to the sum of momentum and pressure thrusts

$$T_{\text{gross}} = T_{\text{momentum}} + T_{\text{pressure}} = 39,222 \text{ N}$$

The momentum drag for flight speed varying from 500 to 4000 km/h is given by the relation:

$$D_{\text{momentum}} = \dot{m}_a U = 40(\text{kg/s}) \times \frac{U(\text{km/hr})}{3.6} = 11.11 \times U \text{ (N)}$$

It is a linear relation in the flight speed U . Flight speed in momentum drag relation and continuity equation will be substituted in km/h.

The net thrust is then (Fig. 3.3)

$$T_{\text{net}} = T_{\text{gross}} - D_{\text{momentum}} = 39,222 - 11.11 \times U \text{ (N)}$$

The net thrust varies linearly with the flight speed. The results are plotted in Fig. 3.4. The net thrust must be greater than the total aircraft drag force during acceleration and equal to the drag at steady cruise flight. Zero net thrust results from the intersection of the gross thrust and ram drag. The flight speed corresponding to zero net thrust represents the maximum possible aircraft's speed.

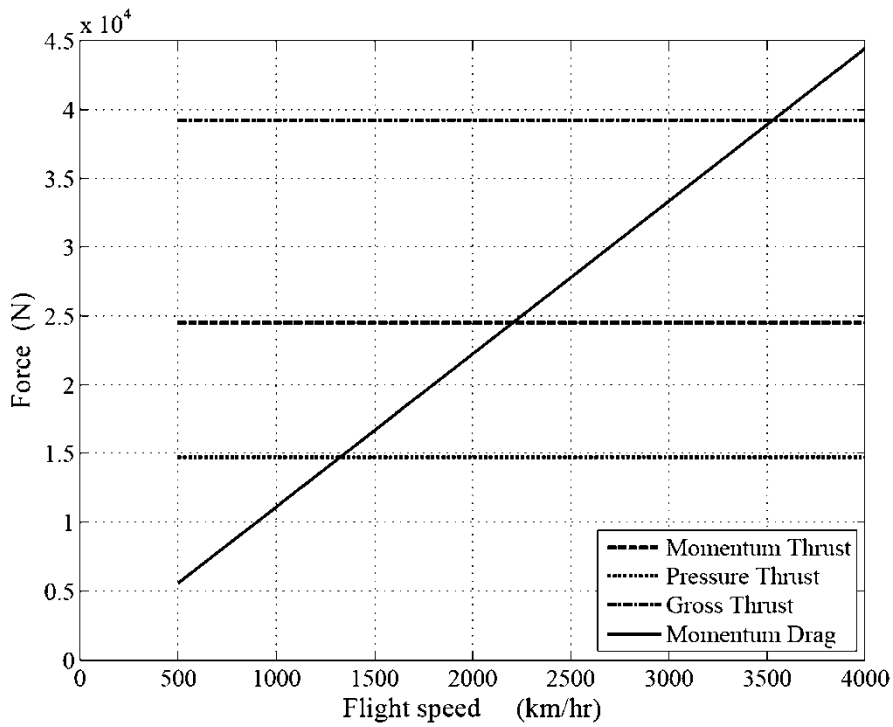


Fig. 3.3 Thrust components and drag with variable flight speed

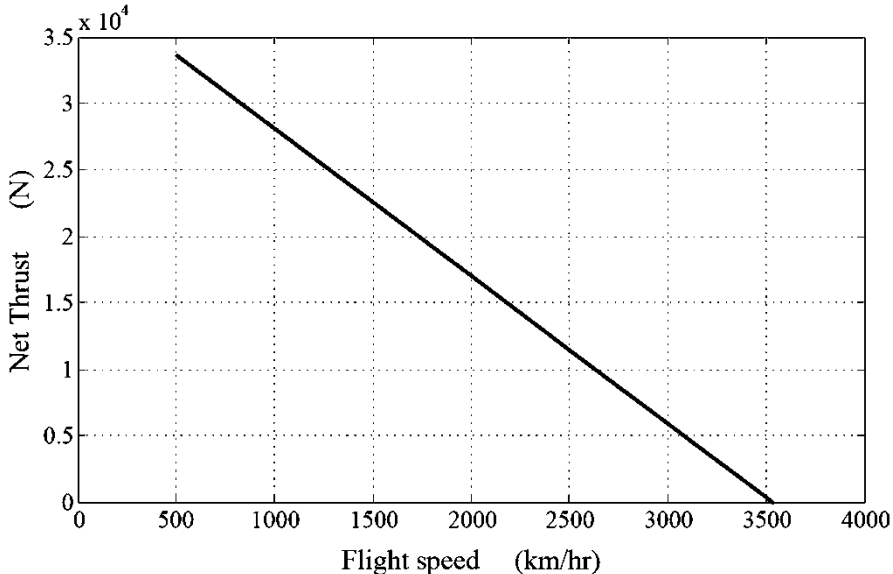


Fig. 3.4 Thrust variations with constant mass flow rate

B. Variable air mass flow rate at altitude 9 km

The mass flow rate varies linearly with the flight speed according to the relation:

$$\dot{m}_a = \rho_a U A_i = \frac{P_a}{R T_a} U A_i = \frac{30.8 \times 10^3}{287 \times 229.74} \times \frac{U}{3.6} \times 0.24 \text{ (kg/s)}$$

$$\dot{m}_a = 0.031141 \times U \text{ (kg/s)}$$

The momentum thrust varies linearly with the flight speed as per the relation

$$T_{\text{momentum}} = \dot{m}_a (1 + f) U_e = 0.031141 \times U \times 1.02 \times 600 = 19.058 \times U \text{ (N)}$$

The pressure thrust is constant and has the same value as in case (1)

$$T_{\text{pressure}} = A_e \times (P_e - P_a) = 0.26 \times (87.5 - 30.8) \times 10^3 = 14,742 \text{ N}$$

The gross thrust is varying linearly with the flight speed

$$T_{\text{gross}} = T_{\text{momentum}} + T_{\text{pressure}} = 19.058 \times U + 14742 \text{ (N)}$$

The momentum drag for flight speed varying from 500 to 4000 km/h is given by the quadratic relation:

$$D_{\text{momentum}} = \dot{m}_a U = 0.031141 \times U \text{ (kg/s)} \times \frac{U \text{ (km/hr)}}{3.6} = 8.65 \times 10^{-3} \times U^2 \text{ (N)}$$

The net thrust is then

$$T_{\text{net}} = T_{\text{gross}} - D_{\text{momentum}} = 19.058 \times U + 14,742 - 8.65 \times 10^{-3} \times U^2 \text{ (N)}$$

The above relations are plotted in Fig. 3.5.

C. Variable mass flow rate at altitudes 3, 6, and 12 km and constant exhaust pressure of $P_e = 87.50 \text{ kPa}$

Air mass flow rate varies linearly with the flight speed according to the relation:

$$\dot{m}_a = \rho_a U A_i = \frac{P_{\text{alt}}}{R T_{\text{alt}}} U A_i = \frac{P_{\text{alt}}}{287 \times T_{\text{alt}}} \times \frac{U}{3.6} \times 0.24$$

$$= 2.32 \times 10^{-4} \times \frac{P_{\text{alt}}}{T_{\text{alt}}} U \text{ (kg/s)}$$

The momentum thrust varies linearly with the flight speed as per the relation

$$T_{\text{momentum}} = \dot{m}_a (1 + f) U_e = 2.32 \times 10^{-4} \times \frac{P_{\text{alt}}}{T_{\text{alt}}} U \times 1.02 \times 600$$

$$= 0.142 \times \frac{P_{\text{alt}}}{T_{\text{alt}}} \times U \text{ (N)}$$

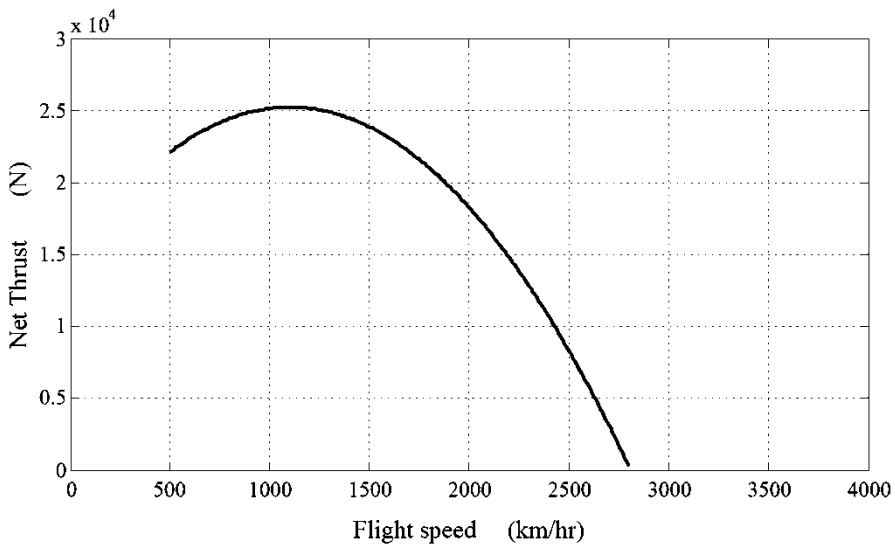


Fig. 3.5 Variations of net thrust with variable mass flow rate

Table 3.1 Values of pressures and temperatures at different altitudes

Altitude (km)	Pressure (kPa)	Temperature (K)
3	70.122	268.66
6	47.2	249.16
9	30.762	229.66
12	19.344	216.66

The pressure thrust is varying with altitude pressure (refer to Table 3.1):

$$T_{\text{pressure}} = A_e \times (P_e - P_{\text{alt}}) = 0.26 \times (87.5 - P_{\text{alt}}) \times 10^3 \text{ (N)}$$

The gross thrust is varying linearly with the flight speed

$$\begin{aligned} T_{\text{gross}} &= T_{\text{momentum}} + T_{\text{pressure}} \\ &= 0.142 \times \frac{P_{\text{alt}}}{T_{\text{alt}}} \times U + 0.26 \times (87.5 - P_{\text{alt}}) \times 10^3 \text{ (N)} \end{aligned}$$

The momentum drag for flight speed varying from 500 to 4000 km/h is given by the quadratic relation:

$$\begin{aligned} D_{\text{momentum}} &= \dot{m}_a U \\ &= 2.32 \times 10^{-4} \\ &\times \frac{P_{\text{alt}}}{T_{\text{alt}}} U(\text{kg/s}) \times \frac{U(\text{km/hr})}{3.6} = 6.44 \times 10^{-5} \times \frac{P_{\text{alt}}}{T_{\text{alt}}} \times U^2 \text{ (N)} \end{aligned}$$

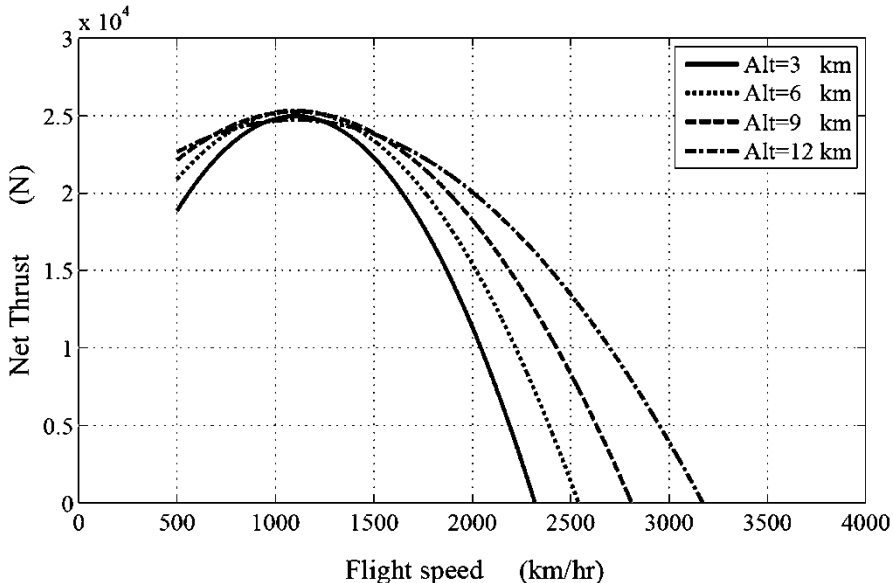


Fig. 3.6 Net thrust variations with variable mass flow rate at different altitudes

The net thrust is then

$$\begin{aligned} T_{\text{net}} &= T_{\text{gross}} - D_{\text{momentum}} \\ &= 0.142 \times \frac{P_{\text{alt}}}{T_{\text{alt}}} \times U + 0.26 \times (87.5 - P_{\text{alt}}) \times 10^3 - 6.44 \times 10^{-5} \times \frac{P_{\text{alt}}}{T_{\text{alt}}} \times U^2 \quad (\text{N}) \end{aligned}$$

The above relation is plotted in Fig. 3.6.

D. *Variable mass flow rate at altitudes 3, 6, 9, and 12 km and variable exhaust pressure based on the relation $P_e/P_{\text{alt}} = 1.25$*

The net thrust is expressed by the relation:

$$\begin{aligned} T_{\text{net}} &= T_{\text{gross}} - D_{\text{momentum}} \\ &= 0.142 \times \frac{P_{\text{alt}}(Pa)}{T_{\text{alt}}(K)} \times U + 0.26 \times (P_e - P_{\text{alt}}) - 6.44 \times 10^{-5} \times \frac{P_{\text{alt}}(Pa)}{T_{\text{alt}}(K)} \times U^2 \quad (\text{N}) \\ T_{\text{net}} &= 0.142 \times \frac{P_{\text{alt}}(Pa)}{T_{\text{alt}}(K)} \times U + 0.26 \times 0.25 \times P_{\text{alt}}(Pa) - 6.44 \times 10^{-5} \times \frac{P_{\text{alt}}(Pa)}{T_{\text{alt}}(K)} \\ &\quad \times U^2 \quad (\text{N}) \end{aligned}$$

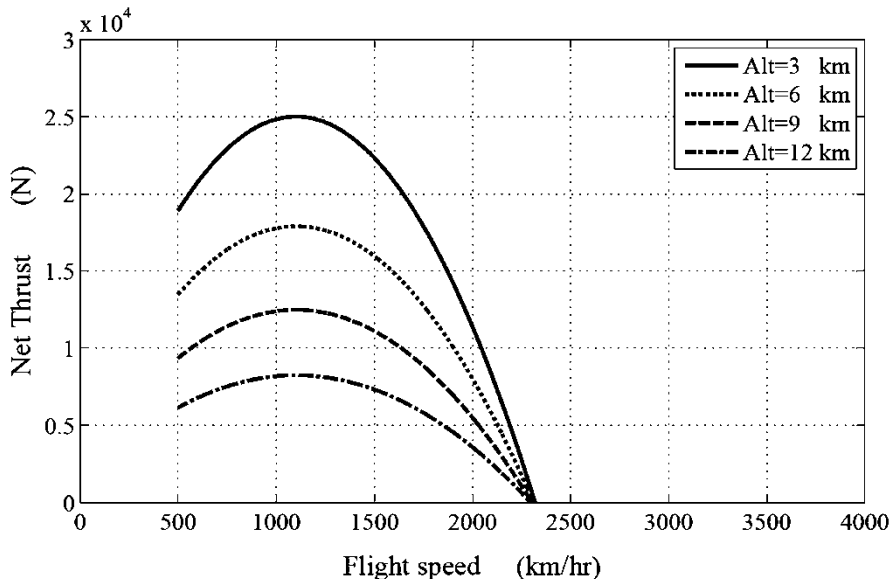


Fig. 3.7 Thrust variations with variable mass flow rate at different altitudes with pressure ratio at exit equals 1.25

For the case of altitude 3 km and flight speed of 600 km/h, then

$$\begin{aligned}
 T_{\text{net}} &= 0.142 \times \frac{70 \times 10^3}{268} \times 600 + 0.26 \times 0.25 \times 70 \times 10^3 (\text{Pa}) - 6.44 \times 10^{-5} \\
 &\quad \times \frac{70 \times 10^3}{268} \times (600)^2 (\text{N}) \\
 T_{\text{net}} &= 22,253 + 4550 - 6055 = 20,748 \text{ N} = 2.0748 \times 10^4 \text{ N}
 \end{aligned}$$

Figure 3.7 illustrates the positive net thrust for different flight speeds and altitudes of 3, 6, 9, and 12 km. It is clarified that the maximum possible flight speed for such an aircraft is nearly 2300 km/h.

It is interesting here to calculate the flight speed that provides a maximum thrust, which is obtained from the relation: $\frac{\partial T_{\text{net}}}{\partial U} = 0$

Since

$$\begin{aligned}
 T_{\text{net}} &= 0.142 \times \frac{P_{\text{alt}}(\text{Pa})}{T_{\text{alt}}(K)} \times U + 0.26 \times 0.25 \times P_{\text{alt}}(\text{Pa}) - 6.44 \times 10^{-5} \times \frac{P_{\text{alt}}(\text{Pa})}{T_{\text{alt}}(K)} \\
 &\quad \times U^2 (\text{N})
 \end{aligned}$$

$$\text{Then } \frac{\partial T_{\text{net}}}{\partial U} = 0.142 \times \frac{P_{\text{alt}}(\text{Pa})}{T_{\text{alt}}(K)} - 2 \times 6.44 \times 10^{-5} \times \frac{P_{\text{alt}}(\text{Pa})}{T_{\text{alt}}(K)} \times U = 0$$

Thus net thrust attains a maximum value at all altitudes when the flight speed is

$$U = \frac{0.142}{2 \times 6.44 \times 10^{-5}} = 1102.5 \text{ km/hr}$$

The above value is also clear in Fig. 3.7.

Example 3.4 A high bypass ratio turbofan engine is powering a civil transport aircraft flying at an altitude 11 km with a speed of 1100 km/h. The total air mass flow rate is 120 kg/s and the bypass ratio is 5.0. Exhaust speeds for the cold and hot streams are, respectively, 1460 and 2000 km/h. Both cold and hot nozzles are unchoked. Calculate the thrust force (fuel-to-air ratio is 0.012).

Solution

From Eq. (3.4), the thrust force for unchoked nozzles is

$$T = \dot{m}_h[(1+f)u_{eh} - u] + \dot{m}_c(u_{ec} - u)$$

Since the bypass ratio $\beta = 5.0$ and the total air mass flow is 120.0 kg/s, then

$$\begin{aligned} \dot{m}_c &= \frac{\beta}{1+\beta}\dot{m}_a = \frac{5}{1+5} \times 120 = 100 \text{ kg/s} \\ \text{and} \quad \dot{m}_h &= \frac{1}{1+\beta}\dot{m}_a = \frac{1}{1+5} \times 120 = 20 \text{ kg/s} \end{aligned}$$

Then the thrust force is

$$\begin{aligned} T &= \{20[(1+0.012)2000 - 1100] + 100(1460 - 1100)\} \times (1000/3600) \\ T &= 15,133 \text{ N} = 15.133 \text{ kN} \end{aligned}$$

Example 3.5 The thrust of a ramjet engine (single exhaust stream athodyd aero-engine) is expressed by the relation:

$$T = \dot{m}_a\{(1+f)u_e - u\}$$

where the exhaust speed is expressed by the relation:

$$u_e = \sqrt{2C_p T_{0\max} \left[1 - (P_a/P_{0\max})^{\frac{\gamma-1}{\gamma}}\right]}$$

It is required to examine the effect of maximum temperature $T_{0\max}$ on thrust force, by considering the following case: $\dot{m}_a = 100 \text{ kg/s}$, $u = 250 \text{ m/s}$, $(P_a/P_{0\max}) = 0.125$, $C_p = 1148 \text{ J/(kg.K)}$, $\gamma = 4/3$, $f = 0.015$, and $T_{0\max} = 1000, 1200, 1400, 1600 \text{ K}$

Table 3.2 Values of exhaust velocity and net thrust at different maximum temperatures

$T_{0\max}$ (K)	1000	1200	1400	1600
u_e (m/s)	965	1957	1142	1220
Thrust T (kN)	72.9	82.2	90.8	98.8

Solution

Since the exhaust speed is given by the relation:

$$u_e = \sqrt{2C_p T_{0\max} \left[1 - (P_a/P_{0\max})^{\frac{\gamma-1}{\gamma}} \right]}$$

Then, from the above given data:

$$\begin{aligned} u_e &= \sqrt{2C_p T_{0\max} \left[1 - (P_a/P_{0\max})^{\frac{\gamma-1}{\gamma}} \right]} = \sqrt{2 \times 1148 \times T_{0\max} \left[1 - (0.125)^{0.25} \right]} \\ &= 30.5 \sqrt{T_{0\max}} \end{aligned}$$

Moreover, the thrust force is then expressed by the relation

$$T = \dot{m}_a \{(1+f)u_e - u\} = 100[(1.015)u_e - 250]$$

Substituting for the different values of maximum temperature, we get the following tabulated results.

It is clear from Table 3.2 that keeping a constant ratio between the maximum and ambient pressures, then increasing the maximum total temperature will increase the generated thrust.

3.3 Factors Affecting Thrust

As seen from Eq. (3.1) for a single stream aero engine (ramjet or turbojet engine), the thrust force depends on the inlet and outlet air mass flow rates, fuel-to-air ratio, flight speed, exhaust speed, and exhaust and ambient pressures [1]. Though it looked like a simple task to identify the factors listed above, each of them is dependent on several parameters. For example, the inlet air mass flow rate influencing both of the momentum thrust and momentum drag is dependent on several variables including the flight speed, ambient temperature and pressure, humidity, altitude, and rotational speed of the compressor. The outlet gas mass flow rate is dependent on the fuel added, air bleed, and water injection. The pressure thrust term depends on the turbine inlet temperature, flight altitude, and the nozzle outlet area and pressure. The momentum thrust is also dependent on the jet nozzle velocity. These parameters [2] and [3] can be further explained as below:

3.3.1 Jet Nozzle

Pressure thrust has finite values only for choked nozzles, where the exit pressure is greater than the ambient pressure. Nozzles are either of the convergent or convergent–divergent (C–D) type. Only convergent nozzles may be choked. For a choked convergent nozzle, the pressure thrust depends on both of the area of the exhaust nozzle and also on the difference between the exit and ambient pressures. Moreover, the exhaust speed is equal to the sonic speed which is mainly influenced by the exhaust gas temperature. If a convergent nozzle is unchoked, then the jet velocity will attain subsonic values. For a convergent divergent (CD) nozzle, the jet speed may attain supersonic values as described in Chap. 2. CD nozzles are seen only in supersonic aircrafts.

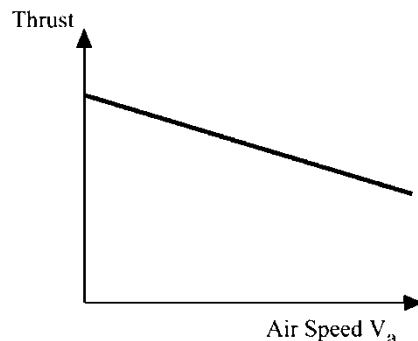
3.3.2 Air Speed

The air speed, sometimes denoted as the approach speed, is equal to the flight speed in the thrust force; Eq. (3.1). Such a parameter has a direct effect on the net thrust. If the exhaust gas velocity is constant and the air velocity is increased, then the difference between both velocities $[(1+f)u_e - u]$ is decreased leading to a decrease also in the net thrust. If the air mass flow and the fuel to air ratio are assumed constants, then a linear decrease in the net thrust is enhanced (Fig. 3.8).

3.3.3 Mass Air Flow

The mass air flow \dot{m}_a is the most significant parameter in the thrust equation. It depends on the air temperature and pressure as both together determine the density of the air entering the engine. In free air, a rise in temperature will decrease the density. Thus air density and mass flow rate is inversely proportional with the air

Fig. 3.8 Variation of thrust force with air speed



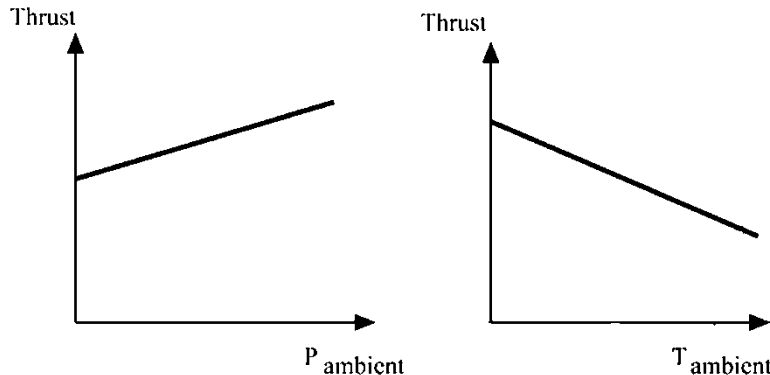


Fig. 3.9 Variation of the thrust force with air temperature and pressure

temperature. On the contrary, an increase in the pressure of a free air increases its density and, consequently, its thrust increases. The effect of both of air temperature and pressure is illustrated in Fig. 3.9. In brief, the density affects the inlet air mass flow and it directly affects thrust.

3.3.4 Altitude

As outlined above, the air temperature and pressure have significant effects on the thrust. As described in Chap. 2, in the International Standard Atmosphere (ISA) temperature decreases by about 3.2 K per 500 m of altitude up to nearly 11,000 m (36,089 ft). The variations of ambient temperature and pressure are given by Eqs. (2.83) and (2.84). These relations are repeated here, but with altitude expressed in meter:

$$T(\text{K}) = 288 - 0.0065 \times z \quad (3.6)$$

$$P \text{ (bar)} = 1.01325 - 0.000112 \times z + 3.8e^{-9} \times z \quad (3.7)$$

After 11,000 m, the temperature stops falling, but the pressure continues to drop steadily with increasing altitude. Consequently, above 11,000 m (36,089 ft), the thrust will drop off more rapidly (Fig. 3.10). This makes the 11,000 m an optimum altitude for long-range cruising at nominal speed, just prior to the rapidly increased effect of altitude on thrust. It may be concluded that the effect of altitude on thrust is really a function of density.

Fig. 3.10 Variation of the thrust force with altitude

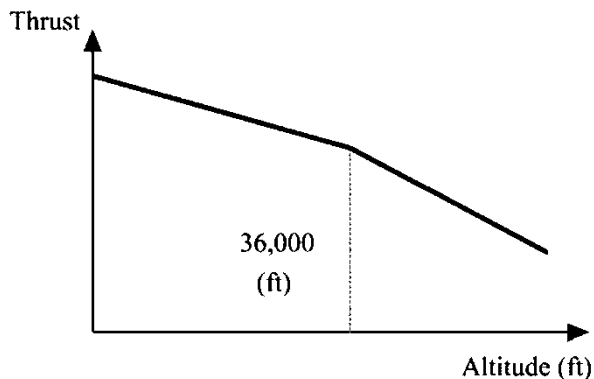
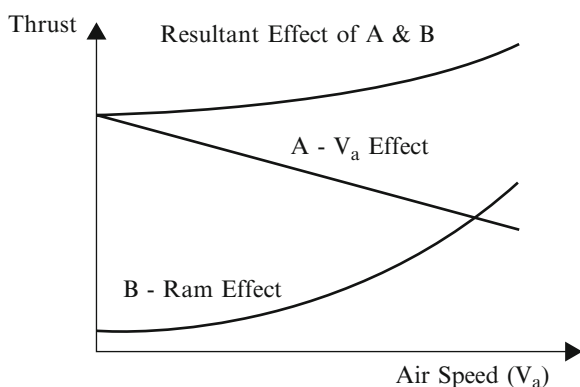


Fig. 3.11 Effect of ram pressure on thrust



3.3.5 Ram Effect

The movement of the aircraft relative to the outside air causes air to be rammed into the engine inlet duct. Ram effect increases the airflow to the engine, which in turn, increases the gross thrust. However, it is not as easy, ram effects combine two factors, namely, the air speed increase and in the same time increases the pressure of the air and the airflow into the engine. As described earlier, the increase of air speed reduces the thrust, which is sketched in Fig. 3.11 as the 'A' curve. Moreover, the increase of the airflow will increase the thrust, which is sketched by the 'B' curve in the same figure. The 'C' curve is the result of combining curves 'A' and 'B'. The increase of thrust due to ram becomes significant as the air speed increases, which will compensate for the loss in thrust due to the reduced pressure at high altitude. Ram effect is thus important in high speed fighter aircrafts. Also modern subsonic jet-powered aircraft fly at high subsonic speeds and higher altitudes to make use of the ram effect.

Finally, it is fruitful to classify the factors affecting thrust into two groups [4]:

1. Factors related to the engine
2. Factors related to the surrounding medium

The first group [1] includes:

1. The rotational speed (rpm), which influences both of the compressor pressure ratio and the turbine work
2. Exhaust nozzle size, which influences the jet velocity
3. Fuel flow rate and turbine inlet temperature, which affect the combustor heat generation
4. Compressor bleed flow, water injection, and components performance, which lead to increase of the specific work

The first group thus contributes to both of the air mass flow rate and jet velocity.

The second group includes:

1. Forward (air) speed, which leads to thrust decrease and more fuel consumption
2. Air density (influenced by the flight altitude, humidity, hot/cold day), which influences the airflow leading to a thrust increase if the airflow is increased and vice versa.

3.4 Engine Performance Parameters

The performance of an aircraft engine may be criticized by its ability to provide the necessary thrust force needed in propelling an aircraft efficiently in its different flight regimes.

The engine performance parameters [1] are identified as:

1. Propulsive efficiency
2. Thermal efficiency
3. Propeller efficiency
4. Overall efficiency
5. Takeoff thrust
6. Specific fuel consumption
7. Aircraft range

Military aircrafts are powered by engines that fulfill its mission requirements. For this reason, the takeoff thrust, maneuverability, and affordability are the critical issues with some sacrifice of its fuel consumption in some types like fighters and interceptors. For both civil and military transports, specific fuel consumption and the aircraft range are the critical design issues. In both types, several efficiencies related to the conversion of heat generated by fuel burning into thrust force are important.

3.4.1 Propulsive Efficiency

It is the efficiency of the conversion of the kinetic energy of air when passes through the engine into a propulsive power. It is identified by manufacturers of aero engine as an external efficiency. It is influenced by the amount of the energy wasted in the propelling nozzle(s) and denoted by (η_p).

It is defined as

$$\eta_p = \frac{\text{Thrust power}}{\text{Power imparted to engine airflow}} \quad (3.8a)$$

or simply

$$\eta_p = \frac{\text{Thrust power}}{\text{Thrust power} + \text{power wasted in the exhaust}} \quad (3.8b)$$

which will be denoted here as the *first* expression for the propulsive efficiency.

Another definition used in many texts is

$$\eta_p = \frac{\text{Thrust power}}{\text{Rate of kinetic energy added to engine airflow}} \quad (3.9)$$

This will be referred to as the *second* expression.

For *ramjet*, *scramjet* and *turbojet* engines, the first expression has the form:

$$\eta_p = \frac{uT}{uT + \frac{1}{2}\dot{m}_e(u_e - u)^2} \quad (3.10a)$$

$$\eta_p = \frac{u\{\dot{m}_a[(1+f)u_e - u] + A_e(P_e - P_a)\}}{u\{\dot{m}_a[(1+f)u_e - u] + A_e(P_e - P_a)\} + \frac{1}{2}\dot{m}_a(1+f)(u_e - u)^2} \quad (3.10b)$$

This expression is normally used by manufacturers of aero engines [3–6] as well as some texts [7, 8].

The second expression is adopted by other authors [9, 10] and expressed as

$$\eta_p = \frac{2uT}{\dot{m}_a[(1+f)u_e^2 - u^2]} \quad (3.11a)$$

$$\eta_p = \frac{2u\{\dot{m}_a[(1+f)u_e - u] + A_e(P_e - P_a)\}}{\dot{m}_a[(1+f)u_e^2 - u^2]} \quad (3.11b)$$

The two expressions are identical if the nozzle is unchoked ($P_e = P_a$). If in addition, the fuel-to-air ratio (f) is negligible, then the following *third* expression is obtained:

$$\eta_p = \frac{2u}{u + u_e} = \frac{2}{1 + (u_e/u)} \quad (3.12)$$

Considering Eqs. (3.3) and (3.12), it is important to notice that [1]:

1. If the exhaust speed is much greater than the air (flight) speed, $u_e \gg u$, then the thrust force will be maximum while the propulsive efficiency attains a very small value approaching zero; or as $\left(\frac{u_e}{u_0}\right) \uparrow$, then $(\eta_p) \downarrow$. This case represents takeoff conditions (where $u \approx 0$) as well as military aircrafts.
2. If the exhaust speed is nearly equal to the flight speed, $u_e/u \approx 1$, then the thrust force will be so small and approaches zero, while the propulsive attains very high value approaching 100 %, or as $\left(\frac{u_e}{u_0}\right) \downarrow$ then $(\eta_p) \uparrow$. Thus civil transport aircrafts require higher efficiency and fly at lower speeds.

The highest propulsive efficiency is typically obtained with a propeller or an unducted fan, as both give a relatively small impulse (Δu) to a relatively large mass flow.

For bypass engines (*turbofan* and *propfan*), the air coming into the engine is splitted into two streams: the first passes through the fan/propfan and is known as the cold stream, while the other passes through the engine core, compressor, combustion chamber, and subsequent modules, and is known as the hot stream. Applying the same principle and employing the first expression, we get the following form:

$$\eta_p = \frac{u(T_h + T_c)}{u(T_h + T_c) + W_h + W_c} \quad (3.13a)$$

where T_h and T_c are the thrust force generated by the hot and cold streams respectively, while W_h and W_c are the wake losses of the hot and cold streams respectively. The thrust force and wake losses for both hot and cold streams are expressed as

$$\begin{aligned} T_h &= \dot{m}_h[(1+f)u_{eh} - u] + A_{eh}(P_{eh} - P_a) \\ T_c &= \dot{m}_c[u_{ec} - u] + A_{ec}(P_{ec} - P_a) \\ W_h &= \frac{1}{2}\dot{m}_h(1+f)(u_{eh} - u)^2 = \frac{1}{2}\dot{m}_{eh}(u_{eh} - u)^2 \\ W_c &= \frac{1}{2}\dot{m}_c(u_{ec} - u)^2 \end{aligned}$$

where $\dot{m}_{eh} = (1+f)\dot{m}_h$

This relation can be written also as

$$\eta_p = \frac{T_u}{T_u + 0.5 \left\{ \dot{m}_{eh}(u_{eh} - u)^2 + \dot{m}_c(u_{ec} - u)^2 \right\}} \quad (3.13b)$$

This is the first expression for the propulsive efficiency in turbofan engine.

The *second* expression, Eq. (3.11a), can be also written using the two hot and cold streams.

$$\eta_p = \frac{2uT}{\dot{m}_h \{(1+f)u_{eh}^2 + \beta u_{ec}^2 - (1+\beta)u^2\}} \quad (3.14a)$$

When the two nozzles of the hot and cold streams are unchoked and the fuel to air ratio (f) is negligible, both expressions yield the following expression:

$$\eta_p = \frac{2u[u_{eh} + \beta u_{ec} - (1+\beta)u]}{u_{eh}^2 + \beta u_{ec}^2 - (1+\beta)u^2} \quad (3.14b)$$

where (β) is the bypass ratio which is the ratio between the mass flow rates of the cold air and hot air, or $\beta = \frac{\dot{m}_c}{\dot{m}_h}$. For turbofan engines, the simple relation (Eq. (3.12)) cannot be applied.

The propulsive efficiency for a turboprop engine can be written also as

$$\eta_p = \frac{Tu}{Tu + 0.5 \left\{ \dot{m}_e (u_e - u_1)^2 + \dot{m}_0 (u_1 - u_0)^2 \right\}} \quad (3.15)$$

The propulsive efficiency for turboprop, turbojet, and turbofan engines is illustrated by Fig. 3.12. Figure 3.13 illustrates the propulsive efficiency for single and contra rotating propfan engines.

Example 3.6 A turbojet engine is powering a fighter airplane. Its cruise altitude and Mach number are 10 km and 0.85, respectively. The exhaust gases leave the nozzle at a speed of 600 m/s and a pressure of 0.75 bar. The outlet area of exhaust nozzle is $A_e = 0.24 \text{ m}^2$. The air mass flow rate is 40 kg/s and fuel to air ratio is 0.02. It is required to calculate:

- (a) The specific thrust (T/\dot{m}_a)
- (b) The propulsive efficiency using the different expressions defined above

Solution

- (a) At altitude 10 km, the ambient temperature and pressure are

$$T_a = 223.3 \text{ K} \text{ and } P_a = 0.265 \text{ bar}$$

This ambient pressure is less than the exit pressure. Thus the nozzle is choked and the pressure thrust is not zero.

The flight speed $u = M\sqrt{\gamma RT_a} = 254.6 \text{ m/s}$

From Eq. (3.3), the specific thrust is

$$\frac{T}{\dot{m}_a} = [(1+f)u_e - u] + (P_e - P_a) \frac{A_e}{\dot{m}_a}$$

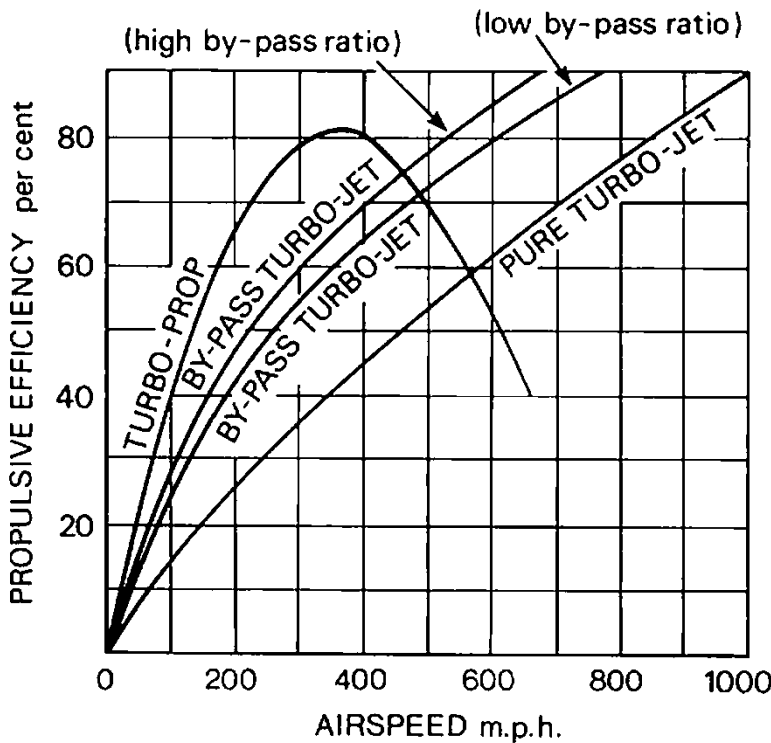


Fig. 3.12 Propulsive efficiency for turboprop, turbojet, and turbofan engines (Reproduced with the permission of Rolls-Royce plc, copyright © Rolls-Royce plc 2007)

$$\frac{T}{\dot{m}_a} = (1.02 \times 600 - 254.6) + (0.75 - 0.265) \times 10^5 \times \frac{0.24}{40}$$

Then $\frac{T}{\dot{m}_a} = 648.4 \text{ N.s/kg}$

(b) The propulsive efficiency is calculated using the different expressions.

The first expression given by Eq. (3.10) can be rewritten as

$$\eta_p = \frac{2(T/\dot{m}_a)u}{2(T/\dot{m}_a)u + (1+f)(u_e - u)^2}$$

Substitution will give

$$\eta_p = \frac{2 \times 648.4 \times 254.6}{2 \times 648.4 \times 254.6 + 1.02 \times (600 - 254.6)^2} = \frac{330165.3}{330165.3 + 121687.2}$$

$$\eta_p = 0.7307 = 73.07 \%$$

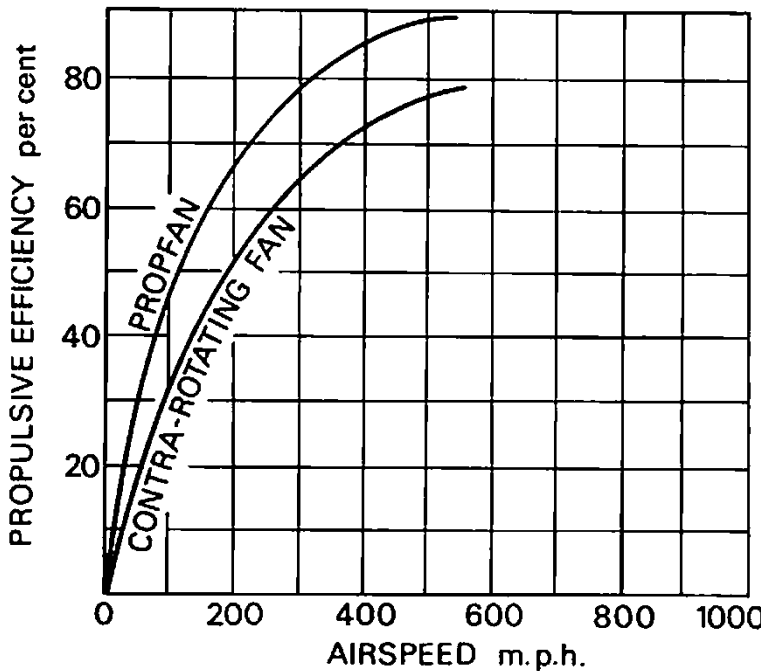


Fig. 3.13 Propulsive efficiency for single- and contra-rotating propfan engines (Reproduced with the permission of Rolls-Royce plc, copyright © Rolls-Royce plc 2007)

Next, the second expression given by Eq. (3.11) can be rewritten as

$$\eta_p = \frac{2(T/\dot{m}_a)u}{(1+f)u_e^2 - u^2}$$

which by substitution gives

$$\eta_p = \frac{2 \times 648.4 \times 254.6}{1.02 \times (600)^2 - (254.6)^2} = 1.092 = 109.2 \text{ \%}$$

This value assures that this expression must *not* be used if the nozzle is choked. Finally using the third expression given by Eq. (3.12) gives

$$\eta_p = \frac{2u}{u_e + u} = 0.5958 = 59.58 \text{ \%}$$

Though this expression is simple but gives a very rough estimate of the propulsive efficiency.

Comment

As depicted in example (3.6), the second expression for the propulsive efficiency provides efficiencies greater than unity. Such astonishing value of a propulsive efficiency greater than unity can be overcome if the effective jet velocity proposed in [1, 6, 11] is employed. The proposed effective jet velocity is expressed as

$$u'_e = u_e + (P_e - P_a) \frac{A_e}{\dot{m}_e} \quad (3.16)$$

Such an effective jet velocity means that a full expansion of the gases to the ambient pressure is assumed. In such a case, the second expression for the propulsive efficiency will be exactly equal to the first expression. This effective velocity was also employed by Rolls Royce [5]. The effective jet velocity is identified by aero engine manufacturers as the fully expanded jet velocity (in the exhaust plume).

Example 3.7 A comparison between turbojet, turbofan, and turboprop engines is considered here. The three engines have the same gas generator (compressor, combustion chamber, and turbine). It is required to calculate both the thrust and propulsive efficiency of them provided the following data:

Engine	Core air mass flow rate (kg/s)	Bypass ratio β	Flight speed (km/h)	Fuel to air ratio	Exhaust speed for hot gases (km/h)	Exhaust speed for cold stream
Turbojet	20	0	1100	0.02	3000	0
Turbofan	20	5	1100	0.015	2000	1460
Turboprop	20	25	1100	0.015	1800	1200

All nozzles are unchoked.

Solution

(A) Turbojet engine

The thrust force is given by Eq. (3.2)

$$\tau = \dot{m}_e [(1+f)u_e - u]$$

$$\tau = 20 \times [(1 + 0.02) \times 3000 - 1000]/3.6 = 10,888 \text{ N} = 10.888 \text{ kN}$$

$$\begin{aligned} \eta_p &= \frac{Tu}{Tu + 0.5 \left\{ \dot{m}_e (u_e - u_1)^2 \right\}} \\ &= \frac{10,888 \times (1100/3.6)}{10,888 \times (1100/3.6) + 0.5 \times 20.04 \times \{(3000 - 1100)/3.6\}^2} = 0.5439 \\ \eta_p &= 54.39 \% \end{aligned}$$

(B) Turbofan engine

Since the bypass ratio $\beta = 5.0$ and the core air mass flow is 20.0 kg/s, then

$$\dot{m}_{\text{fan}} = \beta \dot{m}_{\text{core}} = 5 \times 20 = 100 \text{ kg/s}$$

The thrust force is calculated from Eq. (3.4)

$$\begin{aligned}\tau &= \dot{m}_{\text{core}}[(1+f)u_{eh} - u] + \dot{m}_{\text{fan}}(u_{ec} - u) \\ \tau &= \{20[(1+0.015)2000 - 1100] + 100(1460 - 1100)\} \times (1000/3600) \\ \tau &= 15,166 \text{ N} = 15.166 \text{ kN} \\ \eta_p &= \frac{Tu}{Tu + 0.5 \left\{ \dot{m}_{eh}(u_{eh} - u)^2 + \dot{m}_c(u_{ec} - u)^2 \right\}} \\ \eta_p &= \frac{15,166 \times (1100/3.6)}{15,166 \times (1100/3.6) + 0.5 \left\{ 20.3 \times [(2000 - 1100)/3.6]^2 + 100 \times [(1460 - 1100)/3.6]^2 \right\}} \\ \eta_p &= 0.8033 = 80.33 \%\end{aligned}$$

(C) Turboprop engine

Total air mass flow rate

$$\dot{m}_0 = \beta \times \dot{m}_c = 25 \times 20 = 500 \text{ kg/s}$$

The thrust force is calculated from Eq. (3.5):

$$\begin{aligned}\tau &= \dot{m}_c[(1+f)u_e - u_1] + \dot{m}_0(u_1 - u_0) \\ \tau &= \{20[(1+0.015)1800 - 1200] + 500(1200 - 1100)\} \times (1000/3600) \\ \tau &= 17,372 \text{ N}\end{aligned}$$

The Propulsive Efficiency

$$\begin{aligned}\eta_p &= \frac{Tu}{Tu + 0.5 \left\{ \dot{m}_e(u_e - u_1)^2 + \dot{m}_0(u_1 - u_0)^2 \right\}} \\ \eta_p &= \frac{17,372 \times (1100/3.6)}{17,372 \times (1100/3.6) + 0.5 \left\{ 20.3 \times \left(\frac{1800-1200}{3.6}\right)^2 + 500 \left(\frac{1200-1100}{3.6}\right)^2 \right\}} \\ \eta_p &= 0.9178 \\ \eta_p &= 91.78 \%\end{aligned}$$

Summary of Results

Engine	Thrust force (kN)	Propulsive efficiency η_p %
Turbojet	10.888	54.39
Turbofan	15.166	80.33
Turboprop	17.372	91.78

It is clear from the above example that for the same gas generator, the turboprop engines furnishes the maximum thrust force and highest propulsive efficiency. The least thrust force and minimum propulsive efficiency is attained by a turbojet engine. Turbofan engine delivers a large thrust force and a high propulsive efficiency. It is important to mention here that the thrust of turbofan engine in many cases much greater than turboprop engines as well be described in Chap. 4.

3.4.2 Thermal Efficiency

It is the efficiency of energy conversion within the power plant itself. So it is considered as an internal efficiency, while the propulsive efficiency resembles an external efficiency as stated earlier. Thermal efficiency is denoted by (η_{th}). Two forms for such efficiency are defined for the following two groups of engines.

Ramjet, scramjet, turbojet, and turbofan engines:

$$\eta_{th} = \frac{\text{Power imparted to engine airflow}}{\text{Rate of energy supplied in the fuel}} = \frac{\dot{W}_{out}}{\dot{Q}_{in}} \quad (3.17)$$

It is easy to note that the denominator in Eq. (3.8a) is equal to the numerator in Eq. (3.17).

For a *ramjet* and *turbojet* engines:

Using the *first* expression for the propulsive efficiency, the following first expression for (η_{th}) is obtained:

$$\eta_{th} = \frac{T u + \frac{1}{2} \dot{m}_a (1+f)(u_e - u)^2}{\dot{m}_f Q_R} \quad (3.16)$$

where (Q_R) is the heat of reaction of the fuel used. Other names for Q_R are the calorific value of fuel [9] or the lower heating value (LHV) [4]. It is also alternatively written as Q_{HV} .

Assuming an unchoked nozzle, then

$$\dot{W}_{out} = \frac{1}{2} [(\dot{m}_a + \dot{m}_f) u_e^2 - \dot{m}_a u^2]$$

From the *second* expression for propulsive efficiency, the following second expression for thermal efficiency is obtained:

$$\eta_{th} = \frac{\frac{1}{2}[(\dot{m}_a + \dot{m}_f)u_e^2 - \dot{m}_a u^2]}{\dot{m}_f Q_R} \quad (3.17a)$$

$$\eta_{th} = \frac{[(1+f)u_e^2 - u^2]}{2fQ_R} \quad (3.17b)$$

For an unchoked nozzle and negligible (f), then the following *third* expression is given:

$$\eta_{th} = \frac{u_e^2 - u^2}{2fQ_R} \quad (3.18)$$

For a two stream engines (turbofan and prop fan), the following expression is employed:

$$\eta_{th} = \frac{Tu + \frac{1}{2}\dot{m}_h(1+f)(u_{eh} - u)^2 + \frac{1}{2}\dot{m}_c(u_{ec} - u)^2}{\dot{m}_f Q_R} \quad (3.19)$$

Similarly, assuming unchoked nozzles and negligible (f) to get

$$\eta_{th} = \frac{u_{eh}^2 + \beta u_{ec}^2 - (1+\beta)u^2}{2fQ_R} \quad (3.20)$$

which is the counterpart of Eq. (3.18)

Turboprop and turbo shaft engines:

The output of turboprop or a turbo shaft engine is largely a shaft power. In this case, thermal efficiency is defined as

$$\eta_{th} = \frac{P_{\text{Total}}}{\dot{m}_f Q_R} \quad (3.21)$$

where (P_{Total}) is the total power.

For a *turboprop* engine:

$$P_{\text{Total}} = P_{\text{Propeller}} + P_{\text{Jet}} = \eta_{pr}\eta_{gb}SP + T \times V_j$$

where (SP) is the shaft power, while the jet thrust (T) is given by the relation:

$$T = \dot{m}_a [(1+f)V_j - V_f]$$

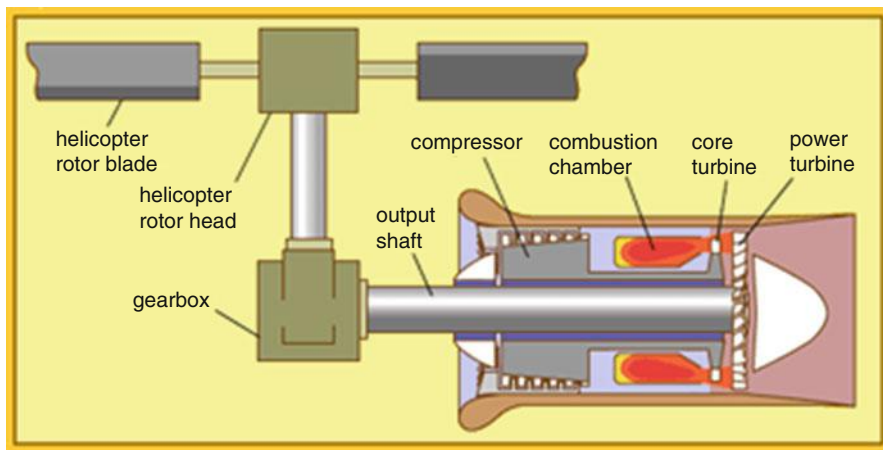


Fig. 3.14 Turboshaft engine powering helicopter's rotor

For a *turbo shaft* engine say driving the rotor of a helicopter:

$$P_{\text{Total}} = P_{\text{Rotor}} = \eta_{\text{rotor}} \eta_{gb} SP$$

Example 3.8 Bell 206 LM helicopter is powered a single Rolls-Royce 250 C30P turboshaft engine, Fig. 3.14, having a takeoff shaft power of 726 hp. The engine has the following data:

Rotor efficiency	0.8
Gearbox efficiency	0.995
Fuel heating value	45,000 kJ/kg
Fuel mass flow rate	102 kg/h

Calculate the thermal efficiency

Solution

Since thermal efficiency is expressed by the relation:

$$\eta_{th} = \frac{P_{\text{Total}}}{\dot{m}_f Q_R}$$

where $P_{\text{Total}} = P_{\text{Rotor}} = \eta_{\text{rotor}} \eta_{gb} SP$,

$$\begin{aligned} \text{Then } P_{\text{Total}} &= P_{\text{Rotor}} = \eta_{\text{rotor}} \eta_{gb} SP = 0.8 \times 0.995 \times 726 = 577.9 \text{ hp} \\ &= 431 \text{ kW} \end{aligned}$$

$$\eta_{th} = \frac{P_{\text{Total}}}{\dot{m}_f Q_R} = \frac{431}{(102/3600) \times 45,000} = 0.338 = 33.8 \text{ \%}$$

3.4.3 Propeller Efficiency

Propellers are used in both of piston and turboprop. Shaft power is converted to thrust power. Propeller efficiency (η_{pr}) is defined as the ratio between the thrust power generated by the propeller ($TP \equiv uT_{pr}$) to the shaft power (SP)

$$\eta_{pr} = \frac{TP}{SP} = \frac{uT_{pr}}{SP} \quad (3.22)$$

when an appreciable amount of thrust is obtained from the exhaust gases T_e in a turboprop engine, an *Equivalent Thrust Power*, ETP is expressed in terms of the shaft power, propeller efficiency, and exhaust thrust power, thus

$$ETP = (SP) \times \eta_{pr} + T_e u \quad (3.23a)$$

Alternatively, an equivalent shaft power (ESP) is used instead of the equivalent thrust power. They are related to each other by the relation:

$$\text{where } ESP = ETP / \eta_{pr} = SP + \frac{T_e u}{\eta_{pr}} \quad (3.23b)$$

Moreover, the exhaust thrust is expressed as

$$T_e = \dot{m}_h [(1+f)u_e - u] \quad (3.24a)$$

The total thrust force is given by the relation:

$$T = T_{pr} + T_e \quad (3.24b)$$

The propeller efficiency is then expressed as

$$\eta_{pr} = \frac{uT}{ESP} \quad (3.25)$$

Such propeller efficiency replaces the propulsive efficiency of other types of aero engines discussed above. More details will be given in Chap. 4.

3.4.4 Overall Efficiency

The product of the propulsive and thermal efficiencies ($\eta_p \times \eta_{th}$) or ($\eta_{pr} \times \eta_{th}$) as appropriate is called the overall efficiency.

In all cases

$$\eta_o = \frac{T u}{\dot{m}_f} Q_R \quad (3.26)$$

Since the overall efficiency depends on speed (u) and the thrust (T) balances the aircraft drag, overall efficiency is actually not a parameter of the engine alone, but characterizes the engine/aircraft combination and its state of operation. The overall efficiency was close to 0.2 in the 1950s, near 0.3 on average for subsonic airliner fleet in the 1990s, and may reach 0.5 for engines of 2015 [12]. The overall efficiency is 0.35 for a B747 aircraft with CF6-80C2B1F engines cruising with Mach 0.86 at 11.9 km altitude and was 0.40 for a Concorde with Olympus 593 engines cruising with Mach 2 at 16.5 km altitude, on 6400 km mission.

For a turbojet with unchoked nozzle and negligible fuel to air ratio (f), then from Eq. (3.12):

$$\eta_o = \eta_{th} \frac{2u}{u + u_e} \quad (3.27a)$$

Example 3.9 Boeing 747-400 aircraft is powered by four PW4062 turbofan engines manufactured by Pratt & Whiney Aircraft Engine Company. Each engine has the following data:

Thrust force	24.0 kN
Air mass flow rate	120 kg/s
Bypass ratio	5.0
Fuel mass flow rate	0.5 kg/s
Operating Mach number	0.85
Altitude	10 km
Ambient temperature	223.2 K
Fuel heating value	40,800 kJ/kg

If the thrust generated from the fan is 75 % of the total thrust, determine:

- (a) Jet velocities of the cold air and hot gases
- (b) Specific thrust
- (c) Propulsive efficiency
- (d) Thermal efficiency
- (e) Overall efficiency

(Assume that the exit pressures of the cold and hot streams are equal to the ambient pressure)

Solution

Since the total air mass flow rate through the engine is $\dot{m}_a = 120 \text{ kg/s}$ and the bypass ratio is 5.0, then the flow rates of the cold (fan) and hot (core) streams are calculated as follows:

$$\begin{aligned}\dot{m}_c &\equiv \dot{m}_{\text{fan}} = \frac{\beta}{1+\beta} \dot{m}_{\text{total}} = \frac{5}{6} \times 120 = 100.0 \text{ kg/s} \\ \dot{m}_h &\equiv \dot{m}_{\text{core}} = \frac{1}{1+\beta} \dot{m}_{\text{total}} = \frac{1}{6} \times 120 = 20.0 \text{ kg/s}\end{aligned}$$

- (a) Subscripts (c) and (h) stands for the cold (or fan) and hot (or core) sections respectively.

$$\text{Fuel-to-air ratio } f = \dot{m}_{\text{fuel}} / \dot{m}_h = \frac{0.5}{20.0} = 0.025$$

$$T_{\text{fan}} = 0.75T = 0.75 \times 24 = 18 \text{ kN}$$

$$T_{\text{core}} \equiv T_h = 0.25T = 6 \text{ kN}$$

$$\text{Flight speed } U = M\sqrt{\gamma RT_a} = 0.85\sqrt{1.4 \times 287 \times 223.2}$$

$$U = 254.5 \text{ m/s}$$

Exit velocity from fan (cold air)

$$\begin{aligned}\text{since } T_{\text{fan}} &= \dot{m}_{\text{fan}} (U_{e_{\text{fan}}} - U) \\ \therefore U_{e_{\text{fan}}} &= \frac{T_{\text{fan}}}{\dot{m}_{\text{fan}}} + U = \frac{18000}{100.0} + 254.5 = 180 + 254.5 \\ U_{e_{\text{fan}}} &= 434.5 \text{ m/s}\end{aligned}$$

Exhaust velocity from engine core (hot gases)

$$\begin{aligned}\text{Since } T_h &= \dot{m}_h [(1+f)U_{e_h} - U] \\ \therefore U_{e_h} &= \frac{[(T_h/\dot{m}_h) + U]}{1+f} = \frac{1}{1.025} \times [(6000/20.0) + 254.5] \\ U_{e_h} &= 541.0 \text{ m/s}\end{aligned}$$

- (b) Specific thrust = $\frac{T}{\dot{m}_a} = \frac{24}{120} = 0.2 \text{ kN} \cdot \text{s/kg} = 200 \text{ m/s}$
 (c) The propulsive efficiency

Since both cold (fan) and hot (core) nozzles are unchoked, then the propulsive efficiency can be expressed as

$$\eta_P = \frac{T \times U}{\frac{1}{2} \dot{m}_h [(1+f)U_{e_h}^2 - U^2] + \frac{1}{2} \dot{m}_c [U_{e_c}^2 - U^2]}$$

$$\eta_P = \frac{2 \times 24,000 \times 254.5}{20.0 [1.025 \times (541)^2 - (254.5)^2] + (100.0) [(434.5)^2 - (254.5)^2]}$$

$$\eta_P = \frac{12.216 \times 10^6}{4.7045 \times 10^6 + 12.402 \times 10^6} = 0.714 = 71.4\%$$

(d) The thermal efficiency

$$\eta_{th} = \frac{\frac{1}{2} \dot{m}_h [(1+f)U_{e_h}^2 - U^2] + \frac{1}{2} \dot{m}_c [U_{e_c}^2 - U^2]}{\dot{m}_{fuel} Q_{HV}}$$

$$\eta_{th} = \frac{17.1065 \times 10^6}{2 \times 0.5 \times 40.8 \times 10^6} = 0.4192$$

$$\eta_{th} = 41.92 \%$$

(e) The overall efficiency

$$\eta_o = \eta_P \eta_{th} = 0.3 = 30.0 \%$$

3.4.5 Takeoff Thrust

An important parameter that defines the ability of an aero engine to provide a static and low speed thrust which enables the aircraft to take off under its own power [1]. Both ramjet and scramjet engines are not self-accelerating propulsion systems from static conditions: they require acceleration to an appreciable velocity by a boost system before they are capable of providing net positive thrust. Thus they are excluded from this discussion.

From Eq. (3.3), the static thrust of a turbojet engine with an unchoked nozzle is expressed by the relation:

$$T_{takeoff} = \dot{m}_a (1+f) u_e \quad (a)$$

From Eq. (3.17a) when $u=0$, then

$$(\eta_{th})_{static} = \dot{m}_a (1+f) \frac{u_e^2}{2 \dot{m}_f Q_R} \quad (b)$$

From equations (a) and (b), then the static or takeoff thrust is given by the relation:

$$T_{\text{takeoff}} = \frac{2\eta_{th}\dot{m}_f Q_R}{u_e} \quad (3.27b)$$

For constant values flow rate and thermal efficiency, then

$$T_{\text{takeoff}} \propto \frac{1}{u_e}$$

The above relation outlines one of the advantages of turboprop engines over turbojet and turbofan engines. Turboprop engines accelerate a large mass flow rate of air to a small exhaust velocity which in turn increases the takeoff thrust. Consequently, aircraft powered by turboprop engines can takeoff from a very short runway.

3.4.6 Specific Fuel Consumption

This performance parameter of the engine has a direct influence on the costs of aircraft trip and flight economics [1]. Fuel consumption is either defined per unit thrust force (for ramjet, turbojet, and turbofan engines) or per horsepower (for example, for turboprop and piston-propeller engines).

(A) Ramjet, turbojet and turbofan engines:

The Thrust Specific Fuel Consumption (*TSFC*) is defined as

$$TSFC = \frac{\dot{m}_f}{T} \quad (3.28a)$$

where the thrust force (*T*) is expressed by Eq. (3.1) for a ramjet/turbojet engine and Eq. (3.4) for a turbofan engine. Values of *TSFC* strongly depend on the flight speed, so its typical values for both turbojet and turbofan are defined for static condition. However, for ramjet reference values for *TSFC* are defined at flight Mach number of 2. Typical values [10] for the above mentioned three engine types are given in Table 3.3.

Some empirical formulae are presented in [13] for thrust specific fuel consumption. These formulae have the form:

$$TSFC = (a + bM_0)\sqrt{\theta} \quad (3.28b)$$

where (a) and (b) are constants that vary from one engine to another, M_0 is the flight Mach number, and θ is the dimensionless ratio (T_a/T_{ref}), which is the ratio between

Table 3.3 Typical TSFC values for different engines at certain Mach numbers

	TSFC	
	kg/N.h	$ib/ib_f \cdot hr$
Turbojet ($M = 0$)	0.075 – 0.11	0.75 – 1.1
Turbofan ($M = 0$)	0.03 – 0.05	0.3 – 0.5
Ramjet ($M = 2.0$)	0.17 – 0.26	1.7 – 2.6

the ambient temperature at the flight altitude and the standard temperature at sea level (288.2 K). For a high bypass ratio turbofan, the values of these constants are $a = 0.4$ and $b = 0.45$.

(B) Turboprop engines

For engines which produce shaft power, fuel consumption is identified by Brake Specific Fuel Consumption (BSFC), or simply SFC, and defined as

$$SFC \equiv BSFC = \dot{m}_f / SP \quad (3.29)$$

When appreciable thrust is produced by the hot gases, the fuel consumption is identified by the Equivalent Brake Specific Fuel Consumption (EBSFC), or simply ESFC, and defined by

$$ESFC = \dot{m}_f / ESP \quad (3.30)$$

Typical values [10] for ESFC are $0.45\text{--}0.60 \left(\frac{\text{lb}/\text{hr}}{\text{hp}} \right)$ or $0.27\text{--}0.36 \left(\frac{\text{kg}}{\text{kW}\cdot\text{hr}} \right)$. The values of the corresponding constants in the empirical relation (3.25b) are $a = 0.2$ and $b = 0.9$ [13].

Example 3.10 A turbojet engine powering a fighter airplane has an unchoked nozzle. The following simplified expressions for thrust and propulsive efficiency may be used:

$$T = \dot{m}_a(u_e - u)$$

$$\eta_p = \frac{2u}{u + u_e}$$

Prove that the propulsive efficiency is expressed by the relation

$$\eta_p = \frac{2u}{2u + (f/TSFC)}$$

Next, calculate the propulsive efficiency for the case of fuel-to-air ratio $f = 0.02$ and $TSFC = 0.1 \text{ kg/N.h}$, at different flight speeds $u = 100, 200, 300, 400, 500, 600, 700 \text{ m/s}$.

Table 3.4 Propulsive efficiency versus flight speed

u (m/s)	100	200	300	400	500	600	700
η_p %	21.74	35.71	45.45	52.63	58.14	62.5	66.04

Solution

$$\text{Since } T = \dot{m}_a(u_e - u) \quad \text{then} \quad u_e = T/\dot{m}_a + u$$

$$\text{Thus } \eta_p = \frac{2u}{u + T/\dot{m}_a + u} = \frac{2u}{2u + T/\dot{m}_a}$$

$$\text{But } TSFC = \dot{m}_f/T$$

$$\text{Then } T/\dot{m}_a = (\dot{m}_f/TSFC)/\dot{m}_a = f/TSFC$$

$$\text{Thus } \eta_p = \frac{2u}{2u + (f/TSFC)}$$

$$\text{From the given data, } \eta_p = \frac{2u}{2u + (f/TSFC)} = \frac{2u}{2u + (0.02/0.1) \times 3600} = \frac{2u}{2u + 720}$$

Substituting for the flight speed, the propulsive efficiency is calculated and tabulated in Table 3.4.

Example 3.11 A turbojet engine is powering an aircraft flying with a speed of 250 m/s at an altitude where the ambient pressure is 20 kPa. A convergent nozzle is used which has an outlet area of 0.5 m². The air mass flow rate is 60 kg/s, fuel to air ratio is 0.02, and the nozzle inlet total conditions are

$$600 \text{ K and } 100 \text{ kPa.}$$

(A) For the cases of full expansion and choked nozzle, calculate:

1. The exhaust velocity and pressure
2. The jet, pressure, and net thrusts

(B) Repeat the above requirements in the following six cases of *under-expanded* flow in the nozzle, where the ratio between the total inlet and exit pressures $P_{0i}/P_e = 2.0, 2.5, 3.0, 3.5, 4.0$ and 4.5 .

(C) Calculate:

1. The incremental decrease in thrust $\Delta\tau = \tau_{\text{critical}} - \tau$, where τ_{critical} is the thrust at choked conditions
2. Calculate the percentage of thrust decrease $\Delta\tau/\tau_{\text{critical}} \%$

(D) Calculate the equivalent jet speed

(E) Plot the below variables versus P_{0i}/P_e (horizontal axis), while the vertical axis may be

1. Jet thrust
2. Pressure thrust
3. Net thrust

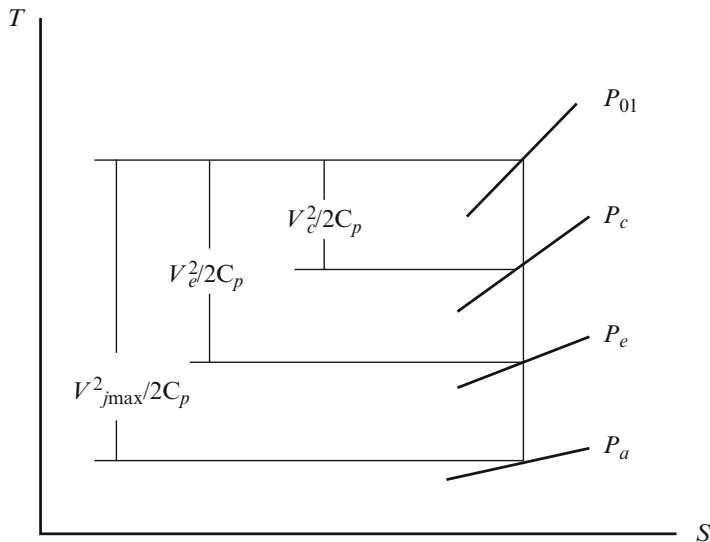


Fig. 3.15 Nozzle behavior for full expansion, choking, and under-expansion

4. Exact propulsive efficiency
5. Approximate propulsive efficiency

Solution

The nozzle flow characteristics are

$$P_{01} = 100 \text{ kPa}, \quad T_{01} = 600 \text{ K}, \quad \gamma_h = 4/3, \quad C_{p_h} = 1.148 \text{ kJ/kgK}, \quad P_a = 20 \text{ kPa}$$

Figure 3.15 illustrates the flow behavior inside the nozzle on T-S diagram.

(A.1) Full expansion

For the case of full expansion, the exhaust speed is the maximum in all cases, while the exhaust pressure is the lowest in all cases. It is calculated as follows:

Conditions

$$\text{Exhaust pressure} = P_a = 20 \text{ kPa}$$

$$\begin{aligned} V_{j\max} &= \sqrt{2C_{p_h}(T_{01} - T_a)} = \sqrt{2C_{p_h}T_{01} \left[1 - \left(\frac{P_a}{P_{01}} \right)^{\frac{\gamma_h - 1}{\gamma_h}} \right]} \\ &= \sqrt{2 \times 1148 \times 600 \left[1 - \left(\frac{20}{100} \right)^{0.25} \right]} \end{aligned}$$

$$\text{Jet speed} \equiv V_{j\max} = 675 \text{ m/s}$$

The exit temperature is

$$T_a = T_{01} \left(\frac{P_a}{P_{01}} \right)^{\frac{\gamma_h}{\gamma_h - 1}} = 600 \left(\frac{20}{100} \right)^{0.25} = 401.2 \text{ K}$$

(A.2) *Choked nozzle*: The exhaust pressure is the maximum, while the exhaust speed attains its minimum value.

$$\frac{P_{01}}{P_c} = \left(\frac{\gamma_h + 1}{2} \right)^{\frac{\gamma_h}{\gamma_h - 1}} = \left(\frac{4/3 + 1}{2} \right)^4$$

$$\frac{P_{01}}{P_c} = 1.8526$$

$$P_c = 53.98 \text{ kPa}$$

$$\frac{T_{01}}{T_c} = \left(\frac{\gamma_h + 1}{2} \right) = \frac{7}{6}$$

$$T_c = 514.3 \text{ K}$$

$$\text{Jet speed} \equiv V_c = a = \sqrt{\gamma_h R T_c} = 443.6 \text{ m/s}$$

(B) *For in-between pressure ratios*

$$\frac{P_{01}}{P_c} < \frac{P_{01}}{P_e} < \frac{P_{01}}{P_a}$$

then

$$\text{Jet speed} \equiv V_e = \sqrt{2C p_h (T_{01} - T_e)} = \sqrt{2C p_h T_{01} \left[1 - \left(\frac{P_e}{P_{01}} \right)^{\frac{\gamma_h - 1}{\gamma_h}} \right]}$$

$$\text{Exhaust pressure} \equiv P_e = \frac{P_e}{P_{01}} \times P_{01}$$

The net thrust is $\tau = \dot{m}_a [(1+f)V_e - V] + A_e (P_e - P_a)$

The jet thrust is $\tau_j = \dot{m}_a [(1+f)V_e - V]$

And the pressure thrust is $\tau_p = A_e (P_e - P_a)$

Computational results are summarized in Table 3.5.

As noticed from Table 3.5, the maximum thrust is achieved in the critical flow case (choked nozzle) and attains a value of 29.14 kN. The minimum thrust is noticed in the full expansion flow case.

(C.1) *Incremental decrease in thrust* $\Delta\tau = \tau_{\text{critical}} - \tau$

(C.2) *Percentage of thrust decrease* $\Delta\tau/\tau_{\text{critical}} \%$

Calculation of the incremental change in thrust and percentage of thrust decrease are calculated and tabulated in Table 3.6, where τ_{critical} is the thrust at choked condition.

Table 3.5 Exhaust speed and pressure and net, jet, and pressure thrusts

P_0/P_e	Critical case (1.8526)	2.0	2.5	3.0	3.5	4.0	4.5	Full expansion (5.0)
V_e (m/s)	444	468	531	575	608	635	657	676
P_e (kPa)	54	50	40	33.3	28.6	25	22.2	20
τ_J (kN)	12.15	13.65	17.5	20.2	22.5	23.9	25.21	26.34
τ_P (kN)	16.99	15.0	10.0	6.7	4.3	2.5	1.11	0
τ (kN)	29.14	28.65	27.5	26.9	26.8	26.4	26.32	26.34

Table 3.6 Incremental decrease in thrust ($\Delta\tau$) and percentage of thrust decrease with variation of exit pressure ($\Delta\tau/\tau_{critical}$ %)

P_{0i}/P_e	Critical case (1.8929)	2.0	2.5	3.0	3.5	4.0	4.5	Full expansion (5.0)
$\Delta\tau$ (kN) ($\tau_{critical} - \tau$)	0	0.49	1.64	2.24	2.34	2.74	2.82	2.8
$\frac{\Delta\tau}{\tau_{critical}}\%$	0	1.68	5.63	7.69	8.03	9.4	9.68	9.61

Table 3.7 Effective jet speed and exact and approximate propulsive efficiency

P_{0i}/P_e	Critical case (1.8526)	2.0	2.5	3.0	3.5	4.0	4.5	Full expansion (5.0)
V_{eff} (m/s)	736	727	708	698	692	690	688.7	689
$(\eta_p)_{exact}\%$ $\left(\frac{2V_f}{V_f + V_{eff}}\right)\%$	50.7	51.2	52.2	52.8	53.1	53.21	53.26	53.25
$(\eta_p)_{approximate}\%$ $\left(\frac{2V_f}{V_f + V_e}\right)\%$	72.1	69.6	64	60.6	58.2	56.5	55.1	54

(D) *The equivalent jet speed* is evaluated as follows:

$$\tau = \dot{m}_a[(1+f)V_e - V] + A_e(P_e - P_a) \equiv \dot{m}_a[V_{eff} - V]$$

$$V_{eff} = (1+f)V_e + \frac{A_e(P_e - P_a)}{\dot{m}_a}$$

$$V_{eff} = 1.02 \times V_e + \frac{0.5}{60}(P_e - 20) \times 10^3$$

$$V_{eff} = 1.02 \times V_e + 8.33 \times (P_e - 20)$$

where the pressure is substituted in kPa.

(E) *The propulsive efficiency* is expressed as

The exact value of propulsive efficiency is calculated from the equation:

$$(\eta_p)_{exact} = \left(\frac{2V_f}{V_f + V_{eff}} \right)$$

The approximate value of propulsive efficiency is also calculated from the equation

$$\eta_p = \frac{2V_f}{V_f + V_e}$$

Effective speed, exact, and approximate propulsive efficiencies are calculated and plotted in Table 3.7.

Figure 3.16 illustrates jet, pressure, and net thrusts for different nozzle pressure ratio.

Figure 3.17 illustrates exact and approximate propulsive efficiency for different nozzle pressure ratios.

3.4.7 Aircraft Range

Aircraft range is a design parameter of the aircraft and based on which the number, location, and capacity of fuel tanks in the aircraft is determined [1]. The aircraft weight is composed of the structural weight, the pay load (including the crew members, food, and service supply), and the fuel weight. During any trip, only the fuel weight is changeable.

Now consider the cruise phase in a flight trip where the aircraft flies at a constant speed. Ignoring the climb and descent phases, it may be assumed that the cruise distance is equal to the trip distance of the aircraft. During cruise, the aircraft is subjected to two vertical forces [lift (L) and weight (mg), which are equal in magnitude] and two horizontal forces [thrust (T) and drag (D), which are also equal in magnitude], refer to Fig. 3.18.

Then

$$T = D = mg(D/L)$$

where (m) is the instantaneous aircraft mass and (g) is the gravitational acceleration. Thus

$$\frac{T}{D} = \frac{L}{mg} = 1$$

Since the rate of fuel consumption is equal to the rate of decrease of the mass of aircraft, then

$$\dot{m}_f = -dm/dt = (-dm/ds) \times (ds/dt) = -udm/ds$$

where (s) is the distance along the flight path.

$$\begin{aligned}\therefore \dot{m}_f &= -u \left(\frac{T}{D} \right) \left(\frac{L}{mg} \right) \frac{dm}{ds} \\ \therefore ds &= -\frac{u}{g \dot{m}_f} \frac{T}{D} \frac{L}{m} dm\end{aligned}$$

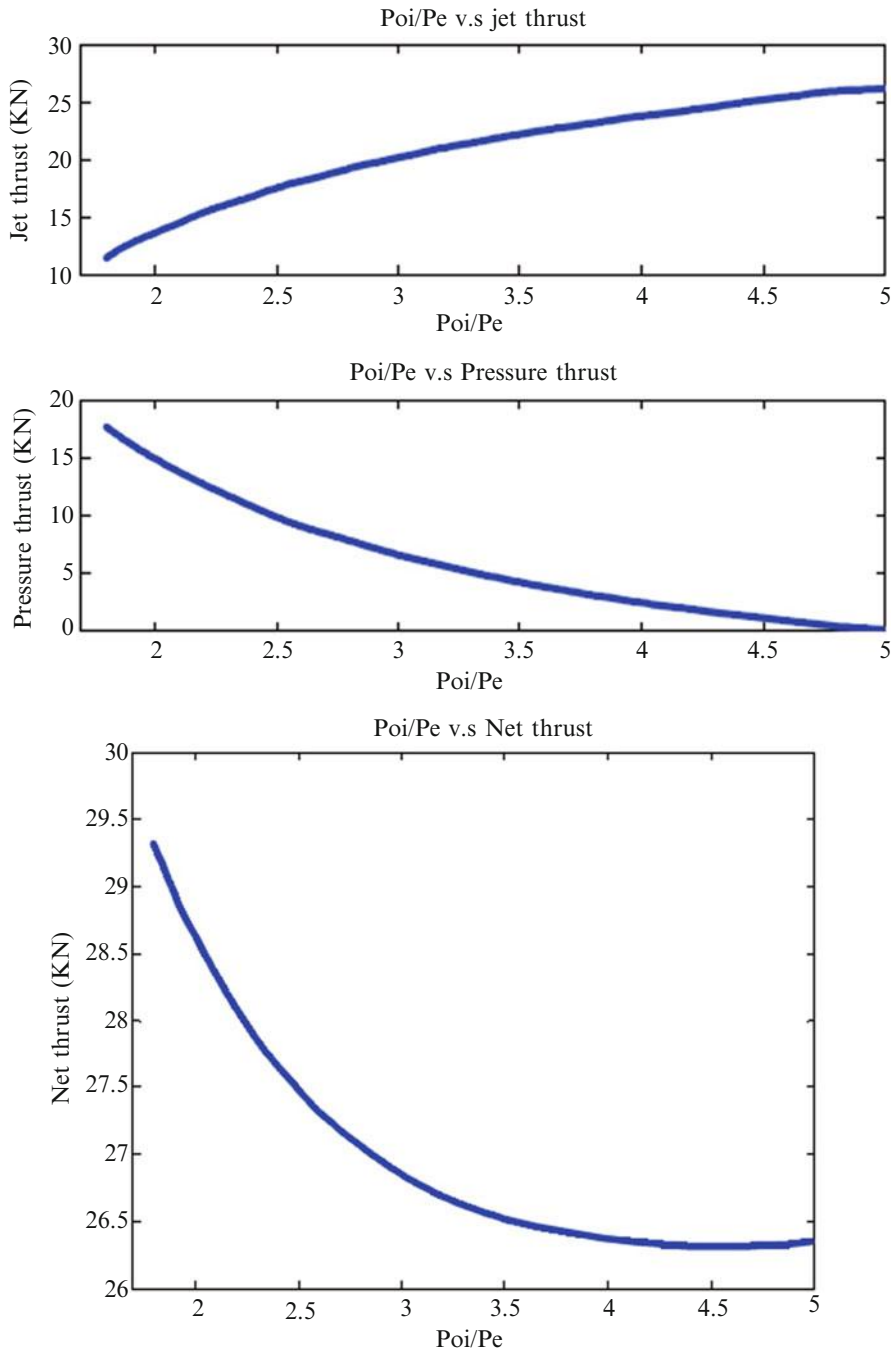


Fig. 3.16 Jet, pressure and net thrusts for different nozzle pressure ratio

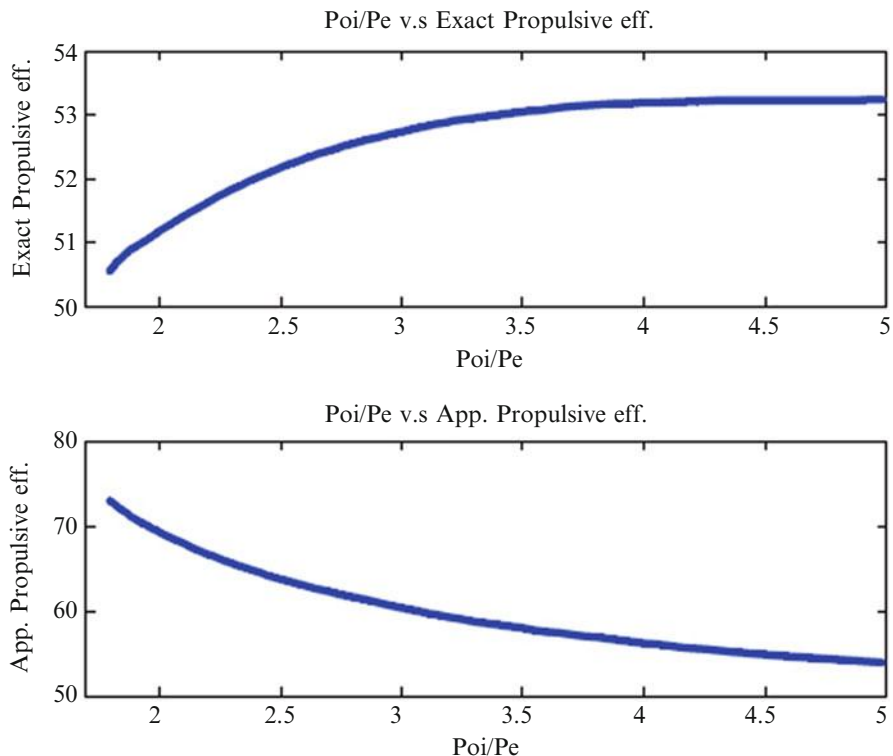


Fig. 3.17 Exact and approximate propulsive efficiency for different nozzle pressure ratio

Integration of the above equation yields the range of aircraft (S) as follows

$$S = \frac{u}{g} \frac{T}{\dot{m}_f} \frac{L}{D} \ln \left(\frac{m_1}{m_2} \right) \quad (3.31)$$

where (m_1) and (m_2) are the initial and final mass of aircraft.

From Eq. (3.25a), the above equation is reformulated as

$$S = \frac{u}{g} \frac{1}{TSFC} \frac{L}{D} \ln \left(\frac{m_1}{m_2} \right) \quad (3.32)$$

The above equation is known *Breguet's* equation, which was derived since 1920. Another expression for the range is obtained from the overall efficiency, Eq. (3.26) and Eq. (3.31), as

$$S = \frac{\eta_o Q_R}{g} \frac{L}{D} \ln \left(\frac{m_1}{m_2} \right) \quad (3.33)$$

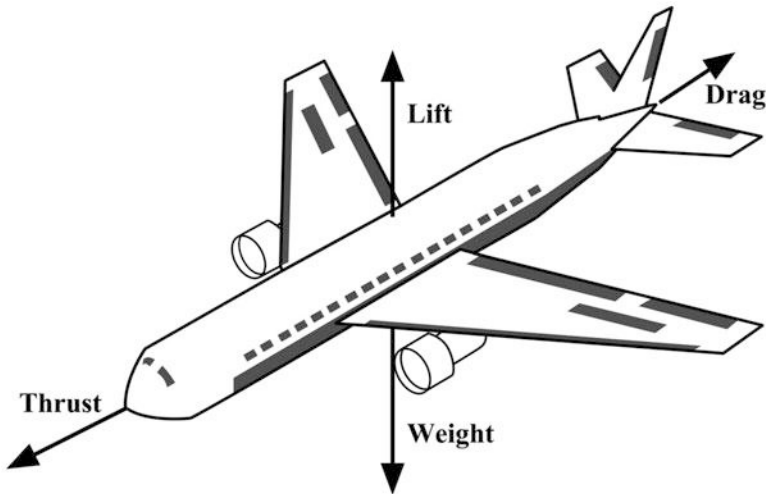


Fig. 3.18 Forces on airplane during cruise

In the above Eqs. (3.32) and (3.33), the ratio between the lift and drag forces may be alternatively written as $\frac{C_L}{C_D}$, where the lift force coefficient is calculated as usual from the relation:

$$C_L = \frac{W}{\frac{1}{2}\rho U^2 S_W}$$

where W and S_W are the aircraft weight and wing area.

The drag coefficient is calculated from the relation:

$$C_D = K_1 C_L^2 + K_2 C_L + C_{D_0}$$

where the constants K_1 , K_2 , and C_{D_0} are typical function of the flight Mach number and wing configuration (flap position, etc.). The C_{D_0} term is the zero lift drag coefficient, which accounts for both frictional and pressure drag in the subsonic flight and wave drag in supersonic flight [13]. The K_1 and K_2 terms account for the drag due to lift. Normally, K_2 is very small and approximately equal to zero in most fighter aircrafts.

It is clear from Eqs. (3.32) and (3.31) that to maximize the range of an aircraft flying at a specified speed [14]:

1. Fly at the maximum lift to drag ratio
2. Have the highest possible overall efficiency
3. Have the lowest specific fuel consumption
4. Have the highest possible ratio between the aircraft weights at the start and end of cruise

For a propeller/reciprocating or turboprop engines, a similar analysis may be followed.

From Eqs. (3.25) and (3.30), then

$$\therefore \frac{uT}{m_f} = \frac{\eta_{pr}}{ESFC}$$

Substituting the above equation in Eq. (3.31), the following equation for the range is obtained

$$S = \frac{\eta_{pr}}{g} \frac{1}{ESFC D} \frac{L}{D} \ln\left(\frac{m_1}{m_2}\right) \quad (3.34)$$

Similarly to maximize the range, the lift to drag ratio, propeller efficiency, and the ratio between the aircraft weight at the start to that at the end of cruise have to be chosen as maximums while the fuel consumption (ESFC) have to be minimum.

Airlines and aircraft manufacturers normally use the following forms for Breguet's relation:

For turbojet/turbofan engines:

$$S = \frac{u L}{c D} \ln\frac{m_1}{m_2} \quad (3.35)$$

and for turboprop engines:

$$S = \frac{\eta L}{c D} \ln\frac{m_1}{m_2} \quad (3.36)$$

where (c) is the specific fuel consumption [15] expressed in ($\text{lbs} \cdot \text{fuel}/\text{lb} \cdot \text{thrust}/\text{hr}$) or

($\text{lbs} \cdot \text{fuel}/\text{ESHP}/\text{hr}$). Another definition is also employed, namely, the *specific range* [16], which is given in miles per pound of fuel (mi/lb)

(a) For a turbojet/turbofan

$$\frac{mi}{lb} = \frac{u}{[c(\frac{D}{L})W]} = \frac{u L}{c D W} \quad (3.37a)$$

If u is in knots, mi/lb will be in nautical miles per pound of fuel.

(b) For a turboprop engine

$$\frac{mi}{lb} = 325 \left(\frac{\eta_{prop}}{c} \right) \left(\frac{L}{D} \right) \left(\frac{1}{W} \right) \quad (3.37b)$$

3.4.8 Range Factor

The range factor is defined as

$$RF = \frac{1}{g} \frac{u}{TSFC} \frac{L}{D} = \frac{1}{g} \frac{u}{TSFC} \frac{C_L}{C_D} \quad (3.38)$$

The minimum fuel consumption for a distance(s) occurs at the condition where the range factor is maximum.

3.4.9 Endurance and Endurance Factor

If the time spent in the air is of interest and not the distance traveled then one is concerned with endurance. Endurance is the longest time an aircraft can spend in flight without landing. The maximum endurance of an aircraft (or the time aloft) refers to a flight condition that requires the minimum fuel power.

The minimum fuel consumption as seen from Eq. (3.39) for a time flight time (t) occurs, when the endurance factor is maximum.

The instantaneous endurance is defined as the amount of time the aircraft will remain aloft from the next increment of fuel burned. This can be expressed by the relation:

$$\begin{aligned} \frac{dE}{dm} &= -\frac{1}{cT} \\ E &= \int_{m_1}^{m_2} \frac{dm}{-cT} = - \int_{m_1}^{m_2} \frac{1}{cD} \frac{L}{D} dm \\ E &= \frac{1}{cD} \frac{L}{D} \ln \frac{m_1}{m_2} \end{aligned} \quad (3.39)$$

and for propeller/turboprop engines:

$$E = \frac{\eta}{cuD} \frac{L}{D} \ln \frac{m_1}{m_2} \quad (3.40)$$

The endurance factor is defined as

$$EF = \frac{1}{g} \frac{1}{TSFC} \frac{L}{D} = \frac{1}{g} \frac{1}{TSFC} \frac{C_L}{C_D} \quad (3.41)$$

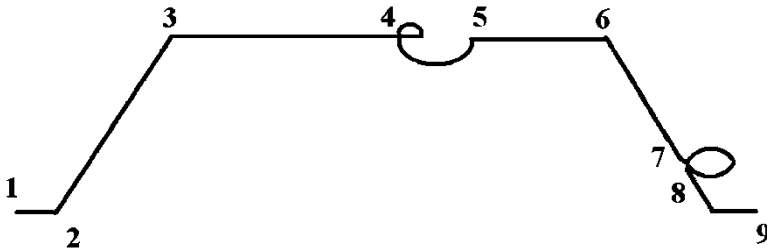


Fig. 3.19 Flight segments of a bomber in a mission

Table 3.8 Mission segments weight fractions [17]

	$\frac{m_{i+1}}{m_i}$
Warmup and takeoff	0.97
Climb	0.985
Landing	0.995

3.4.10 Mission Segment Weight Fraction

For analysis, the various mission segments, or “legs”, are numbered, with (1) denoting the start of the mission. Mission leg “one” is usually engine warmup and takeoff. The remaining legs are sequentially numbered [17]. The simple mission for a passenger aircraft the mission legs are: (1) warmup and takeoff, (2) climb, (3) cruise, (4) loiter, and (5) land (Fig. 3.19). Table 3.8 gives typical weight-fractions for mission legs [17].

Loiter weight fractions are found from the endurance factor; Eq. (3.41)

$$W_2/W_1 = e^{-\frac{E(TSFC)s}{(L/D)}}$$

It is important here to mention that the empty weight fraction ($\frac{W_e}{W_0}$) is expressed by the relation

$$\frac{W_e}{W_0} = AW_0^C K_{vs}$$

The values of the constants (A and C) are given in Table 3.9 for different aircraft.

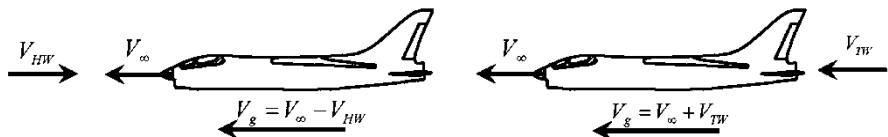
$$\begin{aligned} K_{vs} &= \text{variable sweep constant} = 1.04 \text{ if variable sweep} \\ &= 1.00 \text{ if fixed sweep} \end{aligned}$$

3.4.11 Head- and Tail-Wind

When an aircraft is in flight, it is moving relative to the body of air through which it is flying; therefore maintaining an accurate ground track is not easy unless there is no wind at all which is a very rare occurrence. The pilot must adjust heading to

Table 3.9 Empty weight fraction vs (W_0) [17]

$\frac{W_e}{W_0} = AW_0^C K_{vs}$	A	C
Sailplane-powered	0.91	-0.05
General aviation-single engine	2.36	-0.18
General aviation-twin engine	1.51	-0.10
Agricultural aircraft	0.74	-0.03
Twin turboprop	0.96	-0.05
Flying boat	1.09	-0.05
Jet trainer	1.59	-0.10
Jet fighter	2.34	-0.13
Military cargo/bomber	0.93	-0.07
Jet transport	1.02	-0.06

**Fig. 3.20** Head and tail wind conditions

compensate for the wind, in order to follow the ground track. Initially the pilot will calculate headings to fly for each leg of the trip prior to departure, using the forecast wind directions and speeds supplied by the meteorological authorities for the purpose. These figures are generally accurate and updated several times per day, but the unpredictable nature of the weather means that the pilot must be prepared to make further adjustments in flight. A general aviation (GA) pilot will often make use of either the E6B flight computer – a type of slide rule – or a purpose-designed electronic navigational computer to calculate initial headings. As will be explained in example (3.12), the flight time will depend on both the desired cruising speed of the aircraft and the wind – a tailwind will shorten flight times, a headwind will increase them.

Example 3.12 The range of an aircraft is given by Eq. (3.32) as

$$S = \frac{u}{g TSFC D} \ln\left(\frac{m_1}{m_2}\right)$$

where u is the air relative speed including the effect of wind as shown in Fig. 3.20 for either head- or tail-wind conditions. The shown military aircraft has the following data:

$$\text{Maximum range} = 3700 \text{ km}, \quad \frac{L}{D} = 10, \quad TSFC = 0.08 \frac{\text{kg}}{\text{N.h}}, \\ m_2 = 10,300 \text{ kg},$$

flight speed = 280 m/s.

1. Calculate the mass of fuel consumed during a trip in the following two cases:
 - (i) Head wind = 50 m/s
 - (ii) Tail wind = 50 m/s
2. Calculate the time for such a trip in the above two cases.

Solution

This example illustrates the effect of wind on both fuel consumption and the time of a trip.

1. Fuel consumption

Consider first the case of:

Tail wind

$$u = V_\infty + V_{TW} = 280 + 50 = 330 \text{ m/s}$$

From Eq. (3.32), the range is calculated using the relative speed rather than the airplane speed.

$$S = \frac{u}{g TSFC D} \frac{L}{D} \ln\left(\frac{m_1}{m_2}\right)$$

$$\ln\frac{m_1}{m_2} = \frac{(S)(g)(TSFC)}{(u)(\frac{L}{D})} = \frac{3700 \times 10^3 \times 9.8 \times 0.08}{330 \times 10 \times 3600} = 0.24418$$

$$\frac{m_1}{m_2} = 1.27657$$

$$\text{Fuel consumed} = m_1 - m_2 = m_2 \left(\frac{m_1}{m_2} - 1 \right) = 10,300(1.27657 - 1) = 2848 \text{ kg}$$

For the case of tail wind (i.e., supporting wind) = 2848 kg

Head wind

$$u = V_\infty - V_{TW} = 280 - 50 = 230 \text{ m/s}$$

$$\ln\frac{m_1}{m_2} = 0.35034$$

$$\frac{m_1}{m_2} = 1.4195$$

Fuel consumed = $m_1 - m_2 = m_2(1.4195 - 1) = 4321 \text{ kg}$

For the case of head wind (i.e., opposing wind) = 4321 kg

2. Trip time (t)

$$t = \frac{S}{u}$$

Tail wind

$$\text{Time} = \frac{3700}{330 \times 3.6} = 3.114 \text{ h}$$

Head wind

$$\text{Time} = \frac{3700}{230 \times 3.6} = 4.469 \text{ h}$$

From the above calculation tail wind shortens the trip time and saves fuel, while head wind increases the trip time and fuel consumption. What are the corresponding values for zero wind speed?

3.4.12 Route Planning

Pilot planning a flight under VFR (Visual flight rules) will usually use an aeronautical chart of the area published for the use of pilots. This map will depict controlled airspace, radio navigation aids, and airfields prominently, as well as hazards to flying such as mountains, etc. It also includes sufficient ground detail – towns, roads, wooded areas – to aid visual navigation.

The pilot will choose a route, taking care to avoid controlled airspace that is not permitted for the flight, restricted areas, danger areas, and so on. The chosen route is plotted on the map, and the lines drawn are called the *track*. During flight planning, two points must be taken into consideration:

Point of no return

Critical point

These points will be discussed hereafter.

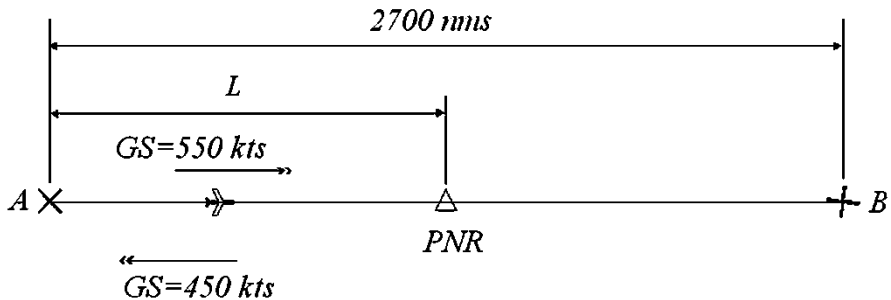


Fig. 3.21 Flight track with departure airport as an alternate

3.4.12.1 Point of No Return

The Point of no Return (*PNR*) is also known as the Point of Safe Return (*PSR*). This is the furthest point along track that a pilot can fly towards the destination and have sufficient fuel to divert to an alternate, with safe reserves on arrival. In other words, it is pilot's last chance to assess his/her prospect of a successful approach and landing at his destination and decide whether to go on or to divert. If any doubt exists, he/she must *divert to the alternate*.

There are a number of methods which can be used to calculate a *PNR/PSR*, but the one most favored uses what are called Specific Fuel Flows (*SFF*).

These are calculated by dividing the planned cruise fuel flow by the expected ground speeds towards the destination and towards the alternate field. Normally, two cases may be expected:

1. When the alternate is the departure field
2. Alternate is on track between the departure point and the destination

Two examples will be given below to illustrate both cases.

Example 3.13 Consider a flight from airport A to airport B, with A as the alternate field (Fig. 3.21). The distance A to B is 2700 nms. Maximum range cruise power will be used, giving a fuel flow (FF) of 800 l/h. The aircraft can carry 8000 l of useable fuel without exceeding the Maximum AUW (All Up Weight (Gross)). The Fixed Reserve is 1400 l. The used fuel for taxi and the climb are 100 and 500 l, respectively. A 15 % of fuel is next maintained to provide a Variable Reserve. At this power setting, the planned TAS (true airspeed) is 500 kts and a 50 kts tailwind is forecast A to B. Calculate the distance of point of no return (PNR) from the departure airport A.

Solution

The ground speed from A to B is

$$V_{AB} = V_0 + V_1 = 550 \text{ kts}$$

For a return to A, the ground speed is

$$V_{BA} = V_0 - V_1 = 450 \text{ kts}$$

Maximum range cruise power will be used, giving a fuel flow (FF) of 800 l/h, and this fuel flow will also be used for a Fixed Reserve and any holding.

To establish the Flight Fuel Available for the PNR calculation, we must subtract from the Useable Fuel the Fixed Reserve (1400 l), the taxi fuel (100 l), and the climb allowance (500 l). The forecast for a possible return to A does not indicate the need for any holding fuel. Therefore, the Flight Fuel Available (FFA) is

$$\text{FFA} = 8000 - (1400 + 100 + 500) = 6000 \text{ l}$$

This figure is now divided by 1.15 to provide a Variable Reserve, giving a final FFA of 5217 l.

Assume that L is the distance from airport A to PNR, and fuel consumption as:

$$Q_1 = \text{Fuel quantity consumed in the root from A to PNR}$$

$$Q_2 = \text{Fuel quantity consumed in the root from PNR to A}$$

Total fuel consumed $Q_1 + Q_2 == 5217 \text{ l}$

$$Q_1 = FF \times T_1 = 800T_1, \quad Q_2 = FF \times T_2 = 800T_2$$

$$T_1 = \frac{L}{V_0 + V_1}, \quad T_2 = \frac{L}{V_0 - V_1}$$

$$Q = Q_1 + Q_2 = FF \times (T_1 + T_2) = FF \times \left(\frac{L}{V_0 - V_1} + \frac{L}{V_0 + V_1} \right)$$

$$Q = FF \times L \times \left(\frac{2V_0}{(V_0 - V_1)(V_0 + V_1)} \right)$$

$$L = Q \times \frac{(V_0 - V_1)(V_0 + V_1)}{2V_0 \times FF} = 5217 \times \frac{450 \times 550}{2 \times 500 \times 800} = 1614 \text{ nms}$$

The PNR is 1614 nms apart from departure airport and 1086 nms apart from arrival airport.

Example 3.14 We will use the previous example of a flight from A to B over a distance of 2700 nms, but with the possible alternate (C) located at 700 nms along track towards A, i.e., the distance from C to B is 2000 nms. The other planning data remains the same as in the previous example, i.e.:

- (a) Flight Fuel Available at A = 5217 l (after allowing for a Variable Reserve)
- (b) Cruise Fuel Flow = 800 l/h
- (c) Ground Speed away from home = 550 kts
- (d) Ground Speed back to home = 450 kts

Calculate the distance between departure airport (A) and PNR.

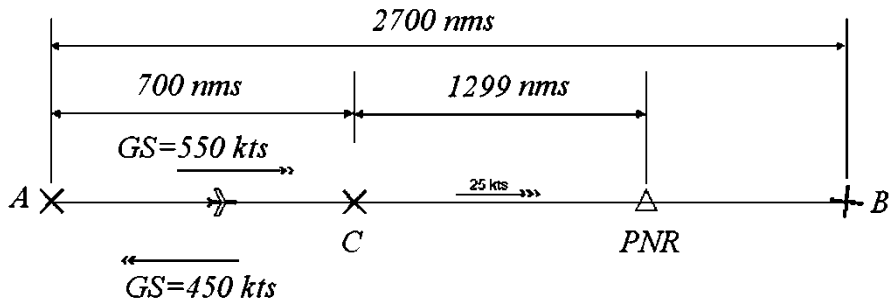


Fig. 3.22 Flight track with alternate on track

Solution

We first determine how much fuel is required to fly from A to overhead C. This is equal to the distance A to C (700 nms) divided by the speed (550 kts) and multiplied by the cruise fuel consumption (800 l/h).

Q = Fuel quantity consumed in the root from A to C

$$Q = FF \times T = 800T = 800 \frac{700}{550} = 1,018 \text{ l}$$

Fuel available to the trip from C to PNR and PNR to C is then

$$Q' = 5217 - 1,018 = 4199 \text{ l}$$

The distance to PNR is L, given by the relation:

$$L = Q' \times \frac{(V_0 - V_1)(V_0 + V_1)}{2V_0 \times FF} = 4199 \times \frac{450 \times 550}{2 \times 500 \times 800} = 1299 \text{ nms}$$

The distance of the PNR from C is therefore 1299 nms. This is 701 nms short of B and 1999 nms away from A. If the aircraft flies beyond this point, there will not be sufficient fuel to return to C with the fixed reserve intact (Fig. 3.22).

3.4.12.2 Critical Point

Similarly, the Equal Time Point, referred to as the ETP (also Critical point (CP)), is the point in the flight where it would take the same time to continue flying straight, or track back to the departure aerodrome. The ETP is not dependant on fuel, but wind, giving a change in ground speed out from, and back to the departure aerodrome. In Nil wind conditions, the ETP is located halfway between the two aerodromes, but in reality it is shifted depending on the wind speed and direction.

While the distance to a PNR is dependent on fuel availability and fuel flow, the distance to a *Critical Point (CP)* is independent of fuel considerations and is based on groundspeeds only.

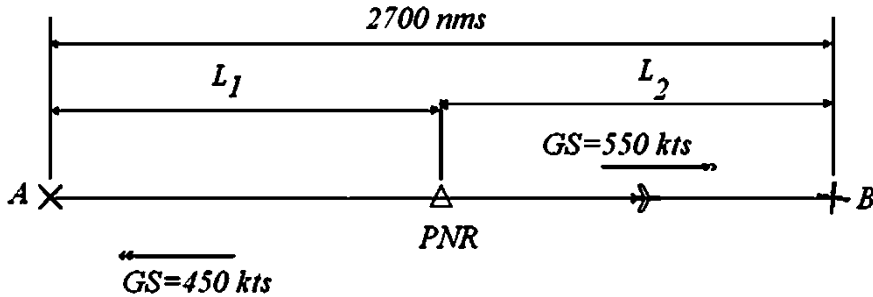


Fig. 3.23 Critical point

As an illustration, we will calculate a CP/ETP for the previous example flight.

Example 3.15 Consider a flight from airport A to airport B. The distance A to B is 2700 nms. At this power setting, the planned TAS (true airspeed) is 500 kts and a 50 kts tailwind is forecast A to B. Calculate the critical point (CP) from the departure airport A (Fig. 3.23).

The ground speed from CP to B is ($V_{AB} = V_0 + V_1 = 550$ kts), while the ground speed for a return to A is ($V_{BA} = V_0 - V_1 = 450$ kts).

T_1 = Flight time from critical point to departure airport A

T_2 = Flight time from critical point to arrival airport B

$$T_1 = \frac{L_1}{V_0 - V_1}, \quad T_2 = \frac{L_2}{V_0 + V_1}$$

$$\text{Since } T_1 = T_2, \quad \text{then } \frac{L_1}{450} = \frac{L_2}{550}$$

$$\frac{L_2}{L_1} = \frac{550}{450} = \frac{11}{9}$$

$$\therefore L_1 + L_2 = 2700$$

$$\therefore L_1 = 1215 \text{ kts} \quad L_2 = 1485 \text{ kts}$$

From this critical point, the time on to B is 2.7 h (1485/550), and the time back to A is also 2.7 h (1215/450).

3.4.13 Specific Impulse

The specific impulse (I_{sp}) is defined as the thrust per unit fuel flow rate, or

$$I_{sp} = \frac{T}{\dot{m}_f g} \tag{3.42}$$

This quantity enters directly into the calculation of the fractional weight change of aircraft (or rocket) during flight. Thus from Eq. (3.31), the range can be expressed in term of the specific impulse as follows

$$S = u I_{sp} \frac{L}{D} \ln \left(\frac{m_1}{m_2} \right) \quad (3.43)$$

The specific impulse is equally applied for both rockets and aircrafts. The units of specific impulse are time (seconds).

Problems

- 3.1 A General Electric J79-GE-15 turbojet engine is one of two propelling a McDonnell F4C airplane is powered by two General Electric J79-GE-15 turbojet engines. F4C has the following characteristics: wing area $S = 49 \text{ m}^2$, engine inlet area $A_I = 0.6 \text{ m}^2$, cruise Mach number $M_0 = 0.82$, and flight altitude of 30,000 ft. The drag coefficient of the aircraft under these conditions is 0.045. Determine:

- (a) The net thrust of the engine
- (b) The mass flow rate through the engine
- (c) The gross thrust of the engine

Then, if the exhaust pressure $P_e = P_0$

- (d) Estimate the exhaust velocity V_e assuming that the turbine exit stagnation temperature (which is the nozzle entry stagnation temperature) as $T_{0e} = 1005.4 \text{ K}$
- (e) Estimate the exit static temperature T_e
- (f) The exit Mach number M_e



Problem 1 McDonnell F4C

- 3.2 A turbojet engine powers an aircraft flying at a speed of 245 m/s, which has an exhaust speed of 560 m/s and a specific thrust of 535 N · s/kg. Using the three different formulae, calculate the propulsive efficiency. What are your comments?

(Neglect the fuel-to-air ratio).

- 3.3 A turbojet engine is powering an aircraft flying at 9 km (ambient temperature and pressure are 229.74 K and 30.8 kPa). It has the following data:

$$\dot{m}_a = 40 \text{ kg/s}, \quad f = 0.02, \quad u_e = 950 \text{ m/s}, \quad P_e = 100.0 \text{ kPa}, \quad A_e = 0.25 \text{ m}^2$$

Plot

- (a) The relation between the propulsive efficiency η_p and the speed ratio (u/u_e)
- (b) The relation between the thrust force and the speed ratio (u/u_e)

The flight speed u – varies from 0 to 500 m/s.

- 3.4 A turbojet engine is being flown at a velocity of 230 m/s. It is burning a hydrocarbon fuel with a heating value of 43,000 kJ/kg. The specific thrust is 500 N/(kg.s), and the thrust specific fuel consumption is 0.08 kg/(N.h). Calculate:

- (a) Fuel-to-air ratio
- (b) Overall efficiency
- (c) Exhaust speed of gases
- (d) Propulsive efficiency
- (e) Thermal efficiency

- 3.5 The GENx high-bypass-ratio turbofan engine at maximum static power ($V_0=0$) on a sea level, standard day ($P_0=101$ kPa, $T_0=288.0$ K) has the following data:

Total air mass flow rate through the engine is 1000 kg/s, bypass ratio is 9.3, the exit velocity from the core is 360 m/s, the exit velocity from the bypass duct is 265 m/s, and the fuel flow rate into the combustor is 3750 kg/h. For the case of exhaust pressures equal to ambient pressure ($P_0=P_e$), estimate the following:

- (a) The thrust of the engine
- (b) The thermal efficiency of the engine (heating value of jet fuel is 43,000 kJ/kg)
- (c) The propulsive efficiency and thrust specific fuel consumption of the engine

- 3.6 A commercial airliner has a dry mass of the aircraft 600 t and has a range of 9000 km using 150 t of hydrocarbon fuel. Estimate the range of the aircraft when burning the same volume of hydrogen (both gaseous and liquid). The hydrocarbon heating value is 43,000 kJ/kg and its density is 804 kg/m³. The gaseous and liquid hydrogen has heating value of 120 MJ/kg. Density of liquid and gaseous hydrogen is 70 kg/m³ and 0.08 kg/m³.

- 3.7 A fighter aircraft flies at speed of 650 m/s at an altitude of 9.0 km. It is powered by a single turbojet engine having an inlet area of 0.35 m^2 . Assuming the exhaust speed is constant and equal to 700 m/s, the fuel to air ratio $f = 0.025$ and the nozzle is unchoked. Calculate:
- The thrust force
 - Propulsive efficiency
- 3.8 What is the equivalent specific fuel consumption (ESFC) of a turboprop engine that consumes 600 kg of fuel per hour and produces 1.2 kN of exhaust thrust and 2300 kW during flight at 425 km/h. The propeller efficiency is 0.9.
- 3.9 The below figure shows space shuttle Endeavor, sitting atop of carrier NASA Boeing 747-400, which is powered by four turbofan engines GE CF6-50E. If the thrust force is expressed by the relation:

$$\tau = \dot{m} (u_e - u)$$

- (i) *Prove that the thrust is a maximum*

$$\text{when : } u = 0.5 u_e$$

- (ii) The carrier Boeing 747-400 is only considered here.



Figure Problem (3.9)

It has the following data:

Gross mass	396,890 kg	Wing area	525 m ²
Drag coefficient	0.035	Exhaust jet speed	600 m/s
Engine thrust force	106 kN	Air density	0.414 kg/m ³
Engine inlet area	3.14 m ²		

Calculate

- Minimum flight speed
- The maximum thrust that the engine can develop if ($u = 0.5u_e$)
- Maximum acceleration

- (iii) Consider the assembly case with space shuttle atop of Boeing 747 as shown in figure. Space shuttle has the following data:

Gross mass	110,000 kg
Wing area	343 m ²
Drag coefficient	0.025

For the same minimum flight speed calculated above, calculate the maximum *acceleration* of the space shuttle-Boeing assembly.

- 3.10 For a two stream engine (turboprop or turbofan engines), prove that the ratio between the exhaust speed of hot stream and the inlet speed (u_{eh}/u) is expressed by the relation:

$$\frac{u_{eh}}{u} = \frac{1 \pm \sqrt{1 - \eta_p C}}{\eta_p}$$

$$\text{where } C = \eta_p \beta \left(\frac{u_{ec}}{u} \right)^2 - 2\beta \left(\frac{u_{ec}}{u} \right) + (1 + \beta)(2 - \eta_p)$$

Four engine types are considered in the below table:

	Turboprop	High bypass ratio turbofan	Low bypass ratio turbofan	Turbojet
β	30.0	10.0	1.0	0
η_p	0.9	0.75	0.62	0.5
$\frac{u_{ec}}{u}$	1.05	1.2	1.4	0

1. Calculate $\left(\frac{u_{eh}}{u} \right)$ for each case
2. Comment

- 3.11 The range of an aircraft is given by Eq. (3.32) as:

$$S = \frac{u}{g} \frac{1}{TSFC D} \ln \left(\frac{m_1}{m_2} \right)$$

where u is the air relative speed including the effect of wind (for either head- or tail-wind conditions). The shown military aircraft has the following data:

Maximum range = 3700 km, $\frac{L}{D} = 10$, TSFC = 0.08 kg/N.h, $m_2 = 10,300$ kg, flight speed = 280 m/s. If the maximum fuel capacity is 4700 kg, what is the maximum value for head wind to reach this destination?

- 3.12 Consider an airliner flying from airport A to airport B, with A as the alternate field. The distance A to B is 6000 km. Maximum range cruise power will be used, giving a fuel flow (FF) of 800 l/h. The aircraft can carry 9000 l of useable fuel without exceeding the Maximum AUW. The Fixed Reserve is 1500 l. The used fuel for taxi and the climb are 100 and 500 l, respectively. A 15 % of fuel is next maintained to provide a Variable Reserve. At this power setting, the planned TAS (true airspeed) is 800 km/h and a 100 km/h tailwind is forecasted A to B. Calculate the distance of point of no return (PNR) from the departure airport A.

References

1. El-Sayed AF (2008) Aircraft propulsion and gas turbine engines. Taylor & Francis, Boca Raton, Florida
2. Crawford R, Schulz R (2008) Fundamentals of air breathing propulsion, University of Tennessee Space Institute, Aero propulsion Short Course, PS-749
3. United Technologies, Pratt Whitney (1988) The aircraft gas turbine engine and its operation, P&W Operation Instruction 200
4. Moustapha H (2010) Turbomachinery and propulsion, Pratt & Whitney Canada Inc., Course Handbook
5. The jet engine, (1996) Rolls Royce Plc
6. Kurzke J (2003) Aero-engine design: a state of the art, preliminary design, Von Karman Institute Lecture Series, Belgium
7. Zucrow MJ (1958) Aircraft and missile propulsion, vol I, Thermodynamics and fluid flow and application to propulsion engines. Wiley, New York
8. Ashby H (1974) Engineering analysis of flight vehicles. Addison-Wesley Publication Co, Reading, Mass
9. Saravanamuttoo HIH, Rogers GFC, Cohen H, Stranzicky PV (2009) Gas turbine theory. Prentice Hall, [Upper Saddle River](#), New Jersey
10. Hill JP, Peterson C (1992) Mechanics and thermodynamics of propulsion, 2nd edn. Addison Wesley Publication Company, Reading, Mass
11. Shepherd DG (1972) Aerospace propulsion. American Elsevier Publishing Company, Inc, New York
12. Schumann U (2000) Influence of propulsion efficiency on contrail formation, vol 4, Aerospace science and technology. Elsevier, France, pp 391–401
13. Mattingly JD (1996) Elements of gas turbine propulsion. McGraw-Hill International Edition, New York
14. Anderson JD Jr (1999) Aircraft performance and design. WCB/McGraw-Hill, Boston
15. Corning G (1979) Supersonic and subsonic CTOL and VTOL airplane design, Box No.14, 4th ed., College Park
16. Shevell R (1983) Fundamentals of flight. Prentice-Hall, Inc, [Upper Saddle River](#), New Jersey
17. Raymer DP (1999). Aircraft design: a conceptual approach (AIAA Education Series), USA

Chapter 4

Piston Engines and Propellers

4.1 Introduction

Air-breathing engines are named so because they need only air for combustion while carrying appropriate fuels. Consequently, these propulsion systems stop working outside the atmosphere.

Aircraft designers endeavor is to achieve higher power (or thrust) and less weight (using advanced composite material). Thus achieve high thrust-to-weight ratio. Other goals are smaller frontal area, reduced emission (CO_2 , SOx , and NOx), small noise footprint, better cooling characteristics, and lower fuel consumption [1]. Moreover, during production, it is recommended to be built with green processes and material.

The main target of this chapter and the succeeding three ones (5–7) is to provide aerodynamics and thermodynamics details of different aero engines powering all types of aircrafts discussed in Chap. 1 as illustrated by Fig. 1.56, which is reproduced again here as Fig. 4.1. We are concerned in these four chapters with internal combustion engines rather than external combustion engines. Internal combustion engines have two broad categories, namely, shaft and reaction engines. Shaft engines are categorized as two groups, namely:

- Intermittent types
- Continuous types

This chapter handles only intermittent combustion engines, namely, reciprocating and rotary types. Continuous combustion engines identified as turbine shaft engines are categorized as turboprop, turboshaft, and propfan engines, which will be handled in Chap. 7. The other main group of internal combustion is the reaction engines. This engine group is either of the Ram Based Cycles (RBC) (also identified as athodyd, which stands for Aero T HermODYnamic Duct) or Turbine Based Cycle (TBC) Engines. Athodyd group (or RBC) includes ramjet, pulsejet, scramjet, and dual combustion ramjet engines, which will be treated in Chap. 5 [1]. Turbine based

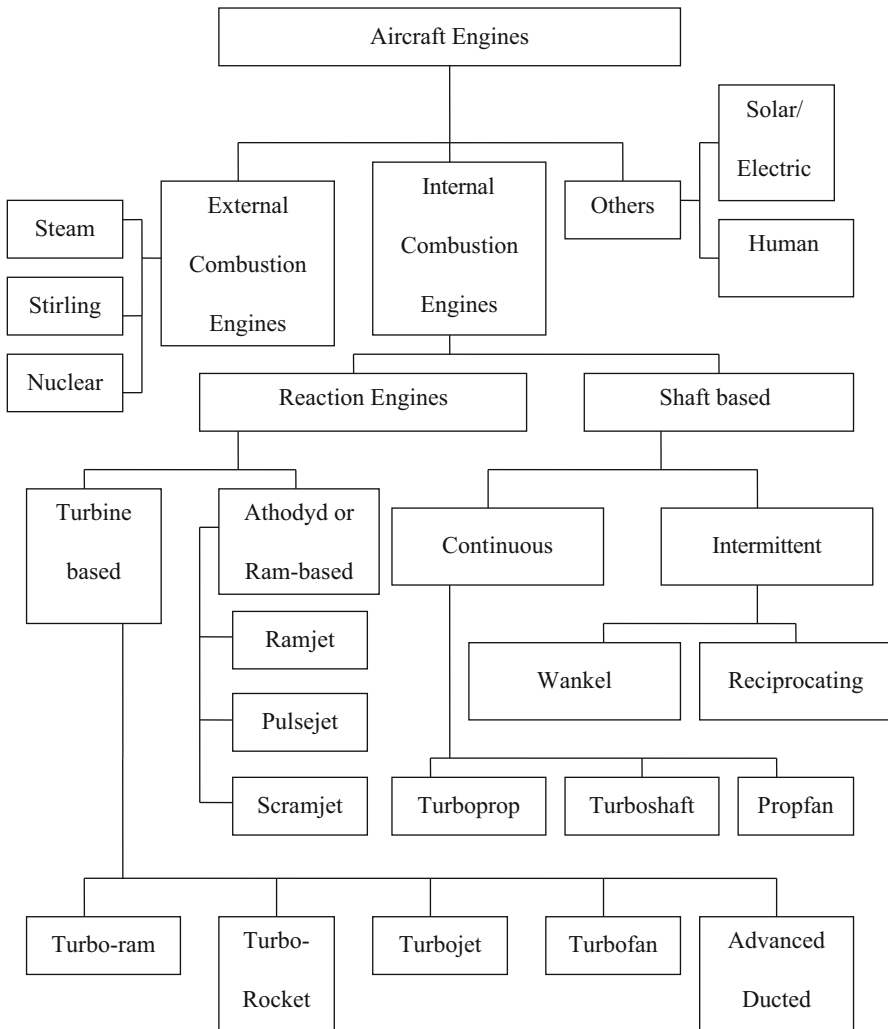


Fig. 4.1 Classification of propulsion systems

engines (or TBC) include turbojet, turbofan, turbo ramjet, turbo rocket, and advanced ducted fan engines, which will be handled in Chap. 6.

All of these engines must fulfill the following basic requirements:

1. Efficiency: the engine must operate at high efficiency under a wide range of atmospheric conditions
2. Economy: the engine must be economic to produce, run, and maintain
3. Reliability: the engine must be able to endure long periods of operation at high power settings without failure

A question arises here is: Why are there different types of engines? The short answer is that each engine is designed to fulfill the mission requirements of

Table 4.1 Jet velocity for different aerospace vehicles

Propulsion system	Jet velocity (m/s)
Helicopter lifting rotor	Up to 30
Propeller	30–200
Remote ducted fan, unducted fan, or propfan	100–300
Turbofan	200–600
Turbojet (sea-level, static)	350–600
Turbojet ($M = 2.0$ at 36,000 ft, approx. 600 m/s)	900–1200
Ramjet ($M = 2.0$ at 36,000 ft, approx. 600 m/s)	900–1200
Ramjet ($M = 4.0$ at 36,000 ft, approx. 1200 m/s)	1800–2400
Solid-propellant rocket	1500–2600
Liquid-propellant rocket	2000–3500
Nuclear rocket (solid core reactor)	9000–10,000
Nuclear rocket (fusion reactor)	25,000
Solar	6000
Arc	20,000
Plasma and ion	30×10^6
Photon	300×10^6

aerospace vehicle to which it is installed. Airliners and cargo planes spend most of their flight operation in a cruise condition. For these airplanes, thrust is not as important as high engine efficiency and low **fuel consumption**. Since thrust depends on both the amount of air/gas moved and its velocity, we can generate high thrust by accelerating a large mass of air/gas by a small amount (propeller coupled to either piston or turboprop engines as well as single/double propfan engines), or by accelerating a small mass of air/gas by a large amount (RBC based and TBC engines). Because of the high aerodynamic efficiency of propellers and fans, it is more fuel efficient to accelerate a large mass of air by a small amount. That is why we find high bypass turbofans and turboprops on cargo planes and airliners.

Most fighter planes or experimental high speed aircrafts require very high excess thrust to accelerate quickly and to overcome the high drag associated with high speeds. For these airplanes, engine efficiency is not as important as very high thrust. Modern military aircraft typically employ afterburners on a low bypass turbofan engines. Future hypersonic aircraft will employ some type of ramjet/scramjet or **rocket propulsion**.

Since thrust force is dependent on jet speed, the higher jet speed is the higher thrust and flight speed of aerospace vehicles. Table 4.1 presents the jet velocity for different aerospace vehicles.

4.2 Intermittent (or Piston) Engines

As illustrated in Fig. 4.1, intermittent combustion (or piston) engines are one of the shaft engines. It is sometimes identified as *Aero Piston Engines* to differentiate it from automotive piston engines. Aero piston engines are classified into three types:

Table 4.2 Aviation statistics (2000–2032)*

Year	Fixed wing				Rotorcraft		Total	
	Piston		Turbine		Piston	Turbine	Piston	Turbine
	Single engine	Multi-engine	Turbo prop	Turbo jet				
2000	149,422	21,091	5762	7001	2680	4470	173,193	17,233
2005	148,101	19,412	7942	9823	3039	5689	170,552	23,454
2010	139,519	15,900	9369	11,484	3588	6514	159,007	27,367
2013	136,650	15,660	9570	12,410	3875	7165	156,185	29,145
2020	132,335	15,175	10,120	16,265	4505	8940	152,015	35,325
2026	132,370	14,745	10,740	20,865	5075	10,650	152,190	42,255
2032	135,340	14,350	11,445	26,935	5705	12,550	155,395	50,930

FAA Aerospace Forecast, Fiscal Years 2012–2032, FAA Report

namely: rotary, reciprocating, and supercharged/turbocharged reciprocating engines. The Wright Flyer that started the era of powered flight in 1903 was powered by a simple four-cylinder piston engine. Aero piston engines were the primary power plant during the first 50 years of flight. Aero piston engines may power small aircrafts and helicopters. Small airplanes have one or more piston-powered engines connected to the propeller(s), which provide thrust to move the aircraft on the ground and through the air. Piston-powered aircrafts/helicopters most commonly use 100 octane low-leaded fuel. Table 4.2 provides astonishing statistics for present and forecast of piston and jet engines in the period 2000–2032. Aircraft powered by jet engines are nearly 10 % of those powered by piston engines in year 2000. However, this ratio is expected to increase to 27.8 % by year 2032. The number of aircraft powered by piston engines drops by 10 % in the interval 2000–2032, while the number of aircrafts powered by jet engines increases by 195 % in the same period. Many of the piston aircraft used for business typically fly relatively short missions of 300–400 miles, at altitudes below 15,000 ft, using very small general aviation airports that are often without air traffic control towers. Helicopters are often attractive to business people because of their ability to land at a variety of heliports and outlying airports. Manufacturers of piston-driven airplanes include the following companies: Cirrus, Cessna, Hawker Beechcraft, Diamond, and Mooney. Manufacturers of helicopters include the following companies: Agusta Westland, Bell, Enstrom Helicopter, Eurocopter, Robinson, and Sikorsky.

Piston engines are sources of power in land, sea, and air applications. They are the only source for nearly all automotives. Very few cars in present days use electrical and/or solar powers. Most locomotives use piston engines. Most maritime applications also use piston engines. In aviation field also, most small aircrafts (whether in capacity or range) are powered by piston engines. However, for both maritime and aviation applications, piston engines cannot propel these vehicle by its own. Piston engines must be coupled to propellers. Marine propellers sometimes called marine screws were invented and employed far before air propellers or air screws. Wright brothers had also designed, tested (in their wind tunnel), and

manufactured the first air propeller in their Flyer I (or 1903 Flyer). Their lightweight four stroke piston engine powered the twin [propellers](#) via a sprocket [chain drive](#).

For this reason, this chapter is divided into two parts: the first one handles aero-piston engines and the second part treats propellers. In both parts, aerodynamics and available power are the main topics.

4.2.1 Milestones

Since 1903 and up to the first jet engines invented by Sir Frank Whittle and Dr. von Ohain, piston engines were the only prime mover for flight vehicles. Later on jet engines took over and became the dominant prime mover or power plants employed in propelling aircrafts. [Appendix A](#) provides a short list for piston engines employed in aviation field, starting from Wrights Brothers.

4.2.2 Types of Aero Piston Engines

Aero piston engines as described earlier are further classified into the following three types:

- Rotary engines
- Reciprocating engines
- Supercharged/turbocharged reciprocating engines

Piston engines are further classified based on number of cylinders, method of cooling, and cylinders' arrangements. Regarding cooling, most aircraft engines are air-cooled. However, a few liquid-cooled engines are in operation. In both cases, excess air is transferred to the surrounding air. In air cooled, heat is transferred directly to the surrounding air. A liquid cooled engine transfer heat from the cylinders to a liquid coolant which in turn transfers the heat to the surrounding air through the radiator.

Two principal types of piston engines are:

- Spark ignition engine (SI), which is also identified as petrol engine or gasoline engine
- Compression-ignition engine (CI), which is also identified as diesel engine

Moreover, piston engines may be specified as:

- Two-stroke engines
- Four-stroke engines

In a spark-ignition engine, a mixture of fuel and air is ignited by a spark plug. In most petrol engines, the fuel and air are usually pre-mixed before compression. The pre-mixing was formerly done in a carburetor, but now it is done by electronically controlled fuel injection, except in small engines. Spark-ignition engines are

advantageous for applications requiring small power (up to about 225 kW; 300 horsepower). In a compression-ignition engine, air is compressed to a high enough pressure and temperature that combustion occurs spontaneously when fuel is injected. Petrol engines run at higher speeds than diesels, partially due to their lighter pistons, connecting rods and crankshaft and due to petrol burning faster than diesel. However, the lower compression ratios of a petrol engine give a lower efficiency than a diesel engine. Compression-ignition engines are more reliable and normally preferred for applications when fuel economy and relatively large amounts of power are required. New diesel engines may bring fuel efficiency and lead-free emissions to small aircraft, representing the biggest change in light aircraft engines in decades. The diesel engine has the highest thermal efficiency of any regular internal or external combustion engine due to its very high compression ratio. In the middle range, spark ignition and compression-ignition engines are used.

4.2.2.1 Rotary Engines

(A) Conventional types

The *rotary engine* was an early type of [internal-combustion engine](#), usually designed with an odd number of cylinders per row in a [radial configuration](#). In rotary engines, the [crankshaft](#) remained stationary and the entire [cylinder block](#) rotated around it. This type of engine was widely used during [World War I](#) and the years immediately preceding that conflict. They have been described as very efficient in terms of power output, weight, cost, manufacture, and reliability.

The rotary engine met these goals with Gnome Omega No. 1 Rotary Engine; Fig. 4.2 as an example. The entire engine rotates with the propeller, providing plenty of airflow for cooling regardless of the aircraft's forward speed. Some of

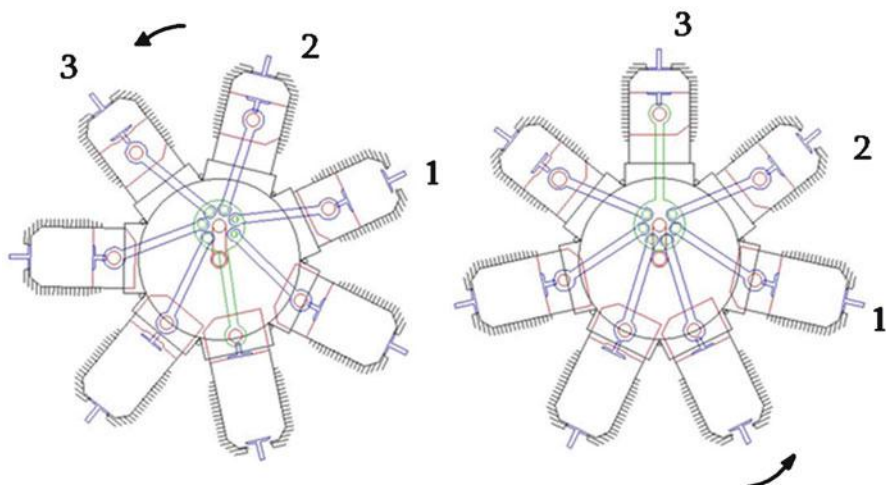


Fig. 4.2 Rotary engine (Gnome engine)

these engines were a two-stroke design, giving them a high specific power and power-to-weight ratio. Unfortunately, the severe gyroscopic effects from the heavy rotating engine made the aircraft very difficult to fly. The engines also consumed large amounts of castor oil, spreading it all over the airframe and creating fumes which were nauseating to the pilots. Engine designers had always been aware of the many limitations of the rotary engine.

(B) Wankel Engines

The *Wankel engine* is a type of internal combustion engine using an [eccentric rotary design](#) to convert pressure into a rotating motion instead of using reciprocating [pistons](#) (Fig. 4.3a). Its [four-stroke cycle](#) (Fig. 4.3b) takes place in a space between the inside of an oval-like [epitrochoid](#)-shaped housing and a rotor that is similar in shape to a [Reuleaux triangle](#) but with sides that are somewhat flatter. The very compact Wankel engine delivers smooth high-[rpm](#) power. It also has high horsepower per displacement compared to other internal combustion engines. The lubrication system is similar to that of the two-stroke engine, and thus it does not need a separate system like the four-stroke engine.

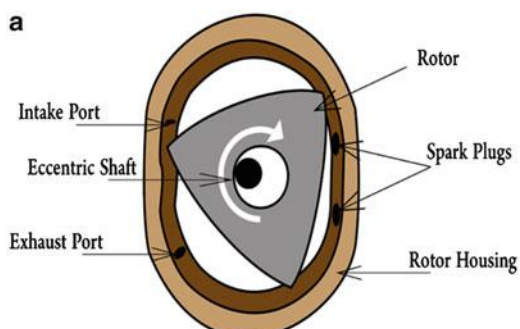
Wankel engine is considered optimum power plant for light aircraft, as it is light, compact, and almost vibrationless and has a high power-to-weight ratio. Further aviation benefits of a Wankel engine include:

- (i) Rotors cannot seize, since rotor casings expand more than rotors
- (ii) Not susceptible to “shock-cooling” during descent
- (iii) Does not require an enriched mixture for cooling at high power

The first Wankel rotary-engine aircraft was the experimental Lockheed Q-Star civilian version of the [United States Army](#)'s reconnaissance QT-2 in 1967. It was later on installed in a variety of [aircrafts](#) including [Diamond DA20](#), [general aviation aircraft](#) designed for [flight training](#). Moreover, Wankels due to their compact size and quiet operation are used in drones or [UAVs](#) (as an example, AAI RQ-7 Shadow) (Fig. 4.4).

Wankel engines are also becoming increasingly popular in homebuilt experimental aircraft, such as the light aircraft [ARV Super2](#) powered by liquid cooled MidWest AE110 twin-rotor Wankel engine (Fig. 4.5).

Fig. 4.3a Wankel engine



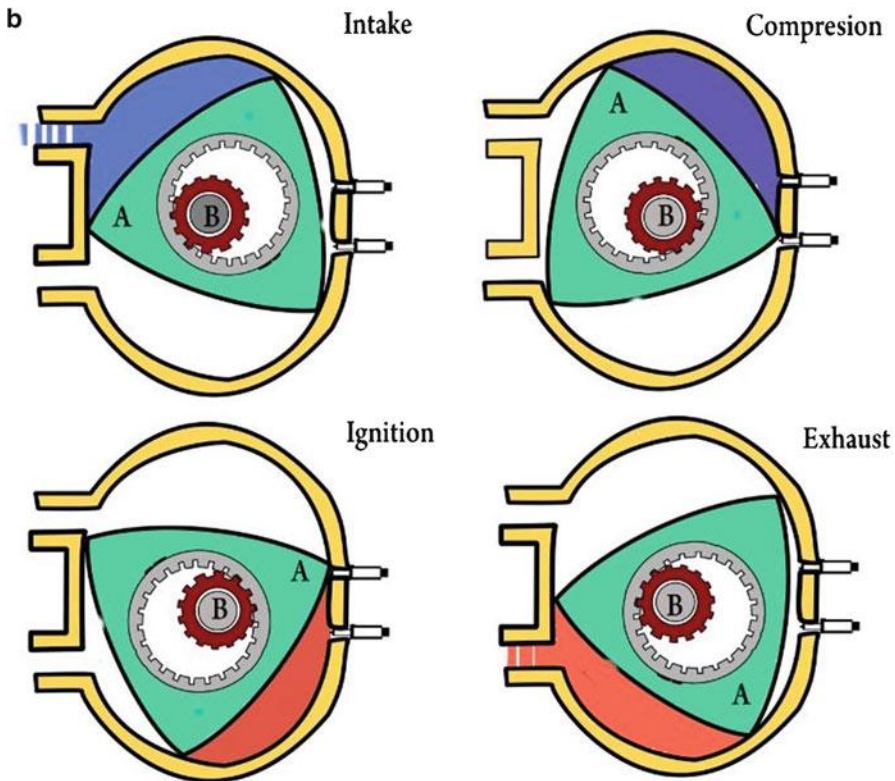


Fig. 4.3b Four strokes of Wankel engine



Fig. 4.4 AAI RQ-7 Shadow AUV



Fig. 4.5 ARV Super2 homebuilt experimental aircraft

Since Wankel engines operate at a relatively high [rotational speed](#) with relatively low torque, propeller aircraft must use a [Propeller Speed Reduction Unit \(PSRU\)](#) to keep their propellers within the proper speed range. For instance, the [MidWest](#) twin-rotor engine (Fig. 4.5) has a 2.95:1 reduction gearbox.

[Pratt & Whitney Rocketdyne](#) developed a diesel Wankel engine for use in a prototype [VTOL flying car](#) called the “Transformer”. The engine based on an earlier UAV diesel Wankel concept called “EnduroCORE”.

4.2.2.2 Reciprocating Engines

Based on cylinder arrangements, we have the following types:

- [Inline engine](#)
- Horizontally [opposed engine](#)
- [V-type engine](#)
- X-type Engine
- H-type Engine
- Radial type engine

(a) *In-line Engines*

This type of engine has cylinders lined up in one row. Mostly, it has an even number of cylinders (Fig. 4.6). Many in-line engines were developed during World War I (WWI), like Hispano-Suiza engine and Benz BZ-4. The biggest advantage of an inline engine is that it allows the aircraft to be designed with a narrow frontal area for low drag. The cylinders are either upright above the crankshaft or inverted, that is, below the crankshaft. An example for *inverted inline* engine is Menasco Pirate, model C-4. Inverted inline engine allows the propeller to be mounted up high for ground clearance and good visibility for pilots. The disadvantages of an inline engine include a poor power-to-weight ratio, because the crankcase and

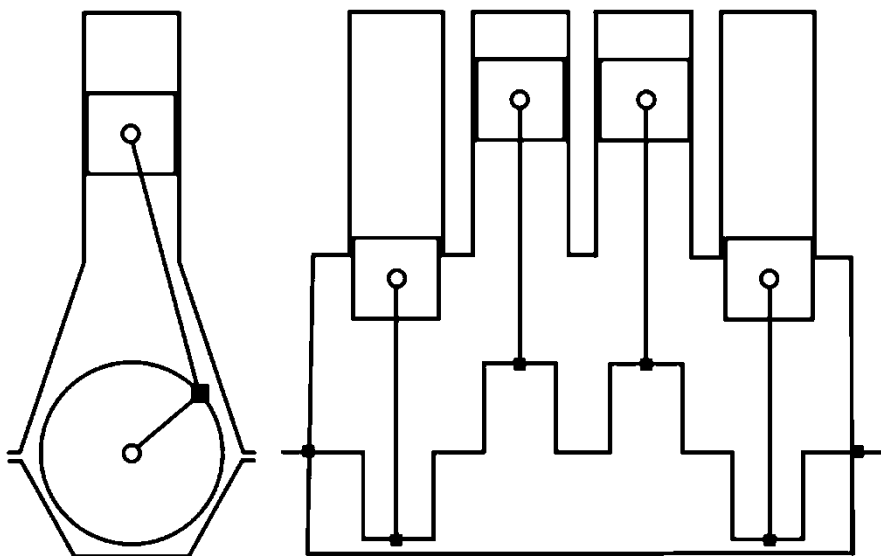


Fig. 4.6 Four-cylinder straight engine scheme

crankshaft are long and thus heavy. An in-line engine may be either air-cooled or liquid-cooled, but liquid-cooling is more common because it is difficult to get enough air-flow to cool the rear cylinders directly. Inline engines were common in early aircraft, including the Wright Flyer. However, the inherent disadvantages of the design soon became apparent, and the inline design was abandoned, becoming a rarity in modern aviation.

(b) *Horizontally Opposed Engines*

A horizontally opposed engine, also called a flat or boxer engine, has two banks of cylinders on opposite sides of a centrally located crankcase. The engine is either air-cooled or liquid-cooled, but air-cooled versions predominate. Opposed engines are mounted with the crankshaft horizontal in airplanes, but may be mounted with the crankshaft vertical in helicopters. Engine is streamlined resulting in less drag and good visibility for pilots. Due to the cylinder layout, reciprocating forces tend to cancel, resulting in a smooth running engine. Opposed, air-cooled four- and six-cylinder piston engines are by far the most common engines used in small general aviation aircraft requiring up to 400 horsepower (300 kW) per engine. Continental O-360 is an example for horizontally opposed engine.

(c) *V-type Engines*

Cylinders in this engine are arranged in two in-line banks, tilted 30–90° apart from each other. The vast majority of V engines are water-cooled. The V design provides a higher power-to-weight ratio than an inline engine, while still providing a small frontal area. Perhaps the most famous example of this design is the legendary Rolls-Royce Merlin engine, a 27-l 60° V12 engine used in, among others,

the Spitfires. Similarly two types of V-engines, namely, upright V-type and inverted V-type, are frequently seen in WWI engines.

(d) *X-type Engines*

X engine comprises twinned V-block engines horizontally opposed to each other. Thus, the cylinders are arranged in four banks, driving a common [crankshaft](#). [Rolls-Royce Vulture](#) is an example of this type, which powered [Avro Manchester](#) bomber and the [Hawker Tornado](#) fighter.

(e) *H-Type Engine*

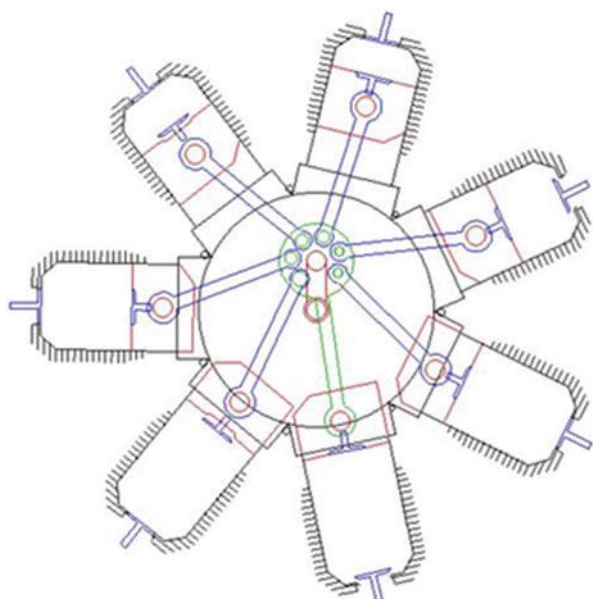
An *H engine* (or H-block) is an [engine configuration](#) in which the [cylinders](#) are aligned so that if viewed from the front they appear to be in a vertical or horizontal letter **H**. An H engine can be viewed as two [flat engines](#), one atop or beside the other. The “two engines” each have their own [crankshaft](#), which are then geared together at one end for power-take-off.

Napier Sabre was a British [H-24-cylinder](#), liquid cooled, piston aero engine, built by [Napier & Son](#) during [World War II](#), which powered the [Hawker Typhoon](#) aircraft, in mid-1941.

(f) *Radial Type Engine*

This type of engine has *one* or *two* rows of cylinders arranged in a circle around a centrally located crankcase (Fig. 4.7). Each row must have an odd number of cylinders in order to produce smooth operation. Rotary and radial engines look strikingly similar when they are not running and can easily be confused, since both have cylinders arranged radially around a central crankshaft. Unlike the rotary

Fig. 4.7 Single-row radial type engine

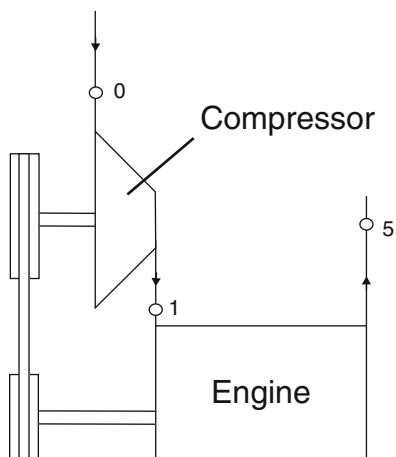


engine, however, radial engines use a conventional rotating crankshaft in a fixed engine block. A radial engine has only one crank throw per row and a relatively small crankcase, resulting in a favorable power-to-weight ratio. Because the cylinder arrangement exposes a large amount of the engine's heat-radiating surfaces to the air and tends to cancel reciprocating forces, radials tend to cool evenly and run smoothly. The lower cylinders, which are under the crankcase, may collect oil when the engine has been stopped for an extended period with a possible hydrostatic lock. In military aircraft designs, the large frontal area of the engine acted as an extra layer of armor for the pilot. However, the large frontal area also resulted in an aircraft with a blunt and aerodynamically inefficient profile.

4.2.2.3 Supercharging and Turbocharging Engines

Superchargers and turbochargers are two types of forced induction employed in piston engines to add large amounts of power to their motor. In aviation fields, supercharging and turbocharging allows piston engines to develop maximum power when operating at high altitudes or boost its power during takeoff. At high altitudes, an un-supercharged engine will lose power because of the reduced density of air entering the induction system of engine. Both superchargers (Fig. 4.8) and turbochargers (Fig. 4.9) have compressors mounted in the intake system and used to raise the pressure and density of the incoming air. The advantage of compressing the air is that it lets the engine stuff more air into a cylinder. More air means that more fuel can be stuffed in too, so more power is obtained from each explosion in each cylinder. The typical boost provided by either a turbocharger or a supercharger is 20–50 kPa. Two types of compressors are used in superchargers and turbochargers. These are either positive displacement or dynamic. Three types of positive displacement compressors are extensively used, namely, the roots, vane, and screw

Fig. 4.8 Supercharger



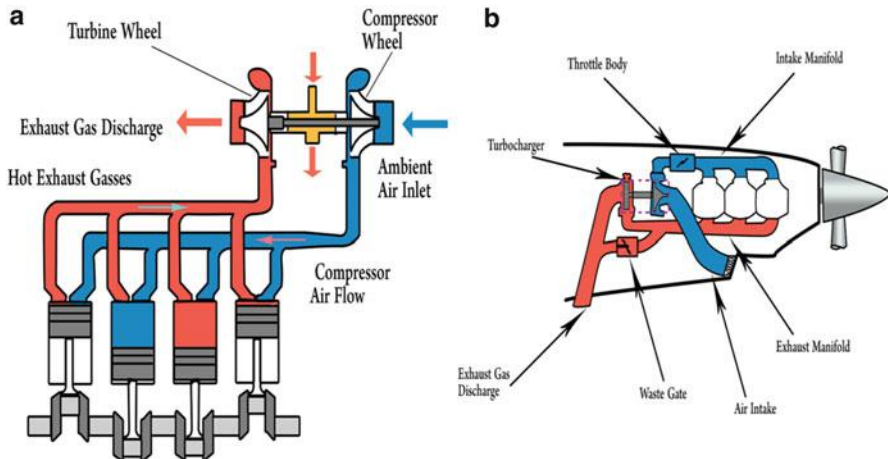


Fig. 4.9 Turbocharger: (a) Typical layout, (b) Turbocharger (Rolls Royce Merlin III engine)

compressor. Two types of dynamic compressors are used, either centrifugal or axial. This power can be supplied by a separate drive for the supercharger or by connecting the supercharger directly to the engine shaft or to gas turbine driven by the engine exhaust gases. As shown in Fig. 4.9, turbochargers consist of a centrifugal compressor coupled to a radial inflow turbine through either vaneless or vaned diffuser housing.

The key difference between a turbocharger and a supercharger is its power supply. Superchargers are mechanically driven directly off the engine through belts, gears, shafts, or chains connected to the engine's crankshaft. It is normally located between the carburetor and inlet manifold. A turbocharger, on the other hand, is powered by a turbine mounted in the exhaust stream, which in turn spins the compressor element situated between the air-intake and the carburetor or injector [2].

There are tradeoffs in both systems. In theory, a turbocharger is more efficient because it is using the “wasted” energy in the exhaust stream for its power source. On the other hand, a turbocharger causes some amount of back pressure in the exhaust system and tends to provide less boost until the engine is running at higher RPMs. Generally, turbocharging is commonly found on high power four-stroke engines, but it can also be used on two-stroke engines. Superchargers are easier to install but tend to be more expensive. A supercharger is a lot safer because of the simplicity of its design.

Super/turbo-chargers are used in the following aircrafts: Spitfire Mark I, Hurricane Mark I, Defiant fighter, Wellington bomber, Halifax bomber, Lancaster bomber, and Mosquito fighter (Table 4.3).

Table 4.3 Supercharger versus turbocharger

Parameter	Supercharger	Turbocharger
Driving method	Compressors is driven by the power taken directly from the engine via belts, gears, or chains	Compressor is driven by a turbine that is driven by the exhaust gases
Advantages	Drives vehicles to faster speeds	High fuel economy
Disadvantages	1. Losses due to mechanical friction	1. Increased engine back pressure
	2. More expensive	2. Less expensive

4.3 Aerodynamics and Thermodynamics of Reciprocating ICE

4.3.1 Terminology for Four-Stroke Engine

Figure 4.10 is a sketch of a reciprocating internal combustion engine consisting of a piston that moves within a cylinder fitted with two valves. The sketch is labeled with some special terms. The *bore* of the cylinder is its diameter. The *stroke* is the distance the piston moves in one direction. The piston is said to be at top dead center (TDC) when it has moved to a position where the cylinder volume is a minimum [3]. This minimum volume is known as the *clearance volume*. When the piston has moved to the position of maximum cylinder volume, the piston is at bottom dead center (BDC). The distance between the TDC and the BDC is the largest distance that the piston can travel in one direction, and it is called the *stroke* of the engine. The volume swept out by the piston as it moves from the top dead center to the bottom dead center position is called the *displacement volume*. The reciprocating motion of the piston is converted to rotary motion by a crank mechanism.

The *compression ratio* (r_c) is defined as the volume at bottom dead center (maximum volume) divided by the volume at top dead center (minimum volume or clearance).

$$r_c = \frac{V_{\max}}{V_{\min}} = \frac{V_{BDC}}{V_{TDC}} \quad (4.1)$$

Notice that the compression ratio is a volume ratio and should not be confused with the pressure ratio [4].

In a four-stroke internal combustion engine, the piston executes four distinct strokes within the cylinder for every two revolutions of the crankshaft. Figure 4.11 gives a pressure–volume diagram such as might be displayed electronically.

1. With the intake valve open, the piston makes an intake stroke to draw a fresh charge into the cylinder. For spark-ignition engines, the charge is a combustible mixture of fuel and air. Air alone is the charge in compression-ignition engines.

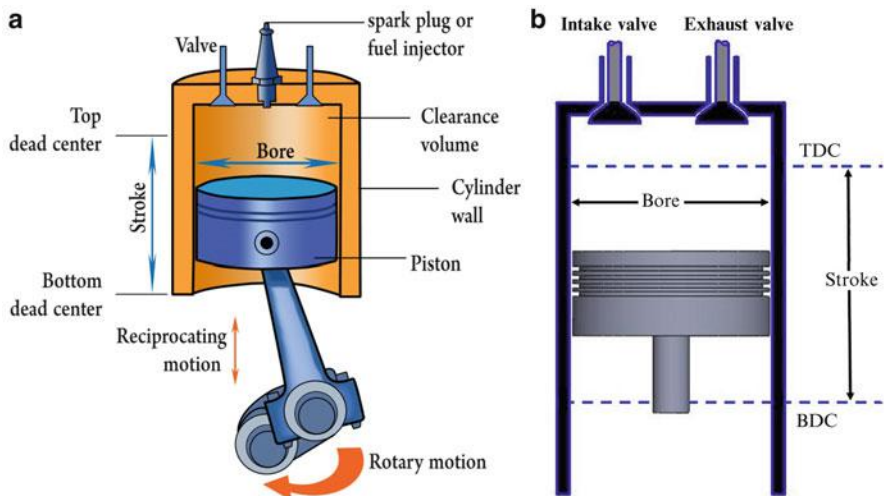


Fig. 4.10 Nomenclature for reciprocating piston-cylinder engines

2. With both valves closed, the piston undergoes a compression stroke, raising the temperature and pressure of the charge. This requires work input from the piston to the cylinder contents. Combustion is induced near the end of the compression stroke in spark-ignition engines by the spark plug. In compression ignition engines, combustion is initiated by injecting fuel into the hot compressed air, beginning near the end of the compression stroke and continuing through the first part of the expansion. Combustion process results in a high-pressure, high-temperature gas mixture.
3. A power stroke follows the compression stroke, during which the gas mixture expands and work is done on the piston as it returns to bottom dead center.
4. The piston then executes an exhaust stroke in which the burned gases are purged from the cylinder through the open exhaust valve.

4.3.2 Air-Standard Analysis

The analysis of real flow within internal combustion engine is very complex due to mechanical and thermal losses associated with friction and combustion process. Other complexities are associated with heat transfer between the gases and the cylinder walls as well as the work required to charge the cylinder and exhaust the products of combustion. Accurate modeling of reciprocating internal combustion engines normally involves computer simulation. To conduct elementary thermodynamic analyses of internal combustion engines, considerable simplification is

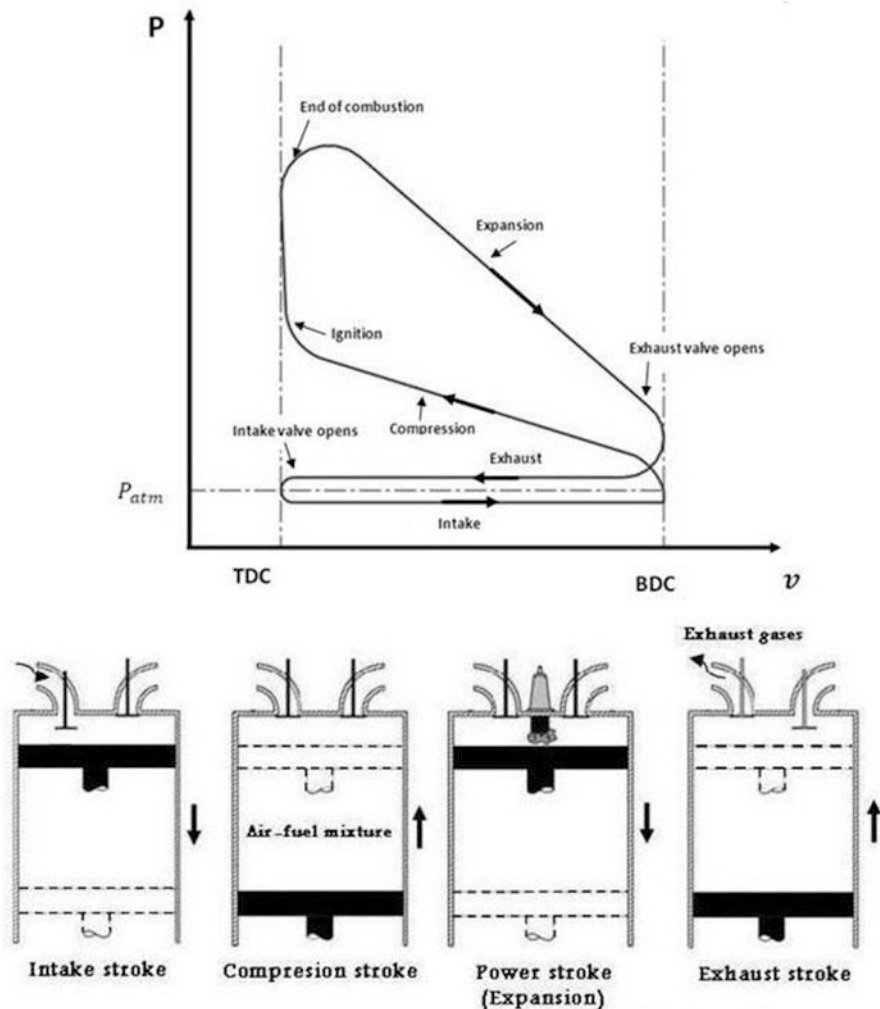


Fig. 4.11 Pressure–volume diagram for a reciprocating internal combustion engine

required. One procedure is to employ an *air-standard analysis* having the following elements:

1. The almost-constant pressure intake and exhaust strokes are assumed to be constant pressure. At WOT (Wide-Open Throttle or fully open throttle valve), the intake stroke is assumed to be at a pressure of one atmosphere. At partially closed throttle or when supercharged, inlet pressure will assume a constant value other than one atmosphere [5]. The exhaust stroke pressure is assumed constant at one atmosphere.
2. All processes are internally reversible.

3. Compression and expansion strokes are approximated by isentropic processes (reversible and adiabatic). Lubrication minimizes the friction between piston and cylinder walls. Heat transfer for any stroke is negligibly small due to its very short time.
4. The combustion process is replaced by a heat addition process from an external source at constant-volume process (Spark-Ignition: SI cycle), a constant-pressure process (Compression-Ignition: CI cycle), or a combination of both (Dual cycle)
5. Exhaust blow-down is approximated by a constant-volume process.

In air-standard cycles, air is considered an ideal gas such that the following ideal gas relations are used:

$$Pv = RT, P = \rho RT, PV = mRT \quad (4.2a)$$

$$dh = C_p dT, du = C_v dT \quad (4.2b)$$

$$a = \sqrt{\gamma RT} \quad (4.3)$$

For isentropic process:

$$Pv^\gamma = \text{constant}, T v^{\gamma-1} = \text{constant}, TP^{(\frac{1-\gamma}{\gamma})} = \text{constant} \quad (4.4)$$

Work done for isentropic process from state (1) to state (2):

$$w_{1-2} = \frac{P_2 v_2 - P_1 v_1}{1 - \gamma} = \frac{R(T_2 - T_1)}{1 - \gamma} \quad (4.5)$$

4.3.3 Engine Cycles

Two cycles will be discussed here. These are Otto and diesel cycles. Otto cycle is the ideal cycle for spark-ignition engines, while diesel cycle is the ideal cycle for compression-ignition cycles.

Specific heats of air are functions of temperature. Temperature within piston engines may vary from room temperature up to several thousands. At the low-temperature of the cycle (during intake and start of compression), specific heat ratio has a value of $\gamma = 1.4$, while at the end of combustion, due to temperature rise, specific heat ratio will be $\gamma = 1.3$. To simplify cycle analysis, *specific heat will be assumed constant* having the average value of $\gamma = 1.35$.

In the next sections, the following values will be used:

$$C_p = 1.108 \text{ kJ/ (kg - K)} \quad C_v = 0.821 \text{ kJ/ (kg - K)} \quad (4.6a)$$

$$R = C_p - C_v = 0.287 \text{ kJ/(kg} - \text{K}), \quad (4.6b)$$

$$\frac{C_p}{C_v} = 1.35 \quad (4.6c)$$

4.3.3.1 Thermodynamic Analysis of Air-Standard Otto Cycle at WOT

The Otto cycle is the ideal cycle for spark-ignition reciprocating engines. It is named after Nikolaus A. Otto, who built in 1876 a successful four-stroke engine in Germany. In most spark-ignition engines, the piston executes four complete strokes (two mechanical cycles) within the cylinder, and the crankshaft completes two revolutions for each thermodynamic cycle. These engines are called four-stroke internal combustion engines. A schematic drawing for the ideal cycle drawn on both P-v and T-s diagrams are shown in Fig. 4.12.

Detailed thermodynamic analysis of Otto cycle

1. Process 0–1: Constant pressure suction (intake) stroke of air at ambient pressure P_0

With the intake valve open and exhaust valve closed, the piston makes an intake stroke to draw a fresh charge (a combustible mixture of fuel and air) into the cylinder

$$P_1 = P_5 = P_0 \quad (4.7a)$$

$$w_{0-1} = P_0(v_1 - v_0) \quad (4.7b)$$

Here specific and total volumes are identified as (v, V) , respectively.

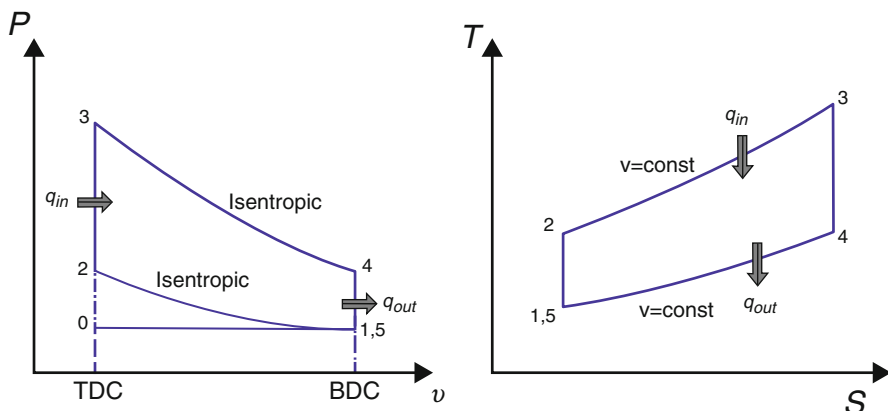


Fig. 4.12 P-v and T-s diagram of ideal Otto cycle

2. Process 1–2: Isentropic compression stroke

With both valves closed, the piston undergoes a compression stroke, raising the temperature and pressure of the charge. This requires work input from the piston to the cylinder contents.

$$T_2 = T_1 \left(\frac{v_1}{v_2} \right)^{\gamma-1} = T_1 \left(\frac{V_1}{V_2} \right)^{\gamma-1} = T_1(r_c)^{\gamma-1} \quad (4.8a)$$

$$P_2 = P_1 \left(\frac{v_1}{v_2} \right)^\gamma = P_1 \left(\frac{V_1}{V_2} \right)^\gamma = P_1(r_c)^\gamma \quad (4.8b)$$

$$q_{1-2} = 0 \quad (4.8c)$$

$$w_{1-2} = \frac{P_2 v_2 - P_1 v_1}{1 - \gamma} = \frac{R(T_2 - T_1)}{1 - \gamma} = (u_1 - u_2) = C_v(T_1 - T_2) \quad (4.8d)$$

3. Process 2–3: Constant-volume heat addition (combustion)

$$T_3 = T_{\max}, P_3 = P_{\max}, v_3 = v_2 = v_{\text{TDC}}, w_{2-3} = 0 \quad (4.9a)$$

Specific heat added is (q_{in}), given by the relation:

$$q_{2-3} = q_{\text{in}} = C_v(T_3 - T_2) = (u_3 - u_2) \quad (4.9b)$$

$$Q_{2-3} = Q_{\text{in}} = m_f Q_{\text{HV}} \eta_c = m_m C_v(T_3 - T_2) = (m_a + m_f) C_v(T_3 - T_2) \quad (4.9c)$$

$$Q_{\text{HV}} \eta_c = (\text{AF} + 1) C_v(T_3 - T_2) \quad (4.9d)$$

Here (Q_{HV}) is the heating value of fuel, while (AF) is the air-to-fuel ratio (m_a/m_f).

Combustion process results in a gas mixture having the maximum-pressure and maximum-temperature. Combustion is induced near the end of the compression stroke by the spark plug.

4. Process 3–4: Isentropic power or expansion stroke

It follows the compression stroke, during which the gas mixture expands and work is done on the piston as it returns to bottom dead center. All valves are closed.

$$T_4 = T_3 \left(\frac{v_3}{v_4} \right)^{\gamma-1} = T_3 \left(\frac{V_3}{V_4} \right)^{\gamma-1} = T_3(r_c)^{\gamma-1} \quad (4.10a)$$

$$P_4 = P_3 \left(\frac{v_3}{v_4} \right)^\gamma = P_3 \left(\frac{V_3}{V_4} \right)^\gamma = P_3(r_c)^\gamma \quad (4.10b)$$

$$q_{3-4} = 0 \quad (4.10c)$$

$$w_{3-4} = \frac{P_4 v_4 - P_3 v_3}{1 - \gamma} = \frac{R(T_4 - T_3)}{1 - \gamma} = (u_3 - u_4) = C_v(T_3 - T_4) \quad (4.10d)$$

5. Process 4–5: Constant volume heat rejection (exhaust blow-down)

Exhaust valve open and intake valve closed:

$$v_5 = v_4 = v_{BDC}, w_{4-5} = 0 \quad (4.11a)$$

$$q_{4-5} = q_{\text{out}} = C_v(T_5 - T_4) = C_v(T_1 - T_4) = (u_5 - u_4) \quad (4.11b)$$

$$Q_{4-5} = Q_{\text{out}} = m_m C_v(T_5 - T_4) = m_m C_v(T_1 - T_4) \quad (4.11c)$$

6. Process 5–0: Constant pressure exhaust stroke at P_0

The piston then executes an exhaust stroke in which the burned gases are purged from the cylinder through the open exhaust valve.

$$P_5 = P_1 = P_0 \quad (4.12a)$$

$$w_{5-0} = P_0(v_0 - v_5) = P_0(v_0 - v_1) \quad (4.12b)$$

Thermal efficiency of Otto cycle

Since Otto cycle is executed in a closed system, and disregarding the changes in kinetic and potential energies, the energy balance for any process is expressed, on a unit-mass basis, as:

$$w_{\text{net}} = (q_{\text{in}} - q_{\text{out}}) \left(\frac{\text{kJ}}{\text{kg}} \right) \quad (4.13)$$

$$\text{with : } w_{\text{net}} = q_{\text{in}} - q_{\text{out}} = (u_3 - u_2) - (u_4 - u_1)$$

The thermal efficiency is defined as:

$$\begin{aligned} \eta_{\text{th, Otto}} &= \frac{w_{\text{net}}}{q_{\text{in}}} = 1 - \frac{q_{\text{out}}}{q_{\text{in}}} = 1 - \frac{(u_4 - u_1)}{(u_3 - u_2)} = 1 - \frac{c_v(T_4 - T_1)}{c_v(T_3 - T_2)} \\ &= 1 - \frac{(T_4 - T_1)}{(T_3 - T_2)} = 1 - \frac{T_1 \left(\frac{T_4}{T_1} - 1 \right)}{T_2 \left(\frac{T_3}{T_2} - 1 \right)} \end{aligned} \quad (4.14a)$$

Since processes 1–2 and 3–4 are isentropic, $v_2 = v_3$ and $v_4 = v_1$.

Thus:

$$\frac{T_1}{T_2} = \left(\frac{v_2}{v_1} \right)^{\gamma-1} = \left(\frac{v_3}{v_4} \right)^{\gamma-1} = \frac{T_4}{T_3} \quad (4.14b)$$

Rearranging

$$\frac{T_4}{T_1} = \frac{T_3}{T_2} \quad (4.14c)$$

From Eqs. (4.14a), (4.14b), and (4.14c), then:

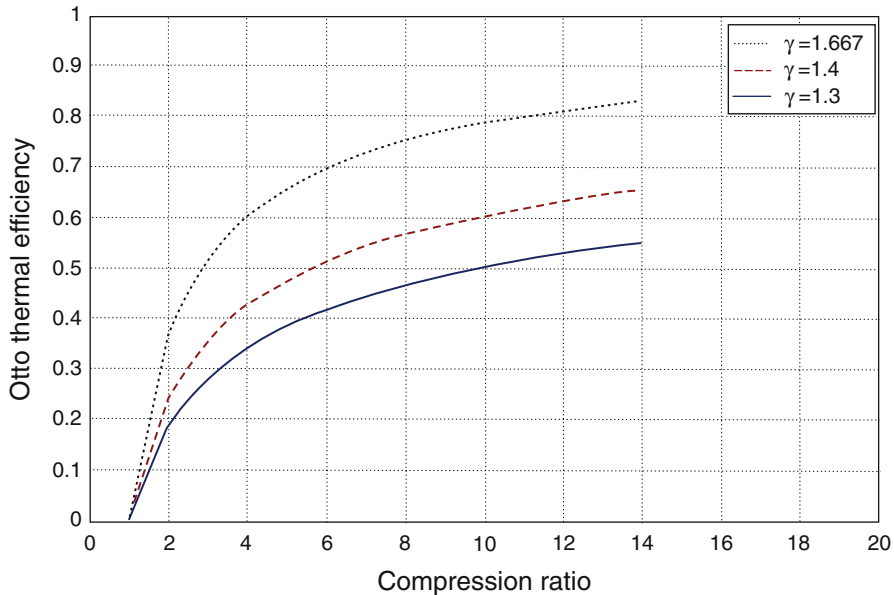


Fig. 4.13 Thermal efficiency of the Otto cycle versus the compression ratio for different values of specific heat ratio (γ) of the working fluid

$$\eta_{\text{th, Otto}} = 1 - \frac{1}{r_c^{\gamma-1}} \quad (4.15)$$

$$\text{where as previously defined} \quad r_c = \frac{v_{\max}}{v_{\min}} = \frac{v_1}{v_2} \quad (4.16)$$

From Eq. (4.14b), thermal efficiency is dependent of both of the compression ratio (r_c) and specific heat ratio (γ). A plot of Otto thermal efficiency versus the compression ratio for different values of (γ) is given in Fig. 4.13.

From Fig. 4.13, it is noticed that:

1. The thermal efficiency curve is rather steep at low compression ratios but flattens out starting with a compression ratio value of about 8. Therefore, the increase in thermal efficiency with the compression ratio is not as pronounced at high compression ratios.
2. For a given compression ratio, an ideal Otto cycle using a monatomic gas (such as argon or helium, $\gamma = 1.667$) as the working fluid will have the highest thermal efficiency. The least specific heat ratio ($\gamma = 1.3$) provides the smallest Otto thermal efficiency.

General Remarks

1. The working fluid in actual engines contains larger molecules such as carbon dioxide, and the specific heat ratio decreases with temperature, which is one of

the reasons that the actual cycles have lower thermal efficiencies than the ideal Otto cycle.

2. For a given compression ratio, the thermal efficiency of an actual spark-ignition engine is less than that of an ideal Otto cycle because of the irreversibilities, such as friction, and other factors such as incomplete combustion.
3. The thermal efficiencies of actual spark-ignition engines range from about 25 to 30 %.

Power generation and fuel consumption

The torque generated in piston engines is normally measured with a dynamometer. The engine is clamped on a test bed and the shaft is connected to the dynamometer rotor. The rotor is coupled to a stator either electromagnetically, hydraulically or by mechanical friction. The stator is balanced with the rotor stationary. The torque exerted by the engine T is:

$$T = F b \quad (4.17)$$

The power P delivered by the engine and absorbed by the dynamometer is given by:

$$P = T \times \omega = 2 \pi N T \quad (4.18)$$

This value of engine power is called BRAKE POWER (P_b), where:

$$P_b(\text{KW}) = 2 \pi N (\text{rev/s}) \times T(\text{N.m}) \times 10^{-3}$$

The indicated power is correlated to the indicated work as illustrated in Fig. 4.14.

The indicated work per cycle per cylinder

$$W_{C,i} = \oint p dv \quad (4.19a)$$

The *net indicated work per cycle per cylinder* $W_{C,i}$ is the work delivered to the piston over the entire four-stroke cycle:

$$W_{c,i} = \text{Area } (A) - \text{Area } (B) \quad (4.19b)$$

The power per cylinder is related to the indicated work per cylinder by:

$$P_i = \frac{W_{C,i} N}{n_R} \quad (4.19c)$$

where (n_R) is the number of crank revolution for each power stroke per cylinder. For four-stroke cycle engine ($n_R = 2$), for two-stroke engine ($n_R = 1$). This power is the indicated power defined as the rate of work transfer from the gas within the cylinder to the piston. From Eq. (4.19a), then:

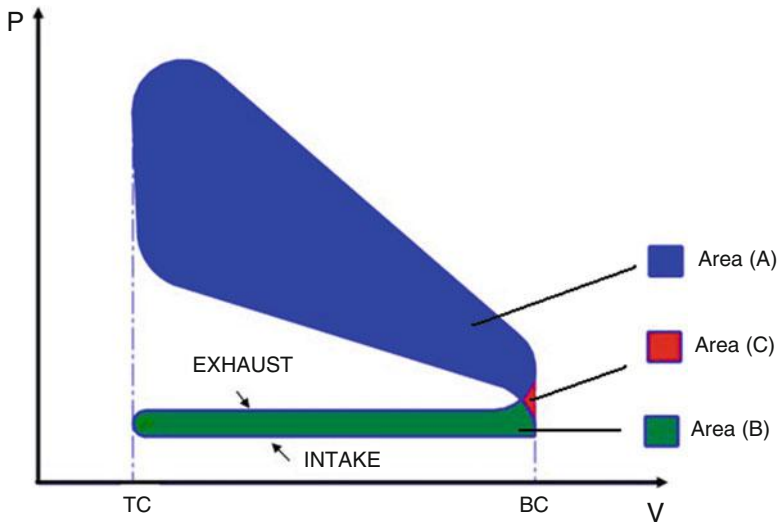


Fig. 4.14 P-v diagram for a four-stroke SI engine

$$W_{C,i} = \frac{P_i n_R}{N} \quad (4.19d)$$

$$\text{For four-stroke engine: } W_{C,i} = \frac{2P_i}{N} \quad (4.19e)$$

$$\text{For two-stroke engine: } W_{C,i} = \frac{P_i}{N} \quad (4.19f)$$

The brake power P_b is related to the indicated power P_i by the relation:

$$P_i = P_b + P_f \quad (4.20)$$

where P_f = Power consumed in:

- Overcoming the friction of the bearings, pistons, and other mechanical components of engine
- Driving accessories
- Induction and exhaust strokes

Figure 4.15 illustrates the brake down of losses in aero piston engines driving an aircraft propeller.

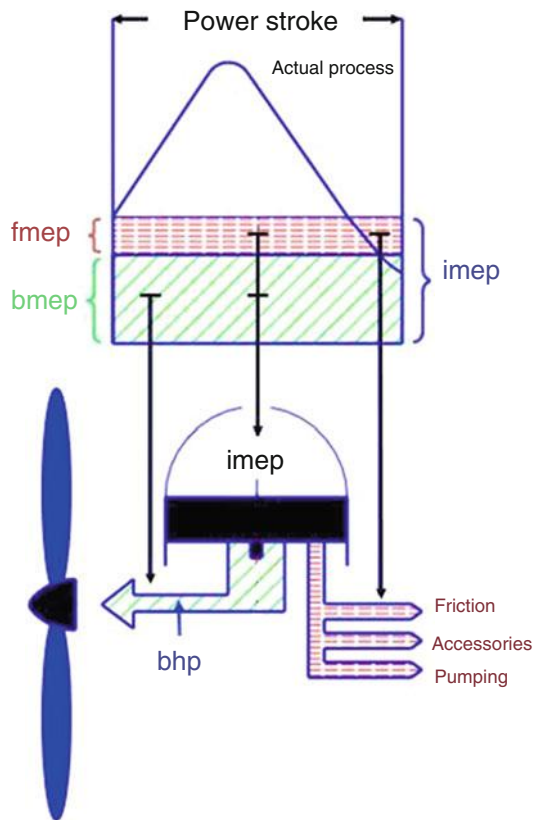
The ratio of brake (or useful) power delivered by the engine to the indicated power is called the mechanical efficiency (η_m) defined as:

$$\eta_m = \frac{P_b}{P_i} \quad (4.21)$$

$\eta_m = 90\%$ for modern automotive engines at speeds below 30–40 rev/s (1800–2400 rev/min) and

$\eta_m = 75\%$ at maximum rated speed

Fig. 4.15 Brake down of losses in aero piston engines driving an aircraft propeller



A parameter used to describe the performance of reciprocating piston engines is the mean effective pressure (*MEP*); Eq. (4.43). The mean effective pressure is a fictitious pressure that, if it acted on the piston during the entire power stroke, would produce the same amount of net work as that produced during the actual cycle (Fig. 4.16). That is

$$W_{\text{net}} = \text{MEP} \times \text{Piston area} \times \text{Stroke} = \text{MEP} \times \text{Displacement volume}$$

Or:

$$\begin{aligned} \text{Mean effective pressure} &= \frac{\text{Net work for one cycle}}{\text{Displacement volume}} \\ &= \frac{W_{\text{net}}}{V_{\max} - V_{\min}} = \frac{w_{\text{net}}}{v_{\max} - v_{\min}} \end{aligned} \quad (4.22)$$

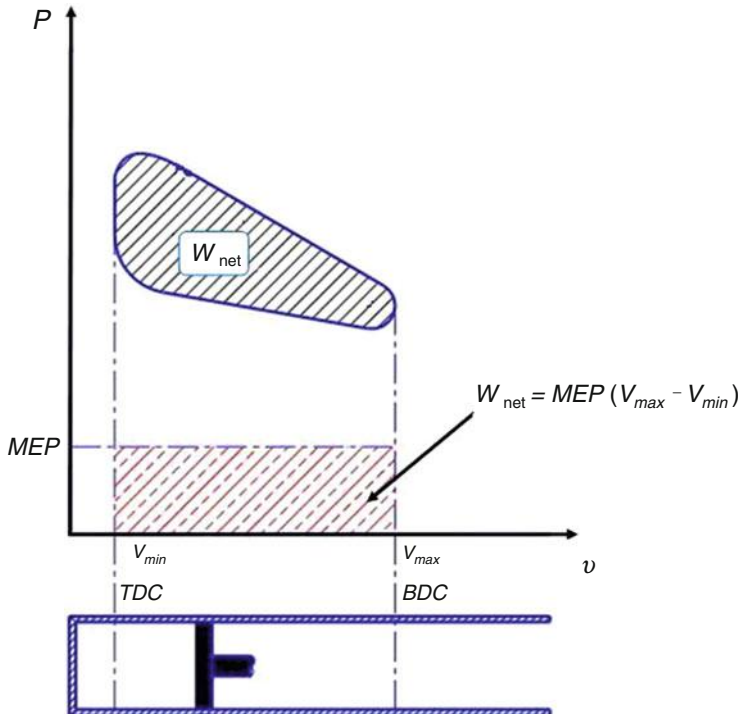


Fig. 4.16 Mean effective pressure

Various mean effective pressure can be defined by using different work terms in Eq. (4.22). If *indicated work* is used, then indicated mean effective pressure is obtained:

$$\text{imep} = \frac{W_{C,i}}{V_d} = \frac{P_i n_R}{N V_d} \quad (4.23)$$

If brake work is used, then *brake mean effective pressure* (BMEP) is obtained:

$$\text{bmeep} = \frac{P_b n_R}{N V_d} \quad (4.24a)$$

Both mean effective pressures are related by:

$$\text{bmeep} = \eta_m \times \text{imep} \quad (4.24b)$$

Also *friction mean effective pressure* is given by:

$$\text{fmep} = \text{imep} - \text{bmepl} \quad (4.25)$$

Moreover, with

$$P_b = 2 \pi N T$$

then

$$\text{bmepl} = \frac{2 \pi T n_R}{V_d} \quad (4.24c)$$

Other expressions for thermal efficiency

Thermal efficiency is also identified as *fuel-conversion efficiency* ($\eta_f \equiv \eta_{th}$). From Eq. (4.14a), thermal efficiency may be expressed as:

$$\begin{aligned} \eta_{th} &= \frac{\text{Indicated power}}{\text{Fuel mass flow rate} \times \text{Heating value}} \\ \eta_{th} &= \frac{P_i}{\dot{m}_f \times Q_{HV}} \end{aligned} \quad (4.26a)$$

In British units, the indicating thermal efficiency is expressed as:

$$\eta_{th} = \frac{\text{ihp} \times 33,000}{(\text{Mass of fuel burned/min}) \times (\text{Heat value}) \times 778} \quad (4.26b)$$

Air/Fuel and Fuel/Air ratios

$$\text{Air/Fuel ratio (A/F)} = \frac{\dot{m}_a}{\dot{m}_f} \quad (4.27a)$$

$$\text{Fuel/Air ratio (F/A)} = \frac{\dot{m}_f}{\dot{m}_a} \quad (4.27b)$$

For normal operating range for
SI engine using gasoline fuel:

$$12 \ll A/F \ll 18 \quad (0.056 \ll F/A \ll 0.083)$$

For CI-engine using diesel fuel:

$$18 \ll A/F \ll 70 \quad (0.014 \ll F/A \ll 0.056)$$

Specific Fuel Consumption

Specific fuel consumption is defined as the fuel flow rate per unit power output, or:

$$\text{SFC} = \frac{\dot{m}_f}{P} \quad (4.28a)$$

Indicated specific fuel consumption:

$$\text{ISFC} = \frac{\dot{m}_f}{P_i} \quad (4.28\text{b})$$

Brake specific fuel consumption:

$$\text{BSFC} = \frac{\dot{m}_f}{P_b} \quad (4.28\text{c})$$

Friction specific fuel consumption:

$$\text{FSFC} = \frac{\dot{m}_f}{P_f} \quad (4.28\text{d})$$

Then from Eq. (4.25), we get:

$$\eta_{\text{th}} = \frac{1}{\text{SFC } Q_{\text{HV}}} \quad (4.29)$$

Thus, specific fuel consumption is inversely proportional to the thermal (or fuel conversion) efficiency for normal hydrocarbon fuels. Introducing several units, then:

$$\eta_{\text{th}} = \eta_f = \frac{1}{\text{SFC } (\text{mg/J})Q_{\text{HV}}(\text{MJ/Kg})} \quad (4.30\text{a})$$

or $\eta_{\text{th}} = \eta_f = \frac{3600}{\text{SFC } (\text{g/KW.hr})Q_{\text{HV}}(\text{MJ/Kg})} \quad (4.30\text{b})$

or $\eta_{\text{th}} = \eta_f = \frac{2545}{\text{SFC } (ib_m/\text{hp.hr})Q_{\text{HV}}(\text{Btu}/ib_m)} \quad (4.30\text{c})$

Typical heating value for the commercial hydrocarbon fuels used in engines:

$$Q_{\text{HV}} = 42 - 44 \text{ MJ/Kg} \quad (4.31\text{a})$$

or $Q_{\text{HV}} = 18,000 - 19,000 \text{ Btu}/ib_m \quad (4.31\text{b})$

Note that low values of SFC are desirable. Typical best values of brake specific fuel consumption are equal or less than:

For SI engines,

$$75 \mu\text{g/J} = 270 \text{ g/KW.h} = 0.47 ib_m/\text{hp.h} \quad (4.32\text{a})$$

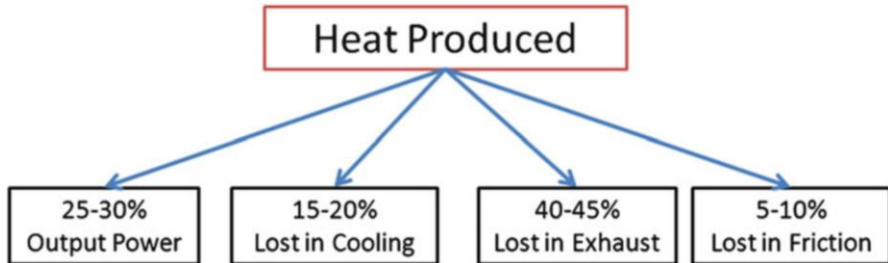


Fig. 4.17 Breakdown of heat produced by combustion

For CI engines,

$$55 \mu\text{g}/\text{J} = 200 \text{ g/KW.h} = 0.32 \text{ lb}_m/\text{hp.h} \quad (4.32\text{b})$$

Figure 4.17 illustrates breakdown for the heat energy generated from fuel consumption.

Volumetric Efficiency (η_V)

Volumetric efficiency is only used with four-stroke cycle engines which have a distinct induction process. It is a measure for the effectiveness of engine's induction process, as the intake system (air filter, carburetor, intake manifold, and intake valve) restricts the amount of air induced to the engine [6]. It is defined as the volume flow rate of air into the intake system divided by the rate at which volume is displaced by the piston:

$$\eta_V = \frac{\dot{V}_a}{V_s} = \frac{2 \dot{m}_a}{\rho_{a,i} V_d N} \quad (4.33\text{a})$$

where $\rho_{a,i}$ is the air density at inlet

\dot{V}_a is the rate of naturally aspirated induced air volume

V_s is the rate at which volume is displaced by the piston

Since piston speed is defined as $\bar{S}_P = 2LN$

where L is the stroke

then

$$\eta_V = \frac{4 \dot{m}_a L}{\rho_{a,i} V_d \bar{S}_P} \quad (4.33\text{b})$$

then

$$\eta_V = \frac{m_a}{\rho_{a,i} V_d} \quad (4.33\text{c})$$

where m is the mass of air inducted into the cylinder per cycle. The maximum value for volumetric efficiency has the following range:

$$(\eta_V)_{\max} = 80 - 90\%$$

Propulsive Efficiency

Piston engine is coupled to propeller(s) to furnish the forwarding thrust force. The propulsive efficiency here is a propeller efficiency which is the ratio of thrust horsepower to the brake horsepower. In average, $\eta_P \equiv \eta_{Pr} = 80\%$.

Thus thrust horsepower constitutes approximately 80 % of the bhp, while the other 20 % is lost in friction and slippage controlling the blade angle of the propeller.

Engine Specific Weight and Specific Volume

$$\text{Specific Weight} = \frac{\text{Engine Weight}}{\text{Rated Power}} \quad (4.34)$$

$$\text{Specific Volume} = \frac{\text{Engine Volume}}{\text{Rated Power}} \quad (4.35)$$

Relationships Between Performance Parameters

From the previous relations, the following performance parameters can be developed:

Power:

$$P = \frac{\eta_f m_a N Q_{HV}(F/A)}{n_R}$$

$$P = \frac{\eta_f \eta_V N V_d Q_{HV} \rho_{a,i}(F/A)}{n_R}$$

Torque:

$$T = \frac{\eta_f \eta_V V_d Q_{HV} \rho_{a,i}(F/A)}{2\pi n_R}$$

Mean-effective pressure:

$$\text{MEP} = \eta_f \eta_V Q_{HV} \rho_{a,i}(F/A)$$

The power per piston area, often called *SPECIFIC POWER*, is:

$$\frac{P}{A_P} = \frac{\eta_f \eta_V N L Q_{HV} \rho_{a,i}(F/A)}{n_R} \quad (4.36a)$$

Introducing mean piston speed: $\bar{S}_P = 2LN$, then:

$$\frac{P}{A_P} = \frac{\eta_f \eta_V \bar{S}_P Q_{HV} \rho_{a,i}(F/A)}{2 n_R} \quad (4.36b)$$

For four-stroke engine:

$$P/A_P = (\text{mep})\bar{S}_P/4 \quad (4.37a)$$

For two-stroke engine:

$$P/A_P = (\text{mep})\bar{S}_P/2 \quad (4.37b)$$

Example 4.1 The following data is for a four-stroke spark ignition engine:

Displacement volume V_d	2.2 l
Bore	87.5 mm
Stroke	92.0 mm
Compression ratio	8.9
Maximum power	65 kW
Speed	5000 rpm
Number of cylinders	4
Mean piston speed	10 m/s
Air flow rate	60 g/s

Calculate

1. Volumetric efficiency based on atmospheric conditions
2. Brake mean effective pressure
3. Specific power

Assume: mixture density = 1.184(g/l)

Solution

1. Volumetric efficiency is calculated using Eqs. (4.33a and 4.33b)

$$\eta_V = \frac{2 \dot{m}_a}{\rho_{a,i} V_d N} = \frac{4 \dot{m}_a L}{\rho_{a,i} V_d \bar{S}_P} = \frac{4 \times 60(\text{g/s}) \times 0.092 \text{ m}}{1.184 (\text{g/l}) \times 2.2 (\text{l}) \times 10(\text{m/s})} = 0.85$$

$$\eta_V = 85\%$$

2. Mean effective pressure is calculated using Eq. (4.24a)

$$\text{bmeep} = \frac{P_b n_R}{V_d N} = \frac{65 \times 10^3 \times 2}{2.2 \times 10^{-3} \times (5000/60)} = 709 \text{ kPa}$$

3. Specific power

Since piston speed is given by:

$$\bar{S}_P = 2LN = 2 \times 0.092 \times 5000/60 = 15.3 \text{ m/s}$$

Mean effective pressure is calculated from Eq. (4.37a) as:

$$P/A_P = (\text{mep})\bar{S}_P/4 = \frac{709 \times 15.3}{4} = 2.7 \text{ MW/m}^2$$

Example 4.2 A four-cylinder 2.0 l, SI engine operates at WOT on a four stroke air standard Otto cycle. The engine has a compression ratio of 8:1, a stroke-to-bore ratio S/B = 1.025 at 3000 rpm and mechanical efficiency of 86 %. Air to fuel ratio AF = 15, fuel heating value is 44,000 kJ/kg. At the start of compression stroke, conditions at the cylinder are 100 kPa and 30 °C. It is assumed that a 4 % exhaust residual is left over from previous cycle.

1. Perform a complete thermodynamic analysis of the engine
2. Calculate thermal efficiency
3. Mean piston speed
4. Brake power
5. Brake specific fuel consumption

Solution

1. Displacement volume for one cylinder

$$V_d = \frac{2.0L}{4} = 0.5 \text{ L} = 0.0005 \text{ m}^3$$

$$\text{Compression ratio } r_c = \frac{V_1}{V_2} = \frac{V_d + V_c}{V_c} = \frac{0.5 + V_c}{V_c} = 8.0$$

$$V_c = 0.714 \text{ L} = 0.0000714 \text{ m}^3$$

Since the displacement volume is expressed as $V_d = \frac{\pi}{4}B^2S = \frac{\pi}{4} \times B^2 \times 1.025B$

Then the bore $B = 0.0853 \text{ m} = 8.53 \text{ cm}$

The stroke $S = 0.0874 \text{ m} = 8.74 \text{ cm}$

Now, let us calculate the air/gas properties at different states.

State (1)

$$T_1 = 30^\circ\text{C} = 303 \text{ K}, P_1 = 100 \text{ kPa}$$

$$V_1 = V_d + V_c = 0.0005714 \text{ m}^3$$

Mass of mixture at state (1) is $m_m = \frac{P_1 V_1}{R T_1} = \frac{100 \times 10^3 \times 0.0005714}{287 \times 303} = 0.000657 \text{ kg}$

State (2)

Since process 1–2 is an isentropic compression, then:

$$P_2 = P_1(r_c)^\gamma = 100 \times (8)^{1.35} = 1656 \text{ kPa}$$

$$T_2 = T_1(r_c)^{\gamma-1} = 303 \times (8)^{0.35} = 627.4 \text{ K}$$

$$V_2 = \frac{mRT_2}{P_2} = \frac{0.000657 \times 0.287 \times 627.4}{1656} = 0.0000714 \text{ m}^3$$

Or simply $V_2 = \frac{V_1}{r_c} = \frac{0.0005714}{8} = 0.0000714 \text{ m}^3$

The mass of mixture (m_m) within the cylinder can be decomposed as follows:

$$m_m = m_a + m_f + m_{ex} = 0.000657 \text{ kg}$$

Where where (m_a) is the mass of fresh air sucked into the cylinder and (m_f) is the mass of fuel mixed with fresh air, while (m_{ex}) is the exhaust residual left in the cylinder.

$$(m_{ex}) = 0.04 m_m = 0.00002628 \text{ kg}$$

Since, AF = $\frac{m_a}{m_f} = 15$, then $0.96m_m = 16 m_f$

$$m_f = 0.00003942 \text{ kg}, \quad m_a = 0.0005913 \text{ kg}$$

State (3): Heat added $Q_{in} = m_f Q_{HV} = 0.00003942 \times 44,000 = 1.73448 \text{ kJ}$

Heat added can be also expressed as:

$$Q_{in} = m_m C_v (T_3 - T_2) = 0.000657 \times 0.821 \times (T_3 - 627.4)$$

Then

$$T_3 = 3842 \text{ K} \equiv T_{\max}$$

$$V_3 = V_1 = 0.0005714 \text{ m}^3$$

For a constant volume process, $P_3 = P_2 \left(\frac{T_3}{T_2} \right) = 10,143 \text{ kPa}$

State (4):

Power stroke; isentropic expansion

$$P_4 = P_3 \left(\frac{1}{r_c} \right)^\gamma = \frac{10,143}{(8)^{1.35}} = 612.3 \text{ kPa}$$

$$T_4 = T_3 \left(\frac{1}{r_c} \right)^{\gamma-1} = \frac{3843}{(8)^{0.35}} = 1856 \text{ K}$$

$$v_4 = \frac{mRT_4}{P_4} = 0.000571 \equiv V_1$$

Work produced in power expansion:

$$W_{3-4} = \frac{mR(T_4 - T_3)}{1 - \gamma} = \frac{0.000657 \times 0.287 \times (1856 - 3843)}{1 - 1.35} = 1.07047 \text{ kJ}$$

Work absorbed in isentropic compression stroke

$$W_{1-2} = \frac{mR(T_2 - T_1)}{1 - \gamma} = \frac{0.000657 \times 0.287 \times (627.4 - 303)}{1 - 1.35} = -0.17476 \text{ kJ}$$

$$W_{\text{net}} = W_{3-4} + W_{1-2} = 0.8957 \text{ kJ}$$

2. Thermal efficiency $\eta_{\text{th}} = W_{\text{net}}/Q_{\text{in}} = 0.5166 = 51.7\%$

Thermal efficiency can be also evaluated from the relation:

$$\eta_{\text{th}} = 1 - \frac{1}{r_c^{\gamma-1}} = 0.517$$

3. Mean piston speed

$$\bar{S}_P = 2LN = 2 \times 0.0874 \times \left(\frac{3000}{60} \right) = 8.74 \text{ m/s}$$

4. Brake power

Net brake work per cylinder for one cycle:

$$W_b = \eta_m W_i = 0.86 \times 0.8957 = 0.77 \text{ kJ}$$

Brake power at 3000 rpm

$$P_b = (W_b N / n_R) \times (\text{number of cylinders})$$

$$P_b = \left(0.77 \times \frac{3000}{60} \times \frac{1}{2} \right) \times (4) = 77 \text{ kW} = 103.4 \text{ hp}$$

5. Brake specific fuel consumption

$$\text{Fuel mass flow rate } \dot{m}_f = \left(\frac{m_f N}{n_R} \right) \times (\text{number of cylinders})$$

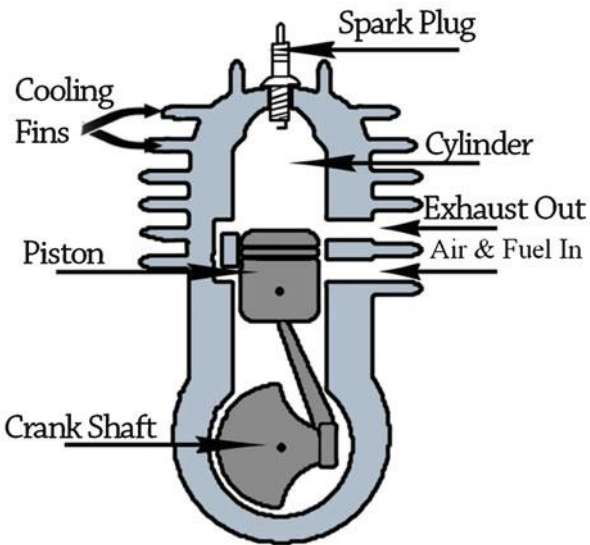
$$\dot{m}_f = \left(0.00003942 \times \frac{3000}{60} \times \frac{1}{2} \right) \times (4) = 0.003942 \text{ kg/s}$$

$$\text{bsfc} = 0.003942 \times 1000 \times \frac{3600}{77} = 184.3 \text{ gm}/(\text{kW.h})$$

4.3.3.2 Two-Stroke Spark Ignition (Otto Cycle) Engines

Two stroke engines are small engines that may be used in ultra-light aircrafts. Similar to four stroke engines, two-stroke engine is constructed with a cylinder, piston, crankshaft, connecting rod, and crankcase.

Fig. 4.18 Two-stroke spark ignition engine



Petrol engine includes a spark plug, while diesel engine replaces the spark plug with fuel injector (Fig. 4.18). The cycle is illustrated in Fig. 4.19 and described as follows:

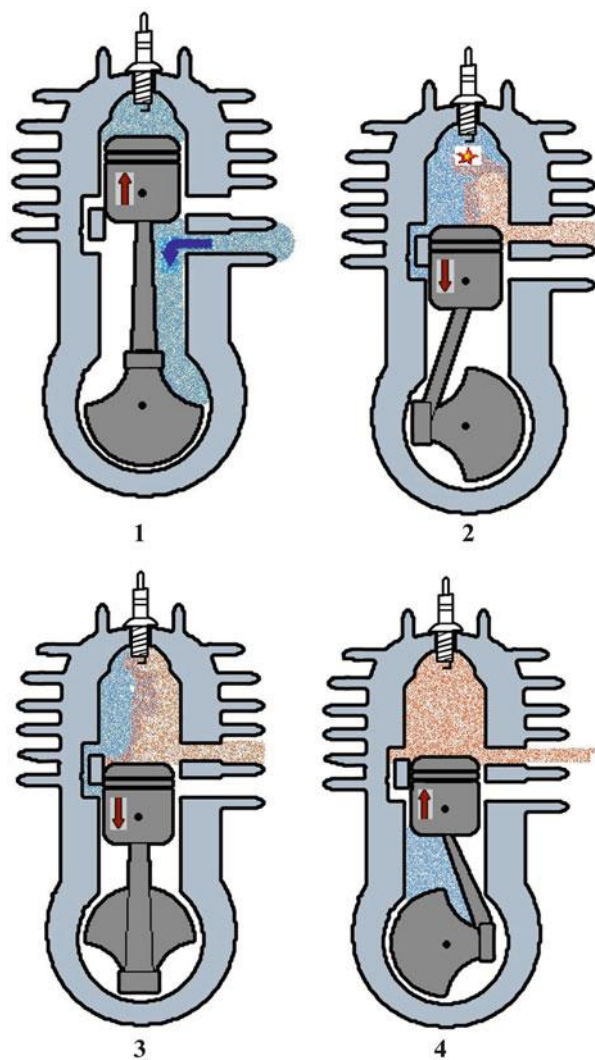
A fresh charge of fuel-air mixture enters when the piston uncovers the intake port while moving upwards (Fig. 4.19)). There is already a fuel-air mixture being compressed in the cylinder head above the piston. At the top of the compression stroke, the compressed fuel-air mixture is ignited by the spark plug Fig. (4.19). The resulting explosion of gases is what drives the piston downwards and more fuel-air mixture has been drawn into the cylinder. As the piston moves downwards, it uncovers the exhaust port. The exhaust gases flow out of that port Fig. (4.19). As the piston moves down even further Fig. (4.19), the transfer port becomes uncovered and the compressed fuel-air mixture in the crankcase rushes into the cylinder head above the piston, helping to displace any remaining exhaust gases. The piston now starts back on its upward stroke.

Table 4.4 presents a quick comparison between two-stroke and four-stroke engines.

4.3.3.3 Four-Stroke Diesel Engines

The Diesel cycle is the ideal cycle for CI reciprocating engines. The CI engine, first proposed by Rudolph Diesel in the 1890s, is very similar to the SI engine discussed in the last section, differing mainly in the method of initiating combustion. In CI engines (also known as diesel engines), the air is compressed to a temperature that is above the auto-ignition temperature of the fuel, and combustion starts as the fuel

Fig. 4.19 Two-stroke Otto cycle

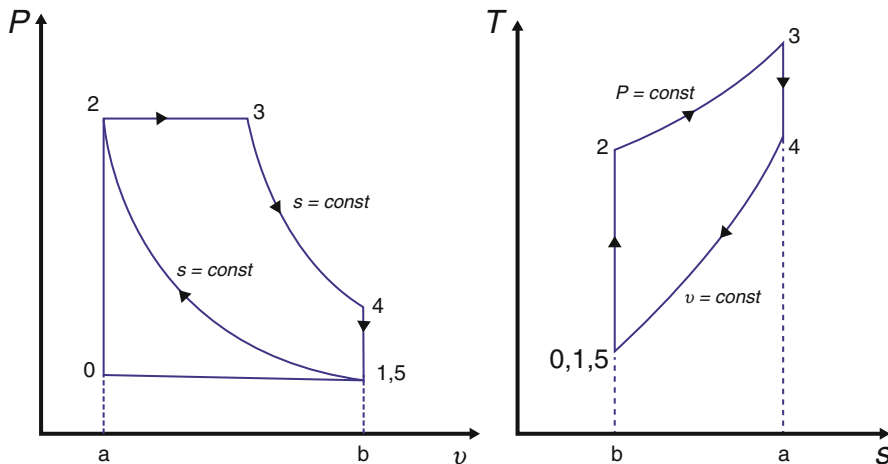


is injected into this hot air. Therefore, the spark plug and carburetor are replaced by a fuel injector in diesel engines. The four strokes of diesel engines are plotted on both P-v and T-s diagrams in Fig. 4.20.

In diesel engines, only air is compressed during the compression stroke, eliminating the possibility of auto-ignition. Therefore, diesel engines can be designed to operate at much higher compression ratios, typically between 12 and 24. Fuels that are less refined (thus less expensive) can be used in diesel engines. The fuel injection process in diesel engines starts when the piston approaches TDC and continues during the first part of the power stroke. Therefore, the combustion process in these engines takes place over a longer interval. Because of this longer

Table 4.4 Two-stroke versus four-stroke engines

	Two-stroke	Four-stroke	
1	Compression ratio	18:1–100:1	10:1–20:1
2	speed	2000–6000	400–3500
3	Power stroke	One working stroke per one revolution of crankshaft	One working stroke per two revolutions of crankshaft
4	Weight and size	Lighter and compact for same power	Heavier and larger
5	Flywheel size	Smaller	Larger
6	Construction	Simpler and easy to manufacture	More complicated due to valve mechanisms
7	Mechanical efficiency	Higher due to few moving parts	smaller
8	Thermal efficiency	Small	Higher
9	Noise	High	smaller
10	Fuel consumption	High	Low
11	Maintenance	Less	High

**Fig. 4.20** Air-standard diesel cycle

duration, the combustion process in the ideal Diesel cycle is approximated as a constant-pressure heat-addition process. In fact, this is the only process where the Otto and the Diesel cycles differ. The remaining three processes are the same for both ideal cycles. That is, process 1–2 is isentropic compression, process 2–3 constant-pressure heat addition, process 3–4 is isentropic expansion, and process 4–1 is constant-volume heat rejection. The similarity between the two cycles is also

apparent by comparing the P-v and T-s diagrams of both cycles illustrated in Figs. 4.12 and 4.20.

Thermodynamic Analysis of Air-Standard Diesel Cycle

1. *Process 0–1:* Constant pressure induction of air at ambient pressure P_0

Intake valve open and exhaust valve closed, Eqs. (4.7a) and (4.7b) are also used here.

2. *Process 1–2:* isentropic compression stroke

Both valves closed, Eqs. (4.8a) through (4.8d) are applied here.

3. *Process 2–3: Constant-pressure heat addition (combustion)*

$$T_3 = T_{\max}, P_3 = P_2, v_2 = v_{\text{TDC}} \quad (4.38a)$$

$$q_{2-3} = q_{\text{in}} = C_p(T_3 - T_2) = (h_3 - h_2) \quad (4.38b)$$

$$Q_{2-3} = Q_{\text{in}} = m_f Q_{\text{HV}} \eta_c = m_m C_p(T_3 - T_2) = (m_a + m_f) C_p(T_3 - T_2) \quad (4.38c)$$

$$Q_{\text{HV}} \eta_c = (\text{AF} + 1) C_p(T_3 - T_2) \quad (4.38d)$$

$$w_{2-3} = q_{2-3} - (u_3 - u_2) = P_2(v_3 - v_2) \quad (4.38e)$$

Cutoff ratio β is defined as the change in volume that occurs during combustion, given by:

$$\beta = V_3/V_2 = v_3/v_2 = T_3/T_2 \quad (4.38f)$$

4. *Process 3–4: Isentropic power or expansion stroke*

All valves are closed; Eqs (4.10a) through (4.10d) are also used here.

5. *Process 4–5: Constant volume heat rejection (exhaust blow-down)*

Exhaust valve open and intake valve closed; Eqs (4.11a) through (4.11c) are also applicable.

6. *Process 5–0: Constant pressure exhaust stroke at P_0*

The piston then executes an exhaust stroke in which the burned gases are purged from the cylinder through the open exhaust valve. Eqs (4.12a) and (4.12b) are used here.

Thermal efficiency of Diesel cycle:

$$\eta_{\text{th, Diesel}} = \frac{w_{\text{net}}}{q_{\text{in}}} = 1 - \frac{q_{\text{out}}}{q_{\text{in}}} = 1 - \frac{C_v(T_4 - T_1)}{C_p(T_3 - T_2)} = 1 - \frac{(T_4 - T_1)}{\gamma(T_3 - T_2)} \quad (4.39a)$$

With Rearrangement,

$$\eta_{\text{th, Diesel}} = 1 - \frac{1}{r_c^{\gamma-1}} [(\beta^\gamma - 1)/\gamma(\beta - 1)] \quad (4.39b)$$

where as previously defined $r_c = \frac{v_{\max}}{v_{\min}} = \frac{v_1}{v_2} = C_p/C_v$, $\beta = v_3/v_2$

Example 4.3 A large CI engine operates on air-standard Diesel cycle using diesel fuel having latent heating value of 41,000 kJ/kg and a combustion efficiency of 98 %. The engine has a compression ratio of 16:1 and cutoff ratio of 3.0. Inlet temperature and pressure are 35 °C and 101 kPa. Calculate:

1. Pressure, temperature, and specific volume at each point of the cycle
2. Air-fuel ratio
3. Thermal efficiency

Solution

State 1:

$$T_1 = 35^\circ\text{C} = 308 \text{ K}, \quad P_1 = 101 \text{ kPa}$$

$$v_1 = \frac{RT_1}{P_1} = \frac{0.287 \times 308}{101} = 0.8752 \text{ m}^3/\text{kg}$$

State 2: Isentropic compression

$$P_2 = P_1(r_c)^\gamma = 101 \times (16)^{1.35} = 4264.6 \text{ kPa}$$

$$T_2 = T_1(r_c)^{\gamma-1} = 308 \times (16)^{0.35} = 627.4 \text{ K}$$

$$v_2 = \frac{RT_2}{P_2} = \frac{0.287 \times 812.8}{4,264.6} = 0.0547 \text{ m}^3/\text{kg}$$

Or simply $v_2 = \frac{V_1}{r_c} = 0.0547 \text{ m}^3/\text{kg}$

$$\text{Work } W_{1-2} = \frac{R(T_2 - T_1)}{1 - \gamma} = \frac{0.287 \times (812.8 - 308)}{1 - 1.35} = -413.94 \text{ kJ/kg}$$

State 3: $v_3 = v_2 \times \beta = 0.1641 \text{ m}^3/\text{kg}$

$$P_3 = P_2 = 4264.6 \text{ kPa}$$

$$T_3 = \frac{P_3 v_3}{R} = \frac{4264.6 \times 0.1641}{0.287} = 2438.4 \text{ K}$$

$$w_{2-3} = P_2(v_3 - v_2) = 4264.6 \times (0.1641 - 0.0547) = 466.5 \text{ kJ/kg}$$

$$q_{\text{in}} = q_{2-3} = C_p(T_3 - T_2) = 1.108 \times (2438.4 - 812.8) = 1801.2 \text{ kJ/kg}$$

State 4: $v_4 = v_1 = 0.8752 \text{ m}^3/\text{kg}$

$$T_4 = T_3 \times \left(\frac{v_3}{v_4} \right)^{\gamma-1} = 2438.4 \times \left(\frac{0.1641}{0.8752} \right)^{0.35} = 1357.2 \text{ K}$$

$$P_4 = P_3 \times \left(\frac{v_3}{v_4} \right)^\gamma = 4264.6 \times \left(\frac{0.1641}{0.8753} \right)^{1.35} = 445.1 \text{ kPa}$$

Air-to-fuel ratio is obtained from Eq (4.38d)

$$\begin{aligned} Q_{\text{HV}}\eta_c &= (AF + 1)C_p(T_3 - T_2) \\ AF &= \frac{Q_{\text{HV}}\eta_c}{C_p(T_3 - T_2)} - 1 = \frac{41,000 \times 0.98}{1.108 \times (2438.4 - 812.8)} - 1 = 21.3 \\ W_{3-4} &= \frac{R(T_4 - T_3)}{1 - \gamma} = \frac{0.287 \times (1,357.2 - 2438.4)}{1 - 1.35} = 886.6 \text{ kJ/kg} \end{aligned}$$

$$W_{\text{net}} = W_{1-2} + W_{2-3} + W_{3-4} = -413.9 + 466.5 + 886.6 = 939.2 \text{ kJ/kg}$$

Thermal efficiency

$$\eta_{\text{th, Diesel}} = 1 - \frac{W_{\text{net}}}{q_{\text{in}}} = 1 - \frac{939.2}{1801.2} = 0.5214 = 52.14\%$$

Or it can be evaluated from the relation:

$$\begin{aligned} \eta_{\text{th, Diesel}} &= 1 - \frac{1}{r_c^{\gamma-1}} [(\beta^\gamma - 1)/\gamma(\beta - 1)] \\ \eta_{\text{th, Diesel}} &= 1 - \frac{1}{(16)^{0.35}} [(3^{1.35} - 1)/(1.35)(3 - 1)] = 0.5214 = 52.14\% \end{aligned}$$

4.3.3.4 Two-Stroke Diesel Engines

In a two stroke cycle CI engine, all the operations are exactly the same as those in two-stroke SI engine except that in this case only air is taken in instead of air fuel mixture and the fuel is injected at the end of compression stroke, a fuel injector being fitted instead of a spark plug.

Summary for piston engines used in Land, Sea, and Air applications

Table 4.5 provides a comparison of piston engines used in land, sea, and air applications.

4.3.3.5 Superchargers/Turbochargers

As stated in Sect. 4.2.2.3, superchargers or turbochargers will increase the power and efficiency of an internal combustion engine through increasing the pressure and density of the inlet air using compressors. Two types of compressors are used,

Table 4.5 Data for piston engines used in different land, sea, and air applications [6]

Class	Services	Power range (KW)	Predominant type		
			D or SI	cycle	Cooling
Road vehicles	Passengers	15–200	D	4	W
	Heavy commercial	120–400	D	4	W
Rail road	Locomotive	400–3000	D	2/4	W
Marine	Ships	3500–22,000	D	2/4	W
Stationary	Electric power	35–22,000	D	2/4	W
Airborne	Airplanes	45–2700	SI	4	A
	Helicopters	45–1500	SI	4	A

SI spark ignition, D diesel, A air cooled, W Water cooled

namely, positive displacement and dynamic. Three types of positive displacement compressors are extensively used; namely, the roots, vane, and screw compressor. Two types of dynamic compressors are used; either centrifugal or axial.

Figure 4.21 illustrates the P -v and T -s diagrams for a supercharger coupled to an aero piston engine performing an Otto cycle. Since the boost pressure (P_1) is greater than the ambient pressure (P_0), then the pumping loop represents a positive work.

Hence to get the net indicated power (P_i), the power represented by pumping loop is to be added:

$$P_i = \text{Area } (1 - 2 - 3 - 4) + \text{Area } (0 - 6 - 1 - 5) \quad (4.40)$$

The power required for driving the supercharger can be calculated by considering flow in as an adiabatic steady flow. The air enters the compressor at a pressure, temperature, and enthalpy (P_0, T_0, h_0). The work supplied to the supercharger is (w). The air leaves the supercharger at a pressure, temperature, and enthalpy (P_1, T_1, h_1). From Fig. 4.22, the work is calculated as:

$$w = h_1 - h_0 = C_p(T_1 - T_0) = \frac{C_p T_0}{\eta_s} \left[\left(\frac{P_1}{P_0} \right)^{\frac{r-1}{r}} - 1 \right] \quad (4.41a)$$

where η_s is the efficiency of supercharger. The power required to drive the supercharger is then equal to

$$P_{\text{supercharger}} = \dot{m}_a C_p (T_1 - T_0) = \frac{\dot{m}_a C_p T_0}{\eta_s} \left[\left(\frac{P_1}{P_0} \right)^{\frac{r-1}{r}} - 1 \right] \quad (4.41b)$$

Assuming a mechanical efficiency for coupling between supercharger and piston engine (η_m), then the power extracted from engine to drive the supercharger is:

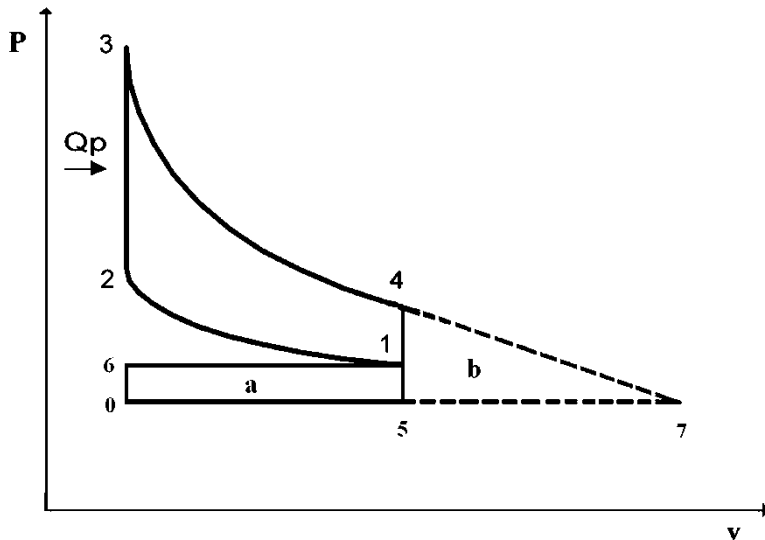


Fig. 4.21 P-v diagram for super/turbo-charger

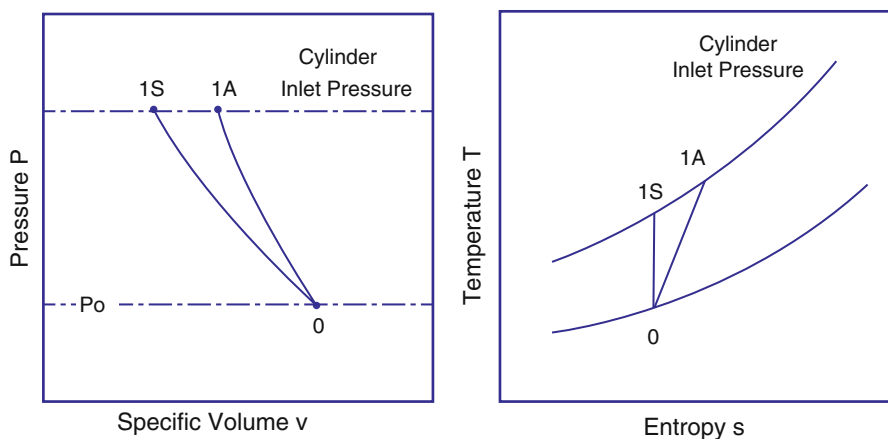


Fig. 4.22 Compression process in compressor of super/turbo-charger

$$P_{\text{supercharger}} = \frac{\dot{m}_d C_p T_0}{\eta_s \times \eta_m} \left[\left(\frac{P_1}{P_0} \right)^{\frac{\gamma-1}{\gamma}} - 1 \right] \quad (4.41c)$$

Example 4.4 A four-stroke diesel engine of 3000 CC capacity develops 15.0 kW per m^3 of free air induced per minute. When running at 3600 rev/min, it has a volumetric efficiency of 90 % referred to free air conditions of 1.01 bar and 25 °C.

Supercharger is added to boost the engine power. It has a pressure ratio 1.75 and isentropic efficiency of 80 % and overall mechanical efficiency as 80 %.

Assuming that at the end of induction, the cylinders contains a volume of charge equal to the swept volume, at the pressure and temperature of the delivery from the blower, *calculate*

1. The increase in indicated and brake powers
2. Recalculate for altitudes 3, 6, and 9 km altitudes
3. Plot the increase in indicated and brake powers versus altitude

Solution

1. Sea Level conditions

$$\text{Swept volume } V_s \equiv V_1 = 3000 \times \frac{3600}{2} = 5.4 \times 10^6 \frac{\text{cm}^3}{\text{min}} = 5.4 \text{ m}^3/\text{min}$$

From Eq (4.33a), the rate of naturally aspirated induced air volume (\dot{V}_a) is

$$\dot{V}_a = V_s \times \eta_V = 5.4 \times 0.9 = 4.86 \text{ m}^3/\text{min}$$

Supercharger:

Inlet conditions of 1.01 bar and $25^\circ\text{C} = 25 + 273 = 298 \text{ K}$

Exit pressure $P_1 = 1.75 \times 1.01 = 1.7675 \text{ bar}$

$$\text{Exit temperature } T_1 = T_0 \left(1 + \frac{\pi_s^{\gamma-1} - 1}{\eta_s} \right) = 298 \left(1 + \frac{1.75^{0.286} - 1}{0.8} \right) = 362.7 \text{ K}$$

The process in the compressor is governed by the relation:

$$\frac{P_1 V_1}{T_1} = \frac{P_0 V_0}{T_0}$$

Using rate of volume flow instead, the above relation can be expressed as:

$$\frac{P_1 V_1}{T_1} = \frac{P_0 V_0}{T_0}$$

$$\text{Thus } V_0 = \frac{\pi_s \times T_0 \times V_1}{T_1} = \frac{1.75 \times 298 \times 5.4}{362.7} = 7.76 \text{ m}^3/\text{min}$$

The inlet air flow rate into supercharger is $7.76 \text{ m}^3/\text{min}$ at pressure = 1.01 bar and temperature 25°C .

The increase in indicated power (ΔP_i) due to increased induction pressure is:

$$(\Delta P)_i = \frac{(P_1 - P_0) \times V_s}{60} = \frac{(1.7675 - 1.01) \times 100 \times 5.4}{60} = 6.8175 \text{ kW}$$

The increase in brake power ($\Delta P)_b$ due to increased induction pressure is:

$$(\Delta P)_b = (\Delta P)_i \times \eta_m = 6.8175 \times 0.8 = 5.454 \text{ kW}$$

Increase in induced air volume = $7.76 - 4.86 = 2.9 \text{ m}^3/\text{min}$

Increase in power due to induced air = $15 \times 2.9 = 43.5 \text{ kW}$

Mass of air delivered by supercharger is:

$$\dot{m}_a = \frac{P_1 V_1}{RT_1} = \frac{1.7675 \times 10^5 \times 5.4}{287 \times 362.7} = 9.17 \text{ kg/min}$$

Power extracted to drive the supercharger is then, Eq (4.41c):

$$(\Delta P)_{\text{supercharger}} = \dot{m}_a \frac{C_p(T_1 - T_0)}{\eta_m} = \frac{9.17 \times 1.005 \times (362.7 - 298)}{0.8 \times 60} = 12.422 \text{ kW}$$

Net increase in indicated power = $43.5 + 6.8175 - 12.422 = 37.8955 \text{ kW}$

Net increase in brake power = $43.5 + 5.454 - 12.422 = 36.532 \text{ kW}$

Net power for original engine (without supercharger) = $15 \times 4.86 = 72.9 \text{ kW}$

2. Altitudes

The above procedure is followed and the results of calculations are arranged in Table 4.6.

A plot for the increase in indicated and brake powers versus altitude is given in the Fig. 4.23.

4.4 Aircraft Propellers

4.4.1 Introduction

Aircraft propellers or *airscrew* convert rotary motion from piston engines or turboprops to provide propulsive force (Fig. 4.24). They may be of fixed or variable *pitch*. In both cases, the propeller accelerates a large quantity of air through a small velocity change. In turboprop engines, 80–90 % of the thrust is produced by a turbine driven propeller and 10–20 % by the jet. While in piston engines, propellers produce 100 % of thrust force.

Propeller has several definitions as follows:

A device having a central revolving hub with radiating blades, for *propelling* an airplane, ship, etc. [7]

A device consisting of a set of two or more twisted, airfoil-shaped blades mounted around a shaft and spun to provide propulsion of a vehicle through air or water.

A type of fan that transmits power by converting *rotational* motion from piston engine or turboprops into *thrust* to pull or push the airplane through the air.

Table 4.6 Variation of power vs. altitude

Altitude km	$V_s \equiv V_1 m^3 /$ min	P_l bar	T/K	\dot{m}_a kg/min	$(\Delta P)_i$ kW	$(\Delta P)_b$ kW	$(\Delta P)_s$ kW	Net increase in indicated power kW	Net increase in brake power kW
0	5.4	1.768	362.7	9.17	6.82	5.45	12.422	37.90	36.53
3	5.4	1.225	326.7	7.06	4.73	3.78	8.595	39.63	38.68
6	5.4	0.823	303.0	5.11	3.17	2.54	5.772	40.90	40.27
9	5.4	0.543	279.2	3.66	2.09	1.67	3.807	41.79	41.37

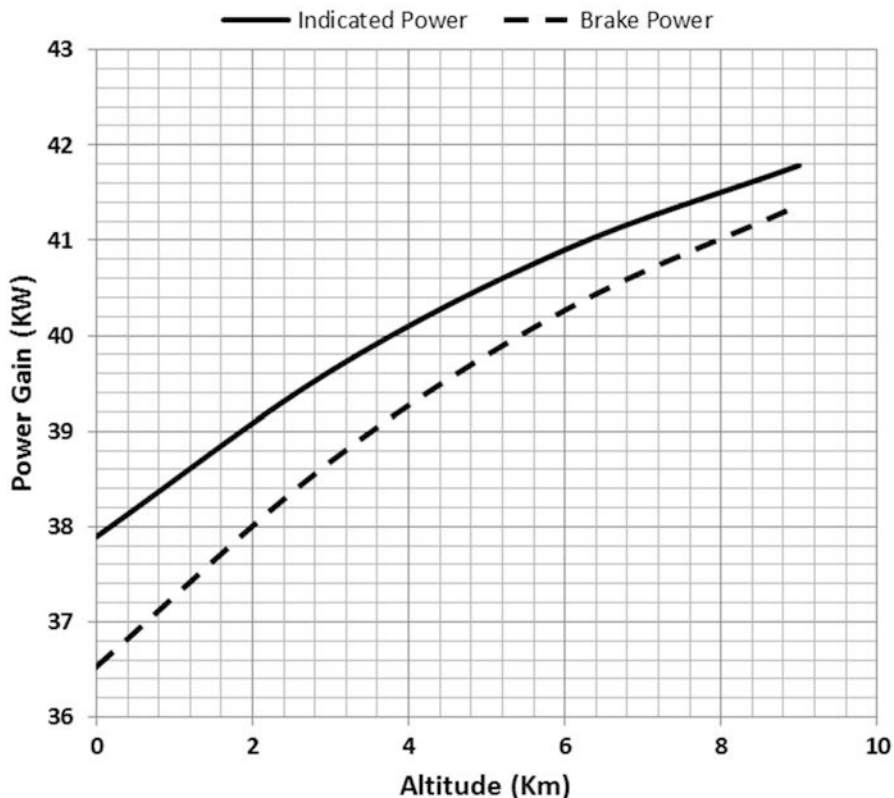


Fig. 4.23 Power gain by supercharger at different altitudes

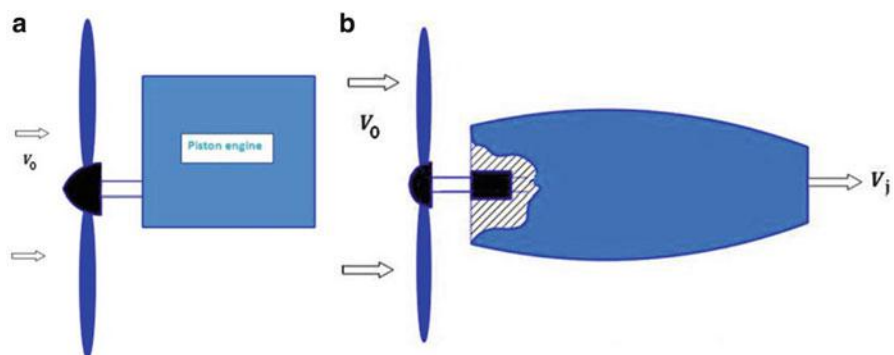


Fig. 4.24 Propeller installed to (a) piston engines (b) turboprop engine

A series of rotating wings (or airfoils) of equal length meeting at a center hub attached to the crankshaft of aircraft engine.

In brief, *propeller history* has the following milestones:

Third century BC: Greek scientist Archimedes figured out how to enclose a long spiral screw inside a cylinder to lift water.

Sixteenth century: Leonardo da Vinci (1452–1519) sketched an upward-facing screw propeller on his design for a *helicopter*, which he never built.

1796: American inventor John Fitch made the first basic propeller, shaped like a screw, for a steamboat.

1836: Englishman Francis Petit-Smith and Swedish-American John Ericsson independently developed modern-style propellers with blades for ships.

1903: The brothers Wilbur and Orville Wright used twisted propellers shaped like airfoils to make the first powered flight, ushering in the modern age of air travel.

1919: Fixed pitch propellers enter service

1924: The constant speed propeller is patented by Dr. H.S. Hele-Shaw and T.E. Beacham

1932: Variable pitch propellers were introduced into air force service

1935: Constant speed propellers become available

1945: Five blade propellers installed to Rolls-Royce RB50 Trent turboprop engine to power Gloster meteor

1980 High speed propellers tested by NASA for propfans to power transport aircraft

4.4.2 Nomenclature

In order to explain the theory and construction of propellers, it is necessary first to define the parts of various types of propellers and give the nomenclature associated with propellers. Figure 4.25 shows a fixed-pitch one-piece wood propeller designed for light aircrafts. Note carefully the hub, hub bore, bolt holes, neck, shank, blade, tip, and metal tipping. In example, fixed propeller is used in the WWI Nieuport 28.

The cross section of a propeller blade is a typical airfoil section as shown in Fig. 4.26.

Figure 4.26 shows two views and various cross sections of a propeller blade. The blade shank is the portion of the blade which is near the butt of the blade. It is usually thick to give it strength, and it is cylindrical where it fits the hub barrel, but the cylindrical portion of the shank contributes little or nothing to thrust. In an attempt to obtain more thrust, some propeller blades are designed so that the airfoil section (shape) is carried all the way along the blade from the tip to the hub. In other designs, the airfoil shape is carried to the hub by means of blade cuffs, which are thin sheets of metal or other material, which function like cowling as shown in Fig. 4.27. The cuff is a hard rubber shape that changes the airfoil of the propeller to a more advantageous shape near the spinner.



Fig. 4.25 Wooden propeller

4.5 Classifications

In this section, classifications for propellers based on different points are identified. It is important to state here that classifications listed here are applied for both piston engines and turboprop engines as well be discussed in Chap. 7. Classifications will be followed hereafter based on different items.

4.5.1 *Source of Power*

As seen in Fig. 4.24, it may be either driven by:

Piston engines (crankshaft of a piston engine)

Turboprops (turbine shaft of a turboprop engine)

4.5.2 *Material*

Wood (solid or laminated) in very early types (Fig. 4.24), which were used exclusively on personal and business aircraft prior to World War II.

Metal (later types)

After 1940, propellers were made of steel, but recent propellers are fabricated from high-strength, heat-treated, aluminum alloy. Metal propeller is similar to the wood propeller, except that the sections are generally thinner.

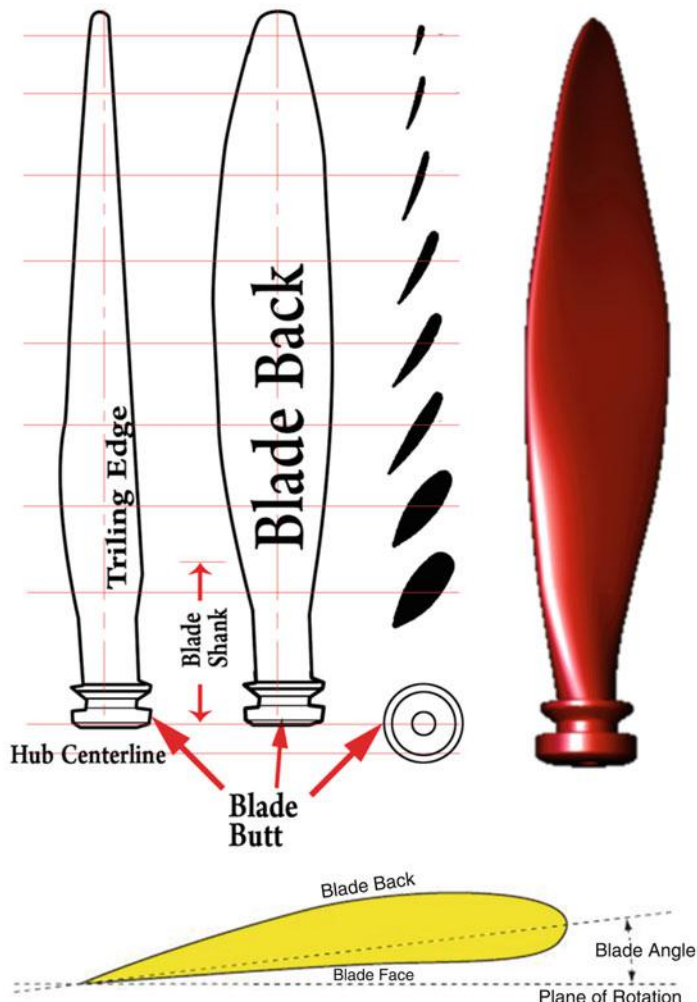


Fig. 4.26 Cross sections of a propeller

Composite materials (most modern designs)

In the 1960s, glass and fiber polymer composite propeller materials were used for manufacturing propellers. Today nearly all the large propellers for aircrafts have carbon fiber blades (Lockheed Hercules C-130 J). These are light weight, have high specific strength, stiffness and excellent fatigue resistance, and its resistance to erosion are three times that of aluminum alloys [8].



Fig. 4.27 Single propeller with cuffs

4.5.3 *Coupling to the Output Shaft*

Direct coupling

Through a *reduction unit*

Refer to Fig. 4.28

4.5.4 *Control*

Fixed pitch (small aircrafts)

Blades are fixed at a certain fixed angle to the hub, usually never changes (it can be altered on the ground only and not during flight). Wright brothers developed the first successful propellers of the fixed pitch type.

Variable pitch (Bigger and more sophisticated planes)

Blades may be rotated about its long axis. It may be subdivided into:

Two-position propeller

Blades are limited to two angles, one for takeoff and climb (low speed operation) and the other for cruising (high speed operation)

Adjustable pitch (ones whose pitch can be altered by the pilot)

Controllable pitch (has automatic mechanism to adjust its own pitch to match the plane's flying speed)

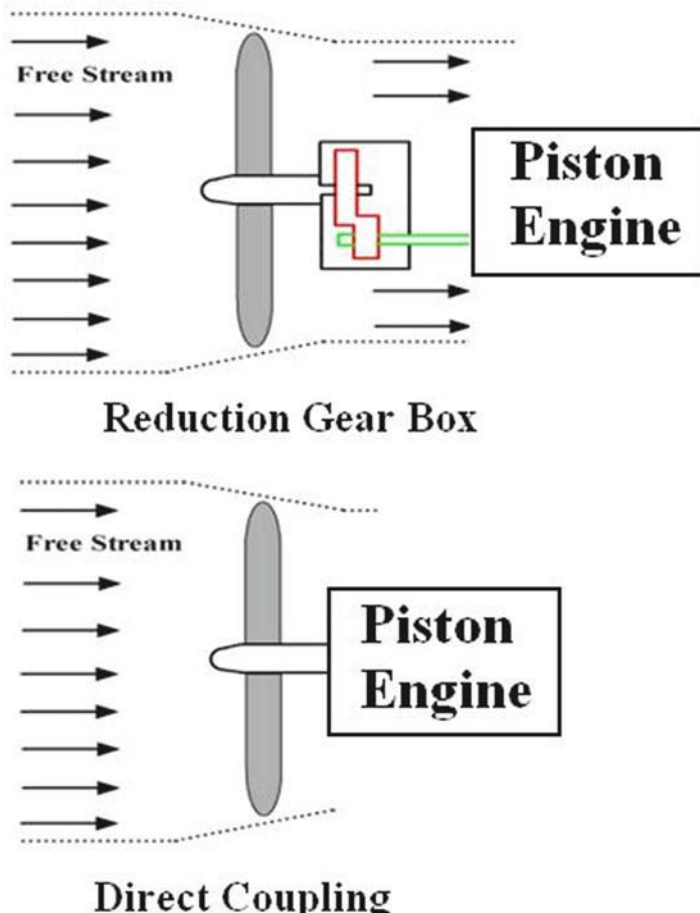


Fig. 4.28 Coupling between propeller and engine

Constant-speed (designed to change pitch automatically, allowing the engine always to turn over at the same (constant) speed)

Feathered (turning the propeller blades so they are edge on, making a very shallow angle to the oncoming air, minimizing air resistance, and allowing the plane either to keep on flying on its remaining engines or glide to a crash landing). On single-engine aircraft, the effect is to increase the gliding distance. On a multi-engine aircraft, feathering the propeller on a failed engine allows the aircraft to maintain altitude with the reduced power from the remaining engines.

Thrust reversal (the pitch of the blades can be reversed so a propeller makes a forward draft of air instead of one moving backward – handy for extra braking (especially if the main *brakes* on the wheels suddenly fail)).

Table 4.7 Fixed pitch versus variable pitch propellers

Basic function (poor performance)	Fixed pitch propeller	Lowest cost
	Ground adjustable propeller	
	In flight adjustable propeller	
Best performance	Constant speed propeller	Most expensive

Table 4.7 illustrates a comparison between fixed and variable pitch propellers from performance and cost points of view.

4.5.5 Number of Propellers Coupled to Each Engine

Single; Fig. 4.26

Double (contra-rotating) (Fig. 4.29)

Contra-rotating propellers, also referred to as *coaxial contra-rotating propellers* or *high-speed propellers*, apply the maximum power of an engine (or engines) to drive two **propellers** in **contra-rotation** (rotation about the same axis in opposite directions). Two propellers are arranged one behind the other, and power is transferred from the engine via a **planetary gear** or **spur gear** transmission.

4.5.6 Direction of Rotation

Nose installation (single engine)

Left-handed propeller

A left-handed propeller is one which when viewed from the cockpit rotates in an anti-clockwise direction, while if viewed from outside the aircraft, positioned at the front, propeller will rotate in a clockwise direction.

Right-handed propeller

A right-handed propeller will be seen to rotate clockwise from the cockpit, and anti-clockwise when viewed from the front of the aircraft.

Wing installation (Even number of engines; two/four/six,...etc.)

Propellers may be:

Same rotation direction (for both wings)

The propellers on both engines of most conventional twin-engine aircraft spin clockwise (as viewed from the pilot seat).

Counter-rotating (right wing has clockwise propeller rotation and left wing has counter clockwise propeller rotation or vice-versa). The advantage of such designs is that counter-rotating propellers balance the effects of **torque** and **p-factor**, eliminating the problem of the **critical engine**.



Fig. 4.29 Contra-rotating propellers on a Rolls-Royce–Griffon–powered [P-51 unlimited racer](#)

Counter-rotating pairs on each wing (Airbus A400M Atlas)

The pair of propellers on each wing of the A400M, Fig. 4.30 turn in opposite directions, with the tips of the propellers advancing from above towards the midpoint between the two engines. This is in contrast to the overwhelming majority of multi-engine propeller driven aircraft where all propellers on the same wing turn in the same direction.

The [Wright Flyer](#) has a single engine and a chain to drive its two propellers in counter-rotation directions.

The following twin-engine aircrafts (one engine per wing) have counter-rotating propellers: [de Havilland Hornet](#), [Lockheed P-38 Lightning](#), [Henschel Hs 129](#), [Piper PA-31 Navajo](#), [Piper PA-34 Seneca](#), [Piper PA-39 Twin Comanche C/R](#), [Piper PA-40 Arapaho](#), and [Piper PA-44 Seminole](#).

The six engines in Messerschmitt Me 323 were fitted – to reduce torque – by a trio of counterclockwise rotation engines mounted on the port wing, and a trio of clockwise rotation engines on the starboard wing, resulting in the props rotating “away” from each other at the tops of their arcs.



Fig. 4.30 Airbus A400 M aircraft (pair of propellers on each wing [turn in opposite directions](#))

4.5.7 Propulsion Method

Pusher (Fig. 4.31)

Puller (tractor) (Fig. 4.32)

Combination of the tractor and pusher types mounted in-line on a small aircraft (refer to Burton [10]) as shown in Fig. 4.33

4.5.8 Number of Blades

One has the option of setting the number of blades (B) for a given application. While one has a minimum of two blades to choose from, one can presently go as high as around eight blades on the high-performance end for an unducted propeller

- Two
- Three
- Four

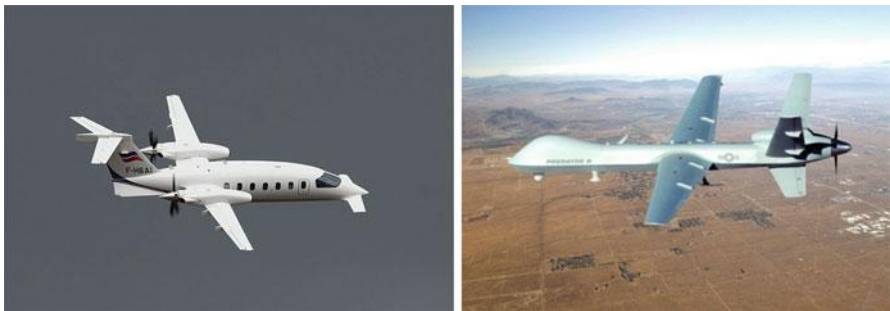


Fig. 4.31 Pusher propeller: (*Left*) Piaggio P-180 Avanti Rennes (*Right*) an AUV

Fig. 4.32 Puller propeller installed to Antonov An-140-100 aircraft



- Six
- Eight

Multiple (greater than four, as an example: eight-bladed Hamilton Sundstrand NP2000) (Fig. 4.34)

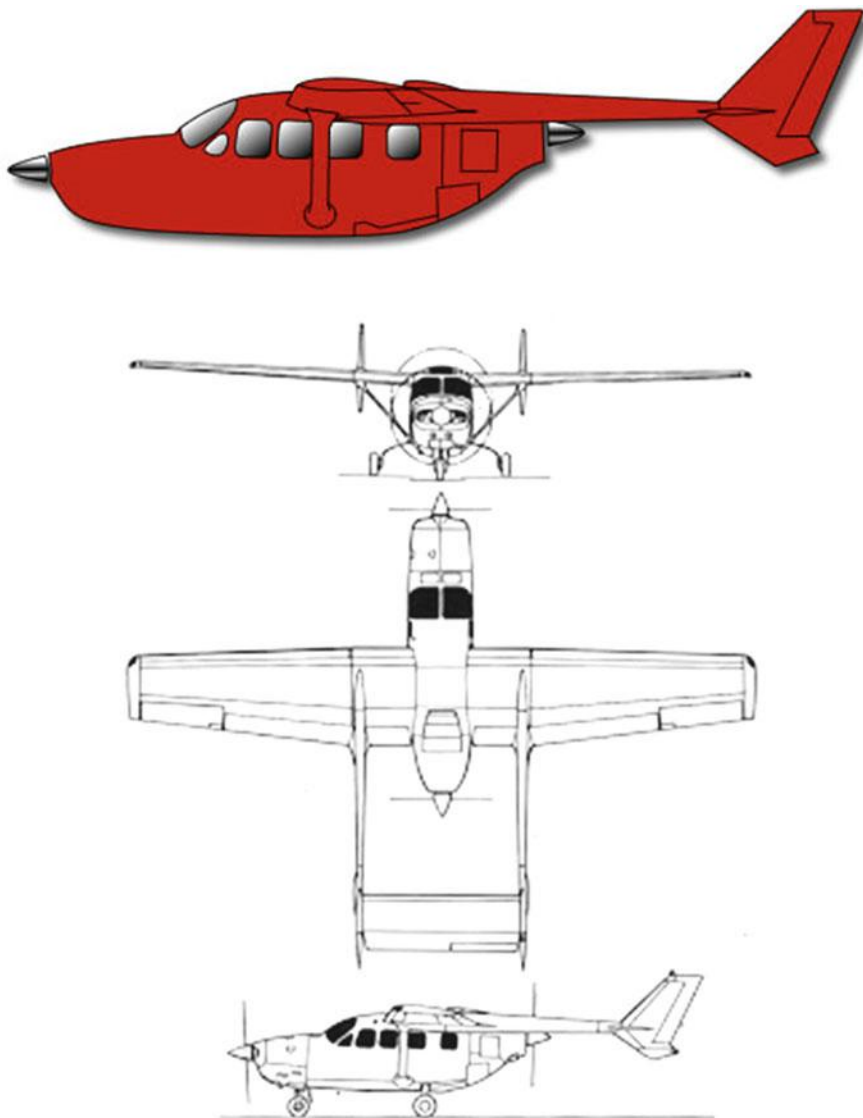


Fig. 4.33 Combination of puller-pusher layout (Cessna 337 Skymaster)

4.6 Aerodynamic Design

Aerodynamic developments of propellers started with the simple Rankine-Froude momentum theory. Next, blade element theories provided more realistic results and lead to practical propeller design calculations. Initially, lumped inflow factors [9] are used to evaluate flow velocities around a blade element.



Fig. 4.34 Hamilton Sundstrand 8-blades NP2000 Propeller for C-130 aircraft

This section will handle only actuator disk and blade element theories. For more advanced work, the reader can review the work of Bocci [11]. Detailed description for advanced methods is highlighted by Douglas Archer and Saarlas [12]. There is also interest in transonic and supersonic propellers, but shockwave losses and noise present severe problems.

4.6.1 Axial Momentum, (or Actuator Disk) Theory

Actuator disk is also sometime denoted as *Rankine-Froude* or *slip stream* Theory (1865). The actuator disk theory replaces the propeller with an infinitely thin plane “actuator” disk, which imparts a certain momentum to the fluid passing through it, thus produces an increase in axial velocity and axial momentum (Fig. 4.35). This theory provides an initial idea regarding the performance of a propeller (say efficiency) but fails to furnish the required design data for the propeller blades.

The following assumptions and definitions are stated:

- Fluid is one dimensional, perfect, incompressible, and isentropic
- Flow has uniform properties (velocity and pressure) across any plane normal to the flow except for the discontinuous jump in pressure across the disk itself.
- Rotation imparted to the flow is neglected.
- The streamlines at the edge of the disk define the outer limit of the contracting streamtube, which passes through the disk and separates it from the surrounding

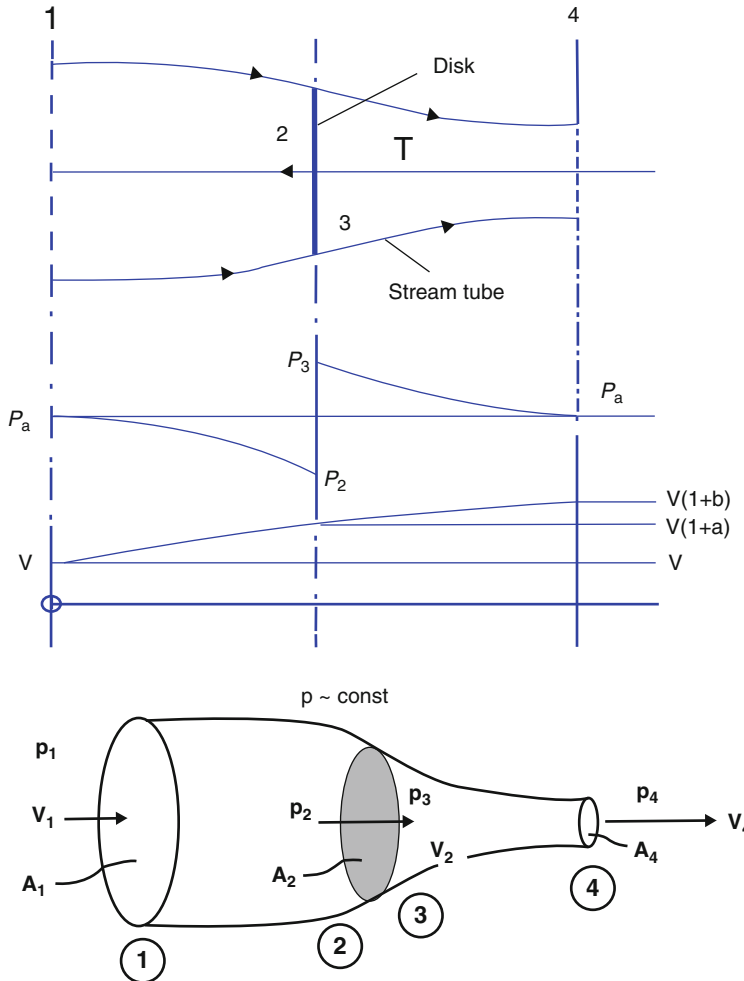


Fig. 4.35 Actuator disk in physical plan and its pressure and velocity distribution.

flow. The streamtube has cylindrical sections in both far upstream and far downstream.

- The flow outside the propeller stream tube has constant stagnation pressure (no work is imparted to it).

Figure 4.35 illustrates fluid streamlines, velocities, and pressures around the plane of the propeller with the following designations for points: (1) Far upstream the propeller

(2) Just in front of the propeller (3) Just after the propeller (4) Far downstream the propeller

The distance between (2) and (3) is assumed infinitesimal.

Along the stream tube between stations 1 and 4, the velocity increases from the free upstream value V_1 , at cross-sectional area A_1 , to the value V_4 in the cross-sectional area A_4 . The static pressure at stations 1 and 4 is the ambient atmospheric value P_a ($P_1 = P_4 = P_a$), while pressure difference builds up across the disc.

The velocity at the disk, $V_2 = V_3$ is written as:

$V_2 = V_1(1 + a)$, where, $aV_1 = V_2 - V_1$, is the increase in velocity through the disk and (a) is called the *axial inflow factor*.

In the fully developed slipstream, the velocity

$V_4 = V_1(1 + b)$, where, $bV_1 = V_4 - V_1$, is the increase in velocity there and (b) is called the *slipstream factor*. So

$$a = \frac{V_2 - V_1}{V_1} \quad (4.42)$$

and

$$b = \frac{V_4 - V_1}{V_1} \quad (4.43)$$

4.6.1.1 Thrust

Apply the Newton second law (conservation of momentum principle) in the axial flow direction to the control region between stations 1 and 4 (Fig. 4.35). The thrust (T) is simply the rate of increase of momentum of the airflow in the downstream direction:

$$T = \dot{m}(V_4 - V_1) \quad (4.44)$$

Dropping the subscript (1) on the free-stream velocity, put $V = V_1$

$$T = \dot{m}[V(1 + b) - V] = \dot{m}bV \quad (4.45)$$

Where \dot{m} is the mass flow through the actuator disk, and

$$\dot{m} = \rho A V_2 = \rho A V(1 + a) \quad (4.46)$$

Eqs. (4.44) through (4.46) give:

$$T = \rho A V_2 (V_4 - V_1) = \rho A V^2 (1 + a) b \quad (4.47)$$

Force balance across the disk requires that

$$T = A \Delta p \quad (4.48)$$

where from Fig. 4.35

$$\Delta p = p_3 - p_2 \quad (4.49)$$

Eliminating (T) from Eqs. (4.47) and (4.48) gives

$$\Delta p = \rho V^2(1 + a)b \quad (4.50)$$

Since the flow is assumed incompressible, then Bernoulli's equation applied between stations (1) and (2) yields:

$$p_a + \frac{1}{2}\rho V^2 = p_2 + \frac{1}{2}\rho V^2(1 + a)^2$$

Applying Bernoulli's equation between stations (3) and (4) yields:

$$p_3 + \frac{1}{2}\rho V^2(1 + a)^2 = p_a + \frac{1}{2}\rho V^2(1 + b)^2$$

So

$$\begin{aligned} p_3 - p_2 &= \Delta p = \frac{1}{2}\rho V^2(1 + b)^2 - \frac{1}{2}\rho V^2 \\ \text{Or : } \Delta p &= \rho V^2 b \left(1 + \frac{b}{2} \right) \end{aligned} \quad (4.51)$$

Eliminating (Δp) from Eqs. (4.50) and (4.51) gives

$$\begin{aligned} 1 + a &= 1 + \frac{b}{2} \\ \text{Thus } a &= \frac{b}{2} \quad \text{or} \quad b = 2a \end{aligned} \quad (4.52)$$

From Eqs. (4.42) and (4.43), it is easily to prove that:

$$V_2 = \frac{V_1 + V_4}{2} \quad (4.53a)$$

Moreover, at zero forward speed ($V = V_1 = 0$), then $(V_4 = 2V_2)_{V=0}$

This simple but important result means that at any speed including zero, one-half of the final increase in velocity in the slipstream has already occurred at the rotor disk itself. Using Eqs. (4.47) and (4.52), the following relations between thrust and the inflow factor (a), or the slipstream factor (b), can be derived:

$$T = \rho A V^2 (1 + a) 2a = \rho A V^2 \left(1 + \frac{b}{2} \right) b \quad (4.54)$$

Equation (4.54) is quadratic in the parameters (a) or (b), which have the solutions:

$$a = -\frac{1}{2} \pm \sqrt{\left(\frac{1}{2}\right)^2 + \frac{T}{2\rho A V^2}} \quad (4.55a)$$

Denoting $v = aV$, where (v) is the induced velocity at the propeller (disk), then

$$v = aV = -\frac{V}{2} \pm \sqrt{\left(\frac{V}{2}\right)^2 + \frac{T}{2\rho A}} \quad (4.55b)$$

Moreover

$$b = -1 \pm \sqrt{1 + \frac{2T}{\rho A V^2}} \quad (4.55c)$$

Denoting $w = bV$, where (w) is the induced velocity far downstream the propeller (disk). Then

$$w = bV = -V \pm \sqrt{(V)^2 + \frac{2T}{\rho A}} \quad (4.55d)$$

4.6.1.2 Propulsive Efficiency

The propulsive efficiency (η_p) of a propeller is the ratio of the available power; or sometimes identified as useful thrust power ($P_A = TV$) to the power delivered to the propeller. For piston engines, this is the shaft brake power (P):

$$\eta_p = \frac{P_A}{P} = \frac{TV}{P} \quad (4.56)$$

For the actuator disk model, this efficiency is an ideal propulsive efficiency because it ignores all losses except that associated with the streamwise kinetic energy. Using Eqs. (4.52) and (4.54) gives

$$\text{Useful thrust power} = TV = \rho A V^3 (1 + a)(2a) \quad (4.57)$$

Power expended on the air = P = rate of change of kinetic energy

$$\begin{aligned} P &= \frac{1}{2} \dot{m} \left[V^2(1+b)^2 - V^2 \right] \\ P &= \rho A V^3 (1+a)^2 (2a) \end{aligned} \quad (4.58)$$

The ratio of these two powers, Eqs. (4.57) and (4.58), for the *ideal* actuator disk model is called the ideal *Froude* efficiency (η_F) and is therefore the upper limit to propeller performance:

$$\eta_F = \frac{1}{1+a} = \frac{V_1}{V_2} = \frac{V}{V+v} \quad (4.59)$$

Equation (4.59) proves that higher efficiency of propulsion can be achieved by large rotors with very small increase in fluid velocity (achieving thrust by large surfaces rather than velocity). Ideal Froude efficiency (η_F) is always greater than the actual propulsive efficiency (η_P).

Example 4.5 The shown figure illustrates Cessna 335/340 aircraft which is powered by two piston engines each produces 2900 N thrust force. Each propeller is three bladed having a diameter of 1.92 m. If service ceiling of airplane is 30,000 ft and cruise speed is 450 km/h.

Calculate

1. Propeller efficiency using actuator disk theory
2. The pressure jump across the propeller



Figure (Example 4.5) Cessna 335/340 aircraft

Solution1. *The propeller efficiency*

Flight speed is

$$V = \frac{450 \times 1000}{3600} = 125 \text{ m/s}$$

The propeller (Froude) efficiency is calculated from Eq. (4.59):

$$\eta_F = \frac{V}{V + v}$$

Where the induced velocity (v) is calculated from Eq. (4.55b):

$$v = -\frac{V}{2} + \sqrt{\left(\frac{V}{2}\right)^2 + \frac{T}{2\rho A}}$$

Air density at an altitude of 30,000 ft is $\rho = 0.458 \text{ kg/m}^3$ and

$$\text{Propeller area } A = \frac{\pi d^2}{4} = \frac{\pi \times (1.92)^2}{4} = 2.895 \text{ m}^2$$

$$v = -\frac{125}{2} + \sqrt{\left(\frac{125}{2}\right)^2 + \frac{2900}{2 \times 0.458 \times 2.895}} = 8.21 \text{ m/s}$$

The propeller efficiency is then calculated as follows:

$$\eta_F = \frac{125}{125 + 8.21} = 93.84\%$$

To evaluate the *pressure difference across the propeller*, we calculate the pressure upstream of propeller from Bernoulli's equation.

$$P_{\text{atm}} - P_2 = \left(\frac{\rho}{2}\right) \left\{ (V + v)^2 - V^2 \right\}$$

The atmospheric pressure at 30,000 ft is 30.09 kPa

$$P_{\text{atm}} - P_2 = \left(\frac{0.458}{2}\right) \left\{ (125 + 8.21)^2 - (125)^2 \right\} = 484.45 \text{ Pa} \quad (1)$$

The pressure downstream of propeller is calculated from Bernoulli's equation:

$$P_3 - P_{\text{atm}} = \left(\frac{\rho}{2}\right) \left\{ (V + 2v)^2 - (V + v)^2 \right\}$$

$$P_3 - P_{\text{atm}} = \left(\frac{0.458}{2}\right) \left\{ (125 + 2 \times 8.2)^2 - (125 + 8.2)^2 \right\} = 515.34 \text{ Pa} \quad (2)$$

Adding equation (1) and (2) to get

$$P_3 - P_2 = 999.8 \text{ Pa} = 1.0 \text{ kPa}$$

This pressure difference can be easily found from Eq. (4.46):

$$\Delta p = \frac{T}{A} = \frac{2900}{2.895} = 1001.7 \text{ Pa} \cong 1.0 \text{ kPa}$$

4.6.2 Modified Momentum or Simple Vortex Model

A practical assessment of propeller performance and design of realistic propellers require inclusion of at least some of the foregoing effects and allowance for blading details. In this simple vortex model, the effect of rotational flow will be discussed hereafter.

Consider a stream tube that passes through the propeller section at radius (r) (Fig. 4.36). The corresponding angular speed at this blade section is (Ωr) where (Ω) is the angular speed of propeller and (r) is the local radius of propeller. When fluid passes through the propeller section, it acquires an angular speed due to the swirling nature of the flow induced by the propeller. Thus the rotational speeds at propeller sections are:

$$u = a_\Omega \Omega r \quad (4.60)$$

where (a_Ω) is the angular induced factor.

The local flow velocity just downstream of the propeller blade is expressed as:

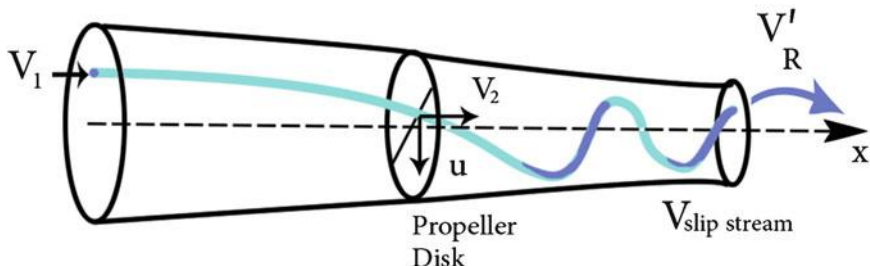


Fig. 4.36 Modified actuator disk

$$V_R = \sqrt{V_2^2 + u^2} = \sqrt{V_1^2(1+a)^2 + (a_\Omega \Omega r)^2}$$

The local flow velocity far downstream of the propeller is expressed as:

$$V'_R = \sqrt{V_4^2 + u^2} = \sqrt{V_1^2(1+b)^2 + (a_\Omega \Omega r)^2}$$

The local propulsive efficiency at any radius (r) based on modified momentum theory η_{mm} is defined as:

$$\begin{aligned} \eta_{mm} &= \frac{T \times V_1}{T \times V_1 + (KE)_{\text{Losses}}} = \frac{\dot{m} (V_4 - V_1) \times V_1}{\dot{m} (V_4 - V_1) \times V_1 + \frac{1}{2} \dot{m} (b^2 V_1^2 + u^2)} \\ &= \frac{b V_1^2}{b V_1^2 + \frac{b^2 V_1^2 + u^2}{2}} \\ \eta_{mm} &= \frac{1}{1 + \frac{b}{2} + \frac{u^2}{2b V_1^2}} = \frac{1}{1 + a + \frac{u^2}{4a V_1^2}} \\ \eta_{mm} &= \frac{1}{1 + a + \frac{a_\Omega^2 \Omega^2 r^2}{4a V_1^2}} \end{aligned} \quad (4.61)$$

4.6.3 Blade Element Considerations

Blade element theory is similar to wing theory. In this theory, the blade is divided into small sections, which are handled independently from each other. Each segment has a chord, a blade angle, and associated airfoil characteristics. This isolated airfoil assumption is found to be substantially correct for two- or three-bladed propellers, except near the hub.

At any given radius (r), the circumferential distance between two successive blades is called spacing (s), while the length of blade section between leading and trailing edges is called chord (c) (Fig. 4.37). Since (s/c) for two- and three-bladed propellers are much greater than unity, this justifies the use of isolated airfoil characteristics in this theory. Multi-blade propellers, for which the (s/c) ratio has fallen to a value of order (1) or less, will have to be treated as cascades.

The forces acting on a small section of the blade (lift and drag) are determined and then integrated over the propeller radius in order to predict the thrust, torque, and power characteristics of the propeller.

The forces acting on a small section of the blade (lift and drag) are first determined, next resolved into two perpendicular components in the axial and

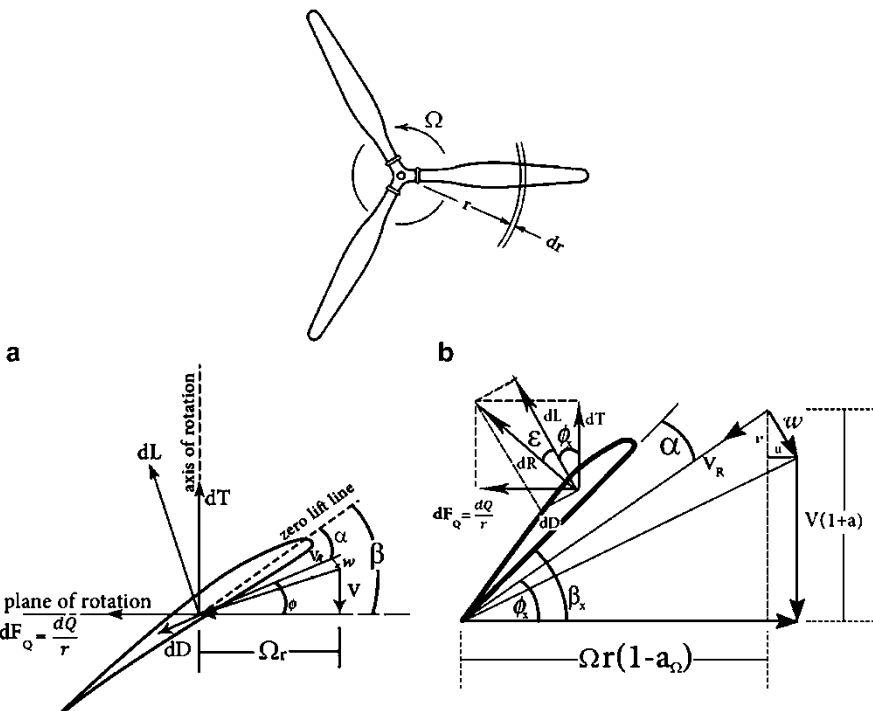


Fig. 4.37 Blade element theory

tangential directions, and finally integrated over the propeller radius in order to predict the thrust, torque, and power characteristics of the propeller.

A differential blade element of chord (c) and width (dr) located at a radius (r) from the propeller axis is shown in Fig. 4.37a. The element is shown acting under the influence of the rotational velocity (\bar{V}_t), forward velocity (\vec{V}'), and the induced velocity (\bar{w}). The resultant or relative velocity (\bar{V}_R) is then expressed by the relation

$$\bar{V}_R = \vec{V}' + \bar{V}_t + \bar{w} \quad (4.62)$$

where the axial velocity and rotational velocities are given by:

$$V' = V(1 + a) \quad (4.63)$$

$$\text{and} \quad V_t = \Omega r(1 - a_\Omega) \quad (4.64)$$

The relative fluid velocity varies from hub to tip, primarily under the influence of the rotational velocity component (Ωr) and the inflow factor (a). Figure 4.37 shows the velocities and forces on a blade element that lies between radial stations

(r) and ($r + \delta r$) and whose local chord length is (c). The section has a geometric pitch angle, or blade angle (β), where

$$\beta = \alpha + \varphi \quad (4.65)$$

With (α) is the local two dimensional incidence angle (or angle of attack) and (φ) is the advance angle, given by

$$\tan \varphi = \frac{V_1(1+a)}{\Omega r(1-a_\Omega)} \quad (4.66)$$

Defining the dimensionless radius $x = \frac{r}{R}$, then

$$\tan \varphi = \frac{V_1(1+a)}{\Omega r(1-a_\Omega)} = \frac{J(1+a)}{\pi x(1-a_\Omega)} \quad (4.67)$$

The blade angle (β) is calculated from the advance of propeller during one revolution (known as geometric pitch (p) as follows

$$\tan \beta = \frac{p}{\pi D} \quad (4.68)$$

Radial pitch distribution will be specified for a given blade, but a representative pitch is quoted at a *reference radius* conventionally taken at either 70 % or 75 % radius. Overall solid body pitch may be varied by rotation of the blade about its radial axis.

4.6.3.1 Thrust and Torque

The axial and tangential forces on a blade element generate the thrust δT and torque $\delta F_Q = \delta Q/r$ contributions of the blade elements and can now be written as:

$$\delta T = \delta L \cos \varphi - \delta D \sin \varphi = (l \cos \varphi - d \sin \varphi) \delta r \quad (4.69)$$

$$\frac{\delta Q}{r} = \delta L \sin \varphi + \delta D \cos \varphi = (l \sin \varphi + d \cos \varphi) \delta r \quad (4.70)$$

(δL and δD) are the lift and drag forces on blade element. Introducing the definitions for lift and drag coefficients (C_l and C_d) as well as dynamic pressure (q), then the lift and drag forces per unit span length (l and d) are expressed as:

$$C_l = \frac{l}{\frac{1}{2} \rho V_R^2 c}, \quad C_d = \frac{d}{\frac{1}{2} \rho V_R^2 c} \quad \text{and} \quad q = \frac{1}{2} \rho V^2 \quad (4.71)$$

Moreover, from Fig. 4.37b, the relative velocity is given by:

$$V_R = \frac{V(1+a)}{\sin \varphi} \quad (4.72)$$

Introducing relations (4.71) and (4.72) into Eqs. (4.69) and (4.70), and assuming the number of blades is (B), we get the following relations for thrust and torque gradients:

$$\frac{\delta T}{\delta r} = Bc q (1+a)^2 \frac{c_l \cos \varphi - c_d \sin \varphi}{\sin^2 \varphi} \quad (4.73)$$

$$\frac{\delta Q}{\delta r} = Brcq (1+a)^2 \frac{c_l \sin \varphi + c_d \cos \varphi}{\sin^2 \varphi} \quad (4.74)$$

With $x = r/R$, the local solidity (σ_r) at station (r) is defined as:

$$\sigma_r = \frac{Bc}{\pi r} \quad (4.75a)$$

The solidity at propeller tip is then

$$\sigma_R = \frac{Bc}{\pi R} = x \sigma_r \quad (4.75b)$$

In the succeeding equations, thrust force is non-dimensionalized by ($\rho n^2 D^4$) to obtain the coefficient; Eq. (4.59a) and the torque will be non-dimensionalized by ($\rho n^2 D^5$) to get the torque coefficient (C_Q); see Eq. (4.60a).

Introducing them into Eqs. (4.73) and (4.74), yield the following relations:

$$\frac{dC_T}{dx} = \frac{\pi}{8} \sigma_R J^2 (1+a)^2 \frac{c_l \cos \varphi - c_d \sin \varphi}{\sin^2 \varphi} \quad (4.76a)$$

$$\frac{dC_Q}{dx} = \frac{\pi}{16} \sigma_R J^2 (1+a)^2 x \frac{c_l \sin \varphi + c_d \cos \varphi}{\sin^2 \varphi} \quad (4.76b)$$

The relation between drag and lift forces on blade element is given by:

$$\tan \epsilon = \frac{l}{d} = \frac{c_l}{c_d} \quad (4.77)$$

Introducing Eq. (4.77) into Eq. (4.76a) and (4.76b) to get:

$$\frac{dC_T}{dx} = \frac{\pi}{8} \sigma_R J^2 (1+a)^2 c_l \frac{\cot \varphi - \tan \epsilon}{\sin \varphi} \quad (4.78)$$

and

$$\frac{dC_Q}{dx} = \frac{\pi}{16} \sigma_R J^2 (1+a)^2 x c_l \cot \varphi \frac{\tan \varphi + \tan \epsilon}{\sin \varphi} \quad (4.79)$$

Integrating Eqs. (4.78) and (4.79) to obtain the thrust (T) and torque (Q).

4.6.3.2 Propulsive Efficiency

Propulsive efficiency for a *blade element* is defined as the ratio between useful work ($V\delta T$) to the supplied torque power ($\Omega\delta Q$), or:

$$\eta_{be} = \frac{V\delta T}{\Omega\delta Q}$$

From Eqs. (4.67) and (4.72) as well as Fig. 4.37b, we get:

$$\begin{aligned} \eta_{be} &= \frac{V\delta T}{\Omega\delta Q} = \frac{1-a_\Omega}{1-a} r \tan \varphi \frac{\delta T}{\delta Q} = \frac{1-a_\Omega}{1-a} \tan \varphi \frac{\delta T}{(\delta Q/r)} \\ \eta_{be} &= \frac{(1-a_\Omega)}{(1-a)} \tan \varphi \frac{c_l \cos \varphi - c_d \sin \varphi}{c_l \sin \varphi + c_d \cos \varphi} = \frac{(1-a_\Omega)}{(1-a)} \tan \varphi \frac{1 - \tan \epsilon \sin \varphi}{\tan \epsilon + \tan \varphi} \\ \therefore \eta_{be} &= \frac{(1-a_\Omega)}{(1-a)} \frac{\tan \varphi}{\tan (\varphi + \epsilon)} \end{aligned} \quad (4.80)$$

As noticed from Eq. (4.80), the local propeller efficiency is dependent on the angle $\epsilon = \tan^{-1}(c_d/c_l)$ and the interference factors (a, a_Ω). Figure 4.38 illustrates the variation of blade element efficiency as a function of the advance angle (φ) and the angle (ϵ).

The following two cases are identified:

1. $\eta_{be} = 100\%$

This is the straight line case when:

$$\epsilon = a = a_\Omega = 0$$

2. $\eta_{be} = \text{variable}$

$$\epsilon \neq 0, a \neq 0, a_\Omega \neq 0$$

In this case, blade element efficiency has zero value when

$$\varphi = 0 \text{ and } \varphi = 90^\circ - \epsilon$$

At an in-between value, the blade element efficiency acquires a maximum value, which can be obtained by differentiating Eq. (4.80) with respect to (φ) and equating the differential to zero, then:

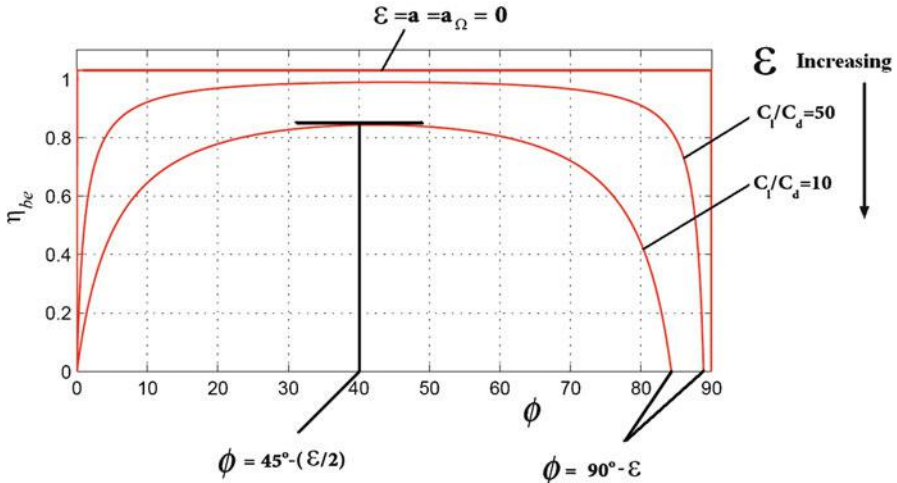


Fig. 4.38 Variation of blade element efficiency versus the angle (ϕ)

$$\phi = 45^\circ - (\varepsilon/2)$$

Several curves are obtained for different ratio of drag to lift coefficients.

4.7 Dimensionless Parameters

There are nine independent variables needed to define the performance of fixed-pitch propeller in subsonic flight, namely: thrust force, torque, power, air density, compressibility, air viscosity, propeller diameter, approach speed, and rotational speed expressed by the variables between brackets, respectively; $(T, Q, P, \rho, \beta, \mu, D, V, n)$. From these nine variables, and with the three fundamental units of mass [M], length [L], and time [T], using dimensional analysis we get six ($6 = 9 - 3$) dimensionless groups or parameters. These are:

1. Thrust coefficient

$$C_T = \frac{T}{\rho n^2 D^4} \quad \text{or} \quad T_c = \frac{T}{\rho V^2 D^2} \quad (4.59/81)$$

2. Torque coefficient

$$C_Q = \frac{Q}{\rho n^2 D^5} \quad \text{or} \quad Q_c = \frac{Q}{\rho V^2 D^5} \quad (4.82)$$

3. Power coefficient

$$C_P = \frac{P}{\rho n^3 D^5} \quad (4.83a)$$

A relation between power and torque coefficients can be derived as follows:

$$C_P = \frac{P}{\rho n^3 D^5} = \frac{2\pi n Q}{\rho n^3 D^5} = 2\pi C_Q \quad (4.83b)$$

4. Advance ratio (or speed coefficient):

$$J = \frac{V}{nD} \quad (4.84)$$

5. Reynolds number $R_e = \frac{VD\rho}{\mu}$

6. Mach number $M = \frac{V}{a} = \frac{V}{\sqrt{\gamma RT}}$

The first four dimensionless quantities are correlated by the following relations:

$$C_T = T_c J^2 \quad (4.85a)$$

and

$$C_Q = Q_c J^2 \quad (4.85b)$$

Another important dimensionless quantity is the *Speed Power Coefficient* denoted as (C_S) and sometimes as (C_{P_S}) is defined as: $C_S = \left(\frac{\rho V^5}{P n^2} \right)^{1/5}$ (4.86a)

Or

$$C_S^5 = \frac{\rho V^5}{P n^2} = \frac{\rho n^3 D^5}{P} \frac{V^5}{n^5 D^5} = \frac{J^5}{C_P} \\ C_S = \frac{J}{(C_P)^{1/5}} \quad (4.86b)$$

As noticed from Eq. (4.86); speed power coefficient eliminates the propeller diameter (D). Now, back to Eqs. (4.55a) and (4.55c) and using Eq. (4.81), we can express the factors (a) and (b) by the relation:

$$b = 2a = -1 \pm \sqrt{1 + \frac{8}{\pi} T_c} \quad (4.87)$$

The actual propulsive efficiency can be expressed in terms of the thrust and power coefficients, Eqs. (4.81) and (4.83b), as follows:

$$\eta_p = \frac{TV}{P} = \frac{TV}{\Omega Q} = \frac{JC_T}{2\pi C_Q} = \frac{JC_T}{C_P} \quad (4.88)$$

As discussed earlier, the maximum value of ideal Froude efficiencies η_F is 100 %, while the peak for actual propulsive efficiency of propellers – Eq. (4.88) – is much less than this value. This is due to the ignored losses in the ideal actuator disk model arising from:

- Rotational flow (whirl) about the rotor axis in the wake
- Profile drag (viscous friction and form drag) of the flow over the propeller blades (near the high-speed zero-thrust condition, profile drag is dominant) [9]
- Interference effects in the hub region between multiple blades and nacelle
- Compressibility effects (shock waves and shock/boundary layer interaction)
- Lateral components of incoming flow that occur when a propeller is yawed

Two other important parameters relevant to propeller power are power loading and activity factor defined as:

Power loading (PL)

$$PL = \frac{P}{D^2} = \frac{C_P \rho n^3 D^5}{D^2} = \frac{C_P}{J^3} \rho V^3 \quad (4.89)$$

Activity factor (AF)

$$AF = 10^5 \int_{root}^{tip} \left[\frac{c}{D} \left(\frac{r}{D} \right)^3 \right] d \left(\frac{r}{D} \right) \quad (4.90)$$

Both of these are a measure of power absorption by the propeller and are used to compare the performance of different propeller designs. (PL) is a simple disk loading, whereas the (AF) is designed to express the capacity of a blade to absorb power. (AF) is dimensionless, with a value of about 80 per blade.

Example 4.6 It is required to design a three-bladed propeller having the following data:

- Power = 260 kW
- Rotational speed = 2500 rpm
- Flight speed = 300 km/h
- Tip Mach number = 0.8 and sonic speed = 340 m/s
- Rotational induction factor is assumed constant and given by: $a_\Omega = 0.001$

Other data are given in the following table:

(r/R)	0.2	0.4	0.6	0.75	0.9
$\frac{c}{R}$	0.1	0.15	0.16	0.18	0.09
C_d	0.05	0.04	0.025	0.015	0.01
$(\frac{dT}{dr})_{3-blades}$ (N/m)	500	2500	4400	5900	3150

It is Required to Calculate

- (A) Radius of propeller
- (B) Propeller efficiency
- (C) At each blade section, calculate:
 - Axial interference factor (a)
 - Lift coefficient C_L
 - Angle of attack (α)
 - Blade angle (β)
 - Local propeller efficiency

Hint: For calculating the angle of attack use one of the following relations:

$$\alpha = \frac{C_L}{2\pi} \text{ for } M_W \cong 0.3 - 0.6$$

$$\alpha = \frac{C_L \sqrt{1-M_W^2}}{2\pi} \text{ for } M_W \cong 0.7 - 0.9$$

Solution

- (A) Radius of propeller

Relative velocity at blade tip is calculated from the relation:

$$W_t = M_t \times a = 0.8 \times 340 = 272 \text{ m/s}$$

$$\text{Since } W_t = \sqrt{V^2 + U_t^2} = 272 \text{ m/s}$$

$$\text{and } V = 300 \times \frac{1000}{3600} = 83.3 \text{ m/s}$$

$$\therefore U_t = \sqrt{W_t^2 - V^2} = \sqrt{(272)^2 - (83.3)^2} = 258.5 \text{ m/s}$$

$$\text{Since } U_t = 2\pi \times n \times R = 2\pi \times \frac{2500}{60} \times R = 258.5 \times R$$

Then

$$R = 1.0 \text{ m}$$

- (B) Propeller efficiency

The thrust is obtained from the rate of thrust distribution along the blades as follows:

$$T = \Sigma \left(\frac{dT}{dr} \right)_{\text{3-blades}} \times dr$$

$$T = \frac{1}{2} [500 \times 0.2 + (500 + 2500) \times 0.2 + (2500 + 4400) \\ \times 0.2 + (4400 + 5900) \times 0.15 + (5900 + 3150) \\ \times 0.15 + 3150 \times 0.1] = 2649.7 \text{ N}$$

Propeller efficiency is calculated from the relation:

$$\eta_p = \frac{TV}{P} = \frac{2649.7 \times 83.3}{260,000} = 84.86\%$$

C. Element of thrust force over a blade element at radius (r) and thickness (dr) is given by:

$$\begin{aligned} dT &= \dot{m} dV = \dot{m} (V_4 - V_1) = [(2\pi r dr) \times \rho \times V(1+a)] \times (2aV) \\ &= dr [4\pi \rho r V^2 (a + a^2)] \\ a^2 + a - \frac{dT/dr}{4\pi \rho r V^2} &= 0 \\ 2a &= -1 \pm \sqrt{1 + \frac{dT/dr}{\pi \rho r V^2}} \end{aligned}$$

From the above equation, we calculate (a) at each blade section.

At section (r/R) = 0.4:

$$\begin{aligned} 2a &= -1 + \sqrt{1 + \frac{dT/dr}{\pi \rho r V^2}} = 0.11088 \\ a &= 0.05544 \\ U &= 2\pi \times \frac{2500}{60} \times 0.4 = 104.7 \text{ m/s} \\ \tan \varphi &= \frac{V(1+a)}{U(1-a_\Omega)} = \frac{83.3 \times 1.05544}{104.7 \times 0.999} = 0.84 \\ \varphi &= 40.04^\circ \end{aligned}$$

From Eq. (4.73) $\frac{\delta T}{\delta r} = Bc\varphi(1+a)^2 \frac{c_l \cos \varphi - c_d \sin \varphi}{\sin^2 \varphi}$, then

$$c_l = \frac{1}{\cos \varphi} \left[\frac{(\delta T/dr) \sin^2 \varphi}{Bc\varphi(1+a)^2} + c_d \sin \varphi \right]$$

$$\text{With } q = \rho V^2 / 2 = 1.224 \times (83.3)^2 / 2 = 4250 \text{ Pa}$$

$$c_l = \frac{1}{\cos 40} \left[\frac{(2500) \sin^2 40}{3 \times 0.15 \times 4250 \times (1.05544)^2} + 0.04 \times \sin 40 \right] = 0.6665$$

$$W = \sqrt{V^2 + U^2} = \sqrt{(83.3)^2 + (104.7)^2} = 133.8 \text{ m/s}$$

$$M_W = \frac{133.8}{340} = 0.394$$

Since $M_W < 0.7$, then

Table 4.8 Calculated propeller properties at different blade sections

(r/R)	0.2	0.4	0.6	0.75	0.9
c	0.1	0.15	0.16	0.18	0.09
a	0.02288	0.05544	0.06449	0.06889	0.03175
U	52.35	104.7	157.05	196.31	235.575
W	98.38	133.8	177.8	213.25	250
M_W	0.289	0.3935	0.523	0.627	0.735
φ	58.45	40	29.5	24.4	20
c_l	0.602	0.6494	0.544	0.4285	0.3299
α	5.486	5.92	4.9647	3.91	2.00
β	63.936	45.92	34.46	28.31	22.0
$\varepsilon = \tan^{-1}(c_d/c_l)$	4.747	3.4344	2.63	2.0	1.74
$\varphi + \varepsilon$	63.197	41.76	32.13	26.4	21.74
$\tan \varphi / \tan(\varphi + \varepsilon)$	0.838	0.9398	0.9008	0.93	0.9129
η_{be}	81.84 %	83.89 %	84.54 %	86.92 %	94.2 %

$$\alpha = \frac{C_l}{2\pi} = 0.1061 \text{ rad} = 6.08^\circ$$

$$\beta = \varphi + \alpha = 40 + 6.08^\circ = 46.08^\circ$$

$$\varepsilon = \tan^{-1}(c_d/c_l) = \tan^{-1}(0.04/0.6665) = 3.4344^\circ$$

$$\varphi + \varepsilon = 43.4344^\circ$$

$$\eta_{be} = \frac{(1 - a_\Omega)}{(1 + a)} \frac{\tan \varphi}{\tan(\varphi + \varepsilon)} = 0.8397 = 83.97 \%$$

Repeating the above procedure for different sections, we get Table 4.8.

Example 4.7 Compare between propulsive efficiencies of a propeller using Froude and modified momentum theory to that obtained using blade element theory for section $(r/R) = 0.4$ in example (4.6).

Solution

The following data is given from example (4.6)

$$V_1 = 83.3 \text{ m/s}, \quad \Omega r = 104.7 \text{ m/s}, \quad a = 0.05544, \quad a_\Omega = 0.001$$

Froude efficiency is calculated from Eq. (4.59) as:

$$\eta_F = \frac{1}{1 + 0.05544} = 94.747 \%$$

Local efficiency from *Modified momentum theory* is calculated from Eq. (4.61) as:

$$\eta_{mm} = \frac{1}{1 + a + \frac{a_0^2 \Omega^2 r^2}{4aV_1^2}} = \frac{1}{1 + 0.05544 + \frac{(0.001 \times 104.7)^2}{4 \times 0.05544 \times (83.3)^2}} = 94.747\%$$

Propeller efficiency was calculated in example (4.6) as:

$$\eta_p = 83.89 \%$$

From the above calculations, the modified momentum theory yielded the same value of local efficiency as global Froude theory.

4.8 Typical Propeller Performance

Experimental testing of propellers started long ago by Wright Brothers during their design of their first airborne flight machine. Extensive experimental work continued and full-scale propeller testing was performed in NACA 20 ft. wind tunnel in NASA Langley. Detailed analyses of 2-, 3-, and 4-bladed propeller having CLARK Y and RAF series airfoil section was published in [14]. During the late 1930s, some NACA 4-digit airfoils were used extensively in propellers. Blade thickness decreases from root to tip along the blade length as shown in Fig. 4.26. The following NACA series are used for sections from hub to tip [19]:

NACA 4424/NACA 4418/NACA 2415/NACA 2412/NACA 2410/NACA 2408/
NACA 1412/NACA 1410/NACA 1408/NACA 0012/NACA 0009

To remind readers with airfoil designations, consider the section *NACA 4428*:

First integer (4) means that airfoil has a maximum camber (maximum value of mean line ordinate) in percentage of chord (4 %)

Second integer (4) means the position of maximum camber in tenths of the chord from leading edge (40 %)

Last two integers (15) denotes the maximum thickness in percentage of the chord (15 %)

After World War II, NACA 16-series airfoils were derived for use at high speeds, particularly for propeller applications [15]. This series has thin profile airfoils and thus has low drag at high speeds. Consequently, it is appropriate to transonic propeller sections near the tip [16]. Continuous efforts continued where computational analyses side by side with experimental ones are performed. A detailed computational analysis of propeller performance using the commercial code FLUENT 6.2 is presented in [17].

In general, the performance of a propeller is indicated by thrust coefficient (C_T), power coefficient (C_P), and efficiency (η_p). These quantities depend on advance ratio (J).

Figure 4.39 presents the propeller efficiency for two-bladed propeller. As clarified it depends on advance ratio (J) and pitch angle (β).

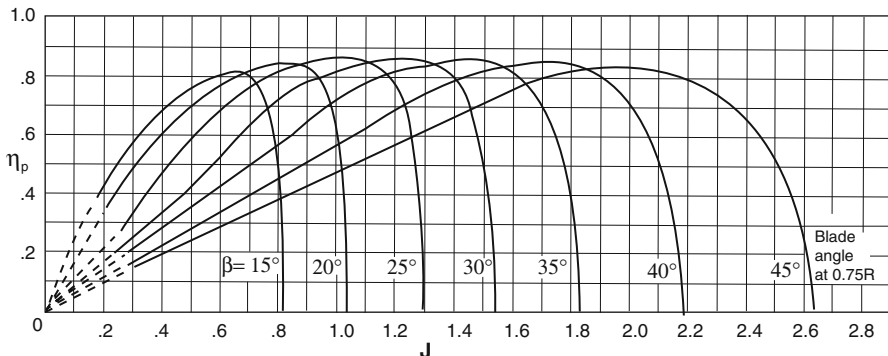


Fig. 4.39 Propeller efficiency η_p versus advance ratio J for two-bladed propeller at different pitch angles (β)

Efficiency values are less than unity as expected, since the available power is less than delivered one due to losses. These losses are attributed to translational and rotational kinetic energy in the wake of propeller as discussed earlier in Froude and modified momentum theories. Skin friction and profile drag of propeller blades add to the previous losses. For high speed propellers where the relative tip speed approaches sonic values, shock waves as well as boundary layer interaction on the suction sides of blade section result in additional losses.

For any pitch angles, propeller efficiency starts by a zero value at $J = 0$, increases to a maximum value and drops again to zero at high finite value of (J). When $J = 0$, then $V = 0$, and consequently the available or thrust power ($P_A \equiv TV = 0$), consequently $\eta_p \equiv P_A/P = 0$

The other case of zero efficiency corresponds to a higher value of advance ratio ($J > 0$), this corresponds to a high flight speed. The corresponding relative speed coincides with the zero lift (which in turn leads to zero thrust and zero efficiency). For higher flight (forward) speed, a negative lift is produced leading to reverse thrust as shown in Fig. 4.40.

The maximum value of η_p is seen to be around 80–85 %. However, the value of (J) at which the maximum of η_p occurs depends on the pitch angle (β). This indicates that for a single pitch or fixed pitch propeller, the efficiency is high (80–85 %) only over a narrow range of flight speeds Fig. 4.39.

At other flight velocities, the propeller will operate at smaller efficiencies which severely influence aircraft performance. For this reason, commercial airplanes use a variable pitch propeller. In such a propeller, the entire blade is rotated through a chosen angle during the flight and the pitch of all blade elements changes. Such propellers have high efficiency over a wide range of speeds. However, propellers with variable pitch arrangements are expensive and heavy. Hence, small (personal) airplanes, where cost of the airplane is an important consideration, employ a fixed pitch propeller. As a compromise, in some designs, propellers with two or three pitch settings are employed.

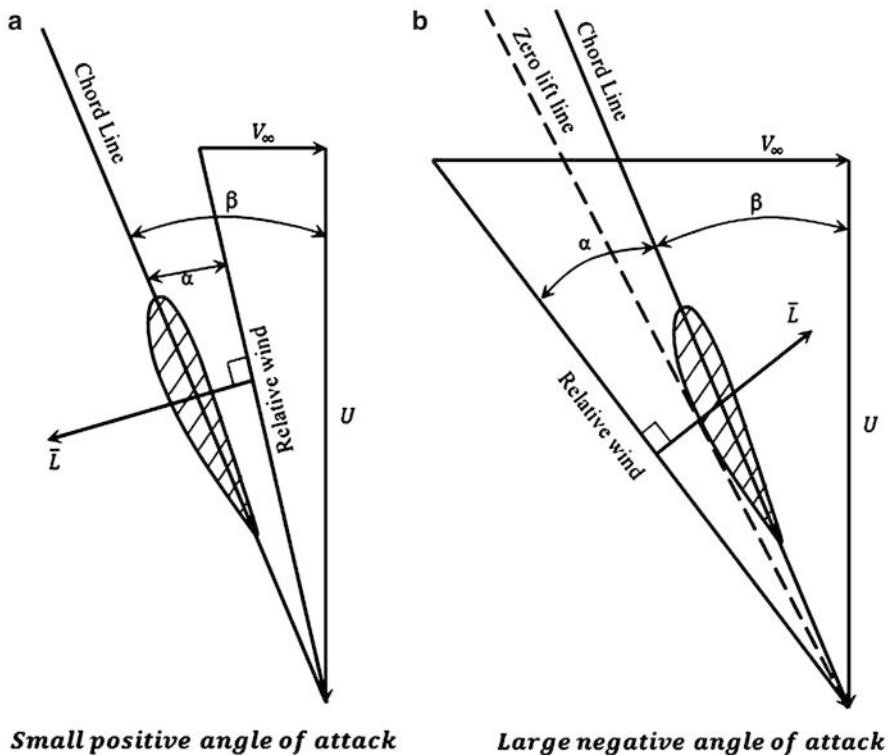


Fig. 4.40 Variation of propeller efficiency with advance ratio

Figure 4.41 presents the variation of thrust coefficient (C_T) versus (J) for two-bladed propeller with different values of (β).

Figure 4.42 presents the variation of power coefficient (C_P) versus J for two-bladed propeller with (β) and (C_T) as parameters.

Figures 4.40 through 4.42 can be combined and plotted in a single figure for each pitch angle (β) as shown in Fig. 4.43. For each pitch angle (β), efficiency has zero value at both $J = 0$ and thrust coefficient ($C_T = 0$). The condition ($C_T = 0$) corresponds to axial interference factor ($a = 0$) and Froude efficiency ($\eta_F = 100\%$).

At small values of pitch angle, the thrust coefficient is greater than power coefficient for any value of advance ratio. On the contrary, at high value of pitch angle, the power coefficient is greater than thrust coefficient at any advance ratio.

Other figures for three- and four-bladed propellers (similar to Figs. 4.39, 4.41, and 4.42) are found in reference [14]. However, recent propellers may have other number of blades (5–8). Performance parameters like thrust coefficient can be obtained from the following equation [18]:

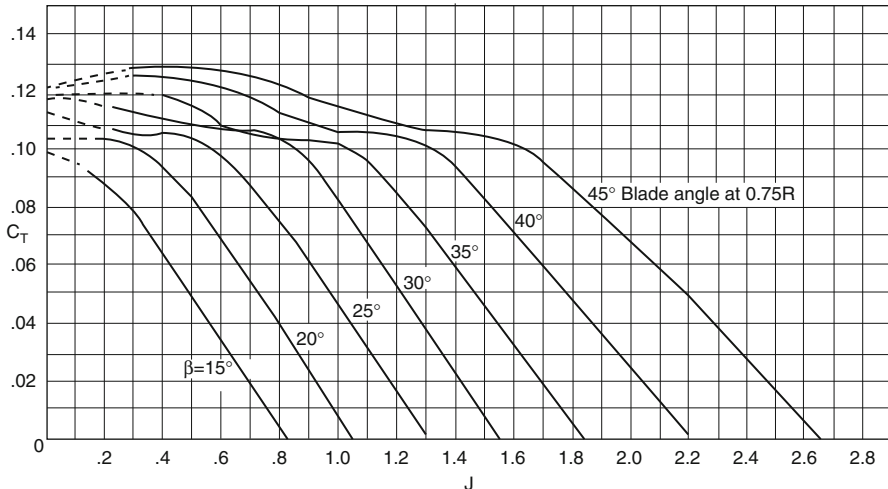


Fig. 4.41 Thrust coefficient (C_T) versus advance ratio (J) for two-bladed propeller with pitch angle parameter (β)

$$C_T|_{B=8} = C_T|_{B=4} + \{C_T|_{B=4} - C_T|_{B=3}\} \times (B - 4) \quad (4.91)$$

Then thrust coefficient for eight-blade propeller:

At preliminary design stages, when the propeller diameter is not yet determined, the speed-power coefficient – Eqs. (4.86a) and (4.86b) – may be used. Thus new plots for speed-power coefficient as well as efficiency are plotted versus the advance ratio. Two methods for plotting these relations are found in Figs. 4.44 and 4.45.

Figure 4.44 provides the locus of maximum efficiency for different speed power coefficient.

Figure 4.45 provides iso-efficiency lines plotted over constant speed-power coefficient and advance ratio parameter. It is quite similar with the compressor map as will be explained later on in turbomachinery sections.

Figure 4.46 provides values of efficiency at different pitch angle corresponding to a constant speed-power coefficient. As noticed from this figure, efficiency increases by increase of pitch angle for same speed-power coefficient value.

Example 4.8 It is required to provide a preliminary design of a *four-bladed propeller* having the following data:

- Power = 1965 kW
- Sea level conditions
- Relative speed at tip is 330 m/s
- Flight speed is 125 m/s
- $\varphi_{\text{root}} = 70^\circ$
- $a_\Omega = 0.00787$

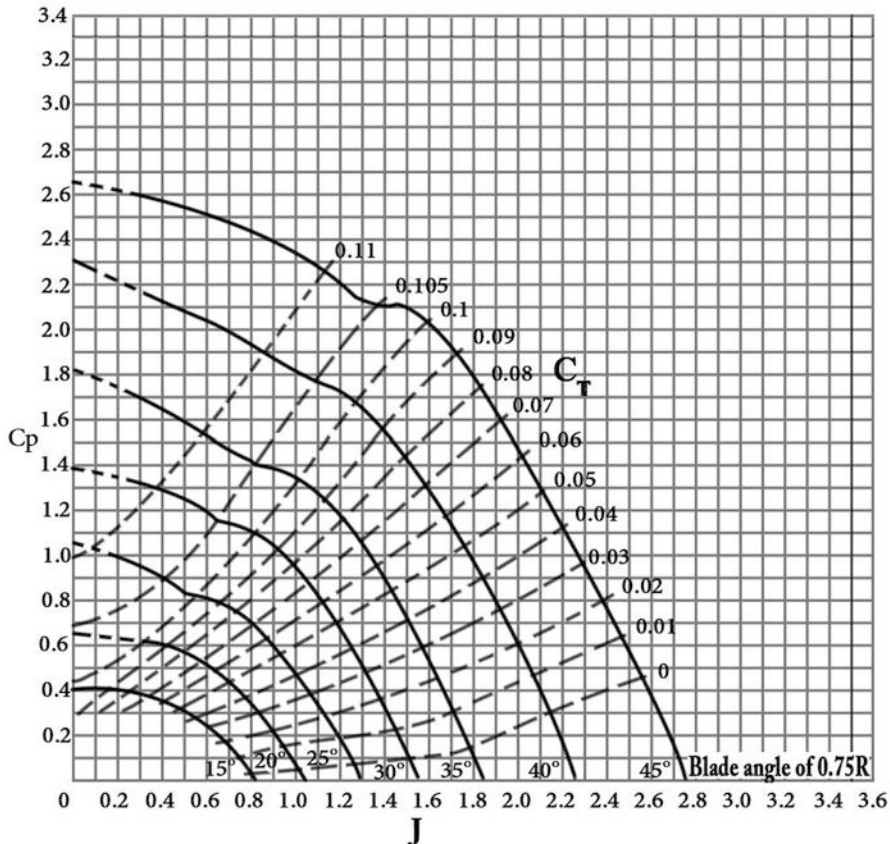


Fig. 4.42 Power coefficient (C_p) versus advance ratio (J) for two-bladed propeller with pitch angle parameter (β) and thrust coefficient (C_T) as parameters

Assume that the chord distribution is linear with the following defined sections:

($c_{0.3h} = c_{0.75h} = 0.054D$ and $c_{0.5h} = 0.074D$, where D is the propeller diameter and h is the blade height). Blade section has a lift and drag coefficients equal to 0.85 and 0.035.

At 0.75 R, it has a pitch angle $\beta = 40^\circ$ and the following data:

- Thrust coefficient $c_T = 0.1764$
- Propeller efficiency $\eta_b = 0.85$

Angle of attack is constant along the blade height; $\alpha = 3^\circ$

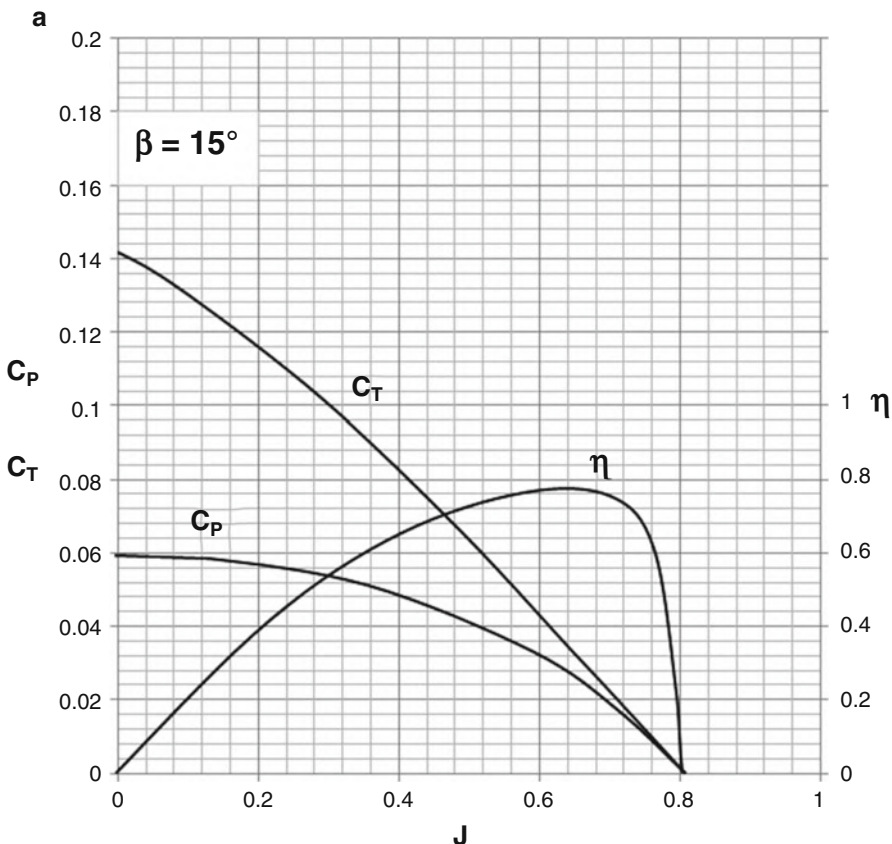


Fig. 4.43 Combined efficiency, thrust, and power coefficient curves versus advance ratio

Calculate

1. Thrust force
2. Propeller diameter and rotational speed
3. Blade height
4. Chord and the advance angle (φ) along the blade length
5. The thrust distribution along the blade height

Solution

1. The thrust force can be obtained from the relation

$$T = \frac{\eta_p P}{V} = \frac{0.85 \times 1765 \times 10^3}{125} = 12,000 \text{ N}$$

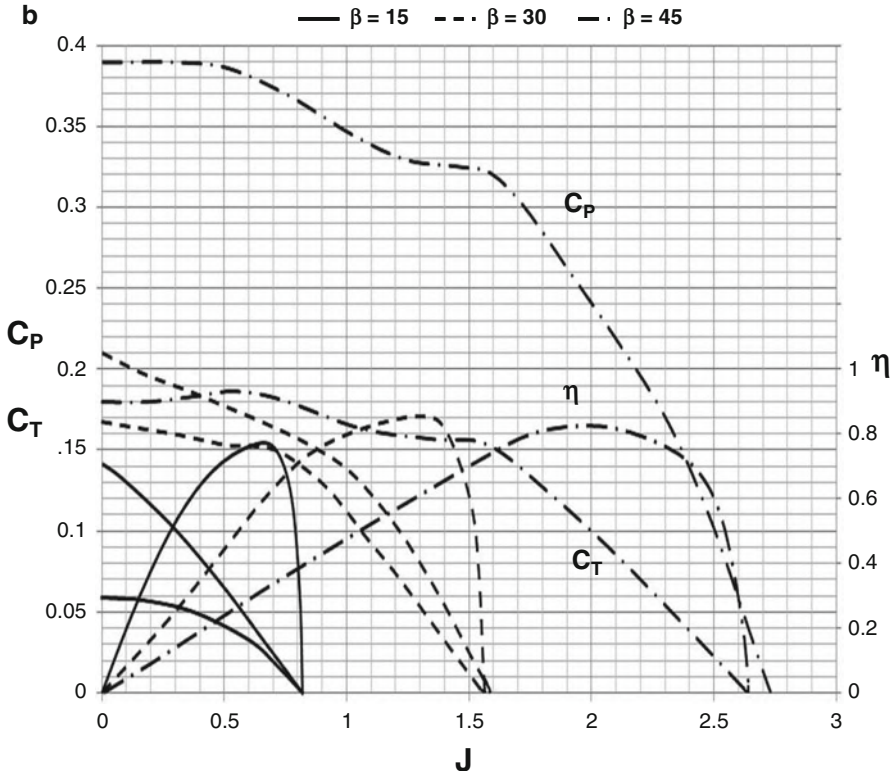


Fig. 4.43 (continued)

(2A) *Rotational speed limit*

$$U_t = \sqrt{W_t^2 - V^2} = \sqrt{330^2 - 125^2} = 305.4 \text{ m/s}$$

$$nD = \frac{U_t}{\pi} = 97.2 \text{ m/s} \quad (\text{a})$$

Advance ratio is $J = \frac{V}{nD} = \frac{125}{97.2} = 1.285$

(2B) *Power limit*

From Eqs. (4.81) and (4.84), we get

$$n = \left(\frac{V}{J}\right)^2 \sqrt{\frac{\rho C_t}{T}} = \left(\frac{125}{1.285}\right)^2 \sqrt{\frac{1.225 \times 0.1764}{12,000}} = 40.155 \text{ rps}$$

and $D = \frac{J}{V} \sqrt{\frac{T}{\rho C_t}} = \frac{1.285}{125} \sqrt{\frac{12,000}{1.225 \times 0.1764}} = 2.423 \text{ m}$

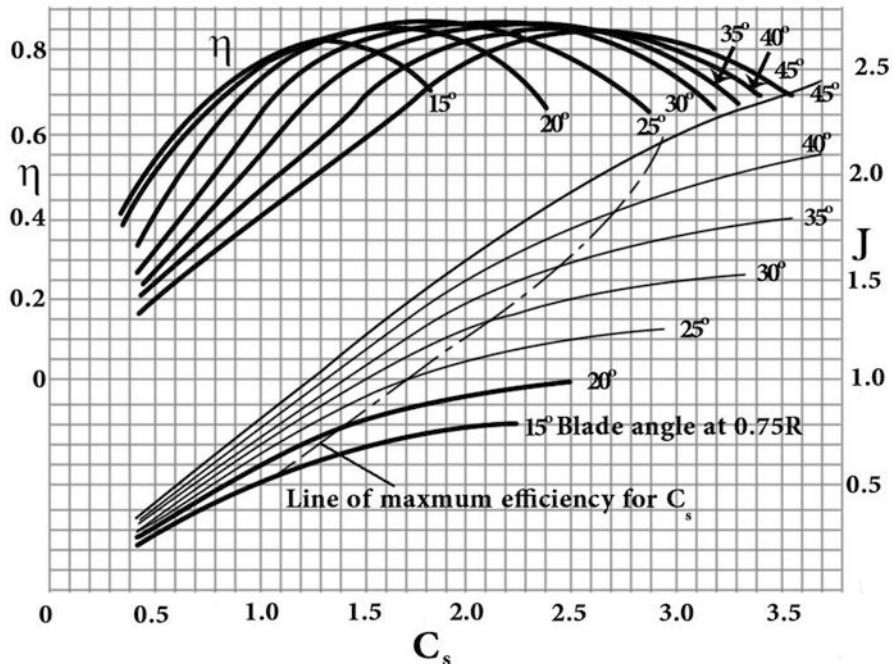


Fig. 4.44 Combined speed-power coefficient and propeller efficiency for different advance ratio and pitch angle parameters

$$T_c = \frac{C_T}{J^2} = 0.1068$$

$$b = 2a = -1 + \sqrt{1 + \frac{8}{\pi} T_c} = 0.1278$$

$$a = 0.0639$$

Forward speed is $V(1 + a) = 125 \times 1.0639 = 132.99$ m/s

Rotational speed is

$$U_t = \Omega r(1 - a_\Omega) = \pi D n(1 - a_\Omega) = \pi \times 97.2 \times (1 - 0.007876) = 302.95 \text{ m/s}$$

$$\tan \varphi_t = \frac{V(1 + a)}{\pi D n(1 - a_\Omega)} = \frac{132.99}{302.95} = 0.4387$$

$$\varphi_t = 23.7^\circ$$

At hub section, assuming the interference factors (a, a_Ω) are constant:

$$\tan \varphi_{\text{root}} = \tan 70 = \frac{V(1 + a)}{U_{\text{root}}(1 - a_\Omega)} = \frac{132.99}{0.99213 U_r} = 2.747$$

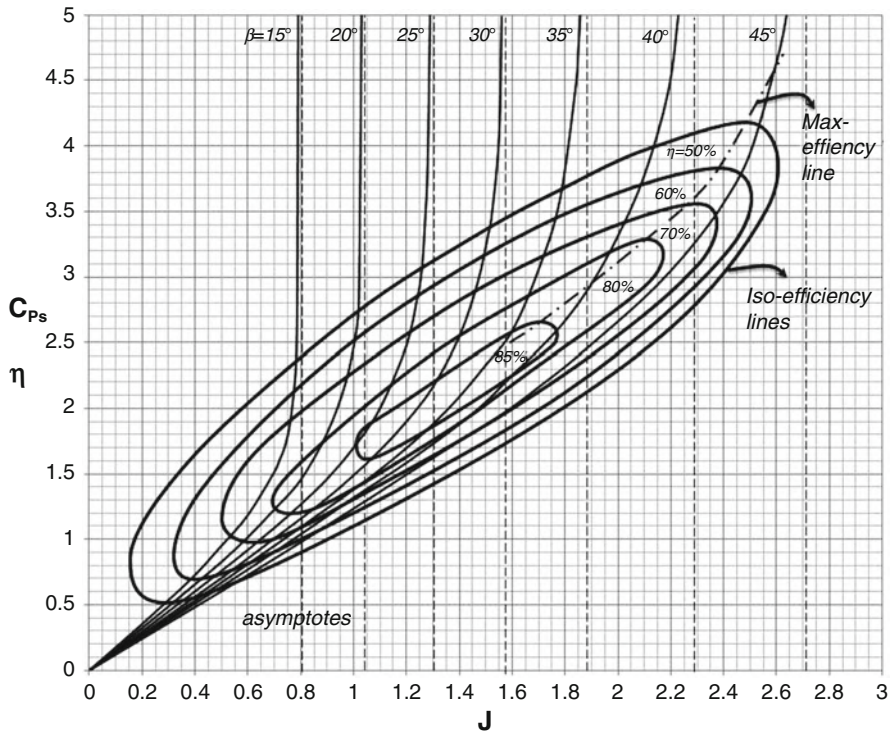


Fig. 4.45 Other version of speed-power coefficient and propeller efficiency curves for different advance ratio and pitch angle parameters

$$U_r = 48.79 \text{ m}$$

$$D_{\text{root}}/D_{\text{tip}} = U_{\text{root}}/U_{\text{tip}} = 0.161$$

$$D_{\text{root}} = 0.39 \text{ m}$$

$$\text{Blade height: } h = \frac{D_{\text{tip}} - D_{\text{root}}}{2} = U_{\text{root}}/U_{\text{tip}} = 1.016 \text{ m}$$

(3A) Chord length:

$$c_{0.3h} = c_{0.75h} = 0.054D = 0.131 \text{ m}$$

and

$$c_{0.5h} = 0.074D = 0.179 \text{ m}$$

Linear variation of chord is displayed in Fig. 4.47. The variation of chord is calculated from the known values at mean blade section 0.3 and 0.75 heights above and tabulated in Table 4.9.

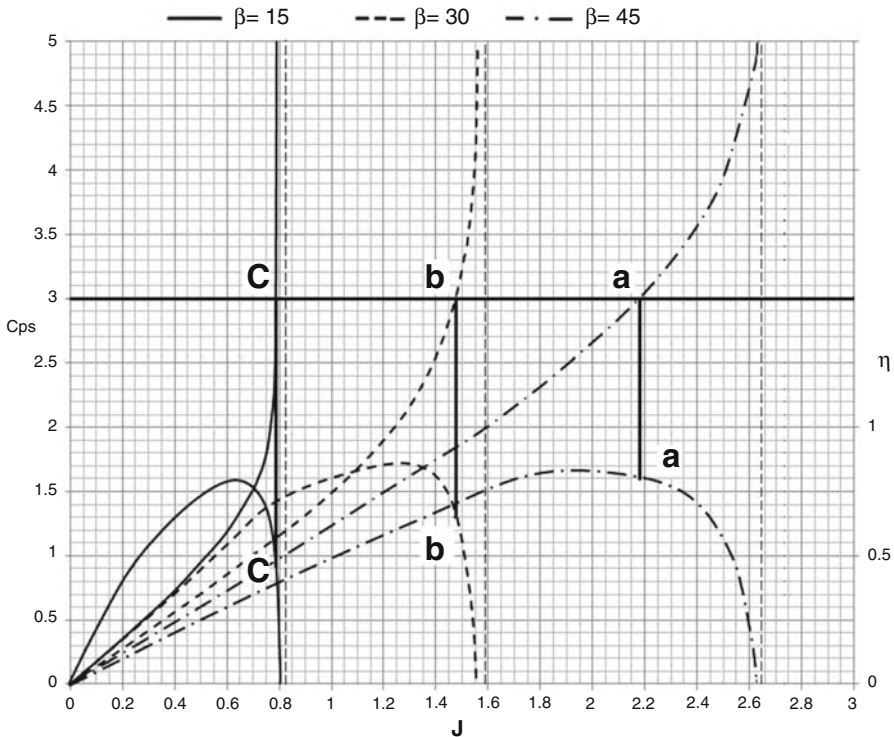


Fig. 4.46 Constant speed-power coefficient and corresponding efficiency values

(3B) Advance angle (φ)

$$\begin{aligned} \text{At root} \quad \varphi_{R=0} &= 70^\circ \\ \text{At } 0.75R: \quad \beta &= 40^\circ \end{aligned}$$

$$\text{thus} \quad \varphi_{0.75R} = \beta - \alpha = 40^\circ - 3^\circ = 37^\circ$$

Also at tip $\varphi_t = 23.7^\circ$

At any location along the blade:

$$\tan \varphi(x) = \frac{(1+a)}{(1-a_\Omega)} \frac{V}{U(x)} = \frac{132.99}{0.99213 U(x)} = \frac{134}{U(x)}$$

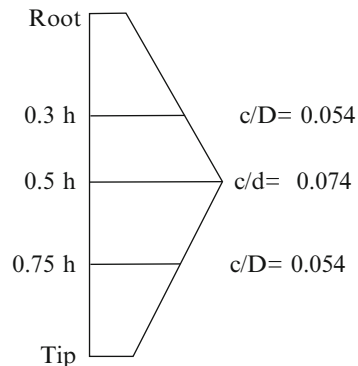
The distribution of angle (φ) will be given in Table 4.9.

Thrust force distribution

Dividing the blade into ten increments, then $\Delta r = \frac{h}{10} = 0.10$ m

From Eq. (4.51), thrust increment for each blade element is expressed by:

Fig. 4.47 Chord distribution



$$\Delta T = Bcq(1+a)^2 \frac{c_l \cos \varphi - c_d \sin \varphi}{\sin^2 \varphi} \Delta r$$

We have

$$Bq(1+a)^2 \Delta r = 4 \times (0.5 \times 1.225 \times 125^2) \times (1.0639)^2 \times 0.1 = 4333 \text{ N/m}$$

Thus $\Delta T(r) = 4333c \frac{c_l \cos \varphi - c_d \sin \varphi}{\sin^2 \varphi}$

The torque distribution will be given in Table 4.9.

$$T = \sum \Delta T = 11,994.24 \text{ N}$$

Since the thrust force was obtained before $T = 12,000 \text{ N}$, the summation of thrust increment obtained in Table (4.9) yields nearly the same design value ($12,000 \text{ N}$); the assumptions set earlier are satisfactory. If not, then an iteration procedure is to be employed by varying one or more of the following variables:

- Flight speed
- Chord length of blade
- Airfoil section, which contributes different lift and drag coefficients.

Example 4.9 An aircraft is flying at a speed of 540 km/h speed at sea level. It is powered by a three-bladed propeller developing 1600 kW . Propeller is connected to a piston engine rotating at 2600 rpm , through a $1:2$ gear box. The propeller is designed with blades of NACA 5869–9 blade sections. At 0.75 R , it has a pitch angle $\beta = 35^\circ$. Use the given chart for speed-power coefficient to compute the propeller diameter and the efficiency of the propeller at this operating condition.

Solution

Density of the air at this sea level operating condition is $\rho = 1.225 \text{ kg/m}^3$

The flight speed as given is $V = 540 \text{ km/h} = 150 \text{ m/s}$

Supplied power is $P = 16,000,000 \text{ W}$

Table 4.9 Generated thrust from different blade sections

Station x/R	C (m)	U (m/s)	φ	$c \times \frac{c_l \cos \varphi - c_d \sin \varphi}{\sin^2 \varphi}$	ΔT (N)
0.1	0.083	74.46	60.9	0.0416	180.25
0.2	0.107	100.12	53.23	0.0801	347.1
0.3	0.131	125.78	46.81	0.1371	594.1
0.4	0.155	151.44	41.5	0.2165	938.1
0.5	0.179	177.1	37.11	0.3229	1399.12
0.6	0.1598	202.76	33.46	0.3626	1571.14
0.7	0.1406	228.42	30.4	0.3928	1702
0.8	0.1214	254.08	27.8	0.4105	1778.7
0.9	0.1022	279.74	25.6	0.4114	1782.6
1.0	0.083	305.4	23.7	0.3926	1701.13

Propeller rotates at (1/2) the engine speed, i.e. at 1470 rpm or 24.5 rps

The speed-power coefficient may be calculated from:

$$C_S = \sqrt[5]{\frac{\rho V^5}{Pn^2}} = 2.5$$

From Fig. 4.48, the maximum efficiency at the calculated speed power coefficient is determined by interpolation and equals 85 % at an advance ratio of 1.6 and pitch angle of 36.

Then, propeller diameter is 3.826 m

Note that Fig. 4.45 provides the same results.

4.9 Conclusion

This chapter focused on aerodynamics of both piston engines and aircraft propellers. Aero piston engines were the first prime mover used in aircrafts since the early Flyer 1903 of Wright brothers and extensively used until now. Both petrol and diesel engines were analyzed. Superchargers used for boosting power in high altitudes were also discussed. Since piston engines alone cannot support aircraft's flight, a propeller is installed either directly or via a reduction gearbox to piston engine. Basic theories for propeller aerodynamics, namely, momentum, modified momentum, and blade-element theories, are reviewed. Propellers will be further reviewed in Chap. 7 handling turboprops as one of the shaft engine types. These will be high speed propellers.

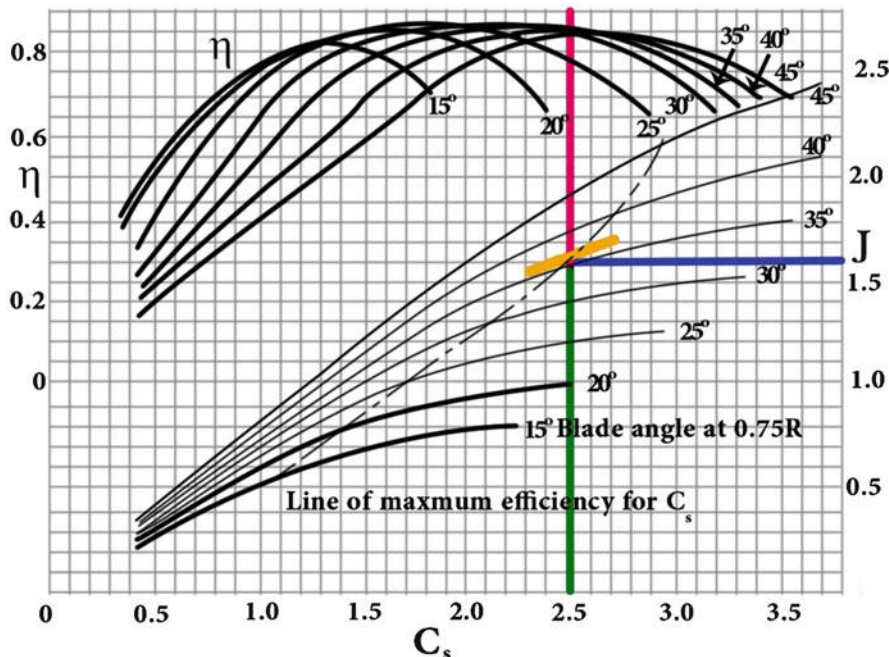


Fig. 4.48 Speed-power coefficient versus advance ratio for NACA 5869-9 three-bladed propeller with spinner blade angle at 0.75 R

Problems

- 4.1 Define the following terms related to reciprocating engines: stroke – bore – top dead center – bottom dead center – clearance volume
- 4.2 What is the benefit of liquid (as opposed to air) to cool aircraft piston engine?
 - (A) A steady operating temperature will be more easily maintained
 - (B) The engine will be lighter
 - (C) The engine will be simpler
 - (D) The cost of engine production will be less
- 4.3 What is the purpose of the “fins” which are arranged about the cylinder and cylinder head of an air-cooled engine?
 - (A) To allow heat to dissipate rapidly
 - (B) To reduce the engine weight
 - (C) To direct air through the engine compartment
 - (D) To support the engine cooling

4.4 Dornier is a light Freighter and Feeder liner aircraft powered by two Lycoming IGSO-540-A1A six cylinder horizontally opposed engines each rated at 260 kW. Assume that *Otto cycle* represents the cycle for such a spark ignition engine. Data of the engine is as follows:

- Compression ratio: 8
- Temperature and pressure at the beginning of compression stroke: 300 K and 95 kPa
- Rate of heat transfer during constant volume stroke: 750 kJ/kg
- Specific heat at constant volume: 0.719 kJ/(kg.K)

Calculate

- (a) The pressure and temperature at the end of heat addition process
 - (b) Network output
 - (c) Air mass flow rate
 - (d) Mean effective pressure
- 4.5 A large CI engine operates on air-standard *Diesel cycle* using diesel fuel having latent heating value of 41,000 kJ/kg and a combustion efficiency of 98 %. Inlet temperature and pressure are 298 K and 1 atmosphere. For a parametric study, it is required to calculate and plot the thermal efficiency versus the pressure ratio in the two cases of cutoff ratio of 3.0 and 4.0. Consider the following values for compression ratio 7.5, 19, 12.5, 15, and 17.5 and maximum temperature of 1500, 1800, and 2100 K.
- 4.6 The pressure and temperature at the start of compression in air-standard *Otto cycle* are 101 kPa and 300 K. The compression ratio is 8. The amount of heat addition is 2000 kJ/kg of air. Determine
- (a) The cycle thermal efficiency
 - (b) The maximum cycle temperature
 - (c) The maximum cycle pressure
 - (d) Mean Effective Pressure.
- 4.7 The shown figure illustrates Beechcraft Baron 58TC light aircraft powered by 2 *Continental O-470* six-cylinder, horizontally opposed, air-cooled aircraft engines.



Figure: Problem (4.7)

It has the following data

- Bore: 127.0 mm
- Stroke: 101.6 mm
- Displacement: 7.8 L
- Power output: 159 kW at 2575 rpm
- Specific power: 20.4 kW/L
- Compression ratio: 7.0:1
- Power-to-weight ratio: 0.90 kW/kg

Calculate

1. Specific speed
2. Brake mean effective pressure
3. Engine weight
4. Fuel conversion efficiency

4.8 The shown figure illustrates *Robinson R44* is a four-seat light helicopter produced by the Robinson Helicopter Company since 1992, with the first delivery in February 1993. It is powered by one [Lycoming IO-540-AE1A5](#) 6 cylinder air-cooled [horizontally opposed engine](#), 183 kW. Engine has the following characteristics:



Figure: Problem (4.8)

- Engine operates on the ideal Otto cycle
- Displacement: 8.9 L
- **Compression ratio:** 8.7:1
- The temperature and pressure at the beginning of the compression process of an air-standard Otto cycle are 290 K and the pressure is 1 atm

Calculate

- (a) Heat supplied per cylinder
- (b) Thermal efficiency
- (c) Mean effective pressure
- (d) Rotational speed

4.9 Consider a cold air-standard Diesel cycle. The below table illustrates properties at different cycle states:

State	T (K)	P (kPa)	v (m^3/kg)
1	300	101	0.849
2	910	4916	0.053
3	1820	4916	0.106
4	790	267	0.849

For $\gamma = 1.4$, $C_p = 1.005 \text{ kJ}/(\text{kg.K})$, determine:

- (a) Heat transfer and work per unit mass for each process
- (b) Thermal efficiency

4.10 The thermal efficiency of Diesel cycle is expressed by the relation:

$$\eta_{\text{th, Diesel}} = 1 - \frac{1}{r_c^{\gamma-1}} \left[\frac{(\beta' - 1)}{\gamma(\beta - 1)} \right]$$

While the thermal efficiency for an Otto cycle is expressed by the relation:

$$\eta_{\text{th, Otto}} = 1 - \frac{1}{r_c^{\gamma-1}}$$

Plot both relations on the same figure for compression ratio ranging from 4 to 12.

4.11 A four-cylinder internal combustion engine has the following design values:

- Maximum brake torque of 200 N.m
- Mid-speed range of 3000 rpm
- Maximum bmepl = 950 kPa

Estimate the engine displacement, bore, and stroke (assume bore and stroke to be equal).

4.12 Consider a six-cylinder ICE having a stroke of 9.5 cm, a bore of 8.0 cm, and compression ratio of 10. The pressure and temperature in the intake manifold are 0.8 atm and 250 K, respectively. The fuel to air ratio is 0.06. Mechanical efficiency of the engine is 75 %. If the crankshaft is connected to a propeller having efficiency of 83 %, calculate the ***available power from propeller*** for engine speed of 3000 rpm. Fuel heating value is 42.9 MJ/kg and Otto cycle is assumed.

4.13 Diesel engine has the following data:

- Fuel used: Diesel
- Type: Vertical cylinder, DI diesel engine
- Number of cylinder: 1
- Bore × Stroke (mm): 87.5×110
- Compression ratio: 17.5:1
- Cutoff ratio of 3.0
- Cooling system: Water cooling
- Speed (rpm): 1500
- Rated brake power (kW): 5.4 @ 1500 rpm
- Ignition system: Compression ignition
- Fuel Chemical formula: $\text{C}_{12}\text{H}_{26}$
- Stoichiometric air/fuel ratio (wt/wt): 14.6
- Lower heating value (kJ/kg): 42800
- Inlet total temperature and pressure: 280 K and 0.95 bar

- 4.14 Write down five conditions for a heat cycle to be considered as an air standard cycle.
- 4.15 The displacement volume of an internal combustion engine is 5.8 l. The processes within each cylinder of the engine are modeled as an air-standard Diesel cycle with a cutoff ratio of 2.4. The state of the air at the beginning of compression is $P_1 = 96 \text{ kPa}$, $T_1 = 300 \text{ K}$, and $V_1 = 6.0 \text{ l}$. Draw the cycle on the P-v diagram, and determine the work per cycle in kJ, the power developed in kW, and the thermal efficiency, if the engine speed is 1600 rpm.
- 4.16 A four-stroke petrol engine operates on an air standard cycle has a volume of (0.46 m^3). Operating conditions at the beginning of compression stroke are 1 bar and 27°C . At the end of compression stroke, the pressure is 11 bar and 220 kJ of heat is added at constant volume. The engine runs at 215 rpm. Determine:
- (i) P , T , and v at all cycle points
 - (ii) Clearance percentages
 - (iii) Thermal efficiency
 - (iv) Net work per cycle
 - (v) Mean effective pressure

- 4.17 Starting from the following definition for propeller efficiency:

$$\eta_P = \frac{\text{Thrust power}}{\text{Thrust power} + \text{Wasted power in jet}} = \frac{TV_1}{TV_1 + \frac{1}{2}\dot{m}(V_4 - V_1)^2}$$

Prove that:

$$\eta_F = \frac{2}{1 + V_4/V_1}$$

- 4.18 Prove that the thrust force generated by a propeller is related to the supplied power by the relation:

$$T = \frac{PC_T}{nDC_P}$$

- 4.19 Prove that the available power of a propeller is expressed by the relation:

$$P = \frac{TV_1}{2} \left(\sqrt{\frac{8T}{\rho V_1^2 \pi D^2} + 1} + 1 \right)$$

- 4.20 Compute the diameter of the flow field in the far wake of propeller of diameter 3.0 m, which produces a thrust of 9.0 kN of thrust at sea level conditions while flying at a speed of 330 km/h

4.21 Which of these statements applies to a propeller that has been “feathered”

- (A) Its leading edges are facing forwards in the direction of flight
- (B) It is operating at its maximum rotational speed
- (C) It is producing maximum power
- (D) Its leading edges are facing 90° to the direction of flight

4.22 On a variable pitch propeller, the largest obtainable pitch angle is known as:

- (A) Fine pitch
- (B) Optimum pitch
- (C) Coarse pitch
- (D) Take-off pitch

4.23 When the airflow over the propeller blades of a failed engine keeps the propeller turning, this is known as:

- (A) Reverse thrust
- (B) Windmilling
- (C) Contra-rotating
- (D) Reverse thrust

4.24 “Blade twist” in a propeller helps to:

- (A) Reduce noise levels
- (B) Make feathering possible
- (C) Make the blade stronger and lighter
- (D) Even out the thrust along the blade

4.25 An aircraft is propelled by a 4.6 m diameter propeller, which produces 36.0 kN of thrust. The aircraft is flying at an altitude where air density is 0.9 kg/m^3 . Using momentum theory, *calculate*:

- (i) The induced velocity through the disk
- (ii) The final velocity of the flow in the far wake
- (iii) Propeller efficiency using actuator disk theory
- (iv) The pressure jump across the propeller

4.26 A three-bladed propeller has the following data:

Generated power = 2250 hp

Sea level conditions

Relative tip speed = 320 m/s

Flight speed = 75 m/s

Blade section has a lift and drag coefficients equal to 0.85 and 0.0425, respectively

Calculate

1. Tip rotational speed
2. Thrust and torque coefficients
3. Propeller efficiency
4. Rotational speed
5. Propeller diameter
6. Reference blade chord

For a preliminary analysis assume that:

- Blade has a constant chord equal to the reference chord (c_{ref}), where $c_{\text{ref}} = 0.06D$ and D is the propeller diameter
 - $a = 0.1$, $a_{\Omega} = 0$
- 4.27 The shown figure illustrates Cessna R172K Hawk XP single engine aircraft. The airplane has a maximum cruise speed 243 km/h. It is powered by a single fuel injected, *Continental IO-360K* 195 hp (145 kW). Propeller has the following characteristics:

Number of blades (B) = 2

Diameter (D) = 2.80 m

Blade chord at $0.75R = 0.16$ m

Rotational speed = 2880 rpm

Inflow factor (a) = 0.05

Lift coefficient = 0.7

It is required to calculate: C_T , C_Q , C_P , η



Figure Problem (4.27)

Hints

1. Divide the propeller blade into five stations having $x = 0.12, 0.34, 0.56, 0.78$, and 1.0
2. Neglect drag coefficient and use the following relations (4.52)

4.28 A four-bladed propeller has the following data:

- Generated power = 3000 hp
- Sea level conditions
- Relative tip speed = 320 m/s
- Flight speed = 75 m/s
- Blade section has a lift and drag coefficients equal to 0.85 and 0.0425, respectively

Calculate

1. Tip rotational speed
2. Thrust and torque coefficients
3. Propeller efficiency
4. Rotational speed
5. Propeller diameter
6. Reference blade chord

For a preliminary analysis assume that:

- Blade has a constant chord equal to the reference chord (c_{ref}), where $c_{ref} = 0.06D$ and D is the propeller diameter
- $a = a_\Omega = 0$
- Neglect drag coefficient

4.29 A propeller of diameter (D) that develops the thrust (T) when operating at an advance ratio (J) and at (N) rpm is to be replaced by a pair of equal propellers of the same diameter, operating at the same advance ratio (J) and producing together the same thrust (T). The velocity (V) being the same in both cases, determine (D') and the rotational speed (N') of these two propellers.

Prove that the power of the two propellers equal to the original power.

References

1. El-Sayed AF (2008) Aircraft propulsion and gas turbine engines, Taylor & Francis, Boca Raton, Florida, USA
2. DOE Fundamentals handbook, mechanical science, volume 1 of 2 (1993) DOE-HDBK-1018/1-93
3. Michael JM, Shapiro HN, Boettner DD, Bailey MB (2011) Fundamentals of engineering thermodynamics, 7th edn. Wiley, New York
4. Cengel YA, Boles MA (2010) Thermodynamics – an engineering approach, 7th edn. McGraw-Hill, New York

5. Pulkabek WW (2004) Engineering fundamentals of the internal combustion engine, 2nd edn. Pearson Prentice Hall, Upper Saddle River, New Jersey
6. Heywood J (1988) Internal combustion engine fundamentals, 1st edn. McGraw-Hill, New York
7. Collins English Dictionary – complete & unabridged 10th edition (2009) © HarperCollins Publishers, Glasgow
8. Burden M, McCarthy R, Wiggins B (2012) Advanced polymer composite propeller blades, Chapter 6, aerospace materials, edited by Brian Cantor, Hazzel Assender and Patrik Grant, IOP, Bristol, Philadelphia, Institute of Physics
9. Glauert H (1947) On the vortex theory of screw propellers. In: Proceedings of the Royal Society of London, A, vol. 123, no 792, April 6, pp 440–465
10. Burton M, The Professional Pilot Study Guide Series, PROPELLERS (1992) Airlife Publishing Ltd, Shrewsbury, pp 6–7
11. Bocci AJ (1977) A new series of aerofoil sections suitable for aircraft propellers, RAeS Aeronaut Q 28:29–73
12. Douglas Archer R, Saarlas M (1996) An introduction to aerospace propulsion. Prentice Hall, Upper Saddle River, New Jersey
13. Ribner HS, Foster SP (1990) Ideal efficiency of propellers: theodorsen revisited AIAA. J Aircr 37(9):810–819
14. Hartman EP, Biermann D (1938) The aerodynamic characteristics of full-scale propellers having 2, 3 and 4 Blades of CLARK Y and R.A.F. 6 airfoil sections, N.A.C.A. report no. 640
15. Lindsey WF, Stevenson DB, Daley BN (1948) Aerodynamic characteristics of 24 NACA 16-series airfoils at mach numbers between 0.3 and 0.8, NACA TN-1546
16. Anderson JD Jr (2011) Introduction to flight, 7th edn. McGraw-Hill, Pub. Co, New York
17. Farghaly MB (2012) Erosion of propeller blades for turboprop engine, M.Sc thesis, Cairo University, Cairo, Egypt
18. Roskam J (1997) Airplane aerodynamics and performance. DARcorporation, Lawrence, Kansas
19. Abbott IH, Doenhoff AEV (1959) *Theory of wing sections*, Pan American and International Copyright conventions, Mineola, N.Y.

Chapter 5

Pulsejet, Ramjet, and Scramjet Engines

5.1 Introduction to Athodyd Engines

Different athodyd engines (where athodyd stands for Aero *T*herm*ODY*namic Duct) will be treated here. These engines are pulsejet, ramjet, and scramjet engines. The latter two are identified as Ram-Based Cycle (RBC) Engines. These engines have no major rotating parts (fan/compressor or turbine) and consist of an entry duct, a combustion chamber, and a nozzle [1].

Pulsejet engine will be treated first. It operates intermittently and has found limited applications [2, 3] as there are great difficulties of its integration into manned aircraft. Its other disadvantages are high fuel consumption, poor efficiency, severe vibration, and high noise. The second engine to be analyzed here is ramjet engine. Ramjet engines are appropriate for supersonic flight speeds though were also used in subsonic flight conditions [4]. Its ram compression of air becomes sufficient to overcome the need for mechanical compression achieved normally by compressors or fans in other TBC engines. The third type is the scramjet engine. Its name *scramjet* is abbreviated from Supersonic Combustion Ramjet. If the flight speed of a ramjet is so high that fuel combustion must occur supersonically, then this ramjet is identified as a scramjet [5]. Scramjet engine operates at the speeds of rockets. Its main difference from a rocket is that it collects air from the atmosphere to burn its fuel rather than carrying its oxidizer on board.

5.2 Pulsejet

5.2.1 Introduction

A pulse jet (or pulsejet) engine is a very simple jet engine, which can be made with a few or no moving parts. It comprises an air intake, a combustion chamber, and an

acoustically resonant exhaust pipe. Intake of air is intermittent, thus combustion occurs in pulses, resulting in a pulsating thrust rather than a continuous one and thus has found limited applications [2].

Consequently, pulsejet engine (PJ) is similar to piston engines in its intermittent combustion nature. In the same time, it is similar to all jet engines in generating thrust via reaction principle for propulsion. Thus, one can say that pulsejet engine resembles a transitional development between older piston engines and subsequent jet engines. The advantages of pulsejet engine are extremely light, simple, cheap, easy to construct, uses both atmospheric oxygen and cheap fuels, and capable of running statically. Another important advantage is the pressure gain across the combustor in contrast to pressure loss in other jet engines. However, its main disadvantages are low reliability, poor fuel economy, severe vibration, poor compression ratio, low specific impulse, and very high noise levels. The high noise levels make them practical only for military applications. The first 50 years of twentieth century showed great interest in pulsejet engines. However, with the improvements in power and efficiency of turbojets, pulse jets ceased to receive attention. Various organizations, both private and public, continued a limited pulse jet research in the period 1940–1970. Recently, however, with the interest in UAV's, various agencies and contractors have started looking for ways to propel these tiny vehicles with an efficient, affordable, and robust power source.

Pulsejets have three types, namely: Valved, Valveless, and Pulse detonation engine (PDE).

The valved type is fitted with a one-way valve, while a valveless engine has no mechanical valves at its intake. The pulse detonation engine is a concept currently in active development to create a jet engine that operates on the supersonic detonation of fuel.

5.2.2 Brief History

1. *Martin Wiberg* (1826–1905) developed the first pulse jet in Sweden. While *V.V. Karavodin* patented in 1906 and completed a working engine in 1907 in Russia, which was a high velocity pulsed gas jet generated by a cyclic combustion of a liquid hydrocarbon fuel/air mixture [6].

Marconnet in 1907 invented his valveless pulsejet engine in France [7], which is composed of an inlet diffuser, combustor, and outlet longer exhaust pipe in order to direct most of the combusted mixtures through exhaust rather than through intake. In 1939, the most infamous pulsejet Schmidt Argus V1 pulsejet was developed by German Paul Schmidt and manufactured by Argus Company. It is known as Schmidt Argus V1 pulsejet. That pulsejet was used to power the Fieseler Fi 103 V-1 “Buzz Bomb” shown in Fig. 5.1. It is an unmanned bomb steered by a gyro. When the fuel ran out, it just dropped down from the sky and explodes on the ground. It had a mass of 4750 lbs and produced 650 lbs of thrust at an altitude of



Fig. 5.1 V-1 flying bomb [8]

3000 ft and at a cruise speed of 400 mph [8]. It could be launched from a 152 ft inclined ramp by a Walter steam (or hydrogen peroxide) catapult, or air-dropped from a carrier aircraft (usually He III Hs of KG 3 and later KG 63). The V-1 pulsejet was the first cruise missile. It was extensively used in bombing England and Belgium during WWII.

In July 1944, captured V-1 components were shipped to USA, where the USAAF and American industry had built their own V-1, designated as the “Jet Bomb 2 (JB-2)” and more informally known as the “Thunderbug”. First successful launch of a JB-2 was on 5 June 1945. The JB-2s were easily launched off a rail with a solid rocket booster. The USAAF also experimented with air-launching the JB-2 from a B-17 bomber, B-24s, and B-29s. Also Ford built the pulse jet engine, designated “PJ-31” in USA.

The US Navy experimented its V-1 variant, the “KUW-1 (later LTV-N-2) Loon”. The submarine USS CUSK was modified to launch the Loon flying bombs in February 1947. In 1948, the surface vessel USS NORTON SOUND was modified for Loon launches and performed four launches in 1949 and 1950.

The Soviets also built copies and derivatives of the V-1.

In 1944, Japan also relied upon Argus pulse jet Fieseler Fi-103 “Reichenberg” (Fi103R) manned V-1 in designing their rocket-powered aircrafts for suicide missions known as Yokosuka MXY7 *Ohka* Japanese flying bomb against Allied naval forces. Carried aloft by G4M ‘Betty’ bombers, the *Ohkas* remained attached until 21 miles off the target [9].

In the 1950s, French operated a target drone based on the V-1 and designated the “Arsenal 5.501”, which differed from the original design in having twin tail fins and radio control.

In the early 1940s, Lt. William Schubert of the US navy designed his valveless pulsejet engine called the “resojet”. Its two main advancements over Marconnet’s design were the combustor entry has sudden expansion and produces higher turbulence for the thorough mixing of the air and fuel molecules. The second is

that the intake geometry was carefully designed so that the exhaust gas does not escape before the pressure inside the chamber falls below atmospheric.

In 1950, *Bertin* and his fellow engineers at SNECMA Corporation (France) developed *Escopette* engine, which is known to be the best performing valveless pulsejet engine in history. Escopette backward bent intake provides additional thrust to the engine [6]. Instead of using a straight exhaust pipe a series of steps of increasing section is used. Escopette engine was intended for commercial applications, thus was extensively tested on French Emouchet SA 104 sailplane in various configurations [6].

In the late 1950s and early 1960s, Lockwood of Hiller aircraft invented his famous U-shaped valveless pulsejet or *Lockwood hillier* engine, which is considered the most effective pulsejet ever. The short pipe is the intake pipe and the long curved shape pipe denotes the exhaust pipe. Lockwood engines are usually variable area throughout the engine. It was used for military purpose (Model HH 5.25–7) to produce a thrust of 280 pounds. Another notable feature in lockwood engine is that the addition of augmenters at the end of the intake as well as exhaust port. Augmenter uses exhaust hot gas to suck in fresh air and increase the thrust.

In the 1970s and 1980s, J.A.C Kentfield (Canada) introduced *recuperator* for thrust augmentation. Instead of making a simple tube bent backwards, he used a flaring cone at the end, which is referred to as secondary thrust augmentation. This method allows the cone to suck in more fresh air and adds to more reaction mass.

It is worth mentioning that after WWII pulsejets have been used to power:

1. Experimental helicopters where these engines were attached to the extreme ends of the rotor blades in the 1950s. They have also been used in both tethered and radio-control model aircraft.
2. Go karts were also powered by pulsejets generating some 100 lb thrust similar to Argus V1 and Lookwood valveless engines
3. Model airplanes where Dyna-jet engines were used and these models reached speeds over 150 mph in the 1950s
4. Boats could reach speed more than 45 mph when powered by two pulsejet engines each 105 lb thrust in the 1950s. Its drawbacks were noise which spread to several miles away as well as its high fuel consumption (6 gallons of gasoline per mile)
5. In the twenty-first century, with the interest in UAVs, various agencies and contractors have started looking for ways to propel these tiny vehicles with an efficient, affordable, and robust power source. Pulsejets are one of these options.
6. The flying bomb concept can be seen today in the modern cruise missile.

5.2.3 Valved Pulsejet

Valved type has an air scoop and a set of one-way valves (check valves which is sometimes denoted as shutter) through which the incoming air passes. Fuel in the form of a gas or liquid aerosol is either mixed with the air in the intake or injected

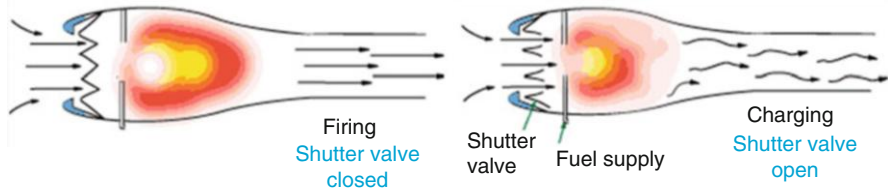


Fig. 5.2 Pulsejet engine during operation

into the combustion chamber. When the air/fuel is ignited, these valves slam shut, thus hot gases leave through the engine's tailpipe, thus creating forward thrust (Fig. 5.2). The cycle frequency is primarily dependent on the length of the engine. For a small model-type engine, the frequency may be typically around 250 pulses per second – whereas for a larger engine such as the one used on the German V1 flying bomb, the frequency was closer to 45 pulses per second. Once the engine is running, it requires only an input of fuel, but it usually requires forced air and an ignition method for the fuel-air mix. The main drawback of valved type is that the valves require regular replacement and represent a weak link in the engine's reliability.

5.2.4 Thermodynamic Cycle

Figure 5.3 illustrates the simple construction of valved type together with its cycle on the temperature entropy diagram. Air is sucked into the combustion chamber through a bank of spring-loaded check one way valves. Next, a carefully adjusted amount of fuel is sprayed into the cold combustion chamber in order to create a mixture and the resultant strong explosion starts the cycle. The fuel flow, injected directly into the combustion chamber, is continuous throughout the cycle with some variation in fuel flow resulting from the pressure in the combustion chamber. This fuel flow fluctuation can be neglected. The resultant high pressure and temperature forces the gases to flow out of the tail pipe at high velocity.

At the end of discharge, the inertia of the gas creates a vacuum in the combustion chamber which together with the ram pressure developed in the diffuser causes sufficient pressure differential to open the check valves. A new charge of air enters the chamber and a new cycle starts. The frequency of the cycle depends on the size of the engine, and the dynamic characteristics of the valves must be matched carefully to this frequency. Small size engines operate as high as 300–400 cycles per second, and large engines operate as low as 40 cycles per second.

Pulsejets operate on the *Humphrey cycle* as shown in Fig. 5.3. The four step cycle starts at state (a) with isentropic compression followed by isochoric heat addition, isentropic expansion, and lastly, isobaric heat rejection as it returns to state (a).

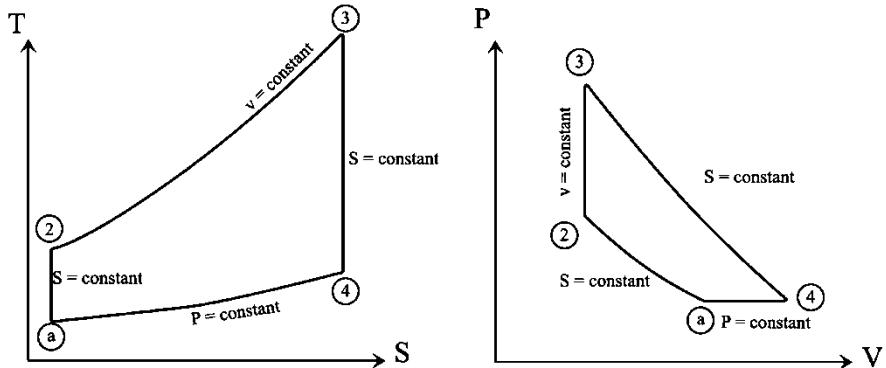
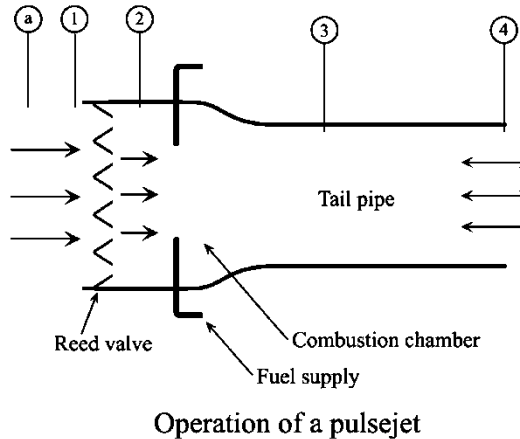


Fig. 5.3 T-s AND P-v diagrams for ideal Humphrey cycle of pulsejet engine

1. Intake or diffuser

This process occurs from state (a) to state (2) as shown in Fig. 5.3. Air is sucked into the combustion chamber through a bank of spring-loaded check (one way) valve. State (a) is far upstream, while state (1) is at the pulsejet inlet, and state (2) is just aft of the check valve upstream of the combustion chamber. Due to ram effect, both the pressure and temperature rise from the ambient conditions to the values at state (1) calculated by the relations:

$$P_{01} = P_{0a} = P_a \left(1 + \frac{\gamma_c - 1}{2} M^2 \right)^{\frac{\gamma_c}{\gamma_c - 1}} \quad (5.1)$$

Here (M) is the flight Mach number and (γ_c) is the specific heat ratio for cold air. If it is assumed that the diffuser is an ideal one (isentropic process), then the total pressure and temperature at state (2) is equal to those at state (1), or:

$$P_{02} = P_{01} \quad (5.2)$$

However, due to losses in the diffuser and check valves, the pressure at state (2) is less than that at (1). Process in diffuser is assumed adiabatic having an isentropic efficiency of (η_d). Then the total pressure will be calculated from the relation:

$$P_{02} = P_a \left(1 + \eta_d \frac{\gamma_c - 1}{2} M_a^2 \right)^{\frac{\gamma_c}{\gamma_c - 1}} \quad (5.3)$$

In all cases (isentropic or adiabatic processes), the stagnation (total) temperatures for states (a), (1), (2) are equal and expressed by the relation:

$$T_{02} = T_{01} = T_{0a} = T_a \left(1 + \frac{\gamma_c - 1}{2} M^2 \right) \quad (5.4)$$

2. Combustion chamber

Fuel is added to the combustion chamber through several fuel injectors placed after the valves and a spark plug mounted on top of engine initiates the combustion process, which occurs at something approaching a constant-volume process [1, 10]. The spark plug igniter is only needed for the initial start-up. Once started, the engine will continue to operate on its own, with hot residual combustion gases subsequently in a cyclic manner igniting incoming fresh fuel-air mixtures in a low–high–low passive pressure cycle. Such combustion occurs in the form of an explosion, which raises the pressure in the combustion chamber to a high level and closes the spring valve at the intake. Thus for such isochoric heat addition, the pressure ratio is

$$P_{03} = P_{02} (T_{03}/T_{02}) \quad (5.5)$$

The mass flow rate of the burnt fuel is calculated from the energy balance of the combustion chamber.

$$(\dot{m}_a + \dot{m}_f) C_{ph} T_{03} = \dot{m}_a C_{pc} T_{02} + \eta_b \dot{m}_f Q_R \quad (5.6)$$

with $f = \dot{m}_f/\dot{m}_a$, η_b is the burners (or combustion chamber) efficiency, and C_{pc} , C_{ph} are the specific heats for the cold air and hot gases

The fuel to air ratio is determined from the relation:

$$f = \frac{C_{ph} T_{03} - C_{pa} T_{02}}{\eta_b Q_R - C_{ph} T_{03}} \quad (5.7)$$

3. Tail Pipe:

The resultant high pressure and temperature forces the gases to flow out of the tail pipe at high velocity. If the gases are assumed to expand isentropically in the tail pipe to the ambient pressure, thus $p_4 = p_a$. The temperature of the exhaust gases is determined from the relation:

$$\left(\frac{T_{03}}{T_4}\right) = \left(\frac{P_{03}}{P_a}\right)^{\frac{\gamma_h - 1}{\gamma_h}} \quad (5.8)$$

The exhaust velocity is now calculated from the relation:

$$U_e = \sqrt{2Cp_h T_{03} \left[1 - \left(\frac{P_a}{P_{03}}\right)^{\frac{\gamma_h - 1}{\gamma_h}}\right]} \quad (5.9)$$

The thrust force is now calculated from the relation:

$$T = m_a[(1+f)U_e - U] \quad (5.10)$$

The specific thrust is (T/m_a) , and the thrust specific fuel consumption (TSFC) is given by the relation

$$TSFC = \frac{\dot{m}_f}{T} = \frac{f}{(T/\dot{m}_a)} \quad (5.11)$$

The thermal efficiency of the cycle is given by the relation:

$$\eta_{th} = 1 - \gamma \frac{T_a}{T_{02}} \left\{ \frac{\left(\frac{T_{03}}{T_{02}}\right)^{\frac{1}{\gamma}} - 1}{\frac{T_{03}}{T_{02}} - 1} \right\} \quad (5.12)$$

Some treatments for Humphrey cycle ignore the first process and consider it as three processes only, namely, an isochoric heat addition process follows isentropic compression and isobaric heat rejection follows isentropic expansion (a-3-4-1).

Example 5.1 A pulsejet engine is employed in powering a vehicle flying at a speed of 640 km/h at sea level. The engine has an inlet area 0.0962 m^2 develops thrust of 3520 N. Fuel heating value is 43,000 kJ/kg. Diffuser, combustion chamber, and nozzle are assumed ideal. It is required to calculate:

- 1. The air mass flow rate 2. The exhaust velocity
- 3. The maximum temperature 4. The fuel to air ratio

Solution

At sea level, the ambient temperature and pressure are 288.0 K and 101.07 kPa.

The flight speed is $U = 640/3.6 = 177.77$ m/s.

The air mass flow rate is $\dot{m}_a = \rho_a U A_i = 20.95$ kg/s.

Diffuser:

For an ideal diffuser, then

$$T_{02} = T_a + \frac{U^2}{2Cp_c} = 303.72 \text{ K}$$

$$P_{02} = P_a \left(\frac{T_{02}}{T_a} \right)^{\frac{\gamma_c}{\gamma_c - 1}} = 1.2044 \times 101 = 121.75 \text{ kPa}$$

The thrust force is expressed by:

$$T = \dot{m} [(1+f)U_e - U]$$

With negligible (fuel to air ratio, f), then

$$T \cong \dot{m} [U_e - U]$$

With negligible (fuel to air ratio, f), then

$$T \cong \dot{m} [U_e - U]$$

$$U_e = \frac{T}{\dot{m}} + U = 345.76 \text{ m/s}$$

Tail pipe:

The exhaust speed is calculated from Eq. (5.18) as

$$U_e^2 = 2Cp_h(T_{0\max} - T_4)$$

$$U_e^2 = 2Cp_h T_{0\max} \left[1 - \left(\frac{P_4}{P_{03}} \right)^{\frac{\gamma_h - 1}{\gamma_h}} \right]$$

Since the flow in both diffuser and tailpipe (nozzle) is assumed isentropic, and combustion process is a constant volume one, then

$$\frac{T_{03}}{T_{02}} = \frac{P_{03}}{P_{02}}$$

Then

$$\left(\frac{P_4}{P_{03}}\right)^{\frac{\gamma_h-1}{\gamma_h}} = \left[\frac{P_4 P_a P_{02}}{P_a P_{02} P_{03}}\right]^{\frac{\gamma_h-1}{\gamma_h}} = 1 \times \left(\frac{T_a}{T_{02}}\right)^{\left(\frac{\gamma_c}{\gamma_c-1}\right)\left(\frac{\gamma_h-1}{\gamma_h}\right)} \left(\frac{T_{02}}{T_{03}}\right)^{\frac{\gamma_h-1}{\gamma_h}}$$

Since $T_{03} = T_{0max}$, then

$$U_e^2 = 2Cp_h T_{0max} \left[1 - \left(\frac{T_a}{T_{02}}\right)^{\left(\frac{\gamma_c}{\gamma_c-1}\right)\left(\frac{\gamma_h-1}{\gamma_h}\right)} \left(\frac{T_{02}}{T_{0max}}\right)^{\frac{\gamma_h-1}{\gamma_h}} \right]$$

Using the results of above calculations, substitute to get the following relation:

$$52.06 = T_{0max} \left[1 - \frac{3.985}{(T_{0max})^{0.25}} \right]$$

The above equation is solved by trial and error, to get

$$T_{0max} = 425 \text{ K}$$

Fuel to air ratio is

$$f = \frac{Cp_h T_{03} - Cp_a T_{02}}{Q_R - Cp_h T_{03}} = \frac{1148 \times 425 - 1005 \times 303}{43,000,000 - 1148 \times 425} = 0.0043$$

It is shown above that fuel to air ratio has a small value that justifies its previous neglecting.

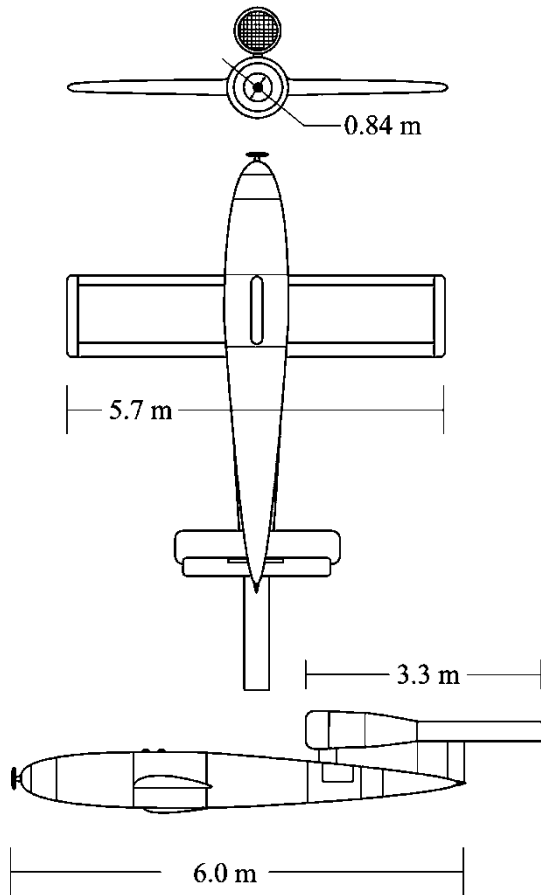
Recalculating for more precise values, since

$$U_e = \frac{(T/\dot{m} + U)}{1+f} = 344.3 \text{ m/s}$$

The difference between this value and first calculated one is only 1.4 m/s, thus the error is 0.4 %. Consequently, the above analysis is very accurate.

Example 5.2 The flying bomb V-1 powered by a pulse jet engine and illustrated in Fig. 5.4 is analyzed here. It has the following data:

- Flight altitude and speed are 2500 m and 220 m/s
- Thrust is 3330 N
- Intake area 0.1 m²
- Fuel is standard 80-octane gasoline having heating value of 40 MJ/kg and density of 0.75 kg/literature
- Fuel consumption 26 l/min
- Burner efficiency 0.92
- Typical flight duration is 1800 s

Fig. 5.4 Flying bomb V-1

Assume specific heat of air $Cp_a = 1.005 \frac{\text{kJ}}{\text{kgK}}$ and specific heat of hot gases $Cp_h = 1.1 \frac{\text{kJ}}{\text{kgK}}$
Calculate

1. Air and fuel mass flow rate
2. Fuel mass flow rate
3. Exhaust speed
4. Maximum temperature and pressure inside the engine
5. Thrust specific fuel consumption (TSFC)
6. Exhaust temperature
7. Fuel tank capacity in gallons

Solution

Air properties at 2500 m altitude are

$$\rho_a = 0.957 \text{ kg/m}^3, T_a = 271.9 \text{ K}, P_a = 74.683 \text{ kPa}$$

1. *Air mass flow rate* into engine

$$\dot{m}_a = \rho_a U A_i = 0.957 \times 220 \times 0.1 = 21.05 \text{ kg/s}$$

2. *Fuel mass flow rate*

$$\begin{aligned}\dot{m}_f &= \rho_f \times \text{Fuel consumption} = 0.75 \left(\frac{\text{kg}}{\text{liter}} \right) \times 26 \left(\frac{\text{liter}}{\text{min}} \right) \\ &= 19.5 \frac{\text{kg}}{\text{min}} = 0.325 \text{ kg/s}\end{aligned}$$

Fuel to air ratio is then

$$f = \frac{\dot{m}_f}{\dot{m}_a} = 0.0154$$

3. *Exhaust speed*

Since the thrust force is expressed by the relation

$$T = \dot{m}_a [(1+f)U_e - U]$$

The exhaust velocity is then calculated from

$$U_e = \frac{T + \dot{m}_a U}{\dot{m}_a (1+f)} = \frac{3330 + 21.05 \times 220}{21.05 \times 1.0154} = 372.5 \text{ m/s}$$

4. *Maximum temperature and pressure inside engine:*

Prior combustion, the temperature, and pressure of air are

$$\begin{aligned}T_{02} &= T_{01} = T_{0a} = T_a + \frac{U^2}{2Cp_a} = 271.9 + \frac{(220)^2}{2 \times 1005} = 303.2 \text{ K} \\ P_{02} &= P_{01} = P_{0a} = P_a \times \left(\frac{T_{02}}{T_a} \right)^{\frac{\gamma}{\gamma-1}} = 74.683 \times \left(\frac{303.2}{279.1} \right)^{3.5} = 99.77 \text{ kPa}\end{aligned}$$

From energy balance in combustion chamber, the maximum temperature in engine is given by

$$T_{03} = \frac{\dot{m}_a C p_a T_{02} + \eta_b \dot{m}_f Q_R}{\dot{m}_a (1+f) \times C p_h} = \frac{21.05 \times 1.005 \times 303.2 + 0.92 \times 0.325 \times 40,000}{21.05 \times 1.0154 \times 1.1}$$

Thus the *maximum temperature* in engine is $T_{03} = 781.5 \text{ K}$

Since combustion takes place at nearly constant volume process, then

$$P_{03} = P_{02} \times \frac{T_{03}}{T_{02}} = 99.77 \times \frac{781.5}{303.2} = 257.2 \text{ kPa}$$

Thus the *maximum pressure* in engine is $P_{03} = 257.2 \text{ kPa}$

5. Thrust specific fuel consumption (TSFC)

$$TSFC = \frac{\dot{m}_f}{T} = \frac{0.325}{3330} = 9.76 \times 10^{-5} \frac{\text{kg}}{\text{s.N}} = 0.351 \frac{\text{kg}}{\text{hr.N}}$$

6. The *exhaust temperature* (T_4)

$$T_4 = T_{03} - \frac{U_e^2}{2Cp_h} = 781.5 - \frac{(372.5)^2}{2 \times 1100} = 718.5 \text{ K}$$

7. Fuel tank capacity

Assuming all fuel is consumed during flight, then

$$\text{Tank capacity} = \dot{m}_f \times \text{flight duration} = 0.325 \times 1800 = 5851$$

$$\text{Tank capacity} = 154.6 \text{ gallon}$$

5.2.5 Valveless Pulsejet

Valveless engine is one of the simplest jet engines in the world as it has no mechanical valves, but it does have aerodynamic valve, which, for the most part, restricts the flow of gases to a single direction just as their mechanical counterparts. Valveless pulsejet engine is sometimes identified as *acoustic jet* engine [11], or *aerovated* and also *intermittent ramjet* [12].

This engine has no moving parts which mean no wear. It is similar to a ramjet in that respect.

Valveless pulse jet is designed to resolve the wear issues of valves in valved type. They have all the advantages and most of the disadvantages of conventional valved pulsejets [1]. Fuel consumption is excessively high, and the noise level is unacceptable for recent standards. However, they do not have the troublesome reed

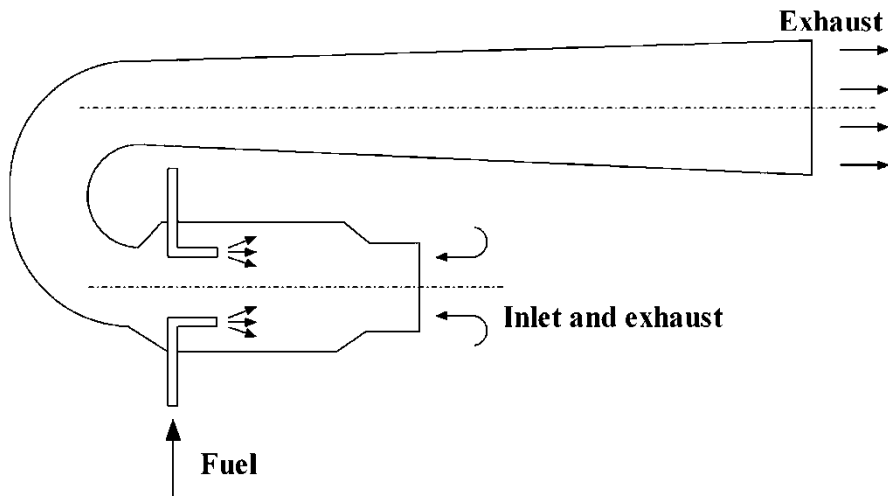


Fig. 5.5 Valveless pulsejet engine

valves that need frequent replacement. They can operate for their entire useful life with practically zero maintenance. They have been used to power model aircraft, experimental go-karts, and even some unmanned military aircraft such as target drones. The intake and exhaust pipes usually face the same direction. This necessitates bending the engine into a "U" shape as shown in Fig. 5.5 or placing a 180°bend in the intake tube.

In this type of pulsejet, combustion process generates two shock wave fronts, one travels down each tube. By properly "tuning" of the system a stable, resonating combustion process can be achieved which yields a considerable thrust.

The engine can be built in many different sizes from a few centimeters in length to huge sizes. The smallest ones are only successful when extremely fast-burning fuels are employed acetylene or hydrogen, for example. Medium- and larger-sized engines can burn almost any flammable material delivered uniformly to the combustion zone, though of course volatile flammable liquids (gasoline, kerosene, various alcohols) and standard fuel gases (propane, butane, MAPP gas) are easiest to use. Because of the deflagration nature of pulsejet combustion, these engines are extremely efficient combustors, producing practically no hazardous pollutants, even when using hydrocarbon fuels. With modern high-temperature metals for the main structure, engine weight can be kept extremely low.

Up to the present, the physical size of successful valveless designs has always been somewhat larger than valved engines for the same thrust value, though this is theoretically not a requirement. An ignition system of some sort is required for engine startup. In the smallest sizes, forced air at the intake is also typically needed for startup.

5.2.6 Pulsating Nature of Flow Parameters in Pulsejet Engines

Several researches were performed to examine the fluctuating nature of flow properties within pulsejets since the 1940s [13]. Experimental investigations are still going on [14, 15] as well as other numerical ones [11]. The fundamental operating frequency of the pulsejet (f : cycles/sec or Hz) is primarily related to the overall length of pulsejet (combustion and tail pipe) and can be expressed as:

$$f \approx \frac{1}{L} \quad (5.13)$$

In acoustic terminology, a conventional pulsejet operates on a ($4L$) wave system. That is to say, four pressure waves (compression–rarefaction–rarefaction–compression; C _R _R _C) moving at or slightly above the local gas sound speed sequentially traverse the duct system (combustor +tailpipe = combustion tube of length $4L$ in one operational cycle. Thus the operational period for one cycle in seconds is approximately:

$$\Delta t_{cyc} \approx \frac{4L}{a} \approx \frac{1}{f} \quad (5.14)$$

Various parameters in pulsejets like air mass flow rate, pressure, temperature, Mach number, and thrust force have pulsating nature. Numerical simulation for various parameters in valved pulsejet was given in [14].

As a trial for idealization of such pulsating behavior, a sinusoidal representation of the combustor pressure profile with time can be suggested [12]. Figure 5.6 illustrates the upper and lower absolute pressure limits about the idealized baseline pressure. Since they are nearly equal in magnitude, then $\Delta P = \mp 100\%$ for a symmetrical cycle (vacuum limit; $P \cong 0$, as the most negative trough point possible in the idealized sinusoidal cycle acting to enforce this limitation on performance).

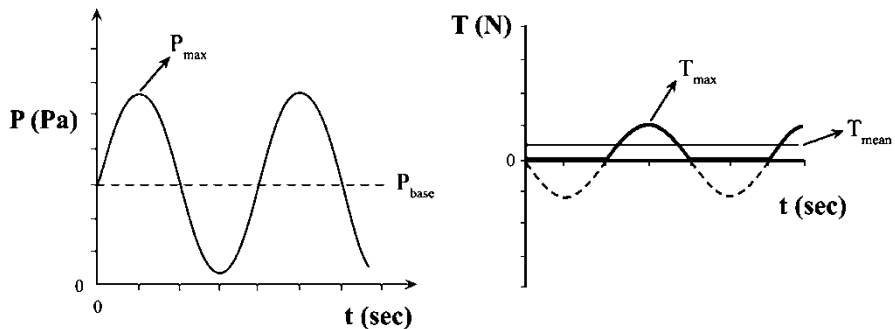


Fig. 5.6 Idealized sinusoidal fluctuations in combustion pressure (P) and thrust force (T) versus time (t)

Analogous to the assumed idealized sinusoidal combustor pressure–time profile of Fig. 5.6, one can assume a corresponding thrust–time profile would then have also a sinusoidal shape as shown in Fig. 5.6. Assuming that no appreciable negative thrust (resulting from backflow during the induction phase of the operational cycle), the remaining positive components of the cyclic thrust profile would produce a net mean thrust of

$$\bar{T} = \frac{T_{\max}}{\pi} \quad (5.15)$$

It is worth mentioning here that the results of numerical calculations in [16] are far from Eq. (5.15). In a case study, the maximum thrust was 110 N while the average was 19.5 N.

5.2.7 Pulse Detonation Engine (PDE)

The pulse detonation engine (PDE) marks a new approach towards non-continuous combustion in jet engines. They are light, easy to manufacture, and promises higher fuel efficiency compared even to turbofan engines. With the aid of latest design techniques and high pulse frequencies, the drawbacks of the early designs promise to be overcome. To date, no practical PDE engine has been put into production, but several test bed engines have been built by Pratt & Whitney and General Electric that have proven the basic concept. Extensive research work is also carried out in different NASA centers. In theory, the design can produce an engine with the efficiency far surpassing gas turbine with almost no moving parts. These systems should be put to use in the near future.

All regular jet engines operate on the *deflagration* of fuel, that is, the rapid but relatively gentle subsonic combustion of fuel. The pulse detonation engine is a concept currently in active development to create a jet engine that operates on the supersonic *detonation* of fuel [1].

Pulse detonation engines (PDEs) are an extension of pulse-jet engines. They share many similarities including the operating Humphrey's cycle. However, there is one important difference between them, namely, PDEs detonate, rather than deflagrate, their fuel. Detonation of fuel is a sudden and violent supersonic combustion of fuel that results in immense pressure which in turn used as thrust. Combustion process in PDE resembles perfectly constant volume combustion, while combustion process in valveless and valved pulsejets is approximated only as a constant volume process [10, 12]. Others identify combustion in PDE as neither constant volume nor constant pressure [17]. Details of test results of both PDE and pulsejet are given in [14]. PDE achieves higher specific impulse in comparison with pulsejet engines for same operating static conditions. The main objective of PDE is to provide an efficient engine that is primarily used for high-speed (about Mach 5) civilian transport as well as many military applications including supersonic

vehicles, cruise missiles, UAVs, SSTO launchers, and rockets. However, their noise and the drop in efficiency at higher Mach number imply that pure PDEs will likely not to be used often for large-scale applications.

The single flight of an aircraft powered by a pulse detonation engine took place at the Mojave Air & Space Port on 31 January 2008 [18]. The aircraft selected for the flight was a heavily modified [Scaled Composites Long-EZ](#), named *Borealis*. The engine consisted of four tubes producing pulse detonations at a frequency of 80 Hz, creating up to 890 Newton of thrust and using a refined [octane](#) as fuel. A small rocket system was used to facilitate the liftoff of the Long-EZ, but the PDE operated under its own power for 10 s at an altitude of approximately 100 ft (30 m). This demonstration showed that a PDE can be integrated into an aircraft frame without experiencing structural problems from the 195 to 200 dB detonation waves.

Pulse detonation engines use intermittent detonation waves to generate thrust. The cycle of PDE is illustrated in Fig. 5.7. Its cycle is also idealized by Humphrey cycle shown in Fig. 5.3. Unlike the pulsejet, combustion in PDE is supersonic, effectively an explosion instead of burning, and the shock wave of the combustion front inside the fuel serves the purpose of shutters of valved pulsejet. A detonation propagating from the closed end of the tube is followed by an unsteady expansion wave (called Taylor wave), whose role is to bring the flow to rest near the closed end of the tube. When the shock wave reaches the rear of engine and exits, the combustion products are ejected in “one go”, the pressure inside the engine suddenly drops, and the air is pulled in front of the engine to start the next cycle.

PDE operation is not determined by the acoustics of the system and can be directly controlled. PDEs typically operate at a frequency of 50–100 Hz, which means that a typical cycle time is on the order of 10–20 ms. Since PDE produces a higher specific thrust than a comparable ramjet engines at low supersonic speeds, it is suitable for use as part of a multi-stage propulsion system. The specific impulse for PDE is plotted versus several other pulse and ramjet engine for comparison as shown in Fig. 5.8. Single-tube supersonic impulse PDE with straight detonation has higher performance than ideal ramjet engines for flight Mach number up to 1.35. The PDE can provide static thrust for a ramjet or scramjet engine or operate in combination with turbofan systems.

PDE can be classified as:

- Pure (standalone)
- Combined cycles
- Hybrid turbomachinery cycles

Pure PDE as the name implies consists of an array of detonation tubes, an inlet, and a nozzle. The applications of pure PDEs are mainly military, as they are light, easy to manufacture, and have higher performance around Mach 1 than current engine technologies. Their noise and the drop in efficiency at higher Mach number imply that pure PDEs will likely not to be used often for large-scale applications.

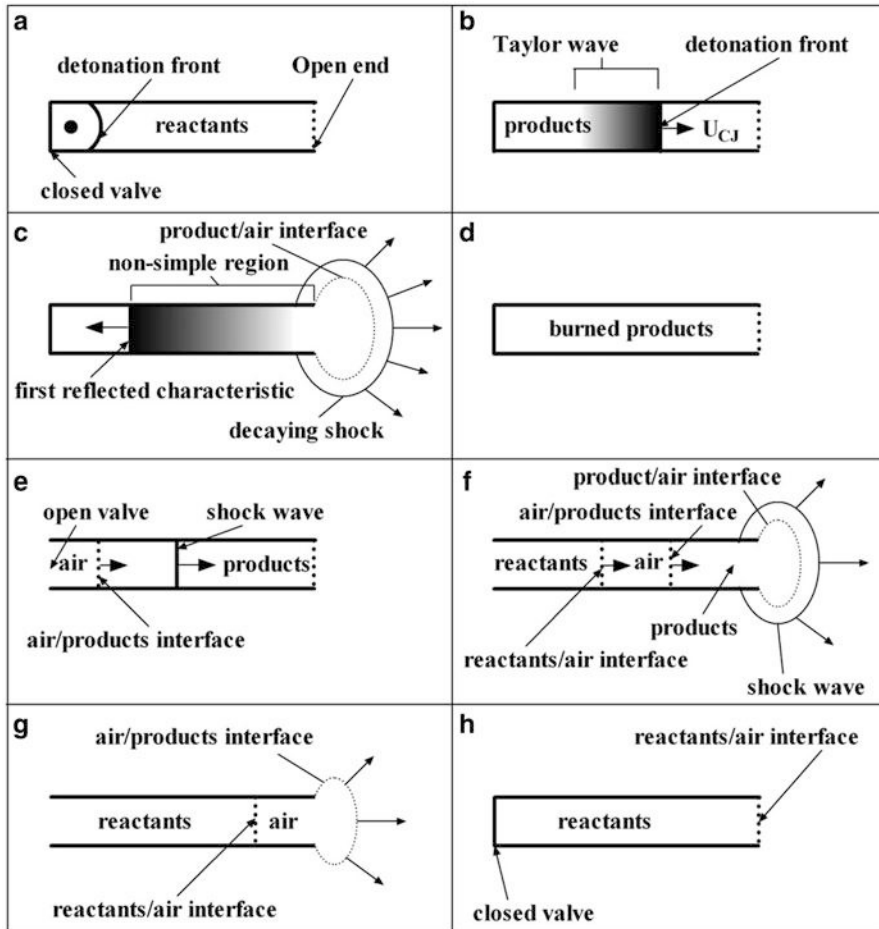


Fig. 5.7 PDE thermodynamic cycle

Combined-cycle PDEs may provide the most exciting possibilities for aviation. Adding a PDE to the flowpath of a ramjet or scramjet would make an engine capable of operating efficiently as high as Mach 5.5. These engines would seem initially suitable for high altitude, high-speed aircraft [19].

Hybrid PDE's make use of detonative combustion in place of constant pressure combustion, usually in combination with turbomachinery.

Hybrid engines are of two types, one in which the PDE replaces the conventional combustor, but has several disadvantages among which providing high temperature flow into turbine blades [20]. An alternate approach involves arranging the PDE combustor in the bypass duct of turbofan engines and mixing the PDE exhaust with the turbine exhaust in a mixer located aft of the turbine, which resembles a mixed turbofan arrangements as well be described in Chap. 6 [21]. In other researches of

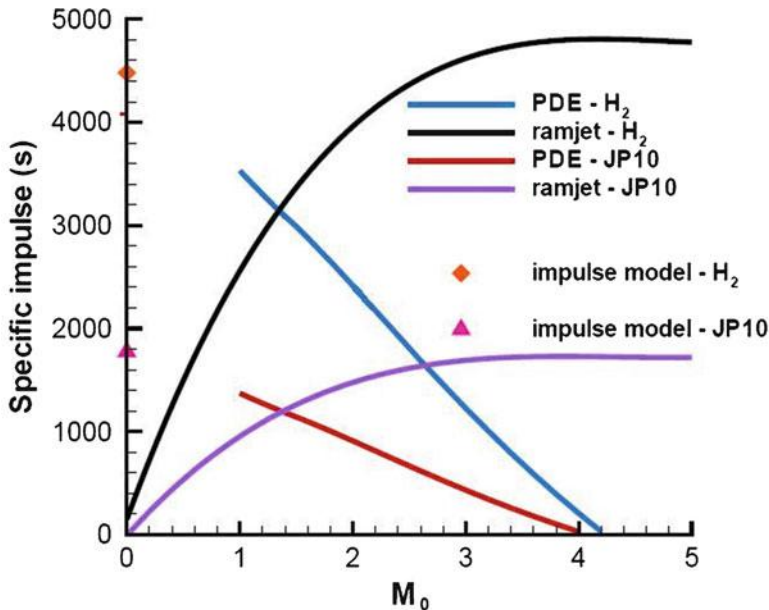


Fig. 5.8 Specific impulse for PDE compared to other engines

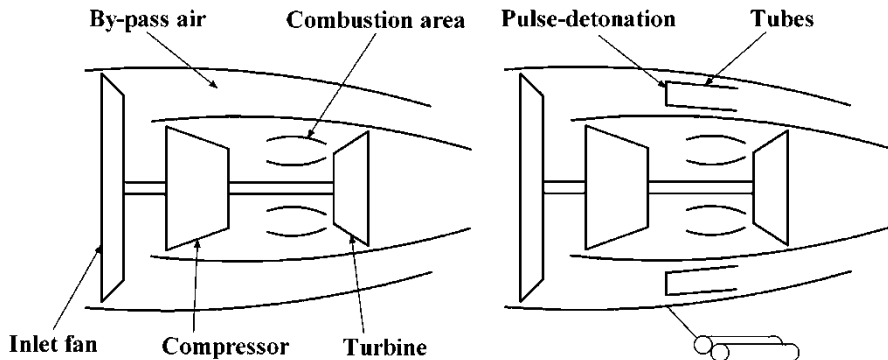


Fig. 5.9 Hybrid turbofan-PDE

hybrid turbofan-PDE: The central core engine would still turn the large fan in front, but the bypass would flow into a ring of PDEs [22, 23] in an unmixed turbofan arrangement as will also be analyzed in Chap. 6. The bypass air enters pulse detonation tubes that surround the standard combustion chamber (Fig. 5.9). The tubes are then cyclically detonated; one detonates while the others fill with air or are primed with fuel. This combination promises to require simpler engine mechanisms and yield higher thrust with lower fuel consumption as examined by GE.

Hybrid PDEs will allow commercial aircraft powered by subsonic gas turbines to be faster, more efficient, and more environmentally friendly. Similarly, hybrid supersonic gas turbines can also be used in military applications. Generally, hybrid PDEs will deliver the same thrust of a turbofan engine but with less fuel consumption. Moreover, they would produce significantly more thrust without requiring additional fuel.

Example 5.3 A PDE is employed in propelling a vehicle flying at a Mach number of 3 at an altitude of 40,000 ft. The engine has an inlet area 0.084 m^2 . The temperature ratio at combustion chamber is

$$\frac{T_{03}}{T_{02}} = 10.1, \text{ fuel heating value is } 43,000 \text{ kJ/kg. Assuming that}$$

- PDE operates on the simplified Humphrey thermodynamic cycle
- Ideal diffuser ($P_{02} = P_{0a}$)
- $\gamma_{air} = 1.4, \gamma_{gas} = 1.18,$

It is required to calculate:

- | | |
|-----------------------------|--|
| 1. The air mass flow rate | 2. The maximum temperature |
| 3. The fuel to air ratio | 4. The exhaust velocity |
| 5. The thrust force | 6. The thrust specific fuel consumption (TSFC) |
| 7. Thermodynamic efficiency | 8. Specific impulse |

Solution

At altitude 40,000 ft, the ambient temperature and pressure are 216.65 K and 18.75 kPa

The flight speed is

$$U = M\sqrt{\gamma RT_a} = 3 \times \sqrt{1.4 \times 287 \times 216.65} = 885.1269 \text{ m/s}$$

$$U = 885.126957 \text{ m/s}$$

The *air mass flow rate* is

$$\dot{m}_a = \rho_a U A_i = \frac{P_a}{RT_a} U A_i = \frac{18.75 \times 1000}{287 \times 216.65} \times 885.1269 \times 0.084 = 22.4205 \text{ Kg/s}$$

$$C_{P_{air}} = \frac{\gamma_{air} R}{\gamma_{air} - 1} = \frac{1.4 \times 287}{1.4 - 1} = 1005 \frac{J}{Kg} K$$

$$C_{P_{gas}} = \frac{\gamma_{gas} R}{\gamma_{gas} - 1} = \frac{1.18 \times 287}{1.18 - 1} = 1881.44 \frac{J}{kg} K$$

Diffuser:

The total temperature at the intake is equal to the total upstream temperature, or

$$T_{02} = T_{0a} = T_a \left(1 + \frac{\gamma_c - 1}{2} M^2 \right) = 216.65 \left(1 + \frac{1.4 - 1}{2} 3^2 \right)$$

$$T_{02} = 606.62 \text{ K}$$

The total pressure at the diffuser outlet also equal to the free stream total pressure as the flow through the diffuser is assumed ideal

$$P_{02} = P_{0a} = P_a \left(\frac{T_{0a}}{T_a} \right)^{\frac{\gamma}{\gamma-1}} = 18.75 \left(\frac{606.62}{216.65} \right)^{3.5} = 688.7385 \text{ kPa}$$

Combustion Chamber

A constant volume process is assumed, and then the *maximum temperature* is

$$T_{03} = 10.1 T_{02} = 6126.862 \text{ K}$$

From Eq. (5.5)

$$P_{03} = 10.1 P_{02} = 6956.25885 \text{ kPa}$$

The *fuel to air ratio* is calculated from Eq. (3.6) as

$$f = \frac{Cp_{\text{gas}} T_{03} - Cp_{\text{air}} T_{02}}{Q_R - Cp_{\text{gas}} T_{03}} = \frac{1.8814 \times 6126.862 - 1.005 \times 606.62}{43,000 - 1.8814 \times 6126.862} = 0.34688$$

$$f = 0.346883$$

The obtained fuel to air ratio is too large which implies great fuel consumption.

Tail pipe:

The *exhaust speed* is calculated from Eq. (5.9) as

$$U_e = \sqrt{2 C_{p_{\text{gas}}} T_{03} \left[1 - \left(\frac{P_a}{P_{03}} \right)^{\frac{\gamma_h - 1}{\gamma_h}} \right]} \quad (5.9)$$

$$= \sqrt{2 \times 1881.44 \times 6126.862 \left[1 - \left(\frac{18.75}{6956.25885} \right)^{\frac{1.18 - 1}{1.18}} \right]}$$

$$U_e = 3701.954 \text{ m/s}$$

The specific thrust is

$$\frac{T}{\dot{m}_a} = (1+f)U_e - U = 4100.960847 \frac{N.s}{kg}$$

The *thrust force* is then $T = \dot{m}_a \times \frac{T}{\dot{m}_a} = 41,160 \text{ N} = 91.94559 \text{ kN}$

The *thrust specific fuel consumption* is calculated from Eq. (5.11)

$$TSFC = \frac{\dot{m}_f}{T} = \frac{0.34688}{91945.59} = 3.77266 \times 10^{-6} \frac{\text{kg}}{\text{N.s}} = 0.00679 \frac{\text{kg}}{\text{N.hr}}$$

The *thermal efficiency* of the cycle is calculated from Eq. (5.12):

For $\gamma = 1.18$, thermal efficiency is:

$$\eta_{th} = 1$$

$$-\gamma \frac{T_a}{T_{02}} \left\{ \frac{\left(\frac{T_{03}}{T_{02}}\right)^{\frac{1}{\gamma}} - 1}{\frac{T_{03}}{T_{02}} - 1} \right\} = 1 - 1.18 \times \frac{216.65}{606.62} \times \left\{ \frac{\left(\frac{6126.862}{606.62}\right)^{0.847} - 1}{\frac{6126.862}{606.62} - 1} \right\} = 71.7\%$$

For $\gamma = 1.4$, then:

$$\eta_{th} = 1$$

$$-\gamma \frac{T_a}{T_{02}} \left\{ \frac{\left(\frac{T_{03}}{T_{02}}\right)^{\frac{1}{\gamma}} - 1}{\frac{T_{03}}{T_{02}} - 1} \right\} = 1 - 1.4 \times \frac{216.65}{606.62} \times \left\{ \frac{\left(\frac{6126.862}{606.62}\right)^{0.714} - 1}{\frac{6126.862}{606.62} - 1} \right\} = 76.8\%$$

The above two values for thermal efficiencies for the two values of specific heats are in complete compliance with the results in [24] for same temperature (pressure) ratio of 10.1.

Specific impulse:

$$I = \frac{T}{\dot{m}_a g} = \frac{91945.59}{0.346883 \times 22.4205 \times 9.81} = 1205.13 \text{ s}$$

5.3 Ramjet

5.3.1 Introduction

A *ramjet* (Stato-Réacteur) is another type of athodyd airbreathing jet engine that was first proposed by *Rene Lorin* in 1913. It uses the forward motion of engine to compress the incoming air, without a rotary compressor. Thus a ramjet is much like a valveless pulsejet but it operates with continuous combustion rather than the series of explosions that give a pulsejet its characteristic noise. Ramjet engine may be either of the *subsonic* or *supersonic* type. In either cases, ramjet depends on the compression of the in-rushing air for its operation, or in other words depends on the flight speed. A vehicle powered by a ramjet cannot develop static thrust and therefore cannot accelerate a vehicle from a standing start. The vehicle must first be accelerated by other means to a sufficiently high speed prior to using a ramjet as a propulsive device. It may be dropped from a plane or launched by rocket assist.

The theoretical upper operating limit for engines with subsonic combustion is not a hard line, but lies somewhere between Mach 4 and Mach 8 depending on the fuel used, usually about Mach 5.5.

Although ramjet can operate at subsonic flight speed, the increasing pressure rise accompanying higher flight speeds renders the ramjet most suitable for supersonic and most efficient at speeds around Mach 3. For this reason, subsonic ramjets are seldom (if ever) used these days. Figure 5.10 illustrates a subsonic ramjet engine (A) and a supersonic engine (B and C).

The ramjet has been called a flying stovepipe, because it is open at both ends and has only fuel nozzles in the middle. A straight stovepipe would not work however; a ramjet must have a properly shaped inlet-diffusion section to produce low-velocity, high-pressure air at the combustion section and it must also have a properly shaped

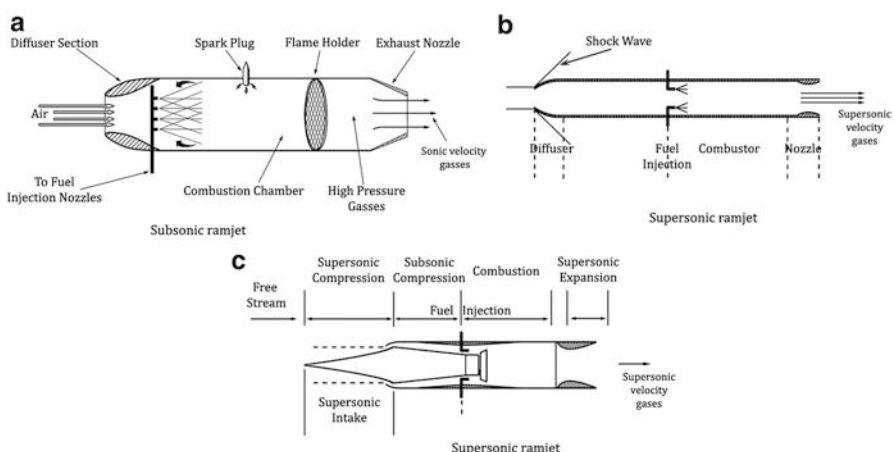


Fig. 5.10 Types of ramjet engines subsonic (a) and supersonic (b and c)

exhaust nozzle. High speed air enters the inlet, is compressed as it is slowed down, is mixed with fuel and burned in the combustion chamber, and is finally expanded and ejected through the nozzle. The air rushing toward the inlet of an engine flying at high speeds is partially compressed by the so-called ram effect. If the flight speed is supersonic, part of this compression actually occurs across a shock wave system that is either external or external-internal to the inlet. When the flight speed is high enough, this compression will be sufficient to operate an engine without a compressor. Once the compressor is eliminated, the turbine is no longer required and it is omitted. Ramjets can operate at speeds above 320 km/h (about 200 mph) or as low Mach number as 0.2. However, the fuel consumption is horrendous at these low velocities. The operation of ramjet does not become competitive with that of a turbojet until speeds of about $M_a = 2.5$ or even more are reached. Ramjets become practical for military applications only (almost exclusively in missiles) at very high or supersonic speeds (up to flight Mach number of 6 for example). The combustion region is generally a large single combustor, similar to afterburner [25]. Combustion process occurs in subsonic speeds. Thus the upper operating flight speeds lies somewhere between Mach 4 and Mach 8 depending on the fuel used, usually about Mach 5.5.

Advantages and disadvantages of ramjet engines may be summarized as follows:

Advantages

- Able to attain high speeds (around Mach 5)
- No moving parts so less wear and tear as well as minimum losses
- Reduced weight and smaller engine
- Lighter and simpler than turbine based engines
- Higher temperatures can be employed

Disadvantages

- Bad performance at lower speeds
- Needs booster to accelerate it to a speed where ramjet begins to produce thrust
- Higher fuel consumption
- Maximum operating altitude is limited
- High temperature material is required

5.3.2 *Applications*

Ramjet engines are used in propelling both of missiles and aircrafts. In the next sections, several examples for applications in both fields are given.

(I) *Missiles Applications*

Ramjet engines are found in most types of missiles as described in the forthcoming subsections.

(A) Air-to-air missiles

Ramjet engines enable medium-range missiles to maintain higher average speed across their engagement envelope and extend their range. Examples are MBDA Meteor (scheduled to enter service in 2015). Others are AIM-120 AMRAAM, Vympel RVV-AE-PD R77M (AA12 Adder), and Gorgon IV.

(B) Air-to-surface missiles

Examples are EADS/AMM, ASMP, ASMP-A, Radouga Kh41 Moskit and Zvezda Kh31P (AS17 Krypton) Radouga 3 M80/82 Moskit (SSN22 Sunburn), CPMEC C301 (coast to ship), and Hsiung Feng 3. Also air-to-ground missile carried by Mirage IV and Mirage 2000 liquid fuel ramjet Mach 2 capability range 20 km.

(C) Surface-to-air missiles

Examples are MBDA and LFK NG (USA), Bloodhound Mk2, Rapier and Sea Dart (UK), Mistral and Eurosam Aster (France), and Aspide (Alenia consortium), SA -4 Ganef (propelled by 4 booster rockets and one liquid fuel ramjet), SA-6 Gainful (solid propellant booster propels it to Mach 1.5 ramjet propels it to Mach 2.8).

(D) Anti-ship missiles

Examples are Machinostroenie 3 K55, Yakhont (SS N26), ANS (liquid fueled ramjet; reaches Mach 4 Range 25 km), and C101 & C103 (ranges 50 and 100 km).

Figure 5.11 illustrates the ramjet engine (7 ft long and 20 inches in diameter) powered Gorgon IV air-to-air missile. It was positioned below the missile which in turn was mounted below the wing of a [P-61 Black Widow](#) for flight testing.

(II) Aircraft Applications

A variant of the pure ramjet engine is coupled to other type of engines (piston/turbojet/turbofan) to power aircrafts to overcome the limitations of the pure ramjet.

Some ramjet engines arranged by country are listed hereafter.

(A) France

Two distinct ramjets were manufactured, namely:

- (i) The *Leduc 0.10* was a research aircraft (achieved Mach 0.84 at 26,000 ft), powered solely by a Leduc ramjet engine, which was designed to separate from the airplane that brought it to altitude (*SNCASE SE.161 Languedoc* four-engined airliner produced by [SNCASE](#) (Sud-Est)). It produced 15.7 kN thrust and flew in October 1947 (Fig. 5.12).
- (ii) The *Nord 1500 Griffon* was an experimental ramjet-powered a Mach 2 fighter aircraft designed and built in the mid-1950s by Nord Aviation. Griffon II a research fighter having a *maximum speed of* Mach 2.19 (or 2330 km/h) was



Fig. 5.11 Ramjet engine positioned below the Missile Gorgon IV



Fig. 5.12 Leduc 0.10

fitted with the definitive *hybrid* engine (turbo-ramjet) composed of ATAR 101E-3 turbojet (34.3 kN) and Nord Stato-Réacteur ramjet (68.0 kN).

(B) Germany

In 1936, [Hellmuth Walter](#) constructed a test engine powered by [natural gas](#). In 1941, [Eugen Sänger](#) of the DFL proposed a ramjet engine with a very high

combustion chamber temperature. He constructed a very large diameter ramjet pipes and carried out combustion tests at flight speeds of up to 200 m/s.

(C) *Japan*

The ATREX engine is an example for AirTurbo Ramjet (ATR), which is a “combined cycle” engine, intended to overcome the limitations of the pure ramjet [26]. It operates as a conventional turbojet at subsonic speeds and a fan assisted ramjet at speeds below Mach 6.

(D) *(Former) Soviet Union*

In the Soviet Union, a theory of *supersonic ramjet* engines was presented in 1928 by [Boris S. Stechkin](#). In August 1939, Yuri Pobedonostsev developed the first ramjet engine for use as an auxiliary motor of an aircraft, the DM-1. The world’s first ramjet-powered airplane flight took place in December 1939, using two DM-2 engines on a modified Polikarpov I-15. Two of his DM-4 engines were installed on the [YaK-7PVRD](#) fighter during World War II.

(E) *United States of America*

1. The *Lockheed X-7* was an unmanned test bed for ramjet. It was carried aloft by a B-29 or B-50 Superfortress carrier aircraft. The booster rocket ignited after launch and propelled the vehicle to a speed of 1000 mph (1625 km/h). The booster was then jettisoned, and the under slung ramjet took over from that point. A total of 130 X-7 flights were conducted from April 1951 to July 1960.
2. The *Lockheed D-21* was a Mach 3+ reconnaissance drone designed to be launched off the back of its M-21 carrier aircraft and was modified to be launched from a Boeing B-52 Stratofortress. Only four operational D-21 flights were made over the People’s Republic of China before the program was canceled in 1971.
3. SR-71 high speed reconnaissance aircraft is powered by a *hybrid* engine, part turbojet, part ramjet (identified as turbo-ram engine).

5.3.3 *Aero-Thermodynamic Analysis of Modules*

In this section, different modules of Ram Based Cycle (RBC) Engines will be described. These three modules are intake (inlet or diffuser), combustor (or burner), and nozzle. First, it will be treated as a black boxes. Aero- and thermo-dynamics of air/gas flow upstream and downstream of each component are sufficient for analysis of each component. These data are necessary and sufficient for calculating engine’s cycle. Thus global parameters like thrust, TSFC, range as well as different efficiencies (propulsive, thermal, and overall) will be defined. Detailed analyses of each component will be discussed in later chapters.

5.3.3.1 Intake (Inlet) Module

Intake is the first component of any air-breathing engine. Intake section may have a circular/oval or rectangular inlet. It also may have a constant or variable area inlet. Supersonic ramjets may contain inlet cones (sometimes called shock cones/inlet center bodies/ spike) or compression ramps for shocks capture during supersonic flight speeds. In such cases, external/internal (mixed) compression intake is selected. These oblique shocks must be terminated by a strong normal shock, to slow down the airflow to a subsonic velocity prior combustion chamber.

Figure 5.13 shows the selected intake configuration together with a system of external/internal (mixed) shock waves. The external compression part starts at the vehicle nose and ends at the intake lip followed by the internal compression part inside the intake.

Subsonic ramjets need simpler inlets having a simple hole in front of a divergent duct. This would also work at slightly supersonic speeds, but a normal shock wave will be developed at inlet and the air will choke. Thus a reasonable pressure drop will be encountered and the inlet will be inefficient.

Pressure rise in the intake simultaneously raises the air temperature. Further diffusion is then required to get the air velocity down to a suitable level for the combustor. Flow of air through the intake will be treated as polytropic compression with a certain isentropic efficiency. Figure 5.14 shows the variation in intake isentropic efficiency with the number of oblique shock waves [27]. Intakes of subsonic ramjets are normally associated with one or multiple oblique shock waves followed by a normal shock. While intakes for supersonic ramjet (scramjet) engines employ only oblique shock waves that generate supersonic combustion. Such intakes will have high efficiencies of the range (90⁺) %.

Figure 5.15 shows the T-S diagram and configuration of the intake between inlet state (A) and exit state (B). The intake model is built up by the definition of isentropic efficiency given by Eq. (5.16). The variation of total temperature and

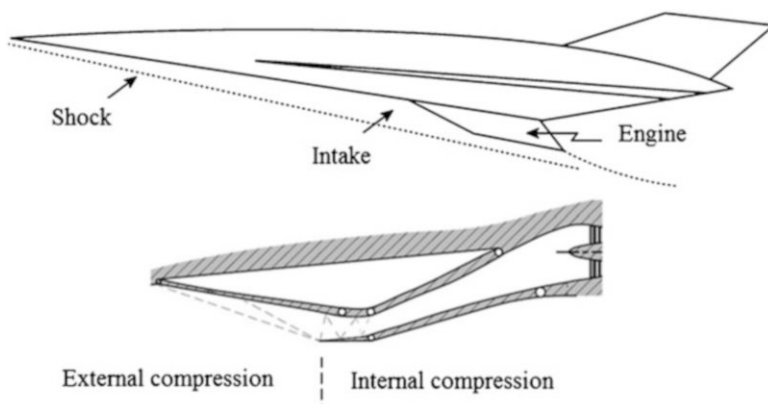
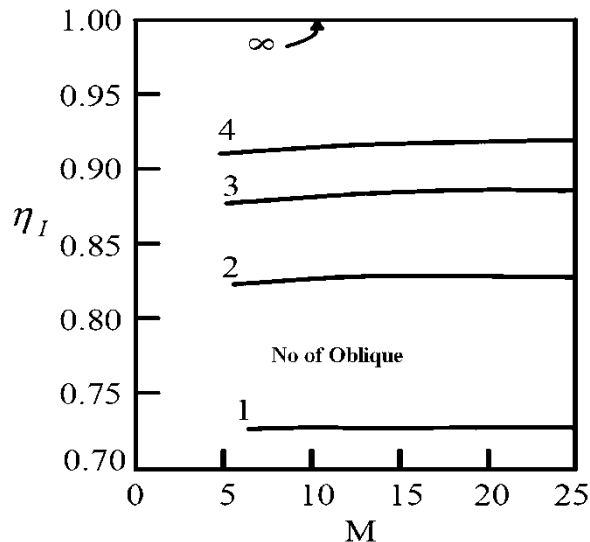


Fig. 5.13 Configuration of intake system

Fig. 5.14 Isentropic efficiency versus Mach number of supersonic intake with different number of oblique shock waves



total pressure within the intake are given by Eqs. (5.17) and (5.18). Block diagram showing the intake module, input data, and output data is shown in Fig. 5.16.

$$\eta_I = \frac{T_{oBS} - T_A}{T_{oB} - T_A} \quad (5.16)$$

$$\frac{T_{oB}}{T_A} = \frac{T_{oA}}{T_A} = \left(1 + \frac{\gamma_a - 1}{2} M_A^2 \right) \quad (5.17)$$

$$\frac{P_{oB}}{P_A} = \left[1 + \eta_I \frac{\gamma_a - 1}{2} M_A^2 \right]^{\frac{\gamma_a}{\gamma_a - 1}} \quad (5.18)$$

With static temperature and pressure expressed as (T, P) , while total conditions are denoted by (T_0, P_o) . Subscripts (A,B) presents inlet and outlet states

5.3.3.2 Combustion Chamber (Or Burners) Module

Combustion chambers are modeled as burners within which energy is generated through chemical reaction. Since there is no downstream turbine, a ramjet combustor can safely operate at stoichiometric fuel to air ratios, which implies a combustor exit stagnation temperature of the order of 2400 K for kerosene. Within the combustion chamber fuel is added, mixed with a part of air, then burnt by one or more ignitors. Remaining air quantity is used for cooling. Combustion process takes place at nearly constant pressure. However, due to friction and fuel-air mixing, a small drop in total pressure will take place inside the burner. The fuel burning will be simulated as heat addition to escape the complication of chemical reaction.

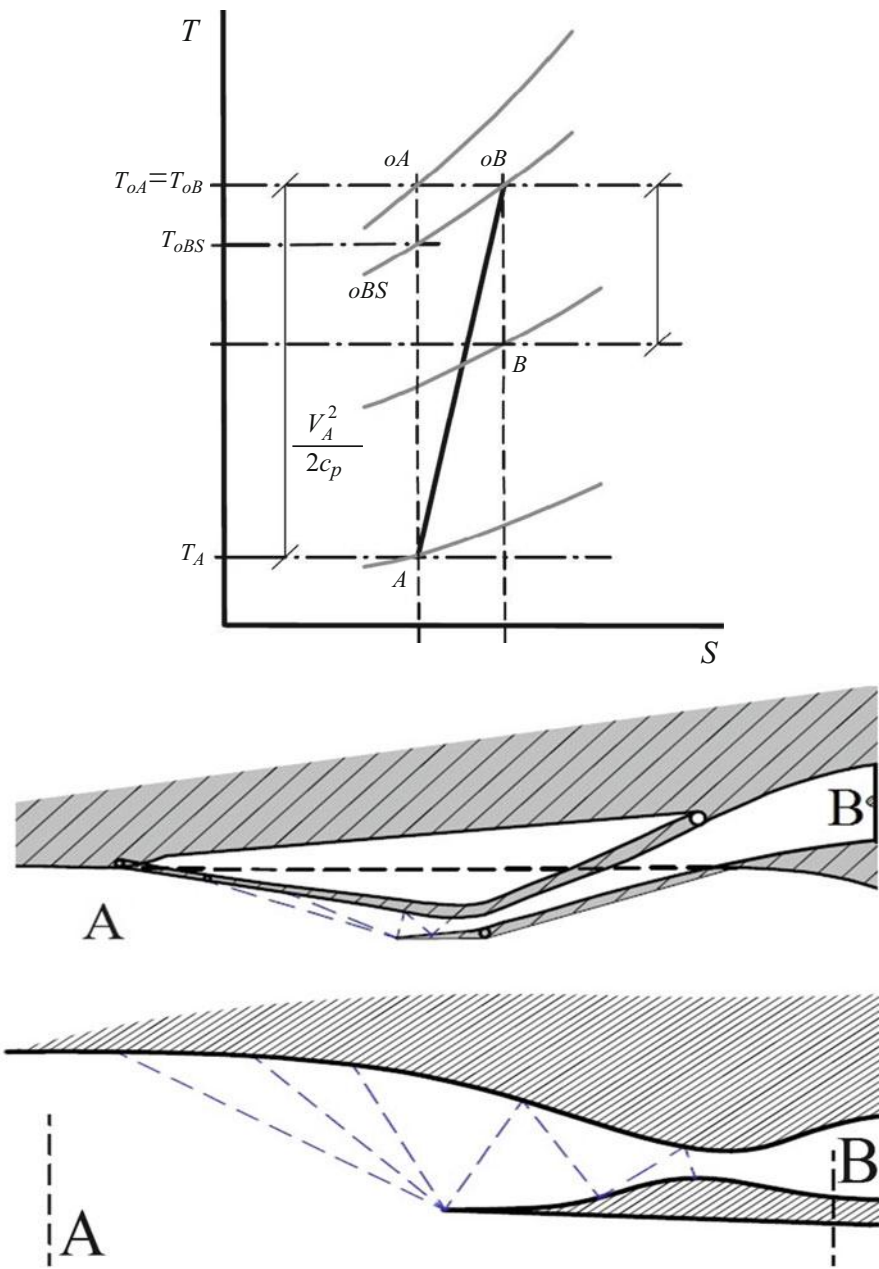


Fig. 5.15 T-s diagram and configuration of supersonic intake

Fig. 5.16 Block diagram for intake

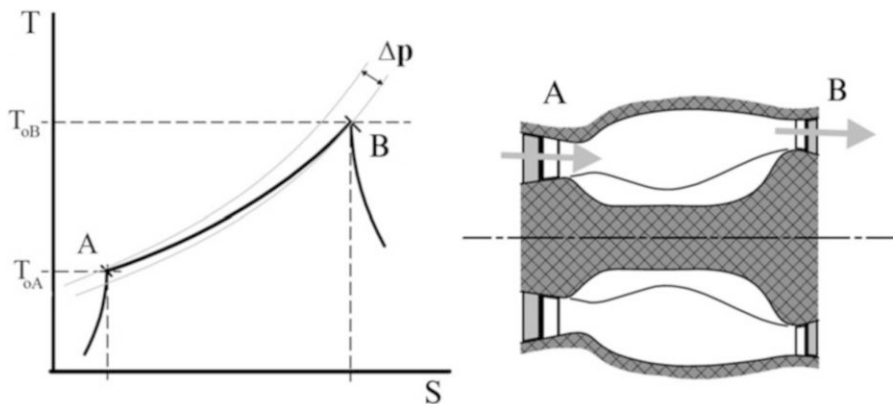
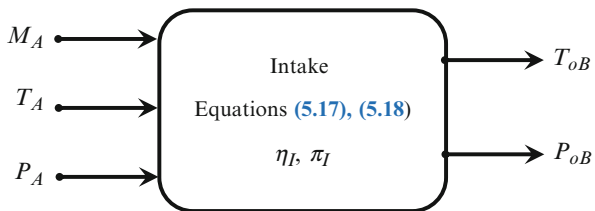


Fig. 5.17 T-s diagram and configuration of combustion chamber

Burning efficiency will be taken into consideration to represent unburned hydrocarbons. According to Zucrow, burning efficiency was nearly 95 % in the 1940s and 1950s [28], while it reached 98 % in the 1960s and reached 99 % in the 1990s. Concerning total pressure losses, it was 5 % in the 1960s and was improved to 2.5 % in the 1990s.

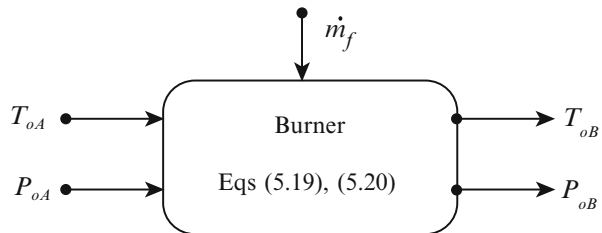
First law of thermodynamics and continuity equation will be used to build the burner model. Figure 5.17 shows the T-S diagram and burner's geometry. Burner's governing equations are given by Eqs. (5.19) and (5.20). Figure 5.18 shows block diagram of combustion chamber. Letters (A) and (B) are used for inlet states of combustion chamber, (ΔP_b) is the total pressure drop in burner while (Q_{HV}) is the heating value of fuel. Burner efficiency is (η_b), air and fuel mass flow rates are respectively (\dot{m}_a, \dot{m}_f).

$$P_{oB} = P_{oA} - \Delta P_b \quad (5.19)$$

$$T_{oB} = \frac{\dot{m}_a C_{pc} T_{oA} + \dot{m}_f \eta_b Q_{HV}}{C_{ph}(\dot{m}_a + \dot{m}_f)} \quad (5.20)$$

For large flight speeds, the temperature level becomes very high at the entrance of the combustion chamber.

Fig. 5.18 Block diagram for combustion chamber



Different types of fuels are used, namely:

- Gaseous (hydrogen as an example)
- Liquid (kerosene, synthetic hydrocarbon fuel; like US made RJ1, RJ4 and French CSD07T, CSD15T)
- Solid (polymers loaded with metal particles like Mg, Al, or B as examples: polyether, polyester, polyurethane). In such solid fuel ramjet, a grain of solid fuel gasifies or ablates and reacts with air.

5.3.3.3 Nozzle Module

Nozzle is the last and the most important component in all jet engines. It converts the pressure and thermal energy into kinetic energy of hot gases jet, which generates the thrust. Nozzles may be of fixed or variable geometry. It also may be convergent or convergent divergent sections. Finally, nozzles also may be choked or unchoked. The flow in nozzle is treated as polytropic expansion with a certain isentropic efficiency. Typical value for nozzle efficiency is taken as 99 % [28]. T-S diagram and nozzle configuration of are shown in Fig. 5.19.

The nozzle model is constructed by applying the first law of thermodynamics and the definition of isentropic efficiency in nozzle Eq. (5.21) between the nozzle inlet state (A) and exit state (B). State (A) is completely defined while only the static pressure is known at state (B) (free-stream static pressure if unchoked and sonic speed if choked). The final form of the nozzle model is given by Eqs. (5.21) and (5.22). Figure 5.20 illustrates a block diagram of nozzle module.

$$\eta_N = \frac{T_{oA} - T_B}{T_{oA} - T_{BS}} \quad (5.21)$$

$$T_B = T_{oA} \left[1 - \eta_N \left(1 - \left[\frac{P_B}{P_{oA}} \right]^{\frac{\gamma_m - 1}{\gamma_m}} \right) \right] \quad (5.22)$$

$$V_B = \sqrt{2C_{pm}(T_{oA} - T_B)} \quad (5.23)$$

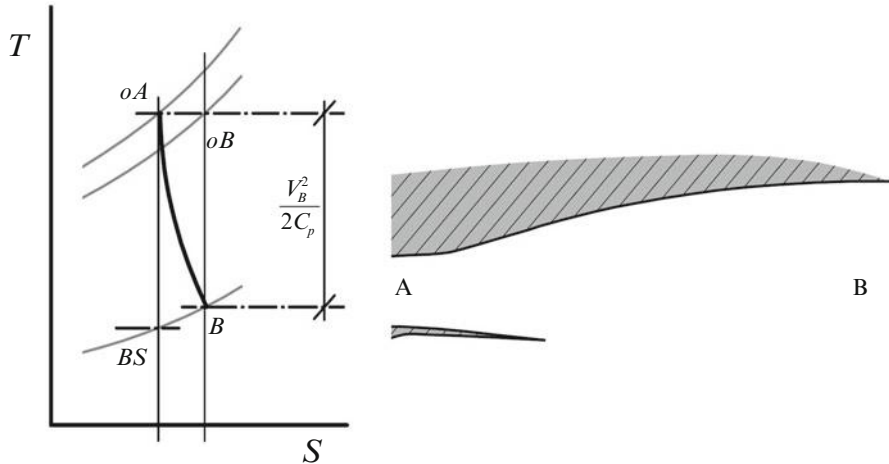
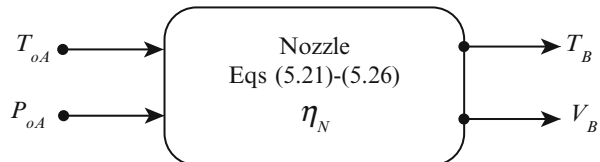


Fig. 5.19 T-s diagram and configuration of nozzle

Fig. 5.20 Block diagram for nozzle



If the nozzle is the convergent type and choked, then Mach number at exit is sonic speed. The exit condition is the critical one. Then the ratio between total and static temperatures is

$$\frac{T_{oA}}{T_B} = \frac{T_{oA}}{T_{cr}} = \frac{\gamma_m + 1}{2} \quad (5.24)$$

Nozzle efficiency is

$$\eta_N = \frac{T_{oA} - T_{cr}}{T_{oA} - T_{BS}} = \frac{1 - (T_{cr}/T_{oA})}{1 - (T_{BS}/T_{oA})} = \frac{1 - \left(\frac{2}{\gamma_m + 1}\right)}{1 - \left(\frac{P_{cr}}{P_{oA}}\right)^{\frac{\gamma_m - 1}{\gamma_m}}} \quad (5.25)$$

The critical pressure ratio is then

$$\frac{P_{oA}}{P_{cr}} = \frac{1}{\left[1 - \left(\frac{1}{\eta_N}\right) \left(\frac{\gamma_m - 1}{\gamma_m + 1}\right)^{\frac{\gamma_m}{\gamma_m - 1}}\right]} \quad (5.26)$$

5.3.4 Aero-thermodynamic Analysis of Ramjet Cycle

To analyze ramjet performance, the different states of its three modules (intake, combustion chamber, and nozzle) are defined here (Fig. 5.21). Intake is located between states (1) to (2), while combustion chamber from (2) to (4) and finally nozzle from (4) to (6).

The cycle of events within the engine is described below (Fig. 5.22). Figure 5.22a illustrates ideal processes, while Fig. 5.22b illustrates actual processes experiencing losses.

State (a), stands for ambient, is far upstream of the engine. Diffusion process takes place in part outside of the engine and in part inside the engine. The first part of diffusion takes place from the far upstream, state (a) to the engine entrance, state (1). The second part of diffusion takes place inside the engine, from state (1) to state (2), where state (2) is at the end of the diffusion section. Air then enters the combustion chamber at subsonic speeds. This is achieved either through a strong normal shock wave or a multiple oblique shock waves followed by a normal shock wave. Fuel is next, injected as fine droplets which mixes rapidly with the mixture and next ignited by a spark. A “flame holder” at state (3) stabilizes the flame and facilitates a good combustion process. The flame holder may be of grill-type, which provides a type of barrier to the burning mixture while allowing hot, expanding

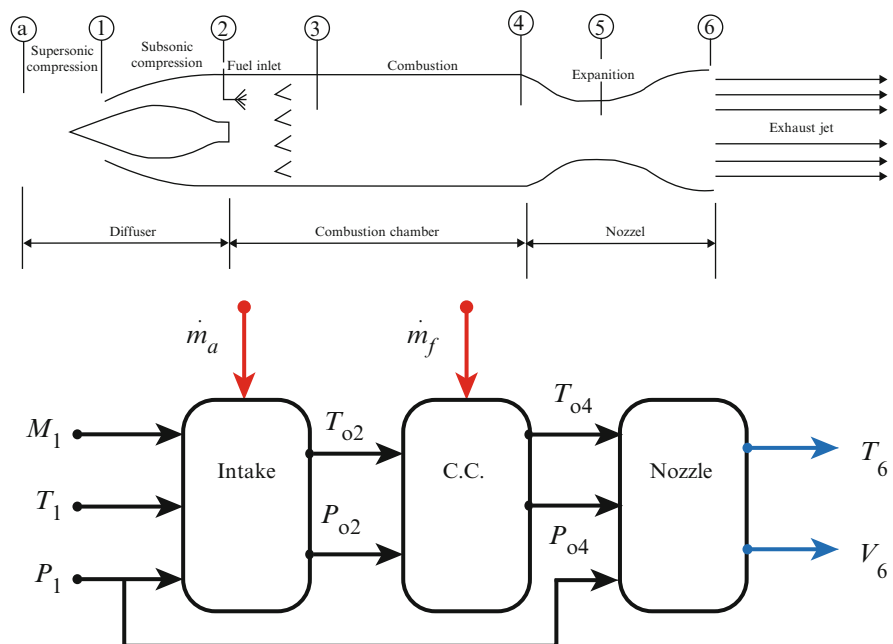


Fig. 5.21 Schematic drawing for a supersonic ramjet engine, its different states, and block diagram

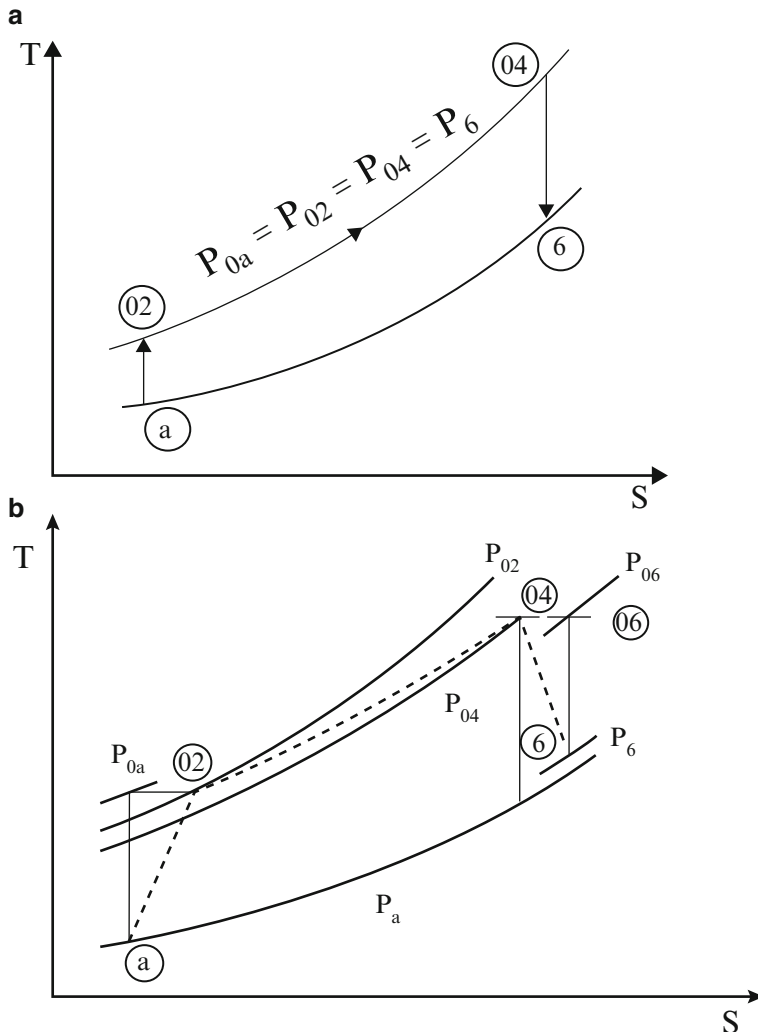


Fig 5.22 Thermodynamic cycle for a ramjet engine: (a) ideal, (b) real

gases to escape through the exhaust nozzle. The high-pressure air coming into the combustion chamber keeps the burning mixture from effectively reacting toward the intake end of the engine. Combustion raises the temperature of the mixture to some 2000–3000 K before the products of combustion expand to high velocities in the nozzle. Though the walls of combustion chambers cannot tolerate temperature much above 1200 K, but they can be kept much cooler than the main fluid stream by a fuel injection pattern that leaves a shielding layer of relatively cool air next to the walls [29]. The expansion process takes place at the third module of the engine, namely the nozzle. Most ramjet engines now have a convergent divergent (C-D)

nozzle as it is installed to supersonic flight vehicles. Expansion starts at the convergent section between state (4) and the nozzle throat, state (5). The nozzle has next a diverging section that ends at state (6). Sometimes state (6) is denoted by (e) resembling the exhaust or exit condition. The nozzle accelerates the flow, thus the exit velocity is greater than the free stream velocity, and so thrust is created.

5.3.4.1 Ideal Cycle

For ideal cycle, all the processes are assumed isentropic (reversible adiabatic) and no pressure drop will be encountered in the three modules of the engine, refer to Fig. 5.22a.

Total pressure is constant in the whole cycle; thus

$$P_{0a} = P_{02} = P_{04} = P_{06} \quad (5.27)$$

Moreover, since neither work nor heat addition or rejection takes place in the intake and nozzle, then from the first law of thermodynamics, equal total enthalpy (and thus total temperature) is presumed. Thus

$$\left. \begin{aligned} T_{0a} &= T_{02} \\ T_{04} &= T_{06} \end{aligned} \right\} \quad (5.28)$$

Nozzle is assumed unchoked, thus a full expansion of the hot gasses within the nozzle to ambient pressure is assumed, therefore

$$P_a = P_6 = P_e \quad (5.29)$$

The relation between total and static conditions (temperature and pressure) at the inlet and outlet of the engine, state (a) and (6 or e) are

$$\left. \begin{aligned} \frac{T_{0a}}{T_a} &= 1 + \frac{\gamma_a - 1}{2} M^2 = \frac{T_{02}}{T_a} \\ \frac{T_{0e}}{T_e} &= \frac{T_{06}}{T_6} = 1 + \frac{\gamma_6 - 1}{2} M_e^2 = \frac{T_{04}}{T_e} \end{aligned} \right\} \quad (5.30)$$

$$\left. \begin{aligned} \frac{P_{0a}}{P_a} &= \left(1 + \frac{\gamma_a - 1}{2} M^2 \right)^{\frac{\gamma_a}{\gamma_a - 1}} \\ \frac{P_{06}}{P_e} &= \left(1 + \frac{\gamma_6 - 1}{2} M_e^2 \right)^{\frac{\gamma_6}{\gamma_6 - 1}} \end{aligned} \right\} \quad (5.31)$$

In Eqs. (4.4) and (4.5) (γ_a, γ_6) are the specific heat ratios for air and exhaust gases respectively. If we assume constant values for (R, γ) within the engine, then from Eqs. (5.27) and (5.29), we get:

$$\frac{P_{06}}{P_e} = \frac{P_{0a}}{P_a} \quad (5.32)$$

Then from Eq. (5.31), we arrive at the relation:

$$M_e = M \quad (5.33)$$

Though inlet and exit Mach numbers are equal, but the exit speed is not equal to the flight speed as it is clear from Eq. (5.34a).

$$u_e = \frac{a_e}{a} u = \sqrt{\frac{\gamma_6 R T_e}{\gamma_a R T_a}} u \quad (5.34a)$$

Again, assuming constant (γ, R) within the engine, then

$$u_e = \sqrt{\frac{T_e}{T_a}} u \quad (5.34b)$$

From Eqs. (5.30) and (5.33), then

$$u_e = u \sqrt{\frac{T_{04}}{T_{0a}}} = u \sqrt{\frac{T_{04}}{T_{02}}} \quad (5.34c)$$

The fuel-to-air ratio (f):

Fuel-to-air ratio is derived from energy balance equation for the combustion process

$$\dot{m}_a h_{02} + \dot{m}_f Q_R = (\dot{m}_a + \dot{m}_f) h_{04}$$

$$Q_R = \text{heating value of the fuel} \quad \text{but} \quad T_{02} = T_{0a}$$

$$\therefore f = \frac{(C_{p4} T_{04}/C_{p2} T_{0a}) - 1}{(Q_R/C_{p2} T_{0a}) - (C_{p4} T_{04}/C_{p2} T_{0a})} \quad (5.35a)$$

For constant (γ, R) within the engine, then the fuel-to-air ratio is expressed by

$$f = \frac{C_p(T_{04} - T_{0a})}{Q_R - C_p T_{04}} \quad (5.35b)$$

The thrust force (T):

Since full expansion in the nozzle is assumed, i.e. $P_e = P_a$, then the thrust force is expressed as

$$T = \dot{m}_a(1+f)u_e - \dot{m}_a u$$

$$\frac{T}{\dot{m}_a} = (1+f)u_e - u = u \left[(1+f) \frac{u_e}{u} - 1 \right]$$

Now, from Eqs. (5.30) and (5.34), another relation can be written as

$$u_e = u \sqrt{\frac{T_{04}}{T_{0a}}} = u \sqrt{\frac{T_{04}}{T_a} \frac{T_a}{T_{0a}}} = u \sqrt{\frac{T_{04}}{T_a}} \sqrt{\frac{1}{1 + \frac{\gamma-1}{2} M^2}} \quad (5.36)$$

Then the thrust force can be expressed as

$$\frac{T}{\dot{m}_a} = M \sqrt{\gamma R T_a} \left[(1+f) \sqrt{\frac{T_{04}}{T_a}} \sqrt{\frac{1}{1 + \frac{\gamma-1}{2} M^2}} - 1 \right] \quad (5.37)$$

The thrust specific fuel consumption is

$$TSFC = \frac{\dot{m}_f}{T} = \frac{f}{T/\dot{m}_a} \quad (5.38)$$

5.3.4.2 Real Cycle

For a real cycle, stagnation pressure drop is encountered in the all modules; intake, combustion chamber and nozzle due to aerodynamic losses. Compression in the diffuser and expansion in the nozzle are adiabatic. Moreover, losses occur during combustion which is accounted for by combustion or burner efficiency. Figure 5.22b illustrates the effect of irreversibilities on the different processes in the cycle. Thus stagnations pressure ratios in diffuser, combustion chamber, and nozzle (r_d, r_c, r_n) are respectively defined as

$$r_d = \frac{P_{02}}{P_{0a}}, \quad r_c = \frac{P_{04}}{P_{02}}, \quad r_n = \frac{P_{06}}{P_{04}}$$

Then the overall stagnation pressure ratio is

$$\frac{P_{06}}{P_{0a}} = r_d r_c r_n \quad (5.39)$$

It will be shown here after that irreversibilities will lead to the inequality of the flight and exhaust Mach numbers. The properties (γ, R) of the fluid through the different parts of the engine are also assumed constant.

Now, since the stagnation pressure of the free stream is expressed as

$$\frac{P_{0a}}{P_a} = \left(1 + \frac{\gamma - 1}{2} M^2\right)^{\frac{\gamma}{\gamma-1}}$$

$$\left(\frac{P_a}{P_{0a}}\right)^{\frac{\gamma-1}{\gamma}} \left(1 + \frac{\gamma - 1}{2} M^2\right) = 1$$

And

$$\frac{P_{06}}{P_6} = \left(1 + \frac{\gamma - 1}{2} M_e^2\right)^{\frac{\gamma}{\gamma-1}}$$

$$\therefore M_e^2 = \frac{2}{\gamma - 1} \left[\left(\frac{P_{06}}{P_6}\right)^{\frac{\gamma-1}{\gamma}} - 1 \right]$$

$$M_e^2 = \left(\frac{2}{\gamma - 1}\right) \left[\left(1 + \frac{\gamma - 1}{2} M^2\right) \left(\frac{P_a}{P_{0a}}\right)^{\frac{\gamma-1}{\gamma}} \left(\frac{P_{06}}{P_6}\right)^{\frac{\gamma-1}{\gamma}} - 1 \right]$$

$$M_e^2 = \left(\frac{2}{\gamma - 1}\right) \left[\left(1 + \frac{\gamma - 1}{2} M^2\right) \left(\frac{P_{06} P_a}{P_6 P_{0a}}\right)^{\frac{\gamma-1}{\gamma}} - 1 \right]$$

Recalling Eq. (5.39), the exhaust Mach number is

$$M_e^2 = \left(\frac{2}{\gamma - 1}\right) \left[\left(1 + \frac{\gamma - 1}{2} M^2\right) \left(r_d r_c r_n \frac{P_a}{P_e}\right)^{\frac{\gamma-1}{\gamma}} - 1 \right] \quad (5.40a)$$

Now, define (m) as

$$m = \left(1 + \frac{\gamma - 1}{2} M^2\right) \left(r_d r_c r_n \frac{P_a}{P_e}\right)^{\frac{\gamma-1}{\gamma}} \quad (5.40b)$$

$$M_e^2 = \left(\frac{2}{\gamma - 1}\right) (m - 1) \quad (5.40c)$$

From Eq. (5.40c), another expression for (m) can be reached:

$$m = \left(1 + \frac{\gamma - 1}{2} M_e^2\right) \quad (5.40d)$$

If $r_d = r_c = r_n = 1$, and $P_e = P_a$, then from Eqs. (5.40b) and (5.40d), we get:

$$M_e = M$$

If heat transfer from the engine is assumed negligible (per unit mass of fluid) then the total exhaust temperature $T_{06} = T_{04}$

$$\begin{aligned}\frac{T_{06}}{T_6} &= \frac{T_{04}}{T_e} = \left(1 + \frac{\gamma - 1}{2} M_e^2\right) \\ u_e &= M_e \sqrt{\gamma R T_e} = M_e \sqrt{\gamma R T_{04} \frac{T_e}{T_{04}}} \\ u_e &= M_e \sqrt{\gamma R T_{04} / \left(1 + \frac{\gamma - 1}{2} M_e^2\right)} \\ u_e &= M_e \sqrt{\gamma R T_{04} / m}\end{aligned}$$

Substituting for M_e from Eq. (5.40c), then

$$u_e = \sqrt{\frac{2\gamma R T_{04} (m - 1)}{(\gamma - 1)m}} \quad (5.41)$$

Since irreversibilities have no effect on total temperatures throughout the engine, then the fuel-to-air ratio can be given by Eq. (5.35a), but modified for burner efficiency (η_b)

$$f = \frac{C_{p4} T_{04} - C_{p2} T_{0a}}{\eta_b Q_R - C_{p4} T_{04}} \quad (5.35c)$$

The specific thrust is expressed by the relation:

$$\frac{T}{\dot{m}_a} = [(1 + f)u_e - u] + \frac{A_e}{\dot{m}_a} (P_e - P_a) \quad (5.42)$$

Then since, $u = M \sqrt{\gamma R T_a}$, then specific thrust will be expressed as

$$\frac{T}{\dot{m}_a} = (1 + f) \sqrt{\frac{2\gamma_e R T_{04} (m - 1)}{(\gamma - 1)m}} - M \sqrt{\gamma R T_a} + \frac{P_e A_e}{\dot{m}_a} \left(1 - \frac{P_a}{P_e}\right) \quad (5.43)$$

From the above derived relations, the specific thrust and thrust specific fuel consumption (TSFC) are plotted in Fig. 5.23 for ideal and real engines. The ratio between specific heats is assumed constant $\gamma = 1.4$. The maximum temperatures investigated are $T_{04} = 2000K$ or $3000K$. The pressure ratios in the diffuser, combustion chamber, and nozzle are respectively $r_d = 0.7$, $r_c = 0.97$, and $r_n = 0.96$. The burner is assumed ideal $\eta_b = 1$ and fuel heating value is $Q_R = 43,000 \text{ kJ/kg}$.

For any given peak temperature, the thrust per unit mass flow rate \dot{m}_a , for real ramjet is less than the ideal. However, the TSFC for real is higher than the ideal. Also for real ramjet, there is a reasonably well-defined minimum TSFC.

Example 5.4 For an *ideal* ramjet engine, assuming negligible fuel-to-air ratio, prove that the specific thrust force is expressed by the relation:

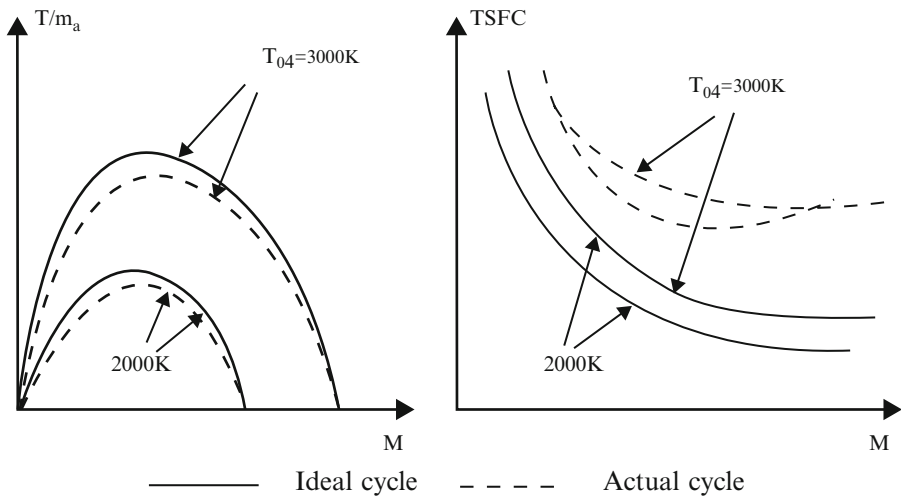


Fig. 5.23 Specific thrust and thrust specific fuel consumption for ideal and real ramjet engines

$$\frac{T}{\dot{m}} = \varphi M \left(\frac{\sqrt{T_{o\max}}}{\sqrt{1 + \frac{\gamma-1}{2} M^2}} - \sqrt{T_a} \right)$$

where $\varphi = \sqrt{\gamma R}$, and the ambient and maximum total temperatures in the cycle are expressed by $(T_a, T_{o\max})$. Moreover, the specific thrust attains a maximum value when the Mach number is expressed by

$$M = \sqrt{\left(\frac{2}{\gamma-1}\right)(\tau^{1/3} - 1)}$$

$$\text{where } \tau = \frac{T_{o\max}}{T_a}$$

Solution

The thrust force is expressed as

$$T = \dot{m} [(1+f)u_e - u]$$

Assuming a negligible fuel-to-air ratio, then

$$T = \dot{m} (u_e - u)$$

Since $u_e = M_e a_e = M_e \sqrt{\gamma R T_e}$

$$T_{\text{omax}} = T_e \left(1 + \frac{\gamma - 1}{2} M_e^2 \right) \quad (1)$$

and $u = Ma = M\sqrt{\gamma RT_a}$

$$\begin{aligned} \frac{T}{\dot{m}} &= (u_e - u) \\ \frac{T}{\dot{m}} &= \left(M_e \sqrt{\gamma RT_e} - M \sqrt{\gamma RT_a} \right) \end{aligned}$$

Since $M_e = M$, then

$$\begin{aligned} \frac{T}{\dot{m}} &= M \sqrt{\gamma R} \left(\sqrt{T_e} - \sqrt{T_a} \right) \\ \varphi &= \sqrt{\gamma R} \end{aligned}$$

From Eq. (1), then

$$\frac{T}{\dot{m}} = \varphi M \left(\frac{\sqrt{T_{\text{omax}}}}{\sqrt{1 + \frac{\gamma-1}{2} M^2}} - \sqrt{T_a} \right) \quad \#$$

At maximum thrust, then $\frac{\partial(T/\dot{m})}{\partial M} = 0$

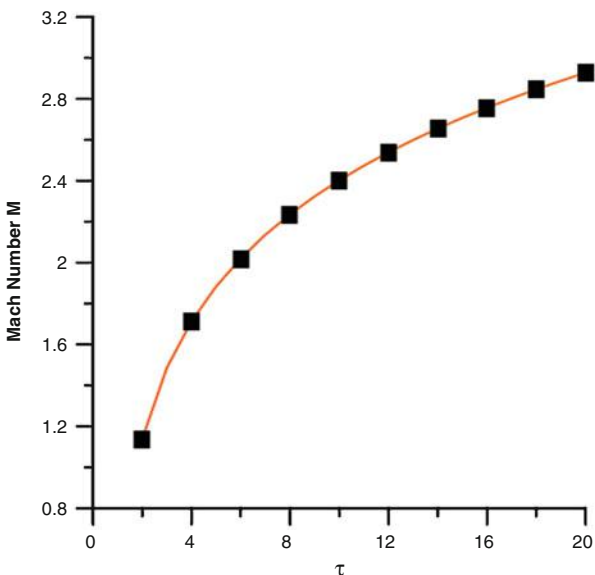
$$\begin{aligned} \frac{\partial(T/\dot{m})}{\partial M} &= \varphi \left(\frac{\sqrt{T_{\text{omax}}}}{\sqrt{1 + \frac{\gamma-1}{2} M^2}} - \sqrt{T_a} \right) - \frac{\varphi M}{2} \frac{\frac{\gamma-1}{2}(2M)}{(1 + \frac{\gamma-1}{2} M^2)^{3/2}} \sqrt{T_{\text{omax}}} = 0 \\ \sqrt{T_{\text{omax}}} \left(1 + \frac{\gamma-1}{2} M^2 \right) - \sqrt{T_a} \left(1 + \frac{\gamma-1}{2} M^2 \right)^{3/2} - \frac{\gamma-1}{2} M^2 \sqrt{T_{\text{omax}}} &= 0 \\ \left(1 + \frac{\gamma-1}{2} M^2 \right)^{3/2} &= \sqrt{\frac{T_{\text{omax}}}{T_a}} = \sqrt{\tau} \end{aligned}$$

Maximum thrust occurs at values of Mach number expressed by the relation

$$M = \sqrt{\left(\frac{2}{\gamma-1} \right) (\tau^{1/3} - 1)}$$

A plot for the Mach number and the corresponding temperature ratio (τ) is illustrated by Fig. 5.24 below.

Fig. 5.24 Plot of Mach number yielding maximum thrust for different ratios of maximum to ambient temperatures



Example 5.5 An ideal ramjet engine (as shown in Fig. 5.21) operates at an altitude where the ambient temperature and pressure are 216.7 k and 10.287 kPa.

The engine has the following data:

Thrust $T = 50.0\text{kN}$; Inlet area $A_i = 0.5\text{m}^2$; propulsive efficiency $\eta_p = 80\%$

Fuel heating value $Q_R = 43\text{ MJ/kg}$

Mach number in the inlet of combustion chamber $M_2 = 0.15$

Assume that $M_2 = M_3 = M_4 = 0.15$, and the specific heat ratio is assumed constant through the engine $\gamma = 1.4$, $C_p = 1005\frac{\text{J}}{\text{kg}\cdot\text{K}}$

Neglecting fuel-to-air ratio, calculate:

1. Flight speed and Mach number (V, M)
2. Exhaust speed and Mach number (V_6, M_6)
3. Maximum total temperature (T_{04})
4. Air mass flow rate
5. Area at the inlet to the combustion chamber (A_2)
6. Area at throat of the nozzle (A_5)
7. Plot static temperature, static pressure, total temperature, and total temperature at different stations of the engine
8. Plot the internal areas at different stations within the engine

Solution

Given data

Ideal cycle

$$T_a = 216.7\text{k}; \quad P_a = 10.287\text{kPa}$$

Thrust force: $F = 50.0 \text{ kN}$; $\eta_p = 0.8$

$$Q_R = 43 \text{ MJ/kg}; \quad M_2 = 0.15$$

$$A_i = 0.5 \text{ m}^2; \quad \gamma = 1.4 \quad \text{Constant}$$

For ideal ramjet cycle with negligible fuel-to-air Air ratio, then

$$M_i = M_6 = M$$

$$\eta_p = \frac{2V_a}{V_a + V_6} = 0.8$$

$$0.8(V_a + V_6) = 2V_a$$

$$V_6 = 1.5V_a$$

$$F = \dot{m}_a(V_6 - V_a) = \rho_a V_a A_i (1.5V_a - V_a) = 0.5 \rho_a V_a^2 A_i$$

$$V_a = \sqrt{\frac{2F}{\rho_a A_i}} = \sqrt{\frac{2F \times RT_a}{P_a A_i}} = \sqrt{\frac{2*50*10^3*287*216.7}{10.287*10^3*0.5}} = 1100 \text{ m/s}$$

Then $V_6 = 1.5V_a = 1650 \text{ m/s}$

$$M_a = \frac{V_a}{\sqrt{\gamma R T_a}} = 3.7278 = M_6$$

$$\text{From Eq. (5.34b), } \frac{T_6}{T_a} = \frac{V_6^2}{V_a^2} = (1.5)^2 = 2.25$$

$$T_6 = \frac{V_6^2}{\gamma R M_6^2} = 487.58 \text{ K}$$

$$T_{o4} = T_{o6} = T_6 \left(1 + \frac{\gamma - 1}{2} M_6^2 \right) = 487.58 \left(1 + \frac{1.4 - 1}{2} \times 3.7278^2 \right) \\ = 1842.71 \text{ K}$$

$$T_{o2} = T_{oa} = T_a \left(1 + \frac{\gamma - 1}{2} M_a^2 \right) = 216.7 \left(1 + \frac{1.4 - 1}{2} \times 3.7278^2 \right) = 818.974 \text{ K}$$

$$T_2 = \frac{T_{o2}}{1 + \frac{\gamma - 1}{2} M_2^2} = \frac{818.974}{1 + \frac{1.4 - 1}{2} \times 0.15^2} = 815.305 \text{ K}$$

$$P_{o6} = P_{o4} = P_{o2} = P_{oa} = P_a \left(1 + \frac{\gamma - 1}{2} M_a^2 \right)^{\frac{1}{\gamma-1}} = 1079.5 \text{ kPa}$$

$$P_2 = \frac{P_{o2}}{\left(1 + \frac{\gamma - 1}{2} M_2^2 \right)^{\frac{1}{\gamma-1}}} = 1062.66 \text{ kPa}$$

$$V_2 = M_2 \sqrt{\gamma R T_2} = 0.15 \sqrt{1.4 \times 287 \times 815.305} = 85.853 \text{ m/s}$$

$$\dot{m}_a = \rho_a V_a A_i = \frac{P_a}{R T_a} V_a A_i = \frac{10,287}{287 \times 216.7} \times 1100 \times 0.5 = 90.973 \text{ kg/s}$$

$$A_2 = \frac{\rho_a V_a A_i}{\rho_2 V_2} = \left(\frac{T_a}{T_2} \right)^{\frac{1}{\gamma-1}} \left(\frac{V_a}{V_2} \right) A_i = \left(\frac{216.7}{815.305} \right)^{\frac{1}{1.4-1}} \times \frac{1100}{85.853} \times 0.5$$

$$A_2 = 0.233 \text{ m}^2$$

$$A_6 = \frac{\rho_a V_a A_i}{\rho_6 V_6} = \frac{P_a}{RT_a} \frac{RT_6}{P_6} \frac{V_a}{V_6} A_i = \frac{T_6}{T_a} \frac{V_a}{V_6} A_i = \left(\frac{V_6}{V_a} \right)^2 \times \frac{V_a}{V_6} \times A_i$$

$$A_6 = \frac{V_6}{V_a} A_i = 1.5 A_i = 0.75 \text{ m}^2$$

$$T_5 = \frac{T_{o4}}{1 + \frac{\gamma-1}{2} M_5^2} = \frac{T_{o4}}{\frac{\gamma+1}{2}} = \frac{1842.71}{\frac{2.4}{2}} = 1535.5 \text{ K}$$

$$P_5 = \frac{P_{o4}}{\left(1 + \frac{\gamma-1}{2} M_5^2\right)^{\frac{\gamma}{\gamma-1}}} = \frac{P_{o4}}{\left(\frac{\gamma+1}{2}\right)^{\frac{\gamma}{\gamma-1}}} = \frac{1079.5}{\left(\frac{2.4}{2}\right)^{\frac{1.4}{0.4}}} = 570.28 \text{ kPa}$$

$$V_5 = a_{5-} \sqrt{\gamma RT_5} = \sqrt{1.4 \times 287 \times 1535.5} = 785.47 \text{ m/s}$$

$$A_5 = \frac{\rho_6 V_6 A_6}{\rho_5 V_5} = \left(\frac{T_6}{T_5} \right)^{\frac{1}{\gamma-1}} \frac{V_6}{\sqrt{\gamma RT_5}} A_6 = \left(\frac{487.58}{1535.5} \right)^{\frac{1}{0.4}} \times \frac{1650}{\sqrt{1.4 \times 287 \times 1535.5}} \times 0.75$$

$$A_5 = 0.0895 \text{ m}^2$$

$$P_4 = \frac{P_{o4}}{\left(1 + \frac{\gamma-1}{2} M_4^2\right)^{\frac{\gamma}{\gamma-1}}}$$

Assuming $M_4 = M_2 = 0.15$

$$P_4 = \frac{P_{o4}}{\left(1 + \frac{\gamma-1}{2} M_4^2\right)^{\frac{\gamma}{\gamma-1}}} = \frac{1079.5}{\left(1 + 0.2 \times 0.15^2\right)^{\frac{1.4}{0.4}}} = 1062.612 \text{ kPa}$$

$$T_4 = T_4 = \frac{T_{o4}}{1 + \frac{\gamma-1}{2} M_4^2} = \frac{1842.71}{1 + 0.2 \times 0.15^2} = 1834.45 \text{ K}$$

The density at state (4) $\rho_4 = \frac{P_4}{RT_4} = \frac{1062.612 \times 10^3}{287 \times 1834.45} = 2.018 \text{ m}^3/\text{kg}$

$$V_4 = M_4 \sqrt{\gamma RT_4} = 0.15 \sqrt{1.4 \times 287 \times 1834.45} = 128.14 \text{ m/s}$$

$$A_4 = \dot{m}_a / \rho_4 V_4 = 90.973 / (2.018 \times 128.14) = 0.3518 \text{ m}^2$$

State	a	2	3	4	5	6
Total temperature, K	818.97	818.97	818.97	1842.7	1842.7	1842.7
Total pressure kPa	1079.5	1079.5	1079.5	1079.5	1079.5	1079.5
Static Temperature, K	216.7	815.305	815.305	1834.45	1535.5	487.58
Static pressure, kPa	10.287	1062.612	1062.612	1062.612	570.28	10.287
Density, m^3/kg	0.1654	4.593	4.593	2.018	1.294	0.0735

(continued)

State	a	2	3	4	5	6
Area, m ²	0.5	0.233	0.233	0.3518	0.0895	0.75
Velocity, m/s	1100	85.853	85.853	128.14	785.47	1650
Mach number	3.7278	0.15	0.15	0.15	1.00	3.7278

The characteristics of air/gas flow within the ramjet engine at different stations are plotted in Figs. 5.25, 5.26, and 5.27.

5.3.5 Nuclear Ramjet

The principle behind the nuclear ramjet was relatively simple: The three basic components of ramjet engines are the same but a nuclear reactor is used to heat the air instead of burning fuel in a combustion chamber. Thus additional components

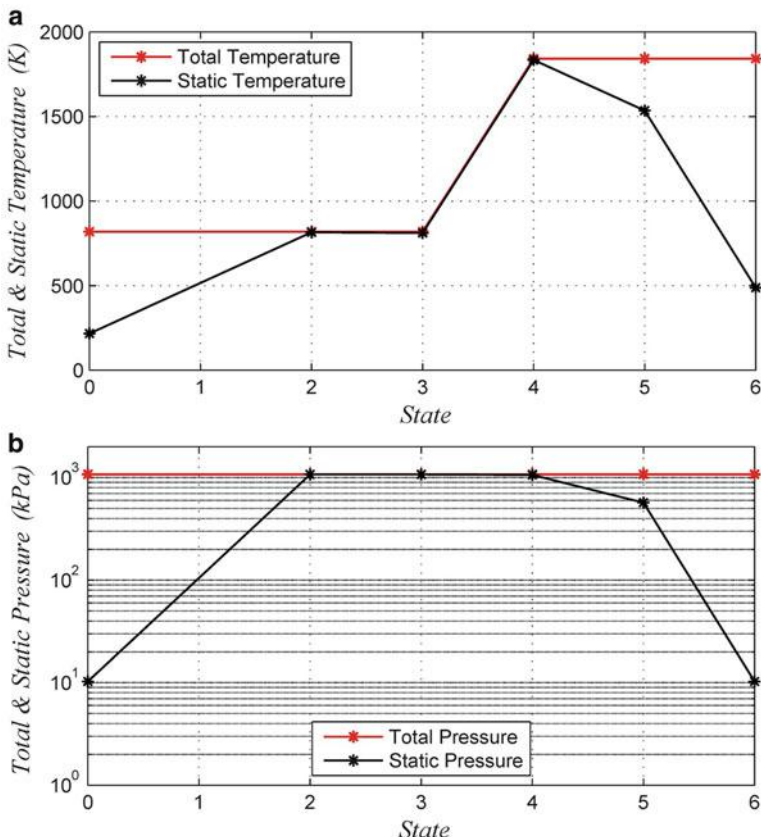


Fig. 5.25 Total and static temperature (a) and pressures (b)

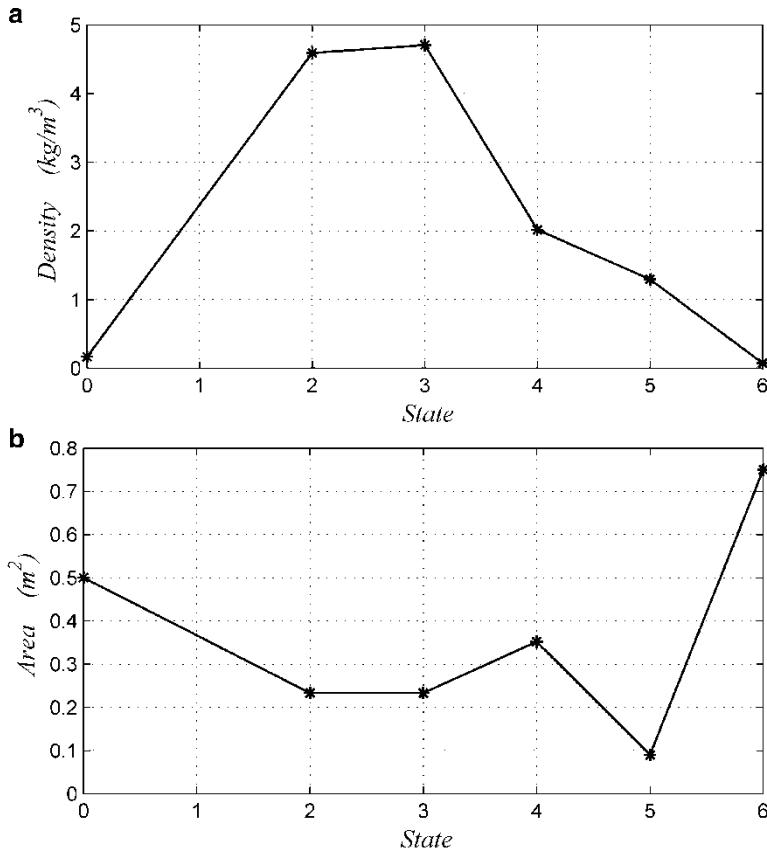


Fig. 5.26 Distribution of density (a) and internal area (b) along the ramjet states

are used in nuclear ramjets, namely, reactor core, radiation shield, and heat exchanger (Fig. 5.28a).

During 1950s and 1960s, there was a government program in the United States to develop **nuclear-powered ramjet** engines for use in **cruise missiles** namely *Project Pluto*. Two experimental engines were tested at the **United States Department of Energy Nevada Test Site (NTS)** in 1961 and 1964. Unlike commercial reactors, which are surrounded by concrete, the Pluto reactor had to be small and compact enough to fly, but durable enough to survive a 7000 mile (11,000 km) trip to a potential target. The nuclear engine could, in principle, operate for months, so a Pluto cruise missile could be left airborne for a prolonged time before being directed to carry out its attack. For many reasons, the project started on 1 January 1957 and cancelled on 1 July 1964.

Hybrid ramjet and scramjet engine are illustrated in Fig. 5.28b. Nuclear ramjet engine is located upstream of a scramjet engine. Exhaust of ramjet engine is pure air

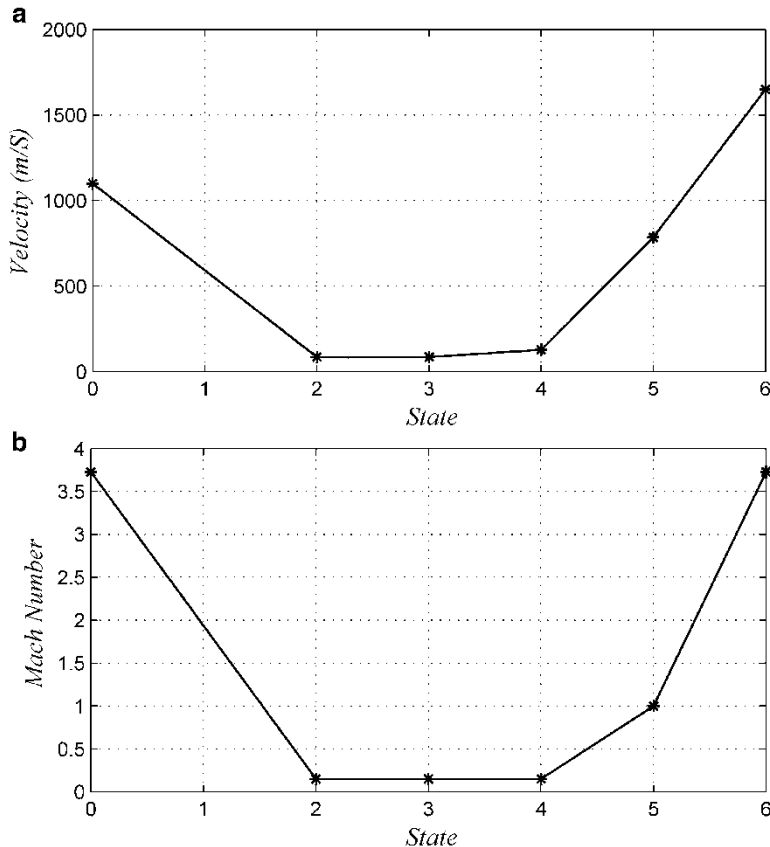


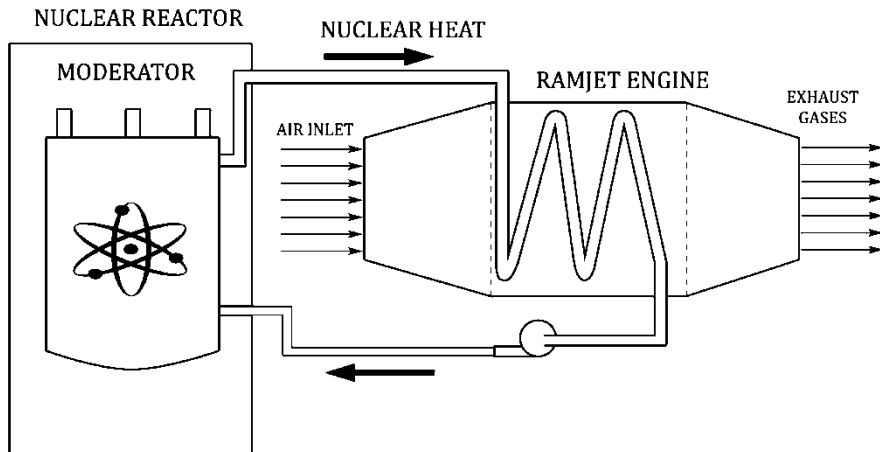
Fig. 5.27 Distribution of velocity (a) and Mach number (b) along the ramjet states

at supersonic speeds which flows into the intake of scramjet and next into a typical combustion chamber where either hydrocarbon or hydrogen fuel is added and burnt.

5.3.6 Double Throat Ramjet Engine

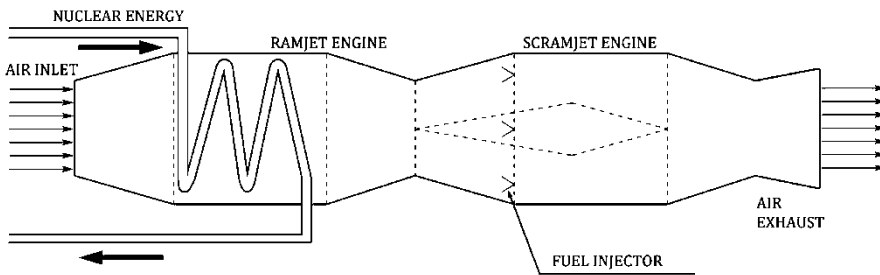
Double throat ramjet (DTR) engine (Fig. 5.29) flow stream needs to contain two throats: the first is to decelerate the flow to subsonic flow before the combustion chamber, and the second is to accelerate the flow to supersonic again in the nozzle.

Thus, DTR is composed of a supersonic-subsonic intake followed by a subsonic combustion chamber and a subsonic-supersonic nozzle. The supersonic flow in the intake is decelerated to subsonic through either a normal shock or a number of oblique shock waves ended by a normal shock wave in the first throat. Subsonic



Nuclear Energy Powered Ramjet

Fig. 5.28a Nuclear energy ramjet



Hybrid Ramjet & Scramjet Engine

Fig. 5.28b Hybrid ramjet and scramjet engine

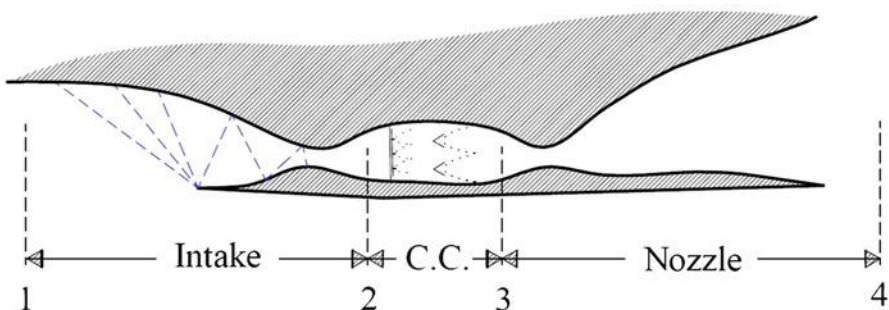
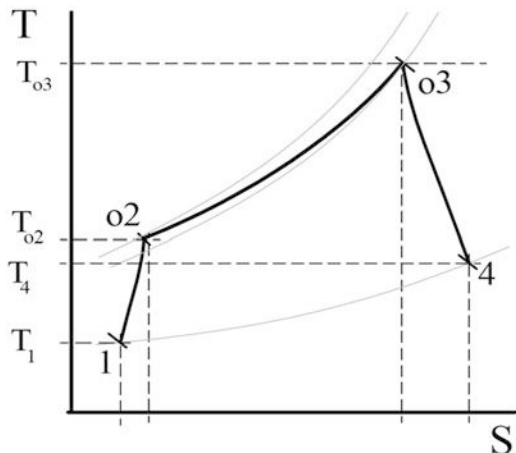


Fig. 5.29 Configuration of double-throat ramjet (DTR) engine

Fig. 5.30 T-s diagram for double-throat ramjet engine



constant pressure combustion chamber will follow. The subsonic flow leaving the combustion chamber is accelerated to supersonic speed in a convergent divergent nozzle (incorporating the second throat). The main parameters affecting the engine performance is the amount of heat added per unit mass of air passing through the engine, which can be calculated from the fuel-to-air ratio in the engine.

Figure 5.29 shows the engine configuration, and Fig. 5.30 shows the T.S diagram of ramjet engine.

5.4 Scramjet

5.4.1 Introduction

A *scramjet* (supersonic combustion *ramjet*) is a variant of a *ramjet airbreathing jet engine* in which combustion takes place in *supersonic* airflow [30–32]. Thus, the airflow through the whole engine remains supersonic. Due to the nature of its design, scramjet operation is limited to *near-hypersonic* velocities. Thus, a scramjet-powered vehicle must be accelerated to the required velocity by some other means of propulsion, such as turbojet, *rail gun*, or rocket engines. In the flight of the experimental scramjet-powered *Boeing X-51A*, the test craft was lifted to flight altitude by a *Boeing B-52 Stratofortress* before being released and accelerated by a detachable rocket to near Mach 5.1 for 210 s on 1 May 2013 for the longest duration hypersonic flight [30, 31].

Scramjet like ramjet is also composed of *three basic components*, namely: inlet (or intake), combustor and nozzle. While scramjets are conceptually simple, actual implementation is limited by extreme technical challenges:

1. Only limited testing can be performed in ground facilities. Long duration, full-scale testing requires flight test speeds above Mach 6.
2. Hypersonic flight within the atmosphere generates immense drag, and temperatures (heat barrier) found on the aircraft and within the engine [2, 3]
3. Maintaining combustion in the supersonic, as the fuel must be injected, mixed, ignited, and burned within milliseconds [33].

Two families of operational application can be seen for high-speed air-breathing propulsion, namely:

- Combined airbreathing/rocket propulsion for space launcher
- Military systems, mainly missiles and drone

Aerospace industries follow now the motto of “The sky is no longer the limit.”

Concerning flight speeds or Mach numbers, scramjet engines are employed for Mach numbers greater than 5.0, ramjet engines are used for a Mach number range of (0.5–5.5), while turbine-based engines are installed to vehicles flying at Mach numbers up to 3.0 [34].

5.4.2 Evolution of Scramjets

The evolution of the scramjet engine started in the 1940s is elegantly reviewed in several articles including those by John Bertin [34], Rife and Cantelon [35], Hallion’s report [36], Waltrup et al. [37] Curran [38], and Segal [39]. These developments will be quickly highlighted here below

- In *1940s*, research and development (R&D) in different institutions in USA and Canada began to develop scramjet powered flights. [37].
- In *1944*, Swithenbank and McGill University, Canada, published early work on scramjet inlets, fuel injection, combustion, and nozzles focusing on hypersonic flight Mach numbers of between 10 and 25.
- In the *1950s and 1960s*, a variety of experimental scramjet engines were built and ground tested in the USA and the UK.
- In *1957*, Avery and Dugger started an analytical and experimental study of scramjet engines and their potential [38].
- In *1958*, Weber and MacKay published an analysis on the feasibility, benefits, and technical challenges to scramjet powered flight (Mach 4–7).
- In *1964*, Dr. [Frederick S. Billig](#) and Dr. Gordon L. Dugger submitted a patent application for a scramjet that was based on Billig’s PhD thesis. This patent was issued in 1981 following the removal of an order of secrecy.
- In the *1980s*, the National Aero-space Plane (X-30) project envisioned a single stage to orbit (SSTO) airplane, which could take off and land horizontally. The plane’s engine was a scramjet engine powered by hydrogen. However, the project was canceled in 1993.

- In 1981, experimental scramjets were made and tested in Australia under the guidance of Professor Ray Stalker in the T3 ground test facility at Australia's national university (ANU).
- In 1991, the first successful flight test of a scramjet was performed by *Russia*. It was an axisymmetric hydrogen-fueled dual-mode scramjet developed by [Central Institute of Aviation Motors \(CIAM\)](#), Moscow, in the late 1970s. The scramjet flight was flown captive-carry atop the [SA-5 surface-to-air missile](#) that included an experiment flight support unit known as the "Hypersonic Flying Laboratory" (HFL), Kholod [40].
- From 1992 to 1998, an additional six flight tests of the axisymmetric high-speed scramjet-demonstrator were conducted by CIAM together with France and then with NASA, USA. Maximum flight velocity greater than Mach 6.4 was achieved and Scramjet operation during 77 s was demonstrated. These flight test series also provided insight into autonomous hypersonic flight controls.
- In 2000 and 2001, the AFRL and P&W ground tested the first uncooled liquid hydrocarbon-fueled scramjet performance test engine (PTE) at simulated flight Mach numbers of 4.5 and 6.5 in 2000 and 2001 [41]. This was followed by the first successful ground test of a flight-weight, fuel-cooled scramjet engine at the same flight conditions in 2003.
- In the interval 2001–2006, the Australian project (*HyShot*) of The [University of Queensland, Australia](#), demonstrated the possibility of supersonic combustion of scramjet engines [42]. Two stage Terrier- Orion Mk70 rocket carrying a scramjet engine in its nosecone. The first successful launch (Hyshot II) was of a University of Queensland scramjet on 30 July 2002. A second successful flight (HyShot III) using a [QinetiQ](#) scramjet was achieved on 25 March 2006. The later QinetiQ prototype is cylindrical with four stainless steel combustors around the outside. The HyShot IV flight on 30 March 2006 launched successfully. The scramjet engine of [HyShot](#) project was not designed to provide thrust to propel a craft.
- In 2004 and making use of the research and development for the X-30, the X-43 hydrogen-fueled hypersonic research aircraft succeeded in its flight test. The X-43 was designed and built to be an unmanned system [41]. A Pegasus booster launched from a B-52 was used to achieve to the correct altitude and speed prior to igniting the X-43 scramjet engine (Fig. 5.31). Thus, the X-43A was able to reach and maintain a record speed of Mach 9.68 at 112,000 ft.
- On 27 May 2010, [NASA](#) and the [United States Air Force](#) successfully flew the [X-51A Waverider](#) for approximately 200 s at Mach 5, setting a new world record hypersonic airspeed. The Waverider flew autonomously before losing acceleration for an unknown reason and destroying itself as planned. The test was declared a success. The X-51A was carried aboard a [B-52](#), accelerated to Mach 4.5 via a solid rocket booster, and then ignited the Pratt & Whitney Rocketdyne scramjet engine to reach Mach 5 at 70,000 ft.
- In May 2013, X-51A reached "4828 km/h" (Mach 5.1) during 210 s flight under scramjet power.
- Other hypersonic programs [43] are available in Germany, India [44], and Brazil [45].

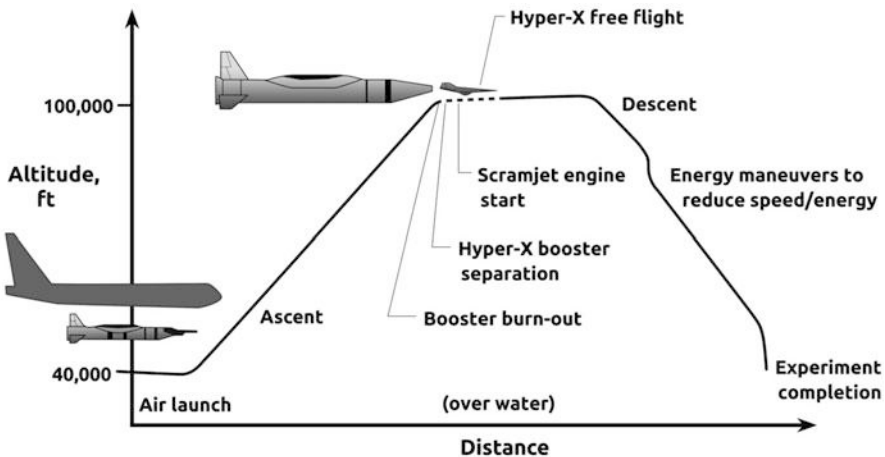


Fig. 5.31 Hyper-X flight envelope

5.4.3 Advantages and Disadvantages of Scramjets

(A) Advantages

1. Does not have to carry oxygen
2. No rotating parts makes it easier to manufacture
3. Has a higher specific impulse (change in momentum per unit of propellant) than a conventional engine; could provide between 1000 and 4000 s, while a rocket only provides 600 s or less
4. Higher speed could mean cheaper access to outer space in the future

(B) Disadvantages

1. Cannot produce efficient thrust unless boosted to high speed, around Mach 5. For a horizontal take-off, scramjet would need either a rocket or combined propulsion systems like turbojet/turbofan to boost it to Mach numbers (2–3) followed by another propulsion method like ramjets or rockets.
2. Testing scramjet designs use extremely expensive hypersonic test chambers or expensive launch vehicles, both of which lead to high instrumentation costs. Launched test vehicles very typically end with destruction of the test item and instrumentation.
3. Lack of stealth as the vehicle would be very hot due to its high speed within the atmosphere and it would be easy to be detected with infrared sensors
4. The increased cooling requirements of scramjet engines result in lower efficiency.

5.4.4 Aero-Thermodynamic Analysis of Scramjets

Scramjet engine is similar to ramjet engine while having supersonic combustion to overcome the overheating problems –thermal barrier – that appear when

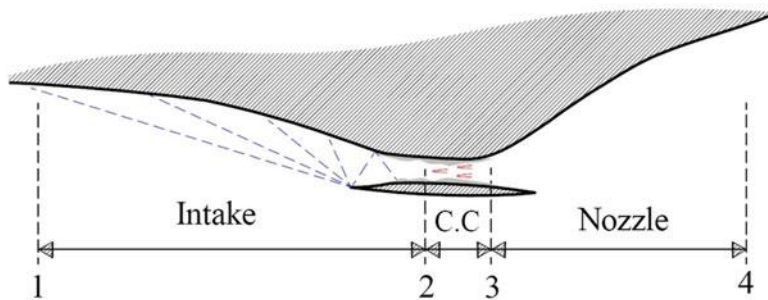
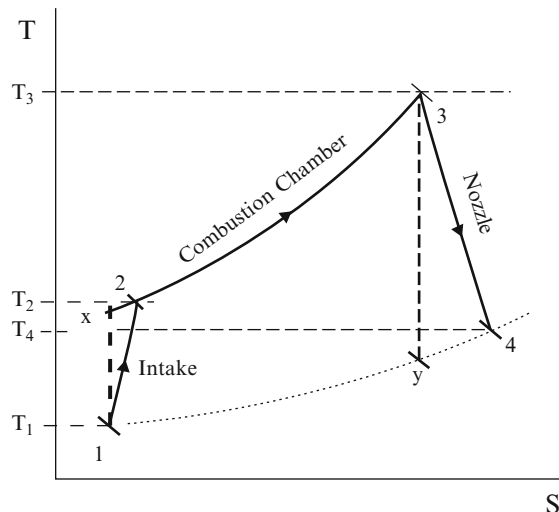


Fig. 5.32 Configuration of scramjet engine

Fig. 5.33 T-s diagram for scramjet engine



decelerating high Mach number flow to subsonic flow. The model for scramjet engine (Fig. 5.32) is composed of supersonic-supersonic intake followed by a constant area supersonic combustion chamber and a divergent nozzle. The flow will not go through chocking or critical conditions to prevent flow deceleration. The parameters affecting the cycle performance are the burner Mach number, the air mass flow rate, and the fuel mass flow rate. The thermodynamic behavior is illustrated by the T-S diagram as shown in Fig. 5.33.

Different states on the engine and T-s diagram are described as follows:

Station 1: Represents the inlet of the intake which is also the beginning of compression process. Since the hypersonic shock-wave angles are small, the ramps (in 2-D inlets) or spikes (for axisymmetric configurations) are long. In many of the suggested configurations, shock waves begin at the vehicle's leading edge. Additional compression takes place inside the inlet duct.

Station 2: Represents the combustion chamber entrance. In a fixed-geometry scramjet, the pressure at the combustion chamber entrance varies over a large range.

Station 3: Represents the combustion chamber exit and the beginning of expansion.

Station 4: Represents the exit from the nozzle; because of the large expansion ratios, the entire aft part of the vehicle may be part of the engine nozzle.

5.4.4.1 Intake

The flow through intake is modeled as variable area supersonic adiabatic flow with isentropic efficiency. The Mach number at intake is used as cycle parameter and is used to obtain contraction ratio through the intake, pressure, and temperature leaving the intake. Definition of Intake isentropic compression efficiency is stated in Eq. (5.44) and Fig. 5.33. The intake output parameters are calculated using Eqs. (5.45), (5.46), and (5.47).

$$\eta_I = \frac{T_x - T_1}{T_2 - T_1} \quad (5.44)$$

$$\frac{A_2}{A_1} = \frac{M_1}{M_2} \left(\frac{1 + 0.5 \times (\gamma_c - 1) M_1^2}{1 + 0.5 \times (\gamma_c - 1) M_2^2} \right)^{\frac{\gamma_c + 1}{2(\gamma_c - 1)}} \quad (5.45)$$

$$T_2 = T_1 \left(\frac{1 + 0.5 \times (\gamma_c - 1) M_1^2}{1 + 0.5 \times (\gamma_c - 1) M_2^2} \right) \quad (5.46)$$

$$P_2 = P_1 \left(1 + \eta_I \left(\frac{T_2}{T_1} - 1 \right) \right)^{\frac{\gamma_c}{\gamma_c - 1}} \quad (5.47)$$

Inlet total pressure recovery is modeled using MIL Spec E-5007D, which provides the following correlations:

$$\frac{P_{02}}{P_{01}} = 1.0 \quad (0 \leq M_1 \leq 1.0) \quad (5.48a)$$

$$\frac{P_{02}}{P_{01}} = 1.0 - 0.0776 (M_1 - 1)^{1.35} \quad (1.0 < M_1 < 5.0) \quad (5.48b)$$

$$\frac{P_{02}}{P_{01}} = 800 / (M_1^4 + 935) \quad (5.0 < M_1) \quad (5.48c)$$

5.4.4.2 Burner

The burner is modeled as constant area Rayleigh flow with the heat addition. Heat added in combustion chamber must be less than the critical value to prevent thermal shocking and flow deceleration. The flow properties downstream the combustion

chamber are obtained using Rayleigh and energy relations that can be expressed by Eqs. (5.49), (5.50), (5.51), and (5.52).

$$T_{o3} = \frac{\dot{m}_f \eta_b Q_{HV}}{C_{ph}(\dot{m}_a + \dot{m}_f)} + \frac{\dot{m}_a C_{pc} T_2}{C_{ph}(\dot{m}_a + \dot{m}_f)} (1 + 0.5 \times (\gamma_c - 1) M_2^2) \quad (5.49)$$

$$\frac{T_{o3}}{T_{o2}} = \frac{M_3^2}{M_2^2} \left(\frac{1 + \gamma_c M_2^2}{1 + \gamma_h M_3^2} \right)^2 \left(\frac{1 + 0.5 \times (\gamma_h - 1) M_3^2}{1 + 0.5 \times (\gamma_c - 1) M_2^2} \right) \quad (5.50)$$

$$P_3 = P_2 \frac{1 + \gamma_c M_2^2}{1 + \gamma_h M_3^2} \quad (5.51)$$

$$T_3 = \frac{T_{o3}}{1 + 0.5 \times (\gamma_h - 1) M_3^2} \quad (5.52)$$

From energy balance in Eq. (5.49), the maximum total temperature in engine (T_{o3}) is determined. Next, the Mach number at exit of combustion chamber is determined by trial and error from Eq. (5.50). Static temperature and pressure at exit of combustion chamber are calculated using Eqs. (5.51) and (5.52).

5.4.4.3 Nozzle

Nozzle flow is modeled as adiabatic expansion with isentropic efficiency which is defined in Eq. (5.53) and Fig. 5.33. Assuming complete expansion in the leaving jet, properties can be calculated using Eqs. (5.54) and (5.55).

Figure 5.34 shows block diagram for scramjet engine.

$$\eta_N = \frac{T_3 - T_4}{T_3 - T_y} \quad (5.53)$$

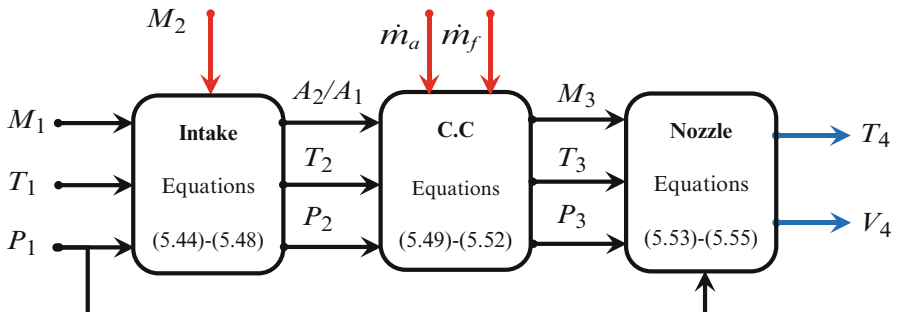


Fig. 5.34 Block diagram for scramjet engine

$$T_4 = T_3 - T_3 \eta_N \left(1 - \left(\frac{P_1}{P_3} \right)^{\frac{\gamma_h - 1}{\gamma_h}} \right) \quad (5.54)$$

$$V_4 = \sqrt{2C_{Ph}(T_{o3} - T_4)} \quad (5.55)$$

5.4.5 Performance Analysis

Cycle performance is defined by evaluating the generated thrust and quantity of burnt fuel. The corresponding propulsive, thermal, and overall efficiencies are next calculated. Finally, the specific impulse of the cycle is evaluated.

The thrust force is expressed by the relation:

$$T = (\dot{m}_a + \dot{m}_f)V_4 - \dot{m}_a V_1 \quad (5.56)$$

The specific thrust is then obtained by division of the thrust by air mass flow rate

$$T / \dot{m}_a = (1+f)V_4 - V_1 \quad (5.57)$$

Thrust specific fuel consumption (TSFC) is obtained from the relation

$$TSFC = \frac{\dot{m}_f}{T} = \frac{f}{T/\dot{m}_a} \quad (5.58)$$

The propulsive efficiency, which is defined as the engine exit energy realized out of the total energy available, will be expressed as

$$\begin{aligned} \eta_{pr} &= \frac{T \cdot V_1}{\Delta(K.E)} = \frac{2V_1((\dot{m}_a + \dot{m}_f)V_4 - \dot{m}_a V_1)}{\dot{m}_a(1+f)V_4^2 - \dot{m}_a V_1^2} \\ \eta_P &= \frac{2V_1 \times V_4(1+f) - 2V_1^2}{(1+f)V_4^2 - V_1^2} \end{aligned} \quad (5.59a)$$

Neglecting the fuel to air ratio ($f \ll 1$), then

$$\eta_P = \frac{2V_1}{V_1 + V_4} \quad (5.59b)$$

Thermal efficiency is defined as the kinetic energy increment across the entire engine normalized by the amount of energy contained in the fuel consumed:

$$\eta_{th} = \frac{\Delta(K.E)}{\dot{Q}_{add}} = \frac{\dot{m}_a(1+f)V_4^2 - \dot{m}_a V_1^2}{2\dot{m}_f \eta_{cc} Q_{HV}} = \frac{(1+f)V_4^2 - V_1^2}{2f \eta_{cc} Q_{HV}} \quad (5.60a)$$

With ($f \ll 1$), then the thermal efficiency can be approximated as

$$\eta_{th} = \frac{V_4^2 - V_1^2}{2f\eta_{cc}Q_{HV}} \quad (5.60b)$$

The overall efficiency is given by the relation

$$\eta_0 = \eta_P \times \eta_{th} \quad (5.61)$$

The specific impulse is defined as thrust-to-air mass flow rate

$$I_{SP} = \frac{T}{\dot{m}g} \quad (5.62)$$

Example 5.6 A scramjet engine is used to power a hypersonic vehicle that flies at an altitude of 27,000 m; flight Mach number is $M_1 = 6$; Mach number at inlet to combustion chamber is $M_2 = 2.5$; fuel-to-air ratio $f = 0.01$; and component efficiencies are as follows:

- Intake efficiency η_I 92 %
- Burner efficiency η_b 95 %
- Nozzle efficiency η_N 97 %

Calculate

1. Specific thrust and thrust specific fuel consumption
2. Thermal efficiency, propulsive efficiency, and overall efficiency
3. Area ratio $\left(\frac{A_2}{A_1}\right)$
4. Specific impulse
5. Predict and plot cycle performance for
 - Mach number ranges from (4) to (7)
 - fuel-to-air ratios of $f = 0.002, 0.006$, and 0.025

Solution

Figures 5.35a and 5.35b illustrate layout and T-s diagram of the scramjet engine.

At altitude 21,000 m

Temperature and pressure are

$$T_1 = 222.66 \text{ K} \quad P_1 = 1823 \text{ Pa}$$

$$V_1 = M_1 \sqrt{\gamma_c R T_1} = 1794.6 \text{ m/s}$$

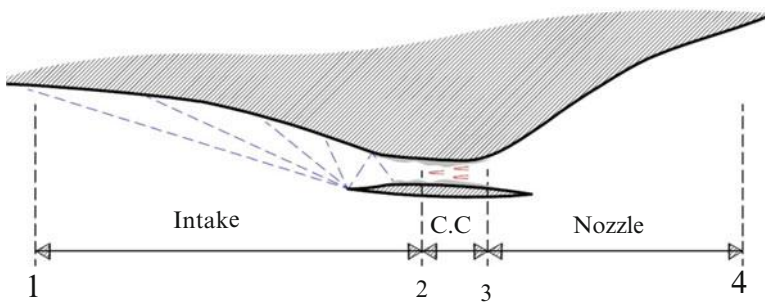
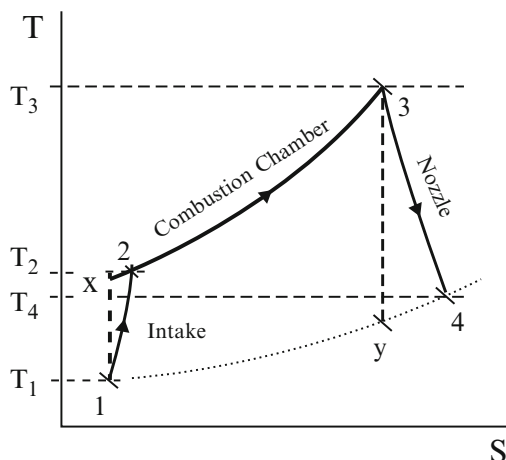


Fig. 5.35a Scramjet engine

Fig. 5.35b T-s diagram for scramjet engine



1. Intake

With: $M_1 = 6.0$ and $M_2 = 2.5$, then the static and total temperatures as well as the static pressure at intake outlet are calculated as follows:

$$T_2 = T_1 \left(\frac{1 + 0.5 \times (\gamma_c - 1) M_1^2}{1 + 0.5 \times (\gamma_c - 1) M_2^2} \right) = 222.66 \left(\frac{1 + 0.5 \times (1.4 - 1) \times 6^2}{1 + 0.5 \times (1.4 - 1) \times 2.5^2} \right) \\ = 811.47 K$$

$$T_{02} = T_2 (1 + 0.5 \times (\gamma_c - 1) M_2^2) = 1,825.812 K \equiv T_{01}$$

$$P_2 = P_1 \left(1 + \eta_I \left(\frac{T_2}{T_1} - 1 \right) \right)^{\frac{\gamma_c}{\gamma_c - 1}} = 1823 \left(1 + 0.92 \times \left(\frac{811.47}{222.66} - 1 \right) \right)^{\frac{1.4}{0.4}} \\ = 136,644 \text{ Pa}$$

$$P_2 = 136.44 \text{ kPa}$$

2. Combustion Chamber

With fuel-to-air ratio ($f = 0.01$) and fuel heating value $Q_{HV} = 119 \text{ MJ/kg}$, then from Eq. (5.49), the maximum total temperature in the combustion chamber and also engine is

$$\begin{aligned} T_{o3} &= \frac{f\eta_b Q_{HV}}{C_{Ph}(1+f)} + \frac{C_{Pc}T_{02}}{C_{Ph}(1+f)} = \frac{f\eta_b Q_{HV}}{C_{Ph}(1+f)} + \frac{C_{Pc}T_2(1+0.5(\gamma_c - 1)M_2^2)}{C_{Ph}(1+f)} \\ &= \frac{0.01 \times 0.95 \times 119E6}{1,148 \times 1.01} + \frac{1,005 \times 811.47 \times (1 + 0.5 \times 0.4 \times 2.5^2)}{1,148 \times 1.01} \\ T_{o3} &= 2,556.8 \text{ K} \end{aligned}$$

Mach number at outlet of combustion chamber (M_3) is calculated from the equation:

$$\begin{aligned} \frac{T_{o3}}{T_{o2}} &= \frac{M_3^2}{M_2^2} \left(\frac{1 + \gamma_c M_2^2}{1 + \gamma_h M_3^2} \right)^2 \left(\frac{1 + 0.5(\gamma_h - 1)M_3^2}{1 + 0.5(\gamma_c - 1)M_2^2} \right) \\ \frac{2556.8}{1,825.8} &= \frac{M_3^2}{2.5^2} \left(\frac{1 + 1.4 \times 2.5^2}{1 + 1.33 \times M_3^2} \right)^2 \left(\frac{1 + 0.5 \times 0.33 \times M_3^2}{1 + 0.5 \times 0.4 \times 2.5^2} \right) \end{aligned}$$

Using trial and error $M_3 = 1.25$

The corresponding static pressure and temperature at nozzle inlet are calculated from the following relations:

$$\begin{aligned} P_3 &= P_2 \frac{1 + \gamma_c M_2^2}{1 + \gamma_h M_3^2} = 136.644 \left(\frac{1 + 1.4 \times 2.5^2}{1 + 1.33 \times 1.25^2} \right) = 432.1 \text{ kPa} \\ T_3 &= \frac{T_{o3}}{1 + 0.5(\gamma_h - 1)M_3^2} = \frac{2556.8}{1 + 0.5 \times 0.33 \times 1.25^2} = 2,028.6 \text{ K} \end{aligned}$$

3. Nozzle

Static temperature and velocity of exhaust (at nozzle outlet) are calculated as follows:

$$\begin{aligned} T_4 &= T_3 - T_3 \eta_N \left(1 - \left(\frac{P_1}{P_3} \right)^{\frac{\gamma_h - 1}{\gamma_h}} \right) \\ &= 2,028.6 - 2,028.6 \times 0.97 \left(1 - \left(\frac{1823}{432.1E3} \right)^{\frac{0.33}{1.33}} \right) \\ T_4 &= 562.4 \text{ K} \end{aligned}$$

$$V_4 = \sqrt{2C_{Ph}(T_{o3} - T_4)} = \sqrt{2 \times 1148(2556.8 - 562.4)} = 2,139.9 \text{ m/s}$$

Thrust force is then

$$T = (\dot{m}_a + \dot{m}_f)V_4 - \dot{m}_a V_1$$

Specific thrust

$$\frac{T}{\dot{m}_a} = (1+f)V_4 - V_1 = 366.72 \frac{\text{N.s}}{\text{kg}}$$

Thrust specific fuel consumption

$$TSFC = \frac{\dot{m}_f}{T} = \frac{f}{\frac{T}{\dot{m}_a}} = 2.73E^{-5} \frac{\text{kg.s}}{\text{N}}$$

Thermal efficiency

$$\eta_{th} = \frac{\Delta(K.E)}{\dot{Q}_{\text{add}}} = \frac{\dot{m}_a(1+f)V_4^2 - \dot{m}_a V_1^2}{2Q_{HV}\dot{m}_f\eta_{cc}} = \frac{(1+f)V_4^2 - V_1^2}{2Q_{HV}f\eta_{cc}} = 62.11\%$$

Propulsive efficiency

$$\begin{aligned} \eta_{pr} &= \frac{T \cdot V_1}{\Delta(K.E)} = \frac{2V_1((\dot{m}_a + \dot{m}_f)V_4 - \dot{m}_a V_1)}{\dot{m}_a(1+f)V_4^2 - \dot{m}_a V_1^2} = \frac{2V_1 \times V_4(1+f) - 2V_1^2}{(1+f)V_4^2 - V_1^2} \\ &= 93.72\% \end{aligned}$$

Overall efficiency

$$\eta_o = \frac{T \cdot V_1}{\dot{Q}_{\text{add}}} = \eta_{pr} \cdot \eta_{th} = 58.21\%$$

Area ratio of intake is

$$\frac{A_1}{A_2} = \frac{M_1}{M_2} \left(\frac{1 + 0.5(\gamma_c - 1)M_1^2}{1 + 0.5(\gamma_c - 1)M_2^2} \right)^{\frac{\gamma_c + 1}{2(\gamma_c - 1)}} = \frac{6}{2.5} \left(\frac{1 + 0.5 \times 0.4 \times 6^2}{1 + 0.5 \times 0.4 \times 2.5^2} \right)^{\frac{2.4}{2 \times 0.4}} = 0.224$$

Specific Impulse

$$I_{SP} = \frac{\frac{T}{\dot{m}_a}}{fg} = \frac{366.72}{0.01 \times 9.81} = 3738 \text{ s}$$

Figure 5.36 presents the requested variables versus flight Mach number.

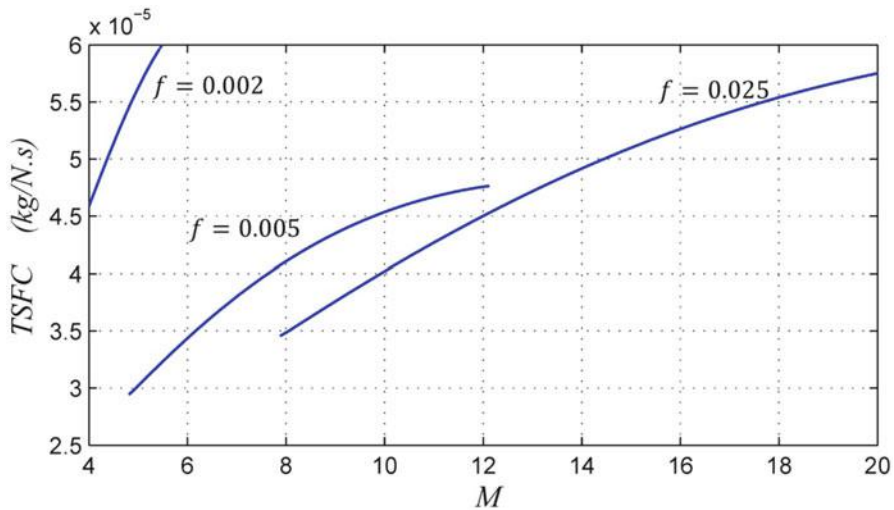


Fig. 5.36a TSFC versus flight Mach number

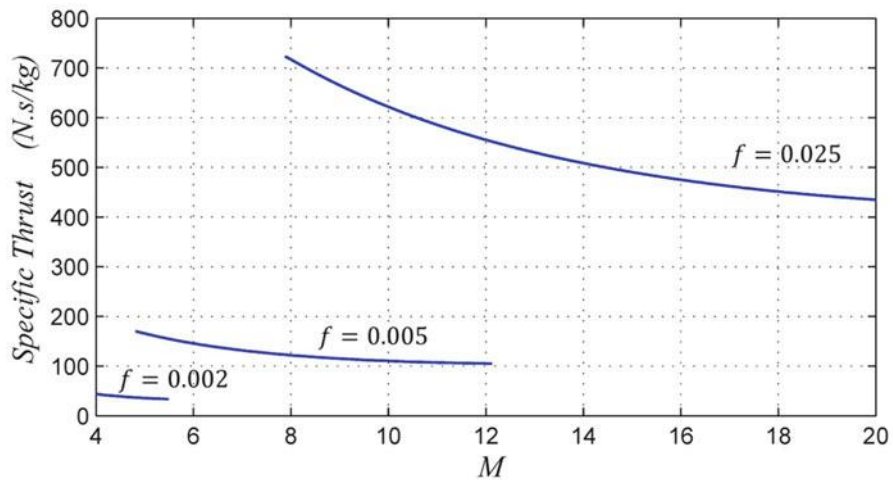


Fig. 5.36b Specific thrust versus flight Mach number

5.4.6 Dual-Mode Combustion Engine (Dual Ram-Scramjet)

5.4.6.1 Introduction

Dual-mode ramjet (DRM), which is also identified as dual-mode scramjets, is a ramjet that operates as ramjet at low supersonic speeds and transforms into a scramjet at high Mach numbers. It normally operates in the lower hypersonic regime between Mach 4 and 8. In ramjet operations, air flow needs to contain two

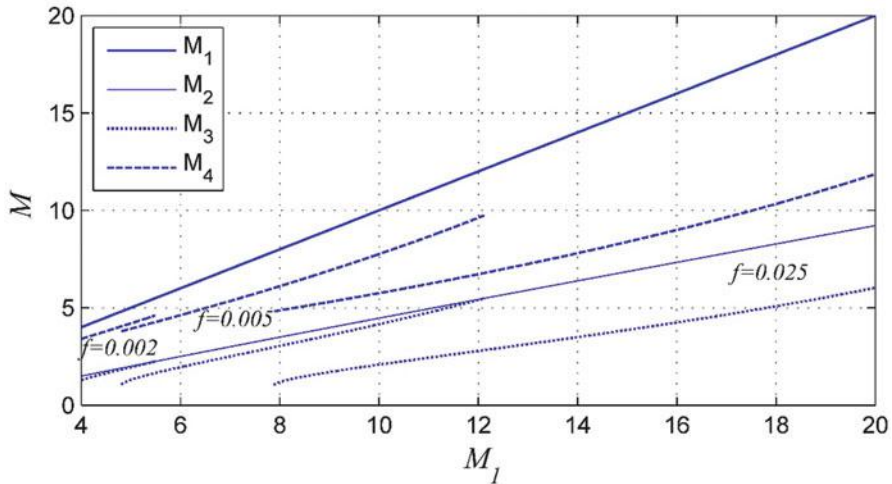


Fig. 5.36c Mach number at different states versus flight Mach number for different fuel to air ratio

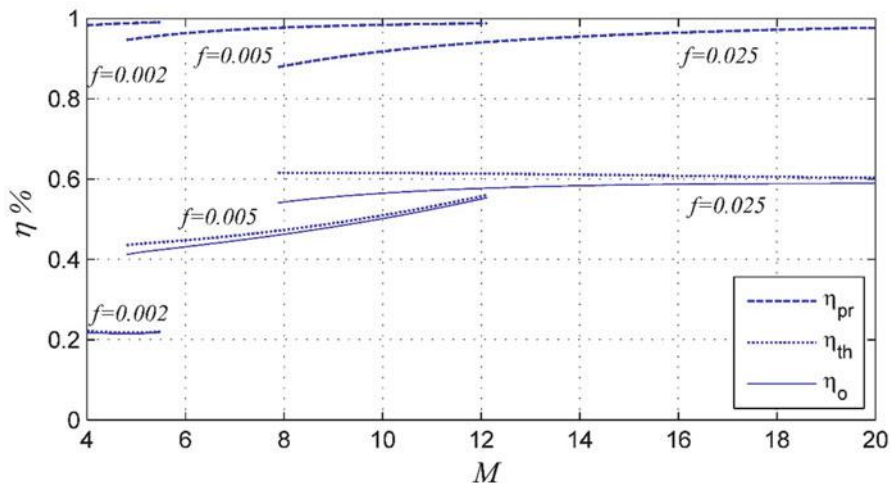


Fig. 5.36d Propulsive, thermal, and overall efficiencies versus flight Mach number for different fuel-to-air ratio

throats: the first is to decelerate the flow to subsonic flow before the combustion chamber, and the second is to accelerate the flow to supersonic again in the nozzle. For a scramjet, these two throats are no longer needed. Thus, a complicated control system is needed to modify scramjet geometry to match flight speed requirements. Aerodynamists suggested a simpler solution, namely, adding a short duct between the inlet and the combustor known as an *isolator* [46] and keeping the other engine

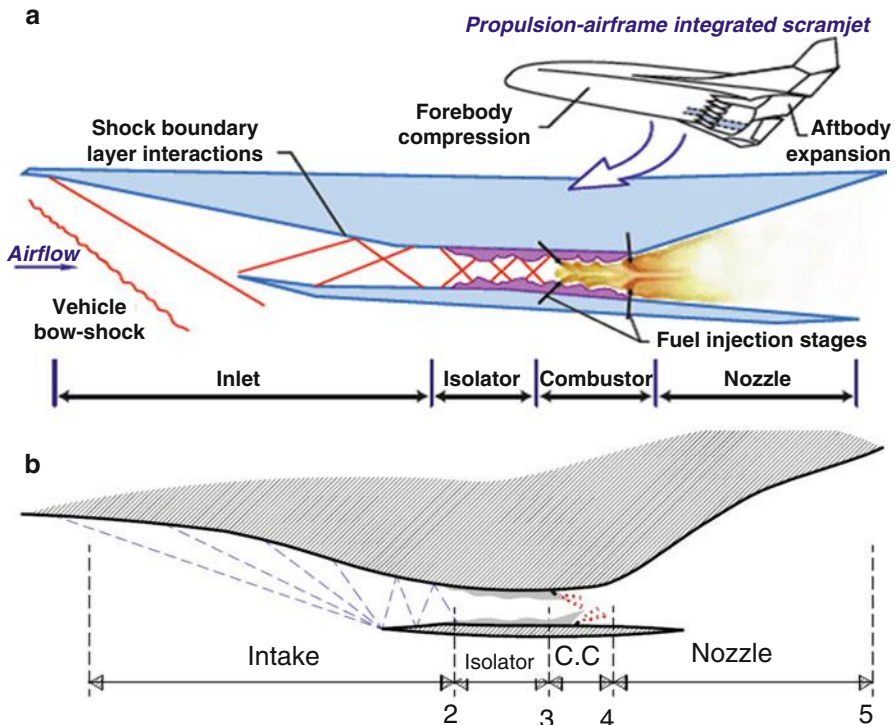


Fig. 5.37 Configuration of dual ram-scramjet engine

geometry unchanged. The isolator is a constant area duct that can maintain normal or oblique shock trains (Figs. 5.37 and 5.38). The main concern in the isolator is that the shock pattern that occurs during subsonic combustion operation does not reach the inlet since this condition can cause the engine to unstart. For high supersonic flight Mach numbers (and correspondingly high combustor Mach numbers), the boundary layers in the isolator will be very thin and no waves of any importance will form in the isolator [47]. The shock train formed in the isolator and its performance depends on the back pressure acting on it and the isolator height to length ratio which is a new parameter affecting the system. Other components are treated the same as in scramjet. The T-s diagram of dual ram-scramjet engine are shown in Fig. 5.39. Static states are displayed in Fig. 5.39a, while total and static states are shown in Fig. 5.39b for both ideal and real processes.

5.4.6.2 Aero-thermodynamics of Dual-Mode Scramjet

Same designations for the states of scramjet as described in Sect. 5.4.4 are used here, thus:

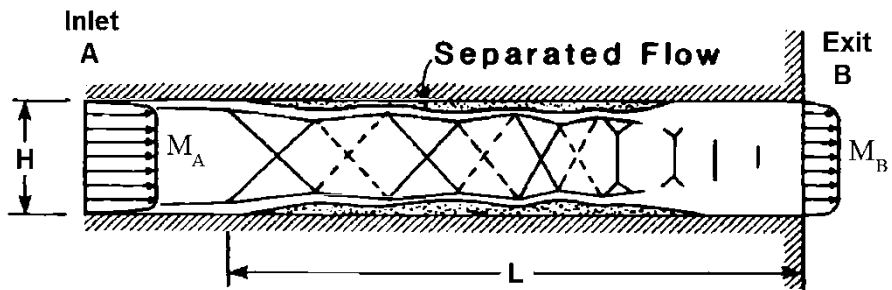


Fig. 5.38 Configuration of isolator [46]

Fig. 5.39a T-s diagram for dual ram-scramjet engine (static states only)

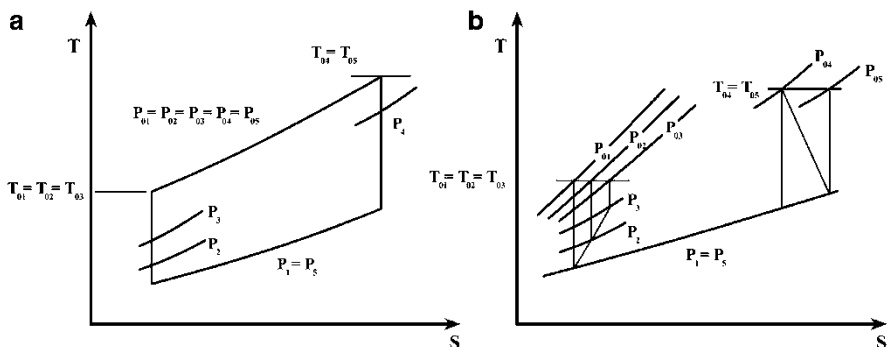
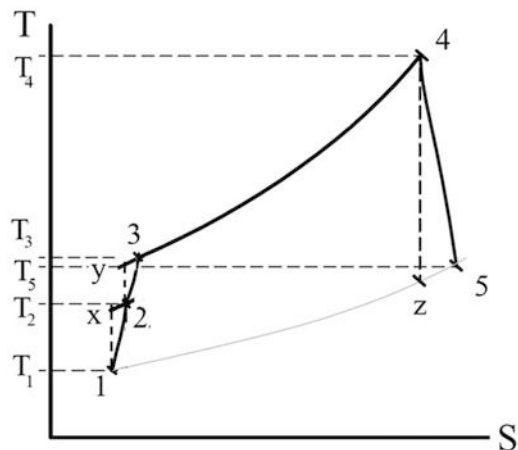


Fig. 5.39b Ideal and real cycle on T-s diagram: (a) ideal cycle, (b) real cycle

Station 1 is downstream of the vehicle forebody shock and represents the properties of the flow that enters the inlet.

Station 2 is at the inlet throat, which is usually the minimum area of the flow path, and the isolator extends between stations 2 and 3.

Station 3 represents the start of the combustor, where fuel and air is mixed and burned.

Station 4 represents the end of the combustor.

Station 5 represents the end of expansion process, which includes an internal expansion within the nozzle and an external expansion to the end of the vehicle.

(A) Intake

The intake is modeled as adiabatic supersonic flow with adiabatic compression efficiency. The governing equations are same as listed in scramjet; Eqs. (5.44), (5.45), (5.46), (5.47), (5.48).

(B) Isolator

The isolator behavior will be governed by Eq. (5.60) that relates isolator outlet pressure ratio to its dimensions, inlet Mach number, and boundary layer parameters at inlet [27]. In Eq. (5.63), L/H are isolator dimensions according to Fig. 5.38, θ is the momentum thickness at isolator inlet, and R_θ is the Reynolds number related to momentum thickness. The maximum pressure ratio that can take place in duct module with no energy addition or subtraction will be equal to the pressure ratio through a normal shock wave. So the pressure ratio in the isolator will be limited to Eq. (5.64). The flow in the isolator will be treated also as adiabatic supersonic flow with adiabatic compression efficiency defined by Eq. (5.65) and Fig. 5.39a. The combustion inlet temperature and Mach number can be calculated through Eqs. (5.66) and (5.67).

$$\frac{L}{H} = \frac{\sqrt{\frac{\theta}{H}}}{\sqrt[4]{Re_\theta}} \cdot \frac{50 \left(\frac{P_3}{P_2} - 1 \right) + 170 \left(\frac{P_3}{P_2} - 1 \right)^2}{M_2^2 - 1} \quad (5.63)$$

$$\frac{P_3}{P_2} = \frac{2\gamma_c}{\gamma_c + 1} \times M_2^2 - \frac{\gamma_c - 1}{\gamma_c + 1} \quad (5.64)$$

$$\eta_{Iso} = \frac{T_y - T_2}{T_3 - T_2} \quad (5.65)$$

$$T_3 = T_2 \left[1 + \frac{1}{\eta_{Iso}} \left(\left(\frac{P_3}{P_2} \right)^{\frac{\gamma_c - 1}{\gamma_c}} - 1 \right) \right] \quad (5.66)$$

$$M_3 = \sqrt{\frac{T_1}{T_3} \left(\frac{2}{\gamma - 1} + M_1^2 \right) - \frac{2}{\gamma - 1}} \quad (5.67)$$

(C) Combustion Chamber

The burner process is modeled as a Rayleigh flow. When the Mach number at combustion chamber is supersonic, the combustion chamber will be similar to the scramjet combustion. Combustion chamber outlet data is obtained using Rayleigh flow and energy Eqs. (5.68), (5.69), (5.70).

$$T_{o4} = \frac{\dot{m}_f \eta_b Q V}{C_{ph}(\dot{m}_a + \dot{m}_f)} + \frac{\dot{m}_a C_{pc} T_3}{C_{ph}(\dot{m}_a + \dot{m}_f)} (1 + 0.5 \times (\gamma_c - 1) M_3^2) \quad (5.68)$$

$$\frac{T_{o4}}{T_{o3}} = \left(\frac{M_4}{M_3} \right)^2 \left(\frac{1 + \gamma_c M_3^2}{1 + \gamma_h M_4^2} \right)^2 \left(\frac{1 + 0.5 \times (\gamma_h - 1) M_4^2}{1 + 0.5 \times (\gamma_c - 1) M_3^2} \right) \quad (5.69a)$$

$$\frac{T_4}{T_3} = \left(\frac{M_4}{M_3} \right)^2 \left(\frac{1 + \gamma_c M_3^2}{1 + \gamma_h M_4^2} \right)^2 \quad (5.69b)$$

$$\frac{P_4}{P_3} = \frac{1 + \gamma_c M_3^2}{1 + \gamma_h M_4^2} \quad (5.70)$$

For subsonic combustion, the amount of heat added will be equal to the critical value to reach a choking condition at combustion chamber exit $M_4 = 1.0$ to convert the flow to supersonic. The combustion chamber outlet data is obtained using Rayleigh flow and energy equation: Eqs. (5.71) and (5.72)

$$T_{o4} = \frac{T_{o3}}{M_3^2} \left(\frac{1 + \gamma_c M_3^2}{1 + \gamma_h} \right)^2 \left(\frac{1 + 0.5 \times (\gamma_h - 1)}{1 + 0.5 \times (\gamma_c - 1) M_3^2} \right) \quad (5.71)$$

$$P_4 = P_3 \frac{1 + \gamma_c M_3^2}{1 + \gamma_h} \quad (5.72)$$

The definition of adiabatic expansion (nozzle) efficiency is Eq. (5.73) and Fig. 5.37a. Assuming complete expansion in the nozzle, output flow can be calculated using Eqs. (5.74) and (5.75).

$$\eta_N = \frac{T_4 - T_5}{T_4 - T_z} \quad (5.73)$$

$$T_5 = T_4 - T_4 \eta_N \left(1 - \left(\frac{P_1}{P_4} \right)^{\frac{\gamma_h - 1}{\gamma_h}} \right) \quad (5.74)$$

$$V_5 = \sqrt{2 C_{ph} (T_{o4} - T_5)} \quad (5.75)$$

Finally, a comparison of specific impulse for different engine types will be given in Fig. 5.40.

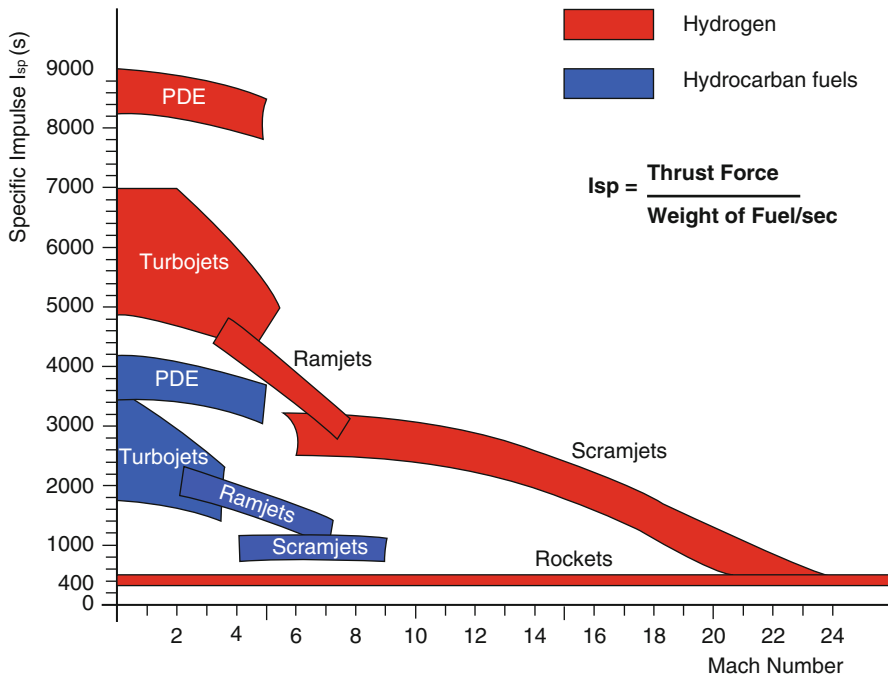


Fig. 5.40 Specific impulse versus flight Mach number for different airbreathing and non-airbreathing engines

Table 5.1 Summary of results

Scramjet at Mach number 6, alt 27 km	
T/m_a (N.s/kg)	366.72
$TSFC$ (kg/N.s)	2.73E ⁻⁵
η_{th}	62.11 %
η_{pr}	93.72 %
η_o	58.21 %

Example 5.7 A scramjet engine is used to power a hypersonic vehicle that flies at an altitude of 27,000 m, Mach number $M = 7$, using Hydrogen fuel (Heating value $Q_{HV} = 120 \text{ MJ/kg}$).

The momentum thickness is $\theta = 3 \text{ mm}$, height of isolator $H = 0.08 \text{ m}$, and Reynolds number based on momentum thickness boundary layer is $Re_\theta = 3 \times 10^5$. Detailed data of its four elements are given in Table 5.1.

Calculate

1. Specific thrust and thrust specific fuel consumption
2. Thermal efficiency, propulsive efficiency, and overall efficiency
3. Mach number of gases leaving scramjet
4. Isolator length (L)

Solution

Figures 5.37 and 5.39 illustrate the considered scramjet and its T-s diagram.

At altitude 27,000 m

Temperature and pressure are

$$T_1 = 222.66 \text{ K} \quad P_1 = 1,823 \text{ Pa} \quad M_1 = 7.0$$

$$V_1 = M_1 \sqrt{\gamma_l R T_1} = 2,093.7 \text{ m/s}$$

$$T_{01} = T_1 [1 + 0.5 \times (\gamma_c - 1) M_1^2] = 2405 \text{ K}$$

$$P_{01} = P_1 [1 + 0.5 \times (\gamma_c - 1) M_1^2]^{3.5} = 7,547 \text{ kPa}$$

1. Intake

$$\begin{aligned} T_2 &= T_1 \left(\frac{1 + 0.5 \times (\gamma_c - 1) M_1^2}{1 + 0.5 \times (\gamma_c - 1) M_2^2} \right) = 222.66 \left(\frac{1 + 0.5 \times (1.4 - 1) \times 7^2}{1 + 0.5 \times (1.4 - 1) \times 3.6^2} \right) \\ &= 669.5 \text{ K} \end{aligned}$$

$$T_{02} = T_2 (1 + 0.5 \times (\gamma_c - 1) M_2^2) = 2,405 \text{ K} = T_{01}$$

$$\begin{aligned} P_2 &= P_1 \left(1 + \eta_I \left(\frac{T_2}{T_1} - 1 \right) \right)^{\frac{\gamma_c}{\gamma_c - 1}} = 1,823 \left(1 + 0.92 \times \left(\frac{669.5}{222.66} - 1 \right) \right)^{\frac{1.4}{0.4}} = 70,918 \text{ Pa} \\ P_2 &= 70.92 \text{ kPa} \end{aligned}$$

$$P_{02} = P \left(1 + 0.5 \times (\gamma_c - 1) M_2^2 \right)^{\frac{\gamma_c}{\gamma_c - 1}} = 6,229 \text{ kPa}$$

2. Isolator

$$\begin{aligned} T_3 &= T_2 \left(\frac{1 + 0.5 \times (\gamma_i - 1) M_2^2}{1 + 0.5 \times (\gamma_{iso} - 1) M_3^2} \right) = 669.5 \left(\frac{1 + 0.5 \times (1.4 - 1) \times 3.6^2}{1 + 0.5 \times (1.37 - 1) \times 2.2^2} \right) \\ T_3 &= 669.5 \times 1.895 = 1,269 \text{ K} \end{aligned}$$

$$\begin{aligned} P_3 &= P_2 \left(1 + \eta_{iso} \left(\frac{T_3}{T_2} - 1 \right) \right)^{\frac{\gamma_{iso}}{\gamma_{iso} - 1}} = 70.92 \left(1 + 0.85 \times \left(\frac{1269}{669.5} - 1 \right) \right)^{\frac{1.37}{0.37}} \\ P_3 &= 70.92 \times 8.13 = 577 \text{ kPa} \end{aligned}$$

$$T_{03} = T_3 [1 + 0.5 \times (\gamma_{iso} - 1) M_3^2] = 2,405 \text{ K}$$

$$P_{03} = P_3 [1 + 0.5 \times (\gamma_{iso} - 1) M_3^2]^{\frac{\gamma_{iso}}{\gamma_{iso} - 1}} = 6,158 \text{ kPa}$$

3. Combustion Chamber

$$\frac{T_{04}}{T_{03}} = \frac{M_4^2}{M_3^2} \left(\frac{1 + \gamma_{iso} M_3^2}{1 + \gamma_b M_4^2} \right)^2 \left(\frac{1 + 0.5(\gamma_b - 1) M_4^2}{1 + 0.5(\gamma_{iso} - 1) M_3^2} \right) = 1.19743$$

$$\begin{aligned}
T_{o4} &= 2,880 \text{ K} = T_{o5} \\
P_4 &= P_3 \frac{1 + \gamma_{iso} M_3^2}{1 + \gamma_b M_4^2} = 577 \left\{ \frac{1 + 1.37 \times 2.2^2}{1 + 1.31 \times 1.6^2} \right\} = 1,011.3 \text{ kPa} \\
T_4 &= \frac{T_{o4}}{1 + 0.5(\gamma_b - 1)M_4^2} = \frac{2880}{1 + 0.5 \times 0.31 \times 1.6^2} = 2062 \text{ K} \\
P_{04} &= P_4 \left\{ 1 + 0.5(\gamma_b - 1)M_4^2 \right\}^{\frac{\gamma_b}{\gamma_b - 1}} = 4,151 \text{ kPa} \\
f &= \frac{C_{Pb}T_{04} - C_{Piso}T_{03}}{\eta_b QV - C_{Pb}T_{04}} = \frac{1.255 \times 2,880 - 1.063 \times 2,062}{0.97 \times 120,000 - 1.255 \times 2,880} = \frac{1,422.5}{112,785.6} \\
&= 0.0126
\end{aligned}$$

4. Nozzle

$$\begin{aligned}
T_5 &= T_{04} \left[1 - \eta_N \left(1 - \left(\frac{P_1}{P_{04}} \right)^{\frac{\gamma_n - 1}{\gamma_n}} \right) \right] = 2,880 \left[1 - 0.97 \left(1 - \left(\frac{1.823}{4151} \right)^{\frac{0.33}{1.33}} \right) \right] \\
&= 496.7 \text{ K}
\end{aligned}$$

Sonic speed at exhasut temperature

$$\begin{aligned}
a_5 &= \sqrt{\gamma_5 R_5 T_5} = 437.7 \text{ m/s} \\
V_5 &= \sqrt{2C_{Pn}(T_{o4} - T_5)} = \sqrt{2 \times 1169 \times (2880 - 437.7)} = 2,389.6 \text{ m/s} \\
M_5 &= 5.46 \\
P_{05} &= P_5 \left\{ 1 + 0.5(\gamma_n - 1)M_5^2 \right\}^{\frac{\gamma_n}{\gamma_n - 1}} = 2359 \text{ kPa} \\
T &= (\dot{m}_a + \dot{m}_f)V_5 - \dot{m}_a V_1
\end{aligned}$$

Specific thrust

$$T / \dot{m}_a = (1+f)V_5 - V_1 = 326 \frac{\text{N.s}}{\text{kg}}$$

Thrust specific fuel consumption

$$TSFC = \frac{\dot{m}_f}{T} = \frac{f}{\frac{T}{\dot{m}_a}} = 3.86 \text{ E}^{-5} \frac{\text{kg.s}}{\text{N}}$$

Propulsive efficiency

$$\eta_{pr} = \frac{T \cdot V_1}{\Delta(K.E)} = \frac{2T \cdot V_1}{\dot{m}_a(1+f)V_5^2 - \dot{m}_aV_1^2} = \frac{2\left(\frac{r}{\dot{m}_a}\right) \cdot V_1}{(1+f)V_5^2 - V_1^2} = 97.6\%$$

$$\text{Or } \eta_{pr} = \frac{2V_1((\dot{m}_a + \dot{m}_f)V_5 - \dot{m}_aV_1)}{\dot{m}_a(1+f)V_5^2 - \dot{m}_aV_1^2} = \frac{2V_1 \times V_5(1+f) - 2V_1^2}{(1+f)V_5^2 - V_1^2} = 97.6\%$$

It is noticed that propulsive efficiency acquired very high values which is mainly due to the small difference between flight speed (2,093.7 m/s) and exhaust speed (2,389.6 m/s).

Thermal efficiency

$$\eta_{th} = \frac{\Delta(K.E)}{\dot{Q}_{add}} = \frac{\dot{m}_a(1+f)V_5^2 - \dot{m}_aV_1^2}{2Q_{HV}\dot{m}_f\eta_{cc}} = \frac{(1+f)V_5^2 - V_1^2}{2Q_{HV}f\eta_b} = 47.68\%$$

Overall efficiency

$$\eta_o = \frac{T \cdot V_1}{\dot{Q}_{add}} = \eta_{pr} \cdot \eta_{th} = 46.53\%$$

3. Mach number of exhaust gases $M_5 = \frac{V_5}{a_5} = 5.46$

4. Isolator length is calculated from the relation

$$\begin{aligned} \frac{L}{H} &= \frac{\sqrt{\frac{\theta}{H}}}{\sqrt[4]{Re_\theta}} \cdot \frac{50\left(\frac{P_3}{P_2} - 1\right) + 170\left(\frac{P_3}{P_2} - 1\right)^2}{M_2^2 - 1} \\ &= \frac{\sqrt{0.002/0.08}}{\sqrt[4]{3 \times 10^5}} \frac{50 \times \left(\frac{577}{70.9} - 1\right) + 170 \times \left(\frac{577}{70.9} - 1\right)^2}{3.6^2 - 1} \\ &= 5.09 \end{aligned}$$

$$\frac{L}{H} = \frac{\sqrt{0.002/0.08}}{\sqrt[4]{3 \times 10^5}} \frac{50 \times \left(\frac{577}{70.9} - 1\right) + 170 \times \left(\frac{577}{70.9} - 1\right)^2}{3.6^2 - 1} = 5.09$$

$$L = 0.407m$$

Results are given in Tables 5.2 and 5.3 as well as Figs. 5.41a, 5.41b, and 5.41c.

Table 5.2 Air and gas properties

Element	γ	R	C_P	M_{inlet}	η (%)
		$\left(\frac{\text{J}}{\text{kg.K}}\right)$	$\left(\frac{\text{J}}{\text{kg.K}}\right)$	Mach number at inlet	
Intake (states 1–2)	1.4	287	1005	7.0	92
Isolator (states 2–3)	1.37	287	1063	3.6	85
Burner (states 3–4)	1.31	297	1255	2.2	97
Nozzle (states 4–5)	1.33	290	1169	1.6	97

5.5 Conclusion

In this chapter, three types of athodyd engines, namely pulsejet, ramjet, and scramjet, are discussed. These engines cover the whole flight domain starting from subsonic to hypersonic speeds. Historical review for the three types is reviewed. The first engine discussed is pulsejet engine. Starting by its first version dates back to the thirties/forties of the last century and ending by its new version, pulse detonation engine (PDE), all thermodynamic and propulsive analyses are given.

Next, ramjet engine is handled. Both subsonic and supersonic types as well as single-throat and double-throat types are discussed. Moreover, its aircraft and missile applications are discussed with numerous examples for each. Nuclear types are also described.

Finally, scramjet engines are discussed. Thermodynamic analysis of both single- and dual-mode is given.

Problems

Pulsejet

5.1 The *Republic-Ford JB-2 Loon* was a United States copy of the German V-1 flying bomb developed in 1944. It was powered by [Ford PJ31 pulsejet](#) (a copy of German [Argus As014](#) pulse-jet engine). JB-2 was air launched for flight test by B-17 bomber during testing of weapon at Eglin Field, 1944. Its specifications are:

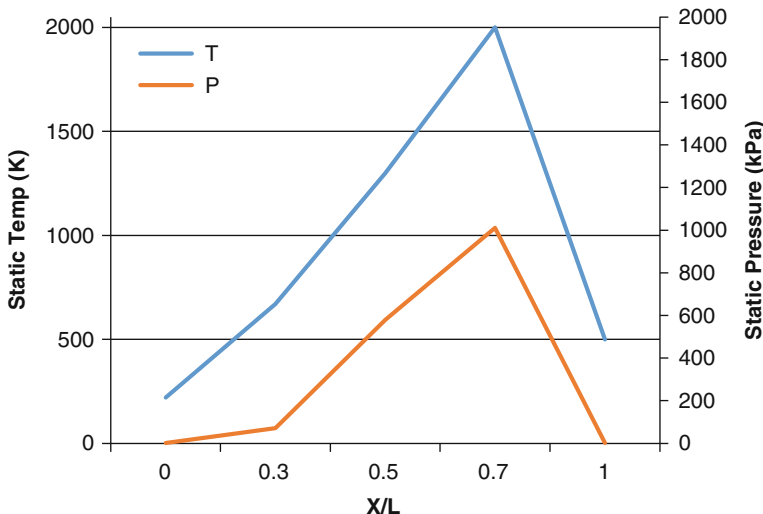
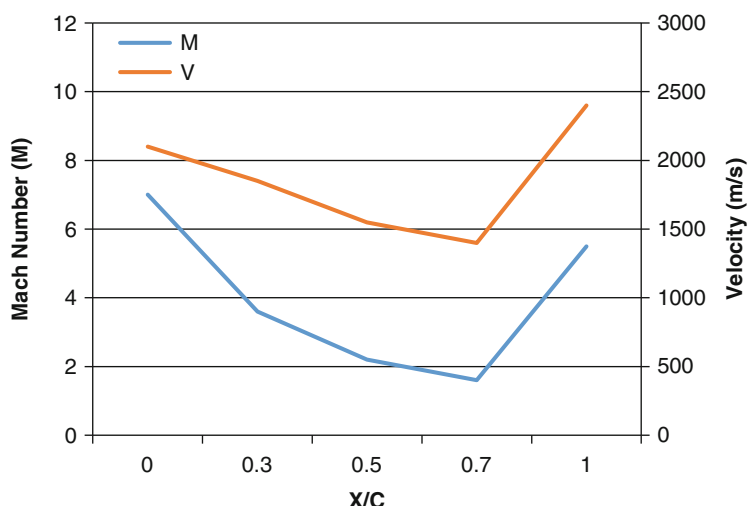
- Thrust 2.9 kN at an altitude of 10,000 ft
- Flight speed 684 km/h
- Intake area 0.148 m²
- Fuel is standard 80-octane gasoline having heating value of 40 MJ/kg and density of 0.75 kg/literature
- Fuel consumption 30 l/min
- Burner efficiency 0.92
- Typical flight duration is 1800 s

Table 5.3 Summary of Flow Properties through Engine

State	State no.	Velocity (m/s)	Mach number	Static temperature (K)	Static pressure (kPa)	Total temperature (K)	Total pressure (kPa)
Inlet	1	2094	7.0	222.66	1,823	2,405	7547
Inlet to isolator	2	1847	3.6	669.5	70.92	2405	6229
Inlet to combustion chamber	3	1554	2.2	1269	577	2405	6158
Inlet to nozzle	4	1433	1.6	2062	1011.3	2880	4151
Exit	5	2389.6	5.46	496.7	1,823	2880	2359

Table 5.4 Overall properties of scramjet engine

Scramjet at Mach number 7, altitude 27 km	
T/m_a (N.s/kg)	326
f	0.0126
TSFC (kg/N. s)	3.86 E ⁻⁵
η_{th}	47.68 %
η_{pr}	97.6 %
η_o	46.53 %
M_5	5.46

**Fig. 5.41a** Static temperature variation along the scramjet flow path**Fig. 5.41b** Mach number variation along the scramjet flow path

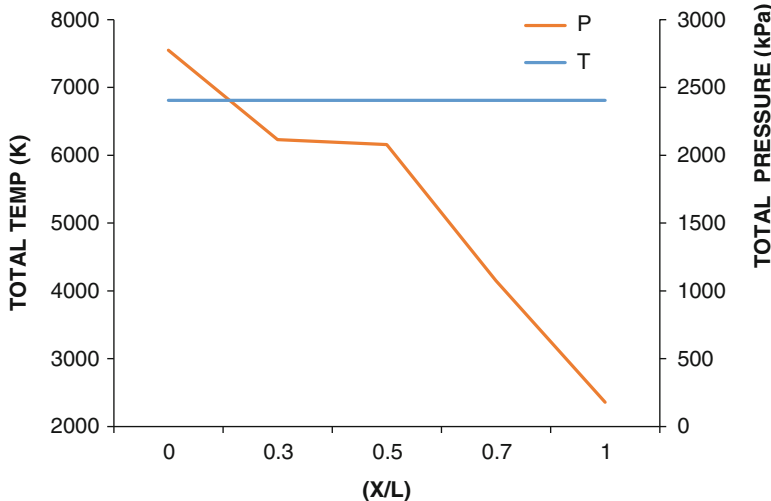


Fig. 5.41c Variation of total temperature and pressure along the scramjet flow path

Assume specific heat of air $Cp_a = 1.005 \frac{\text{kJ}}{\text{kgK}}$ and specific heat of hot gases $Cp_h = 1.1 \frac{\text{kJ}}{\text{kgK}}$

Calculate

- Air and fuel mass flow rate
- Fuel mass flow rate
- Exhaust speed
- Maximum temperature and pressure inside the engine
- Thrust specific fuel consumption (TSFC)
- Exhaust temperature
- Fuel tank capacity in gallons

5.2 KGW-1 (later re-designated as LTV-N-2) was the US Navy's version of American flying bomb *JB-2 Loon*. It was developed to be carried on the aft deck of submarines in watertight containers. The first submarine to employ them was the [SS-348 Cusk](#) which successfully launched its first Loon on 12 February 1947 in [Point Mugu, California](#). It has the following data:

- Static thrust 2200 N with air inlet speed of 180 m/s
- Intake area 0.145 m^2
- Fuel is standard 80-octane gasoline having heating value $Q_R = 40 \text{ MJ/kg}$
- Burner efficiency 0.90
- Typical flight duration is 1800 s
- Exhaust temperature 735 K

Assume specific heat of air $Cp_a = 1.005 \frac{\text{kJ}}{\text{kgK}}$ and specific heat of hot gases $Cp_h = 1.12 \frac{\text{kJ}}{\text{kgK}}$

Calculate

1. Air mass flow rate into engine
 2. Exhaust velocity
 3. Maximum temperature inside the engine
 4. Maximum pressure
 5. Thrust specific fuel consumption (TSFC)
 6. Average range
- 5.3 As described in Sect. 5.2.6, the idealized thrust–time profile that corresponds to the idealized sinusoidal combustor pressure–time profile of Fig. 5.6 would then have also a sinusoidal shape for half of the cycle and zero value for the remaining half as shown in Fig. 5.6. In other words, mathematically, the thrust force may be expressed as

$$T = T_{max} \sin \frac{2\pi t}{\Delta t} \text{ for } 0 \leq t \leq \frac{\Delta t}{2}$$

And $T = 0$ for $\frac{\Delta t}{2} \leq t \leq \Delta t$
where $\Delta t = \frac{1}{f}$ is the time of one cycle.

Prove that the net mean thrust of

$$\bar{T} = \frac{T_{max}}{\pi}$$

Ramjet

- 5.4 For an ideal ramjet, prove that the thermal efficiency is expressed by

$$\eta_{th} = 1 - (1/\tau_r)$$

where $\tau_r = T_{o2}/T_a$

(Hint: Use the following approximations: $f = Cp (T_{o4} - T_{o2})/Q_R$ and $\dot{m}_f \ll \dot{m}_a$)

- 5.5 For an ideal ramjet engine powering an airplane flying at stratosphere region of the standard atmosphere, where $T_a = \text{constant}$, prove that the thrust is expressed by the relation:

$$T = \dot{m}_a (\sqrt{\tau_b} - 1) \text{ where } \tau_b = \frac{T_{03}}{T_{02}}$$

If the maximum temperature $T_{o4} = \text{constant}$ (full-throttle operation), prove that the thrust attains a maximum value when the flight Mach number M_o is given by:

$$M_o = \sqrt{\frac{2}{\gamma - 1} \left(\tau_\lambda^{\frac{1}{3}} - 1 \right)}, \quad \tau_\lambda = \frac{T_{o4}}{T_a}$$

Plot the relation $\left(\frac{T}{\dot{m}_a a_0} \right)$ versus M_0 , for $\tau_\lambda = 7.0, 8.0, 0.9$, where a_0 is the sonic speed at the flight altitude.

- 5.6 A ramjet has low-speed stagnation pressure losses given by $r_d = 0.90$; $r_c = 0.95$; $r_n = 0.96$. The ambient and maximum temperatures are 225 K and 2000 K, respectively. The fuel-to-air ratio is assumed very small such that $f \ll 1$. What is the minimum flight Mach number at which the engine develops positive thrust? Assume the nozzle is unchoked.

Hint: Use the thrust equation:

$$\frac{T}{\dot{m}_a} = (1 + f) \sqrt{\frac{2\gamma_e R_e T_{04}(m-1)}{(\gamma-1)m}} - M \sqrt{\gamma R T_a} + \frac{P_e A_e}{\dot{m}_a} \left(1 - \frac{P_a}{P_e} \right)$$

$$m = \left(1 + \frac{\gamma-1}{2} M^2 \right) \left(r_d r_c r_n \frac{P_a}{P_e} \right)^{\frac{\gamma-1}{\gamma}}$$

- 5.7 A ramjet engine is fitted with a variable geometry intake, where a center body moves forward or backward to adjust the oblique shock wave to the intake lips; Figure (Problem 7). The half angle of the spike is 10°. The flight Mach number M_1 in the supersonic regime varies from M_{minimum} to 3.6. The inlet radius of the intake is 250 mm.

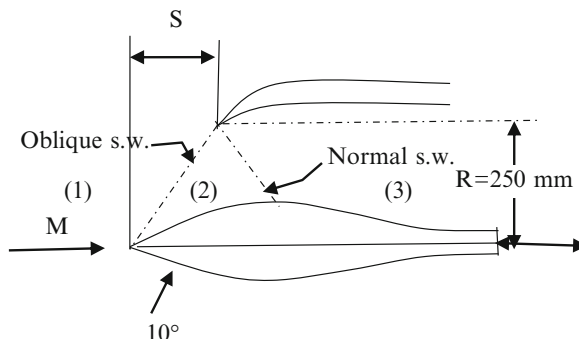


Figure (Problem 7) Variable geometry intake of a ramjet engine

- Find the minimum Mach number $M_{\text{min}} > 1.0$, which corresponds to an attached shock wave to the apex.
- Find the distance (S) wave to the apex of the center body.
- Whether the center body moves forward or rearward when the flight Mach number increases?

- (d) What would be the value of (S) if the Mach number $M_1 = 2.8$? Calculate the distance moved by the spike.

5.8 A ramjet traveling in level flight at an altitude of 20,000 m with a constant speed of 540 m/s. The intake conditions have been simplified to represent the formation of a normal shock wave immediately at the inlet. It is assumed that the pressure external to the engine is everywhere that of the ambient atmosphere. Moreover, the flow is isentropic through inlet (intake) and nozzle is assumed isentropic. Combustion process occurs through the addition of fuel at constant area frictionless duct; the maximum stagnation temperature is 1300 K. Assume that the air-to-fuel ratio is 40/1. For simplicity, take the working fluid as air with $\gamma = 1.4$ for all processes. The areas of the intake and combustion chamber are $A_2 = 0.10 \text{ m}^2$ and $A_3 = 0.19 \text{ m}^2$. For a convergent divergent nozzle, calculate:

- (a) Mass flow rate
- (b) Pressure drop in the combustion chamber
- (c) Nozzle throat area
- (d) Thrust developed by the ramjet if the nozzle expands the gas down to the ambient pressure
- (e) Propulsive efficiency for cases
- (f) TSFC
- (g) Repeat (d) through (f) for a convergent nozzle

5.9 A ramjet engine operates at an altitude where the ambient conditions are $T_a = 205 \text{ K}$ and $P_a = 11.58 \text{ kPa}$. Fuel heating value is 45 MJ/kg. Flight Mach number is $M_0 = 3$. Maximum temperature is 3000 K. If the losses in diffuser are expressed by

$$\pi_s = 1 - 0.075(M_0 - 1)^{1.35}$$

Losses in combustion chamber and nozzle are also given as $r_{cc} = 0.98$ and $r_n = 0.96$

Calculate

- The specific thrust
- TSFC

5.10 An ideal ramjet engine operates at an altitude where the ambient conditions are $T_a = 227 \text{ K}$ and $P_a = 0.3 \text{ bar}$. Flight Mach number is $M_0 = 3$. Maximum temperature is 1300 K. Intake inlet area is $A_i = 0.1 \text{ m}^2$. Calculate:

- (i) Air mass flow rate
- (ii) Thrust force
- (iii) Propulsive, thermal, and overall efficiencies

- 5.11 A ramjet engine is powering an airplane flying with Mach number $M = 4.2$, at an altitude of 50,000 ft, where the ambient temperature and pressure are 205 K and 11.6 kPa, respectively. The fuel heating value is 44 MJ/kg, and the peak temperature is 3000 K. The air mass flow rate is 55 kg/s. The ramjet diffuser losses are given by

$$\frac{P_{02}}{P_{0a}} = 1 - 0.1(M - 1)^{1.5}$$

where M is the flight Mach number. The stagnation pressure ratio across the flame holders (from state 2 to 3) is 0.97, and the stagnation pressure loss in the combustor (from state 3 to 4) is 4 %. The combustion chamber and nozzle efficiencies are 0.98 and 0.94, respectively. Assume the propellant is a perfect gas having $R = 287 \text{ J/(kg.K)}$ throughout, but having $\gamma = 1.4$ from state a (ambient) to state 3 and $\gamma = 1.3$ from states 3 to 6. It is required to calculate:

- (a) The fuel-to-air ratio
 - (b) The nozzle exit area for the two nozzle cases: choked (convergent nozzle) and unchoked (de Laval nozzle)
 - (c) The thrust force in the two above cases
 - (d) d-TSFC in the two above cases
- 5.12 An aircraft propelled by a ramjet engine, flies at an altitude of 5000 m and at a speed of $M_a = 2$. The inlet diameter is $D_1 = 0.9 \text{ m}$, and the maximal engine temperature is $T_{04} = 2000 \text{ K}$. The stagnation pressure losses are $r_d = 0.88$, $r_{cc} = 0.98$, and $r_n = 0.96$.

Assuming that $P_e = P_a$

Other data is $C_p = 1.12 \frac{\text{kJ}}{\text{kg.K}}$; $Q_R = 44 \frac{\text{MJ}}{\text{kg}}$; $T_a = 270 \text{ K}$, $R = 287.43 \frac{\text{J}}{\text{kg.K}}$; and $\rho_a = 0.8 \text{ kg/m}^3$

Compute

- (a) The fuel-to-air ratio (f)
- (b) The thrust force

- 5.13 An ideal ramjet flies at a speed of $V_a = 400 \text{ m/s}$. The ambient conditions are $T_a = 270 \text{ K}$ and $\rho_a = 0.8 \text{ kg/m}^3$. The effective inlet area is $A_i = 0.2 \text{ m}^2$. Compute:

- (b) The thrust of the engine if $\frac{T_{0\max}}{T_{0a}} = 8$ and $f \ll 1$
- (c) What are the magnitude and direction of thrust if the exhaust is deflected 90° without affecting mass flow?

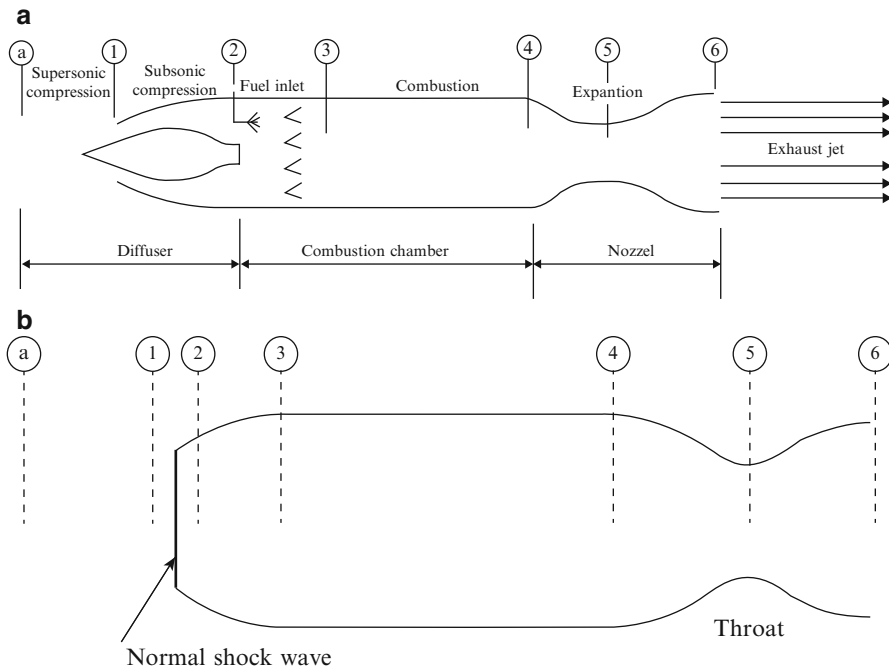
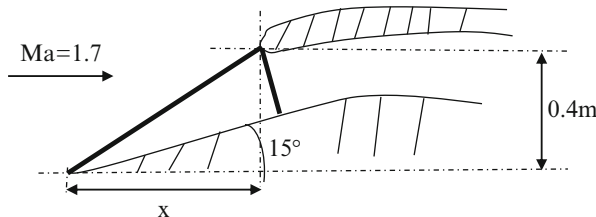


Figure (Problem 13) Two Ramjet Engines (A) Supersonic Intake and (B) Subsonic Intake

5.14 A ramjet operates at an altitude of 10,000 m ($T_a = 223\text{ K}$, $P_a = 0.26\text{ atm}$, $\gamma = 1.4$) at a Mach number of 1.7. The external diffusion is based on an oblique shock and on a normal shock, as described in the shown figure.



Calculate

- Stagnation pressure recovery, $\frac{P_{02}}{P_{0a}}$?
- At what Mach number does the oblique shock become detached?
- What is the distance x , from the cone tip to the outer inlet lip, for the condition described in the figure?
- What is the best turning angle θ in terms of highest pressure ratio, $\frac{P_{02}}{P_{0a}}$?

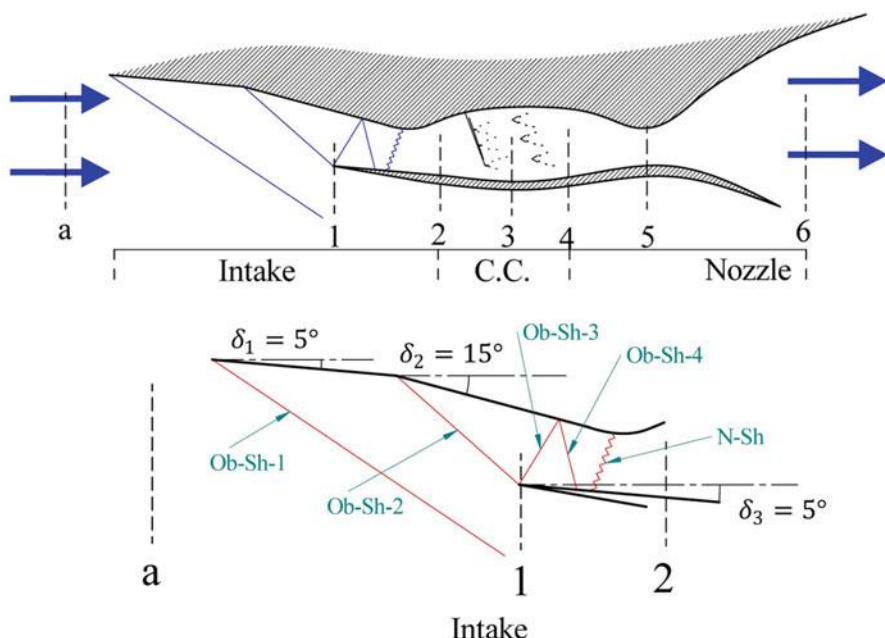


Figure (Problem 14)

5.15 An aircraft powered by ramjet is flying at a speed of $M_a = 2.0$ at an altitude of 16,200 m, where the temperature is 216.6 °K and the pressure is 10.01 kPa. Two layouts for intake (as shown in figure below) are examined:

- (A) Supersonic configuration having an axisymmetric layout and fitted with a spike having a deflection angle 12° .
- (B) Typical subsonic intake with a normal shock just at inlet. The following data applies for both layouts. Combustion chamber has a cylindrical shape with a constant cross sectional area $A_{cc} = 0.2 \text{ m}^2$. The maximum total temperature in the combustion chamber is 2500 K. Heating value of fuel is 45,000 kJ/kg. The burner efficiency is $\eta_b = 0.96$. The nozzle expands to atmospheric pressure for maximum thrust with $\eta_n = 0.96$. The velocity entering the combustion chamber is to be kept as large as possible but the Mach number must not exceed 0.25. Assuming ($\gamma_{\text{air}} = 1.4$, $\gamma_{\text{gases}} = 4/3$), compute:
 - (a) The stagnation pressure ratio of the diffuser (r_d)
 - (b) The inlet Mach number to the combustion chamber
 - (c) The stagnation pressure ratio in the combustion chamber (r_c)
 - (d) The stagnation pressure ratio in the nozzle (r_n)
 - (e) The flight and exhaust speeds
 - (f) Inlet and outlet areas (A_i, A_e)

- (g) The thrust force
- (h) The specific thrust fuel consumption (TSFC)

5.16 A ramjet operates at flight Mach number of $M_a = 2.5$ at an altitude of 16,200 m, where the ambient temperature and pressure are $T_a = 216.6 \text{ K}$ and $P_a = 10.01 \text{ kPa}$. The engine has a 2D inlet fitted with two deflection flaps as shown in figure. The inlet area at state 1 is $A_1 = 0.2 \text{ m}^2$ and the frictional losses in the intake are negligible. The maximum total temperature in the combustion chamber is $T_{\text{Max}} = 2500 \text{ K}$, and the fuel used is hydrogen having a heating value of $Q_R = 119 \text{ MJ/kg}$. The stagnation pressure loss in the combustor $\Delta p_{\text{CC}} = 3\%$ and the burning efficiency $\eta_b = 98\%$. The nozzle expands to atmospheric pressure for maximum thrust nozzle efficiency $\eta_N = 95\%$.

Assume

- The flow is a perfect gas having $R = 0.287 \text{ kJ/kg}$
- $\gamma_c = 1.4$ before combustion and $\gamma_h = 1.33$ after combustion

Calculate

- (a) The stagnation pressure ratio of the intake π_i
- (b) The fuel-to-air ratio
- (c) The stagnation pressure ratio in the nozzle π_N
- (d) The flight and exhaust speeds
- (e) The nozzle exit area
- (f) The thrust force
- (g) The specific thrust TSFC

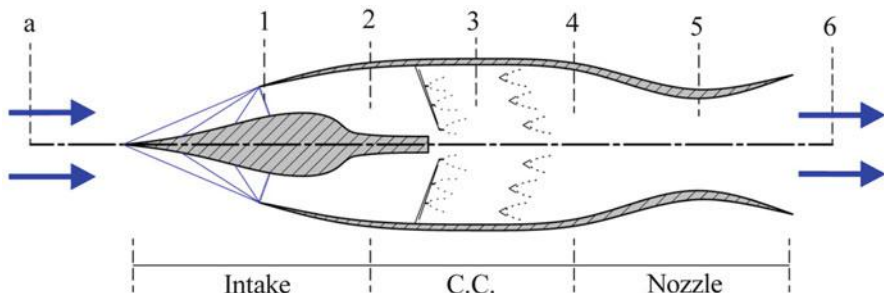


Figure (Problem 16)

5.17 The shown figure illustrates a ramjet engine having the following data:

Flight Mach number $M_a = 2.0$

Flight altitude is sea level where ambient pressure $P_a = 101 \text{ kPa}$

Maximum total temperature $T_{\text{omax}} = 2000 \text{ K}$

Pressure recovery of intake (diffuser) $r_d = 0.90$

Pressure recovery of combustion chamber $r_{cc} = 0.98$

Pressure recovery of nozzle $r_n = 0.96$

Constant properties of fluid inside the engine are assumed:

$$\gamma = 1.4 ; C_p = 1005 \text{ J/(kg K)}$$

- (A) Neglecting fuel mass flow rate, calculate the specific thrust in the following cases:

- (a) All process are ideal
- (b) Losses in intake only
- (c) Losses in intake and combustion chamber
- (d) Losses in intake, combustion chamber, and nozzle

- (B) Repeat the above calculations after calculating the fuel-to-air ratio (f) with fuel heating value: $Q_R = 43 \frac{\text{MJ}}{\text{kg}}$

5.18 The shown figure illustrates a ramjet engine having the following data:

Flight Mach number $M_a = 2.4$

Flight altitude is 61,000 m where ambient pressure $P_a = 18 \text{ kPa}$ and ambient temperature $T_a = 252.5 \text{ K}$

Maximum total temperature $T_{\text{omax}} = 2000 \text{ K}$

Pressure recovery of intake (diffuser) $r_d = 0.80$

Pressure recovery of combustion chamber $r_{cc} = 0.98$

Pressure recovery of nozzle $r_n = 0.96$

Constant properties of fluid inside the engine are assumed:

$$\gamma = 1.4 ; C_p = 1005 \text{ J/(kg K)}$$

- (a) Neglecting fuel mass flow rate, calculate the specific thrust.
- (b) Calculate the specific thrust for the same flight Mach number and pressure losses if the flight altitude has the following values: 0, 20,000, and 40,000 m.

5.19 An ideal ramjet engine has the following data:

Flight Mach number $M_a = 3.0$

Ambient conditions $T_a = 288 \text{ K}$, $P_a = 101 \text{ kPa}$

Maximum total temperature $T_{\text{omax}} = 1300 \text{ K}$

Inlet area $A_i = 0.1 \text{ m}^2$

Calculate

- (a) Air mass flow rate
- (b) Thrust
- (c) Propulsive, thermal, and overall efficiencies

5.20 A ramjet engine has the following data:

Flight Mach number $M_a = 2.0$

Ambient conditions: $T_a = 216.7 \text{ K}$, $P_a = 11.13 \text{ kPa}$

Maximum total temperature $Q_R = 45 \text{ MJ/kg}$

Specific heat ratio $\gamma = 1.4$

Calculate

- (a) Specific thrust
- (b) Propulsive efficiency

5.21 Boeing IM-99/CIM-10 *Bomarc rocket* is designed to fly at a cruising altitude of 60,000 ft (18 km), where the ambient temperature and pressure are 216.5 K and 7.5 kPa. Its liquid-fuel rocket engine boosts the Bomarc to Mach 2.5, when its ramjet engines Marquardt RJ43-MA-3, would take over for the remainder of the flight. For ideal processes and constant properties (γ , C_p),



- (a) Derive an expression for exhaust Mach number
- (b) Prove that it will have a constant value: $M_e = 2.5$
- (c) Calculate the specific thrust if $T_{04} = 2000 \text{ K}$ (ignore fuel)
- (d) Calculate the propulsive efficiency

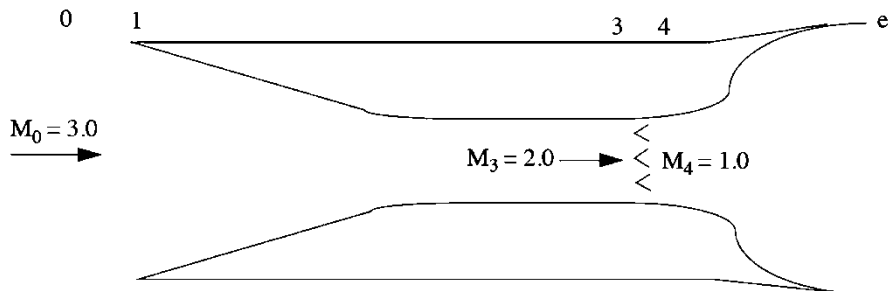
20. For an ideal ramjet engine, neglecting fuel-to-air ratio, prove that the thermal efficiency is expressed by

$$\eta_{th} = \frac{\frac{\gamma-1}{2} M_a^2}{1 + \frac{\gamma-1}{2} M_a^2}$$

SCRAMJET

- 5.22 The shown figure illustrates a scramjet engine powering an aerospace vehicle flying at Mach number of 3.0 at an altitude where the ambient conditions are:

$T_0 = 216 \text{ K}$, $P_0 = 20 \text{ kPa}$. Air is decelerated to Mach number of 2.0 at the inlet of combustion chamber. Heat is added at the combustion chamber to bring the Mach number at the exit of combustion chamber to 1.0. The flow expands to the ambient pressure at exit of nozzle ($P_e = P_a$). Assuming the whole processes in the engine are *ideal* and the flow have constant properties ($\gamma = 1.4$, $R = 287 \frac{\text{J}}{\text{kg.K}}$, $C_p = 1005 \frac{\text{J}}{\text{kg.K}}$).



- (a) Prove that $M_e = M_0$
- (b) Assuming negligible fuel to air ratio ($f \ll 1$), prove that

$$\frac{T}{P_0 A_0} = \gamma M^2 \left(\frac{U_e}{U_0} - 1 \right) + \frac{A_e}{A_0} \left(\frac{P_e}{P_0} - 1 \right)$$

- (c) Assuming Rayleigh flow in combustion chamber, calculate maximum temperature in the engine
- (d) Calculate $\frac{T}{P_0 A_0}$

- 5.23 A scramjet engine is used to power a hypersonic vehicle that flies at an altitude of 25,000 m, Mach number $M = 8$, using hydrocarbon fuel (Heating value $Q_{HV} = 44 \text{ MJ/kg}$).

The momentum thickness is $\theta = 3 \text{ mm}$, height of isolator $H = 0.08 \text{ m}$ and Reynolds number based on momentum thickness boundary layer is $Re_\theta = 3.5 \times 10^5$. Detailed data of its four elements are given in table below:

Air and gas properties

Element	γ	R	C_p	M_{inlet}	$\eta (\%)$
		$\left(\frac{\text{J}}{\text{kg.K}}\right)$	$\left(\frac{\text{J}}{\text{kg.K}}\right)$	Mach number at inlet	
Intake (states 1–2)	1.4	287	1005	8.0	92
Isolator (states 2–3)	1.37	287	1063	4.0	86
Burner (states 3–4)	1.30	297	1275	2.5	97
Nozzle (states 4–5)	1.33	290	1170	2.0	98

Calculate

- (a) Specific thrust and thrust specific fuel consumption
- (b) Thermal efficiency, propulsive efficiency, and overall efficiency
- (c) Mach number of gases leaving scramjet
- (d) Isolator length (L)

References

1. El-Sayed AF (2008) Aircraft propulsion and gas turbine engines. Taylor & Francis/CRC Press, February 2008, p. 97
2. The jet engine, 5th edn. Rolls-Royce plc, p. 3, Reprinted 1996 with revisions
3. Simpson B (2004) The enthusiast's guide to pulsejet engines, 2nd edn. <http://aardvark.co.nz/pjet>, May 2004
4. Fry RS (2004) A century of ramjet propulsion technology evolution. J Propuls Power 20(1), January–February 2004
5. Billing FS (1993) Research on supersonic combustion. AIAA J Propuls Power 9:499–514
6. Narayan GKB (2013) Pulsejet technology. 38th Engine systems symposium – March 2013
7. <http://www.pulse-jets.com/valveless/>
8. Zaloga, V-1 Flying Bomb 1942–52: Hitler's Infamous 'Doodlebug', Osprey Publishing, January 2005
9. <http://www.fiddlersgreen.net/models/aircraft/Yokosuka-Ohka.html>
10. Scott Sayres J Jr (2011) Computational fluid dynamics for pulsejets and pulsejet related technologies. M. Sc. thesis, Raleigh, North Carolina, 2011
11. Roskam J, Lan C-TE (1997) Airplane aerodynamics and design. DAR Corporation, Lawrence, Kansas, p 258
12. Greatrix DR (2012) Powered flight – the engineering of aerospace propulsion. Springer, London/New York
13. Manganiello EJ, Valerino MF, Essig RH (1945) Sea- level performance tests of A 22- inch-diameter pulse-jet engine at various simulated ram pressures, NACA MR No. E5J02, October 1945
14. Litke PJ, Schauer FR, Paxon DE, Bradley RP, Hoke JL. Assessment of the performance of a pulsejet and comparison with a pulsed-detonation engine, AIAA-2005-0228
15. Kailasanathan RKA (2007) Experimental investigation on pulsejet engines. M.Sc. thesis, North Carolina, Rayleigh
16. Geng T, Paxon DE, Zheng F, Kuznetsov AV, Roberts WL (2008) Comparison between numerically simulated and experimentally measured flow field quantities behind a pulsjet. NASA/TM-2008-215432
17. Heiser W, Pratt D (2002) Thermodynamic cycle analysis of pulse detonation engines. J Propuls Power 18:68–76
18. Norris G (2008) Pulse power: pulse detonation engine- powered flight demonstration marks milestone in mojave. Aviat Week Space Technol 168(7):60
19. Povinelli LA. Pulse detonation engine for high speed flight, NASA/TM 2002-211908
20. Irandoust M (2012) A numerical study of reacting flows using finite rate chemistry. Ph. D. thesis, Chalmers University of Technology, Sweden
21. Kumar SA (2011) Parametric and performance analysis of a hybrid pulse detonation/turbofan engine. M.Sc. in Aerospace Engineering, The University of Texas at Arlington
22. Jindal TK (2012) Pulse detonation engine – a next generation propulsion. IJMER 2 (6):4083–4085

23. Mawid MA, Park TW, Sekar B, Arana C (2003) Application of pulse detonation combustion to turbofan engines. *J Eng Gas Turbines Power* 125(1):270–283
24. Coleman ML (2001) Overview of pulse detonation propulsion technology, Chemical propulsion Information Agency (CPIA), Report CPTR 70, April 2001
25. Zucker RD, Biblarz O (2002) Fundamentals of gas dynamics, 2nd edn. Wiley, Hoboken, New Jersey, p 336
26. Sato T, Tanatsugu N, Naruo Y, Omi J, Tomike J, Nishino T (2000) Development study on ATREX Engine. *Acta Astronautica* 47(11):799–808
27. Heiser W, Pratt D (1994) Hypersonic airbreathing propulsion, AIAA education series. American Institute of Aeronautics and Astronautics, Washington, DC
28. Zucrow MJ (1958) Aircraft and missile propulsion volume II: the gas turbine power plant, the turboprop, turbojet, ramjet, and rocket engines. Wiley, New York
29. Hill P, Peterson C (1992) Mechanics and thermodynamics of propulsion, 2nd edn. Addison Wesley Publication Company Inc, Reading, p 155
30. <http://en.wikipedia.org/wiki/Scramjet>
31. Heppenheimer TA (2011) Facing the heat barrier: a history of hypersonics. Books Express Publishing, July 31, 2011
32. National Aerospace Plane (NASP) (2007) Facing the heat barrier: a history of hypersonics – V-2, Sanger, Missile Nose Cones, X-15, Scramjets, Space shuttle, NASA SP-2007-4232. National Aerospace Plane (NASP), Washington, DC, pp X-33–X-34
33. François F (2004) Propulsion systems for hypersonic flight, RTO-EN-AVT-116, Lecture Series on “Critical Technologies for Hypersonic Vehicle Development”, von Kármán Institute, Rhode-St-Genèse, Belgium, 10–14 May, 2004
34. John J (1994) Bertin, hypersonic aerothermodynamics, AIAA education series. American Institute of Aeronautics and Astronautics, Washington, DC
35. Rife JP, Cantelon PL. Speeds up to orbital: a history of the William H. Avery Advanced Technology Development Laboratory, www.jhuapl.edu/techdigest/TD/td2804/rife.pdf
36. Hallion RP (1995) The hypersonic revolution: eight case studies. In: Hallion RP (ed) The history of hypersonic technology, volume II: from scramjet to the national aero-space plane (1964–1986). Wright-Patterson Air Force Base, Ohio
37. Waltrup PJ, White M, Zarlingo F, Gravlin E (1994) History of ramjet and scramjet propulsion development for U.S. navy missiles. *J Hopkins APL Tech Dig* 2:234–244
38. Curran ET (2001) Scramjet engines: the first forty years. *J Propuls Power* 17(6):1138–1148
39. Segal C (2009) The scramjet engine: processes and characteristics. Cambridge University Press, Cambridge/New York
40. Roudakov AS, Schickzman Y, Semenov V, Novelli Ph, Fourt O (1993) Flight testing an axisymmetric scramjet: russian recent advances. 44th congress of the international astronomical federation, 16–22 October, 1993, Graz, Austria
41. Kazmar RR. Airbreathing hypersonic propulsion at Pratt & Whitney – Overview, AIAA-2005-3256
42. <http://www.powershow.com/view/3b57b7-ZGVIM/TECHNICAL%20ADVANCES%20IN%20AIR%20BREATHING%20PROPULSION%20AIR%20BREATHTHIN>
43. http://en.wikipedia.org/wiki/Scramjet_programs
44. Pandey KM (2010) Recent advances in scramjet fuel injection – a review. *Int J Chem Eng Appl* 1(4):294–301
45. Toro PGP, Minucci MA, Rolim T, Follador R, Santos A, Camillo G, Barreta L. Brazilian 14-X hypersonic aerospace vehicle project, AIAA 2012-5851
46. Smart MK. Scramjet isolators, RTO-EN-AVT-185
47. Torrez SM, Dalle DJ, Driscoll JF. Dual mode scramjet design to achieve improved operational stability, AIAA 2010-6957

Chapter 6

Turbine-Based Engines: Turbojet, Turbofan, and Turboramjet Engines

6.1 Introduction

Turbine-based cycle engines (or gas turbine) together with athodyd engines represent the two main categories of reaction engines; refer to Fig. 4.1. Athodyd engines are analyzed in Chap. 5, while gas turbine engines will be analyzed in this chapter. The main difference between athodyd and turbine engines is the presence of turbomachines or rotating modules in turbine engines. There are five main types of gas turbine engines; namely: turbojet, turbofan, advanced ducted fan, turbo-ram, and turbo-rocket. In this chapter only three engines will be treated, namely, turbojet, turbofan, and turboramjet engines. Turbo-rocket engines will be analyzed in late chapters handling rockets.

Aircraft designers have always been limited by the efficiency of the available power plants. Their constant endeavor is to achieve higher thrust, lower fuel consumption, less weight, smaller frontal area, and better cooling characteristics [1].

Both piston engine and gas turbine engine are internal combustion engines. In both, air is compressed, fuel added, and the mixture ignited, and the rapid expansion of the resultant hot gas produces the power or thrust. However, combustion in a piston engine is intermittent, and the expanding gas produces shaft power through a piston and crank shaft arrangements, Chap. 4, whereas in a jet engine combustion is continuous and its power results from expanding gas being forced out of the rear of the engine as described in Chap. 5 and the present chapter.

Jet engines overcome the many drawbacks of piston engines particularly for higher-power engines. Comparison between turbine and reciprocating (piston) engines having the same power will be given hereafter [2].

Advantages of *gas turbines* over piston engines are:

Turbine engines have higher-power-to-weight ratio.

Turbine engines need less maintenance per flying hour.

Turbine engines have less frontal area and consequently less drag force.

Turbine engines do not need any oil dilution or engine preheating before starting. Turbine engines have lower rates of oil consumption.

Advantages of *piston engines* over gas turbines are:

Piston engines are less exposed to foreign object damage.

Piston engines have faster acceleration rates compared to turbine engines.

Piston engines have less operating temperature.

Piston engines have lower fuel consumption specially for low flight speeds.

Piston engines have much less initial costs compared to turbine engines.

6.2 Turbojet

6.2.1 Introduction

The turbojet is the basic engine of the jet age. It resembles the simplest form of gas turbine. It was separately coinvented by the two fathers of jet engines: Frank Whittle from Britain and von Ohain from Germany. The first airplane powered by a turbojet engine was the He178 German aircraft powered by the He S-3 engine on August 27, 1939. Based on von Ohain work, the German engine Junker *Jumo 004* was later developed. It was the world's first turbojet engine in production and operational use as well as the first successful axial compressor jet engine ever built. Some 8000 units were manufactured by Junkers in Germany during late World War II which powered several aircrafts including Messerschmitt Me 262 jet fighter, Arado Ar 234 jet reconnaissance/bomber, and prototypes of the Horten Ho 229. Frank Whittle in England having no knowledge of Ohain's engine built his W.1 turbojet engine which powered the Gloster E28/39 aircraft. Turbojets are rarely flying today due its disadvantage of high noise levels and drastic fuel consumption. Examples for the still flying turbojets powering civil transports are GE CJ610-Learjet 25 series, P&W JT12 Sabre 40, and JetStar Dash 8. Turbojet engines still power old military fighters, cruise and antiship missiles, as well as turboramjet engines. Examples for cruise missiles are AGM-109C/H/I/J/K/L and Microturbo TRI 60, while 3M-54 Klub is an example for antiship missiles and J58 turboramjet engine powering SR-71 aircraft.

As described in Chap. 5, both ramjet and scramjet engines cannot develop takeoff thrust. To overcome this disadvantage, a compressor is installed in the inlet duct so that even at zero flight speed, air could be drawn into the engine. This compressor is driven by the turbine installed downstream of the combustion chamber and connected to the compressor by a central shaft. Addition of these two rotating parts or modules (compressor and turbine) converts the ramjet into a turbojet. The three successive modules, compressor, combustion chamber, and turbine, constitute what is called *gas generator* (Fig. 6.1). The air is squeezed in the compressor to many times its normal atmospheric pressure and then forced into the combustion chamber. Fuel is sprayed into the compressed air, ignited, and burnt continuously in the combustion chamber. This raises the temperature of the

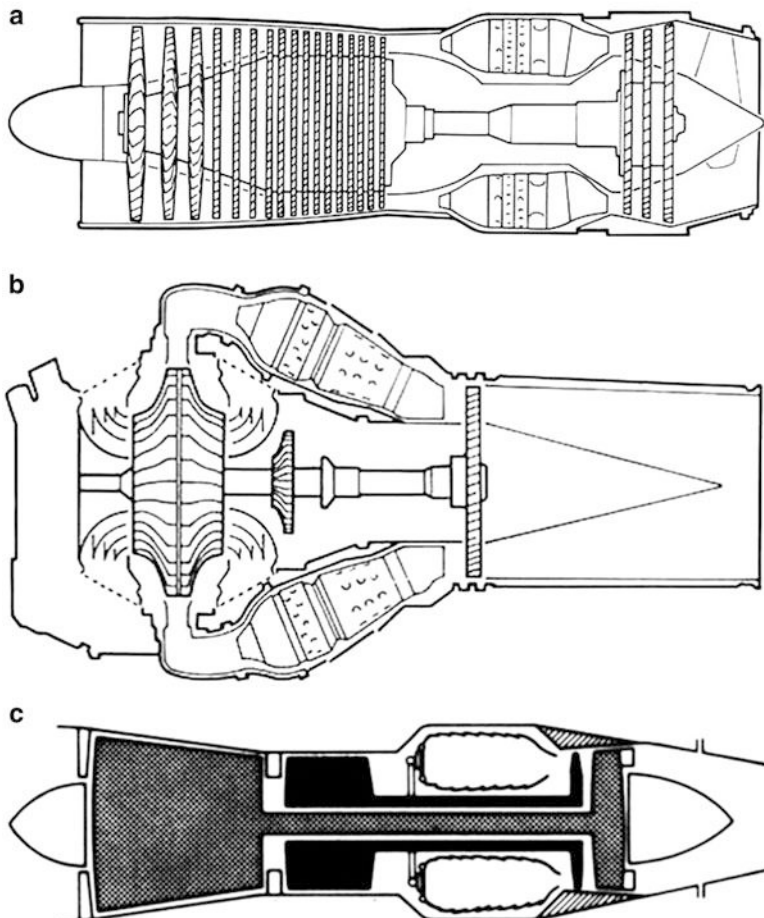


Fig. 6.1 Layout of single- and dual-spool turbojet engine. (a) Single-spool centrifugal flow compressor. (b) Single-spool axial flow compressor. (c) Double-spool axial flow compressor

fluid mixture to about 600° – 800° C. The resulting burning gases expand rapidly rearward and pass through the turbine, which drives the compressor. The turbine extracts energy from the expanding gases to drive the compressor. If the turbine and compressor are efficient, the pressure at the turbine discharge will be nearly twice the atmospheric pressure, and this excess pressure is sent to the nozzle to produce a high-velocity stream of gases. These gases bounce back and shoot out of the rear of the exhaust, thus producing a thrust propelling the plane. This five-module engine (intake, compressor, combustion chamber, turbine, and nozzle) is identified as a single-spool turbojet engine.

Substantial increases in thrust can be obtained by employing an afterburner or an augmenter. It is a second combustion chamber positioned between the turbine and

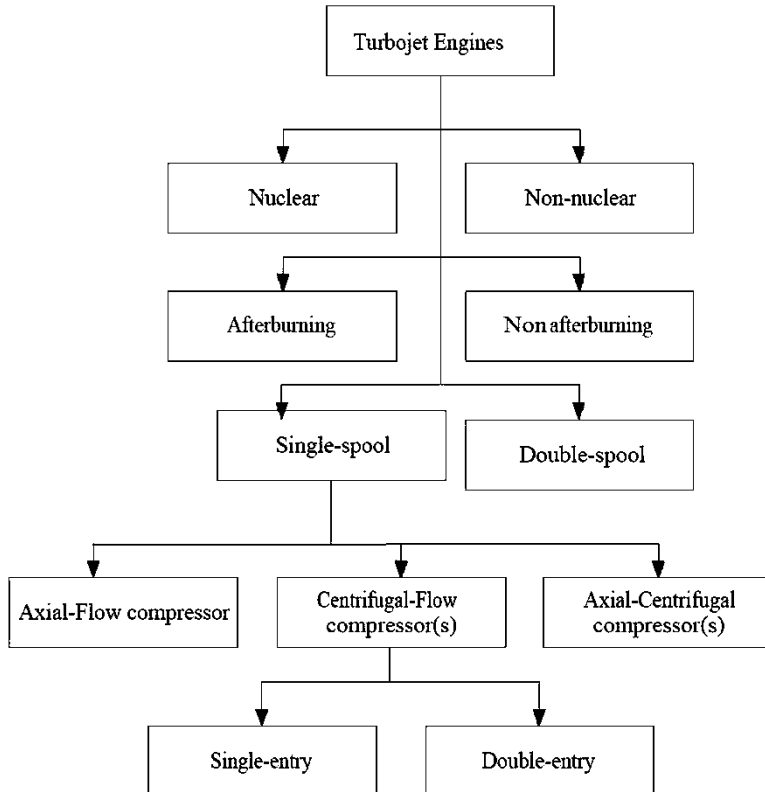


Fig. 6.2 Classification of turbojet engines

the nozzle, which is normally employed in military aircrafts. Moreover, for civil transport, the thrust force may be increased by adding a second spool (or a second set of compressor–turbine combination). Figure 6.1 illustrates two layouts for a single-spool turbojet using either an axial or centrifugal compressors while a third layout for a double-spool engine.

Classification of turbojet engines [1] is shown in Fig. 6.2. Turbojet engines may be a *nuclear* or nonnuclear engine. In the late 1940s and through the 1950s [3], preliminary work was done on developing nuclear-powered rockets and jet engines. In nuclear turbojet engine, a liquid metal is heated by the reactor which passes through a heat exchanger in the combustion chamber.

Both US and USSR nuclear programs developed the American “Crusader” NB-36, version of

B-36 [4], as well as the Russian Tupolev Tu-95 LAL [5]. Both programs were ultimately cancelled due to technical difficulties and growing safety concerns as catastrophic atomic radiation might be encountered in case of crashes/accidents of such nuclear airplanes.

Other classifications for turbojet engines may be *afterburning* or non-afterburning. Afterburning (or reheat) is a method of augmenting the basic thrust of an engine to improve the aircraft takeoff, climb, and (for military aircraft) combat performance.

Afterburner is another combustion chamber added between the turbine and the nozzle that utilizes the unburnt oxygen in the exhaust gas to support combustion. The increase in the temperature of the exhaust gas increases the velocity of the exhaust gases leaving the nozzle and therefore increases the engine thrust by 40 % at takeoff and a much larger percentage at high speeds once the plane is in the air.

A third classification of the turbojet engines is based on their *number of spools*. Turbojets may be single- or two (sometimes identified as double or dual)-spool engines. A single-spool turbojet has one shaft with a compressor and a turbine mounted at either shaft ends, while a two-spool engine has two concentric shafts as well as two compressors and turbines. The first compressor next to the intake is identified as the low-pressure compressor (LPC) which is driven by the low-pressure turbine (LPT). Both together with their shaft are denoted as the low-pressure spool. The high-pressure compressor (HPC) is situated downstream of the low-pressure compressor. Also this compressor is driven by the high-pressure turbine (HPT). Both are coupled by the high-pressure shaft (which is concentric with the low-pressure shaft) and constitute the modules of the high-pressure spool. Figure 6.1 illustrates the layout and modules of the single- and double-spool turbojet engines.

The single-spool engine may be further classified based on the *type of compressor* employed. The compression section may be composed of either a single or double compressors. Moreover, the compressor may be of the axial or centrifugal (radial) type. A single axial or centrifugal compressor is seen in some turbojets. In other cases two compressors assembled in series are found. These compressors may be either two centrifugal compressors or an axial compressor followed by a centrifugal compressor.

Lastly, this classification closes by the *type of entry* associated with the two centrifugal compressors case. Centrifugal compressors may have either a single or double entries if they were assembled in a back-to-back configuration.

6.2.2 Milestones of Turbojet Engines

[Appendix B](#) summarizes important milestones along the history of turbojet engines in both civil and military applications.

6.2.3 Thermodynamic Cycle Analysis of a Single Spool

Single-spool turbojet engine is composed of five modules, namely, intake (or inlet), compressor, combustion chamber, turbine, and nozzle. Afterburning turbojet

incorporates a sixth module, namely, afterburner. Intake, combustion chamber, afterburner (if included), and nozzle are stationary elements, whereas compressor and turbine are rotating elements. Generally, in aero engines and gas turbines, two types of compressors and two types of turbines are found. These are the centrifugal and axial flow compressors (which will be analyzed in Chap. 9) and radial and axial turbines (will be analyzed in Chap. 10). Centrifugal compressor was used in both first engines of von Ohain and Whittle. The axial flow type has several stages of alternate rotating and stationary airfoil blades which can achieve compression ratios in excess of 40:1. Axial turbine consists of one or more stages of alternate stationary and rotating airfoil-section blades. The turbine extracts energy from the hot exhaust gases to drive the compressor. Radial turbines are found in small gas turbines like APU.

The characteristics of the engine that must be known in advance are flight speed (or Mach number), flight altitude, compressor pressure ratio, turbine inlet temperature (TIT) and maximum temperature of the cycle (if the afterburner is operative), type of nozzle (convergent or convergent–divergent), and fuel lowest heating value. Percentage of bled air as well as the power delivered to drive accessories and any aircraft systems must be also specified. Component efficiencies of all modules and pressure drops in stationary modules (inlet, combustor, and afterburner) must also be known. When the cycle is assumed ideal, then all efficiencies are assumed unity (or hundred percent) and all pressure drops are assumed zeros.

Figure 6.3 illustrates a layout with its designation points (Fig. 6.3a) as well as thermodynamic cycle (T-s diagram) for a single-spool turbojet with inoperative afterburner (Fig. 6.3b) and with operative afterburner (Fig. 6.3c).

The cycle different processes are described here:

- (1): air flows from far upstream (where the velocity of air relative to engine is the flight velocity) up to the intake, usually with some deceleration during cruise and acceleration during takeoff (the process is always ideal where: $h_{0a} = h_{01}$).
- (1)–(2): air flows through the inlet (or intake) and ducting system up to the compressor inlet. Since this element is always considered as a diffuser, the air velocity is decreased.
- (2)–(3): air is compressed in a dynamic compressor.
- (3)–(4): air is heated by mixing and burning of fuel within the combustion chamber.
- (4)–(5): products of combustion are expanded through a turbine to obtain power to drive the compressor.
- (5)–(6): gases may or may not be further heated if the afterburner is operative or inoperative.
- (6)–(7): gases are accelerated and exhausted through the exhaust nozzle.

If the engine is not fitted with afterburner, then states 5 and 6 are coincident. The amount of mass flow is usually set by flow choking in the nozzle throat.

The following remarks may be listed:

1. All components are irreversible but they are adiabatic (except burners); thus, isentropic efficiencies for the intake, compressor, turbine, and nozzle are employed.

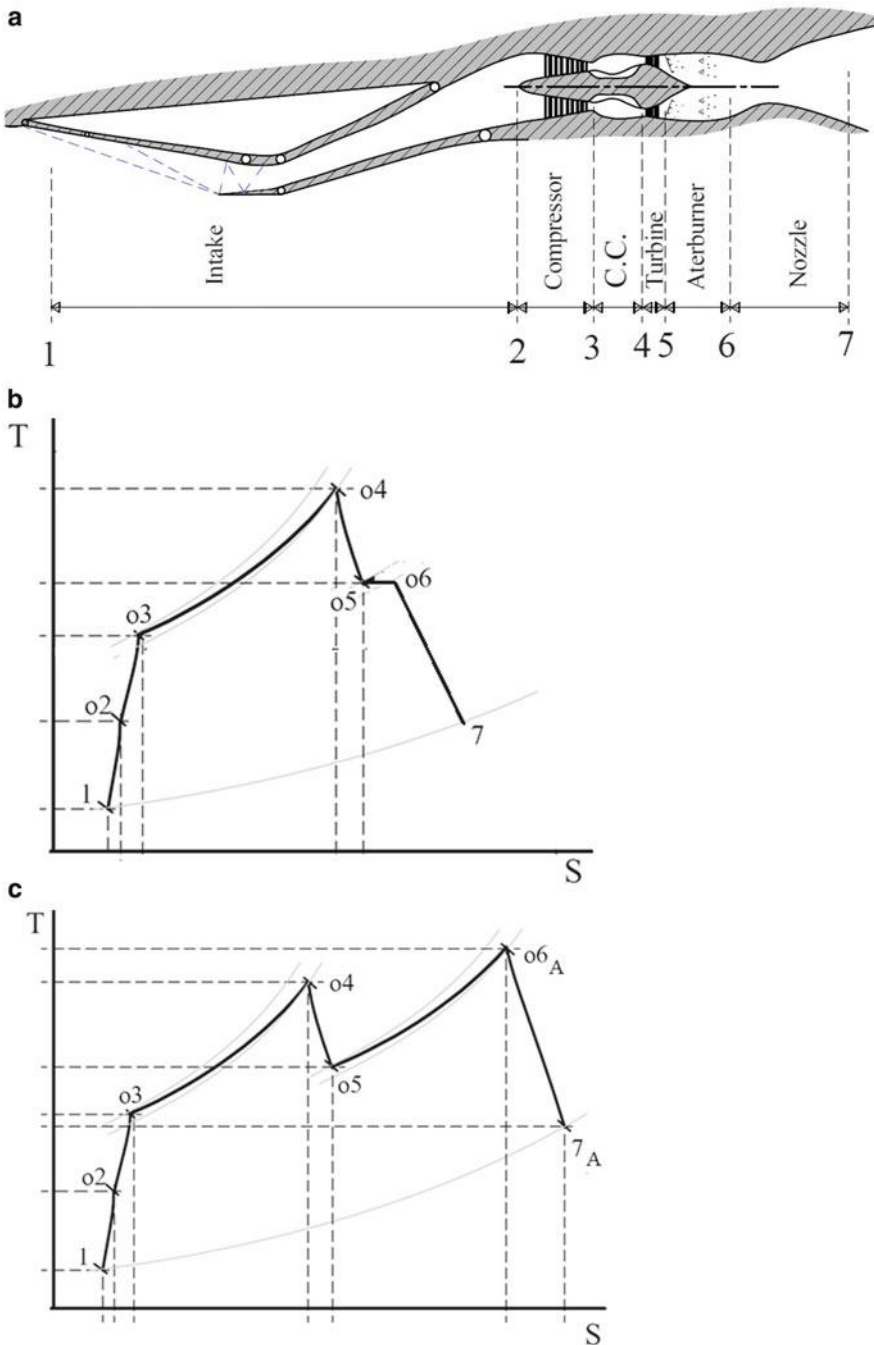


Fig. 6.3 Single-spool turbojet engine. (a) Schematic diagram. (b) T-s diagram of actual cycle with inoperative afterburner. (c) T-s diagram of actual cycle with operative afterburner

2. Friction in the air intake (or diffuser) reduces the total pressure from its free-stream value and increases its entropy. At the intake outlet, the total temperature is higher than the isentropic case, while the total pressure is smaller than the isentropic case which depends on the intake or diffuser efficiency (η_d). Depending on flight Mach number, the diffuser efficiency ranges as $(0.7 < \eta_d < 0.9)$. The specific heat ratio ($\gamma = 1.4$). More details about intakes will be given in Chap. 8.
3. The compression of the air in the compressor increases temperature, pressure, and entropy due to irreversibilities of this process. Such increase in temperature depends on the compressor efficiency (η_c) which ranges from 0.85 to 0.90, while the specific heat ratio ($\gamma = 1.37$). A portion of the compressed air is utilized in cooling the turbine disks, blades, and the supporting bearings through an air bleed system. Thus, the air mass flow rate in the succeeding modules is somewhat smaller than that entering the compressor.
4. The burners are not simple heaters and the chemical composition of the working fluid changes during combustion process. The larger the fuel-to-air ratio (f) the greater is the deviation in the chemical composition of the products of combustion from that of the air. Losses in the combustion process are encountered due to many factors including imperfect combustion, physical characteristics of the fuel, as well as thermal losses due to conduction and radiation. Such losses are handled by introducing the burner efficiency (η_b), where: $0.97 < \eta_b \leq 0.99$. Pressure drop due to skin friction and pressure drag in the combustors (normally 3–6 % of the total pressure of the entering air) must be also taken into account.
5. The expansion process in turbine is very nearly adiabatic. However, due to friction an increase in the entropy is encountered. Moreover, the outlet temperature is higher than that of the isentropic case. Thus, the available power from the turbine is less than that in the isentropic case. The expansion process is associated with the turbine efficiency (η_t), where: $0.90 < \eta_t < 0.95$ and specific heat ratio ($\gamma = 1.33$).
6. The afterburner is similar to the burner. This added fuel is much greater than that added in combustion chamber (burner). Losses in the afterburner are also due to imperfect combustion and thermal losses due to conduction and radiation. Such losses are handled by introducing the burner efficiency (η_{ab}), where: $0.97 < \eta_{ab} \leq 0.99$. Also a total pressure drop is encountered ranging between 3 and 6 %.
7. Finally, the expansion process in the nozzle is similar to that in the turbine and influenced by skin friction. It is also governed by the adiabatic efficiency (η_n), where: $0.95 < \eta_n < 0.98$. The specific heat ratio $\gamma = 1.36$

It is here worth mentioning that air/gas velocities within the gas generator is ignored. The velocities at the inlet to intake and outlet of nozzle are only calculated.

The different processes through the engine modules are described again here.

1. Intake

During cruise, the static pressure rises from (a) to (1) outside the intake and from (1) to (2) inside the intake. The air is decelerated relative to the engine. Since the

velocity at (2) is assumed to be zero and the deceleration is adiabatic, then the total or stagnation pressure at states (0) and (1) are equal and greater than its value at state (2).

The stagnation temperatures for states (a), (1), and (2) are equal and independent from any losses:

$$T_{02} = T_{01} = T_{0a} = T_a \left(1 + \frac{\gamma - 1}{2} M^2 \right) \quad (6.1)$$

Outside the engine, the total pressure remains constant; thus:

$$P_{01} = P_{0a} = P_a \left(1 + \frac{\gamma - 1}{2} M^2 \right)^{\frac{\gamma}{\gamma-1}} \quad (6.2)$$

The pressure recovery within the inlet may be given; thus, the outlet pressure is obtained from the relation:

$$r_d = \frac{P_{02}}{P_{0a}} \quad (6.3a)$$

Alternatively, the efficiency (η_d) of the inlet (also denoted as intake or diffuser) is given. The outlet pressure will be given by:

$$P_{02} = P_a \left(1 + \eta_d \frac{\gamma_c - 1}{2} M_a^2 \right)^{\frac{\gamma_c}{\gamma_c - 1}} \quad (6.3b)$$

2. Compressor

From state (2) to (3), an irreversible adiabatic compression process takes place, which is associated with the isentropic efficiency of the compressor (η_c). Thus, with known pressure ratio (π_c), the pressure and temperature at the outlet of the compressor are evaluated from the relations:

$$P_{03} = P_{02} \times \pi_c \quad (6.4)$$

$$T_{03} = T_{02} \left(1 + \frac{\pi_c^{\frac{\gamma_c - 1}{\gamma_c}} - 1}{\eta_c} \right) \quad (6.5)$$

3. Combustion chamber

In combustion process, fuel is injected in an atomized form, evaporated, and mixed with air. Spark plugs initiate the combustion process. The mass flow rate of the burnt fuel is calculated from the energy balance of the combustion chamber:

$$(\dot{m}_a + \dot{m}_f) C p_h T_{04} = \dot{m}_a C p_e T_{03} + \eta_b \dot{m}_f Q_R$$

The temperature at the outlet of the combustors (inlet of turbine) is determined from metallurgical limits set by the turbine blade material and is known as the turbine inlet temperature ($TIT \equiv T_{04}$) or turbine entry temperature (TET).

With $f = \dot{m}_f / \dot{m}_a$

then the fuel-to-air ratio is determined from the relation:

$$f = \frac{Cp_h T_{04} - Cp_c T_{03}}{\eta_b Q_R - Cp_h T_{04}} \quad (6.6)$$

The stagnation pressure at the outlet of combustion chamber, state (4), is less than its value at the inlet, state (3), because of fluid friction. The pressure drop is either given as a definite value or as a percentage. Thus, the outlet pressure from the combustion chamber is expressed either as:

$$P_{04} = P_{03} - \Delta P_{cc} \quad (6.7a)$$

or

$$P_{04} = P_{03}(1 - \Delta P_{cc}\%) \quad (6.7b)$$

4. Turbine

The power consumed in the compressor is supplied by the turbine. If the ratio of the power needed to drive the compressor to the power available in the turbine is (λ), then the energy balance for the compressor–turbine shaft is:

$$W_c = \eta_m \lambda W_t$$

Here (λ) is of the range 75–85 %. Thus, 15–25 % of the turbine power is used in driving accessories, different actuators in the aircraft systems/cycles. The mechanical efficiency (η_m) is equal or greater than 98 %. Thus, in terms of the temperature differences:

$$\begin{aligned} Cp_c(T_{03} - T_{02}) &= \lambda \eta_m (1 + f) Cp_h (T_{04} - T_{05}) \\ \left(\frac{T_{05}}{T_{04}} \right) &= 1 - \frac{(Cp_c/Cp_h) T_{02}}{\lambda \eta_m (1 + f) T_{04}} \left[\left(\frac{T_{03}}{T_{02}} \right) - 1 \right] \end{aligned} \quad (6.8)$$

The outlet pressure is calculated considering the adiabatic efficiency of the turbine (η_t); thus:

$$\frac{P_{05}}{P_{04}} = \left[1 - \frac{1}{\eta_t} \left(1 - \frac{T_{05}}{T_{04}} \right) \right]^{\gamma_h / (\gamma_h - 1)} \quad (6.9a)$$

Then the turbine and compressor pressure ratios are related by:

$$\left(\frac{P_{05}}{P_{04}}\right) = \left\{ 1 - \frac{(Cp_c/Cp_h)T_{02}}{\lambda(1+f)\eta_m\eta_c\eta_t T_{04}} \left[\left(\frac{P_{03}}{P_{02}}\right)^{\frac{\gamma_c-1}{\gamma_c}} - 1 \right] \right\}^{\frac{\gamma_h}{\gamma_h-1}} \quad (6.9b)$$

$$\text{Or in general : } \pi_t = \left[1 - A \left(\pi_c^{\frac{\gamma_c-1}{\gamma_c}} - 1 \right) \right]^{\frac{\gamma_h}{\gamma_h-1}} \quad (6.9c)$$

$$\text{Where : } A = \frac{(Cp_c/Cp_h)T_{02}}{\lambda(1+f)\eta_m\eta_c\eta_t T_{04}}$$

From equation (6.1)

$$\left(\frac{P_{05}}{P_{04}}\right) = \left\{ 1 - \frac{(Cp_c/Cp_h)T_a}{\lambda(1+f)\eta_m\eta_c\eta_t T_{04}} \left(1 + \frac{\gamma-1}{2} M^2 \right) \left[\left(\frac{P_{03}}{P_{02}}\right)^{\frac{\gamma_c-1}{\gamma_c}} - 1 \right] \right\}^{\frac{\gamma_h}{\gamma_h-1}} \quad (6.9d)$$

5. Afterburner

If the jet engine is without an afterburner, then no work or heat transfer occurs downstream of turbine, station (5). The stagnation enthalpy remains constant throughout the rest of engine. However, if there is an afterburner, we have two cases; either the afterburner is operative or inoperative.

(a) Inoperative afterburner

If the afterburner is inoperative (Fig. 6.3b), no further fuel is burnt, and the stagnation (total) temperature at states (5) and (6) is equal or:

$$T_{06} = T_{05} \quad (6.10)$$

Concerning the total pressure, a similar treatment to the combustion chamber is considered. Thus, based on the value of the pressure drop within the afterburner due to the skin friction and the drag from the flameholders:

$$P_{06} = P_{05} - \Delta P_{ab} \quad (6.11a)$$

$$\text{Or : } P_{06} = P_{05}(1 - \Delta P_{ab}\%) \quad (6.11b)$$

(b) Operative afterburner

For operative afterburner (Fig. 6.3c), a subscript (A) is added to the symbols of the temperature and the pressure to denote operative afterburner. In this case an additional amount of fuel is burnt which raises the temperature to (T_{06A}):

$$T_{06A} = T_{\text{MAX}} \quad (6.12)$$

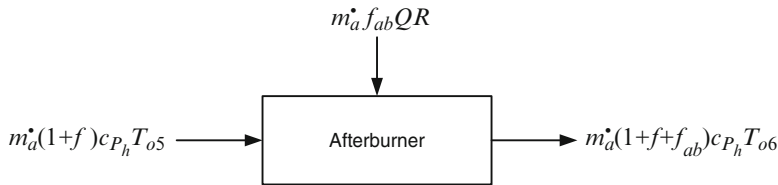


Fig. 6.4 Energy balance for afterburner

It may be higher than the turbine inlet temperature (*TIT*). The reason for such a higher temperature is that the downstream element is the nozzle, which is a nonrotating part. Thus, the walls are subjected only to thermal stresses rather than the combined thermal and mechanical stresses as in the turbine(s). The pressure at the outlet of the afterburner will be also less than its value at the inlet. It is calculated using Eq. (6.11a) and (6.11b) but P_{06A} replaces P_{06} . Conservation of mass and energy are discussed with reference to Fig. 6.4.

There is an additional fuel quantity (\dot{m}_{fab}) added and burnt in the afterburner. Then conservation of mass within the afterburner is expressed by:

$$\dot{m}_6 = \dot{m}_5 + \dot{m}_{fab}$$

Conservation of energy yields:

$$\begin{aligned}\dot{m}_5 h_{05} + \eta_{ab} \dot{m}_{fab} Q_R &= \dot{m}_6 h_{06A} \\ \dot{m}_5 C_{p5} T_{05} + \eta_{ab} \dot{m}_{fab} Q_R &= (\dot{m}_5 + \dot{m}_{fab}) C_{p6A} T_{06A} \\ (1+f) C_{p5} T_{05} + \eta_{ab} f_{ab} Q_R &= (1+f+f_{ab}) C_{p6A} T_{06A}\end{aligned}$$

The afterburner fuel-to-air ratio is calculated from the relation:

$$f_{ab} = \frac{(1+f)(C_{p6A} T_{06A} - C_{p5} T_{05})}{\eta_{ab} Q_R - C_{p6A} T_{06A}} \quad (6.13)$$

6. Nozzle

The two cases of inoperative and operative afterburner are again considered.

(a) Inoperative afterburner

A check for nozzle choking is performed first by calculating the critical pressure. The critical pressure is obtained from the relation:

$$\frac{P_{06}}{P_c} = \frac{1}{\left[1 - \frac{1}{\eta_n} \left(\frac{\gamma_n - 1}{\gamma_n + 1}\right)\right]^{\frac{\gamma_n}{\gamma_n - 1}}} \quad (6.14)$$

The critical pressure is then compared with the ambient pressure. If it is greater or equal to the ambient pressure, then the nozzle is choked ($M_7 = 1$). This means that $P_7 = P_c$ and the nozzle outlet temperature (T_7) is then calculated from the relation:

$$\left(\frac{T_{06}}{T_7}\right) = \left(\frac{\gamma_n + 1}{2}\right) \quad (6.15)$$

The exhaust velocity is then calculated as:

$$V_7 = \sqrt{\gamma_n R T_7} \quad (6.16)$$

On the other hand if the ambient pressure is greater than the critical pressure, then the nozzle is unchoked, and the exhaust pressure is equal to the ambient pressure, $P_7 = P_a$, and the exhaust gases are determined from the relation:

$$V_7 = \sqrt{2Cp_n(T_{06} - T_7)} = \sqrt{2Cp_n\eta_n T_{06} \left[1 - (P_a/P_{06})^{\frac{\gamma_n-1}{\gamma_n}}\right]} \quad (6.17a)$$

$$\text{or} \quad V_7 = \sqrt{\frac{2\gamma_n\eta_n R T_{06}}{(\gamma_n - 1)} \left[1 - (P_a/P_{06})^{\frac{\gamma_n-1}{\gamma_n}}\right]} \quad (6.17b)$$

(b) Operative afterburner

The expansion process in the nozzle starts from state (06A) to state (7). The critical pressure is calculated from the relation:

$$\frac{P_{06A}}{P_c} = \frac{1}{\left[1 - \frac{1}{\eta_n} \left(\frac{\gamma_n-1}{\gamma_n+1}\right)\right]^{\frac{\gamma_n}{\gamma_n-1}}} \quad (6.18)$$

If the nozzle is unchoked, the exhaust pressure will be equal to the ambient one. The jet speed will then be:

$$V_{7ab} = \sqrt{2Cp_n\eta_n T_{06A} \left[1 - (P_a/P_{06A})^{\frac{\gamma_n-1}{\gamma_n}}\right]} \quad (6.19a)$$

If the nozzle is choked, then:

$$V_{7ab} = \sqrt{\gamma_n R T_{7A}} \quad (6.19b)$$

A general relation for the exhaust speed (whether choked or unchoked) may be obtained from Eq. (4.25) by replacing P_a by P_7 ; thus:

$$V_{7ab} = \sqrt{2Cp_n\eta_n T_{06A} \left[1 - (P_7/P_{06A})^{\frac{\gamma_n-1}{\gamma_n}}\right]} \quad (6.20)$$

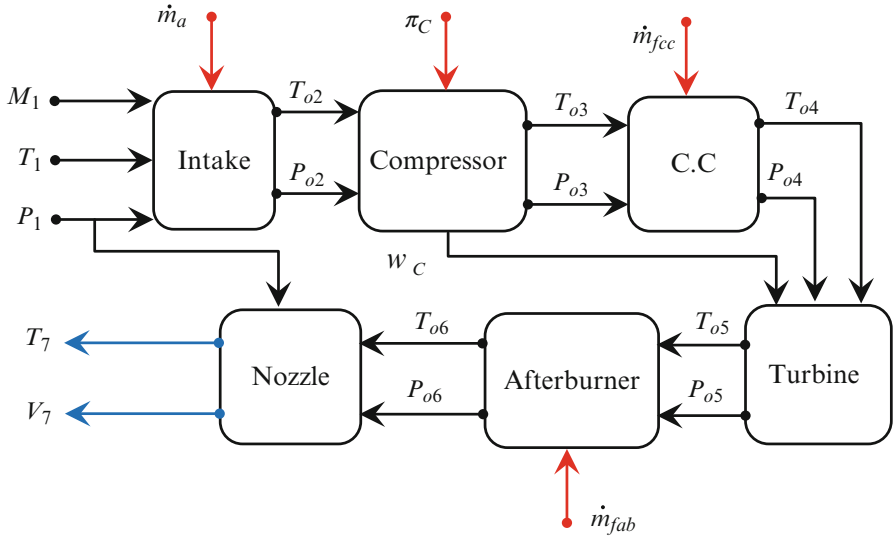


Fig. 6.5 Block diagram for the single-spool afterburning turbojet engine

The previous processes in a single-spool turbojet engines can be illustrated by the block diagram shown in Fig. 6.5 which displays flow information, input, and output data.

6.2.4 Performance Parameters of a Single Spool

The two engine parameters defining the performance of engine are the specific thrust and the specific fuel consumption. The specific thrust is expressed by the relation:

$$\frac{T}{\dot{m}_a} = [(1 + f + f_{ab})V_7 - V] + \frac{A_7}{\dot{m}_a}(P_7 - P_a) \quad (6.21)$$

The thrust specific fuel consumption (TSFC) is given by:

$$TSFC = \frac{\dot{m}_f + \dot{m}_{fab}}{T} \quad (6.22a)$$

Substituting from Eq. (6.21) to get:

$$TSFC = \frac{f + f_{ab}}{(1 + f + f_{ab})V_7 - V + \frac{A_7}{\dot{m}}(P_7 - P_a)} \quad (6.22b)$$

For inoperative afterburner, the same Eqs. (6.21) and (6.22) are used, but the afterburner fuel-to-air ratio f_{ab} is set equal to zero.

6.2.5 Important Definitions

Designers and operators of aero engines normally use the below definitions in their daily work.

(A) *Exhaust gas temperature gauge (EGT)*

Exhaust gas temperature is measured with a **thermocouple-type pyrometer**. By monitoring EGT, the pilot can get an idea of the engine's **air-fuel ratio**. At a **stoichiometric** fuel-to-air ratio, the exhaust gas temperature is different than that in a lean or rich fuel-to-air ratio. High temperatures (typically above 900 °C) can be an indicator of dangerous conditions that can lead to catastrophic engine failure.

(B) *Engine Pressure Ratio (EPR)*

Engine pressure ratio (*EPR*) is the ratio of turbine discharge to compressor inlet pressure. *EPR* is used as an indication of the amount of thrust being developed by a turbine engine. An engine pressure ratio (*EPR*) gauge is used to indicate the power output of turbojet (and turbofan) engines. Pressure measurements are recorded by probes installed in the engine inlet and at the exhaust. Once collected, the data is sent to a differential pressure transducer, which is indicated on a flight deck *EPR* gauge. *EPR* system design automatically compensates for the effects of airspeed and altitude. Changes in ambient temperature require a correction be applied to *EPR* indications to provide accurate engine power settings

(C) *Bleed*

Bleed air in aircraft engine is a **compressed air** that can be taken from within the engine, most often after the compressor stage(s) but before the fuel is injected in the burners. Bleed air has high **temperature** and high **pressure** (typical values are 200–250 °C and 275 kPa). This compressed air is used in aircraft in many different ways, deicing of wing leading edge, pressurizing the cabin, **pneumatic actuators**, starting the remaining engines, and pressurizing **lavatory** water storage tanks. Moreover, it is used in deicing of engine intake and cooling of turbine blades.

Example 6.1 A single-spool turbojet engine powers a military aircraft flying with a Mach number (M) at an altitude where the ambient temperature is (T_a). The compressor pressure ratio is (π) and the turbine inlet total temperature is (T_{04}). Assuming all the processes are ideal, constant air/gas properties (γ, C_p) and constant (T_{04}), and ($f \approx 0$), prove that the maximum thrust force is obtained when:

$$\frac{T_{04}}{T_a} = \left\{ \pi^{\frac{\gamma-1}{\gamma}} \times \left(1 + \frac{\gamma-1}{2} M^2 \right) \right\}^2$$

What will be the value at ground run ($M = 0$)?

Solution

Same state designation of Fig. 6.3 is used here. Air total temperature at the compressor inlet is:

$$T_{02} = T_a \left(1 + \frac{\gamma - 1}{2} M^2 \right)$$

The total temperature at the compressor outlet is:

$$T_{03} = \pi^{\frac{\gamma-1}{\gamma}} T_{02}$$

Neglecting fuel-to-air ratio, assuming constant (C_p), then the energy balance between compressor and turbine yields:

$$\begin{aligned} T_{04} - T_{05} &= T_{03} - T_{02} \\ T_{05} &= T_{04} - (T_{03} - T_{02}) = T_{04} - T_{02} \left(\pi^{\frac{\gamma-1}{\gamma}} - 1 \right) \\ T_{05} &= T_{04} - T_a \left(1 + \frac{\gamma - 1}{2} M^2 \right) \left(\pi^{\frac{\gamma-1}{\gamma}} - 1 \right) \\ V_j^2 &= 2Cp(T_{05} - T_7) \\ V_j^2 &= 2Cp \left[T_{04} - T_a \left(1 + \frac{\gamma - 1}{2} M^2 \right) \left(\pi^{\frac{\gamma-1}{\gamma}} - 1 \right) - T_7 \right] \end{aligned}$$

The ratio between turbine inlet total temperature and exhaust static temperature is:

$$\begin{aligned} \frac{T_{04}}{T_7} &= \left(\frac{P_{04}}{P_7} \right)^{\frac{\gamma-1}{\gamma}} = \left(\frac{P_{03}}{P_a} \right)^{\frac{\gamma-1}{\gamma}} = \left(\frac{P_{03} P_{02}}{P_{02} P_a} \right)^{\frac{\gamma-1}{\gamma}} = \pi^{\frac{\gamma-1}{\gamma}} \left(1 + \frac{\gamma - 1}{2} M^2 \right) \\ V_7^2 &= 2Cp \left[T_{04} - T_a \left(1 + \frac{\gamma - 1}{2} M^2 \right) \left(\pi^{\frac{\gamma-1}{\gamma}} - 1 \right) - \frac{T_{04}}{\pi^{\frac{\gamma-1}{\gamma}} \left(1 + \frac{\gamma - 1}{2} M^2 \right)} \right] \end{aligned}$$

Denoting $\lambda = 1 + \frac{\gamma-1}{2} M^2$, then:

$$V_7^2 = 2Cp \left[T_{04} - T_a \lambda \left(\pi^{\frac{\gamma-1}{\gamma}} - 1 \right) - \frac{T_{04}}{\pi^{\frac{\gamma-1}{\gamma}} \lambda} \right] \quad (\text{A})$$

The thrust force is:

$$T = \dot{m} (V_7 - V)$$

The thrust is a maximum when V_7 is maximum.

Differentiate equation (A) w.r.t. compressor pressure ratio (π), then:

$$2V_7 \frac{\partial V_7}{\partial \pi} = 2Cp \left[-T_a \lambda \left(\frac{\gamma - 1}{\gamma} \right) \left(\pi^{\frac{1}{\gamma}} \right) + \left(\frac{\gamma - 1}{\gamma} \right) \frac{T_{04}}{\pi^{\frac{2\gamma-1}{\gamma}} \lambda} \right]$$

For maximum thrust, then $\frac{\partial V_7}{\partial \pi} = 0$.

$$\text{Thus : } T_a \left(\frac{\gamma - 1}{\gamma} \right) \left(\pi^{\frac{1}{\gamma}} \right) = \left(\frac{\gamma - 1}{\gamma} \right) \left(\frac{1}{\lambda} \right) \left(\frac{T_{04}}{\pi^{\frac{2\gamma-1}{\gamma}} \lambda} \right)$$

$$\left(\frac{T_{04}}{T_a} \right)_{\text{Maximum thrust}} = \left(\pi^{\frac{1}{\gamma}} \lambda \right)^2 \equiv \left[\pi^{\frac{1}{\gamma}} \left(1 + \frac{\gamma - 1}{2} M^2 \right) \right]^2$$

For ground run, $M = 0$; thus:

$$\left(\frac{T_{04}}{T_a} \right)_{\text{Maximum thrust}} = (\pi)^{2(\frac{1}{\gamma})}$$

Example 6.2 A single-spool turbojet engine powers a military aircraft flying with a Mach number (M) at an altitude where the ambient temperature is (T_a). The compressor pressure ratio is (π) and the turbine inlet total temperature is (T_{04}). Assuming all the processes are ideal, prove that the compressor pressure ratio is expressed by the relation:

$$\pi = \left(\frac{T_{04} - \left(\frac{fQ}{C_p} \right)}{\lambda T_a} \right)^{\left(\frac{1}{\gamma-1} \right)}$$

$$\text{Where : } \lambda = 1 + \frac{\gamma - 1}{2} M^2$$

Evaluate the compressor pressure ratio for the two cases: $T_{04} = 1200$ and 1500 K:

$$\text{Assuming : } \frac{Q}{C_p} = 38,300, f = 0.02, M = 0.8 \text{ and } T_a = 300 \text{ K}$$

Assume ($\gamma = 1.4$) = constant.

Solution

Energy balance in combustion chamber is expressed as:

$$\dot{m}_f Q = \dot{m}_a C_p (T_{04} - T_{03})$$

Dividing by \dot{m}_a , then:

$$\frac{fQ}{Cp} = (T_{04} - T_{03}) \quad (\text{A})$$

The outlet total temperature to the compressor is:

$$\begin{aligned} T_{03} &= \pi^{\left(\frac{\gamma-1}{\gamma}\right)} T_{02} \\ \text{Where } T_{02} &= T_a \left(1 + \frac{\gamma-1}{2} M^2 \right) \\ \text{Then } T_{03} &= \pi^{\left(\frac{\gamma-1}{\gamma}\right)} T_a \left(1 + \frac{\gamma-1}{2} M^2 \right) \end{aligned} \quad (\text{B})$$

From equations (A) and (B), then:

$$\pi = \left[\frac{T_{04} - \frac{fQ}{Cp}}{T_a \left(1 + \frac{\gamma-1}{2} M^2 \right)} \right]^{\left(\frac{\gamma}{\gamma-1}\right)}$$

With $\gamma = 1.4$, $Cp = 1005 \text{ J/kg.K}$:

$$\begin{aligned} \text{When } T_{04} = 1200 \text{ K, then } \pi &= \left[\frac{1200 - 0.02 \times 38300}{300 \times (1 + 0.2 \times 0.64)} \right]^{3.5} = 2.389. \\ \text{When } T_{04} = 1500 \text{ K, then } \pi &= \left[\frac{1500 - 0.02 \times 38300}{300 \times (1 + 0.2 \times 0.64)} \right]^{3.5} = 15.03. \end{aligned}$$

Example 6.3 A single-spool turbojet engine has an unchoked nozzle. The fuel-to-air ratio is assumed negligible. Prove that when the thrust is a maximum, then:

$$\begin{aligned} V_e &= 2V_f \\ \eta_p &= \frac{2}{3} \end{aligned}$$

Solution

Since the nozzle is unchoked and the fuel-to-air ratio is negligible, thrust force is expressed by the relation:

$$\begin{aligned} T &= \dot{m} (V_e - V_f) \\ \text{Where } \dot{m} &= \rho V_f A_i \\ \text{Then } T &= \rho V_f A_i (V_e - V_f) \end{aligned}$$

Thrust is a maximum when $\frac{\partial T}{\partial V_f} = 0$.

$$\text{Thus } \frac{\partial T}{\partial V_f} = -\rho V_f A_i + \rho A_i (V_e - V_f) = 0$$

$$-V_f + (V_f - V_e) = 0$$

$$V_e = 2V_f$$

Propulsive efficiency for unchoked and negligible fuel-to-air ratio is expressed by:

$$\eta_p = \frac{2V_f}{V_e + V_f} = \frac{2V_f}{2V_f + V_f} = \frac{2}{3}$$

Example 6.4 A single-spool turbojet engine has an unchoked nozzle.

(A) It is required to prove that:

The thrust force assuming an ideal cycle is expressed by the relation:

$$\frac{T}{P_a A_a} = \frac{2\gamma}{\gamma - 1} (\tau_r - 1) \left[(1 + f) \left\{ \frac{(\tau_r \tau_c \tau_t - 1)}{(\tau_r - 1)} \left(\frac{\tau_\lambda}{\tau_c \tau_r} \right) \right\}^{\frac{1}{2}} - 1 \right]$$

$$\text{Where, } \tau_\lambda = \frac{T_{04}}{T_a}$$

The energy balance between turbine and compressor (neglecting the fuel-to-air ratio) yields the relation:

$$\tau_t = 1 - \frac{\tau_r (\tau_c - 1)}{\tau_\lambda}$$

The maximum thrust is attained if the temperature ratio across the compressor has the value:

$$\tau_{c_{\max}} = \frac{\sqrt{\tau_\lambda}}{\tau_r}$$

Zero thrust is generated if: $\tau_c = \frac{\tau_\lambda}{\tau_r}$

(B) Plot:

The relations $\frac{T}{P_a A_a}$ versus τ_r

The relation $\frac{T}{P_a A_a}$ versus τ_c

The temperature ratio across different modules is expressed as:

$$\text{Ram: } \tau_r = \frac{T_{0a}}{T_a}$$

$$\text{Diffuser (intake): } \tau_d = \frac{T_{02}}{T_{0a}} \quad \text{Compressor: } \tau_c = \frac{T_{03}}{T_{02}}$$

$$\text{Combustion chamber: } \tau_b = \frac{T_{04}}{T_{03}} \quad \text{Turbine: } \tau_t = \frac{T_{05}}{T_{04}}$$

$$\text{Nozzle: } \tau_n = \frac{T_{06}}{T_{05}}$$

Solution

The thrust force equation for an unchoked nozzle ($P_e = P_a$) is:

$$\begin{aligned} T &= \dot{m}_a[(1+f)u_e - u_a] = \rho_a u_a^2 A_a \left[(1+f) \frac{u_e}{u_a} - 1 \right] \\ T &= \frac{P_a}{RT_a} u_a^2 A_a \left[(1+f) \frac{u_e}{u_a} - 1 \right] \\ \frac{T}{P_a A_a} &= \frac{\gamma u_a^2}{\gamma RT} \left[(1+f) \frac{u_e}{u_a} - 1 \right] \\ \frac{T}{P_a A_a} &= \gamma M_a^2 \left[(1+f) \frac{u_e}{u_a} - 1 \right] \quad (\text{A}) \end{aligned}$$

The ratio between exhaust and flight speeds may be correlated as:

$$\frac{u_e}{u_a} = \frac{M_e}{M_a} \sqrt{\frac{T_e}{T_a}} \quad (\text{B})$$

The pressure ratio across different modules is expressed as:

Ram: $\pi_r = \frac{P_{0a}}{P_a}$	Diffuser (intake): $\pi_d = \frac{P_{02}}{P_{0a}}$	Compressor: $\pi_c = \frac{P_{03}}{P_{02}}$
Combustion chamber: $\pi_b = \frac{P_{04}}{P_{03}}$	Turbine : $\pi_t = \frac{P_{05}}{P_{04}}$	Nozzle: $\pi_n = \frac{P_{06}}{P_{05}} = \frac{P_{0e}}{P_{05}}$

The exhaust total pressure may be expressed as:

$$\begin{aligned} P_{0e} &= P_a \frac{P_{0d} P_{02} P_{03} P_{04} P_{05} P_{0e}}{P_a P_{0a} P_{02} P_{03} P_{04} P_{05}} \\ P_{0e} &= P_a \pi_r \pi_d \pi_c \pi_b \pi_t \pi_n \end{aligned}$$

For ideal diffuser, burner, and nozzle, then:

$$\pi_d = \pi_b = \pi_n = 1$$

The exhaust total pressure can be then expressed as:

$$P_{0e} = P_a \pi_r \pi_c \pi_t = P_a \left(1 + \frac{\gamma - 1}{2} M_e^2 \right)^{\frac{\gamma}{\gamma-1}}$$

Since the nozzle is unchoked, then:

$$\begin{aligned} P_a &= P_e \\ \pi_r \pi_c \pi_t &= \left(1 + \frac{\gamma - 1}{2} M_e^2 \right)^{\frac{\gamma}{\gamma-1}} \end{aligned}$$

Moreover, with:

$$\begin{aligned}\pi_r &= \tau_r^{\frac{\gamma}{\gamma-1}}, & \pi_c &= \tau_c^{\frac{\gamma}{\gamma-1}}, & \pi_t &= \tau_t^{\frac{\gamma}{\gamma-1}} \\ P_a &= P_e \\ (\tau_r \tau_c \tau_t)^{\frac{\gamma}{\gamma-1}} &= \left(1 + \frac{\gamma-1}{2} M_e^2\right)^{\frac{\gamma}{\gamma-1}}\end{aligned}$$

Thus:

$$\begin{aligned}\tau_r \tau_c \tau_t &= 1 + \frac{\gamma-1}{2} M_e^2 \\ M_e^2 &= \frac{2}{\gamma-1} (\tau_r \tau_c \tau_t - 1)\end{aligned}\quad (\text{C})$$

Also, ram total temperature is expressed as:

$$\begin{aligned}\tau_r &= 1 + \frac{\gamma-1}{2} M_a^2 \\ M_a^2 &= \frac{2}{\gamma-1} (\tau_r - 1)\end{aligned}\quad (\text{D})$$

Thus, the ratio between exhaust and flight Mach numbers is:

$$\frac{M_e^2}{M_a^2} = \frac{(\tau_r \tau_c \tau_t - 1)}{(\tau_r - 1)} \quad (\text{E})$$

The exhaust total temperature may be further expressed as:

$$\begin{aligned}T_{0e} &= T_a \frac{T_{0a} T_{02} T_{03} T_{04} T_{05} T_{0e}}{T_a T_{0a} T_{02} T_{03} T_{04} T_{05}} \\ T_{0e} &= T_a \tau_r \tau_d \tau_c \tau_b \tau_t \tau_n\end{aligned}$$

With $\tau_d = \tau_n = 1$, then from (C):

$$\begin{aligned}T_{0e} &= T_a \tau_r \tau_c \tau_b \tau_t \\ T_{0e} &= T_e \left(1 + \frac{\gamma-1}{2} M_e^2\right) \\ T_{0e} &= T_e \tau_r \tau_c \tau_t \\ \frac{T_e}{T_a} &= \tau_b = \frac{T_{04}}{T_{03}}\end{aligned}$$

Now, define $\tau_\lambda = \frac{T_{04}}{T_a}$.

Then:

$$\frac{T_e}{T_a} = \frac{T_{04}}{T_{03}} = \frac{T_{04}}{T_a} \frac{T_a}{T_{03}} = \frac{T_{04}}{T_a} \frac{T_{02}}{T_{03}} \frac{T_a}{T_{02}} = \frac{\tau_\lambda}{\tau_c \tau_r} \quad (\text{F})$$

From (A) through (F), then:

$$\frac{T}{P_a A_a} = \frac{2\gamma}{\gamma - 1} (\tau_r - 1) \left[(1 + f) \left\{ \frac{(\tau_r \tau_c \tau_t - 1)}{(\tau_r - 1)} \left(\frac{\tau_\lambda}{\tau_c \tau_r} \right) \right\}^{\frac{1}{2}} - 1 \right] \quad \#$$

Next, assuming that the turbine provides a work just sufficient to rotate the compressor, then:

$$\begin{aligned} \dot{m}_a (T_{03} - T_{02}) &= (\dot{m}_a + \dot{m}_f) (T_{04} - T_{05}) \\ \tau_r (\tau_c - 1) &= (1 + f) \tau_\lambda (1 - \tau_t) \\ \tau_t &= 1 - \frac{\tau_r (\tau_c - 1)}{(1 + f) \tau_\lambda} \end{aligned}$$

Neglecting the fuel-to-air ratio, then:

$$\tau_t = 1 - \frac{\tau_r (\tau_c - 1)}{\tau_\lambda} \quad (\text{G}) \quad \#$$

Now, to maximize the thrust for a certain flight Mach number, from equation (A), the ratio between exhaust and flight speeds ($\frac{u_e}{u_a}$) must be maximum.

From equations (E) through (G):

$$\begin{aligned} \left(\frac{u_e}{u_a} \right)^2 &= \left(\frac{M_e}{M_a} \right)^2 \frac{T_e}{T_a} = \frac{(\tau_r \tau_c \tau_t - 1)}{(\tau_r - 1)} \frac{\tau_\lambda}{\tau_c \tau_r} \\ \left(\frac{u_e}{u_a} \right)^2 &= \frac{1}{(\tau_r - 1)} \left(\tau_t \tau_\lambda - \frac{\tau_\lambda}{\tau_c \tau_r} \right) = \frac{1}{(\tau_r - 1)} \left[\left\{ 1 - \frac{\tau_r (\tau_c - 1)}{\tau_\lambda} \right\} \tau_\lambda - \frac{\tau_\lambda}{\tau_c \tau_r} \right] \\ \left(\frac{u_e}{u_a} \right)^2 &= \frac{1}{(\tau_r - 1)} \left[\tau_\lambda - \tau_r (\tau_c - 1) - \frac{\tau_\lambda}{\tau_c \tau_r} \right] \end{aligned}$$

Now, differentiate the above relation with respect to temperature ratio across the compressor:

$$\begin{aligned} \frac{\partial}{\partial \tau_c} \left(\frac{u_e}{u_a} \right)^2 &= \frac{1}{(\tau_r - 1)} \left[-\tau_r + \frac{\tau_\lambda}{\tau_c^2 \tau_r} \right] = 0 \\ \tau_r &= \frac{\tau_\lambda}{\tau_c^2 \tau_r} \quad \# \\ \tau_{c_{\max}} &= \frac{\sqrt{\tau_\lambda}}{\tau_r} \end{aligned}$$

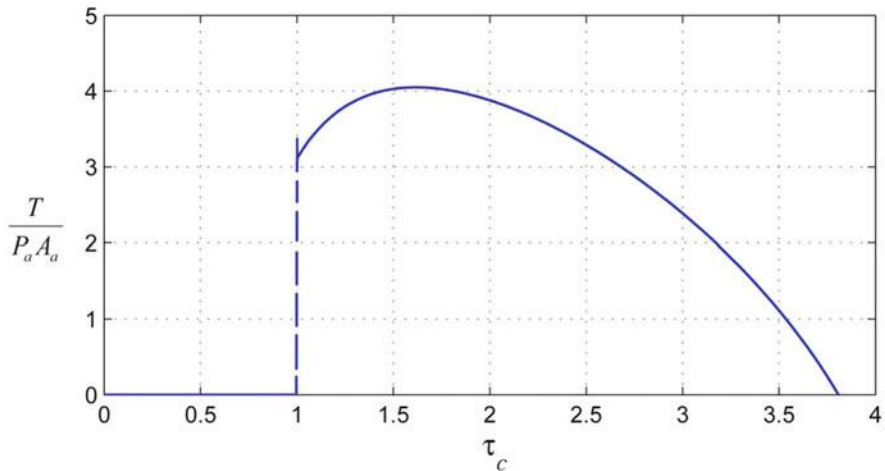


Fig. 6.6 Nondimensional thrust versus temperature ratio in compressor

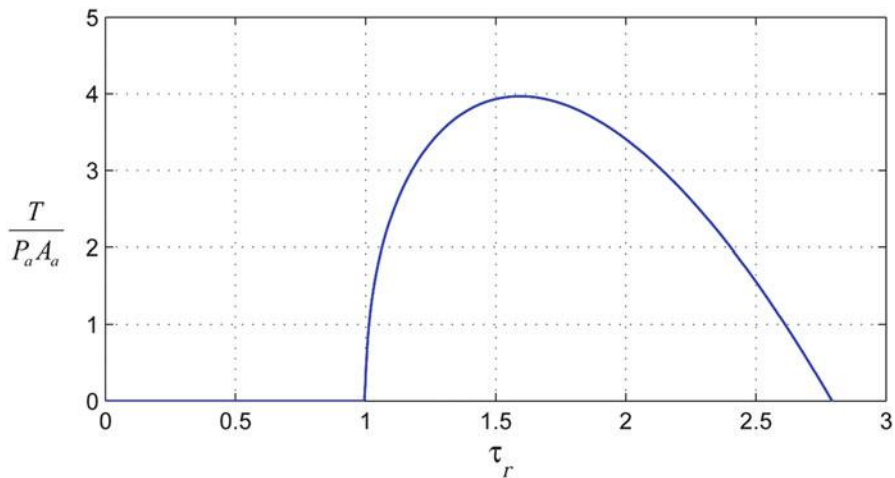


Fig. 6.6b Nondimensional thrust versus ram temperature ratio

The thrust force attains a zero value when $\frac{u_e}{u_a} = 1$, which is achieved when:

$$\tau_c = \frac{\tau_\lambda}{\tau_r} \quad \#$$

Example 6.5 A civil transport aircraft powered by four turbojet engines is flying at a Mach number of 0.85 and an altitude where the ambient temperature is 230 K. The

overall pressure ratio is 20 and the maximum temperature is 1500 K. Due to an *ingested bird*, one engine failed and the aircraft flew by three engines at the same altitude and Mach number. The pilot advanced the throttle lever to increase the rate of fuel flow and thus the turbine inlet temperature. This led to an increase in exhaust gas velocity to compensate for the thrust of the failed engine. The thrust force of the operative engines was thus increased. Calculate:

The original and final exhaust speeds

The new maximum total temperature

Fuel-to-air ratio in both cases (fuel heating value is 42,000 kJ/kg)

Assume that:

All processes are ideal

Constant specific heats and specific heat ratio at all engine modules, such that

$$C_p = 1005 \text{ J/kg/K} \quad \text{and} \quad \gamma = 1.4$$

The works of both compressor and turbine are equal

Air mass flow rate into each engine in both cases is constant

Neglect fuel mass flow rate in thrust and energy balance calculation

Solution

(A) Four operative engines

The flight speed is then: $u = M\sqrt{\gamma RT_a} = 258.5 \text{ m/s}$

Intake

$$T_{02} = T_a \left(1 + \frac{\gamma - 1}{2} M^2 \right) = 263.24 \text{ K}$$

Compressor

The air temperature at compressor outlet is:

$$T_{03} = T_{02} \times \pi^{\frac{\gamma-1}{\gamma}} = 263.24 \times 20^{0.286} = 620 \text{ K}$$

The specific work of compressor is:

$$w = C_p(T_{03} - T_{02}) = C_p T_{02} \left(\pi^{\frac{\gamma-1}{\gamma}} - 1 \right) = 1005 \times 263.24 (20^{0.286} - 1)$$

$$w = 358.62 \text{ kN/kg and } w/C_p = 256.83 \text{ kN/kg}$$

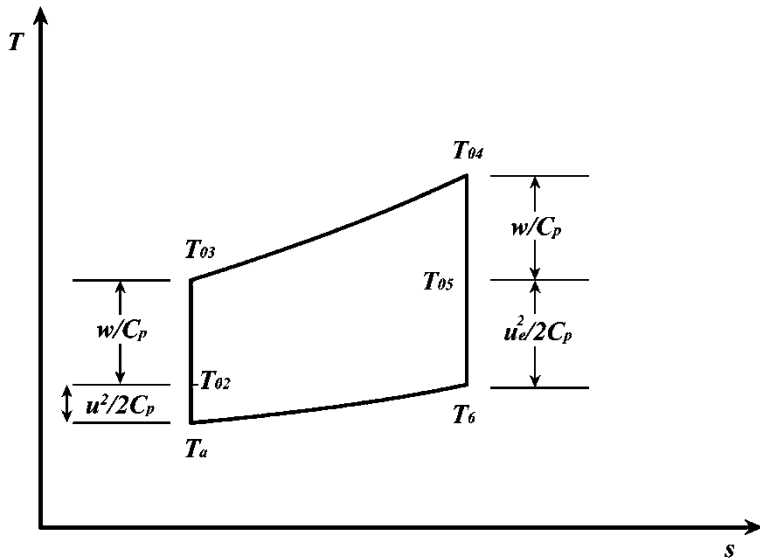


Fig. 6.7a T-s diagram for four engines operating case

Combustion chamber

The fuel-to-air ratio is:

$$f = \frac{C_p(T_{04} - T_{03})}{Q_{HV} - C_p T_{04}} = \frac{1.005(1500 - 620)}{42,000 - 1.005 \times 1500} = 0.02184$$

Turbine

The assumptions of constant specific heat through the engine as well as equal work for both compressor and turbine imply that both air and gas flow rates in compressor and turbine are equal (negligible fuel flow mass). Thus:

$$T_{05} = T_{0\max} - \frac{w}{C_p} = 1500 - 356.84 = 1143.17 \text{ K}$$

Nozzle

Since combustion process is ideal, then:

$$\begin{aligned} \frac{P_{04}}{P_6} &= \frac{P_{03}}{P_a} = \frac{P_{03}P_{02}}{P_{02}P_a} = \frac{P_{03}}{P_{02}} \left(\frac{T_{02}}{T_a} \right)^{\frac{\gamma}{\gamma-1}} = \pi \left(1 + \frac{\gamma-1}{2} M^2 \right)^{\frac{\gamma}{\gamma-1}} \\ \frac{P_{04}}{P_6} &= 20(1 + 0.2 \times 0.85^2) \\ \frac{P_{04}}{P_6} &= 32.076 \end{aligned}$$

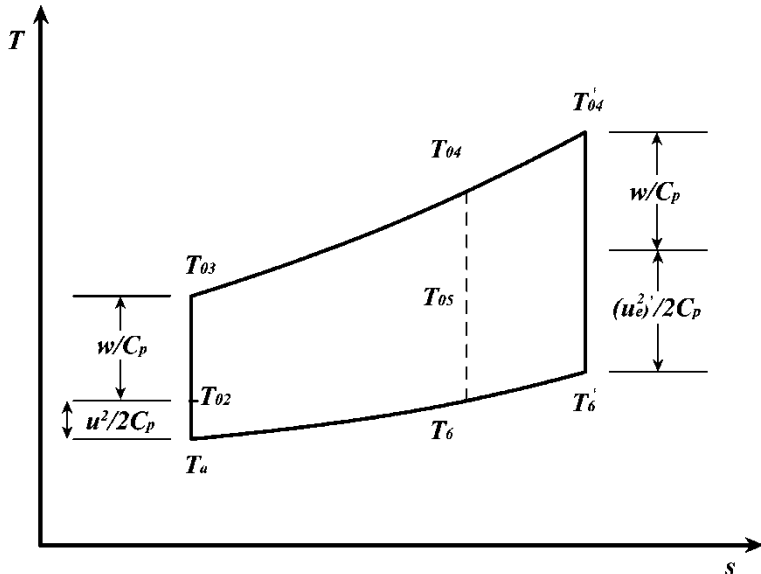


Fig. 6.7b T-s diagram for three engines operating case

$$\text{But } \frac{P_{04}}{P_{05}} = \left(\frac{T_{04}}{T_{05}} \right)^{\frac{\gamma}{\gamma-1}} = \left(\frac{1500}{1143.17} \right)^{3.5} = 2.5878$$

$$\frac{P_{05}}{P_6} = \frac{P_{05}}{P_{04}} \frac{P_{04}}{P_6} = \frac{32.076}{2.5878} = 12.3947$$

$$\text{Also } T_6 = T_{0\max}/(32.076)^{0.286} = 1500/2.6963 = 556.32 \text{ K}$$

The exhaust speed is then:

$$u_e = \sqrt{2C_p(T_{05} - T_6)} = \sqrt{2 \times 1005 \times (1143.17 - 556.32)}$$

$$u_e = 1086 \text{ m/s}$$

Specific thrust is then:

$$T/\dot{m}_a = (1+f)u_e - u \approx u_e - u = 1086 - 258.5 = 827.58 \text{ m/s}$$

(B) Only three engines operative

This case represents a one engine failure; thus, aircraft is powered by three engines only.

For the same flight speed, the aircraft drag is the same which must be equal to the sum of thrust forces generated by operative engines. The pilot had to advance throttle lever to a forward setting leading to a greater fuel flow and consequently higher maximum (turbine inlet) temperature T'_{04} .

For the same compressor–turbine work as in the four-engine case, the exhaust speed is increased to u'_e , such that the corresponding engine thrust, T' , will be governed by the relation:

$$3T' = 4T$$

Assuming the air mass flow rate is maintained constant, thus:

$$\dot{m}'_a = \dot{m}_a$$

And:

$$\begin{aligned} 3\dot{m}'_a(u'_e - u) &= 4\dot{m}_a(u_e - u) \\ 3(u'_e - u) &= 4(u_e - u) \\ u'_e = \frac{4}{3}u_e - \frac{1}{3}u &= \frac{4 \times 1086 - 258.5}{3} = 1316.9 \text{ m/s} \end{aligned}$$

Since the compressor pressure ratio is constant and flight speed is also unchanged, then the overall pressure ratio is unchanged or:

$$\begin{aligned} \frac{T'_{04}}{T'_6} &= \left(\frac{P_{03}}{P_a}\right)^{\frac{\gamma-1}{\gamma}} = (32.076)^{0.286} = 2.6963 \\ T'_{04} &= T'_6 + \frac{u'^2_e}{2C_p} + \frac{w}{C_p} \\ \frac{u'^2_e}{2C_p} + \frac{w}{C_p} &= 1219.6 \text{ K} \\ 2.6963T'_6 &= T'_6 + 1219.6 \\ T'_6 &= 718.92 \text{ K} \\ T'_{04} &= 1938 \text{ K} \end{aligned}$$

The new fuel-to-air ratio is:

$$f = \frac{C_p(T_{04} - T_{03})}{Q_{HV} - C_pT_{04}} = \frac{1.005(1938 - 620)}{42,000 - 1.005 \times 1938} = 0.03307$$

It may be concluded that:

Fuel-to-air ratio had been drastically increased from 0.02184 to 0.03307 (52.3 %).

The maximum temperature (turbine inlet) increased from 1500 K to 1938 K (29.2 %), which most probably led to a turbine overheat.

Practically, pilots normally follow other procedures, among which the flight altitude and speed are reduced which reduce the drag force. Thus, the thrust generated by each engine in the second case is close to its value prior engine failure. In this case the maximum temperature may be kept within the range of 100–110 % of its original value.

6.2.6 Double-Spool Turbojet

The two-spool (or double-spool) engines are composed of two compressors coupled to two turbines through two shafts (or spools) (Fig. 6.8a). Double-spool engines are designed to fulfill the high-thrust requirements for both military and civil aircrafts. The first spool is composed of the low-pressure compressor (LPC) located downstream the intake. It is coupled and driven by the low-pressure turbine (LPT) located upstream of the nozzle or afterburner (if fitted). The second spool is composed of the high-pressure compressor (HPC) located downstream of the LPC and upstream of the combustion chamber. This HPC is driven by the high-pressure turbine (HPT) installed downstream of the combustion chamber and upstream of the LPT. Low-pressure spool rotates at speed (N_1) while high-pressure spool rotates at a higher speed (N_2). Also two-spool turbojet may be fitted with afterburner as shown in Fig. 6.8a. Afterburner is located downstream the LPT and upstream of the nozzle. Most afterburning turbojet engines are fitted to military airplanes. Only supersonic transports (Concorde and Tu-144) are powered afterburning turbojet engines, namely, Rolls-Royce/SNECMA Olympus 593 Mk 610 and Kolesov RD-36-51 engines. Moreover, afterburning turbojets employ variable area intake and nozzle.

It may be concluded that two-spool turbojet engines may be composed of seven or eight modules. These are intake, two compressors, combustion chamber, two turbines, and a nozzle. For afterburning engines, the eighth module is the afterburner.

6.2.7 Thermodynamic Analysis of Double-Spool Turbojet

Real (nonideal) case will be considered here, as the ideal performance can be considered as a special case where the efficiencies are set equal to unity and no pressure losses. Modules of two-spool turbojet engine were listed above.

Intake is identical to the case of single-spool turbojet. Thus, Eqs. (6.1), (6.2), and (6.3) are used and no need to be repeated here. Now the successive elements (LPC through nozzle) will be examined.

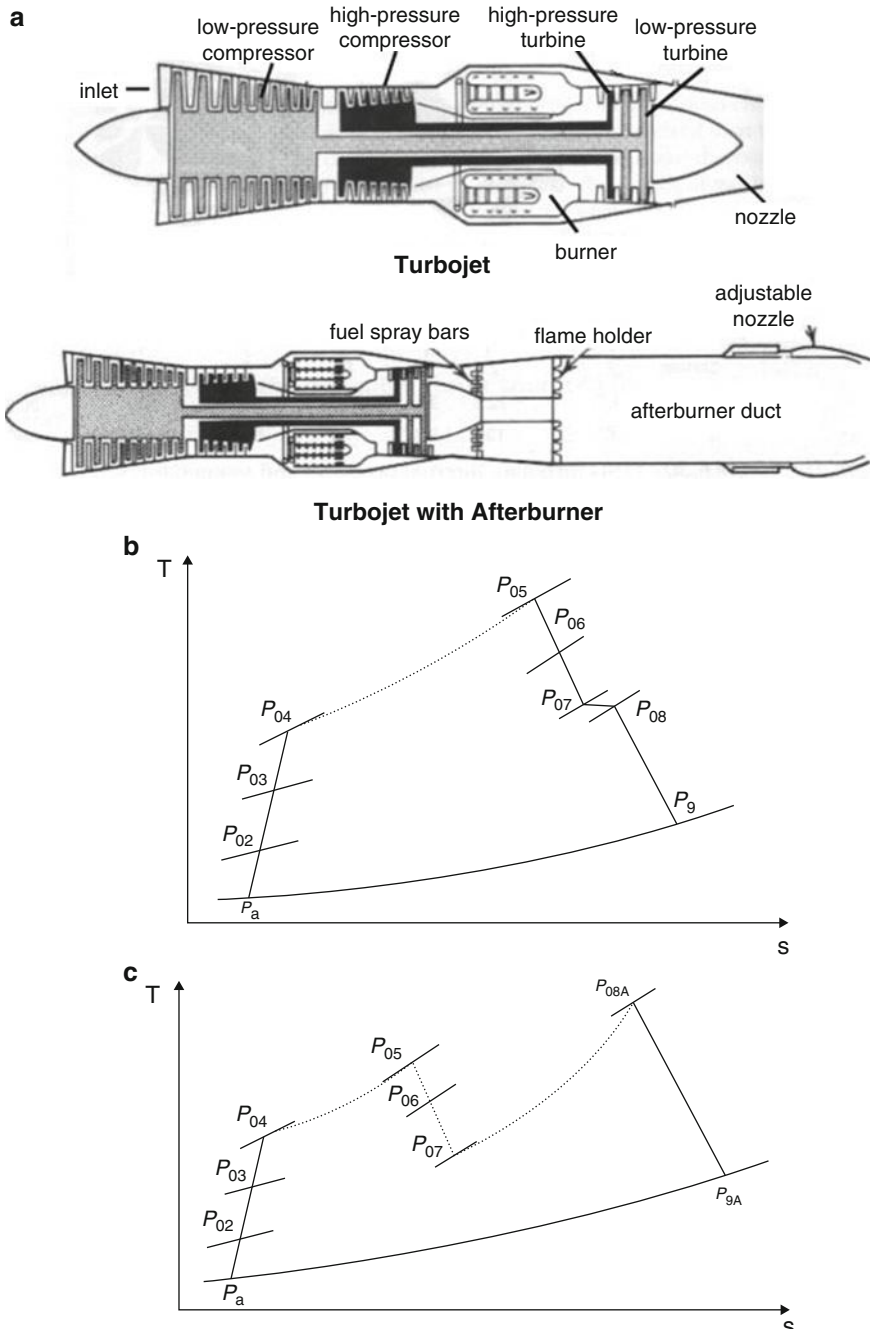


Fig. 6.8 Two (double)-spool turbojet engine. (a) Layout of two-spool turbojet engine (with and without afterburner). (b) T-s diagram for non-afterburning turbojet. (c) T-s diagram for afterburning turbojet

(A) Non-afterburning Engine

1. Low-pressure compressor (LPC)

For a known compressor pressure ratio (π_{c1}) and isentropic efficiency (η_{c1}), then the pressure and temperature at the outlet of the LPC are given by the following relations:

$$P_{03} = P_{02} \times \pi_{c1} \quad (6.23)$$

$$T_{03} = T_{02} \left(1 + \frac{\pi_{c1}^{\frac{\gamma_c-1}{\gamma_c}} - 1}{\eta_{c1}} \right) \quad (6.24)$$

2. High-pressure compressor (HPC)

Similarly, both of the pressure ratio (π_{c2}) and its isentropic efficiency (η_{c2}) are known. Thus, the pressure and temperature at the outlet of the HPC are given by the following relations:

$$P_{04} = (P_{03})(\pi_{c2}) \quad (6.25)$$

$$T_{04} = T_{03} \left[1 + \frac{\pi_{c2}^{\frac{\gamma_c-1}{\gamma_c}} - 1}{\eta_{c2}} \right] \quad (6.26)$$

3. Combustion chamber

The temperature at the end of combustion process T_{05} is generally known. It is the maximum temperature in the cycle if the afterburner is inoperative. A similar analysis to single-spool turbojet yields:

$$P_{05} = P_{04} - \Delta P_{cc} \quad (6.27a)$$

$$\text{Or} \quad P_{05} = P_{04}(1 - \Delta P_{cc}\%) \quad (6.27b)$$

The energy balance for the combustion chamber yields the following relation for the fuel-to-air ratio (f):

$$\begin{aligned} \dot{m}_a(1+f)Cp_h T_{05} &= \dot{m}_a C p_c T_{04} + \eta_b \dot{m}_f Q_R \\ \text{With} \quad f &= \dot{m}_f / \dot{m}_a \\ f &= \frac{(Cp_h/Cp_c)(T_{05}/T_{04}) - 1}{\eta_b(Q_R/Cp_c T_{04}) - (Cp_h/Cp_c)(T_{05}/T_{04})} \end{aligned} \quad (6.28)$$

4. High-pressure turbine (HPT)

The power generated in the high-pressure turbine (HPT) is used in driving the high-pressure compressor (HPC) in addition to some accessories. If the ratio of the

power needed to drive the HPC to the power available from the HPT is (λ_1), then the energy balance for the compressor–turbine shaft is:

$$W_{\text{HPC}} = \lambda_1 \eta_{m1} W_{\text{HPT}}$$

Here (λ_1) is of the range 75–85 % and (η_{m1}) is the mechanical efficiency of high-pressure spool (normally 99 + %). Thus, in terms of the temperatures differences:

$$\begin{aligned} Cp_c(T_{04} - T_{03}) &= \lambda_1(1+f)\eta_{m1}Cp_h(T_{05} - T_{06}) \\ \left(\frac{T_{06}}{T_{05}}\right) &= 1 - \frac{(Cp_c/Cp_h)T_{03}}{\lambda_1(1+f)\eta_{m1}T_{05}} \left[\left(\frac{T_{04}}{T_{03}}\right) - 1 \right] \end{aligned} \quad (6.29)$$

Then the pressure ratios of the high-pressure turbine and high-pressure compressor are related by:

$$\left(\frac{P_{06}}{P_{05}}\right) = \left(1 - \frac{T_{05} - T_{06}}{\eta_{t1}T_{05}}\right)^{\frac{\gamma_t}{\gamma_t - 1}} \quad (6.30)$$

where η_{t1} is the isentropic efficiency of the high-pressure turbine.

5. Low-pressure turbine (LPT)

The power consumed in the LPC is supplied through the LPT in expansion. With (λ_2) identifying the ratio of the power needed to drive the compressor to the power available in the turbine, then the energy balance for the low-pressure spool is:

$$W_{\text{LPC}} = \lambda_2 \eta_{m2} W_{\text{LPT}}$$

Here (λ_2) is of the range 75–85 %. Thus, in terms of the temperatures differences:

$$\begin{aligned} Cp_c(T_{03} - T_{02}) &= \lambda_2 \eta_{m2}(1+f)Cp_h(T_{06} - T_{07}) \\ \left(\frac{T_{07}}{T_{06}}\right) &= 1 - \frac{(Cp_c/Cp_h)T_{02}}{\lambda_2 \eta_{m2}(1+f)T_{06}} \left[\left(\frac{T_{03}}{T_{02}}\right) - 1 \right] \end{aligned} \quad (6.31)$$

Then the turbine and compressor pressure ratios are related by:

$$\left(\frac{P_{07}}{P_{06}}\right) = \left\{ 1 - \frac{(Cp_c/Cp_h)T_{02}}{\lambda_2 \eta_{m2}(1+f)\eta_{c1}\eta_{t1}T_{06}} \left[\left(\frac{P_{03}}{P_{02}}\right)^{\frac{\gamma_c - 1}{\gamma_c}} - 1 \right] \right\}^{\frac{\gamma_h}{\gamma_h - 1}} \quad (6.32)$$

From the diffuser part, Eq. (6.1):

$$\left(\frac{P_{07}}{P_{06}}\right) = \left\{ 1 - \frac{(Cp_c/Cp_h)T_a}{\lambda_2 \eta_{m2}(1+f)\eta_{c1}\eta_{t1}T_{06}} \left(1 + \frac{\gamma - 1}{2} M^2 \right) \left[\left(\frac{P_{03}}{P_{02}}\right)^{\frac{\gamma_c - 1}{\gamma_c}} - 1 \right] \right\}^{\frac{\gamma_h}{\gamma_h - 1}} \quad (6.33)$$

6. Jet pipe

The jet pipe following the low-pressure turbine and preceding the nozzle is associated with a slight pressure drop, while the total temperature remains unchanged:

$$P_{08} = P_{07} - \Delta P_{\text{jet pipe}} \quad (6.34a)$$

$$T_{08} = T_{07} \quad (6.34b)$$

7. Nozzle

First a check for nozzle choking is performed. Thus, the critical pressure is obtained from the relation:

$$\frac{P_{08}}{P_c} = \frac{1}{\left[1 - \frac{1}{\eta_n} \left(\frac{\gamma_h - 1}{\gamma_h + 1}\right)\right]^{\frac{\gamma_h}{\gamma_h - 1}}} \quad (6.35)$$

If the nozzle is unchoked, then the outlet pressure is equal to the ambient pressure. The jet speed is now evaluated from the relation:

$$V_9 = \sqrt{2Cp_h \eta_n T_{08} \left[1 - (P_a/P_{08})^{\frac{\gamma_h - 1}{\gamma_h}}\right]} \quad (6.36a)$$

If the nozzle is choked, then the outlet temperature (T_8) is calculated from the relation:

$$\left(\frac{T_{08}}{T_9}\right) = \left(\frac{\gamma_h + 1}{2}\right)$$

The jet speed is expressed as:

$$V_9 = \sqrt{\gamma_h RT_9} \quad (6.36b)$$

(B) Afterburning Engine

The same treatment for all the modules upstream to the afterburner is applied here. Now, for operating afterburner, the pressure at the outlet to the afterburner is determined from one of the following relations:

$$P_{08A} = P_{07} - \Delta P_{ab} \quad (6.37a)$$

$$\text{Or} \quad P_{08A} = P_{07}(1 - \Delta P_{ab}\%) \quad (6.37b)$$

The maximum temperature in the cycle is obtained at the end of the combustion process:

$$T_{08A} = T_{\text{MAX}}$$

The afterburner fuel-to-air ratio is calculated from the energy balance in the afterburner which gives:

$$f_{ab} = \frac{(1+f)(Cp_{8A}T_{08A}-Cp_7T_{07})}{\eta_{ab}Q_R - Cp_{8A}T_{08A}} \quad (6.38)$$

Nozzle:

The very hot gases leaving the afterburner expand in the nozzle from the state (08A) to state (9). As usual a check for nozzle choking is performed as follows:

$$\frac{P_{08A}}{P_c} = \frac{1}{\left[1 - \frac{1}{\eta_n} \left(\frac{\gamma_h-1}{\gamma_h+1}\right)\right]^{\frac{\gamma_h}{\gamma_h-1}}} \quad (6.39)$$

If the nozzle is unchoked, the jet speed will be:

$$V_{9ab} = \sqrt{2Cp_h\eta_n T_{08A} \left[1 - \left(P_a/P_{08}\right)^{\frac{\gamma_h-1}{\gamma_h}}\right]} \quad (6.40a)$$

If the nozzle is choked, then the exhaust gases leave the nozzle with a temperature of T_{9A} which is calculated from the relation:

$$\left(\frac{T_{08}}{T_{9A}}\right) = \left(\frac{\gamma_h+1}{2}\right)$$

The exhaust speed is then calculated from the relation:

$$V_{9ab} = \sqrt{\gamma_h RT_{9A}} \quad (6.40b)$$

6.2.8 Performance Parameters of Double-Spool Turbojet Engine

By performance parameters, it is meant the specific thrust and the specific fuel consumption as well as the three efficiencies.

The specific thrust is expressed by the relation:

$$\frac{T}{\dot{m}_a} = [(1 + f + f_{ab})V_9 - V] + \frac{A_9}{\dot{m}_a}(P_9 - P_a) \quad (6.41)$$

The thrust specific fuel consumption (*TSFC*) is given by:

$$TSFC = \frac{\dot{m}_f + \dot{m}_{fab}}{T}$$

Substituting from Eq. (6.41), the thrust specific fuel consumption is:

$$TSFC = \frac{f + f_{ab}}{(1 + f + f_{ab})V_9 - V + \frac{A_9}{\dot{m}_a}(P_9 - P_a)} \quad (6.42)$$

For inoperative afterburner, the same Eqs. (6.41) and (6.42) are used, but the afterburner fuel-to-air ratio f_{ab} is set equal to zero.

Turbojet engines resemble a one stream flow engine, and then from Chap. 2, the efficiencies are calculated as follows. The propulsive efficiency is obtained from the relation:

$$\eta_p = \frac{TV}{TV + \frac{1}{2}\dot{m}_e(V_e - V)^2}$$

where the mass and velocity of the gases leaving the nozzle are expressed in general as \dot{m}_e and V_e .

The thermal efficiency is expressed as:

$$\eta_{th} = TV + \frac{\frac{1}{2}\dot{m}_e(V_e - V)^2}{\dot{m}_f Q_R}$$

The overall efficiency is then:

$$\eta_0 = \eta_p \times \eta_{th}$$

Example 6.6 The following data presents some details of a double-spool turbojet engine close to Pratt & Whitney J57:

$$\begin{aligned} \pi_{c1} &= 4.0, & \pi_{c2} &= 3.125, & T_{0 \text{ max}} &= 1143 \text{ K}, & Q_R &= 45 \text{ MJ/kg}, & T_a &= 288 \text{ K} \\ P_a &= 101 \text{ kPa}, & M &= 0.0, & \eta_{c1} = \eta_{c2} &= 0.86, & \eta_{t1} = \eta_{t2} &= 0.9, & \eta_b &= 0.99 \\ \eta_n &= 0.94, & \Delta P_{cc} &= 1\%, & \gamma_c &= 1.4, & \gamma_h &= \frac{4}{3}, & \text{Nozzle exhaust area } A_n &= 0.208 \text{ m}^2 \end{aligned}$$

Afterburner is assumed inoperative with no pressure losses in tailpipe.

Calculate

Air mass flow rate

Thrust force

Thrust specific fuel consumption (*TSFC*)

Propulsive efficiency

Thermal efficiency

Overall efficiency

Solution

Since Mach number is zero, then the above case represents a ground run. Thus:

Intake

$$T_{02} = T_{01} = T_{0a} = T_a = 288 \text{ K}$$

$$P_{01} = P_{0a} = P_a = 101 \text{ kPa}$$

LPC

$$P_{03} = P_{02} \times \pi_{c1} = 4 \times 101 = 404 \text{ kPa}$$

$$T_{03} = T_{02} \left(1 + \frac{\pi_{c1}^{\frac{\gamma_c - 1}{\gamma_c}} - 1}{\eta_{c1}} \right) = 288 \left(1 + \frac{4^{0.286} - 1}{0.86} \right) = 451 \text{ K}$$

HPC

$$P_{04} = P_{03} \times \pi_{c2} = 3.125 \times 404 = 1262.5 \text{ kPa}$$

$$T_{04} = T_{03} \left(1 + \frac{\pi_{c2}^{\frac{\gamma_c - 1}{\gamma_c}} - 1}{\eta_{c2}} \right) = 451 \left(1 + \frac{3.125^{0.286} - 1}{0.86} \right) = 653 \text{ K}$$

Combustion chamber

$$P_{05} = P_{04} (1 - \Delta P_{cc} \%) = 1262.5 \times 0.99 = 1250 \text{ kPa}$$

$$f = \frac{(Cp_h/Cp_c)(T_{05}/T_{04}) - 1}{\eta_b(Q_R/Cp_c T_{04}) - (Cp_h/Cp_c)(T_{05}/T_{04})}$$

$$f = \frac{(1.148/1.005)(1143/653) - 1}{0.99 \times 45,000/(1.005 \times 653) - (1.148/1.005)(1143/653)}$$

$$= \frac{0.999}{65.885} = 0.015169$$

HPT

Assume $\lambda = 1$, then:

$$\begin{aligned}\left(\frac{T_{06}}{T_{05}}\right) &= 1 - \frac{(Cp_c/Cp_h)T_{03}}{\lambda_1(1+f)T_{05}} \left[\left(\frac{T_{04}}{T_{03}}\right) - 1 \right] \\ &= 1 - \left[\frac{(1.005/1.148) \times 451}{1.015169 \times 1143} \right] \left(\frac{653}{451} - 1 \right) = 0.8476\end{aligned}$$

$$T_{06} = 969 \text{ K}$$

$$\left(\frac{P_{06}}{P_{05}}\right) = \left(1 - \frac{T_{05} - T_{06}}{\eta_{t1}T_{05}}\right)^{\frac{\gamma_t}{\gamma_t-1}} = \left(1 - \frac{1143 - 969}{0.9 \times 1143}\right)^4 = 0.4765$$

$$P_{06} = 595.7 \text{ kPa}$$

LPT

Assume also $\lambda_2 = 1$, then:

$$\begin{aligned}\left(\frac{T_{07}}{T_{06}}\right) &= 1 - \frac{(Cp_c/Cp_h)T_{02}}{\lambda_2(1+f)T_{06}} \left[\left(\frac{T_{03}}{T_{02}}\right) - 1 \right] \\ &= 1 - \left[\frac{(1.005/1.148) \times 288}{1.015169 \times 969} \right] \left(\frac{451}{288} - 1 \right) = 0.8549\end{aligned}$$

$$T_{07} = 828.4 \text{ K}$$

$$\left(\frac{P_{07}}{P_{06}}\right) = \left(1 - \frac{T_{06} - T_{07}}{\eta_{t1}T_{06}}\right)^{\frac{\gamma_t}{\gamma_t-1}} = \left(1 - \frac{969 - 828.4}{0.9 \times 969}\right)^4 = 0.495$$

$$P_{07} = 294.9 \text{ kPa}$$

Nozzle

No losses are assumed at tailpipe; thus, conditions at point (7) are equal to those in point (8).

Check nozzle choking:

$$\begin{aligned}\frac{P_{08}}{P_c} &= \frac{1}{\left[1 - \frac{1}{\eta_n} \left(\frac{\gamma_h-1}{\gamma_h+1}\right)\right]^{\frac{\gamma_h}{\gamma_h-1}}} = 1.9336 \\ P_c &= 152.5 \text{ kPa}\end{aligned}$$

Since $P_c > P_a$, then the nozzle is choked and thus: $P_9 > P_c$

The exhaust gas temperature is calculated from the relation:

$$T_9 = T_c = \frac{2T_{08}}{\gamma_h + 1} = 710 \text{ K}$$

The jet speed is expressed as:

$$V_9 = \sqrt{\gamma_h R T_9} = 521.3 \text{ m/s}$$

The density of exhaust gases: $\rho_9 = \frac{P_9}{R T_9} = 0.748 \text{ kg/m}^3$

The gas mass flow rate: $\dot{m}_9 = \rho_9 V_9 A_9 = 0.748 \times 521.3 \times 0.208 = 81.15 \text{ kg/s}$

$$\text{The air mass flow rate : } \dot{m}_a = \frac{\dot{m}_9}{1+f} = 79.94 \text{ kg/s} \quad \#$$

$$\begin{aligned} T &= \dot{m}_a(1+f)V_9 + A_9(P_9 - P_a) \\ &= 81.15 \times 521.3 + 0.208 \times (152.5 - 101) \times 10^3 \end{aligned}$$

$$T = (42.303 + 10.712) \times 10^3 = 53,015 \text{ N} = 53.015 \text{ kN}$$

The thrust specific fuel consumption is:

$$TSFC = \frac{f\dot{m}}{T} = \frac{0.015169 \times 79.94}{53,656} = 21.79 \times 10^{-6} \text{ kg/N.s} = 21.79 \text{ g/N.s} \quad \#$$

The propulsive efficiency is *zero* as this case represents a ground run ($V=0.0$).

The thermal efficiency with $V=0.0$ is expressed as:

$$\eta_{th} = \frac{\dot{m}_e(V_e)^2}{2\dot{m}_f Q_R} = \frac{(1+f)V_e^2}{2fQ_R} = 0.202 = 20.2\%$$

The overall efficiency is also zero as it is the product of both propulsive efficiency (here zero) and thermal efficiency.

Example 6.7 If the afterburner for the two-spool engine described in Example (6.6) is operative. Additional data are:

$$T_{0max} = 1850 \text{ K}, \quad \eta_{ab} = 98\%, \quad \Delta P_{ab} = 2\%$$

Calculate

The new values for thrust force and $TSFC$

The thermal efficiency

The percentage increase in thrust force

The percentage increase in fuel consumption

Solutions

All the calculations in Example (6.6) are applied to the present case of operative afterburner up to the states (8 and 9).

Afterburner

$$f_{ab} = \frac{(1+f)(Cp_{8A}T_{08A}-Cp_7T_{07})}{\eta_{ab}Q_R - Cp_{8A}T_{08A}}$$

$$f_{ab} = \frac{(1+0.015169) \times 1.148 \times (1850 - 828.4)}{0.98 \times 45,000 - 1.148 \times 2000} = \frac{1,191}{41,804} = 0.0285$$

$$P_{08A} = P_{07}(1 - \Delta P_{ab}\%)$$

$$P_{08A} = 289 \text{ kPa}$$

Nozzle

As usual a check for nozzle choking is performed as follows:

$$\frac{P_{08A}}{P_c} = \frac{1}{\left[1 - \frac{1}{\eta_n} \left(\frac{\gamma_h - 1}{\gamma_h + 1}\right)\right]^{\frac{\gamma_h}{\gamma_h - 1}}} = 1.9336$$

Then the critical pressure is $P_c = 149.46 \text{ kPa} > P_a$.

Then the nozzle is also choked. The exhaust gases leave the nozzle with a temperature of T_{9A} calculated as:

$$\left(\frac{T_{08}}{T_{9A}}\right) = \left(\frac{\gamma_h + 1}{2}\right) = 1.167$$

The exhaust temperature is then $T_{9A} = 1585 \text{ K}$, and the exhaust jet speed is calculated from the relation:

$$V_{9ab} = \sqrt{\gamma_h R T_{9A}} = 779 \text{ m/s}$$

The *thrust* is expressed by the relation:

$$T_{ab} = \dot{m}_a[(1+f+f_{ab})V_9] + A_9(P_9 - P_a) = 64,993 + 10,080 = 75,073 \text{ N}$$

$$= 75.073 \text{ kN}$$

The *thrust specific fuel consumption (TSFC)* is given by:

$$TSFC = \frac{\dot{m}_f + \dot{m}_{fab}}{T} = \frac{\dot{m}_a(f+f_{ab})}{T} = 49.82 \text{ g/(kN.s)}$$

Thermal efficiency

$$\eta_{th} = \frac{\dot{m}_e(V_e)^2}{2\dot{m}_f Q_R} = \frac{(1+f+f_{ab})V_e^2}{2(f+f_{ab})Q_R} = 0.161 = 16.1 \text{ \%}$$

Increase in thrust: $\Delta T\%$

$$\Delta T\% = \frac{T_{ab} - T}{T} = \frac{76.045 - 53.656}{53.656} = 41.6 \text{ \%}$$

Increase in fuel consumption ($\Delta f\%$)

$$\Delta f\% = \frac{f_{ab}-f}{f} = \frac{0.0285 - 0.015169}{0.015169} = 87.88\%$$

6.2.9 Micro-turbojet

Small turbojet engine are developed for use in cruise missiles, target drones, and other small unmanned air vehicles (UAVs). Examples are Microturbo TRI 60 which different types (TRI 60-1, 60-2, 60-3, 60-5, 60-20, and 60-30) produce a thrust force ranging from 3.5 to 5.3 kN. This engine is a single spool, having a length of 851 mm (33.5 in), diameter of 348 mm (13.7 in), and dry weight of 61.2 kg (135 lb). March 20, 1983, represents the first-ever flight of a micro-turbojet-powered model aircraft, which had a three-minute flight. This engine measured $4\frac{3}{4}$ " in diameter and $13\frac{1}{2}$ " long and weighed $3\frac{3}{4}$ pounds. At 85,000 rpm it produced over 9 lb of thrust and had a top speed of 97,000 rpm. Twenty years later, commercial engines of roughly similar dimensions and weight are in the 30-lb thrust class when running at 120,000 rpm. The airframe, with its twin-boom high-tail configuration, is remarkably, perhaps inevitably, similar to many of today's trainer aircraft.

The first commercial micro-turbines were made available by JPX in the early 1990s [6]. Shortly after, Germany and the Netherlands sought out to develop a powerful, lightweight, liquid-fueled micro-turbine. AMT and Schreckling Designs were the first two companies to accomplish these goals. Figure 6.9 shows a cross section of micro-turbojet engine (SR-30). Table 6.1 shows some data for micro-turbojet engines.

Figure 6.10 illustrates Harpoon missile which is an air-, surface-, or submarine-launched anti-surface (antiship) missile. It is powered by Teledyne CAE J402 small *turbojet* engine (together with a solid-propellant booster). Teledyne CAE J402 turbojet engine is thoroughly discussed in Example (6.8).

Example 6.8 Harpoon Block II (Fig. 6.10) is the world's premier antiship missile. It uses solid-propellant booster for launch and Teledyne CAE J402 turbojet for cruise. General characteristics of Teledyne turbojet engine:

Inlet diameter: 14.35 cm

Compressor type: single-stage axial compressor and single-stage centrifugal compressor, having overall pressure ratio: 5.6:1

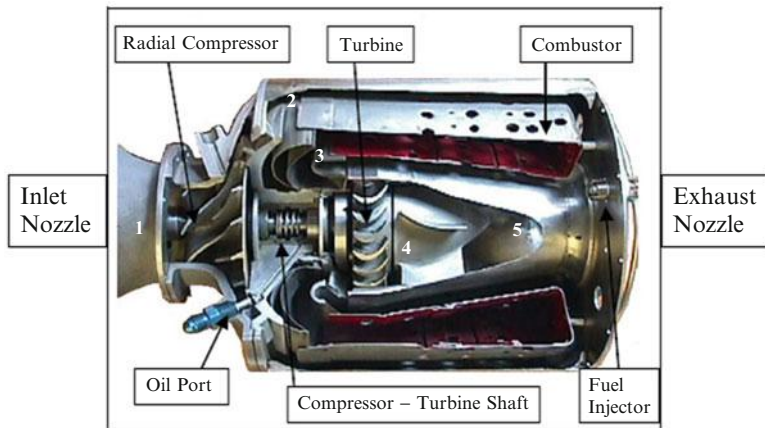


Fig. 6.9 Cross section of micro-turbojet engine (SR-30)

Table 6.1 Some micro-turbojet engines

Manufacturer	Model	Diameter (in)	Length (in)	Weight (Lbs)	Max thrust (Lbf)
AMT	Mercury HP	3.9	8.7	3.1	19.8
SWB	SWB-11 Mamba	3.5	7.3	1.9	11.4
AMT	Pegasus HP	4.7	10.4	5.9	35.3
Jetcat	P160	4.37	12.0	3.4	34
Ram	750 F	4.37	9.4	2.4	16.9
Simjet	85 N+	4.25	9.5	2.4	19.1
Artes/Espiell	JG100	4.33	9.4	2.3	22.5
Kamps		4.33	9.3	2.7	13.5
Phoenix	30/3	4.33	9.8	3.5	20.23
Schreckling	FD 3/64	4.33	NA	1.9	4.95
AMT	Olympus	5.1	10.6	5.3	42.7



Fig. 6.10 Harpoon missile

Maximum thrust: 2.9 kN

Thrust specific fuel consumption: 0.1226 kg/N.hr

When the turbojet is turned on, the missile has a speed of 135 m/s and sea-level conditions (temperature and pressure 288 K and 101 kPa). Assume all processes are ideal as well as constant specific heat and specific heat ratio inside the engine.

Calculate

Fuel-to-air ratio

Exhaust jet speed

The maximum temperature in engine

Fuel heating value

Solution

Inlet area:

$$A_i = \frac{\pi}{4} D^2 = 0.01617 \text{ m}^2$$

$$\dot{m}_a = \rho_a V_f A_i = 1.222 \times 250 \times 0.01617 = 4.94 \text{ kg/s}$$

$$\dot{m}_f = TSFC \times T = \frac{0.1226}{3600} \times 2900 = 0.0988 \text{ kg/s}$$

Fuel-to-air ratio

$$f = \frac{\dot{m}_f}{\dot{m}_a} = 0.02$$

Exhaust jet speed

From the thrust force: $T = \dot{m}_a [(1+f)V_e - V_f]$

Exhaust jet speed is:

$$V_e = \frac{1}{1+f} \left(\frac{T}{\dot{m}_a} + V_f \right) = \frac{1}{1.02} \left(\frac{2900}{4.94} + 250 \right) = 820.6 \text{ m/s}$$

Maximum cycle temperature

The following cycle analysis is performed first:

Sonic speed at sea level:

$$a = \sqrt{\gamma RT} = 340 \text{ m/s}$$

Flight Mach number:

$$M = \frac{V}{a} = 0.397$$

Compressor inlet (state 2):

$$T_{02} = T_a \left(1 + \frac{\gamma - 1}{2} M^2 \right) = 297 \text{ K}$$

$$P_{02} = P_a \left(1 + \frac{\gamma - 1}{2} M^2 \right)^{\frac{1}{\gamma-1}} = 112.6 \text{ kPa}$$

Combustion chamber inlet (state 3):

$$P_{03} = P_{02}\pi_c = 630.5 \text{ kPa} = P_{04}$$

$$T_{03} = T_{02}(\pi_c)^{\frac{1}{\gamma}} = 486 \text{ K}$$

With constant specific heats, then balance between compressor (states 2–3) and turbine (states 4–5) yields:

$$(1+f)C_p(T_{04} - T_{05}) = C_p(T_{03} - T_{02})$$

$$T_{05} = T_{04} - \frac{(T_{03} - T_{02})}{(1+f)} = T_{04} - 186$$

Besides : $\frac{P_{05}}{P_{04}} = \left(\frac{T_{05}}{T_{04}} \right)^{\frac{1}{\gamma-1}}$ (A)

Nozzle (states 5–6):

$$V_e^2 = 2C_p(T_{05} - T_6) = 2C_pT_{05} \left[1 - \left(\frac{P_a}{P_{05}} \right)^{\frac{1}{\gamma-1}} \right]$$

$$\frac{P_a}{P_{05}} = \left(1 - \frac{V_e^2}{2C_pT_{05}} \right)^{\frac{1}{\gamma-1}} = \left[1 - \frac{(820.6)^2}{2 \times 1005} \frac{1}{T_{05}} \right]^{\frac{1}{\gamma-1}} = \left(1 - \frac{335}{T_{04} - 186} \right)^{\frac{1}{\gamma-1}} \quad (\text{B})$$

From (A) and (B), then:

$$\frac{P_a}{P_{04}} = \left[\left(\frac{T_{05}}{T_{04}} \right) \left(1 - \frac{335}{T_{04} - 186} \right) \right]^{\frac{1}{\gamma-1}}$$

$$\begin{aligned}\left(\frac{P_a}{P_{04}}\right)^{\frac{\gamma-1}{\gamma}} &= \left(\frac{T_{04} - 186}{T_{04}}\right) \left(1 - \frac{335}{T_{04} - 186}\right) \\ \left(\frac{101}{630.4}\right)^{0.296} &= \left(\frac{T_{04} - 186}{T_{04}}\right) \left(\frac{T_{04} - 521}{T_{04} - 186}\right) = \frac{T_{04} - 521}{T_{04}} \\ 0.59227 &= \frac{T_{04} - 521}{T_{04}}\end{aligned}$$

Maximum cycle temperature is then:

$$T_{04} = 1278 \text{ K}$$

Fuel heating value

From balance in combustion chamber:

$$\begin{aligned}Q_R &= C_p T_{04} + \frac{C_p(T_{04} - T_{03})}{f} = 1.005 \times 1278 + \frac{1.005 \times (1278 - 486)}{0.02} \\ &= 41082 \text{ kJ/kg} \\ Q_R &= 41.082 \text{ MJ/kg}\end{aligned}$$

6.3 Turbofan

6.3.1 *Introduction*

Turbofan engines are the dominant air-breathing engines in the last 4 decades. They are the most reliable engines ever developed. Turbofans were first termed by Rolls-Royce as *bypass turbojet*. Boeing Company sometimes identifies them as *fanjets* [7]. In turbofan or “bypass” engine, the partly compressed airflow is divided, some into a central part, the gas generator or core, and some into a surrounding casing, the bypass or fan duct. The gas generator acts like a turbojet, while the bypass air is accelerated relatively slowly down the duct to provide “cold stream” thrust. The cold and hot streams mix inside or outside the engine to give better propulsive efficiency, lower noise levels, and improved fuel consumption.

Gas generator in both of turbofan and turbojet engines has three modules, namely, compressor, combustion chamber, and turbine. In turbofan engines, the fan pressurizes air and feeds it aft. Most goes around the engine core through a nozzle-shaped chamber. The rest goes through the engine core where it mixes with fuel and ignites. The hot gases expand through the turbine section and exit the hot nozzle as it exits the engine.

In the 1950s, Rolls-Royce introduced the first turbofan in the world, namely, RB.80 Conway. Conway design and development started in the 1940s, but it was used only in the late 1950s and early 1960s. The Conway powered versions of the Handley Page Victor, Vickers VC10, Boeing 707-420, and Douglas DC-8-40. It had a very low-bypass ratio (BPR designated as β) of 0.25 and maximum thrust of 76.3 kN [8]. In 1964, another RR turbofan engine was produced having also a low-bypass ratio of 0.64. GE led the way of high-bypass ratio turbofan engines in 1965 with the TF39 (BPR 8) to power the C-5 Galaxy [9]. Rolls-Royce developed the first worldwide three-spool turbofan engines RB211 in 1969 having a high-bypass ratio ranging from 4.0 to 5.0 depending on its series [10].

GE still leads HBPR turbofan engines with GE90 (BPR of 9) [11]. The maximum achieved BPR is 12.0:1 which is a record number scored by Pratt and Whitney in 2013 in its PW1500 series, which powered Bombardier CSeries CS100 and CS300 (second half of 2015), and PW 1100G series, which powered Airbus A319neo, A320neo, and A321neo in October 2015 [12]. The PW1400 series will power the Russian Federation airplane [Irkut MC-21](#) in 2017, whereas the PW1700 series will power Embraer [E-Jets E2](#) in 2018.

There are several advantages to turbofan engines over both of turboprop and the turbojet engines. The fan is not as large as the propeller, so the increase of speeds along the blade is less. Thus, turbofan engines power now all civil transports flying at transonic speeds up to Mach 0.9. Also, by enclosing the fan inside a duct or cowling, the aerodynamics is better controlled. There is less flow separation at the higher speeds and less trouble with shock developing. The turbofan may suck in more airflow than a turbojet, thus generating more thrust. Like the turboprop engine, the turbofan has low fuel consumption compared with the turbojet. The turbofan engine is the best choice for high-speed, subsonic commercial airplanes.

6.3.2 Milestones

[Appendix C](#) presents detailed list of milestones of turbofan engines.

6.3.3 Classifications of Turbofan Engines

As described in Chap. 1, numerous types of turbofan exist. Figure 6.11 illustrates a very detailed classification of turbofan engines.

Turbofan engines may be classified based on fan location as either forward or aft fan. Based on a number of spools, it may be classified as single, double, and three (triple) spools. Based on a bypass ratio, it may be categorized as either low- or high-bypass ratio. The fan may be geared or ungeared to its driving low-pressure turbine. Moreover, mixed types (low-bypass types) may be fitted with afterburner or not. Cross matching between different categories is identified in Fig. 6.11.

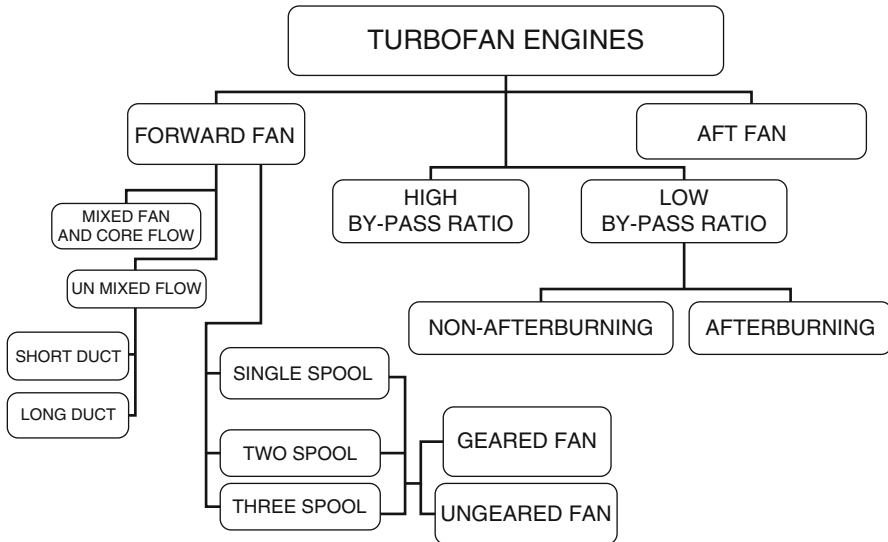


Fig. 6.11 Classification of turbofan engines

High-bypass ratio turbofan ($\beta = 7 - 8$) achieves around 75 % of its thrust from the bypass air and is ideal for subsonic transport aircraft. *Examples in commercial usage are Rolls-Royce Trent series (500/700/800/900/1000 powering in the Airbus A330, A340, A350, and A380), Pratt & Whitney PW1000 G (geared) powering Airbus A320neo, Bombardier CSeries, Embraer E2, Mitsubishi Regional Jet MC-21, and General Electric GE90 series (76B/77B/85B/90B/92B/94B/110B1/115B) powering Boeing 777-300ER, 747.*

A low-bypass ratio turbofan, where the air is divided approximately equally between the gas generator and the bypass duct, is well suited to high-speed military usage. *Examples in military usage are Rolls-Royce RB199 in the Tornado, Pratt & Whitney F100-PW-200 in F-16A/B and F-15, as well as EuroJet Turbo GmbH EJ200 powering the Typhoon.*

It is too lengthy to analyze all types of turbofan engines. So, the following cases will be analyzed:

Double-spool unmixed flow turbofan

Tripe-spool unmixed turbofan

Double-spool mixed turbofan with afterburner

Aft fan engine

First of all, let us define the bypass ratio as:

$$\beta = BPR = \frac{\dot{m}_{\text{cold}}}{\dot{m}_{\text{hot}}} \equiv \frac{\dot{m}_{\text{fan}}}{\dot{m}_{\text{core}}}$$

Table 6.2 Component efficiencies and specific heat ratio for moderate bypass ratio ($\beta = 2.7$) [13]

Module	Efficiency (η)	Specific heat ratio (γ)
Intake (diffuser)	0.97 ($M < 1$)	1.4
	0.85 ($M > 1$)	
Fan	0.85	1.39
Compressor	0.85	1.37
Turbine	0.9	1.33
Core nozzle	0.97	1.36
Fan nozzle	0.97	1.39

Thus, if the air mass through the core (compressor) is (\dot{m}_a), then the bypass air (fan duct) mass flow rate is ($\beta\dot{m}_a$). Typical component efficiencies and specific heat ratios for a supersonic turbofan engine having a bypass ratio, $\beta = 2.7$, are given in Table 6.2.

6.3.4 Forward Fan Unmixed Double-Spool Configuration

The main components here are the intake, fan, fan nozzle, low-pressure compressor (booster), high-pressure compressor, combustion chamber, high-pressure turbine, low-pressure turbine, and turbine nozzle. Two cases are seen for the low-pressure spool, namely:

Fan and low-pressure compressor (LPC) on one shaft and driven by low-pressure turbine

Fan driven by the LPT and the compressor driven by the HPT

Typical examples for the first type are the General Electric CF6 engine series and Pratt & Whitney PW4000 series. Typical example for the second type is GE Rolls-Royce F136 engine.

A schematic diagram for the first type as well as its T-s diagram is shown in Figs. 6.12 and 6.13.

Low-pressure spool is rotating with N_1 speed, while the high-pressure spool is rotating with N_2 speed.

Here below is an analysis for the different modules of the engine:

1. Intake

The inlet module is analyzed quite similar to turbojet engine using Eqs. (6.1), (6.2), and (6.3).

2. Fan

A similar analysis to the compressor section is followed. The appropriate equations are:

$$P_{010} = (P_{02})(\pi_f) \quad (6.43)$$

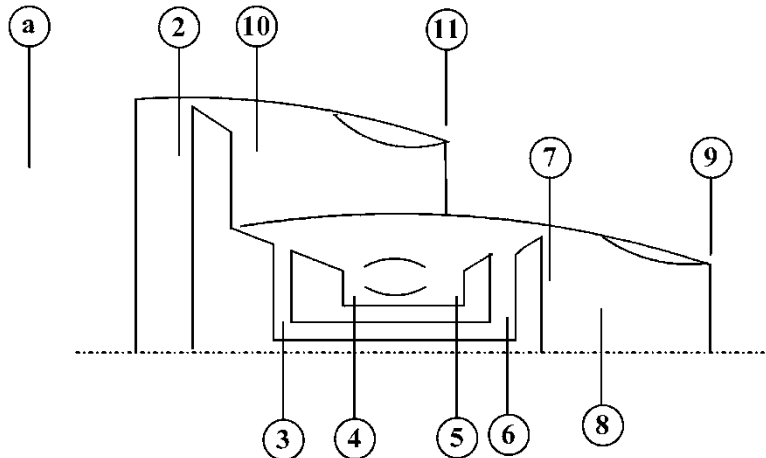


Fig. 6.12 Layout of a double spool where fan and LPC driven by LPT

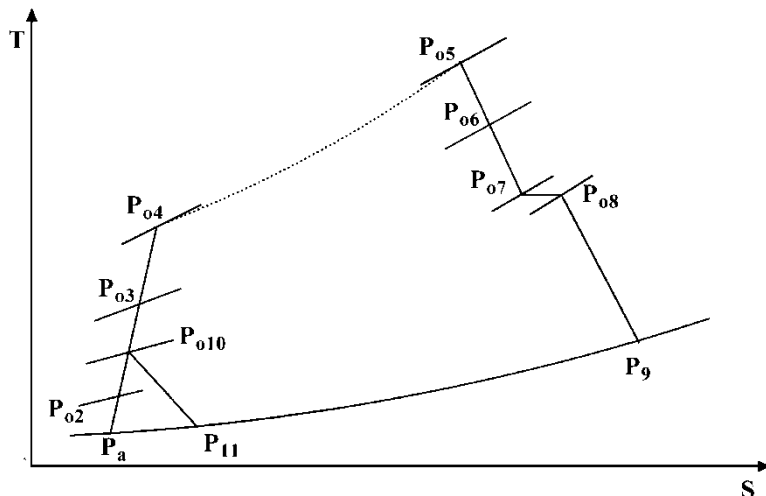


Fig. 6.13 T-s diagram for a double-spool turbofan engine

$$T_{010} = T_{02} \left[1 + \frac{\left(\frac{\gamma-1}{\pi_f^\gamma} - 1 \right)}{\eta_f} \right] \quad (6.44)$$

3. Low-pressure compressor (or booster)

Low-pressure ratio is developed in this compressor (normally less than two):

$$P_{03} = (P_{010})(\pi_{lpc}) \quad (6.45)$$

$$T_{03} = T_{010} \left[1 + \frac{\left(\pi_{\text{hpc}}^{\frac{\gamma-1}{\gamma}} - 1 \right)}{\eta_{\text{hpc}}} \right] \quad (6.46)$$

4. High-pressure compressor

High-pressure ratio is developed by HPC (normally around 10):

$$P_{04} = (P_{03})(\pi_{\text{hpc}}) \quad (6.47)$$

$$T_{04} = T_{03} \left[1 + \frac{\left(\pi_{\text{hpc}}^{\frac{\gamma-1}{\gamma}} - 1 \right)}{\eta_{\text{hpc}}} \right] \quad (6.48)$$

5. Combustion chamber

The pressure at the outlet of the combustion chamber is obtained from the pressure drop in the combustion chamber:

$$P_{05} = P_{04} - \Delta P_{cc} \quad (6.49a)$$

$$\text{Or} \quad P_{05} = P_{04}(1 - \Delta P_{cc} \%) \quad (6.49b)$$

The temperature at the outlet of the combustion chamber is also the maximum temperature in the engine and known in advance. Thus, the fuel-to-air ratio is calculated from the relation:

$$f = \frac{\left(\frac{Cp_h}{Cp_c} \right) \left(\frac{T_{05}}{T_{04}} \right) - 1}{\eta_b \left(\frac{Q_R}{Cp_c T_{04}} \right) - \left(\frac{Cp_h}{Cp_c} \right) \left(\frac{T_{05}}{T_{04}} \right)} \quad (6.50)$$

6. High-pressure turbine (HPT)

To calculate the temperature and pressure at the outlet of the high-pressure turbine, an energy balance between the high-pressure compressor (HPC) and high-pressure turbine (HPT) is performed:

$$\dot{m}_a Cp_c (T_{04} - T_{03}) = \eta_{m1} \lambda_1 [\dot{m}_a (1+f) Cp_h (T_{05} - T_{06})] \quad (6.51a)$$

$$\left(\frac{T_{06}}{T_{05}} \right) = 1 - \frac{(Cp_c/Cp_h) T_{03}}{\lambda_1 \eta_{m1} (1+f) T_{05}} \left[\left(\frac{T_{04}}{T_{03}} \right) - 1 \right] \quad (6.51b)$$

Here also the mechanical efficiency for high-pressure spool is (η_{m1}), and the portion of energy extracted by the HPC from that developed in the HPT is (λ_1). From the

above relation, the temperature at the outlet of the turbine T_{06} is calculated. Moreover, from the known isentropic efficiency of high-pressure turbine η_{hpt} , the outlet pressure from the high-pressure turbine P_{06} is calculated from the relation:

$$P_{06} = P_{05} \left(1 - \frac{T_{05} - T_{06}}{\eta_{\text{hpt}} \times T_{05}} \right)^{\frac{\gamma_h}{\gamma_h - 1}} \quad (6.52)$$

7. Low-pressure turbine

An energy balance between the fan and low-pressure compressor (LPC) from one side and the low-pressure turbine (LPT) on the other side is expressed by the relation:

$$\begin{aligned} \beta \dot{m}_a C p_c (T_{010} - T_{02}) + \dot{m}_a C p_c (T_{03} - T_{02}) \\ = \eta_{m2} \lambda_2 [\dot{m}_a (1 + f) C p_h (T_{06} - T_{07})] \end{aligned} \quad (6.53a)$$

or

$$\begin{aligned} (1 + \beta) \dot{m}_a C p_c (T_{010} - T_{02}) + \dot{m}_a C p_c (T_{03} - T_{010}) \\ = \eta_{m2} \lambda_2 \dot{m}_a (1 + f) C p_h (T_{06} - T_{07}) \end{aligned} \quad (6.53b)$$

$$T_{07} = T_{06} - \frac{C p_c}{\eta_{m2} \lambda_2 (1 + f) C p_h} [(1 + \beta)(T_{010} - T_{02}) + (T_{03} - T_{010})]$$

The pressure at the outlet is obtained from the relation:

$$P_{07} = P_{06} \left(1 - \frac{T_{06} - T_{07}}{\eta_{\text{lpt}} \times T_{06}} \right)^{\frac{\gamma_h}{\gamma_h - 1}} \quad (6.54)$$

Bleed from high-pressure compressor

Now, if there is an *air bleed* from the high-pressure compressor (HPC) at a station where the pressure is P_{03b} , then the energy balance with the high-pressure turbine gives:

$$\begin{aligned} \dot{m}_a C p_c (T_{03b} - T_{03}) + \dot{m}_a (1 - b) C p_c (T_{04} - T_{03b}) \\ = \eta_{m1} \lambda_1 \dot{m}_a (1 + f - b) C p_h (T_{05} - T_{06}) \end{aligned} \quad (6.51c)$$

where $b = \frac{\dot{m}_b}{\dot{m}_a}$ is the air bleed ratio defining the ratio between the air bled from the HPC to the core airflow rate. Moreover, such a bleed has its impact on the energy balance of the low-pressure spool as the air passing through the low-pressure turbine is now reduced:

$$\begin{aligned} (1 + \beta) \dot{m}_a C p_c (T_{010} - T_{02}) + \dot{m}_a C p_c (T_{03} - T_{010}) \\ = \eta_{m2} \lambda_2 \dot{m}_a (1 + f - b) C p_h (T_{06} - T_{07}) \end{aligned} \quad (6.53c)$$

The flow in the jet pipe is frequently associated with a pressure drop mainly due to skin friction.

Thus, the pressure upstream of the turbine nozzle is slightly less than the outlet pressure from the turbine. The temperature, however, is the same. Thus:

$$\begin{aligned} P_{08} &= P_{07}(1 - \Delta P_{\text{jet pipe}}) \\ T_{08} &= T_{07} \end{aligned}$$

8. Turbine nozzle

The exhaust velocities of both of the hot gases from the turbine nozzles are obtained after checks for choking. Thus, if the isentropic efficiency of turbine nozzle is η_{nt} , then the critical pressure is calculated from the relation:

$$\frac{P_{08}}{P_c} = \frac{1}{\left[1 - \frac{1}{\eta_{nt}} \left(\frac{\gamma_h - 1}{\gamma_h + 1}\right)\right]^{\frac{\gamma_h}{\gamma_h - 1}}}$$

For an ideal, $\eta_{nt} = 1$, then the above equation is reduced to:

$$\left(\frac{P_{08}}{P_c}\right) = \left(\frac{\gamma_h + 1}{2}\right)^{\frac{\gamma_h}{\gamma_h - 1}}$$

If $P_c \geq P_a$ then the nozzle is choked. The temperature and pressure of the gases leaving the nozzle are the critical values ($T_9 = T_c$, $P_9 = P_c$). Temperature is obtained from the relation:

$$\left(\frac{T_{08}}{T_9}\right) = \left(\frac{\gamma_h + 1}{2}\right)$$

In this case the gases leave the nozzle at a speed equal to the sonic speed or:

$$V_9 = \sqrt{\gamma_h RT_9} \quad (6.55a)$$

If the nozzle is unchoked ($P_9 = P_a$), then the speed of the gases leaving the nozzle is now given by:

$$V_9 = \sqrt{2Cp_h T_{08} \eta_{nt} \left[1 - \left(\frac{P_a}{P_{08}}\right)^{\frac{\gamma_h - 1}{\gamma_h}}\right]} \quad (6.55b)$$

The pressure ratio in the nozzle is obtained from the relation:

$$\frac{P_{08}}{P_a} = \frac{P_{08}}{P_{07}} \frac{P_{07}}{P_{06}} \frac{P_{06}}{P_{05}} \frac{P_{05}}{P_{04}} \frac{P_{04}}{P_{03}} \frac{P_{03}}{P_{010}} \frac{P_{010}}{P_{02}} \frac{P_{02}}{P_{0a}} \frac{P_{0a}}{P_a}$$

9. Fan nozzle

The critical pressure is calculated from the relation:

$$\frac{P_{010}}{P_c} = \frac{1}{\left[1 - \frac{1}{\eta_{fn}} \left(\frac{\gamma_c - 1}{\gamma_c + 1}\right)\right]^{\frac{\gamma_c}{\gamma_c - 1}}}$$

Also for an ideal nozzle $\eta_{fn} = 1$ and the above equation will be reduced to:

$$\left(\frac{P_{010}}{P_c}\right) = \left(\frac{\gamma_c + 1}{2}\right)^{\frac{\gamma_c}{\gamma_c - 1}}$$

If $P_c \geq P_a$ then the fan nozzle is choked. The temperature and pressure of air leaving the nozzle are ($T_{11} = T_c, P_{11} = P_c$). Temperature is then obtained from the relation:

$$\left(\frac{T_{010}}{T_{11}}\right) = \left(\frac{\gamma_c + 1}{2}\right)$$

Then the gases leave the nozzle at a speed equal to the sonic speed or:

$$V_{11} = \sqrt{\gamma_c R T_{11}} \quad (6.56a)$$

If the nozzle is unchoked ($P_{11} = P_a$), then the speed of the gases leaving the nozzle is now given by:

$$V_{11} = \sqrt{2C_{pc} T_{010} \eta_{fn} \left[1 - (P_a/P_{010})^{\frac{\gamma_c - 1}{\gamma_c}}\right]} \quad (6.56b)$$

$$\frac{P_{010}}{P_a} = \frac{P_{010}}{P_{02}} \frac{P_{02}}{P_a}$$

The thrust force is now obtained from the general relation:

$$\begin{aligned} \frac{T}{\dot{m}_a} &= (1+f)V_9 + \beta V_{11} - U(1+\beta) + \frac{1}{\dot{m}_a} [A_{11}(P_{11} - P_a) + A_9(P_9 - P_a)] \\ &= (1+f)V_9 + \beta(V_{11} - U) - U + \frac{1}{\dot{m}_a} [A_{11}(P_{11} - P_a) + A_9(P_9 - P_a)] \end{aligned} \quad (6.57a)$$

The specific thrust, the thrust force per total air mass flow rate (\dot{M}_{at}), is further evaluated from the relation:

$$\frac{T}{\dot{M}_{at}} = \frac{T}{\dot{m}_h + \dot{m}_c} = \frac{T}{\dot{m}_a(1+\beta)} = \frac{(1+f)}{(1+\beta)} V_9 + \frac{\beta}{(1+\beta)} V_{11} - U + \frac{1}{\dot{m}_a(1+\beta)} [A_{11}(P_{11} - P_a) + A_9(P_9 - P_a)] \quad (6.57b)$$

The thrust specific fuel consumption is:

$$TSFC = \dot{m}_f/T = \frac{\dot{m}_f \dot{m}_a}{\dot{m}_a T} = \frac{f}{T/\dot{m}_a}$$

It is noted from the above equation that the fuel-to-air ratio is calculated as the ratio between fuel flow rate and the airflow through the core of engine and not the total airflow rate through the engine.

The thrust force, specific thrust, and the thrust specific fuel consumption are calculated.

Example 6.9 The Tomahawk is a long-range subsonic cruise missile powered by a solid-fuel rocket booster and the small two-spool turbofan engine [Williams International F107-WR-402](#) (Fig. 6.14). It has the following data:

Flight speed $V_f = 247.22$ m/s

Ambient temperature $T_a = 275$ K

Ambient pressure $P_a = 0.79$ bar

Thrust force $T = 3.1$ kN

Specific fuel consumption = 0.682 kg/kg-h

Bypass ratio = 1

Overall pressure ratio = 13.8

Fan pressure ratio = 2.1

Fan diameter = 0.305 m

Fuel heating value = 43,000 kJ/kg

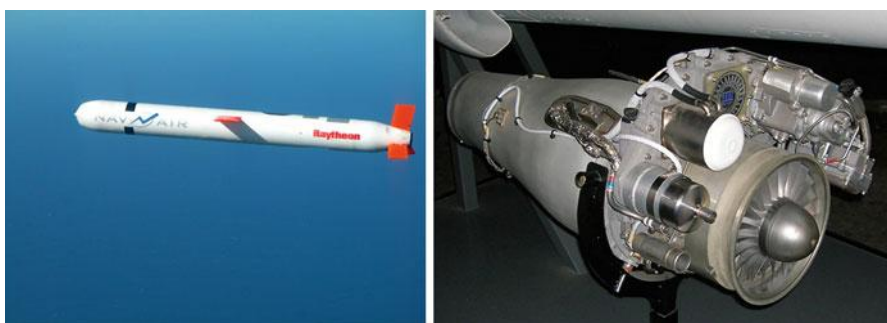
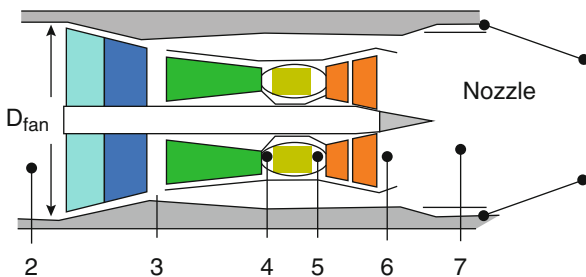


Fig. 6.14a Tomahawk missile and Williams [F107-WR-402](#) turbofan engine

Fig. 6.14b Schematic diagram of Williams F107-WR-402 turbofan engine



Calculate

Air mass flow rate

Fuel-to-air ratio

Exhaust gas speed

Engine maximum temperature

Solution

Air mass flow rate

Flight speed

$$V_f = 247.22 \text{ m/s}$$

$$A = 0.07306 \text{ m}^2$$

$$\rho_a = \frac{P_a}{RT_a} = 1.001 \text{ kg/m}^3$$

$$\dot{m}_a = \rho_a V_f A = 18.08 \text{ kg/s}$$

$$\text{Since } \beta = 1.0, \text{ then } \dot{m}_c = \dot{m}_h = 9.04 \text{ kg/s}$$

$$T/\dot{m}_a = \frac{T}{\dot{m}_a} = 171.46 \text{ m/s}$$

$$TSFC = 0.682 \text{ kg/kgf.h} = \frac{0.682}{9.81 \times 3600} = 0.0000193 \text{ kg/N.s} = 19.3 \text{ g/kN.s}$$

Fuel-to-air ratio

$$TSFC = \frac{\dot{m}_f}{T} = \frac{\dot{m}_f / \dot{m}_h}{T / \dot{m}_h} = \frac{(\dot{m}_f / \dot{m}_h)}{(T / \dot{m}_a) \times (1 + \beta)} = \frac{f}{(T / \dot{m}_a) \times (1 + \beta)}$$

$$f = TSFC \times \left(\frac{T}{\dot{m}_a} \right) (1 + \beta) = 0.0000193 \times 171.46 \times 2 = 0.006618$$

Exhaust gas speed

$$T = [\dot{m}_c + c \dot{m}_h (1+f)^h] V_e - \dot{m}_a V_f$$

$$\frac{T}{\dot{m}_a} = \left[\frac{\beta}{1+\beta} + \frac{(1+f)}{1+\beta} \right] V_e - V_f = \left(\frac{\beta+1+f}{1+\beta} \right) V_e - V_f$$

$$V_e = \frac{(T/\dot{m}_a) + V_f}{\left(\frac{\beta+1+f}{1+\beta} \right)} = \frac{171.4622 + 247.22}{\left(\frac{2.006618}{2} \right)} = 417.3 \text{ m/s}$$

Engine maximum temperature is analyzed from cycle analysis.

Intake

$$M = \frac{V_f}{\sqrt{\gamma R T_a}} = 0.7437$$

$$P_{02} = P_a \left(1 + \frac{\gamma-1}{2} M^2 \right)^{\frac{\gamma}{\gamma-1}} = 114.0522 \text{ kPa}$$

$$T_{02} = T_a \left(1 + \frac{\gamma-1}{2} M^2 \right) = 305.42 \text{ K}$$

Fan

$$P_{03} = P_{02} \pi_f = 239.51 \text{ kPa}$$

$$T_{03} = T_{02} (\pi_f)^{\frac{\gamma-1}{\gamma}} = 377.62 \text{ K}$$

Compressor

$$P_{04} = P_{03} \pi_c = 1574 \text{ kPa}$$

$$T_{04} = T_{03} (\pi_c)^{\frac{\gamma-1}{\gamma}} = 645 \text{ K}$$

Combustion chamber

$$\dot{m}_f Q_R + \dot{m}_h C_{pc} T_{04} = (\dot{m}_h + \dot{m}_f) C_{ph} T_{05}$$

$$T_{05} = \frac{f Q_R + C_{pc} T_{04}}{(1+f) C_{ph}} = \frac{0.006618 \times 43000 + 1.005 \times 645.0}{1.006618 \times 1.148} = 807.2 \text{ K}$$

Maximum temperature is then $T_{0\max} = 807.2 \text{ K}$.

Example 6.10 A two-spool forward unmixed turbofan engine is powering an airliner flying at Mach number 0.9 at an altitude of 10,500 m (ambient pressure,

Table 6.3 Modules results

Module	Fan	LPC	HPC	HPT	LPT
ΔT_0	42	43	355	380	390
π	1.58	1.5	9.75	2.75	3.9

temperature, sonic speed, and air density ratio are 24,475 Pa, 220 K, 297.3 m/s, and 0.3165, respectively). The low-pressure spool is composed of a turbine driving the fan and the low-pressure compressor. The high-pressure spool is composed of a high-pressure compressor and a high-pressure turbine. Air is bled from the outlet of high-pressure compressor. The total temperature difference (in K) and pressure ratios for different modules are recorded and shown in Table 6.3:

Diffuser, fan, and turbine nozzles have isentropic efficiency of 0.9. Maximum cycle temperature is 1500 K. Inlet area is 3.14 m^2 . Assume the following values for the different variables:

$$\eta_b = 0.96, Q_{HV} = 45,000 \text{ kJ/kg}, \gamma_{\text{air}} = 1.4, \text{ and } \gamma_{\text{gases}} = 1.33$$

It is required to calculate:

- (a) Pressure recovery of diffuser r_d
- (b) Total air mass flow rate
- (c) Isentropic efficiency of fan and low-pressure and high-pressure compressors
- (d) The fuel-to-air ratio (f)
- (e) The air bleed ratio (b)
- (f) The bypass ratio (β)
- (g) Area of cold and hot nozzles
- (h) The thrust force

Solution

The modules of the engine and its different processes plotted on the T-s diagram are shown in Figs. 6.12 and 6.13.

Diffuser

$$T_{02} = T_{0a} = T_a \left(1 + \frac{\gamma_c - 1}{2} M_a^2 \right) = 220 \times (1 + 0.2 \times 0.81) = 255.6 \text{ K}$$

$$P_{0a} = P_a \left(1 + \frac{\gamma_c - 1}{2} M_a^2 \right)^{\frac{\gamma_c}{\gamma_c - 1}} = (1 + 0.2 \times 0.81)^{3.5} = 1.69 \text{ Pa}$$

$$P_{02} = P_a \left(1 + \eta_d \frac{\gamma_c - 1}{2} M_a^2 \right)^{\frac{\gamma_c}{\gamma_c - 1}} = (1 + 0.9 \times 0.2 \times 0.81)^{3.5} = 1.61 \text{ Pa}$$

$$P_{02} = 39.4 \text{ kPa}$$

$$\pi_d = \frac{P_{02}}{P_{0a}} = 0.953$$

$$\rho_a = 0.3165 \rho_{s,l} = 0.3877 \text{ kg/m}^3$$

$$V = Ma = 0.9 \times 297.3 = 267.6 \text{ m/s}$$

$$\dot{m}_{\text{total}} = \rho_a V A_{\text{inlet}} = 0.3877 \times 267.6 \times 3.14 = 325.7 \text{ kg/s}$$

Fan

$$T_{02} = 255.6 \text{ K}$$

$$T_{010} = T_{02} + \Delta T_{0f} = 255.6 + 42 = 297.6 \text{ K}$$

$$P_{010} = P_{02} \times \pi_f = 39.4 \times 1.58 = 62.27 \text{ kPa}$$

The fan isentropic efficiency may be expressed as:

$$\eta_f = \frac{T_{010s} - T_{02}}{T_{010} - T_{02}} = \frac{T_{02} \left(\pi_f^{\frac{\gamma_c-1}{\gamma_c}} - 1 \right)}{\Delta T_{0f}} = \frac{255.6}{42} (1.58^{0.286} - 1) = 0.8505 = 85.05 \%$$

Low-pressure compressor

$$T_{03} = T_{010} + \Delta T_{0LPC} = 297.6 + 43 = 340.6 \text{ K}$$

$$P_{03} = P_{010} \times \pi_{LPC} = 62.27 \times 1.5 = 93.04 \text{ kPa}$$

$$\eta_{LPC} = \frac{T_{010} \left(\pi_{LPC}^{\frac{\gamma_c-1}{\gamma_c}} - 1 \right)}{\Delta T_{0LPC}} = \frac{297.6}{43} (1.5^{0.286} - 1) = 0.85095 = 85.1\%$$

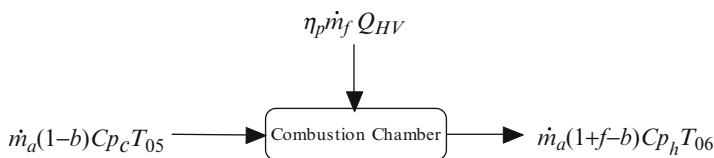
High-pressure compressor

$$T_{04} = T_{03} + \Delta T_{0HPC} = 340.6 + 355 = 695.6 \text{ K}$$

$$P_{04} = P_{03} \times \pi_{HPC} = 93.40 \times 9.75 = 910.65 \text{ kPa}$$

$$\eta_{HPC} = \frac{T_{03} \left(\pi_{HPC}^{\frac{\gamma_c-1}{\gamma_c}} - 1 \right)}{\Delta T_{0HPC}} = \frac{340.6}{355} (9.75^{0.286} - 1) = 0.88079 = 88.1\%$$

Combustion chamber



Fuel-to-air ratio

$$f = \frac{\dot{m}_f}{\dot{m}_h} = \frac{(1-b)(Cp_h T_{05} - Cp_c T_{04})}{\eta_{cc} Q_{HV} - Cp_h T_{05}} = \frac{(1-b)(1.148 \times 1500 - 1.005 \times 695.6)}{0.96 \times 45,000 - 1.148 \times 1500} \\ = 0.02466(1-b)$$

$$f = 0.02466(1-b) \quad (1)$$

Energy balance for high-pressure spool

$$Cp_c(T_{04} - T_{03}) = (1+f-b)Cp_h(T_{05} - T_{06})$$

Substitute from (1)

$$1.005 \times (355) = [1 + 0.02466 \times (1-b) - b] \times 1.148 \times (380)$$

$$b = 20.2\%$$

Bleed = 20.2 %

Comment: Though this bleed ratio looks like a great percentage, however, it will be described in the turbine cooling sections that each blade row may need some 2 % of air mass flow rate for cooling, and the two turbines here have a total of five stages and so ten blade rows. In addition bleeding has its other applications for cabin air conditioning as well as other anti-icing applications.

From equation (1)

$$\text{Fuel-to-air ratio} \quad f = 0.01968$$

This fuel-to-air ratio is a reasonable figure which assures the value previously obtained for the bleed ratio.

Energy balance for low-pressure spool:

$$(1+\beta)Cp_c\Delta T_{0f} + Cp_c\Delta T_{0LPC} = (1+f-b)Cp_hT_{0LPT}$$

$$(1+\beta) \times 1.005 \times 42 + 1.005 \times 43 = (1 + 0.01968 - 0.202) \times 1.148 \times 390$$

$$\beta = 6.649$$

Thus, the *bypass ratio* is

$$\beta = 6.649.$$

Fan airflow rate is then

$$\dot{m}_{\text{fan}} = \frac{\beta}{1+\beta} \dot{m}_{\text{total}} = \frac{6.649}{7.649} \times 325.7 = 283.12 \text{ kg/s.}$$

Core airflow rate is then

$$\dot{m}_{\text{core}} = \frac{1}{1+\beta} \dot{m}_{\text{total}} = \frac{1}{7.649} \times 325.7 = 42.58 \text{ kg/s.}$$

Fan nozzle

The first step in nozzle analysis is to check whether it is choked or not by calculating the pressure ratio:

$$\frac{P_{010}}{P_c} = \frac{1}{\left(1 - \frac{1}{\eta_{f_n} \gamma_c + 1}\right)^{\frac{\gamma_c}{\gamma_c - 1}}} = \frac{1}{\left(1 - \frac{1}{0.9} \frac{1.4 - 1}{1.4 + 1}\right)^{\frac{1.4}{1.4 - 1}}} = 2.0478$$

$$\frac{P_{010}}{P_a} = \frac{62.27}{24.47} = 2.5447$$

Since $\frac{P_{010}}{P_c} < \frac{P_{010}}{P_a}$, then the nozzle is *choked*:

$$P_{11} = P_c = 30.41 \text{ kPa}$$

$$T_{11} = T_c = \frac{2}{\gamma_c + 1} T_{010} = \frac{297.6}{1.2} = 248 \text{ K}$$

$$V_{11} = V_{e \text{ fan}} = \sqrt{\gamma_c R T_{11}} = \frac{297.6}{1.2} = 315.67 \text{ m/s}$$

$$\rho_{11} = \frac{P_{11}}{R T_{11}} = 0.4273 \text{ kg/m}^3$$

$$A_{11} = \frac{\dot{m}_{\text{fan}}}{\rho_{11} V_{11}} = 2.099 \text{ m}^2$$

Turbine nozzle

Here also a check for the choking of turbine nozzle is followed:

$$\frac{P_{08}}{P_c} = \frac{1}{\left(1 - \frac{1}{\eta_m \gamma_h + 1}\right)^{\frac{\gamma_h}{\gamma_h - 1}}} = \frac{1}{\left(1 - \frac{1}{0.9} \frac{1.333 - 1}{1.333 + 1}\right)^{\frac{1.333}{1.333 - 1}}} = 1.9835$$

$$\frac{P_{08}}{P_a} = \frac{84.91}{24.47} = 3.469$$

Since $\frac{P_{08}}{P_c} < \frac{P_{08}}{P_a}$, then the nozzle is *choked*:

$$P_9 = P_c = 42.81 \text{ kPa}$$

$$T_9 = T_c = \frac{2}{\gamma_h + 1} T_{08} = \frac{730}{1.167} = 625.53 \text{ K}$$

$$V_9 = V_{e h} = \sqrt{\gamma_h R T_9} = 489.26 \text{ m/s}$$

$$\rho_9 = \frac{P_9}{R T_9} = 0.23845 \text{ kg/m}^3$$

$$A_9 = \frac{\dot{m}_{\text{core}}(1 + f - b)}{\rho_9 V_9} = 0.298 \text{ m}^2$$

Thrust force (T)

$$\begin{aligned}
 T &= \dot{m}_{\text{fan}} V_{e\text{Fan}} + (1+f-b)\dot{m}_h V_{e\text{h}} - \dot{m}_{\text{total}} V_{\text{flight}} + P_{11}A_{11} + P_9A_9 - P_a A_i \\
 T &= 283.12 \times 315.67 + 0.81768 \times 42.58 \times 489.26 - 325.7 \times 267.6 \\
 &\quad + 10^3(30.4 \times 2.099 + 42.81 \times 0.298 - 24.475 \times 3.14) \\
 \therefore T &= 18.97 \text{ kN}
 \end{aligned}$$

6.3.5 Forward Fan Mixed-Flow Engine

Mixed turbofan engines are always found in either single- or two-spool engines. It was used in the past for military applications only. Nowadays it is used in many civil aircrafts but nearly all military aircrafts. An example for a two-spool engine in civil aircrafts is the CFM56 series. The cold compressed air leaving the fan will not be directly exhausted as previously described, but it flows in a long duct surrounding the engine core and then mixes with the hot gases leaving the low-pressure turbine. Thus, the cold air is heated while the hot gases are cooled. Only one mixed exhaust is found.

6.3.5.1 Mixed-Flow Two-Spool Engine

Most of the mixed turbofan engines now are two-spool ones. If mixed turbofan engines are analyzed versus unmixed turbofan engines, reasonable improvements [14] in the following points are noticed; thrust generated, noise reduction and reverse thrust increase.

Hereafter, a detailed analysis of this category will be given. Figures 6.15 and 6.16 present the engine layout and its temperature–entropy diagram.

The requirements for the mixing process are equal static pressures and also equal velocities. Thus, from the layout designation, these two conditions are specified as $P'_3 = P_7$ and $V'_3 = V_7$ which means that if no pressure losses in the bypass duct connecting the cold and hot streams and no pressure loss in the mixing process, then:

$$P_{010} = P'_{03} = P_{07} = P_{08} \quad (6.58)$$

If losses exist in the fan bypass duct, then:

$$P'_{03} = P_{010} - \Delta P_{\text{fan duct}} \quad \text{and} \quad P_{07} = P_{08} = P'_{03}$$

In the above equation, no pressure drop is considered during the mixing process.

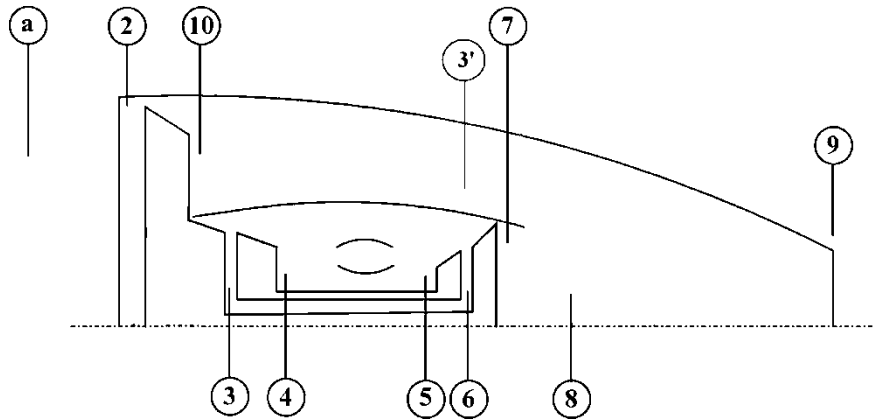


Fig. 6.15 Layout of a mixed two-spool turbofan

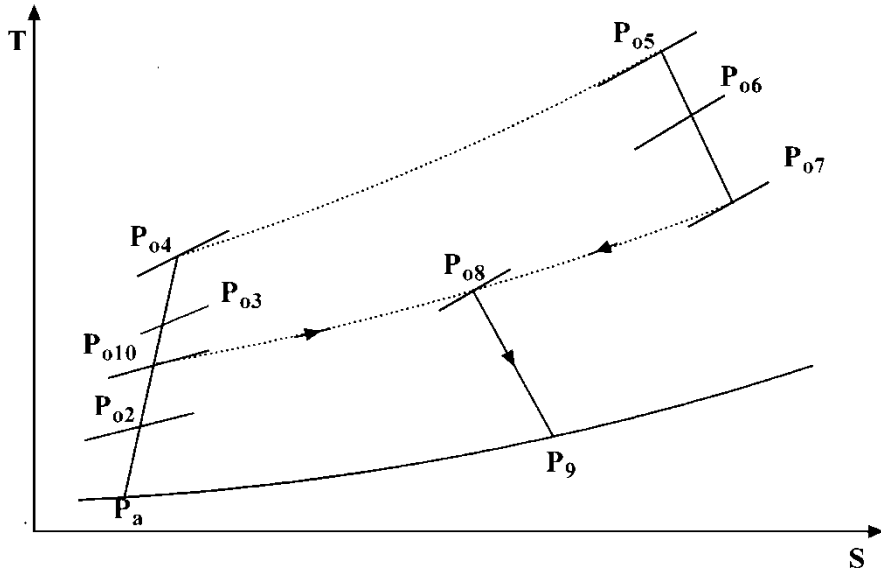


Fig. 6.16 Temperature–entropy diagram for two-spool mixed turbofan

In some engines like the CFM56 series, the mixing process takes place in a mixer preceding the nozzle. It results in a quieter engine than if the mixer was not present.

1. Energy balance for the low-pressure spool

Considering a mechanical efficiency for the low-pressure spool (η_{m1}), then:

$$W_{\text{fan}} + W_{\text{LPC}} = \eta_{m1} \lambda_1 W_{\text{LPT}}$$

or

$$\begin{aligned} \dot{m}_a (1 + \beta) Cp_c (T_{010} - T_{02}) + \dot{m}_a Cp_c (T_{03} - T_{010}) \\ = \eta_{m1} \lambda_1 \dot{m}_a (1 + f) Cp_h (T_{06} - T_{07}) \end{aligned} \quad (6.59)$$

2. Energy balance for the high-pressure spool

Also a second mechanical efficiency for the high-pressure spool is (η_{m2}) assumed:

$$W_{HPC} = \eta_{m2} \lambda_2 W_{HPT}$$

thus:

$$\dot{m}_a Cp_c (T_{04} - T_{03}) = \eta_{m2} \lambda_2 \dot{m}_a (1 + f) Cp_h (T_{05} - T_{06}) \quad (6.60)$$

3. Mixing process

The hot gases leaving the low-pressure turbine and the cold air leaving the fan bypass duct are mixed, giving new properties at state (8). Thus, such a process is governed by the first law of thermodynamics as follows:

$$\begin{aligned} H'_{03} + H_{07} &= H_{08} \\ \beta \dot{m}_h Cp_c T_{03} + \dot{m}_h (1 + f) Cp_h T_{07} &= \dot{m}_h (1 + \beta + f) Cp_h T_{08} \end{aligned}$$

which is reduced to:

$$\beta Cp_c T_{03} + (1 + f) Cp_h T_{07} = (1 + \beta + f) Cp_h T_{08} \quad (6.61)$$

Now for a better evaluation of the gas properties after mixing, we can use mass-weighted average properties of the gases at state (8) as follows:

$$\begin{aligned} Cp_8 &= \frac{(1 + f)Cp_7 + \beta Cp_3}{1 + f + \beta} \\ R_8 &= \frac{(1 + f)R_7 + \beta R_3}{1 + f + \beta} \\ \gamma_8 &= \frac{Cp_8}{Cp_8 - R_8} \end{aligned}$$

Consider the real case of mixing where normally losses are encountered and a pressure drop is associated with the mixing process. Such pressure losses are either given as the value ΔP_{mixing} or as a ratio r_m in the mixing process:

$$\begin{aligned} P_{08} &= P_{07} - \Delta P_{\text{mixing}} && \text{or} \\ P_{08} &= r_m P_{07} && \text{where } r_m < 1 \approx 0.98 \end{aligned}$$

Check nozzle choking as previously outlined. If the nozzle is unchoked, then the exhaust velocity is calculated from the relation:

$$V_9 = \sqrt{\frac{2\gamma_c RT_{08}\eta_n}{(\gamma_c - 1)} \left[1 - \left(P_a/P_{08} \right)^{\frac{\gamma_c-1}{\gamma_c}} \right]}$$

If the nozzle is choked, then $V_9 = \sqrt{\gamma_c RT_9} = \sqrt{\frac{2\gamma_c}{\gamma_c+1} RT_{08}}$

The thrust force is then given by the relation:

$$T = \dot{m}_a [(1 + f + \beta) V_9 - (1 + \beta) U] + A_9 (P_9 - P_a) \quad (6.62)$$

6.3.5.2 Mixed Turbofan with Afterburner

Since more than three decades, most military aircrafts are powered by a low-bypass ratio turbofan fitted with an afterburner [15]. One of the earliest afterburning turbofan engines is the Pratt & Whitney TF30 that powered the F-111 and the F-14A Tomcat. First flight of the TF30 was in 1964 and production continued until 1986. Afterburning gives a significant thrust boost for takeoff particularly from short runways like air carriers, transonic acceleration, and combat maneuvers, but is very fuel intensive. This engine is a mixed low-bypass ratio forward fan one. The mixed flow still has a sufficient quantity of oxygen for another combustion process. Thus, an afterburner is installed downstream of the low-pressure turbine and upstream of the nozzle. Tremendous amounts of fuel are burnt in the afterburner when it is lit. This rises the temperature of exhaust gases by a significant amount which results in a higher exhaust velocity/engine specific thrust. For a turbofan engine, afterburning (or reheat) offers greater gains because of the relatively low temperature, after mixing of the hot and cold streams and the large quantity of the excess air available for combustion. Exhaust nozzle is normally of the variable area type to furnish a suitable media for different operating conditions. Unlike the main combustor, an afterburner can operate at the ideal maximum (stoichiometric) temperature (i.e., about 2100 K). Now, at a fixed total applied fuel-to-air ratio, the total fuel flow for a given fan airflow will be the same, regardless of the dry specific thrust of the engine. However, a high specific thrust turbofan will, by definition, have a higher nozzle pressure ratio, resulting in a higher afterburning net thrust and, therefore, lower afterburning specific fuel consumption.

Though afterburning turbofan engines are mostly two-spool engine, some few single-spool ones are found. An example for single-spool afterburning is the SNECMA M53 developed for the [Dassault Mirage 2000](#) fighter. The engine is in service with different air forces, including the latest Mirage 2000-5 and 2000-9 multirole fighters. It had two variants, M 53-5 and M63-P2, which develop dry thrust, 54.0–64.7 kN, and wet (afterburning thrust) of 86.3–95.1 kN. [Overall](#)

pressure ratio is 9.8:1, bypass ratio is 0.36:1, specific fuel consumption is 0.90 (kg/daN.h), and thrust-to-weight ratio is 6.5.

Examples for other two-spool afterburning turbofans are:

The Pratt & Whitney series F100-220 (thrust: 40 K), F100-229 (48 K), F100-232 (28 K), F119 (65 K)

Eurojet EJ200

General Electric F110

Rolls-Royce Adour Mk.104

Russian engine RD-133

It is interesting to add here that military engines are now so powerful that the latest fighters can *supercruise*; (flying at sustained supersonic speed without the use of the afterburner). Examples are the Lockheed Martin: F-22 Raptor and Eurofighter: Eurofighter Typhoon can accelerate to supersonic speed (without using augmentation) and then sustain such a speed indefinitely in dry thrust. F-22 can supercruise at Mach 1.82, while Eurofighter Typhoon can supercruise at Mach 1.1–1.5.

A. Forward fan mixed afterburning low-bypass turbofan (LBPT) engine

The flow mixing will be the only difference in the cycle from that of afterburning turbojet engine. Figure 6.17 shows the configuration of a single-spool afterburning turbofan engine, while Fig. 6.18 shows its T-s diagram, and Fig. 6.19 shows its block diagram together with its input and output data.

A typical layout of a two-spool afterburning turbofan engine is displayed in Fig. 6.20, while its T-s diagram for an ideal cycle is shown in Fig. 6.21.

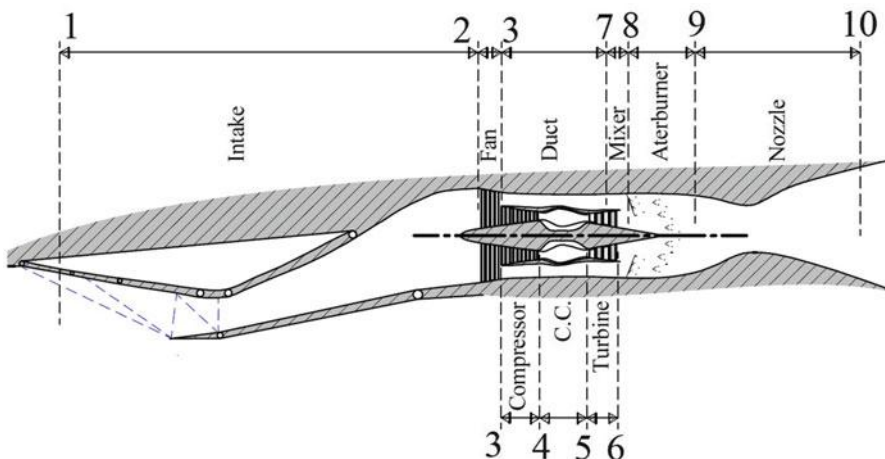


Fig. 6.17 Configuration of mixed turbofan with afterburner

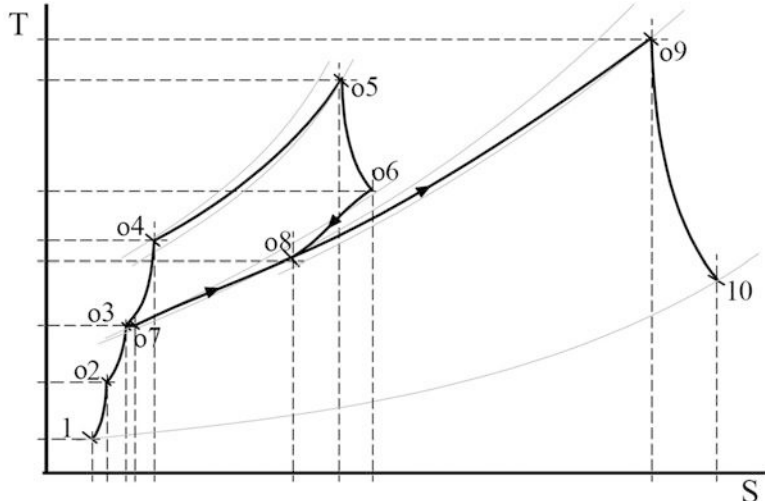


Fig. 6.18 T-s diagram for a single-spool mixed turbofan with afterburner

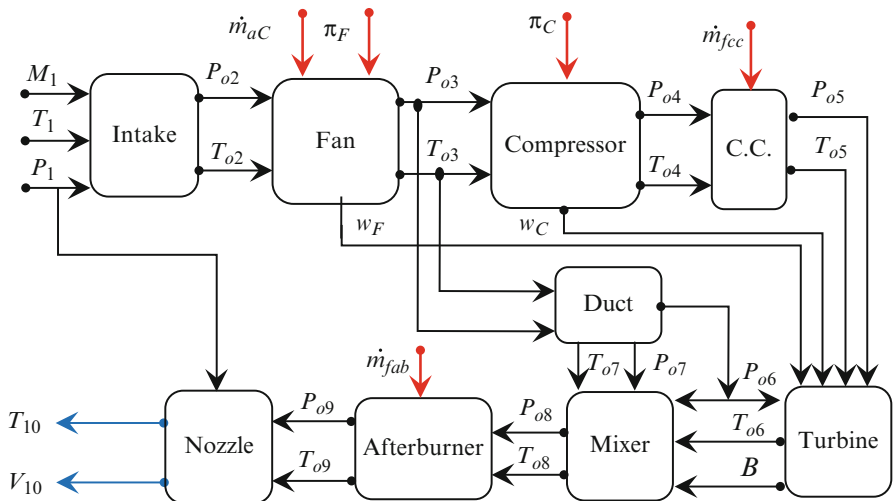


Fig. 6.19 Block diagram for a single-spool mixed afterburning turbofan engine

The same conditions necessary for mixing described above still hold. Thus, the following relation stands for ideal conditions (no pressure losses):

$$P_{010} = P_{07} = P_{08} = P_{011}$$

Normally mixing process is associated with pressure losses, which may be governed by either one of the following equations for losses:

$$P_{08} = P_{07} - \Delta P_{\text{mixing}}$$

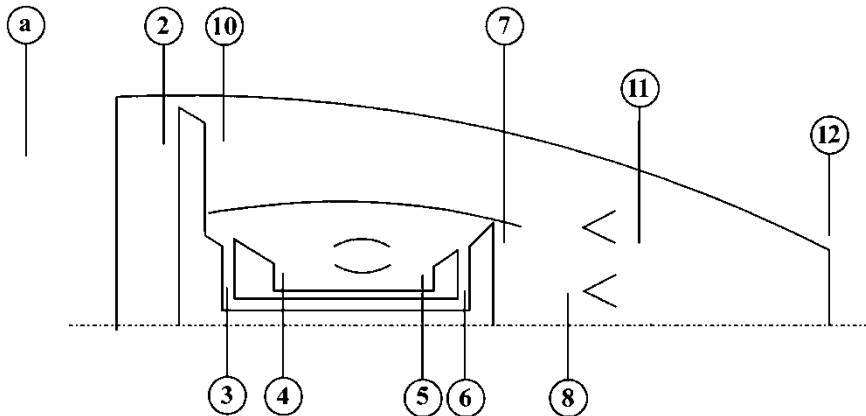


Fig. 6.20 Layout of a typical two-spool mixed afterburning engine

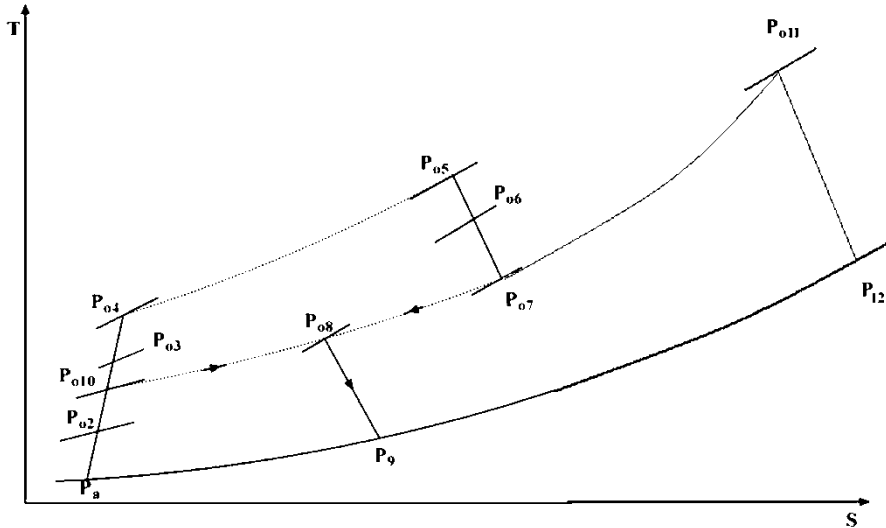


Fig. 6.21 T-s diagram for two-spool mixed afterburning engine

$$\text{Or} \quad P_{08} = r_m P_{07} \quad \text{where } r_m < 1 \approx 0.98$$

Here P_{011} is the total pressure at the outlet of the afterburner, when it is operative. Moreover, the outlet temperature of the afterburner is T_{011} which is known in advance. It is limited by the maximum temperature that the material of afterburner can withstand. However, it could be much higher than the total turbine inlet temperature (TIT) due to the absence of mechanical stresses arising from centrifugal forces created by the rotation of the turbine blades.

Now the mass balance in the afterburner gives the following afterburner fuel-to-air ratio (f_{ab}), where (f_{ab}) defined as:

$$f_{ab} = \frac{\dot{m}_{fab}}{\dot{m}_c + \dot{m}_h} \quad (6.63a)$$

Then the energy balance of the afterburner yields the relation:

$$f_{ab} = \frac{Cp_{11}T_{011}-Cp_8T_{08}}{\eta_{ab}Q_{HV} - Cp_{11}T_{011}} \quad (6.63b)$$

The pressure loss in the afterburner is also governed by the relation:

$$P_{09A} = P_{08} - \Delta P_{ab}$$

Next a convergent-divergent nozzle will enhance a full expansion to the ambient pressure. Thus, the jet speed will be given by the relation:

$$\therefore V_{12} = \sqrt{2Cp_{11}T_{011} \left[1 - \left(\frac{P_a}{P_{011}} \right)^{\frac{\gamma_{11}-1}{\gamma_{11}}} \right]} \quad (6.64)$$

The thrust force is now:

$$T = \dot{m}_e V_{12} - \dot{m}_a V_\infty$$

With the exhaust mass flow rate defined as:

$$\begin{aligned} \dot{m}_e &= m_c + \dot{m}_h (1+f) + \dot{m}_{f_{ab}} \\ \dot{m}_e &= \{\dot{m}_c + \dot{m}_h (1+f)\}(1+f_{ab}) \end{aligned}$$

Then the thrust is now expressed as:

$$T = \{\dot{m}_c + \dot{m}_h (1+f)\}(1+f_{ab})V_{12} - (\dot{m}_c + \dot{m}_h)V_\infty \quad (6.65)$$

6.3.5.3 Geared Turbofan (GTF)

Geared turbofans are of the two-spool unmixed forward fan category (Figs. 6.22 and 6.23). Since the fan is normally part of the low spool, both fan and LPT are turning at the same speed (N_1). This speed, however, often is a compromise. The fan really operates more efficiently at low rotational speeds (rpm), while the rest of the low spool is more efficient at higher speeds. Putting a reduction gear in between these components makes it possible for the fan and the low spool to run at their

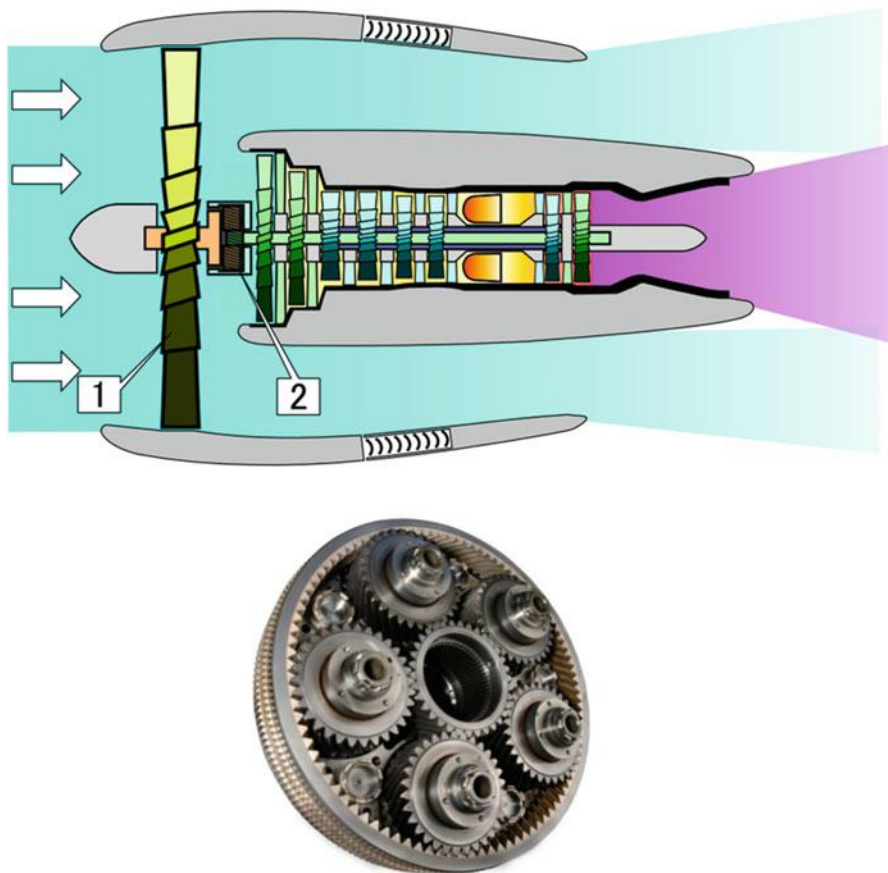


Fig. 6.22 Layout of geared turbofan (*top*) and planetary gearbox (*bottom*). (1) Fan (2) planetary gearbox

optimum speed, namely, N_1 for fan and N_3 for LPT. This in turn will minimize the possibility of formation of shock waves in the fan leading to a higher efficiency. The other advantages are more fuel efficiency, reduced noise levels, reduced emission (CO_2 and NO_x), fewer engine parts (fewer compressors and turbine stages), as well as reduction in overall operating costs. Gearbox used here is of the planetary type as shown in Fig. 6.22. Planetary gearbox is recommended as its length is short to match with minimum size requirements of turbofan engines.

Examples of geared turbofan engines

Low-pressure spool may be either composed of a fan driven by low-pressure turbine or a fan and low-pressure compressor representing the compression section driven by a low-pressure turbine. In either cases, a reduction gearbox is located directly downstream the fan.

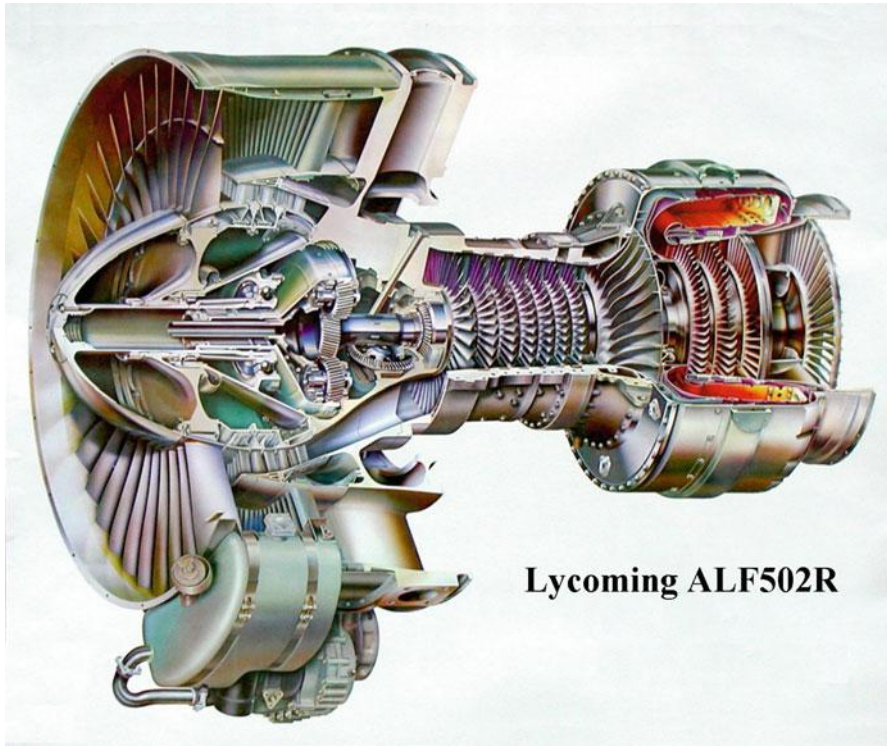


Fig. 6.23 Lycoming ALF502R geared turbofan

An example for geared turbofan is the *Honeywell LF 507* produced by [Lycoming](#), [AlliedSignal](#), and then [Honeywell Aerospace](#). The earlier [ALF 502](#) was certified in 1980 [16]. The improved, higher-thrust LF 507 was used on the [Avro RJ](#) update of the [British Aerospace BAe 146](#). Lycoming ALF502R shown in Fig. 6.23.

A second example is Pratt & Whitney PurePower PW1000G series (PW1100/1200/1400/1500/1700 G/1900) engine which represents the future geared turbofan scheduled for 2015–2018 [17]. It will power A320neo, MRJ, MS-21, and CSeries.

The PurePower PW1000G engine family has a maximum thrust in the range 62–100 kN.

It also has the following advantages;

It improves fuel burnup to 16 % versus today's best engines. That alone could save airlines nearly \$1,400,000 per aircraft per year

It cuts carbon emissions by more than 3500 t per aircraft per year. That's equal to the effect of planting more than 900,000 trees.

It will be ready to power aircraft well with biofuels since it has successfully been tested with alternative fuel.

Its TALON™ X combustor slashes polluting emissions. Thus, it will surpass the most stringent standards (CAEP/6) by 50 % for nitrous oxide (NOx).

It slashes aircraft noise footprints by up to 75 %—a big relief to communities. At up to 20 dB below today's most stringent standard, it is the quietest engine in its class, meaning lower noise fees, shorter flight tracks, extended curfew operation, and quieter cabins.

Now, concerning thermodynamic analysis of geared turbofan, if the mechanical efficiency of gearbox is η_{gb} , then two cases are examined. Firstly, the low-pressure spool is composed of fan and a low-pressure turbine. The fan states are 2 and 3 and the LPT states are 6 and 7. Then energy balance is expressed by the relation:

$$(1 + \beta) \dot{m}_a C p_c (T_{03} - T_{02}) = \eta_{gb} \lambda_1 \eta_{m1} \dot{m}_a (1 + f - b) C p_h (T_{06} - T_{07}) \quad (6.66)$$

where $b = \frac{\dot{m}_b}{\dot{m}_a}$ is the air bleed ratio defining the ratio between the air bled and the HPC to the core airflow rate.

In the second case, the low-pressure turbine (states 6 and 7) drives both fan (states 2 and 10) and low-pressure compressor (states 10 and 3). Then the energy balance equation will be expressed as:

$$\begin{aligned} (1 + \beta) \dot{m}_a C p_c (T_{010} - T_{02}) + \dot{m}_a C p_c (T_{03} - T_{010}) \\ = \eta_{gb} \lambda_1 \eta_{m1} \dot{m}_a (1 + f - b) C p_h (T_{06} - T_{07}) \end{aligned} \quad (6.67)$$

Concerning the high-pressure spool, with an air bled from a station just downstream of HPC and prior of combustion chamber:

$$\dot{m}_a C p_c (T_{04} - T_{03}) = \lambda_2 \eta_{m2} \dot{m}_a (1 + f - b) C p_h (T_{05} - T_{06}) \quad (6.68a)$$

Next, if *air is bled* from at a station within the high-pressure compressor (HPC), identified by the pressure P_{03b} , then the energy balance of the high-pressure spool is given by:

$$\begin{aligned} \dot{m}_a C p_c (T_{03b} - T_{03}) + \dot{m}_a C p_c (1 - b) (T_{04} - T_{03b}) \\ = \lambda_2 \eta_{m2} \dot{m}_a (1 + f - b) C p_h (T_{05} - T_{06}) \end{aligned} \quad (6.68b)$$

6.3.6 Forward Fan Unmixed Three-Spool Engine

The three-spool engine is composed of a low-pressure, intermediate-pressure, and high-pressure spools running at different speeds (N_1 , N_2 , and N_3). The fan and the low-pressure turbine (LPT) compose the low-pressure spool. The intermediate spool is composed of an intermediate-pressure compressor (IPC) and intermediate-pressure turbine (IPT). The high-pressure spool is also composed of a high-pressure compressor (HPC) and high-pressure turbine (HPT). Rolls-Royce

was the first aero engine manufacturer to design, develop, and produce the three-spool turbofan engine. The Rolls-Royce RB211 was the first three-spool engine to enter service (1972). Later on several manufacturers developed and manufactured this type of engines.

The main advantages of three-spool arrangement:

1. Shorter modules and shafts which result in a shorted engine
 - (a) Single-stage fan with no booster stages
 - (b) Fewer overall compressor stages and fewer variable stages
 - (c) Shorter high-pressure compressor
2. Higher efficiencies as each spool is running at its “optimum speed”
3. Greater engine rigidity
4. Lighter weight

The main drawbacks of this three-spool category are that they are more complex to build and maintain [18].

Examples for three-spool engines

1. Rolls-Royce RB211

The first of the whole series was RB211-22 series [18] which first saw service in 1972. Its thrust rating is 169 kN. Several subsequent series were developed with thrust rating of 222–270 kN, featured FADEC (full authority digital engine—or electronics—control), and wide-chord fan (which increases efficiency, reduces noise, and gives added protection against foreign object damage).

2. Rolls-Royce Trent

It is a family of high-bypass developed from RB211 with thrust ratings of 236–423 kN. Its layout provides lighter weight and better performance. It features the wide-chord fan and single crystal high-pressure turbine blades with improved performance and durability. The core turbomachinery is brand new, giving better performance, noise, and pollution levels.

The layout of this engine and the T-s diagram is shown in Figs. 6.24 and 6.25. Air bleed is also extracted from the high-pressure compressor at station (4b), not shown.

1. Energy balance of the 1st spool (fan and LPT)

$$(1 + \beta) \dot{m}_a C_p c (T_{03} - T_{02}) = \eta_{m1} \lambda_1 \dot{m}_a (1 + f - b) C_p h (T_{08} - T_{09}) \quad (6.69)$$

2. Energy balance for the intermediate spool (IPC and IPT)

$$\dot{m}_a C_p c (T_{04} - T_{03}) = \eta_{m2} \lambda_2 \dot{m}_a (1 + f - b) C_p h (T_{07} - T_{08}) \quad (6.70)$$

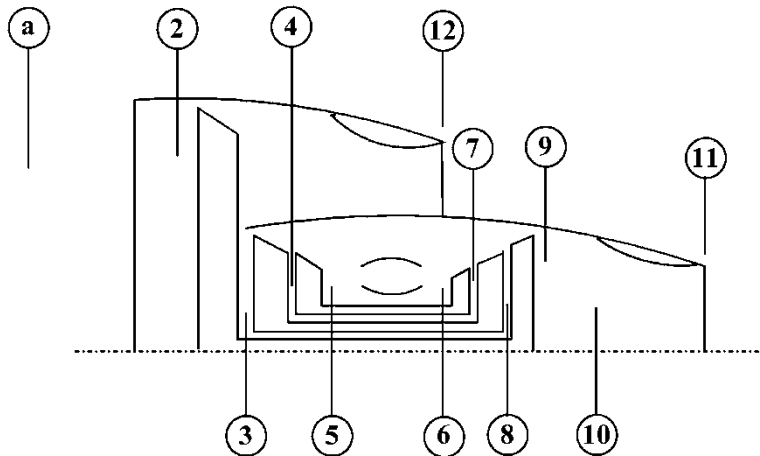


Fig. 6.24 Layout of a three-spool engine

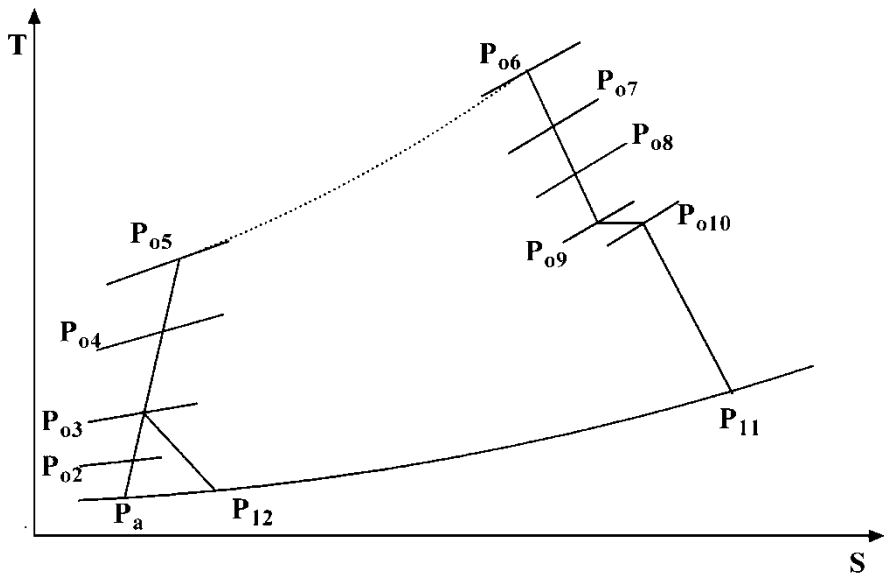


Fig. 6.25 T-s diagram for a three-spool turbofan

3. Energy balance for the high-pressure spool (HPC and HPT) with inter-bleed stage at (4b)

$$\begin{aligned} \dot{m}_a C_p_c (T_{04b} - T_{04}) + (1 - b) \dot{m}_a C_p_c (T_{05} - T_{04b}) \\ = \eta_{m3} \lambda_3 \dot{m}_a (1 + f - b) C_p_h (T_{06} - T_{07}) \end{aligned} \quad (6.71)$$

The same procedure discussed earlier in evaluating the fuel-to-air ratio, jet velocities of the cold air, and hot gases from the fan and turbine nozzles may be followed here. The propulsive, thermal, and overall efficiencies are obtained following the appropriate equations from Chap. 2.

Example 6.11 A. Triple-spool unmixed turbofan engine (Trent 700) is shown in Fig. 6.26. Bleed air having a percentage of 8 % is taken from HP compressor to cool HP and IP turbines as shown in Fig. 6.27. Engine has the following data in Table 6.4 below:

For takeoff operation where Mach number $M = 0.2$ at sea level, calculate:

1. The total temperature at the outlet of the fan and intermediate- and high-pressure compressors
2. The total temperature at the outlet of the high-, intermediate-, and low-pressure turbines

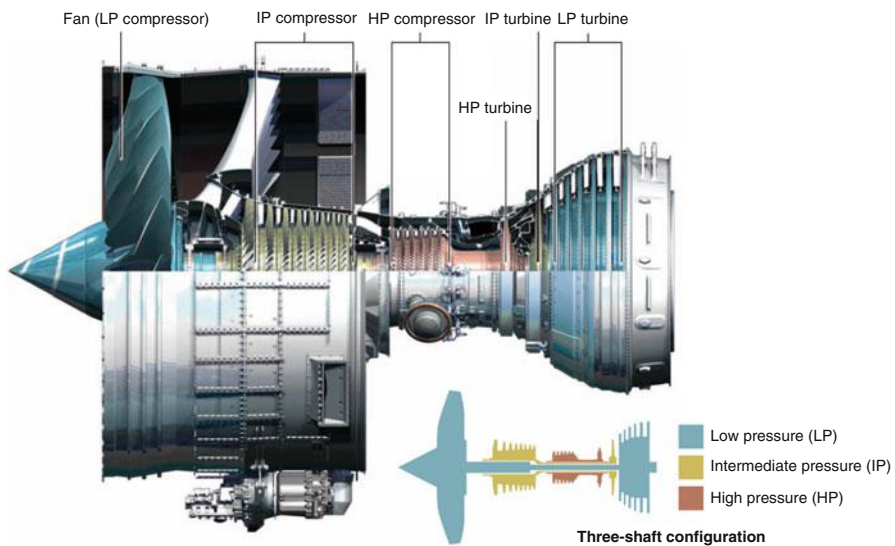


Fig. 6.26 Layout of unmixed three-spool engine (Trent 700)

Fig. 6.27 Layout of three-spool engine and air bleed details

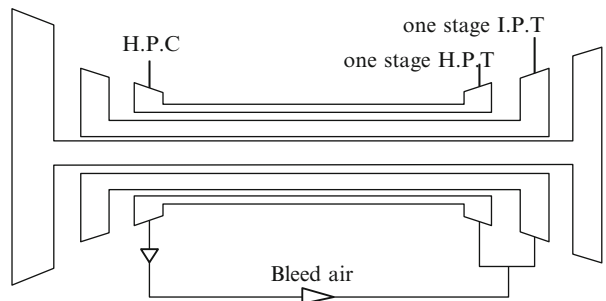


Table 6.4 A triple-spool unmixed turbofan engine operating conditions (Trent 700)

Variable	Value	Variable	Value
η_d	0.88	$\Delta p_{c.c.}$	0.03
η_f	0.9	$\Delta p_{fanduct}$	0
η_c	0.89	c_p_c (J/kg.K)	1005
η_b	0.98	c_p_h (J/kg.K)	1148
η_t	0.93	R (J/kg.K)	287
η_n	0.98	γ_c	1.4
η_m	0.99	γ_h	1.33
λ_1	0.84	B	0.08
λ_2	1	β	5.05
λ_3	1	TIT (K)	1543
M	0.82	π_{IPC}	5.8
π_F	1.45	π_{HPC}	4.2

3. The pressure and temperature at the outlet of cold and hot nozzles
4. Specific thrust, thrust specific fuel consumption, and propulsive, thermal, and overall efficiencies

Solution

At takeoff ($M = 0.2$) at sea level

Cycle analysis from Figs. 6.26 and 6.27:

Diffuser (a–2)

$$P_{02} = P_a \left(1 + \eta_d \frac{\gamma_c - 1}{2} M_a^2 \right)^{\frac{\gamma_c}{\gamma_c - 1}} = 1.0384 \times 10^5 \text{ Pa}$$

$$T_{02} = T_a \left(1 + \frac{\gamma_c - 1}{2} M_a^2 \right) = 290.4653 \text{ K}$$

Fan (2–3)

$$P_{03} = P_{02} \pi_f = 1.5057 \times 10^5 \text{ Pa}$$

$$T_{03} = T_{02} \left(1 + \frac{\frac{\gamma_c - 1}{\gamma_c}}{\eta_f} - 1 \right) = 326.6124 \text{ K}$$

Intermediate-pressure compressor (IPC) (3–4)

$$P_{04} = P_{03} \times \pi_{IPC} = 8.7333 \times 10^5 \text{ Pa}$$

$$T_{04} = T_{03} \left(1 + \frac{\pi_{IPC}^{\frac{\gamma_c-1}{\gamma_c}} - 1}{\eta_{IPC}} \right) = 566.0401 \text{ K}$$

High-pressure compressor (HPC) (4–5)

Bleed air is extracted at an intermediate state defined as:

$$P_{04b} = P_{04} \times \sqrt{\pi_{HPC}} = 1.7898 \times 10^6 \text{ Pa}$$

$$T_{04b} = T_{04} \left(1 + \frac{\pi_{HPC}^{\frac{\gamma_c-1}{2\gamma_c}} - 1}{\eta_{HPC}} \right) = 710.7556 \text{ K}$$

$$P_{05} = P_{04b} \times \sqrt{\pi_{HPC}} = 3.6680 \times 10^6$$

$$T_{05} = T_{04b} \left(1 + \frac{\pi_{HPC}^{\frac{\gamma_c-1}{2\gamma_c}} - 1}{\eta_{HPC}} \right) = 892.4693 \text{ K}$$

Combustion chamber (CC) (5–6)

$$T_{06} = TIT, \quad P_{06} = P_{05} \times (1 - \Delta p_{c.c.}) = 3.5579 \times 10^6 \text{ kPa}$$

$$f = (1 - b) \left(\frac{C_{ph} \times T_{06} - C_{pc} \times T_{05}}{\eta_b \times Q_R - C_{ph} \times T_{06}} \right) = 0.0213$$

High-pressure turbine (HPT) (6–7)

$$T_{07} = T_{06} - \left[\left(\frac{C_{pc}}{\eta_{m1} \times \lambda_1 \times (1 + f - b) \times C_{ph}} \right) \times ([T_{04b} - T_{04}] + (1 - b) \times [T_{05} - T_{04b}]) \right] \\ = 1206.8 \text{ K}$$

$$P_{07} = P_{06} \left(1 - \frac{(T_{06} - T_{07})}{\eta_{HPT} \times T_{06}} \right)^{\frac{\gamma_h}{\gamma_h - 1}} = 1.2134 \times 10^6 \text{ Pa}$$

Intermediate-pressure turbine (IPT) (7–8)

$$T_{08} = T_{07} - \left(\frac{C_{pc} \times [T_{04} - T_{03}]}{\lambda_2 \times \eta_{m2} \times (1 + f - \frac{b}{2}) \times C_{ph}} \right) = 995.3980 \text{ K}$$

$$P_{08} = P_{07} \left(1 - \frac{[T_{07} - T_{08}]}{\eta_{IPT} \times T_{07}} \right)^{\frac{\gamma_h}{\gamma_h - 1}} = 5.2318 \times 10^5 \text{ Pa}$$

Low-pressure turbine (LPT) (8–9)

$$T_{09} = T_{08} - \left(\frac{(1 + \beta) \times C_{pc} \times [T_{03} - T_{02}]}{\lambda_3 \times \eta_{m3} \times (1 + f) \times C_{ph}} \right) = 798.3326 \text{ K}$$

$$P_{09} = P_{08} \left(1 - \frac{[T_{08} - T_{09}]}{\eta_{LPT} \times T_{08}} \right)^{\frac{\gamma_h}{\gamma_h - 1}} = 1.9938 \times 10^5 \text{ Pa}$$

Hot nozzle (10–11)

$$P_{010} = P_{09} (1 - \Delta p_{duct}) = 1.9339 \times 10^5 \text{ Pa}$$

To get critical pressure: $P_c = P_{010} \left(1 - \frac{1}{\eta_n} \left[\frac{\gamma_h - 1}{\gamma_h + 1} \right] \right)^{\frac{\gamma_h}{\gamma_h - 1}} = 1.0309 \times 10^5 \text{ Pa}$

$$\text{Where } P_a = 1.01325 \times 10^5 \text{ Pa}$$

Since $P_C > P_a$, then the hot nozzle is choked:

$$\therefore P_{11} = P_c, \quad T_{11} = T_{010} \left(\frac{2}{\gamma_h + 1} \right) = 685.2640 \text{ K},$$

$$V_{11} = \sqrt{\gamma_h R T_{11}} = 511.4412 \text{ m/s}$$

Cold nozzle (3–12)

The critical pressure: $P_c = P_{03} \left(1 - \frac{1}{\eta_n} \left[\frac{\gamma_h - 1}{\gamma_h + 1} \right] \right)^{\frac{\gamma_h}{\gamma_h - 1}} = 7.8415 \times 10^4 \text{ Pa}$

Since $P_a = 1.01325 \times 10^5 \text{ Pa}$ and then $P_C < P_a$, the cold nozzle is unchoked:

$$P_{12} = P_a, \quad T_{12} = T_{03} \left[1 - \eta_n \left(1 - \left(\frac{P_a}{P_{03}} \right)^{\frac{\gamma_h - 1}{\gamma_h}} \right) \right] = 292.3616 \text{ K},$$

$$V_{12} = \sqrt{2C_{ph}(T_{03} - T_{12})} = 280.4278 \text{ m/s}$$

Specific thrust

$$\begin{aligned}\frac{T}{m_a^\circ} &= \left[\left(\frac{1}{1+\beta} \right) \left[(1+f) \times V_{11} + \beta \times V_{12} + (1+f) \left(\frac{RT_{11}}{P_{11}V_{11}} \right) (P_{11} - P_a) \right. \right. \\ &\quad \left. \left. + \beta \left(\frac{RT_{12}}{P_{12}V_{12}} \right) (P_{12} - P_a) \right] - V \right] \\ &= 253.4724 \text{ N.s/kg}\end{aligned}$$

Where:

T is the thrust force, m_a° is the air mass flow rate.

V is the flight speed, V_{11} is the exhaust hot gas speed.

V_{12} is the exhaust cooled gas speed.

Since the cold nozzle is unchoked, then $P_{12} = P_a$, and the corresponding pressure thrust is zero.

Thrust specific fuel consumption

$$TSFC = \frac{f/(1+\beta)}{T/m_a^\circ} = 1.3898 \times 10^{-5} \text{ kg/(N.s)}$$

Propulsive efficiency

$$\begin{aligned}\eta_p &= \frac{T/m_a^\circ \times V}{T/m_a^\circ \times V + \left[0.5 \left(\frac{1+f}{1+\beta} \right) (V_{11} - V)^2 \right] + \left[0.5 \left(\frac{\beta}{1+\beta} \right) (V_{12} - V)^2 \right]} \\ &= 0.3275\end{aligned}$$

Thermal efficiency

$$\eta_{th} = \frac{T/m_a^\circ \times V + \left[0.5 \left(\frac{1+f}{1+\beta} \right) (V_{11} - V)^2 \right] + \left[0.5 \left(\frac{\beta}{1+\beta} \right) (V_{12} - V)^2 \right]}{\left(\frac{f}{1+\beta} \right) Q_R} = 0.3560$$

Overall efficiency

$$\eta_o = \eta_p \times \eta_{th} = \frac{T/m_a^\circ \times V}{\left(\frac{f}{1+\beta} \right) Q_R} = 0.1166$$

6.4 Turbine-Based Combined-Cycle (TBCC) Engines

6.4.1 Introduction

Long distance airliner flights are troublesome to passengers particularly if it last for more than 6 h. This motivated aerospace industry for working hard in designing and manufacturing airplanes and space planes that will satisfy the greatest human demands for faster and comfortable Earth and space flights. This can be achieved by designing engines that power airplanes/space planes which fly at high speeds (Mach 3.0^+) and high altitudes ($20,000^+$ m). Such propulsion system has to facilitate low subsonic conditions for takeoff/climb flight segments and hypersonic speeds for cruise operation. Such tough requirements can be achieved only through combined-cycle engines (CCE) or sometimes identified as *hybrid engines*. These engines will combine a turbine-based cycle (TBC) (turbojet or turbofan) for low-to-moderate flight speed operation and a ram-based cycle (RBC) (ramjet, scramjet, or dual combustion scram) for high-speed conditions. These are also frequently identified as turbine-based combine cycle (TBCC) engines.

Moreover, such hybrid engines can also be employed in the long-range tactical missiles as well as high-performance unmanned aerial vehicles (UAVs) or unmanned combat aerial vehicles (UCAVs) [39].

Figure 6.28 illustrates such a hybrid engine powering a future super-/hypersonic speed transport.

Figure 6.29a illustrates hybrid engine layout for low-/moderate-speed operation, where turbojet (or turbofan) engine is active, while ramjet/scramjet engine is inoperative. Figure 6.29b illustrates operative ramjet/scramjet engine and inoperative turbojet/turbofan engine during high-speed operation.

Concerning turbine-based cycle, only afterburning category of turbojet or turbofan engines is employed. However, all types of ram, scram, or dual combustion scram are employed as ram-based cycles. These two groups will generate the following six different combinations for the TBCC:

- Turbojet and ramjet (TJRJ)
- Turbojet and scramjet (TJSJ)
- Turbojet and dual combustion scramjet (TJDJ)
- Turbofan and ramjet (TFRJ)
- Turbofan and scramjet (TFSJ)
- Turbofan and dual combustion scramjet (TFDJ)

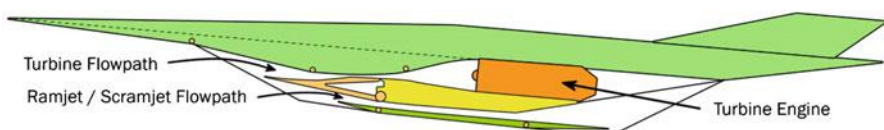


Fig. 6.28 Layout of a hybrid or turbine-based combined-cycle engine (TBCC)

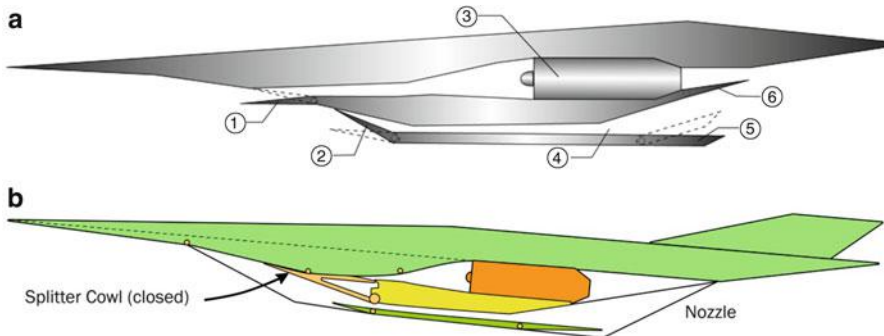


Fig. 6.29 Layout of a turbine-based combined-cycle engine (TBCC). (a) Operative turbojet/turbofan only. (b) Operative ramjet (scramjet) only

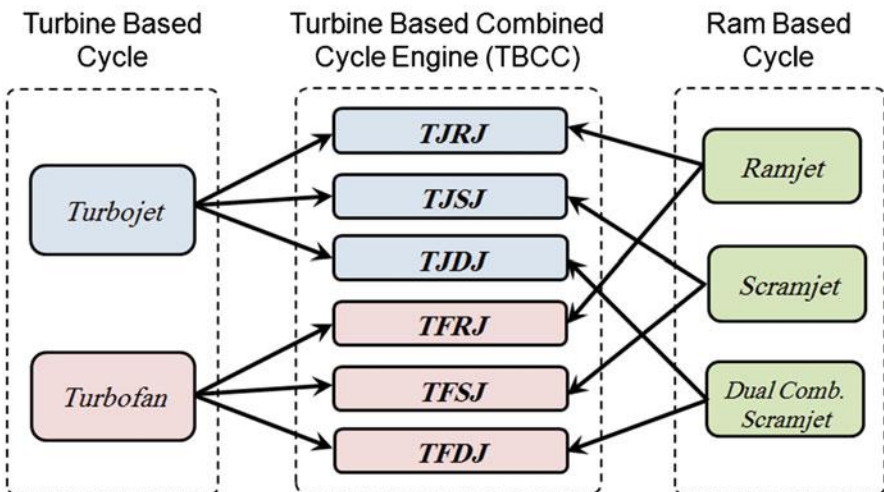


Fig. 6.30 Block diagram of the different configurations of the turbine-based combined cycle [19]

Figure 6.30 shows block diagram of these different combinations of the turbine-based combined cycle [19].

It is worth mentioning here that for an aircraft cruising at Mach 6, a *multistage vehicle* is an alternative for TBCC (or hybrid) engine. A multistage vehicle is composed of two vehicles (or stages), one having turbine engines to enhance takeoff and acceleration to supersonic speeds where the second vehicle (stage) is driven by ramjet or scramjet engines for supersonic/hypersonic flight speeds (Fig. 6.31).

In the following sections, a brief historical review of super-/hypersonic aircrafts followed by mathematical modeling of such complex engine will be given.

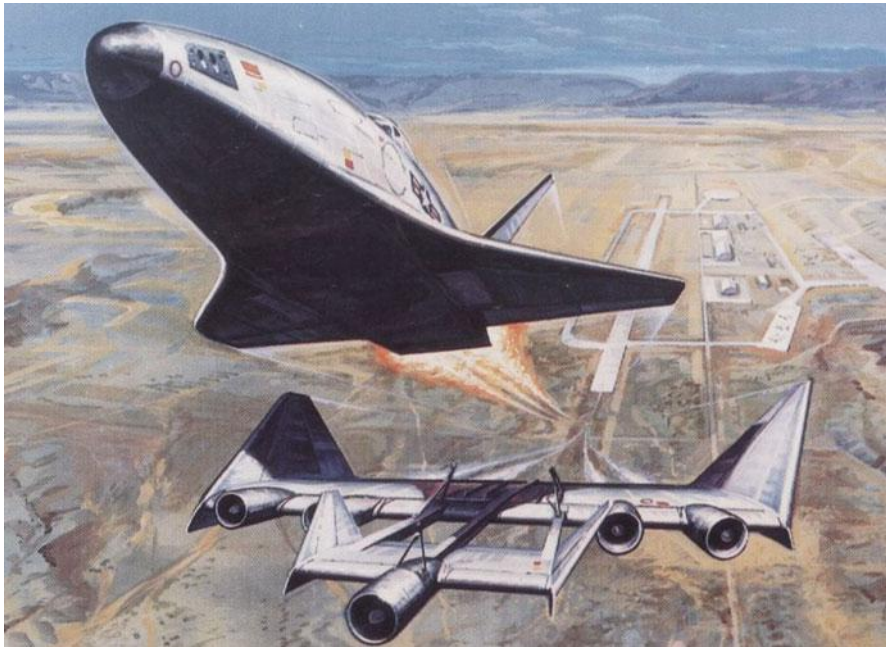


Fig. 6.31 A multistage aircraft concept

6.4.2 Historical Review of Supersonic and Hypersonic Aircrafts

6.4.2.1 Supersonic Aircrafts and Programs

Supersonic aircrafts have been used almost entirely for research and military purposes. Only two airliners, [Concorde](#) and the [Tupolev Tu-144](#), were ever designed for civil use.

Quick highlights will be described as:

On October 14, 1947, the Bell X-1 rocket plane, launched at an altitude of approximately 20,000 ft from the Boeing B-29, became the first airplane to fly faster than the speed of sound [20]. The X-1 reached a speed of 1127 km/h (Mach 1.06) at an altitude of 43,000 ft. However, it was powered by a liquid-fueled [rocket](#).

In 1954, the second generation of Bell X-1 reached a Mach number of 2.44 at an altitude of 90,000 ft.

On December 22, 1964, Lockheed SR-71 Blackbird (Fig. 6.32) entered service. It is a long-range, strategic reconnaissance aircraft which can fly at Mach number of (3+), maximum speed (3530+) km/h at 80,000 ft (24,000 m). It is powered by 2 Pratt & Whitney J58-1, *turboramjet* engines continuous-bleed afterburning turbojet [21]. However, it retired on October 9, 1999.

The Tupolev Tu-144 was the first commercial [supersonic transport](#) aircraft (SST), Fig. 6.33. The design, publicly unveiled in January 1962, was constructed

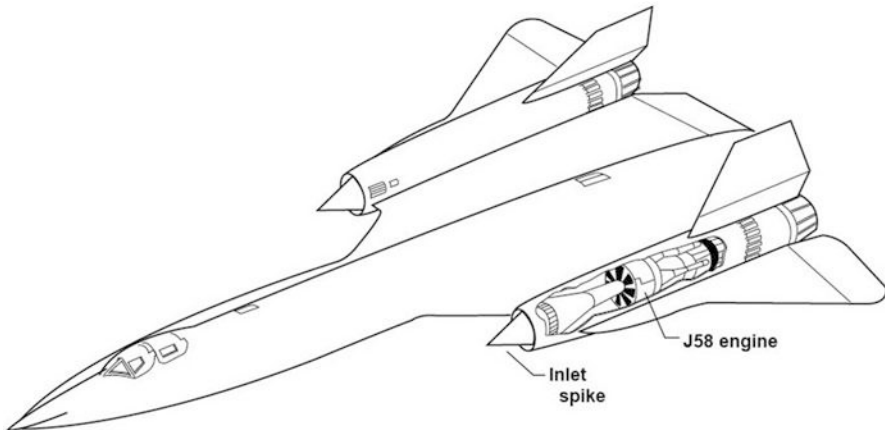


Fig. 6.32 SR-71 aircraft [21]



Fig. 6.33 Tupolev TU-144

in the Soviet Union under the direction of the [Tupolev design bureau](#), headed by [Alexei Tupolev](#). The [prototype](#) first flew on December 31, 1968, near Moscow, two months before the first flight of Concorde. The Tu-144 first went supersonic on June 5, 1969, and, on May 26, 1970, became the first commercial transport to exceed



Fig. 6.34 Concorde supersonic airplane

Mach 2. Tu-144 is powered by $4 \times$ [Kolesov RD-36-51](#) turbojet, 200 kN (44,122 lbf) each. It was withdrawn from service 1985 after only a ten-year line life. However, in 1994, NASA had some developments for TU-144 that led to the first flight of the flying laboratory plane TU-144LL on November 29, 1996. The last time TU-144 was shown was during MAKS 2013 Eleventh International Aviation and Space Salon held from August 27 to September 1, 2013, in Zhukovsky, Moscow region.

Aérospatiale-BAC Concorde was jointly developed and produced by [Aérospatiale](#) and the [British Aircraft Corporation](#) (BAC) (Fig. 6.34). On March 2, 1969, “Concorde” French prototype 001 made its first flight from Toulouse, while on April 9, 1969, “Concorde” British prototype 002 made its first flight from Filton. Concorde entered service in 1976 and continued commercial flights until November 26, 2003. Concorde [powerplant](#) is $4 \times$ [Rolls-Royce/SNECMA Olympus 593](#) Mk 610 afterburning [turbojets](#) having dry thrust 140 kN each while thrust with [afterburner](#) 169 kN each.

Many projects for *SST* were cancelled. Examples are:

(British) [Bristol Type 223](#); (French–American) [Convair BJ-58-9](#), [Boeing 2707–100](#), [Lockheed L-2000](#), [Douglas 2229](#), and [Tupolev Tu-244](#); (Russian–American) [Sukhoi-Gulfstream S-21](#)

Supersonic business jets (SSBJ) are a proposed class of small supersonic aircraft. None has yet flown. Examples are [Aerion SBJ](#), [HyperMach SonicStar](#), [Tupolev Tu-444](#), and [Gulfstream X-54](#). All are still under development.

Examples for *flying strategic bombers* (defined as a heavy bomber that carries a large bomb load over long distances) are [Convair B-58A Hustler](#) (1956), [Tupolev](#)

Tu-22 (1959), **Myasishchev M-50** (1959), **North American XB-70 Valkyrie** (1964), **Tupolev Tu-22M** (1969), **Sukhoi T-4** (1972), and **Rockwell B-1B Lancer** (1986). A next-generation stealthy supersonic strategic bomber is being planned in the USA under the **2037 Bomber** project.

Few examples for *flying supersonic fighters* (sometimes called fast jets) are listed hereafter and arranged by country:

China

Shenyang J-11 (1998), **Shenyang J-15 Flying Shark** (2009), **Shenyang J-16** (2012)

Egypt

Helwan HA-300 (March 7, 1964) and retired May 1969

France

Dassault Mirage 5 (1967), **Dassault Mirage 2000** (1978), **Dassault Rafale** (1986)

Japan

Mitsubishi T-2 (1971), **Mitsubishi F-1** (1975), **Mitsubishi F-2** (1995)

Sweden

Saab 32 Lansen (1952), **Saab 35 Draken** (1955), **Saab JAS 39 Gripen** (1988)

Soviet Union/Russia

Mikoyan MiG-31 (1975), **Mikoyan MiG-35** (2007), **Sukhoi Su-35** (2008)

United States

North American F-100 Super Sabre (1953), **Lockheed Martin F-22 Raptor** (1997),

Lockheed Martin F-35 Lightning II (2006)

It is to be noted that all the above listed aircrafts are powered by either one or more of turbojet or turbofan engines fitted with afterburners.

6.4.2.2 Hypersonic Vehicles

Aircraft or spacecrafts flying at speeds above Mach 5 are often referred to as **hypersonic aircraft**. A very brief review of the work held in the field of hypersonic aviation in different countries is given in [22]. NASA has been working in the design of a lot of hypersonic commercial aircrafts from the 1970s till now. Perhaps one of the most well-known activity concepts is the commercial derivative of the **NASP** project.

Concerning military applications, trends of the 1950s and 1960s indicated that military aircraft had to fly faster and higher to survive, so concepts for high-altitude fighters and bombers cruising at Mach 4 or more were not uncommon. Although the trend soon fizzled and military planners looked to maneuverability and stealth for survival, the military has recently shown renewed interest in hypersonic flight. For example, many have conjectured about the existence of a Mach 5 spy plane, the **Aurora**, that may be a scramjet powered (Fig. 6.35).

The only manned aircraft to fly in the low hypersonic regime was the **X-15** (Fig. 6.36) and the Space Shuttle during reentry. American Robert White flew the X-15 rocket-powered research aircraft at Mach 5.3 thereby becoming the first pilot



Fig. 6.35 Aurora a hypersonic fighter

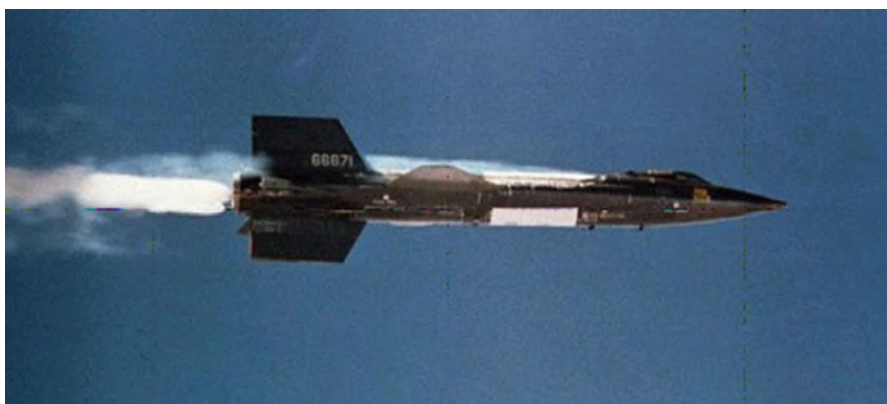


Fig. 6.36 X-15

to reach hypersonic velocities and at a record altitude of 314,750 ft on July 17, 1962. White's mark was later topped by fellow X-15 pilot Pete Knight who flew the craft to a maximum speed of Mach 6.72 in 1967. The record still stands today as the highest velocity ever reached by an aircraft. Recently, an unmanned X-43A used a **scramjet**, to make two hypersonic flights, one at Mach 7, the other at

Mach 10. Because lift and drag depend on the square of the velocity, hypersonic aircraft do not require a large wing area.

6.4.3 Technology Challenges of the Future Flight

The key technology challenges that are derived from the customer requirements and vehicle characteristics are related to economics, environment, or certification [23]:

Environment

Benign effect on climate and atmospheric ozone

Low landing and takeoff noise

Low sonic boom

Economics range, payload, fuel burn, etc.

Low weight and low empty weight fraction

Improved aerodynamic performance

Highly integrated airframe/propulsion systems

Low thrust specific fuel consumption (*TSFC*)

Long life

Certification for commercial operations

Acceptable handling and ride qualities

Passenger and crew safety at high altitudes

Reliability of advanced technologies, including synthetic vision

Technical justification for revising regulations to allow supersonic operations over land

6.4.4 Propulsion System Configurations

6.4.4.1 Introduction

There are two main layouts for the turboramjet (or TBCC) engine, namely:

Wraparound configuration

Over-under configuration

The differences between them are:

The position of the ram with respect to turbojet

The position of the afterburner of the turbojet with respect to the ram

Wraparound turboramjet

The wraparound installation methods are limited for axisymmetric propulsion systems. In such a configuration, the turbojet is mounted inside a ramjet (Fig. 6.37).

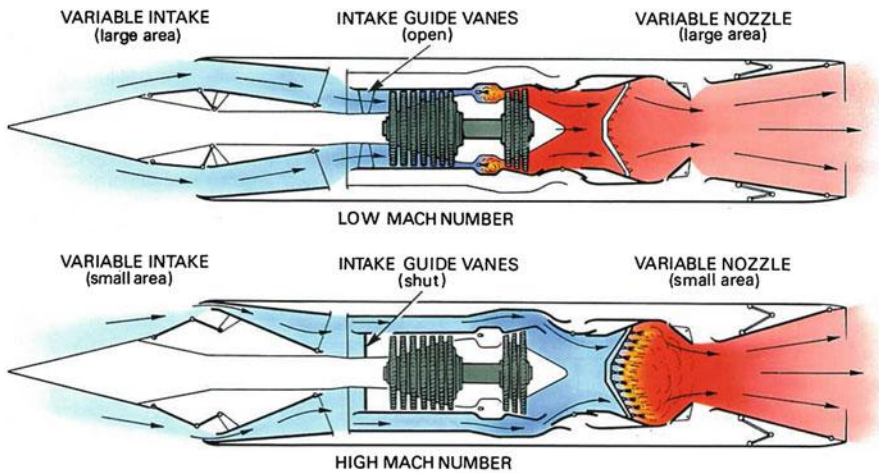


Fig. 6.37 Wraparound turboramjet [26]

Usually both engines share the same intake and nozzle, while the combustion chamber of the ramjet engine may be located in the afterburner of the turbojet engine or separated from it. The flow is divided between the two engines by mean of a number of bypass flaps or movable inlet guide vanes—located just downstream of the diffuser—that control the air mass fraction passing through each engine. The wraparound configuration with ram burner in the afterburner of turbojet was used in the Pratt & Whitney J58 engine that powered the Blackbird SR-71 that flows with speed of Mach 3+ (Fig. 6.32). Figure 6.37 shows wraparound TBCC installed on SR-71 in its two configurations for low and high Mach number operation [26]. During low-speed flight, these controllable flaps close the bypass duct and force air directly into the compressor section of the turbojet. During high-speed flight, the flaps block the flow into the turbojet, and the engine operates like a ramjet using the aft combustion chamber to produce thrust.

The Nord 1500 Griffon II, a French aircraft powered by a SNECMA ATAR 101 E-3 dry turbojet and a wraparound ramjet having a separate combustion chamber, was the first aircraft powered by combined-cycle engine in the 1950s (Fig. 6.38).

Two installation configurations are seen for the wraparound turbo ramjet engines, namely:

Wing like SR-71 [25–27] (Fig. 6.37)

Fuselage like Griffon II (Fig. 6.38)

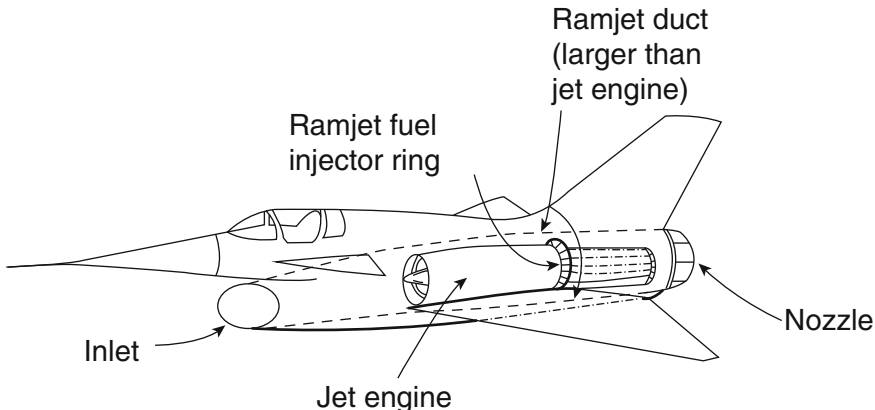


Fig. 6.38 Cutaway in the Nord 1500 Griffon II powered by wraparound TBCC

6.4.4.2 Over–Under Turboramjet

In over–under configuration, the engines are installed one over the other, while the vehicle body serves as part of the intake and the nozzle. In this configuration, the combustion chambers are totally separated. However, two cases are encountered for intakes and nozzles, namely:

- (A) Separate intakes and nozzles (Fig. 6.39)
- (B) Shared intake and nozzle (Fig. 6.40)

The ram-based cycle has a rectangle cross section. The intake(s) and nozzle(s) are rectangle, while they may be shared between the engines. In shared intake and nozzle, the system should contain flaps in the intake to divide the incoming airflow between the two engines and other flaps in nozzle to control the exit area of each engine.

In the late 1980s, the NASA Lewis Research Center discussed analytically and experimentally the performance of over–under TBCC configuration with separated intakes and nozzles and the interaction between the two intakes. Data from this study was presented in [28].

The NASA Lewis Research Center in the mid-1990s extended its studies for over–under TBCC configuration with shared intake and nozzle. Non-afterburning turbojet engines are integrated with a single-throat ramjet. The result is a simple, lightweight system that is operable from takeoff to Mach number 6. Flow in intake, spillage drag, system performance, and modes of operation were discussed in a series of publications ([29] and [30]).

Concerning installation of over–under layouts, the following types are seen:

- Fuselage installation (Fig. 6.41)
- Wing installation (Fig. 6.42)
- Tail installation (Fig. 6.43)

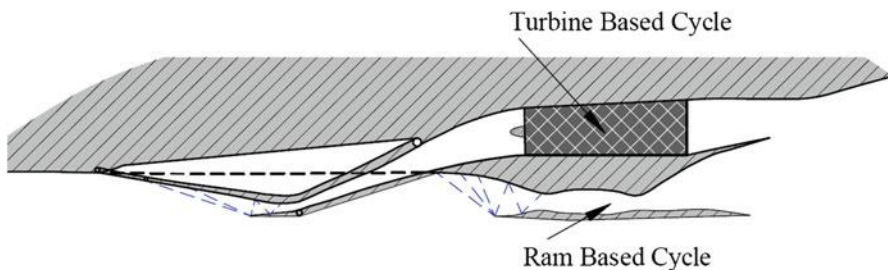


Fig. 6.39 Over-under TBCC configuration with separate intake and nozzle

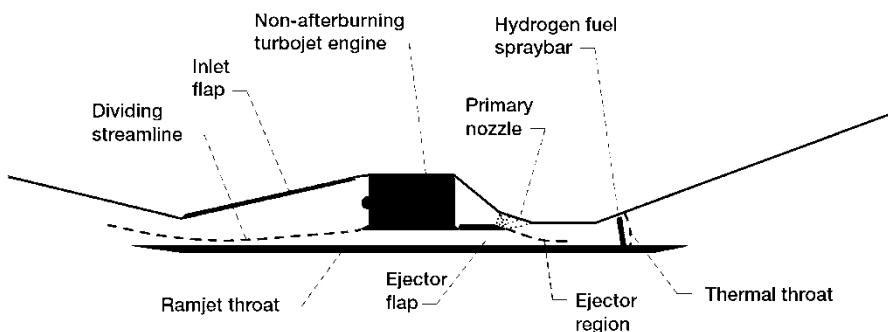


Fig. 6.40 Over-under TBCC configuration with shared intake and nozzle

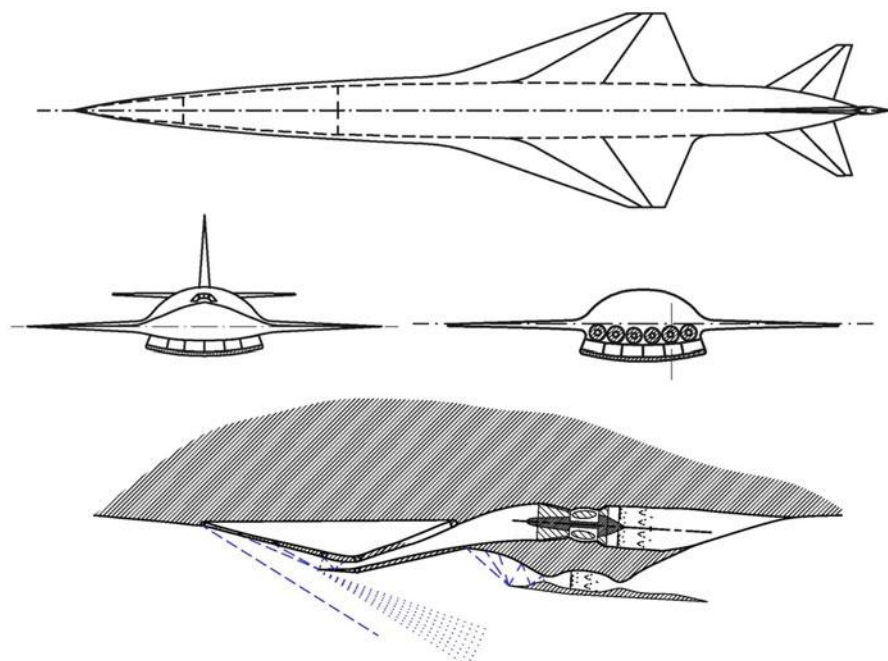


Fig. 6.41 Engine installed to fuselage HYCAT-1 and HYCAT-1A [34]

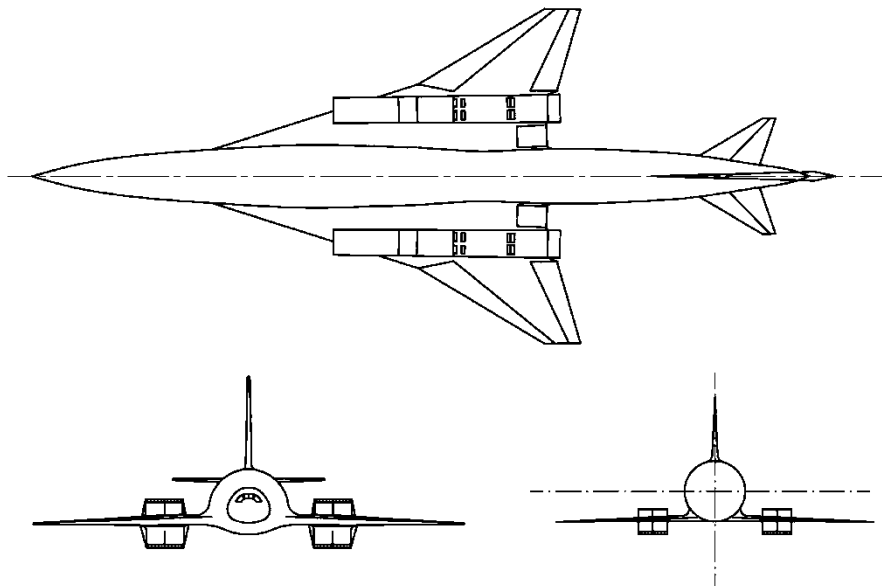


Fig. 6.42 Engine installed to the wing; HYCAT-4 configuration

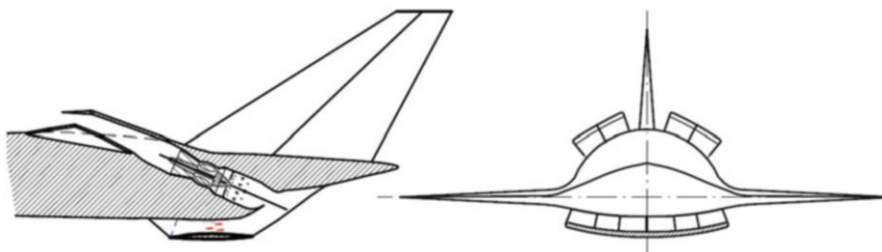


Fig. 6.43 Engine installed to the tail; HYCAT-2 [34]

6.4.5 *Performance of TBCC (or Hybrid Engine)*

As previously described, TBCC (or CCE) is composed of different engines performing different cycles, and each has strong and poor operation range [24] as illustrated in Fig. 6.44. Designer must then specifies which is which to be employed in each flight range and whether this engine will operate alone or in a combined mode with another engine.

Turbine-based engine (turbojet or turbofan) is used during takeoff, climb, as well as low supersonic Mach numbers. However, engine thrust will start to decrease at a certain Mach number depending on the overall pressure ratio of the engine and the bypass ratio for turbofans. In the same time ramjet generates thrust up to Mach numbers of 5–6 but generates zero or small thrust at takeoff or low subsonic speeds.

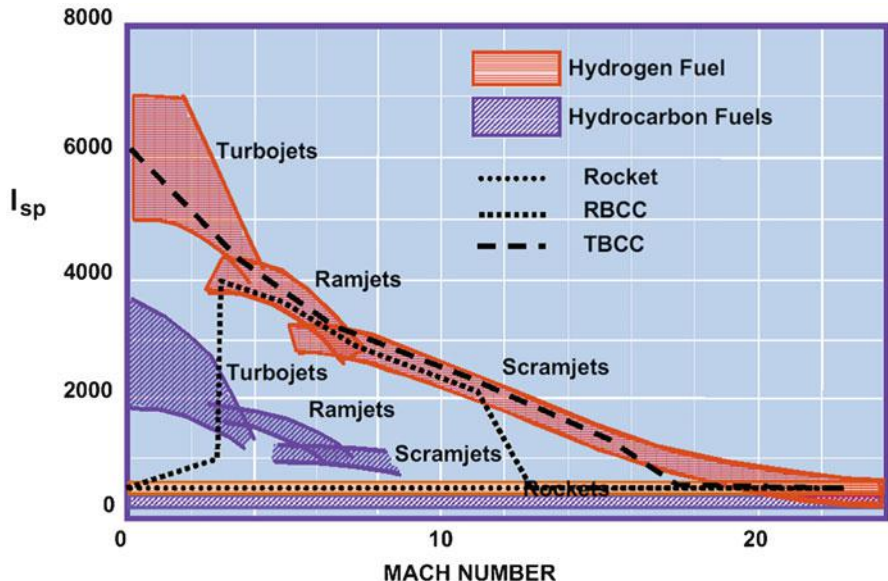


Fig. 6.44 Strong regimes for different propulsion cycles [25]

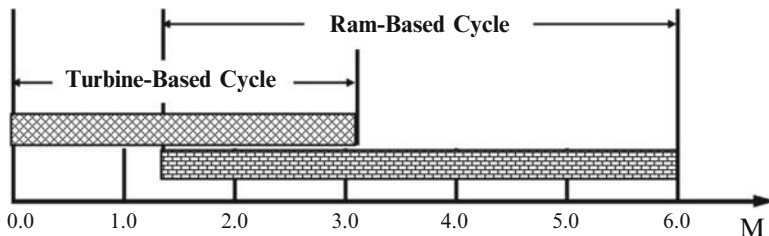


Fig. 6.45 The variation in TBCC with Mach number

As a result, designer set the turbojet/turbofan functioning at takeoff and operating alone up to say 1.5 Mach number. Next, turbojet (or turbofan) engine operates in conjunction with ramjet up to say a 3.0 Mach number. Finally, turbojet (or turbofan) engine is switched off leaving ramjet operating alone up to a Mach number of 6.0. Figure 6.45 shows cycle variation with Mach number for a Mach 6 civil airplane design [31].

Moreover, scramjet keeps generating thrust theoretically up to Mach number of 20. Thus, RBC operates in the scramjet mode for a Mach number range of 6.0–15.0. For space operation, this engine may have a booster rocket to help the engine in the transition region or drive the vehicle alone if it moves in space (the aerospace plane).

6.4.6 Cycle Analysis of Turboramjet (or TBCC) Engine

The analysis for both cases of wraparound and over-under turboramjet is given hereafter.

6.4.6.1 Wraparound Turboramjet

Designation of different states of engine is identified in Fig. 6.46. During low-speed flight, controllable flaps close a bypass duct and force air directly into the compressor section of the turbojet. During high-speed flight, the flaps block the flow into the turbojet, and the engine operates like a ramjet using the aft combustion chamber to produce thrust. In a combined mode, air may be split between both engines. Afterburner of turbojet acts as the combustion chamber of ramjet.

The engine cycle *has* two modes of operation, either working as a simple single-spool turbojet or as a ramjet. A plot for the cycle on the temperature, entropy plane, is illustrated in Fig. 6.47.

6.4.6.1.1 Operation as a Turbojet Engine

In the turbojet mode, a chain description of the different processes through the different modules is described in Table 6.5.

Different processes have been previously described in details. Input data for turbojet cycle will be: ambient pressure and temperature, flight Mach number, pressure ratio of compressor, turbine inlet temperature, maximum temperature in afterburner, type of nozzle, and lowest heating value for fuel used. Moreover, efficiencies of different modules (intake, compressor(s), combustion chamber,

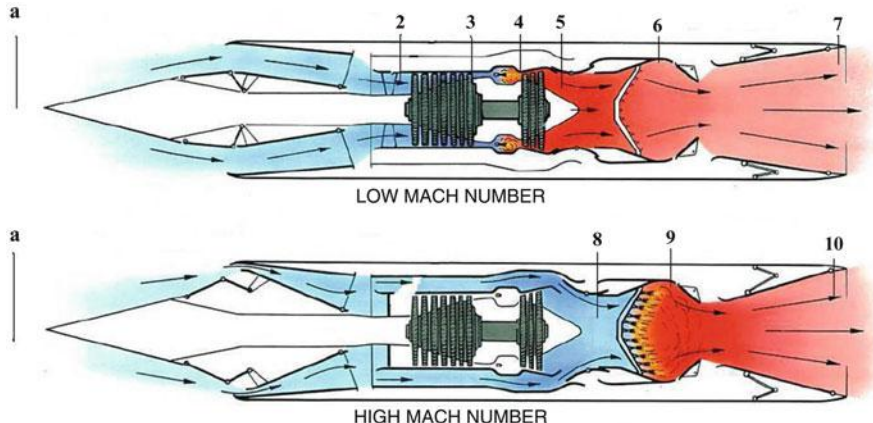


Fig. 6.46 Wraparound turboramjet

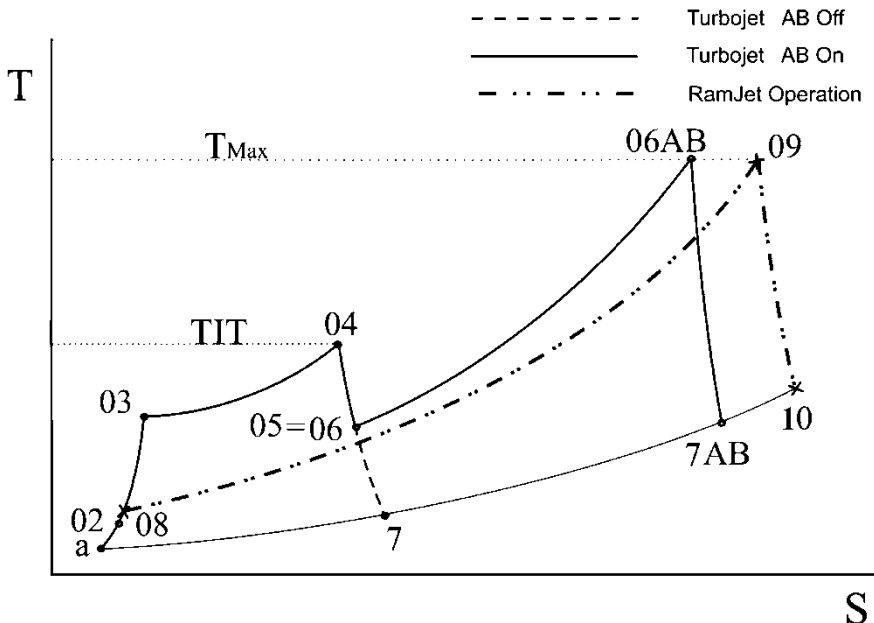


Fig. 6.47 T-s diagram of the wwraparound turboramjet engine

Table 6.5 Modules of afterburning turbojet engine and corresponding processes

Part	States	Processes
Intake	a-2	Compression process with isentropic efficiency η_d
Compressor	2-3	Compression process with isentropic efficiency η_c
Combustion chamber	3-4	Heat addition at constant pressure process, with pressure drop $\Delta P_{c.c.}$ and burner efficiency η_b
Turbine	4-5	Expansion process with isentropic efficiency η_t
Afterburner	5-6	Heat addition at constant pressure process with pressure drop ΔP_{AB} and afterburner efficiency η_{ab}
Nozzle	6-7	Expansion process with isentropic efficiency η_N

turbine(s), afterburner and nozzle, mechanical efficiency) together with pressure drop in intake, combustion chamber, and afterburner. Calculations for temperature, pressure for different states, flight and exhaust speeds, as well as fuel burnt in combustion chamber and afterburner are given by Eqs. (6.1), (6.2), (6.3a), (6.3b), (6.4), (6.5), (6.6), (6.7a), (6.7b), (6.8), (6.9a), (6.9b), (6.9c), (6.9d), (6.10), (6.11a), (6.11b), (6.12), (6.13), (6.14), (6.15), (6.16), (6.17a), (6.17b), (6.18), (6.19a), (6.19b), and (6.20).

Single-spool turbojet engine is discussed here. However, the same procedure can be followed for double-spool turbojet engine.

Cycle performance parameters are calculated as described below:
The specific thrust is:

$$\left(\frac{T}{\dot{m}_a}\right)_{T,J} = (1 + f + f_{AB})V_7 - V \quad (6.72)$$

The thrust specific fuel consumption (*TSFC*):

$$(TSFC)_{T,J} = \frac{(f + f_{AB})}{T/\dot{m}_a} \quad (6.73)$$

The engine propulsive, thermal, and overall efficiencies are:

$$\eta_p = \frac{\frac{T}{\dot{m}_a}V}{\frac{T}{\dot{m}_a}V + \frac{(V_7-V)^2}{2}(1+f+f_{AB})} \quad (6.74)$$

$$\eta_{th} = \frac{\frac{T}{\dot{m}_a}V + \frac{(V_7-V)^2}{2}(1+f+f_{AB})}{Q_{HV}(f+f_{AB})} \quad (6.75)$$

$$\eta_o = \eta_p \times \eta_{th} \quad (6.76)$$

6.4.6.1.2 Operation as a Ramjet Engine

In the ramjet mode, the flow is passing through the processes and states described in Table 6.6.

Different processes have been previously described in details. Input data for ramjet cycle will be: ambient pressure and temperature, flight Mach number, maximum temperature in combustion chamber, type of nozzle, and lowest heating value for fuel used. Moreover, efficiencies of different modules (intake, combustion chamber, and nozzle) together with pressure drop in intake and combustion chamber. Calculations for temperature, pressure for different states, flight and exhaust speeds, as well as fuel burnt in combustion chamber are given by Eqs. 5.19, 5.20, 5.21, 5.22, 5.23, 5.24, 5.25, and 5.26.

Ram cycle performance parameters will be calculated in the same way as in Chap. 5 and given here for the present states.

The thrust per unit air mass flow $\frac{T}{\dot{m}_a}$:

Table 6.6 Different modules of ramjet engine and the corresponding processes

Part	States	Processes
Intake	a–8	Compression process with total pressure ratio r_d
Combustion chamber	8–9	Heat addition at constant pressure with pressure drop $\Delta P_{c.c.}$
Nozzle	9–10	Expansion with isentropic efficiency (η_N).

$$\left(\frac{T}{\dot{m}_a}\right)_{R,J} = (1+f_R)V_{10} - V \quad (6.77)$$

The thrust specific fuel consumption (*TSFC*):

$$(TSFC)_{R,J} = \frac{f_R}{\left(\frac{T}{\dot{m}_a}\right)_{R,J}} \quad (6.78)$$

The engine efficiencies propulsive, thermal, and overall efficiency:

$$\eta_p = \frac{\left(\frac{T}{\dot{m}_a}\right)_{R,J} V}{\left(\frac{T}{\dot{m}_a}\right)_{R,J} V + \frac{(V_{10}-V)^2}{2}(1+f_R)} \quad (6.79)$$

$$\eta_{th} = \frac{\left(\frac{T}{\dot{m}_a}\right)_{R,J} V + \frac{(V_{10}-V)^2}{2}(1+f_R)}{Q_{HV} f_R} \quad (6.80)$$

$$\eta_o = \eta_p \times \eta_{th} \quad (6.81)$$

6.4.6.1.3 Operation as a CCE or Dual Mode

Both turbojet and ramjet are operating simultaneously. The total thrust will be:

$$T = (T)_{T,J} + (T)_{R,J} \quad (6.82)$$

$$T = (\dot{m}_a)_{T,J}[(1+f+f_{AB})V_7 - V] + (\dot{m}_a)_{R,J}[(1+f_R)V_{10} - V] \quad (6.83a)$$

$$T = (\dot{m}_a)_{T,J}(1+f+f_{AB})V_7 + (\dot{m}_a)_{R,J}(1+f_R)V_{10} - (\dot{m}_a)_{TOTAL}V \quad (6.83b)$$

The specific thrust is:

$$\frac{T}{\dot{m}_a} = \frac{T_{total}}{(\dot{m}_a)_{total}} = \frac{(T)_{T,J} + (T)_{R,J}}{(\dot{m}_a)_{T,J} + (\dot{m}_a)_{R,J}} \quad (6.84)$$

The total fuel mass flow rate is:

$$\dot{m}_f = (\dot{m}_a)_{T,J}(f+f_{AB}) + (\dot{m}_a)_{R,J} \times f_R \quad (6.85)$$

The specific thrust fuel consumption is:

$$\frac{(\dot{m}_f)_{Total}}{(T)_{Total}} = \frac{(\dot{m}_f)_{T,J} + (\dot{m}_f)_{R,J}}{(T)_{T,J} + (T)_{R,J}} \quad (6.86)$$

6.4.6.2 Over–Under Turboramjet

For the over–under configuration of turboramjet engine, the engine height is large compared to the wraparound configuration. The reason is clear as the height in this case is the sum of the heights of turbojet and ramjet engines. Usually a part of the engine is to be buried inside the fuselage or inside the wing. Since the engine will operate at high Mach number, it needs a long intake. In the fuselage installation method, the vehicle underbody is completely integrated with the propulsion system as the upstream lower surface serves as an external compression system intake and the downstream surface as an external expansion nozzle (Fig. 6.50).

Three possible configurations for intake may be seen for different flight regimes (Fig. 6.49). In the first case at takeoff and low subsonic flight, the turbojet engine operates alone where a movable inlet ramp is deployed to allow for the maximum airflow rate into its intake and negligible or zero airflow rate into the ramjet engine (Fig. 6.49a). In the second case of higher Mach number, the engine operates at a dual mode where both turbojet and ramjet engines are operative for few seconds until Mach number reaches 2.5 or 3.0. In this case, moveable surfaces allow airflow rates into both engines (Fig. 6.49b). Finally, in the third case of hypersonic speed, the turbojet engine is shut down and only ramjet becomes operative (Fig. 6.49c). An example for such layout is found in the four over–under air-breathing turboramjet engines powering the Mach 5 WaveRider [32].

The complexity of both aerodynamic and mechanical design of two variable throat nozzles and necessary flaps led to another design including only one nozzle [33]. The suggested nozzle uses a single-expansion ramp nozzle (SERN) instead of a conventional, two-dimensional, convergent–divergent nozzle. Figures 6.50 and 6.51 illustrate a layout and T-s diagram of the over–under configuration of the turboramjet engine.

An over–under configuration has also three modes of operation, namely, a turbojet, a ramjet, or a dual mode. Dual mode represents the combined or transition mode in which both of the turbojet and ramjet are operating simultaneously.

6.4.6.2.1 Turbojet Mode

In this mode the engine is working as a simple turbojet engine and develops all the thrust needed by the aircraft. The states and governing equations are the same as the turbojet in the wraparound configuration.

6.4.6.2.2 Dual Mode

Both of the turbojet and ramjet are operating simultaneously. Turbojet starts declining and its developed thrust will be intentionally decreased by reducing the inlet air mass flow rate via its variable geometrical inlet. The ramjet starts working by adding fuel and starting ignition into its combustion chamber. The thrust generated in the ramjet is increased by increasing also the air mass flow rate through its variable area inlet. The generated thrust force will be then the sum of both thrusts of turbojet and ramjet engines. Same equations for wraparound case are to be applied here.

6.4.6.2.3 Ramjet Mode

In this mode, turbojet stops working and its intake is completely closed. All the air mass flow passes through the ramjet intake. With a Mach number increase, the forebody acts as a part of the intake with the foremost oblique shock wave located close to the aircraft nose, as shown in Fig. 6.48. Also same equations for wrap-around case will be employed here.

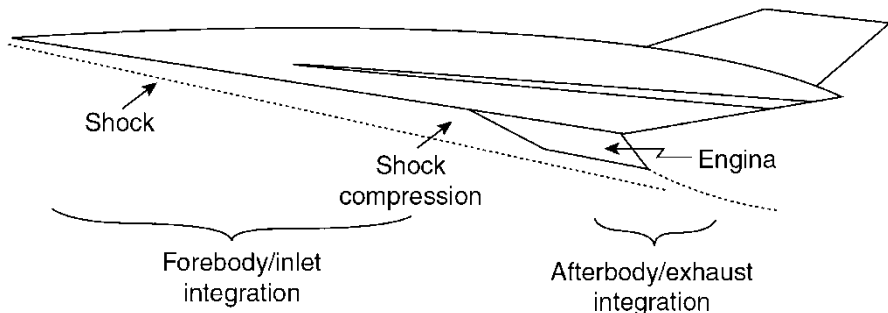


Fig. 6.48 Propulsion system integration with the vehicle body

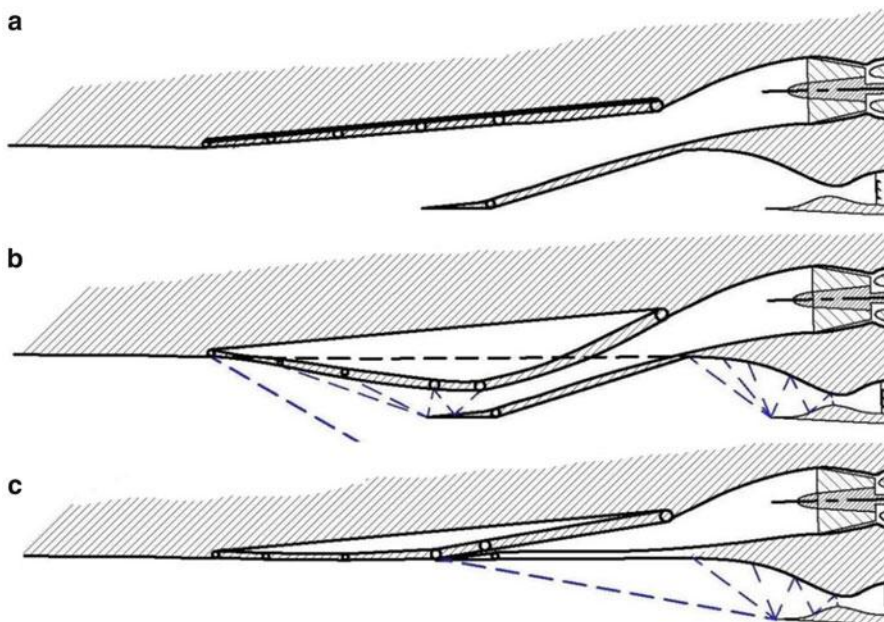


Fig. 6.49 Intake layout with different positions of intake flap at (a) subsonic, (b) low supersonic, and (c) hypersonic speeds [32]

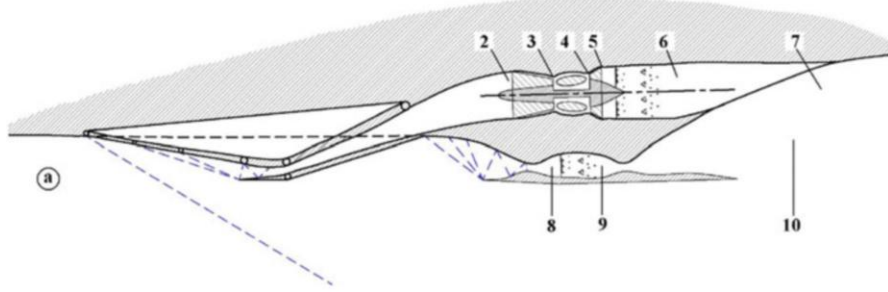


Fig. 6.50 Over–under layout of turboramjet engine

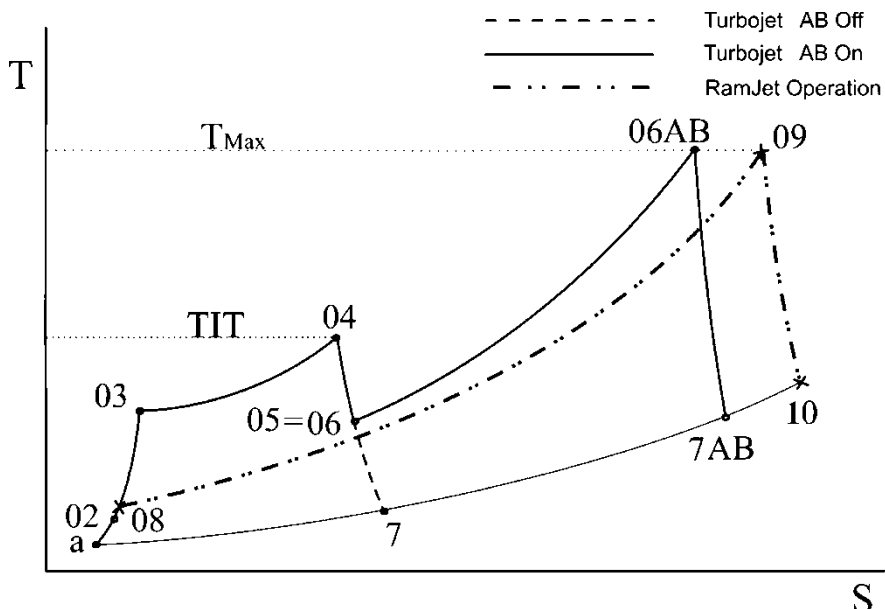


Fig. 6.51 T-s diagram of the over–under layout of turboramjet engine

6.4.7 General Analysis for a Turboramjet Engine

The turbine engine for a turboramjet may be either a turbojet or a of turbofan engine. In the entire previous sections, only turbojet engine was discussed. However, if turbofan engine replaces the turbojet engine, then additional parameters have to be specified, namely, fan pressure ratio and its isentropic efficiency besides bypass ratio together with the other parameters listed in Sect. 6.4.6.1.1. Moreover,

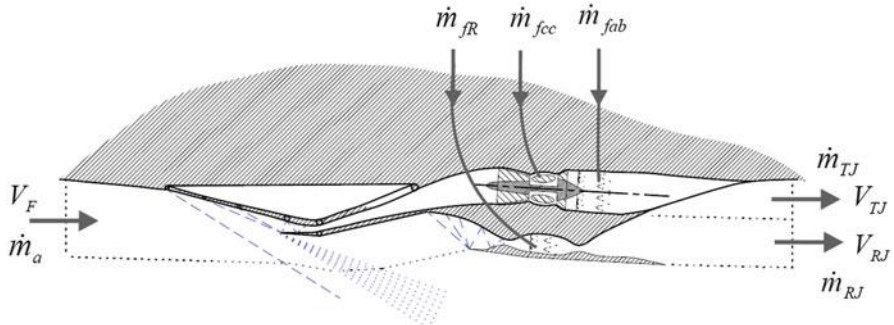


Fig. 6.52 Turboramjet engine and appropriate control volume

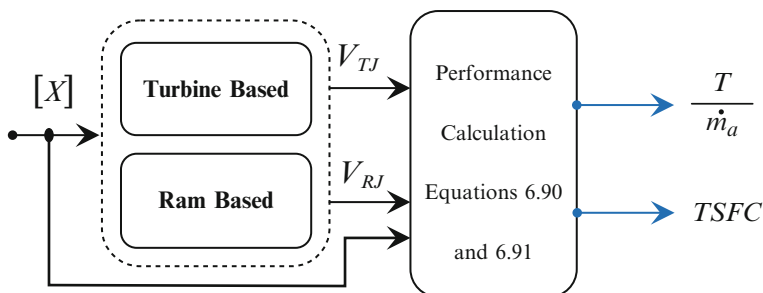


Fig. 6.53 Block diagram for CCE

for high supersonic speed, the ram-based engine will be a scramjet rather than a ramjet engine. Figure 6.52 shows the control volume for the general turbo ramjet engine. Figure 6.53 shows a block diagram of the complete system.

The air mass flow through the turbine-based cycle is \dot{m}_{aTJ} , while the air mass flow through the ram-based cycle is \dot{m}_{aRJ} . From cycle analysis the fuel mass flow rates will be calculated. Apply the mass conservation law (continuity equations for both cycle to reach Eqs. (6.87) and (6.88). Momentum equation defines the thrust force for a full expansion of gases in nozzle(s), Eq. (6.89). The specific thrust and $TSFC$ can be obtained through Eqs. (6.90) and (6.91):

$$\dot{m}_{TJ} = \frac{\dot{m}_a}{\dot{m}_a} \dot{m}_a + \dot{m}_{fcc} + \dot{m}_{fab} \quad (6.87)$$

$$\dot{m}_{RJ} = \frac{\dot{m}_a}{\dot{m}_a} \dot{m}_a + \dot{m}_{fR} \quad (6.88)$$

$$T = \dot{m}_{aTJ} V_{TJ} + \dot{m}_{aRJ} V_{RJ} - \dot{m}_a V_F \quad (6.89)$$

$$\frac{T}{\dot{m}_a} = \left(\frac{\dot{m}_{aTJ}}{\dot{m}_a} + \frac{\dot{m}_{fcc}}{\dot{m}_a} + \frac{\dot{m}_{fab}}{\dot{m}_a} \right) V_{TJ} + \left(\frac{\dot{m}_{aRJ}}{\dot{m}_a} + \frac{\dot{m}_{fR}}{\dot{m}_a} \right) V_{RJ} - V_F \quad (6.90)$$

$$TSFC = \frac{\dot{m}_{fcc}/\dot{m}_a + \dot{m}_{fab}/\dot{m}_a + \dot{m}_{fR}/\dot{m}_a}{T/\dot{m}_a} \quad (6.91)$$

Example 6.12 A conceptual design of a turboramjet engine to power a future supersonic transport; Fig. (6.54), provided the following data:

Flight altitude	20,000 m
Cruise Mach number	3.0
Engines	Two turboramjet engines in over-under installation with separate intakes and nozzles
Hydrogen fuel with heating value	119 MJ/kg

Turbojet engine

Single-spool afterburning

Intake efficiency	η_I	92 %
Compressor pressure ratio	π_C	7
Compressor efficiency	η_C	92 %
Burner efficiency	η_{CC}	99 %
CC pressure ratio	π_{CC}	0.975
Turbine inlet temperature	TIT = 1500 K	
Turbine efficiency	η_T	92 %
Mechanical efficiency	η_m	99 %
Afterburner maximum temperature	= 1750 K	
Afterburner efficiency	η_{Ab}	99 %
Afterburner pressure ratio	π_{Ab}	0.98
Nozzle efficiency	η_N	99 %

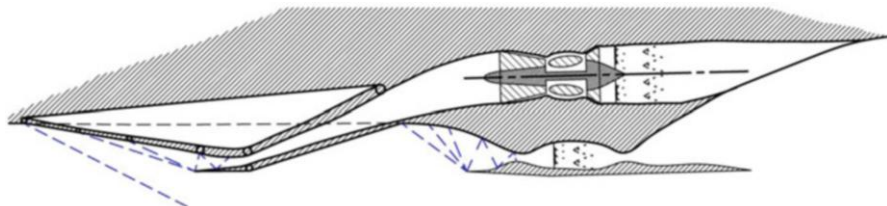


Fig. 6.54 Turboramjet engine

Ramjet engine

Ramjet intake efficiency	η_{RI}	95 %
Ram burner maximum temperature	=	1900 K
Ram burner efficiency	η_{RB}	99 %
Ram burner pressure ratio	π_{RB}	0.98
Ramjet nozzle efficiency	η_{RN}	99 %

The ratio between air mass flow rate in ramjet and turbojet engines is $\dot{m}_{aRI}/\dot{m}_{aTJ} = \alpha_R = 2$.

1. For the combined engine (TBCC), calculate:

- (a) Specific thrust
- (b) Thrust specific fuel consumption
- (c) Thermal efficiency
- (d) Propulsive efficiency
- (e) Overall efficiency

2. Compare the above results with the cases:

- (a) The turbojet engine is operating alone.
- (b) The ramjet engine is operating alone.

3. If the total thrust generated is 150 kN, calculate:

- (a) Air mass flow rate through each engine
- (b) Thrust generated by each engine

Solution

Ambient conditions at 20,000 m altitude are:

$$T_a = 216.66 \text{ k} \quad P_a = 5,475.5 \text{ Pa}$$

Then at flight Mach number $M_1 = 3$.

Turbojet

Layout of afterburning turbojet and the corresponding T-s diagram are illustrated by Fig. (6.55).

(a) Intake 1–2

$$T_{02} = T_{01} = T_a \left(1 + \frac{\gamma_c - 1}{2} M_1^2 \right) = 216.66 \left(1 + \frac{0.4}{2} \times 9 \right) = 606.65 \text{ K}$$

$$P_{02} = P_{01}$$

$$= P_a \left(1 + \eta_I \frac{\gamma_c - 1}{2} M_1^2 \right)^{\frac{\gamma_c}{\gamma_c - 1}} = 5475.5 \left(1 + 0.92 \times \frac{0.4}{2} \times 9 \right)^{\frac{1.4}{0.4}} = 167,190 \text{ Pa}$$

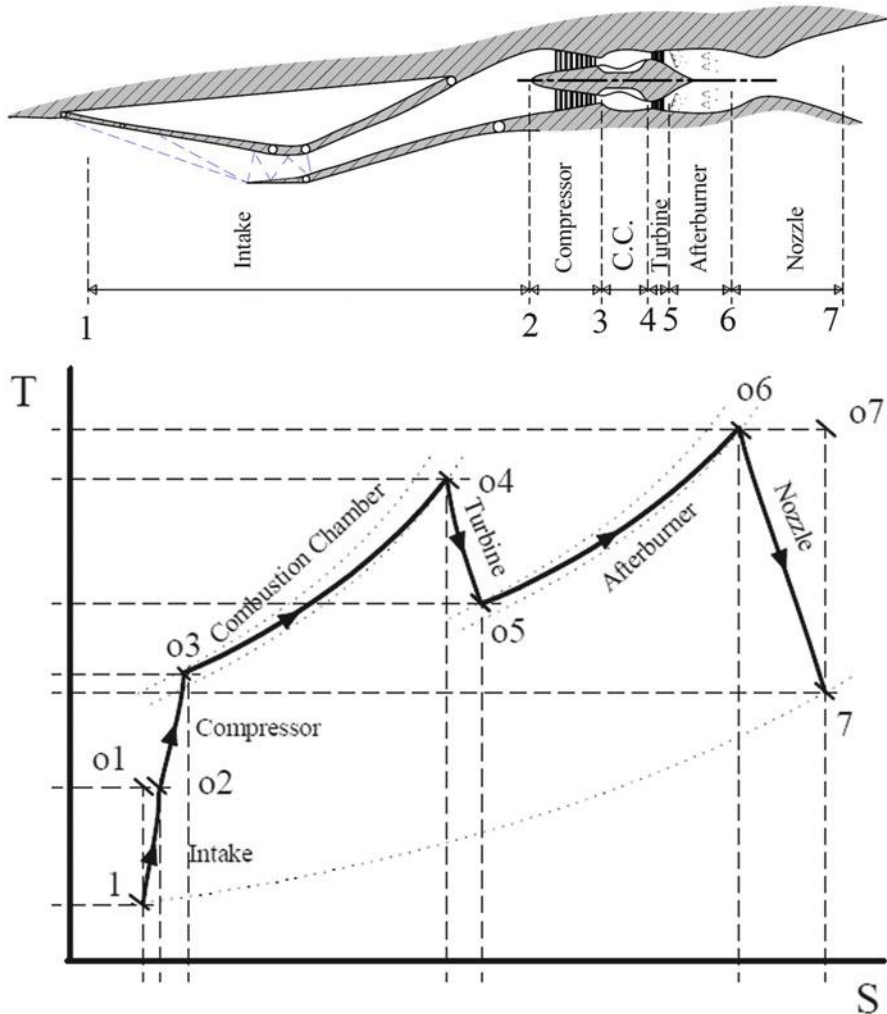


Fig. 6.55 Stations and T-s diagram of turboramjet engine

(b) *Compressor 2–3*

$$P_{03} = P_{02}\pi_C = 1170400 \text{ Pa}$$

$$T_{03} = T_{02} \left[1 + \frac{1}{\eta_C} \left(\pi_C^{\frac{\gamma_c - 1}{r_c}} - 1 \right) \right] = 606.65 \left[1 + \frac{1}{0.92} \left(7^{0.4} - 1 \right) \right] = 1097 \text{ K}$$

(c) *Combustion chamber 3–4*

$$T_{04} = T_{IT} = 1500 \text{ K}$$

$$P_{04} = P_{03}\pi_{CC} = 1141,100 \text{ Pa}$$

$$f = \frac{C_{Ph}T_{04} - C_{Pc}T_{03}}{\eta_{cc}Q_{HV} - C_{Ph}T_{04}} = \frac{1148 \times 1500 - 1005 \times 1097}{0.99 \times 119 \times 10^6 - 1148 \times 1500} = 5.337 \times 10^{-3}$$

(d) *Turbine 4–5*

$$T_{o5} = T_{o4} - \frac{C_{Pc}(T_{o3} - T_{o2})}{\eta_m C_{Ph}(1+f)} = 1500 - \frac{1005(1097 - 606.65)}{0.99 \times 1148(1.005337)} = 1067.85 \text{ K}$$

$$P_{05} = P_{04} \left[1 - \frac{1}{\eta_t} \left(1 - \frac{T_{05}}{T_{04}} \right) \right]^{\frac{\gamma_h}{\gamma_h - 1}} = 1,141,100 \left[1 - \frac{1}{0.92} \left(1 - \frac{1067.85}{1500} \right) \right]^{\frac{4/3}{1/3}} = 253,960 \text{ Pa}$$

(e) *Afterburner 5–6*

$$T_{06} = T_{\text{Max } Tj} = 1750 \text{ K}$$

$$P_{06} = P_{05}\pi_{Ab} = 248,880 \text{ Pa}$$

$$\begin{aligned} f_{Ab} &= \frac{C_{Ph}(T_{06} - T_{05})(1+f)}{\eta_{Ab}Q_{HV} - C_{Ph}T_{06}(1+f)} = \frac{1148(1750 - 1067.85) \times 1.00534}{0.98 \times 10^6 - 1148 \times 1750 \times 1.00534} \\ &= 6.87 \times 10^{-3} \end{aligned}$$

(f) *Nozzle 6–7*

$$P_7 = P_1 = 5475.5 \text{ Pa}$$

$$\begin{aligned} T_7 &= T_{06} \left[1 - \eta_N \left(1 - \left(\frac{P_7}{P_{06}} \right)^{\frac{\gamma_h - 1}{\gamma_h}} \right) \right] = 1750 \left[1 - 0.99 \left(1 - \left(\frac{5475.5}{248,880} \right)^{\frac{1/3}{4/3}} \right) \right] \\ &= 684.74 \text{ K} \end{aligned}$$

$$V_{TJ} = V_7 = \sqrt{2C_{Ph}(T_{06} - T_7)} = \sqrt{2 \times 1148(1750 - 684.74)} = 1563.9 \text{ m/s}$$

Ramjet

Figure (6.56) illustrates the states of a ramjet engine while its T-s diagram is displayed in Fig. (6.57).

(a) *Intake 1r–2r*

$$T_{02r} = T_{01r} = T_a \left(1 + \frac{\gamma_c - 1}{2} M_1^2 \right) = 216.66 \left(1 + \frac{0.4}{2} \times 9 \right) = 606.65 \text{ K}$$

$$\begin{aligned} P_{02r} &= P_{01r} = P_a \left(1 + \eta_{RI} \frac{\gamma_c - 1}{2} M_1^2 \right)^{\frac{\gamma_c}{\gamma_c - 1}} = 5475.5 \left(1 + 0.95 \times \frac{0.4}{2} \times 9 \right)^{\frac{1.4}{0.4}} \\ &= 179,400 \text{ Pa} \end{aligned}$$

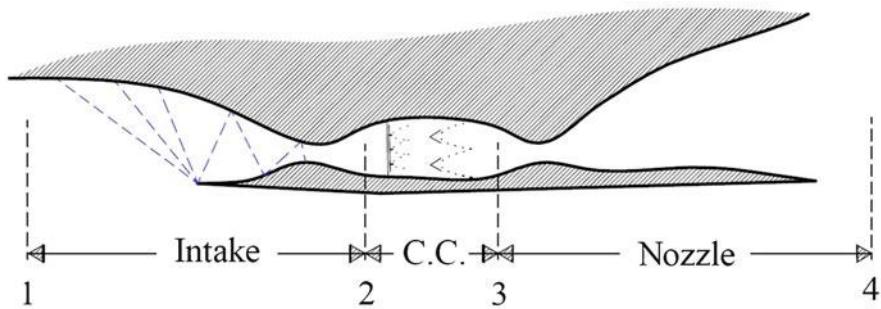


Fig. 6.56 Ramjet operation

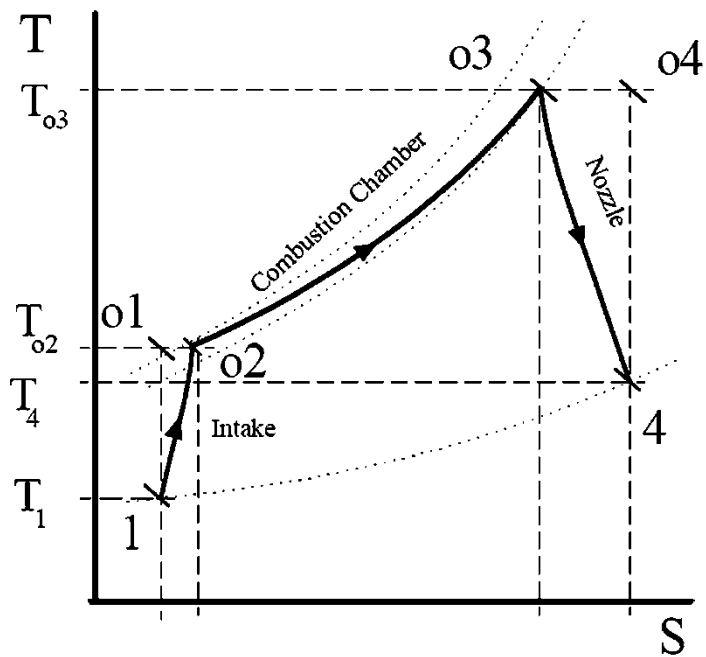


Fig. 6.57 T-s diagram of ramjet operation

(b) *Combustion chamber 2r-3r*

$$T_{03r} = T_{\text{Max } Rj} = 1900 \text{ K}$$

$$P_{03r} = P_{02r}\pi_{Rb} = 175,810 \text{ Pa}$$

$$f_{Rb} = \frac{C_{Ph}T_{03r} - C_{Pc}T_{02r}}{\eta_{Rb}Q_{HV} - C_{Ph}T_{03r}}$$

$$f_{Rb} = \frac{1148*1900 - 1005*606.65}{0.99*119 \times 10^6 - 1148*1900}$$

$$f_{Rb} = 13.59 \times 10^{-3}$$

(c) Nozzle 3r–4r

$$P_{4r} = P_{1r} = 5,475.5 \text{ Pa}$$

$$T_{4r} = T_{03r} \left[1 - \eta_{RN} \left(1 - \left(\frac{P_{4r}}{P_{03r}} \right)^{\frac{\gamma_h-1}{\gamma_h}} \right) \right]$$

$$= 1900 \left[1 - 0.99 \left(1 - \left(\frac{5475.5}{1,75,810} \right)^{\frac{1/3}{4/3}} \right) \right] = 809.2 \text{ K}$$

$$V_{RJ} = V_4 = \sqrt{2C_{Ph}(T_{03} - T_4)} = \sqrt{2 \times 1148(1900 - 809.2)} = 1582.6 \text{ m/s}$$

Performance

$$V_1 = M\sqrt{\gamma_c RT_1} = M\sqrt{\gamma_c RT_1} = 885.15 \text{ m/s}$$

$$\dot{m}_{fTJ} = \dot{m}_{aTJ}(f + f_{Ab})$$

$$\dot{m}_{fRJ} = \dot{m}_{aRJ}f_{Rb}$$

$$\dot{m}_f = \dot{m}_{fRJ} + \dot{m}_{fTJ}$$

$$\dot{m}_a = \dot{m}_{aTJ} + \dot{m}_{aRJ} = \dot{m}_{aTJ}(1 + \alpha_R)$$

$$T = (\dot{m}_{aTJ} + \dot{m}_{fTJ})V_{TJ} + (\dot{m}_{aRJ} + \dot{m}_{fRJ})V_{RJ} - \dot{m}_a V_1$$

$$T = \dot{m}_{aTJ}(1 + f + f_{Ab})V_{TJ} + \dot{m}_{aRJ}(1 + f_{Rb})V_{RJ} - (\dot{m}_{aTJ} + \dot{m}_{aRJ})V_1$$

$$T/\dot{m}_a = \frac{(1 + f + f_{Ab})V_{TJ}}{[1 + \alpha_R]} + \frac{\alpha_R(1 + f_{Rb})V_{RJ}}{[1 + \alpha_R]} - V_1 = 711.7 \text{ N.s/kg}$$

$$TSFC = \frac{\dot{m}_f}{T} = \frac{\dot{m}_{aTJ}(f + f_{Ab}) + f_{Rb}\dot{m}_{aRJ}}{\dot{m}_{aTJ}(1 + f + f_{Ab})V_{TJ} + \dot{m}_{aRJ}(1 + f_{Rb})V_{RJ} - (\dot{m}_{aTJ} + \dot{m}_{aRJ})V_1}$$

$$TSFC = \frac{f + f_{Ab} + \alpha_R f_{Rb}}{(1 + f + f_{Ab})V_{TJ} + \alpha_R(1 + f_{Rb})V_{RJ} - (1 + \alpha_R)V_1}$$

$$= 1.84556 \times 10^{-5} \text{ kg.s/N}$$

$$\eta_{th} = \frac{\Delta K.E}{\dot{Q}_{add}} = \frac{\dot{m}_{aTJ}(1 + f + f_{Ab})V_{TJ}^2 + \dot{m}_{aRJ}(1 + f_{Rb})V_{RJ}^2 - (\dot{m}_{aTJ} + \dot{m}_{aRJ})V_1^2}{2Q_{HV}(\dot{m}_{aTJ}*f*\eta_{cc} + \dot{m}_{aTJ}*f_{Ab}*\eta_{Ab} + \dot{m}_{aRJ}*f_{Rb}*\eta_{Rb})}$$

$$\eta_{th} = \frac{(1 + f + f_{Ab})V_{TJ}^2 + \alpha_R(1 + f_{Rb})V_{RJ}^2 - (1 + \alpha_R)V_1^2}{2Q_{HV}(f*\eta_{cc} + f_{Ab}*\eta_{Ab} + \alpha_R*f_{Rb}*\eta_{Rb})} = \frac{5,200,314.3}{9,267,986.6}$$

$$= 56.11\%$$

$$\begin{aligned}\eta_{pr} &= \frac{T^*V_1}{\Delta K.E} \\ &= \frac{2V_1(\dot{m}_{aTJ}(1+f+f_{Ab})V_{TJ} + \dot{m}_{aRJ}(1+f_{Rb})V_{RJ} - (\dot{m}_{aTJ} + \dot{m}_{aRJ})V_1)}{\dot{m}_{aTJ}(1+f+f_{Ab})V_{TJ}^2 + \dot{m}_{aRJ}(1+f_{Rb})V_{RJ}^2 - (\dot{m}_{aTJ} + \dot{m}_{aRJ})V_1^2} \\ \eta_{pr} &= \frac{2V_1((1+f+f_{Ab})V_{TJ} + \alpha_R(1+f_{Rb})V_{RJ} - (1+\alpha_R)V_1)}{(1+f+f_{Ab})V_{TJ}^2 + \alpha_R(1+f_{Rb})V_{RJ}^2 - (1+\alpha_R)V_1^2} = \frac{3,779,721}{5,200,314.3} \\ &= 72.68 \% \\ \eta_o &= \frac{T^*V_1}{\dot{Q}_{\text{add}}} = \eta_{pr} * \eta_{th} = 40.78 \%\end{aligned}$$

	Turbojet only	Ramjet only	TBCC engine
T/\dot{m}_a (N.s/kg)	697.15	718.95	711.7
TSFC (kg/N.s)	1.7534×10^{-5}	1.89×10^{-5}	1.84556×10^{-5}
η_{th}	59 %	54.81 %	56.11 %
η_{pr}	73.03 %	72.52 %	72.68 %
η_o	43.09 %	39.75 %	40.78 %

(C) From the above table:

$$\text{Total thrust: } T = \dot{m}_{aTJ} \times (T/\dot{m}_a)_{TJ} + \dot{m}_{aRJ} \times (T/\dot{m}_a)_{RJ}$$

$$\text{With } \dot{m}_{aRJ}/\dot{m}_{aTJ} = \alpha_R = 2$$

$$\text{Then } T = \dot{m}_{aTJ} \times [(T/\dot{m}_a)_{TJ} + 2 \times (T/\dot{m}_a)_{RJ}]$$

$$150,000 = \dot{m}_{aTJ} \times [697.15 + 2 \times 718.95]$$

Air mass flow rate through turbojet engine	$\dot{m}_{aTJ} = 70.26 \text{ kg/s}$
Air mass flow rate through ramjet engine	$\dot{m}_{aRJ} = 140.52 \text{ kg/s}$
Thrust generated by turbojet engine	$T_{TJ} = \dot{m}_{aTJ} \times (T/\dot{m}_a)_{TJ} = 48,974 \text{ N}$
Thrust generated by ramjet engine	$T_{RJ} = \dot{m}_{aRJ} \times (T/\dot{m}_a)_{RJ} = 101,026 \text{ N}$

Example 6.13 The turboramjet engine discussed in Example (6.12) will be used in propelling the same aircraft during its operation from flight Mach numbers of 2–4 at same 20,000 m altitude. For Mach number 2, only the turbojet engine will be used while the ramjet is off. At Mach number 4, the ramjet will be only operating while the turbojet will be off.

The drag coefficient for aircraft at different Mach numbers is given in Table 6.7.

Assuming aircraft is moving at constant speeds where thrust and drag forces are equal, calculate:

1. Drag force at Mach numbers of 2 and 4
2. Air mass flow rate for both turbojet and ramjet engines

Table 6.7 Drag coefficient vs. Mach number

M	2.0	3.0	4.0
C_D	0.0569	0.038	0.026

Solution

1. At Mach number = 2

Turbojet engine with lit afterburner is only operating.

Same procedure will be followed as in the previous example. Only final results will be given here:

Module	Intake	Compressor	CC	Turbine	AB	Nozzle
Outlet temperature (K)	390	705.23	1500	1196	1750	870.2
Outlet pressure (Pa)	37,744	264,208	257,603	95,210	93,306	5475.5
Fuel-to-air ratio	—	—	0.008726	—	0.005598	—
Velocity (m/s)	590.1	—	—	—	—	1421.3

The thrust force

$$T = \dot{m}_{aTJ}[(1 + f + f_{Ab})V_{TJ} - V_1] \\ = \dot{m}_{aTJ}[(1 + 0.008726 + 0.005598) \times 1421.3 - 590.1]$$

$$T = 851.56 \dot{m}_{aTJ}$$

$$\text{Since } T = D = 0.5\rho V_1^2 A C_D = 0.5\rho M_1^2 a_1^2 A C_D$$

$$\frac{T_{TJ}}{T_{\text{combined}}} = \left(\frac{M_{TJ}}{M_{\text{combined}}} \right)^2 \frac{(C_D)_{TJ}}{(C_D)_{\text{combined}}} = \left(\frac{2}{3} \right)^2 \times \frac{0.0569}{0.038} = 0.6655$$

Drag and thrust forces are $D_{TJ} = T_{TJ} = 0.6655 \times 150,000 = 99,825 \text{ N.}$

$$\text{But } T = 851.56 \dot{m}_{aTJ}$$

Air mass flow rate through turbojet engine is $\dot{m}_{aTJ} = \frac{99,825}{851.56} = 117.225 \text{ kg/s.}$

2. At Mach number = 4

Ramjet engine is only operating.

Same procedure will be followed as in the previous example. Only final results will be given here:

Module	Intake	CC	Nozzle
Outlet temperature (K)	910	1900	588
Outlet pressure (kPa)	667.118	653.776	5.475
Fuel-to-air ratio	—	0.01095	—
Speed (m/s)	1180	—	1736

$$T = \dot{m}_{aRJ}[(1 + f_{RJ})V_{RJ} - V_1] = \dot{m}_{aRJ}[(1 + 0.01095) \times 1736 - 1180]$$

$$= 574.6 \dot{m}_{aRJ}$$

$$T = 574.6 \dot{m}_{aRJ}$$

$$T = D = 0.5\rho V_1^2 A C_D = 0.5\rho M_1^2 a_1^2 A C_D$$

$$\frac{T_{RJ}}{T_{combined}} = \left(\frac{M_{RJ}}{M_{combined}}\right)^2 \frac{(C_D)_{RJ}}{(C_D)_{combined}} = \left(\frac{4}{3}\right)^2 \times \frac{0.026}{0.038} = 1.216374$$

Drag and thrust forces are $D_{RJ} = T_{RJ} = 1.216374 \times 150,000 = 182,456 N$.

$$\text{But } T_{RJ} = 574.6 \dot{m}_{aRJ}$$

Air mass flow rate through ramjet engine is $\dot{m}_{aRJ} = \frac{182,456}{574.6} = 317.53 \text{ kg/s}$.

6.4.8 Design Procedure

A simplified design procedure for a turboramjet engine will be given here [35–37]. The following steps summarize the procedure for high supersonic/hypersonic cruise aircraft propulsion integration:

1. Mission or flight envelope has to be selected. The cruise altitude is important from fuel economy point of view, while takeoff, climb, and acceleration are critical from the surplus thrust that must be available over the aircraft drag force.
2. Calculate the drag force based on drag coefficient variations with Mach number.
3. The needed thrust force must be greater than the drag value all over its Mach number operation. A margin of 10 % is selected here.
4. Determination of the number of engines based on the maximum thrust suggested for the hybrid engine at its different modes.
5. The performance of each constituents of the hybrid engine is separately determined. For example, if the hybrid engine includes a ramjet, turbojet, and scramjet, each module is examined separately. Thus, the performance of turbojet engine running alone is considered first. The specific thrust and thrust specific fuel consumption are determined for the cases of operative and inoperative afterburner. Next, the performance of the ramjet operating alone also is considered. Since the ramjet operates up to Mach number of 6, liquid hydrogen is considered as its fuel. If a scramjet is available, then its performance is determined separately also.
6. Optimization of the hybrid engine represents the next difficult step. From the specific thrust and thrust specific fuel consumption, the switching points are defined. Thus, in this step, the designer selects at which Mach number the turbojet operates or stops the afterburner and, moreover, at which Mach number

the turbojet must be completely stopped and replaced by the ramjet. If a scramjet is also available, another decision has to be made concerning the switching Mach number from ramjet to scramjet. The switching process duration and the accompanying procedures regarding the air and fuel flow rates and inlet doors actuation are to be carefully defined.

6.4.9 Future TBCC Engine

The *Lockheed Martin SR-72* (Fig. 6.58) is a conceptualized unmanned, hypersonic aircraft intended for intelligence, surveillance and reconnaissance proposed by **Lockheed Martin** to succeed the retired **Lockheed SR-71 Blackbird**. The SR-72 was dubbed by *Aviation Week* as “[son of Blackbird \[38\]](#)”. It could be operational by 2030. Moreover, it would fly at speeds up to Mach 6.

The SR-72 will use a turbine-based combined-cycle (TBCC) system. Thus, a turbine engine will be used from takeoff up to Mach 3, while a dual-mode ramjet engine will accelerate the vehicle to hypersonic speeds. The turbine and ramjet engines share common inlet that provides air to both turbine and ramjet and a common nozzle to discharge exhaust from both engines. Variable inlet and nozzle ramps open and close to match the cycle requirements.

6.5 Conclusion

This chapter is devoted to turbine-based cycle (TBC). Three major types of engines are analyzed, namely, turbojet, turbofan, and turboramjet engines. Application to both airliners and missiles is discussed. Detailed classifications and thermodynamic and performance analyses are discussed.

Problems

6.1 Complete the following table.

Engine	Description	Examples	Application	Advantages	Disadvantages
Turbojet					
Turbofan					
Propfan					
Turboprop					
Turboshaft					

- 6.2 A. What is the difference between a jet engine and a rocket engine?
 B. Can a jet engine use hydrogen fuel instead of a fossil one? If so, is its structure or operation any different from the turbofan or turbojet?

Turbojet

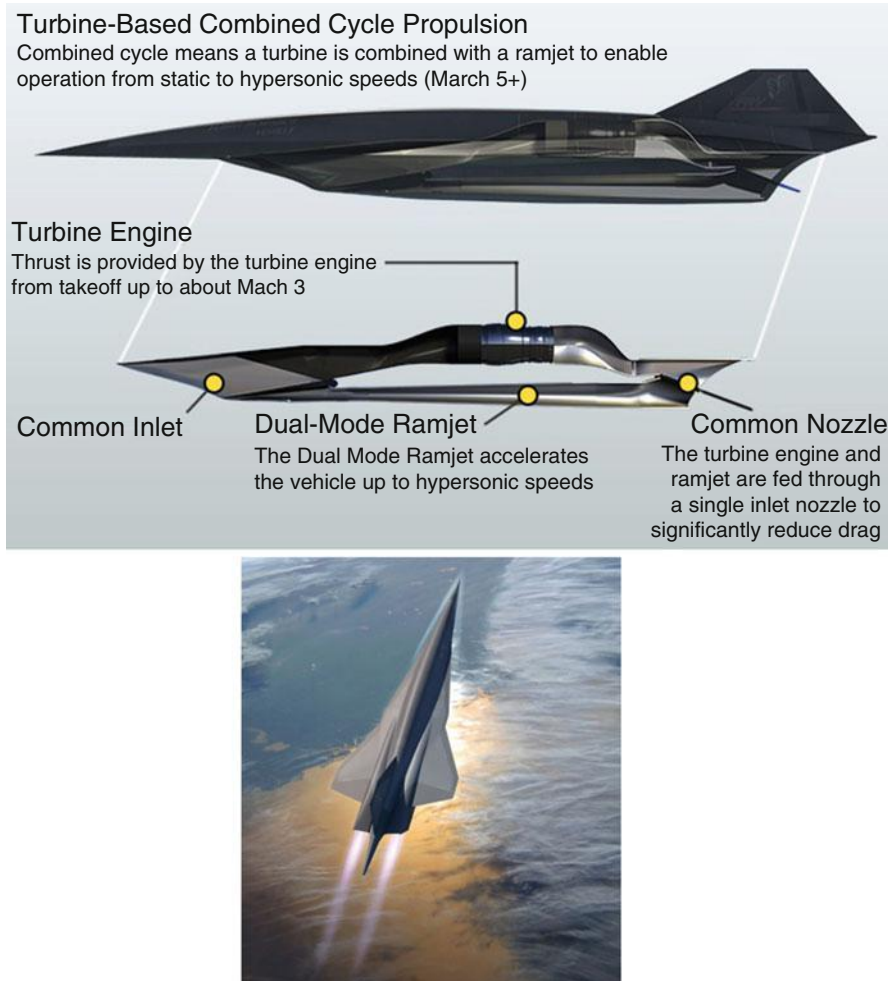


Fig. 6.58 Lockheed martin SR-72

6.3 Choose the correct answer:

- (a) “Afterburning” in a jet engine involves burning additional fuel in the:
- (A) Jet pipe
 - (B) Turbine
 - (C) Combustion chamber
 - (D) Compressor

- (b) The function of the turbine in a turbojet engine is to:
- Vaporize the fuel as much as possible
 - Drive the gas stream into the atmosphere
 - Energize the gas steam
 - Drive the compressor
- (c) Which of these is a turbojet engine?
- Olympus 593
 - Spey
 - Tyne
 - Pegasus

6.4 An aircraft equipped with a *turbojet engine* rolls down the runway at 180 km/h. The engine consumes air at 55 kg/s and produces an exhaust velocity of 160 m/s.

- What is the thrust of this engine?
 - What are the magnitude and direction if the exhaust is deflected 60, 90, and 120° without affecting mass flow?
-

6.5 A turbojet engine propels an aircraft at 600 mph. The fuel heating value is 44 MJ/kg, the speed ratio $\frac{V_e}{V_\infty} = 2$, and the fuel-to-air ratio $f = 0.02$.

Determine:

-
- Propulsion efficiency
 - Thermal efficiency
 - Overall efficiency
-
-
-

6.6 Compare between the ideal performance of ramjet and turbojet engines in the following operating case:

- Flight Mach number for both is 1.5.
- Ambient conditions are $T_a = 216.7$, $P_a = 14.1$ kPa.
- Maximum total temperature: turbojet = 1400 K, ramjet = 2500 K.
- Compressor pressure ratio of turbojet = 10.

Assume

All processes are ideal

Unchoked nozzles

Fuel heating value = 45 MJ/kg

Constant properties ($\gamma = 14$, $C_p = 1.005$ kJ/(kg.K))

Compare the performance of both engines by calculating:

- (a) $TSFC$
- (b) Specific thrust
- (c) Propulsive efficiency
- (d) Thermal efficiency

If the turbojet engine is fitted with an afterburner that develops same maximum temperature as ramjet (2500 K), compute the above four requirements (a–d). Comment:

- 6.7 A twin-engine *turbojet* airplane flies at $M = 0.8$, $L/D = 5$, airplane weight $W = 15$ t.

Operating data:

$$P_a = 1 \text{ bar}, T_a = 288 \text{ K}, \gamma = 1.4, C_p = 1.005 \text{ kJ/kg.K}, Q_R = 43 \text{ MJ/kg}$$

$$TIT = 1400 \text{ K}, \pi_0 = 12, \eta_d = 0.9, \eta_c = 0.92, \eta_b = 0.99, \eta_t = 0.95$$

$$\eta_n = 0.96, \eta_m = 0.99, \Delta P_{cc} = 4 \%,$$

Calculate

- The stagnation pressures and temperatures at each engine station
- The thrust per engine
- $TSFC$

If the afterburner of the jet engine is activated and the fuel flow is $\dot{m}_f = 1.63 \text{ kg/s}$ both in the combustor and the afterburner, calculate the increase in thrust and the change in $TSFC$ because of the operating afterburner.

- 6.8 A General Electric J79-GE-15 *turbojet engine* is one of two engines propelling McDonnell F4C airplanes (wing area $S = 530 \text{ ft}^2$, inlet area for each engine $A_i = 6.5 \text{ ft}^2$) cruising at a constant Mach number $M_0 = 0.84$ at an altitude of 35,000 ft. The drag coefficient of the aircraft under these conditions is 0.044. Assume that the nozzle is unchoked and the turbine exit stagnation temperature is 990 K.

Determine

- (a) Net thrust of the engine
- (b) Gross thrust of the engine
- (c) Weight (or mass) flow through the engine
- (d) Exhaust velocity
- (e) Exit static temperature
- (f) Exit Mach number
- (g) Propulsive, thermal, and overall efficiencies

- 6.9 The airplane SR-71 fitted with two Pratt & Whitney turbojet engine J58 that incorporates an afterburner. All processes are assumed ideal with constant values of both (C_p and γ).

- (A) Draw a schematic diagram for the engine identifying each states by a number from (1–7).
 (B) Draw the corresponding cycle on T-s and P-v diagrams.
 (C) Prove that:

The *thrust ratio* for operative (τ_{AB}) and inoperative afterburner (τ) is expressed by the relation:

$$\frac{\tau_{AB}}{\tau} = \frac{\sqrt{\left(\frac{2}{\gamma-1}\right)\left(\frac{T_{06A}}{T_a}\right)\left[1 - \left(\frac{P_a}{P_{06A}}\right)^{\frac{\gamma-1}{\gamma}}\right]} - M}{\sqrt{\left(\frac{2}{\gamma-1}\right)\left(\frac{T_{05}}{T_a}\right)\left[1 - \left(\frac{P_a}{P_{05}}\right)^{\frac{\gamma-1}{\gamma}}\right]} - M}$$

where subscript (a) denotes ambient conditions and (6A) denotes inlet conditions to nozzle when the afterburner is operative.

Next, when $M = 0$ and outlet temperatures of both compressor and turbine are equal, then:

$$\frac{\tau_{AB}}{\tau} = \frac{\sqrt{\left(\frac{T_{06A}}{T_a}\right)}}{\pi^{\left(\frac{\gamma-1}{2\gamma}\right)}}$$

- 6.10 The below table gives details of temperature and pressure at interior states of an afterburning turbojet engine

	Diffuser inlet	Compressor inlet	Compressor outlet	Turbine inlet	Afterburner inlet	Afterburner outlet	Nozzle outlet
T [K]	220	226	424.3	1300	1082	2200	1650
P [kPa]	23.1	25.1	188.25	182.5	82.5	79	23.1

Assuming *variable values* of both (C_p and γ), calculate:

- (a) Efficiency of diffuser, compressor, and turbine
 - (b) Percentage of pressure drop in combustion chamber and afterburner
 - (c) Total rate of burnt fuel in engine if $Q_R = 44$ MJ/g, $\eta_{burner} = 0.96$ and air mass flow rate = 135 kg/s
 - (d) The thrust force if the inlet area is 0.25 m^2
- 6.11 An aircraft powered by a turbojet engine is flying with 900 km/h. The engine takes 50 kg/s of air and expands the gases to the ambient pressure. The fuel-to-air

ratio is 50 and heating value is 43 MJ/kg. For a maximum thrust condition ($u_f = 0.5 u_e$), calculate:

- (A) Jet velocity
- (B) Thrust
- (C) Specific thrust
- (D) Propulsive and thermal efficiency
- (E) $TSFC$

6.12 An aircraft powered by a turbojet engine is flying with 280 m/s at an altitude of 25 km, where the ambient pressure and temperature are 25.11 kPa and 221.7 K, respectively. The engine takes 200 kg/s of air and burns 6 kg/s of fuel having a heating value of $Q_R = 43,000 \text{ kJ/kg}$, the jet speed is 600 m/s, and exhaust pressure and temperature are 750 K and 30 kPa, respectively.

Calculate the specific thrust ($\frac{T}{m_a}$), the thrust specific fuel consumption (TSFC), propulsive efficiency (η_{pr}), and thermal efficiency (η_{th}).

6.13 A turbojet engine propels an aircraft flying at a Mach number of 0.9 at an altitude of 11 km. Engine has the following data:

Stagnation temperature rise through the compressor = 190 K.

Fuel heating value = 42.8 MJ/kg.

Turbine inlet temperature (TIT) = 1300 K.

Flight speed = half exhaust speed.

Efficiencies: $\eta_d = 0.9$, $\eta_c = 0.8$, $\eta_{cc} = 0.97$, $\eta_t = 0.84$, $\eta_n = 0.97$, $\eta_m = 0.99$

Assume variable specific heat ratio ($\gamma_c = 1.4$, $\gamma_h = \frac{1}{3}, R=287 \text{ J/(kg.K)}$).

Calculate

- (A) Compressor pressure ratio
- (B) Fuel-to-air ratio
- (C) Exhaust Mach number

6.14 The following data apply to a turbojet flying at an altitude where the ambient conditions are 38.25 kPa and 239.4 K.

- Speed of the aircraft: 900 km/h.
- Compressor pressure ratio: 6:1.
- Heat of reaction of the fuel: 43 MJ/kg.
- Turbine inlet temperature: 1400 K.
- Nozzle is choked.
- Nozzle outlet area 0.1 m^2 .

Assuming $\gamma_c = 1.4$, $\gamma_h = \frac{1}{3}$, $R=0.287 \text{ kJ/kg.K}$, calculate:

- Inlet area
- Thrust force
- $TSFC$

- 6.15 A turbojet engine inducts 50 kg of air per second and propels an aircraft with a flight speed of 900 km/h. The fuel-to-air ratio is 0.012 and the heating value of the fuel is 43 MJ/kg. The enthalpy change for the nozzle is 211.25 kJ/kg. Determine:

- The propulsive efficiency
- The thermal efficiency
- *TSFC*
- The propulsive power

- 6.16 Figure (6.59) illustrates a turbojet engine with two pitot tubes for measuring total pressures at inlet to compressor (P_{02}) and outlet from turbine (P_{05}). These measurements are next displayed for the flight crew as exhaust pressure ratio (*EPR* defined as: $EPR = \frac{P_{05}}{P_{02}}$).

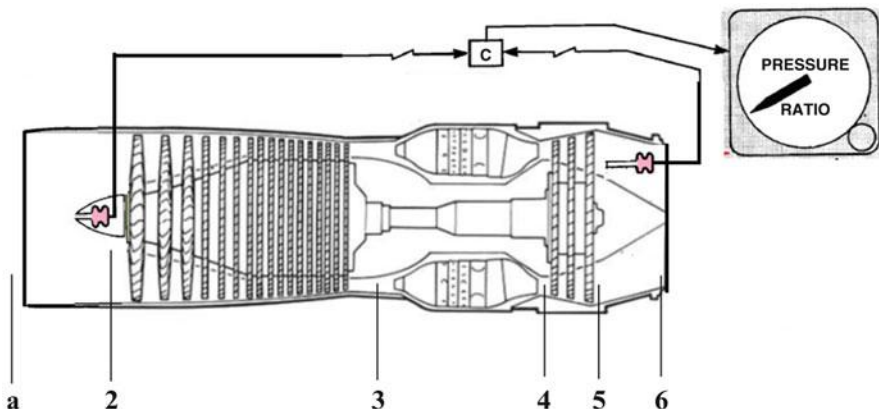


Figure (6.59) Problem (6.16)

Prove that for ideal conditions, exhaust Mach number is expressed by:

$$M_e = \sqrt{\left(\frac{2}{\gamma_h - 1}\right) \left[(EPR)^{\frac{\gamma_h - 1}{\gamma_h}} \left(1 + \frac{\gamma_c - 1}{2} M^2 \right)^{\left(\frac{\gamma_c}{\gamma_c - 1}\right) \left(\frac{\gamma_h - 1}{\gamma_h}\right)} - 1 \right]} \quad (\text{A})$$

Next, if constant properties are assumed ($\gamma_c = \gamma_h = \gamma$), then the above equation is simplified to:

$$M_e = \sqrt{\left(\frac{2}{\gamma - 1}\right) \left[(EPR)^{\frac{\gamma - 1}{\gamma}} \left(1 + \frac{\gamma - 1}{2} M^2 \right) - 1 \right]} \quad (\text{B})$$

Calculate the exhaust Mach number from equation (A) for the case:

$EPR = 1.6$, $M = 2.0$, $\gamma_c = 1.4$, $\gamma_h = 4/3$. Next, recalculate it using the equation (B) for the same data and a constant specific heat ratio $\gamma = 1.4$.

Comment.

Now consider the case: $M = 2$, $\pi_c = 6.0$, $T_a = 288$ K, $T_{\max} = 1400$ K, $\gamma = 1.4$,

$$Q_R = 43 \text{ MJ/kg}$$

Calculate

- (A) *Exhaust Mach number using equation (B)*
- (B) *Turbine pressure ratio*
- (C) *The power delivered to accessories*

6.17 A. Compare between *ramjet* and *afterburning turbojet* engines.

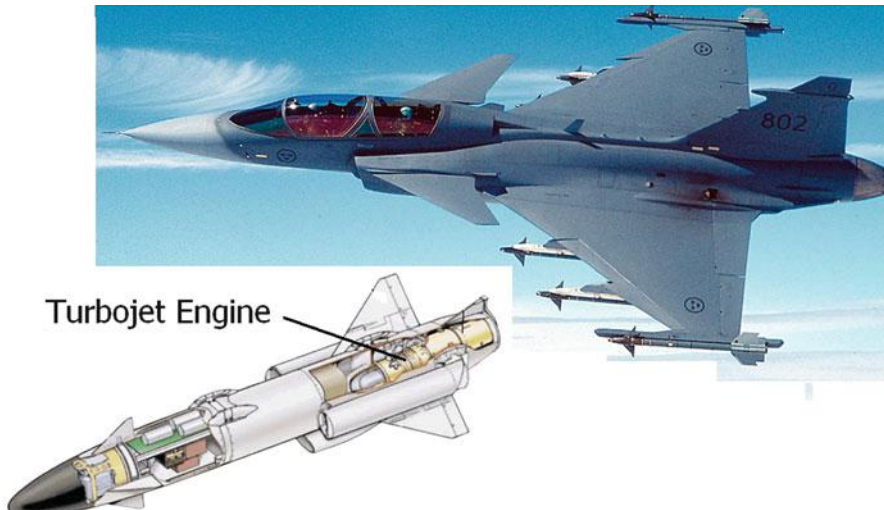


Figure (6.60) Problem (6.17)

B. Gripen multirole fighter (shown in the figure below) is armed with RBS15 MK3 antiship missile which is powered by a French Microturbo TRI 60 engine as shown in Fig. (6.60). It is a *single-spool turbojet* engine with a sustained flight of 0.9 Mach number and nearly sea-level cruise altitude. The engine has the following data:

Thrust force = 4.4 kN	Compressor pressure ratio = 6.3
Air mass flow rate = 8.4 kg/s	$TSFC = 0.11 \text{ kg}/(\text{N.hr})$
Fuel heating value $Q_R = 43 \text{ MJ/kg}$	

Gases expand in nozzle to ambient pressure.

Assuming all processes are ideal and constant values of (γ , C_p), calculate:

- (a) Fuel-to-air ratio
 - (b) Maximum temperature and pressure within the engine
 - (c) Exhaust speed and Mach number
 - (d) Inlet area
- 6.18 The Storm Shadow missile, Fig. (6.61) has been integrated onto the RAF's Tornado GR4 and the Eurofighter Typhoon aircraft. It is a long-range air-to-surface missile that is powered by a single-spool turbojet for sustained flight. For a sea-level cruise operation ($P_a = 101.325 \text{ kPa}$ and $T_a = 298 \text{ K}$), it has the following data:

Flight Mach number = 0.8.

Thrust = 5.4 kN.

Compressor pressure ratio = 6.3.

Fuel-to-air ratio $f = 0.02$.

Fuel heating value $Q_R = 43 \text{ MJ/kg}$.

$P_e = P_a$.

All processes are ideal.

Constant values of (γ , C_p).

Calculate

1. Maximum temperature and pressure within the engine
2. Exhaust speed and Mach number
3. Air mass flow rate
4. Inlet area
5. *TSFC*



Figure (6.61) Eurofighter Typhoon aircraft and Storm Shadow missile

- 6.19 A turbojet is flying with a velocity of 300 m/s at an altitude of 9150 m, where the ambient conditions are 32 kPa and -32°C . The pressure ratio across the compressor is 14, and the temperature at the turbine inlet is 1400 K. Air enters the compressor at a rate of 45 kg/s, and the jet fuel has a heating value of 42,700 kJ/kg. Assuming ideal operation for all components and constant specific heats for air at room temperature, determine:
- The temperature and pressure at the turbine exit
 - The velocity of the exhaust gases
 - The propulsive power developed
 - The propulsive efficiency
 - The rate of fuel consumption

Reexamine this engine if the following efficiencies are considered:

$$\eta_d = 0.92, \eta_c = 0.88, \eta_b = 0.98, \eta_t = 0.9, \eta_n = 0.96$$

What will be the new propulsive power and the rate of fuel consumption?

- 6.20 Compare the specific fuel consumption of a turbojet and a ramjet which are being considered for flight at $M = 1.5$ and 17,000 m altitude (ambient conditions of pressure and temperature, 8.786 kPa and 216.7 K, respectively). The turbojet pressure ratio is 8 and the maximum allowable temperature is 1173 K. For the ramjet the maximum temperature is 2300 K. For simplicity ignore aerodynamic losses in both engines. Conventional hydrocarbon fuels are to be used (heating value 43 MJ/kg). Assume $\gamma = 1.4$ and $C_p = 1.005 \text{ kg/(kg.K)}$.
- 6.21 A turbojet engine propels an aircraft at 300 m/s. The heating value of the fuel is 44 MJ/kg, the speed ratio $\frac{V_f}{V_j} = 0.5$, and the fuel-to-air ratio $\frac{\dot{m}_f}{\dot{m}_a} = 0.02$. Determine:
- The ideal propulsion efficiency
 - The thermal efficiency
 - The overall efficiency

- 6.22 A twin-engine turbojet airplane flies at $M = 0.8$. It has the following data:
 $\eta_d = 0.9, \eta_c = 0.92, \eta_t = 0.95, r_b = 0.95, \eta_n = 0.96, \pi_c = 11, TIT = 1400 \text{ K}, Q_R = 42,000 \text{ kJ/kg}$
 $T_a = 15^{\circ}\text{C}, P_a = 1 \text{ atm.}, \gamma = 1.4, C_p = 1.1 \text{ kJ/(kg.K)}, L/D = 5, \text{Airplane Weight } W = 15 \text{ t}$

Calculate

- The stagnation pressures and temperatures at each engine station
- The thrust per engine
- $TSFC$

- 6.23 In a turbojet engine, prove that for ideal cycle the specific thrust is expressed by the relation:

$$\frac{T}{\dot{m}_a} = a_0 \left\{ \sqrt{\frac{2}{\gamma - 1} \frac{\tau_\lambda}{\tau_r \tau_c} (\tau_r \tau_c \tau_t - 1)} - M_0 \right\}$$

$$\text{Where : } \tau_r = \frac{T_{02}}{T_a}, \tau_c = \frac{T_{03}}{T_{02}}, \tau_\lambda = \frac{T_{04}}{T_a}$$

Next, consider the case of removing the turbine driving the compressor and replacing it by an electric motor, as shown in Fig. (6.62). For an ideal approximation to this new engine, assume that compression and expansion are isentropic, and approximate the effect of combustion as heat addition at constant stagnation (total) pressure. For this model, show the specific thrust is given by:

$$\frac{T}{\dot{m}_a} = a_0 \left\{ \sqrt{\frac{2}{\gamma - 1} \frac{\tau_\lambda}{\tau_r \tau_c} (\tau_r \tau_c - 1)} - M_0 \right\}$$

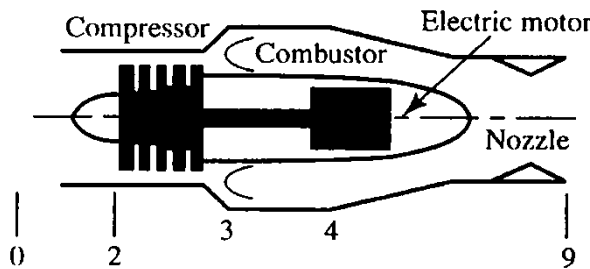


Figure (6.62) Turbojet innovation

Determine the specific thrust for both engines in the following case:

$$T_a = 288 \text{ K}, M_0 = 0.2, T_{0 \max} = 1600 \text{ K}, \pi_c = 4, \gamma = 1.38, C_p = 1.042 \text{ kJ/kg.K}$$

What are your comments?

- 6.24 Compare between the following three engines: turbojet, turbojet with afterburner, and ramjet. Their operating conditions and common features are:

Altitude range: sea level – 40,000 ft.

Mach number range: 0.0–2.0.

Fuel heating value = 43,260 kJ/kg.

Nozzle is convergent.

Intake inlet diameter = 0.6 m.

Typical turbojet engine (without afterburner)

Fuel mass flow rate = air bleed mass flow rate ($m_f^* = m_b^*$).

Maximum fuel-to-air ratio = (stoichiometric ratio/3) or ($f_{\max} \leq 0.068/3$):

$$\Delta P_d = 0, \quad \Delta P_{cc} = 3\%$$

$$\eta_d = \eta_b = \eta_n = 100\%, \quad \eta_c = 87\%, \quad \eta_t = 90\%$$

$$\pi_c = 5.0, \quad TIT = 1100 \text{ K}$$

$$W_c = W_t$$

Turbojet engine with afterburner

Same data as above, together with the following data:

$$f_{ab} = 0.068 - f_{cc}$$

$$\eta_{ab} = 100 \text{ \%}$$

$$\Delta P_{ab} = 4 \text{ \%}$$

Ramjet engine

$$f_{cc} = 0.068$$

$$\Delta P_d = \Delta P_{cc} = 0 \text{ \%}$$

$$\eta_d = \eta_b = \eta_n = 100\%$$

$$(v_{inlet})_{cc} = 175 \text{ ft/s}$$

Plot the following relations for the three engines:

- (a) $f_{\text{total}}, T_{05}/T_{02}, P_{05}/P_{02}, F_j/A_{\text{front}}, F_n/A_{\text{front}}$ versus Mach number (from 0.0 to 2.0)
- (b) Exhaust nozzle area versus Mach number (from 0.0 to 2.0)
- (c) Exhaust nozzle area for Mach number = 0.8 versus altitude (from 0.0 to 40,000 ft)
- (d) F_n/A_{front} versus altitude (from 0.0 to 40,000 ft)
- (e) $TSFC$ versus altitude (from 0 to 40,000 ft)
- (f) $TSFC$ versus Mach number (from 0.0 to 2.0)

Turbofan

- 6.25 The following data apply to a twin-spool turbofan engine, with the fan driven by the LP turbine and the compressor by the HP turbine. Separate hot and cold nozzles are used:

- Overall pressure ratio: 20.0
- Fan pressure ratio: 1.6

- Bypass ratio: 3.5
- Turbine inlet temperature: 1300 K
- Air mass flow: 120 kg/s
- Find the sea-level static thrust and *TSFC* if the ambient pressure and temperature are 1 bar and 288 K. Heat value of the fuel: 43 MJ/kg

6.26 A twin-spool mixed turbofan engine operates with an overall pressure ratio of 18. The fan operates with a pressure ratio of 1.45 and the bypass ratio of 5.0. The turbine inlet temperature is 1400 K. The engine is operating at a Mach number of 0.85 at an altitude where the ambient pressure and temperature are 223.2 K and 0.2645 bar.

Calculate

- The thrust
- *TSFC*
- Propulsive efficiency

6.27 The shown block diagram illustrated in Fig. (6.63) represents a single-spool mixed afterburning turbofan engine flying at altitude 24,000 ft and Mach number 1.8. The fan pressure ratio and mass flow rate are 1.8 and 90 kg/s, respectively. Compressor pressure ratio and mass flow rate are 8.0 and 45 kg/s. Turbine inlet temperature and maximum engine temperature are 1500 and 2600 K. Fuel heating value is 45,000 kJ/kg. Nozzle is of the convergent-divergent type.

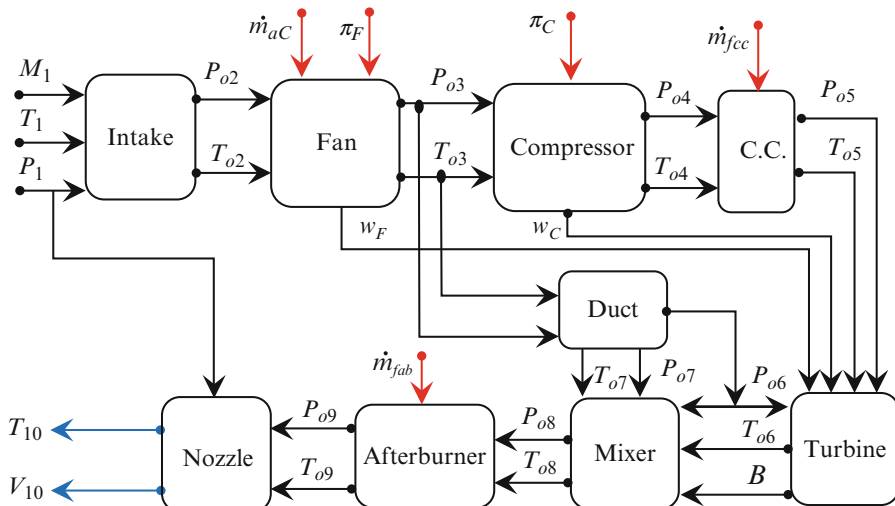


Figure (6.63) Block diagram for a single-spool mixed afterburning turbofan engine

No pressure drop is assumed in combustor, mixer, or afterburner. All other processes are assumed ideal. It is required to:

1. Draw a schematic diagram for engine showing different states
2. Plot T-s diagram for the cycle
3. Calculate bypass ratio
4. Calculate fuel-to-air ratios in combustor and afterburner
5. Calculate the thrust and $TSFC$
6. Calculate the propulsive, thermal and overall efficiencies

6.28 Illustrate how the propulsion efficiency and SFC vary with the flight Mach number for:

1. A conventional turbofan
2. A geared fan with ultrahigh-bypass ratio
3. An unducted fan

Explain the trends in the curves.

6.29 Figure (6.64) shows a fighter airplane propelled by a low-bypass ratio *mixed* afterburning turbofan engine during takeoff from an air carrier. Temperature and pressure of ambient air are 290 K and 101 kPa. Air is ingested into the engine intake at a Mach number of 0.2. Turbofan engine has the following data:

Fan pressure ratio $\pi_f = 1.8$.

Compressor pressure ratio $\pi_c = 5$.

Fuel-to-air ratio in combustion chamber $f = 0.02$.

Afterburner fuel-to-air ratio $f_{ab} = 0.04$.

Fuel heating value $Q_R = 45 \text{ MJ/kg}$.

Percentages of power extracted by fan and compressor from the driving turbines are respectively $\lambda_1 = \lambda_2 = 0.8$.

Assume ideal processes and variable properties: (γ, C_p) .

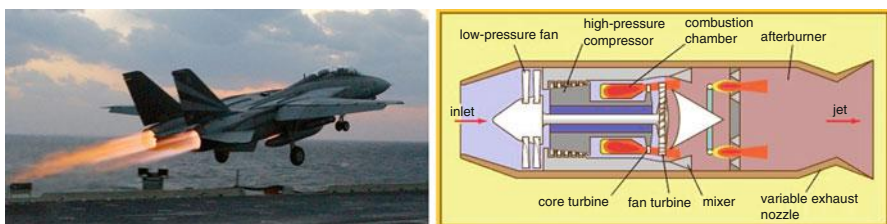


Figure (6.64) Fighter airplane powered by a low-bypass ratio mixed afterburning turbofan engine

Calculate:

1. Bypass ratio
2. Jet speed
3. $TSFC$

6.30 A. Classify turbofan engines

B. Compare between *turbojet* and *turbofan* engines (maximum Mach number, ceiling, noise, fuel consumption)

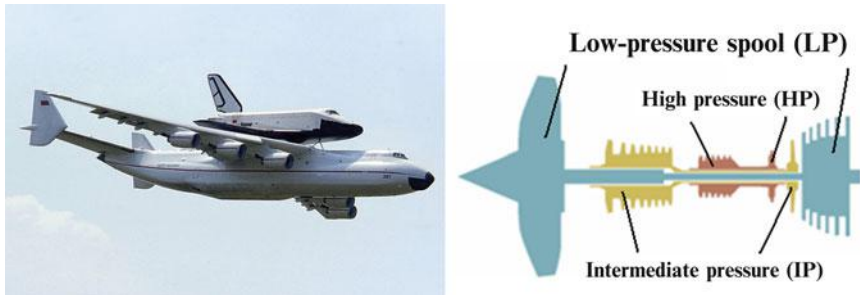


Figure (6.65) Antonov An-225 aircraft (carrying space shuttle) and powered by six engines (Progress D-18T triple-spool unmixed high-bypass ratio turbofan)

C. The shown figure illustrates Antonov An-225 aircraft powered by six engines (Progress D-18T *triple-spool unmixed high-bypass ratio turbofan engine*). Bleed air is 8 % extracted from HP compressor to cool HP turbine (5 %) and IP turbine (3 %). It has the following data:

Parameter	Value	Parameter	Value	Parameter	Value	Parameter	Value
η_d	0.88	$\Delta p_{c.c}$	0.03	π_F	1.35	λ_1	0.84
η_f	0.9	$\Delta p_{fanduct}$	0.0	π_{IPC}	5.0	$\lambda_2 = \lambda_3$	1.0
η_c	0.88	c_{p_c} (J/kg.K)	1005	π_{HPC}	4.1	η_n	0.96
η_b	0.98	c_{p_h} (J/kg.K)	1148	β	5.7	η_m	0.99
η_t	0.92	R (J/kJ/K)	287	TIT (K)	1600	b	8 %
γ_c	1.4	γ_h	4/3				

For *takeoff conditions* ($M = 0.2$) at sea level, calculate:

1. The pressure and temperature at outlet of cold and hot nozzles
2. Specific thrust and thrust specific fuel consumption

6.31 A double-spool turbofan engine; Fig. (6.66), is used to power an aircraft flying at speed of 250 m/s at an altitude of 11,000 m. As shown in the figure below, the low-pressure turbine drives the fan and low-pressure compressor, while the high-pressure turbine drives the high-pressure compressor. The engine has the following data:

- Bypass ratio = 8.
- Total ingested air flow rate = 180 kg/s.
- Overall pressure ratio OPR = 35.
- Fan pressure ratio = 1.6.

- Pressure ratio of high-pressure compressor is four times that of the low-pressure compressor; $\pi_{HPC} = 4 \pi_{LPC}$.
- Turbine inlet temperature = 1650 K.
- Fuel heating value = 43 MJ/kg.

Assuming all processes are ideal and neglecting any pressure drop, it's required to:

1. Find the thrust, $TSFC$, and efficiencies of the engine
2. Plot the velocity and temperature distribution over the engine cross section (rear end)

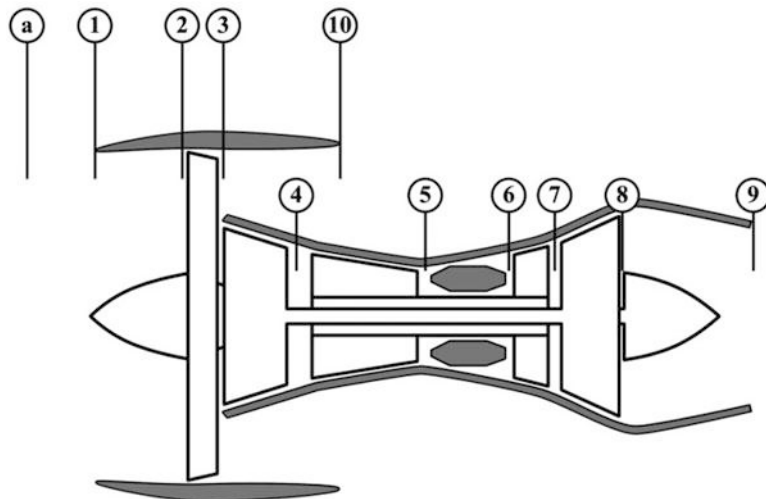


Figure (6.66) Double spool high bypass ratio turbofan engine

- 6.23 A double-spool turbofan engine is used to power an aircraft flying at speed of 250 m/s at an altitude of 11,000 m. As shown in Fig. (6.67), the low-pressure turbine drives the fan and low-pressure compressor, while the high-pressure turbine drives the high-pressure compressor. Inlet and outlet temperature and velocity of engine are plotted beside the engine layout. The engine has the following data:

- Bypass ratio = 8.
- Total ingested air flow rate = 180 kg/s.
- Overall pressure ratio OPR = 35.
- Pressure ratio of high-pressure compressor is four times that of the low-pressure compressor; $\pi_{HPC} = 4 \pi_{LPC}$.
- Fuel heating value = 43 MJ/kg.

Assuming all processes are ideal and neglecting any pressure drop, it's required to find:

1. Whether the nozzles are choked or not
2. Fan pressure ratio
3. TIT
4. The thrust force

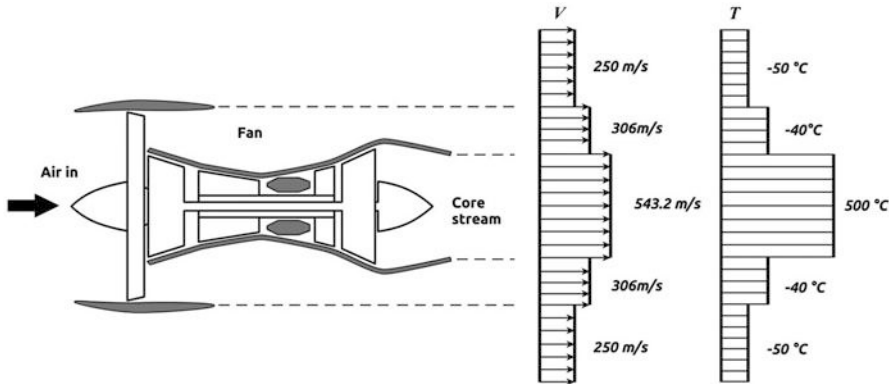


Figure (6.67)

6.33 A single-spool mixed afterburning turbofan engine is to be compared with a single-spool afterburning turbojet engine in its preliminary design stages (Fig. 6.68). The following characteristics are to be considered:

- Ideal processes, $M = 1.2$
- Altitude = 8 km (where $T_a = 236.23$ K and $P_a = 35.651$ kPa): $c_{p_c} = 1.005$ kJ/kg/K, $\gamma_c = 1.4$, $c_{P_n} = 1.148$ kJ/kg/K, and $\gamma_h = \frac{4}{3}$
- Fuel heating value $Q_R = 43,000$ kJ/kg
- Total air flow rate of both engines: $m_a^o = 60$ kg/s

For turbojet

Compressor pressure ratio ($\pi_c = 20$), turbine inlet temperature ($T_{04} = 1400$ K), maximum cycle temperature ($T_{06} = 2200$ K), and unchoked nozzle ($p_7 = p_a$)

For turbofan

Fan pressure ratio ($\pi_f = 2$), compressor pressure ratio ($\pi_c = 10$), turbine inlet temperature ($T_{05} = 1400$ K), maximum cycle temperature ($T_{09} = 2200$ K), and unchoked nozzle ($p_{10} = p_a$)

Calculate

1. Thrust force
2. Propulsive efficiency

3. Thermal efficiency
4. Overall efficiency

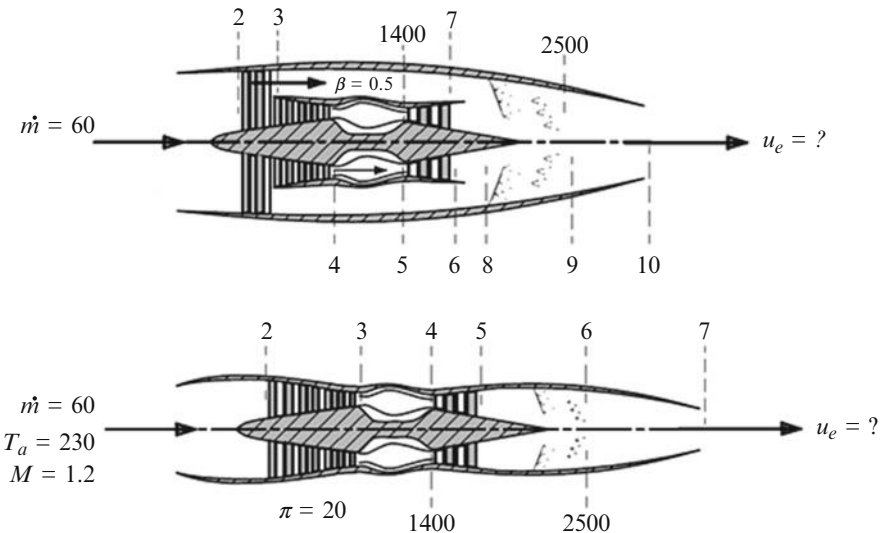


Figure (6.68) Turbojet/Turbofan Layouts

Turboramjet

- 6.34 The drag of a hypersonic future business jet is to be simplified by the following equations:

Flight Mach number	Drag (N)
$M = 0 - 0.75$	$D = 10^5 \cdot (4.1M^2 - 1.1M + 2.1)$
$M = 0.75 - 1.25$	$D = 10^5 \cdot (-9.7M^2 + 20M - 5.9)$
$M = 1.25 - 6$	$D = 10^5 \cdot \left(\frac{21}{M^4} - \frac{37}{M^3} + \frac{26}{M^2} - \frac{5.9}{M} + 2.3 \right)$

Plot the drag versus Mach number

- 6.35 If that aircraft in (6.34) is to be driven by two turbojet engines with afterburner, each has the following parameters:

$$TIT = 1800 \text{ K}, \quad T_{\max} = 2600 \text{ K}, \quad \pi_0 = 12, \quad \eta_d = 0.9, \quad \eta_c = 0.91, \quad \eta_b = 0.99, \quad \eta_t = 0.92$$

$\eta_n = 0.96, \quad \eta_m = 0.99, \quad \Delta P_{cc} = 2 \%, \quad \Delta P_{AB} = 3 \%$. Fuel is hydrocarbon fuel having a heating value of 45.0 MJ/Kg.

Calculate and Plot

- The air mass flow rate (m_a^o)
- The fuel flow rate (m_f^o)
- The thrust specific fuel consumption (TSFC)

The afterburner is on for a Mach range of $M = 0$ to $M = 4$.

Note: the airplane is designed to fly with dynamic pressure $50,000 \text{ N/m}^2$.

- 6.36 The aircraft of problem (6.34) is to be driven by two ramjet engine having the following parameters:

$$T_{\max} = 2600 \text{ K}, \quad \eta_d = 0.9, \quad \eta_b = 0.99, \quad \eta_n = 0.98, \quad \Delta P_{cc} = 2.5 \%,$$

Calculate and Plot

- The air mass flow rate (m_a^o)
- The fuel flow rate (m_f^o)
- The thrust specific fuel consumption (TSFC)

The engine is using also hydrocarbon fuel with heating value of 45 MJ/kg .

- 6.37 The aircraft of problem (6.34) is to be driven by an over-under turboramjet configuration that is constructed of the turbojet in problem (6.34) and the ramjet in problem (6.34) and work on the following regimes.

Regime	Engine condition
$M = 0$ to $M = 0.5$	Turbojet with AB off
$M = 0.5$ to $M = 1.5$	Turbojet with AB on
$M = 1.5$ to $M = 3$	Turbojet with AB off Mass flow in turbojet decreasing from 100 % m_a^o at $M = 1.5$ – 0% m_a^o at $M = 2.5$ Ramjet is operating as a support for the turbojet engine
$M = 3$ to $M = 6$	The turbojet is off The ramjet is driving the A/C alone

Calculate and Plot

- The air mass flow rate (m_a^o)
- The fuel flow rate (m_f^o)
- The thrust specific fuel consumption (TSFC)

Comment!

- 6.38 A wrapharound turboramjet engine has the following data when the turbojet engine was operating and the afterburner was lit at an altitude of 60,000 ft.

Flight Mach number	2.5
Turbine inlet temperature	1300 K
Maximum temperature	2000 K
Air mass flow rate	60 kg/s

If the pilot is planning to switch operation to ramjet and stop the turbojet, what is the procedure he has to follow for this transition time?

If the maximum temperature of the ramjet is 2500 K, what will be the needed air mass flow rate to keep the same thrust as the turbojet mode?

Do you expect a dual mode is visible? Explain why or why not.

- 6.39 Compare between turboramjet and scramjet engines with respect to the following points:

- Flight altitude
- Maximum Mach number
- Fuel consumption

References

1. El-Sayed AF (2008) Aircraft propulsion and gas turbine engines, 1st edn. Taylor & Francis/ CRC Press, Boca Raton, Florida
2. Gill PW (1964) Fundamentals of internal combustion engines. United States Naval Institute, Maryland
3. Wm. B. Cottrell (Ed.) (1952) Reactor program of the aircraft nuclear propulsion project, Oak Ridge National Laboratory, ORNL-1234
4. Colon, Raul (2007) Flying on nuclear, The American effort to build a nuclear powered bomber. The Aviation History On-Line Museum. <http://www.aviation-history.com/articles/nuke-american.htm>
5. Colon R (2009) Soviet experimentation with nuclear powered bombers, <http://www.aviation-history.com/articles/nuke-bombers.htm>, January 3, 2012
6. Lobik DP (1995) Unmanned aerial vehicles: a study of gas turbine applications, M.Sc. Thesis, Naval Postgraduate School
7. www.boeing.com/commercial/safety/propulsion.html
8. <http://enginehistory.org/GasTurbines/Rolls-Royce/R-RConway/index.html>
9. <http://www.bga-aeroweb.com/Engines/General-Electric-TF39.html>
10. <http://www.rolls-royce.com/customers/civil-aerospace/products/civil-large-engines/rb211-535e4.aspx#overview>
11. [http://easa.europa.eu/system/files/dfu/EASA-TCDSE.002_\(IM\)_General_Electric_GE90_series_engines-02-16032004.pdf](http://easa.europa.eu/system/files/dfu/EASA-TCDSE.002_(IM)_General_Electric_GE90_series_engines-02-16032004.pdf)
12. http://www.pw.utc.com/Content/Press_Kits/pdf/ce_pw1700g-1900g_pCard.pdf
13. Papamoschou D, Nielsen E (2008) Fan flow deflection for supersonic turbofan engines, AIAA 2008-39, 46th Aerospace Sciences Meeting and Exhibit, 7–10 January 2008, Reno, Nevada
14. Kurzke J (2007) About simplifications in gas turbine performance calculations, ASME Paper GT2007-27620, Montreal
15. <http://en.wikipedia.org/wiki/Turbofan>
16. Cusick M (1981) Avco lycoming's ALF 502 high bypass fan engine, SAE Technical Paper 810618
17. http://www.pw.utc.com/Content/Press_Kits/pdf/ce_purepower_broch.pdf; https://www.pw.utc.com/Content/PurePowerPW1000G_Engine/pdf/B-1-1_PurePowerEngineFamily_SpecsChart.pdf
18. <http://jetpropulsion.co.uk/jet-engine-projects/rolls-royce-rb-211-22b>
19. Almeldein, Ahmed Z (2010) Propulsion system selection & optimization for a hypersonic civil transport, M.Sc. thesis, Cairo University

20. Jenkins DR, Landis T, Miller J AMERICAN X-VEHICLES An inventory—X-1 to X-50 SP-2003-4531
21. Conners TR Predicted performance of a thrust-enhanced SR-71 aircraft with an external payload NASA-TM-1997-104330
22. William R. Corliss NASA sounding rockets, 1958–1968: a historical summary NASA-SP-1971-4401
23. Morris Jr SJ, Geiselhart KA, Coen PG (1989) Performance potential of an advanced technology Mach 3 turbojet engine installed on a conceptual high-speed civil transport, NASA-TM-4144
24. Stueber TJ, Le DK, Vrana DR. Hypersonic vehicle propulsion system control model development roadmap and activities. NASA-TM-2009-215483
25. Moses PL X-43C planes and status AIAA-2003-7084
26. Rolls-Royce The jet Engine 5th edn, 1996, England
27. Heiser WH, Partt DT (1994) Hypersonic airbreathing propulsion AIAA Education Series
28. Weir LJ, Reddy DR, Rupp GD (1989) Mach 5 inlet CFD and experimental results. In: 25th Joint propulsion conference cosponsored by the AIAA, ASME, SAE, and ASEE, Monterey, July 10–12, NASA-TM-1989-102317, AIAA-1989-2355
29. Trefny CJ, Benson TJ An integration of the turbojet and single-throat ramjet NASA-TM-1995-107085
30. Chang I, Hunter LG CFD study of turbo-ramjet interactions in hypersonic airbreathing propulsion system NASA-CR-1996-202418
31. Bradford JE, Eklund D, Boudreau A (2005) Automated hypersonic launch vehicle design using model center Paper No GT-SSEC.B.1, Georgia Tech Space Systems Engineering Conference (GT-SSEC), November 8–10th, 2005
32. Pegg RJ et al (1993) Design of hypersonic Waverider-Derived airplane, AIAA Paper 93-0401
33. Lam DW Use of the PARC code to estimate the off-design transonic performance of an over/under turboramjet noise, NASA TM-106924, AIAA-95-2616
34. Morris RE, Brewer GD (1979) Hypersonic cruise aircraft propulsion integration study, Vol. I and II, NASA-CR-158926-1 and NASA-CR-158926-2
35. Riebe GD (1983) Aerodynamic characteristics including effect of body shape of A Mach 6 aircraft concept, NASA-TP-2235
36. Pittman, JL, Riebe GD (1980) Experimental and theoretical aerodynamic characteristics of two hypersonic cruise aircraft concepts at Mach Numbers of 2.96, 3.96, and 4.63, NASA-TP-1767
37. Domack CS, Dollyhigh SM, Beissner Jr FL, Geiselhart KA, McGraw Jr ME, Shields EW, Swanson EE (1990) Concept development of a Mach 4 high-speed civil transport, NASA-TM-4223-December-1990
38. Haria R (2013) The day a spy plane broke aviation week, *Aviation Week & Space Technology*, November 5, 2013
39. Krikellas D (2003) Improvement of the performance of a turbo-ramjet engine for UAV and missile applications, M.Sc thesis, Naval Postgraduate School

Chapter 7

Shaft Engines Turboprop, Turboshaft, and Propfan

7.1 Introduction

This chapter introduces three types of shaft aero engines, namely, turboprop, turboshaft, and propfan engines. Piston engines together with these three engine types complete the group of shaft engines. Turboprop engines have their exhaust gases leaving the engine at very low speeds, while the exhaust leaves turboshaft engines at nearly zero speeds. Power rather thrust is the key factor in both. Turboprop engines power many commuter and heavy transport aircrafts flying at moderate subsonic speeds. Turboprop engine is composed of two main parts, namely, gas turbine and propeller. Gearbox couples the propeller to the driving turbine.

Turboshaft engines are employed in most helicopters, some tanks, and boats as well as some race cars. In a turboshaft engine, the gearbox is not connected to a propeller but to some other drive devices, namely, rotor(s) in helicopters and marine screws in boats, etc. Turboshaft engines employed in other applications are identified as industrial gas turbines which are extensively employed in petroleum industry and electrical power station.

Propfan engines combine many features of both turbofan and turboprop engines. However, it is distinct from both. The engine uses a [gas turbine](#) to drive an unshielded [propeller](#) like a turboprop, but the propeller itself is designed with a large number of short, highly twisted blades, similar to the fan of a turbofan engine. Propfan engines have the highest propulsive efficiency among all air-breathing engines including shaft-based, ram-based, and turbine-based engines.

7.2 Turboprop Engines

7.2.1 Introduction

Many bush airplanes (like Cessna Caravan and Quest Kodiak) (Fig. 7.1) which are low-speed transport/cargo aircraft and small commuter aircraft use turboprop propulsion. However, some large military and civil aircrafts, such as the [Lockheed L-188 Electra](#) (Fig. 7.2) and the [Tupolev Tu-95](#), use turboprop engines also. A distinguished application for turboprop engines is the Bell Boeing V-22 Osprey; Fig. (7.3), multi-mission, a tilt-rotor military aircraft that has both a vertical takeoff and landing (VTOL) and short takeoff and landing (STOL) capabilities. It is powered by Rolls Royce Allison T406 turboshafts.

The turboprop uses a gas turbine core to turn a propeller. As mentioned in Chap. 4, propeller engines develop thrust by moving a large mass of air through a small change in velocity. Propellers are very efficient and can use nearly any kind of engine to turn the prop. The propeller is driven through a reduction gear by either the compressor–turbine shaft or a power (or free power) turbine shaft. The [reduction gearbox](#) converts the high [RPM](#)/[low torque](#) output to a low RPM/high torque. Turboprop power is measured in total equivalent power (either measured in horse-power or kilowatts). The major part of this total equivalent power is generated by the propeller, while its minor part is developed from the exhaust gases.

Turboprops have higher propulsive efficiency than turbojet and turbofan engines when they fly under 30,000 ft and speeds below 400–450 mph. This is due to the low jet velocities of both the propeller and exhaust. Propellers become less efficient as the speed of the aircraft increases. In this case, the flow may reach or even exceed



Fig. 7.1 A Cessna 208B SKS Caravan (Courtesy [1])



Fig. 7.2 Lockheed L-188 Electra

sonic speed along the outer portion of its blades giving rise to a substantial increase in drag coefficient and awful decrease in lift coefficient.

Turboprop engines may be single, double, or triple spools. For a single-spool engine, the only one turbine drives the only one compressor and propeller (Fig. 7.4). A two-spool turboprop is composed of one or two compressors and two turbines (high pressure and low pressure). The low-pressure turbine drives either the single compressor or the low-pressure compressor (if two compressors are present) and also drives the propeller (Fig. 7.5). Finally the three-spool engine features three turbines and two compressors. The propeller is driven by the low-pressure turbine (Fig. 7.6). The exhaust velocity of a turboprop is low and contributes little thrust because most of the energy of the core hot gases has gone into turning the drive shaft.

Moreover, the turboprop engine may be either of the pusher or tractor (puller) type. Pusher types are installed to either the wing or fuselage. Two possible wing locations are seen, namely, midwing or wing tip. Concerning fuselage, turboprops are either installed to the aft pylon or aft end [2].

Tractor types have three possible types of installation, namely, wing, fuselage, and tail. Turboprops are either installed to the mid or tip of the wing. Concerning fuselage, two possible locations are seen, namely, forward or aft-fuselage pylon. Finally tail installation shows three possible positions, namely, low, median, or tip of the horizontal tail [3].

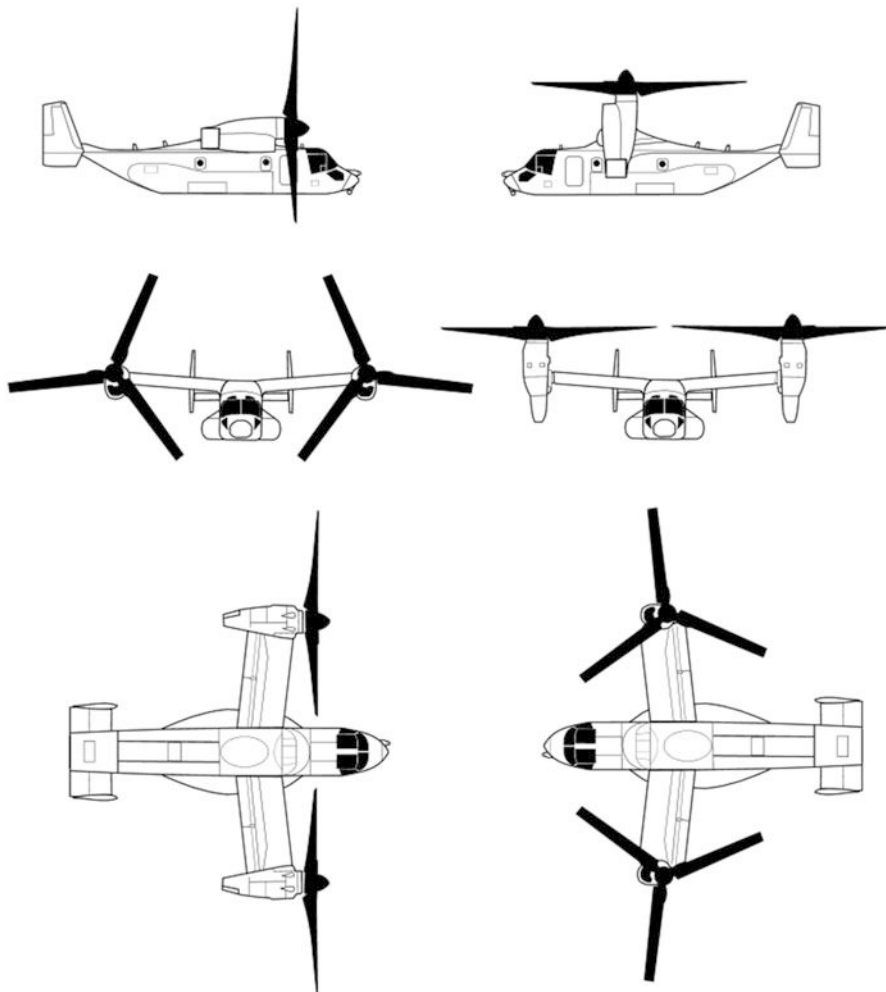


Fig. 7.3 Bell Boeing V-22 Osprey

7.2.2 Milestones

The early name of turboprop engine was “airscrew turbine engine” which was later given the neater title of turboprop.

Hungarian Gyorgy Jendrassik designed the very first working turboprop engine in 1938, called the “Cs-1.” It was produced and flown in Czechoslovakia (1939–1942). The engine was fitted to the Varga XG/XH twin-engined reconnaissance bomber but proved very unreliable.

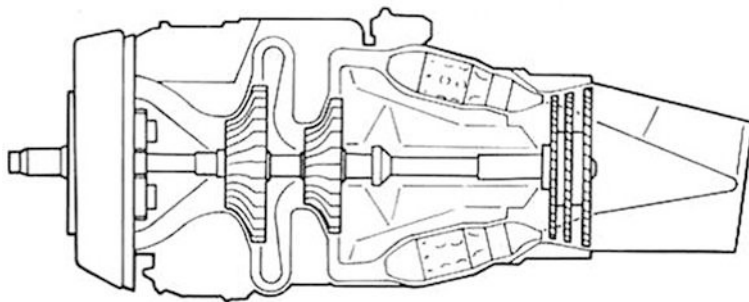


Fig. 7.4 Single-spool turboprop engine (Reproduced by permission from Rolls-Royce plc.)

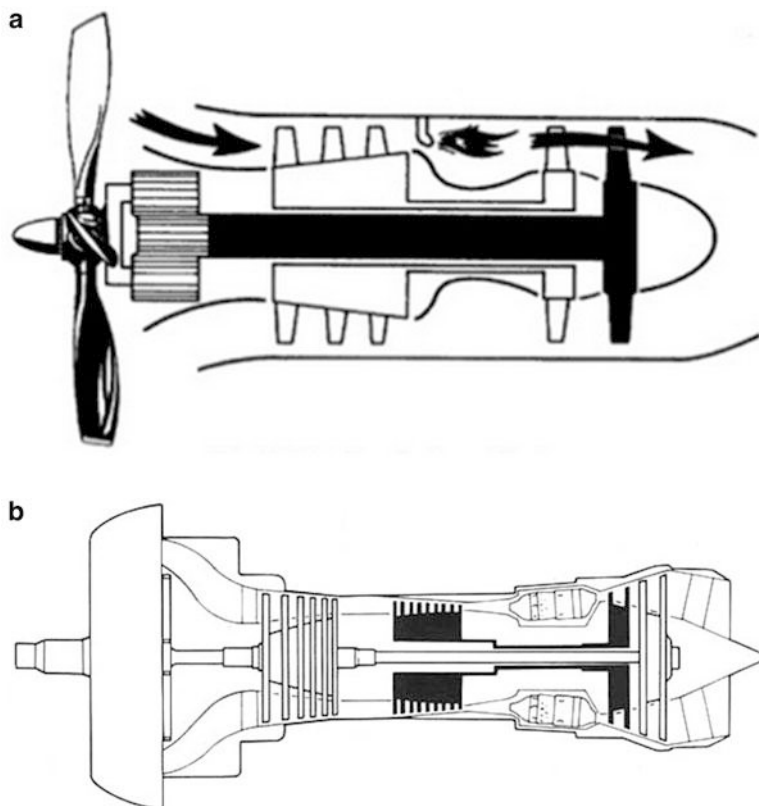


Fig. 7.5 Twin-spool turboprop: (a) LPT drives propeller and (b) LPT drives both LPC and propeller (Fig. 7.5b is reproduced by permission from Rolls-Royce plc.)

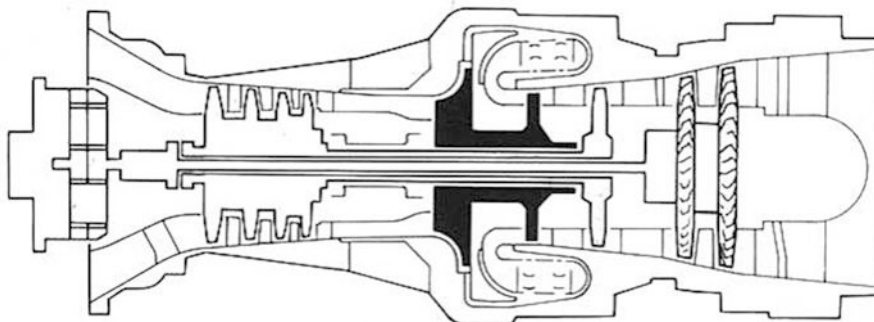


Fig. 7.6 Three-spool turboprop engine (Reproduced by permission from Rolls-Royce plc.)

Since the 1940s, Rolls-Royce built several turboprop engines. Examples are the following:

- RB50 Trent which powered the world's first turboprop-powered aircraft; Gloster Meteor flew on September 20, 1945.
- Clyde (August 1945) which powered [Westland Wyvern TF Mk.2](#) strike aircraft.
- DART which powered several aircrafts including Fairchild Industries' F-27 and Grumman Gulfstream. More than 7100 Darts were sold, flying over 130 million hours.
- Tyne, (April 1955), which is a two-spool engine driving through a double-epicyclic gearbox and a four-blade reverse propeller.
- Merlin (1965–1998) powered Swearingen SA226-T.
- AE2100 which powered Saab 2000.

Another British manufacturer was the Bristol which built:

- Theseus that powered the Avro Lincoln aircraft (July 1945).
- Proteus that flew millions of hours and still drives the biggest hovercraft across the British Channel (Jan 1947).

A third British manufacturer is Armstrong Siddeley, which built:

- Python that powered the Westland Wyvern carrier strike fighter (April 1945)
- Mamba which powered Douglas C-47B Dakota and Double Mamba, which powered the Fairey Gannet (April 1946)

The first American turboprop manufacturer was General Electric which built:

- T-31, the first American turboprop engine that powered Consolidated Vultee XP-81 and first flew on December 21, 1945. The T-31 was mounted in the nose with the J-33 turbojet mounted in the rear fuselage to provide additional thrust. Similar turboprop/turbojet combinations were also used in the Navy XF2R-1 aircraft.
- T-56 turboprop powering the Lockheed Martin C-130-H and C-2A Greyhound.
- T-64 powering de Havilland Canada DHC-5 and Buffalo aircraft.

Another *US* aero engine manufacturer is *Allison* which produced several turboprop engines:

- GMA 2100 powering L100/C-130J
- T56-A-11 powering AC-130A
- T406 turboshaft engine that powers Bell Boeing V-22 Osprey aircraft

A third *US* manufacturer for turboprop engines is *AlliedSignal* (previously Garrett AiResearch) that produced the famous TPF331 turboprop engine, which powered, for example, the Embraer/FAMA CBA-123. It is one of the few pusher turboprops in recent days.

In the *Soviet Union*, the *Kuznetsov Design Bureau* produced in the 1950s the NK-12 turboprop engine that powered Tu-95 strategic bomber, with propellers that had supersonic tip speeds.

A second *Russian* turboprop manufacturer is *Kirill Klimov Experimental Design Bureau*. An example for its engines is Klimov TV7-117 that powers *Ilyushin Il-112* and *Ilyushin Il-114*.

A *Ukrainian* company is *Motor Sich*, which is one of the largest engine manufacturers for airplanes and helicopters worldwide. It produced:

- AI- 20D Series powering the AN-32 aircraft
- AI-24 installed in the AN-24 aircraft servicing short- and medium-haul routes

A *Canadian* famous company *Pratt & Whitney of Canada (PWC)* built a big family of the popular turboprop/turboshaft engine including PT6, PT6A, PT6B, PT6C, PT6D, and ST6 as well as PW100 and PW200. The PT6A comes in 65 different versions with engine power ranging from 500 to 2000 shp. Since the PT6A family entered service in the 1960s, about 40,000 engines have been produced. To date, the PT6A has accumulated about 300 million flying hours and is therefore a highly proven and durable engine. It powers numerous aircraft including Beechcraft 1900, Dornier DO 128-6, Bell412, and Sikorsky S58T.

In *France*, Turbomeca began producing small turboprop engines in 1947 like:

- *Marcadau*, first turboprop built in 1953 generating 400 hp
- *Bastan* in 1957 which develops 800–1100 shp
- *Astazou* in 1957 developing 523–644 hp which is the most famous French turboprop that powered many aircrafts including Mitsubishi MU-2 and *Dornier Do27T-1*

Other worldwide companies include:

Italian Fiat that built the turboprop T64-P4D which powered G222RM

Japanese company *IHI* that built T56-IHI-14 and T58-IHI-110 turboprops, which powered the P-3C and KV-107

EPI Europrop International GmbH created by the four leading European aero engine companies (Industria de Turbo Propulsores, MTU Aero Engines, Rolls-Royce, and Snecma) that produced the three-shaft TP400-D6 turboprop (11,000 shp) which powers Airbus A400M military transport

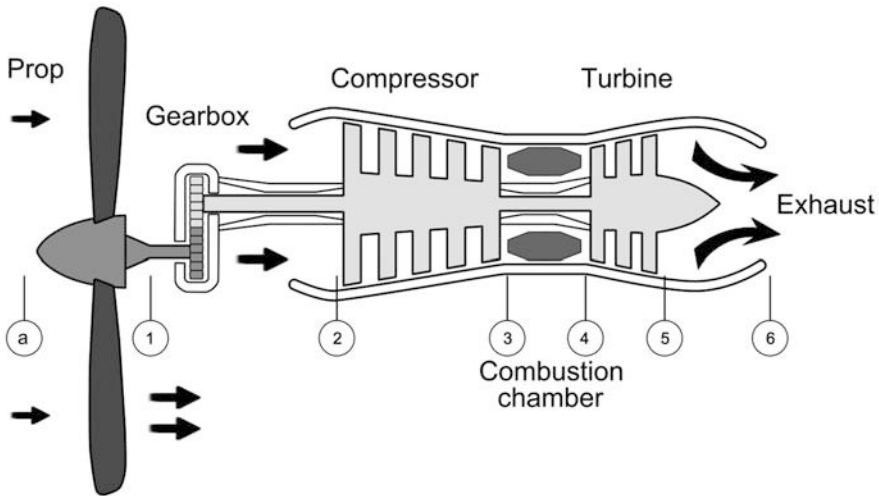


Fig. 7.7 Layout of a single-spool (direct drive turboprop engines)

7.2.3 Thermodynamics Analysis of Turboprop Engines

The different modules of a turboprop engine are the intake or inlet, one or two compressors, a combustion chamber, and one or more (up to three) turbines and the exhaust nozzle.

7.2.3.1 Single-Spool Turboprop

A simplified layout of a single-spool turboprop engine together with its temperature–entropy (T-s) diagram is shown in Figs. 7.7 and 7.8.

The same procedure followed in Chaps. 5 and 6 will be followed here. The flight speed is expressed as $U = M_a \sqrt{\gamma R T_a}$.

The different modules of the engine are treated hereafter.

1. Intake

The intake has an isentropic efficiency (η_d), and the ambient temperature and pressure are (P_a and T_a , respectively), and the flight Mach number is M_a . The temperature and pressure at the intake outlet are T_{02} and P_{02} which may be calculated using the same governing equations described in Chap. 5.

2. Compressor

For a known compressor pressure ratio (π_c) and its isentropic efficiency (η_c), the outlet temperature and pressure are calculated as in Chap. 5. The specific power of the compressor is given by the following relation:

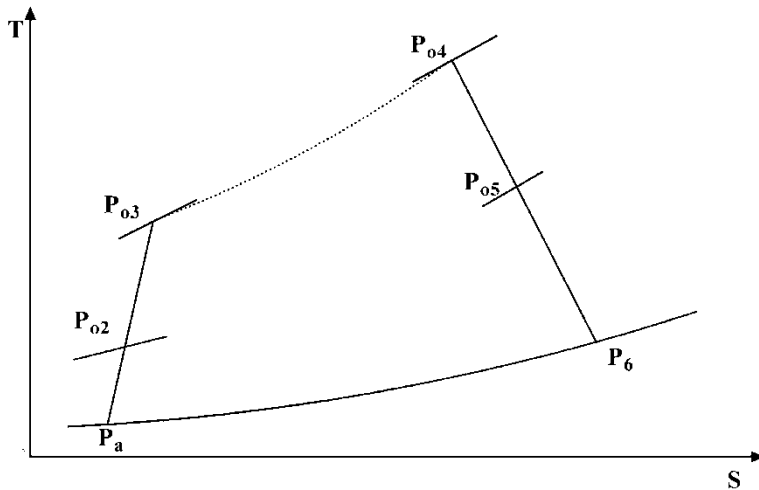


Fig. 7.8 Temperature–entropy diagram of a single-spool turboprop

$$\Delta h_c = Cp_c(T_{03} - T_{02}) \quad (7.1)$$

3. Combustion chamber

With known combustor efficiency of (η_b) and pressure drop in combustor of (ΔP), then the pressure at the outlet of the combustion chamber and fuel-to-air ratio are calculated in the same way as in Chap. 5.

4. Turbine

Since the turbine drives the compressor as well as the propeller and the portion of power transferred to each is not known in advance, then it is not easy here to determine the outlet pressure and temperature of the turbine. Let us first examine the power transmission from the turbine to the propeller as illustrated in Fig. 7.9.

Only a portion of the turbine power is delivered to the propeller. This propeller power is dependent on several efficiencies, namely, the mechanical efficiencies of turbine, compressor, and propeller, namely, (η_m , η_{mc} , η_g) as well as the propeller efficiency (η_{pr}). Figure 7.9 illustrates the enthalpy–entropy diagram for the expansion processes through both the turbine and the exhaust nozzle. It has been shown by Lancaster [4] that there is an optimum exhaust velocity that yields the maximum thrust for a given flight speed, turbine inlet temperature, and given efficiencies. Now define the following symbols as shown in Fig. 7.9.

Δh = enthalpy drop available in an ideal (isentropic) turbine and exhaust nozzle.

$\alpha\Delta h = \Delta h_{is}$ = fraction of Δh that would be available from an isentropic turbine having the actual pressure ratio.

$\Delta h_{ns} = (1 - \alpha)\Delta h$ = the fraction of Δh that may be available from an isentropic nozzle.

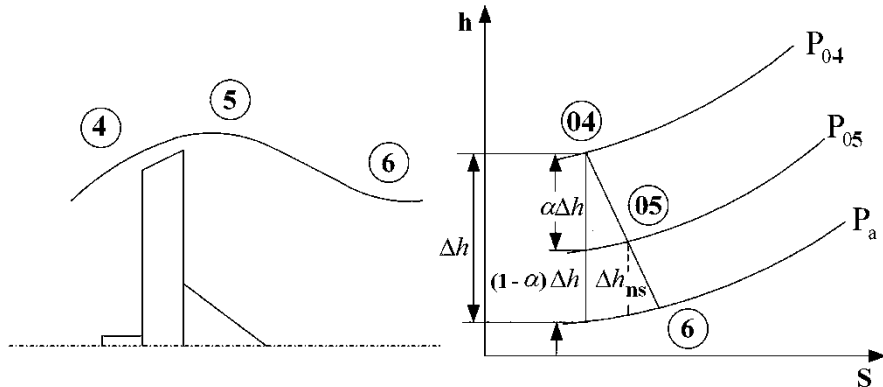


Fig. 7.9 Expansion in the turbine and nozzle of a single-spool turboprop

η_t = isentropic efficiency of turbine.

η_n = isentropic efficiency of the exhaust nozzle.

Now these parameters will be evaluated from the following thermodynamic relations:

$$\Delta h = Cp_t T_{04} \left[1 - \left(\frac{P_a}{P_{04}} \right)^{\frac{\gamma_h-1}{\gamma_h}} \right] \quad (7.2)$$

It was assumed in Eq. (7.2) that the ratios between specific heats within the turbine and nozzle are constant, or

$$\gamma_t = \gamma_n = \gamma_h$$

The exhaust gas speed (U_e) is given by the relation

$$\begin{aligned} \frac{U_e^2}{2} &= \eta_n (1 - \alpha) \Delta h \\ U_e &= \sqrt{2(1 - \alpha) \Delta h \eta_n} \end{aligned} \quad (7.3)$$

The procedure to be followed here is to deduce a mathematical expression for the thrust force generated by the propeller (T_{pr}) from the power generated by the propeller. Adding this thrust to the thrust generated by the exhaust gases then the total thrust is obtained as a function of (α). Differentiate this total thrust with respect to (α), we can obtain the optimum value of α giving the maximum thrust.

The propeller thrust T_{pr} is correlated to the propeller power by the relation

$$T_{pr} = \frac{\dot{m}_a \eta_{pr} \eta_g W_{shaft}}{U}$$

The shaft power is $W_{shaft} = \eta_{mt}(1 + f - b)\Delta h_t - \frac{\Delta h_c}{\eta_{mc}}$

where the turbine specific power is $\Delta h_t = \eta_t \alpha \Delta h$

(\dot{m}_a) is the air induction rate per second, and the fuel-to-air ratio and the bleed ratio are defined as $f = \frac{\dot{m}_f}{\dot{m}_a}$ and $b = \frac{\dot{m}_b}{\dot{m}_a}$

$$T_{pr} = \frac{\dot{m}_a \eta_{pr} \eta_g}{U} \left[(1 + f - b) \eta_{mt} \eta_t \alpha \Delta h - \frac{\Delta h_c}{\eta_{mc}} \right] \quad (7.4)$$

The thrust force obtained from the exhaust gases leaving the nozzle is denoted as (T_n) and is expressed by the relation

$$T_n = \dot{m}_a [(1 + f - b) U_e - U]$$

Total thrust $T = T_{pr} + T_n$

$$\begin{aligned} \frac{T}{\dot{m}} &= \frac{\eta_{pr} \eta_g}{U} \left[(1 + f - b) \eta_{mt} \eta_t \alpha \Delta h - \frac{\Delta h_c}{\eta_{mc}} \right] \\ &+ \left[(1 + f - b) \sqrt{2(1 - \alpha) \eta_n \Delta h} - U \right] \end{aligned} \quad (7.5)$$

Differentiate (7.5) with respect (α), we get the optimum value (α_{opt}) that maximizes the thrust T for fixed component efficiencies, flight speed (U), compressor specific power Δh_c , and expansion power Δh . This optimum value is expressed by Eq. (7.6):

$$\alpha_{opt} = 1 - \frac{U^2}{2\Delta h} \left(\frac{\eta_n}{\eta_{pr}^2 \eta_g^2 \eta_{mt}^2 \eta_t^2} \right) \quad (7.6)$$

This particular value of (α) defines the optimum power split between the propeller and the jet. Substituting this value (α_{opt}) in Eq. (7.5) gives the maximum value of the thrust force. The corresponding value of the exhaust speed is given by the following equation:

$$U_e = U \frac{\eta_n}{\eta_{pr} \eta_g \eta_{mt} \eta_t} \quad (7.7)$$

7.2.3.2 Two-Spool Turboprop

A schematic diagram of a two-spool engine having a free power turbine together with its temperature–entropy diagram is shown in Figs. 7.10 and 7.11. The low-pressure spool is composed of the propeller and the free power turbine, while the high-pressure spool is composed of the compressor and the high-pressure or gas generator turbine.

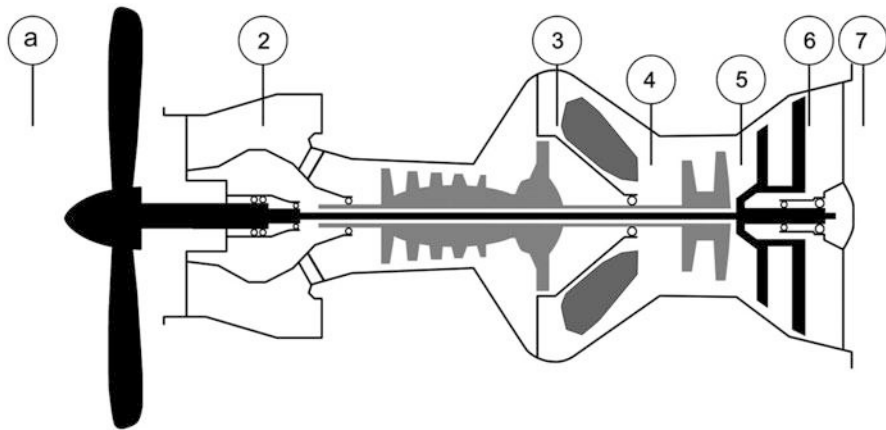


Fig. 7.10 Layout of a free power turbine turboprop engine

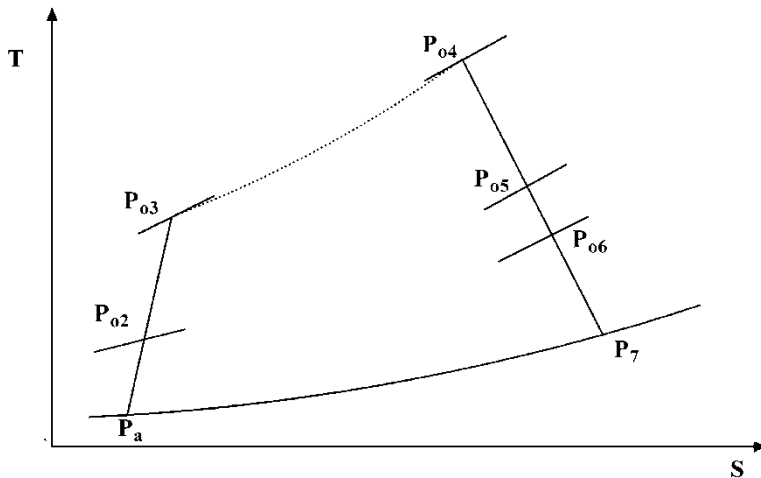


Fig. 7.11 Temperature–entropy diagram for a free power turbine

The different components are examined here:

1-Gas generator turbine

An energy balance between the compressor and this high-pressure turbine gives

$$\eta_{mt} \Delta h_t = \frac{\Delta h_c}{\eta_{mc}} \quad (7.8a)$$

The specific work generated in the turbine of the gas generator is

$$\Delta h_t = Cp_t(T_{04} - T_{05})(1 + f - b) \quad (7.8b)$$

From Eq. (7.8) with known turbine inlet temperature, then the outlet temperature (T_{05}) is calculated from the relation

$$T_{05} = T_{04} - \frac{Cp_c(T_{03} - T_{02})}{Cp_t \eta_{mc} \eta_{mt}(1 + f - b)}$$

Moreover, from the isentropic efficiency of the gas generator turbine, the outlet pressure (P_{05}) is calculated from the relation

$$P_{05} = P_{04} \left[1 - \left(\frac{T_{04} - T_{05}}{\eta_t T_{04}} \right) \right]^{\frac{\gamma_t}{\gamma_t - 1}}$$

5-Free power turbine

The work developed by the free power turbine per unit mass inducted into the engine is

$$\Delta h_{ft} = Cp_{ft}(1 + f - b)(T_{05} - T_{06})$$

As noticed from the above equation and previously explained in Sect. 7.2.3.1, the temperature (T_{06}) is unknown and cannot be calculated. Then a similar procedure will be followed. Referring to Fig. 7.12, which defines the successive expansion processes in the free power turbine and the nozzle, we have

Δh = enthalpy drop available in an ideal (isentropic) turbine and exhaust nozzle, assuming a full expansion to the ambient pressure is assumed in the nozzle ($P_7 = P_a$), it is calculated as

$$\Delta h = Cp_t T_{05} \left[1 - \left(\frac{P_7}{P_{05}} \right)^{\frac{\gamma_t - 1}{\gamma_t}} \right]$$

$\alpha \Delta h = \Delta h_{fts}$ which is the fraction of Δh that would be available from an isentropic free power turbine having the actual pressure ratio

$$\Delta h_{ft} = \eta_{ft} \Delta h_{fts}$$

η_{ft} = isentropic efficiency of the free power turbine.

Following the same procedure described above to determine the optimum α , the propeller thrust and the exhaust thrust are determined from the relations

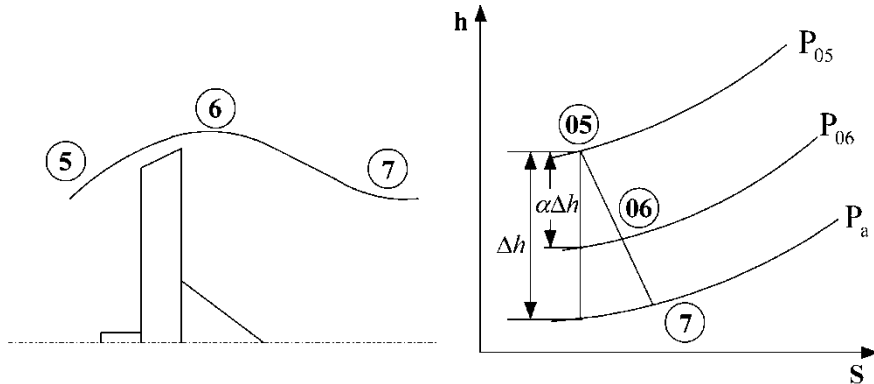


Fig. 7.12 Expansion in the turbine and nozzle of a double-spool turboprop

$$T_{pr} = \frac{\dot{m}_a \eta_{pr} \eta_g}{U} [(1+f-b)\eta_{mft}\eta_{ft}\alpha\Delta h] \quad (7.9)$$

$$T_n = \dot{m}_a [(1+f-b)U_e - U]$$

The total thrust is then $T = T_{pr} + T_n$

$$\frac{T}{\dot{m}} = \frac{\eta_{pr}\eta_g}{U} [(1+f-b)\eta_{mft}\eta_{ft}\alpha\Delta h] + \left[(1+f-b)\sqrt{2(1-\alpha)\eta_n\Delta h} - U \right] \quad (7.10)$$

where

η_{mft} = mechanical efficiency of the free power turbine.

Maximizing the thrust T for fixed component efficiencies, flight speed U and Δh yields the following optimum value of (α_{opt})

$$\alpha_{opt} = 1 - \frac{U^2}{2\Delta h} \left(\frac{\eta_n}{\eta_{pr}^2 \eta_g^2 \eta_{mft}^2 \eta_{ft}^2} \right) \quad (7.11)$$

Again, it can be mentioned that this particular value of (α) defines the optimum power split between the propeller and the jet. Substituting (α_{opt}) in Eq. (7.10) gives the maximum value of the thrust force. The corresponding value of the exhaust speed is given by the following equation:

$$U_e = U \frac{\eta_n}{\eta_{pr} \eta_g \eta_{mft} \eta_{ft}} \quad (7.12)$$

The outlet conditions at the free turbine outlet are easily calculated from the known value of (Δh) and (α_{opt}).

As alternatives to the parameter (α) discussed above, two methods may be followed:

1. Known exhaust speed.
2. Know the ratio between total and static pressures at nozzle outlet (χ); refer to [5].

7.2.4 Equivalent Engine Power

Here two flight phases will be discussed, namely, static run and cruise conditions.

7.2.4.1 Static Condition

During testing (on a test bench) or takeoff conditions, the total equivalent horsepower is denoted by t.e.h.p. and is equal to the s.h.p. of propeller plus the s.h.p. equivalent to the net jet thrust. For estimation purposes it is taken that, under sea-level static conditions, one s.h.p. is equivalent to approximately 2.6 lb of jet thrust [6]. Thus

$$(t.e.h.p.)_{Take-off} = s.h.p. + \frac{jet\ thrust(ib)}{2.6} \quad (7.13a)$$

Switching to SI units, experiments have shown also that [7] the total equivalent power (T.E.P.) in kW is related to the shaft power (S.P.) also in kW by the relation

$$\{T.E.P.(kW)\}_{Take-off} = S.P.(kW) + \frac{jet\ thrust(Newton)}{8.5} \quad (7.13b)$$

The thrust on test bench (ground testing) or during takeoff is given by

$$T = \dot{m}(1+f-b)U_e$$

7.2.4.2 Flight Operation

For a turboprop engine during flight, the equivalent shaft horsepower (e.s.h.p.) is equal to the shaft horsepower plus the jet thrust power as per the following relation:

$$e.s.h.p. = s.h.p. + \frac{T \times U}{\text{constant} \times \eta_{pr}} \quad (7.14a)$$

where the thrust is $T = \dot{m}[(1+f-b)U_e - U]$

The constant in Eq. (6.19a) depends on the employed units, thus

$$e.s.h.p. = s.h.p. + \frac{T(lb) \times U(\text{ft/s})}{550 \times \eta_{pr}} \quad (7.14b)$$

$$e.s.h.p. = s.h.p. + \frac{T(lb) \times U(\text{mph})}{375 \times \eta_{pr}} \quad (7.14c)$$

$$e.s.h.p. = s.h.p. + \frac{T(lb) \times U(\text{knots})}{325 \times \eta_{pr}} \quad (7.14d)$$

$$e.s.h.p. = s.h.p. + \frac{T(lb) \times U(\text{in ft/s})}{550 \times \eta_{pr}} \quad (7.14e)$$

Normally a value of $\eta_{pr} \approx 80\%$ is employed as industrial standards.

7.2.5 Fuel Consumption

As previously explained for turbojet and turbofan engines, the fuel consumption is identified by the thrust specific fuel consumption (*TSFC*) defined as $TSFC = \frac{\dot{m}_f}{T}$ and expressed in terms of $\frac{\text{kg fuel}}{\text{N.hr}}$.

For turboprop engines the fuel consumption is identified by the equivalent specific fuel consumption (*ESFC*) defined as

$$ESFC = \frac{\dot{m}_f}{ESHP} \quad (7.15)$$

and expressed in the following units $\frac{\text{lb fuel}}{\text{hp.hr}}$ or $\frac{\text{kg fuel}}{\text{kW.hr}}$

Typical values for ESFC [8] are $ESFC = (0.45 - 0.60) \frac{\text{lb fuel}}{\text{hp.hr}}$ or $(0.27 - 0.36) \frac{\text{kg fuel}}{\text{kW.hr}}$

Example 7.1 A two-spool turboprop engine with the propeller driven by a free power turbine is considered. It is required to calculate ESHP and ESFC in the following two cases:

(a) Static conditions

$$\dot{m}_f = 1500 \text{ lb/hr}, \quad T = 600 \text{ lb}_f, \quad \text{and} \quad SHP = 2800$$

(b) Flight conditions

$$V = 330 \text{ ft/s}, \quad \dot{m}_f = 1000 \text{ lb/hr}, \quad T = 300 \text{ lb}_f, \quad \text{and} \quad SHP = 2000$$

$$\eta_{pr} = 0.8$$

Solution

- (a) For static or ground run conditions, the equivalent shaft horsepower and equivalent specific fuel consumption are calculated from the relations:

$$\begin{aligned} ESHP &= SHP + \frac{T}{2.5} = 2800 + \frac{600}{2.5} = 3040 \text{ hp} \\ ESFC &= \frac{\dot{m}_f}{ESHP} = \frac{1500}{3040} = 0.4934 \quad \frac{\text{lb}}{\text{ESHP.hr}} \end{aligned}$$

- (b) During flight

$$\begin{aligned} ESHP &= SHP + \frac{T \times V}{550 \times \eta_{pr}} = 2000 + \frac{300 \times 330}{550 \times 0.8} = 2,250 \text{ hp} \\ ESFC &= \frac{\dot{m}_f}{ESHP} = \frac{1000}{2250} = 0.4494 \quad \frac{\text{lb fuel}}{\text{hp.hr}} \end{aligned}$$

Example 7.2 A double-spool turboprop engine is installed to an aircraft flying at a speed of 200 m/s and altitude of 6 km ($T_a = 249$ K and $P_a = 0.472$ bar). The maximum temperature is 1400 K and fuel heating value is 43,600 kJ/kg. It has the following particulars:

$m_a = 14.6 \text{ kg/s}$, $\pi_{LPC} = 8.5$, $\pi_{HPC} = 2.35$, $\Delta P_{CC} = 2\%$, $\eta_d = 0.92$, $\eta_{LPC} = 0.83$, $\eta_{HPC} = 0.85$, $\eta_{mLPC} = \eta_{mLPT} = 0.99$, $\eta_{C.C} = 0.98$, $\eta_{LPT} = 0.9$, $\eta_{HPT} = 0.92$, $\eta_n = 0.95$, $\eta_{pr} \times \eta_g = 0.8$, bleed percentage: $b = 0.0821$, $\alpha = 0.90$ $C_{P_c} = 1.005 \text{ kJ/kg K}$, $C_{P_t} = C_{P_n} = 1.148 \text{ kJ/kg K}$

It is required to calculate the following:

1. Equivalent brake horsepower (E.B.H.P)
2. Ratio between thrust forces generated by propeller and nozzle
3. Optimum alpha

Solution

This two-spool turboprop is composed of the following modules:

Intake (states 1–2), Low-pressure compressor (states 2–3) coupled from both sides to the LPT and propeller, High-pressure compressor (states 3–4), Combustor (states 4–5), High-pressure turbine (states 5–6) drives the HPC, Low-pressure turbine (states 6–7), Nozzle (states 7–8)

Successive analysis of the elements will be given here.

Intake

Sonic speed:

$$a = \sqrt{\gamma_c RT_a} = \sqrt{1.4 \times 287 \times 249} = 316.3 \text{ m/s}$$

$$M = U/a = 0.6323$$

$$T_{02} = T_a \left(1 + \frac{\gamma_c - 1}{2} M^2 \right) = 268.9 \text{ K}$$

$$P_{02} = P_a \left(1 + \eta_d \frac{\gamma_c - 1}{2} M^2 \right)^{\frac{\gamma_c}{\gamma_c - 1}} = 1.0736 \text{ bar} \quad P_a = 0.5067 \text{ bar}$$

Low-Pressure Compressor (States 2–3):

$$P_{03} = P_{02} \times \pi_{LPC} = 8.5 \times 0.5067 = 4.307 \text{ bar}$$

$$T_{03} = T_{02} \left(1 + \frac{\pi_{LPC}^{\frac{\gamma_c - 1}{\gamma_c}} - 1}{\eta_{LPC}} \right) = 268.9 \left(1 + \frac{8.5^{0.286} - 1}{0.83} \right) = 542.4 \text{ K}$$

The specific enthalpy rise is

$$\Delta h_{LPC} = Cp_c(T_{03} - T_{02}) = 274.87 \text{ kJ/kg}$$

High-Pressure Compressor (States 3–4):

$$P_{04} = P_{03} \times \pi_{HPC} = 10.1214 \text{ bar}$$

$$T_{04} = T_{03} \left(1 + \frac{\pi_{HPC}^{\frac{\gamma_c - 1}{\gamma_c}} - 1}{\eta_{HPC}} \right) = 542.4 \left(1 + \frac{2.35^{0.286} - 1}{0.85} \right) = 719 \text{ K}$$

Combustion Chamber (States 4–5):

$$P_{05} = (1 - \Delta P_{cc}) \times P_{04} = 0.98 \times 10.1214 = 9.919 \text{ bar}$$

$$f = (1 - b) \frac{Cp_{cc}T_{05} - Cp_cT_{04}}{\eta_b Q_R - Cp_{cc}T_{05}} = (1 - 0.0821) \frac{1.148 \times 1400 - 1.005 \times 719}{0.98 \times 43,600 - 1.148 \times 1400} \\ = 0.0197$$

High-Pressure Turbine (HPT) (States 5–6):

Energy balance between compressor and turbine

$$Cp_c(T_{04} - T_{03}) = (1 + f - b)Cp_h(T_{05} - T_{06})$$

$$\begin{aligned}
T_{06} &= T_{05} - \frac{Cp_c}{(1+f-b)Cp_h}(T_{04} - T_{03}) \\
&= 1400 - \frac{1.005}{1.148 \times 0.9376}(719 - 452) = 1234.7 \text{ K} \\
\frac{P_{06}}{P_{05}} &= \left[1 - \frac{1}{\eta_{HPT}} \left(1 - \frac{T_{06}}{T_{05}} \right) \right]^{\frac{\gamma_h}{\gamma_h-1}} = \left[1 - \frac{1}{0.92} \left(1 - \frac{1234.7}{1400} \right) \right]^4 = 0.57728 \\
P_{06} &= 5.726 \text{ bar}
\end{aligned}$$

Combined LPT and nozzle (States 6–8):

$$\begin{aligned}
\frac{T_{06}}{T_{8s}} &= \left(\frac{P_{06}}{P_a} \right)^{\frac{\gamma_h-1}{\gamma_h}} = \left(\frac{5.726}{0.472} \right)^{0.25} = 1.8662 \\
T_{8s} &= 661.6 \text{ K} \\
\Delta h &= Cp_h(T_{06} - T_{8s}) = 657.938 \text{ kJ/kg}
\end{aligned}$$

Low-pressure turbine (LPT):

The low-pressure turbine specific power is

$$\begin{aligned}
\Delta h_{LPT} &= \eta_{LPT} \alpha \Delta h \\
\Delta h_{LPT} &= 0.9 \times 0.9 \times 657.938 = 532.929 \text{ kJ/kg} \\
\text{But } \Delta h_{LPT} &= Cp_h(T_{06} - T_{07}) \\
\text{Since } \alpha \Delta h_{LPT} &= Cp_h(T_{06} - T_{07s}) \\
\text{Then } T_{07s} &= T_{06} - \frac{\alpha \Delta h_{LPT}}{Cp_h} = 1234.7 - \frac{0.9 \times 657.938}{1.148} = 718.9 \text{ K} \\
\frac{P_{06}}{P_{07}} &= \left(\frac{T_{06}}{T_{07s}} \right)^{\frac{\gamma_h}{\gamma_h-1}} = \left(\frac{1234.7}{718.9} \right)^4 = 8.7 \\
P_{07} &= 0.658 \text{ bar}
\end{aligned}$$

The shaft specific power is $W_{\text{shaft}} = \eta_{mLPT} (1+f-b) \Delta h_{LPT} - \frac{\Delta h_{LPC}}{\eta_{mLPC}}$

The propeller specific power P_{pr} is given by the relation

$$\begin{aligned}
\frac{P_{pr}}{\dot{m}_a} &= \eta_{pr} \eta_g \left[\eta_{mLPT} (1+f-b) \Delta h_{LPT} - \frac{\Delta h_{LPC}}{\eta_{mLPC}} \right] \\
\frac{P_{pr}}{\dot{m}_a} &= 0.8 \times \left(0.99 \times 0.9376 \times 532.929 - \frac{274.87}{0.99} \right) = 173.625 \text{ kJ/kg}
\end{aligned}$$

$$\frac{P_{pr}}{\dot{m}_a} = 173.625 \text{ kJ/kg}$$

The propeller thrust T_{pr} is correlated to the propeller power by the relation

$$\frac{T_{pr}}{\dot{m}_a} = \frac{P_{pr}}{\dot{m}_a} \times \frac{1}{U} = 868.12 \text{ N/kg}$$

Nozzle

The exhaust gas speed (U_e) is given by the relation

$$\begin{aligned}\frac{U_e^2}{2} &= \eta_n(1 - \alpha)\Delta h \\ U_e &= \sqrt{2(1 - \alpha)\Delta h\eta_n} \\ U_e &= \sqrt{2 \times 0.1 \times 0.95 \times 657,938} = 353.6 \text{ m/s}\end{aligned}$$

The thrust force obtained from the exhaust gases leaving the nozzle is denoted as (T_n) given by the relation

$$\begin{aligned}\frac{T_n}{\dot{m}} &= [(1 + f - b)U_e - U] = 131.5 \text{ N/kg} \\ \text{Total thrust } T &= T_{pr} + T_n \\ T &= \dot{m}_a \left(\frac{T_{pr} + T_n}{\dot{m}_a} \right) = 14.6 \times (868.12 + 131.5) = 14585 \text{ N} = 14.585 \text{ kN}\end{aligned}$$

Total equivalent power is

$$P = T \times U = 14.585 \times 200 = 2917 \text{ kW} = 3911.76 \text{ hp}$$

The ratio between propeller and nozzle thrust is

$$\frac{T_{pr}}{T_n} = \left(\frac{868.12}{131.5} \right) = 6.6$$

Optimum alpha

$$\begin{aligned}\alpha_{opt} &= 1 - \frac{U^2}{2\Delta h} \left(\frac{\eta_n}{\eta_{pr}^2 \eta_g^2 \eta_{mLPT}^2 \eta_{LPT}^2} \right) \\ \alpha_{opt} &= 1 - \frac{0.95}{2 \times 957,938} \left(\frac{200}{0.8 \times 0.99 \times 0.9} \right)^2 = 0.9609\end{aligned}$$

Example 7.3 For turboprop discussed in Example (7.2), plot:

1. The relation between total thrust and alpha
2. The relation between equivalent power and alpha

Solution

Total thrust:

$$\frac{T}{\dot{m}} = \frac{\eta_{pr}\eta_g}{U} \left[(1+f-b)\eta_{mt}\eta_t\alpha\Delta h - \frac{\Delta h_c}{\eta_{mc}} \right] + \left[(1+f-b)\sqrt{2(1-\alpha)\eta_n\Delta h} - U \right]$$

Substitution by the values of different parameters except for (α), we get

$$\frac{T}{\dot{m}} = 2150 \alpha + 1036\sqrt{(1-\alpha)} - 1256$$

Plotting the above equation for specific thrust versus (alpha) to get Fig. 7.13

$$\frac{P}{\dot{m}} = \eta_{pr}\eta_g \left[(1+f-b)\eta_{mt}\eta_t\alpha\Delta h - \frac{\Delta h_c}{\eta_{mc}} \right] + \left[(1+f-b)\sqrt{2(1-\alpha)\eta_n\Delta h} - U \right]$$

$$\frac{P}{\dot{m}} = 429,832 \alpha + 207,291\sqrt{(1-\alpha)} - 304,120$$

Plotting the above equation for specific thrust versus (alpha) to get Fig. 7.14

Fig. 7.13 Total thrust
versus alpha

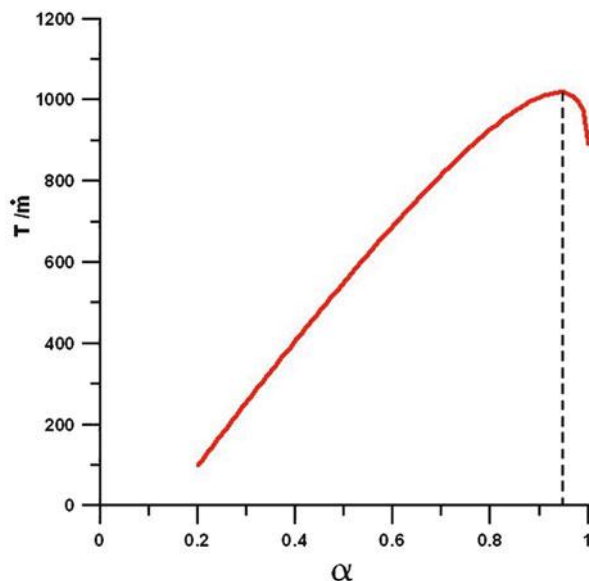
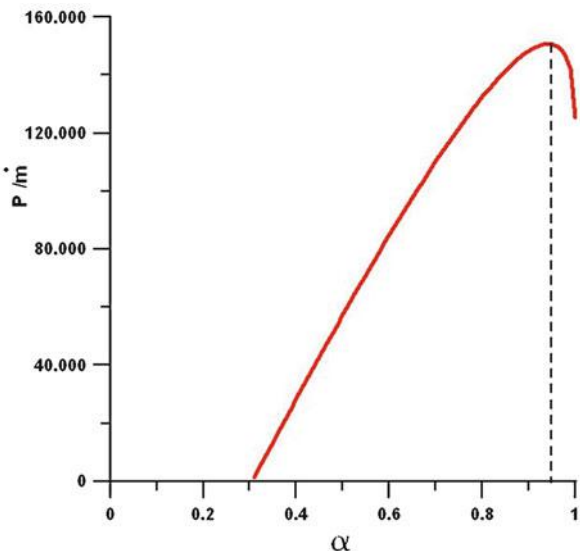


Fig. 7.14 Total power versus alpha



7.2.6 Analogy with Turbofan Engines

Turboprop engines are analogous to high-bypass turbofan engines. The propeller itself is an unducted fan with a bypass ratio equal to or greater than 25. The air flow through the propeller is slightly accelerated and thus acquires speeds slightly higher than the aircraft flight speed. The momentum difference between the inlet and outlet flows through the propeller produces the propeller thrust. Next this accelerated air passes through the engine core and accelerated to higher speeds. The momentum difference between the outlet and inlet core flow results in the core thrust. The thrust force is given by the relation

$$T = \dot{m}_0[(u_1 - u_0)] + \dot{m}_a[(1 + f - b)u_e - u_1] \quad (7.16a)$$

where \dot{m}_a is the core mass flow rate and \dot{m}_0 is the total mass flow rate.

Introducing the bypass ratio into Eq. (6.17a) to get

$$T = \dot{m}_a[\beta u_1 + (1 + f - b)u_e - (1 + \beta)u_0] \quad (7.16b)$$

The specific thrust related to the engine core mass flow rate to get

$$\frac{T}{\dot{m}_a} = [\beta u_1 + (1 + f - b)u_e] + (1 + \beta)u_0 \quad (7.16c)$$

7.3 Turboshaft

7.3.1 *Introduction*

A turboshaft engine is a form of [gas turbine](#) which is optimized to produce shaft power rather than jet thrust. Generally, a turboshaft engine is made up of two major parts assemblies: the “gas generator” and the “power section.” The gas generator consists of one or more [compressors](#), [combustion chamber](#), and one or more [turbines](#). The power section consists of an additional turbine, a [gear reduction](#) system, and the shaft output. The gas generator creates the hot expanding gases to drive the power section. Depending on the design, the engine accessories may be driven either by the gas generator or by the power section. In most designs, the gas generator and power section are mechanically separate so they can each rotate at different speeds.

Turboshaft engines are similar to turboprops, except that the hot gases are expanded to a lower pressure in the turbine, thus providing greater shaft power and little exhaust velocity. They differ primarily in the function of the turbine. Instead of driving a propeller, the turbine is connected to a transmission system that drives helicopter rotors. Other turboshaft engines that will be identified as industrial gas turbine engines are used for land and sea applications. Examples for land applications are electrical generators, compressors, pumps, auxiliary power units, pumping units for natural gas in cross-country pipelines, tanks, and race cars, where power turbine drives transmission system. Examples for marine applications are naval vessels, cargo ships, hydrofoils, hovercrafts, and other vessels, where power turbine drives marine screw. Many aero engine manufacturers produce two versions from an engine one as a turboprop while the other as a turboshaft engine. Examples are the PT6B and PW206 produced by Pratt & Whitney of Canada and AlliedSignal LTS101-600A-3 and Allison 250-C30M.

An unusual example of the turboshaft principle is the [Pratt & Whitney F135-PW-600](#) engines for the [STOVL F-35B](#). In conventional mode it operates as a turbofan, but when powering the [LiftFan](#), it switches partially to turboshaft mode to send power forward through a shaft (like a turboprop) and partially to turbojet mode to continue to send thrust to the rear nozzle.

Turboshaft power is measured in shaft horse power (shp), or kilowatts (KW).

7.3.2 *Examples for Turboshaft Manufacturers and Engines*

[Pratt & Whitney of Canada](#) (PWC) built a great family of its popular turboshaft engine PT6 and PT6A. It powers numerous helicopters including Sikorsky S58T.

[General Electric](#) built several turboshaft engines, including CT58 powering Sikorsky S-61, S-62, and Boeing Vertol CH-47 helicopters and the famous T700/CT7 turboshaft engines, which powers Bell AH-1 W Super Cobra.

Allison Engine Company in the early 1960s built *Allison Model 250*, and since Rolls-Royce acquired Allison in 1995 became the *Rolls-Royce M250*, (US military designations *T63* and *T703*). It powered many helicopters including: [Agusta A109A](#), [Bell 206B/L/LT](#), [Bell 407](#), 230, and 430, and [Boeing AH-6](#).

The *Lycoming* company built Lycoming T-55-L-7C powering the Boeing Vertol Chinook CH-47 helicopter, Bell 309, and [Piper PA-48 Enforcer](#) [9].

Turbomeca built Arrius 2K1 which powers the Eurocopter EC120 Colibri used in tourism over New York City [10].

Rolls-Royce built numerous turboshaft engines such as Gem powering August-Westland Lynx helicopter and AE1107C-Liberty turboshaft that powers Bell Boeing V-22 Osprey.

Rolls-Royce *Turbomeca* RTM322 turboshaft engine that powered AgustaWestland Apache, AgustaWestland [AW101](#) and [NHI NH90](#).

Soloviev Design Bureau built one of the earliest *Russian* turboshaft engines, namely, D-25 V in 1957 having 4780 kW (5500 hp) that powered the Mi-6, Mi-10, and Mi-12 helicopters.

The Ukrainian three-spool turboshaft engine D-136 Series 1 powers the MI-26 transport helicopters that are the largest in the world. Other famous Ukrainian turboshaft engines are the TB3-117 BMA used to power the KA helicopters and the TB3-117 BM powering the MI-17 and MI-8 AMT helicopters.

Example 7.4 Figure 7.15 illustrates a helicopter during hovering close to the ground. A control volume with inlet and outlet dimensions is also shown in figure. The total mass of the helicopter is 2000 kg. The exit static pressure is atmospheric. Assuming the flow is a one-dimensional, steady, and incompressible, calculate:

1. The exit velocity of air V_2
2. The power of the turboshaft engine

Solution

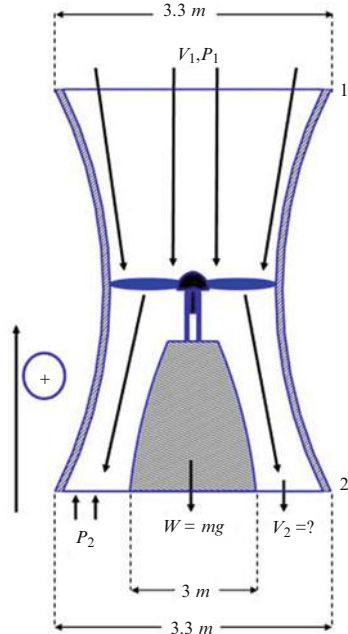
A control volume enclosing the helicopter with states (1) and (2) identifying upstream and downstream of the rotor is shown in Fig. 7.15. Both ends have a diameter of 3.3 m, while the helicopter body at outlet of control volume, state (2), is circular having a diameter of 3.0 m.

Continuity equation:

$$\begin{aligned}\dot{m}_1 &= \dot{m}_2 = \dot{m} \\ \dot{m} &= \rho_1 V_1 A_1 = \rho_2 V_2 A_2\end{aligned}$$

For an incompressible flow, then

$$V_1 = V_2 \left(\frac{A_2}{A_1} \right)$$

Fig. 7.15 Control volume

Momentum equation:

$$\bar{F}_S + \bar{F}_B = \frac{\partial}{\partial t} \int_{C.V.} \bar{V} \rho dV + \int_{C.S.} \bar{V} (\rho \bar{V} \cdot d\bar{A})$$

For a steady flow:

$$\begin{aligned} \bar{F}_S + \bar{F}_B &= \int_{C.S.} \bar{V} (\rho \bar{V} \cdot d\bar{A}) \\ P_{1g}A_1 - P_{2g}A_2 + mg &= \dot{m} (V_2 - V_1) \end{aligned}$$

where P_{1g} and P_{2g} are gauge pressures.

Moreover, from Bernoulli's Equation

$$P_{atm} + \frac{1}{2} \rho V_\infty^2 = P_1 + \frac{1}{2} \rho V_1^2$$

With $V_\infty = 0$

$$P_{1g} \equiv P_1 - P_{atm} = -\frac{1}{2} \rho V_1^2$$

From (A) $P_{1g}A_1 = -\frac{1}{2} \rho V_1^2 A_1 = -\frac{1}{2} \rho V_2^2 A_2 \frac{A_2}{A_1}$

With $P_{2g} = 0$, then from Eqs. (A) and (B)

$$\begin{aligned} m g + P_{1g} A_1 &= \rho V_2 A_2 \left[V_2 - V_2 \left(\frac{A_2}{A_1} \right) \right] \\ m g - \frac{1}{2} \rho V_2^2 A_2 \frac{A_2}{A_1} &= \rho V_2 A_2 \left[V_2 - V_2 \frac{A_2}{A_1} \right] \\ m g &= \rho V_2^2 A_2 \left[1 - \frac{A_2}{2 A_1} \right] \end{aligned}$$

Thus : $V_2 = \sqrt{\frac{m g}{\rho A_2 \left[1 - \frac{A_2}{2 A_1} \right]}}$

Since; $A_1 = \frac{\pi}{4} (3.3)^2 = 8.553$, $A_2 = \frac{\pi}{4} (3.3^2 - 3^2) = 1.484$,

$$\rho = \frac{P}{R T} = \frac{101 \times 10^3}{287 \times 288} = 1.22 \text{ kg/m}^3$$

$$\therefore V_2 = \sqrt{\frac{2000 \times 9.81}{1.22 \times 1.484 \times \left[1 - \frac{1.484}{2 \times 8.553} \right]}} = \sqrt{\frac{19620}{1.6534}} = 108.93 \text{ m/s}$$

From equation (A), $V_1 = V_2 \left(\frac{A_2}{A_1} \right) = 18.9 \text{ m/s}$

Finally, applying the energy equation for the same control volume

$$\dot{Q} + \dot{W} = \int_{CS} \left(\frac{V^2}{2} \right) (\rho \bar{V} \cdot dA) + \frac{\partial}{\partial t} \int_{CV} V^2 \rho dV$$

For adiabatic flow, $\dot{Q} = 0$ and steady conditions $\frac{\partial}{\partial t} \int_{CV} V^2 \rho dV = 0$

$$\therefore \dot{W} = \dot{m} \left(\frac{V_2^2 - V_1^2}{2} \right)$$

Since $\dot{m} = \rho_2 V_2 A_2 = 1.22 \times 108.93 \times 1.484 = 197.22 \text{ kg/s}$

$$\text{then } \dot{W} = \dot{m} \left(\frac{V_2^2 - V_1^2}{2} \right) = \frac{1}{2} \times 197.22 \times [108.93^2 - 18.9^2] = 1134,831 \text{ W.}$$

The power of the turboshaft engine $\dot{W} = 1134.8 \text{ kW}$.

7.3.3 Thermodynamic Analysis of Turboshaft Engines

A turboshaft engine also has two configurations: either the load is driven by the same gas generator shaft (Fig. 7.16) or driven by the free power turbine (Fig. 7.17). The first configuration resembles a single-spool engine while the second is a two-spool one.

The load may be also installed either toward the cold or hot sections. Thermodynamic cycles are plotted on the temperature–entropy (T-s) diagram for single and

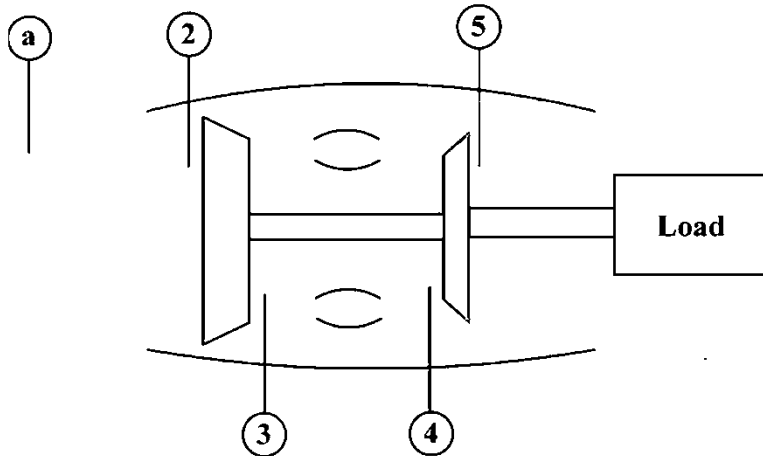


Fig. 7.16 Single-spool turboshaft engine

double spools are shown in Figs. 7.17 and 7.19. It is noted that the hot gases expand in the gas turbine (single spool) or free turbine (double spool) to nearly the ambient pressure. This provides a greater shaft power and little exhaust velocity.

7.3.4 Power Generated by Turboshaft Engines

7.3.4.1 Single-Spool Turboshaft

From Fig. 7.18, the analysis of diffuser, compressor, and combustion chamber is typical to that in turboprop engine.

Turbine

The turbine drives both of the compressor and load. Assuming full expansion in turbine to the ambient pressure, then the specific power delivered to the output shaft (W_{shaft}) is expressed as

$$W_{\text{shaft}} = (1 + f - b)\eta_{mt}W_t - \frac{W_c}{\eta_{mc}} \quad (7.17)$$

where f, b is the fuel-to-air ratio and bleed ratio. The mechanical efficiencies for turbine and compressor are, respectively, η_{mt}, η_{mc} .

This shaft which drives the load (here the rotor of a helicopter) experiences some mechanical losses due to friction in gearbox and bearings, thus

$$W_{\text{load}} = \eta_m W_{\text{shaft}} \quad (7.18)$$

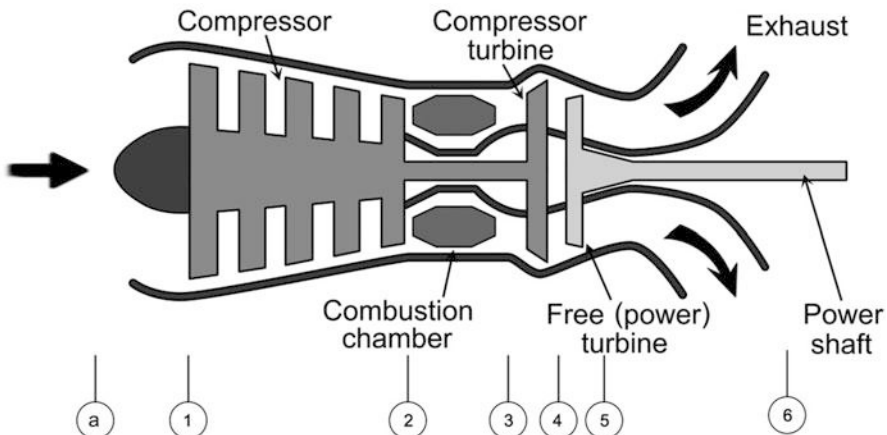


Fig. 7.17 Two-spool turboshaft engine

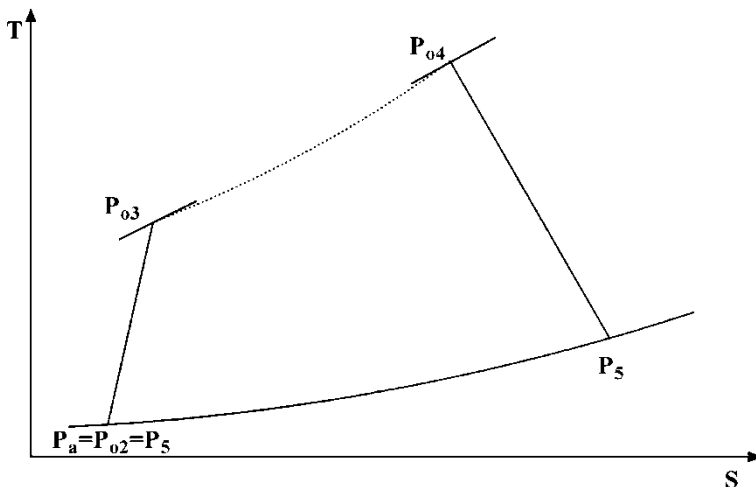


Fig. 7.18 T-s diagram for a single-spool turboshaft

The load power is then

$$P_{load} = \dot{m}_a W_{load} \quad (7.19)$$

7.3.4.2 Double-Spool Turboshaft

The diffuser, compressor, and combustion chamber also will be treated as in turboprop sections.

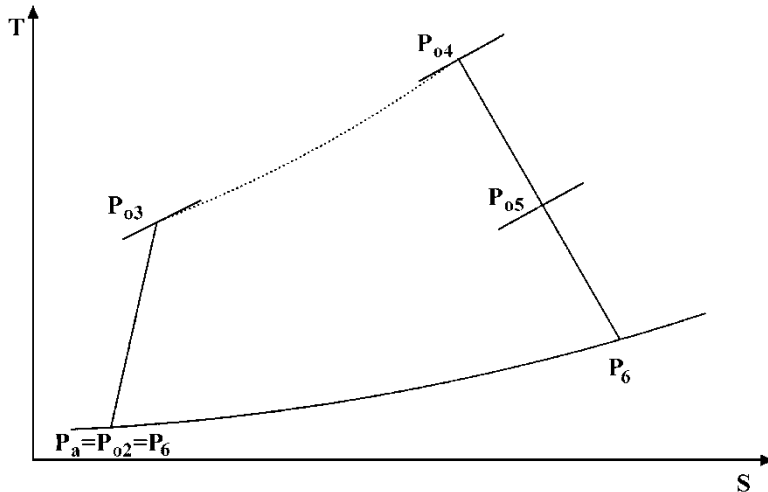


Fig. 7.19 T-s diagram for a double-spool turboshaft

Gas generator turbine

The turbine provides sufficient energy to drive the compressor; thus, the outlet temperature is obtained from the energy balance between the compressor and turbine, or

$$(1 + f - b)\eta_{mt}W_t = \frac{W_c}{\eta_{mc}}$$

$$T_{05} = T_{04} - \frac{Cp_c(T_{03} - T_{02})}{Cp_t\eta_{mc}\eta_{mt}(1 + f - b)} \quad (7.20)$$

and

$$P_{05} = P_{04} \left[1 - \left(\frac{T_{04} - T_{05}}{\eta_t T_{04}} \right)^{\frac{\gamma_t}{\gamma_t - 1}} \right] \quad (7.21)$$

Free power turbine

The gases are assumed to have a complete expansion to the ambient pressure; thus, the power delivered to the load is

$$P_{\text{load}} = \dot{m}_a(1 + f - b)\eta_m Cp_f T_{05} \left[1 - \left(\frac{P_a}{P_{05}} \right)^{\frac{\gamma_t - 1}{\gamma_t}} \right] \quad (7.22)$$

Example 7.5 Figure 7.20 illustrates Bell 206 helicopter that is powered by Allison 250-C20B turboshaft engine. Allison 250-C20 B is a two-spool turboshaft where



Fig. 7.20 Bell 206 helicopter

the gas generator is composed of a compressor driven by a gas turbine, while the power (free) turbine drives the helicopter rotor. The engine data are as follows:

Air mass flow rate is 1 kg/s.

Compressor pressure ratio is 6.2.

Turbine inlet temperature is 1258 K.

Fuel heating value is 43 MJ/kg.

Pressure drop in combustion chamber is 4 %.

Modules efficiencies are $\eta_c = 0.8$, $\eta_b = 0.96$, $\eta_{gt} = \eta_{pt} = 0.82$, $\eta_m = 0.98$.

For a ground operation

Calculate

1. Power delivered to the helicopter rotor
2. Specific fuel consumption

Solution

Figure 7.20 illustrates the layout for the two-spool turboshaft and its state numbering, while Fig. 7.19 illustrates its T-s diagram.

For ground operation:

Intake (a–2):

Outlet conditions $T_{02} = T_a = 288 \text{ K}$, $P_{02} = P_a = 101 \text{ kPa}$

Compressor (2–3):

Outlet conditions $P_{03} = \pi_c P_{02} = 6.2 \times 101 = 622.2 \text{ kPa}$

$$T_{03} = T_{02} \left(1 + \frac{\pi_c^{\frac{\gamma_c - 1}{\gamma_c}} - 1}{\eta_c} \right) = 288 \times \left(1 + \frac{6.2^{0.286} - 1}{0.8} \right) = 535 \text{ K}$$

Combustion chamber (3–4):

$$P_{04} = (1 - \Delta P_{cc}) \times P_{03} = 0.96 \times 622.2 = 601 \text{ kPa}$$

$$f = \frac{Cp_{cc}T_{05} - Cp_cT_{04}}{\eta_b Q_R - Cp_{cc}T_{05}} = \frac{1.148 \times 1258 - 1.005 \times 535}{0.96 \times 43,000 - 1.148 \times 1258} = 0.0228$$

Gas Turbine (States 4–5):

$$Cp_c(T_{03} - T_{02}) = \eta_m(1 + f)Cp_h(T_{04} - T_{05})$$

$$T_{05} = T_{04} - \frac{Cp_c}{\eta_m(1 + f)Cp_h}(T_{03} - T_a)$$

$$= 1258 - \frac{1.005}{0.98 \times 1.0228 \times 1.148}(535 - 288) = 1042 \text{ K}$$

$$\frac{P_{05}}{P_{04}} = \left[1 - \frac{1}{\eta_{gt}} \left(1 - \frac{T_{05}}{T_{04}} \right) \right]^{\frac{\gamma_h}{\gamma_h - 1}} = \left[1 - \frac{1}{0.82} \left(1 - \frac{1042}{1258} \right) \right]^4 = 0.3912$$

$$P_{05} = 235.126 \text{ kPa}$$

Power Turbine (States 5–6):

$$P_6 = P_a = 101 \text{ kPa}$$

$$T_6 = T_{05} \left[1 - \eta_{ft} \left\{ 1 - \left(\frac{P_a}{P_{05}} \right)^{\frac{\gamma-1}{\gamma}} \right\} \right]$$

$$T_6 = 1042 \times \left[1 - 0.82 \left\{ 1 - \left(\frac{101}{235.1} \right)^{0.25} \right\} \right] = 897.3 \text{ K}$$

$$w_{ft} = (1 + f)Cp_h(T_{05} - T_6) = 1.0228 \times 1.148 \times (1042 - 897.3) = 191 \text{ kJ/kg}$$

Power delivered to rotor is

$$P_{\text{rotor}} = \eta_m \dot{m}_a w_{f1} = 0.98 \times 1 \times 191 = 187.2 \text{ kW}$$

Specific fuel consumption

$$SFC = \frac{f\dot{m}_a}{P_{\text{rotor}}} = \frac{0.0228 \times 1}{187.2} = 1.2179 \times 10^{-4} \frac{\text{kg}}{\text{kW.s}} = 0.438 \frac{\text{kg}}{\text{kW.hr}}$$

Example 7.6 Kamov Ka-50 “Black Shark” (Fig. 7.21) is a single-seat Russian attack helicopter. It is powered by two *Klimov TV3-117 turboshaft* engines.

TV3-117 is a two-spool turboshaft engine having the following characteristics:

- Maximum power output: 1640 kW
- Turbine inlet temperature: 990 °C
- **Cruise speed:** 270 km/h
- **Service ceiling:** 5500 m
- Compressor pressure ratio: 9.4
- Fuel heating value: 44 MJ/kg
- Pressure drop in combustion: 2 %
- Modules efficiencies: $\eta_d = 0.92$,

$$\eta_c = 0.84, \eta_b = 0.98, \eta_{gt} = \eta_{pt} = 0.88, \eta_m = 0.99$$



Fig. 7.21 Kamov Ka-50 helicopter

Calculate

1. Air mass flow rate
2. Specific Fuel Consumption (SFC)

Solution

At service ceiling 5500 m: $T_a = 252.3 \text{ K}$, $P_a = 50.5 \text{ kPa}$

Flight speed: $V = \frac{270}{3.6} = 75 \text{ m/s}$

Sonic speed: $a = \sqrt{\gamma R T_a} = \sqrt{1.4 \times 287 \times 252.3} = 318.4 \text{ m/s}$

Flight Mach number: $M = \frac{V}{a} = 0.236$

Intake (a-2):

$$\text{Outlet conditions } T_{02} = T_a \left(1 + \frac{\gamma-1}{2} M^2 \right) = 255.1 \text{ K}$$

$$P_{02} = P_a \left(1 + \eta_d \frac{\gamma-1}{2} M^2 \right)^{\frac{1}{\gamma-1}} = 52.33 \text{ kPa}$$

Compressor (2-3):

$$\text{Outlet conditions: } P_{03} = \pi_c P_{02} = 492 \text{ kPa}$$

$$T_{03} = T_{02} \left(1 + \frac{\pi_c^{\frac{\gamma_c-1}{\gamma_c}} - 1}{\eta_c} \right) = 527.8 \text{ K}$$

Combustion chamber (3-4):

$$T_{04} = 990 + 273 = 1263 \text{ K}$$

$$P_{04} = (1 - \Delta P_{cc}) \times P_{03} = 482.2 \text{ kPa}$$

Fuel-to-Air Ratio

$$f = \frac{Cp_{cc} T_{05} - Cp_c T_{04}}{\eta_b Q_R - Cp_{cc} T_{05}} = \frac{1.148 \times 1263 - 1.005 \times 527.8}{0.98 \times 44,000 - 1.148 \times 1263} = 0.02206$$

Gas Turbine (States 4-5):

$$Cp_c(T_{03} - T_{02}) = \eta_m(1+f)Cp_h(T_{04} - T_{05})$$

$$\begin{aligned}
T_{05} &= T_{04} - \frac{Cp_c}{\eta_m(1+f)Cp_h}(T_{03} - T_{02}) \\
&= 1263 - \frac{1.005}{0.98 \times 1.02206 \times 1.148}(527.8 - 255.1) = 1025 \text{ K} \\
\frac{P_{05}}{P_{04}} &= \left[1 - \frac{1}{\eta_{gt}} \left(1 - \frac{T_{05}}{T_{04}} \right) \right]^{\frac{\gamma_h}{\gamma_h-1}} = \left[1 - \frac{1}{0.88} \left(1 - \frac{1025}{1263} \right) \right]^4 = 0.3814 \\
P_{05} &= 183.9 \text{ kPa}
\end{aligned}$$

Power Turbine (States 5–6):

$$\begin{aligned}
P_6 &= P_a = 50.5 \text{ kPa} \\
T_6 &= T_{05} \left[1 - \eta_{ft} \left\{ 1 - \left(\frac{P_a}{P_{05}} \right)^{\frac{\gamma-1}{\gamma}} \right\} \right] \\
T_6 &= 1025 \times \left[1 - 0.88 \left\{ 1 - \left(\frac{50.5}{183.9} \right)^{0.25} \right\} \right] = 794.9 \text{ K} \\
\frac{P_{\text{rotor}}}{\dot{m}_a} &= (1+f)C_{ph}(T_{05} - T_6) = 1.02206 \times 1.148 \times (1025 - 794.9) = 270 \text{ kJ/kg}
\end{aligned}$$

Since the power of rotor is 1640 kW, then the *air mass flow rate* (\dot{m}_a) is obtained as follows:

$$\dot{m}_a = \frac{P}{P/\dot{m}_a} = \frac{1640}{270} = 6.073 \frac{\text{kg}}{\text{s}}$$

Specific fuel consumption

$$SFC = \frac{f}{P_{\text{rotor}}/\dot{m}_a} = \frac{0.02206 \times 3600}{270} = 0.294 \frac{\text{kg}}{\text{kW.hr}}$$

7.4 Propfan

7.4.1 Introduction

A *propfan* is a modern type of aircraft engine related in concept to both the *turboprop* and *turbofan*, but distinct from both. The engine uses a *gas turbine* to drive an unshielded *propeller* like a turboprop, but the propeller itself is designed

with a large number of short, highly twisted blades, similar to the fan of a turbofan engine.

For this reason, the propfan has been variously described as an *unducted fan (UDF)*, *open rotors (OR)*, or *ultrahigh-bypass (UHB) turbofan*. It is described as “a small diameter, highly loaded multiple-bladed variable-pitch propulsor having swept wide-chord blades with thin advanced airfoil sections, integrated with a contoured nacelle”. Propfan is designed to operate with a turbine engine and using a single-stage reduction gear that results in high performance. The design is intended to offer the performance of a turbofan, with the fuel economy of a *turboprop*.

The most common arrangement of propfan is a two-spool gas generator and aft-located gearbox driving a pusher fan. This fan produces the majority of thrust. It has a number of blades greater than propellers of turboprops and less than those of fan in turbofans. Similarly its bypass ratio is also in-between of turbofan and turboprop engines.

7.4.2 *Historical Hints*

During the 1970s due to the oil crisis in 1973, several projects for developing propfans or unducted fan (UDF) were introduced. The propfan concept was first revealed by Carl Rohrbach and Bruce Metzger of the [Hamilton Standard](#) Division of United Technologies in 1975 and was patented by Robert Cornell and Carl Rohrbach of Hamilton Standard in 1979. Later work by General Electric on similar propulsors was done under the name *unducted fan*, which was a modified [turbofan](#) engine, with the fan placed outside the [engine nacelle](#) on the same axis as the [compressor](#) blades.

Perhaps one of the most significant series of propfan studies was conducted during the late 1970s and early 1980s. This effort culminated in flight tests of the McDonnell Douglas MD-UHB demo aircraft based on the [MD-81](#) airframe. The MD-UHB was used to evaluate advanced, experimental propulsion technologies designed to offer airlines significant improvements in fuel efficiency and lower operational costs.

The propfan concept was intended to deliver 35 % better fuel efficiency than contemporary turbofans. In static and air tests on a modified DC-9, propfans reached a 30 % improvement. This efficiency comes at a price, as one of the major problems with the propfan is noise, particularly in an era where aircraft are required to comply with increasingly strict Stage III and Stage IV noise limitations.

GE introduced its Unducted Fan (UDF) GE36 which featured an aft-mounted open-rotor fan system with two rows of counter-rotating composite fan blades during the mid-1980s. It is of the pusher configuration. The core was based on a GE F404 military turbofan. Exhaust gases were discharged through a seven-stage low-pressure (LP) turbine; each stator ring was designed to move freely in the opposite direction to that of the rotors. The turbine rotors drive one propeller, while

the other prop is connected to the “unearthed” turbine stators and rotates in the opposite direction. So, in effect, the power turbine has 14 stages (Fig. 7.22).

The GE36 flew on the Boeing 727 and MD-80 aircraft and enabled speeds of around Mach 0.75. McDonnell Douglas developed a proof-of-concept aircraft by modifying their MD-80. They removed the JT8D turbofan engine from the left side of the fuselage and replaced it with the GE36 (Fig. 7.22). A number of test flights were conducted which proved the airworthiness, aerodynamic characteristics, and noise signature of the design. The test and marketing flights of the GE-outfitted “Demo Aircraft” concluded in 1988, demonstrating a 30 % reduction in fuel burn over turbofan-powered MD-80, full Stage III noise compliance, and low levels of interior noise/vibration. Due to jet-fuel price drops and shifting marketing priorities, Douglas shelved the program the following year.

In the 1980s, Allison collaborated with Pratt & Whitney on demonstrating the 578-DX propfan, having a reduction gearbox between the LP turbine and the propfan blades. The 578-DX was successfully flight tested on a McDonnell Douglas MD-80 (Fig. 7.24).

The Progress D-27 propfan (Fig. 7.25), developed in the USSR, is even more conventional in layout, with the propfan blades at the front of the engine in a tractor configuration. It is used for propelling Antonov An-180 and An-70 aircrafts in the

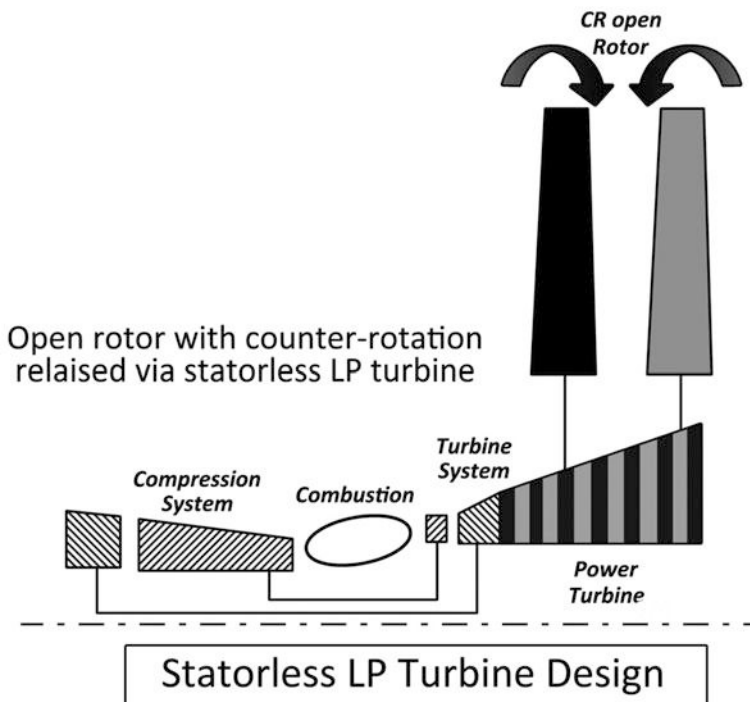


Fig. 7.22 Open rotor with counterrotation achieved via statorless LP turbine



Fig. 7.23 Unducted fan installed in MD-80

1990s. It is worth mentioning that the only flying aircraft powered by a propfan engine is AN-70.

Rolls-Royce is testing its contra-rotating propfan RB3011 which is planned to fly by 2020.

7.4.3 *Classifications of Propfans*

There are two main types of propfans:

1. Tractor type
2. Pusher type

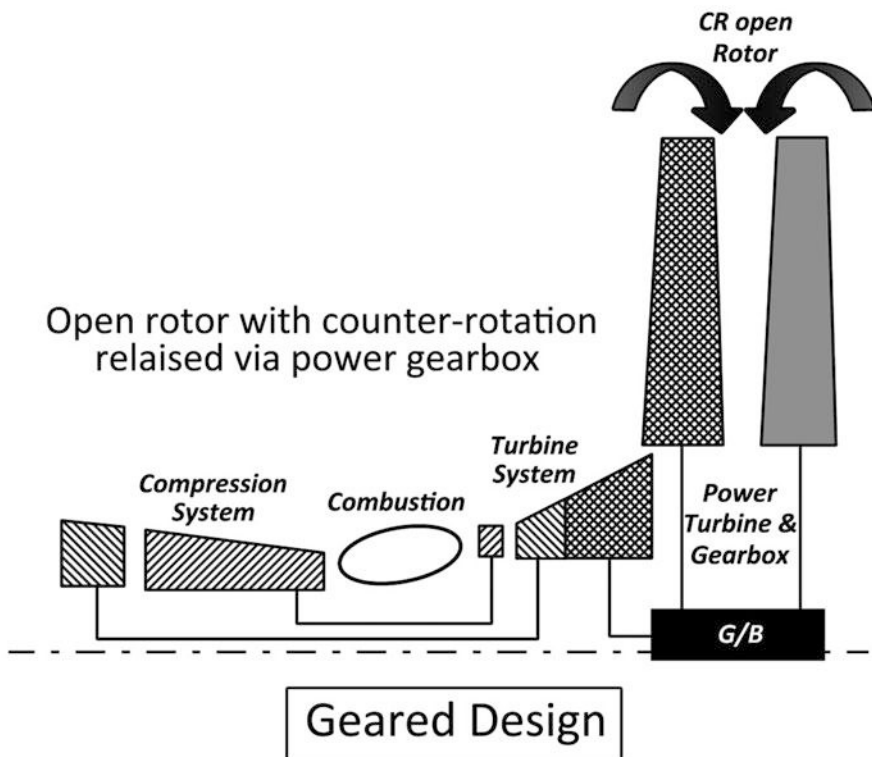


Fig. 7.24 Allison P&W 578DX geared propfan

1. *Tractor (or puller)-type* propfan is similar to forward fan with the fan placed outside the engine nacelle (Fig. 7.23). Propfans are normally of the wing installation type. Also such arrangement dictates a high-wing design.

This type is next divided into

- (A). Single (B). Contra-rotating (or counter-rotating)

An example is the contra-rotating propfan installed to the aircraft AN-70 (Fig. 7.26). *The forward rotor is 8 bladed, while the rear is six bladed.*

2. *Pusher-type* propfan is similar to the aft fan where the fan is coupled to the turbine. It is always of the contra-rotating type (Fig. 7.27). The two fan rows are driven by free power turbine. This type would be more elegant, as the engines would be placed behind the rear pressure bulkhead in the fuselage, minimizing noise. It also would allow for an aerodynamically “clean” wing.

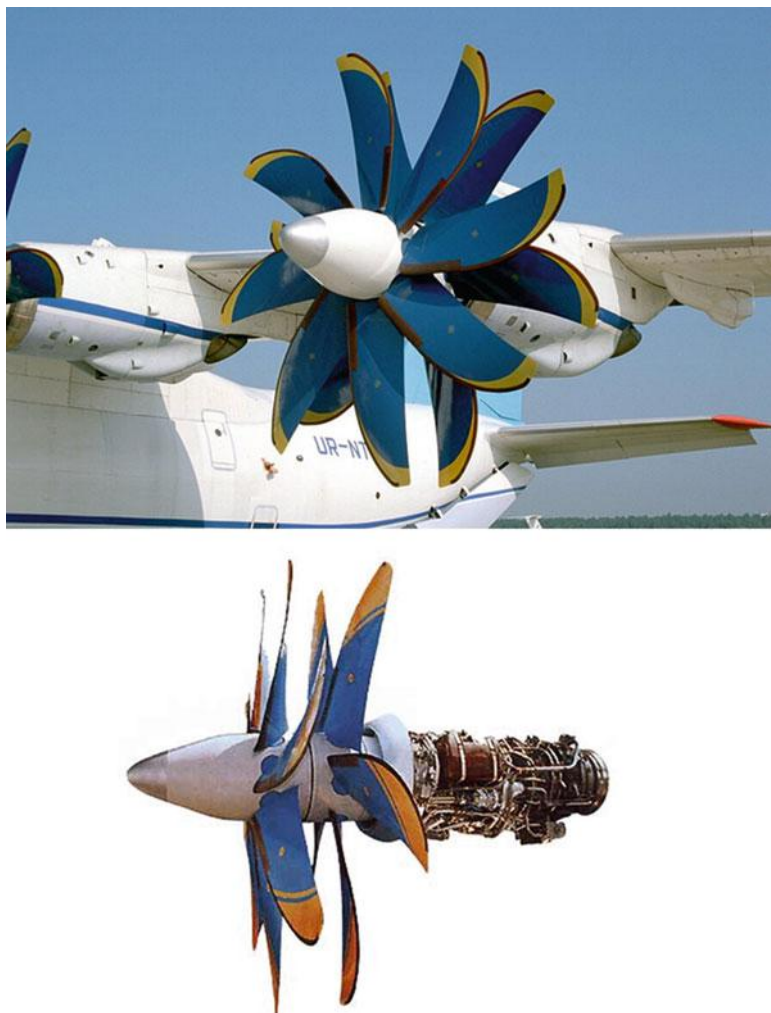


Fig. 7.25 AN-70 aircraft powered by tractor-type contra-rotating propfan

7.4.4 Comparisons Between Turboprop, Propfan, and Turbofan

Propfan engines have the best ever known propulsive efficiency. Single-rotation propfan engines have propulsive efficiency around 80 %, while contra-rotating propfan ones have higher efficiency close to 90 %. The main features of the propfan engines versus both turboprop and turbofan engines are given in the following Table 7.1.

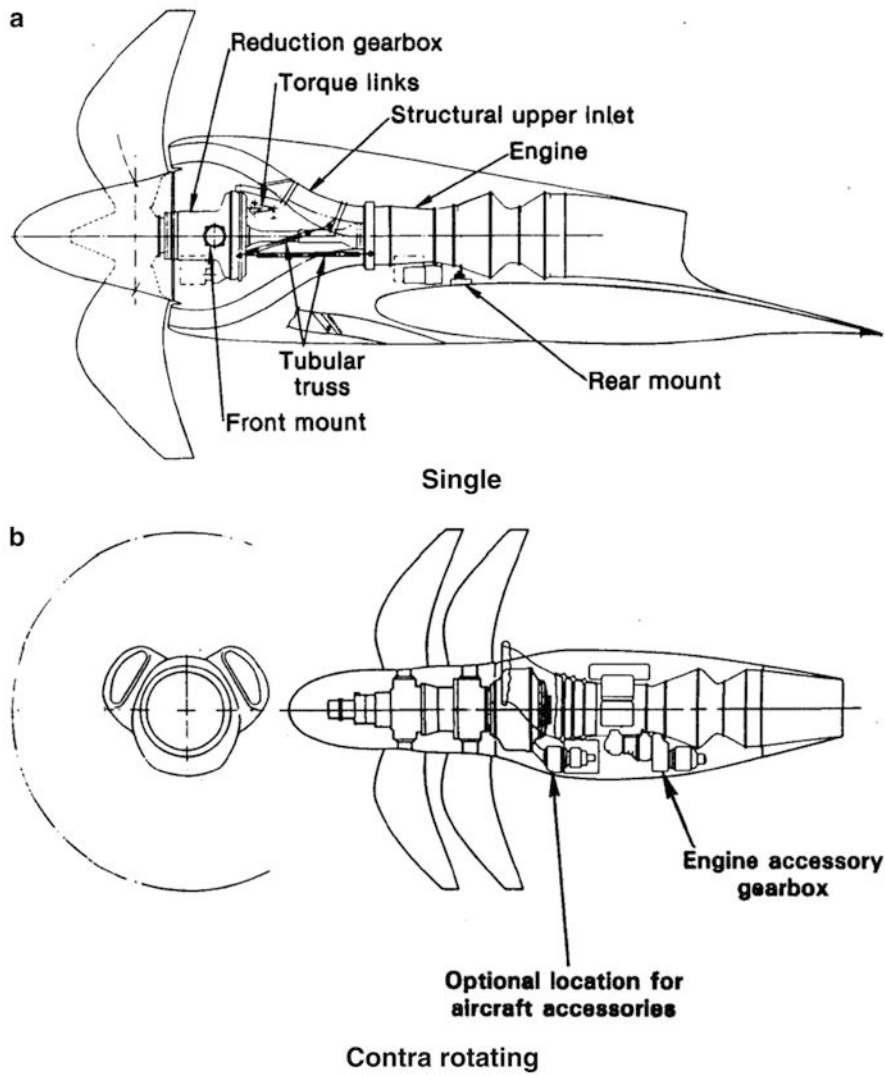


Fig. 7.26 Tractor-type propfan

Propfan engines have the highest propulsive efficiency, the potential to significantly reduce fuel consumption and emission relative to state-of-art high-bypass ratio geared turbofan engines [11] and [12]. Moreover, in terms of benefits to the aircraft operator and the environmental impact, relative to today's aircraft, a future open-rotor-powered aircraft could save approximately \$3 million and 10,000 tons of CO₂ per year per aircraft. Further consideration needs to be given to the trade-off between fuel burn (global) and noise (local).

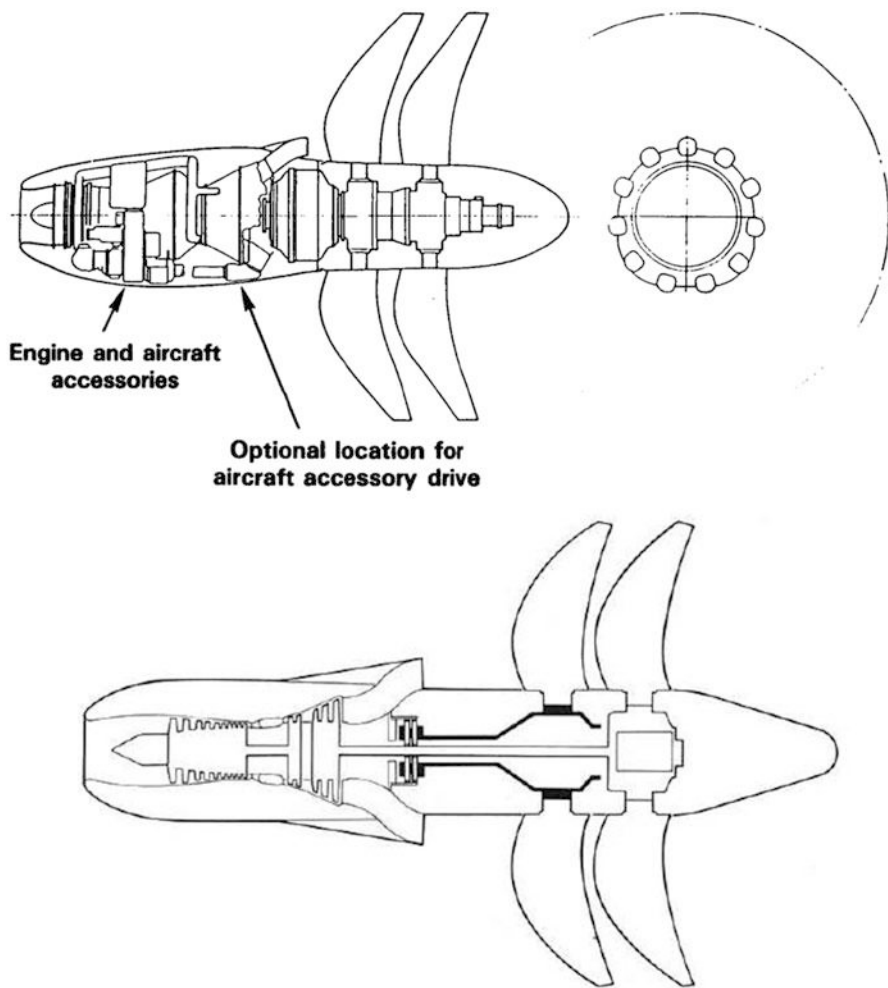


Fig. 7.27 Typical pusher propfan

However, open rotors present many technological challenges [13] and [14], including:

- Noise and vibration (both inside and outside the aircraft cabin)
- Structural reinforcement of the fuselage and wings
- Airworthiness considerations (blade-off, etc.)
- Engine installation and mounting
- Gearbox cooling and reliability
- Design of efficient counter-rotating components
- *Competing technologies:* The efficiency of current technology engines is improving at an average of 1 % a year—which means traditional turbofan engines available in 2020 are likely to be at least 11 % more efficient than 2010 production models, without any major technology risk. Meanwhile, the

Table 7.1 Comparison between Turboprop, Propfan and Turbofan (HBPR) engines

Engine	Turboprop	Propfan	Turbofan (HBPR)
Number of blades	3–6	8–12	20–30
Diameter	Large	Smaller	Smallest
Power/Square of diameter	Small	Larger	—
Blade shape	Nearly straight	Swept or scimitar-like profile	Swept
Maximum thickness	Thick	Thinner	Thinnest
Tip speed	Subsonic	Supersonic	Supersonic
BPR	Nearly 50	25 or more	4–12
Propulsive efficiency	High	Higher	Lower
ESFC(kg/hp.h)	0.19–0.23	0.17	—
Mach number	0.5–0.6	0.68	0.9
Cruise altitude	6000 m	11,000 m	11,000

Pratt & Whitney PW1000G geared turbofan could provide a 22–23 % fuel efficiency gain by 2017, according to the company, while the CFM International non-open-rotor LEAP-X design could provide 16 % lower fuel consumption than the CFM56-7 by 2018. Some manufacturers are skeptical about open-rotor technology.

- *Slower aircraft operating speeds:* An open-rotor-powered aircraft is likely to have a cruising speed 5–10 % slower than a turbofan-powered aircraft.

Example 7.7 A three-spool pusher-type propfan or unducted fan engine (UDF) is fitted to an aircraft flying at a speed of 220 m/s and altitude of 6 km ($T_a = 249.2$ K and $P_a = 47.182$ kPa) (Fig. 7.28). The engine is composed of three spools: intermediate-pressure spool composed of an intermediate-pressure compressor driven by an intermediate-pressure turbine, a high-pressure compressor driven by a high-pressure turbine, and the unducted fan (resembling a low-pressure compressor) driven by a low-pressure turbine. The maximum temperature is 1400 K and fuel having a heating value of 40,000 kJ/kg is used. It has the following particulars:

$\dot{m}_a = 40.0$ kg/s, $\pi_{IPC} = 3.1$, $\pi_{HPC} = 5.6$, $\pi_{UDF} = 1.098$, $\Delta P_{CC} = 6\%$, $\eta_d = 0.92$, $\eta_{IPC} = 0.84$, $\eta_{HPC} = 0.85$, $\eta_{C.C} = 0.965$, $\eta_{IPT} = 0.91$, $\eta_{HPT} = 0.93$, $\eta_{FT} = 0.92$, $\eta_n = 0.96$, $\eta_{UDF} = 0.825$, $(\eta_m)_{UDF} = 0.98$, $\alpha = 0.85$, bleed ratio: $b = 0.12$, $C_{P_c} = 1.005$ kJ/kg K, $C_{P_i} = C_{P_n} = 1.148$ kJ/kg K

It is required to calculate:

1. Bypass ratio β
2. Ratio between thrust force generated by unducted fan and nozzle
3. Total equivalent horsepower
4. Propulsive efficiency

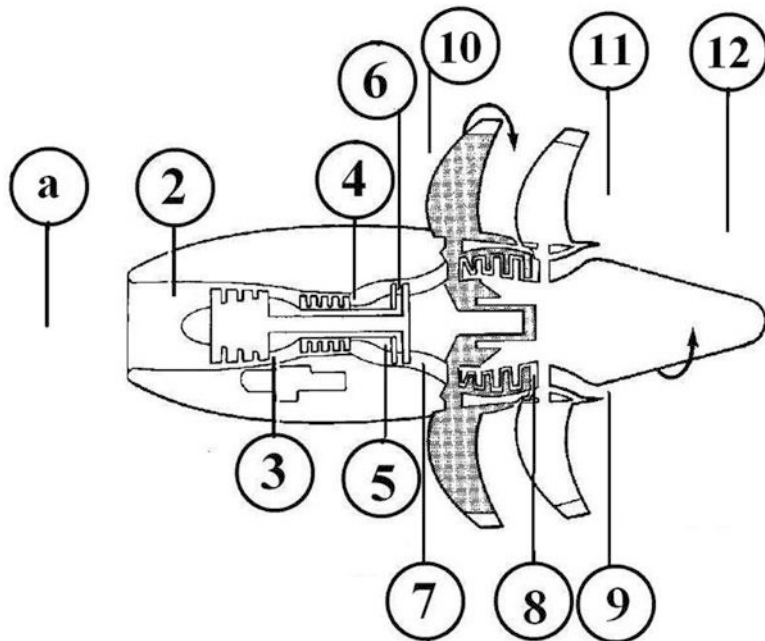


Fig. 7.28 Layout of propfan (UDF) engine

Solution

Figure 7.29 illustrates the T-s diagram for different states identified above.

Intake (States a-2):

The engine is examined during flight at a speed of 220 m/s and altitude of 6.0 km, and then the total conditions at diffuser outlet are calculated as follows:

Sonic speed and flight Mach number are

$$a = \sqrt{\gamma_c R T_a} = \sqrt{1.4 \times 287 \times 249.2} = 316.4 \text{ m/s}$$

$$M = U/a = 0.695$$

$$T_{02} = T_a \left(1 + \frac{\gamma_c - 1}{2} M^2 \right) = 273.3 \text{ K}$$

$$P_{02} = P_a \left(1 + \eta_d \frac{\gamma_c - 1}{2} M^2 \right)^{\frac{1}{\gamma_c - 1}} = 63.56 \text{ kPa}$$

Intermediate-Pressure Compressor (States 2-3):

$$P_{03} = P_{02} \times \pi_{IPC} = 3.1 \times 60.52 = 197 \text{ kPa}$$

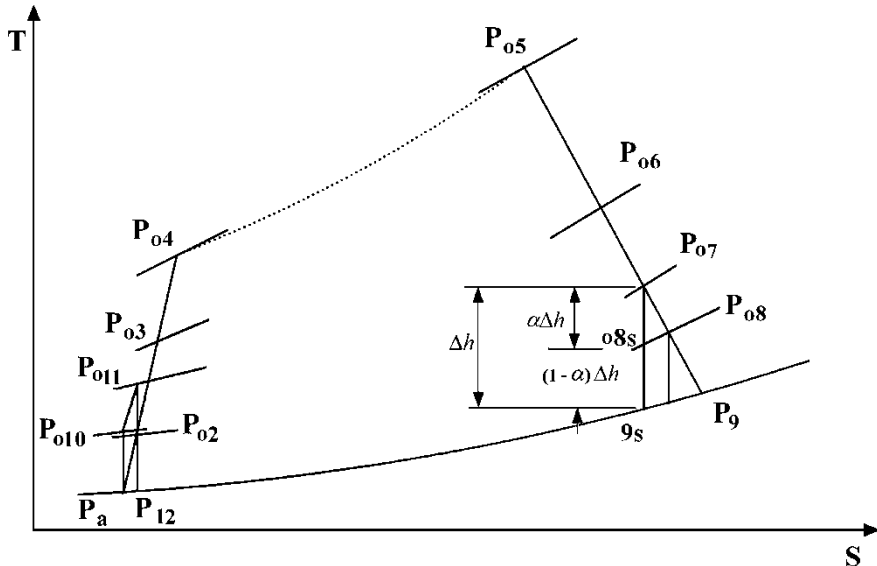


Fig. 7.29 T-s diagram for propfan (UDF) engine

$$T_{03} = T_{02} \left(1 + \frac{\pi_{IPC}^{\frac{\gamma_c-1}{\gamma_c}} - 1}{\eta_{IPC}} \right) = 303 \times \left(1 + \frac{3.1^{0.286} - 1}{0.84} \right) = 397.68 \text{ K}$$

High-Pressure Compressor (States 3–4):

$$P_{04} = P_{03} \times \pi_{HPC} = 1103.2 \text{ kPa}$$

$$T_{04} = T_{03} \left(1 + \frac{\pi_{HPC}^{\frac{\gamma_c-1}{\gamma_c}} - 1}{\eta_{HPC}} \right) = 397.6 \times \left(1 + \frac{5.6^{0.286} - 1}{0.85} \right) = 695.4 \text{ K}$$

Combustion Chamber (States 4–5):

$$P_{05} = (1 - \Delta P_{cc}) \times P_{04} = 0.94 \times 1103.2 = 1037 \text{ kPa}$$

$$f = (1 - b) \frac{Cp_{cc}T_{05} - Cp_cT_{04}}{\eta_b Q_R - Cp_{cc}T_{05}} = (0.88) \frac{1.148 \times 1400 - 1.005 \times 695.4}{0.965 \times 40,000 - 1.148 \times 1400} \\ = 0.0216$$

High-Pressure Turbine (HPT) (States 5–6):

Energy balance for high-pressure spool:

$$\begin{aligned}
 Cp_c(T_{04} - T_{03}) &= (1 + f - b)Cp_h(T_{05} - T_{06}) \\
 T_{06} &= T_{05} - \frac{Cp_c}{(1 + f - b)Cp_h}(T_{04} - T_{03}) \\
 &= 1400 - \frac{1.005}{1.148 \times 0.899}(695.4 - 397.6) = 1110.8 \text{ K} \\
 \frac{P_{06}}{P_{05}} &= \left[1 - \frac{1}{\eta_{HPT}} \left(1 - \frac{T_{06}}{T_{05}} \right) \right]^{\frac{\gamma_h}{\gamma_h - 1}} = \left[1 - \frac{1}{0.93} \left(1 - \frac{1110.8}{1400} \right) \right]^4 = 0.3662 \\
 P_{06} &= 379.75 \text{ kPa}
 \end{aligned}$$

Intermediate-Pressure Turbine (IPT) (States 6–7):

Energy Balance

$$\begin{aligned}
 T_{07} &= T_{06} - \frac{Cp_c}{(1 + f)Cp_h}(T_{03} - T_{02}) \\
 &= 1110.8 - \frac{1.005}{1.148 \times 1.0216}(124.3) = 1004.3 \text{ K} \\
 \frac{P_{07}}{P_{06}} &= \left[1 - \frac{1}{\eta_{IPT}} \left(1 - \frac{T_{07}}{T_{06}} \right) \right]^{\frac{\gamma_h}{\gamma_h - 1}} = \left[1 - \frac{1}{0.91} \left(1 - \frac{1004.3}{1110.8} \right) \right]^4 = 0.6406 \\
 P_{07} &= 243.26 \text{ kPa}
 \end{aligned}$$

Unducted Fan (UDF) (States 10–11):

$$\begin{aligned}
 T_{010} &= T_{02} = 273.3 \text{ K} \\
 P_{010} &= P_a \left(1 + \frac{\gamma_c - 1}{2} M^2 \right)^{\frac{\gamma_c}{\gamma_c - 1}} = 65.15 \text{ kPa} \\
 P_{011} &= P_{010} \times \pi_{UDF} = 71.54 \text{ kPa} \\
 T_{011} &= T_{010} \left(1 + \frac{\pi_{UDF}^{\frac{\gamma_c - 1}{\gamma_c}} - 1}{\eta_{UDF}} \right) = 273.3 \times \left(1 + \frac{1.098^{0.286} - 1}{0.825} \right) = 282.3 \text{ K} \\
 \frac{T_{12}}{T_{011}} &= \left(\frac{P_a}{P_{011}} \right)^{\frac{\gamma_c - 1}{\gamma_c}} = \left(\frac{47.18}{71.54} \right)^{0.286} = 0.8878 \\
 T_{12} &= 250.6 \text{ K} \\
 (U_e)_{UDF} &= \sqrt{2Cp_c(T_{011} - T_{12})} = 252.4 \text{ m/s}
 \end{aligned}$$

Free Turbine (States 7–8) and Hot Gases Nozzle (States 8–9):

$$\frac{T_{07}}{T_{9s}} = \left(\frac{P_{07}}{P_a} \right)^{\frac{\gamma_h-1}{\gamma_h}} = \left(\frac{243.26}{47.18} \right)^{0.25} = 1.5068$$

$$T_{9s} = 666.5 \text{ K}$$

Temperature drop in free turbine:

$$T_{07} - T_{08} = \eta_{FT} \times (T_{07} - T_{08s}) = \eta_{FT} \times \alpha \times (T_{07} - T_{9s})$$

$$= 0.92 \times 0.85 \times (1004.3 - 666.5) = 264.2 \text{ K}$$

$$T_{08} = 740 \text{ K}$$

$$T_{08s} = 717.2 \text{ K}$$

$$\frac{P_{07}}{P_{08}} = \left(\frac{T_{07}}{T_{08s}} \right)^{\frac{\gamma_h}{\gamma_h-1}} = \left(\frac{1004.3}{717.2} \right)^4 = 3.853$$

$$P_{08} = 63.14 \text{ kPa}$$

$$(U_e)_n = \sqrt{2Cp_h \times \eta_n(T_{08} - T_{9s})} = 402.5 \text{ m/s}$$

The thrust force obtained from the exhaust gases leaving the nozzle is denoted as (T_n) given by the relation $T_n = \dot{m} \times [(1+f)(U_e)_n - U] = 7,648 \text{ N}$

Energy Balance

$$\beta Cp_c(T_{011} - T_{010}) = (\eta_m)_{UDF}(1+f)Cp_h(T_{07} - T_{08})$$

$$\beta = (\eta_m)_{UDF}(1+f) \frac{Cp_h(T_{07} - T_{08})}{Cp_c(T_{011} - T_{010})}$$

$$= 0.98 \times 1.0216 \times \frac{1.148 \times (1004.3 - 740)}{1.005 \times (282.3 - 273.3)} = 33.58$$

The thrust force obtained from unducted fan denoted as (T_{UDF}) is given by the relation

$$T_{UDF} = \beta \dot{m} \times [(U_e)_{UDF} - U] = 33.58 \times 40 \times (252.4 - 220) = 43,525 \text{ N}$$

Total thrust $T_{tot} = T_{UDF} + T_n = 51,173 \text{ N}$

The ratio between the unducted fan and nozzle thrusts is

$$\frac{T_{UDF}}{T_n} = \left(\frac{43,525}{7648} \right) = 5.69$$

The unducted fan power is $P_{UDF} = U \times T_{UDF} = 9,575 \text{ kW} = 12,841 \text{ hp}$.

The jet nozzle power is $P_n = U \times T_n = 1683 \text{ kW} = 2256 \text{ hp}$.
 Total equivalent power is

$$P = T_{tot} \times U = 11,258 \text{ kW} = 15,097 \text{ hp.}$$

Propulsive efficiency

$$\eta_p = \frac{T \times U}{T \times U + 0.5 \dot{m} \times \left[(U_{en} - U)^2 + \beta(U_{eUDF} - U)^2 \right]}$$

$$\eta_p = \frac{51,173 \times 220}{51,173 \times 220 + 0.5 \times 40 \times \left[(402.5 - 220)^2 + 33.58 \times (252.4 - 220)^2 \right]}$$

$$\eta_p = \frac{11,258,060}{11,258,060 + 20 \times (33,306 + 1049)} = \frac{11,258,060}{11,945,160} = 0.94247 = 94.247\%$$

Closure

Detailed analyses for three shaft engines, namely, turboprop, turboshaft, and propfan, are given.

Turboprop engines were invented after turbojet to develop a better propulsive efficiency. It is used in bush, commuter, and some heavy transport aircrafts. Propeller provides most of the power, while exhaust gases (having very low speeds) generated about 15 % of total power. Propeller design is the same as those coupled to piston engines. So the only solved example for the giant 8-blades propeller in Airbus A400 aircraft is given. Turboshaft engines are mostly used as prime mover for helicopters. Few are seen in tanks and maritime applications. Turboshaft engines have similar structure to turboprops. Both couple their gas generator to the load through a reduction gearbox (mostly of the planetary type). The load in turboprop is the propeller, while in turboshaft is the helicopter rotor. Moreover, both turboprop and turboshaft engines are either single- or double-spool engines. Few are triple spool. Hovering of helicopters close to ground resembles an important feature, so it was treated as a solved example. Speed of air vehicles powered by both engine types are limited to low to moderate subsonic values.

Propfan engines have similarities with both turbofan and turboprop engines. It combines their best features of high propulsive efficiency and low fuel consumption. R & D for these engines started after the oil crisis of 1973. Several US companies (GE, P&W, and Allison) cooperated to design and manufacture such efficient engines. It proved promising features but were not manufactured outside prototype and testing numbers. The only propfan engine produced in mass numbers is the Russian D-27 engine. A detailed example describing the thermodynamic behavior and performance analysis of a pushing three-spool propfan is given.

Problems

Turboprop

- 7.1 The shown Fig. (7.30) illustrates French military STOL Tactical Transport BREGUET 941S which is powered by four Turbomeca Turmo IID3 turboprops.

The airplane has a maximum speed at sea level of 144 m/s.

Propeller has the following characteristics:

Number of blades (B) = 3

Diameter (D) = 3.0 m

Blade chord at $0.75R$ = 0.16 m

Rotational speed = 2880 rpm

Inflow factor (a) = 0.05

Lift coefficient C_L = 0.7

It is required to calculate C_T , C_Q , C_P , and η_P .

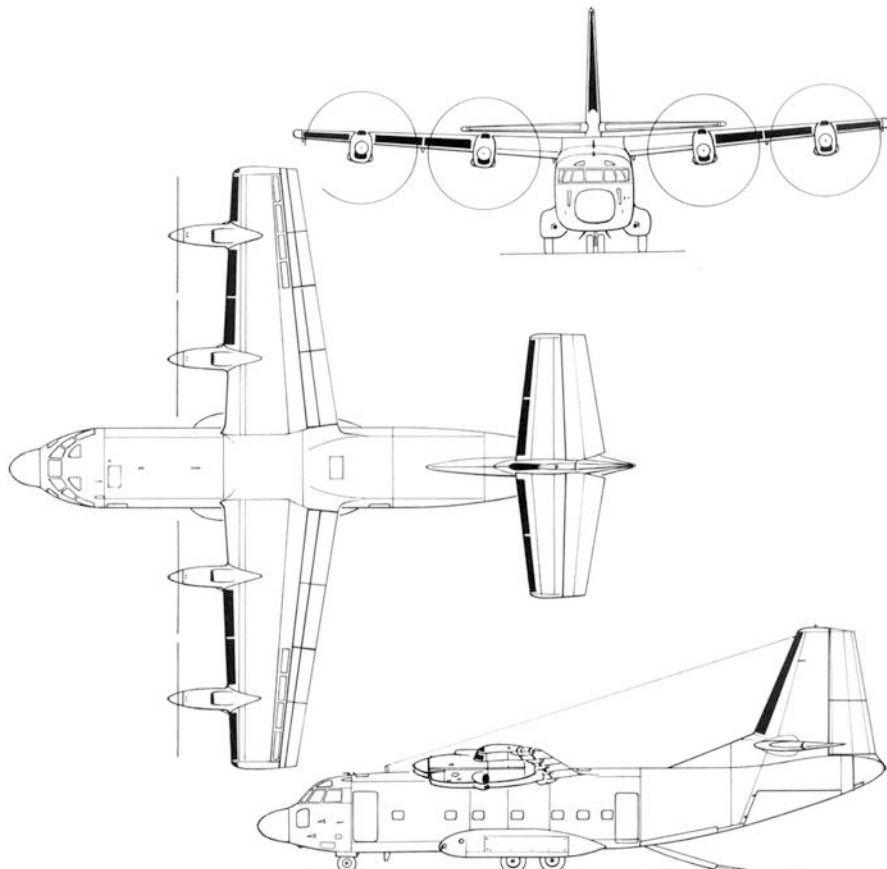


Fig. 7.30 BREGUET 941S

Hints:

1. Divide the propeller blade into five stations having $x = 0.12, 0.34, 0.56, 0.78$, and 1.0.
2. Use the following relations:

$$\frac{dC_T}{dx} = \frac{\pi}{8} \sigma_R J^2 (1+a)^2 C_L \frac{\cot \phi}{\sin \phi}$$

$$\frac{dC_Q}{dx} = \frac{\pi}{16} \sigma_R J^2 (1+a)^2 x \frac{C_L}{\sin \phi}$$

- 7.2 The shown Fig. (7.31) illustrates Antonov AN-12 (CUB) medium-range civil and military Freighter powered by four Ivchenko AI-20 K turboprops. It has the following data:

Cruising speed = 200 m/s

Service ceiling = 33,464 ft

Density ratio (σ) = 0.3345

Power of each engine = 2980 kW

Propeller speed = 2700 rpm

Propeller type: four-bladed Clark Y-section

Diameter (D) = 3.0 m

Blade chord at $0.75R = 0.16$ m

Inflow factor (a) = 0.05

Lift coefficient $C_L = 0.7$

It is required to calculate C_T, C_Q, C_P and η_P



Fig. 7.31 Antonov AN-12 (CUB)

If the propeller is of the variable-pitch type and the cruising speed is increased to 228 m/s, what is the necessary rotation of the propeller?

7.3 Which of these is a turboprop engine?

- (A) Adour
- (B) Dart
- (C) RB 211
- (D) Spey

7.4 A turboprop operates at sea level and moves at 160 m/s (ambient pressure is 101 kPa). It ingests 12 kg/s of air and has negligible fuel flow. The area of the exit is 0.22 m^2 . The exit pressure is 148 kPa, and the exit velocity is 235 m/s. The thrust from the propeller is 14 kN. Find the total developed thrust.

7.5 A turboprop operates at 9000 ft and moves at 160 m/s. The exit velocity is 370 m/s, and the nozzle is unchoked, and exit density is 0.455 kg/m^3 . The fuel flow rate is 0.5 kg/s. The thrust from the propeller is 18 kN, and the total developed thrust is 19.5 kN.

- (a) What is the ingested air mass flow rate?
- (b) If the exit nozzle is round, what is the nozzle exit diameter?

7.6 An ideal turboprop is used to propel an aircraft at 5000 ft. The craft flies with a Mach number of 0.4. The compressor pressure ratio is 6, and the airflow through the core is 12 kg/s. The burner exit total temperature is 1250 K, and the exit Mach number is 0.7. The heating value of the fuel is 41,400 kJ/kg. Find the developed thrust and TSFC.

7.7 An aircraft is to fly at 10,000 ft with a Mach number of 0.5. It is to be propelled with a turboprop and requires 30 kN of thrust per engine. The compressor pressure ratio is 8.0, and the exit total temperature from the burner is 1300 K. The fuel has a heating value of 42 MJ/kg. Assuming ideal operations, how much airflow is required? What are the resulting power of the engine and TSFC?

7.8 A single-spool turboprop is used to propel an aircraft at 3000 m. It flies at Mach 0.55, and the compressor pressure ratio is 5.6. The airflow rate is 8 kg/s. The turbine inlet total temperature is 1200 K, and the heating value of the fuel is 43 MJ/kg. The compressor, burner, turbine, shaft, converging primary nozzle, and propeller have efficiencies of 90, 95, 87, 99.6, 97, and 82 %, respectively. Power is split between the propeller and the jet in the ratio $\alpha = 0.86$. The diffuser and burner have total pressure ratios of 0.93 and 0.96, respectively. Find the following:

- (a) The total thrust
- (b) Total horsepower
- (c) Exit Mach number
- (d) TSFC

- 7.9 A single-spool turboprop engine when running at maximum rpm at sea-level conditions:

($P_a = 101 \text{ kPa}$ and $T_a = 288 \text{ K}$) had the following particulars:

$$\begin{array}{lll} m_a = 12.0 \text{ kg/s} & \pi_c = \frac{P_{03}}{P_{02}} = 7.5 & \Delta P_b = 4\% \\ T_{04} = 1200 \text{ K} & V_J = 240 \text{ m/s} & \\ \eta_c = 0.87 & \eta_{C.C} = 0.98 & \eta_t = 0.9 \\ \eta_n = 0.94 & \eta_m = 0.99 & \eta_{pr} \times \eta_g = 0.78 \\ C_{P_c} = 1.01 \text{ kJ/kg/K} & C_{P_{C.C}} = 1.13 \text{ kJ/kg/K} & C_{P_t} = C_{P_n} = 1.14 \text{ kJ/kg/K} \\ Q_R = 43000 & & \end{array}$$

It is required to calculate the equivalent brake horsepower (E.B.H.P.).

- 7.10 The turboprop considered in problem (12) is reexamined here. The engine is fitted to an aircraft flying at Mach number of 0.6. The maximum temperature is 1200 K, and fuel having a heating value of 43 MJ/kg is used. All other data are unchanged. It is required to calculate the specific equivalent shaft horsepower (S.E.S.H.P.) if the aircraft is flying at sea level and altitudes of 2, 5 and 8 km.
- 7.11 The shown Fig. (7.32) illustrates Bell Boeing V-22 Osprey tilt-rotor multi-mission aircraft which takes off and lands as a helicopter. It is powered by two-spool Rolls-Royce Allison T406 engines with its rotor driven by a free power turbine through a gearbox. Each engine has the following data during takeoff



Fig. 7.32 Bell Boeing V-22 Osprey

Propeller power	4586 kW
Compressor pressure ratio	16.7
Fuel heating value	43.0 MJ/kg
Gas Turbine inlet temperature	1400 K
Gearbox mechanical efficiency	0.95
Propeller efficiency	0.72
Ambient conditions	288 K and 101 kPa
Exhaust speed	200 m/s
Propulsive efficiency	60 % (defined as; $\eta_{\text{propulsive}} = \frac{2V}{V+V_e}$)

Assuming ideal conditions and variable properties ($\gamma_c = 1.4$, $\gamma_h = 4/3$), calculate:

- (A) The speed of air flowing into the intake (V)
- (B) Inlet temperature and pressure for the power turbine driving the propeller
- (C) The air mass flow rate
- (D) ESFC

- 7.12 The V-22 Osprey aircraft shown in previous problem takes off and lands as a helicopter. Once airborne, its engine nacelles can be rotated to convert the aircraft to a turboprop aircraft capable of high-speed and high-altitude flight. It can transport internal and external cargo. The V-22 Osprey is powered by two *turboprop* engines. Each has the following data:

Shaft power	4586 kW
Specific fuel consumption	0.24 kg/kW/h
Compressor pressure ratio	14.1
Compressor isentropic efficiency	0.85
Burner efficiency	0.94
Pressure drop in combustion chamber	2 %
Fuel heating value	45,000 kJ/kg
Turbine inlet temperature	1300 K
Turbines isentropic efficiency	0.92
Gearbox mechanical efficiency	0.98
Propeller efficiency	0.823
Ambient conditions	288 K and 101 kPa

Considering the following value of specific heat ratio ($\gamma_c = 1.4$ and $\gamma_h = 1.3299$), calculate

- (A) The air mass flow rate into the engine
- (B) The ESHP

- 7.13 The total work coefficient (C_W) in turboprop engines is defined as the ratio of propulsive power to the thermal energy of the airflow inducted into the engine, or

$$C_W = \frac{\eta_{pr} P_s + U_0 T}{m_a C_p T_a}$$

Calculate the work coefficient in *problem (13)* for different altitudes

- 7.14 A two-spool turboprop engine with a free power turbine has the following data:

$m_a = 12 \text{ kg/s}$	$H = 6 \text{ km}$
$T_a = 249 \text{ K}$	$P_a = 47.2 \text{ kPa}$
$M_0 = 0.56$	$\pi_C = 6$
$\Delta P_b = 4\%$	$T_{04} = 1180 \text{ K}$
$\eta_d = 0.94$	$\eta_C = 0.87$
$\eta_{C.C} = 0.98$	$\eta_t = \eta_{FPT} = \eta_n = 0.9$
$\eta_g = 0.96$	$\eta_{Pr} = 0.8$
$C_{P_c} = 1.01 \text{ kJ/kg K}$	$C_{P_t} = C_{P_{FPT}} = C_{P_n} = 1.148 \text{ kJ/kg K}$
$Q_R = 44 \text{ MJ/kg}$	

The power in the gases leaving the gas generator turbine is divided between the free power turbine and the nozzle based on the optimum condition $\alpha = \alpha_{opt.}$.

Calculate the equivalent shaft horsepower (ESHP) and the equivalent specific fuel consumption (ESFC)

- 7.15 An aircraft is fitted with a four turboprop engines and flying at a Mach number of 0.6 at altitude of 9 km where the ambient conditions are 30.8 kPa and 229.7 K. When engines are running at maximum rpm, each engine has an ESHP = 1280. The engine components have the following isentropic efficiencies:

Intake (0.9), Compressor (0.86), Burner (0.97), Turbine (0.89), Nozzle (0.95)

Other data are

Compressor pressure ratio	7.5
Combustion chamber pressure drop	3 %
Exhaust velocity	260 m/s
Turbine inlet temperature	1200 K
Fuel Heating Value	44,000 kJ/kg

Calculate the air mass flow rate into the engine.

- 7.16 A turboprop engine has the following specifications:

Air mass flow rate	14 kg/s
Flight Mach no.	M = 0.6
Flight altitude	6 km
Ambient temperature and pressure	249 K and 47.2 kPa
Compressor pressure ratio	6.6
Pressure loss in the combustion chamber	4 %
Maximum total temperature	1150 K
Fuel heating value	43,000 kJ/kg

Efficiencies:

Diffuser = 0.95, compressor = 0.86, Combustion chamber = 0.98,

Turbines and nozzle = 0.93, gearbox=0.96, propeller=0.8

Specific heats at constant pressure:

Compressor = 1.01, combustion chamber = 1.13, turbines = nozzle=1.14 kJ/kg K

Assuming $\alpha = 0.88$, calculate:

- a. ESHP b. ESFC

- 7.17 For a two-stream engine (turboprop or turbofan engines), prove that the ratio between the exhaust speed of hot stream and the inlet speed (u_{eh}/u) is expressed by the relation

$$\frac{u_{eh}}{u} = \frac{1 \pm \sqrt{1 - \eta_p C}}{\eta_p}$$

where

$$C = \eta_p \beta \left(\frac{u_{ec}}{u} \right)^2 - 2\beta \left(\frac{u_{ec}}{u} \right) + (1 + \beta)(2 - \eta_p)$$

η_p = propulsive efficiency

β = bypass ratio

$\frac{u_{ec}}{u}$ = ratio between the exhaust speed of cold stream and the inlet speed

Four engine types are considered in the below table.

	Turboprop	High-bypass ratio turbofan	Low bypass ratio turbofan	Turbojet
β	30.0	10.0	1.0	0
η_p	0.9	0.75	0.62	0.5
$\frac{u_{ec}}{u}$	1.05	1.2	1.4	0

1. Calculate $(\frac{u_{eh}}{u})$ for each case.

2. Comment.

Turboshaft

- 7.18 For which of these applications is the turboshaft engine most suited?

- (A) Low-speed fixed-wing aircraft
- (B) Helicopters
- (C) High-altitude reconnaissance aircraft
- (D) High-speed combat aircraft

7.19 The *Boeing CH-47 Chinook* is an American twin-engine, **tandem rotor heavy-lift helicopter**. Its primary roles are **troop movement**, artillery placement, and battlefield resupply. It is powered by two *Lycoming T55 turboshaft* engines (Fig. 7.33)

T-55 turboshaft engine has the following characteristics:

- Maximum power output: 3631 kW
- Gas Turbine inlet temperature: 1115 °C
- **Cruise speed:** 240 km/h
- **Service ceiling:** 5640 m
- Compressor pressure ratio: 9.32
- Fuel heating value: 44 MJ/kg
- Pressure drop in combustion: 2 %
- Modules efficiencies: $\eta_d = 0.92$, $\eta_c = 0.84$, $\eta_b = 0.98$, $\eta_{gt} = \eta_{pt} = 0.88$, $\eta_r = 0.8$

Calculate:

1. Fuel-to-air ratio
2. Air mass flow rate



Fig. 7.33 Boeing CH-47 Chinook (Courtesy flickr.com)

Fig. 7.34a Mil Mi26 transporting Tupolev Tu-134 airliner



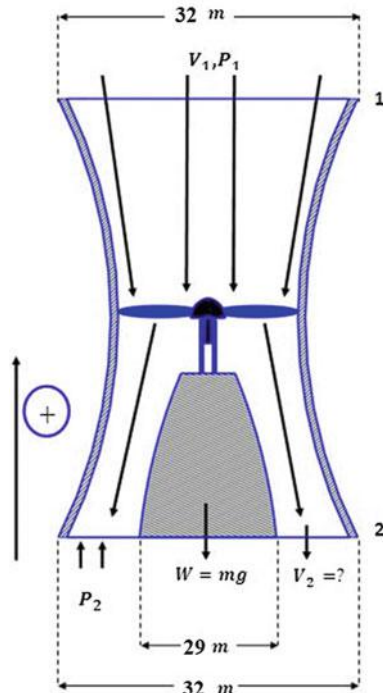
7.20 Figure 7.34a illustrates the world's largest helicopter Mi-26 a Russian multipurpose transport helicopter during lifting and transporting a retired Tupolev Tu-134 airliner. It is powered by two turboshaft engines: Lotarev D-136. Moreover, Fig. 7.34b illustrates its hovering operation close to the ground together with a control volume surrounding it and its inlet and outlet diameters. The total mass of the helicopter is 56,000 kg. The exit static pressure is atmospheric. Assuming the flow is a one-dimensional, steady, and incompressible, calculate:

1. The inlet and exit velocities of air V_1, V_2
2. The power of the turboshaft engine

Propfan

7.21 A three-spool pusher-type propfan, or unducted fan engine (UDF) is fitted to an aircraft flying at a speed of 200 m/s and altitude of 6 km ($T_a = 249.2$ K and $P_a = 47.182$ kPa) (Fig. 7.27). The engine is composed of three spools: intermediate-pressure spool composed of an intermediate-pressure compressor driven by an intermediate-pressure turbine, a high-pressure compressor driven by a high-pressure turbine, and the unducted fan (resembling a low-pressure compressor) driven by a low-pressure turbine. The maximum temperature is 1400 K, and fuel having a heating value of 40,000 kJ/kg is used. It has the following particulars:

Fig. 7.34b Control volume for hovering helicopter



$\dot{m}_a = 36.0 \text{ kg/s}$, $\pi_{IPC} = 3.1$, $\pi_{HPC} = 5.6$, $\pi_{UDF} = 1.098$, $\Delta P_{CC} = 6\%$,
 $\eta_d = 0.92$, $\eta_{IPC} = 0.84$, $\eta_{HPC} = 0.85$, $\eta_{C.C} = 0.965$, $\eta_{IPT} = 0.91$, $\eta_{HPT} = 0.93$,
 $\eta_{FT} = 0.92$, $\eta_n = 0.96$, $\eta_{UDF} = 0.825$, $(\eta_m)_{UDF} = 0.98$, $\alpha = 0.85$, bleed ratio:
 $b = 0.12$, $C_{P_c} = 1.005 \text{ kJ/kg K}$, $C_{P_f} = C_{P_n} = 1.148 \text{ kJ/kg K}$

It is required to calculate the following:

1. The bypass ratio β
2. The ratio between thrust force generated by unducted fan and nozzle
3. The total equivalent horsepower
4. The propulsive efficiency

References

1. Cessna 208B SKS (105090285) by Shawn from Airdrie, Canada – Cessna 208B SKS, Licensed under CC BY-SA 2.0 via Wikimedia Commons. [http://commons.wikimedia.org/wiki/File:Cessna_208B_SKS_\(105090285\).jpg#/media/File:Cessna_208B_SKS_\(105090285\).jpg](http://commons.wikimedia.org/wiki/File:Cessna_208B_SKS_(105090285).jpg#/media/File:Cessna_208B_SKS_(105090285).jpg)
2. Roy HL. A review of advanced turboprop transport activities. In: AGARD conference Proceedings no.366, Aerodynamics and Acoustics of Propellers, pp 1.1–1.16
3. James CP Jr, Glynn RB (1987) Evaluation of installed performance a wing-tip-mounted pusher turboprop on a semispan wing, NASA Tech Paper 2739, August 1987

4. Lancaster OM (1959) Jet propulsion engines. In: Lancaster OM (ed) High speed aerodynamics and jet propulsion, vol 12. Princeton University Press, Princeton, pp 199–267
5. Kerrebrock JL (1992) Aircraft engines and gas turbines, 2nd edn. MIT Press, Cambridge, p 56
6. The jet engine, 5th edn. Rolls-Royce plc, p. 3, Reprinted 1996 with revisions, p 217
7. Saravanamuttoo HIH, Rogers GFC, Cohen H (2001) Gas turbine theory, 5th edn. Prentice Hall, Upper Saddle River, New Jersey, p 137
8. Hill P, Peterson C (1992) Mechanics and thermodynamics of propulsion, 2nd edn. Addison Wesley Publication Company, Inc, Reading, p 155
9. <http://www.minihelicopter.net/CH47Chinook/index.htm>
10. http://www.turbokart.com/about_arrius.htm
11. Strack WC, Knip G, Weisbrich AL, Godston J, Bradley E (1990) Technology and benefits of aircraft counter-rotation propellers. NASA TM-82983
12. Taylor M (2009) Open rotor engine design and validation. Rolls Royce Publication
13. Butterworth-Hayes P (2010) Open rotor research revs up, Aerospace America, AIAA, March 2010, pp 38–42
14. Awker RW (1986) Evaluation of propfan propulsion applied to general aviation. NASA CR-175020

Chapter 8

Stationary Modules Intakes, Combustors, and Nozzles

8.1 Intake

8.1.1 Introduction

All air-breathing engines installed in an aircraft must be provided with an air intake and a ducting system (which is also identified as inlet or diffuser) to diffuse the air from free-stream velocity to a lower velocity acceptable for further processing by other engine components [1]. The intake is the first part of all air-breathing propulsion systems. Both of the words *intake* and *inlet* are used alternatively. *Intake* is normally used in Britain, while *intake* is used in the USA.

Due to the influence of intake flow on overall aircraft performance, responsibility for intake design rests with the aircraft manufacturer, not the engine maker. However, both partners work closely together to arrive at an optimum solution. Both manufacturers cooperate also in testing air intakes. An aircraft will require one or more intakes to capture (collect) the atmospheric air (working fluid) at free-stream Mach number, sometimes change its direction of flow, and supply this flow to the engine with as little distortion as possible, to ensure smooth running and efficient propulsion.

The performance of an inlet must fulfill the following requirements:

- Delivers exact amount of air required for different flight phases and wide spectrum of angles of attack and sideslip
- Diffuses air with maximum static pressure rise and minimum total pressure loss
- Recovers flow distortion or separation at large angles of attack to achieve as uniform flow as possible
- Achieves least possible external drag to the system
- Provides good starting and stability
- Achieves low signatures (acoustic, radar, etc.) for a noise suppression and stealth requirements
- Holds minimum weight and cost while meeting life and reliability goals

Detailed aero-thermal analysis and design of intake for subsonic/supersonic and hypersonic speeds was the topic of a lecture series organized by von Karman Institute [2].

For gas turbine engine (turbojet, turbofan, and turboprop), the airflow entering subsonic compressors or fans must be of low Mach number, of the order 0.4–0.5 or less even if the aircraft speed is supersonic.

For a ramjet also, the inlet reduces the speed to a subsonic value to have a subsonic combustion. Scramjet engine facilitates supersonic combustion, and thus its intake delivers air at supersonic speeds to the combustion chamber. Thus the entrance duct reduces air speed from flight speed to lower values even for scramjet engines.

Inlets may be classified as:

1. Subsonic or supersonic/hypersonic
2. Fixed or variable geometry
3. Two-dimensional or axisymmetric geometry

Inlet performance is either identified by isentropic efficiency or pressure recovery. The last is defined as the ratio, expressed in percent, of the average total pressure of the air entering the engine to that of the free-stream air. The total pressure is the sum of the static, or ambient, pressure of the air and the impact pressure associated with its motion. Modern jet transports may cruise with values of the pressure recovery of 97–98 %. Supersonic aircraft with well-designed, practical inlet and internal flow systems may have pressure recoveries of 85 % or more for Mach numbers in the 2.0–2.5 range.

Noise generated in intake is another issue with extensive research list.

The intake geometry and performance are closely related to the method of power plant installation. The position of the power plant must not affect the efficiency of the air intake. In the following sections, the different methods of power plant installation will be first discussed for both civil and military aircrafts; next subsonic and supersonic/hypersonic intakes will be analyzed. The performance of intakes will be finally discussed.

8.1.2 Power Plant Installation

Power plant installation is sometimes referred to as propulsion–airframe integration. It is the process of locating the power plants and designating their installation to meet many operating requirements while minimizing drag and weight penalties [3]. The installation of the engines influences aircraft safety, structural weight, flutter, drag, control, maximum lift, performance and reliability of engine, maintainability, and aircraft growth potential. Power plant installation influences the design of air-inlet system, cooling arrangement, and mounting structure. These elements are largely the responsibility of the airframe manufacturer. However, the

engine manufacturer is also involved as the engine data must be available to the airframe manufacturer to design a suitable installation.

Hereafter, power plant installation will be discussed for both subsonic and supersonic aircrafts.

8.1.2.1 Subsonic Aircrafts

Power plant installations for both civil and military aircrafts are similar as long as their flight speeds are subsonic or transonic. However, for supersonic aircrafts there are great differences in the installation methods of civil and military aircrafts as well be described later on. Turbojet and turbofan engines have the same methods for installation, while turboprops employ other methods.

(A) *Turbojet and turbofan engines*

Though most of the present-day transport (passenger or cargo) aircrafts are powered by turbofan engines, turbojet engines still have small avenues. The following methods are frequently seen for turbojet and turbofan engines:

1. Wing installation (Even number of engines: 2,4,6, or 8)
2. Fuselage (Even number of engines 2 or 4)
3. Wing and tail combination (Three engines)
4. Fuselage and tail combination (Three engines)

Figure 8.1 illustrates the breakdown of power plant installation for turbojet and turbofan engines in civil applications.

(a) *Wing installation*

The four forms of power plants installed to wings are the following:

- (a) Buried in the wing (2 or 4 engines)
- (b) Pod installation (2, 4, 6, or 8 engines)
- (c) Above the wing (2 or 4 engines)
- (d) Pitot installation (2 or 4 engine)

Buried in the wing

This type of wing installation is found in early aircrafts like the De Haviland Comet 4 and the Hawker Siddeley Nimrod. In both aircrafts, four engines are buried in the wing root (Fig. 8.2).

This method of installation had the following advantages:

1. Minimum parasite drag and probably minimum weight.
2. Minimum yawing moment in case of engine failure that counteracts the asymmetric thrust; thus, the pilot can easily maintain a straight level flight.

However, it has the following disadvantages:

1. It poses a threat to the wing structure in case of failure of a turbine blade or disk.

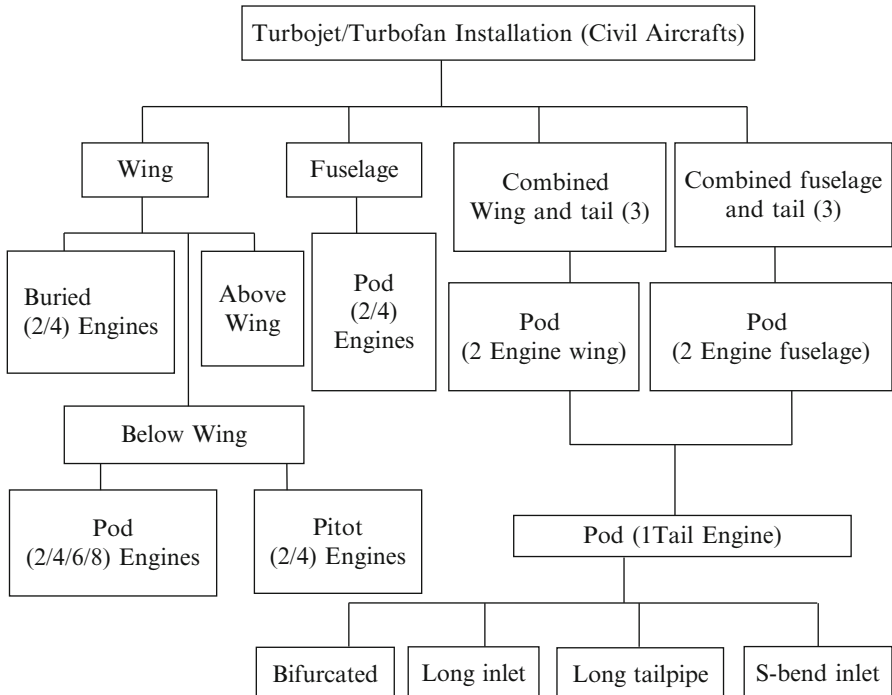


Fig. 8.1 Different methods of installation for turbojet/turbofan engines of civil transports



Fig. 8.2 De Havilland Comet (4 engines buried in the wing)

2. Very difficult to maximize the inlet efficiency.
3. If a larger diameter engine is desired in a later version of the airplane, the entire wing may have to be redesigned.
4. Difficult accessibility for maintenance and repair.
5. It eliminates the flap in the region of the engine exhaust, therefore reducing the maximum lift coefficient $C_{L_{MAX}}$.

Pod installation

In this type engines are attached to the wings via pylons (Fig. 8.3). Most engines nowadays have pod installation; either two or four engines are found in the following aircrafts: Boeing 737, 757, 767, 777, MD-11, and future 787; Airbus A320, A330, A340, A350, and A380; Tristar; and Antonov An-148. Six engines power the Antonov An-225, while eight P&W TF33 turbofan engines power the B-52.

This type of engine installation has the following advantages:

1. Minimize the risk of wing structural damage in case of engine fire or blade/disk failure.
2. Simple to obtain high ram recovery in the inlet since the angle of attack at the inlet is minimized and no wakes are ingested.
3. Easy engine maintenance and replacement due to engine accessibility and being close to the ground.
4. Less noisy.
5. The weight of the engines reduces the wing tip upbending effects of lift allowing a lighter wing structure.
6. It may be a little easier to arrange for a suitable structural fuse that allows the engine to break free from a wing-pylon under-engine seizure or other severe event.

However, it has the following disadvantages:

1. For low-wing aircrafts like Boeing 737, the engines are mounted close to the ground; thus, they tend to suck dirt, pebbles, snow, and so on into the inlet.



Fig. 8.3 Antonov An-225 (6 engines pod installation to wing)



Fig. 8.4 Fokker VFW614 (2 engines above-wing installation)

This is known as foreign object damage (FOD) which may cause serious damage to the engine blades.

2. The high temperature and high dynamic pressure of the exhaust impinging on the flap increase flap loads and weight and may require titanium structure which is more expensive.
3. Pylon–wing interference affects the local velocities near the wing leading edge, thus increases the drag, and reduces the maximum lift coefficient. However, this drawback can be remedied by choosing the nacelle locations sufficiently forward and low with respect to the wing as shown in Figs. 8.3 and 8.4.
4. Strong yaw effect if an engine failed on one side.

Above the wing

Some of these planes are seaplanes like A-40 Albatros powered by two Soloviev D-30KPV engines of 117.7kN thrust each plus two Klimov RD-60 K booster engines of 24.5kN thrust. Others are conventional airplanes like Fokker VFW614 (Fig. 8.4) powered by two turbofan engines and Antonov An-74TK-200 aircraft powered by two turbofan engines D-36, series 3-A. This type of installation has the following advantages:

1. Prevents (or greatly reduces) foreign object ingestion into the engines from the surface of a runway during takeoff and landing
2. Prevents water ingestion into the engine for seaplanes during takeoff and landing
3. Improves wing lift due to the blowing over of the wing's upper surface and inboard flaps by engine streams
4. Reduces noise level at the terrain due to screening engine streams by the wing which copes with the increasingly stringent civilian aviation noise regulations

As at present and in the future, increasingly stringent civilian aviation noise regulations will require the design and manufacture of extremely quiet commercial aircraft. Also, the large fan diameters of modern engines with increasingly higher bypass ratios pose significant packaging and aircraft installation challenges. The design approach that addresses both of these challenges is to mount the engines above the wing. In addition to allowing the performance trend toward large diameters and high-bypass ratio turbofan engines to continue, this approach allows the wing to shield much of the engine noise from people on the ground.

Pitot type

Pitot type is an ideal air intake for a turbojet engine fitted to an aircraft flying at subsonic or low supersonic speeds (Fig. 8.5). Examples are Boeing 707 and Airbus A300 aircrafts. It is a short circular intake. This type of intake makes the fullest use of the ram effect on the air due to forward speed and suffers the minimum loss of ram pressure with changes of the aircraft attitude. However, as sonic speed is approached, the efficiency of this type of air intake begins to fall because of the formation of a shock wave at the intake lip.

(b) Fuselage installation

As described in [3], fuselage installation (which is sometimes identified as *aft-engine* arrangements) is most suitable for small aircrafts where it is difficult to install engines under the wing and maintain adequate wing-nacelle and nacelle-ground clearances.

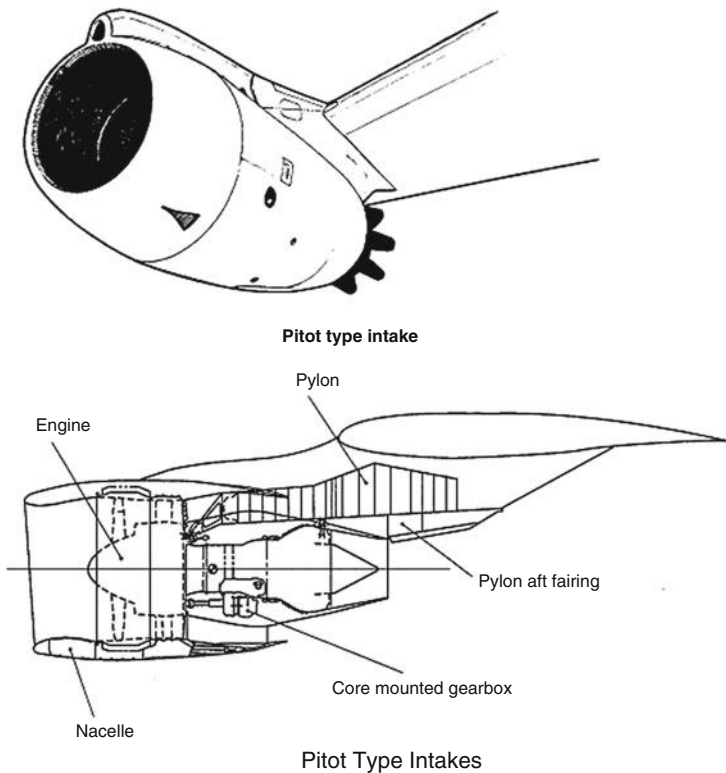
Pod engine installation is employed either on the sides or top of the fuselage using short stub wings. Air gap between the engine and the fuselage minimizes aerodynamic interference. Aircrafts are either powered by two engines (Fig. 8.6) as in the DC-9, MD-80, Gates Learjet Model 25, Fokker F-28, Cessna 550 Citation II, Tu-324 and 334, and Sud Aviation Caravelle 12, or four engines, *as in* the Jetstar and BAC Super VC-10 (Fig. 8.7).

Fuselage installation has the following advantages [3]:

1. Greater maximum lift coefficient and less drag due to elimination of wing–pylon and exhaust–flap interference
2. Less asymmetric yaw after engine failure as the engines are close to the fuselage
3. Lower fuselage height above the ground which permits shorter landing gear and air stair length

However, this installation has the following disadvantages [4]:

1. The center of gravity of the empty airplane is moved aft, well behind the center of gravity of the payload. Thus a greater center of gravity range is required which leads to difficult balance problems and larger tail.
2. On wet runway, the wheels kick water, and the special deflectors on the landing gear may be needed to avoid water ingestion into the engine.
3. At very high angles of attack, the nacelle wake blankets the T-tail and may cause stall which needs a larger tail span.
4. Vibration and noise isolation is a difficult problem.



Piton Type Intakes



Fig. 8.5 Boeing 707 aircraft with 4 pitot tube engines



Fig. 8.6 DC-9 (fuselage 2 engines pod installation)



Fig. 8.7 Super VC-10 (4 engines fuselage pod installation)

It appears that for DC-9 size aircraft, the fuselage installation is to be slightly preferred. In general smaller aircrafts employ fuselage arrangement.

(c) Combined wing and tail installation (Three engines)

Tail installation represents a *center engine* installation. Only one turbofan engine is installed in all available tail combinations with either wing or fuselage arrangement. Examples are found in DC-10 aircrafts. Figure 8.8 illustrates a typical wing and tail installation.

There are four arrangements of center (or tail) engine installation, namely, (A) bifurcated inlet, (B) long inlet, (C) long tail pipe, and (D) "S" bend inlet.

The two usually used are the S-bend and the long inlet configurations (Fig. 8.9). Both installation methods have the following advantages:

1. Mounted very far aft so a ruptured turbine blade or disk will not impact on the basic tail structure.
2. High-thrust reverser without interfering with control surface effectiveness. This is achieved by shaping and tilting the cascades used to reverse the flow.

Moreover, both arrangements also have the following disadvantages:

1. Large inlet losses due to the long length of intake
2. Difficult accessibility for maintenance and repair



Fig. 8.8 DC-10 Combined wing and tail (3 engines pod installation)

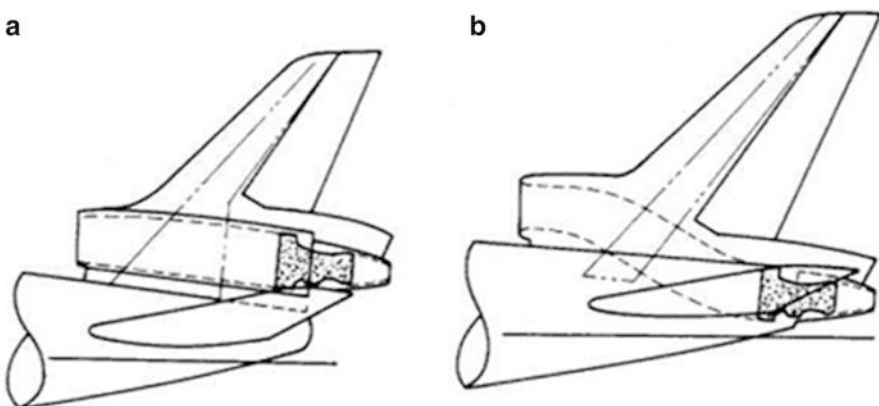


Fig. 8.9 Tail engine installation possibilities

(d) *Combined fuselage and tail installation*

Examples for this type of installation are the Boeing 727 aircraft, Tu-154, and Yak-42D. A typical layout for this configuration is shown in Fig. 8.10.

(B) *Turboprop installation*

Turboprop (or turbo-propeller) engines, however, have limited options. The propeller requirements always place the engine in one of the following positions [5] (Fig. 8.11):

1. Wing installation
2. Fuselage installation, either at the nose or empennage of aircraft for a single-engined aircraft

(a) *Wing installation*

Most present-day turboprops/piston engines are wing mounted to either passenger or cargo transports. Either puller or pusher turboprops may be installed to the wing. Typical wing installation of the puller type is shown in Fig. 8.12. Examples for wing installation are De Havilland DHC-8 commuter airplane powered by two PW120 puller engines, Fokker F-27 powered by two RR Dart engines, and Beechcraft King Air powered by two PT6A engines (Fig. 8.12). In some aircrafts a pair of counter-rotating propellers is installed to each engine. Antonov An-70 is an example for these aircrafts where the aircraft is powered by four engines.

Pusher engine types are less common; examples for pusher turboprops are Rutan Long-EZ and Piaggio GP-166 Avanti aircraft powered by two PT6A. The latter is shown in Fig. 8.13. An example for pusher propeller-piston engine coupling is the famous UAV MQ-1C Sky Warrior powered by a single Thielert Centurion Diesel engine.



Fig. 8.10 Yak-42D (3 engines, pod installation; 2 fuselage and one tail)

Fig. 8.11 Different installation methods for turboprop and piston engines

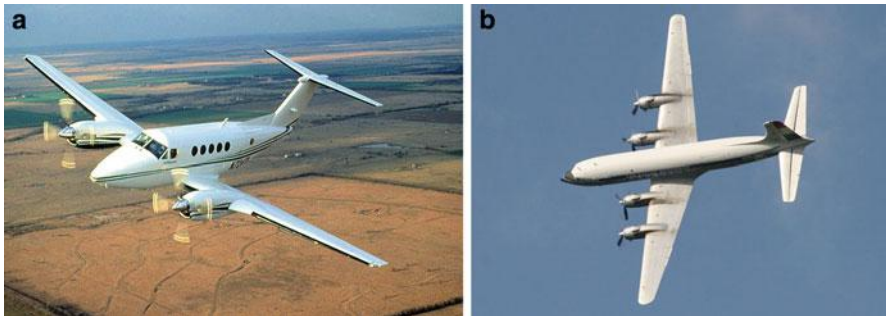
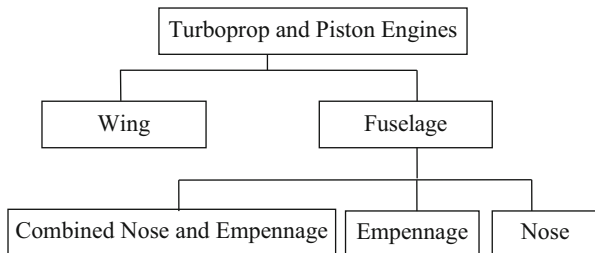


Fig. 8.12 Puller turboprop/piston engines: (a) Beechcraft King Air powered by two PT6A turboprop engines and (b) Douglas DC-6 is a piston-powered airliner

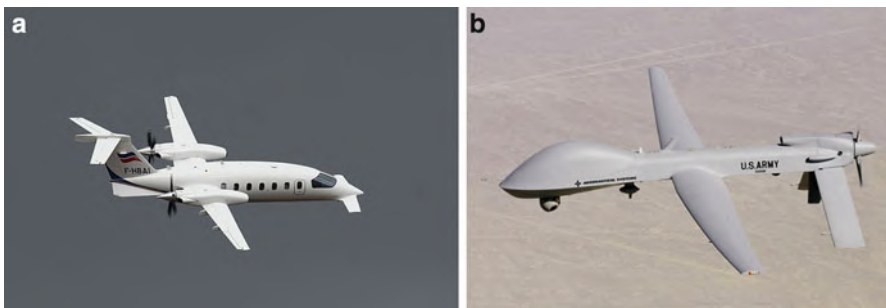


Fig. 8.13 Pusher-type engines: (a) Piaggio GP-166 Avanti aircraft powered by two PT6A and (b) General Atomics MQ-1C Sky Warrior powered by a single Thielert Centurion diesel engine

Pusher propellers have the potential of a quieter ride since the propellers are further from the passengers and because vortices from the propeller tips do not strike the fuselage sides. However, the propellers are operating in a turbulent airflow in the pusher configuration (due to airflow past the wings moving aft in vortex sheets), and high-velocity exhaust gases are discharged directly into the props; thus the resulting external propeller noise is more choppy and raucous than otherwise would be the case.



Fig. 8.14 Dornier Seastar powered by two push–pull turboprop above-wing installation

Figure 8.14 illustrates Dornier Seastar, a parasol-wing flying boat, with its two engines mounted in a single nacelle over the wings in a push–pull configuration.

(b) Fuselage installation

Nose engine installation is always employed in small aircrafts. Turboprop engine fitted to the nose is shown in Fig. 8.15a. The majority of light aircrafts are powered by a single piston engine buried in the fuselage nose, e.g., Cessna 172 (Fig. 8.15b), Beech Bonanza, Piper PA-28R-201 Arrow, and Pilatus PC-9.

Empennage installation is illustrated in Fig. 8.16. An example for turboprop engine is the Jetcruzer 500 with a single Pratt & Whitney Canada PT6A-66 (Fig. 8.16a). For piston engine, an example is Rutan Long-EZ powered by Lycoming O-235 piston engine (Fig. 8.16b).

Finally an example for *combined nose and empennage* installation is employed in aircraft Voyager (Fig. 8.17) with two piston engines, one engine buried in the fuselage nose and the other in the aft fuselage. Both engines were installed along the fuselage center line.

Intake of turboprop engines may have different shapes depending on size and location of the reduction gearbox coupled to the propeller. These inlets may be axial, axisymmetric, axisymmetric through plenum, or a scoop, which in turn



Fig. 8.15 Nose-mounted engines: (a) Pilatus PC-12 powered by a Pratt & Whitney Canada PT6A-67B turboprop and (b) Cessna 172 powered by one Lycoming IO-360-L2A four cylinder, horizontally opposed aircraft engine

may have elliptical, rectangular, U, and annular shapes [5] as illustrated in Fig. 8.18.

Figure 8.19 illustrates an elliptical inlet for a 6-bladed propeller of a puller turboprop engine and a typical annular inlet.

8.1.2.2 Supersonic Aircrafts

Supersonic aircrafts are mostly military ones. Few civil aircrafts are supersonic ones including the Anglo-French Concorde (powered by turbojet engines) and the Russian Tu-144 (powered by turbofan engines). All the remaining supersonic aircrafts are military ones.

(A) Civil transports

The engines of the two civil supersonic transports (SST) are installed in the wing. Concorde is powered by four Rolls-Royce/SNECMA Olympus 593 turbojets (Fig. 8.20), while Tu-144 is powered by four Kolesov RD-36-61 turbojet engines.



Fig. 8.16 Empennage installation: (a) Jetcruzer 500 driven by a single pusher-type turboprop engine and (b) Rutan Long-EZ powered by Lycoming O-235 piston engine

All engines are installed to the lower surface and aft part of the wing. Engine nacelle is flush to the wing surface and has rectangular inlet.

(B) Military aircrafts

Military aircrafts are powered by either turbojet or turbofan engines. Most fighters have one or, at the most, two engines situated inside the fuselage. Rather few ones are powered by wing-type engine installation. Single engine may have single or divided intakes (Fig. 8.21).

A variety of inlet locations and designs have been employed to supply air to subsequent engine modules. Each of these arrangements has both advantages and



Fig. 8.17 Aircraft Voyager, with combined nose and empennage piston engines

disadvantages. Figure 8.22 describes different methods for engine installation employed on fighter aircraft.

(a) *Fuselage installation*

Engines installed in the fuselage may have pitot (or nose), chin, side, and underslung configurations.

Nose (or pitot) inlet employed on the North American F-86 fighter is illustrated in Fig. 8.23. This type of installation enjoys good characteristics through a wide range of angle of attack and sideslip and free from aerodynamic interference effects—such as flow separation—from other parts of the aircraft. The long internal duct leading from the inlet to the engine, however, tends to have relatively high-pressure losses.

The *chin inlet* employed on the F-8 and Eurofighter airplanes shown in Fig. 8.24 has many of the advantages of the simple nose inlet but leaves space in front of the fuselage for radar or guns and has a somewhat shorter internal duct. The proximity of the inlet to the ground introduces a possible risk of foreign object ingestion, and, obviously, a possible damage of its hardware.

Side-mounted inlets may be used on both single- and twin-engine fighters.

Grumman F11F is a single engine, while F-22 Raptor is a twin engine as illustrated in Fig. 8.25. The side-mounted inlet arrangement probably offers the best compromise of all the conflicting aerodynamic, structural, weight, and space requirements, and it is used on many modern combat aircrafts.

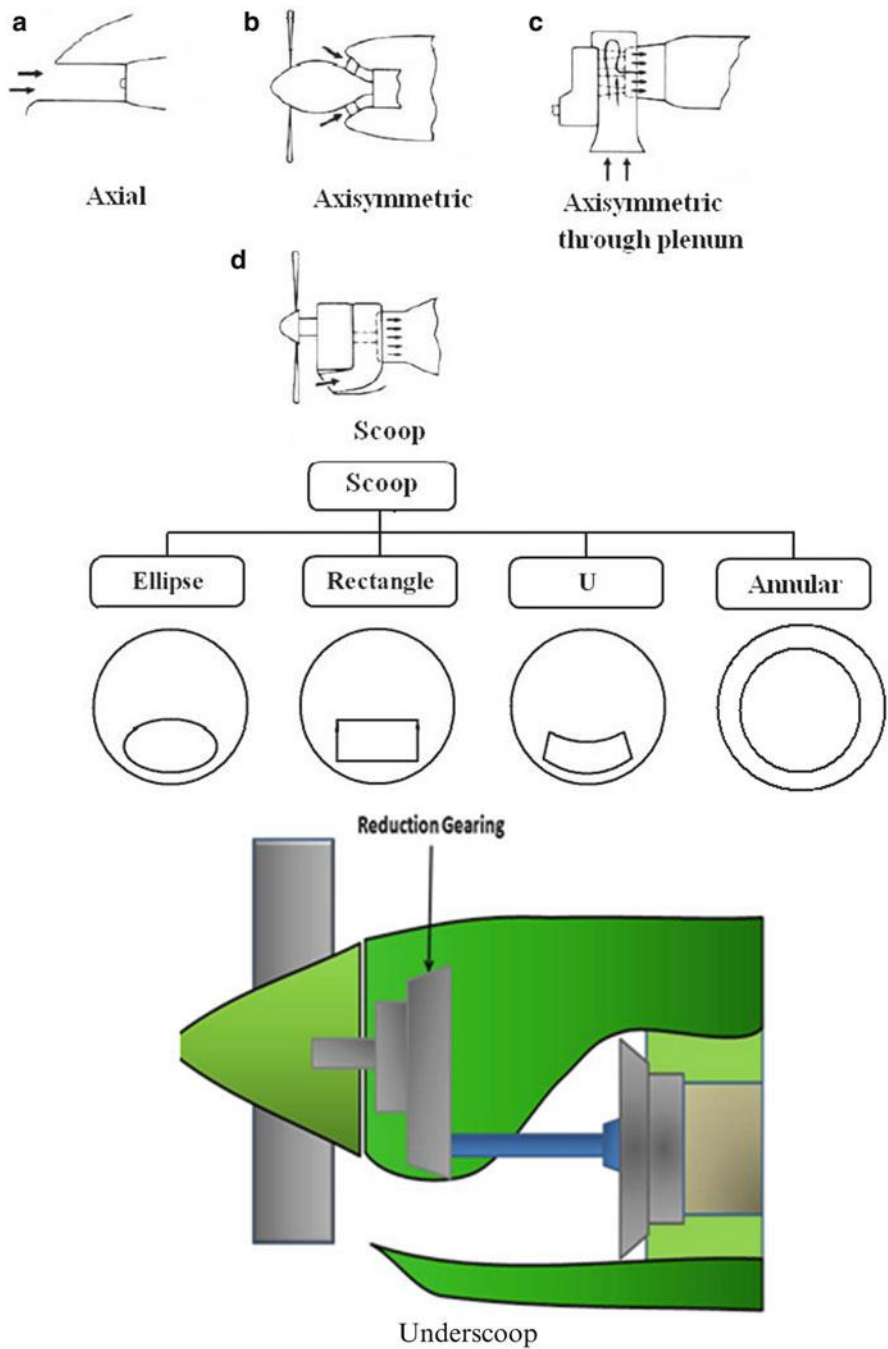


Fig. 8.18 Inlet shapes for turboprop engines

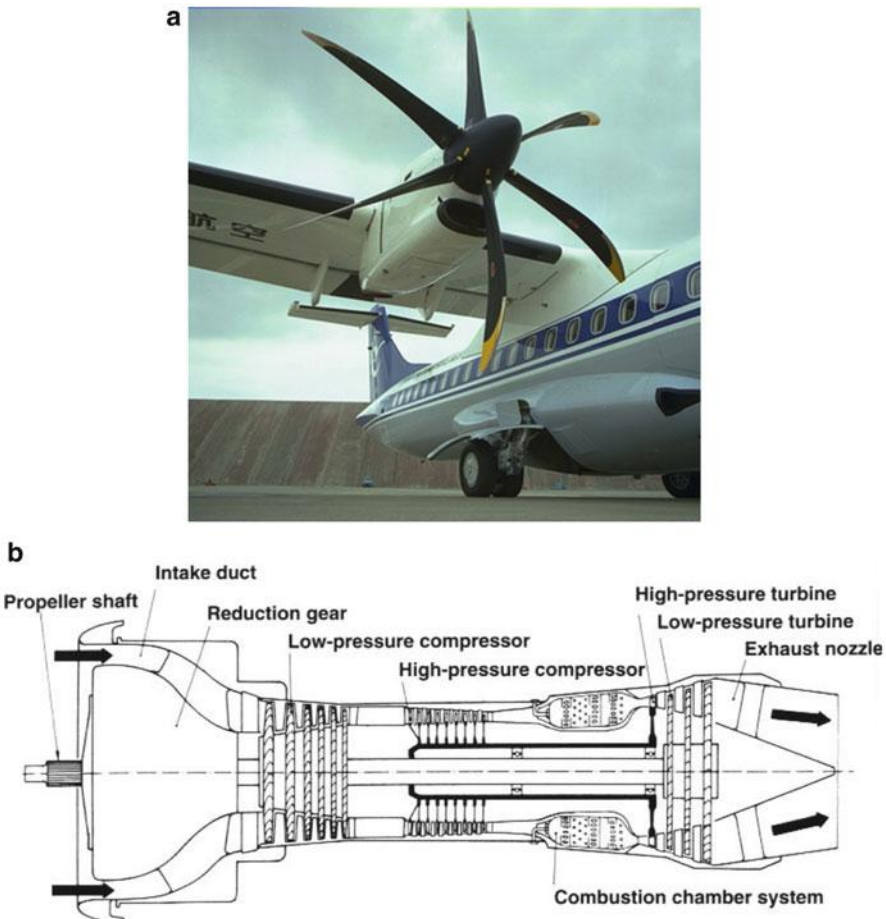


Fig. 8.19 Inlet shape for a turboprop engine: (a) an elliptical inlet and (b) an annular inlet



Fig. 8.20 Supersonic transports

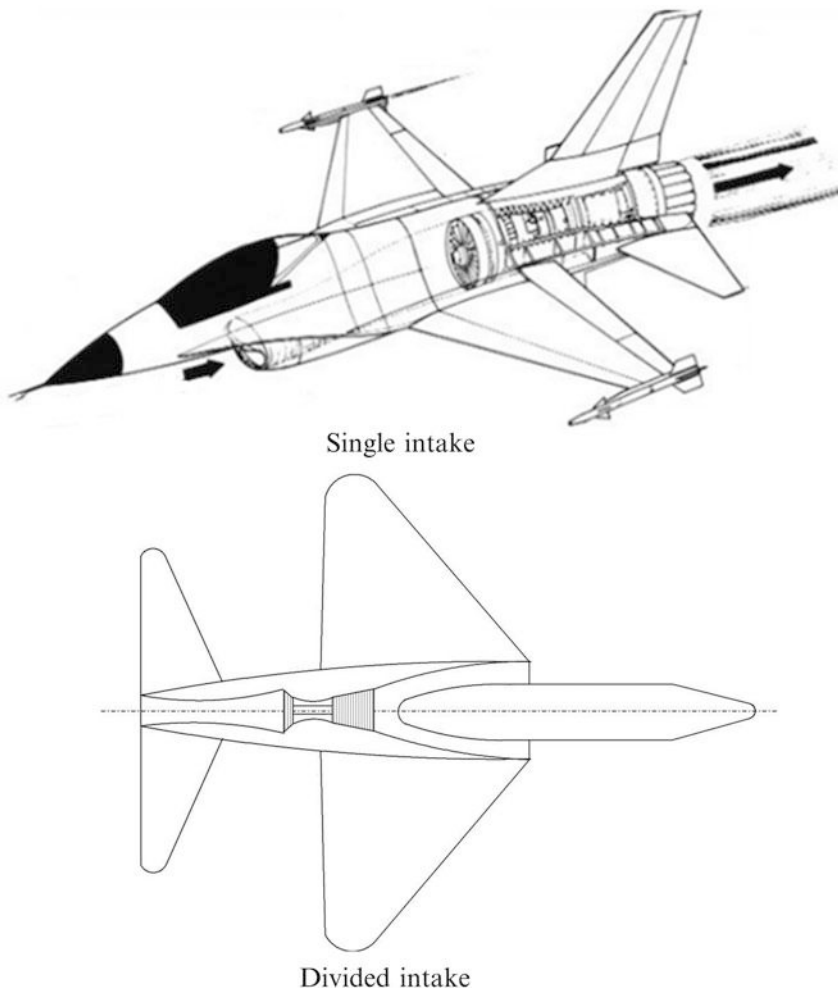


Fig. 8.21 Single and divided intakes

Finally, Fig. 8.26 illustrates an underslung intake as fitted to F16 airplane.

Finally, two engines may be installed to the empennage as shown in Fig. 8.27 illustrating Fairchild A-10A Thunderbolt II.

(b) Wing installation

Wing-root inlet installation shown in Fig. 8.28 is employed on the Vulcan B-2 bomber. Inlets located in this manner offer several advantages. Among these are short and light, internal flow ducts, avoidance of fuselage boundary-layer air ingestion, and freedom to mount guns and radar on the nose of the aircraft. Further, no interference between the cockpit and internal

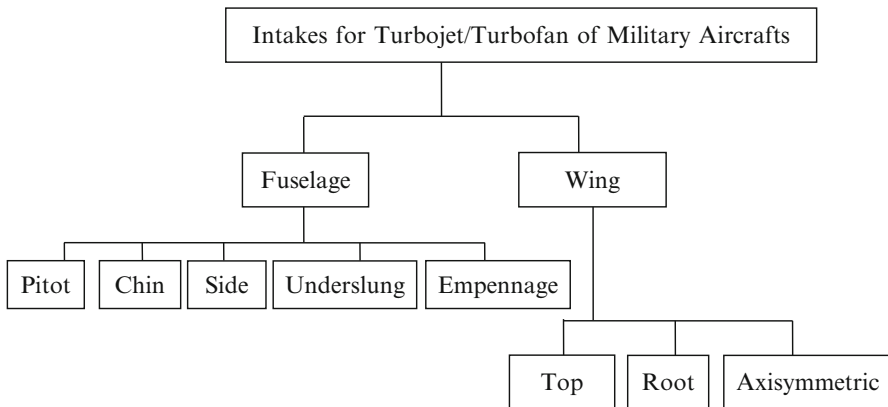
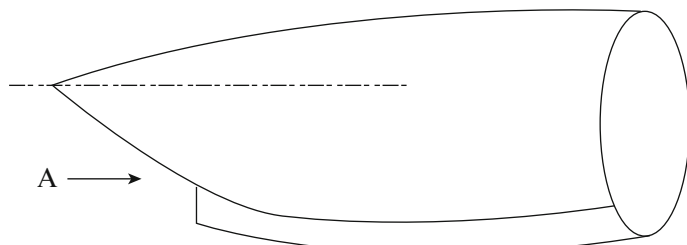


Fig. 8.22 Intakes for turbojet/turbofan engines of fighter aircrafts

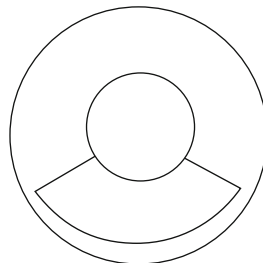


Fig. 8.23 F86 aircraft (single-engine pitot intake)

ducting is encountered in this arrangement. Careful design to avoid flow separation and associated losses must be accomplished. Wing-root intakes are not suitable for modern fighters of high-thrust-to-weight ratio because of the large-size intakes required by these aircrafts and the difficulty of integrating them with the wing.



(c) Chin Inlet



View A (Chin Inlet)

Fig. 8.24 F-8 Crusader (*above*) and Eurofighter (*below*) with chin intakes

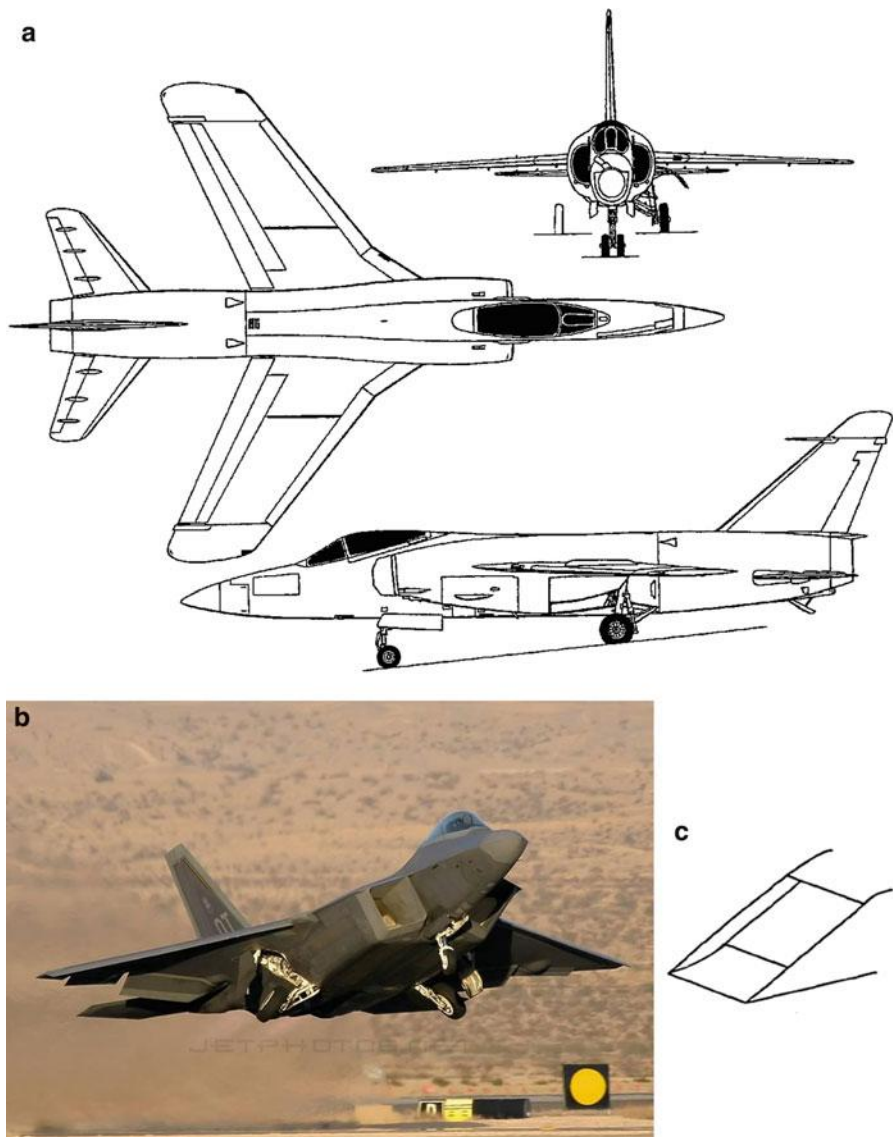


Fig. 8.25 Side-mounted engines: (a) Grumman F11F, (b) F-22 Raptor, and (c) two-dimensional side intakes

Wing top intake is employed in the B-2's four General Electric F118-GE-110 non-afterburning turbofans. They are buried in the wings, with two engines clustered together inboard on each wing (Fig. 8.29). The intakes of the B-2 aircraft have a zigzag lip to scatter radar reflections, and there is a zigzag slot just before each



Fig. 8.26 F16 aircraft fitted with underslung intake



Fig. 8.27 Fairchild A-10-A Thunderbolt II aircraft with 2 engines installed to the empennage

intake to act as a “boundary-layer splitter”, breaking up the stagnant turbulent airflow that tends to collect on the surface of an aircraft.

A unique wing installation is found in the SR-71 aircraft (Fig. 8.30). It is powered by two turboramjet engines having a variable-geometry axisymmetric inlet.



Fig. 8.28 Vulcan B-2 Bomber with 4 engines installed at wing root



Fig. 8.29 B-2 Spirit Stealth Bomber with 4 engines having wing top intake

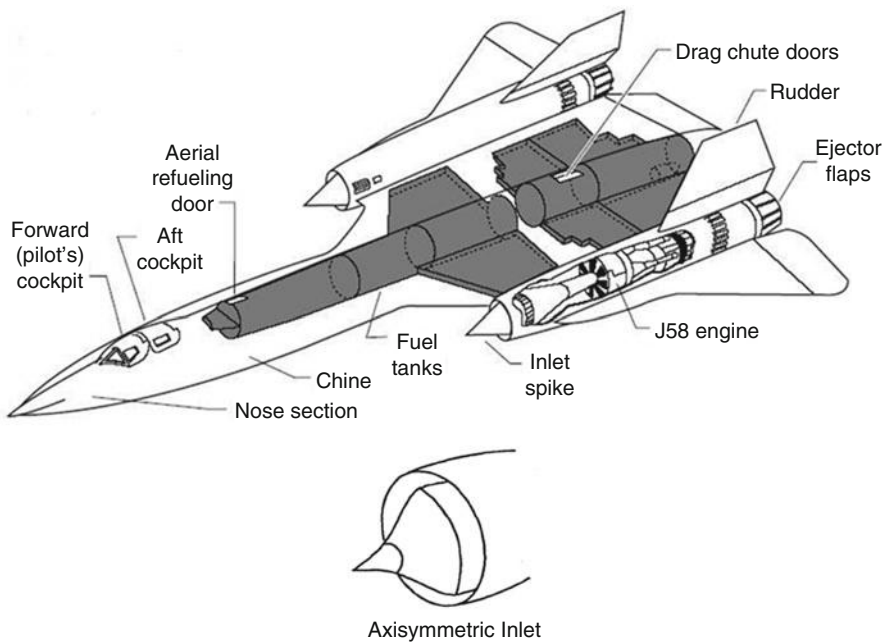


Fig. 8.30 SR-71 aircraft fitted with 2 turboramjet engines having axisymmetric intake



Fig. 8.31 Mi 24A (two engines above cabin with front intake)

8.1.2.3 Helicopters

Two types of intakes are seen:

1. Forward-facing pitot intake
2. Forward-facing side intake
3. Side-facing intake

Figure 8.31 illustrates Mi 24A helicopter powered by two Klimov TV3-117MT turboshafts located side by side above the cabin, having a *forward-facing pitot intake*.



Fig. 8.32 Sikorsky UH-60 helicopter powered by two-side turboshaft engines

Figure 8.32 illustrates Sikorsky UH-60 helicopter powered by two General Electric turboshaft engines sat atop of either side of the middle fuselage having a *forward-facing side intake*.

Side-facing intakes have a very poor pressure recovery compared to the other two types. Thus using a side-facing intake can only be justified due to its effectiveness as an inertial separator to protect against FOD [6].

8.1.2.4 Rockets

Hybrid rockets have both air-breathing and rocket engines. Air-breathing engines may be ramjet, turbojet, or turbofan engines.

(A) Ramjet engines

The Raduga 3M-80 and 3M-82 and Kh-41/ASM-MSS Moskit are all variants of the same 4.5-ton rocket-ramjet missile. *Four intakes* on the sides of the fuselage are employed (Fig. 8.33).

Alternatively, MBDA Meteor has *two rectangular side intakes*. Detailed description of ramjet missile propulsion status is described in [7].

(B) Turbojet engines

Several missiles are powered by turbojet engines (instead of the ramjet ones) together with their basic rocket engines. Examples are the general dynamics AGM-109H/L MRASM. It is a low-cost air-launched derivative of the Tomahawk family. Its propulsion system is a Teledyne CAE variable speed turbojet of the 600 lb class. The power plant has ventral engine inlet/inlet duct assembly. Prior launching the inlet is flush with the missile's skin, but deploys upon reaching a programmed point in the launch sequence.

(C) Turbofan engines

Williams F107-WR100 engine is a small turbofan engine that powers several missiles including Tomahawk (Fig. 8.34) and Boeing AGM-86B air-launched cruise missile (ALCM) (Fig. 8.35).



Fig. 8.33 Raduga 3 M-80, 3 M-82 and Kh-41/ASM-MSS Moskit



Fig. 8.34 Tomahawk missile



Fig. 8.35 Boeing AGM-86B air-launched cruise missile

The F107-WR100 turbofan engine is embedded in the tail for both of Tomahawk and Boeing AGM-86B missiles. Tomahawk uses a ventral engine inlet, while for Boeing AGM-86B, the engine inlet is on the top of the fuselage. Inlet of AGM-86B is usually shielded from GCI radars by the airframe. Prior to launch the vehicle's wings and vertical stabilizer are stowed. They deploy upon release from the launch aircraft. Both Tomahawk and AGM-86B have tail cone exhaust.



Fig. 8.36 Kh-55SM missile



Fig. 8.37 YJ-62 cruise missile

Figure 8.36 illustrates Raduga Kh-55SM missile. The most visible difference between Tomahawk and Kh-55 families of missiles is that Kh-55 uses the two-spool turbofan engine TVD-50 which is mounted in a nacelle and stowed in the aft fuselage. It deploys via a ventral door on a pylon after launch.

Figure 8.37 illustrates the YJ-62 cruise missile. It is also similar to Tomahawk family but employs a unique *fixed* scoop inlet for the air-breathing engine. It is powered by either turbojet or turbofan engine.

8.1.3 Inlet Performance Parameters

Inlet performance is characterized by three factors:

1. *Total (stagnation) pressure recovery (r_d)* is the ratio of the average total pressure at the exit of the inlet to the free-stream total pressure, or

$$r_d = P_{02}/P_{0\infty} \quad (8.1)$$

Modern jet transports may cruise with values of the pressure recovery of 97–98 %. Supersonic aircraft with well-designed, practical inlet and internal flow systems may have pressure recoveries of 85 % or more for Mach numbers in the 2.0–2.5 range. A higher *pressure recovery* indicates a better performing inlet. The maximum possible value of recovery is 1.0.

The *isentropic efficiency* of the intake is denoted by (η_d), which is static-to-total efficiency and is a measure for the losses from the far upstream conditions to the end of inlet (it is the fan/compressor face for turbine or shaft-based engines and the inlet of combustion chamber for ram-based engines). The efficiency is then expressed by the following relation (refer to Fig. 8.38):

$$\begin{aligned} \eta_d &= \frac{h_{02s} - h_\infty}{h_{02} - h_\infty} = \frac{T_{02s} - T_\infty}{T_{02} - T_\infty} = \frac{(T_{02s}/T_\infty) - 1}{(T_{02}/T_\infty) - 1} \\ \therefore \eta_d &= \frac{(r_d)^{\frac{\gamma-1}{\gamma}} [1 + \frac{\gamma-1}{2} M_\infty^2] - 1}{(\frac{\gamma-1}{2}) M_\infty^2} \end{aligned} \quad (8.2)$$

Stagnation pressure ratio is then expressed as

$$r_d = P_{02}/P_{0\infty} = \left[\frac{1 + \eta_d \frac{\gamma-1}{\gamma} M_\infty^2}{1 + \frac{\gamma-1}{\gamma} M_\infty^2} \right]^{\frac{\gamma}{\gamma-1}} \quad (8.3)$$

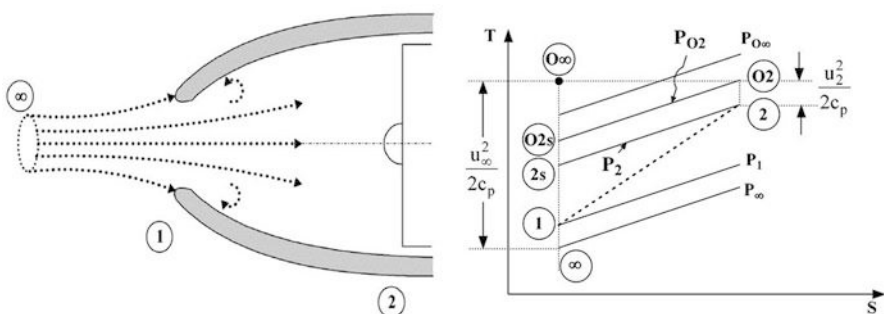


Fig. 8.38 Streamlines and T-s diagram for a subsonic intake

Thus if the isentropic efficiency is known, the pressure recovery can be obtained from Eq. 8.3, while if the pressure recovery is known, the diffuser efficiency can be determined from Eq. 8.2.

However, since the flow upstream of the intake is isentropic, then all the losses are encountered inside the intake, or from state (1) to state (2). In some cases the efficiency is defined for the *internal part of diffuser* (η'_d). In this case, the diffuser efficiency is defined as

$$\begin{aligned}\eta'_d &= \frac{h_{02s} - h_1}{h_{02} - h_1} = \frac{T_{02s} - T_1}{T_{02} - T_1} = \frac{(T_{02s}/T_1) - 1}{(T_{01}/T_1) - 1} \\ \eta'_d &= \frac{(P_{02}/P_1)^{\frac{\gamma-1}{\gamma}} - 1}{(P_{01}/P_1)^{\frac{\gamma-1}{\gamma}} - 1} = \frac{(P_{02}/P_1)^{\frac{\gamma-1}{\gamma}} - 1}{\frac{\gamma-1}{2} M_1^2} \\ (P_{02}/P_1) &= \left(1 + \eta'_d \frac{\gamma - 1}{2} M_1^2\right)^{\frac{\gamma}{\gamma-1}}\end{aligned}\quad (8.4)$$

2. Air distortion at intake outlet

An inlet distortion is often encountered when the real flow is associated with some degree of angle of attack to the engine nacelle. Takeoff, landing, and gust encounter are some typical examples of such situation. The air-to-air refueling is also one of the reasons of inlet distortion.

Such air distortion has its impact on the pressure/velocity across the exit of the inlet, which in turn will influence the compressor/fan face for turbine-based engines or the inlet of combustion chamber for ram-based engines. If air brought from free stream to the compressor face is distorted, then at the exit of the inlet, one portion of the flow may have a higher velocity, or higher pressure, than another portion. The flow may be swirling, or some section of the boundary layer may be thicker than another section because of the inlet shape. The rotor blades of the compressor move in circles around the central shaft. As the blades encounter distorted inlet flow, the flow conditions around the blade change very quickly. The changing flow conditions can cause flow separation in the compressor (a compressor stall) and can cause structural problems for the compressor blades and the whole engine or disrupt the flow through the engine. The simplest method for evaluating compressor distortion takes the maximum measured total pressure minus the minimum measured total pressure divided by the average total pressure. More sophisticated models use mass- or area-weighted averages. Inlet distortion is an important factor because highly distorted flows cause *compressor stalls* that can damage the engine.

One of the strongest *high-cycle fatigue (HCF)* drivers can be caused by intake distortion of the airflow which creates high energy, normally first engine-order (low-pressure shaft speed) driver. Intake distortion may be due to the operation of the aircraft. High-yaw or sideslip maneuvers can grossly distort the inlet flow. Bifurcated intakes often create uneven pressure and velocity distributions at compressor face that induce flutter.

3. *Inlet spillage drag* is a drag that occurs when the engine cannot handle all of the flow that approaches the inlet. The airflow through the engine is set by choked conditions in the nozzle. Any excess flow that approaches the inlet is spilled around the inlet generating additional drag on the airframe. The form of the theoretical spillage drag (D_{spill}) is very similar to the thrust equation and expressed as

$$D_{\text{spill}} = K \dot{m} (V_1 - V_0) + A_1 (P_1 - P_0) \quad (8.5)$$

K ranges from 0.4 to 0.7, but for a given inlet, the value is determined experimentally.

8.1.4 Subsonic Intakes

Most subsonic aircraft intakes have a divergent shape and are sometimes referred to as inlet diffusers because of their effect on pressure. As air flows into a divergent duct, it slows and converts some of its kinetic energy into pressure. Subsonic intakes are found in the turbojet or turbofan engines powering most of the present airliners and military transports (commercial and cargo aircraft). Examples of these engines are the JT8, JT9, PW 4000 series, RB211, Trent series, and V2500 powering many of the Boeing and Airbus aircraft transports. Subsonic intakes are also applied to some combat aircrafts and virtually all jet training aircrafts that operate near the speed of sound.

The surface of the inlet is a continuous smooth curve where the very front (most upstream portion) is called the inlet lip. A subsonic aircraft has an inlet with a relatively thick lip. Concerning turboprop engines the intakes are much complicated by the presence of propeller and gearbox at the inlet of the engine.

Subsonic intakes have fixed geometry, although intakes for some high-bypass ratio turbofan engines are designed with blow in doors. These doors are spring-loaded parts installed in the perimeter of the inlet duct designed to deliver additional air to the aero engine during takeoff and climb conditions as the highest thrust is needed and the aircraft speed is low [8]. The most common type of subsonic intake is the pitot intake. This type of intakes makes the fullest use of ram due to forward speed and suffers the minimum loss of ram pressure with changes of aircraft altitude [9]. However, as sonic speed is approached, the efficiency of this type of air intake begins to fall because of the formation of a shock wave at the intake lip. It consists of a simple forward entry hole with a cowl lip. The three major types of pitot intakes are the following:

- (a) Podded intakes
- (b) Integrated intakes
- (c) Flush intakes

Podded intake is common in transport aircrafts (civil or military). Examples of the commercial aircrafts are Boeing 707, 767, 777, and 787 and Airbus A330, A340, A350, and A380. B-52 is an example for the military aircrafts. The integrated intake is used in combat (military) aircrafts. An example for which is the British Aerospace Harrier. For integrated intakes, the internal flow problems are of dominant concern, due to (a) the duct being longer, usually containing bends and shape changes and (b) the presence of aircraft surface ahead of the intake, wetted by the internal flow [10].

For typical podded intakes, the friction losses are insignificant while the flow separation and minimum external drag are of prime importance. The mass flow rate and the downstream pressure are determined by engine operating conditions: usually by the conditions at the choked turbine exit and by the operating speed of the compressor and turbine.

Because of this variation in mass flow requirements, the inlet may be operating under suction (external acceleration) or spillage (external deceleration).

The internal flow has the shortest and most direct route possible to the engine, and its pressure recovery is almost 100 % [10]. From aerodynamics point of view, the flow in intake resembles the flow in a duct. The duct “captures” a certain stream tube of air, thus dividing the air stream into an internal flow and an external flow. The external flow preserves the good aerodynamics of the airframe, while the internal flow feeds the engine.

The flow characteristics in podded intakes are illustrated in Fig. 8.39 for different flow conditions. Because the inlet does not have thermodynamic work,

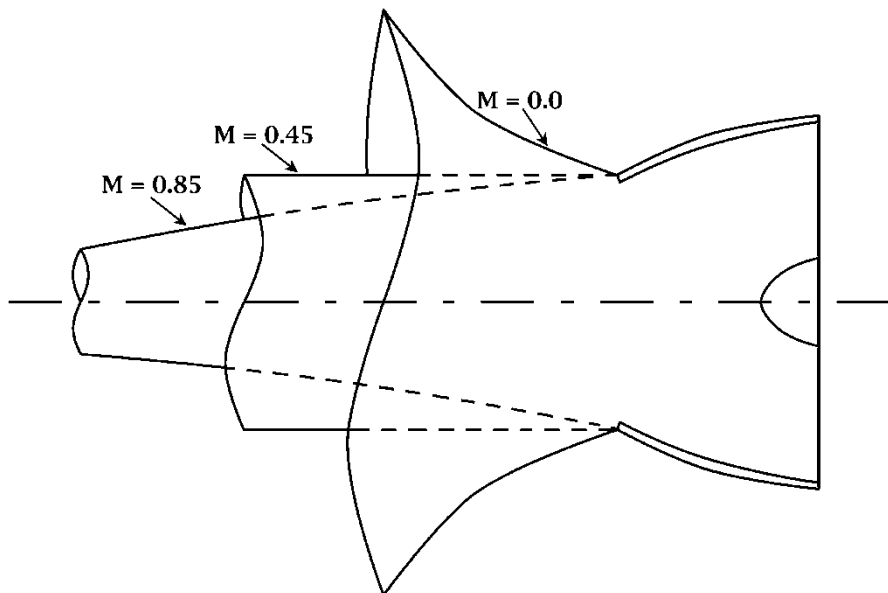


Fig. 8.39 Flow characteristics of podded intakes

the total temperature through the inlet is constant. In ground run and climb (small or zero Mach number), there will be no effective free-stream velocity which results in a large induced flow capture area causing the streamlines to converge into the intake area. The ratio between the upstream capture area to the inlet area approaches infinite. The stream tube has a bell-shape pattern. During climb, the free-stream velocity will be lower than the intake velocity due to the high mass flow rates required. This will also result in a larger entry stream tube area than the intake area (a convergent stream tube pattern). At moderate-speed cruise ($M \geq 0.45$), the entry stream tube will be equal to the intake area, and diffusion takes place inside the inlet. At high cruise and top speeds ($M \geq 0.85$), diffusion takes place partially outside and partially inside the intake.

8.1.4.1 Takeoff and Cruise Operation

Depending on the flight speed and the mass flow demanded by the engine, the inlet may have to operate with a wide range of incident stream conditions. Figure 8.40 shows the performance of subsonic intake during two typical subsonic conditions, namely, takeoff (Fig. 8.40a) and cruise (Fig. 8.40b).

For each operating condition, three plots are given in Fig. 8.36. The first illustrates the stream tube, while the second depicts the pressure and speed variation and the third is a temperature–entropy diagram. The flow in intakes is identified by three states, namely, far upstream which is denoted as (∞) , at the duct entry denoted by (1) and at the engine face denoted (2). The flow outside the engine (from state ∞ to 1) is an isentropic one, where no losses are associated with the total temperature and pressure.

Takeoff and Climb Operation

During low-speed high-thrust operation (e.g., during takeoff and climb), the engine will demand large mass flow and the air stream upstream the intake will be accelerated. The pressure at the inlet face is lower than the ambient pressure, so that air is sucked into the inlet. Boundary-layer separation and compressor stall become more likely [11]. The engine acts as a sink to the flow which rushes in from a wide stream tube, as shown in Fig. 8.39. There is then an external acceleration. Within the inlet, the stream tube will have a divergent shape yielding flow deceleration. Many aircrafts use “bypass doors” which open at takeoff to pull in more air. In high-speed flight, these doors may slide open to let out some of the excess air and thus reduce spillage around the lip of the inlet.

The following conditions are satisfied:

$$u_1 > u_\infty , \quad P_1 < P_\infty , \quad P_{01} = P_{0\infty} , \quad T_{01} = T_{0\infty}$$

$$P_2 > P_1 , \quad P_{02} < P_{0\infty} , \quad u_2 < u_1$$

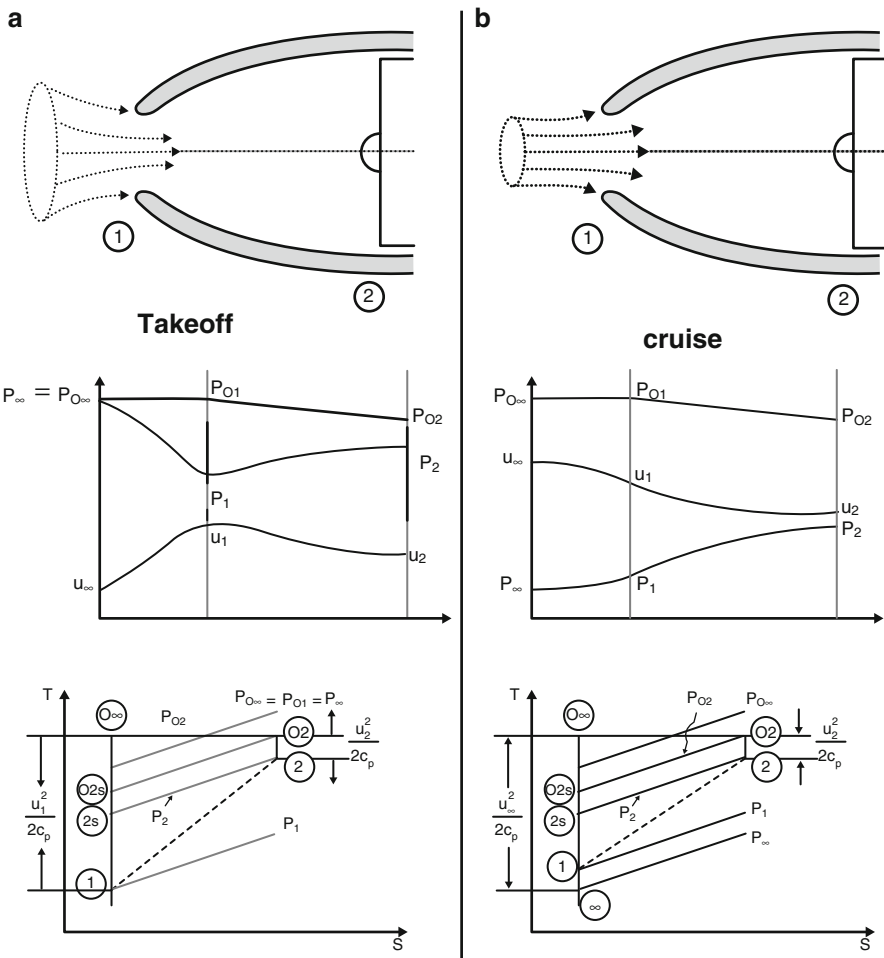


Fig. 8.40 Subsonic inlet during takeoff (a) and cruise (b)

Cruise Operation

For high speed, or cruise condition, the function of intake is to decelerate the air velocity to that which is acceptable to the compressor/fan face. Air is decelerated (diffused) both upstream and within the intake. Since the inlet speed to the engine (compressor/fan) should be nearly constant for different operating conditions, it is a favorable condition for the diffuser because the pressure rise in the diffuser is smaller. Under these conditions the “upstream capture area” A_{∞} is less than the inlet area A_1 , and some flow is spilled over the inlet causing spillage drag. Thus losses are smaller, but external drag is increased.

Table 8.1 Intake performance at different flight segments

	ΔP	ΔP_0	Δu	ΔT_0
Takeoff/Climb	(+)	(-)	(+)	Zero
Cruise	(+)	(-)	(-)	Zero

The following conditions can be stated:

$$u_1 < u_\infty \quad , \quad P_1 > P_\infty \quad , \quad P_{01} = P_{0\infty} \quad , \quad T_{01} = T_{0\infty}$$

$$P_2 > P_1, P_{02} < P_{0\infty}, u_2 < u_1$$

Thus, for cruise conditions, to avoid separation, or to have a less severe loading on the boundary layer, it is recommended to have a low velocity ratio (u_1/u_∞) and consequently less internal pressure rise [12] while

$$\left(\frac{P_2}{P_1}\right)_{\text{takeoff}} > \left(\frac{P_2}{P_1}\right)_{\text{cruise}} \quad (8.6)$$

A summary for intake performance (from far upstream to compressor/fan inlet) may be tabulated in Table 8.1.

The serious problem is the change in M_∞ from zero at takeoff to about 0.8 at cruise.

If optimized for the $M_\infty = 0.8$ cruise, the inlet would have a thin lip to minimize the increase in Mach number as the flow is divided. But this inlet would separate badly on the inside at takeoff and low subsonic conditions because the turn around the sharp lip would impose severe pressure gradients. To compromise, the lip is rounded making it less sensitive to the flow angle, but incurring some loss due to separation in the exterior flow.

When fully developed a good inlet will produce a pressure recovery $P_{o2}/P_{oa} = 0.95 - 0.97$ at its optimum condition.

8.1.4.2 Capture Area for a Turbofan Case Study

Since the mass flow rate is expressed by the relation

$$\dot{m}_\infty = \rho_\infty V_\infty A_\infty = \frac{P_\infty}{RT_\infty} \left(M_\infty \sqrt{\gamma RT_\infty} \right) A_\infty$$

Then

$$A_\infty = \frac{\dot{m}_\infty}{P_\infty M_\infty} \sqrt{\frac{RT_\infty}{\gamma}}$$

or

$$A_\infty = \frac{\lambda}{M_\infty} \quad \text{where} \quad \lambda = \frac{\dot{m}_\infty}{P_\infty} \sqrt{\frac{RT_\infty}{\gamma}}$$

If a turbofan engine during ground ingests airflow at the rate of $\dot{m}_\infty = 561 \text{ kg/s}$ through an inlet area (A_1) of 0.3 m^2 and if the ambient conditions (T_∞, P_∞) are

Table 8.2 Stream tubes of airflow entering the engine inlet at different Mach numbers

M_∞	0.05	0.1	0.2	0.3	0.4	0.5	0.6	0.7	0.8	0.9
$\frac{A_\infty}{A_1}$	9.0	4.5	2.25	1.5	1.125	0.9	0.75	0.64	0.56	0.5
$\frac{D_\infty}{D_1}$	3.0	2.12	1.5	1.22	1.06	0.95	0.87	0.8	0.75	0.71

288 K and 101 kPa respectively, then the area ratio ($A_\infty = A_1$) for different free stream Mach numbers is calculated as follows:

$$\lambda = \frac{\dot{m}_\infty}{P_\infty} \sqrt{\frac{RT_\infty}{\gamma}} = \frac{561}{101,000} \sqrt{\frac{287 \times 288}{1.4}} = 1.35$$

$$\frac{A_\infty}{A_1} = \frac{0.45}{M_\infty} \quad (\text{A})$$

From Eq. A, the capture area is equal to the engine inlet area ($A_\infty/A_1 = 1$) when $M_\infty = 0.45$.

From relation (4), Table 8.2 is constructed. Figure 8.39 illustrates stream tubes of airflow entering the engine inlet at different Mach numbers.

As shown in Fig. 8.39, the upstream “capture area” can be estimated under ideal, isentropic flow conditions. The ideal conditions mean that the flow is frictionless and that there are no flow disturbances in or out of the diffuser. We start from the mass flow rate balance.

$$\rho_\infty V_\infty A_\infty = \rho_1 V_1 A_1$$

The area ratio is then expressed by the relation

$$\frac{A_\infty}{A_1} = \frac{P_1}{P_\infty} \frac{T_\infty}{T_1} \frac{V_1}{V_\infty} = \frac{P_1}{P_\infty} \frac{T_\infty}{T_1} \frac{M_1}{M_\infty} \sqrt{\frac{T_1}{T_\infty}} = \frac{P_1/P_{01}}{P_\infty/P_{01}} \sqrt{\frac{T_\infty/T_{0\infty}}{T_1/T_{0\infty}} M_1}$$

$$\frac{A_\infty}{A_1} = \left(\frac{1 + \frac{\gamma-1}{2} M_\infty^2}{1 + \frac{\gamma-1}{2} M_1^2} \right)^{\frac{\gamma}{\gamma-1}} \left(\frac{1 + \frac{\gamma-1}{2} M_1^2}{1 + \frac{\gamma-1}{2} M_\infty^2} \right)^{\frac{1}{2}} \frac{M_1}{M_\infty}$$

$$\frac{A_\infty}{A_1} = \left(\frac{1 + \frac{\gamma-1}{2} M_\infty^2}{1 + \frac{\gamma-1}{2} M_1^2} \right)^{\frac{\gamma+1}{2(\gamma-1)}} \frac{M_1}{M_\infty} \quad (8.7)$$

Next, within the inlet, continuity equation is then

$$\rho_2 V_2 A_2 = \rho_1 V_1 A_1$$

Friction within the inlet is counted for via pressure recovery factor

$$\pi_d \equiv \frac{P_{02}}{P_{01}}$$

The area ratio is then may be expressed as

$$\begin{aligned} \frac{A_2}{A_1} &= \frac{P_1 T_2 V_1}{P_2 T_1 V_2} = \frac{P_1 M_1}{P_2 M_2} \sqrt{\frac{T_2}{T_1}} = \frac{P_1/P_{01} P_{01}}{P_2/P_{02} P_{02}} \sqrt{\frac{T_2/T_{02} M_1}{T_1/T_{01} M_2}} \\ \frac{A_2}{A_1} &= \left(\frac{1 + \frac{\gamma-1}{2} M_2^2}{1 + \frac{\gamma-1}{2} M_1^2} \right)^{\frac{\gamma}{\gamma-1}} \times \frac{1}{\pi_d} \times \left(\frac{1 + \frac{\gamma-1}{2} M_1^2}{1 + \frac{\gamma-1}{2} M_2^2} \right)^{\frac{1}{2}} \frac{M_1}{M_2} \\ \frac{A_2}{A_1} &= \left(\frac{1 + \frac{\gamma-1}{2} M_2^2}{1 + \frac{\gamma-1}{2} M_1^2} \right)^{\frac{\gamma+1}{2(\gamma-1)}} \times \frac{1}{\pi_d} \times \frac{M_1}{M_2} \end{aligned} \quad (8.8)$$

From Eqs. 8.7 and 8.8,

$$\frac{A_\infty}{A_2} = \left(\frac{1 + \frac{\gamma-1}{2} M_\infty^2}{1 + \frac{\gamma-1}{2} M_2^2} \right)^{\frac{\gamma+1}{2(\gamma-1)}} \frac{M_2}{M_\infty} \times \pi_d \quad (8.9)$$

Equation 8.9 relates the ratio of the capture area to the compressor/fan entrance area, for the given flight Mach number, M_∞ , and the required Mach number, M_2 , at the compressor/fan inlet.

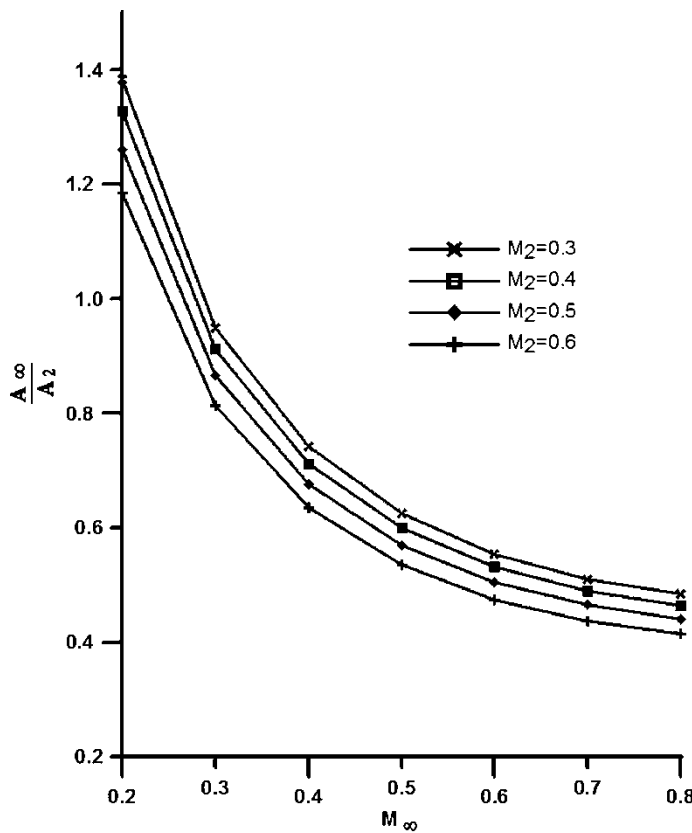
Figure 8.41 shows the plot of Eq. 8.9 for various M_2 . It can be seen that a large capture area is required during low-speed operations (acceleration), as noted above, while the area ratio becomes less than one (deceleration) at normal cruise Mach numbers.

Figure 8.42 shows the plot of Eq. 8.9 for a constant value of M_2 (0.3) and different values of inlet pressure recovery (π_d).

Since the inlet resembles diffuser geometry, a quick review of the diffuser performance is highlighted hereafter. Figure 8.43a illustrates a typical conical diffuser. Three parameters define its geometry, namely, aspect ratio (AR), either its wall length (L) or its axial length (N) is used as a characteristic length. The third parameter is the divergence angle (2θ), though it is not an independent variable but is related to other parameters by the following relation for conical diffusers:

$$AR = 1 + 2 \frac{L}{R_1} \sin \theta + \left(\frac{L}{R_1} \sin \theta \right)^2 \quad (8.10)$$

Figure 8.43 illustrates the different shapes of diffuser. Figure 8.44a illustrates the geometry of a conical/annular diffuser, while Fig. 8.44b illustrates the typical flow pattern for the first stall in the diffuser. Generally flow ideally follows diffuser contours; however, as boundary layer thickens, small separation region is first seen



**Relation Between Area Ratio and Mach Number of the Stream,
at different M_2 , and at $\pi_d=0.95$**

Fig. 8.41 Area ratio as a function of the flight Mach numbers, for various M_2 and constant pressure recovery factor $\pi_d = 0.95$; Eq. 8.9

in corners. It occupies nearly (1/5) of the diffuser wall or less, and no (or little) reverse flow is encountered.

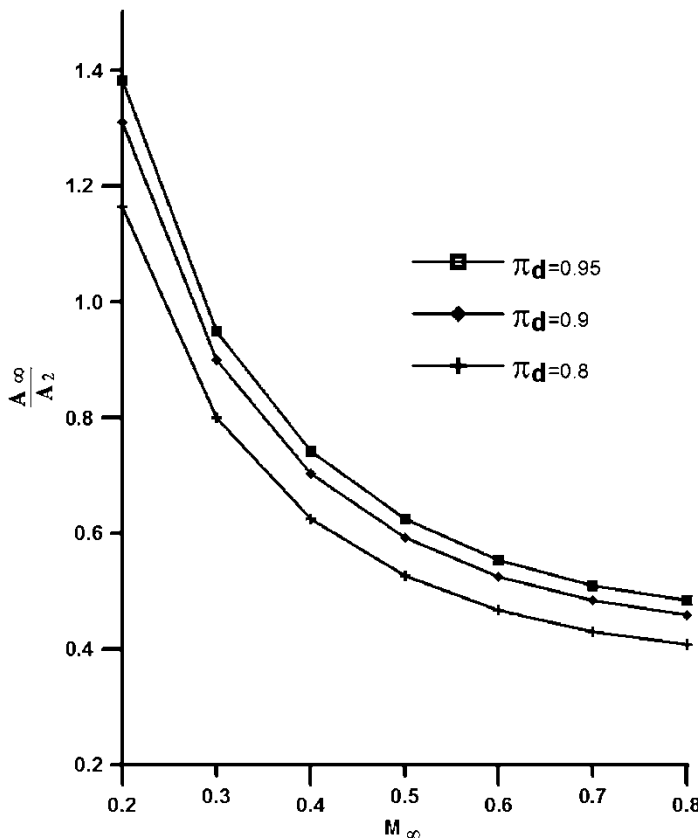
Figure 8.45 illustrates first stall characteristics for diffusers of different geometries [13]. It is clear from this figure that stall may occur in annular diffusers under less severe geometries than in conical diffusers.

Example 8.1 During takeoff conditions, a turbofan engine has the following conditions:

Total air mass flow rate of engine

$$\dot{m} = 1155.43 \text{ kg/sec}, P_{\infty} = 101.325 \text{ kPa}, T_{\infty} = 288 \text{ K}$$

Mach numbers: far upstream $M_{\infty} = 0.25$, intake inlet $M_1 = 0.58$, and intake outlet $M_2 = 0.50$.



**Relation Between Area Ratio and Mach Number of the Stream,
at different π_d , and at $M_2=0.3$.**

Fig. 8.42 Area ratio as a function of the flight Mach numbers, for various pressure recovery factor and constant M_2 ; Eq. 8.9

Determine the diameters at far upstream (d_∞), intake inlet section (d_1) and intake outlet section (d_2) assuming the pressure recovery $\pi_d = 0.95$.

Solution

(a) *Far upstream (state ∞)*

$$\dot{m} = \rho_\infty V_\infty A_\infty = \frac{P_\infty}{R T_\infty} * M_\infty * \sqrt{\gamma R T_\infty} * A_\infty$$

$$1155.43 = \frac{101.325 \times 1000}{287 \times 288} \times 0.25 \times \sqrt{1.4 \times 287 \times 288} \times A_\infty$$

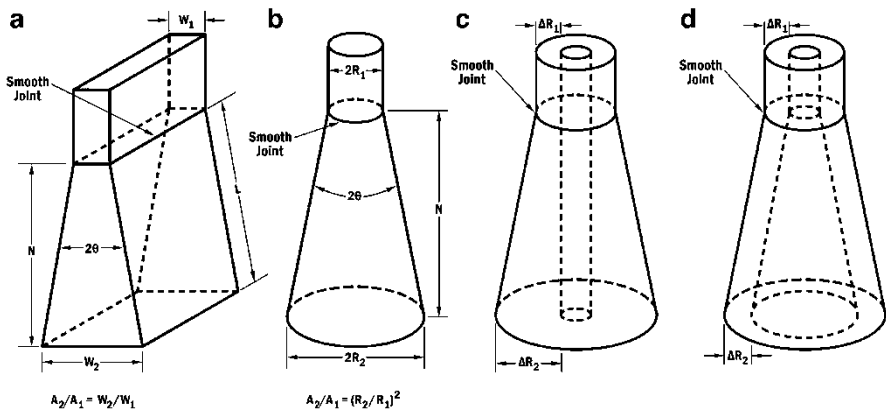


Fig. 8.43 Different shapes of diffuser: (a) two dimensional, (b) conical, (c) straight-core annular, and (d) equiangular annular

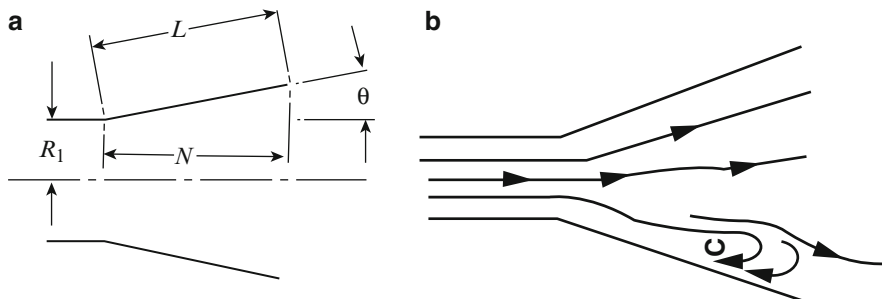


Fig. 8.44 Conical/annular diffuser: (a) geometry and (b) typical flow pattern for first stall

$$A_\infty = 11.0 \text{ m}^2$$

$$d_\infty = 3.742 \text{ m}$$

$$V_\infty = M_\infty \sqrt{\gamma R T_\infty} = 0.25 \sqrt{1.4 \times 287 \times 288}$$

$$V_\infty = 85.04 \text{ m/s}$$

$$T_{O\infty} = T_\infty \left(1 + \frac{\gamma - 1}{2} M_\infty^2 \right)$$

$$T_{O\infty} = 288 \left(1 + \frac{1.4 - 1}{2} * 0.25^2 \right)$$

$$T_{O\infty} = 293.14 \text{ K}$$

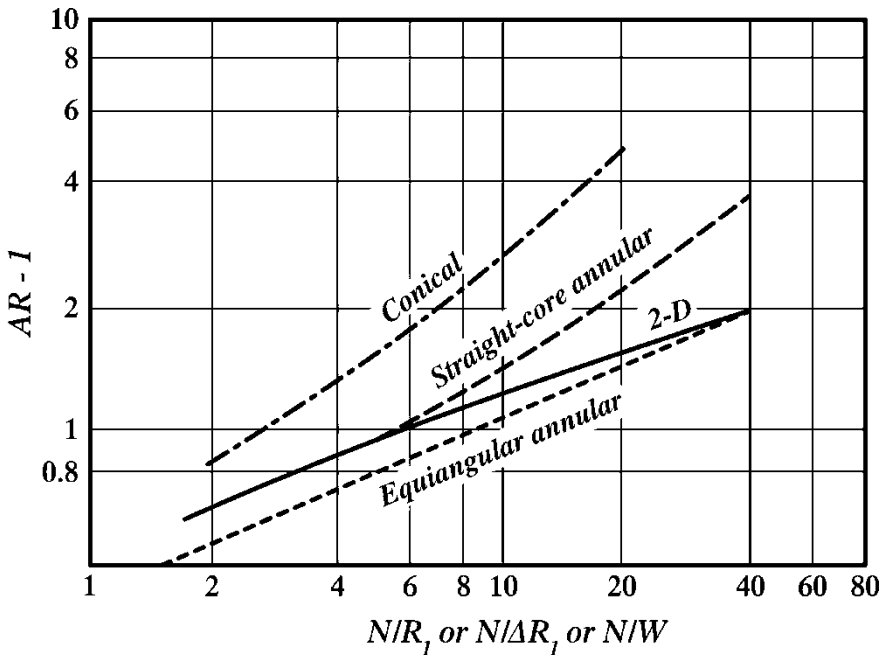


Fig. 8.45 Diffuser characteristics

$$P_{O\infty} = P_\infty \left(1 + \frac{\gamma - 1}{2} M_\infty^2 \right)^{\frac{1}{\gamma-1}}$$

$$P_{O\infty} = 101.84 \text{ kPa}$$

(a) At inlet section of intake (nose lips; state 1)

$$T_{O1} = T_{O\infty} = 293.14 \text{ K}$$

$$P_{O1} = P_{O\infty} = 101.84 \text{ kPa}$$

From Eq. 8.7, then the area ratio is

$$\frac{A_\infty}{A_1} = \left(\frac{1 + \frac{\gamma-1}{2} M_\infty^2}{1 + \frac{\gamma-1}{2} M_1^2} \right)^{\frac{1}{2(\gamma-1)}} \frac{M_1}{M_\infty} = 1.98$$

$$A_1 = 5.55 \text{ m}^2$$

$$d_1 = 2.658 \text{ m}$$

(b) At outlet section of intake (state 2)

From Eq. 8.8, then the area ratio is

$$\frac{A_2}{A_1} = \left(\frac{1 + \frac{\gamma-1}{2} M_2^2}{1 + \frac{\gamma-1}{2} M_1^2} \right)^{\frac{\gamma+1}{2(\gamma-1)}} \times \frac{1}{\pi_d} \times \frac{M_1}{M_2} = 1.1626$$

$$A_2 = 6.452 \text{ m}^2$$

$$d_2 = 2.866 \text{ m}$$

(b) Length of intake (L)

since

$$\frac{A_2}{A_1} = 1.1626$$

then

$$\frac{A_2}{A_1} - 1 = 0.1626$$

From Fig. 8.45

$$\frac{N}{R_1} = 0.58$$

$$N = 0.7708 \text{ m}$$

Assuming the diffuser has an included angle $2\theta = 12^\circ$

$$L = \frac{N}{\cos \theta} = \frac{0.6645}{\cos \theta} = 0.775 \text{ m}$$

Alternatively, from the diffuser shape,

$$\frac{D_0 - D_i}{2L} = \tan \theta$$

$$L = \frac{2.822 - 2.658}{2 \tan 6} = 0.78 \text{ m}$$

8.1.4.3 Case Study

Numerical Modeling for Subsonic Intake of a High-Bypass Ratio Turbofan Engine

Fluent 6.0 software provided by Fluent Inc. is used here to simulate the flow field within the intake of high-bypass ratio turbofan engine. Typical engines are CF6 and V2500 illustrated in Fig. 8.46.

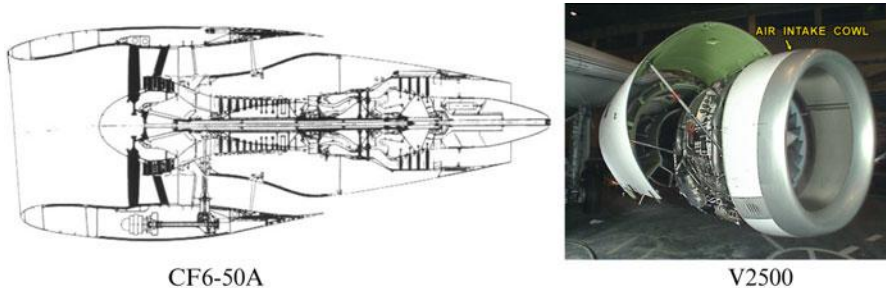


Fig. 8.46 High-bypass ratio turbofan (HBPR) engine

The equations governing the airflow are the conservation of mass, conservation of momentum, conservation of energy equations, and some other auxiliary equations: Sutherland's equation for viscosity and Spalart–Allmaras [14] for turbulence modeling.

The numerical procedure follows the following steps:

1. Division of the computational domain into discrete control volumes using a computational grid
2. Integration of the governing equations on the individual control volumes to construct algebraic equations for the discrete dependent variables such as velocities, pressure, temperature, and conserved scalars
3. Linearization of the discretized equations and solution of the resultant linear equation system to yield updated values of the dependent variables

Figure 8.47 shows the dimensions of the intake and following fan [15]. The axial length of the intake is 155.55 cm, and the nose is simplified as a hemisphere of radius 40.57 cm.

The computational domain in the study includes both the fan and the intake zones. Due to the large dimensions of both the intake and the fan combination, it was very difficult to solve overall the domain. Since the fan includes 38 blades, a periodic sector of an angle ($360/38$) was generated separately for both the fan and the intake zones. The two zones were merged together to form the required computational domain using Gambit preprocessor. Both the fan and the intake zones were meshed separately and next merged using the Tmerge utility. Due to complex geometry of both the fan and intake sectors, unstructured tetrahedral grid is used. Number of cells for intake and fan blocks is 49,000 and 282,000, respectively. The number of nodes for intake and fan blocks is 11,350 and 59,400, respectively.

The results of the computed airflow properties (Mach numbers, total and static pressures, as well as the total and static temperatures) through intake are presented in Figs. 8.48 and 8.49. Two flight conditions are discussed: cruise and takeoff

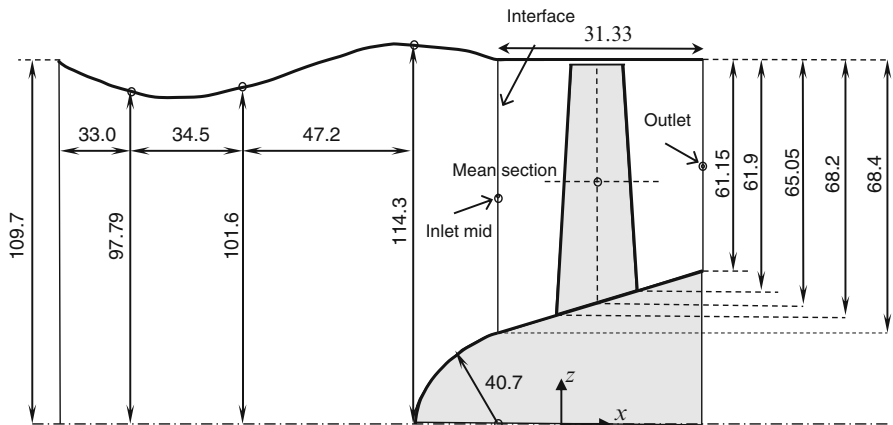


Fig. 8.47 Detailed dimensions of the intake and fan (all dimensions in cm)

conditions. These results include the variation of the flow properties in an axisymmetric section through the intake.

Cruise Conditions

Figure 8.48 shows the variation of the flow properties at an axisymmetric section in the intake and fan nose at the cruise conditions (11,000-m altitude, 0.85 flight Mach number, and 100 % fan speed). The contours of the Mach number are shown in Fig. 8.48a. One can observe that the Mach number varies in both axial and radial directions. At inlet to the intake, the Mach number decreases in the radial outward direction from about 0.5 at the center line to about 0.2 near the intake casing. Moving axially toward the fan, the passage convergence at nearly the first third causes a rapid increase in the Mach number. At this location the Mach number increases radially outward from about 0.5 to 0.67 due to flow acceleration. Next, the intake passage divergence results in a decrease in the Mach number in both the axial and radial directions. At the fan inlet, the Mach number is nearly uniform with a value of about 0.5. The contours of static pressure and temperature are shown in Fig. 8.48b, c, respectively. It is noticed that these contours have a reverse behavior compared with the Mach number contours. The maximum static pressure (about 37.4 kPa) and maximum static temperature (about 261 K) are shown at the fan nose stagnation streamline.

Takeoff Conditions

The airflow results at the takeoff conditions are shown in Fig. 8.49. Figure 8.49 shows the contours of the Mach number, static pressure, and static temperature at an axisymmetric section in the intake. One notices lower values of the Mach number and higher values of both static pressure and temperature compared with the cruise conditions given in Fig. 8.47.

Fig. 8.48 Variation of the flow field properties across the intake (cruise). (a) Contours of absolute Mach number, (b) contours of static pressure (Pa), and (c) contours of static temperature (K)

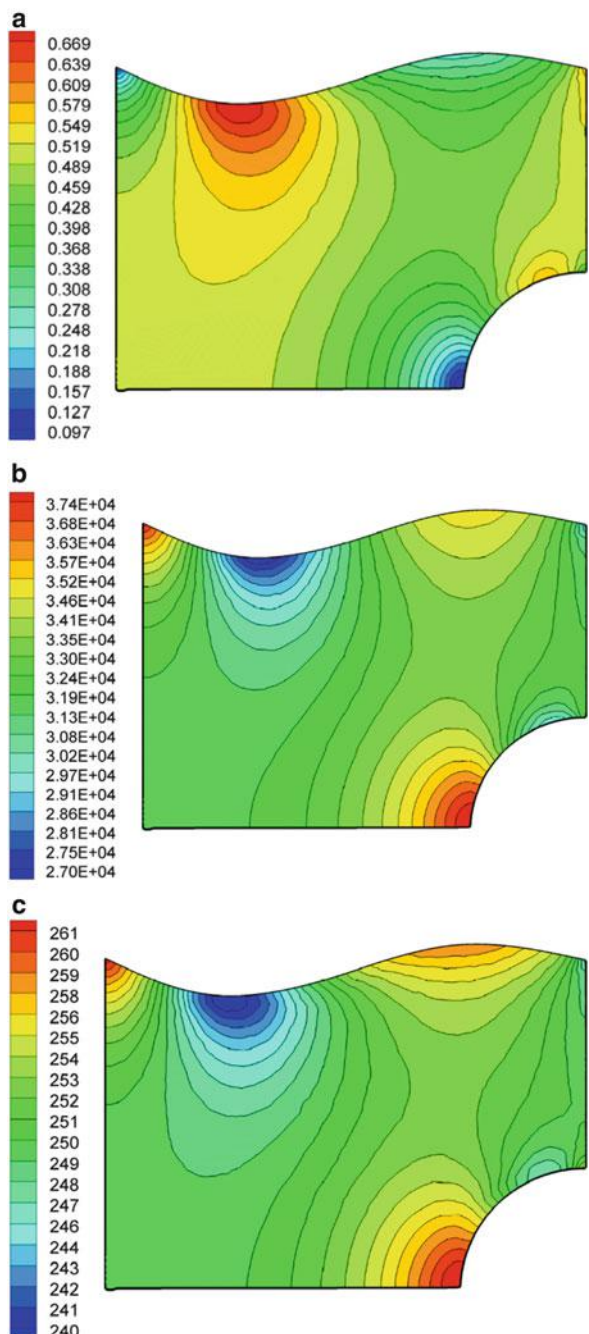
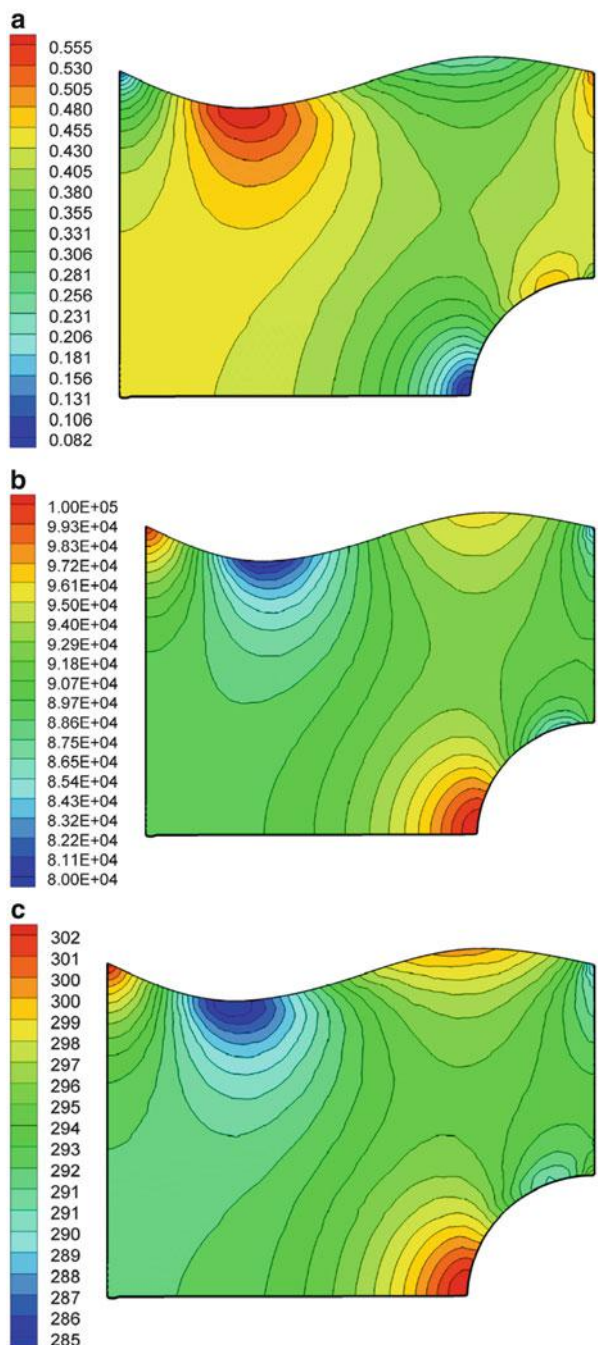


Fig. 8.49 Variation of the flow field properties across the intake (takeoff). (a) Contours of absolute Mach number, (b) contours of static pressure (Pa), and (c) contours of static temperature (K)



8.1.5 Supersonic Intakes

The design of inlet systems for supersonic aircraft is a highly complex matter involving engineering trade-offs between efficiency, complexity, weight, and cost. A typical supersonic intake is made up of a supersonic diffuser, in which the flow is decelerated by a combination of shocks (one or more oblique followed by a normal) and a subsonic diffuser, which reduces the Mach number from high subsonic value after the normal shock to the value acceptable to the engine [16]. Subsonic intakes which have thick lips are quite unsuitable for supersonic speeds. The reason is that a normal shock wave ahead of the intake is generated which will yield a very sharp static pressure rise without change of flow direction and correspondingly big velocity reduction. The adiabatic efficiency of compression through a normal shock wave is very low as compared with oblique shocks. At Mach 2.0 in the stratosphere, adiabatic efficiency would be about 80 % or less for normal shock waves, whereas its value will be about 95 % or even more for an intake designed for oblique shocks.

8.1.5.1 Classification of Supersonic Intakes Based on Geometry

Generally supersonic intakes [5] and [8] may be classified into two types, namely, fixed and variable geometry (Fig. 8.50). Podded installations are inappropriate for fighters.

(A) Fixed Geometry

It may have one of the following three configurations:

1. Two dimensional
2. Axisymmetric
3. Chin

(B) Variable geometry

With the maturing of supersonic flight, the demands for variable-geometry intakes and longer intake ducts gradually pushed engines further back, allowing more room in the center fuselage for fuel over the CG. One of the aircrafts which set the trend to fully rear-mounted engines was the MiG-21, with its short afterburner. Since then aircrafts like the F-111, MiG-25, F-14, F-18, and Tornado have featured this location, which ensures that the exhaust is aft of the empennage, yielding low drag when the reheat is off and reducing heating and acoustic effects when reheat is on.

Variable geometry may have also one of the following three configurations:

1. Translating center body
2. Variable-geometry center body
3. Variable-geometry cowl

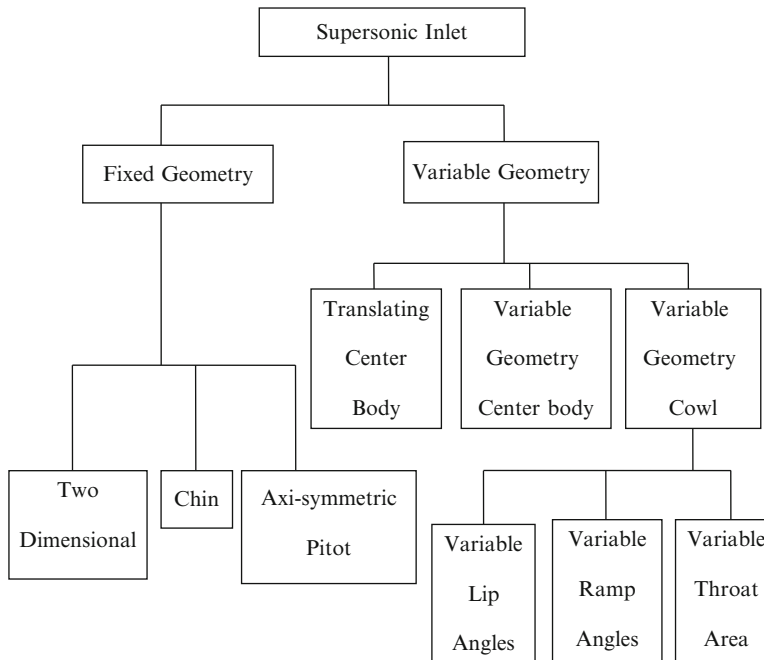


Fig. 8.50 Classification of supersonic inlets

This last one may be either variable lip angle, variable ramp angle, or variable throat angle.

The adjustable ramps provide further compression along with the desired variation of the throat area with Mach number. The angle of the ramps varies automatically in a prescribed manner as the Mach number changes.

Figure 8.51 illustrates both axisymmetric intake for Mig-21 and two-dimensional (2-D) intake for F-14. SR-71 is another example for axisymmetric intake. Axisymmetric intake uses axisymmetric central cone to shock the flow down to subsonic speeds. The two-dimensional intakes have rectangular cross sections; examples are the F-14 and F-15 fighter aircrafts. For variable-geometry axisymmetric intakes, the central cone may move fore and aft to adjust the intake area. The inlet area in the case of rectangular section is adjusted through hinged flaps (or ramps) that may change its angles.

For flight at Mach numbers much beyond 1.6, variable-geometry features must be incorporated in the inlet to achieve high-inlet pressure recoveries together with low external drag.

The General Dynamics F-111 airplane has a quarter-round inlet equipped with a translating center body or spike (Fig. 8.52). The inlet is bounded on the top by the wing and on one side by the fuselage. An installation of this type is often



Fig. 8.51 Axisymmetric and two-dimensional supersonic intakes

referred to as an *armpit* inlet. The spike automatically translates fore and aft as the Mach number changes. The throat area of the inlet also varies with the Mach number. This is accomplished by expansion and contraction of the rear part of the spike.

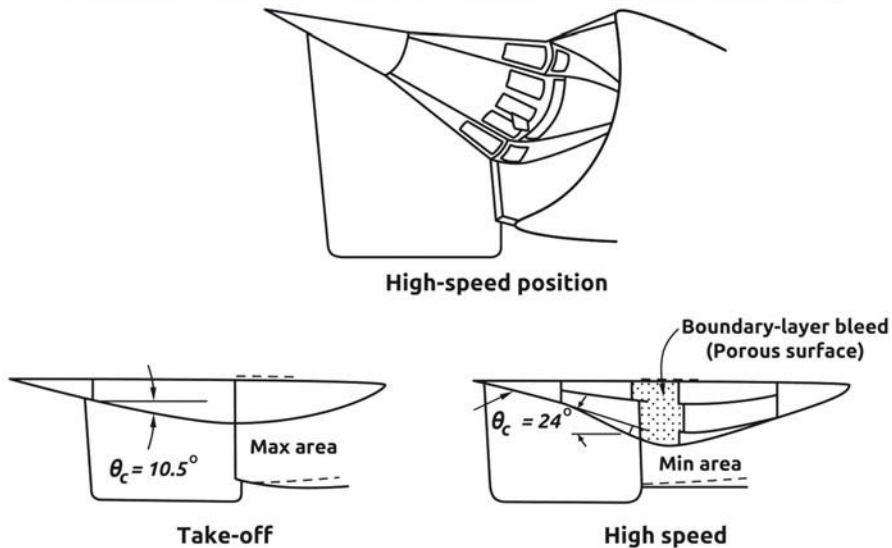


Fig. 8.52 F-111 fighter fitted by “armpit” intakes

8.1.5.2 Classification of Supersonic Intakes Based on Shock Wave Pattern

Concerning shock wave pattern, there are three types, namely, internal, external, or mixed compression. As shown in Fig. 8.53, three patterns for shock waves are seen, namely, external, internal, and combined external/internal. The set of shocks situated between the forebody and intake lip are identified as external shocks, while the shocks found between the nose lip and the intakes throat are called

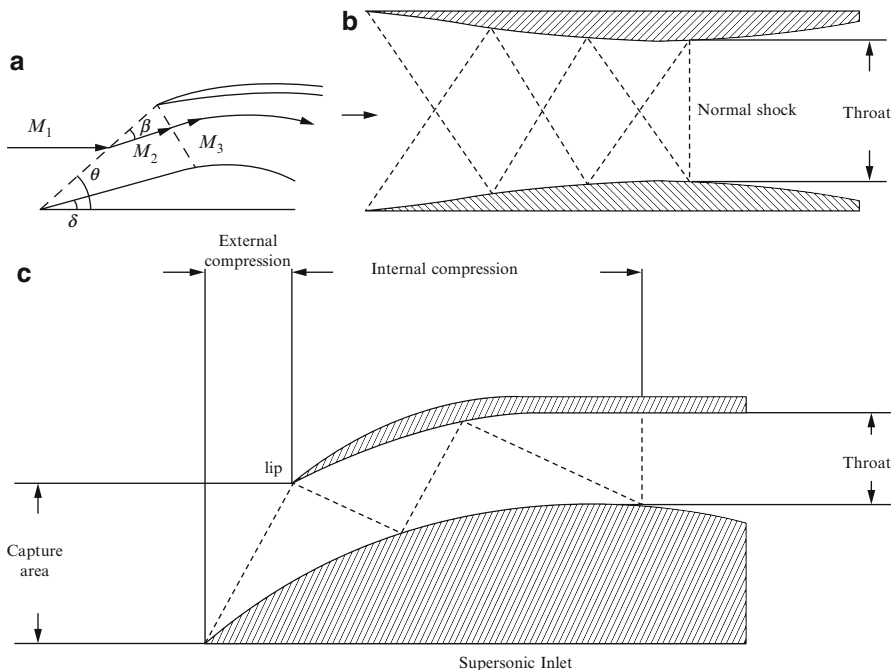


Fig. 8.53 Types of supersonic intakes. (a) External, (b) internal, and (c) external and internal compression supersonic intake

internal shocks. The third type combines both shock patterns (external and internal) and denoted as mixed-compression intakes.

(A) *External compression intake (inlet)*

The forebody intake is frequently used for “external compression intake of wedge or cone form” [10].

External compression intakes complete the supersonic diffusion process outside the covered portion of the inlet where the flow is decelerated through a combination of oblique shocks (may be a single, double, triple, or multiple). These oblique shocks are followed by a normal shock wave that changes the flow from supersonic to subsonic flow. Both of the normal shock wave and the throat are ideally located at the cowl lip. The supersonic diffuser is followed by a subsonic diffuser, which reduces the Mach number from high subsonic value after the last shock to the value acceptable to the engine. The simplest form of staged compression is the single oblique shock, produced by a single-angled wedge or cone projects forward of the duct, followed by a normal shock as illustrated in Fig. 8.53a. The intake in this case is referred to as a *two-shock* intake. With a wedge the flow after the oblique shock wave is at constant Mach number and parallel to the wedge surface. With a cone the flow behind the conical shock is itself conical; the Mach number is constant along rays from the apex and varies along streamline.

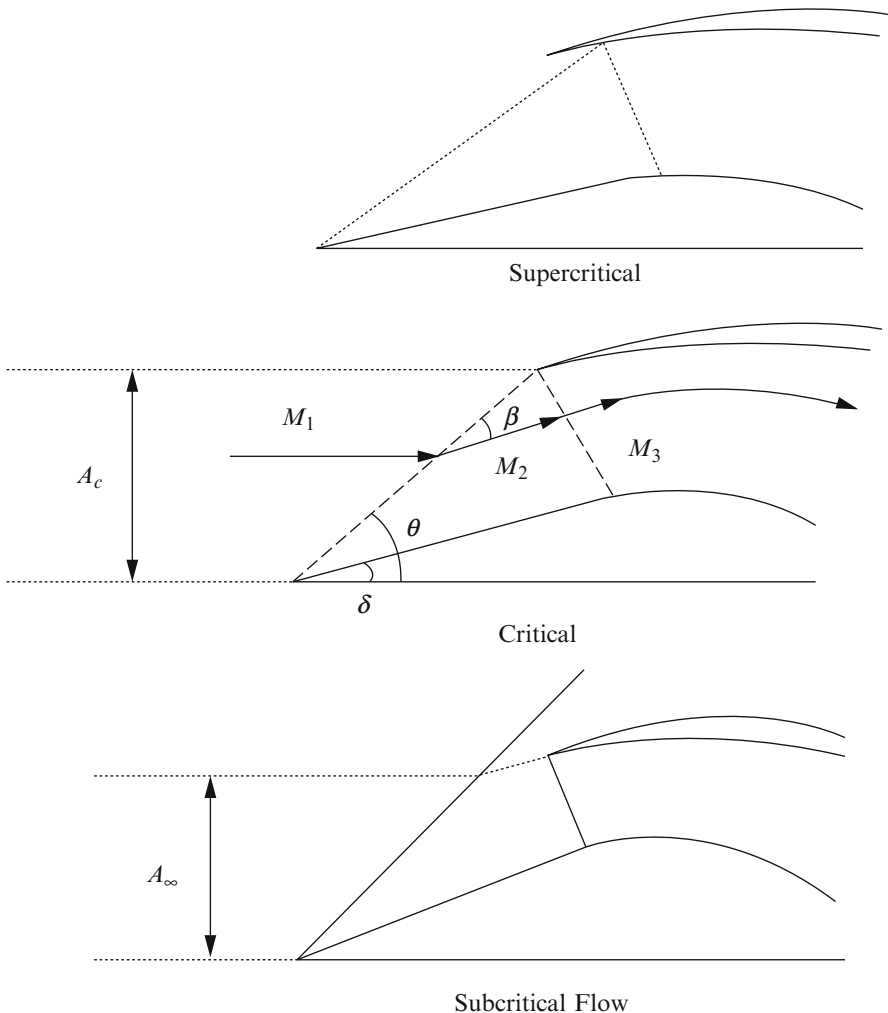


Fig. 8.54 Types of flow in an external compression intake

In a single oblique shock external compression intake, the capture area (A_c) for supersonic intakes is defined as the area enclosed by the leading edge, or “highlight,” of the intake cowl, including the cross-sectional area of the forebody in that plane (Fig. 8.54). The maximum flow ratio is achieved when the boundary of the free-stream tube (A_∞) arrives undisturbed at the lip. This means

$$\frac{A_\infty}{A_c} = 1.0$$

This condition is identified as the *full flow* [10] or the *critical flow* [8]. This condition depends on the Mach number, angle of the forebody, and the position of the tip. In this case, the shock angle (θ) is equal to the angle subtended by the lip at the apex of the body and corresponds to the maximum possible flow through the intake. This is the design point for constant area. At Mach numbers (or speeds) below the value of the critical (design) value, the mass flow is less than that at the critical condition, and the oblique shock wave occurs in front of the cowl lip and this case is identified as *subcritical*. It is noticeable here that

$$\frac{A_\infty}{A_c} < 1.0$$

Moreover, the outer drag of the intake becomes very large and smaller pressure recovery is obtained. If air speeds are greater than the design value, then the oblique shock will impinge inside the cowl lip, and the normal shock will move to the diverging section. This type of operation is referred to as the *supercritical* operation.

The two-shock intake is only moderately good at Mach 2.0 and unlikely to be adequate at higher Mach numbers [8]. The principle of breaking down an external shock system can be extended to any desired number of stages. The next step is the three-shock intake where two oblique shocks are followed by a normal shock, where the double wedge and double cone are the archetypal forms (Fig. 8.55).

Continuing the process of breaking down the external shock system, three or more oblique shocks may be used ahead of the normal shock. For a system of $(n - 1)$ oblique shocks, the pressure recovery factor will be

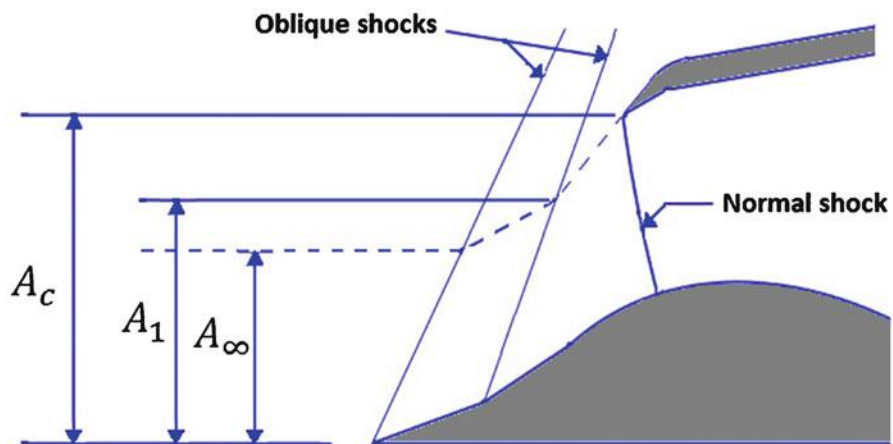


Fig. 8.55 Three shocks for double-cone (or double-wedge) geometry

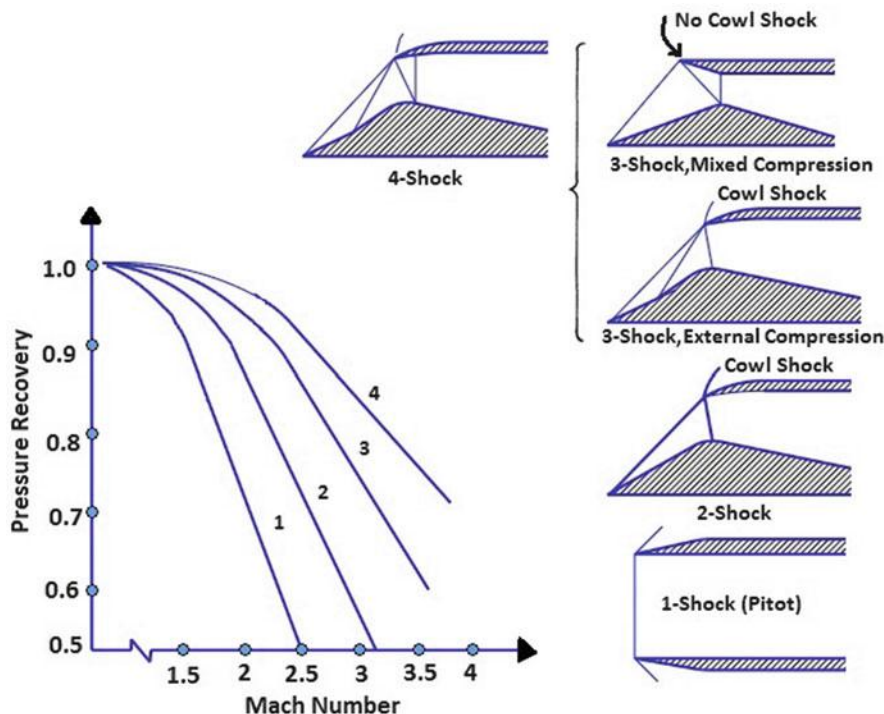


Fig. 8.56 Various types of intake geometry and their effect on pressure recovery

$$\frac{P_{0n}}{P_{0\infty}} = \frac{P_{01}}{P_{0\infty}} \frac{P_{02}}{P_{01}} \frac{P_{03}}{P_{02}} \frac{P_{04}}{P_{03}} \cdots \cdots \frac{P_{0n-1}}{P_{0n-2}} \left(\frac{P_{0n}}{P_{0n-1}} \right)_{\text{normal shock}} \quad (8.11)$$

Two remarks are to be mentioned here:

1. As the number of oblique shocks increases, the pressure recovery factor increases (Fig. 8.56).
2. Up to Mach 2, equal deflections of the successive wedge angles give the best results, while for higher Mach numbers, the first deflection angle needs to be the smallest and the last the largest [8].

Extending the principle of multi-shock compression to its limit leads to the concept of *isentropic compression*, in which a smoothly contoured forebody produces an infinitely large number of infinitely weak oblique shocks. In this case the supersonic stream is compressed with no losses in the total pressure.

(B) Internal compression inlet (intake)

The internal compression inlet locates all the shocks within the covered passage way (Fig. 8.53b). The terminal shock wave is also a normal one which is located near or at the throat.

A principal difference between internal and external compression intakes is that with internal compression, since the system is enclosed, oblique shocks are reflected from an opposite wall which have to be considered. The simplest form is a three-shock system. The single wedge turns the flow toward the opposite wall. The oblique shock is reflected from the opposite wall, and the flow passing the reflected shock is restored to an axial direction. A normal shock terminates the supersonic as usual. For asymmetrical intake, as shown in Fig. 8.53b, there are four oblique shocks. The reflected shocks are part of the symmetrical four-shock intersection system.

Again here there are three flow patterns resembling critical (design), subcritical, and supercritical cases. The inlet is said to be operating in the critical mode, when the normal shock wave is located at the throat resulting in the highest pressure recovery factor. In subcritical operation, the terminal (normal) shock wave is located upstream of the throat, or in the converging part of the diffuser. Supercritical mode occurs when the terminal shock is located downstream of the throat, or in the diverging part of the diffuser.

Subcritical flow operation is an unstable mode [10]. The terminal shock may move upstream, or ahead of the cowl lip producing a condition called unstart. During unstart condition, the pressure recovery factor will drop, and flow will spill over the cowl, which will produce high drag.

The internal compression for the above reason, internal supersonic compression intakes operate in the supercritical mode rather than the critical one. This represents a margin of stability if the inlet flow is suddenly changed.

(C) *Mixed compression intakes*

These intakes use a combined external and internal compression system (Fig. 8.53c). In the present days, all the supersonic intakes are of the mixed-compression type.

8.1.6 *Hypersonic Inlets*

Inlets for hypersonic aircraft present the ultimate design challenge. For ramjet-powered aircraft, the inlet must bring the high-speed external flow down to subsonic conditions in the burner. Scramjet intakes are highly integrated with the fuselage of the aircraft. On the X-43A, the inlet includes the entire lower surface of the aircraft forward of the cowl lip. Thick, hot boundary layers are usually present on the compression surfaces of hypersonic inlets. The flow exiting a scramjet inlet must remain supersonic. The two types of hypersonic engines are the following:

1. All-around turboramjet
2. Above-below turboramjet

Refer to Chap. 6 for details and figures illustrating both types.

8.1.7 Performance Parameters

Supersonic intakes have the same performance parameters discussed in subsonic intakes. It may be listed as follows:

1. The total pressure recovery, which measures the amount of the free-stream flow conditions that are “recovered.” The pressure recovery ($r_d = P_{02}/P_{0\infty}$) which depends on a wide variety of factors, including the shape of the inlet, the speed of the aircraft, the airflow demands of the engine, and aircraft maneuvers. Recovery losses associated with the *boundary layers* on the inlet surface or flow separations in the duct are included in the inlet efficiency factor η_i

$$\eta_i = P_{02}/P_{01} \quad (8.12)$$

For subsonic flight speeds, these losses are the only losses. For Mach number less than unity, the Military Specifications value of recovery is the inlet efficiency, or

$$\text{For } M < 1 \quad \eta_i = P_{02}/P_{0\infty}$$

At supersonic flight speeds, there are additional losses created by the shock waves necessary to reduce the flow speed to subsonic conditions for the compressor.

$$\text{For } M > 1 \quad \frac{P_{02}}{P_{0\infty}} = \eta_i \times \left[1 - 0.075(M - 1)^{1.35} \right] \quad (8.13)$$

Actual inlet performance may be greater. The magnitude of the recovery loss depends on the specific design of the inlet and is normally determined by wind tunnel testing.

1. There is another performance parameter called *spillage drag*. Spillage drag occurs when an inlet “spills” air around the outside instead of conducting the air to the compressor face. It is also expressed by Eq. 8.5.
2. Supersonic intakes when operating at off-design conditions also cause distortion at the front face of engine. As the air is brought from free stream to the compressor face, the flow may be distorted by the inlet. The amount of disruption of the flow is characterized by a numerical inlet distortion index. At the *compressor face*, one portion of the flow may have a higher velocity or higher pressure than another portion. The flow may be swirling, or some section of the boundary layer may be thicker than another section because of the inlet shape. The changing flow conditions can cause flow separation in the compressor, a *compressor stall*, and can cause structural problems for the compressor blades.

A good inlet must produce high-pressure recovery, low spillage drag, and low distortion.

Example 8.2 Air is flowing through a diffuser in a jet engine that is operating under steady-state conditions. At the inlet, $T_i = 10^\circ\text{C}$, $P_i = 101\text{ kPa}$, $V_i = 200\text{ m/s}$, and the cross-sectional area of the inlet is $A_i = 0.4\text{ m}^2$. The air leaves the diffuser with a velocity that is very small compared with the inlet velocity (i.e., $V_e \ll V_i$). Assuming that we can model the air as an ideal gas and that the velocity is normal to cross-sectional area at the inlet and exit, determine the following:

- The mass flow rate \dot{m} through the diffuser
- The temperature of the air leaving the diffuser (T_e)

Solution

- Mass flow rate \dot{m}

Control volume:

We'll take our control volume around the diffuser.

Assumptions:

- Steady-state flow $\Rightarrow \frac{d}{dt}(\dot{m}_{cv}) = \frac{d}{dt}(\dot{E}_{cv}) = 0$
- One inlet/One exit $\Rightarrow \dot{m}_i = \dot{m}_e$
- $V_i \gg V_e \Rightarrow \Delta KE \approx \frac{1}{2}V_i^2$
- Ignore the change in gravitational P.E. $\Rightarrow \Delta PE = 0$
- No moving mechanical parts in CV $\Rightarrow \dot{W}_{cv} = 0$
- Since the air is moving quickly, there is little time for significant heat transfer out of the device $\Rightarrow \dot{Q}_{cv} = 0$
- The air as an ideal gas

The mass flow rate is then expressed by the relation

$$\dot{m}_e = \dot{m}_i = \frac{P_i A_i V_i}{R_{\text{air}} T_i} = \frac{101,000 \times 0.4 \times 200}{287 \times (273 + 10)} = 99.48 \text{ kg/s}$$

- Exit temperature (T_e)

In general, since we have an ideal gas, then the specific enthalpy is independent of pressure.

From previous assumptions,

$$\dot{Q}_{cv} = \dot{W}_{cv} = \Delta g z = 0$$

$$0 = 0 - \dot{m} \Delta \left(h + \frac{V^2}{2} + 0 \right)$$

$$h_e + \frac{V_e^2}{2} = h_i + \frac{V_i^2}{2}$$

$$h_e = h_i + \frac{V_i^2}{2} = C_p T_i + \frac{V_i^2}{2} = 1005 \times (273 + 10) + \frac{(200)^2}{2} = 1005 \times T_e$$

$$T_e = 303 \text{ K} = 30^\circ\text{C}$$

Example 8.3 Atmospheric air is ingested into the inlet of an air-breathing engine at -45°C , 60 kPa with a velocity of 900 km/h. Air leaves the diffuser with a velocity of 20 m/s. Find the diffuser exit temperature and the maximum pressure possible.

Solution

Energy equation:

$$\begin{aligned} h_e + \frac{V_e^2}{2} &= h_i + \frac{V_i^2}{2} \\ h_e - h_i &= C_p(T_e - T_i) = \frac{V_i^2 - V_e^2}{2} \\ 1005 \times (T_e - (-45)) &= 0.5 \times \left[\left(\frac{900}{3.6} \right)^2 - (20)^2 \right] \end{aligned}$$

$$T_e = 14.1^\circ\text{C} = 258.9 \text{ K}$$

$$T_i = 273 - 45 = 228 \text{ K}$$

The maximum possible pressure is obtained if the flow in the diffuser is an isentropic (constant entropy).

$$P_e = P_i (T_e/T_i)^{\gamma-1} = 60 \times \left(\frac{258.9}{228} \right)^{3.5} = 93.61 \text{ kPa}$$

Example 8.4 The shown fighter plane is flying at Mach number of 2.0 and altitude of 15,200 m. The aircraft is powered by an engine of the pitot intake type having a chin inlet. An oblique shock wave of angle 40° is attached to the nose of the fuselage, followed by a normal shock wave just at the inlet of intake. The subsonic diffuser portion of intake has a pressure recovery of $\pi_{\text{subsonic}} = 0.98$.

Calculate the following:

1. Overall pressure recovery for air entering the intake
2. Air mass flow rate
3. Inlet conditions to the fan of the turbofan engine powering the aircraft

Solution

Several compressible relations are employed in this example [17] and [18].

$$P_1 = 11.815 \text{ kPa}, T_1 = 216.5 \text{ K}$$

$$P_{01} = P_1 \times \left(1 + \left(\frac{\gamma - 1}{2}\right) M_1^2\right)^{\frac{\gamma}{\gamma-1}} = 7.824 \times P_1 = 92.445 \text{ kPa}$$

$$T_{01} = T_1 \times \left[1 + \left(\frac{\gamma - 1}{2}\right) M_1^2\right] = 389.7 \text{ K}$$

First shock is an oblique shock wave:

$$M_{1n} = M_1 \sin \theta = 2 \sin 40 = 1.2855$$

$$M_{1t} = M_1 \cos \theta = 2 \cos 40 = 1.532$$

From normal shock relations

$$M_{2n}^2 = \frac{(\gamma - 1)M_{1n}^2 + 2}{2\gamma M_{1n}^2 - (\gamma - 1)} = \frac{0.4 \times 1.2855^2 + 2}{2.8 \times 1.2855^2 - 0.4} = 0.6295$$

$$M_{2n} = 0.7934$$

$$M_{1t} = M_{2t} = 1.532$$

$$M_2 = \sqrt{M_{2n}^2 + M_{2t}^2} = 1.725$$

Moreover, from normal shock relations

$$\frac{P_2}{P_1} = \frac{1 + \gamma M_{1n}^2}{1 + \gamma M_{2n}^2} = \frac{1 + 1.4 \times 1.2855^2}{1 + 1.4 \times 0.7934^2} = 1.761$$

$$P_2 = 20.807 \text{ kPa}$$

$$\frac{T_2}{T_1} = \frac{1 + \left(\frac{\gamma-1}{2}\right) M_{1n}^2}{1 + \left(\frac{\gamma-1}{2}\right) M_{2n}^2} = \frac{1 + 0.2 \times 1.2855^2}{1 + 0.2 \times 0.7934^2} = 1.18169$$

$$T_2 = 255.836 \text{ K}$$

$$\frac{P_{02}}{P_{01}} = \left(\frac{1 + \gamma M_{1n}^2}{1 + \gamma M_{2n}^2}\right) \left(\frac{1 + \left(\frac{\gamma-1}{2}\right) M_{2n}^2}{1 + \left(\frac{\gamma-1}{2}\right) M_{1n}^2}\right)^{\frac{\gamma}{\gamma-1}} = 1.761 \times \left(\frac{1}{1.18169}\right)^{3.5} = 0.9817$$

$$P_{02} = 90.76 \text{ kPa}$$

Intake normal shock

From states (2) to (3)

$$M_3^2 = \frac{(\gamma - 1)M_2^2 + 2}{2\gamma M_2^2 - (\gamma - 1)} = \frac{0.4 \times 1.725^2 + 2}{2.8 \times 1.725^2 - 0.4} = 0.4022$$

$$M_3 = 0.634$$

$$\frac{P_{03}}{P_{02}} = \left(\frac{1 + \gamma M_2^2}{1 + \gamma M_3^2} \right) \left(\frac{1 + (\frac{\gamma-1}{2}) M_3^2}{1 + (\frac{\gamma-1}{2}) M_2^2} \right)^{\frac{\gamma}{\gamma-1}} = 3.3056 \times 0.2557 = 0.8453$$

$$P_{03} = 76.72 \text{ kPa}$$

$$\frac{P_3}{P_2} = \frac{1 + \gamma M_2^2}{1 + \gamma M_3^2} = \frac{1 + 1.4 \times 1.725^2}{1 + 1.4 \times 0.634^2} = 3.3056$$

$$P_3 = 68.78 \text{ kPa}$$

$$\frac{T_3}{T_2} = \frac{1 + (\frac{\gamma-1}{2}) M_2^2}{1 + (\frac{\gamma-1}{2}) M_3^2} = \frac{1 + 0.2 \times 1.725^2}{1 + 0.2 \times 0.634^2} = 1.476$$

$$T_3 = 377.72 \text{ K}$$

$$\rho_3 = \frac{P_3}{RT_3} = \frac{68,780}{287 \times 377.72} = 0.6345 \text{ kg/m}^3$$

Speed at inlet of intake $V_3 = M_3 \sqrt{\gamma RT_3} = 0.634 \times \sqrt{1.4 \times 287 \times 377.72} = 247 \text{ m/s}$

Inlet area of intake $A_3 = \frac{\pi D_3^2}{4} = 1.094 \text{ m}^2$

Air mass flow rate $\dot{m} = \rho_3 V_3 A_3 = 0.6345 \times 247 \times 1.094 = 171.44 \text{ kg/s}$

Overall pressure recovery of intake

$$\pi_d = 0.9817 \times 0.8453 \times 0.98 = 0.8133$$

Inlet total conditions in intake

$$P_{04} = 0.8133 \times 92.455 = 75.1855 \text{ kPa}$$

$$T_{04} = T_{01} = 389.7 \text{ K}$$

Example 8.5 Figure 8.57 illustrates a divided intake having two circular inlets; each has a diameter of 0.3 m (section A-A). The branched part of intake ends with an elliptical section (B-B) having major and minor diameters of 0.6 m and 0.5 m. Air then continues to diffuse to the engine inlet (section C-C) that has a circular shape with a diameter of 0.6 m.

1. If the air velocity at engine inlet (section C-C) is 60 m/s, calculate the air-inlet velocity at the inlet and outlet of the divided section (sections A-A and B-B, respectively).
2. If the ambient conditions are $T_a = 288 \text{ K}$, $P_a = 101 \text{ kPa}$, calculate the inlet total temperature and pressure at section A-A.

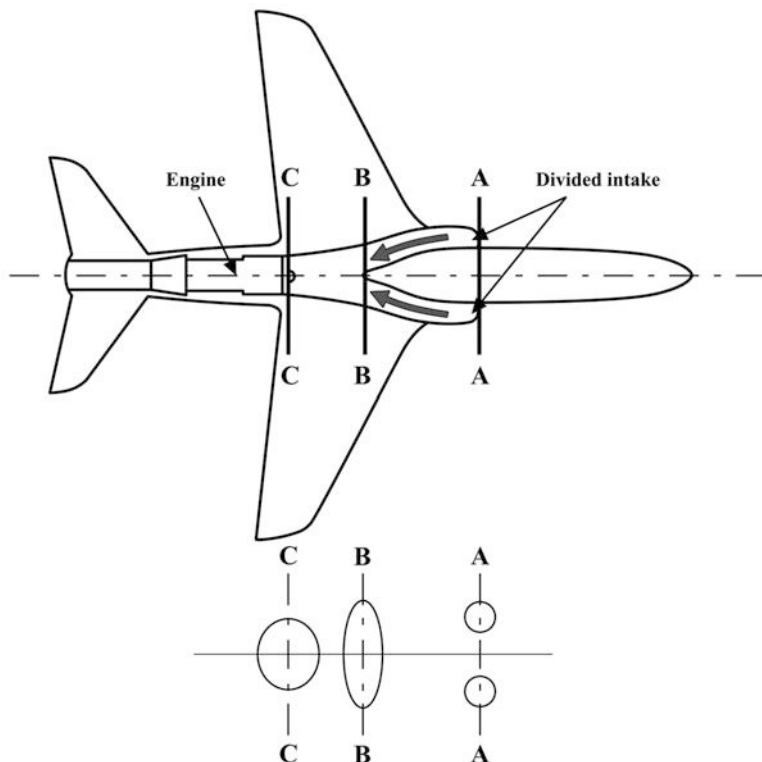


Fig. 8.57 A divided intake having two circular inlets

3. Assume the total pressure drops in the branching and the succeeding diffuser parts up to the engine inlet are, respectively, 2 % and 1 %; calculate the total pressure and temperature at section C-C.

Solution

Denote the areas at different sections (A-A), (B-B), and (C-C) by A_A , B_B , C_C then

$$A_A = 2 \times \frac{\pi D_{A-A}^2}{4} = 2 \times \pi \times \frac{0.3^2}{4} = 0.1414 \text{ m}^2$$

$$A_B = \frac{\pi \times 0.5 \times 0.6}{4} = 2 \times \pi \times \frac{0.3^2}{4} = 0.2356 \text{ m}^2$$

$$A_C = \frac{\pi D_{C-C}^2}{4} = \pi \times \frac{0.6^2}{4} = 0.2828 \text{ m}^2$$

1. Continuity equation

For a nearly incompressible flow and assuming uniform axial speed, then continuity can be expressed as

$$A_A \times V_A = A_B \times V_B = A_C \times V_C$$

With $V_C = 60 \text{ m/s}$, then velocity at section B-B is

$$V_B = 60 \times \frac{0.2828}{0.2356} = 72 \text{ m/s}$$

Velocity at section A-A is then

$$V_A = 60 \times \frac{0.2828}{0.1414} = 120 \text{ m/s}$$

2. Total temperature at inlet (section A-A)

$$T_{0A} = T_A + \frac{V_{A-A}^2}{2C_p} = 288 + \frac{120^2}{2 \times 1005} = 295.2 \text{ K}$$

Mach number at inlet

$$M = \frac{V_{A-A}}{\sqrt{\gamma RT_A}} = \frac{120}{\sqrt{1.4 \times 287 \times 288}} = 0.3528$$

Total pressure at inlet

$$P_{0A} = P_A \left(1 + \frac{\gamma-1}{2} M^2\right)^{\frac{\gamma}{\gamma-1}} = 1.0899 \times 101 = 110.08 \text{ kPa}$$

3. Total pressure at engine inlet

$$P_{0C} = P_{0A} \times 0.98 \times 0.99 = 106.8 \text{ kPa}$$

Total temperature is constant through the whole sections of inlet

$$T_{0A} = T_{0B} = T_{0C} = 295.2 \text{ K}$$

Remarks The assumption of uniform speeds in the different inlet passages is a rather rough one. More precise calculation employing a parabolic shape of velocity profiles is expressed in [19].

8.2 Combustion Systems

8.2.1 Introduction

The purpose of the combustion system is to increase the thermal energy of a flowing air/gas stream by combustion, which is an exothermic chemical reaction between the injected fuel and the oxygen in the flowing stream. Combustion process takes place in the main burner (or the combustor) and the afterburner (or the augmenter/reheater) for supersonic aircraft.

The function of the main burner [20] or combustion chamber is to provide:

1. Complete combustion
2. Moderate total pressure loss
3. Stability of combustion process (freedom from flameout)
4. In-flight relight ability
5. Proper temperature distribution at exit with no “hot spots”
6. Short length and small cross section
7. Wide operating range of mass flow rates, pressures, and temperatures
8. Satisfaction of established environmental limits for air pollutants

The amount of fuel added to the air will depend upon the temperature rise required which ranges from 850 to 1700 °C by the materials from which the turbine blades and nozzles are made [21]. The air has already been heated to 200 – 550°C by the work done during compression. Since the gas temperature required at the turbine varies with engine thrust for (turbine-based engines), and engine power for shaft-based engines, the main combustion chamber must also be capable of maintaining stable and efficient combustion over a wide range of engine operating conditions.

8.2.2 Types of Combustion Chamber

Combustion chambers (or burners) may be classified as follows:

- Main burner or afterburner
- Subsonic or supersonic types depending on the speed of airflow within burners
- Direct or a reverse-flow direction

Subsonic combustion chamber may be further classified into three types, namely, multiple cans, tubo-annular, and annular ones (Fig. 8.58).

8.2.2.1 Subsonic Combustion Chambers

(A) *Multiple cans*

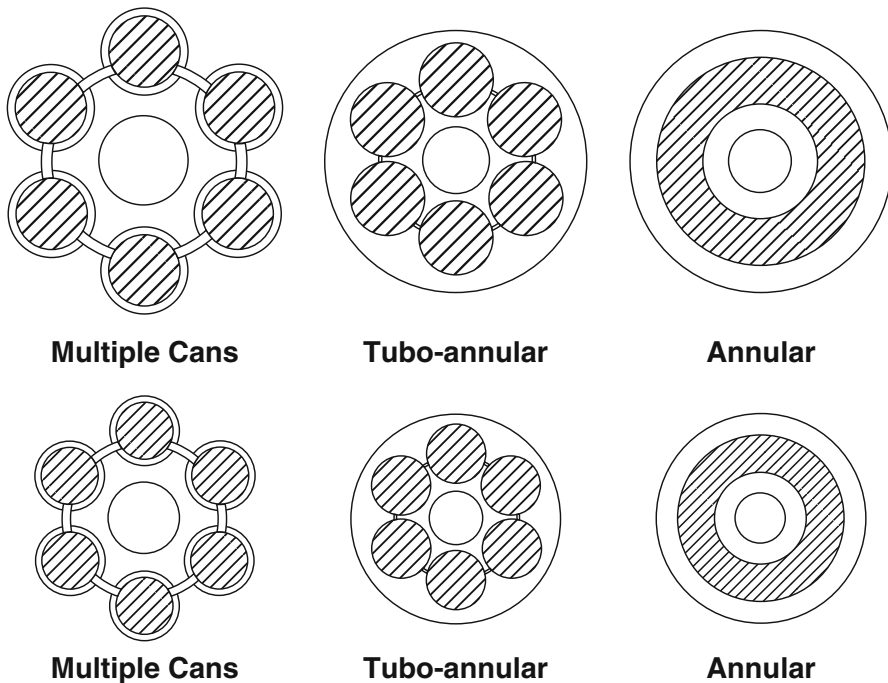


Fig. 8.58 Different types of subsonic combustion chambers

This type is sometimes identified as tubular or can-type combustion chamber. It is used on centrifugal compressor engines (like Jumo 004, Rolls-Royce Nene, Dart and Derwent, as well as Pratt & Whitney Canada PT6 and PW150 turboprop engines). It also was used in the earlier types of axial flow compressor engines. It is a direct development of the early Whittle W2B reverse-flow combustion chamber (Fig. 8.59).

The chambers are disposed around the engine, and the compressor delivery air is directed by separate ducts to pass into these individual chambers. Each combustion chamber has an inner flame tube around which there is an air casing. The separate flame tubes are all interconnected. This allows all tubes to operate at the same pressure and also allows combustion to propagate around the flame tubes during engine starting.

The number of combustion chamber is varying from seven to sixteen per engine. The present trend is to have fewer numbers (8 or 10).

The *advantages* of the tubular type are the following:

- Mechanically robust.
- Fuel-flow and airflow patterns are easily matched.
- Rig testing necessitates only small fraction of total engine air mass flow.
- Easy replacement for maintenance.

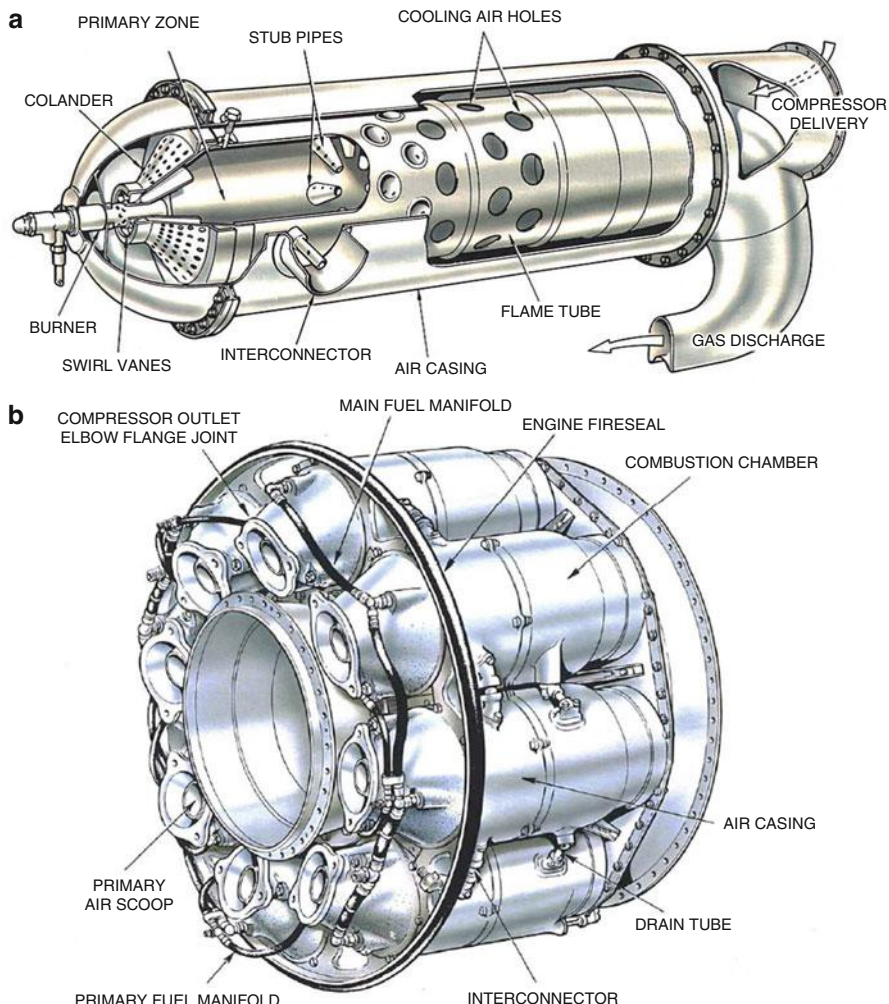


Fig. 8.59 Can and multiple can combustion chamber. (a) Early reverse-flow whittle combustion chamber and (b) multiple can (Reproduced with the permission of Rolls-Royce plc, copyright © Rolls-Royce plc)

The disadvantages are the following:

- Bulky and heavy
- High-pressure loss
- Requires interconnectors that incur problem of light round
- Large frontal area and high drag

For these disadvantages, nowadays tubular (can) type is used in jet engines incorporating centrifugal compressors, auxiliary power units (APUs), and automotives.

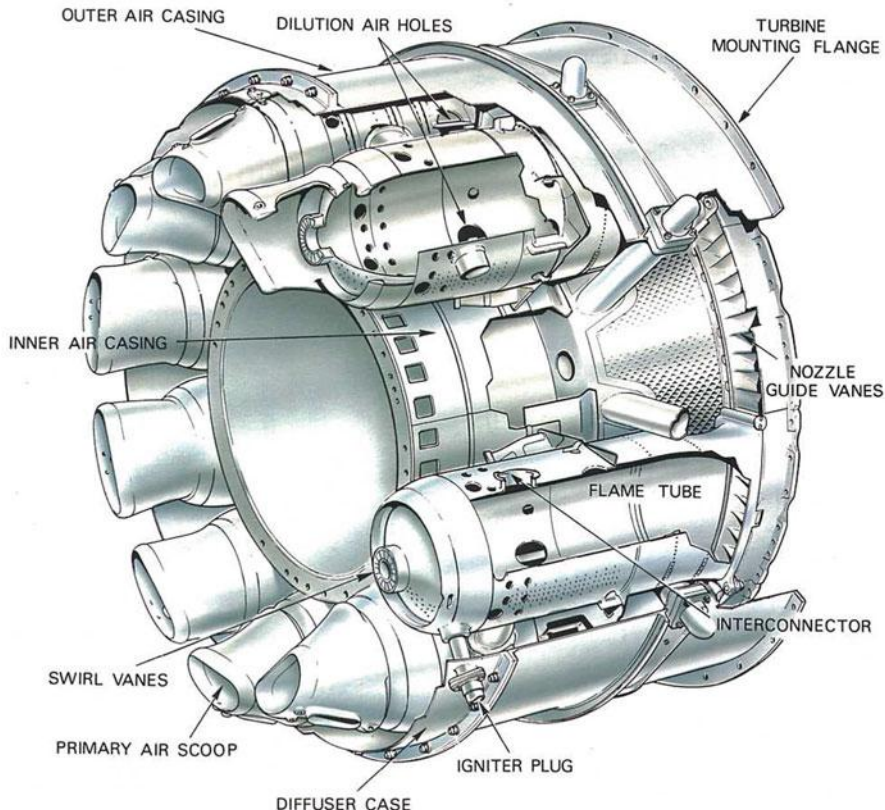


Fig. 8.60 Tubo-annular combustion chamber (Reproduced with the permission of Rolls-Royce plc, copyright © Rolls-Royce plc)

(B) *Tubo-annular combustion chamber*

This type may also be identified as can-annular or cannular. It consists of a series of cylindrical burners arranged within common single annulus as shown in Fig. 8.60. Thus it bridges the evolutionary gap between the tubular (multiple) and annular types. It combines the compactness of the annular chamber with the best features of the tubular type.

The combustion chambers are enclosed in a removable shroud that covers the entire burner section. This feature makes the burners readily available for any required maintenance. The flow of air through the holes and louvers of the can-annular system is almost identical with the flow through other types of burners. Reverse-flow combustors are mostly of the can-annular type. Reverse-flow combustors make the engine more compact. Engines fitted with tubo-annular combustors include the Allison 501-K, the GE J73 and J79, Pratt & Whitney J57, J75, and JT3 as well as RR Avon, Conway, Olympus, Tyne, and Spey. Moreover, General Electric and Westinghouse use this type in their industrial gas turbines.

Advantages of can-annular types are the following:

- Mechanically robust
- Fuel-flow and airflow patterns are easily matched.
- Rig testing necessitates only small fraction of total engine air mass flow.
- Shorter and lighter than tubular chambers.
- Low-pressure loss.

Their disadvantages are the following:

- Less compact than annular
- Requires connectors
- Incurs problem of light round

(C) Annular combustion chamber

This type of combustion chamber consists of a single flame tube, completely annular in form, which is contained in an inner and outer casing. The chamber is

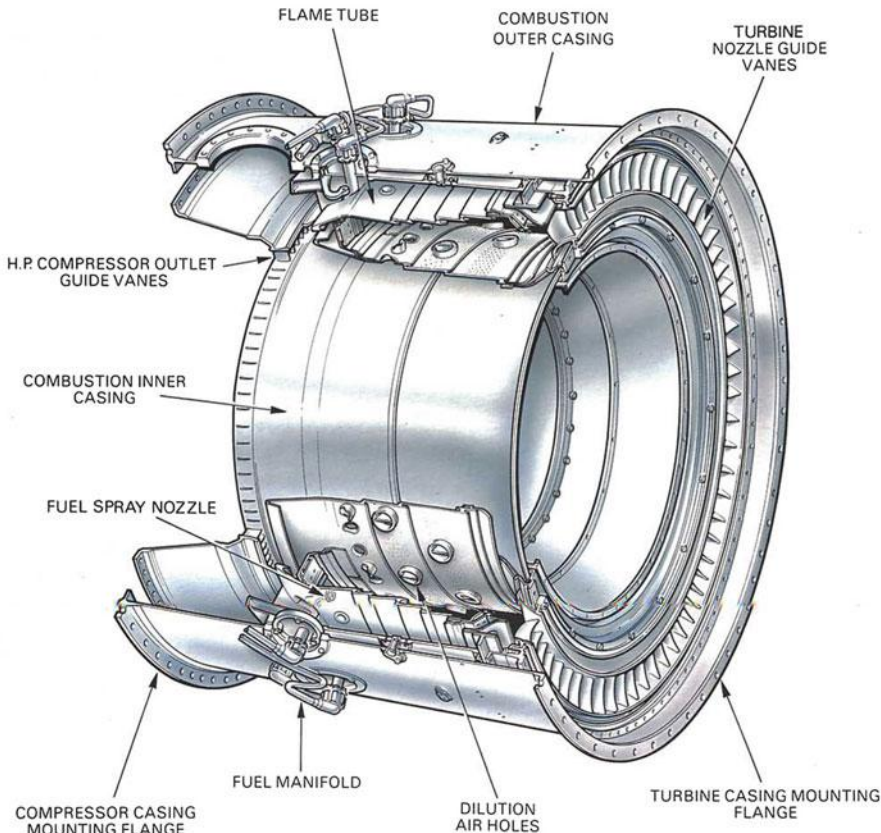


Fig. 8.61 Annular type combustor (Reproduced with the permission of Rolls-Royce plc, copyright © Rolls-Royce plc 2007)

being open at the front to the compressor and at the rear to the turbine nozzles (refer to Fig. 8.61).

Normally, this type is used in many engines using axial flow compressor and also others incorporating dual-type compressors (combinations of axial flow and centrifugal flow). In the 1940s annular liners was confined to engines of low-pressure ratio, such as the BMW 003, the Metrvick Beryl, and the Westinghouse J30. However, by the 1960s, the annular layout became the automatic choice for all new aircraft engines. From this period and until now, the annular combustors were fitted to the General Electric CF6, GE90, P&W JT9D, PW 4000, RR RB211 and Trent series, and V2500 engines. Moreover, several industrial gas turbines like ABB and Siemens plants of over 150 MW use annular combustors also.

The advantages of annular type may be summarized as follows:

- Minimum length and weight (its length is nearly 0.75 of cannular combustor length).
- Minimum pressure loss.
- Minimum engine frontal area.
- Less wall area than cannular and thus cooling air required is less; thus the combustion efficiency raises; the unburnt fuel is reduced and oxidizes the carbon monoxide to nontoxic carbon dioxide, thus reducing air pollution.
- Easy light round.
- Design simplicity.
- Combustion zone uniformity.
- Permitting better mixing of the fuel and air.
- Simple structure compared to can burners.
- Increased durability.

However, it has the following disadvantages:

- Serious bucking problem on outer liner.
- Rig testing necessitates full engine air mass flow.
- Must remove the engine from aircraft to disassemble for maintenance and overhaul.

8.2.3 Components of Combustion Chamber

As illustrated in Fig. 8.62, combustion chamber has the following components:

Casing (or case)

The case is the outer shell of the combustor which has a fairly simple structure needing little maintenance. The case is protected from thermal loads by the air flowing in it, so thermal performance is of limited concern. However, the casing serves as a pressure vessel that must withstand the difference between the high pressures inside the combustor and the lower pressure outside. That mechanical (rather than thermal) load is a driving design factor in the case.

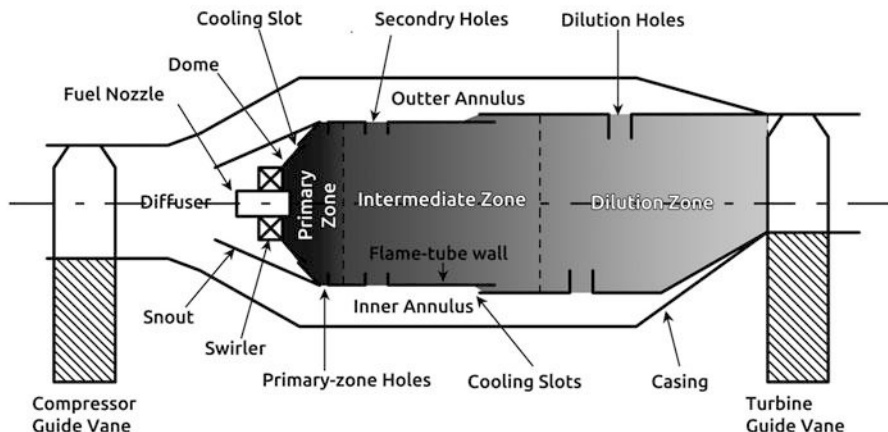


Fig. 8.62 Components of combustion chamber

Diffuser

The purpose of the diffuser is to slow the high speed, highly compressed air from the [compressor](#) to a velocity optimal for the combustor. Reducing the velocity results in an unavoidable loss in total pressure, so one of the design challenges is to limit the loss of pressure as much as possible. Furthermore, the diffuser must be designed to limit the flow distortion as much as possible by avoiding flow separation. Like most other gas turbine engine components, the diffuser is designed to be as short and light as possible.

Liner

The liner contains the combustion process and introduces the various airflows (intermediate, dilution, and cooling; see [Airflow paths](#) below) into the combustion zone. The liner must be designed and built to withstand extended high temperature cycles. For that reason liners tend to be made from [super alloys](#) like [Hastelloy X](#). Some combustors also make use of [thermal barrier coatings](#). However, air cooling is still needed in either cases. In general, there are two main types of liner cooling, namely, film and transpiration methods. In film cooling cool air is injected from outside of the liner to just inside of the liner. This creates a thin film of cool air that protects the liner, reducing the temperature at the liner from around 1800 K to around 830 K. Transpiration cooling is a more modern approach that uses a [porous](#) material for the liner, thus allows a small amount of cooling air to pass through it, providing better performance than film cooling. Transpiration cooling results in a much more even temperature profile as the cooling air is uniformly introduced. Film cooling air is generally introduced through slats or louvers, resulting in an uneven profile where it is cooler at the slat and warmer between the slats.

More importantly, transpiration cooling uses much less cooling air (on the order of 10 % of total airflow, rather than 20–50 % for film cooling). Since less air is used for cooling, more air is available for combustion, which is more and more important for high performance, high-thrust engines.

Snout

The snout is an extension of the dome (Fig. 8.62) that acts as an air splitter, separating the primary air from the secondary airflows (intermediate, dilution, and cooling air).

Dome/swirler

The dome and swirler are the part of the combustor that the primary air flows through as it enters the combustion zone. Their role is to generate turbulence in the flow to rapidly mix the air with fuel. The swirler establishes a local low-pressure zone that forces some of the combustion products to recirculate, creating the high turbulence. However, the higher the turbulence, the higher the pressure loss will be for the combustor. Thus the dome and swirler must be carefully designed so as not to generate more turbulence than is needed to sufficiently mix the fuel and air.

Fuel injector

The fuel injector is responsible for introducing fuel to the combustion zone and, along with the swirler, is responsible for mixing the fuel and air. There are four primary types of fuel injectors: pressure-atomizing, air-blasting, vaporizing, and premixing/pre-vaporizing injectors. Pressure-atomizing fuel injectors rely on high fuel pressures (as much as 3400 kPa to atomize the fuel). Simplicity is its main advantage but it has several disadvantages. The fuel system must be robust enough to withstand such high pressures, and the fuel tends to be [heterogeneously](#) atomized, resulting in incomplete or uneven combustion which has more pollutants and smoke.

Air-blast injector, the second type, “blasts” a sheet of fuel with a stream of air, atomizing the fuel into homogeneous droplets. This type of fuel injector led to the first smokeless combustors. The air used is just some amount of the primary air that is diverted through the injector, rather than the swirler. This type of injector also requires lower fuel pressures than the pressure-atomizing type.

The vaporizing fuel injector, the third type, is similar to the air-blast injector in that primary air is mixed with the fuel as it is injected into the combustion zone. However, the fuel-air mixture travels through a tube within the combustion zone. Heat from the combustion zone is transferred to the fuel-air mixture, vaporizing some of the fuel (mixing it better) before it is combusted. This method allows the fuel to be combusted with less [thermal radiation](#), which helps protect the liner. However, the vaporizer tube may have serious durability problems with low fuel flow within it.

The premixing/pre-vaporizing injectors work by mixing or vaporizing the fuel before it reaches the combustion zone. This method allows the fuel to be very uniformly mixed with the air, reducing emissions from the engine. Fuel autoignition is its main disadvantage, which if happens will result in a seriously damaged combustor.

Igniter

Most igniters in gas turbine applications are electrical spark igniters, similar to [automotive spark plugs](#). The igniter needs to be in the combustion zone where the fuel and air are already mixed, but it needs to be far enough upstream so that it is not damaged by the combustion itself.

Once the combustion is initially started by the igniter, it is self-sustaining and the igniter is no longer used. In can-annular and annular combustors, the flame can propagate from one combustion zone to another, so igniters are not needed at each

one. In some systems ignition-assist techniques are used. One such method is oxygen injection, where oxygen is fed to the ignition area, helping the fuel easily combust. This is particularly useful in some aircraft applications where the engine may have to restart at high altitude.

8.2.4 Aerodynamics of Combustion Chamber

Aerodynamic processes play a vital role in the design and performance of gas turbine combustion systems. The aerodynamic design of combustor provides its size and performance analysis. In the next sections, flow through diffuser and liner holes will be thoroughly analyzed.

8.2.4.1 Aerodynamics of Diffusers

In its simplest form, a diffuser is merely a divergent passage in which the flow is decelerated and the reduction in velocity head is converted into a rise in static pressure. Ideal diffuser achieves the required velocity reduction in the shortest possible length with minimum loss in total pressure as well as uniform and stable flow conditions at its outlet. The different types of diffusers (Fig. 8.43) are as follows:

1. Two dimensional
2. Equiangular
3. Straight-core annular
4. Conical

These straight-walled diffusers may be defined in terms of three geometric parameters, namely, area ratio (AR), geometrical length (either the wall length L or axial length N), and the divergence angle (2θ). The area ratio is expressed by the following relations:

For two dimensional

$$AR = 1 + 2 \frac{L}{W_1} \sin \theta \quad (8.14)$$

For conical

$$AR = 1 + 2 \frac{L}{R_1} \sin \theta + \left(\frac{L}{R_1} \sin \theta \right)^2 \quad (8.15)$$

For annular

$$AR = \frac{\Delta R_2}{\Delta R_1}$$

where ΔR_1 is the annulus height at diffuser inlet.

For straight-core annular, the area ratio is then

$$AR = 1 + 2 \frac{L}{\Delta R_1} \sin \theta + \left(\frac{L}{\Delta R_1} \sin \theta \right)^2 \quad (8.16a)$$

For can-annular and annular diffuser,

$$AR = 1 + 2 \frac{L}{\Delta R_1} (\sin \theta_i + \sin \theta_0) + \left(\frac{L}{\Delta R_1} (\sin \theta_i + \sin \theta_0) \right)^2 \quad (8.16b)$$

The first systematic study of flow pattern in 2-D straight-walled diffusers was carried out by Kline et al. [22]. As the divergence angle increased, different flow patterns were seen including no appreciable stall, transitory stall, fully developed stall, and jet flow in which the main flow is separated from the wall. The first appreciable stall for different types of diffusers is plotted in Fig. 8.45. It was measured by Howard et al. [13] and in good agreements with the data obtained by McDonald and Fox [23] and Reneau et al. [24].

For one-dimensional incompressible flow,

$$\dot{m} = \rho_1 A_1 U_1 = \rho_2 A_2 U_2$$

Hence,

$$\frac{A_2}{A_1} = \frac{U_1}{U_2} = AR \quad (8.17)$$

The pressure recovery coefficient is calculated as

$$C_p = (P_2 - P_1)/q_1$$

Where

$$q_1 = \rho U_1^2$$

The static pressure rise in diffuser is given by

$$\begin{aligned} P_1 + q_1 &= P_2 + q_2 + \Delta P_{\text{diff}} \\ P_2 - P_1 &= q_1 \left(1 - \frac{1}{AR^2} \right) - \Delta P_{\text{diff}} \end{aligned}$$

In ideal diffuser, there are no losses, then

$$C_{p_{\text{ideal}}} = \frac{(P_2 - P_1)_{\text{ideal}}}{(P_2 - P_1)_{\text{ideal}}} = q_1 \left(1 - \frac{1}{AR^2} \right) \quad (8.18)$$

Overall effectiveness of diffuser is expressed by

$$\eta = \frac{C_{p\text{measured}}}{C_{p\text{ideal}}} = \frac{C_p}{\left(1 - \frac{1}{AR^2}\right)} \quad (8.19)$$

Figure 8.63 illustrates performance of conical diffusers. The (C_p^*) is the locus of points that define the diffuser divergence angle (2θ) producing the maximum pressure recovery in a prescribed non-dimensional length.

Example 8.6 A conical diffuser of a combustion chamber has the following data:

- Area ratio (AR) = 1.6
- Divergence angle = 12°
- Air density = 5.42 kg/m^3
- Inlet velocity of air $V_i = 133.304 \text{ m/s}$
- Mass flow rate of air (Diffuser) = 4 kg/s

Calculate the following:

1. Diffuser geometry
2. Overall effectiveness

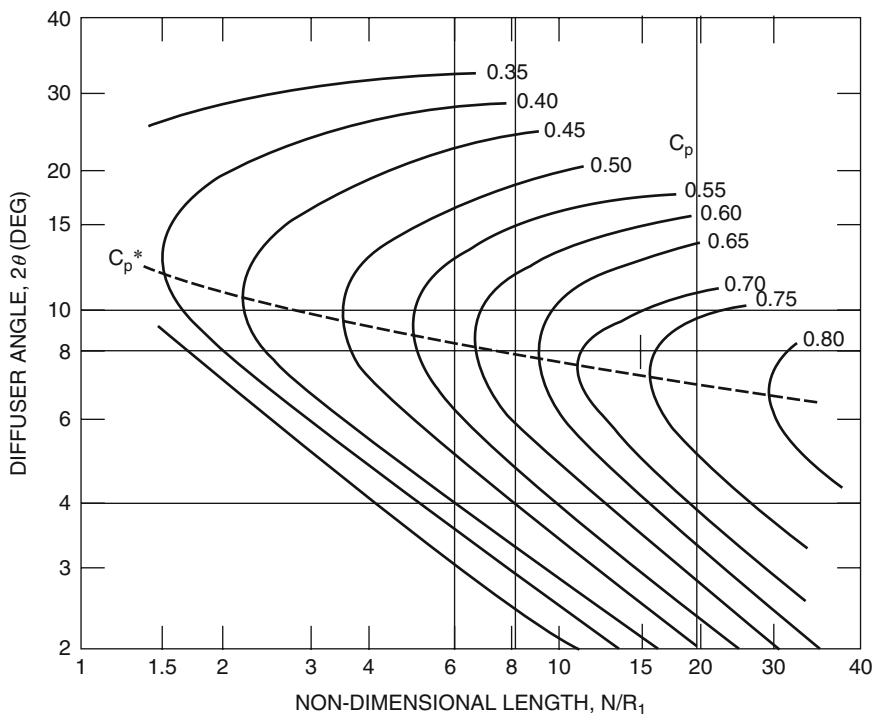


Fig. 8.63 Performance chart for conical diffusers

Solution

Inlet area of diffuser

$$A_i = \frac{m_d^\circ}{V_i * \rho_i} = 5.7209 * 10^{-3} \text{ m}^2$$

$$r_i = 0.0426 \text{ m}$$

$$R_i = 0.0426 \text{ m}$$

Using area ratio to get exit area of diffuser

$$\text{AR} = A_e / A_i = 1.6$$

Therefore, $A_e = 9.1535 * 10^{-3} \text{ m}^2$

$$R_e = 0.0551 \text{ m}$$

Calculation of the wall length of diffuser

For a conical diffuser

$$\text{AR} = 1 + 2\frac{L}{R_i} \sin \theta + \left[\frac{L}{R_i} \sin \theta \right]^2$$

$$\text{Let } x = \frac{L}{R_i} \sin \theta$$

$$\text{AR} = 1 + 2x + x^2$$

$$(1 - \text{AR}) + 2x + x^2 = 0$$

$$2x + x^2 - 0.6 = 0$$

$$L = 0.085 \text{ m}$$

$$N = L \times \cos \theta = 0.0855 \text{ m}$$

Performance of diffuser

From figure (CC.8), with $\text{AR} - 1 = 0.6$ and $N / R_i = 2.004$

Then : $Cp_{\text{measured}} = 0.457$

$$Cp_{\text{ideal}} = 1 - \left(\frac{1}{\text{AR}} \right)^2 = 0.60935$$

$$\eta = \frac{Cp_{\text{measured}}}{Cp_{\text{ideal}}} = 0.75$$

Overall effectiveness

$$\eta = 0.75$$

8.2.5 The Chemistry of Combustion

In this section, a brief introduction for the chemistry and thermodynamics of combustion of generic hydrocarbon fuels, (C_xH_y), in which the oxidizer is the oxygen contained in atmospheric air will be given. Atmospheric air contains approximately 21 % oxygen (O_2) by volume. The other 79 % of “other gases” is mostly nitrogen (N_2), so we will assume air to be composed of 21 % oxygen and 79 % nitrogen by volume [25]. Thus each mole of oxygen needed to oxidize the hydrocarbon is accompanied by $79/21 = 3.76$ moles of nitrogen. Using this combination the molecular mass of air becomes 29 [kg/kmol]. The nitrogen will not normally undergo any chemical reaction.

The basic combustion process can be described by the fuel (the hydrocarbon) plus oxidizer (air or oxygen) called the *reactants*, which undergo a chemical process while releasing heat to form the *products* of combustion such that mass is conserved.

There are three cases for combustion depending on the oxygen percentage in the process:

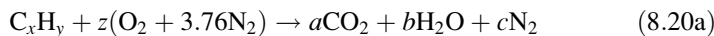
- Theoretical air (or stoichiometric air)
- Extra air (or lean mixture)
- Less air (or rich mixture)

In the simplest combustion process, (*stoichiometric combustion*) all the carbon in the fuel forms carbon dioxide (CO_2), and all the hydrogen forms water (H_2O) in the products.

If we supply less than theoretical air (rich combustion), then the products could include carbon monoxide (CO); thus, it is normal practice to supply more than theoretical air to prevent this occurrence.

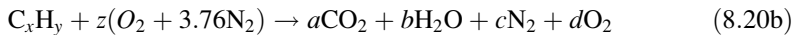
Finally in the case of Excess Air (Lean Combustion) oxygen will appear in the products.

The general chemical relation for *stoichiometric* combustion will be

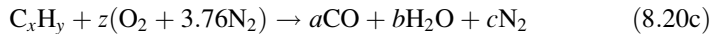


The variable (z) is known as the stoichiometric coefficient for the oxidizer (air). Stoichiometric combustion is defined as the complete combustion of a hydrocarbon fuel and converted it into carbon dioxide and water vapor, in this case all the latent heat of combustion of the fuel.

The general chemical relation for *excess air* (lean mixture) will be



The general chemical relation for *less air* (rich mixture) will be



Because the composition of the combustion products is significantly different for fuel-lean and fuel-rich mixtures, and because the stoichiometric fuel-to-air ratio depends on fuel composition, the ratio of the actual fuel-to-air ratio to the stoichiometric ratio (or its inverse) is a more informative parameter for defining mixture composition. The fuel-to-air equivalence ratio Φ ,

$$\Phi = \frac{(F/A)_{\text{actual}}}{(F/A)_{\text{Stoich.}}} \quad (8.21\text{a})$$

For fuel-lean mixtures $\Phi < 1$

For stoichiometric mixtures $\Phi = 1$

For fuel-rich mixtures $\Phi > 1$

Equation 10.4a can be rewritten in terms of the fuel-to-air ratio (f) as

$$\Phi = \frac{f}{f_{\text{stoich}}} \quad (8.21\text{b})$$

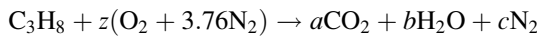
To prevent excessive temperatures at the exit of the main burner or the afterburner and protect its walls, the overall F/A ratio must be much less than stoichiometric ratio where $\Phi < 1$

Example 8.7 Consider a stoichiometric mixture of *propane* (C_3H_8) and air, calculate the air-to-fuel ratio in the following cases:

- (A) Stoichiometric flow
- (B) Less air (60 % of stoichiometric)

Solution

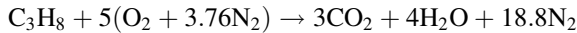
The general chemical relation for stoichiometric mixture will be



Since this reaction yields four unknowns (z , a , b , and c), thus we need four equations to solve. We obtain the four equations from balancing the number of atoms of each element in the reactants (carbon, hydrogen, oxygen, and nitrogen)

with the number of atoms of those elements in the products. This means that no atoms are destroyed or lost in a combustion reaction.

Element	Amount in reactants	=	Amount in products	Reduced equation
Carbon (C)	3		a	$a = 3$
Hydrogen (H)	8		$2b$	$b = 4$
Oxygen (O)	$2z$		$2a + b$	$z = a + b/2 = 5$
Nitrogen (N)	$2(3.76)z$		$2c$	$c = 3.76z = 18.8$



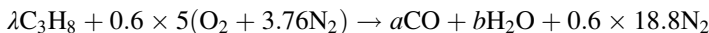
$$(A/F)_{\text{stoch}} = \frac{m_{\text{air}}}{m_{\text{fuel}}} = \frac{23.8 \text{ [kmol]} \times 29 \text{ [kg/kmol]}}{1 \text{ [kmol]} \times (3 \times 12 + 8 \times 1) \text{ [kg/kmol]}}$$

$$(A/F)_{\text{stoch}} = 15.686 \frac{\text{kg - air}}{\text{kg - fuel}}$$

Thus:

$$\left(\frac{F}{A}\right)_{\text{Stoich}} = 0.06374$$

(B) Less air (rich mixture)



Then

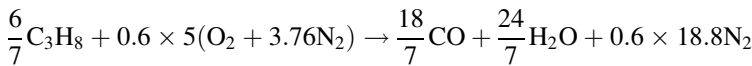
$$a = 3\lambda$$

$$b = 4\lambda$$

$$a + b = 6$$

Thus

$$\lambda = 6/7, \quad a = 18/7 \quad b = 24/7$$



$$(A/F)_{\text{rich}} = \frac{m_{\text{air}}}{m_{\text{fuel}}} = \frac{0.6 \times 23.8 \text{ [kmol]} \times 29 \text{ [kg/kmol]}}{\frac{6}{7} \text{ [kmol]} \times (3 \times 12 + 8 \times 1) \text{ [kg/kmol]}}$$

$$(A/F)_{\text{rich}} = 10.98 \frac{\text{kg - air}}{\text{kg - fuel}}$$

$$\left(\frac{F}{A}\right)_{\text{rich}} = 0.091$$

8.2.6 The First Law Analysis of Combustion

The main purpose of combustion is to produce heat through a change of enthalpy from the reactants to the products. From the first law equation in a control volume bounding the combustion chamber, ignoring kinetic and potential energy changes and assuming no work is done [25], we have the combustion heat expressed as:

$$Q_{cv} = \sum_p N_p h_p - \sum_r N_r h_r \quad (8.22)$$

where the summations are taken over all the products (p) and the reactants (r). Also (N) refers to the number of moles of each component, and (h) in [kJ/kmol] refers to the molar enthalpy of each component.

Since there are a number of different substances involved, we need to establish a common reference state to evaluate the enthalpy, the common choice being 25 °C and 1 atm which is normally denoted with a superscript o.

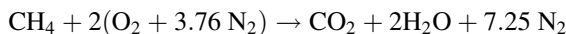
Example 8.8 Consider the complete combustion of methane (CH₄) with theoretical air. If the enthalpy of formation of the reactants and products are as follows:

Substance	Chemical expression	h_{fo} [kJ/kmol]
Carbon dioxide	CO ₂ (g)	-393,520
Water vapor	H ₂ O(g)	-241,820
Water	H ₂ O(l)	-285,820
Methane	CH ₄ (g)	-74,850

where (g) refers to gas and (l) refers to liquid, calculate the lower and higher heating values of CH₄.

Solution

The chemical relation for complete combustion of CH₄ is



Two notes can be mentioned here:

1. The enthalpy of formation of basic elements O₂ and N₂ is zero.
2. The *Enthalpy of Formation* (h_{fo}) has negative sign means as the process is *Exothermic*, i.e., heat is given off when the compound is formed.

Assume here that there is sufficient heat transfer such that both the reactants and the products are at 25 °C and 1 atm pressure and that the lower heating value is obtained when the water product is vapor, while the higher heating value is obtained when water product is liquid.

Since there is no sensible enthalpy change, the energy equation (8.22), the higher heating value becomes

$$Q_{cv} = \sum_p N_p h_{fop} - \sum_r N_r h_{for} = 1(-393,520) + 2(-285,820) - 1(-74,850)$$

$$Q_{cv} = -890,310 \frac{\text{kJ}}{\text{kmol fuel}}$$

Now, on a unit mass basis

$$q_{cv} = \frac{Q_{cv}}{M_{CH_4}} = \frac{-890,310}{(12+4)} = -55,644 \frac{\text{kJ}}{\text{kg fuel}}$$

The lower heating value is then

$$Q_{cv} = \sum_p N_p h_{fop} - \sum_r N_r h_{for} = 1(-393,520) + 2(-241,820) - 1(-74,850)$$

$$Q_{cv} = -802,310 \frac{\text{kJ}}{\text{kmol fuel}}$$

Now, on a unit mass basis

$$q_{cv} = \frac{Q_{cv}}{M_{CH_4}} = \frac{-890,310}{(12+4)} = -50,144 \frac{\text{kJ}}{\text{kg fuel}}$$

This heat (q_{cv}) is called the *enthalpy of combustion* or the *heating value* of the fuel. If the products contain liquid water, then it is the *higher heating value* (as in the above example); however if the product contains water vapor, then it is the *lower heating value* of the fuel. The enthalpy of combustion is the largest amount of heat that can be released by a given fuel.

8.2.7 Combustion Chamber Performance

A combustion chamber must be capable of allowing fuel to burn efficiently over a wide range of operating conditions without incurring a large pressure loss. So, the combustion chamber performance can be evaluated by some conditions or performance as follows [5]:

1. Pressure loss
2. Combustion efficiency
3. Combustion stability
4. Combustion intensity

8.2.7.1 Pressure Losses

The sources of pressure drop or loss are either cold or hot losses. Cold losses arise from sudden expansion, wall friction, turbulent dissipation, and mixing. Cold losses can be measured by flowing air without fuel through all the slots, holes, orifices, etc. The hot losses (fundamental losses) are due to temperature increase. Generally, the fundamental loss due to heat addition in aero engine will be low compared with the losses due to friction and mixing. Experiments have shown that the overall pressure loss can be expressed by the relation

$$\text{Pressure loss factor (PLF)} = \frac{\Delta P_0}{m^2 / (2\rho_1 A_m^2)} = \overline{K_1} + \overline{K_2 \left(\frac{T_{02}}{T_{01}} - 1 \right)} \quad (8.23)$$

Where “ m ” is the air mass flow rate, “ A_m ” is the maximum cross-sectional area of chamber, “ ρ_1 ” is the inlet density, and K_1 and K_2 are determined by measurement of the performance of the system.

Typical values of PLF at design operating conditions for can, can-annular, and annular combustion chamber are 35, 25, and 18, respectively.

8.2.7.2 Combustion Efficiency

The main objective of the combustor is to transfer all the energy of the fuel to the gas stream. In practice this will not occur for many reasons, for example, some of the fuel may not find oxygen for combustion in the very short time available, so it needed to define the efficiency of the combustion.

To obtain high efficiency from the combustor, the following conditions must be achieved:

- Fuel and air have adequate time and adequate space to mix and react.
- Completely vaporized fuel and mixed with air before burning.

The combustion efficiency may be expressed as [26]

$$\eta_b = f(\text{airflow rate})^{-1} \left(\frac{1}{\text{evaporation rate}} + \frac{1}{\text{mixing rate}} + \frac{1}{\text{reaction rate}} \right)^{-1} \quad (8.24)$$

Defining burner (or combustion chamber) efficiency is obtained from low-pressure tests on several types of combustion chambers.

As stated in [21] and illustrated in Fig. 8.64, the combustion efficiency of most gas turbine engines at sea-level takeoff conditions is almost 100 %. It is reduced to 98 % at altitude cruise.

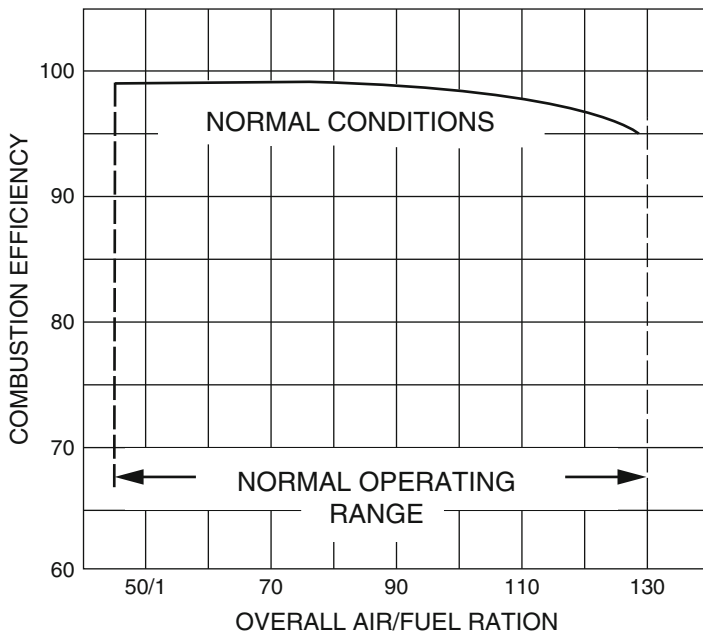


Fig. 8.64 Combustion efficiency (Reproduced with the permission of Rolls-Royce plc, copyright © Rolls-Royce plc)

8.2.7.3 Combustion Stability

Combustion stability means smooth burning and the ability of the flame to remain alight over a wide operating range. For any particular type of combustion chamber, there are both a rich and a weak limit to the air/fuel beyond which the flame is extinguished.

Actually when a new system is tested, the stability limits will be investigated which represent the highest and lowest fuel-to-air ratios at which combustion will take place. Normally the limits will be well away from the normal operating point. The range of stable operation will be reduced with the increase of air velocity, and if the air mass flow rate is increased beyond a certain value, flame will be extinguished. A typical stability loop is illustrated in Fig. 8.65.

There are two reasons that cause instability of combustion. The first is when the fuel-air mixture becomes too lean or too rich such that the temperatures and reaction rates drop below the level necessary to effectively heat and vaporize the incoming fuel and air. The second reason is when the velocity of gas stream “U” becomes higher than the flame speed “S” which causes a blow out of the flame. Stability loops provide two basic kind of information.

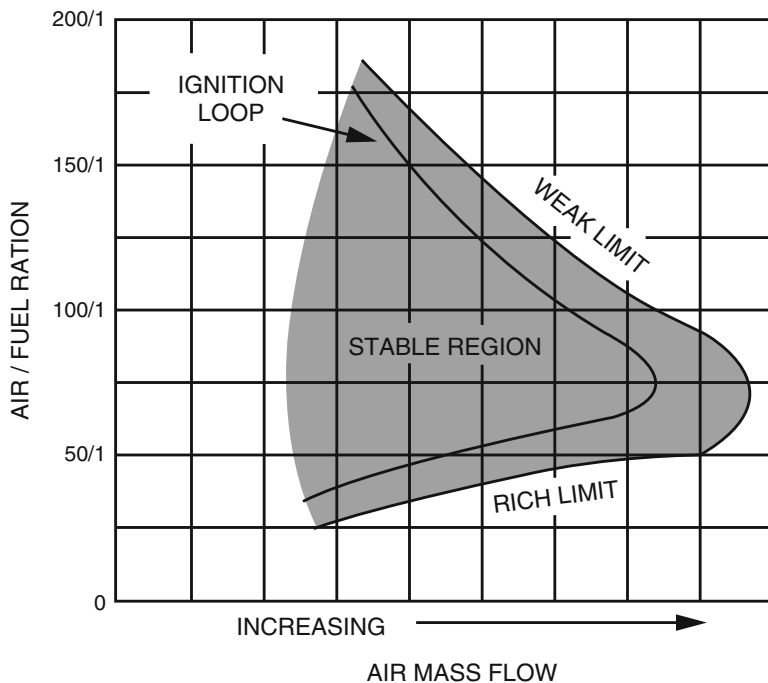


Fig. 8.65 Combustion stability limits (Reproduced with the permission of Rolls-Royce plc, copyright © Rolls-Royce plc)

8.2.8 Material

The walls and internal parts of the combustion chamber must be capable of resisting the very high gas temperature in the primary zone. In practice, this is achieved by using the best heat-resisting materials available. Normally the selected material must withstand severe operating conditions together with the possible corrosion. The most commonly used materials at the present are high-temperature casting superalloy containing nickel, chromium, cobalt, and/or nickel-iron, Inconel 738/Inconel 738 LC, Inconel 939/Inconel 939 LC, Inconel 713/Inconel 713 LC, C1023, Mar M 002, and/or CM 274LC.

8.2.9 Aircraft Fuels

Jet fuel or aviation turbine fuel (ATF) is a type of **aviation fuel** designed for use in aircraft powered by **gas turbine engines**. These jet fuels are denoted as Jet-A (used only in the USA and some parts of Canada) or Jet-A1 (used in the rest of the world).

A third type is identified as Jet B which is used for its enhanced cold-weather performance. However, Jet B's lighter composition makes it more dangerous to handle. For this reason it is rarely used, except in very cold climates.

Military organizations around the world use a different classification system of JP (for "Jet Propellant") numbers. It is designated as JP-i, where (i) stands for its type and changes from 1 to 10. Some are almost identical to their civilian counterparts and differ only by the amounts of a few additives; Jet-A1 is similar to [JP-8](#) and Jet B is similar to [JP-4](#). Other military fuels are highly specialized products and are developed for very specific applications.

Aviation biofuel is a [biofuel](#) used for [aircraft](#) to reduce air pollution and particularly its carbon footprint. In July 2011, biofuels were approved for commercial use in aviation. Since then, some airlines have experimented with using of biofuels on commercial flights. The focus of the industry has now turned to second generation [sustainable biofuels \(sustainable aviation fuels\)](#) that do not compete with food supplies nor are major consumers of prime agricultural land or freshwater.

- Green Flight International was the first airline to fly jet aircraft on 100 % biofuel. The flight from [Reno Stead Airport](#) in Stead, Nevada was in an [Aero L-29 Delfín](#).
- A consortium consisting of Boeing, NASA's [Glenn Research Center](#), [MTU Aero Engines](#) (Germany), and the US [Air Force Research Laboratory](#) is working on the development of jet fuel blends containing a substantial percentage of biofuel.
- [British Airways](#) and Solena Group are establishing a sustainable jet fuel plant in [East London](#), UK as BA plans to use the biofuel to power part of its fleet.
- Twenty-four commercial and military biofuel flights have taken place using [Honeywell](#) "Green Jet Fuel," including a Navy F/A-18 Hornet.
- In 2011, [United Continental Holdings](#) was the first US airline to fly passengers on a commercial flight using a blend of sustainable, advanced biofuels and traditional petroleum-derived jet fuel. [Solazyme](#) company produced the world's first 100 % algae-derived jet fuel, Solajet, for both commercial and military applications.

The fuel specification for aircraft engines is more severe than for all other types of gas turbine.

Several requirements by different sources have to be fulfilled. Some are set by aircraft and engine, others set by fuel system and finally those set by combustion chamber itself.

Operation requirements set by aircraft and engine

It must fulfill the conditions: low cost and high availability; low fire risk; high heat content for maximum range and/or payload; high thermal stability (to avoid filter plugging, sticking of control valves, etc.); low vapor pressure, to minimize vaporization losses at high altitude; and finally high specific heat, to provide effective heat absorption on high-speed aircraft.

Fuel system requirements

It includes pumping ability (fuel must remain liquid phase and flow freely to the atomizer), freedom from filter clogging by ice or wax crystals, freedom from vapor locking, as well as high lubricity for minimum pump wear.

Combustion chamber requirements

It should be free from vanadium, alkali metals such as sodium as well as contaminants that cause blockage of small passage in fuel nozzle, and good atomization. It must provide rapid vaporization, minimum carbon formation and exhaust smoke, less carbon content to avoid excessive carbon deposits in the combustion chamber, and relatively small amount of ash.

8.2.10 Emissions and Pollutants

Recently, control of emissions has become one of the most important factors in the design of aero engines and industrial gas turbines. The pollutants appearing in the exhaust will include:

- Oxides of nitrogen (NOx)
- Carbon monoxide (CO)
- Unburned hydrocarbons (UHC)
- Oxides of sulfur (SO_x), the most common of which is SO₂

NO_x emissions

The oxides of nitrogen can react in the presence of sunlight to produce “smog” which can be seen as a brownish cloud. Oxides of nitrogen also cause acid rain, in combination with moisture in the atmosphere, and ozone depletion at high altitudes, which may result in a reduction in the protection from ultraviolet rays provided by the ozone layer, leading to increases in the incidence of skin cancer. NOx emissions also react with hydrocarbons to form ground-level ozone. NOx also cause lung irritation and lower resistance to respiratory infections.

GE developed low-emissions combustor (LEC) on its CF6-80C, GE90, CF34, and GP7000 engine families which used the existing case and fuel nozzles, optimized mixing for reduced NOx and smoke, and controlled fuel spray and cooling to cut unburned hydrocarbons. For a larger NOx cut, GE introduced the dual-annular combustor (DAC) as an option for CFM56-5B and CFM56-7B engines. The DAC has two combustion zones or stages, a rich pilot stage optimized for emissions during ignition and low power conditions and then a lean main stage optimized for low NOx production for high power conditions.

UHC may also contain carcinogens,

CO emission

CO is fatal if inhaled in significant amounts. It has cardiovascular effects, especially in those persons with heart conditions (e.g., decreased time to onset of exercise-induced angina). It also has similar health effects on animals as on humans.

SO₂ emissions

When sulfur dioxide combines with water, it becomes the primary component in acid rain. Many respiratory problems can be a result of SO₂ inhalation. Bronchoconstriction can be caused by any amount of SO₂ larger than 1 ppm, and 10 ppm can cause eye, throat, and nose irritation which can lead to chronic bronchitis. Much larger amounts of sulfur dioxide can be lethal. SO₂ emissions are a result of the combustion of sulfur and oxygen, and one sulfur and two oxygen combine.

8.2.11 Afterburner

8.2.11.1 Introduction

Afterburners or augmentation devices were first added to aircraft gas turbine engines to increase their thrust during takeoff or brief periods of acceleration and supersonic flight [27]. In a gas turbine engine, the maximum gas temperature at the turbine inlet is limited by structural considerations to values less than half the adiabatic flame temperature at the stoichiometric fuel-to-air ratio. As a result, the gas leaving the turbine contains most of its original concentration of oxygen. This oxygen can be burned with additional fuel in a secondary combustion chamber located downstream of the turbine where temperature constraints are relaxed. The increased total temperature produced at the nozzle by this additional heat addition results in an increased exit velocity and thrust. The advantage of using the afterburning gas turbine engine cycle is that the weight of the augmented engine is much less than the weight of a turbojet engine producing the same maximum thrust. However, when the afterburner is used for a small part of a flight, the weight reduction is more important than the increase in fuel consumption.

The afterburner as described previously is a second combustion chamber located downstream of the turbine and is fitted to supersonic aircrafts (mostly military) to develop a greater thrust force. Afterburner consists of only two fundamentals parts:

1. The fuel injectors
2. The flameholders

An afterburner is quite similar to the combustion chamber in ramjet engines. Both have a maximum temperature much greater than conventional combustion chambers. The gas stream enters the afterburner zone at very high speeds (250–400 m/s), and though diffused, its speed is still high enough to be blown away. For this reason, the AB is provided with flameholders downstream of the spray bars. The flameholders have the different forms. The V-gutter flameholder type has been widely used as it has the advantages of low-flow blockage, low total pressure loss (dry loss), simple, light weight, and has a good development history.

The specific design requirements for afterburner are larger temperature rise and easy ignition.

Firstly the afterburner is not subjected to the physical and temperature limits as in the case of combustion chamber. The temperature rise is limited by the amount of oxygen that is available for combustion and limited by the liner and nozzle cooling air. Moreover, combustion takes place easily because 75 % of the air (oxygen) entering the AB, no longer needed for cooling, is still available for burning with fuel.

8.2.11.2 Thermodynamic Analysis of Afterburner (Rayleigh Flow)

As a first investigate the process of heat addition in simple, one-dimensional channel flow. The calculation will be carried out with the assumption that the heat is added uniformly across the channel. This type of flow is identified crude approximation for the processes occurring in the combustion chamber of an afterburner; it is convenient to Rayleigh flow. With subscripts 1 and 2, identify the inlet and outlet of the afterburner; the ratio between total temperatures and pressures at outlet to inlet states are function of inlet Mach number. These are

$$\frac{T_{02}}{T_{01}} = \left(\frac{1 + \gamma M_1^2}{1 + \gamma M_2^2} \right)^2 \left(\frac{1 + [(\gamma - 1)/2]M_2^2}{1 + [(\gamma - 1)/2]M_1^2} \right) \left(\frac{M_2^2}{M_1^2} \right) \quad (8.25a)$$

$$\frac{P_{02}}{P_{01}} = \left(\frac{1 + \gamma M_1^2}{1 + \gamma M_2^2} \right)^2 \left(\frac{1 + [(\gamma - 1)/2]M_2^2}{1 + [(\gamma - 1)/2]M_1^2} \right)^{\frac{\gamma}{\gamma-1}} \quad (8.26a)$$

If the second state is denoted by a super *, at which heat addition has been sufficient to drive the Mach number to 1 ($M_2 = 1$), thus, $T_{02} \equiv T_0^*$ and $T_{01} \equiv T_0$

$$\frac{T_0^*}{T_0} = \left(\frac{1 + \gamma M_1^2}{1 + \gamma} \right)^2 \left(\frac{[(\gamma + 1)/2]}{1 + [(\gamma - 1)/2]M_1^2} \right) \left(\frac{1}{M_1^2} \right) \quad (8.25b)$$

$$\frac{P_0^*}{P_0} = \left(\frac{1 + \gamma M_1^2}{1 + \gamma} \right)^2 \left(\frac{[(\gamma + 1)/2]}{1 + [(\gamma - 1)/2]M_1^2} \right)^{\frac{\gamma}{\gamma-1}} \quad (8.26b)$$

These relations as well as others are defining ratios between static pressures, and temperatures at outlet and inlet as a function of inlet Mach number are available in Gas Dynamics books [28].

Example 8.9 An afterburner has an inlet Mach number and total temperature of $M = 0.2$ and $T_0 = 500\text{ K}$. It is required to:

1. Calculate the maximum temperature and pressure ratio in the afterburner if the exit Mach number is 1.0.
2. Calculate the exit Mach number and pressure ratio if the maximum temperature is 2000 K.

Solution

Case (1)

This case represents a choked flow, ($M_2 = 1, T_{02} = T_0^*$)

From Eq. 8.25b or gas dynamic tables,

$$\frac{T_0^*}{T_0} = 5.8$$

Thus

$$T_{02} = 5.8 \times 500 = 2400 \text{ K}$$

Moreover, pressure recovery is $\pi_{ab} = \frac{P_{02}}{P_{01}} = \frac{P_0^*}{P_0} = \frac{1}{1.2346} = 0.81$

Case 2

$$\frac{T_{02}}{T_{01}} = \frac{2000}{500} = 4$$

Since

$$\frac{T_0^*}{T_{02}} = \frac{T_0^*}{T_{01}} \frac{T_{01}}{T_{02}} = \frac{5.8}{4} = 1.45$$

$$\frac{T_{02}}{T_0^*} = 0.689$$

The corresponding Mach number is then $M_2 = 0.5$

$$\text{Pressure recovery in afterburner } \pi_{ab} = \frac{P_{02}}{P_0^*} \frac{P_0^*}{P_{01}} = \frac{1.114}{1.2346} = 0.923$$

8.3 Exhaust Nozzle

8.3.1 Introduction

The third stationary module to be examined here is the exhaust nozzle for any airliner or aerospace vehicle (an aerospace plane, orbital launch vehicle, or interplanetary spacecraft). In all cases, a nozzle is used to extract the maximum thrust from high-pressure exhaust gases generated by the propulsion system. *Figure 8.66 illustrates both convergent and convergent-divergent nozzles.*

Early turbojet and turboprop engines employ simple fixed-geometry convergent nozzles.

Unmixed **turbofan** engines mostly employed in airliners have two nozzles for cold and hot streams. Hot gases (core flow) are exhausted from the center convergent nozzle, while the cold air (fan flow) is exhausted from a *co-annular* nozzle as shown in Fig. 8.67. Mixing of the two flows provides some thrust enhancement, and these nozzles also tend to be quieter than convergent nozzles.

Military **turbofan** engines employ a single center convergent-divergent nozzle which exhausts the mixed flow from fan and low-pressure turbine.

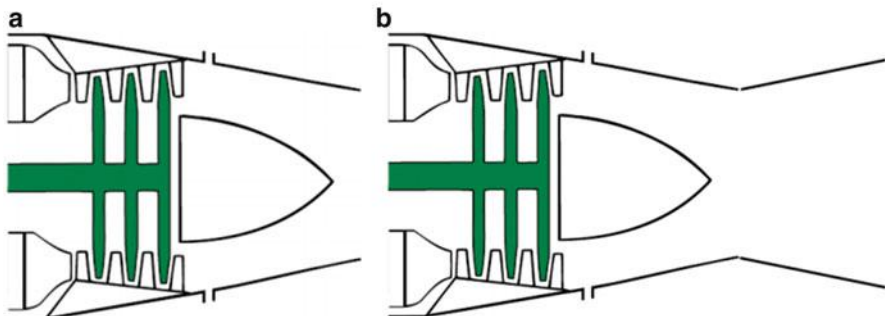


Fig. 8.66 Convergent (a) and convergent–divergent (b) nozzles

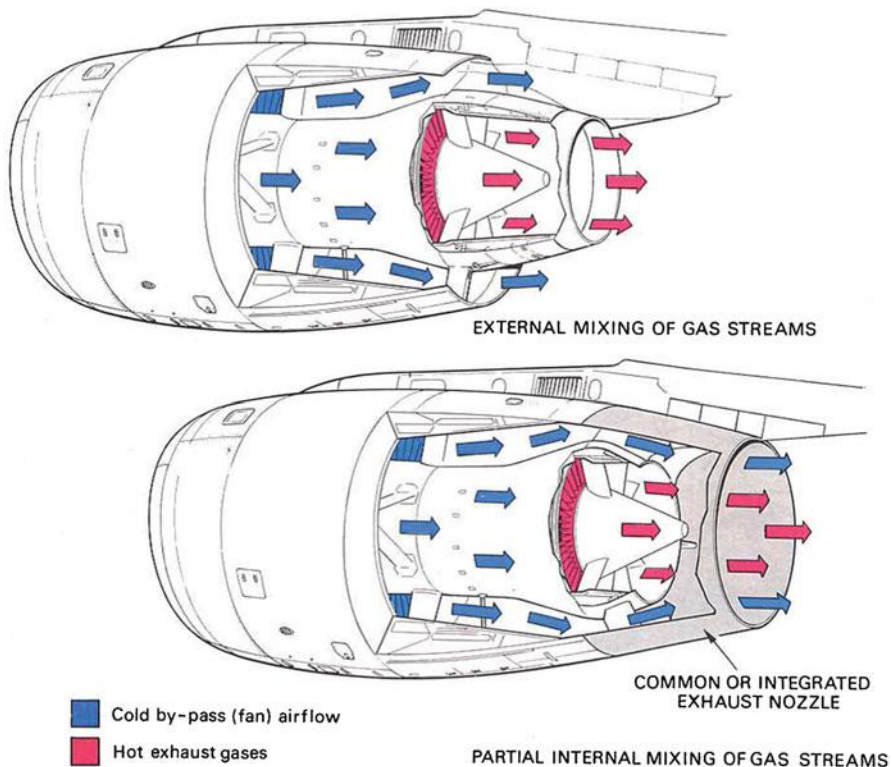


Fig. 8.67 High-bypass ratio engine exhaust systems (Reproduced with the permission of Rolls-Royce plc, copyright © Rolls-Royce plc)

The main *functions* of the nozzles are as follows:

- Provide the required throat area to match the mass flow and exit conditions of the engine.

- (b) Efficiently expand the high-pressure, high-temperature gases at the engine exhaust to atmospheric pressure, converting the available thermal energy to kinetic energy.
- (c) Provide the required thrust in each flight phase with a minimum installed drag.
- (d) Provide the reversed thrust when needed.
- (e) Minimize noise.
- (f) Minimize infrared radiation (IR) for military aircrafts.
- (g) Provide vectored force for VTOL and quick maneuverability of military aircrafts.

Exhaust nozzle may be classified based on simplicity as:

- A simple fixed area
- A complex variable area

A second classification may be:

- Convergent (normally employed in subsonic aircraft)
- Convergent-divergent (C-D) nozzle (adequate performance in supersonic aircraft as well as rockets)

Moreover, it may be classified based on geometry as:

- Axisymmetric
- Two dimensional

The majority of jet-powered aircrafts use axisymmetric nozzles which direct thrust purely along the axis of the engine. Two-dimensional nozzles can direct the thrust along the axis of the engine (as axisymmetric ones) as well as deflecting the thrust to produce inclined thrust force. In later case, thrust force can be deflected up and down in the vertical plane including the engine axis to develop a pitching up or down motion of the aircraft. Examples of these are the American F-35, [F-22 Raptor](#), and Russian [Su-37](#). If the 2-D nozzle is deflected to the right or left direction in a horizontal plane containing engine axis, this will generate right or left yawing motion. A nozzle combining both abilities is a 3-D type, while only one plane of motion is a 2-D type.

The rocket has an alternative option for maneuver. Modern rockets, like the Space Shuttle and the Saturn V, use a system called *gimbaled thrust*. In a gimbaled thrust system, the exhaust [nozzle](#) of the rocket can be swiveled from side to side. As the nozzle is moved, the direction of the [thrust](#) is changed relative to the [center of gravity](#) of the rocket. Figure 8.68 shows three possible cases. The middle rocket shows the “normal” flight configuration in which the thrust force is along the center line of the rocket and through the center of gravity of the rocket. If the nozzle is deflected to the left, then the thrust vector generates a torque about the center of gravity and the rocket will be turned to the left. Such angle of deflection of nozzle is called the gimbal angle. On the rocket at the right, the nozzle has been deflected to the right, and the nose is moved to the right.

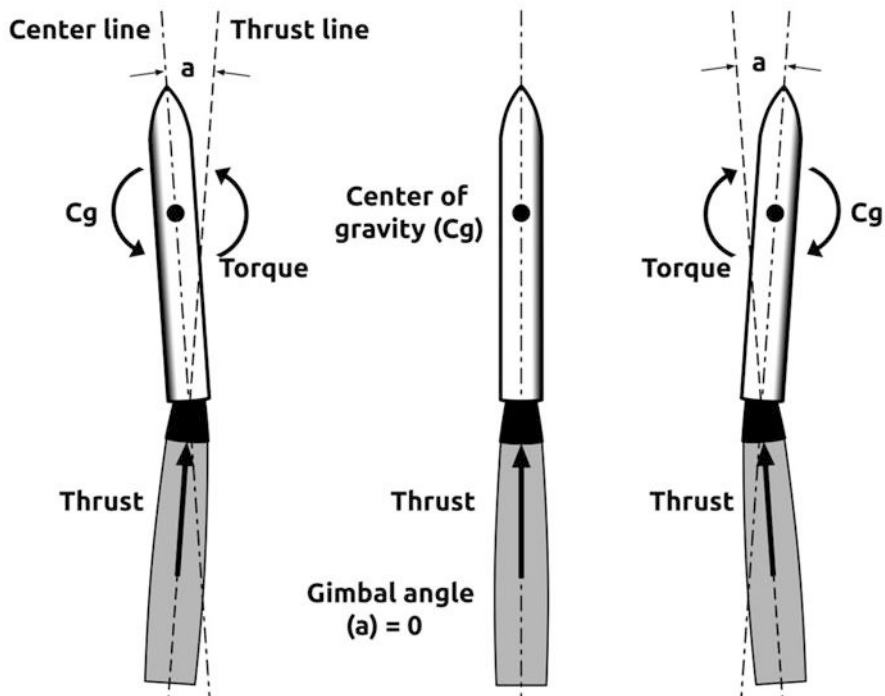


Fig. 8.68 Gimbaled thrust in rockets

8.3.2 Operation of Nozzles

8.3.2.1 Convergent Nozzle

A convergent nozzle is fitted to all airliners which fly at subsonic or transonic speeds. Thus it is either of the axisymmetric or annular geometry. All subsonic/transonic turbojets and turboprop engines have one axisymmetric convergent nozzle. Mixed-flow turbofans fitted to airliners have also one axisymmetric convergent nozzle.

8.3.2.2 Convergent-Divergent Nozzle

Afterburning turbofans and turbojets are fitted with a variable-geometry convergent-divergent C-D nozzle. In this nozzle, the subsonic flow is accelerated in the converging section up to the minimum area or *throat*. *It reaches a sonic speed exactly at the throat*. Decreasing flow area in the converging section results in subsonic (Mach number < 1) acceleration of the gas. The area decreases until the minimum or “throat” area is reached. Here the gas velocity reaches a sonic speed

(Mach number of one). Then the nozzle accelerates the flow supersonically (Mach number > 1) by providing a path of increasing flow area. The variable geometry causes these nozzles to be heavier than a fixed-geometry nozzle, but variable geometry provides efficient engine operation over a wider airflow range than a simple fixed nozzle.

8.3.3 Performance Parameters of Nozzles

The main parameters governing performance of nozzles are as follows:

1. Pressure ratio
2. Efficiency
3. Area ratio

Pressure ratio in a nozzle is the ratio of outlet total pressure $P_{0\text{outlet}}$ to inlet total pressure $P_{0\text{inlet}}$. Thus

$$\pi_n = \frac{P_{0\text{outlet}}}{P_{0\text{inlet}}}$$

Nozzle efficiency is defined as the ratio between the differences between total inlet temperature $T_{0\text{inlet}}$ and the static exit temperature T_e and the difference between the total inlet temperature $T_{0\text{inlet}}$ and the isentropic static exit temperature $T_{e\text{isentropic}}$. Thus

$$\eta_n = \frac{T_{0\text{inlet}} - T_e}{T_{0\text{inlet}} - T_{e\text{isentropic}}} = \left(\frac{V_e}{V_{e\text{isentropic}}} \right)^2$$

Choked nozzle is checked by calculating the following critical pressure P_c as follows:

$$\frac{P_{0\text{inlet}}}{P_c} = \frac{1}{\left(1 - \frac{1}{\eta_n} \frac{\gamma-1}{\gamma+1} \right)^{\frac{\gamma}{\gamma-1}}}$$

Nozzle is choked if

$$\frac{P_{0\text{inlet}}}{P_c} < \frac{P_{0\text{inlet}}}{P_{\text{ambient}}}$$

Thus

$$P_c > P_{\text{ambient}}$$

and

$$P_e = P_c$$

Table 8.3 Mach number corresponding to different area ratios

Subsonic		Supersonic	
	$1.0 < \frac{A}{A^*} < 1.34$	$1.34 < \frac{A}{A^*} < \infty$	$1.0 < \frac{A}{A^*} < 2.9$
M	$1 - 0.88 \left\{ \ln \left(\frac{A}{A^*} \right) \right\}^{0.45}$	$\frac{1 + 0.27 \times \left(\frac{A}{A^*} \right)^{-2}}{1.728 \times \left(\frac{A}{A^*} \right)}$	$1 + 1.2 \left\{ \left(\frac{A}{A^*} \right) - 1 \right\}^{0.5}$

Thus $V_e = \sqrt{\gamma RT_c} = \sqrt{\frac{2\gamma}{\gamma+1} RT_{0 \text{ inlet}}}$

Thrust equation is also

$$T = \dot{m} [(1+f)V_e - V_f] + (P_e - P_{\text{ambient}})A_e$$

From isentropic relations and conservation of mass equation applied to both of exit section and any interior section at station (x), then

$$\frac{A}{A^*} = \frac{1}{M} \left(\frac{2 + (\gamma - 1)M^2}{\gamma + 1} \right)^{\frac{\gamma+1}{2(\gamma-1)}} \quad (8.27)$$

It is not easy to determine the Mach number corresponding to any area ratio (A/A^*), from [29], then Table 8.3 is deduced for $\gamma = 1.4$.

The most important parameter in nozzle design is *expansion area ratio*, ϵ , defined as

$$\epsilon = \frac{A_{\text{exit}}}{A_{\text{throat}}} = \frac{A_e}{A^*} \quad (8.28)$$

Area ratio for convergent nozzle is unity, while for convergent–divergent nozzles in aircrafts is greater than unity. For rockets and space vehicles, it could be as large as 50.

The exhaust speed that can be achieved is governed by the nozzle area ratio which in turn is determined by the design ambient pressure. Low ambient pressure leads to a high nozzle exit area, higher gas exit velocity, and hence, more thrust.

Other design factors are nozzle weight, length, manufacturability, cooling (heat transfer), and aerodynamic characteristics.

Example 8.10 Airflows through a convergent–divergent nozzle having a circular cross-sectional area $A(x)$ expressed by the relation $A(x) = 0.15 + x^2$, where $A(x)$ is in square meters and (x) is in meters. The duct extends from $x = -0.6$ m to $x = +1.8$.

- (a) Draw a layout for the nozzle.
- (b) If the inlet air speed is *subsonic*, plot the variation of the following variables:

- (i) Mach number
- (ii) Static to total temperature $\frac{T}{T_o}$
- (iii) Static to total pressure $\frac{P}{P_o}$
- (iv) Static to total density $\frac{\rho}{\rho_0}$

Solution

Since $A(x) = \pi r^2 = 0.15 + x^2$, then

$$r = \left(\frac{0.15 + x^2}{\pi} \right)^{0.5}$$

Area at nozzle throat $A^* = 0.15$, then

$$\frac{A}{A^*} = \left(\frac{0.15 + x^2}{0.15} \right) \rightarrow (1)$$

From isentropic flow in a variable area duct

$$\frac{A}{A^*} = \frac{1}{M} \left[\frac{2 + (\gamma - 1)M^2}{(\gamma + 1)} \right]^{\frac{(\gamma+1)}{2(\gamma-1)}} \rightarrow (2)$$

From (1) and (2), we get the Mach number along the nozzle using formulae in Table 8.3.

Moreover, pressure and temperature ratios are obtained from isentropic relations:

$$\frac{P}{P_o} = \left[\frac{1}{\left(1 + \frac{\gamma-1}{2} M^2 \right)^{\frac{\gamma}{\gamma-1}}} \right] \rightarrow (3)$$

$$\frac{T}{T_o} = \left[\frac{1}{\left(1 + \frac{\gamma-1}{2} M^2 \right)} \right] \rightarrow (4)$$

$$\frac{\rho}{\rho_0} = \left[\frac{1}{\left(1 + \frac{\gamma-1}{2} M^2 \right)^{\frac{1}{\gamma-1}}} \right] \rightarrow (5)$$

The requested information are calculated and tabulated in Table 8.4. The convergent section is located in the region $x = -0.6$ m up to $x = 0$, while the divergent section extends from $x = 0$ to $x = 1.8$ m. Flow is subsonic in the convergent section, next attains sonic speed at throat, and continues acceleration in the divergent section to reach supersonic speeds.

Table 8.4 Geometry and Mach number distribution at different axial position in a convergent divergent nozzle

x (m)	-0.6	-0.4	-0.2	0	0.6	1.2	1.8
A	0.51	0.31	0.19	0.15	0.51	1.59	3.39
r (m)	0.4	0.314	0.246	0.219	0.4	0.711	1.039
$\frac{A}{A^*}$	3.4	2.067	1.267	1	3.4	10.6	22.6
M	Subsonic	0.1742	0.2977	0.5399			
	Supersonic				1	2.7597	4.0307
$\frac{T}{T_0}$	Subsonic	0.994	0.98258	0.9449			
	Supersonic				0.8333	0.3963	0.2353
$\frac{P}{P_0}$	Subsonic	0.979	0.9404	0.8201			
	Supersonic				0.5283	0.03919	0.00632
							0.0021

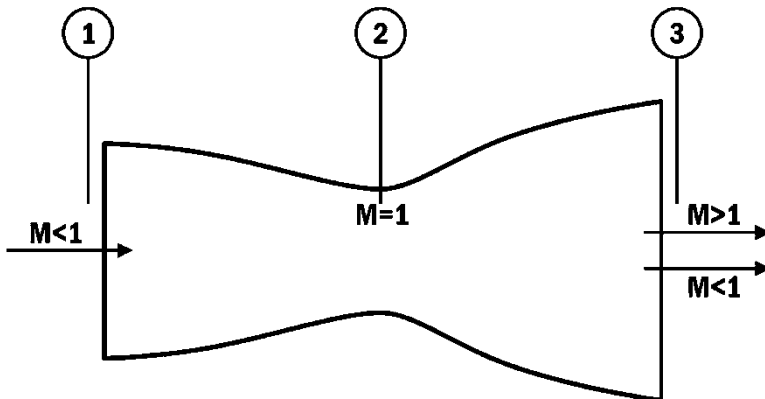


Fig. 8.69 A layout for the convergent–divergent nozzle

Figure 8.69 illustrates a layout for the convergent–divergent nozzle.

Figure 8.70 illustrates the variation of radius, area, and area ratio (A/A^*) along the convergent–divergent nozzle. Figure 8.71 illustrates the variation of temperature ratio (T/T_0), pressure ratio (P/P_0), and density ratio (ρ/ρ_0) along the convergent–divergent nozzle. Figure 8.72 illustrates the variation of Mach number along the convergent–divergent nozzle. Figure 8.73 illustrates T - s diagram for flow along the convergent–divergent nozzle.

Example 8.11 It is required to design the fan and core nozzles of high-bypass ratio turbofan engines based on the following takeoff conditions:

Ambient temperature and pressure: 288 K and 101 kPa.

Total mass flow rate: 1040 kg/s.

Bypass ratio: 9.1.

Fuel mass flow rate: 3.5 kg/s.

Pressure recovery of cold and hot nozzles: 98 %.

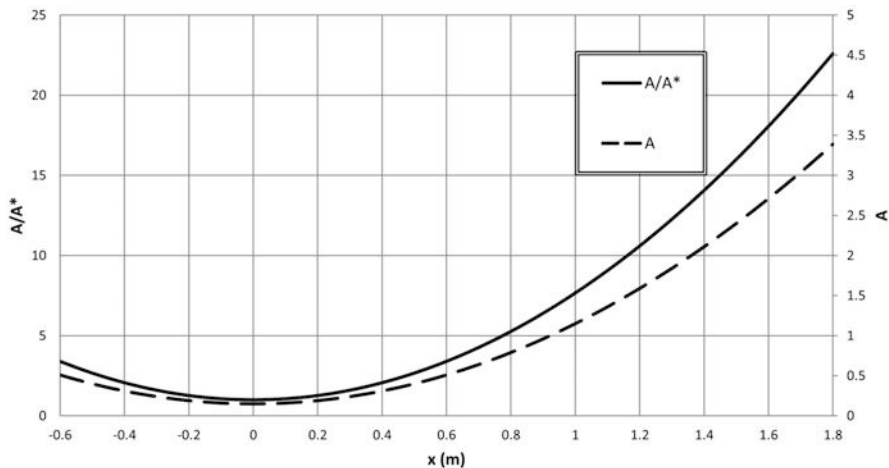


Fig. 8.70 Variation of radius, area, and area ratio (A/A^*) along the convergent–divergent nozzle

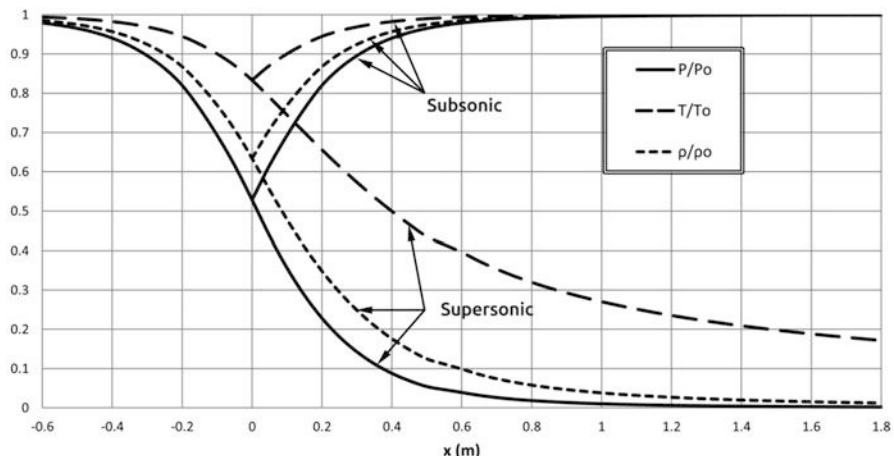


Fig. 8.71 Variations of temperature ratio (T/T_0), pressure ratio (P/P_0), and density ratio (ρ/ρ_0) along the convergent–divergent nozzle

Cold nozzle is choked.

Outer radius of cold nozzle is constant from inlet to outlet = 1.42 m.

Inner radius at inlet of hot nozzle is 0.4 m.

Inner radius at outlet of hot nozzle is 0.35 m.

Axial length (L) of tail cone:

$$L = (r_{\text{inlet}} - r_{\text{outlet}}) / \tan \theta$$

Where θ is the nozzle angle, usually assumed 10–15°.

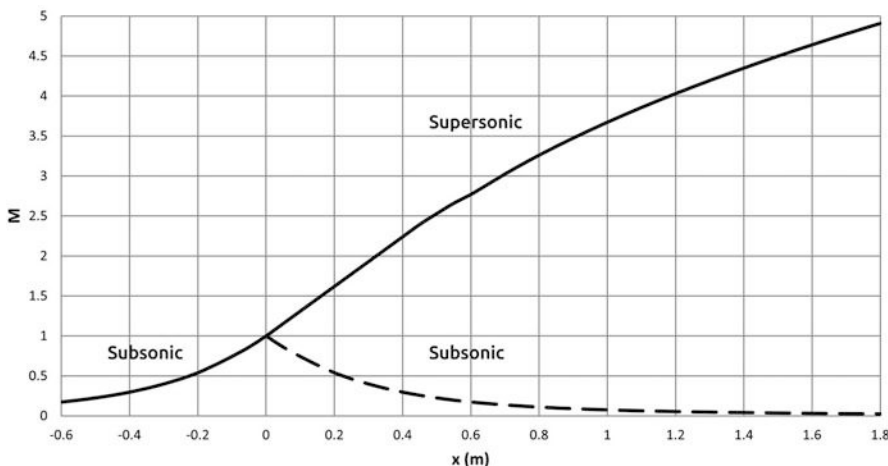


Fig. 8.72 Variation of Mach number along the convergent–divergent nozzle

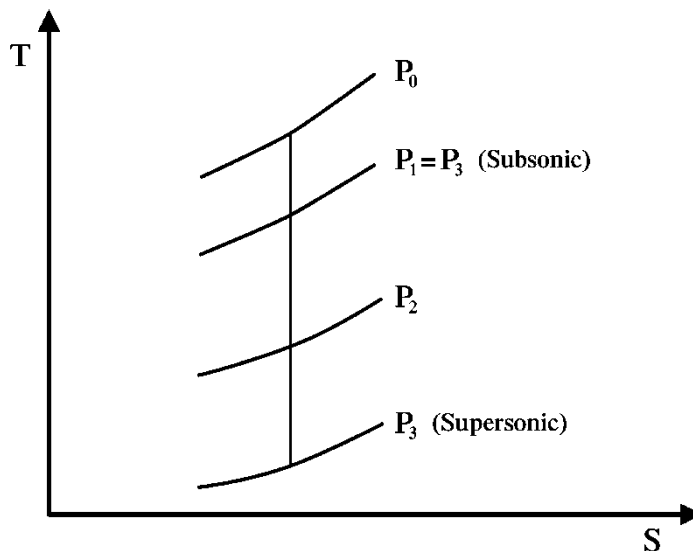


Fig. 8.73 T - s diagram for flow along the convergent–divergent nozzle

	Cold nozzle	Hot nozzle
Inlet total temperature (K)	320	792
Inlet total pressure (kPa)	142	146
Inlet speed (m/s)	187	245
Outlet speed (m/s)	–	390
Specific heat (kJ/kg/K)	1.005	1.148
Specific heat ratio	1.4	4/3

Calculate the following:

1. Inner radii of cold nozzle at inlet and outlet
2. Outer radii of hot nozzle at inlet and outlet
3. Calculate the length of both cold and hot nozzles

Solution

Cold nozzle

$$T_i = T_{0i} - \frac{C_i^2}{2C_{pc}} = 320 - \frac{187^2}{2*1005} = 300.7 \text{ K}$$

$$\frac{P_i}{P_{0i}} = \left(\frac{T_i}{T_{0i}} \right)^{\frac{\gamma_c}{\gamma_c - 1}} = 142 * \left(\frac{300.7}{320} \right)^{3.5} = 114.2 \text{ kPa}$$

$$\rho_i = \frac{P_i}{R*T_i} = \frac{114.2*103}{287*300.7} = 1.323 \frac{\text{kg}}{\text{m}^3}$$

$$\dot{m} = \rho_i * C_{ai} * A_i$$

$$A_i = \frac{\dot{m}}{\rho_i * C_i} = \frac{1040}{1.323 * 187} = 4.2 \text{ m}^2$$

$$A_i = \pi(r_o^2 - r_i^2)$$

$$r_i = \sqrt{r_0^2 - \frac{Ai}{\pi}} = 0.806 \text{ m}$$

Outlet (exit)

$$T_{oe} = 320 \text{ K}$$

$$P_{oe} = 142 * 0.98 = 139.2 \text{ kPa}$$

$$V_{ec} = \sqrt{\frac{2\gamma}{\gamma + 1} RT_0} = 327 \text{ m/s}$$

$$T_e = \frac{2}{\gamma + 1} T_{oe} = 266.7 \text{ K}$$

$$\frac{P_e}{P_{oe}} = \left(\frac{T_e}{T_{oe}} \right)^{\frac{\gamma_c}{\gamma_c - 1}} = 139.2 \left(\frac{266.7}{320} \right)^{3.5}$$

$$P_e = 73.6 \text{ kPa}$$

$$\rho_e = \frac{P_e}{R*T_e}$$

$$\rho_e = \frac{73.6*10^3}{287*266.7} = 0.9611 \text{ kg/m}^3$$

$$\dot{m} = \rho_e * V_{ec} * A_{ec}$$

$$A_{ec} = \frac{\dot{m}}{\rho_e * V_{ec}} = \frac{1040}{0.9611 * 327} = 3.31 \text{ m}^2$$

$$r_i = \sqrt{r_0^2 - \frac{Ai}{\pi}} = \sqrt{1.41^2 - \frac{3.31}{\pi}} = 0.967 \text{ m}$$

Assuming $\theta = 12^\circ$, then

$$L = \frac{|r_{\text{inlet}} - r_{\text{outlet}}|}{\tan \theta} = \frac{0.967 - 0.806}{\tan 12} = 0.757 \text{ m}$$

Hot nozzle

Inlet

$$T_{0i} = 792 \text{ K}$$

$$P_{oi} = 146 \text{ kPa}$$

$$Ci = 245 \frac{\text{m}}{\text{s}}$$

$$\dot{m}_h = \left[\frac{1}{1 + \beta} \right] \dot{m}_t = \left[\frac{1}{1 + 9.1} \right] * 1040 = 103 \text{ kg/s}$$

$$\dot{m}_{\text{nozzle}} = \dot{m}_h + \dot{m}_f = 103 + 3.5 = 106.5 \frac{\text{kg}}{\text{s}}$$

$$Ti = Toi - \frac{Ci^2}{2Cp}$$

$$Ti = 792 - \frac{245^2}{2 * 1148}$$

$$Ti = 765.85 \text{ k}$$

$$\frac{P_i}{P_{oi}} = \left(\frac{T_i}{T_{oi}} \right)^{\frac{\gamma_h}{\gamma_h - 1}}$$

$$P_i = 146 * \left(\frac{765.85}{792} \right)^4 = 127.65 \text{ kPa}$$

$$\rho_i = \frac{P_i}{R * T_i} = \frac{127.65 * 10^3}{287 * 765.85} = 0.58 \frac{\text{kg}}{\text{m}^3}$$

$$\dot{m}_{\text{nozzle}} = \rho_i * C_i * A_i$$

$$A_i = \frac{106.5}{0.58 * 245} = 0.748 \text{ m}^2$$

$$r_0 = \sqrt{r_i^2 + \frac{Ai}{\pi}} = \sqrt{0.4^2 + \frac{0.748}{\pi}} = 0.63 \text{ m}$$

Outlet (exit)

$$T_{oe} = 792 \text{ K}$$

$$P_{oe} = 146 \times 0.98 = 143 \text{ kPa}$$

$$V_e = 390 \frac{\text{m}}{\text{s}}$$

$$T_e = 792 - \frac{390^2}{2*1148} = 725.75 \text{ K}$$

$$P_e = P_{oe} \left(\frac{T_e}{T_{oe}} \right)^{\frac{\gamma}{\gamma-1}} = 143 \left(\frac{725.75}{792} \right)^4 = 100.8 \text{ kPa}$$

Hot nozzle is unchoked

$$\rho_e = \frac{P_e}{R*T_e}$$

$$\rho_e = \frac{P_e}{R*T_e} = \frac{100.8*10^3}{287*725.75} = 0.484 \frac{\text{kg}}{\text{m}^3}$$

$$A_e = \frac{\dot{m}_{\text{nozzle}}}{\rho_e * C_e} = \frac{106.5}{0.484*245} = 0.898 \text{ m}^2$$

$$r_0 = \sqrt{r_i^2 + \frac{Ai}{\pi}} = \sqrt{0.4^2 + \frac{0.898}{\pi}} = 0.66 \text{ m}$$

Assuming $\theta=10^\circ$, then

$$L = \frac{|r_{\text{inlet}} - r_{\text{outlet}}|}{\tan \theta} = \frac{0.66 - 0.63}{\tan 10} = 0.17 \text{ m}$$

8.3.4 High-Speed Vehicles

Supersonic and hypersonic vehicles employ convergent–divergent nozzles. These have three main types [30]:

- Cone
- Bell
- Annular

Hereafter, the main characteristics of these types will be briefly described.

8.3.4.1 Conical Nozzles

The conical nozzle was used in early rockets due to its simplicity and ease of construction. The main geometrical parameters for a conical nozzle are half-angle α , length L , and throat diameter D^* . The ratio of exit to throat area is

$$\frac{A_e}{A^*} = \left(\frac{D^* + 2L \tan \alpha}{D^*} \right)^2 \quad (8.29)$$

The length of nozzle is also expressed as

$$L = \frac{D^* \left(\sqrt{\frac{A_e}{A^*}} - 1 \right)}{2 \tan \alpha} \quad (8.30)$$

The length of the nozzle is then calculated knowing the area ratio, throat diameter, and desired nozzle half angle. Throat diameter D^* is fixed by combustion chamber conditions and desired thrust. Moreover, the nozzle length and mass are strongly dependent on α .

Figure 8.74 illustrates three conical nozzles having constant (A_e/A^*) and different (L/D^*). The longest nozzle (case a) has nearly uniform axial outlet speed. Case (b) has almost axial flow at nozzle outlet. Case (c) is the shortest nozzle, where the flow has a reasonable radial velocity component with possible separation.

Soviet nozzles look more conical.

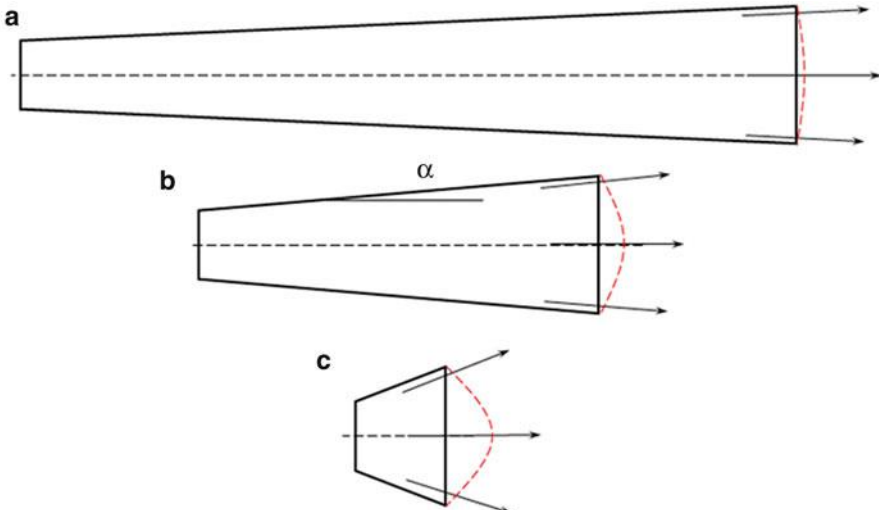


Fig. 8.74 Three conical nozzles having constant (A_e/A^*) and different (L/D^*)

Example 8.12 Calculate the length of a nozzle for area ratio of 50 and half angle $f 20^\circ$ and 10° .

Solution

From Eq. 8.30

$$\frac{L}{D^*} = \frac{\left(\sqrt{\frac{A_e}{A^*}} - 1\right)}{2 \tan \alpha}$$

If $\alpha = 20^\circ$

$$\frac{L}{D^*} = 8.34$$

If $\alpha = 10^\circ$

$$\frac{L}{D^*} = 17.2$$

Reducing α from 20° to 10° would more than double the length and consequently mass of the divergent portion of the nozzle. However, small angle produces a great thrust as it maximizes the axial component of exit velocity and produce higher specific impulse. On the contrary, large angle reduces performance as it causes flow separation.

8.3.4.2 Bell Nozzles

Bell is the most commonly used nozzle shape. It offers significant advantages over conical nozzle. Concerning length, it is nearly 10–25 % shorter than conic as illustrated in Fig. 8.75. Thus it has less weight. It has also better performance as its contour avoids oblique shocks thus has better performance. However, its shape is only optimum at one altitude.

Bell consists of two sections: near throat and divergent section. It diverges at relatively large angle. Degree of divergence tapers off further downstream. Near nozzle exit, divergence angle is very small $\sim 2^\circ$ – 8° [31].

Performance of bell nozzles depends on flight altitude (refer to Fig. 8.76). At optimum (intermediate) altitude the exhaust gases are ideally expanded ($P_e = P_a$); exhaust plume is a column-shaped producing the maximum efficiency. At lower altitudes and sea level, nozzle is overexpanded ($P_e < P_a$), but gases do not expand beyond $P_e = 0.4P_a$. Exhaust plume is pinched by high ambient air pressure. At high altitudes, the nozzle is underexpanded where $P_e > P_a$. The exhaust plume continues to expand past the nozzle exit. Efficiency is reduced for low and high altitudes.

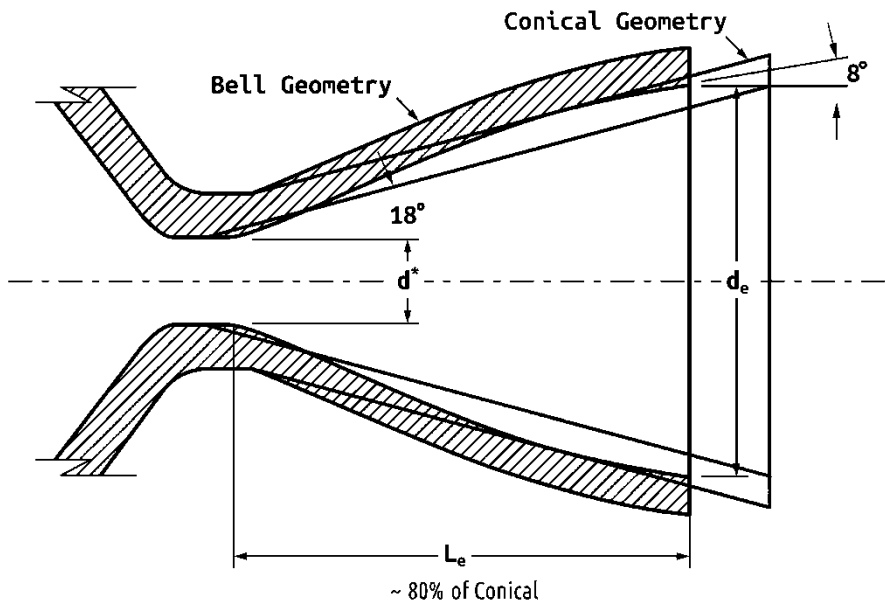


Fig. 8.75 Bell versus conical nozzle

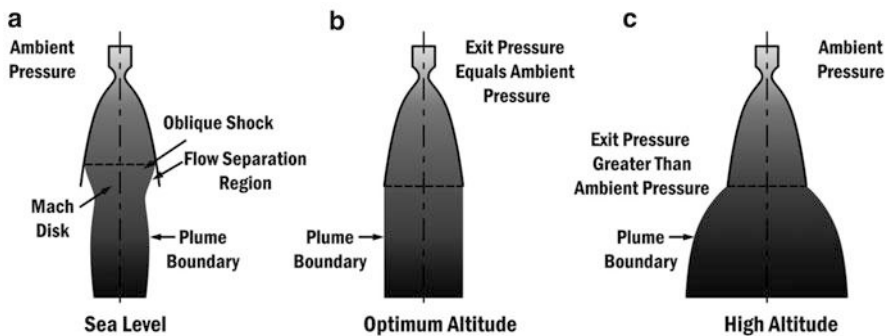


Fig. 8.76 Plume shapes for different altitudes

Advantages of bell-shaped nozzle

1. Mechanical design is simple as tangential stresses are dominant which is easiest to design for.
2. Cooling is easy as it is fabricated with walls of simple tubular construction that enables cooling in a straightforward way.
3. Matching to combustion chamber is simple as it is most naturally a simple cylinder.

Disadvantages of bell-shaped nozzle

Overexpansion case leads to both thrust loss and flow instability as well as uncertainty or unsteadiness of the thrust direction.

Generally US nozzle designs tend to have bell shapes and usually designed by method-of-characteristics methods.

8.3.4.3 Annular Nozzles

Annular nozzles are sometimes known as the plug or “altitude-compensating” nozzles. It recently received significant research attention. However, it is least employed due to its greater complexity. Plug refers to the center body that blocks flow from what would be center portion of traditional nozzle.

Annular nozzles are classified as two major types depending on the method in which they expand exhaust, namely, outward or inward.

Radial outflow nozzles

Examples of this type are the expansion-deflection (E-D), reverse-flow (R-F), and horizontal-flow (H-F) nozzles.

Radial inflow nozzles

Examples of this type are spike nozzles and linear aerospike nozzle for X-33.

Brief notes will be given hereafter for some of the annular nozzles.

(A) Radial outflow nozzles

Figure 8.77 shows an example of an expansion-deflection (E-D) nozzle, which works much like a bell nozzle. Exhaust gases are forced into a converging throat before expanding in a bell-shaped nozzle. Flow is deflected by a plug, or center body, that forces the gases away from the center of nozzle which thus stays attached to nozzle walls. Center-body position may move to optimize performance. As altitude or back pressure varies, flow is free to expand into “void” which allows the nozzle to compensate for altitude.

Expansion ratio

$$\epsilon = \frac{A_{\text{exit}} - A_{\text{plug}}}{A_{\text{throat}}}$$

Another parameter

$$\text{Annular diameter ratio} = D_{\text{plug}}/D_{\text{throat}}$$

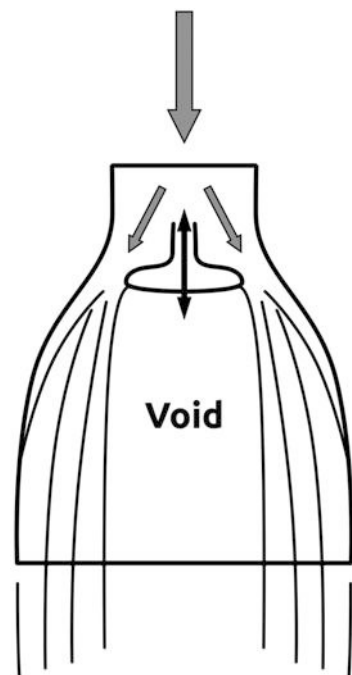
This ratio is used as a measure of nozzle geometry for comparison with other plug nozzle shapes.

(B) Radial inflow nozzles

Radial inflow nozzles [32] are often referred to as

- Spike nozzles
- Aerospike or truncated aerospike

Fig. 8.77 An expansion-deflection (E-D) radial outflow nozzle



Spike nozzle is named for prominent spike center body. It may be thought of as a bell turned inside out. Each of the spike nozzles features a curved, pointed spike. Spike shape allows exhaust gases to expand through isentropic process. Isentropic spike may be most efficient but tends to be prohibitively long and heavy.

Aerospike or truncated aerospike which is generated by removing pointed spike altogether and replace with a flat base. The main disadvantage of “flat” plug is turbulent wake forms aft of base at high altitudes resulting in high-base drag and reduced efficiency. However, it may be alleviated by introducing a “base bleed,” or secondary subsonic flow. Circulation of this secondary flow and its interaction with the engine exhaust creates an “aerodynamic spike” that behaves much like the ideal, isentropic spike.

Problems

- 8.1 The following table lists data for a triple-spool unmixed turbofan engine operating conditions:

Properties	Value	Properties	Value
π_{pr}	[variable]	$\Delta p_{c.c}$	0.03
η_f	0.9	$\Delta p_{\text{fan duct}}$	0
η_c	0.89	$cp_c(\text{J/kg.K})$	1005
η_b	0.98	$cp_h(\text{J/kg.K})$	1148

(continued)

Properties	Value	Properties	Value
η_t	0.93	R (J/kg, K)	287
η_n	0.98	γ_c	1.4
η_m	0.99	γ_h	1.33
λ_1	0.84	b	0.08
λ_2	1	β	5.05
λ_3	1	$TIT(K)$	1543
M	[variable]	π_{IPC}	5.8
π_F	1.45	π_{HPC}	4.2

It is required to examine the influence of intake pressure recovery ($\pi_{pr} = 0.92, 0.95, 0.99$) on performance parameters. Plot the following relation:

1. The thrust specific fuel consumption versus Mach number ($M = 0.0\text{--}0.9$)
2. The specific thrust versus Mach number ($M = 0.0\text{--}0.9$)
3. The propulsive efficiency versus Mach number ($M = 0.0\text{--}0.9$)
4. The thermal efficiency versus the Mach number ($M = 0.0\text{--}0.9$)
5. The thrust specific fuel consumption versus altitude (1.0–11.0 km) for a Mach number ($M = 0.5$)
6. The specific thrust versus altitude (1.0–11.0 km) for a Mach number ($M = 0.5$)
7. The propulsive efficiency versus altitude (1.0–11.0 km) for a Mach number ($M = 0.5$)
8. The thermal efficiency versus altitude (1.0–11.0 km) for a Mach number ($M = 0.5$)

8.2 A nozzle is required to produce a flow of air at 400 m/s at 400 K and 100 kPa. It is estimated that the nozzle has an isentropic efficiency of 94 %. What nozzle inlet pressure and temperature is required assuming the inlet kinetic energy is negligible?

8.3 A jet engine operates at an altitude of 10 km where ambient temperature and pressure are 223 K and 26.5 kPa at a Mach number of 1.7. The engine mass flow is limited by a throat area $A_t = 500 \text{ cm}^2$. The external diffusion is based on an oblique shock followed by a normal shock as shown in figure.

Calculate the following:

Stagnation pressure recovery P_{02}/P_{0a} at what Mach number does the oblique shock become detached?

What is the distance x , from the cone tip to the outer inlet lip, for the conditions described in figure?

What is the best turning angle θ in terms of highest pressure ratio, P_{02}/P_{0a} ?

8.4 Consider air entering a supersonic engine intake at Mach 3 at an altitude of 10 km (ambient temperature and pressure of 223 K and 26.5 kPa). The intake has a protruding wedge which deflects the flow by 30 °. The flow is further

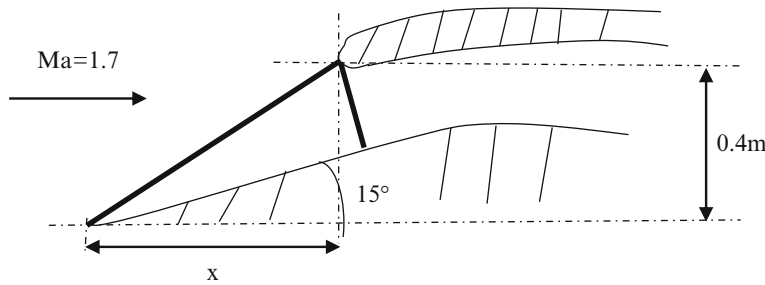


Figure: Problem (8.3)

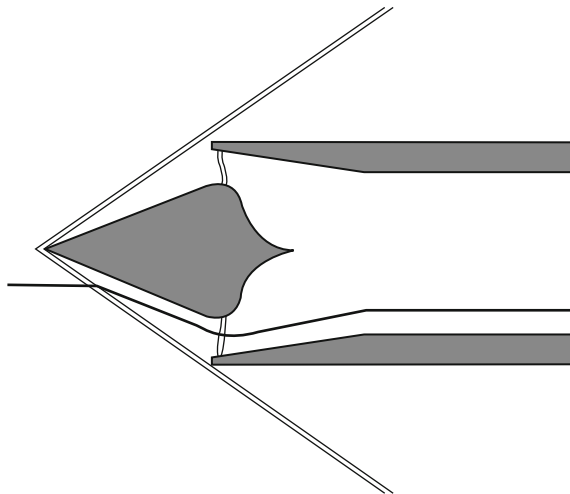


Figure: Problem (8.4)

decelerated to subsonic speed through a normal shock wave that follows the first oblique shock. The flow continues its deceleration in the succeeding subsonic diffuser to reach Mach 0.2.

Calculate the following:

(A) Mach number, total temperature, and pressure in the two regions:

- Between the first oblique shock and normal shock
- Between the normal shock and the diffuser end

(B) Pressure recovery of the intake

8.5 A fighter aircraft (F-111A) is flying at an altitude of 13,700 m where the ambient pressure and temperature are, respectively, 14,794 Pa and 216.66 K, as shown in Fig. (80). The F-111 is powered by two Pratt & Whitney TF30 afterburning turbofan engines. The engine has the one-quarter circle ($r = 0.846$ m) axisymmetric external compression inlets under the wing, as shown in Fig. (81). The aircraft inlet has approximate two-dimensional inlet



Figure A: Problem (8.5): A fighter aircraft (F-111A)

where air enters the intake with a Mach number of 2.2. The intake diffuser has two oblique shock waves followed by a normal shock wave, as shown in Fig. (82). The deflection angle of spike is 12.5° which is followed by a second deflection of 10° .

($\gamma = 1.4$ and $R = 287 \text{ J/kg.K}$)

Calculate the following:

- (a) The total pressure and temperature of air entering the first oblique shock wave
- (b) The first oblique shock wave angle (θ_1)
- (c) The pressure recovery along the first oblique shock
- (d) The Mach number after the first oblique shock wave
- (e) The second oblique shock wave angle (θ_2)
- (f) The Mach number after the second oblique shock wave
- (g) The pressure recovery along the second oblique shock
- (h) The Mach number after the normal shock wave
- (i) The pressure recovery along the normal shock wave
- (j) The total pressure recovery (where pressure recovery for subsonic intake=0.98)
- (k) The external distance of spike (X)

- 8.6 During cruise flight, the ambient conditions and the intake conditions in a turbofan engine are as follows:

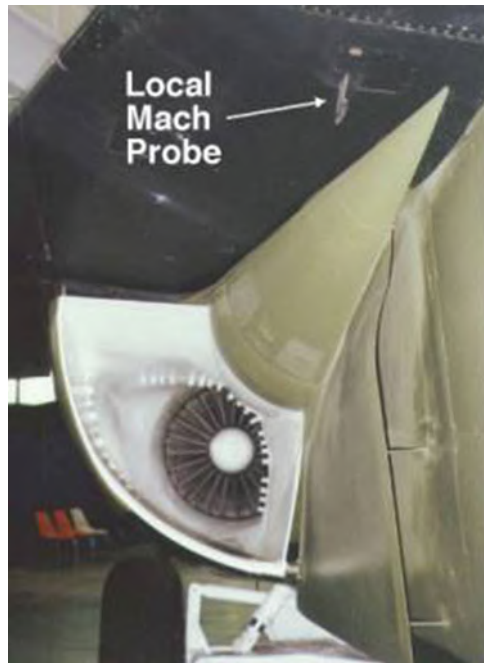


Figure B: Problem (8.5): Supersonic intake of fighter aircraft (F-111A)

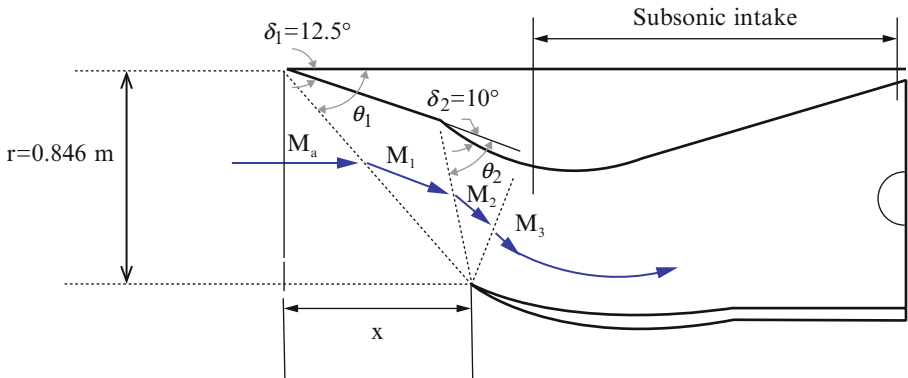


Figure C: Problem (8.5): A fighter aircraft (F-111A) supersonic intake with two oblique shock waves followed by a normal shock wave

$$P_{\infty} = 23.8 \text{ kPa}, T_{\infty} = 218.6 \text{ K}$$

Total air mass flow rate of engine $\dot{m} = 120 \text{ kg/s}$,

Mach numbers

Far upstream $M_{\infty} = 0.87$, at inlet diffuser $M_c = 0.8$, and fan inlet $M_f = 0.50$

Assuming the diffuser pressure recovery $\pi_d = 0.93$,

- (a) Determine the diameters at far upstream (d_∞), intake inlet section (d_i), and intake outlet section (or fan inlet section d_f)
- (b) Diffuser length L

7. Consider the complete combustion of a hydrocarbon fuel with the composition of $C_nH_{2n\mp 2}$.

- (a) Prove that the air-to-fuel ratio on a molar basis is

$$\left(\frac{3n \mp 1}{2}\right) \times (4.76) \frac{\text{kmole of air}}{\text{kmole of fuel}}$$

- (b) Prove that the air-to-fuel ratio on a mass basis is:

$$\left(\frac{3n \mp 1}{2}\right) \times (4.76) \times 28.97 \times \frac{1}{12n + 2n \mp 2} \frac{\text{kg of air}}{\text{kg of fuel}}$$

- (c) Write down the combustion equation for the hydrocarbon fuels.



- (d) Evaluate the air-to-fuel ratios in the above three fuels.

8.7 Write down the combustion equation for CH_4 fuel. Calculate the stoichiometric air-to-fuel ratio. Calculate the equivalence ratio in the two cases of air-to-fuel ratio of 10 and 40.

8.8 Consider the complete combustion of octane (C_8H_{18}) with theoretical air. If the enthalpy of formation of the reactants and products are as follows: where (g) refers to gas and (l) refers to liquid. Calculate the lower and higher heating values of C_8H_{18} .

Substance	Chemical expression	h_{fo} [kJ/kmol]
Carbon dioxide	$CO_2(g)$	-393,520
Water vapor	$H_2O(g)$	-241,820
Water	$H_2O(l)$	-285,820
Methane	$C_8H_{18}(g)$	-208,447

8.9 Prove that the mass of gases (\dot{m}) flowing in the convergent-divergent nozzle of an afterburning jet engine is expressed by

$$\dot{m} = \frac{1}{\left(1 + \frac{\gamma-1}{2} M^2\right)^{\frac{\gamma+1}{2(\gamma-1)}}} \sqrt{\frac{\gamma}{R}} \frac{P_0}{\sqrt{T_0}} A$$

Where P_0 , T_0 are the total pressure and temperature at a nozzle section having an area of A . For chocking conditions, the Mach number is unity at throat section (A_{th}), and the above relation is reduced to

$$\dot{m} = \left(\frac{2}{\gamma + 1} \right)^{\frac{\gamma+1}{2(\gamma-1)}} \sqrt{\frac{\gamma}{R}} \sqrt{T_0} A_{th}$$

Assuming that the mass flow rate and total pressure is the same in the two cases of operative and inoperative afterburner, prove that the ratio of the nozzle throat area in the two cases of operative and inoperative afterburner is

$$\left(\frac{A_{\text{operative}}}{A_{\text{inoperative}}} \right)_{th} = \sqrt{\frac{T_{o \text{ operative}}}{T_{o \text{ inoperative}}}} \quad (\text{A})$$

Using the above relation, calculate the throat area ratio the maximum total temperature rises from 1000 K (when afterburner is off) to 2200 K (when afterburner is on).

- 8.10 Prove that the ratio of throat area for operative and afterburner can be more precisely expressed as

$$\left(\frac{A_{\text{operative}}}{A_{\text{inoperative}}} \right)_{th} = \frac{1 + f + f_{ab}}{1 + f} \sqrt{\frac{\dot{\gamma}}{\gamma}} \sqrt{\frac{T_0}{T'_0}} \frac{P_0}{P'_0} \frac{\left(\frac{\dot{\gamma}+1}{2} \right)^{\frac{\dot{\gamma}+1}{2(\dot{\gamma}-1)}}}{\left(\frac{\gamma+1}{2} \right)^{\frac{\gamma+1}{2(\gamma-1)}}} \quad (\text{B})$$

Where (' \cdot) indicates operative afterburner conditions.

Recalculate the area ratio in *problem (10)* in the following case:

$$f = 2\%, f_{ab} = 3\%, \gamma = \frac{4}{3}, \dot{\gamma} = 1.3, \frac{P_0}{P'_0} = 1.03$$

What is the error percentage between equations (A) and (B)?

- 8.11 The mass flow rate of gases entering nozzle is $25/\text{m}^3$. The inlet total pressure = 200 kPa and inlet total temperature = 900 K. The exit pressure = 80 kPa, and isentropic efficiency = 92 %. Determine the density of gases at the exit and the exit area.

(Specific heat is 1100 J/kg/K and gas constant is 287 J/kg/K)

References

1. Mahoney JJ (1990) Inlet for supersonic missiles, AIAA education series. American Institute of Aeronautics and Astronautics, Washington, DC, p 1
2. Engine intake aerothermal design: subsonic to high speed applications, (RTO-EN-AVT-195), 14–16 November 2011, von Karman Institute, Rhode-St-Genèse, Belgium
3. Shevel RS (1983) Fundamentals of flight. Prentice-Hall, Inc, Englewood Cliffs, p 348

4. Ilan K, Shevel R (2001) Aircraft design: synthesis and analysis, Digital Textbook version 0.99, January 2001, Stanford University, p 374
5. El-Sayed AF (2008) Aircraft propulsion and gas turbine engines. Taylor & Francis/CRC Press, Boca Raton
6. Wyatt DD (1958) A review of supersonic air intake problems. In: Fabri J (ed) Air intake problems in supersonic propulsion. Pergamon Press, New York, p 21
7. Hewitt PW, Waltz B, Vandiviere S (2002) Ramjet tactical missile propulsion status, Defense Technical Information Center Compilation Part Notice, AIAA 2002 Missile Sciences Conference 5–7 November 2002
8. Bathie WW (1996) Fundamentals of gas turbines, 2nd edn. Wiley, New York, p 330
9. The jet engine, 5th edn. Rolls-Royce plc, p 245. Reprinted 1996 with revisions
10. Seddon J, Goldsmith EL (1989) Intake aerodynamics, AIAA education series. Blackwell Science, Oxford/Malden, p 19
11. Hill P, Peterson C (1992) Mechanics and thermodynamics of propulsion, 2nd edn. Addison Wesley Publication Company, Inc, Reading, p 219
12. Power plant, vol II. Boeing publication D6-1420, pp 2–36
13. Howard JHG, Thornton-Trump AB, Henseler HJ (1967) Performance and flow regimes for annular diffusers, ASME Paper 67-WA/FE-21. ASME, New York
14. Thomas T, Michael P, Rudiger M (2002) Aerodynamic optimization of an aeroengine bypass duct OGV-pylon configuration. In: Proceedings of the ASME turbo EXPO 2002, June 2002, Amsterdam, The Netherlands
15. Hassan Z (2002) Particulate flow and erosion of the intakes of turbofan engines. M. Sc. thesis, Zagazig University, Egypt
16. Kerrebrock JL (1992) Aircraft engines and gas turbines, 2nd edn. MIT Press, Cambridge, p 121
17. Compressible flow data book for data book for engineering tripos, 2004 edition, Cambridge University Engineering Department
18. Ames Research Staff (1953) Equations, tables and charts for compressible flow, NACA report 1153
19. Ranjan P, Upadhyay RR, Jain A (2011) Flow control in twin air-intakes using vortex generators. Recent Researches in Applied and Computational Mathematics. www.wseas.us/e-library/conferences/2011/Lanzarote/.../MATH-15.pdf
20. Mattingly JD, Heiser WH, Pratt DT (2002) Aircraft engine design, vol 2. AIAA, Reston
21. The jet engine, 5th edn. Rolls-Royce plc, p. 3, Reprinted 1996 with revisions
22. Kline SJ, Abbott DE, Fox RW (1959) Optimum design of straight-walled diffusers. J Basic Eng 81:321–331
23. McDonald AT, Fox RW (1966) An experimental investigation of incompressible flow in conical diffusers. Int J Mech Sci (Elsevier, Philadelphia) 8:125–139
24. Reneau LR, Johnson JP, Kline SJ (1967) Performance and design of straight, two-dimensional diffusers. J Basic Eng 95:141–150
25. http://www.ohio.edu/mechanical/thermo/Applied/Chapt.7_11/Chapter11.html
26. Lefebvre AH (1999) Gas turbine combustion, 2nd edn. Taylor & Francis, Washington, DC, p 39
27. Johnson RL, Cullom RR (1977) Altitude test of several afterburner configurations on a turbofan engine with a hydrogen heater to simulate an elevated turbine discharge temperature, NASA TP 1068. NASA, Washington, DC
28. Zucker RD, Biblarz O (2002) Fundamental gas dynamics, 2nd edn. Wiley, Hoboken, p 366
29. White FM (1986) Fluid mechanics, 4th edn. McGraw-Hill, 1997, Washington, New York
30. <http://www.aerospaceweb.org/design/aerospike/shapes.shtml>
31. Kirk DR. Rocket nozzles, MAE 4262: Rocket and mission analysis, Nozzles, PPT
32. <http://rohanverse.webnode.com/aerospike-engine/>

Chapter 9

Centrifugal and Axial Compressors

9.1 Introduction

This chapter and Chap. 10 treat the rotating modules of both aero engines and gas turbines. These modules are compressible turboachinery (or turbomachines). Let us first introduce a definition for turbomachines. The word (*turbo*) or (*turbines*) is of Latin origin, meaning “that which spins or whirls around.” Though compressible turbomachines may be fans, compressors, blowers, aircraft propellers, gas, and steam turbines, only compressors, fans, and turbines found in aero engines (or gas turbines) will be discussed in this book. Though the working fluid for a compressible turbomachine may be air, gases, vapor, or steam, only air and gases will be considered here as they are the operating media in both aero engines and gas turbines.

Fans and compressors transfer energy from a rotor to a fluid, while turbines transfer energy from a fluid to a rotor. Turbomachines are governed by the basic conservation equations, namely, conservation of mass and energy as well as Newton’s second law of motion (or Euler’s energy equation) for compressible fluids.

Turbomachines will be classified in Table 9.1.

Two types of turbomachinery will be analyzed in this chapter; namely:

- (a) Centrifugal compressor
- (b) Axial compressor

9.2 Centrifugal Compressor

9.2.1 Introduction

Brown [1] classified compressors as either intermittent flow or continuous flow ones. Intermittent flow compressors are positive displacement ones. They are

Table 9.1 Classification of turbomachinery

Item	Types		
Casing or housing	<i>Open</i>	<i>Enclosed</i>	
	Wind turbines – aircraft propellers – marine screws	Compressors – fans – blowers – pumps – gas turbines – steam turbines – hydraulic turbines	
Working fluid	<i>Compressible</i>	<i>Incompressible</i>	
	Air (fans – compressors – blowers – wind turbines – aircraft propellers)	Water (hydraulic pumps/turbines – marine screw)	
	Gas (gas turbine)	Liquid (fuel pump – oil pump – oxygen pumps – hydrogen pumps – turbopumps – liquid natural gas)	
Energy transfer	<i>Absorb power</i>	<i>Produce power</i>	
	(Increases the fluid pressure or head)	(Decreases pressure or head)	
	Ducted fans, compressors, propellers, marine screws and pumps	Hydraulic, steam, wind and gas turbines	
Flow path through rotor	<i>Axial</i>	<i>Mixed flow</i>	<i>Radial</i>
	(Outlet flow is mainly parallel to the axis of rotation)	(Outlet flow is partly radial and partly axial)	(Outlet flow is mainly in a plane perpendicular to the rotation axis)
	Axial compressor – axial fan – axial gas turbine – aircraft propeller – kaplan turbine	Francis turbine	Centrifugal pump – centrifugal compressor – radial inflow turbine
Pressure (or) enthalpy changes through rotor	<i>Reaction</i>	<i>Impulse</i>	
	Pressure (or enthalpy) is partially changed (increased/decreased) in both rotor and stator of a stage	Pressure (or enthalpy) is changed only through the stator of a stage	
	Most turbomachines	Pelton turbine – some gas and steam turbine stages	

classified as either reciprocating or rotary types, as thoroughly discussed in Chap. 4. Continuous flow compressors are classified as either ejectors or dynamic compressors. Dynamic compressors are further classified as centrifugal (radial) flow, mixed flow, or axial flow compressors.

Comparing intermittent to continuous flow compressors, two points may be noticed. Firstly, the pressure ratio of intermittent compressors may reach 200 while for continuous compressors it is only 20. Secondly, the mass flow rate of intermittent types is too small compared to continuous types.

Based on the previous section, dynamic compressors are identified as enclosed, compressible turbomachinery that absorb power and mostly of the reaction type. These may also be of the axial, radial, or mixed types. Mixed flow compressors are rarely found.

Dynamic compressors work by converting velocity to pressure in a continuous flow. They are efficient, compact and handle large quantities of working fluid. Considering air as the working fluid at 1.013 bar and 288 K, the inlet flow is typically 150 kg/s per square meter of inlet area at Mach 0.4 [2]. The intake diameters of various types range from 0.1 m (4 in.) to 2.44 m (8 ft). The range of mass flow varies from about 1.2 to 700 kg/s. The isentropic efficiency ranges typically from 0.7 to 0.9.

In this Sect. 9.2, the aerodynamic and mechanical designs of centrifugal compressors are discussed. Axial compressors will be treated in the succeeding Sect. 9.3.

Centrifugal compressors and radial inflow turbines are identified as radial turbomachines. Surprisingly, radial turbomachines have a long history and predate axial flow compressors and turbines [3]. Centrifugal compressors were employed in the first jet engines developed by Frank Whittle and von Ohain due to the experience gained in the design of superchargers, which provided higher efficiency values compared to axial compressors. With the development of aero engines, axial compressors have nearly replaced centrifugal compressors. Thus, centrifugal compressors are found in small turbofan engines such as AlliedSignal 731, Garrett F109, GE Honda (HF120), and small turboprop/turboshaft engines such as the Rolls-Royce DART, Honeywell Aerospace TPE331–14, and the famous Pratt & Whitney of Canada PT6. They are also found in auxiliary power units (APU) of many civil transport airplanes such as Garrett GTCP-85 for DC8 and 9, MD-80, Boeing 707, 737 airplanes, as well as Sunstrand Turbomach APS 200 for Airbus A321.

Other applications for the centrifugal compressors are the aircraft cabin air conditioning such as the Hamilton Standard 777 (ACTCS) and the multipurpose small power units (MPSPU) represented by SunStrand Turbomach T-100. Micro-gas turbines also resemble new application for centrifugal compressors. In a few gas turbine engines, centrifugal compressor is used for the final stage of compression downstream of multistage of axial compressor. This arrangement is called *axial–centrifugal* compressor similar to those in the General Electric T700 engine, Pratt & Whitney Canada PT6, and Honeywell engine T53 [4].

Centrifugal compressors in aero engines provide small to moderate air flows (up to nearly 50 kg/s). They have either single or double stages (sometimes identified as impellers in tandem). The pressure ratio per stage ranges from 4:1 to 8:1; while for double (two) stages in series, a pressure ratio of 15:1 is found in Pratt & Whitney PW100.

Centrifugal compressors are used in many industrial applications such as refineries, chemical and petrochemical plants, natural gas processing and transmission plants, very large-scale refrigeration, and iron and steel mills. Two other important applications for centrifugal compressors are air-conditioning and refrigeration and HVAC and automotive engine turbochargers (GTCP-85) and superchargers.

Comparing centrifugal and axial compressor, we can say that centrifugal compressors have the following advantages: light weight, low cost, rigidity, high pressure ratio per stage, easily made in relatively small sizes (thus suitable for

handling small volume flows), simplicity, better resistance to foreign object damage (FOD), less susceptibility to loss of performance by buildup of deposits on the blade surfaces, and the ability to operate over a wider range of mass flow at a particular speed. The disadvantages of the centrifugal compressor are that it is generally less efficient than axial compressor (perhaps 4–5 % less), and it has a larger cross section (frontal area) compared with the cross section of the inlet flow.

Comparing centrifugal compressors to piston compressors, we can also say that centrifugal compressor has not any parts that perform reciprocating movement, consequently centrifugal compressor has very quiet run. In view of its quiet run and because centrifugal compressor has not any part that appose, except of bearings, centrifugal compressor is very reliable. Next advantage is the fact that specific mass of centrifugal compressor is decreasing with its increasing capacity.

In conclusion, we can say that design of centrifugal compressor is interdisciplinary process including aerodynamics, thermodynamics, stress analysis, vibration analysis, selection of materials, and so on. During design stage, possibilities and requirements of manufacturing must be taken into account.

9.2.2 Layout of Compressor

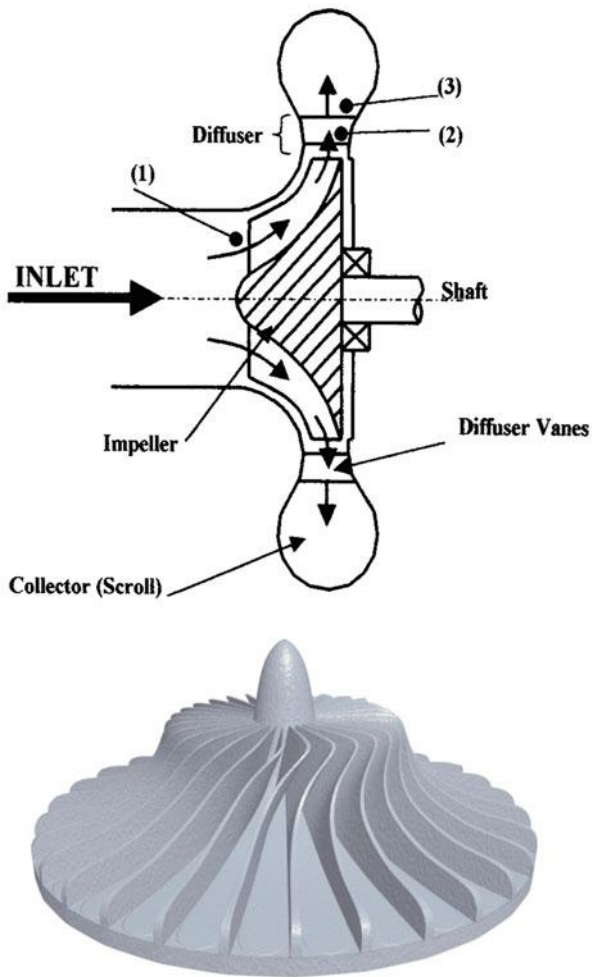
Generally centrifugal compressor is called so because the flow through the compressor is turned perpendicular to the axis of rotation. This type of compressors is composed of three main elements, namely:

1. Rotating part or impeller
2. Stationary part or stator
3. Manifold or a collector (denoted by scroll or volute)

9.2.2.1 Impeller

Air is drawn at the center or eye of the impeller, then accelerated through the fast spinning speed of the impeller and finally thrown out at tip. At the eye (inlet), the vanes are curved to induce the flow: this axial portion is called the inducer or rotating guide vanes and may be integral with or separated from the main impeller. These vanes are cast, forged, or machined integrally with the impeller hub. The number of vanes is usually a prime number, typically from 19 to 37, to avoid vibration problems [2]. The outer curve of the vanes is sealed by the shroud, which may be part of the stationary structure or may rotate with the rotor. Typical impeller proportions are that the eye root diameter is about half the eye tip diameter, and the tip (outlet) diameter is nearly twice the eye tip diameter. The impeller material is often aluminum, with titanium or steel for smaller, high-duty machines.

Fig. 9.1 Layout and stations of a centrifugal compressor



9.2.2.2 Diffuser

The diffuser represents a part of the fixed structure of the compressor that reduces the kinetic energy, thereby increases the static pressure. The diffuser is either a vaneless passage or a vaneless passage followed by a vaned section. The vaned diffuser represents a large group including the vanes together with the cascade, channel, and pipe types; Fig. 9.2 [2].

All diffusers have an initial vaneless gap outboard of the impeller in which the flow settles. The vaneless diffuser is bulky and can be inefficient in comparison to the other types. The cascade may involve one, two, or three rows of vanes, with performance similar to that of axial cascades. Vaned diffusers may use curved or straight vanes, having a longer path length than the cascade diffuser. Vaned diffuser may be made variable, the vanes pivoting about an axis as shown in Fig. 9.2 to

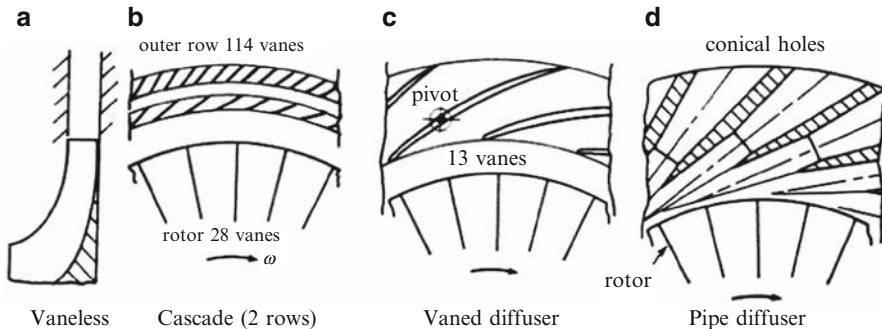


Fig. 9.2 Types of diffuser element of a centrifugal compressor

accommodate different incident flow angles through the speed range. Vaneless, cascade, and vaned diffusers collect the flow in a one volute type collector, which is suitable for industrial applications.

Channel and pipe diffusers are suitable for aero engines and gas turbines. Both diffusers collect the flow in separate passages that diverge slowly. The pipe consists of a conical hole while the channel has a rectangular section with one pair of opposed walls diverging at $10\text{--}11^\circ$ while the others are parallel. The pipe and channel diffusers may feed separate combustors or may merge downstream. Recently, it had been shown that the pipe-type diffuser is more efficient than the conventional rectangular channels [4]. Overall isentropic efficiencies of over 85 % are claimed for compressors using new pipe diffuser.

9.2.2.3 Scroll or Manifold

The final element of centrifugal compressors is either a manifold or a scroll. Centrifugal compressors with manifolds are used when the compressor is a part of a gas generator – in either a gas turbine or an aero engine – and thus the compressor is followed by a combustion chamber. In case of industrial applications, including oil and gas industry, chemical industries and petrochemicals, etc., the working fluid is collected in a scroll or volute. The working fluid leaving the stators is collected in a spiral casing surrounding the diffuser called a *volute* or *scroll*. The area of the cross section of the volute increases along the flow path in such a way that the velocity remains constant. The possible shapes of volute are shown in Fig. 9.3.

9.2.3 Classification of Centrifugal Compressors

Centrifugal compressors may be classified as

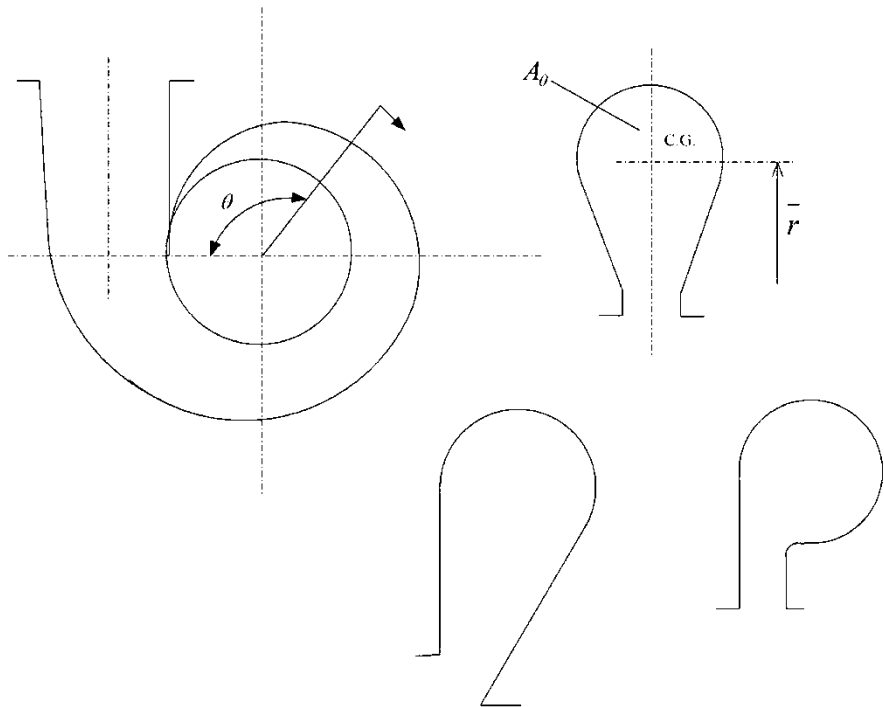


Fig. 9.3 Different shapes of volute (Scroll)

1. *Single or multiple stages:* For aero engines, centrifugal compressors have either single stage or double (two or tandem) stages. In some cases, two (or double) stages are mounted on the same shaft, handling the fluid in series to boost its final pressure. In industrial gas turbines such as pipeline compressors, there are up to five stages.
2. *Single entry (or single-face) or double (dual) entry (or double-face):* The principal differences between the single entry and dual entry are the size of the impeller and the ducting arrangement. The single-entry impeller permits ducting directly to the inducer vanes, as opposed to the more complicated ducting needed to reach the rear side of the dual-entry type; figure (9.4). Although slightly more efficient in receiving air, single-entry impellers must be of greater diameter to provide sufficient air. Dual-entry impellers are smaller in diameter and rotate at higher speeds to ensure sufficient airflow. Most gas turbines of modern design use the dual-entry compressor to reduce engine diameter.
3. *Shrouded or unshrouded impeller:* Unshrouded impeller means that there is a clearance between the ends of the impeller vanes and a stationary shroud, while shrouded impeller means that there is a rotating shroud fixed to the impeller vanes. Shrouding reduces the losses due to leakage of air from the pressure side to the suction side of the blade. However, it increases the friction and weight of

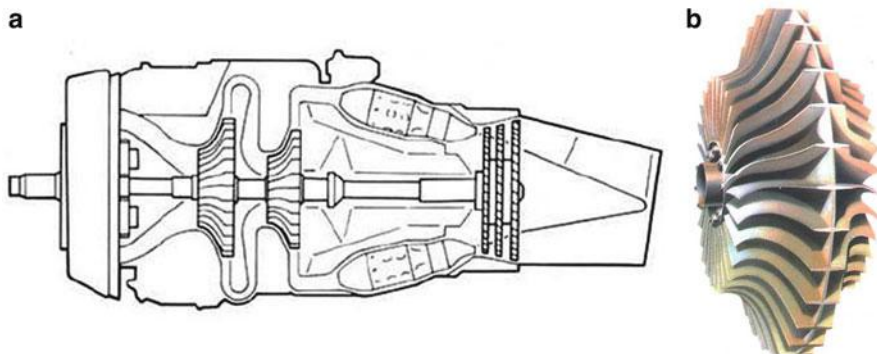


Fig. 9.4 Single entry (a) and double entry (b) layouts

the impeller. For gas turbine and turbocharger applications, the impeller is usually unshrouded and the stationary cover is referred to as the shroud. For large process compressors, the impeller is often constructed with an integral shroud.

4. The impeller may have a *non-, semi-, and full-inducer section*. For full-inducer impeller, the impeller vanes are continued around into the axial direction and the compressor resembles an axial compressor at inlet.
5. The impeller vanes may be *radial* at outlet or they may be inclined *backward* or *forward*, thus identified as backward-leaning (commonly now described as backswept) or forward-leaning compressor.
6. The impeller layout may be *open*, *semi-closed*, or *closed*. Open type is built with blades in a radial direction without enclosing covers on either front or backsides, normally found in turbochargers. Semi-closed types are built with blades in a radial direction with an enclosed cover on the backside that extends to the periphery of the blades, normally found in air compressors. The closed type is built with backward- or forward-leaning blades and has enclosing covers on both the front and backside, normally found in multistage compressors.
7. Impeller may include only *full vanes* or *full plus half vanes* (splitter blades). Such splitter blades are located toward the tip to improve the flow pattern where the full vanes are widely spaced.
8. Intake or inlet passage to the compressor may or may not be fitted with *inlet guide vanes* (IGV). IGVs are designed to give either *positive* or *negative prewhirl*. IGVs giving a positive prewhirl are frequently found in high-speed compressors, say in aero engines, to minimize the possibility of air reaching or exceeding the sonic speed. In this case, possible shock waves formed will lead to great losses in the intake. Negative prewhirl is employed to increase the inlet relative speed at some applications. These IGVs may also be set at fixed angle or they can be rotated to vary the inlet flow angle.

9. Outlet through a *collector* (denoted as scroll or volute) or a *manifold*. In the aviation field, the air leaving the compressor must be directed toward the combustion chamber with the minimum ducting losses. The diffuser is either constructed or ended by a 90° bend to satisfy this requirement. If the compressor is used in other industrial applications, then the air leaving the successive passages of the stators is collected in a scroll or volute and ducted from a single pipe.
10. Exit may or may not be fitted with *exit guide vanes* (EGVs).
11. The *casings* of the compressor may be *horizontally split* casings, *vertically split* casings, or bell casings.

9.2.4 Governing Equations

Aero-thermodynamic relations that govern the flow in centrifugal compressors will be discussed here. In turbomachinery, normally its analysis relies upon the following steps:

1. Identify a control volume for the module or stage and locate different states
2. Plot the processes within turbomachines on both of temperature-entropy (T-s) and pressure-volume (P-v) charts or one of them
3. Draw velocity diagrams at inlet and outlet states of rotor (or impeller)
4. Write down the governing equations, namely, gas law (or equation of state), conservation of mass (or continuity equation), conservation of energy (or energy equation), and Newton's second law (or force-balance equation)

Layout of centrifugal compressor shown in Fig. 9.1 defines three states, namely, the impeller inlet (state 1), impeller outlet (state 2), and diffuser outlet (state 3). These states are also plotted on the T-S diagram in Fig. 9.5. Each state is defined by two points, namely, the static and total (stagnation) conditions. Thus, two pressure lines (static and total) are seen for each state. The compression processes are assumed adiabatic irreversible; thus entropy increase is found in each process.

The velocity triangles at the inlet and outlet of the impeller are shown in Fig. 9.6. The velocity triangles in any turbomachine are governed by the relation

$$\vec{C} = \vec{U} + \vec{W} \quad (9.1)$$

where \vec{C} , \vec{U} , and \vec{W} are the absolute, rotational, and relative velocities, respectively. The inlet velocity triangle is drawn in the axial-tangential plane. As shown in figure, the flow approaching the eye may be axial (C_1) with a typical velocity of 150 m/s for air or may have a swirl angle (in case of prewhirl as will be discussed later). The rotational speed is (U_1) which varies with radii from eye hub to tip since (U_1). The relative velocity is (W_1), which varies in magnitude and direction from eye hub to tip due to variation of (U_1). This requires the inducer vane to be twisted to align with the flow at all radii. It is normal for the relative Mach number at the

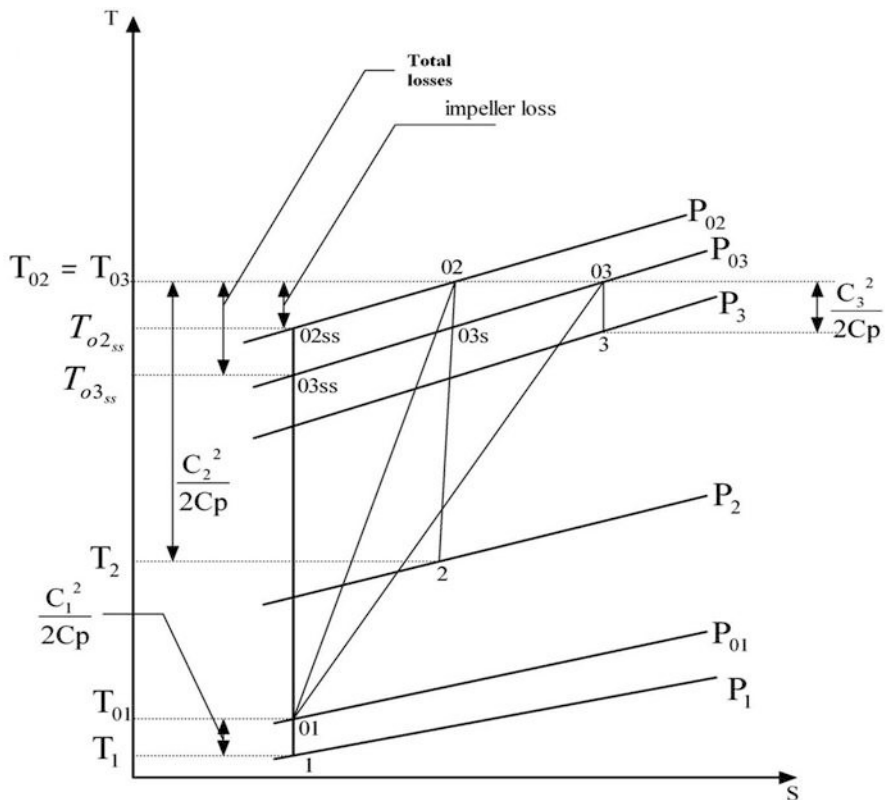


Fig. 9.5 T-s diagram for a centrifugal compressor

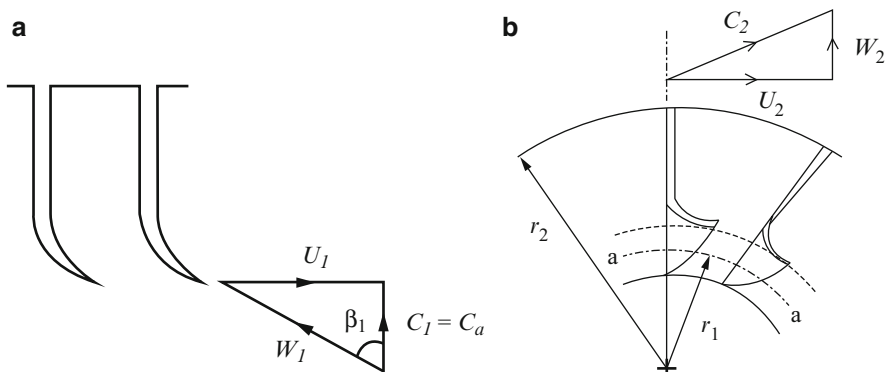


Fig. 9.6 Velocity triangles at inlet and outlet of impeller: (a) velocity triangle at impeller inlet; (b) velocity triangle at impeller outlet

Table 9.2 Various parameters at different states of compressor

	State (1)	State (2)	State (3)
	Impeller inlet	Tip (outlet) of impeller	Stator outlet
T	T_1	$T_2 > T_1$	$T_3 > T_2$
P	P_1	$P_2 > P_1$	$P_3 > P_2$
T_0	T_{01}	$T_{02} \gg T_{01}$	$T_{03} = T_{02}$
P_0	P_{01}	$P_{02} \gg P_{01}$	$P_{03} < P_{02}$
C	C_1	$C_2 \gg C_1$	$C_3 < C_2$ $C_3 \approx C_1$
U	U_1	$U_2 > U_1$	—
W	W_1	$W_2 < W_1$	—

eye tip to be below 0.9, which falls to below 0.5 for most of the subsequent passage length to minimize frictional losses. At the impeller outlet, the air leaves the passage with a relative velocity (W_2), which when added vectorially to the tangential speed (U_2), will give the absolute velocity (C_2). This absolute velocity (C_2) is greater than (C_1) as a result of the work input to the rotor shaft. It is interesting to note here that the outlet velocity triangle is at another plane, namely, the radial-tangential plane. As shown in Fig. 9.6, the tip tangential velocity (U_2) at outlet is equal to the whirl velocity (C_{u2}). However, in most cases, (U_2) is slightly greater than (C_{u2}) and the difference is called the *slip*.

Changes in thermodynamic properties and velocities at the three states of the compressor are summarized in Table 9.1. At state (1), impeller inlet, the static and total temperatures are T_1 and T_{01} , while the static and total pressures are P_1 and P_{01} . The absolute, relative, and rotational velocities are C_1 , W_1 , and U_1 .

Same symbols are used in state (2). Since state (3) resembles a stator outlet, there will be neither rotational or relative speeds (U , W).

As described in Table 9.2, both the total temperature and total pressure increase in the impeller due to energy addition to the air. Moreover, since the impeller is a rotating diffuser then the static pressure rises while the relative speed decreases ($W_2 < W_1$). Moreover, the diffuser converts the kinetic energy into pressure energy. Thus, the total temperature at the inlet and outlet of the stator are equal from the first law of thermodynamics, while the outlet total pressure is less than the inlet total pressure due to friction. The static pressure rises in the diffuser while the absolute velocity decreases as found in any diffusing passage.

From Fig. 9.5, the temperature rise in the compressor is:

$$\Delta T_0 = T_{03} - T_{01} \quad (9.1)$$

The pressure ratio of compressor (π_c) is defined as

$$\pi_c = \frac{P_{03}}{P_{01}} = \left(\frac{T_{03}}{T_{01}} \right)^{\gamma/(\gamma-1)}$$

The isentropic efficiency of the compressor is defined as

$$\eta_c = \frac{T_{03s} - T_{01}}{T_{03} - T_{01}} = \frac{T_{01}[(T_{03s}/T_{01}) - 1]}{T_{03} - T_{01}}$$

The pressure ratio of the compressor is

$$\pi_c = \frac{P_{03}}{P_{01}} = \left[1 + \eta_c \frac{T_{03} - T_{01}}{T_{01}} \right]^{\gamma/(\gamma-1)} = \left[1 + \eta_c \frac{\Delta T_0}{T_{01}} \right]^{\gamma/(\gamma-1)} \quad (9.2)$$

Where, (η_c) is the isentropic efficiency of compressor. Generally, two approaches are used for determining stage efficiency at the preliminary design stage.

- An approach that at first sight appears to be less dependent upon empiricism is to formulate a general 1D compressor model that includes some loss estimation for the principal flow elements of the stage.
- The most comprehensive method includes models for IGV, impeller, vaneless space and vaned diffuser. The loss models are tuned so that the method obtains reasonable agreement with a representative range of test cases.

Switching to the governing equations for a moving fluid, these will be:

1. Conservation of mass or continuity equation
2. Momentum equation or Newton's second law
3. Conservation of energy or the first law of thermodynamics

These equations will be examined hereafter.

9.2.4.1 Conservation of Mass (Continuity Equation)

For a steady flow, the mass rates of fluid entering and leaving a control volume are identical. Thus, considering a control volume between the impeller inlet (State 1) and outlet (State 2), the continuity equation is written as

$$\dot{m}_1 = \dot{m}_2$$

Air mass flow rate (\dot{m}) is at inlet:

$$\dot{m} = \rho_1 C_{a1} \times \text{Inlet area} = \rho_1 C_{a1} \left[\left(\frac{\pi}{4} \right) (D_{1t}^2 - D_{1r}^2) \right] \quad (9.3)$$

where ρ_1 and C_{a1} are the density and axial velocity at the inlet section, and D_{1r} and D_{1t} are the eye root and tip diameters at inlet.

At exit:

$$\dot{m} = \rho_2 C_{r2} A_2 = \rho_2 C_{r2} [b(\pi D_2 - nt)] \quad (9.4a)$$

where ρ_2 and C_{r2} are the density and radial velocity at the impeller tip, n is the number of blades, and t is the thickness of blade at impeller outlet and (b) is the axial width of the impeller.

9.2.4.2 The Momentum Equation or Euler's Equation for Turbomachinery

Newton's second law of motion applied to the fluid passing through a control volume states that the rate of change of momentum of the fluid is equal to the net applied force on the fluid in the control volume, or

$$\vec{F} = \frac{d}{dt} (m \vec{C})$$

For a steady flow between States 1 and 2, this can be written as

$$\vec{F} = \dot{m} (\vec{C}_2 - \vec{C}_1)$$

The above equation is used to obtain the torque arising from the net force, which is related to the angular momentum of the fluid within the control volume by multiplying the above equation by the appropriate radii; thus:

$$\vec{T} = \vec{r} \otimes \vec{F} = \dot{m} (\vec{r}_2 \otimes \vec{C}_2 - \vec{r}_1 \otimes \vec{C}_1)$$

The above vectorial equation is reduced to the following scalar relation for the torque about the axis of rotation:

$$T = \dot{m} [r_2 C_{u2} - r_1 C_{u1}]$$

Or the final form known as *Euler's equation* is given by the relation

$$T = \dot{m} [(rC_u)_2 - (rC_u)_1] \quad (9.5a)$$

where C_{u1} and C_{u2} are the swirl velocities at the inlet (mean section) and outlet to the impeller. The mean inlet radius and the impeller tip radius are r_1 and r_2 , respectively.

Since the power is equal to torque times the rotational speed, the power (\mathcal{P}) is expressed as:

$$\mathcal{P} = T \times \omega = \dot{m} \omega \{(rC_u)_2 - (rC_u)_1\} = \dot{m} \{(UC_u)_2 - (UC_u)_1\} \quad (9.6a)$$

For the case when the flow *enters the impeller axially, there is no swirl velocity at the inlet ($C_{u1} = 0$)*, then Euler equation is reduced to

$$T = \dot{m} r_2 C_{u2}. \quad (9.5b)$$

Moreover, the power (\mathcal{P}) will be expressed as:

$$\mathcal{P} = T \times \omega = \dot{m} \omega (r C_u)_2 = \dot{m} (U C_u)_2 \quad (9.6b)$$

The power needed to drive the compressor is greater than the power derived above. A part of this power is consumed in overcoming the friction between the casing and the air carried round by the vanes, the disk friction or the windage, and the bearing friction. Thus, the power input to the compressor (\mathcal{P}_i) is equal to the power derived above but multiplied by a power input factor, ψ

$$\mathcal{P}_i = \psi \dot{m} \{(U C_u)_2 - (U C_u)_1\} \quad (9.7a)$$

Where $\psi = 1.035 - 1.04$

Sometimes this power input factor is replaced by reciprocal of mechanical efficiency, or $(\psi = \frac{1}{\eta_m})$.

For zero inlet swirl, this power will be

$$\mathcal{P}_i = \psi \dot{m} (U C_u)_2 = \frac{\dot{m} (U C_u)_2}{\eta_m} \quad (9.7b)$$

9.2.4.3 The Energy Equation or the First Law of Thermodynamics

The first law of thermodynamics states that the net change of energy of a fluid undergoing any process is equal to the net transfer of work and heat between the fluid and its surroundings; thus

$$\frac{\dot{Q} - \dot{W}}{\dot{m}} = (h_2 - h_1) + \frac{1}{2} (C_2^2 - C_1^2) + g(z_2 - z_1)$$

In most turbomachines, the potential energy is negligible. Moreover, turbomachines are adiabatic. Thus the heat term is negligible, by adjusting the sign of the rate of work, and since $H_{02} = H_{03}$, then

$$\frac{\dot{W}}{\dot{m}} = \left(h_2 + \frac{1}{2} C_2^2 \right) - \left(h_1 + \frac{1}{2} C_1^2 \right) = H_{02} - H_{01} = H_{03} - H_{01}$$

Since the rate of work is the power ($\mathcal{P}_i = \dot{W}$), the left-hand side (which is the mechanical input power per unit mass flow rate) is equal to the specific enthalpy rise through the compressor. Thus from Eq. (9.7a)

$$Cp(T_{03} - T_{01}) = \psi \{(UC_u)_2 - (UC_u)_1\} \quad (9.8a)$$

The temperature rise in the compressor is then

$$\Delta T_0 = \frac{\psi \{(UC_u)_2 - (UC_u)_1\}}{Cp} \quad (9.9a)$$

Or for zero inlet swirl

$$Cp(T_{03} - T_{01}) = \psi(UC_u)_2 \quad (9.8b)$$

$$\Delta T_0 = \frac{\psi(UC_u)_2}{Cp} \quad (9.9b)$$

The pressure ratio of compressor (π_c) as defined by Eq. (9.2), and then can be formulated as

$$\pi_c \equiv \frac{P_{03}}{P_{01}} = \left(1 + \eta_c \frac{\psi \{(UC_u)_2 - (UC_u)_1\}}{CpT_{01}} \right)^{\frac{\gamma}{\gamma-1}} \quad (9.10)$$

For *zero inlet swirl* ($C_{ul} = 0.0$), then

$$\pi_c \equiv \frac{P_{03}}{P_{01}} = \left(1 + \eta_c \frac{\psi U_2 C_{u2}}{CpT_{01}} \right)^{\frac{\gamma}{\gamma-1}} \quad (9.11a)$$

Since in the *ideal case* (or zero slip as will be shortly discussed)

$$U_2 = C_{u2}$$

Then, for zero inlet swirl, the torque Eq. (9.5b) will be expressed as

$$T = \dot{m} r_2 U_2 \quad (9.12)$$

The power from Eq. (9.6b) is

$$\mathcal{P} = \dot{m} U_2^2 \quad (9.13)$$

The input power from Eq. (9.7b) is

$$\mathcal{P}_i = \psi \dot{m} U_2^2 \quad (9.14)$$

The temperature rise from Eq. (9.9b) is

$$\Delta T_0 = \frac{\psi U_2^2}{C_p} \quad (9.9b)$$

The pressure ratio from Eq. (9.11a) is then

$$\pi_c = \left[1 + \eta_c \frac{\psi U_2^2}{C_p T_{01}} \right]^{\gamma/(\gamma-1)} \quad (9.11b)$$

From the above relation, it is justified to say that centrifugal compressor has the following performance characteristics, often called “the three fan laws”:

1. Flow is proportional to impeller speed.
2. Pressure ratio across an impeller is proportional to the square of the impeller speed.
3. Power absorbed by the impeller varies with the cube of the impeller speed.

9.2.5 Slip Factor (σ)

If the flow at impeller discharge is perfectly guided by the impeller blades, then the tangential component of the absolute velocity (swirl velocity) is equal to the rotational velocity ($C_{u2} = U_2$) in the case of radial type impeller. In practice, the flow cannot be perfectly guided by a finite number of blades and it is said to slip. Thus, at the impeller outlet, the swirl velocity is less than the impeller rotational speed ($C_{u2} < U_2$). The classical explanation for the slip phenomenon [3] uses the concept of the relative eddy. As the flow into the impeller is normally irrotational, that is, has no initial rotation, then at the impeller discharge the flow relative to the impeller must rotate with an angular velocity equal and opposite to the impeller; Fig. 9.7.

By combining this relative eddy and the radial through flow, the resultant relative velocity vector has a component in the direction opposite to the impeller rotation.

The slip factor is denoted by σ and is defined as

$$\sigma = \frac{C_{u2}}{U_2} \quad (9.15)$$

Though Stodola and Busemann derived formulae for this slip factor, the correlation proposed by Stanitz [5] has a wide range of application. Stanitz formula is expressed as

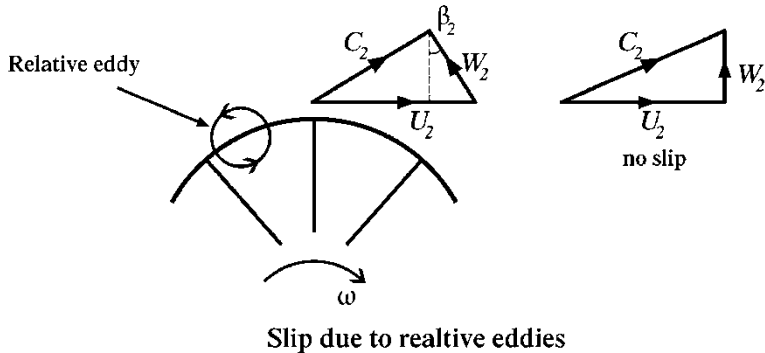


Fig. 9.7 Slip factor for radial impeller

$$\sigma = 1 - \frac{0.63\pi}{n} \quad (9.16)$$

where n is the number of blades. It was considered satisfactory for both radial blades, forward- and backward-leaning blades having blade angles ranging from -45° to $+45^\circ$. As the number of vanes of impeller is increased, then the slip factor is also increased; slip lag at the tip of the impeller reduces.

The effect of slip is to reduce the magnitude of the swirl velocity from the ideal case. This in turn will reduce the pressure ratio. In this way, slip will also reduce the compressor power consumption. The detrimental effect of slip is that the impeller must be larger or the rotational speed must be higher to deliver the same pressure ratio. This leads to increased stress level and it will also lead to increased relative velocity that will lead to increased friction loss and a reduced efficiency.

Then from Eq. (9.8a), the temperature rise will be

$$\Delta T_0 = \frac{\psi \{ \sigma U_2^2 - (U C_u)_1 \}}{C_p} \quad (9.8b)$$

For zero inlet swirl, from Eq. (9.9a)

$$\Delta T_0 = \frac{\sigma \psi U_2^2}{C_p} \quad (9.9c)$$

The pressure ratio for zero inlet swirl will be

$$\pi_c = \left(1 + \frac{\eta_c \psi \sigma U_2^2}{C_p T_{01}} \right)^{(\gamma/\gamma-1)} \quad (9.11c)$$

From Eq. (9.11c), with $C_p = \gamma R / (\gamma - 1)$ and $a_{01}^2 = \gamma R T_{01}$, the pressure ratio can be expressed as

$$\pi_c = \left(1 + \frac{(\gamma - 1)\eta_c \psi \sigma U_2^2}{a_{01}^2} \right)^{\gamma/(\gamma-1)} \quad (9.11d)$$

where a_{01} is the total sonic speed or the sonic speed referred to the total temperature at the compressor inlet.

Note that when there is no slip, the slip factor (σ) is equal to unity and this yields the maximum temperature rise and pressure ratio that may be achieved by this compressor. These values are expressed by the relations

$$\begin{aligned} (\Delta T_0)_{\max} &= \frac{\psi U_2^2}{C_p} \sqrt{b^2 - 4ac} \\ (\pi_c)_{\max} &= \left(1 + \frac{\eta_c \psi U_2^2}{C_p T_{01}} \right)^{\gamma/(\gamma-1)}. \end{aligned}$$

Further discussions for Power Input factor, Slip Factor and Efficiency will be given here:

- Power input factor and slip factor are neither independent of one another nor of efficiency.
- The *power input factor* represents an increase in the work input above that needed for deriving the impeller (rotating element) of compressor.
- This increment increase is absorbed in overcoming frictional loss
- Power input factor should be as close as possible to unity.
- Low values of power input factor imply that the impeller is very efficient.
- However, the value of compressor efficiency also depends on friction losses in the diffuser which does not affect power input factor.
- The *slip factor* limits the capacity of the compressor and this should be as high as possible.
- A high value of slip factor requires higher number of vanes.
- Higher number vanes will increase frictional losses and hence increase the value of power input factor and decrease the value of *efficiency*.
- A suitable compromise must be found, and present day practice is 19–21 vanes to get a slip factor value of 0.9.

Historical trends showed that its value was 70 % in 1950, raised to 75 % in 1960, then to 82 % in 1980, reached 85 % in 2000, and finally scored 87 % by 2010. Its projected value is 90 % in 2040.

Equations (9.5) through (9.16) are assembled in Table (9.3) as a conscious quick reference.

Example 9.1 A single-sided centrifugal compressor has the following data:

Inlet stagnation pressure	110 kPa	Mass flow rate	10 kg/s
Inlet stagnation temperature	300 K	Inducer tip diameter	0.36 m
Impeller exit Mach number	1.1	Inducer hub diameter	0.18 m
Compressor isentropic efficiency	0.8	Impeller outlet diameter	0.52 m
Power input factor	1.05	Slip factor	0.92

Table 9.3 Summary of governing relations for radial impeller

Conditions	Ideal	Real	Real
	No slip	With slip	With slip
	No inlet swirl	No inlet swirl	With inlet swirl
Temperature rise	$\frac{\psi U_2^2}{C_p}$	$\frac{\psi \sigma U_2^2}{C_p}$	$\frac{\psi \{ \sigma U_2^2 - (UC_u)_1 \}}{C_p}$
ΔT_0	Maximum value		Minimum value
Pressure ratio	$\left(1 + \eta_c \frac{\psi U_2^2}{C_p T_{01}}\right)^{\frac{\gamma}{\gamma-1}}$	$\left(1 + \eta_c \frac{\psi \{ (UC_u)_2 \}}{C_p T_{01}}\right)^{\frac{\gamma}{\gamma-1}}$	$\left(1 + \eta_c \frac{\psi \{ (UC_u)_2 - (UC_u)_1 \}}{C_p T_{01}}\right)^{\frac{\gamma}{\gamma-1}}$
π_c	Maximum value		Minimum value
Torque	$\dot{m} r_2 U_2$	$\dot{m} r_2 C_{u2}$	$\dot{m} (r_2 C_{u2} - r_1 C_{u1})$
T	Maximum value		Minimum value
Consumed power	$\dot{m} U_2^2$	$\dot{m} U_2 C_{u2}$	$\dot{m} (U_2 C_{u2} - U_1 C_{u1})$
\mathcal{P}	Maximum value		Minimum value
Input power	$\dot{m} \psi U_2^2$	$\dot{m} \psi U_2 C_{u2}$	$\dot{m} \psi (U_2 C_{u2} - U_1 C_{u1})$
\mathcal{P}_i	Maximum value		Minimum value

Assume that the impeller outlet radial velocity equals the inlet axial velocity. Calculate:

- (a) Absolute velocity at impeller exit.
- (b) The compressor pressure ratio
- (c) The axial width of the impeller at outlet
- (d) The blade angle at the inducer tip

Solution

$$\begin{aligned} T_{01} &= 300 \text{ k} & P_{01} &= 110 \text{ kPa} & M_2 &= 1.1 \\ m &= 10 \text{ kg/s} & d_t &= 0.36 & d_h &= 0.18 \text{ m} \\ D_2 &= 0.52 \text{ m} & \sigma &= 0.92 & \psi &= 1.05 \end{aligned}$$

- (a) *Absolute velocity at impeller exit*

Continuity equation at impeller inlet:

$$\begin{aligned} \dot{m} &= \rho_1 C a_1 A_1 \\ A_1 &= \pi (r_t^2 - r_h^2) = \pi [(0.18)^2 - (0.09)^2] = 0.07634 \text{ m}^2 \end{aligned}$$

Since both of ρ_1 and $C a_1$ are unknowns, *iterative* procedure is to be followed.

1. Let $\rho_1 = \frac{P_{01}}{R T_{01}} = \frac{110 \times 10^3}{287 \times 300} = 1.2776 \text{ kg/m}^3$
2. Calculate ($C a_1$) from the continuity equation; ($\dot{m} = \rho_1 C a_1 A_1$), thus $C a_1 = 102.53 \text{ m/s}$
3. Since $C_1 = C a_1 = 102.53 \text{ m/s}$

4. Calculate static temperature at inlet; $T_1 = T_{0'} - \frac{C_1^2}{2C_p} = 294.77 \text{ K}$
5. Calculate the static pressure at inlet; $P_1 = P_{01} \left(\frac{T_1}{T_{01}} \right)^{\frac{\gamma}{\gamma-1}} = 103.43 \text{ kPa}$
6. Calculate air density from the relation; $\rho_1 = \frac{P_1}{RT_1} = 1.2226 \text{ kg/m}^3$
7. Compare the calculated density with the previously assumed (or calculated) one. If the difference is within engineering limits, this value will be final. If not, the above procedure is repeated until convergence.

Table 9.4 provides the results of four iterations.

Then the final converged results are:

$$\rho_1 = 1.2171 \text{ kg/m}^3$$

$$T_1 = 294.24 \text{ K}$$

$$Ca_1 = C_1 = 107.62 \text{ m/s}$$

$$P_1 = 102.78 \text{ kPa}$$

At the impeller exit

$$Cr_2 = Ca_1 = 107.62 \text{ m/s}$$

$$\text{Since } M_2 = \frac{C_2}{\sqrt{\gamma RT_2}}, \quad \text{then} \quad C_2 = M_2 \sqrt{\gamma RT_2}$$

Moreover, static and total temperatures are related by

$$T_{o2} = T_2 + \frac{C_2^2}{2C_p} = T_2 \left(1 + \frac{\gamma RM_2^2}{2C_p} \right)$$

$$\text{Moreover, } T_{o2} - T_{o1} = \psi \sigma \frac{U_2^2}{C_p} = \frac{\psi \sigma}{C_p} \left(\frac{C_{U2}}{\sigma} \right)^2 = \frac{\psi}{\sigma C_p} C_{u2}^2 = \frac{\psi}{\sigma C_p} (C_2^2 - C_{r2}^2)$$

$$T_2 \left(1 + \frac{\gamma RM_2^2}{2C_p} \right) - T_{01} = \frac{\psi}{\sigma C_p} (C_2^2 - C_{r2}^2) = \frac{\psi}{\sigma C_p} (\gamma RM_2^2 T_2 - C_{r2}^2)$$

Solving the above equation to get:

$$T_2 = 451.9 \text{ K} \quad T_{o2} = 516.5 \text{ K} \quad C_2 = 1.1 \sqrt{1.4 \times 287 \times 415.9} \\ C_2 = 449.67 \text{ m/s}$$

(a) Absolute velocity at impeller exit = $C_2 = 449.67 \text{ m/s}$

The rotational speed at impeller tip is obtained from the relation:

$$T_{o2} - T_{01} = \psi \sigma \frac{U_2^2}{C_p}, \quad \text{thus} \quad 516.5 - 300 = 1.05 \times 0.92 \frac{U_2^2}{1005}$$

Table 9.4 Iterative procedure for evaluating density and axial inlet velocity

Iteration No	1	2	3	4
$C_{a1} = \frac{\dot{m}}{\rho_1 A_1}$ (m/s)	102.53	107.14	107.58	107.62
$C_1 = C_{a1}$ (m/s)	102.53	107.14	107.58	107.62
$T_1 = T_0' - \frac{C_1^2}{2 C_p}$ (K)	294.77	294.29	294.24	294.24
$P_1 = P_{01} \left(\frac{T_1}{T_{01}} \right)^{\frac{\gamma}{\gamma-1}}$ (kPa)	103.43	102.84	102.78	102.78
$\rho_1 = \frac{P_1}{R T_1}$ (kg/m ³)	1.2226	1.2176	1.2171	1.2171

$$U_2 = 474.6 \text{ m/s}$$

(b) *The compressor pressure ratio*

$$\pi_c = \frac{P_{03}}{P_{01}} = \left[1 + \eta_c \psi \sigma \frac{U_2^2}{C_p T_{01}} \right]^{\frac{\gamma}{\gamma-1}}$$

$$\pi_c = \frac{P_{03}}{P_{01}} = \left[1 + 0.8 \times 1.05 \times 0.92 \frac{(474.6)^2}{1005 \times 300} \right]^{\frac{1.4}{0.4}} = 4.93$$

(c) *The axial width of the impeller at outlet*

Since $m^\bullet = \rho_2 C r_2 A_2$

Assuming losses in impeller = losses in diffuser, then

$$\eta_i = \frac{1 + \eta_c}{2} = \frac{1 + 0.8}{2} = 0.9$$

Pressure ratio of impeller is

$$\frac{P_{02}}{P_{01}} = \left[1 + \eta_i \psi \sigma \frac{U_2^2}{C_p T_{01}} \right]^{\frac{\gamma}{\gamma-1}}$$

$$\frac{P_{02}}{P_{01}} = \left[1 + 0.9 \times 1.05 \times 0.92 \frac{(474.6)^2}{1005 \times 300} \right]^{\frac{1.4}{0.4}} = 5.764$$

$$P_{02} = 634 \times 10^3 \text{ Pa}$$

Static pressure at impeller outlet:

$$P_2 = P_{02} \left(\frac{T_2}{T_{02}} \right)^{\frac{\gamma}{\gamma-1}} = 634 \times 10^3 \left(\frac{415.9}{516.5} \right)^{3.5} = 297 \times 10^3 \text{ Pa}$$

Density of air at impeller outlet:

$$\rho_2 = \frac{P_2}{RT_2} = \frac{297 \times 10^3}{287 \times 415.9} = 2.4882 \text{ kg/m}^3$$

Continuity equation at impeller outlet: $m^\bullet = \rho_2 C_{r2} A_2$

$$\text{Then : } 10 = 2.4882 \times 107.62 \times A_2$$

$$\therefore A_2 = 0.037344 \text{ m}^2$$

$$\text{But } A_2 = \pi D_2 b, \text{ thus } b = 2.286 \text{ cm}$$

(d) *The blade angle at the inducer tip*

$$\tan \alpha_t = \frac{C_{a1}}{U_{1t}}$$

To evaluate the rotational speed, since

$$U_2 = \pi D_2 N$$

$$474.6 = \pi \times 0.52 \times N, \text{ then } N = 290.52 \text{ rps}$$

At inducer tip, the rotational speed is

$$U_{1t} = \pi D_{1t} N = \pi \times 0.36 \times 290.52 = 328.57 \text{ m/s}$$

$$\tan \alpha_t = \frac{C_{a1}}{U_{1t}} = \frac{107.62}{325.57}$$

$$\alpha_t = 18.14^\circ$$

9.2.6 Types of Impeller

The impeller may also be classified based on blading into three types, namely, straight radial, forward leaning, or backward leaning. Figure 9.8 shows three types schematically, together with typical velocity triangles in the radial plane for the outlet of each type. The three velocity triangles have the same rotational speed U_2 and same radial velocity component $C_r = W_r$. As a first approximation, the relative fluid velocity leaving the impeller W_2 is assumed parallel to the blade. The angle of

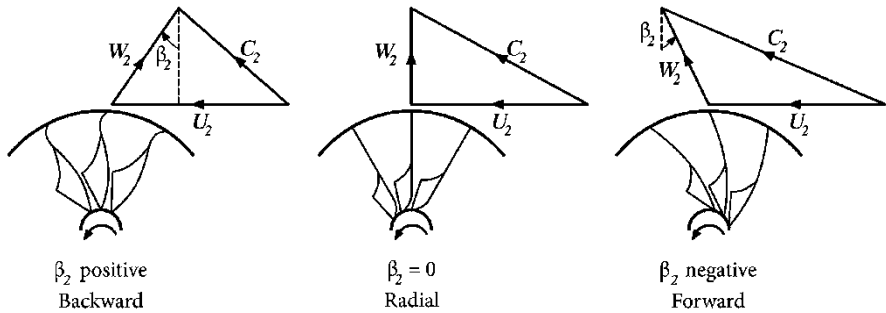


Fig. 9.8 Different shapes of centrifugal blades and outlet velocity triangles

the blade at exit with respect to the tangential direction is denoted by (β_2) and is acute for a backward-leaning blade (Fig. 9.8). The swirl (or tangential) component of the absolute velocity is

$$C_{u2} = U - W_{r2} \tan \beta_2 \quad (9.17a)$$

The angle (α_2) is the angle between the absolute speed at impeller outlet (C_2) and the tangential direction, and

$$C_{u2} = C_{r2} \tan \alpha_2 \text{ and } \frac{C_{r2}}{U_2} = \frac{1}{\tan \alpha_2 + \tan \beta_2}$$

Thus

$$\frac{C_{u2}}{U_2} = \frac{\tan \alpha_2}{\tan \alpha_2 + \tan \beta_2} \quad (9.17b)$$

From Eq. (9.8a),

$$\frac{\Delta T_0}{T_{01}} = \frac{\psi \{(UC_u)_2 - (UC_u)_1\}}{CpT_{01}} = \frac{\psi(\gamma - 1)[U_2(U_2 - W_{r2} \tan \beta_2) - U_{1m}C_{u1}]}{\gamma RT_{01}}$$

With negligible mechanical losses ($\psi = 1.0$), thus

$$\begin{aligned} \frac{\Delta T_0}{T_{01}} &= \frac{(\gamma - 1)U_2^2}{a_{01}^2} \left[\left(1 - \frac{W_{r2}}{U_2} \tan \beta_2 \right) - \left(\frac{U_{1m}}{U_2} \right)^2 \left(\frac{C_{u1}}{U_{1m}} \right) \right] \\ \frac{\Delta T_0}{T_{01}} &= \frac{(\gamma - 1)U_2^2}{a_{01}^2} \left[\left(1 - \frac{W_{r2}}{U_2} \tan \beta_2 \right) - \left(\frac{r_{1m}}{r_2} \right)^2 \left(\frac{C_{u1}}{U_{1m}} \right) \right] \end{aligned}$$

If the flow enters the impeller axially, then $C_{u1} = 0$ and the temperature relation above is expressed as

$$\frac{\Delta T_0}{T_{01}} = \frac{(\gamma - 1)U_2^2}{a_{01}^2} \left(1 - \frac{W_{r2}}{U_2} \tan \beta_2 \right)$$

$$\frac{\Delta T_0}{(\gamma - 1)(U_2/a_{01})^2 T_{01}} = \left(1 - \frac{W_{r2}}{U_2} \tan \beta_2 \right) \quad (9.18)$$

From continuity Eq. (9.4a) and neglecting the blade thickness (t), thus

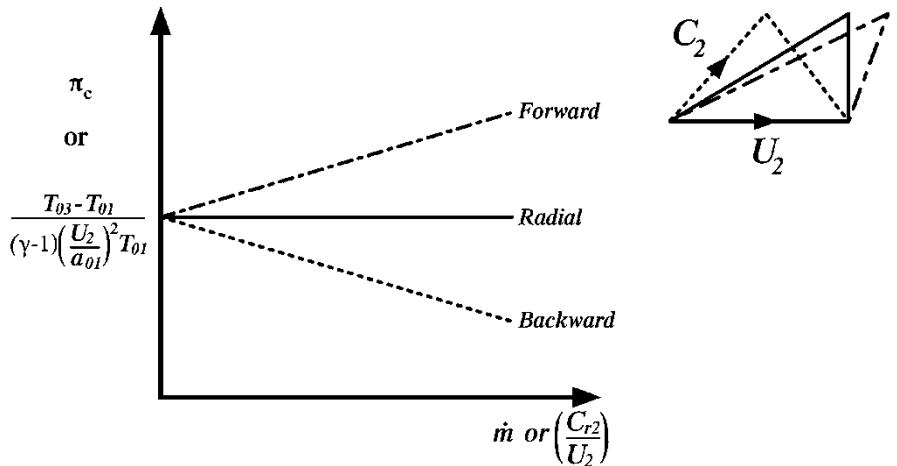
$$W_{r2} = \frac{\dot{m}}{\pi \rho_2 b D_2} \quad (9.4b)$$

The variable, $\left(\frac{\Delta T_0}{(\gamma - 1)(U_2/a_{01})^2 T_{01}} \right)$, represents the relative stage temperature rise and consequently an index for pressure ratio, while the variable W_{r2}/U_2 (which is equivalent to C_{r2}/U_2) represents the mass flow parameter for a certain rotational speed. Plotting relation (9.18) yields a straight line provided that the blade angle (β_2) is constant; Fig. 9.9.

The pressure ratio for any of the three impeller types may be expressed by the relation:

$$\pi = \left(1 + \eta_c \frac{\Delta T_0}{T_{01}} \right)^{\frac{\gamma}{\gamma-1}} = \left\{ 1 + \frac{\eta_c (\gamma - 1) U_2^2}{a_{01}^2} \left[\left(1 - \frac{W_{r2}}{U_2} \tan \beta_2 \right) - \left(\frac{r_{1m}}{r_2} \right)^2 \left(\frac{C_{u1}}{U_{1m}} \right) \right] \right\}^{\frac{\gamma}{\gamma-1}} \quad (9.19a)$$

Moreover, from Eqs. (9.17a) and (9.17b), the pressure ratio can be expressed as



Pressure ratio for different impeller blading

Fig. 9.9 Variation of pressure ratio with impeller blading

$$\pi = \left\{ 1 + \frac{\eta_c(\gamma - 1)U_2^2}{a_{01}^2} \left[\left(\frac{C_{u2}}{U_2} \right) - \left(\frac{r_{1m}}{r_2} \right)^2 \left(\frac{C_{u1}}{U_{1m}} \right) \right] \right\}^{\frac{\gamma}{\gamma-1}}$$

$$\pi = \left\{ 1 + \frac{\eta_c(\gamma - 1)U_2^2}{a_{01}^2} \left[\left(\frac{\tan \alpha_2}{\tan \alpha_2 + \tan \beta_2} \right) - \left(\frac{r_{1m}}{r_2} \right)^2 \left(\frac{C_{u1}}{U_{1m}} \right) \right] \right\}^{\frac{\gamma}{\gamma-1}} \quad (9.19b)$$

At the same mass flow rate and tip speed, U_2 , the rotor with *forward-leaning* blades will do more work on the fluid. Thus, at the first sight it looks that it will produce the highest pressure ratio compared to the radial or backward-leaning blades. However, its positive slope is not an advantageous as the higher pressure ratio and temperature rise will lead to dynamic instability [6]. Moreover, the resulting absolute velocity at exit C_2 is maximum (for the same W_{r2} and U_2), which increases the necessary pressure rise in the diffuser. For these reasons, forward-leaning blades are not suitable for high-speed compressors and never used for aircraft engines. For radial blades ($\beta_2 = 0.0$), a horizontal line is obtained, which means that the pressure ratio is independent from the mass flow rate. For backward-leaning (backswept) blades, the above relation yields a straight line having a negative slope. Since the absolute velocity (C_2) for backward is less than that for both straight radial and backward-leaning blades, it develops higher efficiency than straight radial blades. This means less stringent diffusion requirements in both the impeller and the diffuser, tending to increase the efficiency of both components [5]. The backswept angle may be in the range 30–40°. The use of backswept vanes gives the compressor a wider operating range of the airflow at a given rotational speed, which is important for matching the compressor to its driving turbine.

Table 9.5 A comparison between different types of impeller [7]

Type of Impeller	Radial	Forward	Backward
Advantages	1. Reasonable compromise between low-energy transfer and high absolute outlet velocity	1. Low-outlet kinetic energy (or - low-diffuser inlet Mach number)	1. High-energy transfer
	2. No complex bending stress		2. High efficiency
	3. Easy manufacturing		
Disadvantages	1. Surge margin is relatively narrow	1. Low-energy transfer	1. High-outlet kinetic energy (or high-diffuser inlet Mach number)
		2. Complex bending stress	2. Surge margin is less than radial vanes
		3. Hard manufacturing	3. Complex bending stress
			4. Hard manufacturing

A comparison between different impellers is given in Table 9.5.

It is important to say here that impeller's tip speed not only influencing aerodynamics of compressor but also its allowable stresses. Maximum tip speed depends on impeller's material as follows:

- Cast aluminum can be used up to a tip speed of around 200–300 m/s.
- Forged machined aluminum can be used up to a tip speed of about 500 m/s.
- Titanium can be used up to a tip speed of 650–700 m/s.

Titanium aluminide and titanium metal matrix composites are currently being researched for the higher tip speeds.

9.2.7 Impeller Isentropic Efficiency

The pressure ratio of the *impeller* is defined in a way similar to the whole compressor and expressed as

$$\frac{P_{02}}{P_{01}} = \left[1 + \eta_{\text{imp}} \frac{\psi C_{u2} U_2}{C_p T_{01}} \right]^{\gamma/(\gamma-1)} \quad (9.20)$$

This value is greater than the pressure ratio of the compressor due to the losses in the diffuser.

The impeller isentropic efficiency is related to the compressor efficiency. Now, if the losses in the impeller are equal to a certain fraction of the total losses, say λ , then from the T–S diagram (Fig. 9.5), the impeller loss and the compressor loss are, respectively, $(T_{02} - T_{02\text{SS}})$ and $(T_{02} - T_{03\text{SS}})$.

The impeller efficiency is defined as $\eta_{\text{imp}} = (T_{02\text{ss}} - T_{01}) / (T_{03} - T_{01})$. From this definition and compressor efficiencies

$$\frac{T_{02} - T_{02\text{SS}}}{T_{02} - T_{03\text{SS}}} = \frac{1 - \eta_{\text{imp}}}{1 - \eta_c} = \lambda \quad (9.21)$$

$$\eta_{\text{imp}} = 1 - \lambda + \lambda \eta_c$$

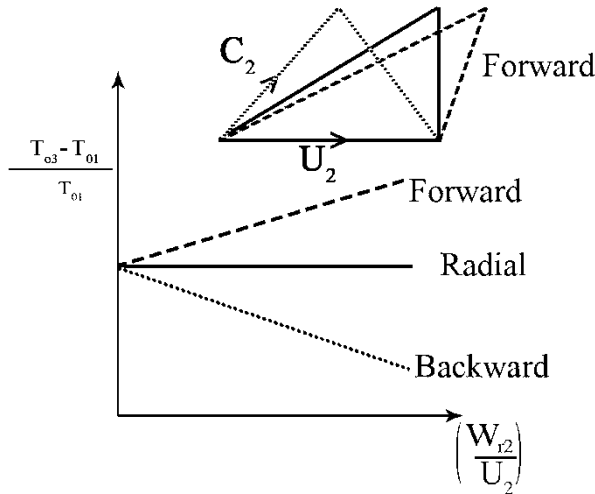
For the case of equal losses in impeller and diffuser

$$\eta_{\text{imp}} = 0.5(1 + \eta_c). \quad (9.22)$$

Example 9.2 The nearby figure illustrates the velocity triangles for the three different types of impellers, namely, radial, forward, and backward leaning ones. Moreover, the relation between temperature rise and radial velocity component at impeller outlet (state 2) is plotted in non-dimensional form. Assuming the flow enters axially, prove that the relation between both parameters is expressed in the form:

$$\frac{T_{03} - T_{01}}{T_{01}} = A + B \left(\frac{W_{r2}}{U_2} \right)$$

where (A) and (B) are constants.



Next, consider the following case for a forward impeller:

$$\frac{W_{r2}}{U_2} = 0.2, \quad D_2 = 0.5 \text{ m},$$

$$P_{01} = 101 \text{ kPa}, \quad T_{01} = 300 \text{ K}$$

$$\eta_c = 0.84 \text{ and } \beta_2 = 30^\circ$$

$$U_2 = 400 \text{ m/s}, \quad b_2 = 0.1 \text{ m}$$

where (β_2) is the angle between the relative velocity (W_2) and radial direction, assuming *no slip*,

(a) *Calculate:*

1. The values of the constants (A) and (B)
2. The mass flow rate and compressor pressure ratio and draw a sketch for the velocity triangle at impeller outlet

(b) If the outlet velocity ratio is doubled; $\left(\frac{W_{r2}}{U_2} = 0.4 \right)$,

1. *Draw the new velocity triangle*

2. *Calculate the new mass flow rate and compressor pressure ratio*

Solution

A-1

$$\text{Power} = m \cdot Cp(T_{03} - T_{01}) = m (U_2 Cu_2 - U_1 Cu_1)$$

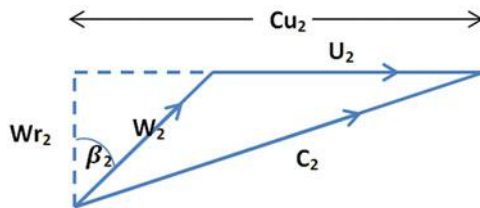
$$\therefore Cp \Delta T_0 = (U_2 Cu_2 - U_1 Cu_1)$$

Since the flow enters the impeller in axial direction.

$$\therefore U_1 Cu_1 = 0$$

$$\therefore Cp \Delta T_0 = U_2 Cu_2 \quad [1]$$

From the nearby figure:



$$Cu_2 = U_2 + Wr_2 \tan (\beta_2)$$

Substituting in Eq. (1)

$$\therefore Cp \Delta T_0 = U_2 (U_2 + Wr_2 \tan (\beta_2)) = U_2^2 + U_2 Wr_2 \tan (\beta_2)$$

$$\therefore \Delta T_0 = \frac{U_2^2 + U_2 Wr_2 \tan (\beta_2)}{Cp}$$

$$\therefore \frac{\Delta T_0}{T_{01}} = \frac{U_2^2 + U_2 Wr_2 \tan (\beta_2)}{Cp T_{01}} = \frac{U_2^2}{Cp T_{01}} + \frac{U_2 Wr_2 \tan (\beta_2)}{Cp T_{01}}$$

$$\therefore \frac{\Delta T_0}{T_{01}} = \frac{U_2^2}{T_{01} Cp} + \frac{U_2^2 \tan (\beta_2)}{T_{01} Cp} \left(\frac{Wr_2}{U_2} \right) = A + B \left(\frac{Wr_2}{U_2} \right)$$

$$\text{where } A = \frac{U_2^2}{T_{01} Cp} \quad \text{and} \quad B = \frac{U_2^2 \tan (\beta_2)}{T_{01} Cp}$$

A-2

The values of constants (A and B)

$$A = \frac{U_2^2}{T_{01} Cp} = \frac{400^2}{300 \times 1005} = 0.53068$$

$$B = \frac{U_2^2 \tan(\beta_2)}{T_{01} Cp} = \frac{400^2 \tan(30)}{300 \times 1005} = 0.3064$$

Since:

$$\frac{\Delta T_0}{T_{01}} = A + B \left(\frac{Wr_2}{U_2} \right) = 0.53068 + 0.3064 \times 0.2 = 0.59196$$

$$\therefore \Delta T_0 = 0.59196 \times 300 = 177.588 \text{ K}$$

$$\therefore T_{03} = T_{02} = 477.588 \text{ K}$$

$$\pi_c = \left(1 + \frac{\eta_c \Delta T_0}{T_{01}} \right)^{\gamma/\gamma-1} = (1 + 0.84 \times 0.59196)^{3.5}$$

$$\pi_c = 4.107$$

$$Wr_2 = Cr_2 = 0.2 \times 400 = 80 \text{ m/s}$$

$$Cu_2 = U_2 + Wr_2 \tan(\beta_2) = 400 + 80 \tan(30) = 446.188 \text{ m/s}$$

$$C_2 = \sqrt{Cu_2^2 + Cr_2^2} = 453.3 \text{ m/s}$$

$$\therefore T_2 = T_{02} - \frac{C_2^2}{2 Cp}$$

$$\therefore T_2 = 477.588 - \frac{453.3^2}{2 \times 1005} = 375.357 \text{ K}$$

Let losses in the impeller = 0.5 total losses

$$\therefore \eta_i = \frac{1 + \eta_c}{2} = 0.92$$

$$\therefore \frac{P_{02}}{P_{01}} = \left(1 + \frac{\eta_i \Delta T_0}{T_{01}} \right)^{\gamma/\gamma-1} = (1 + 0.92 \times 0.59196)^{3.5} = 4.579934$$

$$\therefore P_{02} = 4.579934 \times 101 = 462.57 \text{ kPa}$$

$$\therefore P_2 = P_{02} \left(\frac{T_2}{T_{02}} \right)^{\gamma/\gamma-1} = 462.57 \left(\frac{375.357}{477.588} \right)^{3.5} = 199.09 \text{ kPa}$$

$$\therefore \rho_2 = \frac{P_2}{R T_2} = \frac{199.09 \times 1000}{287 \times 375.357} = 1.848 \text{ kg/m}^3$$

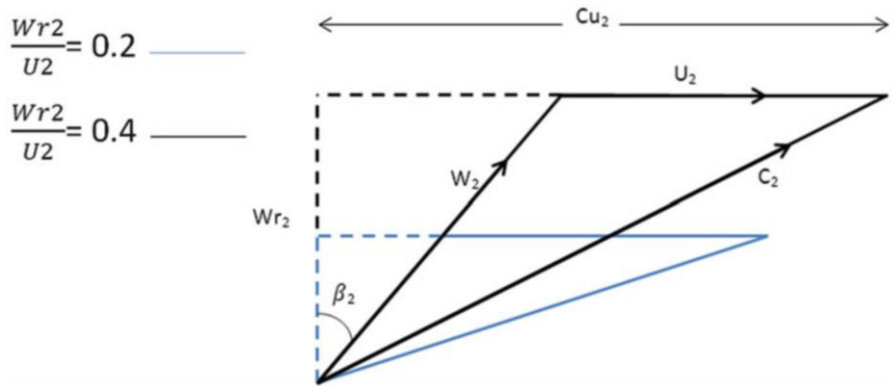
$$\therefore m = \rho_2 W_{r2} \pi D_2 b$$

$$\therefore \dot{m} = 1.848 \times 80 \times \pi * 0.5 \times 0.1 = 23.2236 \text{ kg/s}$$

B-1

The radial velocity at impeller outlet is doubled, and the rotational speed (U_2) is remained constant. Thus

$$\left(\frac{Wr_2}{U_2} \right) = 0.4$$



$$\frac{\Delta T_0}{T_{01}} = A + B \left(\frac{Wr_2}{U_2} \right) = 0.53068 + 0.3064 \times 0.4 = 0.65324$$

$$\therefore \Delta T_0 = 0.65324 \times 300 = 195.972 \text{ K}$$

$$T_{03} = T_{02} = 495.972 \text{ K}$$

$$\pi_c = \left(1 + \frac{\eta_c \Delta T_0}{T_{01}} \right)^{\gamma/\gamma-1} = (1 + 0.84 \times 0.65324)^{3.5}$$

$$\pi_c = 4.6228$$

$$Wr_2 = Cr_2 = 0.4 \times 400 = 160 \text{ m/s}$$

$$Cu_2 = U_2 + Wr_2 \tan(\beta_2) = 400 + 160 \tan(30) = 492.376 \text{ m/s}$$

$$C_2 = \sqrt{Cu_2^2 + Cr_2^2} = 517.72 \text{ m/s}$$

$$\therefore T_2 = T_{02} - \frac{C_2^2}{2 Cp} = 477.588 - \frac{453.3^2}{2 \times 1005} = 362.62 \text{ K}$$

Assuming also losses in the impeller=half of the total losses, then impeller isentropic efficiency is also

$$\eta_i = 0.92$$

$$\frac{P_{02}}{P_{01}} = \left(1 + \frac{\eta_i \Delta T_0}{T_{01}}\right)^{\gamma/\gamma-1} = (1 + 0.92 \times 0.65324)^{3.5} = 5.1922$$

$$P_{02} = 4.579934 \times 101 = 524.4122 \text{ kPa}$$

$$P_2 = P_{02} \left(\frac{T_2}{T_{02}}\right)^{\gamma/\gamma-1} = 462.57 \left(\frac{375.357}{477.588}\right)^{3.5} = 175.248 \text{ kPa}$$

$$\therefore \rho_2 = \frac{P_2}{R T_2} = \frac{199.09 \times 1000}{287 \times 375.357} = 1.684 \text{ kg/m}^3$$

$$\dot{m} = \rho_2 W r_2 \pi D_2 b = 1.684 \times 160 \times \pi \times 0.5 \times 0.1 = 42.321 \text{ kg/s}$$

Conclusion

Doubling the radial velocity at impeller outlet leads to

1. Increasing the mass flow rate by 82 %
2. Increasing total temperature rise by 10.35 %
3. Increasing the pressure ratio by 13.37 %

9.2.8 Radial Impeller

Impeller has no inducer section. The blade starts and ends in the radial plane. Thus both velocity triangles are drawn in the $(r - \theta)$ plane. Figure 9.10 illustrates both blade shape and velocity triangles at inlet and outlet [19].

Example 9.3 Air is compressed in a centrifugal compressor having the following properties:

Rotational speed = 5400 rpm

Mass flow rate = 20 kg/s

Air density at impeller inlet = 1.115 kg/m^3

Air density at impeller outlet = 1.45 kg/m^3

Impeller inlet radius = 0.3 m

Impeller outlet radius = 0.56 m

Power consumed in driving the impeller = 750 kW, and entry is radial with a component of 60 m/s which is Constant throughout

Calculate

1. The width at inlet and outlet
2. Temperature rise in compressor
3. Angles: $\alpha_1, \alpha_2, \beta_2, \beta_2$

Solution

1. Continuity equation:

$$\dot{m} = 20 \text{ kg/s} = \rho_1 C_1 A_1 = 1.115 \times 60 \times A_1$$

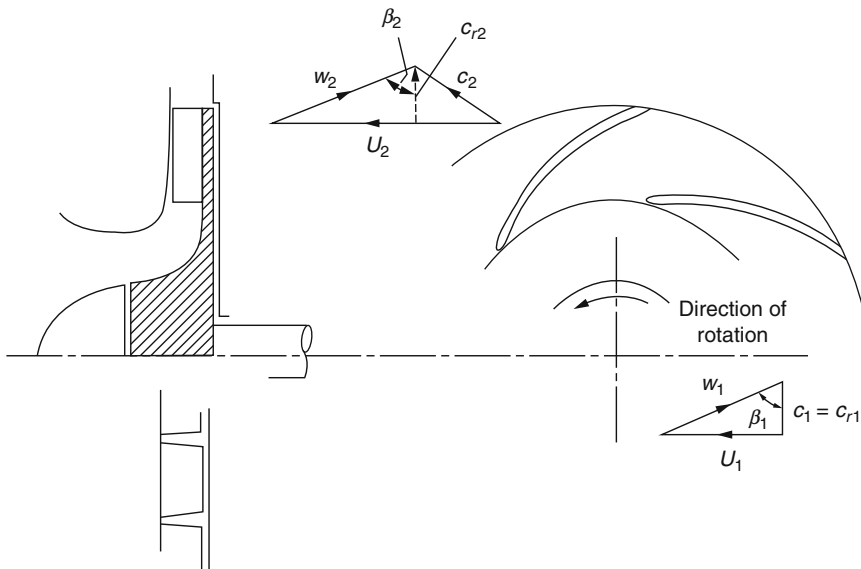


Fig. 9.10 Radial impeller

$$A_1 = \frac{20}{66.9} = 0.2989 \text{ m}^2$$

$$A_1 = 2\pi r_1 b_1$$

Width of impeller at inlet is

$$b_1 = \frac{0.2989}{2\pi \times 0.3} = 0.1586 \text{ m}$$

Similarly impeller blade width at outlet is

$$b_2 = \frac{\dot{m}}{\rho_2 C_{r2} \times 2\pi r_2} = \frac{20}{1.45 \times 60 \times 2 \times \pi \times 0.56} = 0.065 \text{ m}$$

Rotational speeds:

$$U_1 = 2\pi r_1 N = 2\pi \times 0.3 \times \frac{5400}{60} = 169.6 \text{ m/s}$$

$$U_2 = 2\pi r_2 N = 2\pi \times 0.56 \times \frac{5400}{60} = 316.7 \text{ m/s}$$

Power:

$$\mathcal{P} = \dot{m} U_2 C_{u2} \quad (\text{A})$$

$$C_{u2} = \frac{750 \times 10^3}{20 \times 316.7} = 118.4 \text{ m/s}$$

2. Temperature rise

$$\mathcal{P} = \dot{m} C_p \Delta T_0 \quad (\text{B})$$

From (A) and (B):

$$\Delta T_0 = \frac{U_2 C_{u2}}{C_p} = 37.3 \text{ K}$$

$$W_{u2} = U_2 - C_{u2} = 316.7 - 118.4 = 198.3 \text{ m/s}$$

3. Flow angles

$$\tan \beta_1 = \frac{U_1}{C_1} = \frac{169.6}{60} = 2.8267$$

$$\beta_1 = 70.52^\circ$$

$$\alpha_1 = 0.0$$

$$\tan \beta_2 = \frac{W_{u2}}{C_{r2}} = \frac{198.3}{60} = 3.305$$

$$\beta_2 = 73.17^\circ$$

$$\tan \alpha_2 = \frac{C_{u2}}{C_{r2}} = \frac{118.4}{60} = 1.973$$

$$\alpha_2 = 63.12^\circ$$

9.2.9 Diffuser

The function of the diffuser is to decelerate the flow leaving the impeller, thus reducing the absolute velocity of the gas at impeller exit from (C_2) to a lower velocity (C_3) as shown in Fig. 9.5. The static pressure of the air/gas at impeller exit is further raised by passing through the diffuser. The amount of deceleration and the static pressure rise ($P_3 - P_2$) in the diffuser depend on the degree of reaction and the efficiency of the diffusion process. An efficient diffuser must have minimum losses ($P_{02} - P_{03}$) but maximum efficiency.

There are broadly two types of diffuser, namely, vaneless and vaned. The vaned diffuser has many types, including not only the diffuser having fixed or pivoting vanes but also the cascade, channel, and pipe types; Fig. 9.2. All diffusers have an

initial vaneless gap outboard of the impeller in which the flow settles. The vaneless diffuser is bulky and can be inefficient compared with the other types. The cascade may involve one, two, or three rows of vanes, with performance similar to that of axial cascades. Vaned diffusers may use curved or straight vanes, having a longer path length than the cascade diffuser. Vaneless, cascade, and vaned diffusers collect the flow in a one volute type collector. The channel and pipe diffusers collect the flow in separate slowly diverging passages, sometimes with corner vanes at their outlet. The pipe diffuser consists of a conical hole while the channel type being rectangular in section with one pair of opposed walls diverging at 10° – 11° while the others are parallel.

The pipe and channel diffusers may feed separate combustors or may merge downstream. The channel type is sometimes known as the vane-island or wedge-type diffuser. The blunt end causes as much loss as 5 % of the overall efficiency. The pipe-type diffuser is more efficient than the rectangular channels. The passages are formed by drilling holes tangentially through a ring surrounding the impeller, and after the throat the passages are conical. Overall isentropic efficiencies of over 85 % are obtained for compressors using this pipe diffuser. Of all the types of diffuser, the vaned diffuser may be made variable, the vanes pivoting about an axial axis.

In general, the performance of diffuser is examined by considering the pressure coefficient

$$C_p = \frac{P_3 - P_2}{P_{02} - P_2} \quad (9.23)$$

where stations 2 and 3 are the inlet and outlet of the diffuser, respectively. The pressure coefficient is sometimes identified as the pressure rise coefficient and given by the symbol C_{pr} .

9.2.9.1 Vaneless Diffuser

As the name implies, the air/gas in a vaneless diffuser is diffused in the vaneless space around the impeller before it leaves the stage of compressor through a volute casing. The air/gas in the vaneless diffuser gains static pressure rise simply due to the diffusion process from a smaller diameter (d_2) to a larger diameter (d_3). The corresponding areas of cross sections in the radial direction are

$$\begin{aligned} A_2 &= \pi d_2 b_2 = 2\pi r_2 b_2 \\ A_3 &= \pi d_3 b_3 = 2\pi r_3 b_3 \end{aligned} \quad (9.24)$$

Such a flow in the vaneless space is axisymmetric inviscid. Since no external torque is applied, the angular momentum is constant, or

$$r_2 C_{u2} = r_3 C_{u3} \quad (9.25)$$

From the continuity equation, at the entry and exit section of the vaneless diffuser,

$$\begin{aligned}\rho_2 C_{r_2} A_2 &= \rho_3 C_{r_3} A_3 \\ \rho_2 C_{r_2} (2\pi r_2 b_2) &= \rho_3 C_{r_3} (2\pi r_3 b_3) \\ \rho_2 C_{r_2} r_2 b_2 &= \rho_3 C_{r_3} r_3 b_3\end{aligned}\quad (9.26)$$

For a small pressure rise across the diffuser, $\rho_2 \approx \rho_3$, therefore

$$C_{r_2} r_2 b_2 = C_{r_3} r_3 b_3$$

For a constant width (parallel wall) diffuser $b_2 = b_3$

$$C_{r_2} r_2 = C_{r_3} r_3 \quad (9.27)$$

From Eqs. (9.25) and (9.27),

$$\therefore \frac{C_{u3}}{C_{u2}} = \frac{C_{r_3}}{C_{r_2}} = \frac{C_3}{C_2} = \frac{r_2}{r_3} \quad (9.28)$$

Equation (9.28) shows that for incompressible fluid, the diffusion is directly proportional to the diameter ratio (d_3/d_2). This leads to a relatively large-sized diffuser, which is a serious disadvantage of the vaneless type, which leads to an impractically large compressor to be used in aeronautical applications. Moreover, Eq. (9.28) gives

$$\alpha_2 = \alpha_3 = \tan^{-1} \frac{C_{u_2}}{C_{r_2}} = \tan^{-1} \frac{C_{u_3}}{C_{r_3}} = \alpha \quad (9.29)$$

Thus, the streamlines for incompressible flow in a vaneless diffuser of constant axial width make a constant angle with the radial direction α .

9.2.9.2 Vaned Diffuser

To save space, vanes are employed to reduce the fluid angular momentum and thereby reduce C_u more rapidly. Conical diffusers are mostly used in aircraft engines. The static pressure rise coefficient for a conical diffuser ($C_{P_r} \equiv (P_3 - P_2)/P_{02} - P_2$) may be approximated by

$$C_{P_r} \approx 2 \frac{(P_{03} - P_{02})}{\rho_{02} C_2^2} + \left[1 - \frac{P_{03}}{P_{02}} \left(\frac{C_3}{C_2} \right)^2 \right] \quad (9.30)$$

9.2.10 Prewhirl

The tangential component of velocity at the inlet to the impeller is usually zero as the flow enters the impeller axially. If prewhirl (or inlet guide) vanes are installed to

the inlet duct before the impeller, then the incoming air has a tangential component of velocity. This velocity component depends on the vane outlet angle. Prewirl may be positive or negative as shown in Fig. 9.11.

Positive prewirl reduces the inlet relative velocity, while negative prewirl increases the inlet relative velocity. In aero engines, positive prewirl is frequently used to reduce the inlet relative speed. The objective here is to avoid the formation of shock waves on the blade suction side. The designer of compressor seeks for a small inlet area of the engine to reduce the drag force. At the same time, the air mass flow rate is chosen as maximum as possible to maximize the thrust force. Both factors led to an increase in the axial absolute velocity at inlet, and this in turn increases the relative velocity. Since the relative velocity is maximum at the tip radius of the inlet then when accelerated, there is always a tendency for the air to break away from the convex face of the curved part of the impeller vane. Here a shock wave might occur, which upon interaction with the boundary layer over the convex surface of blades, causes a large increase in boundary layer thickness. Thus, excessive pressure loss occurs.

The value of the inlet relative Mach number must be in the range from 0.8 to 0.85 to avoid the shock wave losses described previously, or

$$M_1 = \frac{W_1}{\sqrt{\gamma R T_1}} \approx 0.8 - 0.85$$

where T_1 is the static inlet temperature. Though this Mach number may be satisfactory on ground operation, it may be too large at high altitudes as the ambient temperature decreases with altitude. For this reason, IGVs are added to decrease the Mach number. These IGVs are attached to the compressor casing to provide a positive prewirl that decreases the magnitude of the maximum relative velocity (W_1) at the eye tip.

The IGVs, sometimes denoted as swirl vanes, may swivel about radial axes to vary the swirl angle with speed. Keeping W_1 aligned with the inducer leading edge results in a minimum incidence or shock losses. Thus, they widen the operating speed range, increase efficiency, and reduce the relative Mach number at the eye tip, but they also reduce the mass flow by reducing the inlet area.

Assuming that the axial velocity is uniform from the root to the tip of the eye, then the maximum relative Mach number at the eye tip; Fig. 9.11 is given by the relation:

$$M_{1\max} = \frac{W_{1\max}}{a_1} = \sqrt{\frac{C_{a1}^2 + (U_{1t} - C_{a1} \sin \alpha_1)^2}{\gamma R T_1}} \quad (9.31)$$

where U_{1t} is the rotational speed at the eye tip and (α_1) is the prewirl angle, which is the angle between the absolute velocity leaving the IGV and the axial direction.

Another advantage of the prewirl is that the curvature of the impeller vanes at the inlet will be reduced and so the radius of curvature will increase. Thus, the

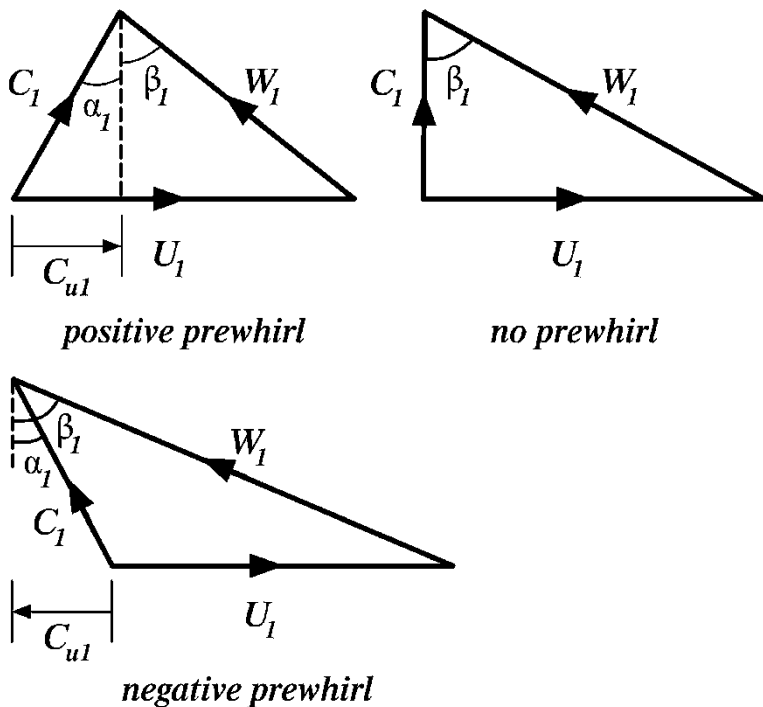


Fig. 9.11 Velocity triangles for different types of prewhirl

bending stress is decreased. The reason is that the inducer of the impeller resembles a curved beam. The bending stress for curved beams is inversely proportional to the radius of curvature [8].

Example 9.4 An aircraft engine flying at 10,500 m is fitted with a single-sided centrifugal compressor. At the compressor inlet, the total pressure and temperature are $P_{01} = 0.34$ bar and $T_{01} = 243$ K, axial speed is $C_{a1} = 120$ m/s and rotational speed is 270 rps. The intake duct of the impeller eye contains fixed vanes, which give the air a *positive* prewhirl of $\alpha_1 = 25^\circ$ at all radii. The inner and outer diameters of the eye are 18 and 33 cm, respectively; the diameter of the impeller periphery is 54 cm. Assuming that the impeller has radial blades at outlet, isentropic efficiency of the compressor is 0.8, the slip factor is 0.9, and the power input factor is 1.04,

Estimate

1. The compressor pressure ratio and stagnation pressure at the compressor outlet
2. The compressor pressure ratio and stagnation pressure at the compressor outlet if the impeller has a backward leaning blades at outlet having an angle $\beta_2 = 30^\circ$ (assume $W_{r2} = C_{a1}$)

3. The compressor pressure ratio and stagnation pressure at the compressor outlet if the impeller has a forward leaning blades at outlet having an angle $\beta_2 = -30^\circ$ (assume $W_{r2} = C_{a1}$)
4. The compressor pressure ratio and stagnation pressure at the compressor outlet if the impeller has a forward leaning blades at outlet ($\beta_2 = -30^\circ$), while the compressor has a negative prewhirl at the same angle ($\alpha_1 = -25^\circ$) and ($W_{r2} = C_{a1}$)

Solution

Case (1): Positive prewhirl $\alpha_1 = 25^\circ$ and radial blades

Compressor rotational speed $N = 270 \text{ rps}$ $C_{a1} = 120 \text{ m/s}$
 Conditions at compressor inlet $P_{01} = 0.34 \text{ bar}$ $T_{01} = 243 \text{ K}$

$$d_{1h} = 18 \text{ cm}, \quad d_{1t} = 33 \text{ cm}$$

$$D_2 = 54 \text{ cm} \quad \eta_c = 0.8 \quad \psi = 1.04 \quad \sigma = 0.9$$

Rotational speeds:

At inlet: $U_1 = 2\pi r_1 N$, where

$$r_1 = r_{mean} = \frac{d_{1h} + d_{1t}}{4} = 0.1275 \text{ m}$$

$$U_1 = 2\pi \times r_1 \times N = 2\pi \times 0.1275 \times 270 = 216.3 \text{ m/s}$$

At outlet: $U_2 = \pi D_2 N = \pi \times 0.54 \times 270 = 458 \text{ m/s}$

Conditions at inlet:

$$C_1 = \frac{C_{a1}}{\cos 25} = \frac{120}{\cos 25} = 127.7 \text{ m/s}$$

For a positive prewhirl with $\alpha_1 = 25^\circ$, then

$$C_{u1} = C_1 \sin(25) = 127.7 \sin(25) = 54.0 \text{ m/s}$$

$$\frac{P_{03}}{P_{01}} = \left[1 + \eta_c \Psi \frac{\sigma U_2^2 - U_1 C_{u1}}{C_P T_{01}} \right]^{\frac{\gamma}{\gamma-1}}$$

$$\frac{P_{03}}{P_{01}} = \left[1 + 0.8 \times 1.04 \times \left(\frac{0.9 \times (458)^2 - 216.3 \times 54.0}{1005 \times 243.0} \right) \right]^{\frac{14}{0.4}}$$

$$\frac{P_{03}}{P_{01}} = 5.22$$

$$P_{03} = 5.22 \times 0.34 \times 10^5 = 1.775 \text{ bar}$$

Case (2): Positive prewhirl and backward-leaning blades at impeller outlet; $\beta_2 = 30^\circ$

$$C_{u2} = U_2 - W_{r2} \tan \beta_2 = 458 - 120 \tan 30 = 388.7 \text{ m/s}$$

$$\frac{P_{03}}{P_{01}} = \left[1 + 0.8 \times 1.04 \times \left(\frac{0.9 \times (388.7)^2 - 216.3 \times 54.0}{1005 \times 243.0} \right) \right]^{\frac{1.4}{0.4}} = 3.44$$

$$P_{03} = 3.44 \times 0.34 \times 10^5 = 1.17 \text{ bar}$$

Case (3): Positive prewhirl and forward-leaning blades at impeller outlet; $\beta_2 = -30^\circ$

$$C_{u2} = U_2 - W_{r2} \tan \beta_2 = 458 - 120 \tan (-30) = 527.3 \text{ m/s}$$

$$\frac{P_{03}}{P_{01}} = \left[1 + 0.8 \times 1.04 \times \left(\frac{0.9 \times (527.3)^2 - 216.3 \times 54.0}{1005 \times 243.0} \right) \right]^{\frac{1.4}{0.4}} = 8.02$$

$$P_{03} = 8.02 \times 0.34 \times 10^5 = 2.726 \text{ bar}$$

Case (4): Negative prewhirl ($\alpha_1 = -25^\circ$) and forward-leaning blades at impeller outlet; $\beta_2 = -30^\circ$

$$C_{u1} = C_{a1} \tan \alpha_1 = 120 \tan (-25) = -54.0 \text{ m/s}$$

$$C_{u2} = U_2 - W_{r2} \tan \beta_2 = 458 - 120 \tan (-30) = 527.3 \text{ m/s}$$

$$\frac{P_{03}}{P_{01}} = \left[1 + 0.8 \times 1.04 \times \left(\frac{0.9 \times (527.3)^2 - 216.3 \times (-54.0)}{1005 \times 243.0} \right) \right]^{\frac{1.4}{0.4}} = 12.82$$

$$P_{03} = 12.82 \times 0.34 \times 10^5 = 4.357 \text{ bar}$$

As calculated above:

- Maximum pressure ratio is obtained for the case of negative prewhirl and forward-leaning blades at impeller outlet
- Minimum pressure ratio is obtained for the case of positive prewhirl and backward-leaning blades at impeller outlet

A summary of results are listed in Table 9.6.

Table 9.6 Summary of results

Case	1	2	3	4
P_{03}/P_{01}	5.22	3.44	8.02	12.82
$P_{03}(\text{bar})$	1.775	1.170	2.726	4.357

9.2.11 Discharge System

The discharge system as described earlier is either a manifold, a crossover duct (an inverted U-shaped passage), or a collector (scroll or volute). Aero engines and many gas turbines require the discharged air to be turned into axial direction for transmission to the combustion chamber. Multistage compressors have inverted U-shaped passage to turn the flow from radially outward to radially inward, and then to axial direction for transmission to the inlet of the next stage. In many industrial gas turbines and turbochargers, the fluid is collected in one pipe for delivery to the subsequent modules of the system.

Very little work treated the volute. Figure 9.3 illustrates the volute shape. In general, the cross-sectional area of the volute must increase with the azimuth angle to accommodate the increasing flow. The cross-sectional area of the volute may be very close to the circular shape. However, other shapes for the volute are shown in the figure. The simplest method of volute design assumes that the angular momentum of the flow remains constant ($rC_u = K$). The area at any azimuth angle A_θ at any angle θ is expressed as

$$\frac{A_\theta}{\bar{r}} = Q \frac{\theta}{2\pi K} \quad (9.32)$$

where \bar{r} and Q are the radius of the centroid of the cross section of the volute and volume flow, respectively.

9.2.12 Compressor Map

In this section, the characteristic behavior of a centrifugal compressor operating between inlet station 1 and outlet station 2 will be discussed. Changing the nomenclature a little, the overall stagnation pressure ratio will be P_{02}/P_{01} . For any compressor, the stagnation pressure at outlet and the overall compressor efficiency are dependent on other physical properties as follows:

$$P_{02}, \eta_c = f(\dot{m}, P_{01}, T_{01}, \gamma, R, D, N, \text{ and } \nu)$$

where subscripts 01 and 02 denote the compressor inlet and outlet total conditions, the mass flow rate is denoted by \dot{m} , specific heat ratio and gas constant are γ and R , and the kinematic viscosity ν . On the basis of Buckingham's theory, there are nine physical quantities and four basic dimensions; hence, the number of dimensionless

quantities is $9-4=5$. The dimensionless analysis will give the following relationship:

$$\frac{P_{02}}{P_{01}}, \eta_C = f\left(\frac{\dot{m}\sqrt{\gamma RT_{01}}}{P_{01}D^2}, \frac{ND}{\sqrt{RT_{01}}} \frac{ND^2}{v}, \gamma\right). \quad (9.33)$$

The specific heat ratio γ does not vary much with compressing the air. The viscous effects are insensitive to the variation of Reynolds number, ND^2/v , if the Reynolds number itself is high. Since the Reynolds number range is sufficiently high, the compressor performance can be adequately described by

$$\frac{P_{02}}{P_{01}}, \eta_C = f\left(\frac{\dot{m}\sqrt{\gamma RT_{01}}}{P_{01}D^2}, \frac{ND}{\sqrt{RT_{01}}}\right) \quad (9.34)$$

Moreover, for a given air compressor if both the diameter and gas constant are fixed, then the performance can be described by the following pseudo-dimensionless variables:

$$\frac{P_{02}}{P_{01}}, \eta_C = f\left(\frac{\dot{m}\sqrt{T_{01}}}{P_{01}}, \frac{N}{\sqrt{T_{01}}}\right) \quad (9.35)$$

To account for the air properties at *different altitudes* (when this compressor is part of an aero engine), the right-hand side variables refer to the standard day conditions. Thus, the performance relation above is described by

$$\frac{P_{02}}{P_{01}}, \eta_C = f\left(\frac{\dot{m}\sqrt{\theta}}{\delta}, \frac{N}{\sqrt{\theta}}\right) \quad (9.36)$$

$$\theta = \frac{T_{01}}{(T_{01})_{\text{std day}}} \quad \text{and} \quad \delta = \frac{P_1}{(P_1)_{\text{std day}}} \quad (9.37)$$

where $(T_{01})_{\text{std day}} = 288.15 \text{ K}$ and $(P_1)_{\text{std day}} = 101.325 \text{ kPa}$.

The compressor performance is defined (either experimentally or numerically) and plotted in what is called a *compressor map*. This map has the vertical axis as the pressure ratio, or the compressor efficiency, and the mass flow parameter as the horizontal axis for varying rotational speed parameter. If the performance of a compressor is to be defined experimentally, then the test rig provides capabilities for both speed and air mass flow rate. For each rotational speed, the air mass flow is varied and the corresponding pressure ratio and efficiency are determined. Next, the rotational speed is changed and another set of experiments is followed by changing the mass flow rate and so on. A schematic representation of the compressor map is shown in Fig. 9.12.

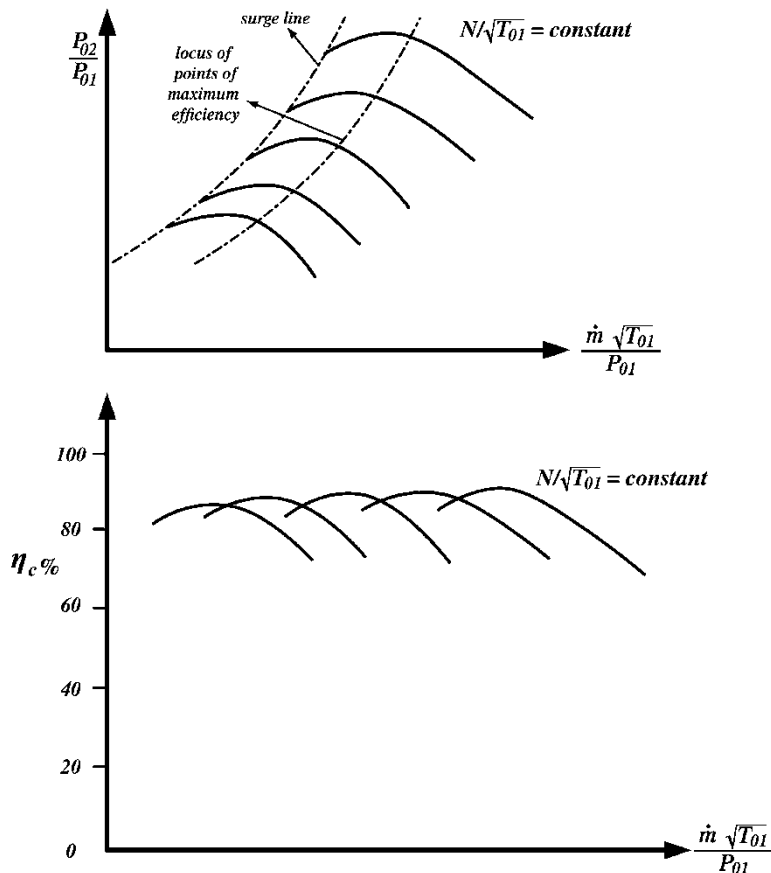


Fig. 9.12 Compressor map

In general, three forms for this map are found:

1. The actual values for the mass and speed parameters are used ($\dot{m} \sqrt{T_{01}}/P_{01}$, $N/\sqrt{T_{01}}$).
2. The values of the mass and speed parameters but referred to the design point values, or,

$$\left(\frac{(\dot{m} \sqrt{T_{01}}/P_{01})}{(\dot{m} \sqrt{T_{01}}/P_{01})_d} \right) \quad \text{and} \quad \left(\frac{(N/\sqrt{T_{01}})}{(N/\sqrt{T_{01}})_d} \right)$$

in such a case at the design point the values of both parameters are unity and other range is from 0.4 to 1.1 (Fig. 9.13).

3. The values of these parameters are referred to the standard day temperature and pressure, or $((\dot{m} \sqrt{\theta}/\delta), N/\sqrt{\theta})$. This form of map is usually used by manufacturers of aero engines (Fig. 9.14) [9].

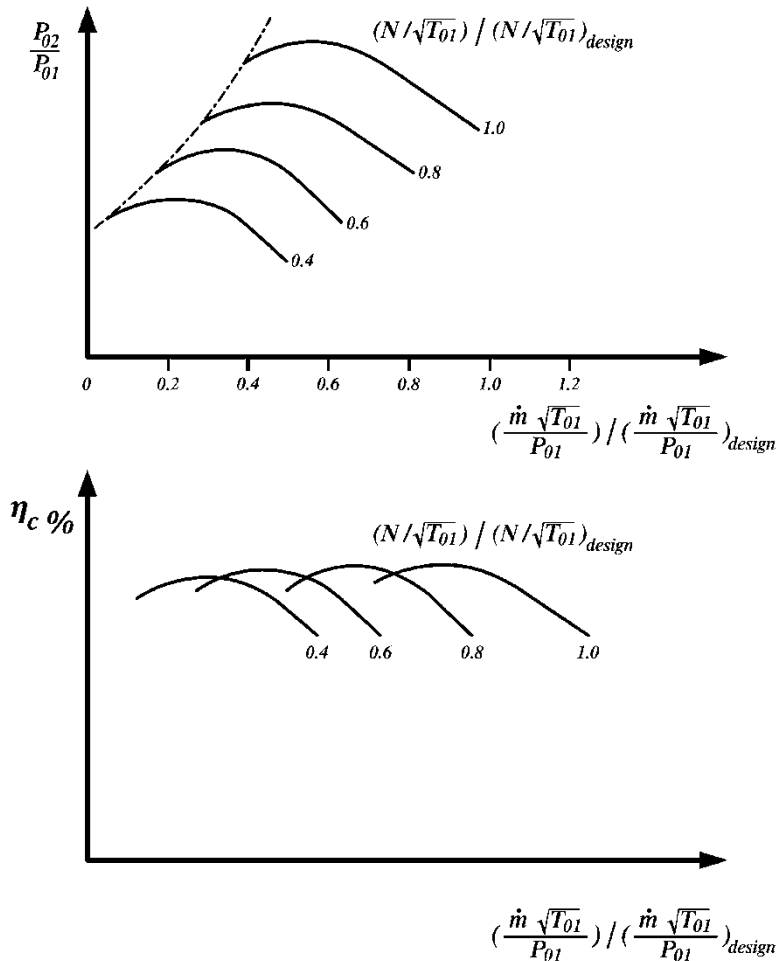


Fig. 9.13 Compressor map referred to design conditions

Each speed line (or corrected speed) has two limiting points, namely, *surge* and *choke* points. The choking point is the extreme right point on the curve. It represents the maximum delivery obtainable at a certain mass flow rate, beyond which no further mass flow rate can be obtained and choking is said to occur. The left point on the constant speed curve represents *surging*. Surging is associated with a drop in delivery pressure with violent aerodynamic pulsation, which is propagated into the whole machine [6]. Surging may be described as follows. If the operating point is on the part of the speed line having a positive slope, then a decrease in the mass flow will be accompanied by a drop in the delivery pressure. If the pressure downstream the compressor does not fall quickly enough, the air will tend to reverse and flow

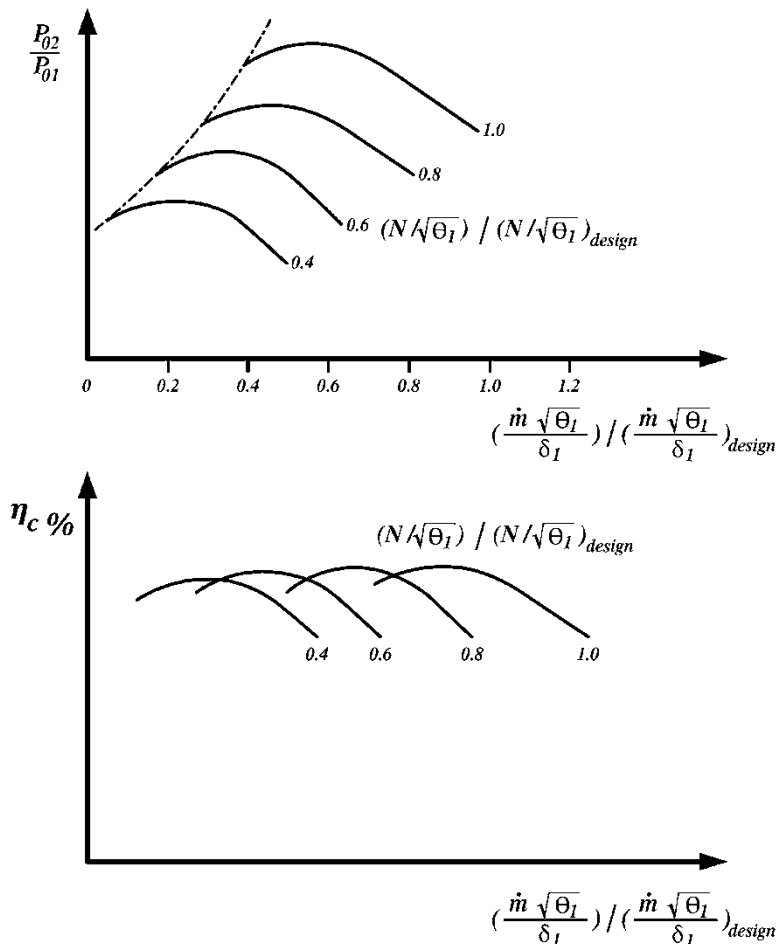


Fig. 9.14 Compressor map referred to sea level conditions

back in the direction of the resulting pressure gradient. This leads to a rapid drop in the pressure ratio. Meanwhile, the pressure downstream the compressor has also fallen, so that the compressor will be able to pick up again and repeat the cycle of events that occurs at high frequency.

9.2.13 Surge

The phenomenon of surge is an unstable condition resulting in flow reversals and pressure fluctuations in the system connected to compressor. This condition occurs when there is sufficient aerodynamic instability within the compressor that the

compressor is unable to produce adequate pressure to deliver continuous flow to the downstream modules. Normally, surge is associated with excessive vibrations and an audible sound [10]. Usually, operation in or near surge is accompanied by pulsating noise level increase, pressure fluctuations, and lateral vibration amplitude increase and may damage the whole compressor. This instability causes stalling of a stage or stages of the compressor. The stalling can occur at the inducer of the impeller, in the radial portion of the impeller, in the diffuser, or in the volute. If stalling is of sufficient strength, the stage will become unstable, and this can lead to surge of compressor. During surge, flow reversal occurs resulting in reverse bending on nearly all compressor components. The higher the pressure or energy level, the more damaging the surge forces will be. As flow is reduced at constant speed, the magnitude of relative velocity decreases proportionally, causing the flow angle to decrease. Additionally, the incidence angle increases, which can result in flow separation at the low pressure side of the blade leading edge. This flow separation frequently starts at one or more blades and continuously shifts around the impeller blades. This occurs at relatively low speeds just before full surge occurs. At higher speeds, the compressor generally goes directly from stable operation to flow separation on all blades and full reverse flow.

Rotating stall can also originate in the diffuser. The point at which a compressor surges can be controlled somewhat by the designer adjusting the diffuser area to increase the relative speed and flow angle. Of course, higher velocities result in higher frictional losses, so a designer must balance between desired surge point and stage efficiency during the design process [11].

Vanes in the diffuser shorten the flow path through the diffuser, reducing frictional losses and controlling the radial velocity component of the gas. Due to lower friction, pressure ratio and efficiency are enhanced, but the operating range is reduced.

9.3 Axial Flow Compressor

9.3.1 *Introduction*

Axial compressors are compressors in which the air flows mainly parallel to the rotational axis. Axial flow compressors have large mass flow capacity, high reliability, and high efficiencies, but have a smaller pressure rise per stage (1.1:1–1.4:1) than centrifugal compressors (4:1–5:1). However, it is easy to link together several stages and produce a multistage axial compressor having pressure ratios up to 40:1 in recent compressors. Integrally bladed rotors (known as blisks) permit blade speeds significantly above conventional rotors and hence stage pressure ratios greater than 1.8 [12]. Axial compressors are widely used in both aero-engines and industrial gas turbines. Almost all present-day jet engines use axial-flow compressors, the notable exception being those used in helicopters, where the smaller size of

the centrifugal compressor is useful. The fan in turbofan engines is also an axial compression module which is treated as an axial compressor having a fewer number of blades of very large height, wide chord, and large twist. These fans may be a single or up to three stages in low bypass turbofan engines (mostly in military applications). Jet engines nowadays use two or three axial compressors (in double- or triple-spool engines) for higher pressure ratios. Nearly all the turbojet engines are of the two spool type, which have two compressors identified as low- and high-pressure compressors. Two spool turbofan engines have the fan as the low pressure spool. Sometimes this fan represents the first stage of the low pressure compressor. The fan in this case is followed by a few stages of an axial compressor (identified as booster), which represents the first module of the engine core. In other turbofans, the fan by its own represents the low pressure compressor which is followed by the high pressure compressor. Three spool turbofan engines have the fan, intermediate pressure, and high pressure compressors. The low pressure compressor turns at the lowest rpm while the high pressure compressor turns at the highest speed.

Since day one of the gas turbine engine, the compressor was the key component for the success and always required high development efforts and costs. The importance of the compressors for modern high bypass ratio engines is demonstrated by the fact that 50–60 % of the engine length and up to 40–50 % of the weight, 35–40 % of the manufacturing, and 30 % of the maintenance costs is covered by the compression system. The advances in compressors allow the aero engines to operate with core engine thermal efficiency in the range of 50 % while the propulsive efficiency approaches 80 % [4].

A typical axial compressor depicted in Fig. 9.15 has a series of rotating *rotor* blades followed by a stationary ‘stator’ set of blades that are concentric with the axis of rotation. The compressor blades/vanes are relatively flat in section. Each pair of rotors and stators is referred to as a *stage*. The stator blades are required in order to ensure reasonable efficiency; without them the gas would rotate with the rotor blades resulting in a large drop in efficiency. The axial compressor compresses the working fluid (here only air will be treated) by first accelerating the air and then diffusing it to obtain a static pressure increase. The air is accelerated in the rotor and then diffused in the stator. This is illustrated in Fig. 9.15 where the absolute velocity (*C*) increases in the rotor and decreases in the diffuser. For successive stages, a saw-teeth pattern for the velocity is obtained, while the static pressure continuously increases in both of the rotor and stator rows of all stages.

If the compressor is a part of turbofan engine, it is preceded by a row of inlet guide vanes (IGVs). Compressor will be ended by a final ring of stator blades (vanes) called the outlet guide vanes (OGVs), as they guide the flow to the axial direction to suit the compressor outlet. Typically, compressor casing is made of light weight titanium. However, in recent engines (like Pratt & Whitney 4084 engine), the casing is made of the ‘Thermax’ alloy of Inconel to allow for the expansion of the casing and keeping acceptable tip clearance margin. The rotor blades (like the stator ones) have airfoil section like the aircraft wing, but they are highly twisted from root to tip to obtain the optimum angle-of-attack to the flow everywhere along the blade length. The reason for that twist is that the root section

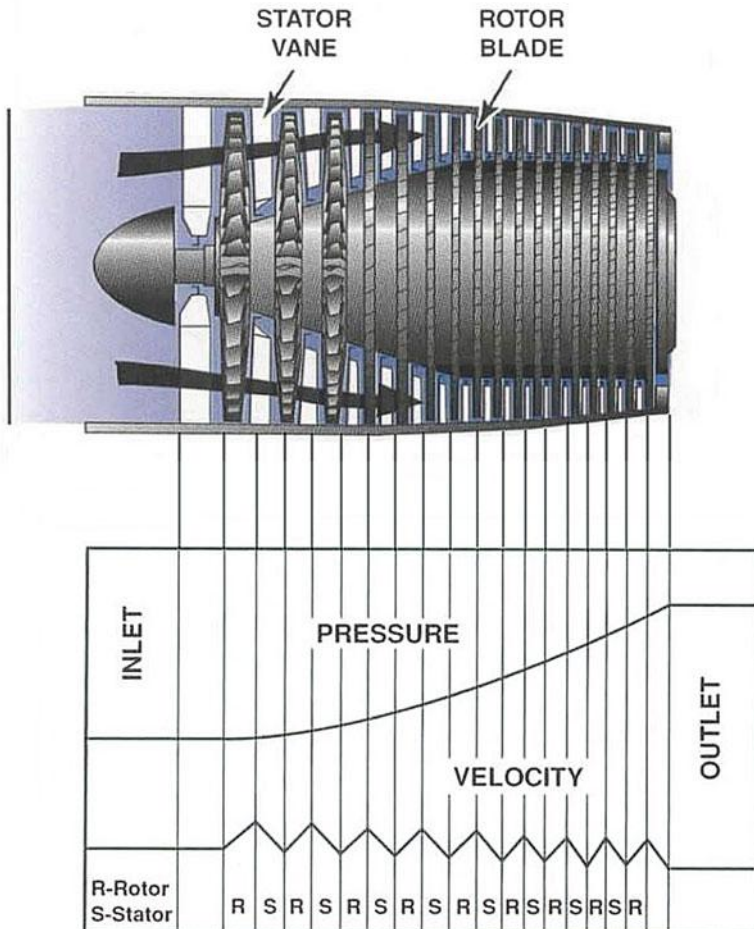


Fig. 9.15 Layout of an axial compressor

travels much slower than the tip section. Thus for a constant axial velocity, the relative velocity and angle change from root to tip.

The length of the blades decreases progressively downstream in the same proportion as the pressure increases. The rotor blades are attached by a dovetail root, pin fixing, fir tree, and straddle T root [13]. These sets of rotor are mounted on the rotor shaft through drums, individual discs, bolted discs, or clamped. The disks are assembled with a number of tie-bolts, with the bolt-circle diameter selected to produce a dynamically stiff rotor and good torque transmission. As the flow usually has a constant axial velocity through the compressor, the cross sectional area of the annular passage reduces towards the outlet (or from the front to the rear). This is due to the decrease of the volume of air (thus increasing the density) as compression progresses from stage to stage.

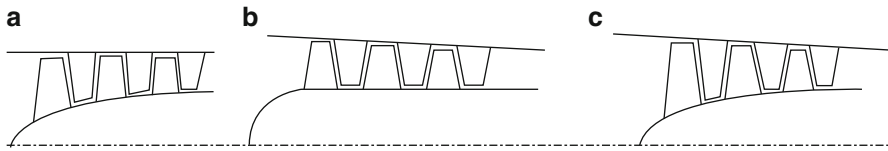


Fig. 9.16 Variations of the annulus section

Three different layouts are possible; Fig. 9.16. The first maintains a constant casing diameter and increasing the hub diameter of successive stages (9.16a). This design provides the maximum Mach number and pressure ratio. In the second pattern, the hub radius is kept constant and the casing diameter is increased, which provides the best geometry of a compressor (9.16b). The third pattern has a constant mean diameter, where the casing diameter is decreased and the hub diameter is increased (9.16c). This typical layout is generally employed in deriving the basic theory of axial compressors.

9.3.2 Comparison Between Axial and Centrifugal Compressors

The centrifugal compressor achieves part of the compression process by causing the fluid to move outward in the centrifugal force field produced by the rotation of the impeller. Thus the pressure rises due to the change in potential energy of the fluid in the centrifugal force field of the rotor. On the contrary, the pressure rise in axial flow compressor rotors and stators is achieved by the exchange of kinetic energy with thermal energy in a diffusion process. The pressure rise in a centrifugal compressor is therefore less limited by the problems of boundary layer growth and separation in adverse pressure gradients. For this reason, the centrifugal compressor first attained a range of pressure ratio and efficiency useful for turbojet engines and was used in the von Ohain engine (1939) and Whittle engine (1941).

The essential feature of air flow in the impeller of a centrifugal compressor is that all the fluid leaves the rotor at a constant radius rather than over a range of radii as in the axial compressor.

9.3.2.1 Advantages of the Axial-Flow Compressor Over the Centrifugal Compressor

1. Smaller frontal area for a given mass rate of flow (may be 1/2 or 1/3), thus the aerodynamic drag or nacelle housing the engine is smaller as shown in Fig. 9.17.
2. Much greater mass flow rates as seen in present day axial compressors for high bypass ratio turbofan engines [14]. In these cases mass flow rates may reach

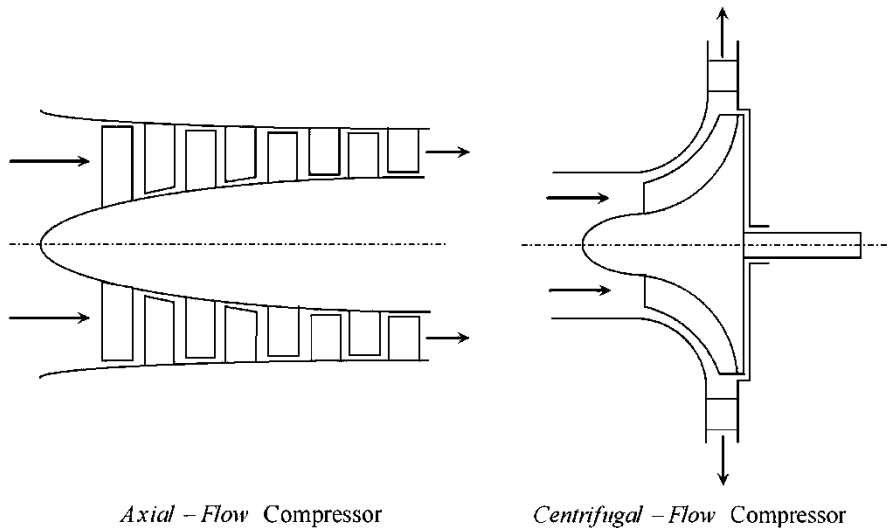


Fig. 9.17 Layouts of axial and centrifugal compressors

1000 kg/s, while centrifugal compressors have mass flow rates less than 100 kg/s.

3. Flow direction at discharge is more suitable for mitigating, thus suitable for large engines.
4. May use cascade experiment research in developing compressor.
5. Somewhat higher efficiency at high pressure ratio (perhaps 4–5 % higher than centrifugal compressor)
6. Higher maximum pressure ratio, which was about 17:1 in the 1960s and presently exceeded 50:1 and even reached 52 for the combined three compressors in RR Trent 1000 turbofan engines [14].

9.3.2.2 Advantages of Centrifugal-Flow Compressor Over the Axial-Flow Compressor

1. Higher stage pressure ratio (5:1 or even 10:1), while the maximum value for research axial stage is only 2.4:1
2. Simplicity and ruggedness of construction
3. Shorter length for the same overall pressure ratio
4. Generally, less severe stall characteristics
5. Less drop in performance with the adherence of dust to blades
6. Cheaper to manufacture for equal pressure ratio
7. Flow direction of discharge air is convenient for the installation of an intercooler and/or heat exchanger in gas turbines

8. Wider range (margin) of stable operation between surging and choking limits at a given rotational speed as shown in Fig. 9.18

9.3.2.3 Main Points for Comparison Between Centrifugal and Axial Compressors

Table 9.7 lists the main points for comparison between axial and centrifugal compressors.

9.3.3 Mean Flow (Two-Dimensional Approach)

The flow is considered occurring in the tangential plane at the mean blade height where the peripheral rotation velocity is U ; Fig. 9.19. This two-dimensional approach means that the flow velocity will have two velocity components one axial denoted by subscript (a) and one peripheral denoted by subscript (u). The radial velocity component is neglected here. The mean section for both of the axial compressor and axial turbine as shown in Fig. 9.19 illustrates that the hub-to-tip ratio of axial compressor is much smaller than its value in axial turbine.

For a constant mean radius, the velocity triangles at the inlet and outlet of a single stage are shown in Fig. 9.20. Subscript (1) denotes state of air upstream of the rotor, while symbol (2) denotes conditions downstream of rotor and upstream of

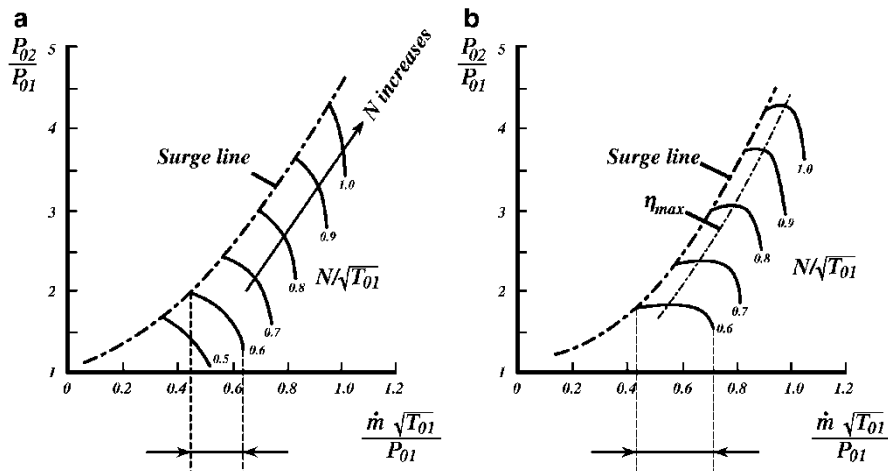


Fig. 9.18 Compressor maps for axial and centrifugal compressors: (a) Axial compressor map; (b) Centrifugal compressor map

Table 9.7 Comparison between axial and centrifugal compressors

	Axial compressor	Centrifugal compressor
Dimensions (frontal area)	Smaller	Larger
Dimensions (length)	Longer	Shorter
Number of blades per stage	Great	Less
Weight	Heavier	Lighter
RPM	Low	High
Efficiency	High (85 % or greater)	Moderate (75–80 %)
Pressure ratio per stage	Small (maximum of 2.4:1)	High (5:1–10:1)
Overall pressure ratio	Higher (30:1)	Much smaller (<10)
Mass flow rate	Higher ($\leq 10000 \text{ kg/s}$)	Smaller ($\leq 100 \text{ kg/s}$)
Flow direction at outlet	Axial	Radial
Manufacturing and its cost	Difficult and expensive	Simple and cheaper
Balance	Difficult	Easier
Construction	Complex	Simple
Rapid change of inlet mass flow	Cannot accept	Can accept
Maintenance and its cost	Difficult and expensive	Simple and cheap
Balancing	More difficult due to blade scatter effect	Easier owing to support bearings
FOD	Less resistant	Good resistant
Fouling	Greatly influenced	Less influenced
Reliability	Lower	Higher
Operating range (between choking and surge points)	Narrow	Wide
Ruggedness	Fragile	Strong
Material	<p><i>Rotor</i></p> <p>Front stages (steel alloy)</p> <p>Mid stages (aluminum alloy)</p> <p>Rear stages (titanium alloys)</p> <p>Drum or discs: steel</p> <p><i>Casing</i></p> <p>Magnesium alloy at the front</p> <p>Steel at the rear</p>	<p><i>Impeller</i> (aluminum alloy)</p> <p>Inlet section (steel)</p>
Application	All aero engines	Small aero engines and APU

stator. State (3) denotes conditions downstream of the stator of one stage and upstream of the rotor of next stage.

The air approaching the rotor with an absolute velocity (C_1) at an angle (α_1) to the axial direction when combined to the rotational speed (U) gives the relative velocity (W_1) at an angle (β_1) to the axial, refer to Fig. 9.20. After passing through

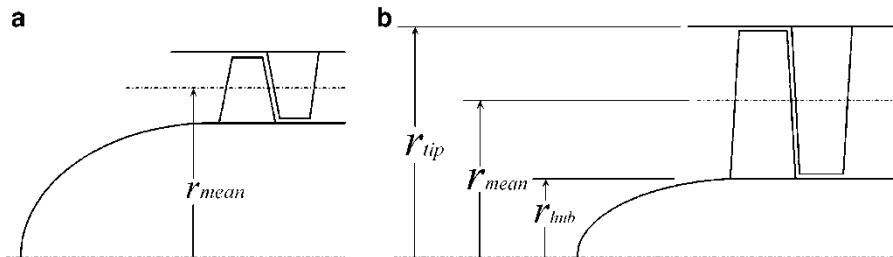


Fig. 9.19 Mean tangential plane for both axial compressor and axial turbine: (a) Axial turbine High hub to tip ratio (large r_h/r_t); (b) Axial compressor Low hub to tip ratio (small r_h/r_t)

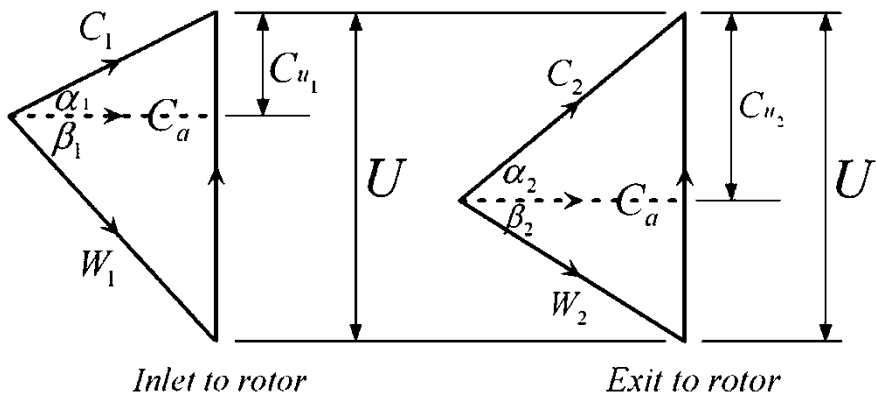


Fig. 9.20 Velocity triangles at the inlet and outlet of a constant mean radius stage

the diverging passages formed between the rotor blades which do work on the air, its absolute velocity (C_2) will increase ($C_2 > C_1$), while its relative velocity W_2 decreases ($W_2 < W_1$) and the flow exit angle β_2 will be less than the flow inlet angle β_1 , ($\beta_1 < \beta_2$). This turning of flow towards the axial direction is necessary to increase the effective flow area.

Since the relative velocity is decreased due to diffusion ($W_2 < W_1$), then the static pressure increases ($P_2 > P_1$), i.e., a pressure rise will be developed in the rotor.

The absolute velocity of the flow leaving the rotor is C_2 . The flow then passes through the stator passages which are also diverging, thus the absolute velocity is decreased due to diffusion and the static pressure is increased, i.e. $C_3 < C_2$ and $P_3 > P_2$. The flow angle at the outlet of the stator will be equal to the inlet angle to the rotor in most design cases, i.e. $\alpha_3 = \alpha_1$

From Fig. 9.20, the following kinematical relations are derived:

$$\frac{U}{C_{a_1}} = \tan \alpha_1 + \tan \beta_1 \quad (9.38a)$$

$$\frac{U}{C_{a_2}} = \tan \alpha_2 + \tan \beta_2 \quad (9.38b)$$

If the axial velocity is constant at inlet and outlet of the stage, then $C_{a1} = C_{a2} = C_a$.

The kinematical relations in Eqs. (9.38a) and (9.38b) will be

$$\frac{U}{C_a} = \tan \alpha_1 + \tan \beta_1 = \tan \alpha_2 + \tan \beta_2 \quad (9.38c)$$

9.3.3.1 Types of Velocity Triangles

The separate velocity triangles are superimposed either on the common base, namely, the blade rotational speed (U) or superimposed with a common apex, Fig. 9.21a. These velocity diagrams assume equal axial velocities at inlet and outlet, implying that the density is varying inversely with area. Figure 9.21b illustrates the case of variable inlet and outlet axial speeds.

In all cases, the term $(C_{u_2} - C_{u_1}) \equiv \Delta C_u$ represents the essential element in the energy transfer.

9.3.3.2 Variation of Enthalpy Velocity, and Pressure an Axial Compressor

The gain in energy of the air/gas in a compressor stage influences the different air parameters as described hereafter. The total enthalpy (and also the total temperature) increases in the rotor and remains constant in the stator. The total pressure increases in the rotor and slightly decreases in the stator due to friction. *Static* pressure (and static temperature) increase in both of the rotor and stator. The absolute velocity increases in the rotor and then decreases in the stator. For successive stages, the absolute speed has a saw shape as illustrated in Fig. 9.15.

The energy equation (or the first law of thermodynamics) is expressed in terms of the inlet and outlet conditions of a stage, states (1) and (3) respectively as

$$q_{13} + h_{01} = w_{13} + h_{03}$$

Since an adiabatic process is assumed ($q_{13} = 0$), then the change in total enthalpy will be equal to the work done on the rotor, or

$$\Delta h_0 = U_2 C_{u2} - U_1 C_{u1} \quad (9.39a)$$

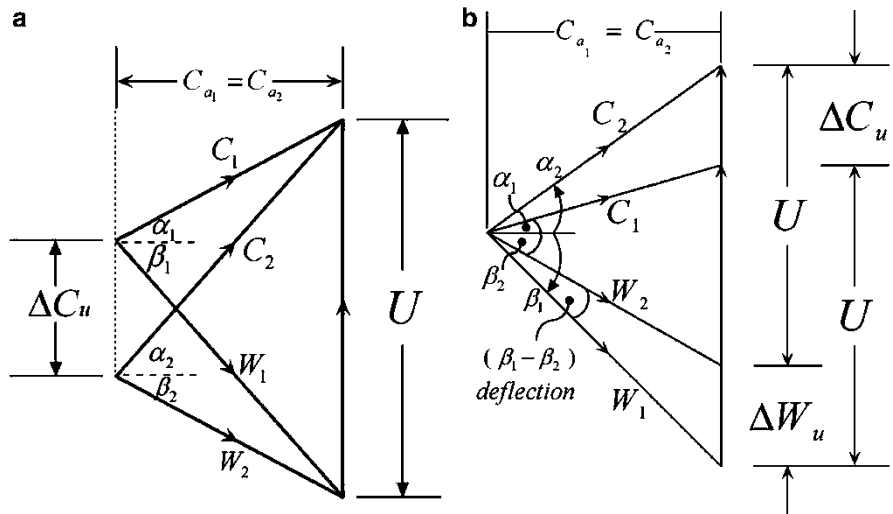


Fig. 9.21a Common base velocity triangles: (a) Combined velocity diagram with common base; (b) Combined velocity diagram with common apex

$$\Delta h_0 = U_2 C_{a2} \tan \alpha_2 - U_1 C_{a1} \tan \alpha_1 \quad (9.39b)$$

For an axial compressor, with constant mean radius at inlet and outlet of the rotor, or $U_1 = U_2 = U$, and $C_{a1} = C_{a2}$, then Euler's equation for turbomachinery is again expressed for axial compressors as

$$\Delta h_0 = U(C_{u2} - C_{u1}) = w_{13} \quad (9.40)$$

All the energy transfer between the fluid and rotor accounted for by the difference between the two (UC_u) terms. Now from the velocity triangles shown in Figs. 9.21a and 9.21b, Euler equation can be mathematically expressed in different form.

$$\begin{aligned} C_a^2 &= C^2 - C_u^2 \\ W_a^2 &= W^2 - W_u^2 = W^2 - (U - C_u)^2 \end{aligned}$$

Since

$$\begin{aligned} C_a &= W_a \\ \therefore C^2 - C_u^2 &= W^2 - U^2 + 2UC_u - C_u^2 \\ \therefore UC_u &= \frac{1}{2}(C^2 + U^2 - W^2) \\ \therefore U_1 C_{u1} &= \frac{1}{2}(C_1^2 + U_1^2 - W_1^2) \\ U_2 C_{u2} &= \frac{1}{2}(C_2^2 + U_2^2 - W_2^2) \end{aligned}$$

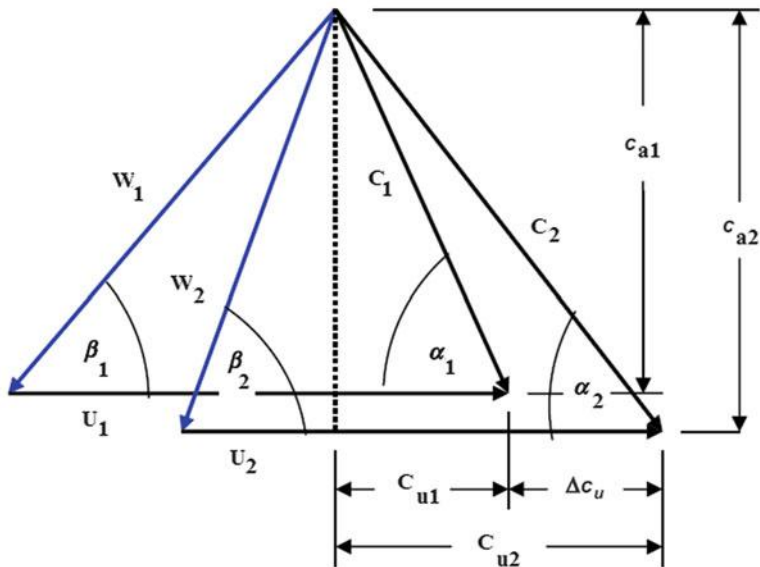


Fig. 9.21b Combined velocity triangles with a common apex and variable axial speed velocity triangles

$$\begin{aligned}\therefore \Delta h_0 &= (UC_u)_2 - (UC_u)_1 \\ \therefore \Delta h_0 &= \frac{1}{2} (C_2^2 - C_1^2 + U_2^2 - U_1^2 + W_1^2 - W_2^2)\end{aligned}\quad (9.41)$$

This equation is an alternative form of the basic energy by definition. The total and static enthalpies are correlated by the relation:

$$\begin{aligned}\Delta h_0 &= h_{02} - h_{01} = h_2 + \frac{C_2^2}{2} - h_1 - \frac{C_1^2}{2} \\ \therefore \Delta h &= h_2 - h_1 = \frac{1}{2} (U_2^2 - U_1^2 + W_1^2 - W_2^2)\end{aligned}\quad (9.42)$$

From Eq. (9.40), the specific work input is equal to the change in the total enthalpy across the stage, or

$$w_s \equiv w_{13} \equiv \Delta h_0 \equiv h_{03} - h_{01} \equiv h_{02} - h_{01} = U(C_{u2} - C_{u1}) = C_p \Delta T_0$$

where h_0 is the total enthalpy, or

$$\begin{aligned}w_s &= \Delta h_0 = C_p(T_{03} - T_{01}) = C_p \Delta T_0 = U \Delta C_u \\ \therefore \Delta T_0 &= \frac{U \Delta C_u}{C_p}\end{aligned}$$

or

$$\frac{\Delta T_0}{T_{01}} = \frac{U \Delta C_u}{C_p T_{01}} \quad (9.43)$$

ΔC_u can be expressed in the following three forms:

$$\Delta C_u \equiv C_{u2} - C_{u1} = C_{a2} \tan \alpha_2 - C_{a1} \tan \alpha_1$$

Or

$$\Delta C_u = C_{a2} \tan \beta_1 - C_{a1} \tan \beta_2$$

Or

$$\Delta C_u = U - (C_{a1} \tan \alpha_1 + C_{a2} \tan \beta_2)$$

If

$$C_{a1} = C_{a2} = C_a$$

$$\therefore \Delta C_u = U \left[1 - \frac{C_a}{U} (\tan \alpha_1 + \tan \beta_2) \right] \text{ or}$$

$$\Delta C_u = C_a (\tan \beta_1 - \tan \beta_2) \equiv C_a (\tan \alpha_2 - \tan \alpha_1)$$

The stage temperature rise is now expressed as

$$\Delta T_0 = \frac{UC_a}{C_p} (\tan \alpha_2 - \tan \alpha_1) = \frac{UC_a}{C_p} (\tan \beta_1 - \tan \beta_2) \quad (9.44a)$$

and

$$\frac{\Delta T_0}{T_{01}} = \frac{U^2}{C_p T_{01}} \left[1 - \frac{C_a}{U} (\tan \alpha_1 + \tan \beta_2) \right] \quad (9.45a)$$

or

$$\frac{\Delta T_0}{T_{01}} = \frac{UC_a}{C_p T_{01}} (\tan \beta_1 - \tan \beta_2) = \frac{UC_a}{C_p T_{01}} (\tan \alpha_2 - \tan \alpha_1) \quad (9.45b)$$

The specific work is also given by the relation:

$$w_s = UC_a (\tan \alpha_2 - \tan \alpha_1) = UC_a (\tan \beta_1 - \tan \beta_2) \quad (9.46)$$

Figure 9.22 illustrates the Mollier chart (temperature–entropy) variation for the compression process through the stage. If the whole processes were isentropic, the final stagnation pressure for the same work input would be $P_{0\max}$. However, due to losses in the rotor and stator, the pressure at the outlet of the rotor is less than the maximum value and the pressure for air leaving the stator is also less than the pressure at the outlet of the rotor, or $P_{03} < P_{02} < P_{0\max}$.

If the stage total-to-total efficiency (η_{st}) is defined as:

$$\eta_{st} = \frac{h_{03ss} - h_{01}}{h_{03} - h_{01}}$$

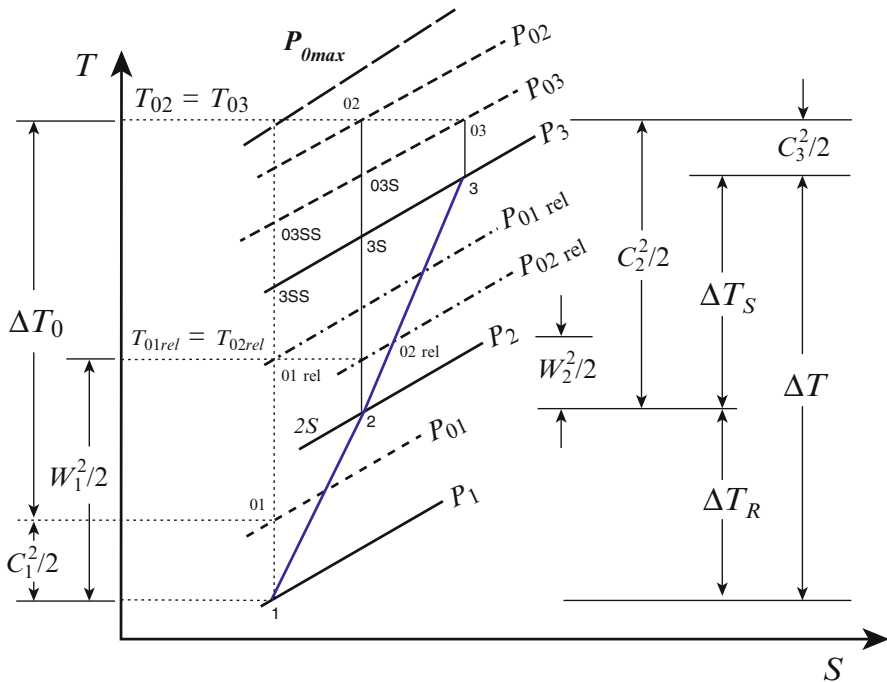


Fig. 9.22 Temperature-entropy diagram for a compressor stage

$$\therefore \eta_{st} = \frac{T_{03ss} - T_{01}}{T_{03} - T_{01}} = \frac{T_{03ss} - T_{01}}{\Delta T_0} = \frac{\frac{T_{03ss}}{T_{01}} - 1}{\frac{\Delta T_0}{T_{01}}}$$

$$\therefore \frac{T_{03ss}}{T_{01}} - 1 = \eta_{st} \frac{\Delta T_0}{T_{01}}$$

Since $\frac{P_{03}}{P_{01}} = \left(\frac{T_{03ss}}{T_{01}} \right)^{\frac{\gamma}{\gamma-1}}$

Then $\pi_{\text{stage}} = \frac{P_{03}}{P_{01}} = \left(1 + \eta_{st} \frac{\Delta T_0}{T_{01}} \right)^{\frac{\gamma}{\gamma-1}}$

But $\left(\frac{\Delta T_0}{T_{01}} \right)_{\text{stage}} = \frac{UCa}{CpT_{01}} (\tan \alpha_2 - \tan \alpha_1)$

Then $\pi_{\text{stage}} = \left[1 + \eta_{st} \frac{UCa (\tan \alpha_2 - \tan \alpha_1)}{CpT_{01}} \right]^{\frac{\gamma}{\gamma-1}} \quad (9.47a)$

In actual stage, temperature rise will be less than the above value due to the three dimensional (3D) effects in compressor annulus. Axial velocity changes both in the

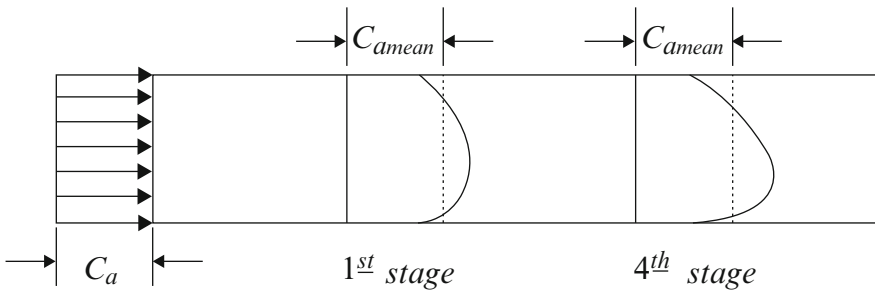


Fig. 9.23 Variations of the axial velocity through successive stages

radial direction for any stage (from root to tip of blades) as well as in the axial direction from one stage to another.

Analysis of experimental results showed that it is necessary to multiply the changes in swirl velocity (ΔC_u) by a factor less than unity identified as the *work done factor* (λ). The axial velocity is peaky as the flow proceeds, setting down to a fixed profile at about fourth stage, as shown in Fig. 9.23. The value of the work done factor starts by 0.98 for the first stage and decreases to 0.93 and 0.88 for the second and third stages, respectively. For the fourth and subsequent stages, its value is constant and equals 0.83.

The stage temperature rise pressure ratio, Eq. (9.47a) should be modified to be:

$$\therefore \Delta T_0 = \frac{\lambda}{C_p} UC_a (\tan \alpha_2 - \tan \alpha_1) = \frac{\lambda}{C_p} UC_a (\tan \beta_1 - \tan \beta_2) \quad (9.44b)$$

$$\pi_S = \left[1 + \frac{\lambda \eta_{st}}{C_p T_{01}} UC_a (\tan \alpha_2 - \tan \alpha_1) \right]^{\frac{\gamma}{\gamma-1}} \quad (9.47b)$$

Thus the pressure ratio across the stage could be determined. For a single stage axial compressor, the temperature rise for efficient operation is always limited as $(\Delta T_0/T_{01}) \ll 1$. Then Eq. (9.47b) may be approximated to:

$$\frac{P_{03}}{P_{01}} = \pi_{stage} \approx 1 + \frac{\gamma}{\gamma-1} \eta_{st} \frac{\Delta T_0}{T_{01}} = 1 + \frac{\gamma}{\gamma-1} \lambda \eta_{st} \frac{UC_a}{C_p T_{01}} (\tan \alpha_2 - \tan \alpha_1) \quad (9.47c)$$

It is highly desirable to achieve high work input per compressor stage in order to minimize the total number of stages necessary to provide the desired overall compression ratio.

Example 9.5 Air at 1 bar and 15 °C enters a three stage axial compressor with a velocity of 120 m/s. There are no inlet guide vanes, and flow enters axially to all stages and has a constant axial velocity throughout. In each stage, the rotor turning angle is 25°. The annular flow passages are shaped so that the mean blade radius

everywhere is 20 cm. The rotor speed is 9000 rpm. The polytropic efficiency is constant at 0.9. The blade height at the inlet is 5 cm.

Draw the velocity triangles and ignoring work done factor *calculate*:

1. Specific work for each stage
2. The mass flow rate
3. The power necessary to run the compressor
4. Pressure ratio for each stage
5. The overall compressor pressure ratio
6. The blade height at the exit from the third stage

Solution

1. The given data are: $P_{01} = 1$ bar, $r_m = 0.2$ m, $N = 9000$ r.p.m, $\eta_s = 0.9$, $\beta_1 - \beta_2 = 25^\circ$, $h_{\text{inlet}} = 0.05$ m, Number of stages = 3, $C_1 \equiv C_{a1} = 120$ m/s,

Since the flow is axial in all stages, then $\alpha_1 = \text{zero}$, $C_{u1} = \text{zero}$, $\Delta C_u = C_{u2}$

The inlet total temperature is $T_{01} = 15 + 273 = 288$ K with $U_m = 2\pi r_m N = 188.496$ m/s

$$\text{then } \tan \beta_1 = \frac{U}{C_{a1}}$$

$$\beta_1 = 57.52^\circ = \text{constant for all stages}$$

$$\beta_2 = \beta_1 - 25 = 32.52^\circ = \text{constant also for all stages, then}$$

since

$$\tan \beta_2 = \frac{U - C_{u2}}{C_{a2}}$$

then

$$C_{u2} = 111.989 \text{ m/s} \equiv \Delta C_u$$

The axial compressor is composed of three identical stages having same identical velocity triangles as shown in Fig. 9.24. Thus the temperature rise per stage as well as the specific work is constants for the three stages.

The specific work per stage is

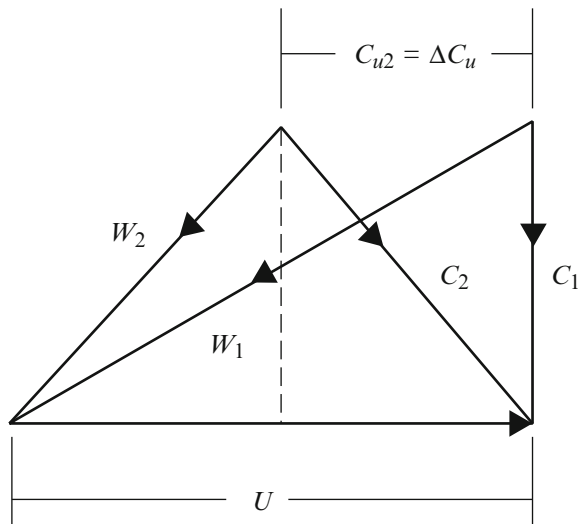
$$w_s = U \Delta C_u = 21.11 \text{ kJ/kg} \equiv \text{Constant for all stages}$$

$$[\text{or } w_s = U \Delta C_u = UC_a (\tan \beta_1 - \tan \beta_2) = 21.11 \text{ Constant for all stages}]$$

$$[\text{or } w_s = U \Delta C_u = UC_a (\tan \beta_1 - \tan \beta_2) = 21.11 \text{ kJ/kg}]$$

The specific work for the whole compressor is $W_s = 3w_s = 3 \times 21.11 = 63.33$ kJ/kg

Fig. 9.24 Velocity triangles for all stages



$$2. \text{ The mass flow rate } \dot{m} = \rho_1 C_{a1} A_1$$

At the compressor inlet, the static temperature: $T_1 = T_{01} - \frac{C_1^2}{2C_p} = 280.836 \text{ K}$ and the static pressure: $P_1 = \frac{P_{01}}{\left(\frac{T_{01}}{T_1}\right)^{\frac{\gamma-1}{\gamma}}} = 0.916 \text{ bar}$

$$\text{The density } \rho_1 = \frac{P_1}{RT_1} = 1.136 \text{ kg/m}^3$$

$$\text{The annulus area } A = 2\pi r_m h = 0.0628 \text{ m}^2$$

$$\therefore \dot{m} = \rho_1 C_{a1} A = 8.565 \text{ kg/s}$$

$$3. \text{ Total Power} = \dot{m} W_S = 542.42 \text{ kW}$$

$$4. \text{ The temperature rise per stage is } \Delta T_{0S} = \frac{w_s}{C_p} = 21 \text{ K} \equiv \text{Constant for all stages}$$

Pressure ratio of stage # 1

$$\pi_1 = \left(1 + \eta_s \frac{\Delta T_{0S}}{T_{01}}\right)^{\frac{\gamma}{\gamma-1}=1.249}$$

Pressure ratio of stage # 2

$$\pi_2 = \left(1 + \eta_s \frac{\Delta T_{0S}}{T_{01} + \Delta T_{0S}}\right)^{\frac{\gamma}{\gamma-1}=1.231}$$

Pressure ratio of stage # 3

$$\pi_3 = \left(1 + \eta_s \frac{\Delta T_{0S}}{T_{01} + 2\Delta T_{0S}} \right)^{\gamma/\gamma-1=1.215}$$

1. Overall pressure ratio $\pi_{\text{comp}} = \pi_1 \times \pi_2 \times \pi_3 = 1.87$
2. The pressure at the outlet of the compressor is $P_{03})_{S3} = \pi_C \times P_{01})_{S1} = 1.87 \text{ bar}$
The temperature at the exit of the compressor is $T_{03})_{S3} = T_{01})_{S1} + 3\Delta T_{0S} = 351 \text{ K}$

With $C_3 = C_1$

$$T_3)_{S3} = T_{03})_{S3} - \frac{C_3^2}{2Cp} = 343.836 \text{ K}$$

$$P_3)_{S3} = \frac{P_{03})_{S3}}{\left[(T_3/T_{03})^{\gamma/\gamma-1} \right]_{S3}} = 1.74 \text{ bar}$$

$$\rho_3 = \frac{P_3}{RT_3})_{S3} = 1.763 \text{ kg/m}^3$$

Since $\dot{m} = (\rho_3 C_3 A_3)_{S3} = [\rho_3 C_3 (2\pi r_m h_3)]_{S3}$
then $(h_3)_{S3} = 3.2 \text{ cm}$

9.3.4 Basic Design Parameters

The pressure ratio per stage is expressed by the relation:

$$\pi_s = \left[1 + \eta_s \frac{\lambda UC_a}{CpT_{01}} (\tan \beta_1 - \tan \beta_2) \right]^{\gamma/\gamma-1}$$

To obtain high pressure ratio per stage it is needed to have

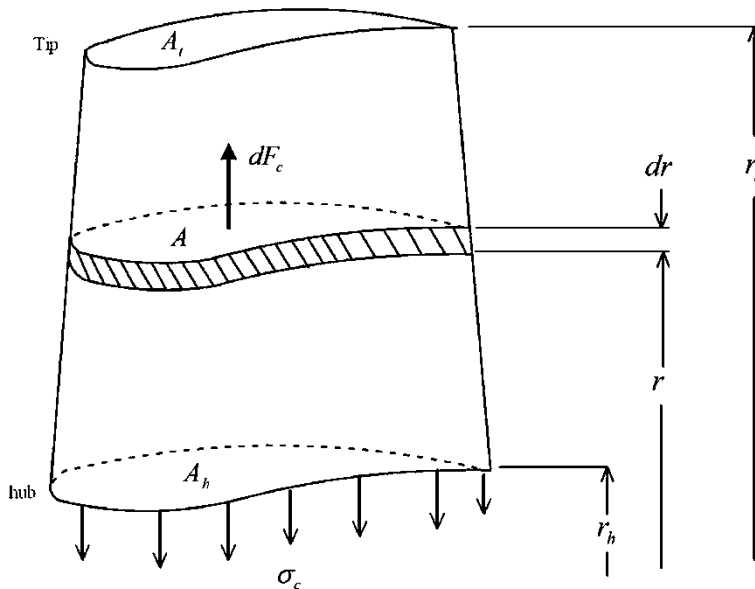
1. High blade speed (U)
2. High axial velocity (C_a)
3. High fluid deflection $\beta_1 - \beta_2$ in the rotor blade
4. High stage efficiency

However, the increase in the rotational speed is limited by the maximum acceptable tensile stress at the rotor hub. Furthermore, the increase in the rotational and axial velocities; (U and C_a) is limited by the tip Mach number. Compressors of the 1960s had a maximum tip Mach number less than 0.8 which has nearly been doubled for the present transonic compressors; 1.4–1.7 [15]. The fluid deflection has upper limits determined by the diffusion factor or de Haller parameters. Stage efficiency has several loss limitations.

9.3.4.1 Centrifugal Stress

Centrifugal stress depends on the rotational speed (ω), blade material density (ρ_b), and height of blade. The maximum centrifugal stress occurs in the root. As shown in Fig. 9.25, the centrifugal force arising from any element of blade is evaluated as:

$$dF_c = \omega^2 r \delta m$$



Centrifugal stress

Fig. 9.25 Nomenclature for centrifugal stress on a rotor blade

where (ω) and (r) are the rotational speed and the radius of any blade element having a mass of (δm) and length of (dr).

$$\delta m = \rho_b A dr$$

Then the maximum centrifugal stress at the root is the summation of the centrifugal forces of all the elements of the blade from the hub to the tip divided by the blade cross sectional area at the root, or

$$\begin{aligned} (\sigma_c)_{\max} &= \frac{\omega^2}{A_{\text{root}}} \int_{r_h}^{r_t} r \delta m \\ &= \frac{\rho_b \omega^2}{A_{\text{root}}} \int_{r_h}^{r_t} r A dr \end{aligned} \quad (9.48)$$

Special Cases

1. The blade has a *constant area* (A) along the blade height then the maximum stress will be

$$(\sigma_c)_{\max} = \frac{\rho_b}{2} (2\pi N)^2 (r_t^2 - r_r^2)$$

$$\sigma_{\max} = 2\pi N^2 \rho_b A$$

Where $A = \pi (r_t^2 - r_r^2)$ = annulus area

$$\begin{aligned} U_t &= \omega r_t = 2\pi N r_t \\ (\sigma_c)_{\max} &= \frac{\rho_b U_t^2}{2} \left[1 - \left(\frac{r_r}{r_t} \right)^2 \right] \end{aligned}$$

or

$$\begin{aligned} (\sigma_c)_{\max} &= \frac{\rho_b U_t^2}{2} [1 - \zeta^2] \\ \text{where } \zeta &= \frac{r_r}{r_t} \end{aligned} \quad (9.49)$$

2. For *linear variation* of cross sectional area with radius

$$\begin{aligned} (\sigma_{ct})_{\max} &= \frac{\rho_b U_t^2}{2} (1 - \zeta^2) K & (9.50) \\ K &= 1 - \frac{(1-d)(2-\zeta-\zeta^2)}{3(1-\zeta^2)} \end{aligned}$$

where $d = A_{\text{tip}}/A_{\text{root}}$ and $K = 0.55 - 0.65$ for tapered blades

3. If the area is *inversely proportional* to the radius, or $A = \frac{\text{constant}}{r}$

$$\text{since } r_r A_r = r_t A_t = r A = K$$

$$\begin{aligned} \therefore \sigma_{c_{\max}} &= \frac{\rho_b \omega^2}{A_r} \int_{r_r}^{r_t} r A dr = \frac{\rho_b \omega^2 K}{A_r} \int_{r_r}^{r_t} dr \\ \sigma_{c_{\max}} &= \rho_b U_t^2 (\zeta - \zeta^2) = \rho_b U_t^2 \zeta (1 - \zeta) & (9.51) \end{aligned}$$

The same equations are applied for both fans and compressors. For fans, the blade height is long which develops large tip rotational speed and the hub-to-tip ratio is small, thus high tensile stresses are expected at blade root.

9.3.4.2 Tip Mach Number

For different compressor layouts (Fig. 9.16), the maximum Mach number in the axial compressor occurs at the blade tip of the rotor inlet of the first stage. This is due to the maximum value of relative speed (W_1) and the minimum static temperature and so sonic speed at inlet. For the first stage, the axial velocity is equal to the inlet absolute velocity and has a constant value along the annulus. The corresponding maximum Mach number is

$$\begin{aligned} M_{tip} = M_{1_{\max}} &= \frac{W_{1_{\max}}}{a} = \frac{\sqrt{C_1^2 + U_{tip}^2}}{\sqrt{\gamma R T_1}} = \sqrt{\frac{C_1^2 + U_{tip}^2}{\gamma R \left(T_{01} - \frac{C_1^2}{2C_p}\right)}} \\ M_{1_{\max}} &= U_{tip} \sqrt{\frac{\left(C_1/U_{tip}\right)^2 + 1}{\gamma R \left(T_{01} - \frac{C_1^2}{2C_p}\right)}} & (9.52) \end{aligned}$$

Thus from Eq. (9.52), for a specified tip Mach number and rotational speed, the axial velocity at inlet can be determined.

For a transonic compressor, an acceptable value for the maximum Mach number at the tip is $M_{1_{\max}} \cong 1.3$, while for the fan in turbofan engines much higher Mach

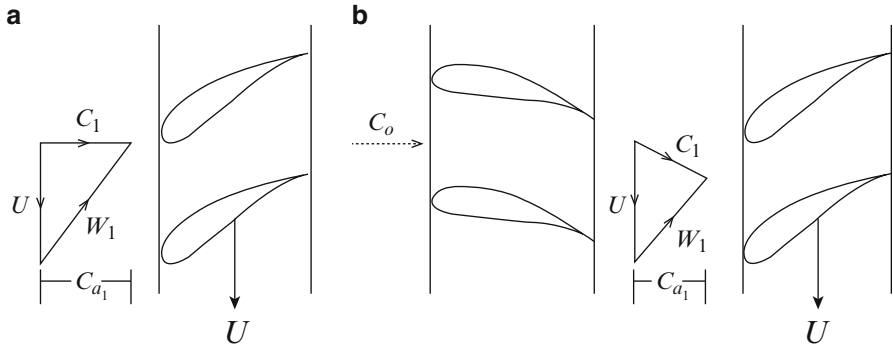


Fig. 9.26 Inlet velocity triangle with and without inlet guide vanes: (a) Rotor without IGV; (b) Rotor with IGV

number is expected and allowed, thus $M_{1\text{tip}} = 1.5 - 1.7$. A challenging design is to increase the rotational speed U and keep the Mach number within the acceptable limits. This is achieved by adding inlet guide vanes (an additional row of stator vanes) upstream of the first stage of the compressor as shown in Fig. 9.26 to add a swirl component to the inlet speed (C_1) and thus reduces the relative speed (W_1). Note that the passages of the inlet guide vanes are *nozzles* to increase the absolute speed ($C_1 > C_0$) and thus keeps a constant axial velocity C_a

The maximum relative Mach number at rotor tip is

$$(M_{1\text{rel}})_{\max} = \frac{W_{1\max}}{\sqrt{\gamma RT_1}} = \sqrt{\frac{(U - C_1 \sin \alpha_1)^2 + (C_1 \cos \alpha_1)^2}{\gamma R \left(T_{01} - \frac{C_1^2}{2C_p}\right)}}$$

where α_1 is the angle between the absolute velocity and axial direction. Thus the maximum relative Mach number can be rewritten as:

$$(M_{1\text{rel}})_{\max} = \sqrt{\frac{U^2 + C_1^2 - 2UC_1 \sin \alpha_1}{\gamma R \left(T_{01} - \frac{C_1^2}{2C_p}\right)}} \quad (9.53)$$

9.3.4.3 Fluid Deflection

By fluid deflection, it is meant the difference between the outlet and inlet angles; $(\beta_2 - \beta_1)$ for the rotor and $(\alpha_3 - \alpha_2)$ for a stator. Excessive deflection which means a high rate of diffusion will lead to blade stall. To maximize the specific work, the difference between the flow angles in the rotor must attain its maximum allowable value. If the inlet relative velocity maintains a constant angle (β_1), then the outlet relative angle (β_2) will control stall or install conditions. Since a constant axial

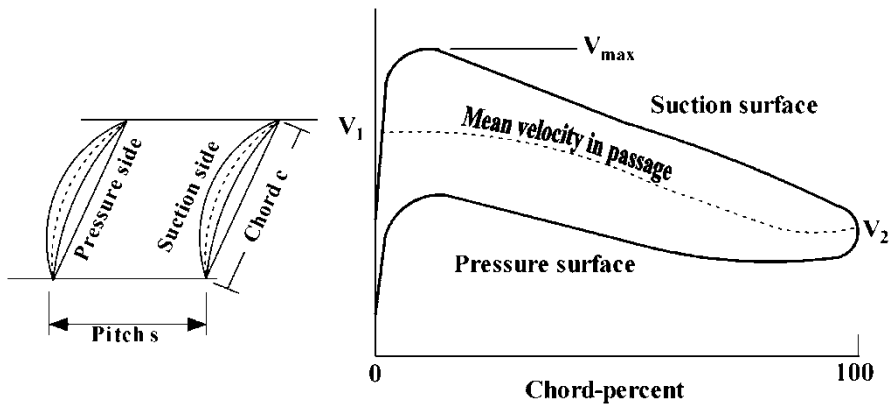


Fig. 9.27 Velocity distribution in the passage of a cascade

velocity is assumed, then the relative angle is a measure of the magnitude of the relative velocities (W_1, W_2). Thus a criterion known as the *diffusion factor* (DF) developed by NACA is adopted [15]. Another and earlier method for assessing the diffusion was the *de Haller number*, defined as, V_2/V_1 . The limit for installed operation is ($V_2/V_1 < 0.72$). Because of its simplicity, it is still used until now in preliminary design. However, for final design calculations, the *diffusion factor* (DF) is preferred. The velocity distribution over the suction and pressure sides of a typical passage of cascade is shown in Fig. 9.27. The velocities V_1, V_2, V_{\max} are respectively the velocities at the inlet and outlet of the cascade as well as the maximum velocity over the suction surface. The diffusion factor (DF) is defined as:

$$DF \approx \frac{V_{\max} - V_2}{V_1} \approx 1 - \frac{V_2}{V_1} + \frac{\Delta C_u}{2\sigma V_1} \quad (9.54a)$$

where $\sigma = \frac{c}{s}$ is the solidity

A more precise expression if the mean radii at the inlet and outlet of the blade are not equal is expressed as [16]:

$$DF = 1 - \frac{V_2}{V_1} + \frac{\Delta(rC_u)}{2\sigma r V_1} \quad (9.54b)$$

Values of DF in excess of 0.6 are thought to indicate blade stall and a value of 0.45 might be taken as a typical design choice [16].

For both rotor and stator, Eq. (9.54) can be expressed as:

$$(DF)_r = 1 - \frac{W_2}{W_1} + \frac{\| W_{u2} - W_{u1} \|}{2\sigma_r W_1} \quad (9.54c)$$

$$(DF)_s = 1 - \frac{C_3}{C_2} + \frac{\| C_{u3} - C_{u2} \|}{2\sigma_s C_2} \quad (9.54d)$$

Example 9.6 Air enters axially the first stage of an axial compressor with velocity ($C_1 \equiv C_{a1}$). The rotor blade has a constant cross sectional area from hub to tip. The maximum inlet relative Mach number at rotor tip is expressed by the relation:

$$M_{1\max} \equiv \frac{W_{1t}}{\sqrt{\gamma RT_1}}$$

- (A) It is required to prove that the maximum stress at blade root is expressed by the relation:

$$\sigma_{\max} = \frac{1}{2} \rho_b (1 - \zeta^2) \left[\gamma R M_{1\max}^2 \left(T_{01} - \frac{C_1^2}{2Cp} \right) - C_1^2 \right]$$

where the rotor blade material density is (ρ_b), hub-to-tip ratio is (ζ), and the inlet total temperature is (T_{01}).

- (B) If the rotor is manufactured from *Hot Rolled Steel Alloy G10950* having the following properties $\rho_b = 3000 \text{ kg/m}^3$, $\zeta = 0.5$, and the air flow properties are

$$M_{1\max} = 1.2, T_{01} = 300 \text{ K}, C_1 = 100 \text{ m/s},$$

Calculate the maximum stress at blade root (σ_{\max})

- (C) Calculate the factor of safety, if the rotor yield strength is $S_y = 460 \text{ MPa}$

Solution

Maximum Mach number is at tip section:

$$M_{1\max} \equiv \frac{W_{1t}}{\sqrt{\gamma RT_1}}$$

$$\text{Thus } M_{1\max}^2 \equiv \frac{W_{1\text{tip}}^2}{\gamma RT_1}, \text{ with } T_1 = T_{01} - \frac{C_1^2}{2Cp}$$

$$\gamma R M_{1\max}^2 = \frac{W_{1\text{tip}}^2}{T_{01} - \frac{C_1^2}{2Cp}} = \frac{C_1^2 + U_t^2}{T_{01} - \frac{C_1^2}{2Cp}}$$

$$U_t^2 = \gamma R M_{1\max}^2 \left(T_{01} - \frac{C_1^2}{2Cp} \right) - C_1^2 \quad (\text{a})$$

The stress for a constant cross sectional rotor blade is expressed by Eq. (9.49), namely:

$$\sigma = \frac{1}{2} \rho_b U_t^2 (1 - \zeta^2) \quad (\text{b})$$

From (a) and (b), then the maximum stress at the blade root is:

$$\sigma = \frac{1}{2} \rho_b (1 - \zeta^2) \left[\gamma R M_{1\max}^2 \left(T_{01} - \frac{C_1^2}{2C_p} \right) - C_1^2 \right] \quad / \text{Ans.}/$$

Substituting by the given data, then:

$$\begin{aligned} \sigma &= \frac{1}{2} \times 3000 \times (1 - 0.25) \left[1.4 \times 287 \times 1.44 \left(300 - \frac{100^2}{2 \times 1005} \right) - 100^2 \right] \\ \sigma &= 180.786 \text{ MPa} \end{aligned}$$

Since the yield strength is $S_y = 460$ MPa

Then, the factor of safety is f.o.s = $\frac{S_y}{\sigma} = \frac{460}{180.786} = 2.544$

9.3.5 Design Parameters

The following three design parameters are frequently used in the parametric study of a repeating axial stage:

1. Flow coefficient ϕ
2. Stage loading Ψ
3. Degree of reaction Λ

The *flow coefficient* is defined as the ratio between the axial and the rotational speeds, or,

$$\phi = \frac{C_a}{U} \quad (9.55)$$

The *stage loading* is defined as the ratio between the total enthalpy rise per stage to the square of the rotational speed, or

$$\psi = \frac{\Delta h_0}{U^2} = \frac{w_s}{U^2} = \frac{\Delta C_u}{U} \quad (9.56)$$

The *degree of reaction* of a compressor stage has several definitions. For an incompressible flow, the degree of reaction is defined as the ratio of the static pressure rise in the rotor to the static pressure rise in the stage [17], or

$$\Lambda = \frac{p_2 - p_1}{p_3 - p_1}$$

For a compressible flow, the degree of reaction is defined as the ratio of the static enthalpy (or temperature) rise in the rotor to the enthalpy (or temperature) rise in the whole stage, or

$$\Lambda = \frac{h_2 - h_1}{h_3 - h_1} = \frac{\Delta T_R}{\Delta T_R + \Delta T_S} \quad (9.57)$$

A third definition [18] states that the degree of reaction is equal to the change of the static enthalpy rise across the rotor as a fraction of the change in the absolute enthalpy rise in a stage, $\Lambda = \frac{h_2 - h_1}{h_{03} - h_{01}} = \frac{h_2 - h_1}{h_{02} - h_{01}}$

The expression given in Eq. (9.57) will be only employed in this book.

The following general relation will be derived for the degree of reaction assuming that the axial velocities are not equal ($C_{a2} \neq C_{a1}$); Fig. 9.21b. Since the absolute velocities at the inlet and outlet of the stage are assumed equal, i.e., $C_1 = C_3$, then the static and total temperature rise in a stage are also equal, or $\Delta T = \Delta T_0$. The temperature rise in the stage is

$$\Delta T \equiv \Delta T_0 = \frac{U(C_{u2} - C_{u1})}{C_p}$$

As known, the rothalpy (I) is defined as $I = h_{0\text{rel}} - \frac{1}{2}U^2$

where

$$h_{0\text{ rel}} = h + \frac{W^2}{2}$$

Since equal mean radii at rotor inlet and inlet is assumed, i.e., $U_2 = U_1$, and $h_{01\text{rel}} = h_{02\text{rel}}$, then the rothalpy at rotor inlet and outlet is equal: $I_2 = I_1$

Or

$$h_1 + \frac{1}{2}W_1^2 = h_2 + \frac{1}{2}W_2^2$$

The temperature rise within the rotor is

$$\Delta T_R = T_2 - T_1 = \frac{W_1^2 - W_2^2}{2C_p}$$

With

$$W^2 = C_a^2 + (U - C_u)^2$$

$$\Delta T_R = \frac{C_{a1}^2 + (U - C_{u1})^2 - C_{a2}^2 - (U - C_{u2})^2}{2C_p}$$

$$\Delta T_R = \frac{C_{a1}^2 - C_{a2}^2 + 2U(C_{u2} - C_{u1}) - C_{u2}^2 + C_{u1}^2}{2C_p}$$

The degree of reaction is then

$$\Lambda = 1 + \frac{C_{a1}^2 - C_{a2}^2}{2U(C_{u2} - C_{u1})} - \frac{C_{u1} + C_{u2}}{2U} \quad (9.58a)$$

When the axial velocities at rotor inlet and outlet are assumed equal, then $C_{a2} = C_{a1}$, then Eq. (9.58a) is reduced to the following relation

$$\Lambda = 1 - \frac{C_{u1} + C_{u2}}{2U} \quad (9.58b)$$

In terms of the flow angles, then Eq. (9.58b) may be rewritten as

$$\Lambda = 1 - \frac{C_a}{2U} (\tan \alpha_1 + \tan \alpha_2) = 1 - \frac{\phi}{2} (\tan \alpha_1 + \tan \alpha_2) \quad (9.58c)$$

From Eq. (9.38c) with some manipulation, we arrive at the following expressions for the degree of reaction:

$$\Lambda = \frac{1}{2} - \frac{C_a}{2U} (\tan \alpha_1 - \tan \beta_2) = \frac{1}{2} - \frac{\phi}{2} (\tan \alpha_1 - \tan \beta_2) \quad (9.58d)$$

$$\Lambda = \frac{C_a}{2U} (\tan \beta_1 + \tan \beta_2) = \frac{\phi}{2} (\tan \beta_1 + \tan \beta_2) \quad (9.58e)$$

From Eq. (9.58e), another expression for the degree of reaction is obtained

$$\Lambda = \frac{1}{U} \left(\frac{C_a \tan \beta_1 + C_a \tan \beta_2}{2} \right)$$

$$\Lambda = \frac{1}{U} \left(\frac{W_{u1} + W_{u2}}{2} \right)$$

$$\Lambda = \frac{W_{u\text{mean}}}{U} = \frac{C_a \tan \beta_m}{U} = \phi \tan \beta_m \quad (9.58f)$$

Three special cases are found here:

1. $\Lambda = 0 \%$
2. $\Lambda = 50 \%$
3. $\Lambda = 100 \%$

Now consider the case of 50 % reaction. In this case, the stage provides the best efficiency. If the degree of reaction is much different from 50 %, one of the blade rows must tolerate greater pressure rise than the other. Now, from Eq. (9.58d),

$$\therefore \tan \alpha_1 = \tan \beta_2$$

$$\therefore \alpha_1 = \beta_2$$

Moreover, from Eq. (9.38c)

$$\begin{aligned} \frac{U}{C_a} &= \tan \alpha_1 + \tan \beta_1 = \tan \alpha_2 + \tan \beta_2 \\ \therefore \alpha_2 &= \beta_1 \end{aligned}$$

This means that these velocity triangles are symmetrical. It is interesting to notice that if the degree of reaction is greater than 50 %, then $\beta_2 > \alpha_1$ and the velocity triangles will be skewed in the direction of the rotational speed [19]. The static enthalpy rise across the rotor exceeds that of the stator (this is also true for the static pressure). If the degree of reaction is less than 50 %, then $\beta_2 < \alpha_1$ and the velocity triangles will be skewed in the opposite direction of the rotational speed. The stator enthalpy rise (and pressure) exceeds that in the rotor.

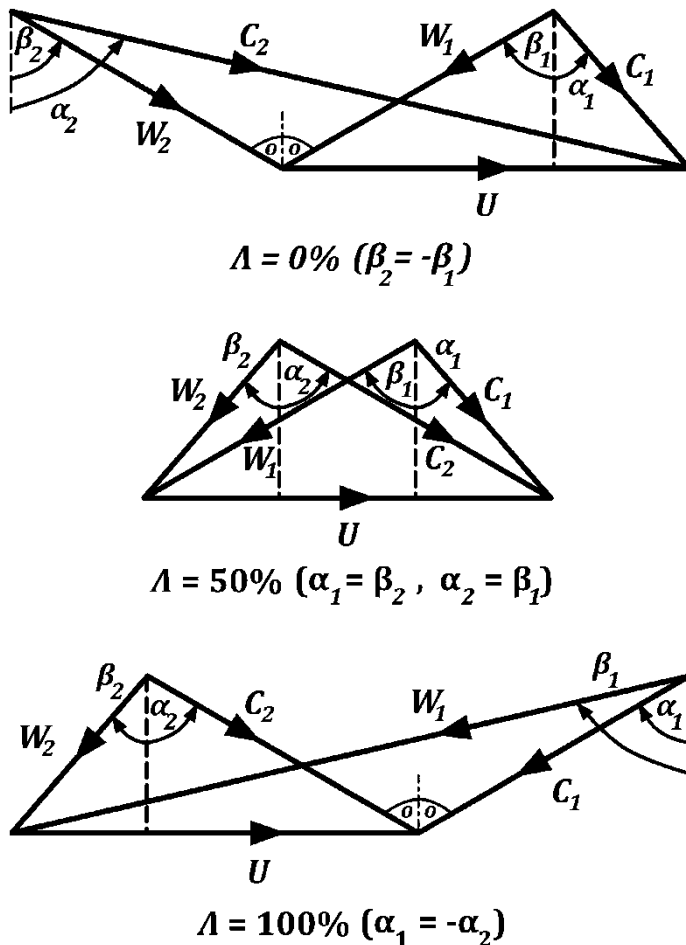
The case of zero degree of reaction is known as *impulse blading*. From Eq. (9.58e), the magnitude of the relative angles at inlet and outlet of the rotor are equal but have opposite signs $\beta_2 = -\beta_1$. There is no contribution for the rotor row here. All the enthalpy (or pressure) rises in the stator blade row. The rotor just redirects the incoming flow, such that the outlet angle is equal in magnitude to the inlet angle with opposite sign.

The case of 100 % degree of reaction necessitates that $\alpha_2 = -\alpha_1$. All the enthalpy (and static pressure) rises in the rotor while the stator has no contribution. The three cases described above are illustrated in Fig. 9.28.

9.3.6 Real Flow in Axial Compressor

In reality, air/gas flow in turbomachinery (compressor/turbine) is a 3D turbulent flow [20]. Some of the 3D effects are due to compressibility, radial variation of density, pressure, and work input/output as well as radial variation in blade thickness, twist, and geometry. Secondary flow and tip leakage as well as boundary layers over blades, hub, and casing complicate such 3D pattern particularly if coupled to shock waves. Non-uniform inlet flow due to upstream blade rows together with air bleed assures 3D of flow. Finally, presence of two-phase flow like injection of water, rain, ice, sand, and volcanic ash also reflects 3D issues.

Since the equations of motion governing such complicated turbulent flow through complex geometry turbomachinery are highly nonlinear, hence most of



Velocity triangles for 0%, 50% & 100% reaction

Fig. 9.28 Velocity triangles for different degrees of reaction

the analytical solutions available are for simple flows. These solutions involve several assumptions depending on the type of machinery and the geometry of the blade-row and flow parameters. Numerical solutions for the governing equations started in the late sixties [21]. The 3D flow in turbomachines is either solved by techniques classified as either axisymmetric solutions or non-axisymmetric solutions.

The axisymmetric solution is used to predict radial or spanwise variation of properties of flow far upstream and downstream of blade rows.

Neither non-axisymmetric nor axisymmetric solutions are appropriate to the present book. However, what is discussed in previous sections was only a 2D

flow, where radial (i.e. spanwise) velocities did not exist. It was assumed that the radial variations in the flow parameters through the compressors annulus are negligible. For a compressor in which the blade height is small relative to the mean diameter, i.e., those with high hub/tip ratios (of the order of 0.8 or more), this assumption is reasonable. But for blades with low hub-to-tip ratio (say 0.4, as in the case of the fan of a turbofan engine), radial variations are important. A step further in describing flow field within blade passage will be discussed in the following sections that may be identified as *quasi-3D* flow analysis. Alternatively, it is called a simplified radial equilibrium equation (SRE)

9.3.7 Simplified Radial Equilibrium Equation (SRE)

It is assumed that all the radial motion of the particle takes place within the blade row passages, while in the axial spacing (gab) between the successive blade rows (rotor/stator combination), radial equilibrium is assumed. Thus the axisymmetrical stream surface in the spacing between the blade rows has now a cylindrical stream surface shape. Thus, the radial component of velocity is neglected in the spaces between blade rows as

$$C_r \ll C_a, \quad C_r \ll C_u, \quad \text{thus} \quad C_r \approx 0$$

For steady flow, when the continuity and three-momentum equations are solved over these cylindrical surfaces, they are simplified considerably, and the resulting radial momentum equation is called the *simplified radial equilibrium equation* (SRE). Only the radial equilibrium equation is relevant because the flow does not vary in either the tangential and axial direction. Thus for a steady inviscid flow in the cylindrical surface and absence of any body force, the variables, C_u , C_a , h and h_0 , are function of the radius (r). Therefore, the radial component of the angular momentum equation is given by Eq. (9.59) identified as the *radial equilibrium* equation:

$$\frac{1}{\rho} \frac{dp}{dr} = \frac{c_u^2}{r} \quad (9.59)$$

The stagnation enthalpy is written now as

$$h_0 = h + \frac{C^2}{2} = h + \frac{C_a^2}{2} + \frac{C_u^2}{2} \quad (C_r \approx 0)$$

$$\frac{dh_0}{dr} = \frac{dh}{dr} + C_a \frac{dC_a}{dr} + C_u \frac{dC_u}{dr}$$

The thermodynamic relation

$$dh = T \ ds + \frac{dp}{\rho}$$

$$\frac{dh}{dr} = T \frac{ds}{dr} + \frac{dT}{dr} ds + \frac{1}{\rho} \frac{dp}{dr}$$

Neglecting second order terms and substituting from Eq. (9.59), then

$$\begin{aligned}\frac{dh}{dr} &= T \frac{ds}{dr} + \frac{1}{\rho} \frac{dp}{dr} = T \frac{ds}{dr} + \frac{C_u^2}{r} \\ \frac{dh_0}{dr} &= T \frac{ds}{dr} + \frac{C_u^2}{r} + C_a \frac{dC_a}{dr} + C_u \frac{dC_u}{dr}\end{aligned}$$

The term $T \frac{ds}{dr}$ represents radial variations across the annulus and may be significant only in detailed design and when the flow is supersonic and shock losses occur. Neglect entropy gradient

$$\frac{dh_0}{dr} = C_a \frac{dc_a}{dr} + C_u \frac{dC_u}{dr} + \frac{C_u^2}{r} \quad (9.60)$$

Equation (9.60) is denoted as the *vortex energy equation* which is also applicable (as the radial equilibrium equation) only in the axial space between a pair of blade rows. Equation (9.60) is an ordinary differential equation and can be easily solved when all the variables except one are known. For example, for isentropic flow, if C_u and h_0 are known or prescribed, then Eq. (9.60) can be solved for C_a

9.3.7.1 Free Vortex Method

Free vortex method is one of the simplest design methods in axial compressors. It is based on the general Eq. (9.60) with the following simplifications

- Assuming *constant specific work* at all radii, $\frac{dh_0}{dr} = 0$

$$\therefore C_a \frac{dC_a}{dr} + C_u \frac{dC_u}{dr} + \frac{C_u^2}{r} = 0$$

- Assuming *constant axial velocity* at all radii, $\frac{dC_a}{dr} = 0$

$$\begin{aligned}\therefore C_u \frac{dC_u}{dr} + \frac{C_u^2}{r} &= 0 \\ \frac{dC_u}{C_u} &= -\frac{dr}{r}\end{aligned}$$

Integrating, to get

$$rC_u = \text{constant} \quad (9.61)$$

Thus the whirl velocity component of the flow varies inversely with radius, which is known as *free vortex*.

It is clear that if the following three variables (h_0 , C_a , rC_u) are not varying in the radial direction, then the radial equilibrium equation, $\frac{1}{\rho} \frac{dp}{dr} = \frac{C_u^2}{r}$ is satisfied. The resulting blading is denoted free vortex blading. Though it represents a simple mathematical treatment for blade twist, but it has two main disadvantages; namely the large variation of the degree of reaction and the large blade twist along blade span (or height).

The degree of reaction from Eq. (9.58b) can be further expressed as

$$\begin{aligned} \Lambda &= 1 - \frac{rC_{u1} + rC_{u2}}{2rU} \\ \text{but } \frac{U}{U_m} &= \frac{r}{r_m} \\ \Lambda &= 1 - \frac{\text{Constant}}{2U_m r^2 / r_m} \\ \Lambda &= 1 - \frac{\text{constant}}{r^2} \end{aligned} \quad (9.62)$$

A great variation in the degree of reaction from the blade hub to tip is depicted by Eq. (9.62). Moreover, some suspect that at the blade root where its radius is a minimum, a negative reaction is possible. One note is remaining here is that the free vortex relation; Eq. (9.61) is applied twice at stations 1 and 2. The following example illustrates the above points.

Example 9.7 Consider a free vortex design for a compressor stage having a degree of reaction at the mean section equals to 0.5, hub-to-tip ratio of 0.6, and the flow angles $\alpha_{1m} = 30^\circ$, $\beta_{1m} = 60^\circ$. Calculate the absolute and relative angles at the hub (α_h , β_h) and tip (α_t , β_t) for both stations 1 (upstream of the rotor) and 2 (downstream of the rotor). Calculate also the degree of reaction at both hub and tip.

Solution

Since the degree of reaction is 50 % at the mean section, then $\alpha_{1m} = \beta_{2m}$ and $\alpha_{2m} = \beta_{1m}$

Since the hub-to-tip ratio is equal to 0.6, then at both stations (1) and (2),

$$\begin{aligned} r_t &= \frac{5}{4}r_m \quad \text{and} \quad r_h = \frac{3}{4}r_m \\ U_t &= U_m \frac{r_t}{r_m} \quad U_t = \frac{5}{4}U_m \end{aligned}$$

$$U_h = U_m \frac{r_h}{r_m} \quad U_h = \frac{3}{4} U_m$$

For a free vortex design, $rC_u = \text{Constant}$ at stations 1 and 2

$$\begin{aligned} r_h C_{uh} &= r_m C_{um} & C_{uh} &= \frac{r_m}{r_h} C_{um} \\ r_t C_{ut} &= r_m C_{um} & C_{ut} &= \frac{r_m}{r_t} C_{um} \end{aligned}$$

The swirl velocity components are $C_{uh} = \frac{4}{3} C_{um}$ $C_{ut} = \frac{4}{5} C_{um}$

Then, for both stations 1 and 2

$$\begin{aligned} C_{u1h} &= \frac{4}{3} C_{u1m} & C_{u2h} &= \frac{4}{3} C_{u2m} & U_h &= \frac{3}{4} U_m \\ C_{u1t} &= \frac{4}{5} C_{u1m} & C_{u2t} &= \frac{4}{5} C_{u2m} & U_t &= \frac{5}{4} U_m \\ \tan \alpha_h &= \frac{C_{uh}}{C_a} = \frac{4}{3} \frac{C_{um}}{C_a} = \frac{4}{3} \tan \alpha_m \\ \tan \alpha_t &= \frac{C_{ut}}{C_a} = \frac{4}{5} \frac{C_{um}}{C_a} = \frac{4}{5} \tan \alpha_m \\ \tan \beta_h &= \frac{U_h - C_{uh}}{C_a} = \frac{(3/4)U_m - (4/3)C_{um}}{C_a} \\ \text{but } \frac{U_m}{C_a} &= \tan \alpha_m + \tan \beta_m \quad \text{and} \quad \frac{C_{um}}{C_a} = \tan \alpha_m \\ \therefore \tan \beta_h &= \frac{3}{4} \tan \beta_m - \frac{7}{12} \tan \alpha_m \end{aligned}$$

Similarly

$$\begin{aligned} \frac{U_m}{C_a} &= \tan \alpha_m + \tan \beta_m \quad \text{and} \quad \frac{C_{um}}{C_a} = \tan \alpha_m \\ \tan \beta_t &= \frac{U_t - C_{ut}}{C_a} = \frac{(5/4)U_m - (4/5)C_{um}}{C_a} \\ \therefore \tan \beta_t &= \frac{9}{20} \tan \alpha_m + \frac{5}{4} \tan \beta_m \end{aligned}$$

From Eqs. (9.38a) and (9.58e), the degree of reaction at any radius may be expressed as

$$\Lambda = \frac{\tan \beta_1 + \tan \beta_2}{2(\tan \alpha_1 + \tan \beta_1)}$$

Final results for this case study are listed in Table 9.8

Table 9.8 Characteristics of a single stage axial compressor based on free vortex design method (all angles in degrees)

	α_1	β_1	α_2	β_2	Λ	$\beta_1 - \beta_2$
Hub	37.6	43.9	66.6	-30	0.11	73.9
Mean	30	60	60	30	0.5	30
Tip	24.8	67.5	54.2	56.3	0.68	11.3

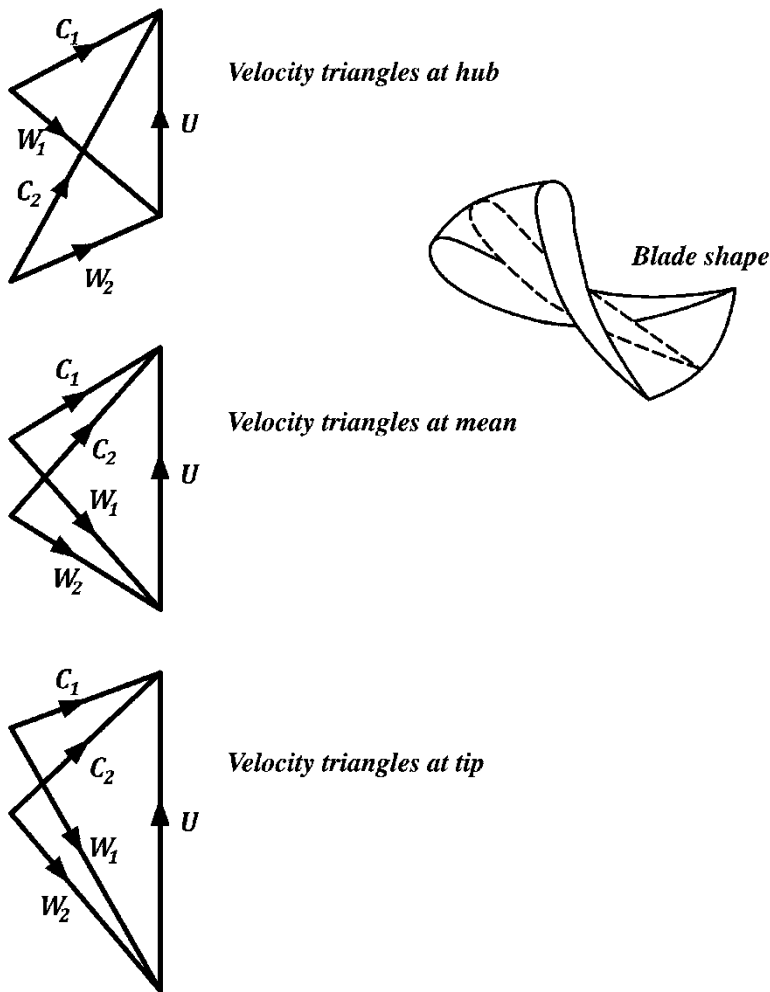


Fig. 9.29 Free vortex velocity triangle and blade shape

The difference in the angles ($\beta_1 - \beta_2$) at different stations along the blade span represents the blade twist. Thus adopting free vortex design yields a highly twisted blade, which implies high structural loading, and a great variation in the degree of reaction from hub to tip, which represent a less safe design blading. The velocity triangles and the blade twist are shown in Fig. 9.29.

Example 9.8 For an axial compressor stage, using the vortex energy equation

$$\frac{1}{r^2} \frac{d}{dr} (r^2 C_u^2) + \frac{d}{dr} (C_a^2) = 0$$

Prove that, if the flow is represented by a free vortex, $rC_u = \text{constant}$, then

1. $C_a = \text{constant}$
2. $\tan \alpha_{1h} = \left(\frac{1+\zeta}{2\zeta}\right) \tan \alpha_{1m}$
3. $\tan \beta_{1h} = \frac{2\zeta}{\zeta+1} \tan \beta_{1m} + \frac{(3\zeta+1)(\zeta-1)}{2\zeta(1+\zeta)} \tan \alpha_{1m}$

where

ζ is the hub-tip ratio

α_1 is the angle between the inlet absolute velocity and the axial direction

β_1 is the angle between the inlet relative velocity and the axial direction

Subscripts (h) and (m) refer to the hub and mean sections, respectively.

Solution

1. For $rC_u = \text{Constant}$

$$\therefore \frac{d}{dr} (rC_u) = 0$$

Then from the vortex energy equation

$$\frac{1}{r^2} \frac{d}{dr} (r^2 C_u^2) + \frac{d}{dr} (C_a^2) = \frac{d}{dr} (C_a^2) = 0$$

Thus

$$C_a^2 = \text{Constant}$$

$$\therefore C_a = \text{Constant}$$

2. Since $\tan \alpha_{1h} = \frac{C_{u1h}}{C_a}$, $\tan \alpha_{1m} = \frac{C_{u1m}}{C_a}$ and $C_a = \text{constant}$

Then

$$\frac{\tan \alpha_{1h}}{\tan \alpha_{1m}} = \frac{C_{u1h}}{C_{u1m}}$$

$$\tan \alpha_{1h} = \frac{C_{u1h}}{C_{u1m}} \tan \alpha_{1m} \quad (1)$$

but

$$rC_u = \text{Constant}, \text{ or } r_h C_{uh} = r_m C_{um}$$

Then at state (1)

$$r_h C_{u1h} = r_m C_{u1m}$$

$$\frac{C_{u1h}}{C_{u1m}} = \frac{r_m}{r_h}$$

Then from equation (1):

$$\begin{aligned} \therefore \tan \alpha_{1h} &= \frac{r_m}{r_h} \tan \alpha_{1m} \\ \frac{r_m}{r_h} &= \frac{r_h + r_t}{2r_h} = \frac{\frac{r_h}{r_t} + 1}{2\frac{r_h}{r_t}} = \frac{1 + \zeta}{2\zeta} \\ \tan \alpha_{1h} &= \frac{1 + \zeta}{2\zeta} \tan \alpha_{1m} \end{aligned} \quad (2)$$

3. From the kinematical relations

$$\begin{aligned} \tan \alpha_{1h} + \tan \beta_{1h} &= \frac{U_h}{C_a} \\ \tan \alpha_{1m} + \tan \beta_{1m} &= \frac{U_m}{C_a} \\ \therefore \frac{\tan \alpha_{1h} + \tan \beta_{1h}}{\tan \alpha_{1m} + \tan \beta_{1m}} &= \frac{U_h}{U_m} \\ \tan \alpha_{1h} + \tan \beta_{1h} &= \frac{U_h}{U_m} (\tan \alpha_{1m} + \tan \beta_{1m}) \\ \tan \beta_{1h} &= \frac{U_h}{U_m} (\tan \alpha_{1m} + \tan \beta_{1m}) - \tan \alpha_{1h} \end{aligned}$$

Since

$$\frac{U_h}{U_m} = \frac{r_h}{r_m} = \frac{2\zeta}{\zeta + 1}$$

and from equation (2): $\tan \alpha_{1h} = \frac{1+\zeta}{2\zeta} \tan \alpha_{1m}$

$$\begin{aligned} \therefore \tan \beta_{1h} &= \frac{2\zeta}{\zeta + 1} (\tan \alpha_{1m} + \tan \beta_{1m}) - \frac{1 + \zeta}{2\zeta} \tan \alpha_{1m} \\ \tan \beta_{1h} &= \frac{2\zeta}{1 + \zeta} \tan \beta_{1m} + \left[\frac{2\zeta}{\zeta + 1} - \frac{1 + \zeta}{2\zeta} \right] \tan \alpha_{1m} \\ \tan \beta_{1h} &= \frac{2\zeta}{\zeta + 1} \tan \beta_{1m} + \frac{4\zeta^2 - (1 + \zeta)^2}{2\zeta(1 + \zeta)} \tan \alpha_{1m} \\ \tan \beta_{1h} &= \frac{2\zeta}{\zeta + 1} \tan \beta_{1m} + \frac{(3\zeta + 1)(\zeta - 1)}{2\zeta(1 + \zeta)} \tan \alpha_{1m} \end{aligned}$$

Example 9.9 Air enters axially into the first stage of an axial compressor. It has the following data:

Hub and tip radii: $r_h = 0.25$ m, $r_t = 0.5$ m.

Axial velocity is expressed by the relation: $C_a(r) = 100 + 24r$ (m/s)

Stage temperature rise: $\Delta T_0 = 30$ K, rotational speed: $N = 9000$ rpm

Air density: $\rho_a = 1.225$ kg/m³

Specific work is assumed constant along the blade height. It is required to

1. Calculate mass flow rate
2. Calculate at hub section the angles: α_{1h} , α_{2h} , β_{1h} , β_{2h}
3. Draw the velocity triangles at hub and tip

Solution

$$1. \text{ Air mass flow rate } \dot{m} = \rho C_a A = \int_{r_h}^{r_t} \rho \times (100 + 24r) \times 2\pi r dr$$

$$\dot{m} = 2\pi\rho [50r^2 + 8r^3]_{r_h}^{r_t}$$

$$\dot{m} = 2\pi \times 1.225 \times \left\{ 50 \times (0.5)^2 - (0.25)^2 + 8(0.5)^3 - (0.25)^3 \right\}$$

$$\dot{m} = 78.89 \text{ kg/s}$$

2. Since flow enters axially, then

$$\alpha_{1h} = \alpha_{1t} = 0$$

Rotational speed:

$$U(r) = 2\pi N r$$

$$U_h = 2\pi N r_h = 2\pi \left(\frac{9000}{60} \right) (0.25) = 235.62 \text{ m/s}$$

$$U_t = 2\pi N r_t = 2\pi \left(\frac{9000}{60} \right) (0.5) = 471.24 \text{ m/s}$$

$$\text{Axial velocity : } C_a(r) = 100 + 24r$$

$$\therefore C_{ah} = 100 + 24(0.25) = 106 \text{ m/s}$$

$$\therefore C_{at} = 100 + 24(0.5) = 112 \text{ m/s}$$

$$\beta_{1h} = \tan^{-1} \left(\frac{U_h}{C_{ah}} \right) = \tan^{-1} \left(\frac{235.62}{106} \right) = 65.78^\circ$$

$$\beta_{1t} = \tan^{-1} \left(\frac{471.24}{112} \right) = 76.63^\circ$$

For constant specific work:

$$W_s = Cp\Delta T_0 = U(C_{u2} - C_{u1}) = UC_{u2}$$

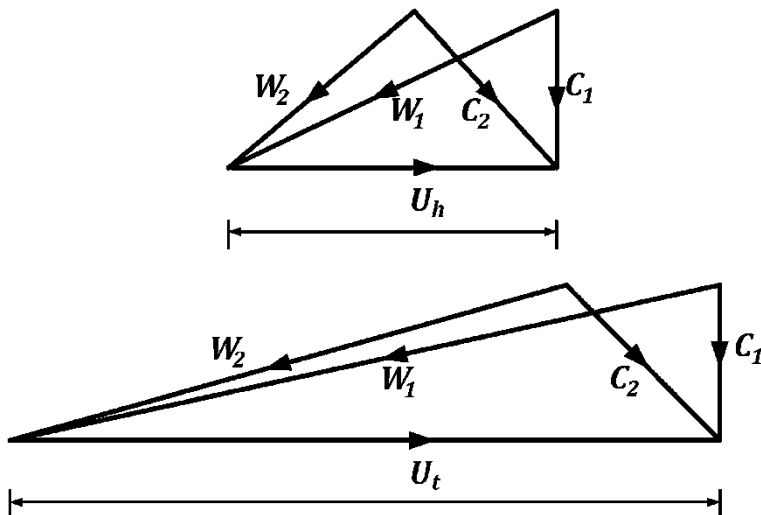
$$C_{u2} = \frac{C_p \Delta T_0}{U}$$

$$(C_{u2})_h = \frac{1005 \times 30}{235.62} = 128 \text{ m/s}$$

$$(C_{u2})_t = \frac{1005 \times 30}{471.24} = 64 \text{ m/s}$$

$$\alpha_{2h} = \tan^{-1}\left(\frac{C_{u2h}}{C_{ah}}\right) = \tan^{-1}\left(\frac{128}{106}\right) = 50.36^\circ$$

$$\alpha_{2t} = \tan^{-1}\left(\frac{C_{u2t}}{C_{at}}\right) = \tan^{-1}\left(\frac{64}{112}\right) = 29.74^\circ$$



Example 9.10 A two-spool turboshaft engine is used to power a helicopter. The overall pressure ratio is 12:1. The low pressure compressor is of the axial type and has five stages, while the high pressure compressor is a single stage centrifugal compressor. Both compressors have same mean inlet diameters. The polytropic efficiency of both compressors is 0.90. The axial compressor has the following data:

Stage temperature rise	30 K	Constant mean diameter	25 cm
Degree of reaction	50 %	Constant axial velocity	160 m/s
Stator outlet angle	20°	Constant work done factor	0.89
Ambient total temperature	300 K	Ambient total pressure	101 kPa

The centrifugal compressor has the following data:

Impeller tip diameter	35 cm	Slip factor	0.9
Power input factor	1.04		

Assuming axial velocity at the eye of the impeller, it is required to:

- (A) Calculate the required rotational speed of each spool.
- (B) Draw velocity triangles at mean section of axial compressor as well as at the inlet and outlet of centrifugal compressor.
- (C) For a free vortex design of axial compressor, calculate the degree of reaction at blade tip of first stage if the hub-to-tip ratio is 0.5.

Solution

(a) Axial Compressor

The specific power is expressed by the relation

$$W \equiv Cp\Delta T_0 = \lambda CaU(\tan \beta_1 - \tan \beta_2)$$

$$\frac{Cp\Delta T_0}{\lambda CaU} = (\tan \beta_1 - \tan \beta_2) \quad (1)$$

The degree of reaction is $\Lambda = \frac{Ca}{2U}(\tan \beta_1 + \tan \beta_2)$

$$\frac{2U\Lambda}{Ca} = (\tan \beta_1 + \tan \beta_2) \quad (2)$$

With $\Lambda = 0.5$, then multiply equations (1) and (2) to get

$$\frac{Cp\Delta T_0}{\lambda C_a^2} = (\tan \beta_1 + \tan \beta_2)(\tan \beta_1 - \tan \beta_2) = \tan^2 \beta_1 - \tan^2 \beta_2$$

Since
$$\frac{Cp\Delta T_0}{\lambda C_a^2} = \frac{1005 \times 30}{0.89 \times (150)^2} = 1.5056$$

Then
$$\tan^2 \beta_1 - \tan^2 \beta_2 = 1.5056$$

Moreover, the stator outlet angle is equal to the absolute inlet angle; $\alpha_3 = \alpha_1$
Since for a 50 % degree of reaction

$$\alpha_1 = \beta_2 = 20^\circ, \quad \text{and} \quad \alpha_2 = \beta_1$$

Then
$$\tan^2 \beta_1 - \tan^2 20 = 1.5056$$

$$\tan^2 \beta_1 = 1.63809$$

$$\begin{aligned}\tan \beta_1 &= 1.2798 \\ \therefore \beta_1 &= 52.0^\circ = \alpha_2 \\ \therefore U &= Ca(\tan \beta_1 + \tan \beta_2),\end{aligned}$$

Then

$$U = 150(\tan 52.0 + \tan 20) = 246.6 \text{ m/s}$$

$$\begin{aligned}U &= \frac{2\pi N}{60} \times r_m \\ 246.6 &= \frac{2\pi N}{60} \times 0.125\end{aligned}$$

$$N = 18,838 \text{ rpm} = 314 \text{ rps} \quad (\text{rotational speed of axial compressor})$$

$$T_{on} = T_{01} + n \times \Delta T_0 \text{ stage} = 300 + 5 \times 30 = 450 \text{ K}$$

$$\begin{aligned}\text{The pressure ratio of axial compressor : } \pi_{\text{axial}} &= \frac{P_{0n}}{P_{01}} = \left[\frac{T_{0n}}{T_{01}} \right]^{\frac{\gamma \eta_p}{\gamma - 1}} \\ \pi_{\text{axial}} &= \frac{P_{0n}}{101} = \left[\frac{450}{300} \right]^{\frac{1.4 \times 0.90}{0.4}} = 3.5866 \\ P_{0n} &= 101 \times 3.5866 = 362.2 \text{ kPa}\end{aligned}$$

(b) Centrifugal Compressor

$$\pi_{\text{centrifugal}} = \frac{\pi_{\text{overall}}}{\pi_{\text{axial}}} = \frac{12}{3.5866} = 3.3458$$

The efficiency of centrifugal compressor is calculated from the relation:

$$\begin{aligned}\eta_c &= \frac{\left[\pi_{\text{centrifugal}} \right]^{\frac{\gamma-1}{\gamma}} - 1}{\left[\pi_{\text{centrifugal}} \right]^{\frac{\gamma-1}{\gamma \eta_p}} - 1} \\ \eta_c &= \frac{\left[3.3458 \right]^{\frac{0.4}{1.4}} - 1}{\left[3.3458 \right]^{\frac{0.4}{1.4 \times 0.90}} - 1} = 0.883 \\ \pi_{\text{centrifugal}} &= \frac{P_{03}}{P_{01}} = \left(1 + \frac{\eta_c \psi (\sigma U_2^2 - C u_1 U_1)}{C p T_{01}} \right)^{\frac{\gamma}{\gamma-1}}\end{aligned}$$

For axial flow at inlet of centrifugal compressor, then $C u_1 = 0$

$$3.3458 = \left(1 + \frac{0.883 \times 1.04 \times 0.9 \times U_2^2}{1005 \times 450} \right)^{\frac{1.4}{0.4}}$$

$$U_2^2 = 225750.1$$

$$U_2 = 475.1 \text{ m/s}$$

$$U_2 = \frac{2\pi N}{60} \times r_2$$

$$475.1 = \frac{2\pi N}{60} \times \frac{0.35}{2}$$

$N = 25,925 \text{ rpm} = 432 \text{ rps}$ (rotational speed of centrifugal compressor)

(B) Velocity triangles

1. Centrifugal Compressor

Velocity triangle at inlet

Since air enters axially the centrifugal compressor, then the values of velocities at inlet are:

Rotational speed at mean radius of inlet (U_1) is

$$U_1 = \pi d_{1m} N = \pi \times 0.25 \times 475.1 = 373.1 \text{ m/s}$$

With $C_1 = 150.0 \text{ m/s}$, then the relative velocity (W_1) is

$$W_1 = \sqrt{C_1^2 + U_1^2} = 402.2 \text{ m/s}$$

Velocity triangle at outlet

$$U_2 = \pi d_2 N = \pi \times 0.35 \times 432 = 475 \text{ m/s}$$

$$C_{u2} = \sigma U_2 = 0.9 \times 475 = 427.5 \text{ m/s}$$

$$C_{r2} = W_{r2} = C_{a1} = C_1 = 150.0 \text{ m/s}$$

$$C_2 = \sqrt{C_{u2}^2 + C_{r2}^2} = 453.0 \text{ m/s}$$

$$W_2 = \sqrt{(U - C_{u2})^2 + W_{r2}^2} = 157.3 \text{ m/s}$$

2. Axial Compressor

From previous calculations, we got the following results for mean section:

$$C_{a1} = C_{a2} = 150 \text{ m/s}$$

$$U = 246.6 \text{ m/s}$$

$$\alpha_1 = \beta_2 = 20^\circ$$

$$\beta_1 = \alpha_2 = 52.0^\circ$$

C- At tip section, with a free vortex blading, thus

$$rC_{u1} = \text{constant} \quad \text{and} \quad rC_{u2} = \text{constant}$$

$$r_t = \frac{d_m}{1 + \zeta} = \frac{0.25}{1.5} = 0.167 \text{ m}$$

$$r_m = \frac{0.25}{2} = 0.125 \text{ m}$$

$$U_t = U_m \frac{r_t}{r_m} = 246.6 \times \frac{0.167}{0.125} = 329.5 \text{ m/s}$$

$$Cu_{1m} = C_{a1} \tan \alpha_{1m} = 150 \times \tan 20 = 54.6 \text{ m/s}$$

$$Cu_{2m} = C_{a1} \tan \alpha_{2m} = 150 \times \tan 52 = 192 \text{ m/s}$$

$$Cu_{1t} = Cu_{1m} \frac{r_m}{r_t} = 54.6 \times \frac{0.125}{0.167} = 40.87 \text{ m/s}$$

$$Cu_{2t} = Cu_{2m} \frac{r_m}{r_t} = 192 \times \frac{0.125}{0.167} = 143.7 \text{ m/s}$$

$$\Lambda_t = 1 - \frac{Cu_{1t} + Cu_{2t}}{2U_t} = 1 - \frac{40.87 + 143.7}{2 \times 329.5} = 0.72$$

Example 9.11 Air flow enters axially into the first stage of an axial compressor. It is required to

1. Draw the velocity triangles
2. Prove that the stage pressure ratio can be expressed by the relation

$$\pi_s = \left[1 + \left(\frac{\tan \alpha_2}{\tan \beta_1} \right) \left(\frac{\eta_s U^2}{C_p T_{01}} \right) \right]^{\frac{\gamma}{\gamma-1}}$$

3. Calculate (π_s) if $T_{01} = 300 \text{ K}$, $\Delta T_0 = 20 \text{ K}$ in the following cases:

$C_a(\text{m/s})$	160	170	180	190
η_s	0.9	0.88	0.86	0.84

Plot (π_s) versus (\dot{m}) for the case of inlet area $A = 0.2 \text{ m}^2$ and air density

$$\rho = 1.225 \text{ kg/m}^3$$

Solution

1. The velocity triangles are shown here: Inlet velocity triangle is the right angle one, while the second triangle represents the outlet velocity triangle.
2. The stage pressure ratio is expressed by the relation

$$\pi_s = \left(1 + \eta_s \frac{\Delta T_0}{T_{01}} \right)^{\frac{\gamma}{\gamma-1}}$$

The stage specific work is given by

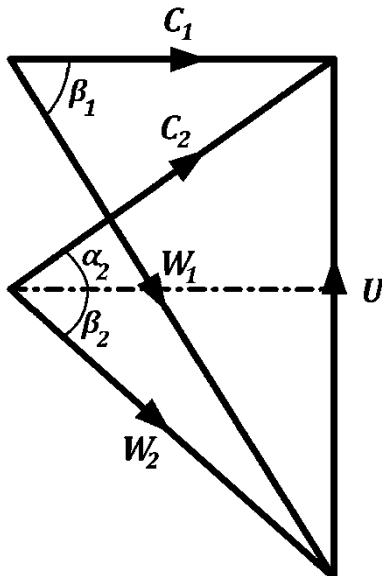
$$W_s = Cp\Delta T_0 = U\Delta C_u = UC_a \tan \alpha_2$$

Thus

$$\Delta T_0 = \frac{UC_a \tan \alpha_2}{Cp}$$

With $C_a = C_1 = U / \tan \beta_1$, then

$$\Delta T_0 = \frac{U^2 \tan \alpha_2}{Cp \tan \beta_1}$$



The stage pressure ratio is then can be written as

$$\pi_s = \left[1 + \left(\frac{\tan \alpha_2}{\tan \beta_1} \right) \left(\frac{\eta_s U^2}{Cp T_{01}} \right) \right]^{\frac{\gamma}{\gamma-1}}$$

3. The stage pressure ratio is calculated from the relation

$$\pi_s = \left(1 + \eta_s \frac{\Delta T_0}{T_{01}} \right)^{\frac{\gamma}{\gamma-1}}$$

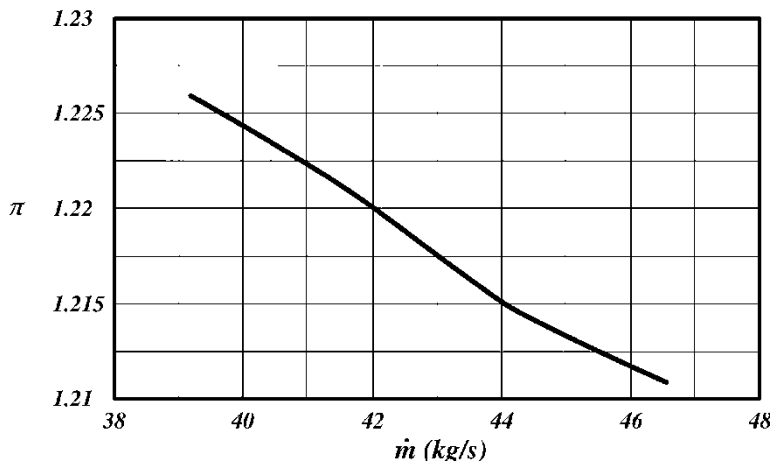
Mass flow rate is calculated from the relation

$$\dot{m} = \rho C_a A$$

The pressure ratio and mass flow rate are calculated and given in the following table:

C_a (m/s)	160	170	180	190
\dot{m} (kg/s)	39.2	41.65	44.1	46.55
η_s	0.9	0.88	0.86	0.84
π_s	1.226	1.221	1.215	1.211

A plot of pressure ratio versus mass flow rate is given in the below figure



With $T_{01} = 300$ K, $\alpha_2 = 30^\circ$

9.3.7.2 General Design Procedure

The disadvantages of the free vortex method mentioned above motivate searching for other design methods. Thus the design is based on arbitrarily chosen radial distribution of any two variables of the three (h_0 , C_a , C_u), then the variation of the other is determined from Eq. (9.60). However, it is always preferred to employ a constant specific work at all radii along the blade together with an arbitrary whirl velocity distribute for C_{u1} , C_{u2} that is compatible with the constant specific work condition. Next, the variation of the axial velocity C_a and the degree of reaction Λ

with the radius r are calculated. Equation (9.60) is to be solved twice at both stations (1) and (2) to obtain the radial variation of the axial velocities C_{a1}, C_{a2} .

The designer usually prescribes the whirl velocity somewhere between a *forced-vortex* and a *free vortex* design according to the relation:

$$C_{u1} = aR^n - \frac{b}{R} \quad C_{u2} = aR^n + \frac{b}{R} \quad (9.63)$$

where

$$R = \frac{r}{r_m} = \frac{U}{U_m}$$

The value (a) is determined from the degree of reaction

$$\Lambda = 1 - \frac{C_{u1} + C_{u2}}{2U}$$

At the mean section, the degree of reaction will be

$$\Lambda_m = 1 - \frac{C_{u1m} + C_{u2m}}{2U_m}$$

Substitute the values of the whirl velocities at the mean section from Eq. (9.63), then

$$\begin{aligned} \Lambda_m &= 1 - \frac{\left(aR_m^n + \frac{b}{R_m}\right) + \left(aR_m^n - \frac{b}{R_m}\right)}{2U_m}, \quad R_m = 1 \\ \therefore \Lambda_m &= 1 - \frac{a}{U_m} \\ a &= U_m(1 - \Lambda_m) \end{aligned} \quad (9.64)$$

The constant (b) is calculated from the condition of constant specific work

$$\begin{aligned} \Delta h_0 &= \text{constant} \equiv h_{02} - h_{01} \\ W_s &\equiv \Delta h_0 = U(C_{u2} - C_{u1}) \\ \Delta h_0 &= U_m R \left(aR^n + \frac{b}{R} - aR^n + \frac{b}{R} \right) \\ \Delta h_0 &= 2bU_m \\ b &= \frac{\Delta h_0}{2U_m} \end{aligned} \quad (9.65)$$

The values of (a) and (b) are *constants and independent* from the radius (r) as verified by Eqs. (9.64) and (9.65).

The total enthalpy upstream of the stage (h_{01}) is assumed constant and independent from the radius (r). Since the specific work, $W_s \equiv h_{02} - h_{01}$, is assumed constant, then the downstream enthalpy (h_{02}) is also constant. Now Eq. (9.60) is to be solved both at state (1) and (2). In both cases the L.H.S. of Eq. (9.60) is zero. The equation to be solved is now reduced to

$$C_a \frac{dC_a}{dr} + C_u \frac{dC_u}{dr} + \frac{C_u^2}{r} = 0$$

The above equation will be integrated at both stations (1) and (2) from the mean radius to any station (r). Note that at the mean radius

$$R_m = 1, \quad C_{u1m} = a - b \quad \text{and} \quad C_{u2m} = a + b$$

The resulting values for the axial velocities at any radius in stations (1) and (2) are calculated. These results are assembled in Table 9.9 together with the values of the whirl speeds and the degree of reaction.

As stated in [20], for exponential method, the loading as well as the blade twists is moderate. The new blade design trend is towards low-aspect ratio blading. The velocity triangles for any type of blading except $n = -1$ is plotted in Fig. 9.30. At hub ($C_{a2} > C_{a1}$), while at tip ($C_{a1} > C_{a2}$).

Example 9.12 If the whirl velocities in an axial stage are expressed as

$$C_{u1} = aR^n - \frac{b}{R} \quad C_{u2} = aR^n + \frac{b}{R}$$

Prove that if a constant specific work is assumed and the exponent, $n = 2$, then

$$C_{a1}^2 - C_{a2}^2 = 12ab(R - 1)$$

Solution

Since the vortex energy equation is expressed by

$$\frac{dh_o}{dr} = C_a \frac{dC_a}{dr} + C_u \frac{dC_u}{dr} + \frac{C_u^2}{r}$$

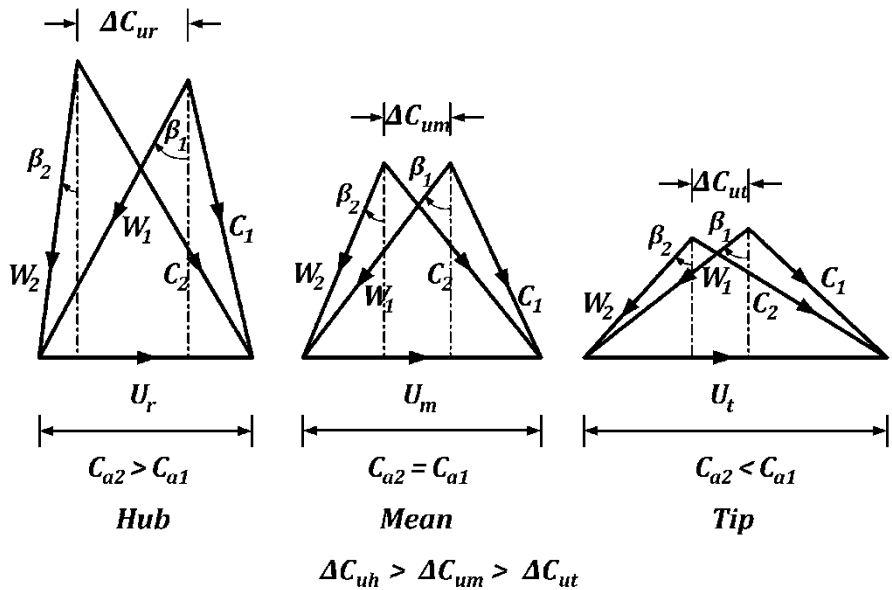
Assumption

Since the specific work = constant the radial direction

$$-C_a \frac{dC_a}{dr} = C_u \frac{dC_u}{dr} + \frac{C_u^2}{r}$$

Table 9.9 Governing equations for different design methods

Blading	C_a	C_u	
		Λ	$a = U_m(1 - \Lambda_m)$ $b = Cp\Delta T_{0s}/2U_m$
Free vortex $n = -1$	$C_{a1} = C_{alm}$ $C_{a2} = C_{a2m}$ $C_{alm} = C_{a2m}$	$\Lambda = 1 - \frac{a}{U_m R^2}$ $\Lambda = 1 - \frac{(1 - \Lambda_m)}{R^2}$	$C_{u1} = \frac{a - b}{R}$ $C_{u2} = \frac{a + b}{R}$
Exponential $n = 0$	$C_{a1}^2 - C_{a1}^2 m = -2 \left[\frac{a^2 \ell n R + \frac{ab}{R} - ab}{U_m} \right]$ $C_{a2}^2 - C_{a2}^2 m = -2 \left[\frac{a^2 \ell n R - \frac{ab}{R} + ab}{U_m} \right]$ $C_{alm} = C_{a2m}$	$\Lambda = 1 + \frac{a}{U_m} - \frac{2a}{U_m R}$ $\Lambda = 1 + \left(1 - \frac{2}{R} \right) (1 - \Lambda_m)$	$C_{u1} = a - \frac{b}{R}$ $C_{u2} = a + \frac{b}{R}$
First power $n = 1$	$C_{a2}^2 - C_{a1}^2 = 4ab \left(\frac{1}{R} - 1 \right)$	$\Lambda = 1 + \frac{2a \ell n R}{U_m} - \frac{a}{U_m}$ $\Lambda = 1 + (2 \ell n R - 1)(1 - \Lambda_m)$	$C_{u1} = dR - \frac{b}{R}$ $C_{u2} = dR + \frac{b}{R}$



Velocity triangles $n \neq -1$

Fig. 9.30 Velocity triangles at hub, mean and tip stations for $n \neq -1$

$$\begin{aligned}
 -C_a dC_a &= C_u dC_u + \frac{C_u^2}{r} dr \\
 R &= \frac{r}{r_m} \\
 - \int_{C_{am}}^{C_a} C_a dC_a &= \int_{C_{um}}^{C_u} C_u dC_u + \int_1^R C_u^2 \frac{dR}{R} \\
 -\frac{1}{2} [C_a^2 - C_{a_m}^2] &= \frac{1}{2} [C_u^2 - C_{u_m}^2] + I
 \end{aligned}$$

$$n = 2$$

$$\begin{aligned}
 C_{u1} &= aR^2 - \frac{b}{R} \\
 C_{u2} &= aR^2 + \frac{b}{R} \\
 -\frac{1}{2} [C_{a1}^2 - C_{a1m}^2] &= \frac{1}{2} [C_{u1}^2 - C_{u1m}^2] + \int_1^R \left(aR^2 - \frac{b}{R} \right)^2 \frac{dR}{R}
 \end{aligned}$$

$$\begin{aligned}
-\frac{1}{2} [C_{a1}^2 - C_{a1m}^2] &= \frac{1}{2} \left[\left(aR^2 - \frac{b}{R} \right)^2 - (a-b)^2 \right] + \int_1^R \left(a^2 R^3 - 2ab + \frac{b^2}{R^3} \right) dR \\
-\frac{1}{2} [C_{a1}^2 - C_{a1m}^2] &= \frac{1}{2} \left[\left(aR^2 - \frac{b}{R} \right)^2 - (a-b)^2 \right] + \left[\frac{a^2 R^4}{4} - 2abR - \frac{b^2}{2R^2} \right]_1^R \\
-\frac{1}{2} [C_{a1}^2 - C_{a1m}^2] &= \frac{1}{2} \left[\left(a^2 R^4 - 2abR + \frac{b^2}{R^2} \right) - (a^2 - 2ab + b^2) \right] \\
&\quad + \left[\left(\frac{a^2 R^4}{4} - 2abR - \frac{b^2}{2R^2} \right) - \left(\frac{a^2}{4} - 2ab - \frac{b^2}{2} \right) \right] \\
C_{a1}^2 - C_{a1m}^2 &= \left(\frac{3}{2}a^2 - 6ab \right) - \left(\frac{3}{2}a^2 R^4 - 6abR \right)
\end{aligned}$$

Similarly

$$C_{a2}^2 - C_{a2m}^2 = \left(\frac{3}{2}a^2 + 6ab \right) - \left(\frac{3}{2}a^2 R^4 + 6abR \right)$$

Since

$$C_{a1m} = C_{a2m}$$

$$C_{a1}^2 - C_{a2}^2 = 12ab(R - 1)$$

From the above equation, the following conclusions are deduced

$R < 1$	$R = 1$	$R > 1$
$C_{a1} < C_{a2}$	$C_{a1} = C_{a2}$	$C_{a1} > C_{a2}$

9.3.8 Conceptual Design Procedure for Axial Compressor

Compressors are designed by the *indirect method* [22]. That is, first one defines the flow path (casing and hub) radii and decides the thermodynamic, aerodynamic properties as well as work input that air must have at each axial location (station) along the flow path. An iterative analysis is conducted in which the continuity, momentum, energy, and state equations are satisfied at each station. Then one designs the blade and vanes to achieve the desired thermodynamic and aerodynamic properties. The designer is constrained to achieve the overall pressure ratio and mass flow rate. The full design details are given in [23, 24].

Steps for such a conceptual design of an axial compressor will briefly described here.

- (A) Quasi-3D analysis of compressor
- (B) Experimental testing of blades

(C) Off-design performance analysis

The first step (quasi-3D) starts by a 2D analysis (axial-tangential) and then extended to define flow properties at different stations along blade height (radial), thus provides a quasi-3D flow field. Details of such step are as follows:

1. Choice of the compressor's data: rotational speed (rpm) and axial velocity as well as annulus dimensions based on previous experiences. These data are used to determine the inlet and outlet dimensions of the compressor
2. Determine number of stages (assuming efficiency)
3. Calculate air angles for each stage at the mean section
4. Determine the variation of air angles from root to tip based on type of blading (free vortex – exponential – first power).

The second step (experimental testing) is decomposed into the steps:

1. Selection of compressor blading using experimentally cascade data
2. Check efficiency (previously assumed) using cascade data
3. Investigation of compressibility effects

The final step is to estimate off-design performance and rig testing prior production.

9.3.8.1 Choice of Compressor's Data

(A) *Speeds criteria*

From past experience of subsonic/transonic compressor design [22], the maximum tip speed and axial velocity have the following typical values:

$$U_t \approx 350 \text{ m/s}$$

$$C_a \approx 150 - 200 \text{ m/s}$$

(B) *Hub-tip ratio*

Typical values for the hub-tip ratio of the first stage of a compressor are

$$\zeta \equiv \frac{r_h}{r_t} \approx 0.4 - 0.6$$

Generally hub-tip ratio at inlet $\zeta > 0.3$ and at outlet $\zeta < 0.9$, for fan $\zeta \geq 0.2$

(C) *Mach numbers criteria*

The following values are suggested:

Axial Mach number $M_a \approx 0.5 (< 0.7)$

Relative Mach number: at tip $M_{1\text{tip}} < 1.2$ for the high pressure compressor (HPC), for fan $M_{1\text{tip}} < 1.8$

Relative Mach number: at hub $M_{1\text{hub}} < 0.9$

However, if this compressor is a part of an aero-engine powering a supersonic or future hypersonic aircraft, the total temperature at the inlet to compressor approaches or exceeds 1000 K. In this case, the static temperature is very close to the total values, which leads to very high values for sonic speeds. Thus the Mach number values suggested above develops unaffordable stresses in the blades. Consequently, these values are drastically reduced even to half its suggested values. Alternatively, specific values for the mean blade and axial speeds are to be employed.

For the first stage, the flow is axial or, $C_1 = C_{a1}$, then the axial Mach number is calculated as

$$\begin{aligned} C_1 &= M_1 \sqrt{\gamma R T_1} \\ C_1 &= M_1 \sqrt{\frac{\gamma R T_{01}}{1 + \frac{\gamma-1}{2} M^2}} \end{aligned} \quad (9.66)$$

Similarly, the relative speed at the blade tip is

$$W_1 = M_{1\text{rel}} \sqrt{\frac{\gamma R T_{01}}{1 + \frac{\gamma-1}{2} M^2}} \quad (9.67)$$

The rotational speed is then $U_t^2 = W_{1\text{tip}}^2 - C_1^2$

$$U_t^2 = \left[(M_{1\text{rel}}^2) - M_1^2 \right] \left(\frac{\gamma R T_{01}}{1 + \frac{\gamma-1}{2} M^2} \right) \quad (9.68)$$

The outer diameter and the rotational speed are related by the equation

$$r_t = \frac{U_t}{2\pi N}$$

If either the tip speed or the rotational speed is specified (or have some constraint), then the hub-tip ratio is calculated from the continuity equation as follows:

$$\dot{m} = \rho_1 C_{a1} A = \rho_1 C_{a1} \pi (r_t^2 - r_h^2)$$

$$\zeta^2 = 1 - \frac{m}{\rho_1 C_{a1} \pi r_t^2}$$

The density is calculated as follows:

$$C_1 = C_{a1}, T_1 = T_{01} - \frac{C_1^2}{2C_p}, P_1 = P_{01} \left(\frac{T_1}{T_{01}} \right)^{\frac{\gamma}{\gamma-1}} \quad (9.69)$$

$$\therefore \rho_1 = \frac{P_1}{RT_1}$$

A check is requested here for the hub-tip ratio to be within the specified range.

Here a decision has to be made concerning the type of *variation of the compressor passage* at its successive stages. One has to decide whether the compressor will have a constant mean, constant tip, or constant hub radius through all stages.

Next to determine the outlet dimensions of the compressor, assume the stage efficiency (or the polytropic efficiency) of the compressor is η_s , then the outlet temperature of the compressor is calculated as

$$\frac{T_{02}}{T_{01}} = \left(\frac{P_{02}}{P_{01}} \right)^{\frac{n-1}{n}},$$

where $\frac{n-1}{n} = \frac{1}{\eta_s} \frac{\gamma - 1}{\gamma}$

Assume that air leaves the stator of the last stage of the compressor axially. Denoting this outlet station of the compressor as state (2), thus exit speed $C_2 = C_a = C_1$, which was previously calculated by Eq. (9.66). The static pressure and temperature will be

$$T_2 = T_{02} - \frac{C_2^2}{2C_p}, \quad P_2 = P_{02} \left(\frac{T_2}{T_{02}} \right)^{\frac{\gamma}{\gamma-1}}$$

The density and the annulus area are $\rho_2 = \frac{P_2}{RT_2}$, $A_2 = \frac{\dot{m}}{\rho_2 C_{a2}}$

If the constant mean radius option is selected, then the mean radius is already known and the blade height at outlet is calculated as follows $h = \frac{A_2}{2\pi r_m}$; the tip and root radii at outlet are calculated from the relations

$$r_t = r_m + \frac{h}{2} \quad r_r = r_m - \frac{h}{2}$$

If the constant casing radius option is selected, then the tip radius is already known and the blade height at outlet is calculated as follows, $h = \frac{A_2}{2\pi r_m}$, the root and mean radii at outlet are calculated from the relations

$$r_h = r_t - h \quad \text{and} \quad r_m = r_t - \frac{h}{2}$$

The compressor efficiency is related to the polytropic (stage) efficiency by the relation

$$\eta_c = \frac{\pi_c^{(\gamma-1)/\gamma} - 1}{\pi_c^{(\gamma-1)/\gamma \eta_s} - 1}$$

Table 9.10 Results for a preliminary design of an axial compressor

M_1	0.5	0.55	0.6
$T_1(\text{K})$	307	304	301
$P_1(\text{kPa})$	119	115	111
$\rho_1(\text{kg/m}^3)$	1.349	1.317	1.28
$C_1(\text{m/s})$	175.6	192.2	209
$W_1(\text{m/s})$	386.3	386	382
$U_t(\text{m/s})$	344.1	335	320
r_t	0.304	0.296	0.283
ζ	0.522	0.531	0.506

Example 9.13 A preliminary design of the low pressure axial compressor which is connected to an axial turbine of a small turbojet engine is requested. The compressor has an inlet total temperature and pressure of 322.2 K and 141 kPa. The mass flow rate is 50 kg/s. The turbine rotational speed is 180 rev/s and has a tip diameter of 0.285 m. Assume the flow to be axial at the compressor inlet.

Solution

Based on the suggested inlet Mach numbers, assume that the relative tip Mach number $M_{1tip}=1.1$ and the axial Mach number $M_a=0.5$. The procedure is as follows:

1. Calculate the static temperature and pressure and then the density at inlet
2. Calculate the axial, relative, and rotational speeds
3. Calculate the tip radius and from which calculate the hub-tip ratio
4. If the tip diameter is far from the turbine outer diameter, the axial Mach number is to be changed within its design range

The results for the example is arranged in Table 9.10, where the axial Mach number varies from 0.5 to 0.6.

Since from turbine calculations

$$N = 180 \text{ rps} \quad \text{and} \quad (r_t)_{\text{turbine}} = 0.285 \text{ m}$$

Choose $M_1=0.6$, where $\zeta=0.5$ and $r_t=0.283 \text{ m}$, which is close to the tip radius of the turbine. The corresponding blade rotational speed at tip is $U_t=320 \text{ m/s}$

The mean radius is $r_m = \frac{1+\zeta}{2} r_t = 0.213 \text{ m}$. The hub radius is 0.143 m. The mean rotational speed U_m or simply U is 241 m/s.

Example 9.14 A helicopter gas turbine requires an overall compressor pressure ratio of 12:1. This is to be obtained using two spool layouts consisting of a five-stage axial compressor (on the first spool) followed by a single stage centrifugal compressor (on the second spool). The polytropic efficiency of both compressors is 0.90. The axial compressor has the following data:

Stage temperature rise of	30 K	The mean diameter of each stage is	25 cm
Degree of reaction of	50 %	Constant axial velocity of	160 m/s
Stator outlet angle of	20°	The work done factor is constant of 0.89	
The ambient total temperature	300 K	The ambient total pressure	101 kPa

The centrifugal compressor has the following data:

Impeller tip diameter of power input factor	35 cm 1.04	Slip factor Assuming axial velocity at the eye of the impeller	0.9
--	---------------	---	-----

- (D) Calculate the required rotational speed of each spool
- (E) Draw velocity triangles at mean section of axial compressor, inlet and outlet of centrifugal compressor
- (F) For a free vortex design of axial compressor, calculate the degree of reaction at blade tip of first stage if the hub-to-tip ratio is 0.5

Solution

(a) Axial compressor

$$C_p \Delta T_0 = \lambda C_a U (\tan \beta_1 - \tan \beta_2)$$

$$\frac{C_p \Delta T_0}{\lambda C_a U} = (\tan \beta_1 - \tan \beta_2) \quad (1)$$

$$\Lambda = \frac{C_a}{2U} (\tan \beta_1 + \tan \beta_2)$$

$$\frac{2U\Lambda}{C_a} = \frac{U}{C_a} = (\tan \beta_1 + \tan \beta_2) \quad (2)$$

Multiply equations (1) and (2) to get:

$$\frac{C_p \Delta T_0}{\lambda C_a^2} = (\tan \beta_1 + \tan \beta_2)(\tan \beta_1 - \tan \beta_2) = \frac{1005 \times 30}{0.89 \times (150)^2} = 1.5056$$

$$\tan^2 \beta_1 - \tan^2 \beta_2 = 1.5056$$

Since the stator outlet angle is equal to the absolute inlet angle $\alpha_3 = \alpha_1$
Also for a degree of reaction $\Lambda = 0.5 \Rightarrow \alpha_1 = \beta_2 = 20^\circ \alpha_2 = \beta_1$

$$\text{Then } \tan^2 \beta_1 - \tan^2 20 = 1.5056$$

$$\tan^2 \beta_1 = 1.63809$$

$$\tan \beta_1 = 1.2798 \quad \beta_1 = 52.0^\circ = \alpha_2$$

$$\therefore U = Ca(\tan \beta_1 + \tan \beta_2),$$

$$\text{Then } U = 150(\tan 52.0 + \tan 20) = 246.6 \text{ m/s}$$

$$U = \frac{2\pi N}{60} \times r_m$$

$$246.6 = \frac{2\pi N}{60} \times 0.125$$

$$N = 18,838 \text{ rpm} = 314 \text{ rps (rotational speed)}$$

$$T_{\text{on}} = T_{01} + n \times \Delta T_{0 \text{ stage}} = 300 + 5 \times 30 = 450 \text{ K}$$

$$\frac{P_{0n}}{P_{01}} = \left[\frac{T_{0n}}{T_{01}} \right]^{\frac{\gamma \eta_p}{\gamma - 1}}$$

$$\pi_{\text{axial}} = \frac{P_{0n}}{101} = \left[\frac{450}{300} \right]^{\frac{1.4 \times 0.90}{0.4}} = 3.5866$$

$$P_{0n} = 101 \times 3.5866 = 362.2 \text{ kPa}$$

(b) *Centrifugal compressor*

$$\pi_{\text{centrifugal}} = \frac{\pi_c}{\pi_{\text{axial}}} = \frac{12}{3.5866} = 3.3458$$

The efficiency of centrifugal compressor is calculated from the relation

$$\eta_c = \frac{\left[\pi_{\text{centrifugal}} \right]^{\frac{\gamma-1}{\gamma}} - 1}{\left[\pi_{\text{centrifugal}} \right]^{\frac{\gamma-1}{\gamma \eta_p}} - 1}$$

$$\eta_c = \frac{\left[3.3458 \right]^{\frac{0.4}{1.4}} - 1}{\left[3.3458 \right]^{\frac{0.4}{1.4 \times 0.90}} - 1} = 0.883$$

$$\pi_{\text{centrifugl}} = \frac{P_{03}}{P_{01}} = \left(1 + \frac{\eta_c \psi (\sigma U_2^2 - C u_1 U_1)}{C p T_{01}} \right)^{\frac{\gamma}{\gamma-1}}$$

$$3.3458 = \left(1 + \frac{0.883 \times 1.04 \times 0.9 \times U_2^2}{1005 \times 450} \right)^{\frac{1.4}{0.4}}$$

$$U_2^2 = 225750.1$$

$$U_2 = 475.1 \text{ m/s}$$

$$U_2 = \frac{2\pi N}{60} \times r_2$$

$$475.1 = \frac{2\pi N}{60} \times \frac{0.35}{2}$$

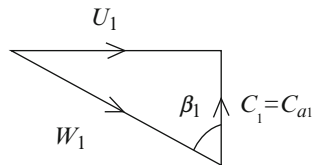
$$N = 25,925 \text{ rpm} = 432 \text{ rps}$$

(B) Velocity triangles

1. Centrifugal compressor

Velocity triangle at inlet

Rotational speed at mean radius of inlet



$$U_1 = \pi d_{1m} N = \pi \times 0.25 \times 475.1 = 373.1 \text{ m/s}$$

$$C_1 = 150.0 \text{ m/s}$$

$$W_1 = \sqrt{C_1^2 + U_1^2} = 402.2 \text{ m/s}$$

Velocity triangle at outlet

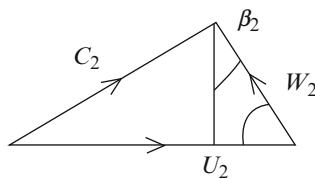
$$U_2 = \pi d_2 N = \pi \times 0.35 \times 432 = 475 \text{ m/s}$$

$$C_{u2} = \sigma U_2 = 0.9 \times 475 = 427.5 \text{ m/s}$$

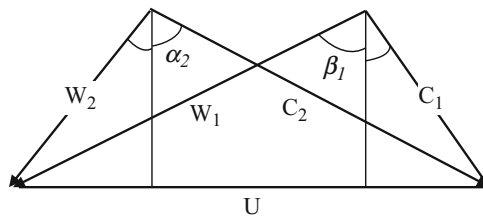
$$C_{r2} = W_{r2} = C_{a1} = C_1 = 150.0 \text{ m/s}$$

$$C_2 = \sqrt{C_{u2}^2 + C_{r2}^2} = 453.0 \text{ m/s}$$

$$W_2 = \sqrt{(U - C_{u2})^2 + W_{r2}^2} = 157.3 \text{ m/s}$$



2. Axial compressor



$$C_{a1} = C_{a2} = 150 \text{ m/s}$$

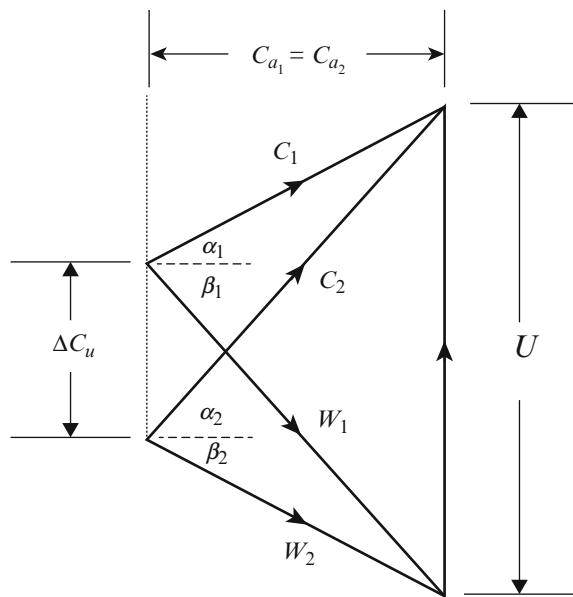
$$U = 246.6 \text{ m/s}$$

$$\alpha_1 = \beta_2 = 20^\circ$$

$$\frac{U}{C_a} = \tan \alpha_1 + \tan \beta_1 = \frac{246.6}{150} = 1.644$$

$$\tan \beta_1 = 1.644 - \tan \alpha_1 = 1.28$$

$$\beta_1 = 52.0^\circ$$



C) Free vortex at mean radius of axial compressor

$$rC_{u1} = \text{constant} \quad rC_{u2} = \text{constant}$$

$$r_t = \frac{d_m}{1 + \zeta} = \frac{0.25}{1.5} = 0.167 \text{ m}$$

$$r_m = \frac{0.25}{2} = 0.125 \text{ m}$$

$$Cu_{1m} = C_{a1} \tan \alpha_1 = 150 \times \tan 20 = 54.6 \text{ m/s}$$

$$Cu_{2m} = C_{a1} \tan \alpha_2 = 150 \times \tan 52 = 192 \text{ m/s}$$

$$Cu_{1t} = Cu_{1m} \frac{r_m}{r_t} = 54.6 \times \frac{0.125}{0.167} = 40.87 \text{ m/s}$$

$$Cu_{2t} = Cu_{2m} \frac{r_m}{r_t} = 192 \times \frac{0.125}{0.167} = 143.7 \text{ m/s}$$

$$U_t = U_m \frac{r_t}{r_m} = 246.6 \times \frac{0.167}{0.125} = 329.5 \text{ m/s}$$

$$\Lambda_t = 1 - \frac{Cu_{1t} + Cu_{2t}}{2U_t} = 1 - \frac{40.87 + 143.7}{2 \times 329.5} = 0.72$$

9.3.8.2 Determine Number of Stages (Assuming Stage Efficiency)

To determine the number of stages, the overall temperature rise within the compressor is first determined as $\Delta T_{\text{comp}} = T_{02} - T_{01}$. Secondly, the stage temperature rise is determined. Divide both values to obtain the number of stages. This figure will be rounded to the nearest integer.

The stage temperature rise will be obtained from (9.44) as follows:

$$\Delta T_0 = \frac{UC_a}{C_p} (\tan \beta_1 - \tan \beta_2)$$

Since the rotor de Haller number $DH_r = \frac{W_2}{W_1}$, then for constant axial velocity,

$$DH_r = \frac{\cos \beta_1}{\cos \beta_2} = \frac{\sec \beta_2}{\sec \beta_1} = \sqrt{\frac{1 + \tan \beta_2^2}{1 + \tan \beta_1^2}}$$

$$\therefore \tan \beta_2 = \sqrt{(DH_r)^2 (1 + \tan \beta_1^2) - 1} \quad (9.70)$$

$$\Delta T_0 = \frac{UC_a}{C_p} \left(\tan \beta_1 - \sqrt{(DH_r)^2 (1 + \tan \beta_1^2) - 1} \right) \quad (9.71)$$

As a guide from past experience [16], the temperature rise per stage for the available compressor has the following range:

$$\Delta T_{0s} = 10 - 30 \text{ K} \quad \text{subsonic stages}$$

$$\Delta T_{0s} = 45 - 55 \text{ K} \quad \text{transonic stage}$$

$$\Delta T_{0s} \geq 80 \text{ K} \quad \text{supersonic stage}$$

Then the number of stages is determined as

$$n = \frac{(\Delta T_0)_{\text{compressor}}}{(\Delta T_0)_{\text{stage}}}$$

Again, the above values for temperature rise per stage are only as a guide for the present day compressors. Aero-engine manufacturers are working hard to increase these values to reach 70 or 80 degrees for transonic compressors.

9.3.8.3 Calculation of Air Angles for Each Stage at the Mean Section

For a constant mean diameter and known axial and mean blade speeds (C_a, U_m), the angles $\alpha_1, \beta_1, \alpha_2$ and β_2 will be calculated for each stage. The degree of reaction at the mean section will be also calculated and checked for reasonable values.

(A) First stage

The first stage is characterized by an axial inlet flow ($\alpha_1 = 0$), thus the relative inlet velocity and angle are calculated from the relations:

$$W_1 = \sqrt{U_m^2 + C_a^2}$$

$$\tan \beta_1 = U_m / C_a$$

for simplicity U_m will be written here as U . The outlet relative angle is to be calculated from Eq. (9.70), where the rotor de Haller number is selected equal or greater than 0.72.

The absolute angle at the rotor outlet is calculated from Eq. (9.38) as follows:

$$\tan \alpha_2 = \frac{U}{C_a} - \tan \beta_2$$

which is the inlet angle to the stator, the outlet angle to the stator (α_3) may be calculated from de Haller number of the stator defined as

$$DH_s = \frac{C_3}{C_2} = \frac{\cos \alpha_2}{\cos \alpha_3}$$

The value of de Haller number of stator has to be carefully selected otherwise it may yield an imaginary value for α_3 (if $\cos \alpha_3 > 1.0!!$). Thus, it must satisfy the condition:

$$DH_s > \cos \alpha_2 \quad (9.72)$$

Thus

$$\cos \alpha_3 = \frac{\cos \alpha_2}{DH_s} \quad (9.73)$$

A better value for the stage temperature rise can now be calculated by incorporating the work done factor (λ), Eq. (9.44b) as follows:

$$\Delta T_{0s} = \frac{\lambda U_m C_a (\tan \beta_1 - \tan \beta_2)}{C_p} \quad (9.44b)$$

The value of the work done factor for different stages is given by the following table:

Stage number	1st	2nd	3rd	4th
λ	0.98	0.93	0.88	0.83

The pressure ratio is calculated from the relation

$$\pi_s = \left(\frac{P_{03}}{P_{01}} \right)_s = \left(1 + \frac{\eta_s \Delta T_{01}}{T_{01}} \right)^{\frac{\gamma}{\gamma-1}} \quad (9.74)$$

The degree of reaction is calculated from Eq. (9.58e) as follows:

$$\Lambda = \frac{C_a}{2U} (\tan \beta_1 + \tan \beta_2) \quad (9.58e)$$

(B) Stages from (2) to (n-1)

The procedure is straight forward as follows:

1. The inlet total conditions to any stage (i) are

$$(P_{01})_{\text{stage}(i)} = (P_{01})_{\text{stage}(i-1)} \left(\frac{P_{03}}{P_{01}} \right)_{\text{stage}(i-1)}$$

$$(T_{01})_{\text{stage}(i)} = (T_{01})_{\text{stage}(i-1)} + (\Delta T_{01})_{\text{stage}(i-1)}$$

2. The flow is no longer axial, but the outlet angle α_3 for any stage will be equal to the inlet absolute angle α_1 of the next angle. In general,

$$(\alpha_1)_{\text{stage}(i)} = (\alpha_3)_{\text{stage}(i-1)}$$

3. The inlet relative angle β_1 is obtained as

$$\tan \beta_1 = \frac{U}{C_a} - \tan \alpha_1$$

4. The outlet relative angle β_2 is obtained from Eq. (9.70) with a de Haller number equal to 0.72.

5. The absolute outlet angle α_2 is calculated from the relation

$$\tan \alpha_2 = \frac{U}{C_a} - \tan \beta_2$$

6. The stage temperature rise ΔT_{0s} is calculated from Eq. (9.44b) using appropriate work done factor.

7. The stage pressure ratio π_s is calculated from the relation (9.44b).

8. The degree of reaction Λ is calculated from Eq. (9.58e).

9. The appropriate de Haller number DH_s for the stator is calculated from Eq. (9.72).

10. The stator outlet angle α_3 is calculated from Eq. (9.73).

The above procedure is repeated for all stages up to the last stage.

(C) Last stage

1. The pressure ratio of the stage is evaluated from the overall pressure ratio of the compressor and the product of the stage pressure ratios of all the previous $(n - 1)$ stages as follows:

$$\pi_{\text{last}} = \frac{\pi_c}{\prod_1^{n-1} \pi_i}$$

2. The corresponding temperature rise is obtained from the relation

$$(\Delta T_0)_{\text{last}} = \frac{(T_{01})_{\text{last}}}{\eta_s} \left(\pi_{\text{last}}^{\frac{\gamma-1}{\gamma}} - 1 \right)$$

4. The inlet relative angle β_1 is calculated as in section (B) – steps 2 and 3 above

5. The relative outlet blade angle is obtained from the relation

$$\tan \beta_2 = \tan \beta_1 - \frac{C_p \Delta T_0}{\lambda U C_a}$$

Check for the rotor de Haller number.

6. The outlet absolute angle α_2 is calculated as above, step 5.
7. The degree of reaction Λ is calculated from Eq. (9.58) as above.
8. The outlet absolute angle α_3 is assumed zero and check the stator de Haller number.

9.3.8.4 Variation of Air Angles from Root to tip Based on Type of Blading (Free Vortex – Exponential – First Power)

The three methods that estimate the variations of air properties in the radial direction from blade hub to tip are applied here. The procedure is as follows:

1. Calculate the dimensions at the rotor inlet and outlet for each stage.
2. Calculate the values of the constants (a) and (b) from Eqs. (9.64) and (9.65).
3. Use Table 9.9 to calculate the variations in axial and whirl velocities as well as the degree of reaction.

Now to calculate the dimensions upstream and downstream, the rotor states (1) and (2); the dimensions at state (3) are first calculated from the continuity equation. The air density is calculated from the perfect gas law, and then the annulus area is calculated as the axial speed (at mean section is already known).

$$\rho_3 = \frac{P_3}{RT_3}, \quad A_3 = \frac{\dot{m}}{\rho_3 C_a}$$

Next, calculate the blade height (h):

$$h_3 = \frac{A}{2\pi r_m}$$

If the compressor is designed with constant mean radius, then the root and tip radii are calculated as

$$r_{r3} = r_{m3} - \frac{h_3}{2} \quad r_{t3} = r_{m3} + \frac{h_3}{2}$$

The corresponding hub and tip radii at the rotor outlet are the mean value of those at states (1) and (3), as shown in Fig. 9.31.

$$r_{r2} = \frac{r_{r1} + r_{r3}}{2} \quad r_{t2} = \frac{r_{t1} + r_{t3}}{2}$$

It remains to calculate the corresponding non dimensional radii ($R = r/r_m$) at the root and tip at states (1) and (2). After calculating the constants (a) and (b), the whirl velocities (C_{u1} and C_{u2}) are calculated for any design methods from the known

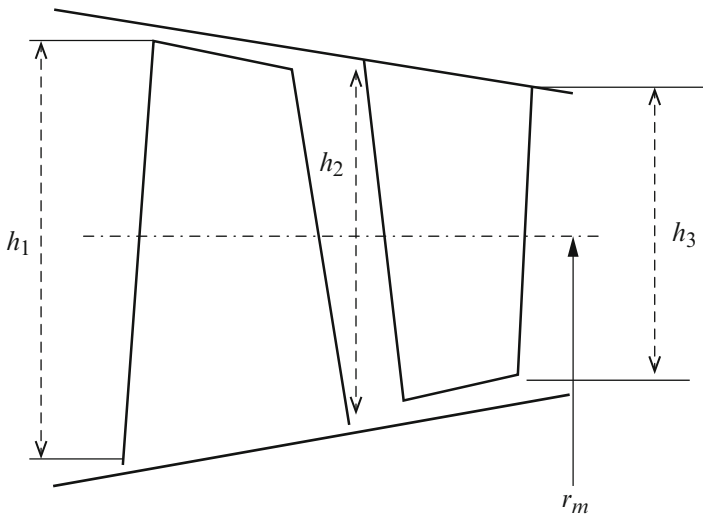


Fig. 9.31 A single stage geometry

values at the mean radius. Moreover, the axial velocities C_{a1} and C_{a2} are calculated for any design method other than the free vortex. The degree of reaction is also calculated. It is important to have as high degree of reaction at the hub as possible.

9.3.9 Blade Design

Blades design or selection from available airfoil series may be performed through experimentation or numerical analyses. The objective is to obtain information on the effect of different blade geometries on air flow angles, pressure losses, and energy transfer across blade rows. Only experimentation will be reviewed here. Cascade wind tunnels are used for testing a compressor blade row to be sure that it satisfies the following objectives:

1. To turn air through the required angles $(\beta_1 - \beta_2)^2$ for rotor and $(\alpha_2 - \alpha_3)$ for stator, to maximize the stage pressure ratio
2. To achieve the diffusion process with optimum efficiency or in other words minimum loss of stagnation pressure

Experiments are generally performed in a straight cascade wind tunnel; Fig. 9.32, that is composed of a row of geometrically similar blades equally spaced and parallel to each other. The height and length of cascade in a cascade wind tunnel are made as large as the available air supply will allow eliminating the interference effects due to the tunnel walls. Cascade is mounted on a turntable so that its angular direction with respect to the inflow duct (α_1) can be set in any

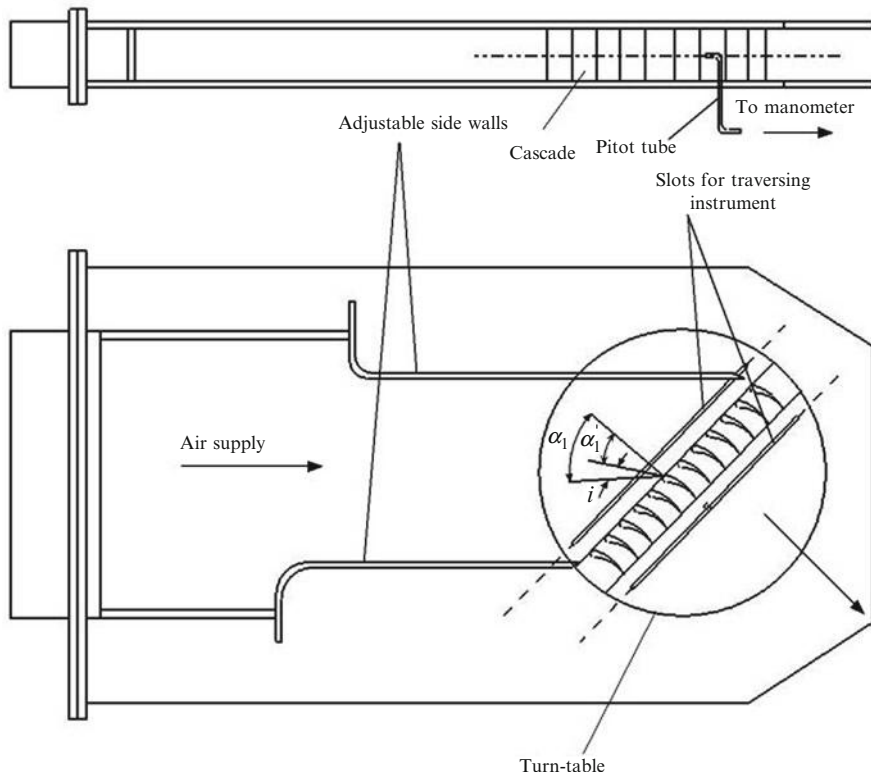


Fig. 9.32 Cascade wind tunnel

desired value and thus the incidence angle (i) may be varied. Vertical traverses over two planes usually a distance of one blade chord upstream and downstream of the cascade are provided pitot tubes and yaw meters to measure the pressure and air flow angles.

Pressure and velocity measurements are made by the usual L-shaped pitot-static tubes. Air direction is found by either claw or cylindrical yaw meters.

Important parameters in cascade design and testing are as follows:

Air deflection angle	$\epsilon = \alpha_1 - \alpha_2$
Solidity	$\sigma = \text{chord}/\text{spacing} (\frac{c}{s})$
Aspect ratio	height/chord (h/c)
Stagnation pressure loss	$\frac{P_{01} - P_{02}}{\frac{1}{2}\rho V_1^2} = \frac{w}{\frac{1}{2}\rho V_1^2}$

An averaging for this stagnation pressure loss (expressed hereafter as, $\frac{\bar{w}}{\frac{1}{2}\rho V_1^2}$) and also an average for the deflection angle ($\bar{\epsilon}$) is evaluated at this particular incidence angle. Repeating measurements for different incidence angles yield Fig. 9.33. The

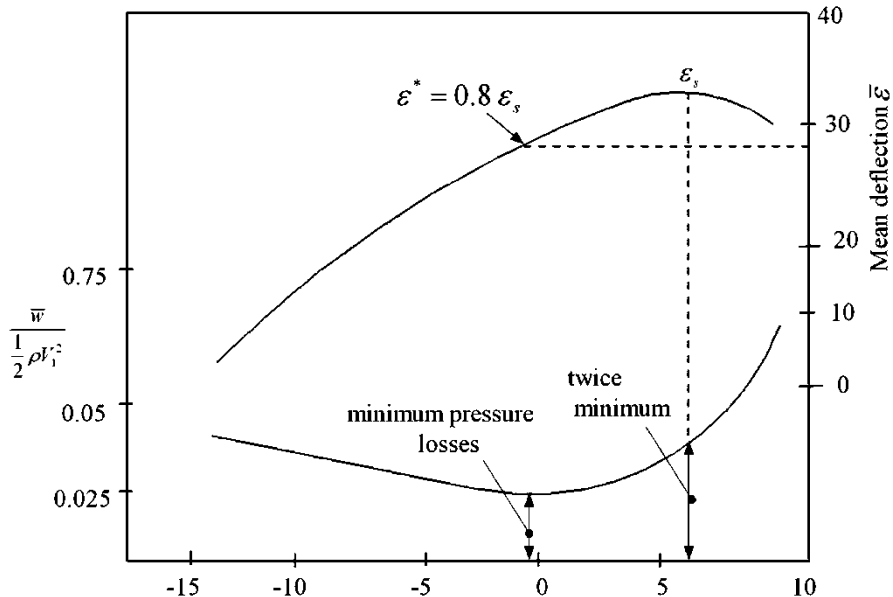


Fig. 9.33 Mean deflection and mean stagnation pressure loss curves

deflection increases with angle of incidence up to a maximum angle, $\bar{\epsilon}_s$, known as the stall or separation point. Since this angle may not be well defined, it is taken as the angle of incidence where the mean pressure loss is twice the minimum. The practice has been to select a deflection which corresponds to a definite proportion of the stalling deflection. This proportion found to be most suitable as 80 %, thus the selected or nominal deflection $\bar{\epsilon}^* = 0.8\bar{\epsilon}_s$.

This nominal deflection angle ($\bar{\epsilon}^*$) is mainly dependent on pitch/chord (s/c) ratio and air outlet angle (α_2). Cumulative results of different cascade tests are plotted in Fig. 9.34. For known flow angles, the deflection angle is calculated. Next from this deflection angle and the flow outlet angle, the ratio of (s/c) can be obtained. Since the blade height is known, then assuming the height/chord ratio is known (typical present day ratio is $h/c = 3$ for subsonic compressor), then the blade chord is known and the spacing (s) is calculated. The number of blades is simply calculated as

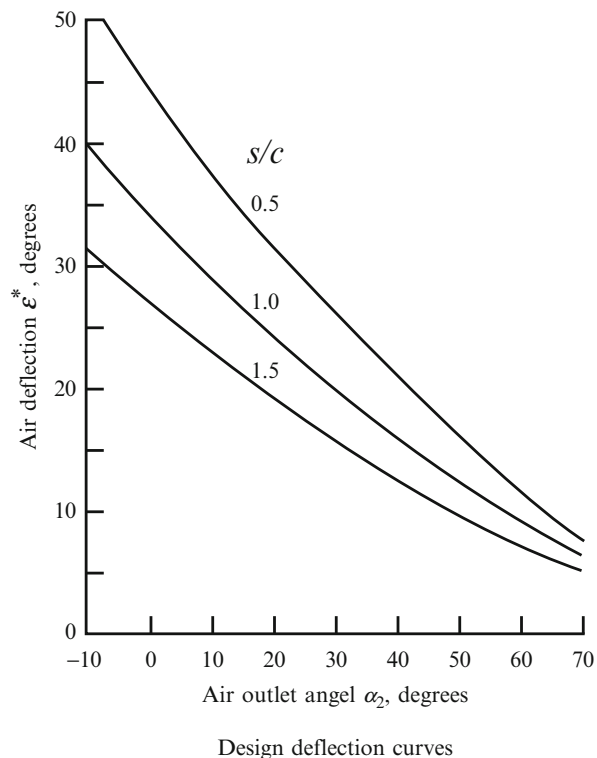
$$n = 2\pi r_m/s$$

It is recommended to avoid numbers with common multiples for the blades in successive rows (rotor/stator or stator/rotor) to avoid introducing resonant forcing frequencies.

Curve fitting of the deviation angle; Fig. 9.34 yields the following expression [25]:

$$\bar{\epsilon}^* = A + B\alpha_2 + C\ln\left(\frac{s}{c}\right) + D\alpha_2^2 + E\left(\ln\left(\frac{s}{c}\right)\right)^2 + F\alpha_2\ln\left(\frac{s}{c}\right) \quad (9.75)$$

Fig. 9.34 Cascade nominal deflection versus outlet angle



where

$A = 33.5293$	$B = -0.530812$	$C = -15.2599$
$C = 0.0020961$	$E = -0.677212$	$F = 0.187148$

Applies for $0 < \alpha_2 < 70^\circ$, $0.5 < s/c < 1.5$ ($0.666 < \sigma < 0.2$)

The blade inlet angle (α'_1) could be determined from the air inlet angle, assuming zero incidence angle $\alpha'_1 = \alpha_1$ ($i = 0$). However, the blade outlet angle (α'_2) cannot be determined from flow outlet angle α_2 , until the deviation angle δ ($\alpha_2 - \alpha'_2$) has been determined. The deflection angle is determined from the empirical relation

$$\delta = m \theta \sqrt{\frac{s}{c}} \quad (9.76a)$$

where

$$m = 0.23 \left(\frac{2a}{c} \right)^2 + 0.1 \left(\frac{\alpha_2^\circ}{50} \right) \quad (9.76b)$$

and blade camber angle $\theta = \alpha'_1 - \alpha'_2$

a = distance of point of maximum camber from the leading edge of the blade and the angle α_2 is in degrees. For circular arc $2a/c = 1$, then

$$m = 0.23 + 0.1 \left(\frac{\alpha_2^\circ}{50} \right) \quad (9.76c)$$

For inlet guide vanes IGV

$$\delta = 0.19 \theta (\text{s/c}) \quad (9.76d)$$

For a circular arc blade camber, the blade setting angle ζ is given by the relation

$$\zeta = \alpha'_1 - \frac{\theta}{2} \quad (9.77)$$

The axial chord of any blade row is then $c_a = c \cos \zeta$. The chord of blade in a subsonic compressor is one third of the blade height $c = h/3$. The gap between two successive blade rows is $w = c_a/4$. Thus the axial length of one stage (including a rotor-gap-stator-gap) will be equal to $l = \frac{5}{4} \{(c_a)_r + (c_a)_s\}$

The same procedure can be followed for any other blade ratios. The length of the compressor is then the sum of axial lengths of all compressor stages.

9.3.10 Choice of Airfoil Type

After the radial distribution of air angles and velocities are determined, the blading can be designed. First, incidence and deviation angles are selected so that the slope of the airfoil mean line (camber line) at the leading and trailing edges can be established [22]. For minimum losses, incidence angle (i) must be in the range $-5^\circ \leq i \leq 5^\circ$. The deviation angle is calculated from Eq. (9.58e), which is also in the range $5^\circ \leq \delta \leq 20^\circ$. Mean line shape and thickness are selected to achieve the desired airfoil loadings. The pressure increase is achieved by the diffusion process. The amount of diffusion is monitored by computing the diffusion factor, Eq. (9.54). Values of diffusion factor greater than 0.65 mean flow separation is imminent.

The nature and type of blading depends on the application and Mach number [26]. Subsonic blading usually consists of circular arcs, parabolic arcs, or combinations thereof. Many countries developed their own profiles (e.g., United States, Britain, Japan, West Germany) for subsonic flows. One of the famous American profiles is *NACA 65 series* blades. The NACA 65 series designation is as follows: NACA 65 (x) y , or 65- x - y , here x is 10 times the design lift coefficient of an isolated airfoil and y is the maximum thickness in percent of chord. Moreover, the famous British profile is the C-series. An example for the C-series is 10C4/20P40, where blade is 10 % thick C4 profile with a 20° camber angle and a parabolic camber line

having maximum camber at 40 % of the chord. A 10C4/20C40 blade would be similar, but with a circular arc. Another British series is the RAF 27 profiles. The NACA 65 series and similar British profiles are used in low subsonic flows [23].

9.3.11 Compressor Map

Compressor performance is usually presented in the form of compressor map as described in the Sect. 9.2.12 for centrifugal compressor. The design point is only a single point on the compressor map, which is characterized by a certain rotational speed, mass flow parameter, pressure ratio, and efficiency. However, compressor has to perform efficiently in other operating conditions, frequently identified as *off-design conditions*, namely, engine starting, idling, reduced power, maximum power, acceleration, and deceleration.

Consequently, compressor has to operate satisfactorily over a wide range of rotational speed (RPM) and inlet conditions. But since the annulus area and compressor blading are chosen to satisfy the design point condition only, then at other conditions they will not function correctly [4]. Comparing maps for axial and centrifugal compressors, it is noticed that for a fixed value of $\frac{N}{\sqrt{T_{01}}}$, the range of mass flow rate is narrower in axial compressor than that in a centrifugal compressor. At high rotational speed, the lines become very steep and ultimately may be vertical.

Surge point occurs before the constant speed curves reach a maximum value. Stage characteristics are similar to overall characteristics but much lower pressure ratio. Mass flow is limited by choking in various stages.

Since the axial velocity is maintained constant, then the annulus area is inversely proportional to the air density and thus the annulus area of the compressor decreases from the front to the rear stages.

9.3.11.1 Stall and Surge

Stall is a situation of abnormal airflow through a single or multiple stages of the compressor. Surge is the situation of stalling of the whole compressor. Surge results in a loss of engine power. This power failure may only be momentary or may shut the engine down completely causing a flameout, as shown in Fig. 9.35 for civilian and military aircrafts. The appropriate response to compressor stalls varies according the engine type and situation, but usually consists of immediately and steadily decreasing thrust on the affected engine. The most likely cause of a compressor stall is a sudden change in the pressure differential between the intake and combustion chamber. The following factors can induce compressor stall:

Engine over-speed, engine operation outside specified engineering parameters, turbulent or disrupted airflow to the engine intake and contaminated or damaged engine components.



Fig. 9.35 Compressor surge leading to a flameout: (a) Boeing 777 aircraft; (b) Sukhoi T-50 PAK FA

Rotating stall and surge phenomena in axial flow compressors are the most serious problem in compressor. Severe performance and reliability problems arise if the compressor is unable to recover from stall. Surge and rotating stall can be described as follows [22].

Rotating stall is defined as a breakdown at one or more compressor blades [22]. A rotating stall is a stagnated region of air which moves in the opposite circumferential direction of rotor rotation, but at 50–70 % of the blade speed [27]. If the throttle is

closed or the back pressure is increased, the blade loading or the incidence is increased. Then the adverse pressure gradient on the suction surfaces increases the boundary layer growth which leads to separation and stall. Not all the blade passages will stall at the same time. Stalling of a blade passage will lead to increase of the incidence angle of the next passage in the opposite direction of rotation.

There may be several stall cells in a blade row rotating in the same time. As described in [28], part span is usually encountered in the front stages of the compressor with large aspect ratio blades and low speeds. It is usually encountered during take-off or start up. Full span stall occurs in the medium speed range and its effect is much more damaging. In brief, rotating stall does not move axially in either direction although it may cause pressure waves to move upstream (compression wave) or downstream (rarefaction waves).

The compressor *surge* occurs when there is complete breakdown of the flow field in the entire engine (not just blading). Upon surge, a compression component will unload by permitting the compressed fluid in downstream stages to expand in the upstream direction forming waves strong enough to lead to flow reversal. The compressor can recover and begin again to pump flow. However, if surge cause is not removed, the compressor will surge again and will continue the surge/recovery cycle until some relief is provided. Otherwise, surge will result in violent oscillations in pressure, propagation of pressure waves, and the failure of the entire compression system.

An important parameter called *surge margin* (very similar to the factor of safety in mechanical system design) is defined as

$$\text{Stall margin} = \left\{ \frac{(P_{02}/P_{01})_{\text{stall}}}{(P_{02}/P_{01})_{\text{design point}}} \times \frac{\left(\dot{m} \sqrt{T_{01}/P_{01}}\right)_{\text{design point}}}{\left(\dot{m} \sqrt{T_{01}/P_{01}}\right)_{\text{stall}}} - 1 \right\} \%$$

When surge occurs in an operating engine, it causes at the least a stoppage of the airflow through the compressor [27], which leads to a straightforward expulsion of air out the intake. In civil transports, this is evidenced by a loud bang emanating from the engine as the combustion process “backfires”. Passengers will feel successive “cannon shots” of fire balls spaced about 3/4 a second apart. In particular, the occupants seated next to the failed engine will be temporarily deaf in one ear and all the other cabin occupants will complain of ringing ears. Surge also may be accompanied by an increased exhaust gas temperature and yawing of the aircraft in the direction of the affected engine. Moreover, all the Mach 0.70+ airflow reverse direction from inside the engine. It projects a fireball from the power generating core combustor of the engine out the front of the engine (surge phase). However that fire ball is driven back into the engine by the forward speed of the aircraft and the residual inertia of the rotating fan (for turbofan engines). The airflow tries to re-establish normal direction in the engine at this point due to the rotating inertia of the engine rotors (recovery phase). The pilot will think the controls have “whip sawed” him as the forces of the airplane are redistributed and then he forces them back to where they should be. The cabin will fill with a haze from the contaminated hot bleed air [4].

Violent fan or compressor surge might completely destroy the engine and set it on fire. But absent such structural damage, the engine will usually recover and continue to run.

If the engine has been damaged too much (e.g. broken blades and parts), the airflow will not resume a normal path and the engine disintegrates; Fig. 9.36. If the engine is only partially damaged, it will give 1 or 2 more cannon shots 3/4 seconds apart before the engine completely disintegrates.

In supersonic aircraft, the consequences can be more serious because the blockage due to surge can generate a shock wave in the inlet which may produce overpressures large enough to damage the structure.

9.3.11.2 Surge Control Methods

As described above, surge causes serious problems both to compressor, engine, and aircraft. Though it is unavoidable but its recovery is affordable. Since rotating stall represents the onset of surge, if stall could be avoided surge will not be seen. However, this is an impossible task due to the different operating conditions for the compressors installed in aero engines powering airplanes during any trip or mission. For compressors in industrial power plants, different conditions are found during starting, idling, acceleration, deceleration, etc. [4]. Foreign object debris (FOD) is another serious circumstance that influences the fluid mass flow rate. Compressor designers proposed and designed some methods for surge control. Designers may replace the single spool engine by two spool engine. Each spool (and consequently compressor) rotates at a different speed. Moreover, they developed the variable geometry compressor and air bleed system to counteract surge during engine run. The later techniques are activated by the engine control unit



Fig. 9.36 Damaged blades of centrifugal compressor (*left*) and axial compressor (*right*)

(ECU), which represents a computerized control system that has its inputs from sensors within the engine.

(A) Multi-spool compressor

Since reduction in compressor speed from design value will cause an increase of incidence in the first stage and a decrease of incidence in the last stage. The incidence could be maintained at the design value by decreasing the speed of the first stages and increasing the speed of the last stage; these conflicting requirements can be met by splitting the compressor into two (or more) sections each driven by separate turbine at different rotational speeds. Examples for the small two spool engines are General Electric CFE738 and Pratt & Whitney Canada PW600. Examples for high bypass ratio two spool turbofan engines are General Electric: CF6, GE90, GEnx, Pratt & Whitney: JT9D and PW4000, IAE V2500, engine alliance GP7000, CFM international CFM56 turbofan engines. Examples for three spools are Rolls Royce RB211 and Trent family as well as Russian three spool engines; Lotarev D-36, Lotarev/Progress D-18T and Progress D-436, Kuznetsov NK-25 and NK-321. Recently, geared fan provides even better surge control and reduced supersonic losses. Examples for geared fan turbofans are Honeywell TFE731, ALF 502/507, and the recent Pratt & Whitney PW1000G.

Typical map for the low pressure compressors is illustrated in Fig. 9.37. It may encounter surge during deceleration. On the contrary, high pressure compressor may surge during acceleration; Fig. 9.38.

(B) Variable vanes

Variable stator vanes (VSV) may be employed to avoid stalling of stages susceptible to surge, namely, the front or last stages of compressors. Furthermore,

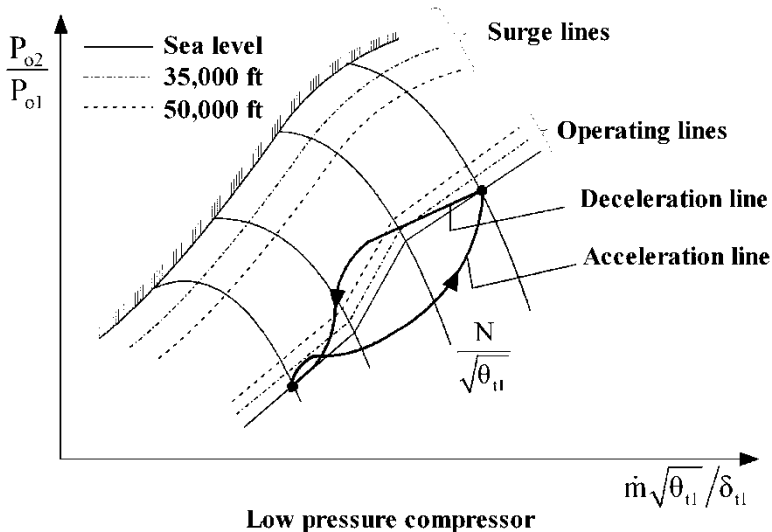


Fig. 9.37 Map for low pressure compressor (Courtesy Pratt & Whitney [29])

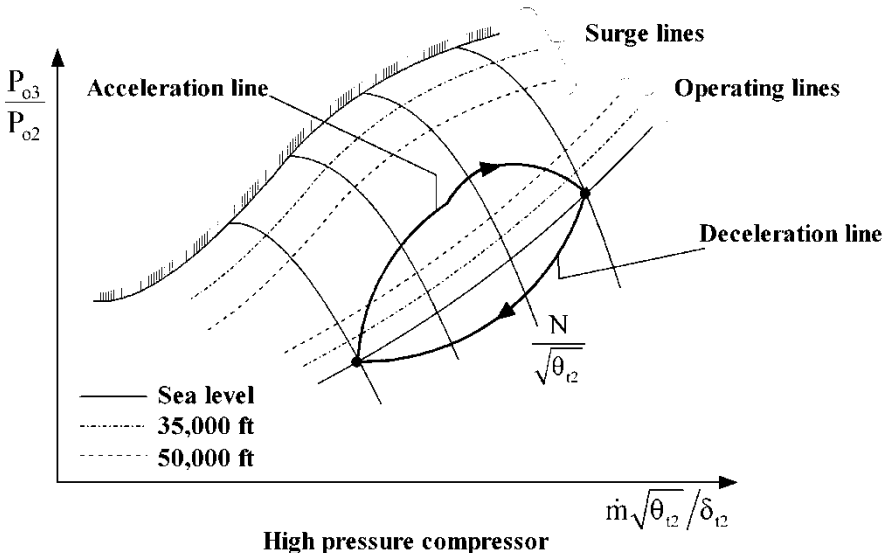


Fig. 9.38 Map for high pressure compressor (Courtesy Pratt & Whitney [29])

with the tendency of the back end stages to be more lightly loaded (due to lower Mach numbers), the stall problem is not as severe in the back stages [30]. As a result, variable stators are normally confined to the front stages and their principle use is to provide acceptable starting and/or low speed acceleration of the engine. Positive stall is encountered when the inlet relative angle β_1 , and consequently the incidence angle are increased. To reduce this value, two methods are employed. In the first, the inlet guide vanes or the stators of the first stages are rotated away from the axial direction to increase the absolute angle at inlet α_1 and thus reduces the relative inlet angle β_1 . As an alternative, the rear part of the blade is rotated, thus becoming over cambered, to do the same job as the completely rotated stators; Fig. 9.39.

(C) Air bleed

Bleeding of air downstream of a stalled stage or stages will allow the air mass flow to increase ahead of the bleed location. This increase in airflow will in turn increase the axial speed and thus results in a reduction of the rotor incidence and install the blade, Fig. 9.40. The flow to the back stages will thereby reduce.

9.4 Centrifugal and Axial Compressors Material

The materials of compressors used in aero engines and gas turbines should have high strength, ductility, and temperature resistance. In addition, compressors in aircraft engines must have low density or high strength/weight ratios. Table 9.11

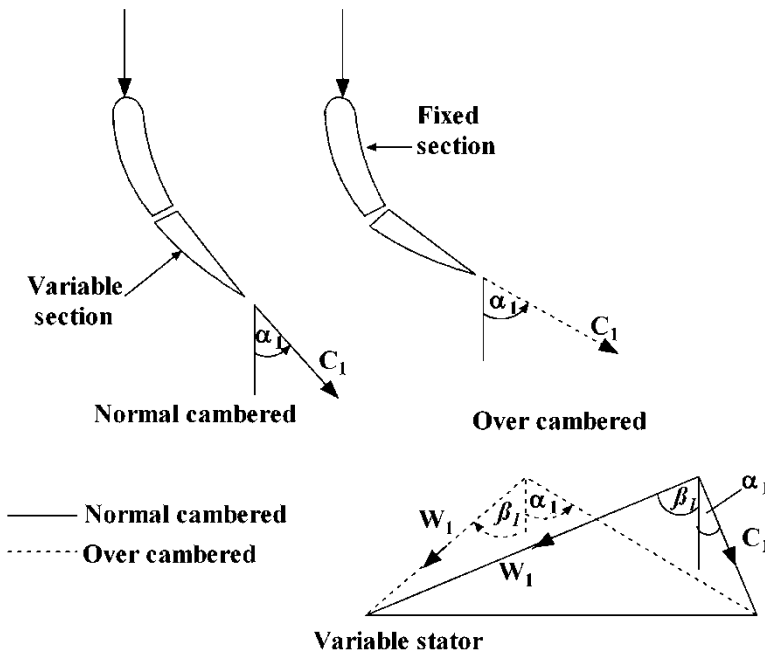


Fig. 9.39 Variable stator blades

provides a short list of materials used in different components of both centrifugal and axial compressors together with their trade names.

9.5 Closure

In this chapter, details of aerodynamic design and mechanical design of compressors are given. Centrifugal compressors having different impeller types (radial, forward and backswept) are discussed. Moreover, different types of diffuser are approached. Two-dimensional aerodynamic analysis is only adopted. Velocity triangles provide insight of the compression process within the impeller.

Two and quasi-3D aerodynamic analysis of axial compressors is given. Critical normal stresses at blade root are discussed for rotor blades having constant or variable cross sectional area along blade height. Details of aerodynamic design of a multi-stage axial compressor are thoroughly discussed.

Compressor maps of both compressors are discussed and methods for controlling surge are highlighted.

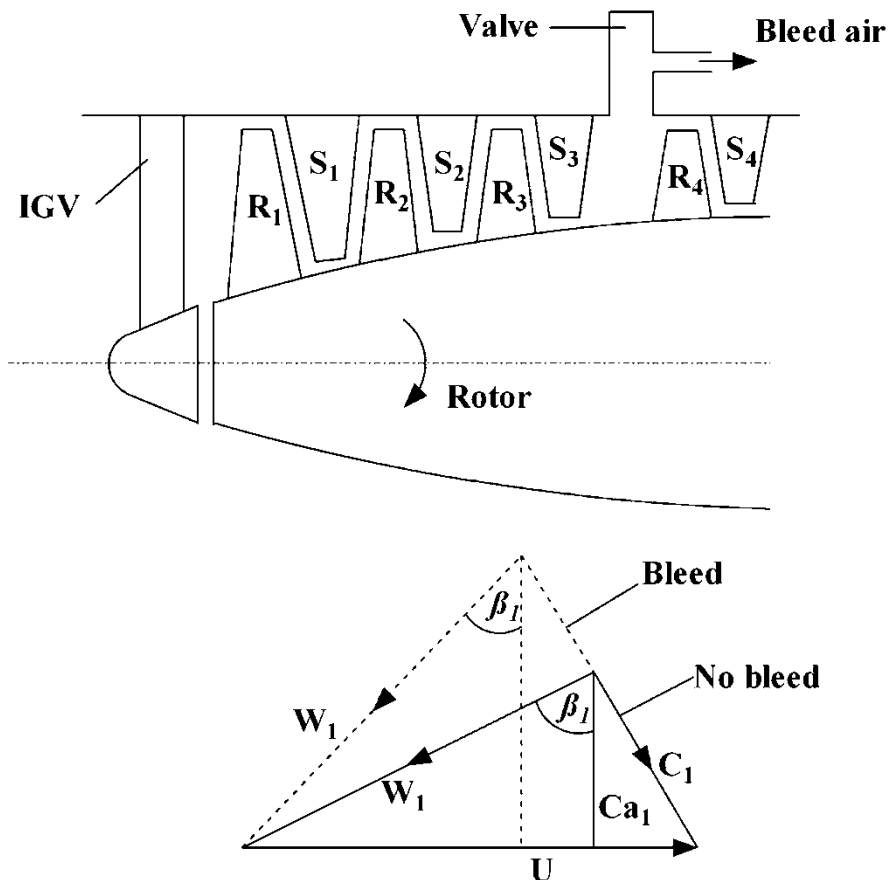


Fig. 9.40 Bleed as a surge controller

Problems

9.1(A) Explain why

1. Positive prewhirl is used in centrifugal compressors of aircraft engines
2. Backward-swept impellers are used in most centrifugal compressors
3. Axial compressors are used in recent industrial gas turbines
4. Blade height in last stages of an axial compressor is shorter than first stages

- (B) Compare between axial compressor and propeller
 (C) Compare between axial compressor and axial turbine

9.2 The shown figure illustrates *two* layouts for a centrifugal compressor. It is required to

- (a) Draw the front view of compressor (looking in direction of arrow 1)
- (b) Draw the velocity triangles in both cases
- (c) Draw a schematic diagram for impeller (case B) with splitters and describe advantages and disadvantages of splitters

Table 9.11 Material commonly used in centrifugal and axial compressors

Component	Material	Trade name
Impeller (centrifugal compressor)	Stainless steel	AISI 416, 17-4 PH
	Titanium alloys	Ti-6Al-4V
Stator vanes (axial compressor)	Aluminum	RR 58
	Titanium	Ti-6Al-4V
	Stainless steel	AISAI 410, A286 Chromalloy, Jethete M. 152, Greek Ascoloy, FV 535, FV500, 18/8
Rotor blades (axial compressor)	Aluminum	RR 58
	Titanium	6 Al-4V, TBB
	Stainless steel	A286, Greek Ascoloy, FV535, FV520, 17-4 Ph, 403
	Precipitation hardening super alloy	Inco 718, Nimonic 901
Discs, drum (axial compressor)	Titanium	Ti-6Al-4V, TBA (IMI 679), IMI 381
	Steel	4340, FV 448, b5-f5, 9310
	Stainless steel	AISI 410, AISI 416, 17-4 Ph, Jethete M. 152, Chromalloy (FV 535)
	Precipitation hardening super alloy	Incoloy 901, Inco 718, Nimonic 901
Shafts, hubs	Steel	Hykoro, 4340, 9310, B5-F5
	Precipitation hardening super alloy	Inco 718

- (d) Describe when vaneless diffuser is used
- (e) Draw the inlet velocity triangles for the cases of positive and negative prewhirl
- (f) Draw the T-s diagram for the diffuser

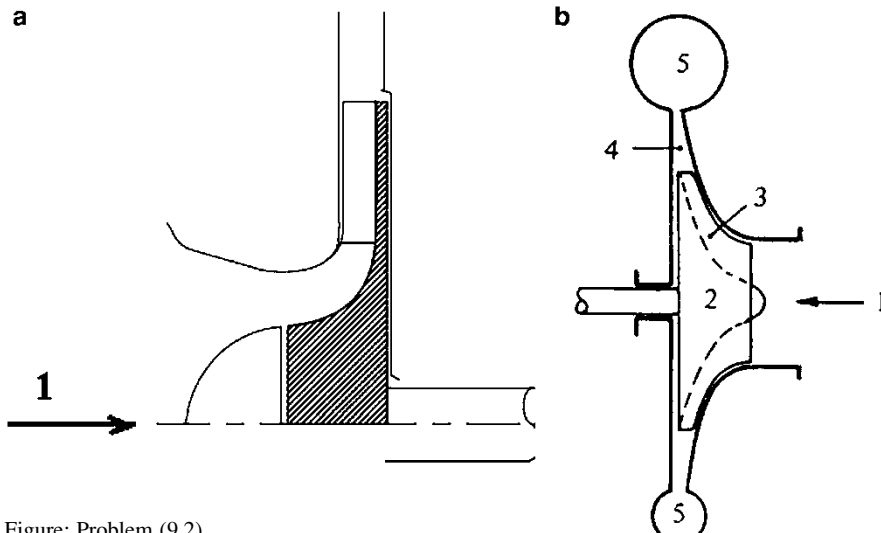


Figure: Problem (9.2)

- 9.3 A small turbojet engine is composed of an intake, centrifugal compressor, combustion chamber, an axial turbine, and an exhaust nozzle. The centrifugal compressor (states 1-2-3) has the following data:

$T_{01} = 300 \text{ K}$	$P_{01} = 100 \text{ kPa}$	$P_{03}/P_{01} = 3.0$
$P_2/P_1 = 1.94$	$P_3/P_2 = 1.48$	$C_1 = 106 \text{ m/s}$
Maximum inlet relative Mach number $W_{1\max}/a_1 = 0.84$		
Maximum absolute Mach number at outlet $C_2/a_2 = 0.9$		
$D_h = 20.6 \text{ mm}$	$D_s = 60.3 \text{ mm}$	$D_2 = 102 \text{ mm}$
$\psi = 1.04$	Number of blades = 18	

Assuming no prewhirl, it is required to

- (a) Calculate air mass flow rate
 - (b) Calculate the rotational speed
 - (c) Calculate the temperature rise in the compressor
 - (d) Prove that: $C_2 = \sqrt{\frac{2\gamma R M_2^2 T_{02}}{2+(\gamma-1)M_2^2}}$
 - (e) Calculate the compressor efficiency
 - (f) Calculate the percentage of losses in the impeller to the total losses in the compressor
 - (g) Calculate the impeller efficiency
- 9.4 Draw the pressure ratio relation versus the blade Mach number ($M_u = U_2/a_{01}$) as expressed by the relation:

$$\pi = \left(1 + \eta_c \frac{\Delta T_0}{T_{01}}\right)^{\frac{\gamma}{\gamma-1}} = \left\{1 + \eta_c(\gamma - 1)M_u^2 \left[\left(1 - \frac{W_{r2}}{U_2} \tan \beta_2\right) - \left(\frac{r_{1m}}{r_2}\right)^2 \left(\frac{C_{u1}}{U_{1m}}\right)\right]\right\}^{\frac{\gamma}{\gamma-1}}$$

In the following cases:

- (a) $C_{u1} = 0.0$, $\beta_2 = 0.0$, for the following three cases: $\eta_c = 0.7, 0.8, 0.85$
- (b) $C_{u1} = 0.0$, $\beta_2 = 20.0$, for the following three cases: $\eta_c = 0.7, 0.8, 0.85$
- (c) $C_{u1} = 0.0$, $\beta_2 = -20.0$, for the following three cases: $\eta_c = 0.7, 0.8, 0.85$
- (d) Repeat the above cases with $\left(\frac{W_{r2}}{U_2} = 0.7\right)$, $\left(\frac{C_{u1}}{U_{1m}}\right) = 1.0$ and $\frac{r_{1m}}{r_2} = 0.5$

Consider the blade Mach number (M_u) varies from (0.8 to 1.4) and $\gamma = 1.4$.

- 9.5 A centrifugal compressor used in a small turbojet engine which is fitted with a can type combustion chamber. Measurement of the pressure, temperature, and velocity components at different locations in the compressor is listed in the following table:

Location	1 (Impeller inlet)	2 (Impeller outlet)	3 (Stator outlet)	4 (Combustor inlet)
$T_o(\text{K})$	292	380	380	380
$P_o(\text{kPa})$	86	190	175	172

(continued)

Location	1 (Impeller inlet)	2 (Impeller outlet)	3 (Stator outlet)	4 (Combustor inlet)
$T(K)$	289	341	353	376
$P(kPa)$	84	135	152	172
$C_u(m/s)$	—	265	218	—
$C_r(m/s)$	—	29	23	—
$C_a(m/s)$	59	—	—	18

Other data are

Power input factor	$\psi = 1.04$,	Rotational speed $N = 210$ rps
Eye tip diameter	$D_{1tip} = 0.3$ m	eye hub diameter = 0.14 m

If the flow in the stator is assumed to be a free vortex flow, it is required to:

- (a) Draw the velocity triangles at impeller inlet and outlet.
 - (b) Calculate the percentage of the impeller losses out of the total losses in compressor.
 - (c) Calculate the air mass flow rate into the compressor.
 - (d) Calculate the diffuser outlet diameter and width.
 - (e) Calculate the power needed to drive the compressor.
 - (f) If air leaving the compressor is assembled in eight circular manifolds to direct the air to the eight cans of the combustion chamber, calculate the diameter of each manifold.
- 9.6 Three cases for an impeller of a centrifugal compressor, namely radial, forward, and backward are considered. They have outlet relative angle ($\beta_2 = 0, 20, -20$) for radial, backward, and forward impellers, respectively (refer to Fig. 9.8).

The design parameters are as follows:

Inlet total temperature	$T_{o1} = 290$ K	Impeller outlet diameter	$D_2 = 0.50$ m
Inlet total pressure	$P_{o1} = 101$ kPa	Eye hub diameter	$d_{1h} = 0.15$ m
Mass flow rate	$m^* = 10.0$ kg/s	Eye tip diameter	$d_{1t} = 0.30$ m
Rotational speed	$N = 275$ rev/s	Impeller isentropic efficiency	$\eta = 0.92$
Power input factor	$\psi = 1.04$		

The impeller losses are half of total compressor losses. Assume the inlet axial velocity is equal to the radial velocity ($C_a = C_r$).

- (a) Calculate the pressure ratio for the three types of compressors.
- (b) If the mass flow rate is decreased such that the new axial velocity at the inlet is reduced by 30 % ($C'_a = 0.7C_a$) and due to losses at the inducer, the impeller adiabatic efficiency is decreased to 0.88, calculate the new pressure ratio and power for the three cases. Comment on the results.

- 9.6 Consider a centrifugal compressor fitted with an upstream inlet guide vane to provide positive prewhirl. The maximum permissible inlet relative Mach number at shroud is $(M_{1\ rel})_{shroud} = 0.95$. The corresponding absolute and relative angles at shroud are $\alpha_{1\ shroud} = 25^\circ$, $\beta_{1\ shroud} = 55^\circ$. Inlet total conditions are $T_{01} = 290\text{K}$, $P_{01} = 101\text{ kPa.}$, and shroud inlet radius is 0.12 m

Calculate

- (a) Axial speed at inlet (C_a)
- (b) Rotational speed (Ω)
- (c) If the inlet guide vanes are removed and the flow enters axially (axial velocity is maintained constant), what is the new value of the rotational speed that maintain the same value of maximum inlet relative Mach number as 0.95

- 9.7 A single-sided centrifugal compressor is to deliver 14 kg/s of air when operating at pressure ratio of 4:1 and a rotational speed of 200 rps. The inlet stagnation conditions are 288 K and 1.0 bar. Assuming a slip factor of 0.9, a power input factor of 1.04 and an overall isentropic efficiency of 0.8, estimate the overall diameter of the impeller.

If the Mach number is not to exceed unity at the impeller tip, and 50 % of the losses are assumed to occur in the impeller, find the minimum possible axial depth of the diffuser

- 9.8 An aircraft engine incorporates a single-sided centrifugal compressor. The aircraft flies with a speed of 230 m/s at an altitude where the pressure is 0.23 bar and the temperature 217 K. The intake duct of the impeller eye contains fixed vanes which give the air prewhirl of 25° at all radii. The inner and outer diameters of the eye are 18 and 33 cm, respectively; the diameter of the impeller periphery is 54 cm and the rotational speed is 270 rps.

Estimate the stagnation pressure at the compressor outlet when the mass flow is 4.0 kg/s. Neglect losses in the inlet duct and fixed vanes, and assume that the isentropic efficiency of the compressor is 0.8. Take the slip factor is 0.92 and the power input factor as 1.04.

- 9.9 The following results were obtained from a test on a small single-sided centrifugal compressor

Compressor delivery stagnation pressure	2.97 bar	Mass flow	0.6 kg/s
Compressor delivery stagnation temperature	429 K	Rotational speed	766 rps
Static pressure at impeller tip	1.92 bar	Impeller diameter	16.5 cm
Axial depth of the vaneless diffuser	1.0 cm	Ambient pressure	0.99 bar
Number of impeller vanes	17	Ambient temperature	288 K

Calculate

- (a) The isentropic efficiency of the compressor
- (b) The stagnation pressure at impeller tip
- (c) The fraction of the overall losses, which occur in the impeller

9.10 A *two-stage* centrifugal compressor has the following data:

	First stage	Second stage
Power input factor	1.04	1.04
Slip factor	0.90	0.92
Overall diameter of the impeller (m)	0.60	0.60
Eye root diameter (m)	0.16	0.16
Eye tip diameter (m)	0.32	0.28
Isentropic efficiency	0.78	0.80

The rotational speed is 250 rev/s, the air mass flow rate is 10 kg/s, and inlet stagnation conditions are $T_{01} = 298$ K, $P_{01} = 1.14$ bar. The total pressure drop in the inverted U-shape duct between the two stages is 5 %. The first stage is identified by states from 1 to 3, while the second stage is identified by states from 4 to 6.

Calculate

- (a) The overall pressure ratio of the compressor.
- (b) If $\rho_1 = 1.24 \text{ kg/m}^3$, $C_{a1} = C_{a2}$, $C_{a4} = C_{a5}$, calculate the diffuser depth for each stage.
- (c) The power needed to drive the compressor.

9.11 A double-sided centrifugal compressor has the following characteristics:

Mass flow rate 60 kg/s, which is divided equally between the front and back faces of impeller

Power input factor $\psi = 1.04$

Number of impeller blades $n = 22$

Rotational speed $N = 320$ rps

Isentropic efficiency $\eta_c = 0.82$

Inlet total temperature and pressure $T_{01} = 296$ K, $P_{01} = 1.05$ bar

Power required driving the compressor 10.0 MW

Absolute Mach number at impeller outlet $M_2 = 1.18$

Eye tip diameter is double the eye root diameter

Assuming that $C_{r2} = C_{a1}$, calculate:

1. Temperature rise in compressor ΔT_0
2. Impeller diameter D_2
3. The absolute velocity at impeller outlet C_2
4. Axial velocity at impeller inlet C_{a1}
5. Eye root and tip diameters
6. Pressure drop in the stator ($P_{01} - P_{03}$)

9.12 The shown figure illustrates a two-stage centrifugal compressor with its design conditions listed in the following table.

	First stage	Second stage
Rotational speed (rpm)	75,000	65,500
Adiabatic efficiency	0.84	0.862
Slip factor	0.9	0.9
Impeller tip radius (cm)	5.9	5.6

Figure: Problem (9.12)

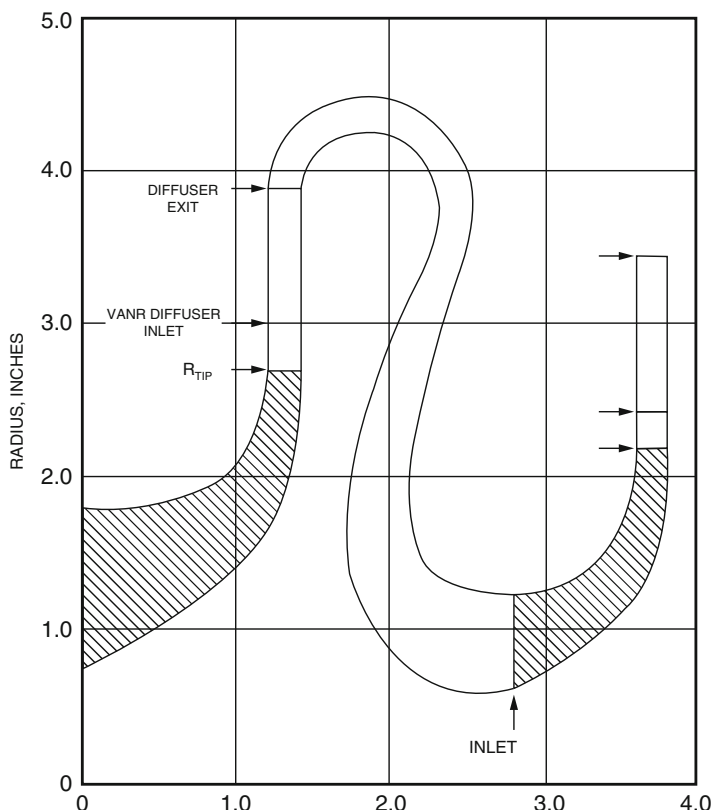
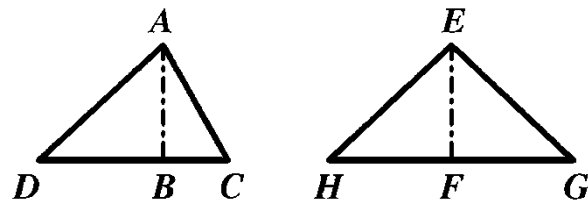


Figure: Problem (9.12)

If the inlet total temperature is: $T_{01} = 288 \text{ K}$, Calculate:

1. Pressure ratio for each stage
2. Overall pressure ratio
3. Efficiency of two-stage centrifugal compressor

9.13 The shown figure illustrates velocity triangles at inlet and outlet for two cases of a centrifugal compressor and an axial compressor.

$$\text{With } AB = EF = C_1 = W_2$$

$$\text{and } BC < BD, \quad FG = FH$$

- (A) Which of these cases represents an axial compressor?
- (B) PROVE that both compressors have the same specific work.
- (C) Consider the case of axial compressor with the following data:

$$(T_{01})_{\text{rel}} = 315 \text{ K}, T_2 = 311 \text{ K}, T_{02} = 340 \text{ K}, N = 7150 \text{ rpm}$$

Calculate

1. Specific work (w)
2. Mean radius (r_m)
3. Degree of reaction (Λ)
4. Loading factor (Ψ)

9.14 The shown figure illustrates a combined axial-centrifugal compressor. Each is composed of a single stage. Inlet conditions are

$$T_{01} = 300 \text{ K}, P_{01} = 101 \text{ kPa}$$

Both stages are rotating at the same rotational speed (N).

Overall pressure Ratio is 10.0.

Other data are

Axial compressor

Mean inlet radius: $r_1 = 0.4 \text{ m}$ Stage efficiency: $\eta_1 = 0.85$

Outlet swirl velocity: $C_{u2} = 100 \text{ m/s}$ Angles: $\alpha_1 = 0^\circ, \alpha_2 = 45^\circ$

Rotor blade height at inlet: $h_1 = 0.15 \text{ m}$

Centrifugal compressor

Mean inlet radius: $r_4 = 0.4 \text{ m}$ Impeller outlet radius: $r_5 = 0.6 \text{ m}$

Power input factor $\psi = 1.04$ slip factor $\sigma = 0.961$

Stage efficiency: $\eta_2 = 0.8$

Velocities relations: $C_1 = C_3 = C_4 = C_{r5} = W_{r5}$

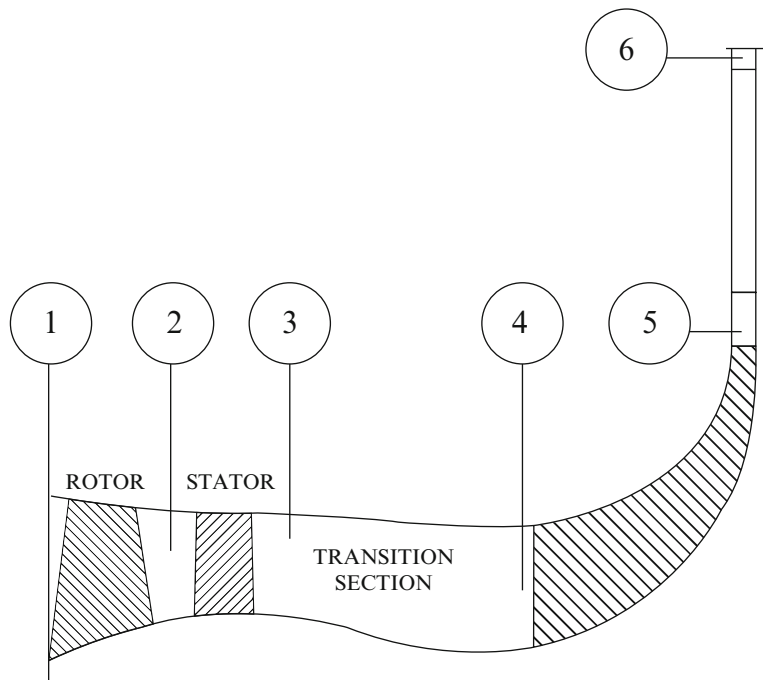


Figure: Problem (9.14)

(A) *Calculate*

1. Rotational speed (N)
2. Air mass flow rate through compressor
3. Hub and tip radii of centrifugal compressor at inlet
4. Width of impeller at outlet
5. Power needed to drive the compressor

(B) *Draw*

1. Velocity triangles for axial compressor stage
2. Velocity triangles at inlet and outlet of centrifugal compressor

(C) *Compare* between axial and centrifugal compressors (in general)

- 9.15 A helicopter gas turbine requires an overall compressor pressure ratio of 15:1. This is to be obtained using *two spool* layouts consisting of a five-stage *axial* compressor (on the first spool) followed by a single stage *centrifugal* compressor (on the second spool). The polytropic efficiency of both compressors is 0.90.

The axial compressor has the following data:

Stage temperature rise	40 K	Mean diameter of each stage	25 cm
Degree of reaction	50 %	Constant axial velocity	160 m/s
Stator outlet angle	20°	Work done factor is constant 0.89	
Ambient total temperature	300 K	Ambient total pressure	101 kPa

The centrifugal compressor has the following data:

Impeller tip diameter	40 cm	Slip factor	0.9
Power input factor	1.04		

Assume inlet velocity at the eye of the impeller is axial and constant

1. Calculate the required rotational speed of each spool.
2. Draw velocity triangles at mean section of axial compressor, inlet and outlet of centrifugal compressor.
3. For a free vortex design of axial compressor, calculate the degree of reaction at blade root of first stage if the hub-to-tip ratio is 0.5.

9.16 A centrifugal compressor is fitted with inlet guide vanes to generate a positive prewhirl at inlet. It is required to prove that the specific work is governed by the following relations.

- (a) If the swirl velocity is governed by a forced vortex; $C_{u1} = Ar_1$, then the specific work w is expressed as

$$w = \sigma U_2^2 - (U_{1t}C_{u1t} + U_{1t}C_{u1h} + U_{1h}C_{u1h})/3$$

- (b) If the swirl velocity is governed by a free vortex; $C_{u1} = B/r_1$, then the specific work w is expressed as

$$w = \sigma U_2^2 - \omega B$$

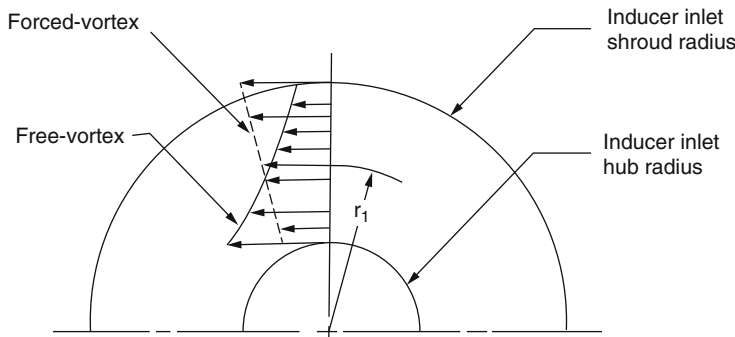


Figure: Problem (9.16)

- (c) If the swirl velocity is *constant*; $C_{u1} = \lambda$, then the specific work w is expressed as

$$w = \sigma U_2^2 - U_{1m} C_{u1}$$

A, B and λ are constants, ω is the rotational speed (rad/s)

9.17. A centrifugal compressor has inlet velocities:

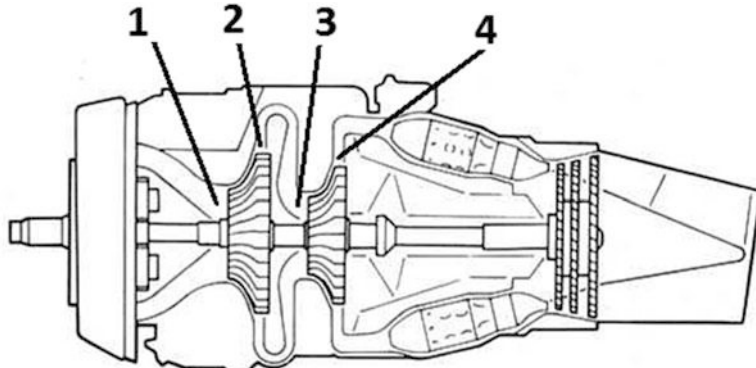
$$C_1 = 150 \text{ m/s}, W_1 = 250 \text{ m/s}, U_1 = 200 \text{ m/s}$$

and outlet velocities of:

$$C_2 = 390 \text{ m/s}, W_2 = 150 \text{ m/s}, U_2 = 350 \text{ m/s},$$

The blade angle at impeller tip with the radial direction $\beta_2' = \beta_2 + 5^\circ$, where β_2 is the flow angle measured from the radial direction.

- (a) What is the type of impeller? (forward – radial – backward)
- (b) Calculate the slip factor
- (c) Calculate the stage temperature rise



9.18 The shown figure illustrates a Turboprop engine where the compressor section is composed of two centrifugal compressors. Air enters both stages in the axial direction, where $C_1 = C_3$

Data for the *first stage*:

$$\begin{aligned} T_{01} &= 288 \text{ K}, & P_{01} &= 101 \text{ kPa}, & \pi_1 &= 3, & \sigma_1 &= 0.94, & \eta_1 &= 0.86, \\ \psi_1 &= 1.04, & D_{1t} &= 0.5 \text{ m}, & D_2 &= 0.8 \text{ m}, & \xi_{\text{inlet}} &= 0.65, & (M_{1 \text{ rel}})_{\text{tip}} &= 1.0 \end{aligned}$$

Data for the *second stage*:

$$\frac{\dot{m} \sqrt{\theta_3}}{\delta_3} = 6.0$$

where $\theta_3 = T_{03}/288$ and $\delta_3 = P_{03}/101$

$$\pi_2 = 3.5, \quad \sigma_2 = 0.94, \quad \eta_2 = 0.87, \quad \psi_2 = 1.04, \quad D_4 = 0.7 \text{ m}$$

Calculate:

1. Air mass flow rate
2. Inlet velocity C_1
3. Rotational speed (s^{-1})
4. Power required for driving the compressor

For an axial compressor stage, prove that

$$\begin{aligned}\tan \alpha_1 &= \frac{(1 - \Lambda) - (\psi/2)}{\phi} \\ \tan \alpha_2 &= \frac{(1 - \Lambda) + (\psi/2)}{\phi} \\ \tan \beta_1 &= \frac{\Lambda + (\psi/2)}{\phi} \\ \tan \beta_2 &= \frac{\Lambda - (\psi/2)}{\phi}\end{aligned}$$

For an axial compressor stage, prove that

$$\begin{aligned}\left(\frac{C_1}{U}\right)^2 &= ((1 - \Lambda) - (\psi/2))^2 + \phi^2 \\ \left(\frac{C_2}{U}\right)^2 &= ((1 - \Lambda) + (\psi/2))^2 + \phi^2 \\ \left(\frac{W_1}{U}\right)^2 &= \left(\left(\frac{\psi}{2}\right) + \Lambda\right)^2 + \phi^2 \\ \left(\frac{W_2}{U}\right)^2 &= \left(\left(\frac{\psi}{2}\right) - \Lambda\right)^2 + \phi^2\end{aligned}$$

- 9.19 For an axial compressor stage having $C_{a1} \neq C_{a2}$ and $U_1 \neq U_2$. Prove that the degree of reaction is expressed by the relation:

$$\Lambda = 1 - \frac{\phi}{2} \left(\frac{A^2 \sec^2 \alpha_2 - \sec^2 \alpha_1}{AB \tan \alpha_2 - \tan \alpha_1} \right)$$

$$\text{where } \phi = \frac{C_{a1}}{U_1}, A = \frac{C_{a2}}{C_{a1}} \quad \text{and} \quad B = \frac{U_2}{U_1}$$

The stage temperature rise of an axial compressor stage ($\Delta T_{0\text{axial}}$) and a centrifugal compressor stage ($\Delta T_{0\text{centrifugal}}$) are to be compared provided the following conditions:

Flow enters axially for both stages

Degree of reaction of axial compressor at mean radius $\Lambda_m = 0.5$

Product of power input factor and slip factor for centrifugal compressor $\psi\sigma = 1.0$

Prove that $(\Delta T_{0\text{axial}})/(\Delta T_{0\text{centrifugal}}) = (U_m/U_2)^2$

where (U_m) is the rotational speed at mean radius of axial compressor and (U_2) is the rotational speed at impeller tip radius of centrifugal compressor.

If the rotational speed is the same for both compressor stages, then the temperature rise ratio will be

$$(\Delta T_{0\text{axial}})/(\Delta T_{0\text{centrifugal}}) = (r_m/r_2)^2$$

Plot the above relation if the radii ratio varies in the range:

$$(r_m/r_2) = 1.0 - 4$$

9.20 For any axial flow compressor having (n) stages; if the pressure rise per stage is constant in all stages,

PROVE that

$$\frac{\Delta T_{0(i+1)}}{\Delta T_{0i}} = \frac{T_{0(i+1)}}{T_{0i}}$$

and

$$\frac{T_{0n}}{T_{01}} = \frac{\Delta T_{0n}}{\Delta T_{01}}$$

Where (ΔT_{0i}) and ($\Delta T_{0(i+1)}$) are the temperature rises for stages (i) and ($i+1$)

(ΔT_{0i}) and ($\Delta T_{0(i+1)}$) are the inlet total temperatures to stages (i) and ($i+1$)

9.21 The *high pressure compressor (HPC)* is composed of six stages. It has the following data:

- Inlet total temperature is 538 K – Inlet total pressure is 7.23 bar
- Inlet absolute speed = Axial flow speed = 172 m/s – Mean radius is 0.35 m
- Rotational speed at tip radius of first stage is 536 m/s – Stage efficiency 0.91
- Rotational speed at mean radius 490 m/s

- Stage temperature rise is constant and equals 69 K
- Rotor blades are to be designed using *first power method*, and the governing equations are listed below:

$C_{u1} = aR - \frac{b}{R}$	$a = U_m(1 - \Lambda_m)$	$\Lambda = 1 + \frac{2a\ell nR}{U_m} - \frac{a}{U_m}$	$C_{a1}^2 - C_{a1}^2 m = -2[a^2(R^2 - 1) - 2ab\ell nR]$
$C_{u2} = aR + \frac{b}{R}$	$b = \frac{\Delta h_0}{2U_m}$	$\Lambda = 1 + (2\ell nR - 1)(1 - \Lambda_m)$	$C_{a2}^2 - C_{a2}^2 m = -2[a^2(R^2 - 1) + 2ab\ell nR]$ $C_{a2}^2 - C_{a1}^2 = -8ab\ell nR$ $C_{a1m} = C_{a2m}$

1. Prove that: if $C_{u1} = 0$, then $a = b$

2. Calculate:

- Compressor efficiency
- Hub-to-tip ratio of first stage
- Absolute angle at mean radius (α_{2m}) for first stage
- Absolute angle at hub radius(α_{2h}) for first stage using *first power design*

- 9.22 The map of a multi-stage axial compressor is shown in the nearby figure. Curve (SC) represents one of the constant speed lines, where S is the surge point and C is the choking point. Line (EF) is the surge line and line (ADB) is the operating line. Point D is the operating point.

The equation of the curve SDC is given by

$$\left(\frac{\pi}{4.8}\right)^2 + \left(\frac{\lambda}{3}\right)^2 = 1$$

The equation of the operating line ADB is

$$\pi = 1.0 + \lambda$$

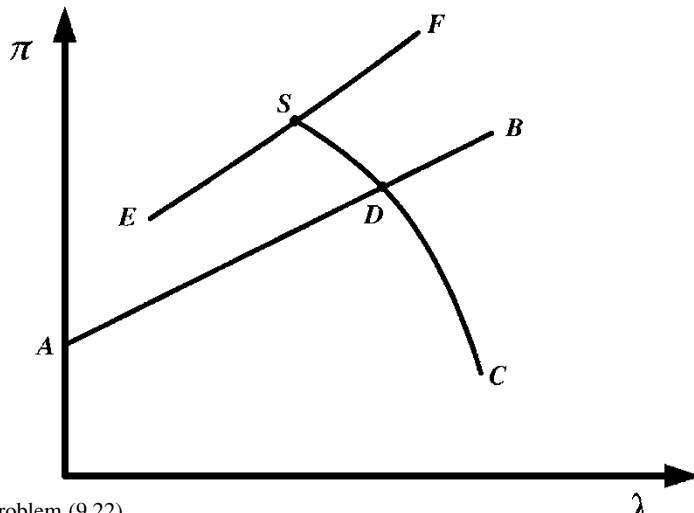


Figure: Problem (9.22)

where $= \frac{\dot{m} \sqrt{T_{01}}}{P_{01}}$, where mass flow rate (\dot{m}) is expressed in (kg/s), temperature (T_{01}) in (K), and pressure (P_{01}) in (kPa). The compressor has a constant mean radius.

1. If the inlet conditions are $T_{01} = 300$ K and $P_{01} = 101$ kPa, calculate the mass flow rate and pressure ratio at operating point (D).

2. First stage

It has the following characteristics: $C_{a1} = C_1 = 150$ m/s, and the tip rotational speed is $U_t = 360$ m/s; stage efficiency is constant for all stages; $\eta_s = 0.84$, hub-tip ratio at inlet $\zeta = 0.5$ and de Haller number for rotor is 0.8. Calculate:

- (a) Tip and hub radii at inlet
 - (b) Number of stages
 - (c) Pressure ratio of first stage
 - (d) Degree of reaction at mean section of first stage
3. Last stage It has the following characteristics, stage temperature rise is same as first stage, de Haller number for stator is 0.8 and flow leaves the compressor axially; $C_a = C_3 = 150$ m/s. Calculate the degree of reaction at mean section.

- 9.23 An axial compressor stage is to be designed based on free vortex method. It has the following data: Hub-to-tip ratio = 0.6 and hub radius = 0.3 m, rotational speed = 6000 rpm, air density = 1.6 kg/m³. Flow angles at root section: $\alpha_1 = 25^\circ$, $\beta_1 = 55^\circ$, $\alpha_2 = 55^\circ$, $\beta_2 = 25^\circ$.

Calculate

- (a) Axial speed
- (b) Air mass flow rate
- (c) Flow angles at mean section
- (d) Specific work
- (e) Degree of reaction at tip section

- 9.24 An axial compressor stage has the following data:

$$\zeta = 0.6, \Lambda_m = 0.6, \alpha_{1m} = 30^\circ, \beta_{1m} = 55^\circ$$

- (a) Use exponential method (with $a = 100$ m/s, $b = 40$ m/s) to calculate:
 - (i) Degree of reaction at root
 - (ii) Flow angles at hub and tip
- (b) Repeat calculations in (a), using free vortex method
- (c) Compare between both methods

9.25 An axial compressor stage has the following data:

$$\Lambda = 0.5, \alpha_1 = 45^\circ, \alpha_2 = 60^\circ, C_a = 150 \text{ m/s}$$

It is required to calculate the rotational speed (U), stage temperature rise (ΔT_0), and flow deflection angle ($\beta_1 - \beta_2$). If the axial speed and rotational speed are maintained constant, recalculate the degree of reaction and flow deflection angle in the following two cases:

- (a) $\alpha_1 = 30^\circ$
- (b) $\alpha_1 = 0^\circ$

Comment!

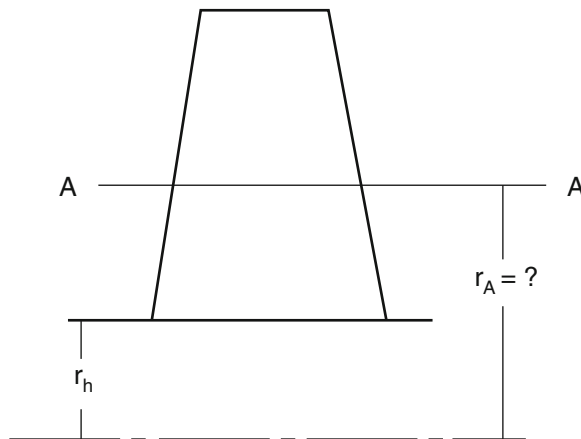
9.26 An axial compressor stage is to be designed by *free vortex* method. Flow enters the stage axially $\alpha_1 = 0$. It has the following data:

Degree of reaction at hub $\Lambda_h = 0.2$

Hub-tip ratio ($\zeta = 0.4$)

Data at section A-A:

- Radius is r_A
- Degree of reaction: $\Lambda_A = 0.5$
- de Haller number = 0.72
- Axial speed = 150 m/s



It is required to

- (a) Calculate radius ratio r_A/r_{tip}
- (b) Calculate the flow angles at hub: $\alpha_{1h}, \beta_{1h}, \alpha_{2h}, \beta_{2h}$
- (c) Calculate the degree of reaction at hub and tip
- (d) Calculate de Haller number at root and tip
- (e) Calculate the stage temperature rise
- (f) Draw a radial projection for the rotor blade

- 9.26 A ten-stage axial compressor has a constant tip radius of 0.27 m and stage efficiency; $\eta_s = 0.92$. Other data is

Inlet conditions:

$T_{01} = 288$ K, $P_{01} = 101$ kPa, Inlet Mach number; $M_1 = 0.5$, inlet hub-to-tip ratio $\xi_1 = 0.5$

Outlet conditions:

Outlet absolute Mach number; $M_2 = 0.3$, outlet hub-to-tip ratio $\xi_2 = 0.8$

Other operating conditions:

Rotational speed; $N = 280$ rps, flow enters the compressor axially with speed (C_1) and leaves the compressor also axially with speed (C_2) where

$$C_1 = C_2 = C_a$$

Air enters the *last stage* also in the axial direction.

It is required to *calculate*:

- (a) Absolute speed at inlet; C_1
- (b) Static and total temperature at outlet; T_2, T_{02}
- (c) Total temperature rise in the compressor; ΔT_0
- (d) Pressure ratio of compressor; π_c
- (e) De Haller number of rotor and stator of last stage
- (f) Relative outlet Mach number (M_2)_{rel}

- 9.27 An eight-stage axial compressor has the following inlet conditions:
 $T_{01} = 296$ K,

$P_{01} = 1.0$ bar, $\eta_s = 0.92$, $\gamma = 1.4$. It is to be designed by three different methods as follows:

- (a) Constant stage total temperature rise ($\Delta T_{0i} = 25$ K)
- (b) Constant stage pressure ratio $\pi_{si} = 1.3$
- (c) Constant total pressure rise per stage $\Delta P_{0i} = (P_{03} - P_{01})_i = 0.3$ bar

Use the following relations:

$$\begin{aligned}\pi_{si} &= \left(1 + \eta_s \frac{\Delta T_{0i}}{T_{0i}}\right)^{\frac{\gamma}{\gamma-1}} \\ \Delta T_{0i} &= T_{0i} \left(\frac{\pi_{si}^{\frac{\gamma-1}{\gamma}} - 1}{\eta_s} \right) \\ \Delta P_{0i} &= (P_{03} - P_{01})_i = P_{0i} \left(1 + \eta_s \frac{\Delta T_{0i}}{T_{0i}}\right)^{\frac{\gamma}{\gamma-1}} - 1\end{aligned}$$

Tabulate your results in the following table.

Stage		1	2	3	4	5	6	7	8
Constant $\Delta T_{0i} = 25$ K	T_{0i} (K)	296							
	T_{0i} (K)	25	25	25	25	25	25	25	25
	π_{si}	1.3							
	ΔP_{0i} (bar)	0.3							
Constant $\pi_{si} = 1.3$	T_{0i} (K)	296							
	ΔT_{0i} (K)	25							
	$\pi_{si} = 1.3$	1.3	1.3	1.3	1.3	1.3	1.3	1.3	1.3
	ΔP_{0i} (bar)	0.3							
Constant $\Delta P_{0i} = 0.3$ bar	T_{0i}	296							
	ΔT_{0i} (K)	25							
	π_{si}	1.3							
	ΔP_{0i} (bar)	0.3	0.3	0.3	0.3	0.3	0.3	0.3	0.3

References

1. Brown RN (1981) Compressors-selection and sizing, Gulf Publication Co., Chapter 1
2. Harman RTC (1981) Gas turbine engineering, applications, cycles and characteristics. Wiley, New York, p 7
3. Whitfield A, Baines NC (1990) Design of turbomachines. Longman Scientific & Technical, New York, p 3
4. El-Sayed AF (2008) Aircraft propulsion and gas turbine engines. Taylor & Francis/CRC Press, Boca Raton, FL
5. Staintz JD (1952) Some theoretical aerodynamic investigations of impellers in radial and mixed flow centrifugal compressors. Trans ASME 74:473
6. Hill P, Peterson C (1992) Mechanics and thermodynamics of propulsion, 2nd edn. Addison Wesley Publication Company, Inc, Boston, p 431
7. Boyce MP (2006) Gas turbine engineering handbook, 3rd edn. Gulf Professional Publishing, Oxford, p 225
8. Shigley JE, Mischke CR (1989) Mechanical engineering design, 5th edn. McGraw Hill Book Co, New York, p 65
9. The aircraft gas turbine and its operations, P&W Oper. Inst. 200, Part No. P&W 182408, 1988, pp 3–81
10. Cousins WT (1997) The dynamic stall and surge behavior of axial-centrifugal compressors, Ph.D. dissertation, Virginia Polytechnic Institute and State University
11. Hanlon PC (ed) (2001) Compressor handbook, McGraw-Hill, New York City
12. Steffens K (2014) Advanced compressor technology – key success factor for competitiveness in modern aero engines, MTU aero engines internal report
13. Harman RTC (1981) Gas turbine engineering, applications, cycles and characteristics. Wiley, New York, p 78
14. Hunecke K, (2003) Jet engines, fundamentals of theory, design and operation, motor books International Publishers & Wholesalers, 1st edn, 6th impression, Minneapolis, MN
15. Cumpsty NA (1989) Compressor aerodynamics. Longman Scientific & Technical, New York, p 48

16. Saravanamuttoo HIH, Rogers GFC, Cohen H, Straznicky PV (2009) Gas turbine theory, 6th edn. Prentice Hall, Harlow, p 198
17. Brown RN (1981) Compressors-selection and sizing, Gulf Publication Co., Houston, p 219
18. Glassman A (ed) (1975) Turbine design, NASA SP-290, vol I, p 32
19. Dixon SL, Hall CA (2010) Fluid mechanics and thermodynamics of turbomachinery, 6th edn. Butterworth/Heinemann, New York, p 155
20. Lakshminarayana B (1996) Fluid dynamics and heat transfer of turbomachinery. Wiley, New York, p 261
21. Marsh H (1968) A computer program for the through flow fluid mechanics in an arbitrary turbomachine using a matrix method, British ARC R&M 3509
22. Wisler DC (1988) Advanced compressor and fan systems. GE aircraft engines, Cincinnati, Ohio, USA, General Electric Co. USA, All Rights Reserved
23. Johnson IA, Bullock RO (eds) (1965) Aerodynamic design of axial flow compressors, NASA SP-36
24. Chmielniak T, Lepszy S, Rulik S (2011) Algorithm for design calculation of axial flow gas turbine compressor – comparison with GTD-350 compressor design. *Mech Mech Eng* 15 (3):207–216, Technical University of Lodz
25. Howell AR (1945) Fluid dynamics of axial compressors. In: Proceedings of institution of mechanical engineers, vol 153. Westminster, London
26. Hobbs DE, Weingold HD (1983) Development of controlled diffusion airfoils for multistage compressor applications', American Society of Mechanical Engineering, International gas turbine conference and EXHIBIT, 28th, Phoenix,, AZ, 27–31, 11 pp
27. Kerreebrock JL (1992). Aircraft engines and gas turbines, 2nd edn, The MIT Press, Cambridge, Mass., p 264
28. Day J (1992), Stall and surge in axial flow compressors, VKI Lecture Series 1992–02
29. United Technologies' Pratt Whitney (1988) The aircraft gas turbine engine and its operation, P&W Operation Instruction 200, pp 3–81
30. Wirkowski P (2010) Modelling the characteristics of axial compressor with variable stator vanes. *J KONES Powertrain Transport* 17(2):497–504

Chapter 10

Turbines

10.1 Introduction

Turbines are a class of turbo machinery used to convert the energy in a flowing fluid into mechanical energy by the use of rotor mechanisms. Turbines, in general, convert either thermal or kinetic energy of the fluid into work to drive compressors/fans, accessories in turbine-based engines, or drive propellers/helicopter rotors or electrical generators in shaft-based engines. Gas turbines and steam turbines are thermal turbo machinery.

There are two basic types of gas turbines, namely, axial and radial flow turbines.

Application areas of interest include propulsion and power systems of all types and sizes including air breathing engines for both conventional and lift (VTOL) propulsion, rocket turbo-pump systems and space auxiliary power units driven by high energy propellants, and inert gas and metal vapor space power systems [1].

Most of the aircraft engines and industrial gas turbines employ the axial flow turbines. The radial turbine can handle low mass flows more efficiently than the axial flow machines. Axial flow turbine is similar to axial compressor, as both are composed of several stages. Turbine expansion takes place in “stages” with each stage composed of a row of stationary blades (nozzles) followed by a row of moving blades (rotors).

The efficiency of a well-designed turbine is higher than that of a compressor. The main reason is that in compressors, the fluid undergoes a pressure rise and a flow deceleration accompanied by viscous losses and possible flow separation, while in turbines the flow is accelerated and thus boundary layer thickness/losses are minimized and flow separation is avoided.

First stage turbine nozzle sees the hottest temperatures; referred to as TIT (Turbine Inlet Temperature) or TRIT (Turbine Rotor Inlet Temperature). Modern engines run TRIT as high as 1200 °C (or even higher). Consequently, turbine blades have to be cooled by cold air driven from compressor through a bleed system.

Turbine stators are subjected to thermal stresses, while rotor blades are subjected to both mechanical and thermal stresses.

10.2 Axial Flow Turbines

10.2.1 Flow Features

The axial flow turbine can be classified as (1) impulse and (2) reaction. As described in Chap. 9, in reaction turbines, pressure drop of expansion takes place in the stator as well as in the rotor-blades. In the impulse turbine, the gases will be expanded only in the nozzle. Figure 10.1 shows a single stage of a multi-stage axial flow turbine or a one-stage turbine.

The stage comprises a row of nozzle guide vanes (NGVs) followed by a row of rotor blades mounted on a disc. Rotor blades may be shrouded or unshrouded. For a multi-stage turbine, the blading is arranged sequentially in an annulus with the discs connected via conical drive features forming the drum.

Gases approach the stator (or nozzle) with an absolute velocity (C_1), and normally in an axial direction, thus the absolute angle to the axial direction ($\alpha_1 = 0$). The nozzle (either a convergent or convergent divergent) accelerates these hot gases, thus leave the stator passage at a speed (C_2) and angle α_2 ; ($C_2 > C_1$). Moreover, the static pressure and temperature decrease.

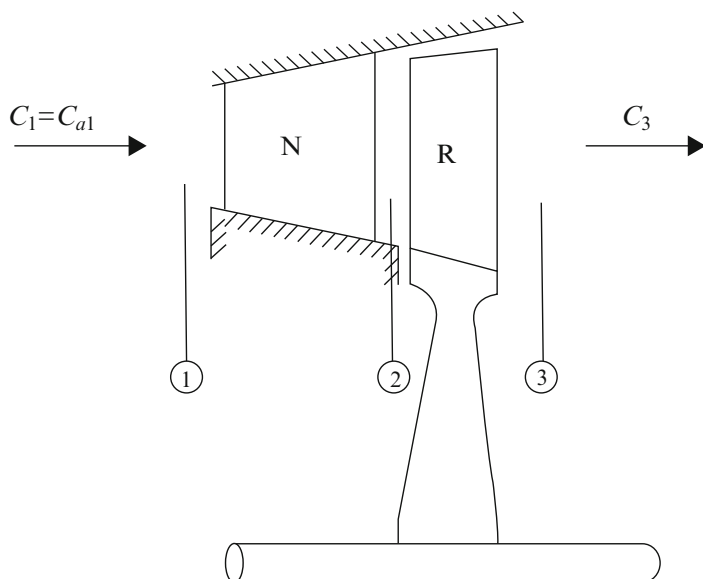


Fig. 10.1 An axial turbine stage

Flow next enters the rotor blade row with a relative speed (W_2) and relative angle β_2 and is also accelerated to (W_3) and relative angle β_3 , ($W_3 > W_2$). Finally gases leave the rotor with an absolute speed ($C_3 \approx C_1$) and angle ($\alpha_3 \approx \alpha_1$). Static pressure and temperature keeps its reduction through successive stages. The analysis of a turbine stage is very similar to that of a compressor stage as will be emphasized here. The relation between absolute, relative, and rotational speeds is expressed as

$$\vec{C} = \vec{W} + \vec{U} \quad (10.1)$$

The blade speed \tilde{U} increases from root to tip and hence velocity diagrams will be different for root, tip, and any other radii points. For short blades, 2-D mean flow design is valid but for long blades, 3-D approach (which incorporates variations from hub to tip) must be adopted in design phase. At first, we shall consider the mean diameter of the annulus. Velocity triangles at rotor's inlet and outlet are shown in Fig. 10.2. Assembled inlet and outlet velocities triangles are shown in Fig. 10.3. Gas with an absolute velocity C_1 making an angle α_1 , (measured from the axial direction) enters the nozzle (or stator) blades and leaves the nozzles or stator blades with an absolute velocity C_2 and angle α_2 . Flow then enters the rotor blade row with relative velocity W_2 and relative angle β_2 and leaves with relative velocity W_3 and relative angle β_3 . Details of gas flow characteristics through a turbine stage are summarized in Table 10.1.

Note that the velocity diagram of the turbine differs from that of the compressor, in that the change in tangential velocity in the rotor; ΔC_u , is in the direction opposite to the blade speed U . The reaction to this change in the tangential momentum of the fluid is a torque on the rotor in the direction of motion [2]. In a similar way to the axial compressor, if the axial velocity is constant at inlet and outlet of the stage

$$C_{a2} = C_{a3} = C_a \quad (10.2)$$

Then

$$\frac{U}{C_a} = \tan \alpha_2 - \tan \beta_2 = \tan \beta_3 - \tan \alpha_3 \quad (10.3)$$

10.2.2 Euler Equation

Euler's equation in turbo machinery represents the conservation of angular momentum, from which the specific work is expressed by the relation

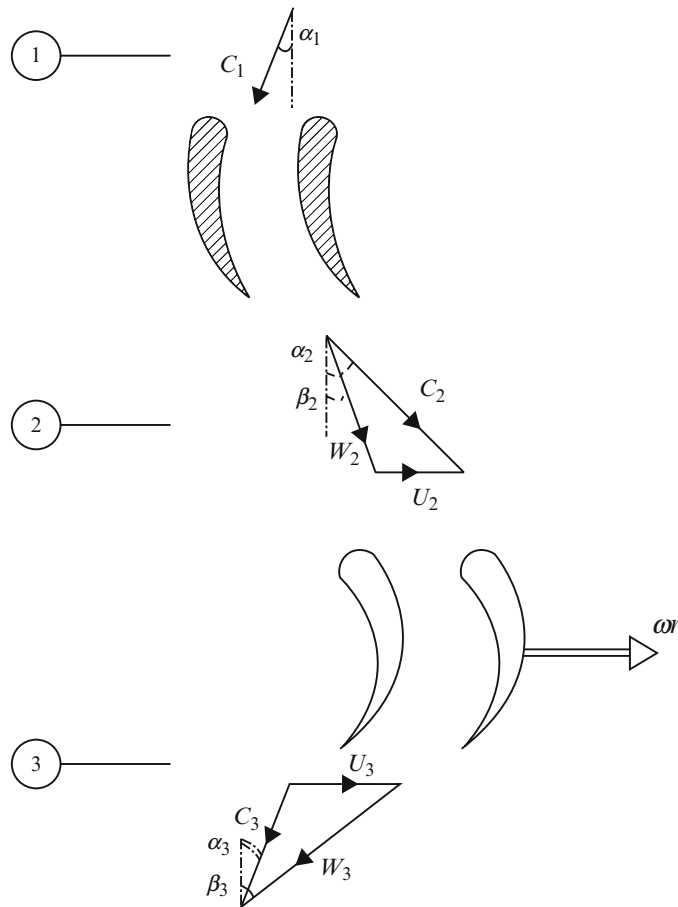


Fig. 10.2 Velocity diagrams along an axial turbine stage

$$W_s = (\vec{U} \cdot \vec{C}_u)_3 - (\vec{U} \cdot \vec{C}_u)_2$$

Since the swirl velocities \vec{C}_{u3} and \vec{C}_{u2} are in opposite directions, then

$$W_s \equiv C_p \Delta T_0 = UC_a (\tan \alpha_2 + \tan \alpha_3) = UC_a (\tan \beta_2 + \tan \beta_3) \quad (10.4)$$

Work done factor used in the designing of axial flow compressor is not applied in turbines, as the flow is accelerating thus growth of the boundary layer along the annulus walls is negligible.

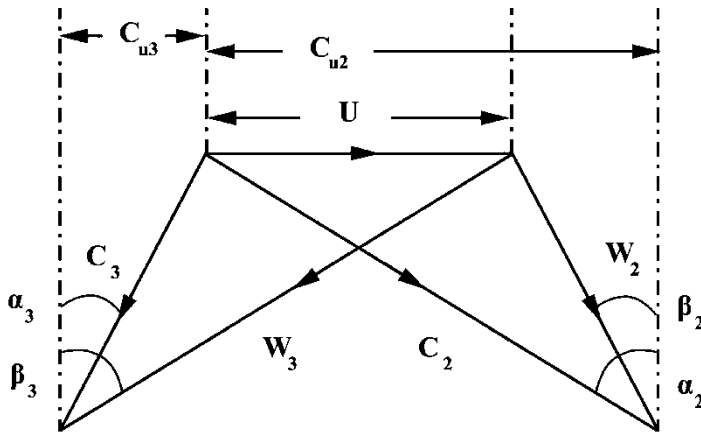


Fig. 10.3 Compound velocity triangles along an axial turbine rotor

10.2.3 Efficiency and Pressure Ratio

The expansion processes in the stator and rotor of an axial turbine is drawn on the T-s diagram Fig. 10.4.

Total-to-total stage efficiency is normally used when the leaving kinetics energy is utilized either in the next stage of the turbine or in propelling nozzle. It is defined as

$$\eta_{\text{stage}} = \frac{T_{01} - T_{03}}{T_{01} - T'_{03}} = \frac{\Delta T_{0\text{stage}}}{T_{01} \left[1 - \left(\frac{P_{03}}{P_{01}} \right)^{\frac{1-\gamma}{\gamma}} \right]} \quad (10.5a)$$

Stage temperature rise is related to stage efficiency by the relation

$$\Delta T_{0s} = \eta_s T_{01} \left[1 - \left(\frac{1}{\pi_s} \right)^{\frac{1-\gamma}{\gamma}} \right] \quad (10.5b)$$

Stage pressure ratio is also expressed as

$$\pi_s = \frac{P_{01}}{P_{03}} = \left(1 - \frac{\Delta T_0}{\eta_s T_{01}} \right)^{\frac{1-\gamma}{\gamma}} \quad (10.5c)$$

Table 10.1 Flow characteristics through a turbine stage

state	C	W	α	β	T	P	T_0	P_0	$T_{0\text{rel}}$
1	C_1	—	$\alpha_1 \approx 0$	—	T_1	P_1	T_{01}	P_{01}	—
2	$C_2 > C_1$	W_2	α_2	β_2	$T_2 < T_1$	$P_2 < P_1$	$T_{02} = T_{01}$	$P_{02} < P_{01}$	$T_{02\text{rel}}$
3	$C_3 \leq C_1 (C_3 \approx C_1)$	$W_3 \geq W_2$	$\alpha_3 \approx 0$	$\beta_2 \geq \beta_3$	$T_3 < T_2$	$P_3 \leq P_2$	$T_{03} \leq T_{02}$	$P_{03} \leq P_{02}$	$T_{03\text{rel}} = T_{02\text{rel}}$

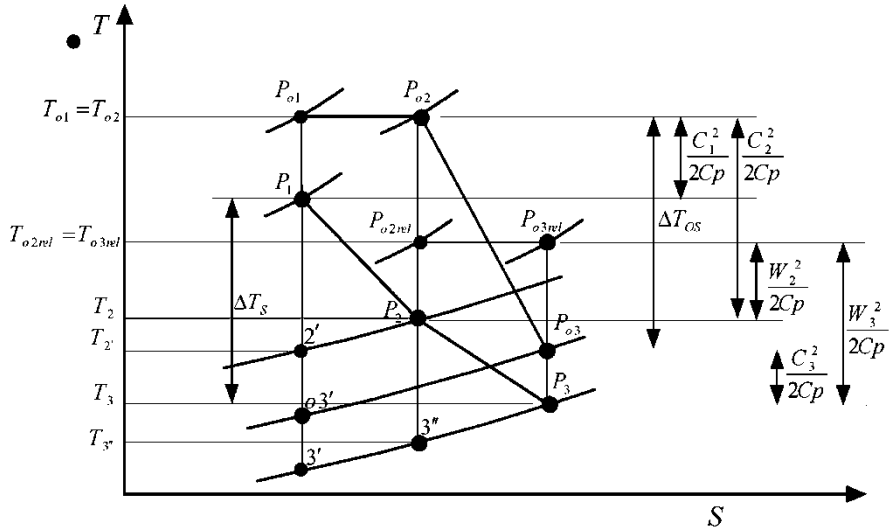


Fig. 10.4 Mollier chart (T-s) diagram of an axial turbine stage

10.2.4 Loss Coefficients in Nozzle and Rotor

Loss coefficient is expressed either as an enthalpy loss coefficient (λ) or pressure loss coefficient (Y). Referring to Fig. 10.4, the enthalpy loss coefficient [3] of the stator (nozzle) is expressed as

$$\lambda_N = \frac{T_2 - T'_2}{C_2^2/2C_P} \quad (10.6)$$

The enthalpy loss in the rotor is also expressed as

$$\lambda_R = \frac{T_3 - T''_3}{W_3^2/2C_P} \quad (10.7)$$

Next in terms of pressure, nozzle (stator) loss is expressed as

$$Y_N = \frac{P_{01} - P_{02}}{P_{02} - P_2} \quad (10.8)$$

Rotor pressure loss is expressed as

$$Y_R = \frac{P_{02rel} - P_{03rel}}{P_{03rel} - P_3} \quad (10.9)$$

In general, the enthalpy and pressure losses are nearly equal for both stator and rotor; thus

$$\lambda_N = Y_N \quad \text{and} \quad \lambda_R = Y_R \quad (10.10)$$

10.2.5 Performance Parameters

10.2.5.1 Blade Loading Coefficient (Or Temperature Drop Coefficient)

The temperature drop or blade loading coefficient is expresses as

$$\psi = \frac{C_p \Delta T_{0s}}{U^2/2} = \frac{2C_a(\tan \alpha_2 + \tan \alpha_3)}{U} = \frac{2C_a(\tan \beta_2 + \tan \beta_3)}{U} \quad (10.11a)$$

10.2.5.2 Flow Coefficient

The flow coefficient has the same definition as in the axial compressor, namely,

$$\phi = \frac{C_a}{U} \quad (10.12)$$

Combining blade loading and flow coefficients, then Eq. (10.11a) can be expressed as

$$\psi = 2\phi(\tan \alpha_2 + \tan \alpha_3) = 2\phi(\tan \beta_2 + \tan \beta_3) \quad (10.11b)$$

10.2.5.3 Degree of Reaction

The degree of reaction is defined in terms of static enthalpy change as

$$\Lambda = \frac{T_2 - T_3}{T_1 - T_3}$$

$$\Lambda = \frac{\text{Static enthalpy drop in rotor}}{\text{Static enthalpy drop in stage}}$$

Since the relative total enthalpy at inlet and outlet of rotor is equal, then

$$h_2 + \frac{W_2^2}{2} = h_3 + \frac{W_3^2}{2}$$

$$T_2 - T_3 = \frac{1}{2C_p}(W_3^2 - W_2^2)$$

For equal inlet and outlet absolute speeds $C_1 = C_3$, thus

$$\Delta T = \Delta T_0, \quad \Delta T_{\text{stage}} = \frac{U \Delta C_u}{C_p}$$

Thus the degree of reaction is then

$$\Lambda = \frac{(W_3^2 - W_2^2)}{2U \Delta C_u} \quad (10.13a)$$

Next, since, $W_2^2 = C_2^2 + U_2^2 - 2U_2 C_{u2}$

$$\text{And} \quad W_3^2 = C_3^2 + U_3^2 - 2U_3 C_{u3}$$

$$\text{Then} \quad W_3^2 - W_2^2 = C_3^2 - C_2^2 + U_3^2 - U_2^2 - 2U_3 C_{u3} + 2U_2 C_{u2}$$

If $U_2 = U_3 = U$, then

$$W_3^2 - W_2^2 = C_3^2 - C_2^2 + 2U(C_{u2} - C_{u3})$$

$$W_3^2 - W_2^2 = C_3^2 - C_2^2 + 2U \Delta C_u$$

Then from Eq. (10.13a),

$$\Lambda = 1 - \frac{(C_2^2 - C_3^2)/2}{U \Delta C_u} \quad (10.13b)$$

Now, if $C_{u2} = C_{u3}$

Then

$$T_2 - T_3 = \frac{1}{2C_p} (W_3^2 - W_2^2) = \frac{C_a^2}{2C_p} (\sec^2 \beta_3 - \sec^2 \beta_2) = \frac{C_a^2}{2C_p} (\tan^2 \beta_3 - \tan^2 \beta_2)$$

and; $\Delta T_{\text{stage}} = \frac{U \Delta C_u}{C_p} = \frac{UC_a(\tan \beta_2 + \tan \beta_3)}{C_p}$

$$\Lambda = \frac{C_a}{2U} (\tan \beta_3 - \tan \beta_2) \quad (10.13c)$$

Introducing the flow coefficient, then degree of reaction will be expressed as

$$\Lambda = \frac{\phi}{2} (\tan \beta_3 - \tan \beta_2) \quad (10.13d)$$

Thus for *impulse* turbine stage, with equal axial speed ($C_{u2} = C_{u3}$), then

$$\Lambda = 0 \quad \text{and} \quad \beta_3 = -\beta_2, \quad W_2 = W_3, \quad T_2 = T_3$$

Velocity triangles are skewed.

From Eq. (10.3), then

$$\Lambda = \frac{1}{2} - \frac{\phi}{2} (\tan \alpha_2 - \tan \beta_3) \quad (10.13e)$$

When $\Lambda = \frac{1}{2}$, the velocity triangles are *symmetrical*:

$$\alpha_2 = \beta_3, \quad \alpha_3 = \beta_2, \quad T_2 = (T_1 + T_3)/2$$

Degree of reaction can be also expressed as

$$\Lambda = 1 - \frac{\phi}{2} (\tan \alpha_2 - \tan \alpha_3) \quad (10.13f)$$

When $\Lambda = 1$, then $\alpha_2 = \alpha_3, \quad T_1 = T_2$

Velocity triangles are skewed.

For *unequal axial speeds*:

$$\Lambda = 1 + \frac{C_{a3}^2 - C_{a2}^2}{2U(C_{u3} + C_{u2})} - \frac{C_{u2} - C_{u3}}{2U} \quad (10.13g)$$

Example 10.1 A single stage axial turbine have the following characteristics:

$$T_{01} = 1144 \text{ K}, P_{01} = 1300 \text{kPa}, \Delta T_0 = 140 \text{ K}, U_m \\ = 320 \text{ m/s, flow coefficient}$$

$$\phi = 1,$$

Nozzle losses coefficient $\lambda_N = 0.05$, $\alpha_1 = 0^\circ$, $\alpha_3 = 10^\circ$ assuming $C_1 = C_3$
Calculate

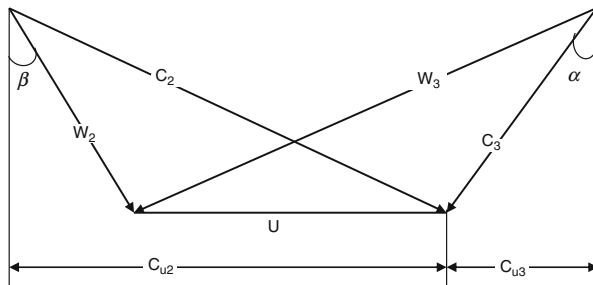
- (i) Angles α_2, β_2 and β_3
- (ii) Variables ψ, Λ
- (iii) The density at the nozzle outlet (ρ_2)

Solution

- (i) The flow coefficient is expressed as

$$\phi = \frac{C_a}{U} = 1$$

$$C_a = U = 320 \text{ m/s}$$



From Eq. (10.3),

$$\tan \beta_3 - \tan \alpha_3 = \frac{U}{C_a}$$

$$\tan \beta_3 - \tan (10) = 1$$

$$\text{Thus } \beta_3 = 49.6^\circ$$

Moreover, from Eq. (10.4),

$$\Delta T_0 = \frac{UC_a}{C_P} (\tan \beta_2 + \tan \beta_3)$$

$$140 = \frac{320 * 320}{1148} (\tan \beta_2 + \tan (49.6))$$

$$\text{Then } \beta_3 = 21.5^\circ$$

Again from Eq. (10.3):

$$\tan \alpha_2 - \tan \beta_2 = \frac{U}{C_a}$$

$$\tan \alpha_2 - \tan (21.5) = 1$$

$$\text{Thus } \alpha_2 = 54.3^\circ$$

(ii) From Eq. (10.11b),

$$\Psi = 2\phi(\tan \beta_2 + \tan \beta_3)$$

$$\Psi = 2 * 1 * (\tan (21.5) + \tan (49.6)) = 3.138$$

From Eq. (10.13), $\Lambda = \frac{\phi}{2}(\tan \beta_3 - \tan \beta_2)$

$$\Lambda = \frac{1}{2} * (\tan(49.6) - \tan(21.5)) = 0.39$$

(iii) From Fig. 10.3, $C_2 = \frac{C_a}{\cos \alpha_2} = \frac{320}{\cos(54.3)} = 548.4 \text{ m/s}$

$$T_2 = T_{02} - \frac{C_2^2}{2C_P} = 1144 - \frac{(548.4)^2}{2*1148} = 1013 \text{ K}$$

$$\text{Since } \lambda_N = \frac{C_P(T_2 - T'_2)}{\dot{C}_2^2 / _2}$$

$$C_P(T_2 - T'_2) = \frac{1}{2} \lambda_N C_2^2$$

$$1148 * (1013 - T'_2) = \frac{1}{2} * 0.05 * (548.4)^2$$

$$T'_2 = 1006.45 \text{ K}$$

$$P_2 = P_{01} \left(\frac{T'_2}{T_{01}} \right)^{\frac{\gamma}{\gamma-1}} = 1300 * \left(\frac{1006.45}{1144} \right)^{\frac{1.33}{0.33}} = 778.77 \text{ kPa}$$

$$\rho_2 = \frac{P_2}{RT_2} = \frac{778.77 * 10^3}{287 * 1013} = 2.678 \text{ kg/m}^3$$

Example 10.2 In the previous example, the gas mass flow rate and total-to-total efficiency are

$$\dot{m} = 120 \text{ kg/s},$$

$$\eta_t = 0.9$$

For the same gas turbine data,

- (a) Check whether the nozzle is choked or not
- (b) Calculate:

1. Nozzle throat area
2. The stator and rotor blade areas: A_1, A_2, A_3
3. The blade heights: h_1, h_2, h_3

Solution

- (a) Mach number at nozzle outlet:

$$M_2 = \frac{C_2}{\sqrt{\gamma RT_2}} = \frac{548.4}{\sqrt{\frac{4}{3} \times 287 \times 1013}} = \frac{548.4}{622.6} = 0.8808$$

The nozzle is thus *un choked*

(b) Dimensions of nozzle and rotor blade rows

1. *Throat area (A_t)*

$$A_t = \frac{\dot{m}}{\rho_2 C_2} = \frac{120}{2.678 \times 548.4} = 0.0817 \text{ m}^2$$

2. *Inlet area (A_1)*

$$C_1 = C_{a1} = 320 \text{ m/s}$$

$$T_1 = T_{01} - \frac{C_1^2}{2C_p} = 1144 - \frac{(320)^2}{2 \times 1148} = 1099.4 \text{ K}$$

$$P_1 = P_{01} \left(\frac{T_1}{T_{01}} \right)^{\frac{\gamma}{\gamma-1}} = 1300 \left(\frac{1099.4}{1144} \right)^4 = 1108.8 \text{ kPa}$$

$$\rho_1 = \frac{P_1}{RT_1} = 3.514 \text{ kg/m}^3$$

$$A_1 = \frac{\dot{m}}{\rho_1 C_1} = 0.1067 \text{ m}^2$$

Nozzle outlet area (A_2)

$$A_2 = \frac{\dot{m}}{\rho_2 C a_2} = \frac{120}{2.687 \times 320} = 0.14 \text{ m}^2$$

Rotor outlet area (A_3)

From Eq. (10.5c)

$$\pi_s = \frac{P_{01}}{P_{03}} = \left(1 - \frac{\Delta T_0}{\eta_s T_{01}} \right)^{\frac{1-\gamma}{\gamma}} = \left(1 - \frac{140}{0.9 \times 1144} \right)^4 = 0.5573$$

$$P_{03} = 724.5 \text{ kPa}$$

$$T_{03} = T_{01} - \Delta T_0 = 1144 - 150 = 994 \text{ K}$$

$$C_3 = \frac{C_a}{\cos \alpha_3} = \frac{320}{\cos (10)} = 324.94 \text{ m/s}$$

$$T_3 = T_{03} - \frac{C_3^2}{2C_p} = 994 - \frac{(324.94)^2}{2 \times 1148} = 948 \text{ K}$$

$$P_3 = P_{03} \left(\frac{T_3}{T_{03}} \right)^{\frac{\gamma}{\gamma-1}} = 724.5 \left(\frac{948}{994} \right)^4 = 599.5 \text{ kPa}$$

$$\rho_3 = \frac{P_3}{RT_3} = 2.2 \text{ kg/m}^3$$

$$A_3 = \frac{\dot{m}}{\rho_3 C a_3} = \frac{120}{2.2 \times 320} = 0.17 \text{ m}^2$$

3. Blade heights

$$h = \frac{A}{\pi D_m}$$

$$h_1 = \frac{A_1}{\pi D_m} = \frac{0.1067}{\pi \times 0.8} = 0.04245 \text{ m} = 4.245 \text{ cm}$$

$$h_2 = \frac{0.14}{\pi \times 0.8} = 0.0557 \text{ m} = 5.57 \text{ cm}$$

$$h_3 = \frac{0.17}{\pi \times 0.8} = 0.0676 \text{ m} = 6.76 \text{ cm}$$

Example 10.3 A single stage axial flow turbine has a mean radius of 0.30 m and blade height of 0.06 m. The hot gasses enter the turbine stage at 1900 kPa and 1200 K, and the absolute velocity leaving the stator (C_2) is 600 m/s making 65° with the axial direction (α_2). The rotor inlet and outlet blade angles (β_2 and β_3) are 25° and 60° , respectively. Draw the velocity triangles and calculate:

- (i) The rotor rotational speed
- (ii) The stage pressure ratio if its efficiency is 0.88
- (iii) Flow coefficient, loading coefficient, and degree of reaction
- (iv) The mass flow rate
- (v) The power delivered by the turbine [$\gamma = 4/3$, $R = 290 \text{ J/kgK}$, and ϕ is constant through the stage]

Solution

(i) Since the axial velocity is defined as

$$C_a = C_2 \cos \alpha_2 = 600 \cos 65 = 253.57 \text{ m/s}$$

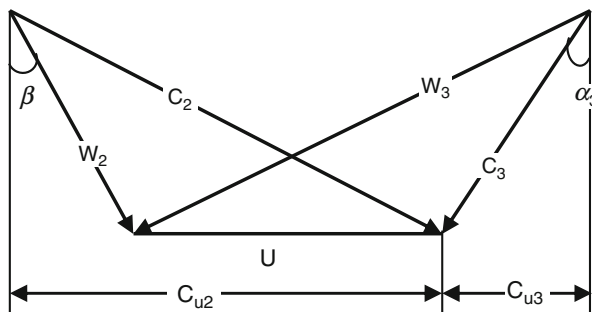
$$U = C_a(\tan \alpha_2 - \tan \beta_2)$$

$$U = 253.57 (\tan 65 - \tan 25) = 425.5 \text{ m/s}$$

The rotational speed is defined as

$$U = \pi ND/60 \text{ or } N = 60U/\pi D$$

$$\text{Thus, } N = 60 * 425.5 / \pi * 0.6 = 13,545 \text{ rpm}$$



(ii) Stage temperature drop is given by

$$\Delta T_{0\text{stage}} = \frac{UC_a}{C_p} (\tan \beta_2 + \tan \beta_3)$$

$$\text{With } C_p = \gamma R / (\gamma - 1) = 1168.8 \text{ J/kgK}$$

$$\Delta T_{0\text{stage}} = \frac{425.5 * 253.37}{1168.8} (\tan 25 + \tan 60)$$

$$\Delta T_{0\text{stage}} = 202.77 \text{ K}$$

From Eq. (10.5c); stage pressure ratio is then

$$\pi_s = \frac{P_{01}}{P_{03}} = \left(1 - \frac{202.77}{0.88 \times 1200} \right)^{-0.25} = 2.35$$

$$(iii) \quad \phi = \frac{C_a}{U} = 0.6$$

$$\Psi = \frac{2C_p \Delta T_{0\text{stage}}}{U^2} = \frac{2 * 1168.8 * 202.77}{(425.5)^2} = 2.62$$

$$\Lambda = \Phi(\tan \beta_3 - \tan \beta_2)/2 = 0.41$$

$$(iv) \quad (\tan \beta_3 - \tan \alpha_2) = \frac{U}{C_a}$$

$$\tan 60 - \tan \alpha_3 = \frac{425.5}{253.57}$$

Thus $\alpha_3 = 3.1^\circ$

$$C_3 = \frac{C_a}{\cos \alpha_3} = \frac{253.57}{\cos 3.1} = 253.94 \text{ m/s}$$

Assuming: $C_1 = C_3$

$$T_1 = T_{01} - \frac{C_1^2}{2C_p} = 1200 - \frac{(253.94)^2}{2*1168.8} = 1172.4 \text{ K}$$

$$P_1 = P_{01} \left(\frac{T_1}{T_{01}} \right)^{\frac{\gamma}{\gamma-1}} = 1900 * 10^3 \left(\frac{1172.4}{1200} \right)^4 = 1731 * 10^3 \text{ Pa}$$

$$\rho_1 = \frac{P_1}{R T_1} = \frac{1731 * 10^3}{290 * 1172.4} = 5.09 \text{ kg/m}^3$$

$$A_1 = \pi D_m h = \pi * 0.6 * 0.06 = 0.1131 \text{ m}^2$$

$$\dot{m} = \rho_1 C_a A_1 = 5.09 * 253.57 * 0.1131 = 145.97 \text{ kg/m}^3$$

$$\text{Power} = \dot{m} C_p * \Delta T_{0\text{stage}}$$

$$\text{Power} = 145.97 * 1.1688 * 202.77 = 34600 \text{ kW}$$

$$\text{Power} = 34.6 \text{ MW}$$

Example 10.4 The high pressure turbine of the CF6 engine is composed of two stages. The following data refer to the first stage of the turbine.

Degree of reaction, Λ_m	0.5	Mass flow rate	600 kg/s
Flow coefficient, ϕ	1.0	Mean radius, r_m	0.38 m
Flow angles	$\alpha_1=0^\circ, \alpha_3=20^\circ$	Rotational speed, N	7200 rpm

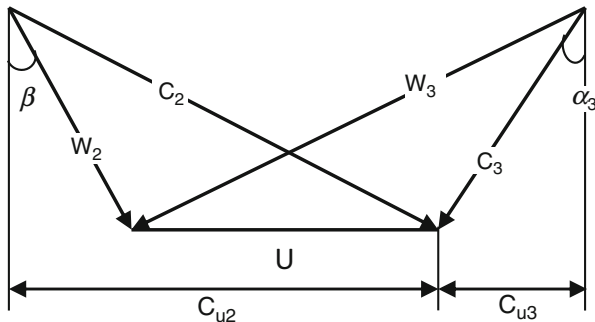
Draw the velocity triangles then calculate:

- (a) The angles β_2 , and β_3 .
- (b) The temperature drop coefficient ψ and the temperature drop of first stage
- (c) Recalculate as in (a) and (b) when the mean degree of reaction $\Lambda_m = 0$
- (d) Recalculate as in (a) and (b) when the mean degree of reaction $\Lambda_m = 1.0$

Solution

$$U = 2\pi r_m \frac{N}{60}$$

$$U = 2\pi * 0.38 * \frac{7200}{60} = 286.5 \text{ m/s}$$



(a) Case (I) $\Lambda_m = 0.5$

$$\beta_2 = \alpha_3 = 20^\circ$$

$$\phi = \frac{C_a}{U} = 1$$

$$C_a = U = 286.5 \text{ m/s}$$

$$\Lambda = \frac{C_a}{2U} (\tan \beta_3 - \tan \beta_2)$$

$$0.5 = \frac{286.5}{2*286.5} (\tan \beta_3 - \tan (20))$$

$$\tan \beta_3 - \tan (20) = 1$$

$$\tan \beta_3 = 1 + \tan (20) = 1.36397$$

$$\beta_3 = 53.75^\circ$$

$$(b) \Psi = \frac{2C_a}{U} (\tan \beta_2 - \tan \beta_3)$$

$$\Psi = \frac{2*286.5}{286.5} (\tan (20) - \tan (53.75))$$

Thus $\Psi = 3.46$

$$\Delta T_0 = \frac{\Psi U^2}{2C_P} = \frac{3.46 \times (286.5)^2}{2 \times 1148} = 123.7 \text{ K}$$

(c) Case (2): $\Lambda_m = 0$

$$\beta_2 = -\beta_3 \quad \text{and} \quad \alpha_3 = 20^\circ$$

$$\frac{U}{C_a} = \tan \beta_3 - \tan \alpha_3$$

$$\tan \beta_3 = \varphi + \tan \alpha_3 = 1.36397$$

$$\Psi = \frac{2 C_a}{U} (\tan \beta_2 + \tan \beta_3) = 2 \times 2 \times 1.36397 = 5.45588$$

$$\Delta T_0 = \frac{\Psi U^2}{2 C_P} = \frac{5.45588 \times (286.5)^2}{2 \times 1148} = 195 \text{ K}$$

(d)

$$\Lambda_m = 0$$

$$\alpha_3 = \alpha_2 = 20^\circ$$

$$\frac{U}{C_a} = \tan \beta_3 - \tan \alpha_3$$

$$\tan \beta_3 = \varphi + \tan \alpha_3 = 1.36397$$

$$\beta_3 = 53.75^\circ$$

$$\frac{U}{C_a} = \tan \alpha_2 - \tan \beta_2$$

$$\tan \beta_2 = \tan \alpha_2 - \varphi = \tan 20 - 1 = -0.636$$

$$\Psi = \frac{2 C_a}{U} (\tan \beta_2 + \tan \beta_3) = 2 \times (-0.636 + 1.36397) = 1.4559$$

$$\Delta T_0 = \frac{\Psi U^2}{2 C_P} = \frac{1.4559 \times (286.5)^2}{2 \times 1148} = 52 \text{ K}$$

Summary

Λ_m	0	0.5	1
Ψ	5.45588	3.46	1.4559
ΔT_0 (K)	195	123.7	52

Example 10.5 Gases at a total temperature of 1400 K and a total pressure of 2.23 MPa enters the nozzle row of a turbine stage in the axial direction at the rate of 22.7 kg/s. Other data are

Turbine rotor speed 14,000 rpm

Mean blade diameter 48.3 cm

$$C_2 = 470 \text{ m/s}, \quad \alpha_2 = 72^\circ, \quad C_3 = 215 \text{ m/s}, \quad \alpha_3 = 22^\circ$$

- (a) Construct the velocity diagrams at the mean blade diameter.
- (b) Calculate the absolute Mach number M_2
- (c) Calculate the specific work and power developed by this stage.
- (d) Calculate the total-to-total expansion ratio. (P_{01}/P_{03})
- (e) Calculate the degree of reaction.

$$(\gamma = 1.33 \text{ and } R = 287 \text{ J/kg.k})$$

Solution:

- (a) Velocity triangles

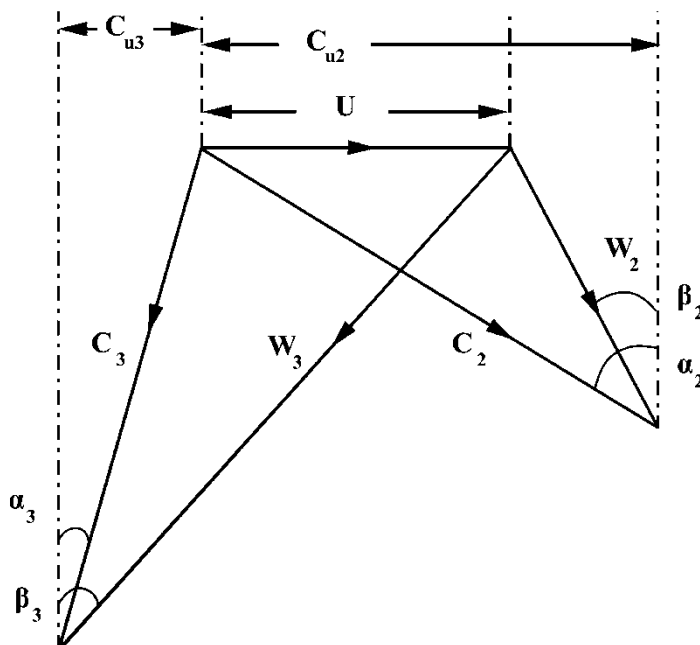
$$U_m = \pi D_m N = \pi * 0.483 * 14000 / 60 = 354.057 \text{ m/s}$$

$$\because \cos \alpha_2 = \frac{C_{a2}}{C_2} \quad \therefore C_{a2} = 145.24 \text{ m/s}$$

$$\because \cos \alpha_3 = \frac{C_{a3}}{C_3} \quad \therefore C_{a3} = 199.34 \text{ m/s}$$

Based on the above calculations, $C_{a2} \neq C_{a3}$

Velocity triangles have the shown pattern.



(b) *Absolute Mach number (M_2)*

$$\begin{aligned}\because T_2 &= T_{02} - \frac{C_2^2}{2C_p} = 1400 - \frac{(470)^2}{2*1148} = 1303.79 \text{ K} \therefore M_2 = \frac{C_2}{\sqrt{\gamma RT_2}} \\ &= 0.6655\end{aligned}$$

(c) *Specific work and power of stage*

$$W = U\Delta C_u = U(C_{u2} + C_{u3}) = 354.(C_2 \sin \alpha_2 + C_3 \sin \alpha_3) = 187 \text{ kJ/kg}$$

$$\text{Power} = \dot{m} W = 22.7 * 186.778 = 4239.864 \text{ kW}$$

(d) *Expansion ratio (P_{01}/P_{03})*

$$\begin{aligned}\because W &= C_p \Delta T_0 \quad \therefore \Delta T_0 = 162.698 \text{ K} \\ \because \Delta T_0 &= \eta_t T_{01} \left[1 - \left(\frac{1}{P_{01}/P_{03}} \right)^{(\gamma-1)/\gamma} \right] \\ \therefore \frac{P_{01}}{P_{03}} &= 1.6391\end{aligned}$$

(e) *Degree of reaction*

$$\Lambda = 1 - \frac{C_2^2 - C_3^2}{2U\Delta C_u} = 0.533$$

10.2.6 Free Vortex Design

Since the blade speed U is not constant and varies from root to tip, velocity triangles vary from root to tip. Twisted blading designed to take account of the changing gas angles is called vortex blading. As discussed in axial flow compressor (Chap. 9), the momentum equation is

$$\frac{1}{\rho} \frac{dP}{dr} = \frac{C_u^2}{r}$$

For constant enthalpy and entropy, the equation takes the form across the annulus:

$$\frac{dh_0}{dr} = C_a \frac{dC_a}{dr} + C_u \frac{dC_u}{dr} + \frac{C_u^2}{r}$$

for constant total enthalpy and axial velocity, then

$$\frac{dh_0}{dr} = \frac{dC_a}{dr} = 0$$

Thus

$$\frac{dC_u}{C_u} = -\frac{dr}{r}$$

And integrating to get

$$rC_u = \text{constant} \quad (10.14)$$

Equation 11.14 is applied at inlet and outlet to rotor blade row, thus:

$$rC_{u2} = \text{constant} \quad (10.15a)$$

$$rC_{u3} = \text{constant} \quad (10.15b)$$

These equations can be applied at any radius (r) as

$$C_{u2} = C_{u2m} \left(\frac{r_m}{r} \right)_2 \quad (10.16a)$$

$$C_{u3} = C_{u3m} \left(\frac{r_m}{r} \right)_3 \quad (10.16b)$$

The above equations can be rewritten interms of axial speed as

$$rC_{u2} = rC_{a2} \tan \alpha_2 = \text{constant}$$

$$rC_{u3} = rC_{a3} \tan \alpha_3 = \text{constant}$$

Since $C_{a2} = C_{a3} = C_a$, the absolute angles (α)at any radius (r) are then

$$\tan \alpha_2 = \left(\frac{r_m}{r} \right)_2 \tan \alpha_{2m} \quad (10.17a)$$

$$\tan \alpha_3 = \left(\frac{r_m}{r} \right)_3 \tan \alpha_{3m} \quad (10.17b)$$

Since

$$\tan \beta_2 = \tan \alpha_2 - \frac{U}{C_a}$$

and

$$\tan \beta_3 = \tan \alpha_3 + \frac{U}{C_a}$$

The relative angles (β)at any radius (r) are then

$$\tan \beta_2 = \left(\frac{r_m}{r} \right)_2 \tan \alpha_{2m} - \left(\frac{r}{r_m} \right)_2 \frac{U_m}{C_a} \quad (10.18a)$$

$$\tan \beta_3 = \left(\frac{r_m}{r} \right)_3 \tan \alpha_{3m} + \left(\frac{r}{r_m} \right)_3 \frac{U_m}{C_a} \quad (10.18b)$$

Example 10.6 The following data apply to a single-stage turbine designed on free-vortex theory:

Inlet stagnation temperature T_{01}	1200 K
Inlet stagnation pressure P_{01}	800 kPa
Isentropic efficiency	0.9
Stage stagnation temperature drop ($\Delta T_0 \equiv T_{01} - T_{03}$)	150 K
Mass flow rate	36 kg/s
Mean blade speed U_m	320 m/s
Rotational speed N	250 rps
Outlet velocity C_3	400 m/s

The outlet velocity is axial ($\alpha_3 = 0$).

Calculate

1. The blade height and radius ratio of the annulus at rotor outlet
2. Swirl components at hub, mean, and tip section of state 2 (rotor inlet) and state 3 (rotor outlet) if the blade height at rotor inlet is 80 % of blade height at rotor outlet
3. Angles α_2 at hub, mean, and tip sections
4. Angles β_2 and β_3 at mean and hub

Solution

1. Blade height and annulus at outlet

$$T_{03} = T_{01} - \Delta T_0 = 1200 - 150 = 1050 \text{ K}$$

$$T_3 = T_{03} - \frac{C_3^2}{2C_p} = 1050 - \frac{(400)^2}{2 \times 1148} = 980.313 \text{ K}$$

$$\begin{aligned} \because \Delta T_0 &= \eta_t T_{01} \left[1 - \left(\frac{1}{P_{01}/P_{03}} \right)^{(\gamma-1)/\gamma} \right] \\ \therefore 150 &= 0.9 * 1200 \left[1 - \left(\frac{1}{P_{01}/P_{03}} \right)^{1/4} \right] \\ \therefore \frac{P_{01}}{P_{03}} &= 1.818709 \quad \therefore P_{03} = 439.8724 \text{ kPa} \end{aligned}$$

$$\begin{aligned} \therefore \frac{P_3}{P_{03}} &= \left(\frac{T_3}{T_{03}} \right)^{\gamma/(\gamma-1)} & \therefore \frac{P_3}{439.8724} &= \left(\frac{980.313}{1200 - 150} \right)^4 \\ \therefore P_3 &= 334.215 \text{ kPa} \end{aligned}$$

$$\therefore U_m = 2\pi N r_m \quad \therefore 320 = 2\pi * 250 * r_m \quad \therefore r_m = 0.203718 \text{ m}$$

$$\therefore \dot{m} = \rho A C_a = \rho_3 A_3 C_{a3}$$

$$\therefore 36 = \frac{P_3}{R T_3} * 2\pi r_m h_3 * 400.$$

$$\therefore 36 = \frac{334.215 * 10^3}{287 * 980.313} * 2\pi * 0.203718 * h_3 * 400$$

$$\therefore h_3 = 0.05919 \text{ m}$$

$$\begin{aligned} \therefore r_{t3} &= r_m + \frac{h_3}{2} = 0.203718 + \frac{0.05919}{2} = 0.2333 \text{ m} \\ \therefore r_{h3} &= r_m - \frac{h_3}{2} = 0.203718 - \frac{0.05919}{2} = 0.174123 \text{ m} \\ \therefore \zeta_3 &= \left(\frac{r_h}{r_t} \right)_3 = 0.7463 \end{aligned}$$

2. Swirl components

Since the outlet flow is axial, then $C_{u3} = 0$

$$\therefore C_p \Delta T_0 = U \Delta C = U C_{u2}$$

$$(C_{u2})_m = \frac{C_p \Delta T_0}{U} = \frac{1148 \times 150}{320} = 538 \text{ m/s}$$

Blade height at state 2:

$$h_2 = 0.8h_3 = 0.0474 \text{ m}$$

$$r_{h2} = r_m - \frac{h_2}{2} = 0.18 \text{ m}$$

$$r_{t2} = r_m + \frac{h_2}{2} = 0.2274 \text{ m}$$

From Eq. (11.16a),

$$C_{u2t} = C_{u2m} \left(\frac{r_m}{r_t} \right)_2 = 538 \times \frac{0.2037}{0.2274} = 482 \text{ m/s}$$

$$C_{u2h} = C_{u2m} \left(\frac{r_m}{r_h} \right)_2 = 538 \times \frac{0.2037}{0.18} = 609 \text{ m/s}$$

3. Flow angles: α_2 and α_3

From Eq. (11.16b)

$$\begin{aligned} C_{u3h} &= C_{u3m} = C_{u3t} = 0 \\ \tan \alpha_{2m} &= \frac{C_{u2}}{C_a} = \frac{538}{400} = 1.345 \end{aligned}$$

Thus

$$\alpha_{2m} = 53.37^\circ$$

From Eq. (11.17a),

$$\begin{aligned} \tan \alpha_{2h} &= \left(\frac{r_m}{r_h} \right)_2 \tan \alpha_{2m} = \frac{0.2037}{0.18} \times 1.345 = 1.522 \\ \alpha_{2h} &= 56.69^\circ \\ \tan \alpha_{2t} &= \left(\frac{r_m}{r_t} \right)_2 \tan \alpha_{2m} = \frac{0.2037}{0.2274} \times 1.345 = 1.205 \\ \alpha_{2t} &= 50.3^\circ \end{aligned}$$

4. Flow angles (β_2 and β_3)

Since

$$\begin{aligned} \frac{U}{C_a} &= \tan \alpha_2 - \tan \beta_2 \\ \tan \beta_{2m} &= \tan \alpha_{2m} - \frac{U_m}{C_a} = 0.545 \\ \beta_{2m} &= 28.6^\circ \end{aligned}$$

From Eq. (10.18a),

$$\begin{aligned} \tan \beta_{2h} &= \left(\frac{r_m}{r_h} \right)_2 \tan \alpha_{2m} - \left(\frac{r_h}{r_m} \right)_2 \frac{U_m}{C_a} = \frac{0.2037}{0.18} \times 1.345 - \frac{0.18}{0.2037} \times 0.8 = 0.815 \\ \beta_{2h} &= 39.19^\circ \end{aligned}$$

Since

$$\frac{U}{C_a} = \tan \beta_3 - \tan \alpha_3$$

With $\alpha_3 = 0$, then $\frac{U}{C_a} = \tan \beta_3$

At mean section; $\tan \beta_{3m} = \frac{320}{400} = 0.8$

Thus

$$\beta_{3m} = 38.66^\circ$$

At hub, with $\alpha_3 = 0$, and from Eq. (10.18b)

$$\tan \beta_{3h} = \left(\frac{r_h}{r_m} \right)_3 \frac{U_m}{C_a} = \frac{0.1741}{0.2037} \times 0.8 = 0.683$$

$$\beta_{3h} = 34.4^\circ$$

Example 10.7 An axial turbine stage has a degree of reaction $\Lambda = 0.5$ and $\beta_3 = \tan^{-1}(\frac{4}{3})$.

(A) For a constant axial speed, draw the velocity triangle in the two cases:

- (i) $U = C_a$ (ii) $U = 2C_a$

(B) Which of the following cases develops the maximum power:

- (i) $U = 0$
- (ii) $U = C_a$
- (iii) $U = 2C_a$

(C) What will be the maximum power that can be extracted from the turbine if the rotational speed varies between $U = 0$ and $= 2C_a$?

(D) For what rotational speed does this axial turbine stage begin to act like a compressor?

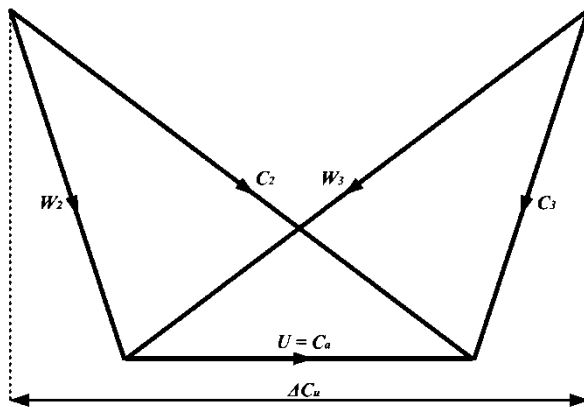
(E) Plot the relation between non-dimensional specific work (w/C_a^2) and non-dimensional rotational speed (U/C_a)

Solution

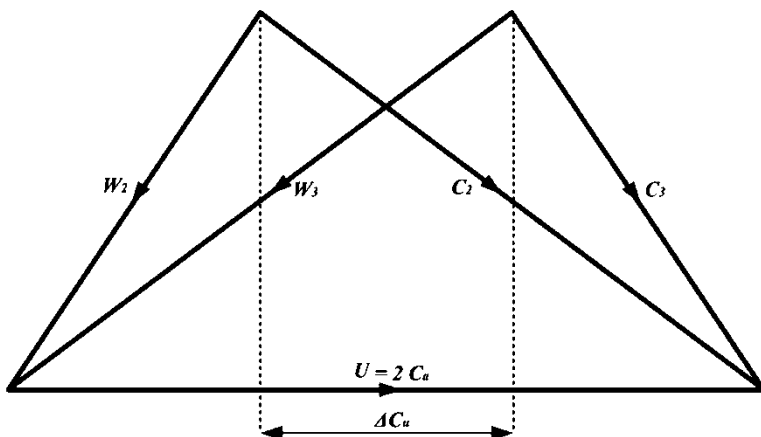
Part 1:

(A)

Case 1. The velocity triangle in the case: $U = C_a$, is shown below



Case 2. The velocity triangles in the case: $U = 2C_a$, is shown below:



(B) The specific work is given by the relation:

$$W = U(C_{u3} + C_{u2})$$

For a constant axial speed and degree of reaction, $\Lambda = 0.5$, then:
 $\alpha_2 = \beta_3 = \tan^{-1}\left(\frac{4}{3}\right) = \text{constant}$. Then

$$C_{u2} = C_a \tan \alpha_2 = \text{constant}$$

and

$$C_{u3} = C_a \tan \alpha_2 - U$$

Then,

$$\begin{aligned} w &= U(C_a \tan \alpha_2 - U + C_a \tan \alpha_2) \\ w &= U(2C_a \tan \alpha_2 - U) \end{aligned}$$

Now consider the three cases,

$$(i) \quad U = 0$$

$$W = U(2C_a \tan \alpha_2 - U) = 0$$

$$(ii) \quad U = C_a$$

$$W = U(2C_a \tan \alpha_2 - U)$$

$$W = C_a(2C_a \tan \alpha_2 - C_a) = C_a^2(2 \tan \alpha_2 - 1)$$

$$W = C_a^2 \left(2 \cdot \frac{4}{3} - 1 \right) = 1.6667 C_a^2$$

$$(iii) \quad U = 2 C_a$$

$$W = 2 C_a(2C_a \tan \alpha_2 - 2C_a) = 4C_a^2(\tan \alpha_2 - 1)$$

$$W = 4C_a^2 \left(\frac{4}{3} - 1 \right) = 1.333 C_a^2$$

then case (ii) gives maximum power extraction

(C) For maximum power extraction,

$$w = U(2C_a \tan \alpha_2 - U)$$

$$\frac{dw}{dU} = (2C_a \tan \alpha_2 - U) + U^*(-1)$$

$$\frac{dw}{dU} = 2C_a \tan \alpha_2 - 2U = 0$$

$$U = C_a \tan \alpha_2$$

This rotational speed that gives maximum power extraction is $U = C_a \tan \alpha_2$
For this case the work would be

$$w = C_a \tan \alpha_2 (2C_a \tan \alpha_2 - C_a \tan \alpha_2)$$

$$w = C_a^2 \cdot \frac{4}{3} \left(2 \cdot \frac{4}{3} - \frac{4}{3} \right)$$

$$w = 1.7778 C_a^2$$

(D) For the turbine to act as a compressor, the work must have a negative sign

$$w = U(2C_a \tan \alpha_2 - U)$$

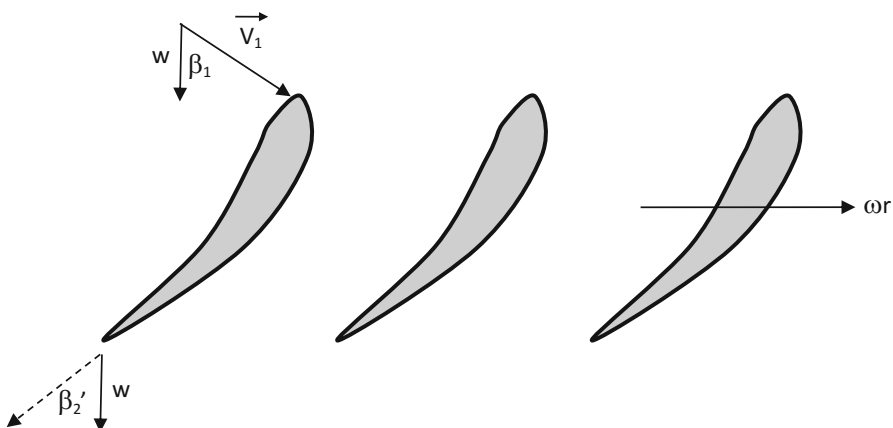
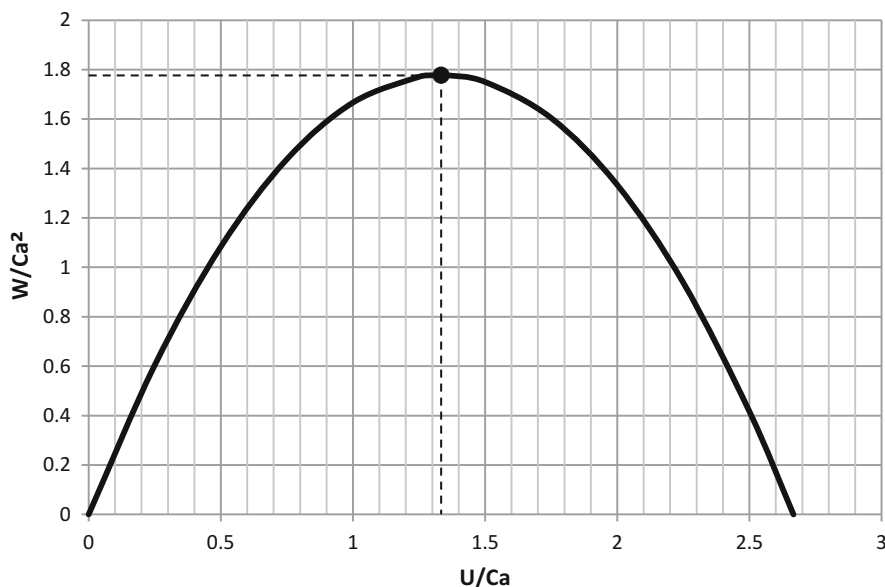
Then U must be greater than $[2C_a \tan (\alpha_2)]$

$$U > 2C_a \tan \alpha_2$$

$$U > 2.667 C_a$$

(E) A plot for power versus the rotational speed is given below. The turbine start to act as a compressor when

$$U = 2.667 C_a$$



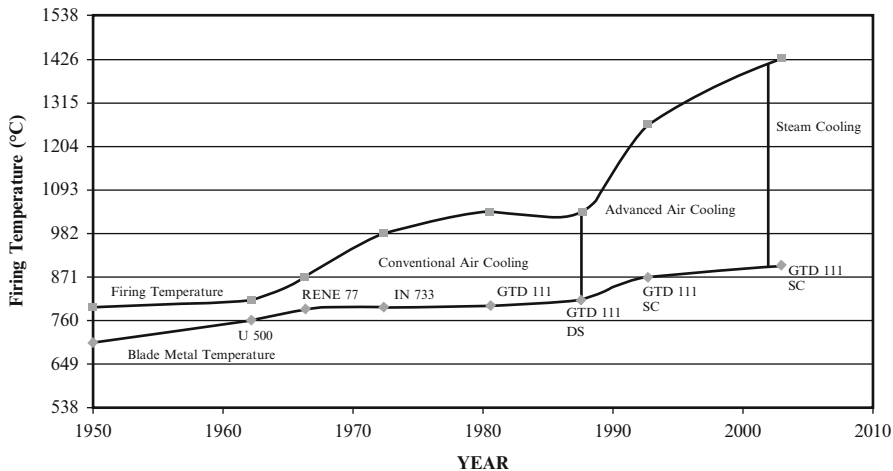


Fig. 10.5 Firing temperature increase with blade material improvement

10.2.7 *Turbine Cooling Techniques*

The turbine inlet temperatures of gas turbines have increased considerably over the past years and will continue to do so. This trend has been made possible by advancement in materials and technology, and the use of advanced turbine blade cooling techniques [4]. The first stage stator blade is subjected to the highest temperature and so must withstand the severest thermal stresses while the first rotor must withstand the combined thermal and mechanical stresses. Figure 10.5 shows the trend of firing temperature and blade alloy capability.

Since 1950, turbine stators (nozzles) material temperature capability has advanced approximately (472 °C), approximately (10 °C) per year. The importance of this increase can be appreciated by noting that an increase of (56 °C) in turbine firing temperature can provide a corresponding increase of 8–13 % in output and 2–4 % improvement in simple-cycle efficiency. Advances in alloys and processing, while expensive and time-consuming, provide significant incentives through increased power density and improved efficiency. Cooling air is bled from the compressor and is directed to the stator, the rotor, and other parts of the turbine rotor and casing to provide adequate cooling. The effect of the coolant on the aerodynamics depends on the type of cooling involved, the temperature of the coolant compared to the mainstream temperature, the location and direction of coolant injection, and the amount of coolant. A number of these factors are being studied experimentally in annular and two-dimensional cascades.

The concepts underlying the following five basic air-cooling schemes are (Fig. 10.6):

1. Convection
2. Impingement

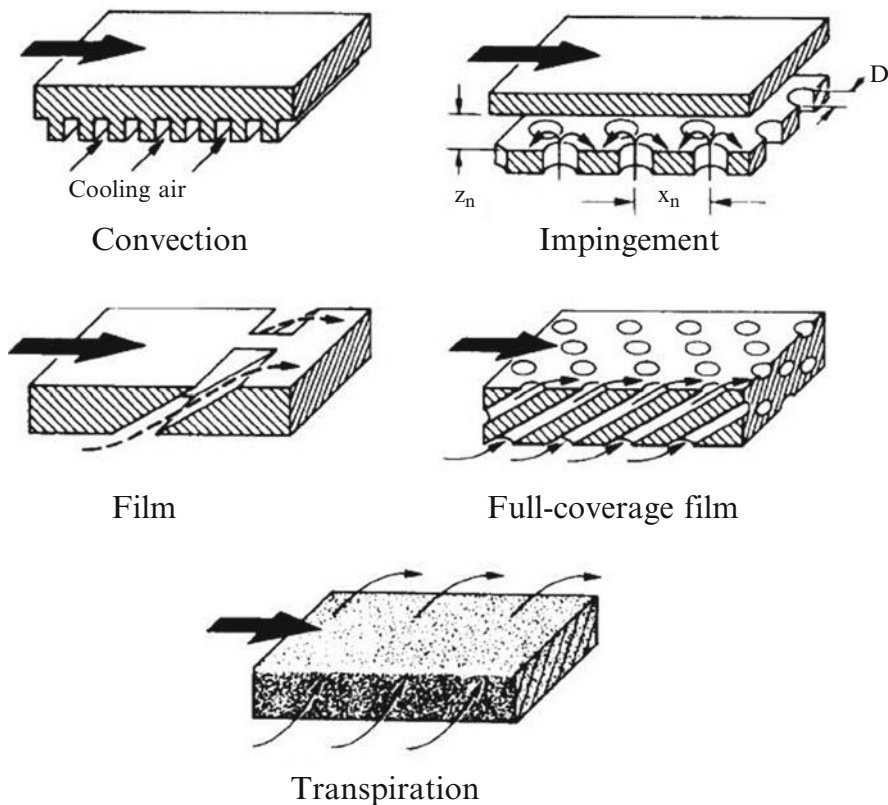


Fig. 10.6 Different cooling techniques

3. Film cooling
4. Full coverage film cooling
5. Transpiration

Until the late 1960s, convection cooling was the primary means of cooling gas turbine blades; some film cooling was occasionally employed in critical regions. Film cooling in the 1980s and 1990s was used extensively.

10.2.7.1 Convection Cooling

This form of cooling is achieved by designing the cooling air to flow inside the turbine blade or vane, and remove heat through the walls. Usually, the air flow is radial, making multiple internal passes from the hub to the blade tip.

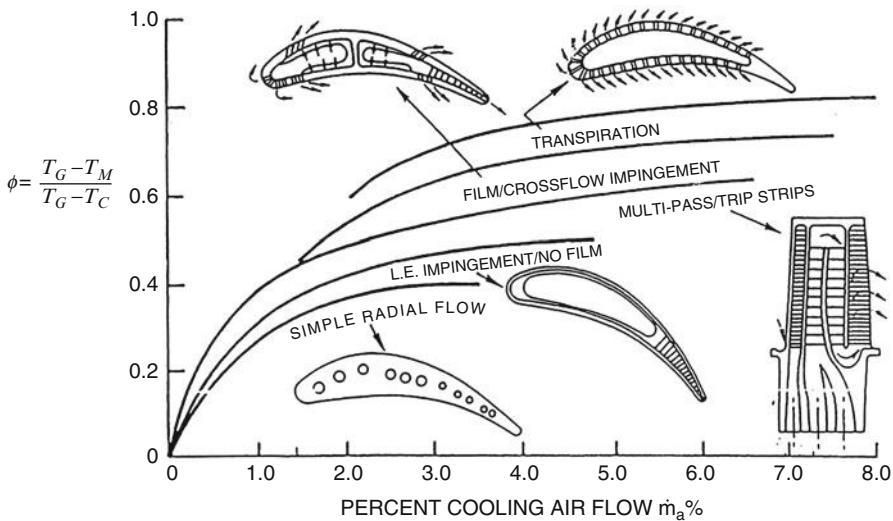


Fig. 10.7 Different cooling techniques

10.2.7.2 Impingement Cooling

In this high-intensity form of convection cooling, the cooling air is blasted on the inner surface of the airfoil by high-velocity air jets, permitting an increased amount of heat to be transferred to the cooling air from the metal surface. This cooling method can be restricted to desired sections of the airfoil to maintain even temperatures over the entire surface. For instance, the leading edge of a blade needs to be cooled more than the mid-chord section or trailing edge.

10.2.7.3 Film Cooling

This type of cooling is achieved by allowing the working air to form an insulating layer between the hot gas stream and the walls of the blade, which protect turbine blades from hot gases at very high temperatures.

10.2.7.4 Transpiration Cooling

Cooling by this method requires the coolant flow to pass through the porous wall of the blade material. The heat transfer is directly between the coolant and the hot gas. Transpiration cooling covers the entire blade with coolant flow (Fig. 10.7).

10.2.8 Guide Lines for Axial Turbine Design

Some recommended practices for axial turbine parameters [5] will be discussed hereafter.

1. Inlet Mach number

To minimize losses in upstream ducting and assure gas acceleration in NGV:

$$(M_1)_{\text{1st stage}} < 0.2 \quad \text{and} \quad (M_1)_{\text{next stages}} \geq (M_1)_{\text{1st stage}}$$

2. Rotor blade inlet hub relative Mach number

To ensure acceleration relative to the rotor and avoid possible separation at rotor inlet, then

$$(M_{w2})_{\text{hub}} < 0.7 \quad \text{and} \quad \alpha_2 = 65^\circ - 73^\circ$$

3. Stage expansion ratio

For the highest efficiency,

- Expansion ratio per stage should be between 2:1 and 3:1
- The highest expansion ratio from a single stage turbine is 4.5:1.

4. Flow coefficient (ϕ)

The flow coefficient versus stage loading for different efficiency is plotted in Fig. 10.8.

5. Hub-tip ratio

To minimize secondary losses and the losses due to tip clearance, the hub-tip ratio is in the range:

$$0.5 < \zeta < 0.85$$

6. Aspect ratio (AR)

Aspect ratio based on axial chord $\left(\frac{h}{C_a}\right)$ should be in the range:

$$AR = 2.5 - 3.5$$

For low pressure turbines (LPT), it may be larger $AR = 6$

7. Axial gap (g)

To avoid blade vibration difficulties, axial gap should be approximately 0.25 times the upstream axial chord.

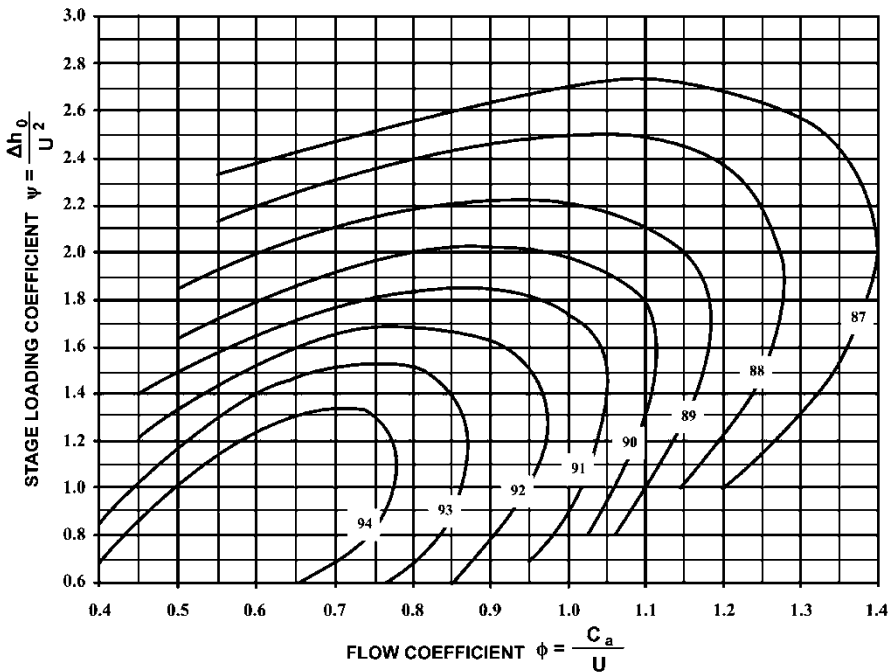


Fig. 10.8 Smith chart (Loading factor versus flow coefficient for different efficiencies)

8. Reaction (Λ)

For best efficiency: $\Lambda \approx 0.5$

If blade temperature is borderline with respect to creep or oxidation: $\Lambda = 0.3$

Hub reaction should be $\Lambda > 0.2$

9. Tip speed (U_{tip})

For high pressure turbine (HPT) due to disc stress limits: $U_{\text{tip}} \approx 400 \text{ m/s}$

For the last stage of an LPT: $U_{\text{tip}} \approx 350 \text{ m/s}$

10. Final stage exit Mach number

To avoid breakdown in flow in turbine's downstream diffusing duct (exhaust, jet pipe, or inter-turbine duct), the final stage Mach number should be in the range:

$$M_{\text{exit}} = 0.3 - 0.55$$

11. Final stage turbine exit swirl angle

To minimize downstream duct pressure loss, the exit swirl angle should be in the range:

$$\alpha_{\text{exit}} = 5^\circ - 20^\circ$$

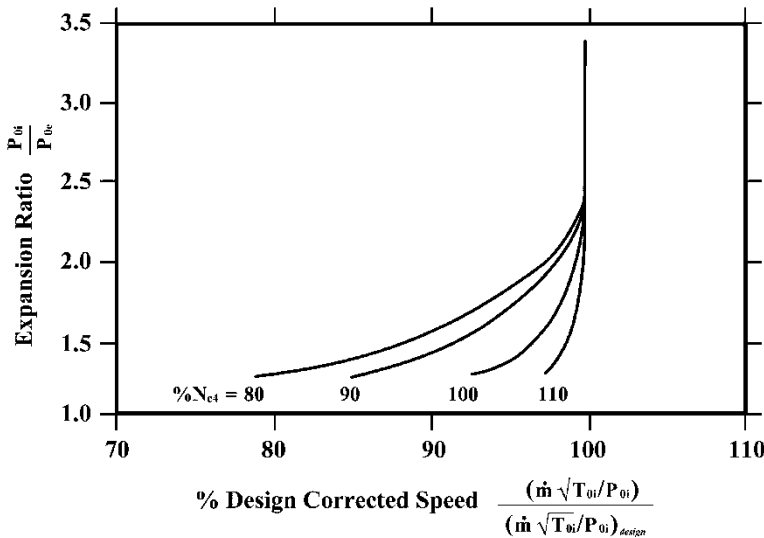


Fig. 10.9 Turbine map

10.2.9 Turbine Map

Turbine map is generated to define performance of turbine under all off design conditions. As described previously for compressors, this map plots the expansion ratio (P_{0i}/P_{0e}) versus mass flow parameter ($\dot{m} \sqrt{T_{0i}/P_{0i}}$) or ($\dot{m} \sqrt{\theta_{0i}/\delta_{0i}}$) for different rotational speed parameter ($N/\sqrt{T_{0i}}$) or ($\frac{N}{\sqrt{\theta_{0i}}}$). Alternatively, turbine map can be drawn with respect to design conditions. Thus its parameters will be the corrected mass flow parameter ($\dot{m} \sqrt{T_{0i}/P_{0i}} / (\dot{m} \sqrt{T_{0i}/P_{0i}})_{design}$) and the speed will be the corrected speed ($N/\sqrt{T_{0i}} / (N/\sqrt{T_{0i}})_{design}$). Additionally, isentropic efficiency is plotted (as an alternative to expansion ratio) versus the mass flow parameter for different rotational speeds.

For each referred speed line, there is a maximum flow capacity which cannot be exceeded. This operating regime is termed choke. For the map shown in Fig. 10.9, the choking capacity is the same for all referred speed lines. This is usually the case when choking occurs in the NGV.

10.3 Radial Flow Turbine

10.3.1 Introduction

Radial turbines are similar to centrifugal compressors as both have mixed flow directions. Fluid enters and leaves in two perpendicular directions. For radial turbines, the flow enters radially and leaves axially close to the axis of rotation. This turning of the flow takes place in the rotor passage, which is relatively long and narrow. For small mass flows, the radial turbine is more efficient than the axial one. The radial turbine develops a high-pressure ratio per stage than the axial one. However, multi-staging of axial turbine can also develop necessary high overall pressure ratios. The radial flow turbines are used in turbochargers for small gas turbines, turbochargers for cars, buses and trucks, railway locomotives and diesel power generators, cryogenic and process expanders, APUs in aircrafts and rocket engine turbopumps [6]. They are very compact and run at very high speeds.

A third type of gas turbines is the mixed flow machine. It is characterized by a combination of axial and radial motion of the fluid relative to the rotor.

Radial inflow turbine is composed of four elements, namely, volute (or scroll), nozzle vanes, rotor, and a discharge diffuser (sometimes identified as exducer) (Fig. 10.10). Flow enters the diffuser at a large radius and leaves it at a smaller radius.

10.3.2 Aero-Thermodynamics of Radial Inflow Turbine

Aerodynamic behavior of gas flow within the turbine passages is demonstrated by its velocity triangles. Thermodynamic behavior is illustrated by its Mollier chart or T-s diagram.

10.3.2.1 Velocity Triangles

The velocity triangles for a radial turbine with prewhirl in the inlet volute is shown in Fig. 10.11, while T-s diagram is plotted in Fig. 10.12.

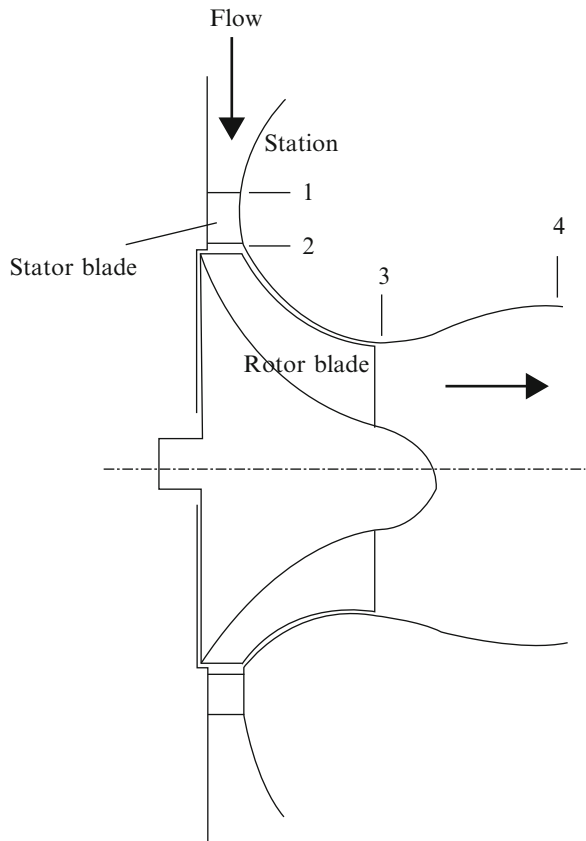
As no work is done in the nozzle, we have

$$h_{01} = h_{02} \quad (10.19)$$

The stagnation pressure drops from P_{01} to P_{02} due to irreversibilities. The specific work is given by Euler's turbine equation:

$$W = U_2 C_{u2} - U_3 C_{u3} \quad (10.20a)$$

Fig. 10.10 Radial inflow turbine



The specific work can be expressed in terms of enthalpy drop as

$$W = U_2 C_{u2} - U_3 C_{u3} = h_{02} - h_{03} = C_p(T_{01} - T_{03}) \quad (10.20b)$$

If the flow at the rotor inlet is radial then the relative angle β_2 is zero (thus $U_2 = C_{u2}$), then

$$W = U_2^2 - U_3 C_{u3} \quad (10.20c)$$

If the whirl velocity is zero at exit (outlet flow is axial), then from Eq. (10.20a):

$$W = U_2 C_{u2} \quad (10.20c)$$

If the flow is radial at inlet and axial at outlet, then from Eq. (10.20c):

$$W = U_2^2 \quad (10.20d)$$

Fig. 10.11 Velocity diagram at inlet and outlet of radial inflow turbine

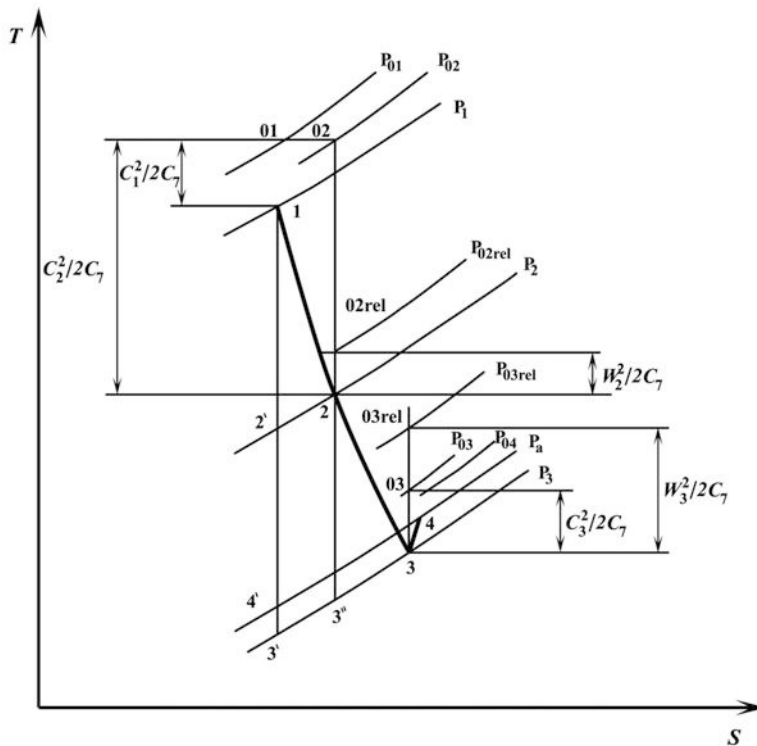
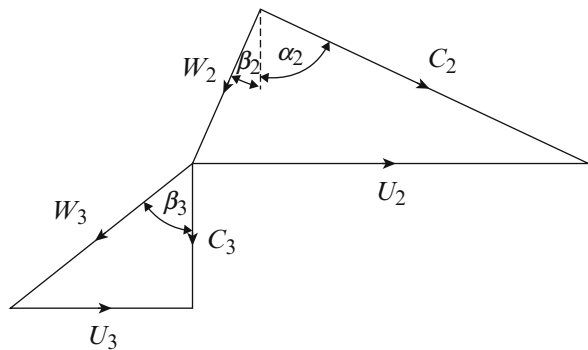


Fig. 10.12 Mollier chart for radial inflow turbine

10.3.2.2 Spouting Velocity C_0

The term spouting velocity C_0 (originating from hydraulic turbine practice) is defined as the velocity that has an associated kinetic energy equal to the isentropic enthalpy drop from turbine inlet stagnation pressure P_{01} to the final exhaust pressure. The exhaust pressure here can have several interpretations depending

upon whether total or static conditions are used in the related efficiency definition and upon whether or not a diffuser is included with the turbine. Thus, if the flow is assumed ideal isentropic through the turbine with a perfect diffuser, then define the specific work output as

$$\frac{C_0^2}{2} = h_{01} - h_{4s} \quad (10.21)$$

Where C_0 is the *spouting velocity* defined as the velocity equivalent of the isentropic enthalpy drop, then from Eq. (10.20d):

$$U_2^2 = \frac{C_0^2}{2}$$

This *velocity ratio* is identified as

$$\nu = \frac{U_2}{C_0} = 0.707 \quad (10.22)$$

In practice $\frac{U_2}{C_0}$ lies in the range: $0.68 < \frac{U_2}{C_0} < 0.71$

When no diffuser is used and if total conditions are used instead of static ones, then the spouting velocity is defined as

$$\frac{C_0^2}{2} = h_{01} - h_{03ss} = C_p(T_{01} - T_{03ss}) \quad (10.23)$$

where T_{03ss} is the total temperature when both stator and rotor are isentropic. Also the speed ratio has the same characteristics identified by Eq. (10.22).

10.3.2.3 Efficiencies

For a radial inflow turbine, three efficiencies are defined:

1. The turbine total-to-static efficiency is defined as

$$\eta_{ts} = \frac{T_{01} - T_{03}}{T_{01} - T'_3} = \frac{\Delta T_0}{T_{01} - T'_3} \quad (10.24)$$

2. The total-to-total efficiency is defined as

$$\eta_{tt} = \frac{T_{01} - T_{03}}{T_{01} - T_{03s}} = \frac{\Delta T_0}{T_{01} - T_{03s}} \quad (10.25)$$

3. The combined turbine and diffuser efficiency is

$$\eta_0 = \frac{T_{01} - T_{03}}{T_{01} - T'_4} = \frac{\Delta T_0}{T_{01} - T'_4} \quad (10.26)$$

Total-to-total efficiency is in the region of 80–90 %.

10.3.2.4 Losses

(a) Nozzle Loss coefficient

Nozzle loss coefficient is defined as

$$\lambda_N = \frac{T_2 - T'_2}{C_2^2/C_p} \quad (10.26a)$$

Assuming that: $T_2 - T'_2 = T''_3 - T'_3$, then

$$\lambda_N = \left[\frac{T''_3 - T'_3}{(C_2^2/C_p)} \right] \left(\frac{T'_2}{T_3} \right) \quad (10.26b)$$

(b) Loss coefficient in rotor

Rotor loss coefficient is defined as

$$\lambda_R = \frac{T_3 - T''_3}{W_3^2/C_p} \quad (10.27)$$

The turbine total-to-static efficiency, Eq. (10.24), can be expressed in terms of the nozzle and rotor loss coefficients:

$$\eta_{ts} = \left[1 + \frac{1}{2C_p(T_{01}-T_{03})} \left(C_3^2 + \lambda_R W_3^2 + \lambda_N \frac{T'_3 C_2^2}{T_2} \right) \right]^{-1} \quad (10.28)$$

The term $\left(\frac{T'_3}{T_2} \right)$ can be calculated from the relation:

$$\frac{T'_3}{T_2} = 1 - \frac{U_2^2}{2C_p T_2} \left[1 + \left(\frac{r_3}{r_2} \right)^2 \left\{ (1 + \lambda_R) \operatorname{cosec}^2 \beta_3 - 1 \right\} - \cot^2 \alpha_2 \right] \quad (10.29)$$

where

$$T_2 = T_{01} - \frac{U_2^2}{2C_p} \operatorname{cosec}^2 \alpha_2 \quad (10.30)$$

10.3.2.5 Dimensionless Parameters

1. Stage loading

The stage loading coefficient can be expressed as

$$\psi = \frac{\Delta h_0}{U_2^2} = \frac{U_2 C_{u2} - U_3 C_{u3}}{U_2^2}$$

Thus

$$\psi = \frac{\Delta h_0}{U_2^2} = \left(\frac{C_{u2}}{U_2} \right) - \left(\frac{r_3}{r_2} \right) \left(\frac{C_{u3}}{U_3} \right) \quad (10.31a)$$

Since $C_{u3} \approx 0$, then

$$\psi \approx \frac{C_{u2}}{U_2} \quad (10.31b)$$

2. Flow coefficient

The flow coefficient is defined in as

$$\phi = \frac{C_{a3}}{U_2} \quad (10.32)$$

3. Rotor meridional velocity ratio

The rotor meridional velocity ratio ξ

$$\xi = \frac{C_{r2}}{C_{a3}} \approx 1.0 \quad (10.33)$$

4. Specific speed

The concept of specific speed was applied almost exclusively to incompressible flow machines as an important parameter in the selection of the optimum type and size of unit.

Specific speed is defined as

$$N_s = \frac{N\sqrt{Q}}{(\Delta h_{0s})^{3/4}} \quad (10.34)$$

According to Balje [8], one suggested value of volume flow rate is that at the outlet (Q_3). Then the specific speed can be expressed as

$$N_s = \frac{\sqrt{Q_3}}{\left(\frac{1}{2}C_0^2\right)^{3/4}} \left(\frac{U_2}{\pi D_2}\right) \sqrt{\frac{U_2}{\pi D_2 N}}$$

$$N_s = \left(\frac{\sqrt{2}}{\pi}\right)^{3/2} \left(\frac{U_2}{C_0}\right)^{3/2} \sqrt{\frac{Q_3}{ND_2^3}}$$

Since $\frac{U_2}{C_0} = 0.707$, then

$$N_s = 0.18 \sqrt{\frac{Q_3}{ND_2^3}} \text{ revolution} \quad (10.35)$$

and

$$\Omega_s = 1.131 \sqrt{\frac{Q_3}{ND_2^3}} \text{ rad} \quad (10.36)$$

Figure 10.13 illustrates the relation between total-to-static efficiency and specific speed for different stator exit angle α_2 .

10.3.3 Recommended Design Values for Radial Inflow Turbines

Based on design and field experience, the following values for different parameters are suggested:

1. Stage loading (ψ), in the range 0.8–1.0
2. Flow coefficient (ϕ), in the range 0.3–0.4
3. Total-to-total or total-to-static efficiency, equal to or greater than 0.7
4. Meridional velocity ratio (ξ) is selected as unity in most cases
5. The ratio between the rotor exit hub to inlet radii (r_{3h}/r_2), in the range 0.25–0.35

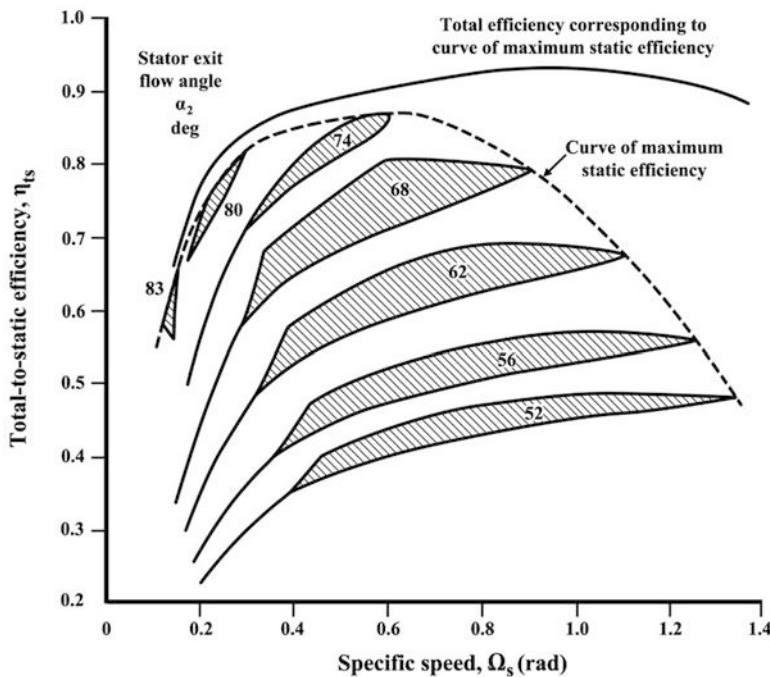


Fig. 10.13 Effect of specific speed on total-to-static efficiency [7]

Table 10.2 Comparison between axial and radial turbines

Axial turbine	Radial turbine
Used for large engines	Used for small engines
Large mass flow rates	Small mass flow rates
Better efficiencies	Lower efficiencies
Low pressure ratio per stage	High pressure ratio per stage
Higher overall pressure ratios	Lower overall pressure ratios
Multi-staging is easier	Multi-staging is more difficult
Expensive	Cheap
Difficult to manufacture	Easy to manufacture

10.3.4 Radial Versus Axial Turbines

Finally, a comparison between axial and radial turbines is given in Table 10.2.

Example 10.8 A radial inflow turbine has the following characteristics and operating conditions:

Inlet total temperature 1000 K
 Inlet total pressure 2.0 bar

Rotor tip rotational speed 500 m/s
 Rotational speed 140,000 rpm

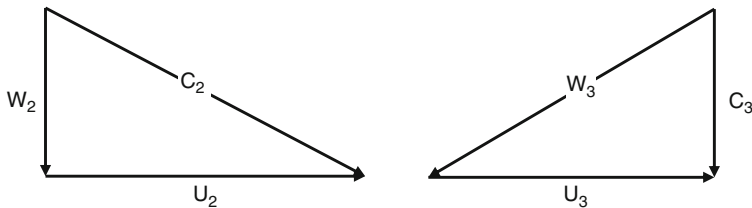
$$\frac{D_{3s}}{D_2} = 0.7, \quad \alpha_2 = 62^\circ, \quad \beta_2 = \alpha_3 = 0$$

$$\frac{U_2}{C_0} = 0.707, \quad \frac{D_{3h}}{D_{3s}} = 0.4, \quad \frac{b_2}{D_2} = 0.0873$$

Calculate:

- (a) Specific speed
- (b) Geometrical dimensions of turbine $D_2, b_2, D_{3h}, D_{3s}, D_{3av}$
- (c) The outlet total and static temperature and outlet static pressure (T_{03}, T_3, P_3)
- (d) Rate of mass flow (\dot{m})
- (e) Rotor inlet static temperature and pressure (T_2, P_2)

Solution



- (a) Specific speed

From Fig. 10.13, the curve total-to-static efficiency, and for $\alpha_2 = 62^\circ$, then $\Omega_S = 0.9$ rad

- (b) Geometrical dimensions

$$(1) \text{ Since } U_2 = \pi D_2 \frac{N}{60}, \text{ then } 500 = \pi * D_2 * \frac{140000}{60}$$

$$\text{Thus } D_2 = 0.06821 \text{ m}$$

$$(2) \text{ Since } \frac{b_2}{D_2} = 0.0873, \text{ then } \frac{b_2}{0.06821} = 0.0873$$

$$\text{Thus } b_2 = 0.00595 \text{ m}$$

$$(3) \text{ Since } \frac{D_{3s}}{D_2} = 0.7, \text{ then } \frac{D_{3s}}{0.06821} = 0.7$$

$$\text{Thus } D_{3s} = 0.04775 \text{ m}$$

$$(4) \text{ Since } \frac{D_{3h}}{D_{3s}} = 0.4, \text{ then } \frac{D_{3h}}{0.04775} = 0.4$$

Thus

$$D_{3_h} = 0.0191 \text{ m}$$

$$(5) \text{ Since } D_{3_{av}} = \frac{D_{3_h} + D_{3_s}}{2} = \frac{0.0191 + 0.04775}{2}$$

Thus

$$D_{3_{av}} = 0.033425 \text{ m}$$

(c) *The outlet conditions*

(1) Since $\alpha_3 = 0$, then the specific work is

$$W = C_P (T_{01} - T_{03}) = U_2 C_{u_2}$$

$$C_P (T_{01} - T_{03}) = U_2^2$$

$$1148 (1000 - T_{03}) = (500)^2$$

$$T_{03} = 782.23 \text{ K}$$

$$(2) \text{ Since } \Omega_S = 1.131 \sqrt{\frac{Q_3}{N D_2^3}}, \text{ then: } 0.9 = 1.131 \sqrt{\frac{Q_3}{\frac{140000}{60} (0.06821)^3}}$$

Thus

$$Q_3 = 0.4689 \text{ m}^3/\text{s}$$

Volume flow rate is $Q_3 = C_{a3} \frac{\pi}{4} (D_{S3}^2 - D_{h3}^2)$

$$0.4689 = C_{a3} \frac{\pi}{4} ((0.04775)^2 - (0.0191)^2)$$

$$C_{a3} = 312 \text{ m/s} = C_3$$

$$T_3 = T_{03} - \frac{C_3^2}{2 C_P}$$

$$T_3 = 782.23 - \frac{(312)^2}{2 * 1148}$$

$$T_3 = 740 \text{ K}$$

(3) Since $\frac{U_2}{C_0} = 0.707$, then $\frac{500}{C_0} = 0.707$ Thus $C_0 = 701.2 \text{ m/s}$

$$\frac{C_0^2}{2} = C_P T_{01} \left[1 - \left(\frac{P_3}{P_{01}} \right)^{\frac{\gamma-1}{\gamma}} \right]$$

$$\frac{(707.2)^2}{2} = 1148 * 1000 \left[1 - \left(\frac{P_3}{P_{01}} \right)^{0.25} \right]$$

$$\left(\frac{P_3}{P_{01}} \right)^{0.25} = 0.78217$$

Thus $\frac{P_3}{P_{01}} = 0.374$, and $\frac{P_3}{2} = 0.374$

$$P_3 = 0.7486 \text{ bar}$$

(d) *Mass flow rate*

$$\dot{m} = \rho_3 Q_3 = \frac{P_3}{R T_3} * Q_3 = \frac{0.7486*10^5}{287*740} * 0.4689$$

Mass flow rate: $\dot{m} = 0.1652 \text{ kg/s}$

(e) *The rotor inlet conditions*

$$(1) \text{ Since } \sin \alpha_2 = \frac{U_2}{C_2}, \text{ then } \sin (62) = \frac{500}{C_2}$$

Thus

$$C_2 = 566.3 \text{ m/s}$$

Since

$$T_{02} = T_{01} = 1000 \text{ K}$$

$$\text{Moreover } T_2 = T_{02} - \frac{C_2^2}{2 C_p} = 1000 - \frac{(566.3)^2}{2 * 1148}$$

$$T_2 = 860 \text{ K}$$

$$(2) \text{ Since } \tan \alpha_2 = \frac{U_2}{C_{r2}}, \text{ then } \tan 62 = \frac{500}{C_{r2}}$$

Thus

$$C_{r2} = 265.85 \text{ m/s}$$

$$A_2 = \pi D_2 b_2 = \pi \times 0.06821 \times 0.00595 = 0.001275 \text{ m}^2$$

With

$$\dot{m} = \rho_2 C_{r2} A_2$$

Then

$$0.1616 = \rho_2 * 265.85 * 0.001275$$

Thus :

$$\rho_2 = 0.47675 \text{ kg/m}^3$$

Now

$$\rho_2 = \frac{P_2}{RT_2}, \text{ thus } 0.47675 = \frac{P_2}{287 * 860.3}$$

$$P_2 = 1.177 \text{ bar}$$

Example 10.9 A small inward flow radial gas turbine comprising a radial vaned impeller, a ring of nozzle blades, and an axial diffuser, operates at its design point with a total-to-total efficiency of 0.91. At turbine entry, the stagnation pressure and temperature of the gas are 410 kPa and 1100 K, respectively. The flow leaving the turbine is diffused to a pressure of 101 kPa and has a negligible final velocity. Given that the flow is just choked at the nozzle exit, *determine*:

- (a) The impeller peripheral speed
- (b) The flow outlet angle from the nozzle

The working fluid is hot gases having $\gamma = 1.333$ and $R = 287 \text{ J/kg.K}$.

Solution

$$\begin{aligned} P_{01} &= 410 \text{ kPa}, & T_{01} &= 1100 \text{ K}, & \eta_{tt} &= 0.91 \\ P_{03} &= 101 \text{ kPa}, & M_2 &= 1 \end{aligned}$$

(a) *Impeller peripheral speed*

Since the outlet total pressure is given by $P_{03} = P_{01} \left(1 - \frac{\Delta T_0}{T_{01} \eta_{tt}}\right)^{\gamma/\gamma-1}$

$$\begin{aligned} 101 &= 410 \left(1 - \frac{\Delta T_0}{1100 \times 0.91}\right)^4 \\ 0.70451 &= 1 - \frac{\Delta T_0}{1100 \times 0.91} \\ \Delta T_0 &= 295.7855 \text{ K} \end{aligned}$$

$$W = C_P(T_{01} - T_{03}) = U_2 C_{u2} - U_3 C_{u3}$$

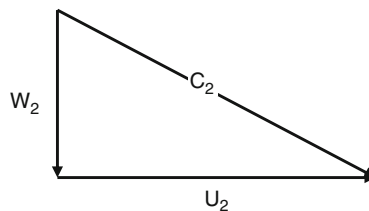
$$C_P(T_{01} - T_{03}) = U_2 \times U_2 - U_3 \times 0$$

$$C_P \Delta T_0 = U_2^2$$

$$U_2^2 = 1148 \times 295.7855$$

$$U_2 = 582.72 \text{ m/s}$$

(b) *Flow outlet angle from the nozzle*



$$T_{02} = T_2 \left[1 + \frac{\gamma - 1}{2} M_2^2 \right]$$

For choked nozzle, then

$$T_2 = \frac{2T_{02}}{\gamma + 1} = \frac{2 \times 1100}{1.333 + 1} = 942.86 \text{ K}$$

$$C_2 = \sqrt{\gamma R T_2}$$

$$C_2 = \sqrt{1.333 \times 287 \times 942.86} = 600.67 \text{ m/s}$$

$$\sin \alpha_2 = \frac{U_2}{C_2} = \frac{582.72}{600.67}$$

$$\alpha_2 = 75.96^\circ$$

10.4 Gas Turbine Engine Matching

10.4.1 Introduction

Turbine is coupled either to a compressor or to a fan, thus forming an engine spool. Each compressor/turbine has a certain design point where the rotational speed (N), pressure ratio (π_c, π_t), and mass flow rate (\dot{m}) are specified. It is requested to operate efficiently over the complete range of speed and power output for aero engine or power plant. These conditions are identified as the *off-design conditions* and resemble starting, idling, reduced power, maximum power, acceleration, and deceleration.

10.4.2 Compatibility Conditions

The steady state performance of an engine at each speed (N) is determined by:

1. Operating Speed

$$\frac{N}{\sqrt{(T_{oi})_{turbine}}} = \frac{N}{\sqrt{(T_{oi})_{compressor}}} \times \sqrt{\frac{(T_{oi})_{compressor}}{(T_{oi})_{turbine}}}$$

where (i) stands for inlet condition. Now, abbreviating compressor as (c) and turbine as (t), the above equation can be rewritten as

$$\frac{N}{\sqrt{(T_{oi})_t}} = \frac{N}{\sqrt{(T_{oi})_c}} \times \sqrt{\frac{(T_{oi})_c}{(T_{oi})_t}}$$

2. Mass flow rate

$$\frac{\dot{m}_t \sqrt{(T_{oi})_t}}{(P_{0i})_t} = \frac{\dot{m}_c \sqrt{(T_{oi})_c}}{(P_{0i})_c} \times \frac{(P_{0i})_c}{(P_{0e})_c} \times \frac{(P_{0e})_c}{(P_{0i})_t} \times \sqrt{\frac{(T_{oi})_t}{(T_{oi})_c}} \times \frac{\dot{m}_t}{\dot{m}_c}$$

where (e) stands for outlet condition and the

compressor's pressure ratio is $\pi_c = \frac{(P_{0e})_c}{(P_{0i})_c}$,

combustion chamber pressure ratio is $\pi_{cc} = \frac{(P_{0i})_c}{(P_{0e})_c} = 1 - \frac{\Delta P_{cc}}{(P_{0e})_c}$

Moreover; from conservation of mass (or continuity of flow)

$$(\dot{m})_t = (\dot{m})_c \times (1 + f - b)$$

where:

f = fuel to air ratio

b = bleed to air ratio

3. Conservation of energy (or power balance)

It depends upon which module is coupled to turbine, a compressor/fan or a power consumed load as will be described hereafter.

10.4.3 Single Shaft Gas Turbine Engine

Figure 10.14 illustrates a schematic diagram of a single-shaft gas turbine. The load could be an electrical generator, a marine screw, a rotor of a helicopter, or a propeller of a turboprop engine.

The following steps summarize the matching procedure:

1. Select a rotational speed (N); thus, from the known ambient conditions calculate $(N/\sqrt{T_{01}})$, which defines the speed line on the compressor map.
2. Assume the compressor pressure ratio (P_{02}/P_{01}) , thus from the compressor map, the operating point is completely defined; i.e., the mass flow parameter $(\dot{m}\sqrt{T_{01}}/P_{01})$ and compressor efficiency (η_c) as shown in Fig. 10.15.
3. The compressor mass flow rate is calculated from the relation

$$\dot{m}_1 = \frac{\dot{m}\sqrt{T_{01}}}{P_{01}} \times \frac{P_{01}}{\sqrt{T_{01}}}$$

4. The turbine mass flow rate is then obtained from the relation

$$(\dot{m})_3 = (\dot{m})_1 \times (1 + f - b)$$

5. Calculate the compressor specific work from the relation

$$w_c = \frac{C_{pc}T_{01}}{\eta_c} \left[\left(\frac{P_{02}}{P_{01}} \right)^{\frac{\gamma-1}{\gamma}} - 1 \right]$$

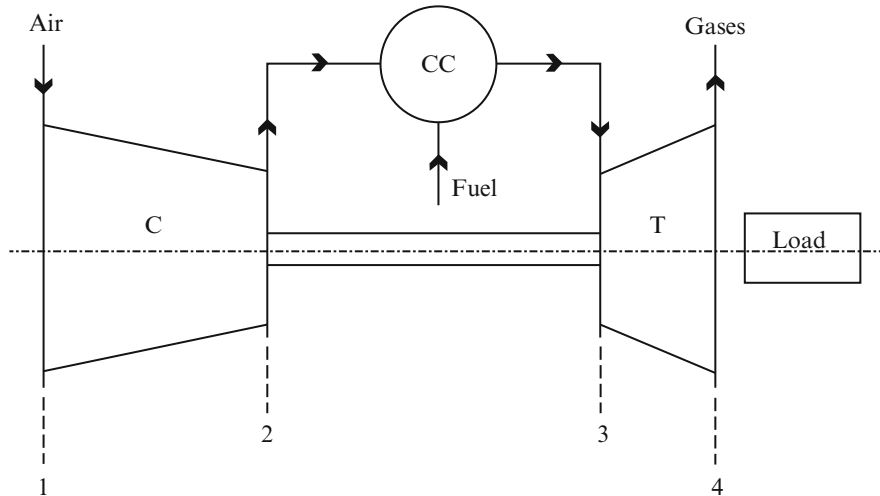


Fig. 10.14 Layout of a single-shaft gas turbine

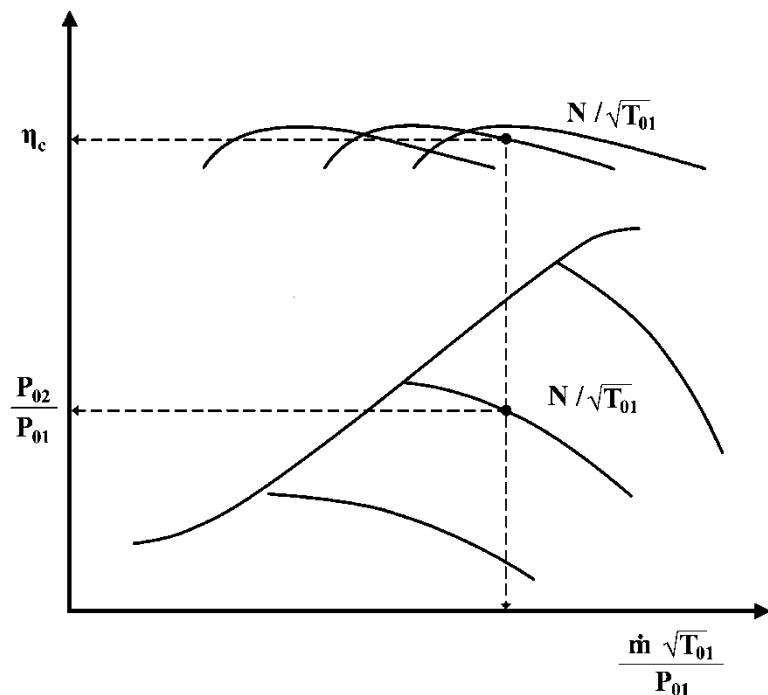


Fig. 10.15 Operating point on compressor map

6. The inlet total pressure of the turbine is obtained from the pressure loss in combustion chamber (ΔP_{cc}); thus

$$P_{03} = P_{02}(1 - \Delta P_{cc})$$

7. Assume turbine inlet temperature (T_{03}); thus, calculate ($N/\sqrt{T_{03}}$)

$$N/\sqrt{T_{03}} = N/\sqrt{T_{01}} \times \sqrt{\frac{T_{01}}{T_{03}}}$$

this determines the speed line on turbine map.

8. The turbine mass flow parameter is determined as follows:

$$\frac{\dot{m}_3\sqrt{T_{03}}}{P_{03}} = \frac{\dot{m}_1\sqrt{T_{01}}}{P_{01}} \times \sqrt{\frac{T_{03}}{T_{01}}} \times \frac{P_{01}}{P_{02}} \times \frac{P_{02}}{P_{03}} \times \frac{\dot{m}_3}{\dot{m}_1}$$

9. From this mass parameter and the operating speed line, the turbine efficiency can be determined from turbine map. The specific work generated in the turbine is then

$$w_t = \eta_t C_{pt} T_{03} \left[1 - \frac{1}{\left(\frac{P_{03}}{P_{04}} \right)^{\frac{\gamma-1}{\gamma}}} \right]$$

10. The net power (P) is then evaluated from the relation

$$\mathcal{P} = \dot{m}_3 w_t - \frac{\dot{m}_1 w_c}{\eta_m}$$

11. A check is next performed between this gained power and the needed power for driving the load. If they are unequal, the above procedure is repeated by assuming another value for compressor's pressure ratio. Interpolation may be employed to define the correct pressure ratio when several iterations did not provide the exact load requirements.

10.4.4 Off-Design of Free Turbine Engine

In this case, the gas turbine incorporates two turbines, namely, the gas generator turbine and the free (power) turbine. The power of the gas generator turbine is exactly equal to that of the compressor. The remaining power in the gases leaving

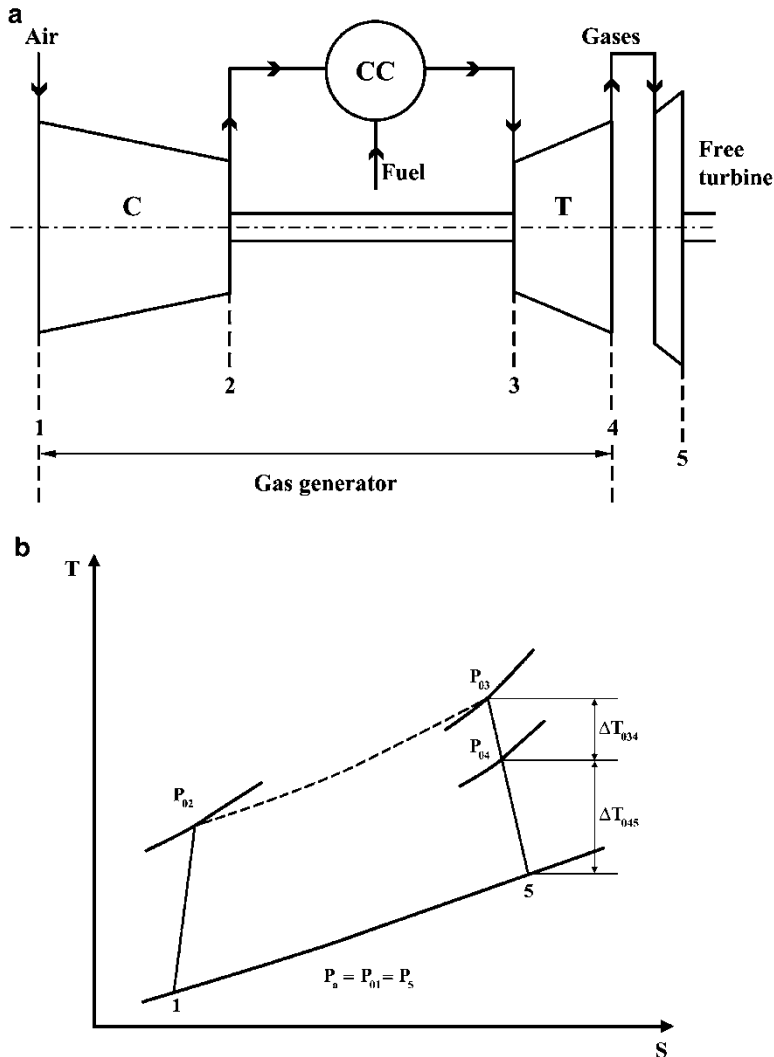


Fig. 10.16 Free power turbine (a) Layout (b) Temperature–entropy diagram

the first gas (generator) turbine is absorbed by the second (free) turbine and used to drive the load (Fig. 10.16).

The analysis to be followed here is divided into two steps:

- Matching between the compressor and turbine of the gas generator
- Off-design analysis of the free turbine

10.4.4.1 Gas Generator

The following steps are followed:

1. Select a constant speed line on compressor map (Fig. 10.15) and choose any point on this line; thus, the compressor parameters ($\frac{N}{\sqrt{T_{01}}}$, $\frac{P_{02}}{P_{01}}$, $\frac{\dot{m}_1 \sqrt{T_{01}}}{P_{01}}$, η_c) are determined
2. The compressor-specific work is determined from

$$W_c = \frac{C_{pc} T_{01}}{\eta_c} \left[\left(\frac{P_{01}}{P_{01}} \right)^{\frac{\gamma_c - 1}{\gamma_c}} - 1 \right]$$

3. Guess a value of the turbine pressure ratio; P_{04}/P_{03} , thus, the value of the turbine mass flow parameter, $\frac{\dot{m}_3 \sqrt{T_{03}}}{P_{03}}$ is determined. The turbine mass flow rate is determined from equation

$$\dot{m}_3 = \dot{m}_1 (1 + f - b)$$

4. Turbine mass flow parameter is expressed as

$$\frac{\dot{m}_3 \sqrt{T_{03}}}{P_{03}} = \frac{\dot{m}_1 \sqrt{T_{01}}}{P_{01}} \times \sqrt{\frac{T_{03}}{T_{01}}} \times \frac{P_{01}}{P_{02}} \times \frac{P_{02}}{P_{03}} \times \frac{\dot{m}_3}{\dot{m}_1}$$

The equation can be rearranged to determine the first value for turbine temperature ratio (T_{03}/T_{01})_A as follows:

$$\left(\frac{T_{03}}{T_{01}} \right)_A = \left[\frac{\dot{m}_3 \sqrt{T_{03}}}{P_{03}} \times \frac{P_{02}}{P_{01}} \times \frac{P_{03}}{P_{02}} \times \frac{\dot{m}_1}{\dot{m}_3} \right]^2$$

5. Thus, the turbine inlet temperature (T_{03}) is defined. From which the speed line i. $(N/\sqrt{T_{03}})$ and turbine efficiency (η_t) are determined.
6. From the energy balance between compressor and turbine of the gas generator, calculate another value for $(T_{03}/T_{01})_B$ from the following relation:

$$\left(\frac{T_{03}}{T_{01}} \right)_B = \frac{\dot{m}_1}{\dot{m}_3} \frac{C_{Pc}}{\eta_c \eta_t C_{Pt}} \left[\frac{(P_{02}/P_{01})^{\frac{\gamma_c - 1}{\gamma_c}} - 1}{1 - \frac{1}{(P_{03}/P_{04})^{\frac{\gamma_t - 1}{\gamma_t}}}} \right]$$

7. If values of $\left(\frac{T_{03}}{T_{01}}\right)_A$ and $\left(\frac{T_{03}}{T_{01}}\right)_B$ are not equal, another value for the turbine pressure ratio is assumed and the above procedure is repeated until convergence is satisfied.

10.4.4.2 Free Power Turbine

Matching procedure for a free power turbine is described as follows:

1. Select a constant speed line on the compressor map $N/\sqrt{T_{01}}$, (Fig. 10.17).
2. Select a point on this speed line, thus different parameters of compressor ($\frac{P_{02}}{P_{01}}$, $\frac{\dot{m}_1 \sqrt{T_{01}}}{P_{01}}$, η_c) is defined.
3. Follow the same procedure described above for matching between this point and a corresponding point on the gas generator turbine.
4. Calculate the pressure ratio of the free power turbine from

$$\frac{P_{04}}{P_a} = \frac{P_{04}}{P_{03}} \frac{P_{03}}{P_{02}} \frac{P_{02}}{P_{01}} \frac{P_{01}}{P_a}$$

5. Determine a first value for the mass flow parameter from the free turbine map $\left(\frac{\dot{m}_4 \sqrt{T_{04}}}{P_{04}}\right)_A$
6. Compare this value with the value calculated from equation

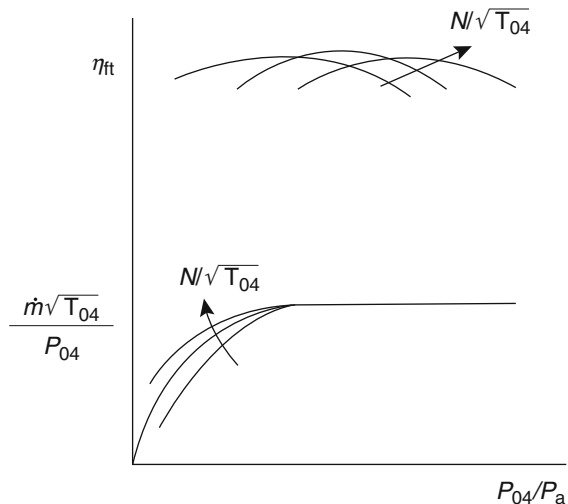
$$\left(\frac{\dot{m}_4 \sqrt{T_{04}}}{P_{04}}\right)_B = \frac{\dot{m}_3 \sqrt{T_{03}}}{P_{03}} \times \frac{P_{03}}{P_{04}} \times \sqrt{\frac{T_{04}}{T_{03}} \times \frac{\dot{m}_4}{\dot{m}_3}}$$

7. If agreement is not reached, the above procedure is repeated by selecting another point on the same speed line of compressor and repeat the procedure until convergence is achieved.
8. Repeat the above procedure for other constant speed lines of the compressor map.
9. The power generated from the free power turbine is

$$\begin{aligned}\mathcal{P} &= \dot{m}_4 C_{p4} (\Delta T_0)_{45} \\ \mathcal{P} &= \dot{m}_4 C_{p4} \eta_{ft} T_{04} \left[1 - \left(\frac{P_{04}}{P_a} \right)^{\frac{1-\eta}{\eta}} \right]\end{aligned}$$

10. The mass flow rate can be obtained from the known output conditions of the gas generator turbine.

Fig. 10.17 Free power turbine map



$$\dot{m}_4^* = \frac{\dot{m} \sqrt{T_{04}}}{P_{04}} = \frac{P_{04}}{\sqrt{T_{04}}}$$

Example 10.10 A single shaft aero engine has an air mass flow rate = 40 kg/s. Other data are

Compressor

Inlet total temperature and pressure are 270 K and 1.1 bar

Bleed ratio is 5 % and fuel to air ratio is 2 %

Compressor map data:

$\frac{P_{02}}{P_{01}}$	$\frac{\dot{m}_1 \sqrt{T_{01}}}{P_{01}}$	η_c
3.5	850	0.86
4.0	750	0.87
4.5	600	0.88

Combustion chamber

Pressure drop in combustion chamber is 3 %.

Turbine

Turbine is choked having a constant mass flow parameter of 368 and efficiency of 0.9. Turbine inlet temperature (TIT) = 1100 K

Calculate the available power.

Solution

The flow compatibility is given by the following relation:

$$\frac{\dot{m}_3 \sqrt{T_{03}}}{P_{03}} = \frac{\dot{m}_1 \sqrt{T_{01}}}{P_{01}} \frac{P_{01}}{P_{02}} \frac{P_{02}}{P_{03}} \frac{\dot{m}_3}{\dot{m}_1} \sqrt{\frac{T_{03}}{T_{01}}} \quad (1)$$

The relation between turbine mass flow rate and compressor mass flow rate is given by

$$\dot{m}_3 = \dot{m}_1(1 + f - b), \dot{m}_3 = 40(1 + 0.02 - 0.05), \dot{m}_3 = 38.8 \text{ kg/sec} \quad (2)$$

The relation between compressor exit pressure and turbine inlet pressure is given by

$$P_{03} = P_{02} (1 - \Delta P_{cc}), P_{03} = P_{02} (1 - 0.03), P_{03} = 0.97 P_{02} \quad (3)$$

Substituting from equations (2) and (3) into (1), and substituting by $T_{03} = 1100 \text{ K}$ and $T_{01} = 470 \text{ K}$,

$$\begin{aligned} \left(\frac{\dot{m}_3 \sqrt{T_{03}}}{P_{03}} \right) &= \left(\frac{\dot{m}_1 \sqrt{T_{01}}}{P_{01}} \right) \left(\frac{P_{01}}{P_{02}} \right) \left(\frac{P_{02}}{0.97 P_{02}} \right) \left(\frac{38.8}{40} \right) \sqrt{\frac{1100}{270}} \\ \left(\frac{\dot{m}_3 \sqrt{T_{03}}}{P_{03}} \right) &= 2.02 \left(\frac{\dot{m}_1 \sqrt{T_{01}}}{P_{01}} \right) \left(\frac{P_{01}}{P_{02}} \right) \end{aligned} \quad (4)$$

Since the turbine is choked, then the mass flow parameter will always be constant and equals 368,

$$\begin{aligned} 368 &= 2.02 \left(\frac{\dot{m}_1 \sqrt{T_{01}}}{P_{01}} \right) \left(\frac{P_{01}}{P_{02}} \right) \\ \left(\frac{\dot{m}_1 \sqrt{T_{01}}}{P_{01}} \right) &= 182.36 \left(\frac{P_{02}}{P_{01}} \right) \end{aligned} \quad (4)$$

The mass flow parameter is calculated from equation (4) for different pressure ratios and tabulated along with the values given in the data above in the following table.

$$\frac{P_{02}}{P_{01}} \quad \frac{\dot{m}_1 \sqrt{T_{01}}}{P_{01}}$$

From data From eqn. 4

3.5	850	638.26
4.0	750	9.44
4.5	600	820.60

The two sets of compressor mass flow parameters are plotted.

From the figure, equilibrium between the turbine and the compressor occur at $\frac{P_{02}}{P_{01}} = 4.05$ and mass flow parameter = 738, where the compressor efficiency = 0.88 (Fig. 10.18).

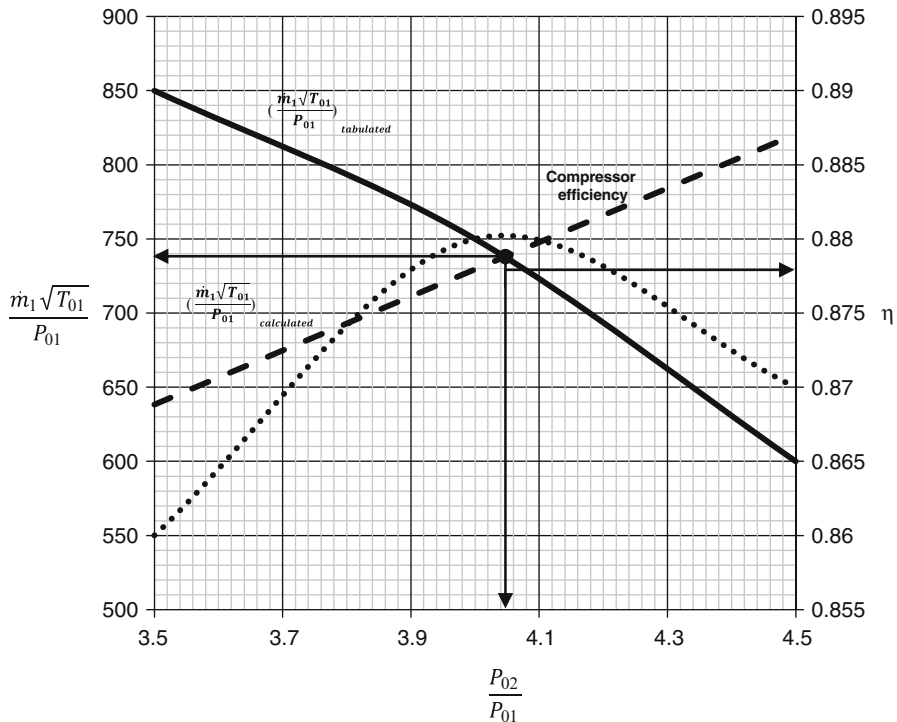


Fig. 10.18 Compressor map

The corresponding turbine pressure ratio is given by

$$\frac{P_{02}}{P_{01}} = \frac{P_{03}/P_{04}}{(1 - \Delta P_{cc})}$$

$$4.05 = \frac{P_{03}/P_{04}}{(1 - 0.03)}$$

$$\frac{P_{03}}{P_{04}} = 3.9285$$

The available power is given by,

$$\mathcal{P} = \dot{m}_3 W_t - \dot{m}_1 W_c$$

$$\mathcal{P} = \dot{m}_3 \eta_t C_{pt} T_{03} \left[1 - \frac{1}{\left(\frac{P_{03}}{P_{04}} \right)^{\gamma_t - 1/\gamma_t}} \right] - \frac{\dot{m}_1 C_{pc} T_{01}}{\eta_c} \left[\left(\frac{P_{03}}{P_{04}} \right)^{\gamma_c - 1/\gamma_c} - 1 \right]$$

$$\begin{aligned}\mathcal{P} &= 38.8 * 0.9 * 1.148 * 1100 \left[1 - \left(\frac{1}{3.9285} \right)^{0.25} \right] \\ &\quad - \frac{40 * 1.005 * 270}{0.88} \left[(4.05)^{0.286} - 1 \right]\end{aligned}$$

Power $\mathcal{P} = 6708 \text{ kW}$

Problems

(A) Axial Flow Turbine

10.1 A single-stage axial flow gas turbine has the following data:

Inlet stagnation temperature T_{01}	1200 K
Stator outlet angle, α_2	60°
Rotor blade inlet angle, β_2	20°
Rotor blade outlet angle, β_3	60°

Calculate

- (a) The flow coefficient
 - (b) The stage-loading coefficient
 - (c) The degree of reaction
 - (d) If the blade speed $U=360 \text{ m/s}$, calculate:
 - (i) The stage total temperature drop
 - (ii) The stage pressure ratio if its efficiency is 0.9
- 10.2 An axial flow gas turbine stage has a flow coefficient of 0.65° , a constant axial velocity and the gas leaves the stator blades at an angle of 65° to axial direction. Calculate:
- (a) The blade-loading coefficient
 - (b) The rotor blade relative flow angle
 - (c) The degree of reaction
- 10.3 A single stage axial flow gas turbine has a mean radius of 30 cm. The hot gases enter the turbine stage at 1900 kPa and 1200 K, and the absolute velocity leaving the stator (C_2) is 600 m/s making 65° with the axial direction (α_2). The rotor inlet and outlet blade angles (β_2 and β_3) are 25° and 60° , respectively. Draw the velocity triangles and calculate:
- (a) The rotor rotational speed (rpm).
 - (b) The stage pressure ratio if its efficiency is 0.88.
 - (c) The flow coefficient, loading coefficient, and degree of reaction.
 - (d) The power delivered by the turbine if mass flow rate is 50 kg/s.

10.4 A single stage axial flow turbine, with axial leaving velocity, has the following data:

Static temperature at stator inlet	=750 K
Gas velocity at stator inlet	=165 m/s
Blade mean velocity	=300 m/s
Degree of reaction at mean radius	=0.5

Plot the velocity triangles, determine:

- (a) The fluid angle (α_2)
- (b) The stage-loading coefficient
- (c) The flow coefficient
- (d) The stage total pressure ratio if $\eta_s = 0.9$

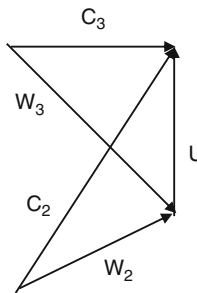
10.5 In a zero reaction gas turbine, the blade speed at the mean diameter is 290 m/s. Gas leaves the nozzle ring at an angle 65^0 to the axial direction while the inlet stage temperature is 1100 K. The following pressures were measured at various locations:

At nozzle entry, stagnation pressure	400 kPa
At nozzle exit, stagnation pressure	390 kPa
At nozzle exit, static pressure	200 kPa
At rotor exit, static pressure	188 kPa

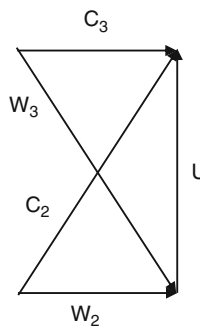
Assuming the magnitude and the direction of velocities at entry and at exit of the stage are the same; determine the total-to-total efficiency of the stage.

10.6 The figure shows velocity diagrams for *impulse* (zero reaction) and 50 % reaction turbine stages at different rotor speeds. In both cases, the rotor absolute inlet velocity C_2 is 450 m/s at an angle $\alpha_2 = 65^0$, and the absolute exit angle C_3 is axial. Complete the following table:

Quantity	Impulse	50%reaction
U		
Φ		
Ψ		
β_1		
β_2		
$\Delta T_{0 \text{ stage}}$		
Work		



Impulse

**50% reaction**

10.7 A small axial flow gas turbine with equal stage inlet and outlet velocities has the following design data based on the mean diameter:

Inlet temperature T_{01}	1200 K	Inlet pressure P_{01}	350 kPa
Axial velocity C_a	260 m/s	Blade speed U	350 m/s
Nozzle efflux angle, α_2	60°	Stage exit angle α_3	12°
Mass flow rate	18 kg/s		

Calculate

- The rotor blade angles
- The blade loading coefficient and degree of reaction.
- The power output.
- The nozzle throat area required if the throat is situated at the nozzle outlet and nozzle losses coefficient is 0.05.

10.8 A single-stage axial flow gas turbine with convergent nozzles has the following data:

Inlet stagnation temperature T_{01}	1250 K	Mass flow rate	25 kg/s
Inlet stagnation pressure P_{01}	420 kPa	Mean blade speed, U	340 m/s

Stage stagnation temperature drop	160 K	Rotational speed, N	15,000 rpm
Pressure ratio, P_{01}/P_{03}	1.9	Flow coefficient, Φ	0.75
Angle of gas leaving stage, α_3	12°	Nozzle coefficient, λ_N	0.05

If the axial velocity remains constant and the gas velocities at inlet and outlet are the same determine at the mean radius:

- (a) The blade angles
- (b) The stage efficiency
- (c) The blade-loading coefficient and degree of reaction
- (d) The required nozzle inlet area
- (e) The annulus area at rotor inlet and outlet
- (f) The blade height at the above locations

10.9 The following data apply to a single-stage axial flow gas turbine

Inlet stagnation temperature T_{01}	1400 K	Mass flow rate	36 kg/s
Inlet stagnation pressure P_{01}	8.0 bar	Mean blade speed, U	320 m/s
Stage stagnation temperature drop	150 K	Rotational speed, N	250 rev/s
Isentropic stage efficiency	0.9	Outlet velocity, C_3	400 m/s

Assuming that the outlet velocity is axial, calculate:

- (a) The stage specific work and the stage power
- (b) Draw the velocity triangle and determine the blade and flow angles
- (c) The stage pressure ratio
- (d) The inlet rotor and exit Mach numbers
- (e) The blade height at rotor inlet and exit if $\lambda_N = 0.05$

10.10 A single-stage axial flow gas turbine with convergent nozzles has the following data:

Inlet stagnation temperature T_{01}	1500 K	Mass flow rate	18.75 kg/s
Inlet stagnation pressure P_{01}	3.4 bar	Mean blade speed, U	298 m/s
Stage stagnation temperature drop	144 K	Rotational speed, N	200 rps
Nozzle losses coefficient, λ_N	0.05	Flow coefficient, Φ	0.95
Isentropic stage efficiency	0.9		

The convergent nozzle is choked. Calculate:

- (a) The pressure ratio in the turbine
- (b) The flow angles α_2 , β_2 , α_3 and β_3

- (c) The blade-loading coefficient
 (d) The degree of reaction
 (e) The blade height and annulus radius ratio at stations 1,2, and 3.
- 10.11 The following particulars relate to a single-stage turbine of a free vortex design:
- | | | | |
|---------------------------------------|---------|------------------------|---------|
| Inlet stagnation temperature T_{01} | 1250 K | Outlet velocity, C_3 | 275 m/s |
| Inlet stagnation pressure P_{01} | 3.8 bar | Root blade speed, U | 300 m/s |
| Pressure ratio, P_{01}/P_{03} | 2.0 | Isentropic efficiency | 0.88 |
- The turbine is designed for zero reaction ($\Lambda=0$) at the root radius and the velocities at inlet and outlet (C_1 and C_3) are both equal and axial. Calculate:
- The nozzle efflux angle α_2 and the blade inlet angle β_2 at the root radius.
 - If the tip to root radius ratio of the annulus at exit from the nozzle blades is 1.4, determine the nozzle efflux angle and degree of reaction at the tip radius.
 - Assuming a nozzle blade losses coefficient of 0.05, calculate the static pressure at inlet and outlet of the rotor blades at root radius.
- 10.12 A single stage axial flow gas turbine has a degree of reaction at mean radius $\Lambda_m=0.5$. If the free vortex design is considered, what is the minimum hub-to-tip ratio (ζ) such that the degree of reaction remains positive along the blade height.
- 10.13 The data below apply to a single-stage axial flow gas turbine designed on free vortex theory. The outlet velocity is axial and the turbine is designed with a constant annulus area through the stage.
- | | | | |
|--|---------|---------------------------------|------------|
| Inlet stagnation temperature T_{01} | 1325 K | Mass flow rate | 30 kg/s |
| Inlet stagnation pressure P_{01} | 800 kPa | Mean blade speed, U | 330 m/s |
| Stage stagnation temperature Drop | 160 K | Rotational speed, N | 15,000 rpm |
| Isentropic stage efficiency | 0.9 | Outlet velocity, C_3 | 390 m/s |
| Angle of gas leaving stage, α_3 | 12^0 | Nozzle coefficient, λ_N | 0.05 |
- Calculate
- The stage pressure ratio
 - The flow and blade angles at the mean radius
 - The flow coefficient, loading stage coefficient, and degree of reaction
 - The blade height at inlet and exit from the rotor
 - The flow and blade angles at root and tip radius using free vortex design
- 10.14 A multi-stage axial turbine of the impulse type has a constant mean diameter (D_m).

- (a) Prove that the specific work is expressed by the relation:

$$W_s = U_m \sum_{i=1}^{i=n} \Delta C_{ui}$$

where ΔC_{ui} is the change of swirl velocities of stage (i) and (n) is the number of stages.

- (b) If the impulse turbine is composed of two stages, mean rotor speed ($U_m = 400\text{m/s}$), axial velocity is constant in each stage, $(C_a)_{\text{stage 1}} = 450\text{m/s}$ and $(C_a)_{\text{stage 2}} = 400\text{m/s}$. The relative angle for the first stage is $\beta = 60^\circ$ and for the second stage is $\beta = 55^\circ$, calculate the specific work.

- 10.15 The *high pressure turbine* (HPT) of a high bypass ratio turbofan engine is a single stage. It has the following data:

- Inlet total temperature is 1563 K – Stage efficiency 0.92
- Inlet total pressure is 43.6 bar – Rotational speed at mean radius is 490 m/s
- Stage temperature drop is 352 K – Absolute outflow angle $\alpha_3 = 25^\circ$
- Flow coefficient $\phi = 0.8$

Calculate:

1. Stage pressure ratio
2. Absolute Mach numbers M_1, M_2, M_3
3. Parameters ψ and Λ
4. Angles $\alpha_2, \beta_2, \beta_3$

- 10.16 An axial turbine stage has the following data at mean section:

$$C_{a2} = 260\text{m/s}, \quad C_{a3} = 130\text{m/s}, \quad U = 360\text{m/s}, \quad \alpha_2 = 65^\circ, \quad \beta_3 = 66.54^\circ$$

- (a) Calculate flow coefficient at inlet and outlet of rotor ϕ_2, ϕ_3
- (b) Temperature drop in stage ΔT_0
- (c) Calculate the relative velocities at inlet and outlet of rotor W_2, W_3
- (d) Calculate the degree of reaction using the relation:

$$\Lambda = 1 + \frac{C_{a3}^2 - C_{a2}^2}{2U(C_{u3} + C_{u2})} - \frac{C_{u2} - C_{u3}}{2U}$$

- 10.17 An axial turbine of the reaction type is running at design rotational speed (N) and has the following characteristic:

$$\beta_2 = 0, \quad \Lambda = 0.5$$

Draw the velocity triangles and prove that the specific power is

$$W_s = U^2$$

During a part load operation, the speed is reduced to (N'). The axial speed is unchanged ($C'_a = C_a$) and the rotor outlet angle is also unchanged ($\beta'_3 = \beta_3$).

For this part load operation, prove that the developed power (P') and torque (τ') are related to the full load operation parameters power and torque (P, τ) by the relations:

$$\frac{P'}{P} = 2\left(\frac{N'}{N}\right) - \left(\frac{N'}{N}\right)^2$$

$$\frac{\tau'}{\tau} = 2 - \frac{N'}{N}$$

Plot the relations: $\frac{P'}{P}$ versus $\frac{N'}{N}$ and $\frac{\tau'}{\tau}$ versus $\frac{N'}{N}$

- 10.18 (a) Why cooling is needed in turbines?
 (b) An axial turbine stage has the following characteristics: Mass flow rate = 18 kg/s, inlet total conditions: $T_{01} = 1000K$, $P_{01} = 400\text{ kPa}$, temperature drop $\Delta T_0 = 151\text{ K}$. The nozzle is choked ($P_2 = P_c$). At rotor inlet: annulus area: $A_2 = 0.08\text{ m}^2$, $\alpha_2 = 60^\circ$ and $U_2 = 350\text{ m/s}$. Stage efficiency $\eta_s = 0.92$. The axial speed is assumed constant through the rotor. Specific heat ratio is $\gamma = 4/3$.
- (A) Draw the stage, velocity triangles, and plot the expansion process on T-s diagram
 (B) Calculate:
 (a) The velocities (C_2) and (C_{a2})
 (b) The flow angles (β_2, α_3 and β_3)
 (c) The degree of reaction (Λ)
 (d) Stage pressure ratio (P_{01}/P_{03})
 (e) The *maximum tensile stress* for a constant cross sectional area rotor blade is given by the relation

$$\sigma_{\max} = 2\pi\rho_b N^2 A$$

If the blade is manufactured from Inconel 718, where its material density $\rho_b = 8220\text{ kg/m}^3$, rotational speed $N = 300\text{ rps}$ and $A = 0.08\text{ m}^2$, calculate the corresponding maximum stress.

- (f) Describe two methods for *turbine cooling*. If film cooling is used, what do you expect for the maximum stress calculated above?
 (B) *Radial turbines*

- 10.19 A radial turbine is proposed as the gas expansion element in a chemical plant. The pressure and temperature conditions through the stage at the design point are to be as follows:

Upstream of the nozzle: $P_{01} = 700\text{ kPa}$, $T_{01} = 1150\text{ K}$

Nozzle exit: $P_2 = 530\text{ kPa}$, $T_2 = 1030\text{ K}$

Rotor exit: $P_3 = 385\text{ kPa}$, $T_3 = 915\text{ K}$, $T_{03} = 925\text{ K}$

The ratio of rotor exit mean diameter to rotor inlet tip diameter is chosen as 0.45 and the rotational speed is 25,000 rpm. Assuming the relative flow at rotor inlet is radial, and the absolute flow at rotor exit is axial. The gases have a molecular weight of 40 and a ratio of specific heats of 1.6. Determine the following:

- (a) The total-to-static efficiency of the turbine
- (b) The rotor diameter

- 10.20 A small radial inflow turbine develops 60 kW power when its rotor is running at 60,000 rpm. The pressure ratio P_{01}/P_3 is 2.0. The inlet total temperature is 1200 K. The rotor has an inlet tip diameter of 12 cm and rotor exit tip diameter of 7.5 cm. The hub-tip ratio at exit is 0.3. The mass flow rate of gases is 0.35 kg/s. They enter the rotor radially and leave axially and have the following inlet and outlet angles $\alpha_2 = 70^\circ$ and $\beta_2 = 40^\circ$. The nozzle loss coefficient (λ_N) = 0.07. It is required to calculate:

- (a) The isentropic efficiency (η_{is})
- (b) The rotor loss coefficient (λ_R)

- 10.21 A radial inflow turbine runs at 60,000 rpm. The inlet conditions are $T_{01} = 1000\text{ K}$, $P_{01} = 400\text{ kPa}$. The turbine pressure ratio $\frac{P_{01}}{P_3} = 2.3$, mass flow rate is 0.3 kg/s. The rotor tip diameter $D_2 = 0.12\text{ m}$, and specific heat ratio $\gamma = 1.35$. Other data is $\beta_2 = C_{u3} = 0$, $W_2 = C_3$, $\alpha_2 = 75^\circ$ and $\frac{P_{02}}{P_{01}} = 0.98$.

Calculate:

- (a) Ratio of tip speed to spouting velocity $\left(\frac{U_2}{C_0}\right)$
- (b) The power produced by the turbine
- (c) The total-to-total efficiency

Matching of turbomachines

- 10.22 The following data refer to the compressor and turbine of high pressure spool at its design speed.

Compressor characteristic			Turbine characteristic		
P_{02}/P_{01}	$\dot{m} \sqrt{T_{01}}/P_{01}$	η_C	P_{03}/P_{04}	$\dot{m} \sqrt{T_{03}}/P_{03}$	η_t
6.5	330	0.80	3.2	110	0.92
6.0	350	0.79	2.8	110	0.92
5.6	370	0.77	2.4	110	0.92

The combustion pressure loss is 5 % of the compressor delivery pressure and the inlet conditions of compressor are 7.23 bar and 540 K. Mechanical losses can be neglected. The inlet total temperature for turbine is 1570 K. The non-dimensional flows are based on \dot{m} in kg/s, and P in bar and T in K, all pressures and temperatures being stagnation values.

Calculate

1. The characteristics of the design point of axial compressor
2. The characteristics of the design point of turbine when the *power of compressor and turbine are equal*

- 10.23 A triple spool turbofan engine in takeoff conditions where the ambient conditions is 288 K and 1 bar, has a bypass ratio equals 10. Gases enter the LPT which drives the front fan at temperature of 900 K. Assuming the gases enter turbine at pressure (P_{03}) of fourfolds that of the air exiting the fan (P_{02}).

Fan map data:

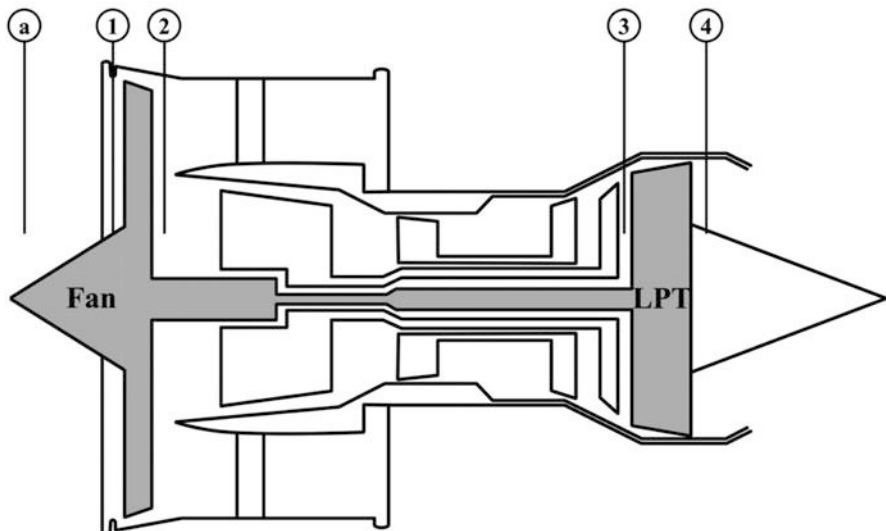
$\frac{P_{02}}{P_{01}}$	$\frac{\dot{m}_1 \sqrt{T_{01}}}{P_{01}}$	η_f
1.2	12,000	0.88
1.5	10,000	0.90
1.8	9000	0.91

Turbine map:

- Choked turbine
- Mass flow parameter 400
- Efficiency 0.91

Calculate

1. The fan operating point (mass flow parameter, pressure ratio)
2. The fan air flow rate
3. The turbine pressure ratio

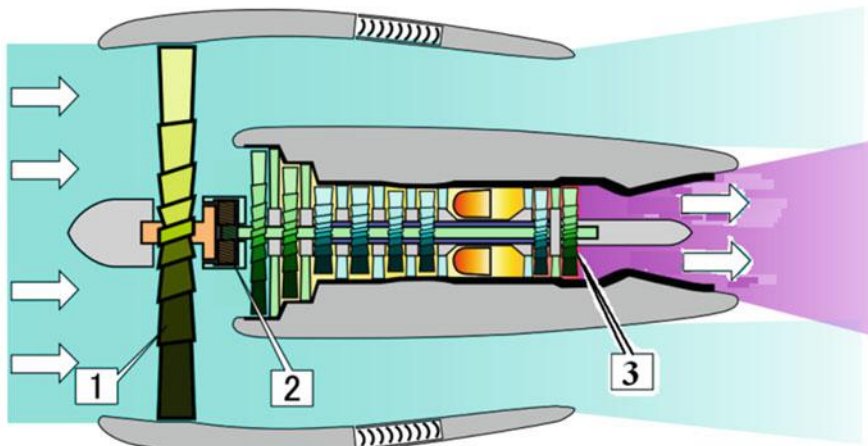


10.24 The below figure illustrates a *Geared turbofan*. The fan (1) is driven by low pressure turbine (3), through a reduction gearbox (2). The fan rotates at smaller speed than that of low pressure turbine to decrease losses. Part of the power generated by turbine (3) is used to drive the fan. Matching between fan (1) and low pressure turbine (3) has the following characteristics:

1. Mass flow ratio $\frac{\dot{m}_1}{\dot{m}_3} = \beta$
2. Speed ratio $\frac{N_3}{N_1} = \lambda$
3. Power ratio $P_3/P_1 = \delta$

where all the variables (β, λ, δ) are greater than unity and the inlet and outlet states of fan are denoted by (1,2), while inlet and outlet states of turbine are (3,4).

- (a) Draw the fan and turbine maps.
- (b) State the three compatibility conditions.



References

1. Glassman AJ, Moffitt TP (1972) New technology in turbine aerodynamics. 1st Turbomachinery symposium, College Station, TX, 24–26 October 1972
2. Stewart WL (1961) A study of axial flow turbine efficiency characteristics in terms of velocity diagram parameters. Winter annual meeting, ASME, November 26 – December 1, 1961
3. Ainley DG, Mathieson GCR (1957) A method of performance estimation for axial-flow turbines, R.& M. No. 2974, Aeronautical Research Council, London, December 1951
4. Meherwan P (2006) Boyce, gas turbine engineering handbook, 3rd edn. Gulf Professional Publishing is an imprint of Elsevier, chapter 9, pp 354–387
5. Walsh PP, Fletcher P (2004) Gas turbine performance, 2nd edn. Blackwell Science, Oxford, pp 204–207
6. Moustapha H, Zelesky MF, Baines NC, Japikse D (2003) Axial and radial turbines, Concepts ETI, Inc., Wilder, VT, 2003, p 199
7. Glassman AJ. Turbine design applications, NASA SP-290, p 279
8. Balje OE (1981) Turbomachinery: a guide to design, selection and theory, 1st edn. Wiley, New York, June 17, 1981

Chapter 11

Rocket Propulsion

11.1 Introduction

In Chap. 1, propulsion systems were classified as either air-breathing or non-air-breathing (rocket) engines. All engines discussed so far belong to the category of air-breathing engines. In this chapter non-air-breathing engines (or rockets) will be discussed. Non-air-breathing engines carry oxidizer as well as fuel on board.

A rocket is a propulsive device that produces a thrust force F on a vehicle by ejecting mass at a high relative velocity. Rockets can be classified into chemical and nonchemical rockets. Chemical rockets can be further categorized into many types. The most famous of them are liquid, solid, and hybrid types. Nonchemical rockets are also classified into several types including electrical, thermal, solar, and nuclear rockets. Some flight vehicles use a dual-mode engine, which has an air-breathing mode (either ramjet, turbojet, or turbofan engine) and a non-air-breathing or rocket mode. One of the latest applications is SABRE [1].

Schematics of rocket engines are shown in Fig. 11.1. Chemical rockets consist of a container or containers for propellant, a combustion chamber (frequently identified as thrust chamber), an exhaust nozzle, an igniter, a navigational equipment, a payload, etc. Chemical rocket propellants are either solid or liquid. In a liquid system, the fuel and oxidizer are separately stored and are sprayed under high pressure (1900–5500 kPa) into the combustion chamber, where burning takes place that produces gases at high temperature (around 4000 K). Products of combustion expand through the nozzle to high velocities which in turn generates very high thrust.

When solid propellants are used, both fuel and oxidizer are contained in the same casing or combustion chamber. The propellant charge is called the “grain” and it contains the entire chemical ingredients for complete burning. Once ignited, it usually burns smoothly at a nearly constant rate on the exposed surface of the charge. Because there are no feed systems or valves such as there are in liquid units, solid-propellant rockets are relatively simple in construction.

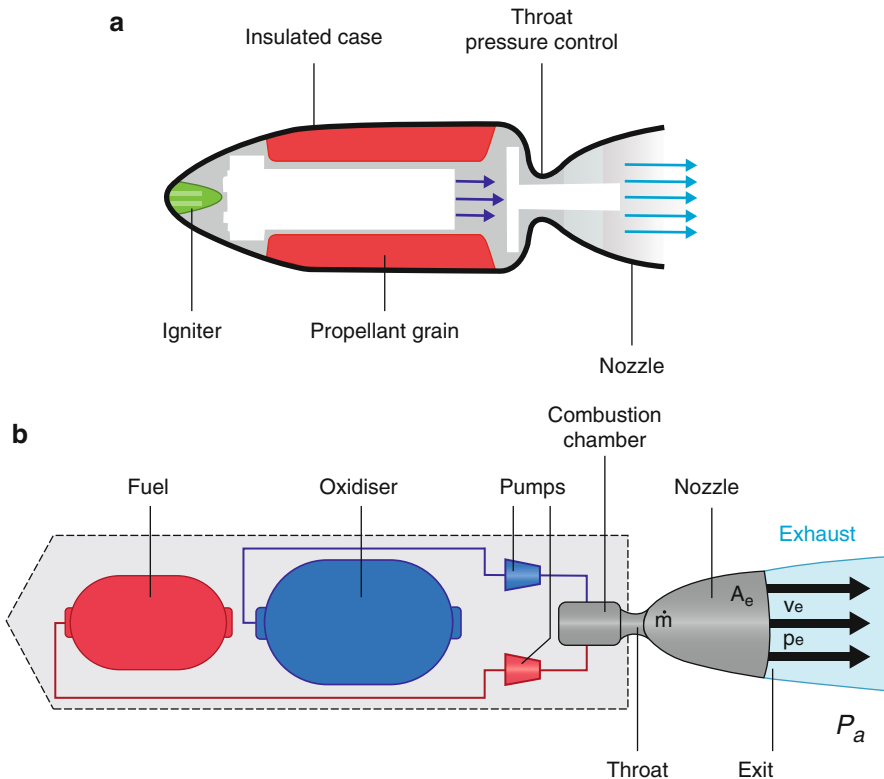


Fig. 11.1 Basic parts of a rocket engine: (a) solid-propellant rocket and (b) liquid-propellant rocket

Thus, the earliest rockets were solid-fuel rockets powered by [gunpowder](#); they were used in warfare by the [Chinese](#), [Indians](#), [Mongols](#), and [Arabs](#), as early as the thirteenth century [2].

Rockets have the following advantages over air-breathing engines [3]:

1. Thrust is essentially independent of speed and altitude.
2. Thrust per frontal area is the largest among all known propulsion systems, while supercharged reciprocating engine is the smallest.
3. Thrust per weight of engine is the largest of all known propulsion systems.
4. No altitude ceiling (or depth floor).

11.2 History

11.2.1 Important Events

Different books, publications, and websites give timeline of rocket history. These include Sutton [4], Turner [5], Yehia [6], and NASA [7]. Details of milestones of

rocket invention are given in Appendix D. A brief history for important dates is given hereafter. Archytas, a Greek who lived in Southern Italy, used reaction principle in flying wooden pigeon (400 B.C.). A second Greek who lived in Alexandria, Egypt, named Hero (10–67 A.D.), invented his aeolipile machine which applies the reaction principle of rocketry. In the first century A.D., Chinese put gunpowder (made from saltpeter, sulfur, etc.) in bamboo tubes and tossed them in fire mostly for fireworks in religious and other festive celebrations. Chinese Feng Jishen (970 A.D.) is considered the real inventor of rockets. In 1232 Chinese repelled the Mongol invaders during the battle of Kai-Keng by a barrage of arrows of flying fire (resemble simple form of a solid-propellant rocket). In 1200s Tatars and Moors used rockets in their invasion to Europe. In 1650 Kazimierz Siemienowicz (a Polish artillery expert) published a series of drawings for a staged rocket. Foundations for modern rocketry were laid by Sir Isaac Newton through his three laws of motion. Konstantin Tsiolkovsky (1857–1935), a Russian mathematician, developed the rocket equation and wrote on multistage rockets, artificial satellites, and space travel. In 1923 his native Hermann Oberth published a book on rocket travel into the outer space. The world's first liquid-fueled rocket launched on March 16, 1926 was created and built by the American Robert Hutchings Goddard (1882–1945). Goddard and his team launched 34 rockets between 1926 and 1941, achieving altitudes as high as 2.6 km and speeds as high as 885 km/h. He conducted practical experiments in rocketry. He developed the single and multi-stage rocket engines for both rocket- and jet-assisted takeoff (JATO) aircraft in 1945. Wernher von Braun assistant of Oberth in 1930 performed early experiments in testing a liquid-fueled rocket with about 15 pounds of thrust. The V-2 (1942) was the world's first long-range ballistic missile (Fig. 11.2). It was a liquid-propellant rocket developed during the Second World War in Germany to attack allied cities. In 1957 Soviet Union stunned the world by launching an Earth-orbiting artificial satellite called Sputnik I. Their succeeding satellite, Sputnik II, carried a dog named Laika on board. In the same year (1957), Jupiter-C rocket carried the US satellite Explorer I into the space. April 12, 1961, dates the first human's journey into the outer space when Russian Yuri Alekseyevich Gagarin ([Soviet](#) pilot and [cosmonaut](#)) with his [Vostok spacecraft](#) completed an [orbit](#) of the [Earth](#). Allan Shepard was the first American astronaut to ride to the space inside a Mercury space capsule on top of a Redstone rocket on May 5, 1961.

[Apollo 11](#) was the [space flight](#) launched by a [Saturn V](#) rocket (111 meter high) from [Kennedy Space Center](#) on July 20, 1969, and [landed](#) the first humans on the [Moon](#), Americans [Neil Armstrong](#) and [Buzz Aldrin](#), at 20:18 UTC. Armstrong became the first to step onto the lunar surface 6 h later on July 21 at 02:56 UTC.

Since then, both Russia (previously Soviet Union) and the USA competed in space invasion through many rockets and spacecrafts which were launched for the Moon and Venus.

Between 1981 and 2011, a total of 135 missions for the space shuttle (Fig. 11.3), which is a crewed, partially reusable [low Earth-orbital spacecraft](#), was operated by the US National Aeronautics and Space Administration (NASA).

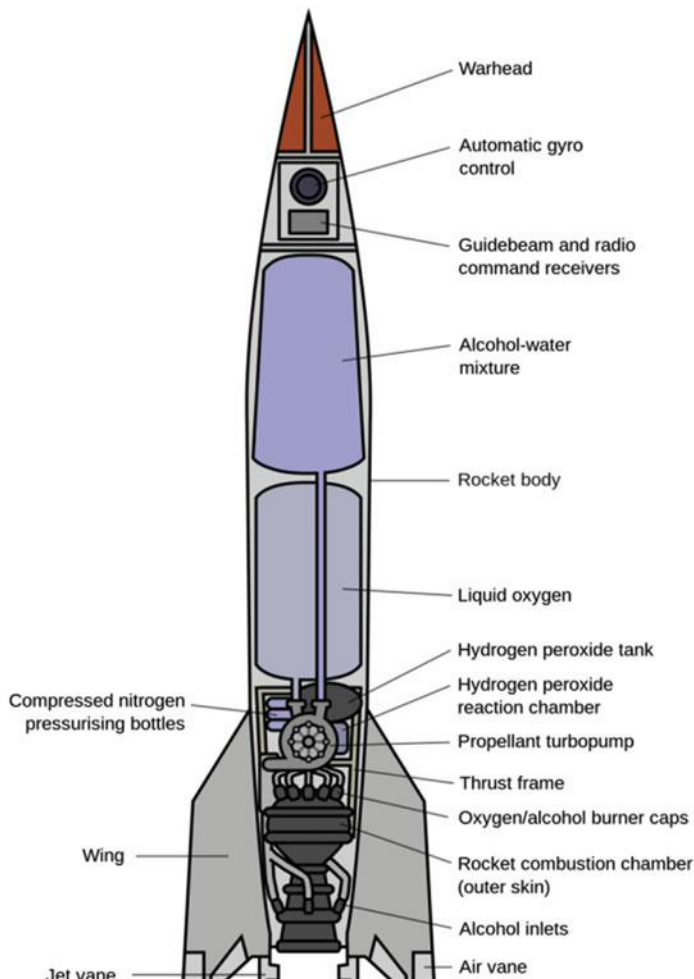


Fig. 11.2 V2 rocket

Ariane rocket family is a series of European civilian launch vehicles. France and Germany are the main contributors, while Belgium, Denmark, Italy, the Netherlands, Spain, Norway, Sweden, and Switzerland have minor participation. Ariane 1 was launched in 1978, while Ariane 5 started its launching in 1996 and will continue up to 2021. Arianespace launches Ariane rockets from the Guiana Space Center at Kourou in French Guiana.



Fig. 11.3 Space shuttle

11.2.2 Future Plans of Rocket and Space Flights (2014 and Beyond)

- NASA's Dawn spacecraft to enter orbit around Ceres.
- NASA's MAVEN spacecraft to enter orbit around Mars.
- NASA to send three small landers on the surface of the Moon.
- The USA to launch the Next Gen NEAR mission aiming to land on an asteroid.
- European Rosetta spacecraft to enter orbit around comet Churyumov-Gerasimenko.
- India's unmanned probe to enter orbit around Mars.
- The Rosetta spacecraft to drop the Philae lander on the surface of comet Churyumov-Gerasimenko.
- Japan to launch Hayabusa-2 spacecraft on a mission to a carbon-rich asteroid.
- Bigelow and Boeing companies to start assembling a 690-cubic-meter space station in the Earth orbit NASA to launch a visible-light coronagraph to search for planets outside the solar system.
- Ariane 6 is planned to be launched in 2021.
- Brazil to conduct its fourth attempt to orbit a satellite with a domestically built vehicle from Alcantara.
- Russia to launch the [Luna-Glob](#) spacecraft toward the Moon.
- China to test-fly the Chang Zheng 5 (CZ-5) rocket, capable of delivering 25 tons to the low Earth orbit.

11.3 Classifications of Rockets

11.3.1 Method of Propulsion

Rockets can be classified based on propulsion methods using one of the following methods (Fig. 11.4):

- Chemical (solid, liquid, and hybrid).
- Electrical (electrostatic, electrothermal, and electromagnetic).
- Solar (solar sail rocket, solar-heated rocket).
- Nuclear (nuclear fission rocket, nuclear fusion rocket, photon rocket).
- Combination of rocket engine and air-breathing engine (like ramjet, turbojet, or turbofan engines). Tomahawk surface-to-surface missile combines solid-propellant booster rocket for liftoff and a small turbojet for sustained flight.

11.3.2 Types of Missiles

- Cruise missile
- Ballistic missile

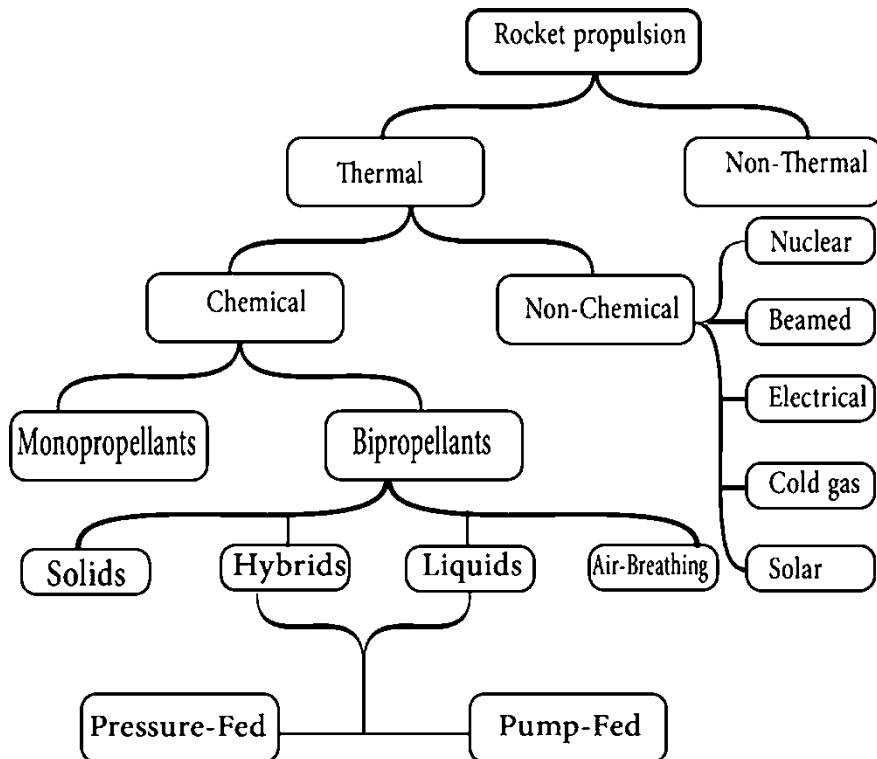


Fig. 11.4 Classification of rockets

11.3.3 Launch Mode

Launch mode can be defined as how and in which way the missile will be fired. The major types of rocket may be classified as the following five categories:

- Surface-to-surface missile SSM
- Surface-to-air missile SAM
- Air-to-surface missile ASM
- Air-to-air missile AAM
- Anti-tank missile ATM

Surface-to-surface missile (SSM) includes sea-to-sea missile, sea-to-surface (Coast) missile, and surface (Coast)-to-sea missile. Surface-to-air missile includes antiballistic missile (ABM).

11.3.4 Range

Range means how long a missile will fly and hit the target, distance. As per range, there are five types of missiles:

- Battlefield short range (up to 150 km)
- Short-range missile (150–799 km)
- Medium-range missile (800–2399 km)
- Intermediate-range ballistic missile (2400–5499 km)
- Intercontinental ballistic missile (over 5500 km)

11.3.5 Number of Stages

- Single-stage rockets
- Multistage rockets

11.3.6 Applications

Based on application, rockets are classified as:

- Space rockets
- Military rockets (missiles)
- Weather or sounding rockets
- Aircraft propulsion, turbo-rocket engines, and ramjet–rocket engines
- Booster rockets
- Sustainer rockets
- Retro-rockets

11.4 Rocket Performance Parameters

The main rocket performance parameters are:

- Thrust
- Specific impulse
- Total impulse
- Effective exhaust velocity
- Thrust coefficient
- Characteristic velocity

11.4.1 Thrust Force

The thrust force for an air-breathing engine was derived in Chap. 3 and expressed as

$$T = \dot{m}_e u_e - \dot{m}_a u + (P_e - P_a) A_e$$

Figure 11.5 illustrates the control volume selected in deriving the thrust equation for both air-breathing and non-air-breathing (rocket) engines.

The following *assumptions* are followed for analyzing the flow in an ideal rocket:

Steady flow of gases within rocket engine; thus mass flow rate through the whole rocket (\dot{m} = constant). All the species of the working fluid are gaseous. Any condensed phases (liquid or solid) in the nozzle flow have negligible volume. There is no heat transfer across the rocket walls; therefore, the flow is adiabatic.

For non-air-breathing engine, no inlet air is ingested into the engine; thus the inlet momentum term vanishes ($\dot{m}_a u = 0$). The thrust equation is reduced to the relation

$$T = \dot{m} u_e + (P_e - P_a) A_e \quad (11.1a)$$

The thrust force is independent of vehicle speed. It depends on the atmospheric pressure (P_a) as well as the exhaust parameters: mass flow rate (\dot{m}), speed (u_e), and pressure (P_e).

In the vacuum of space ($P_a = 0$), the thrust is expressed as

$$T = \dot{m} u_e + P_e A_e \quad (11.1b)$$

For a given design of nozzle, the value of exit pressure (P_e) is fixed. Thus, during flight through the atmosphere, the ambient pressure (P_a) decreases continuously. As a result, the thrust increases with altitude. However, beyond a certain altitude, the variation is negligible and the thrust is nearly constant as illustrated in Fig. 11.6.

11.4.2 Effective Exhaust Velocity (V_{eff})

The thrust force can be related to the effective velocity (as described earlier in Chap. 3).

With

$$T = \dot{m} u_e + (P_e - P_a) A_e = \dot{m} V_{\text{eff}}$$

Thus,

$$\frac{V_{\text{eff}}}{\dot{m}} = u_e + (P_e - P_a) A_e \quad (11.2a)$$

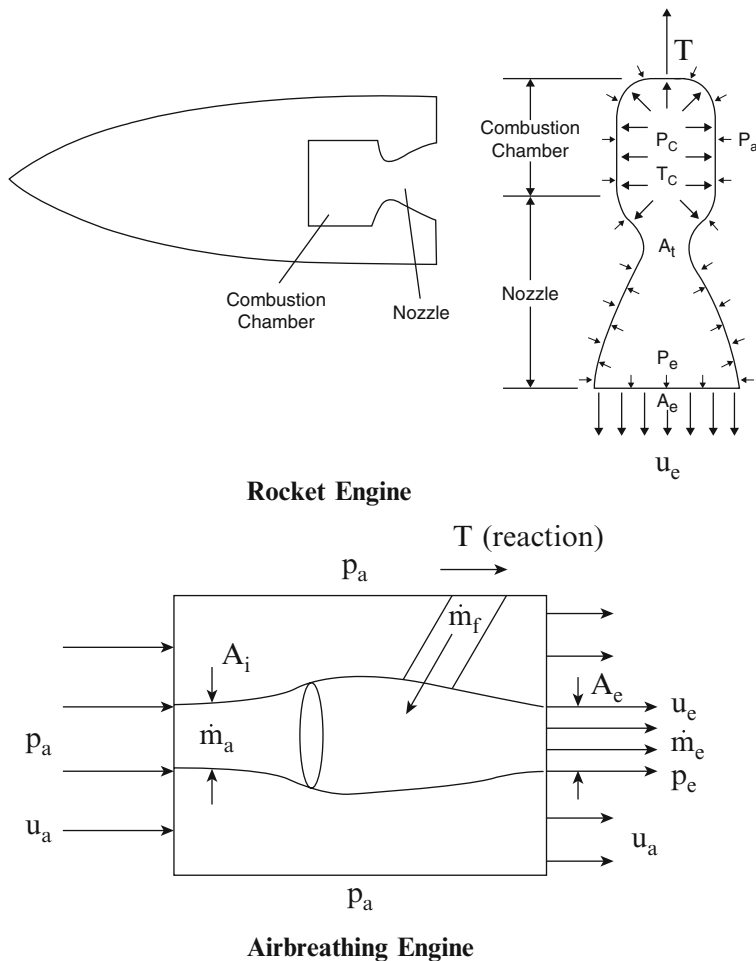


Fig. 11.5 Control volume for a rocket and air-breathing engines

The same equation was derived earlier for air-breathing engines.

The mass flow rate is expressed by $\dot{m} = \rho_e u_e A_e$:

$$V_{\text{eff}} = u_e \left[1 + \frac{(P_e - P_a)A_e}{u_e(\rho_e u_e A_e)} \right]$$

$$V_{\text{eff}} = u_e \left[1 + \frac{(P_e - P_a)A_e}{u_e(\rho_e u_e A_e)} \right]$$

$$V_{\text{eff}} = u_e \left[1 + \frac{P_e}{\rho_e u_e^2} \left(1 - \frac{P_a}{P_e} \right) \right]$$

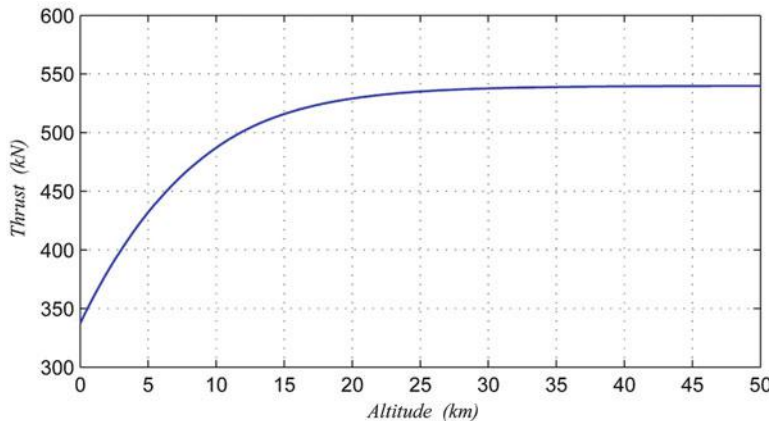


Fig. 11.6 Variation of thrust with altitude

$$\begin{aligned} V_{\text{eff}} &= u_e \left[1 + \frac{RT_e}{\gamma RT_e M_e^2} \left(1 - \frac{P_a}{P_e} \right) \right] \\ V_{\text{eff}} &= u_e \left[1 + \frac{1}{\gamma M_e^2} \left(1 - \frac{P_a}{P_e} \right) \right] \end{aligned} \quad (11.2b)$$

The effective velocity ($V_{\text{eff}} = u_e$) when ($P_e = P_a$). Generally in Eq. (11.2a),

$$\frac{(P_e - P_a)A_e}{\dot{m}} \ll u_e$$

Thus,

$$V_{\text{eff}} \cong u_e$$

Example 11.1 A rocket powered by a liquid-propellant rocket motor has the following data:

Thrust force of 450 kN at *sea level*

Propellant consumption rate = 150 kg/s

Gas exit static pressure = 70.0 kPa

Exhaust area = 0.5 m²

If the exhaust speed is kept constant, calculate the effective exhaust speeds and thrust force in the following cases:

1. Sea-level operation ($P_a = 101$ kPa).
2. At an altitude of 3 km, ambient pressure is ($P_a \sim 70$ kPa)
3. In space operation ($P_a = 0.0$ kPa)

Solution

The thrust force is

$$T = \dot{m} u_e + (P_e - P_a) A_e$$

$$u_e = \frac{T - (P_e - P_a) A_e}{\dot{m}}$$

Case (1)

Sea-level operation

$$u_e = \frac{450,000 - (70.0 - 101) \times 10^3 \times 0.5}{150} = 3103 \text{ m/s}$$

The effective exhaust speed

$$V_{\text{eff}} = u_e + \frac{(P_e - P_a) A_e}{\dot{m}} = 3103 + \frac{(70.0 - 101) \times 10^3 \times 0.5}{150} = 3000 \text{ m/s}$$

Case (2)

If the ambient pressure is equal to exhaust gas pressure of nozzle ($P_e = P_a$), then the thrust force

$$V_{\text{eff}} = u_e + \frac{(P_e - P_a) A_e}{\dot{m}} = u_e = 3103 \text{ m/s}$$

The thrust force is then

$$T = \dot{m} V_{\text{eff}} = 150 \times 3103 = 465,450 \text{ N} = 465.45 \text{ kN}$$

Case (3)

In space where $P_a = 0$, then the effective exhaust speed:

$$V_{\text{eff}} = u_e + \frac{P_e A_e}{\dot{m}} = 3103 + \frac{70 \times 10^3 \times 0.5}{150} = 3336.3 \text{ m/s}$$

The thrust force:

$$T = \dot{m} V_{\text{eff}} = 150 \times 3336.3 = 500,445 \text{ N} = 500.445 \text{ kN}$$

The above results are summarized in Table 11.1.

Table 11.1 Comparison between effective exhaust velocity and thrust at three altitudes

Altitude	Ambient pressure (kPa)	Effective exhaust velocity : $V_{\text{eff}} \left(\frac{\text{m}}{\text{s}} \right)$	Thrust T (kN)
Sea level	101	3000	450.00
3 km	~ 70 kPa	3103	465.45
Space	0	3336.3	500.45

Comments

In case (1), the nozzle is somewhat too long for sea-level conditions which is indicated by the fact that (P_e) is smaller than (P_a) . Thus a pressure “undershoot” and an exhaust velocity “overshoot” occurred. The “penalty” of incorrect nozzle length simply appears as the negative pressure thrust term. From Eq. (11.1), the difference in thrust between space and sea level resides in the term $(A_e P_a)$. Since the nozzle selected was too long at sea level, this thrust increase $(A_e P_a)$ during rocket ascent will be obtained in two steps. First, the *negative* thrust term $(P_e - P_a) A_e$ has to be reduced to zero (case (2)), when the rising vehicle reaches an altitude of 3 km having equal exit and ambient pressures ($P_e = P_a = 70$ kPa). This represents an ideal expansion in nozzle as described in Chaps. 2 and 8. Next, as the vehicle continues to ascend farther and eventually reaches “empty space” ($P_a = 0$) (case (3)), the pressure thrust will attain a positive value equal to $(P_e A_e)$. The combined effect of the two phases is simply the elimination of $(P_a A_e)$ provided the nozzle is filled at all times.

11.4.3 Exhaust Velocity (\mathbf{u}_e)

The propellants enter the combustion chamber, mix, and are ignited. The gas produced is heated by chemical energy released during combustion and expands through nozzle. Applying the first law of thermodynamics, the change in enthalpy of exhaust gases is equal to its kinetic energy. The temperature of gases in *combustion chamber* (T_c) will be equal to the total temperature of gases exhausting the nozzle ($T_c = T_{oe}$). The change in specific enthalpy is:

$$Cp(T_{0e} - T_e)$$

where (Cp) is the specific heat at constant pressure. The gain in kinetic energy of exhaust gases per unit mass is ($\frac{1}{2} u_e^2$). Equating both quantities, then

$$\begin{aligned} u_e^2 &= 2Cp(T_{oe} - T_e) \\ u_e &= \sqrt{2Cp(T_{oe} - T_e)} \end{aligned}$$

$$u_e = \sqrt{2CpT_{oe} \left(1 - \frac{T_e}{T_{oe}}\right)}$$

Assuming isentropic expansion, then $TP^{\frac{\gamma-1}{\gamma}}$ = constant. Moreover, the specific heat can be expressed as $Cp = \frac{\gamma}{\gamma-1}R = \frac{\gamma}{\gamma-1}\frac{\bar{R}}{M}$

where (R) is the gas constant, (\bar{R}) is the universal gas constant, and (M) is the molecular weight of the exhaust gases:

$$u_e = \sqrt{2\frac{\gamma R}{\gamma-1}T_{oe} \left[1 - \left(\frac{P_e}{P_{oe}}\right)^{\frac{\gamma-1}{\gamma}}\right]} \quad (11.3a)$$

or

$$u_e = \sqrt{2\frac{\gamma}{\gamma-1}\frac{\bar{R}}{M}T_{oe} \left[1 - \left(\frac{P_e}{P_{oe}}\right)^{\frac{\gamma-1}{\gamma}}\right]} \quad (11.3b)$$

The maximum exhaust speed occurs when ($P_e = 0$); thus

$$u_{e\max} = \sqrt{2\frac{\gamma R}{\gamma-1}T_{oe}} \equiv \sqrt{2\frac{\gamma R}{\gamma-1}T_c} \quad (11.3c)$$

From Eq. (11.3), the mass flow rate is then

$$\dot{m} = \rho_e u_e A_e = \rho_e A_e \sqrt{\frac{2\gamma R}{\gamma-1}T_{oe} \left[1 - \left(\frac{P_e}{P_{oe}}\right)^{\frac{\gamma-1}{\gamma}}\right]} \quad (11.4a)$$

$$\dot{m} = \rho_e u_e A_e = \rho_e A_e \sqrt{\frac{2\gamma}{\gamma-1}\frac{\bar{R}}{M}T_{oe} \left[1 - \left(\frac{P_e}{P_{oe}}\right)^{\frac{\gamma-1}{\gamma}}\right]} \quad (11.4b)$$

11.4.4 Important Nozzle Relations

Combustion chamber is frequently identified in rocket literature as thrust chamber. Gases leave chamber flows at nearly zero speed and then accelerated in a convergent-divergent nozzle. It reaches sonic speed at throat and keeps its accelerating motion to attain supersonic or even hypersonic speeds at its exit.

Though flow in nozzle was previously described, a brief review of its governing equations is reviewed here. The total temperatures and pressures in the combustion chamber and nozzle are equal ($T_c = T_{oe}$ and $P_c = P_{oe}$); then the temperature, pressure, and area at nozzle throat (Mach number is unity) are given by the relations:

$$\frac{T^*}{T_{oe}} = \frac{2}{\gamma + 1} \quad (11.5)$$

$$\frac{P^*}{P_{oe}} = \frac{1}{[(\gamma + 1)/2]^{\frac{\gamma}{\gamma-1}}} \quad (11.6)$$

$$A^* = \frac{\dot{m} \sqrt{RT^*/\gamma}}{P^*} \quad (11.7)$$

The nozzle throat diameter is given by

$$D^* = \sqrt{4A^*/\pi} \quad (11.8)$$

The mass flow rate is expressed as

$$\dot{m} = \rho^* u^* A^* = \rho_e u_e A_e \quad (11.9)$$

$$\frac{\dot{m} \sqrt{T_{oe}}}{A^* P_{oe}} = \sqrt{\frac{\gamma}{R} \left(\frac{2}{\gamma + 1} \right)^{\frac{\gamma+1}{2(\gamma-1)}}} \quad (11.10)$$

At exit, the static pressure, temperature, Mach number, and velocity are given by the relations:

$$\frac{P_e}{P_{0e}} = \left(\frac{1}{1 + \frac{\gamma-1}{2} M_e^2} \right)^{\frac{\gamma}{\gamma-1}} \quad (11.11)$$

$$\frac{T_e}{T_{0e}} = \frac{1}{1 + \frac{\gamma-1}{2} M_e^2} \quad (11.12)$$

$$M_e^2 = \left(\frac{\gamma + 1}{(P_e/P^*)^{\frac{\gamma-1}{\gamma}}} - 2 \right) \left(\frac{1}{\gamma - 1} \right) \quad (11.13a)$$

$$u_e = M_e \sqrt{\gamma R T_e} = \sqrt{\frac{2\gamma}{\gamma - 1} R T_{0e} \left(1 - \left(\frac{P_e}{P_{0e}} \right)^{\frac{\gamma-1}{\gamma}} \right)} \quad (11.13b)$$

$$u_{e\max} = \sqrt{\frac{2\gamma}{\gamma - 1} R T_{oe}} \quad (11.13c)$$

The density, exhaust area, and diameter at exit are then:

$$\rho_e = \frac{P_e}{RT_e} \quad (11.14)$$

$$A_e = \frac{\dot{m}}{\rho_e V_e} \quad (11.15a)$$

The exhaust diameter:

$$D_e = \sqrt{4A_e/\pi} \quad (11.15b)$$

The area ratio defined as the ratio between exit area and throat area is given by:

$$\frac{A_e}{A^*} = \frac{1}{M_e} \left(\frac{2}{\gamma + 1} + \frac{\gamma - 1}{\gamma + 1} M_e^2 \right)^{\frac{\gamma+1}{2(\gamma-1)}} \quad (11.16)$$

11.4.5 Characteristic Velocity (C^*)

Characteristic velocity is defined as:

$$C^* = \frac{P_{0e} A^*}{\dot{m}} = \frac{\sqrt{\gamma R T_{0e}}}{\gamma \left(\frac{2}{\gamma + 1} \right)^{\frac{\gamma+1}{2(\gamma-1)}}} \quad (11.17a)$$

11.4.6 Thrust Coefficient (C_F)

The thrust coefficient is defined as:

$$C_F = \frac{T}{P_{0e} A^*} \quad (11.18a)$$

Now from Eqs. (11.1a), (11.3a), and (11.10),
then:

$$C_F = \sqrt{\left(\frac{2\gamma^2}{\gamma - 1} \right) \left(\frac{2}{\gamma + 1} \right)^{\frac{\gamma+1}{\gamma-1}} \left[1 - \left(\frac{P_e}{P_{oe}} \right)^{\frac{\gamma-1}{\gamma}} \right]} + \left(\frac{P_e - P_a}{P_{oe}} \right) \frac{A_e}{A^*} \quad (11.18b)$$

A plot for *thrust coefficient versus the area ratio ($\frac{A_e}{A^*}$)* for different pressure ratio $\left(\frac{P_o}{P_{oe}}\right)$ and a constant specific heat $\gamma = 1.2$, is shown in Fig. 11.7.

The first term is the contribution of exit velocity, while the second term is the contribution of the exit pressure. For a perfect expansion of nozzle ($P_e = P_a$), the optimum thrust coefficient is then:

$$C_{F, \text{opt}} = \sqrt{\left(\frac{2\gamma^2}{\gamma - 1}\right) \left(\frac{2}{\gamma + 1}\right)^{\frac{\gamma+1}{\gamma-1}} \left[1 - \left(\frac{P_e}{P_{oe}}\right)^{\frac{\gamma-1}{\gamma}}\right]} \quad (11.18c)$$

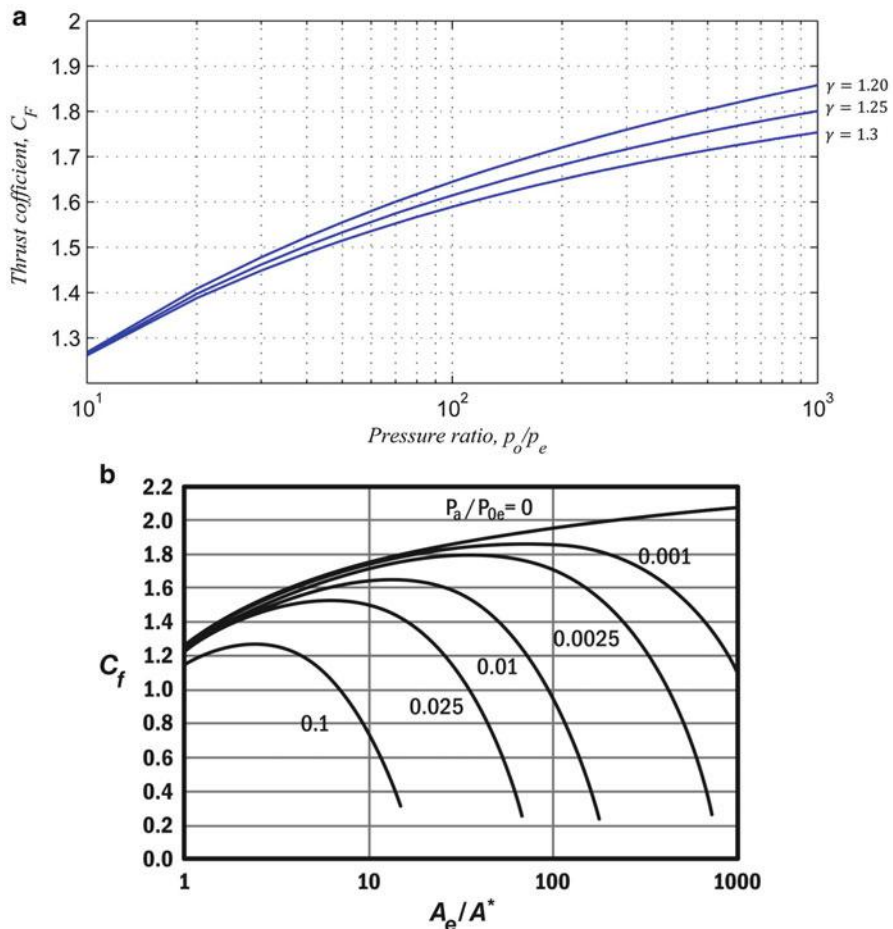


Fig. 11.7 Variation of thrust coefficient versus (a) pressure ratio and (b) area ratio ($\gamma = 1.2$)

Since the ideal thermal efficiency of a Brayton cycle operating between the two pressures P_e and P_{oe} is expressed as:

$$\eta_{th} = 1 - \left(\frac{P_e}{P_{oe}} \right)^{\frac{\gamma-1}{\gamma}}$$

For a very large total pressure (P_{oe}) and low exit pressure (P_e), then

$$\eta_{th} \cong 1 \text{ and} \\ C_{F, \text{ opt, Max}} = \sqrt{\left(\frac{2\gamma^2}{\gamma-1} \right) \left(\frac{2}{\gamma+1} \right)^{\frac{\gamma+1}{\gamma-1}}} \quad (11.18D)$$

11.4.7 Total Impulse (I_t)

Figure 11.8 depicts typical thrust-time profiles for the three cases of propellant burning. Neutral burning generates approximately a constant thrust profile, while the two cases of increasing and decreasing thrust profile are identified as progressive and regressive profiles, respectively.

Total impulse is the thrust force integrated over the burning time (t):

$$I_t = \int_0^t T dt \quad (11.24)$$

For a constant thrust and negligible start and stop transients, then:

$$I_t = Tt \quad (11.25)$$

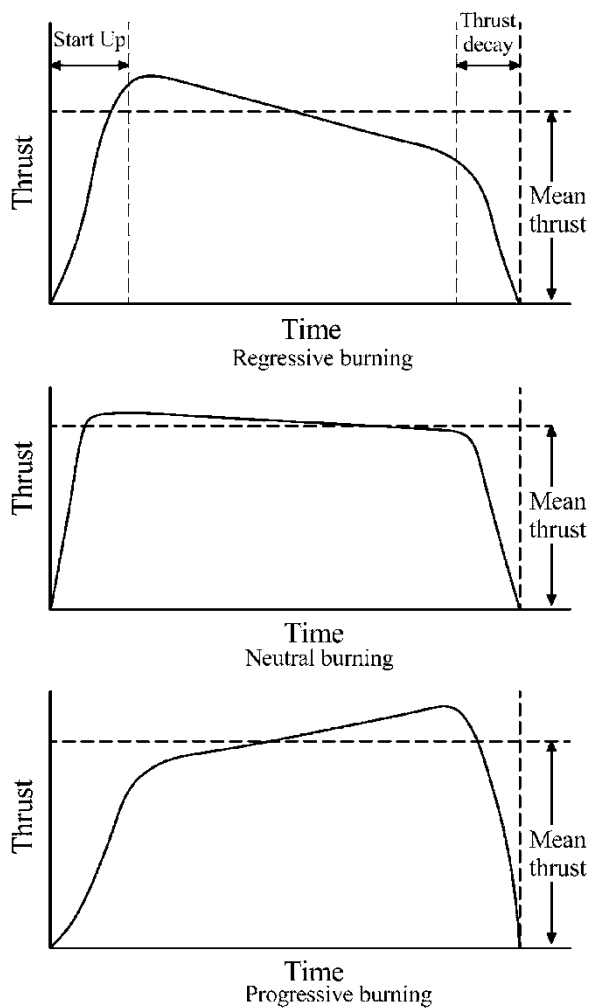
11.4.8 Specific Impulse (I_{sp})

$$I_{sp} = \frac{I_t}{g \int_0^t \dot{m} dt} = \frac{\int_0^t T dt}{g \int_0^t \dot{m} dt}$$

For a constant thrust and propellant mass flow rate, then

$$I_{sp} = \frac{I_t}{m_p g} = \frac{Tt}{\dot{m} t g} = \frac{T}{\dot{m} g} \quad (11.19)$$

Fig. 11.8 Typical thrust-time curves



where m_p = total propellant mass:

$$m_p = \dot{m} t$$

Now with

$$T = \dot{m} V_{\text{eff}}$$

then

$$I_{sp} = \frac{\dot{m} V_{\text{eff}}}{\dot{m} g} = \frac{V_{\text{eff}}}{g} \text{ (seconds)} \quad (11.20)$$

Table 11.2 Typical values of rocket engine properties

T_c (K)	P_c (MPa)	M (kmol/kg)	c^* ($\frac{\text{m}}{\text{s}}$)	A_e/A^*	γ	C_F	I_{sp} (s)
2000–4600	1–26	2–30	900–2500	15–280	1.1–1.6	1.3–2.9	150–480

Table 11.3 Thrust-time characteristics

Time (s)	0	0.5	1.0	2.0	2.5	3.0	3.25	3.3
Thrust (N)	6750	9000	7875	8100	8100	7650	8100	0

Back to the characteristic velocity (C^*), it can be expressed as

$$C^* = \frac{I_{sp} g}{C_F} \quad (11.17b)$$

Table 11.2 represents typical values of characteristic properties of rocket engines [4] and [8].

Example 11.2 Table 11.3 gives the following data for a rocket engine:

The total propellant mass $m_p = 13.2$ kg.

Determine the total impulse, specific impulse, the average thrust and effective speed, and propellant mass flow rate of the rocket motor.

Solution

Total impulse is the thrust force integrated over the burning time (t):

$$I_t = \int_0^t T dt$$

The total impulse is the area under the curve of thrust versus time. Since the thrust is given at discrete time intervals and not as a mathematical relation, total impulse is approximated by trapezoidal area. Total impulse is the sum of trapezoidal area.

The area of each trapezoid is calculated based on:

$$\text{Area} = \text{base} \times (\text{height 1} + \text{height 2})/2$$

Total impulse is then

$$\begin{aligned} I_t &= 0.5 \times [0.5 \times (6750 + 9000) + 0.5 \times (9000 + 7875) + 1.0 \times (7875 + 8100) \\ &\quad + 0.5 \times (8100 + 8100) + 0.5 \times (8100 + 7650) + 0.25 \times (7650 + 8100) \\ &\quad + 0.05 \times (8100 + 0)] \end{aligned}$$

$$\begin{aligned} I_t &= 0.5 \times (8,325 + 8,437.5 + 15,975 + 8100 + 7875 + 3937.5 + 405) \\ &= 26,100 \end{aligned}$$

$$I_t = 0.5 \times 53,055 = 26,527.5 \text{ N.s}$$

Note that accuracy of the calculation improves as the number of trapezoids used increases:

$$\text{Specific impulse : } I_{sp} = \frac{I_t}{m_p g} = \frac{26,527.5}{13.2 \times 9.8065} = 204.9 \text{ s}$$

$$\text{Average thrust : } T = \frac{I_t}{t} = \frac{26,527.5}{3.3} = 8,039 \text{ N}$$

$$\text{Effective speed : } V_{\text{eff}} = I_{sp} \times g = 204.9 \times 9.8065 = 2,009.7 \text{ m/s}$$

$$\text{Propellant mass flow rate : } \dot{m} = \frac{m_p}{t} = \frac{13.2}{3.3} = 4.0 \text{ kg/s}$$

Example 11.4 Calculate the specific thrust for the three cases discussed in Example (11.1).

Solution

Since the specific impulse is expressed as

$$I_{sp} = \frac{V_{\text{eff}}}{g}$$

Results are listed in Table 11.4.

Example 11.3 A rocket motor has a combustion chamber with temperature 3500 K and pressure 22 atmospheres. The throat area is 0.1 m^2 . The exit pressure is equal to atmospheric pressure at altitude of 20 km. Specific heat ratio $\gamma = 1.23$ and specific heat at constant pressure $C_p = 2520 \text{ J/kg/K}$. Calculate:

Exit velocity

Mass flow through the motor

Thrust force

Specific impulse

Solution

Ambient pressure at altitude 20 km is:

$$P_e = 5.475 \text{ kPa}$$

Table 11.4 Effective velocity and specific impulse at three altitudes

Altitude	Effective velocity V_{eff} ($\frac{\text{m}}{\text{s}}$)	Specific impulse I_{sp} (s)
Sea level	3000	305.9
3 km	3103	316.4
Space	3336.3	340.2

$$P_{oe} = 22 \times 101.325 = 2229.15 \text{ kPa}$$

With $\frac{\gamma-1}{\gamma} = \frac{0.23}{1.23} = 0.187$, then:

$$R = \frac{\gamma - 1}{\gamma} Cp = 0.187 \times 2520 = 471.2 \frac{\text{J}}{\text{kg.K}}$$

Exhaust velocity

$$u_e = \sqrt{2CpT_{oe} \left(1 - \left(\frac{P_e}{P_{oe}} \right)^{\frac{\gamma-1}{\gamma}} \right)} = \sqrt{2 \times 2520 \times 3500 \left(1 - \left(\frac{5.475}{2229.15} \right)^{0.187} \right)}$$

$$u_e = 3450.48 \frac{\text{m}}{\text{s}}$$

Here the effective speed \equiv equivalent speed = 3450.48 m/s.

Mass flow rate

$$\dot{m} = \rho_e u_e A_e$$

First evaluate the static temperature:

$$T_e = T_{oe} \left(\frac{P_e}{P_{oe}} \right)^{\frac{\gamma-1}{\gamma}} = 3500 \left(\frac{5.475}{2229.15} \right)^{0.187} = 1137.74 \text{ K}$$

$$\rho_e = \frac{5475}{471.24 \times 1137.74} = 0.0102 \text{ kg/m}^3$$

Exhaust Mach number: $M_e = \frac{u_e}{\sqrt{\gamma RT_e}} = \frac{3450.48}{\sqrt{1.23 \times 471.24 \times 1137.74}} = 4.2489$

Area ratio between throat and exhaust sections, Eq. (11.16), is

$$\frac{A_e}{A^*} = \frac{1}{M_e} \sqrt{\left[\left(\frac{2}{\gamma+1} \right) \left(1 + \frac{\gamma-1}{2} M_e^2 \right) \right]^{\frac{\gamma+1}{\gamma-1}}}$$

$$A_e = \frac{0.1}{4.2489} \sqrt{\left[\left(\frac{2}{2.23} \right) \left(1 + 0.115 \times (4.2489)^2 \right) \right]^{\frac{2.23}{0.23}}} \\ = 0.023535 \times (2.75885)^{4.848}$$

$$A_e = 3.22376 \text{ m}^2$$

$$\dot{m} = \rho_e u_e A_e = 0.0102 \times 3450.48 \times 3.22376 = 113.45 \text{ kg/s}$$

Thrust force

$$T = \dot{m} u_e + (P_e - P_a) A_e$$

Since $P_e = P_a$, then

$$T = \dot{m} u_e = 113.45 \times 3450.48 = 391491.1$$

$$T = 391.49 \text{ kN}$$

Specific impulse

$$I_{sp} = \frac{T}{\dot{m} g} = \frac{\dot{m} u_e}{\dot{m} g} = \frac{u_e}{g} = \frac{3450.48}{9.80665}$$

$$I_{sp} = 351.85 \text{ s}$$

11.4.9 Specific Propellant Consumption

Specific propellant consumption

$$SPC = \frac{1}{I_s} = \frac{\dot{m} g}{T} = \frac{\dot{w}}{T} = \frac{g}{V_{\text{eff}}} \text{ sec}^{-1} \quad (11.21)$$

11.4.10 Mass Ratio (MR)

Mass ratio is defined as the final mass (m_f) after rocket operation (or after propellants were consumed) divided by the initial mass (m_0) before rocket operation:

$$MR = \frac{m_f}{m_0} \quad (11.22)$$

11.4.11 Propellant Mass Fraction (ζ)

Propellant mass fraction (ζ) is the ratio of propellant mass (m_p) to the initial mass (m_0):

$$\zeta = \frac{m_p}{m_0} = \frac{m_0 - m_f}{m_0} = \frac{m_p}{m_p + m_f} \quad (11.23)$$

11.4.12 Impulse-to-Weight Ratio

$$\frac{I_t}{w_o} = \frac{I_{sp}t}{(m_f + m_p)g} = \frac{I_{sp}}{\left(\frac{g m_f}{t}\right) + \dot{m}g} \quad (11.24)$$

Example 11.4 Prove that

$$\zeta = 1 - MR$$

Solution

$$\begin{aligned} \zeta &= \frac{m_p}{m_o} = \frac{m_o - m_f}{m_o} = 1 - \frac{m_f}{m_o} = 1 - MR \\ \zeta &= 1 - MR \end{aligned}$$

11.4.13 Efficiencies

Though efficiencies are not commonly used in rocket design as in aircrafts, it is useful to understand energy conversion processes. Similar to air-breathing engines, rocket engines also have both internal and external efficiencies. Internal energy is normally identified as thermal efficiency, while external efficiency is also denoted as propulsive efficiency. The product of both also is identified as overall efficiency. For chemical rockets, energy stored in fuel is released via a specific chemical reaction process. This available energy depends in the combustion efficiency. However, a part of this energy is lost through heat dissipation from combustor. The remaining energy is now available to the nozzle, but, also, not all of which is convertible into kinetic energy.

The efficiency of converting this chemical energy into kinetic energy is identified as internal or thermal efficiency. This kinetic energy of the exhaust gases is employed in propelling the rocket. The efficiency of converting this kinetic energy into thrust power is identified as external or propulsive efficiency:

(A) Thermal efficiency (η_{th})

The maximum energy available per unit mass of chemical propellant is the heat of the combustion (Q_R). The power input to a chemical engine is

$$P_{\text{chem}} = \dot{m} Q_R$$

The actual power of combustion is obtained by multiplying the combustion efficiency (η_c) by the power input P_{chem} . Combustion efficiency is approximately 94–99 %.

Thermal (or internal) efficiency of a rocket propulsion system is an indication of the effectiveness of converting the chemical power input to the propulsion device into engine output power:

$$\text{Engine output power} = \text{Propulsion (or thrust) power} + \text{Power loss in exhaust gases}$$

$$\text{Thus, engine output power} = Tu + \frac{\dot{m}(V_{\text{eff}} - u)^2}{2} = \dot{m} V_{\text{eff}} u + \frac{\dot{m}(V_{\text{eff}} - u)^2}{2}$$

$$\text{Engine output power} = \dot{m} \times (V_{\text{eff}}^2 + u^2)/2$$

$$\begin{aligned} \eta_{\text{th}} \equiv \eta_{\text{int}} &= \frac{\text{Engine power output}}{\text{Available chemical power developed by combustion}} \\ \eta_{\text{th}} \equiv \eta_{\text{int}} &= \frac{Tu + \frac{\dot{m}(V_{\text{eff}} - u)^2}{2}}{\eta_c P_{\text{chem}}} = \frac{Tu + \frac{\dot{m}(V_{\text{eff}} - u)^2}{2}}{\eta_c \dot{m} Q_R} \\ \eta_{\text{th}} \equiv \eta_{\text{int}} &= \frac{\dot{m} \times (V_{\text{eff}}^2 + u^2)/2}{\eta_c \dot{m} Q_R} \end{aligned} \quad (11.25a)$$

Thus, the thermal efficiency is then expressed as

$$\eta_{\text{th}} \equiv \eta_{\text{int}} = \frac{(V_{\text{eff}}^2 + u^2)}{2\eta_c Q_R} \quad (11.25b)$$

(B) Propulsive efficiency (η_p)

For a rocket flying at a speed of (u) and gases exhaust speed (u_e), then the propulsive efficiency is expressed as in air-breathing engines:

$$\eta_p = \frac{\text{Propulsion (or thrust) power}}{\text{Engine output power}}$$

$$\text{Propulsion power} = Tu$$

$$\text{Engine output power} = \text{propulsion power} + \text{power lost in exhaust}$$

$$\eta_p = \frac{T u}{T u + \dot{m} (V_{\text{eff}} - u)^2 / 2} \quad (11.26a)$$

$$\eta_p = \frac{\dot{m} V_{\text{eff}} u}{\dot{m} V_{\text{eff}} u + \dot{m} (V_{\text{eff}} - u)^2 / 2}$$

$$\eta_p = \frac{V_{\text{eff}} u}{V_{\text{eff}} u + (V_{\text{eff}} - u)^2 / 2} = \frac{V_{\text{eff}} u}{\frac{1}{2} (V_{\text{eff}}^2 + u^2)}$$

$$\eta_p = \frac{2 V_{\text{eff}} u}{V_{\text{eff}}^2 + u^2} = \frac{2 \left(\frac{u}{V_{\text{eff}}} \right)}{1 + (u/V_{\text{eff}})^2}$$

$$\eta_p = \frac{2\sigma}{1 + \sigma^2} \quad (11.26b)$$

where $\sigma = \frac{u}{V_{\text{eff}}}$, the flight to effective jet velocity ratio.

The propulsive efficiency $\eta_p = 1$ (or 100%), when $u = V_{\text{eff}}$, or : $\sigma = 1$. Figure 11.9 illustrates the propulsive efficiency versus the velocity ratio (u/C).

The following striking remarks can be deduced from Fig. 11.9:

- (a) Propulsive efficiency can reach 100 % in rockets which is never attained in air-breathing engines.
- (b) Rockets can operate with exhaust speed less than the flight speed ($u/V_{\text{eff}} > 1.0$); on the contrary all air-breathing engines operate with flight speed less than exhaust speed ($u/V_{\text{eff}} < 1.0$), as propellant material in rocket is carried within its interior; thus, it has a zero initial speed, while air-breathing engine has finite air speed coming into its core and then next accelerated to a higher value within the exhaust nozzle.
- (c) Overall efficiency (η_0)

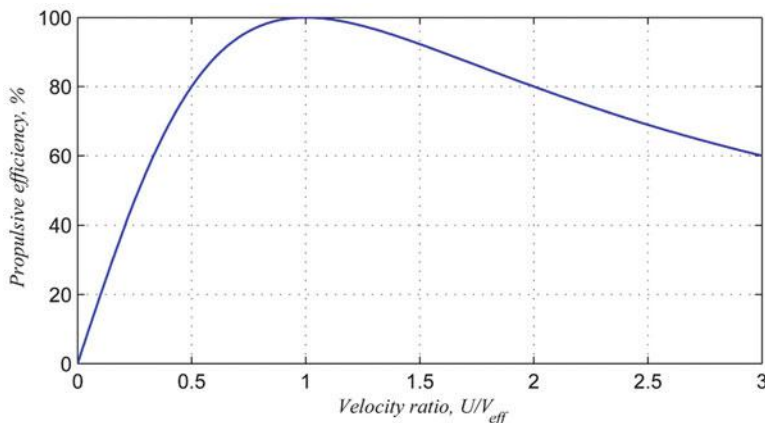


Fig. 11.9 Propulsive efficiency versus the velocity ratio (u/V_{eff})

$$\eta_0 = \frac{\text{ThrustPower}}{\text{Power developed by combustion}}$$

$$\eta_0 = \frac{T u}{\dot{m} Q_R} = \frac{\dot{m} V_{\text{eff}} u}{\dot{m} Q_R} = \frac{V_{\text{eff}} \times u}{Q_R} \quad (11.27a)$$

In general the overall efficiency is equal to the product of thermal and propulsive efficiencies or

$$\eta_0 = \eta_{th} \eta_p \quad (11.27b)$$

It is worth mentioning here that the overall efficiency can be also obtained by multiplying Eqs. (11.25a) and (11.26a).

11.5 The Rocket Equation

11.5.1 Single-Stage Rocket

The equation of motion of a rocket is derived here. Newton's second law of motion is used. The forces governing the motion of a rocket are thrust (T), drag (D), lift (L), and gravitational force (mg). Here (m) is the instantaneous rocket mass. First it is assumed that both thrust and drag are aligned in the flight direction. Flight direction is inclined an angle (θ) to the vertical direction (Fig. 11.10).

The forces acting on the rocket may be resolved in the flight direction to give

$$m \frac{du}{dt} = T - D - mg \cos \theta \quad (11.28)$$

The thrust force in the above equation can be either expressed as

$$T = \dot{m} V_{\text{eff}}$$

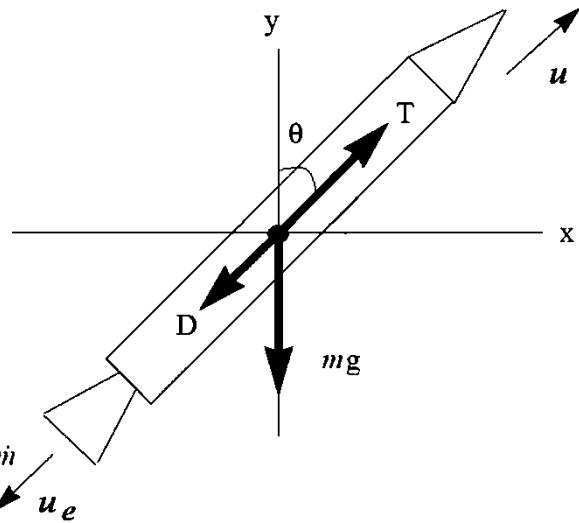
or $T = \dot{m} g I_{sp}$

Thus, from Eq. (11.28), $m \frac{du}{dt} = \dot{m} V_{\text{eff}} - D - mg \cos \theta$.

Noting that a large fraction (typically 90 %) of the mass of a rocket is propellant, thus it is important to consider the change in mass of the vehicle as it accelerates. Since the rate of mass flow through the nozzle is equal to the negative rate of change of rocket mass, thus

$$\dot{m} = -\frac{dm}{dt}$$

Fig. 11.10 Forces on rocket



$$m \frac{du}{dt} = -\frac{dm}{dt} V_{eff} - D - mg \cos \theta$$

$$du = -\left(\frac{dm}{m}\right) V_{eff} - \left(\frac{D}{m}\right) dt - g \cos \theta dt$$

Integrating the above equation over a period of time equal to the burning time (τ_b), to get the increment change in rocket velocity:

$$\frac{\Delta u}{V_{eff}} = \ln \frac{m_0}{m_0 - m_p} - \int_o^{\tau_b} \frac{D}{m V_{eff}} dt - \int_o^{\tau_b} \frac{g \cos \theta}{V_{eff}} dt \quad (11.29a)$$

$$\frac{\Delta u}{V_{eff}} = \ln \frac{1}{MR} - \int_o^{\tau_b} \frac{D}{m V_{eff}} dt - \int_o^{\tau_b} \frac{g \cos \theta}{V_{eff}} dt \quad (11.29b)$$

Here as mentioned previously, (m_0) is the rocket initial mass and (m_p) is the propellant burnt mass. Moreover, the first integral in the RHS is the drag loss, while the second integral is the gravity loss.

Consider the following simple cases:

(A) Negligible drag

$$\frac{\Delta u}{V_{eff}} = \ln \frac{1}{MR} - \int_o^{\tau_b} \frac{g \cos \theta}{V_{eff}} dt$$

Assuming also constant gravitational acceleration and ($\theta = 0$), then :

$$\Delta u = V_{eff} \ln \frac{m_0}{m_0 - m_p} - g \int_o^{\tau_b} dt = g I_{sp} \ln \frac{m_0}{m_0 - m_p} - gt$$

$$\Delta u = g \left(I_{sp} \ln \frac{m_0}{m_0 - m_p} - t \right) \quad (11.30a)$$

$$\Delta u = g \left(I_{sp} \ln \frac{1}{MR} - t \right) \quad (11.30b)$$

(B) *Negligible drag and gravity loss*

The increment change in rocket velocity is then:

$$\Delta u = V_{\text{eff}} \ln \frac{m_0}{m_0 - m_p} = V_{\text{eff}} \ln \frac{m_0}{m_f} \quad (11.31a)$$

Also it can be expressed as

$$\Delta u = g I_{sp} \ln \frac{m_0}{m_0 - m_p} \quad (11.31b)$$

Alternatively it may be expressed as

$$\Delta u = V_{\text{eff}} \ln \frac{1}{MR} \quad (11.32a)$$

or

$$\Delta u = g I_{sp} \ln \frac{1}{MR} \quad (11.32b)$$

Equations (11.31) and (11.32) are known as *Tsiolkovsky rocket equation*.

A plot of Tsiolkovsky for different effective speeds is shown in Fig. 11.11.

Another important parameter is the burn time. Since the final mass is related to original mass by the relation,

$$m_f = m_0 - m_p = m_0 - \dot{m} t$$

Then from Eq. (11.31a),

$$m_0 = m_f e^{\frac{\Delta u}{V_{\text{eff}}}} \quad (11.33)$$

Moreover,

$$m_0 = (m_0 - \dot{m} t) e^{\frac{\Delta u}{V_{\text{eff}}}}$$

Burning time is then

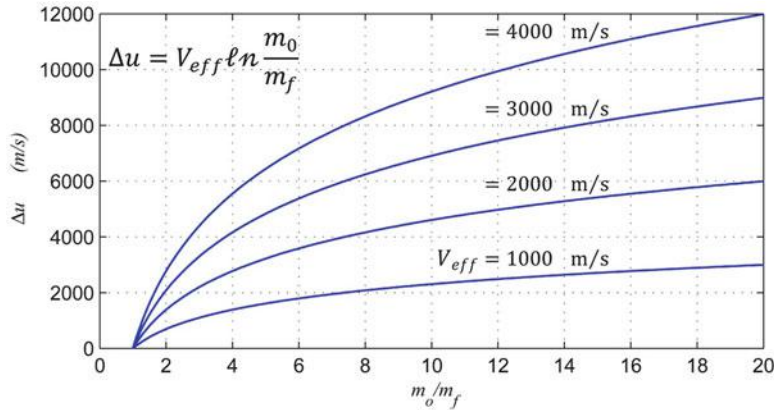


Fig. 11.11 Tsiolkovsky rocket equation

$$t = \frac{m_0}{\dot{m}} \left(1 - \frac{1}{e^{\frac{\Delta u}{V_{eff}}}} \right) \quad (11.34)$$

Introducing the payload ratio or fraction (λ) and structural (dead) weight ratio or structural fraction (δ),

$$\lambda = \frac{m_L}{m_0} \text{ and } \delta = \frac{m_s}{m_0}$$

where:

m_s is the structural mass of the rocket if single stage or (i_{th}) stage alone including the mass of its engine, controllers, and instrumentation as well as any residual propellant which is not expended by the end of the burn.

m_L : is the payload mass (which may be a satellite, space probe, or astronauts/cosmonauts).

Note that

$$m_0 = m_L + m_s + m_p$$

Divide by (m_0), to get:

$$1 = \lambda + \delta + \zeta \quad (11.35)$$

Thus,

$$\frac{m_0}{m_0 - m_p} = \frac{m_0}{m_d + m_L} = \frac{1}{\lambda + \delta} \quad (11.36)$$

Then from Eq. (11.31a),

$$\Delta u = V_{\text{eff}} \ln \frac{1}{\lambda + \delta} = g I_{sp} \ln \frac{1}{\lambda + \delta} \quad (11.37)$$

Example 11.5 A spacecraft's dry mass is 75,000 kg and the effective exhaust gas velocity of its main engine is 3100 m/s. How much propellant must be carried if the propulsion system is to produce a total (Δu) of 700 m/s?

Solution

Since

$$\Delta u = V_{\text{eff}} \ln \frac{m_0}{m_f}$$

$$m_0 = m_f e^{\frac{\Delta u}{V_{\text{eff}}}} = 75,000 \times e^{\frac{700}{3100}} = 94,000 \text{ kg}$$

The propellant mass is $m_p = m_0 - m_f = 94,000 - 75,000 = 19,000 \text{ kg}$.

11.5.2 Multistage Rockets

A multistage (or multistage) rocket is a [rocket](#) that uses two or more *stages*, each of which contains its own [engines](#) and [propellant](#) [9]. Thus we have two or more rockets stacked on top of or attached next to each other. Multistaging is used in space launch vehicles and long-range ballistic missiles. Two-stage rockets are quite common. However, rockets with as many as five separate stages have been successfully launched. An example is the Saturn V rocket which used three distinct stages in order to send its payload of astronauts and equipment toward the Moon.

Rocket staging has two types (Fig. 11.12):

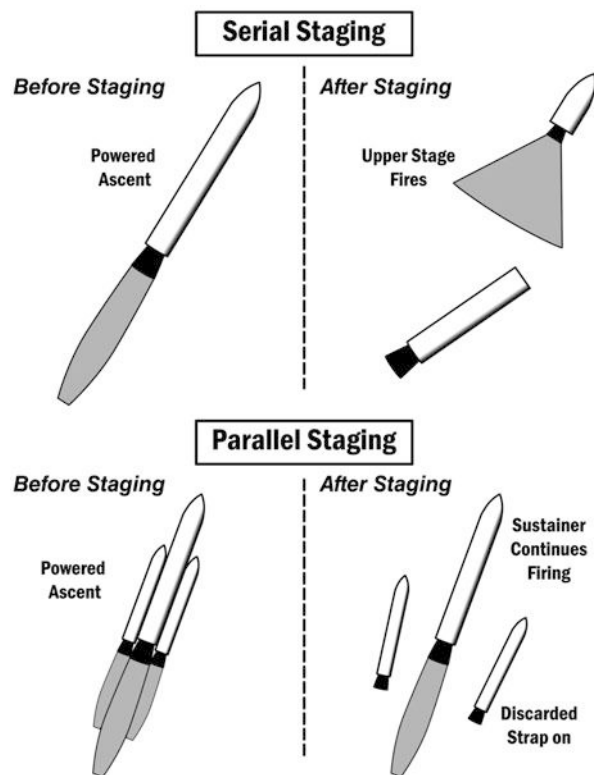
- Series
- Parallel

For serial staging (sometimes identified as tandem or vertical staging), the *first stage* is at the bottom and is usually the largest; the second stage and subsequent upper stages are above it, usually decreasing in size. The first-stage engines are every time electronically ignited. As this stage runs out of propellant, the upper retaining cap splits, sending hot gas onto the next stage, burning it, and throwing the lower stage back to the Earth. This leaves a smaller rocket, with the second stage on the bottom, which then fires. It operates at high altitude and thus under very minimal atmospheric pressure. This process is repeated until the final stage's motor burns to completion.

Both Saturn V and Explorer I are examples for series staging.

A popular method for producing a large first stage has been to cluster several rockets together to provide greater combined thrust without having to build a larger rocket. *Clustering* is the act of using two or more motors in a group (or cluster) and

Fig. 11.12 Serial and parallel staging of rockets



having them all ignite simultaneously, as opposed to *staging*, which ignites motors in succession (one after the other). The Saturn IC is an example of engine clusters fed from a single set of propellant tanks (Fig. 11.13).

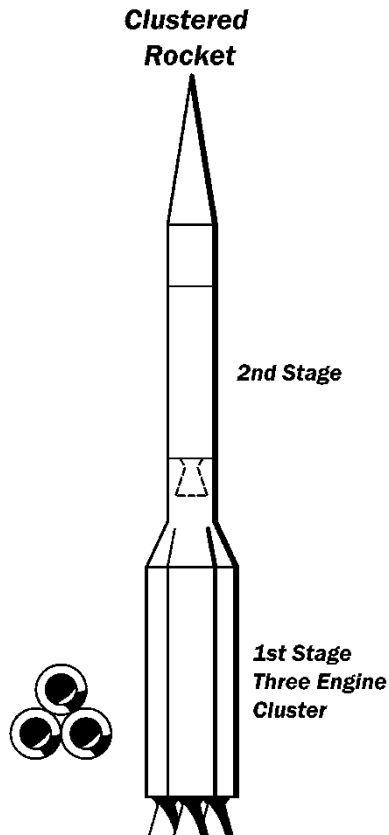
In parallel staging (Fig. 11.12) schemes, **solid** or **liquid** rocket boosters are used to assist with liftoff. These are sometimes referred to as “stage 0.” In the typical case, the first-stage and booster engines fire to propel the entire rocket upwards. When the boosters run out of fuel, they are detached from the rest of the rocket and fall away. The first stage then burns to completion and falls off. For example, the Atlas is parallel staged; it has two booster engines that are fired along with the central sustainer engine at launch.

11.5.3 Rocket Equation for a Series Multistage Rocket

If (*i*) refer to the *i*th of a total of (*N*) stages, then the total change in velocity is

$$\Delta u = \sum_{i=1}^N \Delta u_i = \sum_{i=1}^N (V_{\text{eff}})_i \times \ln\left(\frac{m_0}{m_f}\right)_i = \sum_{i=1}^N (V_{\text{eff}})_i \times \ln\left(\frac{1}{\text{MR}}\right)_i \quad (11.38a)$$

Fig. 11.13 Clustered rocket



$$\Delta u = \sum_{i=1}^N (V_{\text{eff}})_i \times \ln \frac{1}{\lambda_i + \delta_i} \quad (11.38b)$$

$$\Delta u = g \sum_{i=1}^N (I_{sp})_i \times \ln \left(\frac{m_0}{m_0 - m_p} \right)_i = g \sum_{i=1}^N (I_{sp})_i \times \ln \left(\frac{m_0}{m_f} \right)_i \quad (11.38c)$$

$$\Delta u = g \sum_{i=1}^N (I_{sp})_i \times \ln \frac{1}{\lambda_i + \delta_i} \quad (11.38d)$$

When the effective speed (V_{eff}) and mass ratios are the same for all the stages, this simplifies to

$$\Delta u = N \times V_{\text{eff}} \times \ln \left(\frac{1}{\text{MR}} \right) \quad (11.39)$$

Moreover, the payload of the i th stage is the sum of all the succeeding stages. Thus, the overall payload ratio (λ_0) is equal to the product of all payloads (λ_i). Thus,

$$\lambda_0 = \prod_{i=1}^N \lambda_i \quad (11.40)$$

11.5.4 Rocket Equation for a Parallel Multistage Rocket

For (k) stages, we have the *total thrust* as the sum of all engines:

$$T_t = \sum_{i=1}^K \dot{m}_i (V_{\text{eff}})_i$$

Total mass flow is $\dot{m}_t = \sum_{i=1}^k \dot{m}_i$.

Thrust force is then

$$T_t = \dot{m}_t (V_{\text{eff}})_{\text{ave}}$$

where $(V_{\text{eff}})_{\text{ave}}$ is the average exhaust speed and given by

$$(V_{\text{eff}})_{\text{ave}} = \frac{T_t}{\dot{m}_t} = \frac{\sum_{i=1}^K \dot{m}_i (V_{\text{eff}})_i}{\sum_{i=1}^k \dot{m}_i}$$

The rocket equation is then

$$\Delta u = (V_{\text{eff}})_{\text{ave}} \times \ln \left(\frac{m_0}{m_f} \right) \quad (11.41)$$

11.5.5 Advantages of Staging

For a multistage rockets and boosters once the fuel is exhausted, the space and structure which contained it and the motors themselves are dropped being no longer useful. Thus the rocket lightens itself. The thrust of next stages is able to provide more acceleration than if the earlier stage were still attached or a single, large rocket. Thus, rocket performance is improved by eliminating dead weights.

Each stage can use a different type of rocket motor that is appropriate for its particular operating conditions. Thus, the lower-stage motors are designed for use

at atmospheric pressure, while the upper stages can use motors suited to near-vacuum conditions. Lower stages tend to require more structure than the upper as they need to bear their own weight plus that of the stages above them; optimizing the structure of each stage decreases the weight of the total vehicle and provides further advantage.

The capability of the rocket to reduce thrust in mid-flight thus avoids severe acceleration for both men and instruments.

11.5.6 Disadvantages of Staging

Staging requires the vehicle to lift motors which are not yet being used; this means that the first stages must produce higher thrusts than they supposed to do.

Staging also makes the entire rocket more complex and harder to build.

In addition, each staging event is a significant point of failure during a launch, with the possibility of separation failure, ignition failure, and stage collision.

Example 11.6 A three-stage rocket is designed to place a small satellite into the low Earth orbit, having a payload weight of 200 kg (Fig. 11.14). Data for the rocket is given in Table 11.5 below. Calculate the increase in its speed (Δu).

Solution

Calculations will be done using the relation

$$\Delta u = g \sum_{i=1}^N (I_{sp})_i \times \ln\left(\frac{m_0}{m_0 - m_p}\right)_i$$

As seen from Table 11.5, most of the weight of the rocket is the weight of the propellants.

First stage:

Since the payload is carried atop the third stage into orbit, the total mass of the first stage is

$$m_{01} = m_{t1} + m_{t2} + m_{t3} + m_L$$

$$m_{01} = 14,000 + 4500 + 1000 + 200 = 19,700 \text{ kg}$$

$$m_{01} - m_{p1} = 19,700 - 12,800 = 6900 \text{ kg}$$

$$(I_{sp})_1 \times \ln\left(\frac{m_{01}}{m_{01} - m_{p1}}\right) = 285 \times \ln\left(\frac{19,700}{6900}\right) = 285 \times 1.049 = 299 \text{ s}$$

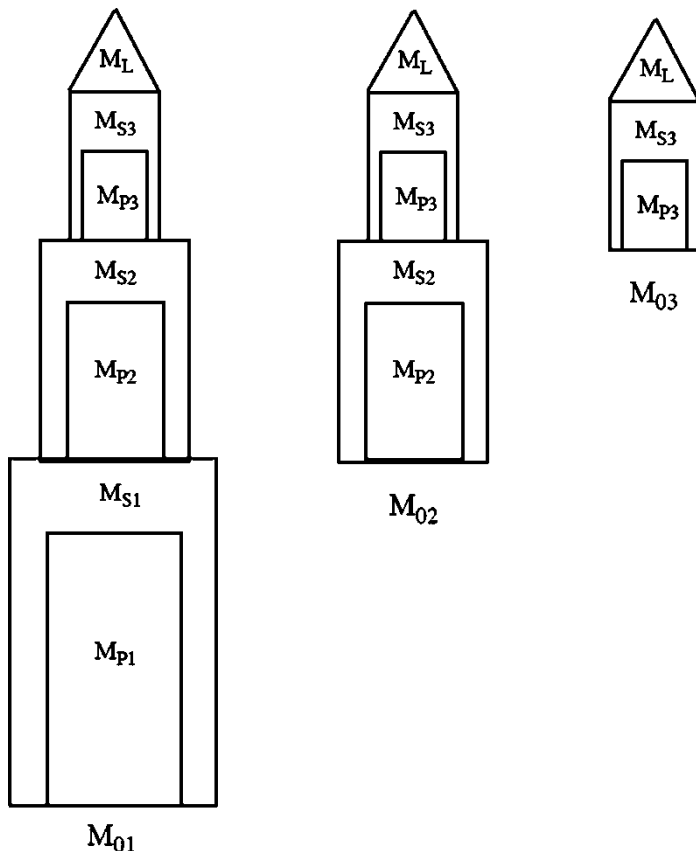


Fig. 11.14 Three multistage rockets

Table 11.5 Specific impulse, propellant and total mass of a three stage rocket

Stage number	Specific impulse (I_{sp}) second	Total mass kg	Propellant mass kg
1	230	14,000	12,800
2	250	4500	3700
3	250	1000	700

Second stage:

As the propellant of the first stage is burned off during [powered ascent](#), the near-empty tank and structure of the first stage are dropped off to reduce the weight of the vehicle to achieve [orbital velocity](#). Smaller amount of propellant is retained in the second- and third-stage tanks.

Thus

$$m_{02} = m_{t2} + m_{t3} + m_L$$

$$m_{02} = 4500 + 1000 + 200 = 5700 \text{ kg}$$

$$m_{02} - m_{p2} = 5700 - 3700 = 2000 \text{ kg}$$

$$(I_{sp})_2 \times \ln\left(\frac{m_{02}}{m_{02} - m_{p2}}\right) = 265 \times \ln\left(\frac{5700}{2000}\right) = 265 \times 1.0473 = 277.5 \text{ s}$$

Third stage:

The second stage is dropped off also; thus,

$$m_{03} = m_{t3} + m_L$$

$$m_{03} = 1000 + 200 = 1200 \text{ kg}$$

$$m_{03} - m_{p3} = 1,200 - 700 = 500 \text{ kg}$$

$$(I_{sp})_3 \times \ln\left(\frac{m_{03}}{m_{03} - m_{p3}}\right) = 290 \times \ln\left(\frac{1200}{500}\right) = 290 \times 0.875 = 253.8 \text{ s}$$

$$\Delta u = 9.81 \times (219 + 277.5 + 253.8) = 8152.8 \frac{\text{m}}{\text{s}} = 8.15 \text{ km/s}$$

Example 11.7 The shown figure illustrates European rocket *Ariane 5*, used to deliver payloads into the [geostationary transfer orbit](#) (GTO) or [low Earth orbit](#) (LEO). Initially at liftoff of an Ariane 5 launch vehicle, two P230 solid-propellant boosters plus the main Vulcain engine are ignited. The two different components of the launch vehicle have the following characteristics:



Engine	Vulcain (main engine)	Booster P230
Type	Liquid propellant	Solid propellant
Thrust (kN)	1114	6470
Specific impulse (second)	430	275

Calculate

1. Effective velocity for each engine
2. Exhaust mass flow rate
3. Average effective exhaust velocity
4. Average specific impulse

Solution

As described previously, Ariane 5 has two boosters (stage 0) employing solid-propellant engines and a liquid-propellant engine. Thus, the propulsion system here resembles parallel staging:

1. Effective velocity

$$I_{sp} = \frac{V_{\text{eff}}}{g}$$

$$V_{\text{eff}} = g I_{sp}$$

For the main engine (Vulcain),

$$(V_{\text{eff}})_{\text{Vulcain}} = 9.81 \times 430 = 4,218 \text{ m/s}$$

For Booster (P230),

$$(V_{\text{eff}})_{\text{P230}} = 9.81 \times 275 = 2,698 \text{ m/s}$$

2. Exhaust mass flow rate

$$\dot{m} = \frac{T}{V_{\text{eff}}}$$

For the main engine (Vulcain),

$$(\dot{m})_{\text{Vulcain}} = \frac{T}{V_{\text{eff}}} = 264 \text{ kg/s}$$

For Booster (P230),

$$(\dot{m})_{\text{P230}} = \frac{T}{V_{\text{eff}}} = 2398 \text{ kg/s}$$

3. Average effective exhaust velocity

$$(V_{\text{eff}})_{\text{ave}} = \frac{T_t}{\dot{m}_t} = \frac{(1,114 + 2 \times 6,470) \times 1000}{264 + 2 \times 2398} = 2777 \text{ m/s}$$

4. Average specific impulse

$$(I_{Sp})_{\text{ave}} = \frac{(V_{\text{eff}})_{\text{ave}}}{g} = 283 \text{ s}$$

11.6 Chemical Rocket Engines

11.6.1 Introduction

All types of rocket propulsion engines contain a chamber, an igniter, and a nozzle. Chemical rocket is unique in being a carrier to the whole energy source necessary for its acceleration.

The chemical reaction of propellant chemicals (usually a fuel and an oxidizer) takes place in the chamber and produces gases. The energy due to this high-pressure reaction permits the heating of the product gases to a very high temperature (2000–3500 °C). These hot gases subsequently are expanded in the convergent-divergent nozzle and accelerated to high velocities (2000–4500 m/s). The nozzle design, shape, and size are critical for the efficient function of the propulsion system.

Chemical rockets are either:

- Solid propellant
- Liquid propellant
- Hybrid propellant

11.6.2 Performance Characteristics

The engine's main components are composed of two elements, namely, a combustion chamber and a CD nozzle. Figure 11.15 illustrates these two modules as well as the corresponding processes on T-s diagram. Combustion process is assumed a heat addition process at constant pressure or with certain total pressure drop (ΔP_c). Flow in nozzle expansion is assumed an isentropic expansion or an adiabatic process with

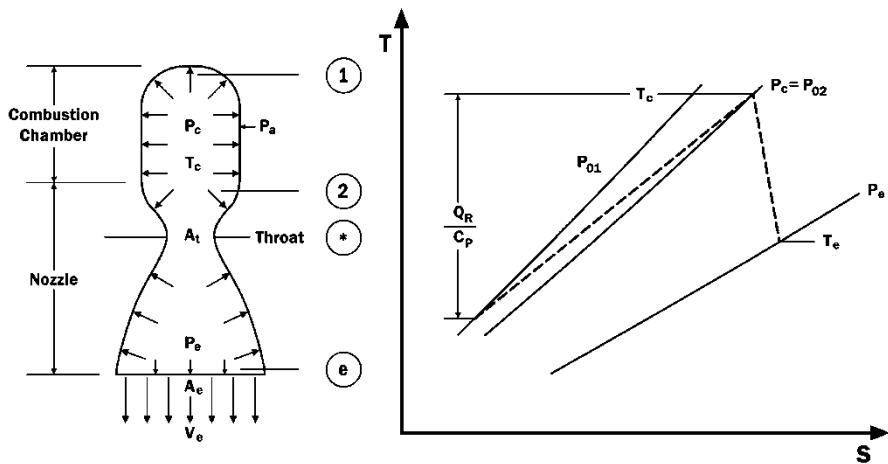


Fig. 11.15 Rocket engine

certain isentropic efficiency. Thus flow in both modules can be described as follows:

Combustion chamber:

$$\Delta P_c = P_{01} - P_c$$

where P_c ; is the combustion chamber or chamber total pressure. If $\Delta P_c = 0$, then: $P_{01} = P_c$.

Heat added:

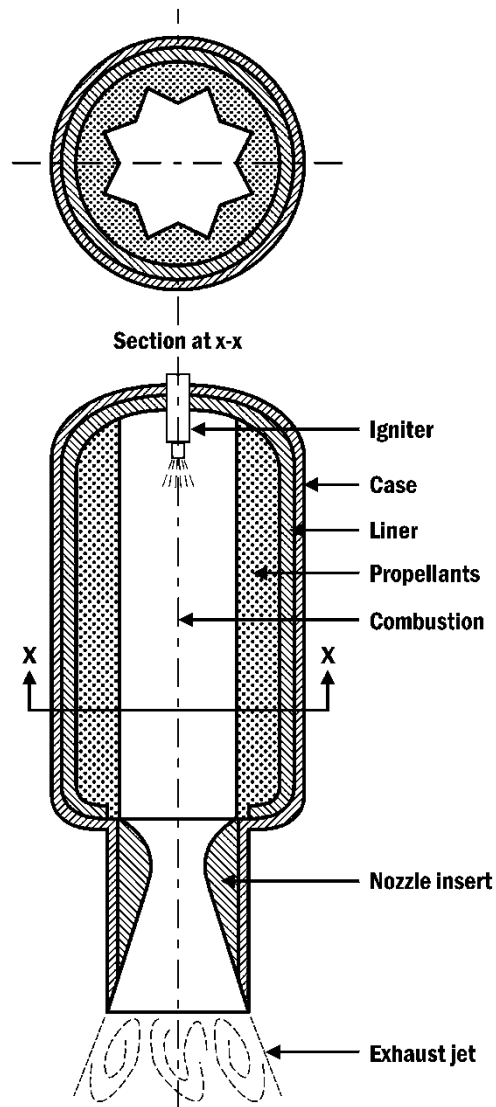
$$\dot{m}_p Q_R = \dot{m}_p C_p (T_{02} - T_{01}) \equiv \dot{m}_p C_p (T_c - T_{01})$$

11.7 Solid Propellant

11.7.1 Introduction

Solid-propellant rockets are the oldest type of rocket and date back to ancient China. They are relatively simple in construction as shown in Fig. 11.16. The term motor is used for solid rocket, while the term engine is used for liquid rocket. Solid rocket engines are used on air-to-air and air-to-ground missiles and on model rockets and as boosters for satellite launchers. A simple solid **rocket motor** consists of a casing, **propellant charge** (identified as grain), **igniter**, and **nozzle**. This grain contains both of the solid fuel and solid oxidizer components combined within a cylindrical combustion chamber or case. The propellant is casted into the rocket

Fig. 11.16 Typical solid-propellant rocket motor



shell having a central cavity of different shapes including star shaped that serves as combustion chamber (Fig. 11.16).

Thrust-burning time profile depends on this cavity. A liner provided between the case and the propellant protects the case from high temperatures developing inside the propellant layers.

An electrical signal is sent to the igniter which creates hot gases that ignite the main propellant grain. Once the flame front is established, combustion is self-sustaining. The rate of burning is proportional to the exposed surface area. As the

Table 11.6 Advantages and disadvantages of solid rocket engine

Advantages	Disadvantages
Compact and smaller in size compared with liquid rocket	Once ignited cannot be shut off
Do not require propellant feeding system or turbopumps as liquid rocket	Used only once
High thrust-to-weight ratio	
Require little maintenance	
Safe and reliable and thus can sit for years before firing	

propellant burns, a “flame front” is produced which moves into the propellant until all the propellant is burned. The hot exhaust gases produced in combustion are used to propel the rocket.

Solid propellant must have the following features:

1. High chemical energy to generate maximum thrust and specific impulse
2. High density to enable packing a large quantity of propellant in a small volume
3. Low molecular weight thus the exhaust gases achieve high acceleration
4. Easy to ignite
5. Burns steadily at predictive rate
6. Easy to fabricate
7. Smoke-free and nontoxic

Space Shuttle Solid Rocket Boosters (SRBs) are the largest solid-propellant motors ever flown and first designed for reuse. Each measures 12.17-ft diameter and 149.16-ft length. It generates 3,300,000 lb sea-level thrust. Its weight with propellant is 1,300,000 lb. Its propellant is ammonium perchlorate/aluminum and has 11 point star shape in forward motor segments and double truncated cone in aft segments. Burn time is 75 s and its expansion ratio is 11.3. After burnout at approximately 150,000 ft, the spent cases separate from the vehicle and arcing up to approximately 220,000 ft before parachuting to the ocean for recovery and reuse.

Table 11.6 presents advantages and disadvantages of solid rockets.

11.7.2 Composition of a Solid Propellant

There are basically *three types of propellant grains*, namely:

1. Homogeneous or colloidal propellants

Fuel and oxidizer are contained in the same molecule which decomposes during combustion. Typical examples are nitroglycerine (NG) and nitrocellulose (NC). Most propellants are double based (few single-based and triple-based propellants are found). Double-based propellants are combinations of nitroglycerine (NG) and nitrocellulose (NC), $[C_3H_5(NO_2)_3 - C_6H_7O_2(NO_2)_3]$, with small quantity of additives. It has nontoxic and smokeless exhausts.

2. Composite or heterogeneous propellants

These are mixtures of oxidizing crystals and a powered fuel (usually aluminum) held together in a binder (synthetic rubber or plastic). Sometimes light metal powders are added to increase the energy of the combustion process and fuel density. They are more stable than homogenous and preferred in long-term stored rockets. However, addition of light metals makes their exhaust toxic and smoky.

3. Composite modified double-based propellants

They are a heterogeneous combination of the double-based homogenous (colloidal) propellants and composite propellants.

11.7.3 Basic Definitions

Hereafter, some definitions are introduced here concerning grain:

1. *Cylindrical grain*: A grain in which the internal cross section is constant along the axis regardless of perforation shape.
2. *Perforation*: The central cavity port or flow passage of a propellant grain; its cross section may be cylindrical, tubular, rod, star shape, etc. (Fig. 11.17). All have a circular outer boundary due to rocket casing shape.
3. *End-burning* (or cigarette-burning) grain is the most common and is used.
4. *Neutral burning*: Motor burn time during which thrust, pressure, and burning surface area remain approximately constant, typically within about +15 % (Fig. 11.18).
5. *Progressive burning*: Burn time during which thrust, pressure, and burning surface area increase (Fig. 11.18).

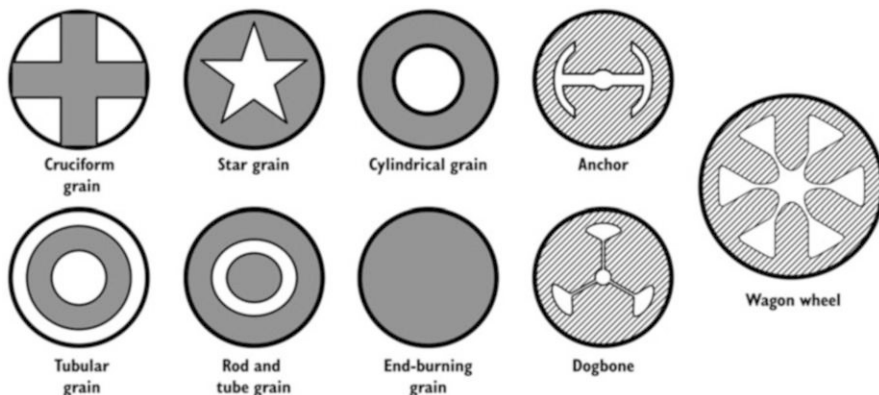


Fig. 11.17 Grains cross sections

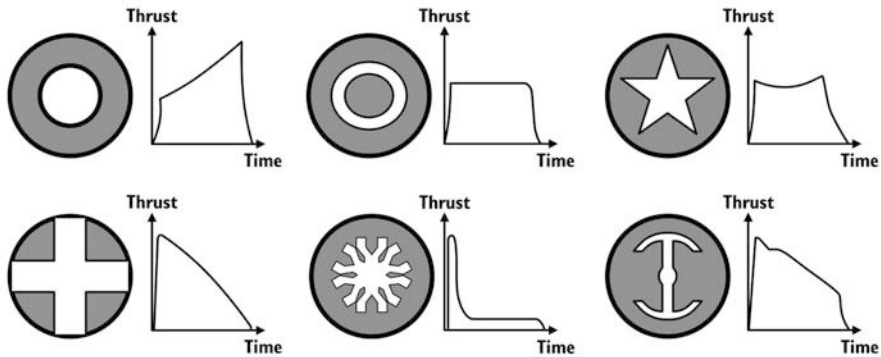


Fig. 11.18 Thrust profile for different grain cross sections

6. *Regressive burning*: Burn time during which thrust, pressure, and burning surface area decrease (Fig. 11.18).
7. *Stoichiometric mixture* of fuel and oxidizer is the correct proportions for complete combustion. Thus the fuel is identified as oxygen balanced. If the propellant contains insufficient oxygen for complete burning, it is called *under-oxidized*, and if it contains much oxygen, it is called *over-oxidized*.

Sliver: Unburned propellant remaining (or lost, that is, expelled through the nozzle) at the time of web.

11.7.4 Burning Rate

Burning rate in a full-scale motor depends on [9]:

1. Propellant composition
2. Combustion chamber pressure
3. Initial temperature of the solid propellant prior to start
4. Combustion gas temperature
5. Velocity of the gas flow parallel to the burning surface
6. Motor motion (acceleration and spin-induced grain stress)

The burning rate r for a solid propellant is:

Burning rate is defined as the recession of the propellant surface in a direction perpendicular to this burning surface per unit time. At any given initial temperature, the empirical relationship between pressure and burning rate known as *Vielle's law* may be written as

$$\dot{r} = aP_c^n \quad (11.42a)$$

where:

(\dot{r}) = the burn rate, usually given in millimeter per second

(P_c) = the chamber pressure given in MPa

(n) = the burning rate pressure exponent or combustion index, which is independent of initial grain temperature and describes effect of chamber pressure on the burning rate

(a) = an empirical constant influenced by the initial propellant temperature prior to ignition (T_p). Also it is known as the temperature coefficient which is dimensional quantity. It is expressed by the relation

$$a = \frac{A}{T_1 - T_p} \quad (11.43)$$

where both of (A) and (T_1) are empirical constants.

Thus

$$\dot{r} = \frac{A}{T_1 - T_p} P_c^n \quad (11.42b)$$

Here, some features of the exponent (n) [9]:

- For stable operation, (n) has values greater than 0 and less than 1.0.
- Most propellants have $(n = 0.2\text{--}0.6)$.
- If $n = 0$, no change in burning rate over a wide pressure range.
- When the (n) value is low and comes closer to zero, burning can become unstable and may even extinguish itself.
- As (n) approaches 1, burning rate and chamber pressure become very sensitive to one another, and disastrous rises in chamber pressure can occur in a few milliseconds.
- Some propellants display a negative (n) which is important for “restartable” motors, burning rate, and chamber pressure.

The mass flow rate of gas generation from the motor, refer to Fig. 11.19, is

$$\dot{m}_g = \rho_p A_b \dot{r} \quad (11.44)$$

where:

ρ_p = solid-propellant density

A_b = area of the burning surface

\dot{r} = burn rate or surface regression speed

\dot{m}_g = rate of gas generation at the propellant surface

The total burned mass of propellant (m_g) can be determined by integrating Eq. (11.43):

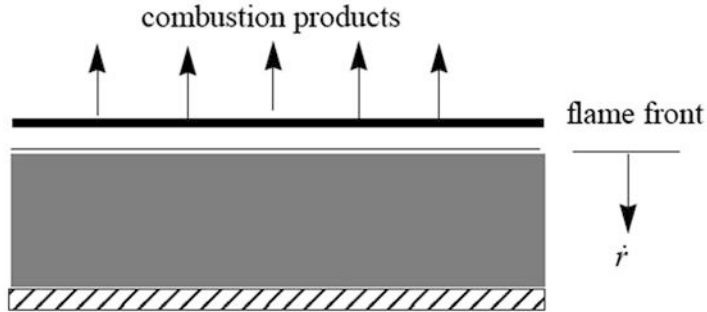


Fig. 11.19 Surface regression and gas generation

$$\dot{m}_g = \int \dot{m}_g dt = \rho_p \int A_b \dot{r} dt \quad (11.45)$$

From the principle of conservation of matter, the rate of propellant mass flow is to equal the rate of mass flow through the exhaust nozzle. Then from Eq. (11.45), with $P_c = P_{0e}$ and

$T_c = T_{0e}$ then

$$C^* = \frac{P_c A^*}{\dot{m}} = \sqrt{\frac{RT_c}{\gamma \left(\frac{2}{\gamma+1}\right)^{\frac{\gamma+1}{\gamma-1}}}} \quad (11.22a)$$

$$\dot{m}_g \equiv \rho_p A_b \dot{r} = \dot{m} = \frac{A^* P_c}{C^*} = A^* P_c \sqrt{\frac{\gamma}{RT_c} \left(\frac{2}{\gamma+1}\right)^{\frac{\gamma+1}{\gamma-1}}} \quad (11.46)$$

$$P_c = \frac{\rho_p A_b \dot{r} C^*}{A^*} = \rho_p C^* a P_c^n \frac{A_b}{A^*}$$

The pressure of combustion chamber is then

$$P_c = \left[\rho_p C^* a \left(\frac{A_b}{A^*} \right) \right]^{\frac{1}{1-n}} \quad (11.47)$$

The ratio between the burnt area and throat area is

$$\frac{A_b}{A^*} = \frac{P_c}{\rho_p \dot{r}} \sqrt{\frac{\gamma}{RT_c} \left(\frac{2}{\gamma+1}\right)^{\frac{\gamma+1}{\gamma-1}}} \quad (11.48a)$$

Since $P_c \equiv P_{0e}$, then from Eq. (11.40),

$$\frac{A_b}{A^*} = \frac{P_c^{(1-n)}}{\rho_p a} \sqrt{\frac{\gamma}{RT_c}} \left(\frac{2}{\gamma+1} \right)^{\frac{\gamma+1}{\gamma-1}} \quad (11.48b)$$

Example 11.8 The grain in such solid propellant is a hollow cylinder having a length (L), an inner radius (d), and an outer radius (D). Prove that for a combined end and radial burning of a solid-propellant rocket; prove that the rate of change of combustion pressure (P_c) is expressed by both of the equations:

$$\frac{dP_c}{dt} = \left(\frac{8P_c}{1-n} \right) \left(\frac{\dot{r}}{D} \right) \left(\frac{\left(\frac{L}{D} - \frac{d}{D} \right)}{4 \left(\frac{d}{D} \right) \left(\frac{L}{D} \right) + 1 - \left(\frac{d}{D} \right)^2} \right)$$

and

$$\frac{dP_c}{dt} = \left(\frac{8P_c^{n+1}}{1-n} \right) \left(\frac{a}{D} \right) \left(\frac{\left(\frac{L}{D} - \frac{d}{D} \right)}{4 \left(\frac{d}{D} \right) \left(\frac{L}{D} \right) + 1 - \left(\frac{d}{D} \right)^2} \right)$$

With $\dot{r} = aP_c^n$ as the burning rate, evaluate this rate in the following case:

$$\dot{r} = 10P_c^{0.6} \text{ (mm/s)}, P_c = 7.0 \text{ MPa}, \frac{L}{D} = 10, \frac{d}{D} = 0.4 \text{ and } L = 1.8 \text{ m}$$

Solution

For radial burning $A_b = \pi dL$.

$$\text{For end burning } A_b = \frac{\pi}{4} (D^2 - d^2).$$

For a combined radial and end burning, then

$$\begin{aligned} A_b &= \pi dL + \frac{\pi}{4} (D^2 - d^2) \\ \frac{dA_b}{dt} &= \pi L \frac{d(d)}{dt} + \pi d \frac{dL}{dt} + \frac{\pi}{4} \left[-2d \frac{d(d)}{dt} \right] \end{aligned} \quad (\text{a})$$

Due to the regression in the radial direction,

$$\frac{d(d)}{dt} = 2\dot{r}$$

Also, due to the regression in the axial direction,

$$\begin{aligned} \frac{dL}{dt} &= -\dot{r} \\ \frac{dA_b}{dt} &= \pi L (2\dot{r}) + \pi d (-\dot{r}) + \frac{\pi}{4} \left[-2d (2\dot{r}) \right] = 2\pi \dot{r} (L - d) \end{aligned}$$

$$\begin{aligned}\frac{1}{A_b} \frac{dA_b}{dt} &= \frac{2\pi \dot{r} (L - d)}{\pi d L + \frac{\pi}{4} (D^2 - d^2)} = \frac{8\dot{r}(L-d)}{4dL+D^2-d^2} \\ \frac{1}{A_b} \frac{dA_b}{dt} &= \frac{8\dot{r}(L-d)}{4dL+D^2-d^2} = \frac{8\dot{r}\left(\frac{L}{D}-\frac{d}{D}\right)}{4\left(\frac{d}{D}\right)\left(\frac{L}{D}\right)+1-\left(\frac{d}{D}\right)^2}\end{aligned}\quad (\text{b})$$

Since the combustion pressure is expressed by

$$P_c = \left(\frac{A_b}{A^*} \frac{a\rho_p}{\sqrt{\frac{\gamma}{RT_c} \left(\frac{2}{\gamma+1} \right)^{\frac{\gamma+1}{\gamma-1}}}} \right)^{\frac{1}{1-n}}$$

differentiating w.r.t. time, then

$$\frac{dP_c}{dt} = \frac{P_c}{1-n} \frac{1}{A_b} \frac{dA_b}{dt} \quad (\text{c})$$

From Eqs. (b) and (c), then

$$\frac{dP_c}{dt} = \left(\frac{8P_c}{1-n} \right) \left(\frac{\dot{r}}{D} \right) \left(\frac{\left(\frac{L}{D} - \frac{d}{D} \right)}{4\left(\frac{d}{D}\right)\left(\frac{L}{D}\right)+1-\left(\frac{d}{D}\right)^2} \right)$$

Substituting for (\dot{r}), then

$$\frac{dP_c}{dt} = \left(\frac{8P_c^{n+1}}{1-n} \right) \left(\frac{a}{D} \right) \left(\frac{\left(\frac{L}{D} - \frac{d}{D} \right)}{4\left(\frac{d}{D}\right)\left(\frac{L}{D}\right)+1-\left(\frac{d}{D}\right)^2} \right)$$

Now from the relation

$$\frac{dP_c}{dt} = \left(\frac{8 \times 7^{1.6}}{1-0.6} \right) \left(\frac{10 \times 10^{-3}}{1.8} \right) \left(\frac{10 - 0.4}{4(0.4)(10) + 1 - (0.4)^2} \right) = 1.4247 \text{ MPa/s}$$

This time rate of change for pressure of combustion chamber represents a *progressive-type* burning.

Example 11.9 A solid-propellant rocket has the following data:

Combustion chamber temperature = Combustion chamber pressure =

2600 K, 18 MPa

Propellant density = 1600 kg/m³, Grain diameter = 10 mm

Exhaust gas constant $R = 400 \text{ J/(kg.K)}$, Gas-specific heat ratio $\gamma = 1.2$

Vielle's law constants $a = 4.0$, $n = 0.6$, Burn time = 12 s

Exit pressure = 100 kPa

Calculate

- The nozzle throat diameter
- Characteristic velocity
- Optimal thrust coefficient
- Thrust force
- The mass flow rate and total burnt mass of the propellant
- The specific impulse
- The total impulse

Solution

- (a) From Eq. (11.47)

$$\frac{A_b}{A^*} = \frac{P_c^{(1-n)}}{\rho_p a} \sqrt{\frac{\gamma}{RT_c}} \left(\frac{2}{\gamma + 1} \right)^{\frac{\gamma+1}{\gamma-1}}$$

$$\frac{A_b}{A^*} = \frac{18^{0.4}}{1600 \times 4} \sqrt{\frac{1.2}{400 \times 2600}} \left(\frac{2}{2.2} \right)^{\frac{2.2}{0.2}} = 6.735 \times 10^{-4}$$

$$\frac{d^*}{d_b} = 38.5$$

Throat diameter = 0.385 m and throat area $A^* = 0.1164 \text{ m}^2$.

- (b) The characteristic velocity

$$C^* = \sqrt{\frac{RT_c}{\gamma \left(\frac{2}{\gamma+1} \right)^{\frac{\gamma+1}{\gamma-1}}}} = \sqrt{\frac{400 \times 2600}{1.2 \times \left(\frac{2}{2.2} \right)^{\frac{2.2}{0.2}}}} = 1,723 \text{ m/s}$$

- (c) Optimal thrust coefficient

From Eq. (11.18c)

$$C_{F, opt} = \sqrt{\left(\frac{2\gamma^2}{\gamma - 1} \right) \left(\frac{2}{\gamma + 1} \right)^{\frac{\gamma+1}{\gamma-1}} \left[1 - \left(\frac{P_e}{P_{oe}} \right)^{\frac{\gamma-1}{\gamma}} \right]}$$

$$C_{F,\text{opt}} = \sqrt{\frac{2 \times 1.2^2}{0.2} \times \left(\frac{2}{2.2}\right)^{11} \times \left[1 - \left(\frac{100}{18,000}\right)^{\frac{0.2}{1.2}}\right]} = 1.71$$

(d) The thrust force

$$T = C_{F,\text{opt}} P_c A^* = 1.71 \times 18 \times 10^6 \times 0.1164 = 3.58 \times 10^6 \text{ N}$$

$$T = 3580 \text{ kN}$$

(e) The mass flow rate of the exhaust gases is calculated from Eq. (11.15) as

$$\dot{m} = \frac{A^* P_c}{\sqrt{T_c}} \sqrt{\gamma} \left(\frac{2}{\gamma + 1} \right)^{\frac{\gamma+1}{2(\gamma-1)}} \\ = \frac{0.1164 \times 18 \times 10^6}{\sqrt{2600}} \times \sqrt{\frac{1.2}{400}} \times \left(\frac{2}{2.2} \right)^{\frac{2.2}{0.4}} = 1332.4 \text{ kg/s}$$

The total burnt mass of propellant is

$$m = \dot{m} \times t_b = 15,989 \text{ kg}$$

(f) The specific impulse

$$I_{sp} = \frac{T}{\dot{m} g} = \frac{3.58 \times 10^6}{1332.4 \times 9.81} = 274 \text{ s}$$

(g) The total impulse

$$I_t = \bar{T} t_b$$

where \bar{T} is the average thrust over the burning duration. Assuming $\bar{T} = 3.58 \times 10^6 \text{ N}$, then

the total impulse will be

$$I_t = 3.58 \times 10^6 \times 12 = 4.296 \times 10^7 \text{ N.s}$$

Example 11.10 If the solid-propellant rocket in example (11.17) has a reduced combustion chamber pressure = 9 MPa, but maintaining the same combustion chamber temperature = 2600 K, what would be the new burning time?

Solution

Since the propellant mass flow rate depends on combustion chamber pressure, then

$$\dot{m} \sim P_c$$

Moreover, the total burnt mass of propellant is defined by

$$m = \dot{m} \times t_b$$

$$t_b \sim \frac{1}{P_c}$$

or

$$\frac{t_{b2}}{t_{b1}} = \frac{P_{c1}}{P_{c2}}$$

Burning time is then

$$t_{b2} = \frac{12 \times 18}{9} = 24 \text{ s}$$

A plot for pressure variation versus burning time for the two cases of combustion chamber pressure is illustrated in Fig. 11.20.

Example 11.11 Tests of solid-propellant grain showed the following results:

Test number	Chamber pressure P_c (MPa)	Burn rate (mm/s)
1	18	23.8
2	8	12.5

Calculate

- (a) The combustion pressure if the burning rate is 20 mm/s
- (b) The propellant consumption rate per square meter of burning surface if the combustion pressure is 15 MPa, the density of propellant $\rho_p = 1700 \text{ kg/m}^3$, and the grain diameter is 0.2 m

Solution

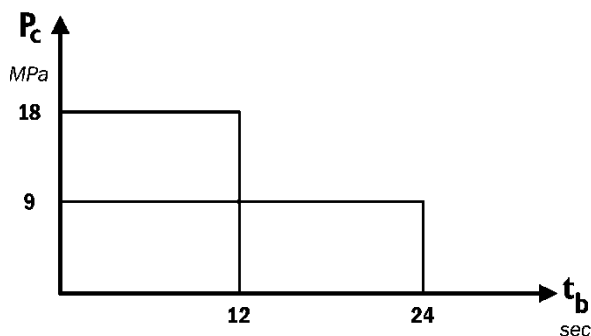
- (a) Since the burning rate is expressed by the relation

$$\dot{r} = aP_c^n$$

then,

$$\begin{aligned} \frac{\dot{r}_1}{\dot{r}_2} &= \left(\frac{P_{c1}}{P_{c2}} \right)^n \\ \ln \left(\frac{\dot{r}_1}{\dot{r}_2} \right) &= n \ln \left(\frac{P_{c1}}{P_{c2}} \right) \end{aligned}$$

Fig. 11.20 Variation of combustion pressure versus burning time



$$n = \frac{\ln\left(\frac{P_{c1}}{P_{c2}}\right)}{\ln\left(\frac{\dot{r}_1}{\dot{r}_2}\right)} = \frac{\ln\left(\frac{18}{9}\right)}{\ln\left(\frac{23.8}{12.5}\right)} = \frac{0.9109}{0.6439} = 1.415$$

Moreover,

$$\alpha = \frac{\dot{r}}{P_c^n} = \frac{12.5}{(8)^{1.415}} = 0.66$$

Now the combustion chamber or a burning rate of 20 mm is

$$P_c = \left(\frac{\dot{r}}{\alpha}\right)^{\frac{1}{n}} = \left(\frac{20}{0.66}\right)^{\frac{1}{1.415}} = 11.143 \text{ MPa}$$

- (b) For a grain diameter of 0.2 m, the mass flow rate of propellant is given by Eq. (11.43) as

$$\dot{m}_g = \rho_p A_b \dot{r}$$

Then, the propellant consumption rate per square meter of burning surface is

$$\frac{\dot{m}_g}{A_b} = \rho_p \dot{r} = 1700 \times 20 \times 10^{-3} = 34.0 \frac{\text{kg}}{\text{s}/\text{m}^2}$$

11.7.5 Characteristics of Some Solid Propellants

Table 11.7 lists some important characteristics of solid propellants [9].

Symbols:

Al, aluminum

PBAA, polybutadiene–acrylic acid polymer

AP, ammonium perchlorate

PBAN, polybutadiene–acrylic acid–acrylonitrile terpolymer

Table 11.7 Typical properties of liquid propellant engine

Propellant type	Specific impulse I_{sp} (s)	Chamber temperature (K)	Metal content (wt %)	Pressure exponent n	Burning rate (mm/s)	Density kg/m ³
DB	220–230	2530	0	0.3	11.43	1605
DB/AP/Al	260–265	3870	20–21	0.4	19.81	1800
DB/AP-HMX/Al	265–270	3975	20	0.49	13.97	1800
PVC/AP	230–240	2820	0	0.38	11.43	1688
PVC/AP/Al	260–265	3370	21	0.35	11.43	1772
PS/AP	230–240	2870	0	0.43	8.9	1716
PU/AP/Al	260–265	3265–3615	16–200	0.15	6.86	1772
CTPB/AP/Al	260–265	3370–3475	15–17	0.4	10.16	1772
HTBP/AP/Al	260–265	3370–3475	4–17	0.4	10.16	1855

CTPB, carboxy-terminated polybutadiene

PS, polysulfide

DB, double based

PU, polyurethane

HMX,

PVC, polyvinyl chloride

cyclotetramethylenetetrinitramine

HTPB, hydroxyl-terminated polybutadiene

11.8 Liquid-Propellant Rocket Engines (LREs)

11.8.1 Introduction

A liquid-propellant rocket engine (LRE) is a reaction engine using the liquid propellants (fuel and oxidizer) stored on a flight vehicle board. Since propellant mass flow rates are extremely large for high-thrust engines, liquids are desirable as they have high density; thus, the volume of the propellant tanks is relatively low. After combustion, the liquid rocket propellant (LRP) is converted into gaseous state and discharges from the engine and creates thrust:

- High-pressure tanks (one or more)
- Pumps
- Turbines
- Gears
- Bearings
- Feeding lines (plumbing or piping)
- Regulators, valves, and control devices
- Thrust chamber or thruster (one or more combustion chambers)
- Nozzle

A liquid-propellant rocket propulsion system consists of one or more tanks to store the propellants, one or more thrust (combustion) chambers, a feed mechanism to force the propellants from the tanks into the thrust chamber (propellant pumps, turbines, pressurizing device), power source to furnish the energy for the feed mechanism, suitable plumbing or piping system to transfer the liquids, a structure to transmit the thrust force, and control devices to initiate and regulate the propellant flow and thus the thrust and nozzles.

Liquid-propellant rockets can be **throttled**, be control of mixture ratio, shut down, and be restarted.

Some commonly used liquid fuels are liquid hydrogen, UDMH, hydrazine, alcohol, etc.

Some common oxidizers are liquid oxygen, red fuming nitric acid (RFNA), liquid fluorine, WFNA, etc. Most of the liquid propellants are toxic and require very high combustion temperature which demands special materials for handling system and cooling of the walls of chamber and exhaust nozzle. For better mixing and efficient combustion, the fuel and the oxidizer are atomized into small droplets through the injectors and then mixed, evaporated, and ignited. Ignition is achieved by chemical, pyrotechnical, and electrical means. The propellant can often be hypergolic. The ignited propellants burn under high pressure, sometimes greater than MPa.

Upon combustion high-temperature gaseous combustion products (CPs) are formed and discharged through the nozzle. Temperature of CP continuously decreases, while its velocity increases to sonic speed at the nozzle throat and supersonic speeds (2700–4500 m/s) at nozzle exit.

11.8.2 Applications

LRE is the main type of engines for booster rockets and space modules. It is widely used in high-altitude research rockets, long-range ballistic missiles, guided antiaircraft missiles, and combat missiles. Examples of such LRE are:

- The *three space shuttle main engines (SSMEs)*, which are sequentially started at launch, combust a mixture of propellants consisting of hydrogen and oxygen, which are stored and delivered in a cryogenic liquid state from the external tank (ET)
- US Saturn V booster rocket first-stage (F-1) engine
- The Russian “Energy” booster rocket (RD-170) engine

11.8.3 Propellant Feed System of LREs

The propellant feed system of a liquid rocket engine determines how the propellants are delivered from the tanks to the thrust chamber. The functions of the propellant feed system in both types are:

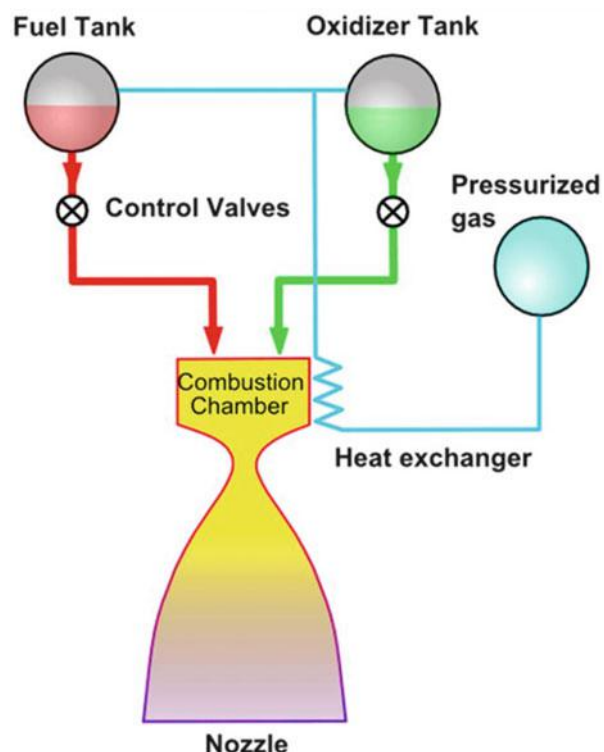
1. Raising the pressure of the propellants
2. Feeding the propellant to the thrust chambers

LREs are generally classified based on the propellant feed system as either pressure fed or pump fed. Pressure fed is performed using gas pressurization, while pump fed relies upon pumps [10]. These two systems are shown in Fig. 11.21:

(A) Pressure-fed rocket engines

A high-pressure gas like helium or nitrogen stored in a high-pressure tank at a very high pressure (say 35 MPa) is used to force the propellants to the thrust chamber. Pressurization gas is warmed by heat exchanger to avoid its cooling down.

Fig. 11.21 Propellant feed systems and pressure-fed engine



The advantages of this system are its simplicity, reliability, and avoidance of turbomachinery. Moreover, procedure for engine cutoff and restart are very simple. However, its great disadvantage is their large and heavy tanks.

Due to the above advantages, this type of system is typically used for space propulsion applications and auxiliary propulsion applications requiring low system pressures and small quantities of propellants. Maneuvering and attitude control thrusters of satellites and space probes are mostly pressure fed since they are restarted thousands of times. Other famous applications are all engines of Apollo CSM and Apollo LM.

(B) Pump-fed rocket engines

The pump-fed system is used for high-pressure, high-performance applications. Several thousand horsepower engines are needed to drive feeding pumps. The selection of a particular feed system and its components is governed primarily by the application of the rocket, duration, number or type of thrust chambers, mission, and general requirements of simplicity of design, ease of manufacture, low cost, and minimum inert mass.

The main elements of liquid rockets are:

There are two categories of liquid-propellant rocket engines, namely:

- Boosting propulsion (hours, days, and months in space)
- Auxiliary propulsion (10 years or more in space)

11.8.4 Liquid Propellants

Liquid propellants are classified into two types:

- (a) Monopropellant
- (b) Bipropellant

In rare cases, [tri-propellant rockets](#) using three types of propellant are used.

The above classification is written as mono-, bi-, and multiphase propellants.

11.8.4.1 Monopropellant

Monopropellant contains an oxidizing agent and combustible matter in a single substance (Fig. 11.22a). It may be a mixture of several compounds, or it may be a homogeneous material, such as hydrogen peroxide H_2O_2 , ethylene oxide $(CH_2)_2O$, and hydrazine N_2H_4). Monopropellants are stable at ordinary atmospheric conditions but decompose and yield hot combustion gases when heated or catalyzed.

It has the following features:

1. Monopropellant is passed through a catalyst.
2. Catalyst causes a reaction, which generates heat.

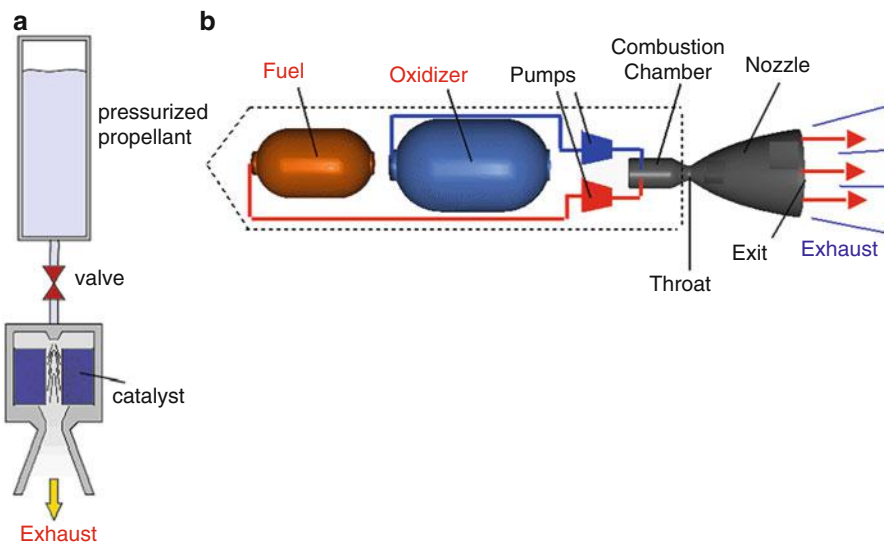


Fig. 11.22 Liquid-propellant engine: (a) monopropellant engine and (b) bipropellant engine

Table 11.8 Advantages and disadvantages of monopropellant liquid fuel rocket engine

Advantages	Disadvantages
1. Simple design	1. Most fuels are toxic
2. Robust design	2. Catalyst lifetime issues
3. Reliable	3. Low thrust
4. Not a lot of plumbing	4. Low exhaust speeds
5. Flight heritage	5. Low specific impulse
6. Can turn them off	

3. The heated products of this reaction are expelled through a nozzle.
4. Exhaust speed = 2.3 km/s.
5. Usually used for altitude control of spacecraft.

Table 11.8 illustrates the advantages and disadvantages of monopropellant.

Some monopropellants are called *hypergolic* if the propellants ignite smoothly on contact with each other. An example is hydrazine.

11.8.4.2 Bipropellant

The *bipropellant* rocket unit has two separate liquid propellants: an oxidizer and a fuel (Fig. 11.22b). They are stored separately and are not mixed outside the combustion chamber [9]. The majority of liquid-propellant rockets have been manufactured for bipropellant applications. It has the following features:

Table 11.9 Advantages and disadvantages of bipropellants liquid fuel rocket engine

Advantages	Disadvantages
1. Typically, more efficient than solid or hybrid rockets	1. More complex than hybrid or solid rockets
2. High exhaust velocity (3.6–4.4 km/s)	2. Cryogenic systems often needed (icing issues)
3. Throttled	3. Difficulty storing
4. Can turn them off	4. System complexity
5. Lots of flight heritage	

Table 11.10 Bipropellant engines

Fuel	Oxidizer	Example
Liquid hydrogen H ₂ (LH ₂)	Liquid oxygen O ₂ (LOX)	Space shuttle main engine
		Saturn V upper stage
		Delta IV first stage
		Centaur
		Ariane second stage
RPI	LOX	Atlas rockets
Liquid hydrocarbon (Kerosene)		Delta
		Titan rockets
		Voyager 1 and 2
Aerozine 50	Dinitrogen tetroxide	Apollo service module
		Lunar module
		Titan rockets
		Voyager 1 and 2
MMH (Monomethyl hydrazine CH ₃ NHNH ₂)	Dinitrogen tetroxide	Space shuttle orbital maneuvering system (OMS)
MMH (Monomethyl hydrazine CH ₃ NHNH ₂)	Dinitrogen tetroxide	Space shuttle orbital maneuvering system (OMS)

1. The fuel and oxidizer are pumped into the combustion chamber.
2. Often use turbopumps.
3. Power tapped off of main combustion.
4. Injectors mix propellant to provide stable and thorough combustion.
5. Heat is generated from combustion.
6. Heated products are expelled out the nozzle.

Table 11.9 lists the advantages and disadvantages of bipropellants.

Also some bipropellants are called *cryogenic* if it has to be kept at a low temperature to remain in a liquid state in propellant tanks. Examples are liquid hydrogen (LH₂), liquid oxygen (LOX), liquid methane, and liquid fluorine.

Some bipropellants are also *hypergolic* like nitrogen tetroxide.

Table 11.10 provides some data for some bipropellant engines and its applications.

11.8.5 Fundamental Relations

The propellant *mixture ratio* for a bipropellant is the ratio at which the oxidizer and fuel are mixed and react to give hot gases. The mixture ratio (r) is defined as the ratio of the oxidizer mass flow rate \dot{m}_o and the fuel mass flow:

$$r = \frac{\dot{m}_o}{\dot{m}_f}$$

The total propellant mass (\dot{m}) is

$$\dot{m} = \dot{m}_o + \dot{m}_f$$

And the oxygen and fuel mass flow rates are related to the propellant mass flow rate by the equations

$$\begin{aligned}\dot{m}_o &= r\dot{m}/(r+1) \\ \dot{m}_f &= \dot{m}/(r+1)\end{aligned}$$

Since the thrust force is expressed by the relation:

$$T = \dot{m} V_{\text{eff}}$$

For full expansion in nozzle, then:

$$u_e = V_{\text{eff}}$$

From Eq. (11.18b), with the chamber total pressure and temperature are equal to the nozzle exit conditions, then:

$$u_e = \sqrt{2CpT_c \left(1 - \left(\frac{P_e}{P_c} \right)^{\frac{\gamma-1}{\gamma}} \right)} = \sqrt{2 \frac{\gamma}{\gamma-1} RT_c \left[1 - \left(\frac{P_e}{P_c} \right)^{\frac{\gamma-1}{\gamma}} \right]} \quad (11.18b)$$

Example 11.12 A liquid oxygen–liquid hydrogen rocket engine has a mixture ratio of 3.5. The combustion chamber temperature and pressure are 3500 K and 22 atmospheres. The exit area is 3.224 m^2 . The exit pressure is equal to atmospheric pressure at altitude of 20 km. Specific heat ratio $\gamma = 1.23$ and specific heat at constant pressure $Cp = 2520 \text{ J/kg/K}$. This example is a continuation for Example 11.5, which had the following results:

$$P_{oe} = 2229.15 \text{ kPa}, \quad u_e = 3450.48 \frac{\text{m}}{\text{s}}, \quad \rho_e = 0.0102 \text{ kg/m}^3$$

$$\dot{m} = 113.45 \text{ kg/s}, T = 391.5 \text{ kN}, I_{sp} = 351.85 \text{ s}$$

(a) Calculate the oxygen and fuel mass flow rate.

If the propellant mass flow rate is constant, examine the effects of:

(b) Nozzle efficiency (η_n) varies from 93 to 99 %.

(c) Pressure drop in the combustion chamber (ΔP_c) varies from 1 to 5 %

on the exhaust speed, thrust force, and specific impulse.

Solution

(a) Since the mixture ratio is 3.5, then:

the *oxygen* mass flow rate is calculated as

$$\dot{m}_o = \frac{r\dot{m}}{r+1} = \frac{3.5 \times 113.45}{3.5 + 1} = 88.24 \text{ kg/s}$$

The *hydrogen fuel* mass flow rate is then:

$$\dot{m}_f = \frac{\dot{m}}{r+1} = \frac{113.45}{4.5} = 25.21 \text{ kg/s}$$

(b) *Effect of nozzle efficiency* ($\eta_n = 93 - 99 \%$)

The exit velocity is recalculated after adding the nozzle efficiency from the relation

$$u_e = \sqrt{2\eta_n C_p T_{oe} \left(1 - \left(\frac{P_e}{P_{oe}} \right)^{\frac{\gamma-1}{\gamma}} \right)}$$

When nozzle efficiency $\eta_n = 93 \%$,

$$u_e = \sqrt{2 \times 0.93 \times 2520 \times 3500 \left(1 - \left(\frac{5.475}{2229.15} \right)^{0.187} \right)} = 3327.5 \text{ m/s}$$

Propellant mass flow rate is constant = 113.45 kg/s.

Thrust is $T = \dot{m} u_e = 113.45 \times 3327.5 = 377,505 \text{ N} = 377.5 \text{ kN}$.

Specific impulse:

$$I_{sp} = \frac{u_e}{g} = \frac{3327.5}{9.80665}$$

$$I_{sp} = 339.3 \text{ s}$$

Other values for nozzle efficiency are calculated and tabulated in Table 11.4. As shown in Table 11.12; the worst performance is associated with the smallest nozzle efficiency of 93 %. In such a case, a drop in both of thrust and specific impulse by 3.6 % is encountered.

(c) *Effect of pressure drop in combustion chamber*

Since the exhaust velocity is expressed by

$$u_e = \sqrt{2CpT_c \left(1 - \left(\frac{P_e}{P_{0e}} \right)^{\frac{\gamma-1}{\gamma}} \right)}$$

Here

$$P_{0e} = P_c (1 - \Delta P_c \%)$$

For a combustion pressure drop of 5 %, then

$$P_{0e} = 2229.15 \times (1 - 0.05) = 2117.7 \text{ kPa}$$

The exhaust speed is then:

$$u_e = \sqrt{2 \times 2520 \times 3500 \left(1 - \left(\frac{5.475}{2117.7} \right)^{0.187} \right)} = 3442.5 \text{ m/s}$$

$$T = \dot{m} u_e = 113.45 \times 3442.5 = 390,552 \text{ N} = 390.55 \text{ kN}$$

Specific impulse:

$$\begin{aligned} I_{sp} &= \frac{u_e}{g} = \frac{3442.5}{9.80665} \\ I_{sp} &= 351.04 \text{ s} \end{aligned}$$

As is noticed, even for the maximum value of pressure drop (5 %), nearly no changes in exhaust velocity and specific impulse if the nozzle efficiency kept constant (100 %) (Table 11.11).

Table 11.11 Effect of nozzle efficiency and pressure drop in combustion chamber on rocket characteristics

	Effects of nozzle efficiency				Effect of pressure drop in CC	
	93 %	95 %	97 %	99 %	100 %	100 %
Nozzle efficiency	93 %	95 %	97 %	99 %	100 %	100 %
Combustion pressure drop ΔP_c	0	0	0	0	0	5 %
Exhaust velocity (m/s)	3327.5	3363	3398	3444	3450.5	3442.5
Thrust (kN)	377.5	381.5	385.5	390.7	391.5	390.55
Specific impulse (seconds)	339.3	342.93	346.49	351.19	351.85	351.04

Table 11.12 Combustion chamber pressure versus pump discharge pressure for different turbopump systems

Turbopump system	Combustion chamber pressure (psia)	Pump discharge pressure (psia)
Expander cycle	150–1000	500–3500
Gas generator cycle	10–1500	100–2500
Staged combustion cycle	1000–3000	2000–6500

11.8.6 Pump-Fed System

The main element in pump-fed system is the turbopumps. A turbopump is a [gas turbine](#) that comprises basically two main components: a rotodynamic [pump](#) that delivers fuel or oxidizer to the thrust chamber and a driving [turbine](#), usually both mounted on the same shaft or sometimes geared together. The purpose of a turbopump is to produce a high-pressure fluid for feeding a [combustion chamber](#) where propellants react and produce high-temperature gases.

The main challenges in the design of turbopumps are to deliver very high power in a small machine, which implies high pressure (up to 55 MPa), large mass flow rate (some 2500 kg/s), and small weight turbomachinery.

A turbopump can comprise either a single/multistage [centrifugal pump](#) or multistage [axial flow pump](#). Pumps should rotate at tens of thousands revolutions per minute. Turbopumps may also include booster pumps.

Pumps are driven by a gas turbine to form together turbopumps. These pumps raise the pressure of cryogenic fluid to higher than the combustion chamber pressure. The gas driving the turbine may be a generator in a gas generator by pre-burning some amount of the propellant, by burning separate propellant (like hydrogen peroxide in the RD-107/108 engines on the Soyuz), or by gasification of some propellant in the cooling jacket of the thrust chamber and the nozzle.

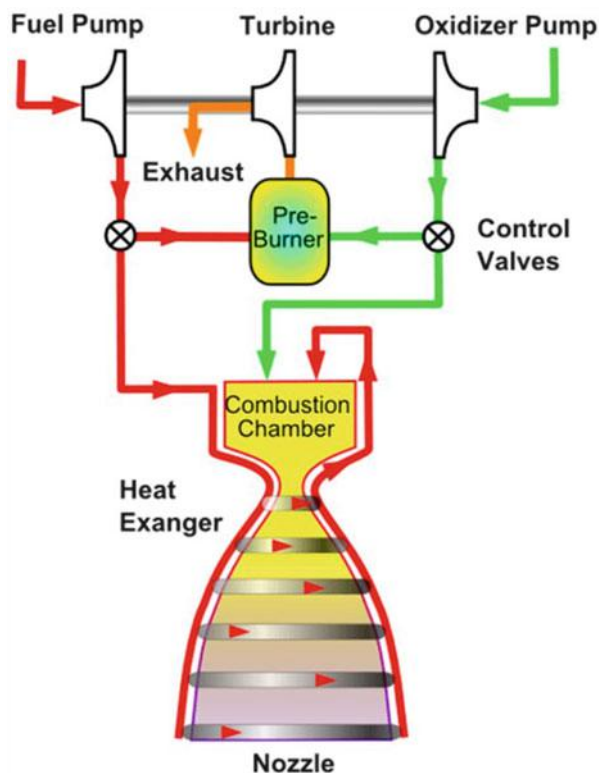
Advantages of turbopumps:

1. High specific impulse due to its high pressure in thrust chamber
2. Compact and light weight compared to pressure-fed engines
3. More efficient thus spend less propellant

Disadvantages of turbopumps:

1. Complexity
2. More expensive compared to pressure fed
3. Less reliable compared to pressure fed
4. Turbopumps are used in all stages of launch vehicles. The following Soviet flight vehicles used turbopumps: Lunar probes E8 (Lunokhods, soil sample missions), Lunar modules for the man expeditions, space stations Salyut, and Soyuz manned spacecraft.

Fig. 11.23a Gas generator engine



Important data of RD-170/171 turbopump are:

Propellants: LOX/kerosene

Mass flow rate: ~ 2.4 tons/s

Pressure of thrust chamber: ~ 250 bar

Turbine power: ~ 200 MW

Rotational speed: $\sim 14,000$ rpm

Pressure of gases driving the turbine: $\sim 500^\circ\text{C}$

Figure 11.23 illustrates three kinds of turbopump systems used for pump-fed liquid-propellant rocket. Figure 11.23a shows a *gas generator cycle*. A part of the fuel and oxidizer is burnt in a separate combustion chamber identified as *pre-burner*. The products of combustion of this small chamber are used to drive the turbine before exhausted to ambient pressure. For this reason it is identified as open cycle [11]. The gas turbine has a high-pressure ratio. To minimize weight, a small number of stages are employed; thus, a moderate turbine efficiency is attained. Combustion pressure is also moderate, of the order of 5.0 MPa. Examples are the Japanese LE-5 engine which was used in the second stage of H-1 rocket, Vulcain 2 engine ([European first-stage rocket engines](#) for the [Ariane 5](#)), and many US engines including Rocketdyne J-2 and the F-1 engines.

Fig. 11.23b Staged combustion cycle

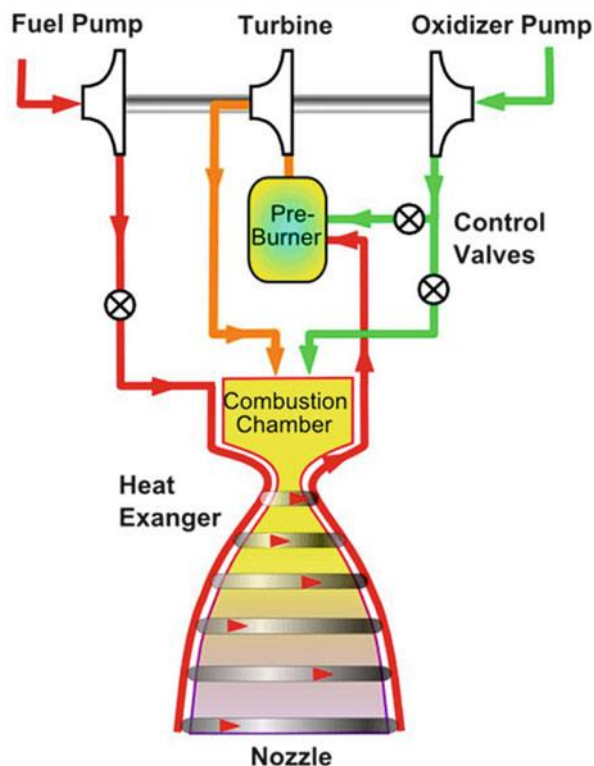


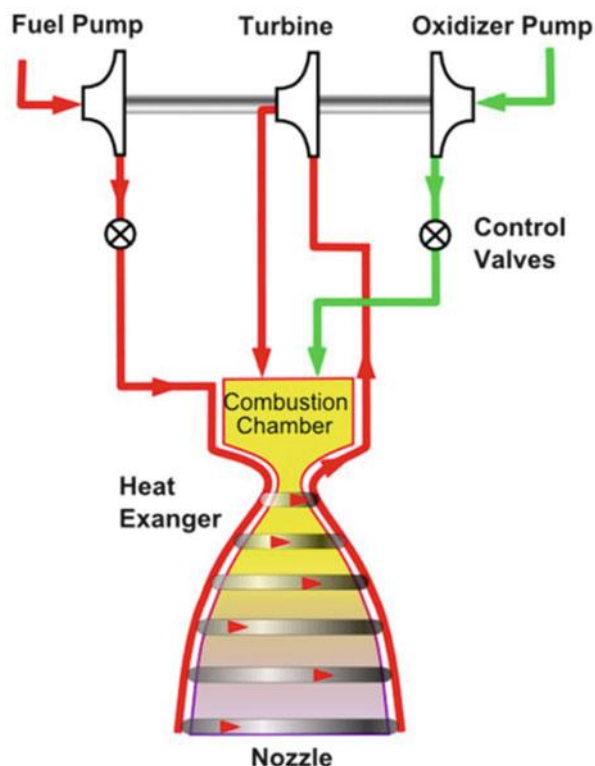
Figure 11.23b shows a *staged combustion* [12] cycle. The turbine exhaust gases are not dumped but fed into the main combustion chamber. So all propellant and all heat pass through the thrust chamber and nothing are wasted. The fuel–oxidizer ratio in main engine need not be the same as in the pre-burner. The turbine pressure ratio is less than that of the gas generator case. Since the turbine driving gas is not efficiently changed into a thrust like the gas generator cycle, high engine performance is not obtained. High chamber pressure is achieved compared with the previous gas generator, here more than 40 MPa. This system first appeared in USSR. Next, it was employed in the Japanese LE-5A and LE-5B. Moreover, the space shuttle main engine (SSME) uses staged combustion arrangements, but separate turbine is used for both fuel (hydrogen) and oxygen turbopumps.

The third type is the “expander” configuration shown in Fig. 11.23c.

Its advantages are making use of all propellant and not requiring a separate gas turbine.

The gas employed in driving the turbine is produced from the fuel vaporized in the cooling jacket of the thrust chamber and nozzle. The cycle may be opened or closed. For open cycle, a small portion of fuel is used to drive the turbine and next is dumped. In closed cycle (shown in Fig. 11.23c), fuel is redirected into thrust

Fig. 11.23c Expander cycle



chamber after leaving the turbine. An example is SNECMA VINCI upper-stage engine. A comparison between the above three cycles (gas generator, expander, and staged combustion) is given in [4] and summarized here:

1. The gas generator cycle is the easiest to control and least sensitive since it works against atmospheric or low pressure. The turbine is a low-flow high-pressure ratio machine. The discharge pressure of the pump is slightly above chamber pressure.
2. In the expander cycle, the heat source is the nozzle cooling. All the flow that passes through the turbine is injected into the chamber. Chamber pressure depends on how much pumping power can be delivered given the heat input. This makes it sensitive to the turbine efficiency. Turbine discharge pressure is higher than the chamber pressure.
3. A staged combustion cycle allows for extremely high chamber pressures. As a consequence the discharge pressure from the pumps has to be extremely high. Thus multiple pumps are used in some cases.

Table 11.12 gives a summary for reasonable choices of cycle for different chamber pressures along with the resulting pump discharge pressure as described in NASA SP-8107 [13].

11.8.7 Rocket Pumps

The principal requirements of a rocket engine pumps are reliability, light weight, high delivery rate at maximum pressure head, smooth flow *for a wide range* of operating conditions, and high efficiency. As described in compressor sections, the used pump types are *centrifugal* flow, axial flow, and mixed flow pumps which consist essentially of two basic elements: the *rotor* and the stator. Centrifugal pumps are generally designed with a single stage, while axial pumps are primarily of multistage design. However, multistage *centrifugal* pumps with crossover-type volutes have also been considered.

The selection of a pump configuration is influenced by operational, hydrodynamic, and mechanical considerations. Pumps have the same working principle as compressors, namely, accelerating the fluid flow by imparting kinetic energy to it in the rotor and then decelerating or “diffusing” it in the stator. This results in increased fluid pressure head. More details concerning different pumps are given below:

1. Single-stage centrifugal pumps

Almost all existing chemical and nuclear rockets have centrifugal turbopumps, due to its simplicity, reliability, wide operating range, and ability to handle large flows at high pressures efficiently. Regarding head and flow rate, centrifugal pumps can generate more than 100,000 ft and up to 30,000 gpm at 5800 rpm [14].

The elements of a centrifugal pump are rotor and stator assemblies. The rotor assembly usually includes an inducer, an impeller, and a shaft, while the stator assembly consists of a casing with stationary diffuser vanes, a volute with discharge outlet, shaft bearings, and seals. An inducer is an axial flow-type impeller which increases the static pressure of the entering fluid sufficiently.

The succeeding element is the impeller which is basically a rotating wheel. Fluid is admitted axially into the impeller which may have either forward-leaning, radial, or backward-leaning geometry the same as in a centrifugal compressor.

2. Multistage centrifugal pumps

For higher-pressure rises, multistage centrifugal pumps can be designed. The basic construction of a multistage pump is similar to that of a single-stage pump, except that proper channeling of the fluid between stages is added [15].

3. Multistage axial pumps

Axial types become competitive to centrifugal ones when multistaging and maximum efficiency are of paramount consideration [16]. This design is well suited to liquid hydrogen service which entails the problems of extremely low fluid temperature and density. Low fluid density results in high-volume flow and in high-pressure-head rise requirements. For such applications a multistage axial flow pump is generally superior with respect to construction and performance. Elements of an axial flow pump are the rotor and stator assemblies. Rotor assembly

Table 11.13 Rocketdyne SSME turbopumps

Feature		Low-pressure turbopump		High-pressure turbopump	
Pump	Type	Hydrogen	Oxygen	Hydrogen	Oxygen
	Number of stages	1	1	3	1 (double entry)
	Flow rate (kg/s)	70.3	424	67.7	407
	Inlet pressure (kPa)	207	689.5	1724	8280
	Outlet pressure (MPa)	2.0	2.863	42.1	49.7
	Efficiency%	71.3	67.7	75	72
	rpm	15,400	5050	34,386	27,263
Turbine	Type	Axial gas turbine	Axial hydraulic	Axial	Axial
	No. of stages	2	6	2	2
	Turbine inlet temperature	-17 (F)	-272 (F)	997 (K)	3620 (K)
	Turbine inlet pressure (MPa)			33.6	34.7
	Flow rate (kg/s)	13.2	84.8	74.1	27.3
	Pressure ratio	1.3	-	1.48	1.53
	Efficiency%	58	67.7	81.1	74.6
	rpm	15,400	5050	34,360	22,220
	Power (kW)	2486	1203	47,039	17,062

which accelerates the flow consists of an inducer, a cylindrical rotor with multiple rows of rotating blades, and a rotor shaft. The stator assembly which converts the fluid velocity head into the pressure head includes a cylindrical casing with rows of stationary blades spaced between inducer and rotating blades, a volute casing, bearings, and seals [17]. The axial speed of flow is kept constant throughout the various stages of the pump.

Typical information for turbopumps is given in Table 11.13. It lists many features of the four turbopumps available in the SSME.

11.8.8 Pump Materials and Fabrication Processes

The first set of pumps used in turbopumps was made of aluminum [18]. Next, as the pressures went up, pumps were made of titanium, steel alloys, and then superalloys like Inconel or Hastelloy. In the early 2000, a few pump impellers were beginning to be made by powder metallurgy processes with new material properties. Old pumps manufactured some 65 years ago are two to four times as heavy as and considerably larger than a modern newly designed version with better materials.

11.8.9 Axial Turbine

The turbines which provide shaft power to the propellant pumps derive their energy from the expansion of a high-pressure and high-temperature gas to lower pressures and temperatures.

As described in turbine sections, turbines are either impulse or reaction turbines. Impulse turbines can be either single or multistages. Reaction turbines are usually multistage.

Example 11.13 An axial turbine is used as a power source in a rocket turbopump. The turbine is a single stage of the impulse type. It has a mean diameter $d_m = 0.24\text{ m}$ and a rotational speed $N = 14,000\text{ rpm}$. Hot gases flow at the rate of 90 kg/s into the turbine having a total temperature and pressure of $T_{01} = 960\text{ K}$ and $P_{01} = 7.5\text{ MPa}$. The turbine pressure ratio and efficiency are $\pi_t = 1.5$ and $\eta_t = 0.85$.

Flow in the stator is assumed ideal and flow has an axial absolute exit velocity from the rotor blade row.

The working fluid is a molecular weight $M = 26.5$ and specific heat ratio $\gamma = 1.3$:

1. Draw the velocity diagram for rotor blade row.
2. Calculate the blade height of rotor at inlet and outlet.

Solution

For impulse turbine then

$$W_2 = W_3, P_2 = P_3$$

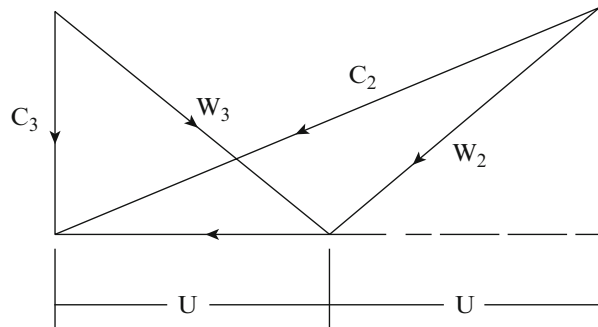
Flow leaves axially; then $\alpha_3 = 0$.

Velocity triangles are shown in Fig. 11.24.

Flow in stator is ideal; then

$$T_{01} = T_{02} \text{ and } P_{01} = P_{02}$$

Fig. 11.24 Velocity triangles for impulse turbine with axial exit



The gas constant :

$$R = \frac{\bar{R}}{M} = \frac{8314}{26.5} = 313.7 \frac{\text{J}}{\text{kg.K}}$$

Specific heat :

$$C_p = \frac{\gamma R}{\gamma - 1} = 1359.5 \frac{\text{J}}{\text{kg.K}}$$

The absolute outlet velocity from stator is calculated from the relation

$$\begin{aligned} C_2 &= C_0 = \sqrt{2C_P T_{01} \left(1 - \frac{1}{\pi_t^{\frac{\gamma-1}{\gamma}}} \right)} \\ C_2 &= C_0 = \sqrt{2 \times 1359.5 \times 960 \left(1 - \frac{1}{1.5^{\frac{0.3}{1.3}}} \right)} = 483 \text{ m/s} \\ U_2 &= \frac{\pi d_2 N}{60} = \frac{\pi \times 0.24 \times 14,000}{60} = 176 \text{ m/s} \end{aligned}$$

From velocity triangle

$$\begin{aligned} \sin \alpha_2 &= \frac{2U_2}{C_2} = \frac{2 \times 176}{483} \\ \alpha_2 &= 46.8^\circ \end{aligned}$$

Then

$$C_3 = C_a = C_2 \cos \alpha_2 = 330.9 \text{ m/s}$$

Assuming $C_1 = C_3$, then $C_1 = 330.9 \text{ m/s}$.

Static temperature at stator outlet:

$$T_2 = T_{01} - \frac{C_2^2}{2C_P} = 960 - \frac{(483)^2}{2 \times 1359.5} = 874.2 \text{ K}$$

Static pressure at stator outlet:

$$P_2 = \frac{P_{01}}{\pi_t} = \frac{7.5}{1.5} = 5.0 \text{ MPa}$$

Density at stator outlet:

$$\rho_2 = \frac{P_2}{RT_2} = \frac{5 \times 10^6}{313.7 \times 874.2} = 18.23 \text{ kg/m}^3$$

$$\dot{m} = \rho_2 C_a A_2$$

$$A_2 = \pi d_m h_2$$

$$h_2 = \frac{\dot{m}}{\rho_2 C_a \pi d_m} = \frac{90}{18.23 \times 330.9 \times \pi \times 0.24} = 0.0198 \text{ m}$$

The tip diameter is then

$$d_{t2} = d_m + h_2 = 0.24 + 0.0198 = 0.2598 \text{ m}$$

The rotational speed at tip is then

$$U_{2t} = U_{2m} \times \frac{d_t}{d_m} = 176 \times \frac{0.2598}{0.24} = 190.5 \text{ m/s}$$

The speed ratio is then

$$\frac{U_{2t}}{C_0} = \frac{190.5}{483} = 0.394$$

Turbine efficiency is defined as

$$\begin{aligned} \eta_t &= \frac{T_{01} - T_3}{T_{01} - T_2} \\ 0.85 &= \frac{960 - T_3}{960 - 874} \\ T_3 &= 887 \text{ K} \end{aligned}$$

With $P_2 = P_3 = 5 \text{ kPa}$, then the density at rotor outlet

$$\rho_3 = \frac{P_3}{RT_3} = \frac{5 \times 10^6}{313.7 \times 887} = 17.97 \text{ kg/m}^3$$

Blade height at rotor outlet is then

$$h_3 = \frac{\dot{m}}{\rho_3 C_3 \pi d_m} = \frac{90}{17.97 \times 330.9 \times \pi \times 0.24} = 0.02 \text{ m}$$

11.9 Hybrid Propulsion

11.9.1 Introduction

Hybrid-propellant engines represent an intermediate group between solid- and liquid-propellant engines. One of the substances is solid, usually the fuel, while

the other, usually the oxidizer, is liquid, although reverse hybrids such as liquid hydrogen burning with solid oxygen have been studied (Fig. 11.25). Such engines have performance similar to that of solid propellants, but the combustion can be moderated, stopped, or even restarted. It has better specific impulse than solid rocket ones.

The liquid oxidizer is injected onto the solid, whose fuel case also serves as the combustion chamber. An igniter starts the combustion process, which develops heat to vaporize the surface layer of solid fuel. The expanding hot fuel gas expands away from the solid surface and meets the spray of liquid oxidizer. Combustion process continues in a self-sustaining manner.

Typically the fuel is a polymeric hydrocarbon solid such as HTPB (which stands for hydroxyl-terminated polybutadiene), and the oxidizer can be any of the oxidizers used with liquid-bipropellant engines (hydrogen peroxide H_2O_2). HTPB has slow burning rates; thus, a number of holes, or ports, exposing more surface area of the fuel for burning are added. Unfortunately, so many holes make the solid fuel structurally weak and subject to dangerous breakup as the combustion chamber builds up pressure and gas flow (Fig. 11.26).

Several hybrid propulsion programs were initiated in the late 80s and early 90s. The Joint Government/Industry Research and Development (JIRAD) program involved the testing of 11- and 24-inch diameter hybrid motors at the Marshall

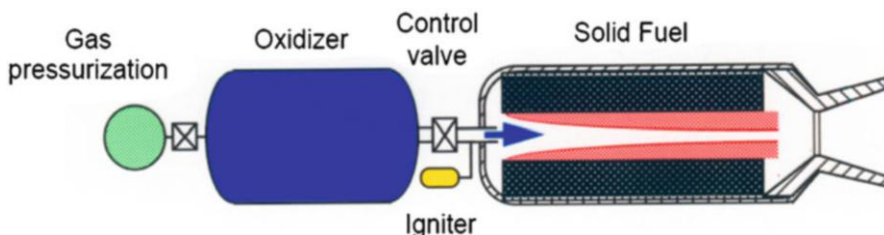


Fig. 11.25 Hybrid rocket engine

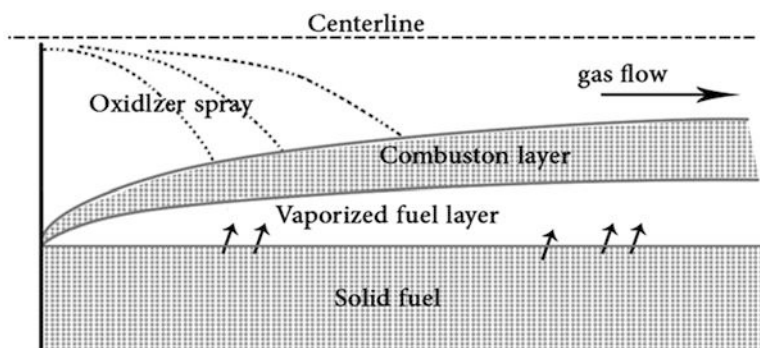


Fig. 11.26 Combustion process in a hybrid motor

Table 11.14 Fuel–oxidizer combinations for hybrid-propellant rockets

Number	Fuel	Oxidizer
1	Beryllium hydride (Be-H ₂)	Fluorine (F ₂)
2	Lithium hydride (Li H)	Chlorine trifluoride (ClF ₃)
3	Lithium hydride (Li H)	Nitrogen tetroxide (N ₂ O ₄)
4	Hydrocarbon (CH ₂) _n	Nitrogen tetroxide (N ₂ O ₄)

Space Flight Center. Another hybrid program initiated during the early 90s was DARPA's Hybrid Technology Options Project (HyTOP). The Hybrid Propulsion Demonstration Program (HPDP) began in March 1995 which included the design and fabrication of a 250,000-pound thrust test-bed. The most recent advance in hybrid rockets occurred in the fall of 2004 when SpaceShipOne carried a pilot to over 328,000 ft in a new era in space tourism.

Some fuel–oxidizer combinations for hybrid-propellant rockets are shown in Table 11.14.

11.9.2 Mathematical Modeling

The surface recession rate may be described by a general empirical relation:

$$\dot{r} = a \left(\frac{\dot{m}}{A} \right)^n \quad (11.49)$$

where (a) is a constant, (\dot{m}) is the *combined* oxidizer and fuel mass flux, A is the cross-sectional area of the combustion chamber, and the exponent (n) has the range $0.6 < n < 0.8$.

Assuming that the fuel has a cylindrical area (A_b) with diameter (D) and length (L), the rate of fuel mass generation is

$$\dot{m}_f = \rho_f A_b \dot{r} = \rho_f \pi D L \dot{r} \quad (11.50a)$$

where ρ_f is the fuel density.

Now following the procedure of Loh [19], who assumed that the recession rate is proportional to the oxidizer only and not to the combined mass flow of fuel and oxidizer, then from (c), the fuel regression rate is

$$\dot{m}_f = \rho_f \pi D L a \left(\frac{\dot{m}_o}{A} \right)^n \quad (11.50b)$$

Substituting for cross-sectional area, A , then

$$\dot{m}_f = \rho_f \pi D L a \left(\frac{4\dot{m}_o}{\pi D^2} \right)^n$$

Now, it is interesting to notice that if $n = 0.5$, then the rate of fuel mass recession is

$$\dot{m}_f = 2a\rho_f L \sqrt{\pi \dot{m}_o} \quad (11.51)$$

which is independent of the fuel diameter (D), which means that the fuel mass flow is constant even though D is increasing as the fuel is consumed.

Example 11.14 A hybrid rocket has the following data:

Propellant density = 1600 kg/m³, Thrust force = 55 kN

Specific impulse $I_{sp} = 275$ s, $O/F = 1.0$

Constants: $a = 0.001$, $n = 0.6$, Burn time = 10 s

Initial propellant diameter $D(0) = 0.1$ m

Calculate:

- (a) The solid-propellant length
- (b) The final propellant diameter

Solution

The propellant flow rate:

$$\begin{aligned} \dot{m} &= \frac{T}{g I_{sp}} \\ \dot{m} &= \frac{55,000}{9.8 \times 275} = 20.4 \text{ kg/s} \end{aligned}$$

Since the ratio between oxidizer to fuel flow rates

$$O/F = 1.0, \text{ then } \dot{m}_f = \dot{m}_o = 10.2 \frac{\text{kg}}{\text{s}}.$$

From Eq. (11.50a),

$$L = \frac{\dot{m}_f}{2a\rho_f \sqrt{\pi \dot{m}_o}} = \frac{10.2}{2 \times 0.001 \times 1600 \times \sqrt{10.2\pi}} = 0.56 \text{ m}$$

From Eq. (c), with $n = 0.5$,

$$\dot{r} = a \left(\frac{\dot{m}_o}{A} \right)^{0.5} = 2a \sqrt{\frac{\dot{m}_o}{\pi D^2}}$$

Moreover $\dot{r} = \frac{1}{2} \frac{dD}{dt}$

Then $\frac{1}{2} \frac{dD}{dt} = 2a \sqrt{\frac{\dot{m}_o}{\pi D^2}}$

$$D \frac{dD}{dt} = 4a \sqrt{\frac{\dot{m}_o}{\pi}}$$

Integrating the above equation from $t = 0$ to $t = t_b$, then

$$D^2(t_b) - D^2(0) = 8at_b \sqrt{\frac{\dot{m}_o}{\pi}}$$

With $t_b = 10$ s, then

$$D^2(t_b) = 0.1^2 + 8 \times 0.001 \times 10 \times \sqrt{\frac{10.2}{\pi}} = 0.1541$$

$$D(t_b) = 0.393 \text{ m}$$

11.9.3 Advantages and Disadvantages of Hybrid Engines

The main advantages of hybrid rockets are:

1. Lighter than the corresponding liquid-propellant types due to fewer propellant pumping equipment and higher fuel density.
2. The regression rate is independent of the chamber pressure which is an important characteristic in the motor design.
3. Inherently safe due to the nonexplosive character of the fuel. Thus in the event of a structural failure, oxidizer and fuel cannot mix intimately leading to a catastrophic explosion that might endanger personnel or destroy a launch pad.
4. Thrust control is comparatively easier because only the flow of liquid oxidizer need be regulated.
5. Greater choices in the selection of grain configuration compared to solid-propellant rockets.
6. Less constituents as it uses only one liquid containment and delivery systems.
7. Less complexity due to omission of a regenerative cooling system for both the chamber and nozzle.

8. A large cost saving could be realized both in manufacture and launch operation as the fuel could be fabricated at any conventional commercial site.

Additional advantages over the solid rocket are:

- (a) Greatly reduced sensitivity to cracks and de-bonds in the propellant.
- (b) Better specific impulse.
- (c) The products of combustion are environmentally benign unlike conventional solids that produce acid-forming gases such as hydrogen chloride.

11.10 Nuclear Rocket Propulsion

Nuclear rockets have never developed or flown due to the grave risk of spreading radioactive debris if an accident occurred [19] [20].

Nuclear sources include:

- Radioactive isotope decay
- Fission reactor
- Fusion reactor

Nuclear rocket engines may be divided into two general classes based on the type of reactor used:

- (A) Solid-core systems
(B) Fluid-core systems, which may be further subdivided based on its core into:

- Liquid core
- Gas core
- Plasma

Solid-core reactor systems have been under active investigation since 1955 [19]. These engines utilize reactors with graphite, metal, or metal–carbide cores capable of operating at temperatures ranging from 2000 to 3000° K.

Such solid-core rocket engine is an adaptation of liquid-propellant engine, but with the combustion chamber replaced by reactor (which resembles a heat exchanger) and the oxidizer-feeding system eliminated.

It includes a propellant tank, feeding system (may be of the gas generator, staged combustion, or expander system), reactor, and a convergent–divergent nozzle.

Nuclear thermal propulsion (NTP) has the following main advantages:

1. High specific impulse capability which reduces the in-orbit mass requirements for staging high ΔV missions
2. High-thrust level which increases interplanetary trip times
3. Ability to utilize any gaseous propellant and thus has the best potential for using in situ planetary propellant resources

Table 11.15 Characteristics of propellants for nuclear propulsion

Propellant	T_c , (K)	Molecular weight M	Max I_{sp} , s
H ₂	2800	2	1000
C ₃ H ₈	2800	5.8	530
NH ₃	2800	8.5	460

Both of the specific impulse and thrust are proportional to exhaust speed u_e , which in turn is proportional to chamber temperature T_c and inversely proportional to the molecular weight M or

$$u_e \sim \sqrt{\frac{T_c}{M}} \quad (11.52)$$

Equation (11.50b) indicates the desirability of using hydrogen ($M_{H_2} = 2$) as a propellant. Its low molecular weight is the source of the superiority of the nuclear engine over its chemical rival. Table 11.15 demonstrates these facts for some nuclear propellants.

Due to close similarity between the fluid-core nuclear engine and liquid-propellant engine, same analyses for feeding systems including turbopumps and nozzle will not be repeated again here. However, it is worth to say that these components differ from similar components found in liquid chemical rockets only in the modifications required to allow them to survive and function properly in the reactor radiation environment.

11.11 Electric Rocket Propulsion

11.11.1 Introduction

Electric propulsion is defined as “the acceleration of gases for spacecraft propulsion by electric heating and/or by electric and magnetic body forces” [21]. Electric thrusters typically use much less propellant than chemical rockets because they have a higher exhaust speed and higher [specific impulse](#) over long periods compared with chemical rockets. Thus, electric propulsion can work better than chemical rockets for deep space missions. However, electric propulsion is not usually suitable for launches from the Earth’s surface, because of its very small thrust.

Historically, the idea of [electric propulsion](#) for spacecraft was introduced by [Konstantin Tsiolkovsky](#) in 1911 [22]. The first in-space demonstration of electric propulsion was an [ion engine](#) carried on board the Space Electric Rocket Test-I ([SERT-I](#)) spacecraft, launched on July 20, 1964. Russian satellites have used electric propulsion for decades, while only recently other countries used electric propulsion. However, presently it is extensively used. As of 2013, over

200 spacecraft operated around the world use electric propulsion for station keeping, orbit raising, or primary propulsion. In the future, the most advanced electric thrusters may be able to impart velocity increase Δv of nearly 100 km/s which is enough to take a spacecraft to the outer planets of the [solar system](#). A useful overview of electric propulsion for spacecraft was presented in [23].

Electric propulsion thrusters for spacecraft may be grouped in three families based on the type of force used to accelerate the ions of the plasma, namely:

- Electrostatic
- Electrothermal
- Electromagnetic

11.11.2 *Electrostatic Rockets*

In *electrostatic* thrusters, discrete particles are charged by electron bombardment and then accelerated by electrostatic [Coulomb forces](#). Electrostatic propulsion depends on the attraction or repulsion of electrically charged particles (by electron bombardment) and uses this effect to accelerate a stream of positively charged ions in order to produce thrust [24]. Spacecraft SERT-II (Space Electric Rocket Test-II) used electrostatic ion propulsion and operated for 10,000 h in space. Its different types are:

- (a) Ion thrusters (ITs)
- (b) Field emission electric propulsion (FEEP)
- (c) Colloidal thrusters

11.11.3 *Electrothermal Rockets*

Electrothermal rockets are very similar in principle to chemical and nuclear rocket as the propellant is a fluid (like hydrazine) which is heated in some chamber prior to its acceleration in a nozzle to convert its thermal energy to a directed stream that delivers reactive thrust power to the vehicle.

Heating may be achieved by either:

- (a) An electrical heating through the chamber wall or a heater coil (resistojets)
- (b) An electrical arc through the fluid (arcjets)
- (c) Inductively and radiatively heated devices, wherein some form of electrodeless discharge or high-frequency radiation heats the flow

11.11.4 Electromagnetic Rockets

Electromagnetic propulsion devices depend on the creation of a magnetic force on a conducting fluid (gas or plasma), by passing it through a field with crossed electric and magnetic fields. Its different types are:

- (a) Magneto plasma dynamic (MPD) thrusters
- (b) Hall thrusters (HTs)
- (c) Pulsed plasma thrusters (PPTs)
- (d) Pulsed inductive thrusters (PITs)

A brief comparison between the above three families may be summarized as:

1. Electrostatic thruster generates the highest specific impulse (from 2000 to over 10,000 s) and efficiency (from 60 to >80 %) and the smallest thrust (5 μN – 0.5 N)). Example for electrostatic thruster is the Deep Space-1 ion engine [25].
2. Resistojet electrothermal types develop the minimum specific impulse (<5 00s) and moderate thrust (0.05–5 N), exhaust velocity \sim 3.5 km/s, and efficiency \sim 80 %. But the electrothermal arcjet has a specific impulse (<7 00s), higher exhaust velocity \sim 5–6 km/s, and lower efficiency \sim 40 %.
3. Electromagnetic (MHD) type generates the maximum thrust (25–200 N) and a very high specific impulse (2000–5000 s) and efficiency (30–50 %).

Problems

11.1 A rocket with a mass of 1500 kg is placed vertically on the launching ramp. If the rate at which the propellants are consumed is equal to 3 kg/s, find the rocket exhaust velocity required if the rocket just begins to rise.

11.2 A rocket supersonic nozzle is to be designed with a combustion chamber pressure of 3.6 MPa and an ambient pressure of 100 kPa. Find the ratio between the thrust at sea level and the thrust in space (0 kPa). Assume that $R = 04 \left(\frac{\text{kJ}}{\text{kg}\cdot\text{K}} \right)$ and $\gamma = 1.3$.

11.3 A rocket has the following characteristics:

- Initial mass = 200 kg
- Mass after rocket operation = 130 kg
- Mass of payload and structure = 110 kg
- Specific impulse = 280 s
- Rocket operation = 3.4 s

Calculate

- Mass ratio
- Propellant mass flow rate
- Thrust
- Exit velocity
- Total impulse

- 11.4 A rocket flies at 7200 km/h where the ejected propellant mass flow rate is 4.0 kg/s. The propellant heating value is 7.0 MJ/kg. It is required to draw the propulsive, thermal, and overall efficiencies for a flight to effective jet velocity ratio $\sigma = 0 - 3$.
- 11.5 A rocket is fired from a flying airplane. The Mach number of aircraft is 0.8; speed of exhaust gases from rocket relative to fixed station on ground is 2500 m/s. Exhaust gases from rocket have a pressure of 80 kPa and density 0.6 $\frac{\text{kg}}{\text{m}^3}$.

Diameter of nozzle exit is 200 cm². If the aircraft is flying at 5, 10, and 15 km, calculate:

- (a) Exhaust speed
- (b) Effective exhaust speed
- (c) Thrust force

- 11.6 Prove that the thrust force of a rocket motor is expressed by the relation

$$\frac{T}{P_{0t}A_t} = \sqrt{\left(\frac{2\gamma^2}{\gamma-1}\right)\left(\frac{2}{\gamma+1}\right)^{\frac{\gamma+1}{\gamma-1}} \left[1 - \left(\frac{P_e}{P_{0t}}\right)^{\frac{\gamma-1}{\gamma}}\right] + \left(\frac{P_e}{P_{0t}} - \frac{P_a}{P_{0t}}\right) \frac{A_e}{A_t}}$$

where:

P_{0t} = total pressure in combustion chamber

P_e = nozzle exit pressure

A_t = nozzle throat area

A_e = nozzle exit area

γ = ratio of specific heats

- 11.7 Given the following data for a rocket:

Time (s)	0	0.5	1.0	2.0	2.5	3.0	3.25	3.3
Thrust (N)	4500	6000	5250	5400	5400	5100	5400	0

determine the total impulse of the motor.

- 11.8 Given the following data for a flying model rocket:

Time (s)	0	0.3	0.5	1.0	1.5	2.0	2.1
Thrust (N)	0	14	7	7	7	7	0

determine the total impulse of the motor.

- 11.9 Prove that if the payload ratio (λ) and the structural ratio (ϵ) are defined as

$$\lambda = \frac{m_L}{m_0 - m_L} \text{ and } \epsilon = \frac{m_s}{m_0 - m_L}$$

then

$$\lambda = \frac{e^{-\left(\frac{\Delta u}{V_{\text{eff}}}\right)} - \epsilon}{1 - e^{-\left(\frac{\Delta u}{V_{\text{eff}}}\right)}}$$

Next, plot (λ) versus $(\frac{\Delta u}{V_{\text{eff}}})$ for $\epsilon = 0.05 - 0.20$ and $\frac{\Delta u}{V_{\text{eff}}} = 1.5 - 3.0$.

- 11.10 Calculate the total speed (Δu) of a three-staged rocket having the following data:

Stage	Structural mass (m_s) tons	Propellant mass (m_p) tons	Effective speed (V_{eff}) m/s
1	5	40	2400
2	1	10	2600
3	0.2	1	3000

The payload mass that has to be put into orbit is 800 kg:

- (a) If a simple single-stage-to-orbit (SSTO) rocket having the same payload, total structural mass, and total propellant mass is used, calculate the rocket speed.
- (b) What is the gain in rocket speed when a three-stage case is used compared to the SSTO rocket?
- 11.11 A two-stage rocket has the following data: first-stage propellant mass 120,000 kg, first-stage dry mass 9000 kg, second-stage propellant mass 30,000 kg, second-stage dry mass 3000 kg, and payload mass 3000 kg. The specific impulses of the first and second stages are 260 s and 320 s, respectively. Calculate the rocket's total ΔV :

Stage	Propellant mass (m_p) ton	Dry mass (m_s) tons	Specific impulse (sec)
1	120	30	270
2	30	3	315

If the payload mass is 3000 kg, calculate the total speed (Δu) of this two-staged rocket.

- 11.12 A rocket engine which has an exhaust velocity of 3000 m/s is used accelerate a vertically launched rocket vehicle to a speed of 3800 m/s. Find the approximate ratio of the propellant mass to the dry vehicle mass required.
- 11.13 A single-stage rocket has the following design parameters:

- Combustion chamber temperature = 4000 K
- Combustion chamber pressure = 6 MPa
- Nozzle throat area = 0.0008 m²
- Nozzle exit area = 0.01 m²
- Propellant mass = 30 kg
- Total mass at takeoff = 45 kg
- Gas constant = 300 J/kg K
- Ratio of specific heats = 1.35

Calculate

- (a) The specific impulse I_{sp}
- (b) Takeoff thrust
- (c) The rocket height assuming the rocket is launched vertically and aerodynamic drag is neglected

11.14 Determine the ratio of the burning area to the nozzle throat area for a solid-propellant rocket motor with the following characteristics:

- Burning rate data: $n = 0.4$, $a = 0.0076$
- Chamber pressure: 6.895 MPa
- Propellant weight density: 1722 kg/m³
- Specific heat ratio of combustion products 1.19
- Gas constant $(R = 400 \frac{\text{J}}{\text{kg.K}})$
- Propellant flame temperature: 3055 K

11.15 The low-pressure oxygen turbopump (LPOTP) has the following data:

$$p_{0i} = 689.5 \text{ kPa}, p_{0e} = 2.895 \text{ MPa}, \dot{m}_{o2} = 70 \frac{\text{kg}}{\text{s}}$$

$$\eta_{o2} = 0.677, \rho_{o2} = 1140 \frac{\text{kg}}{\text{m}^3}$$

The low-pressure fuel turbopump (LPFTP) has the following data:

$$p_{0i} = 207 \text{ kPa}, p_{0e} = 2.0 \text{ MPa}, \dot{m}_f = 13.15 \frac{\text{kg}}{\text{s}}$$

$$\eta_f = 0.713, \rho_f = 70.8 \frac{\text{kg}}{\text{m}^3}$$

If the mechanical efficiency for power transmission from turbine to the pump in both turbopumps is equal and has a numeric value $\eta_m = 0.99$,

calculate the turbine power in both turbopumps.

11.16 An axial turbine is used as a power source in a rocket turbopump. The turbine is a single stage and of the impulse type. The maximum tip speed $U_t = 500 \text{ m/s}$, and a rotational speed $N = 72600 \text{ rpm}$. Liquid oxygen flows at the rate of 5.27 kg/s into the turbine having a total temperature and pressure of $T_{01} = 1000 \text{ K}$, $P_{01} = 10 \text{ MPa}$. The exit static pressure $P_2 = 1.0 \text{ MPa}$, and turbine efficiency $\eta_t = 0.55$. Flow in the stator is assumed ideal and flow has an axial absolute exit velocity from the rotor blade row. The working fluid has a specific heat $C_P = 7757 \frac{\text{J}}{\text{kg.K}}$ and specific heat ratio $\gamma = 1.357$:

1. Calculate the spouting velocity.
2. Calculate the power generated.
3. Rotor tip diameter.

- 11.17 The thrust-time profiles for the three cases of propellant burning are expressed by the following expressions:

Neutral profile $T = 6000 \text{ N}$

Progressive profile $T = 6000 + 500t$

Regressive profile $T = 6000 - 600t$

For a burning time of 3 s in all cases, calculate the total impulse.

- 11.18 A rocket has the following data:

Thrust = 9000 N, propellant combustion = 3.9 kg/s, rocket speed $u = 420 \text{ m/s}$, heat of combustion : $Q_R = 7.0 \text{ MJ/kg}$, and combustion efficiency $\eta_c = 99\%$.

Calculate:

Effective exhaust velocity

Thermal (internal) efficiency

Propulsive (external) efficiency

Overall efficiency

Specific propellant consumption

- 11.19 A spacecraft having a mass of 5000 kg is traveling at a velocity of 8000 m/s in the Earth orbit. Its engine burns fuel to accelerate it to a velocity of 12,000 m/s placing it on an escape trajectory. The engine expels mass at a rate of 10 kg/s and an effective velocity of 4000 m/s. Calculate the duration of the burn.

- 11.20 A small three-stage rocket is designed, having a payload weight of 10 kg (Fig. 11.14). Data for the rocket is given in Table 11.16. Calculate the increase in its speed (Δu).

- 11.21 In the previous problem, launching of Ariane 5 was analyzed. It is required to calculate the total change in rocket velocity when it is used to deliver payloads into the **low Earth orbit** (LEO). Details of masses of its 0 stage (boosters), first stage, and second stage are given in Table 11.17.

Payload or mass to LEO = 10.5 ton.

- 11.22 Deduce two relations for rate of change of burning area in the following burning cases:

1. End burning only (the hollow core of solid propellant remains uniform during burning).

Table 11.16 Data for a three-stage rocket

Stage number	Specific impulse (I_{sp}) second	Structural mass (m_{si}) kg	Propellant mass (m_{pi}) kg
1	285	40	50
2	265	22	15
3	290	12	9

Table 11.17 Data for a booster and two-stage rocket

Stage	0 stage (two boosters)	First stage	Second stage
Propellant mass (ton)	237	170	15
Dry mass (ton)	268	16.3	4.7
Specific impulse I_{Sp} (s)	283		446

2. Radial burning only (the length of propellant remains constant during burning).
 3. Recalculate the rate of change of combustion chamber having the same data in Example (11.14) in the two above cases.
- 11.23 A solid rocket motor burns along the face of a central cylindrical channel 10 m long and 1 m in diameter. The propellant has a burn rate coefficient of 5.6, a pressure exponent of 0.4, and a density of 1760 kg/m³. Calculate the burn rate and the product generation rate when the chamber pressure is 7.0 MPa.
- 11.24 The shown Fig. 11.27 illustrates a turbopump of the gas generator type. It has the following data:

Fuel pump

$$p_{01} = 0.15 \text{ MPa}, p_{02} = 3.5 \text{ MPa}, \dot{m}_f = 25 \frac{\text{kg}}{\text{s}}, \eta_{fp} = 0.7, \rho_f = 800 \frac{\text{kg}}{\text{m}^3}$$

Oxygen pump

$$p_{06} = 0.2 \text{ MPa}, p_{07} = 3.5 \text{ MPa}, \dot{m}_{O2} = 60 \frac{\text{kg}}{\text{s}}, \eta_{O2} = 0.66, \rho_{O2} = 1150 \text{ kg/m}^3$$

Turbine

$$p_{010} = 1.3 \text{ MPa}, T_{010} = 800 \text{ K}, \\ \dot{m}_{10} = 1.7 \frac{\text{kg}}{\text{s}}, \eta_t = 0.72, C_p = 1.06 \frac{\text{kJ}}{\text{kg.K}}, \gamma = 1.3$$

Mechanical efficiency $\eta_m = 0.99$

Combustion chamber

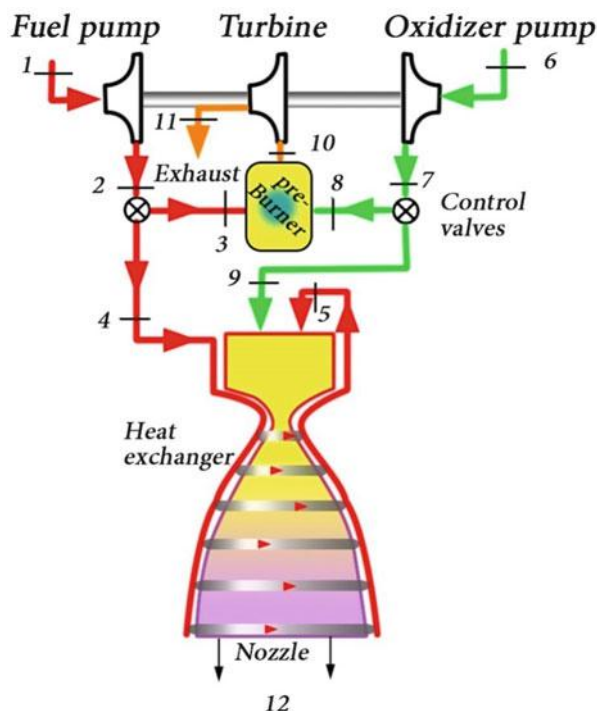
$$p_c = p_{05} = p_{09} = 3.0 \text{ MPa}, T_c = 3000 \text{ K}$$

Nozzle

Full expansion to ambient pressure

$$p_{12} = p_a = 0.1 \text{ MPa}, \eta_n = 0.9, C_p = 1.05 \frac{\text{kJ}}{\text{kg.K}}, \gamma = 1.28$$

Fig. 11.27 Layout of a turbopump of the gas generator type



Calculate

1. The turbine exhaust pressure
2. The exhaust velocity
3. Thrust force

References

1. <http://www.reactionengines.co.uk/index.html>
2. Gruntman M (2004) Blazing the trail: the early history of spacecraft and rocketry, chapters 1–2. AIAA
3. Lyon JM (1991) Introduction to rocket propulsion, technical report RD-PR-91-17, Dec 1991, US Army Missile Command
4. Sutton GP, Oscar B (2010) Rocket propulsion elements, 8th edn. Wiley, New York
5. Turner MJL (2009) Rocket and spacecraft propulsion- principles, practice and new development, 3rd edn. Springer, Berlin/New York
6. Yehia SM (1982) Fundamentals of compressible flow with aircraft and rocket propulsion, SI 8th edn. New Age International Publisher, New Delhi
7. <http://history.msfc.nasa.gov/rocketry/>

8. Haidn OJ (2008) Advanced rocket engines, RTO-EN-AVT-150, Paper 6
9. Multi-stage rockets. Valkyrie report no 5105
10. Hill P, Peterson C (1992) Mechanics and thermodynamics of propulsion, 2nd edn. Addison-Wesley Publishing Co, Reading
11. Demyanenko Y, Dmitrenko A, Ivanov A, Pershin V. Turbopumps for gas generator and staged combustion cycle rocket engines, AIAA 2005–3946
12. Mårtensson H, Andersson S, Trollheden S, Brodin S. Rocket engines: turbomachinery, advances on propulsion technology for high-speed aircraft. Educational Notes RTO-EN-AVT-150, Paper 5, pp 5-1–5-28
13. Turbopump systems for liquid rocket engines (1974) NASA/SP-8107, August, 1974
14. Liquid rocket engine: a centrifugal flow turbopumps, NASA SP 8109
15. Huzel DK, Huang DH (1967) Design of liquid propellant rocket engines, NASA SP-125. NASA, Washington, DC
16. Huppert MC, Rothe K (1974) Axial pumps for propulsion systems, fluid mechanics, acoustics and design of fluid machinery, vol 2, NASA SP-304. NASA, Washington, DC, pp 623–654
17. Balje OM (1959) Study of turbine and turbopump design parameters: vol. IV- low specific speed turboprop study, S/TD No. 1735, No.20. The Sundstrand Corporation, Rockford
18. Sutton GP (2006) Turbopumps, a historical perspective. In: 42nd AIAA/ASME/SAE/ASEE Joint propulsion conference & exhibit, Sacramento, California, 9–12 July 2006
19. Loh WHT (1968) Jet, rocket, nuclear, ion and electric propulsion, theory and design. Springer, New York
20. Ragsdale R (1990) Open cycle gas core nuclear rockets. In: Proceedings of the nuclear thermal propulsion workshop, NASA Lewis Research Center, pp 343–357
21. Jahn RG (1968) Physics of electric propulsion. McGraw-Hill, New York
22. Van Pel M (2009) Space tethers and space elevators. Springer, New York, p 24
23. Martinez-Sanchez M, Pollard JE (1998) Spacecraft electric propulsion: an overview. *J Propuls Power* 14(5):688–699
24. Goebel DM, Katz I (2008) Fundamentals of electric propulsion: ion and hall thrusters. Wiley, Hoboken
25. Brophy JR (2002) NASA's deep space 1 ion engine. *Rev Sci Instrum* 73:1071–1078

Appendices

Appendix A

Short list of milestones for aircrafts powered by piston engines

	Manufacturer	Engine	Max. power	Aircraft	Propeller
1903	Wrights brothers	In-line 4 stroke water cooled	12 hp	Flyer I	Two pusher propellers each two-bladed
1908	Societe des Moteurs Gnome et Rhône	Gnome Omega rotary engine	110 hp	Sopwith Camel replica	
1925	Pratt & Whitney	R1340 Wasp	542 hp	Boeing 247, Fokker F32	
1929	Pratt & Whitney	R-985 Wasp Junior	440–600 hp	Bell XV-3 , Grumman G-21 , Goose	
1933	Rolls-Royce Meteor	Royce Merlin 45 engine liquid-cooled supercharged V-12	1470 hp	Avro Lancaster, de Havilland Mosquito, Supermarine Spitfire, Hawker Hurricane	3–5 blades propellers varying from fixed to constant speed types
1934	de Havilland	Gipsy Six/inline engine	200 hp	de Havilland Dragon Rapide	2 propellers Puller type
1937	Pratt & Whitney	R-2800 Double Wasp	2100 hp	Curtiss P-60 , Sikorsky S-60	Contra-rotating propeller
1944	Pratt & Whitney	R-4360 “Wasp Major”	3500	Hughes H-4 Hercules (8 engines)	Four-bladed Hamilton Standard , propeller dia. 17 ft 2 in (5.23 m)

(continued)

	Manufacturer	Engine	Max. power	Aircraft	Propeller
1945	Pratt & Whitney	R-2800-34 W Double Wasp two-row radial engine	2100 hp	Grumman F8F Bearcat	Aero Products four-bladed 12 ft 4 in propeller
1954	Wright Aeronautical	One Wright R182084 radial piston engine	1525 hp	Sikorsky S58	Helicopter 4-bladed rotor
1962, 1971	Continental Motors	Continental IO-360	195–210 hp	Piper PA-34 Seneca, Cirrus SR20	3-bladed puller
1998–now	SMA Engines	SR305-230 four-cylinder/ four-stroke diesel	(227 hp) at 2200 rpm	Cessna 182	3-bladed constant speed
2004	Diamond Aircraft Industries	Thielert Centurion turbocharged diesel engine	135 hp each	Diamond DA42, Cessna 172 Skyhawk TD	3-bladed puller
2008	IndUS Aviation	Jabiru 2200, 3300, Continental O-200A	120 hp	Light-sport aircraft (LSA SkySkooter (T-111), the Thorpedo DP	Puller propeller
	General Atomics	Rotax 912 4-cyl. liquid-cooled horizontally opposed with a two-stage turbocharger,	100 hp	Apollo Jet Star, Skyleader 200	2-bladed pusher propeller

Appendix B

Milestone of turbojet engines

Year	Manufacturer	Engine name	Maximum power	Aircraft name
1939	Dr. von Ohain (first turbojet)	He S3	1100 lbf	He 178
1939	German Aircraft Manufacturer	Jumo 004	10.8 kN	Me 262
1941	British Thomson-Houston (BTH) (first british turbojet)	Power Jet (or Whittle WI)	850 lbf	Gloster E28/39
October 2, 1942	General Electric (first US turbojet)	IA	1250 lb 5560 N	Bell XP-59A Airacomet
1942	General Electric	J33	20.4 kN	Convair XF-92, Lockheed P-80

(continued)

Year	Manufacturer	Engine name	Maximum power	Aircraft name
1943	<i>Reichsluftfahrtministerium, RLM</i>	Junkers Jumo 004-B	2000 lb	German: Me 262, Ar 234 A/B, Ju 278, He 343, Me P1101, Ho IX/Go 229, and Ta 183 V-1 and French So 6000 (Triton)
1945	<i>Rolls-Royce</i>	RB82	10.8 kN	Vickers 825
1946	Rolls-Royce	Nene	22.2 kN	Hawker P.1052, Vickers VC.1 Viking
1947	Kirill Klimov	VK-1	15.9 kN	MiG 15, MiG 17, Ilyushin II-28
1947	Kirill Klimov	RD-500	26.5 kN	Lavochkin La-15, Lavochkin La-23, Lavochkin La-30
1952	Pratt & Whitney	J57	53.5 kN	B-52 Stratofortress KC-135 Stratotanker B-57 Canberra Boeing 707 Douglas DC-8 F-8 Crusader F-100 Super Sabre
1956	Pratt & Whitney	J52-P8A	41 kN	Douglas A-4 Skyhawk
1956	Sergei Tumansky	R-11F2S	60.3 kN	MiG 21, Sukhoi Su-15
1957	General Electric	J47 ^a	29 kN	B-36, B-45, B-47, F86, XB-51
1958	General Electric	J79	Dry: 47 kN Wet: 69 kN	Lockheed F-104, Convair B-58 Hustler
1958	Pratt&Whitney	J58	Dry:120 kN Wet: 150 kN	Lockheed A-12, Lockheed SR-71
1958	Pratt & Whitney	J57	53.5 kN 76.5 kN with afterburner	Boeing 707, Boeing B-52 Stratofortress, Vought F-8
1963	General Electric	J71	58 kN	F105, F3H-2
1964	General Electric	J85	79 kN	Cessna A-37, F-5E Tiger II
1967	Lyulka	Lyulka AL-21	Dry: 76.4 kN Wet: 109.8 kN	MiG-19S and MiG-19PF
1967	General Electric	GE4 ^b	Dry: 220 kN 281 kN with afterburning	Boeing 2707
1968	Kolesov	RD-36-51	Wet: 200 kN	Tu-144

(continued)

Year	Manufacturer	Engine name	Maximum power	Aircraft name
1969	Rolls-Royce/SNECMA	Mk 610	Dry: 140 kN Wet: 169 kN	Concorde
1960s-Now	General Electric	CJ610 ^c	12.7–13.8 kN	Aero Commander 1121 Jet Commander – HFB-320 Hansa Jet – Learjet 23, 24, 25, 28, 29

^aGE's J47 turbojet is the first jet engine certified for use on a commercial transport (number built is 36,500)

^bGeneral Electric's GE4 prototype turbojet is the world's most powerful jet engine which was designed for the US Supersonic Transport. It establishes a new thrust record of 63,200 pounds

^cCJ610 turbojet, derivative of J85 engine, certificated by FAA for commercial use Compact, lightweight design makes it suitable for small single and multi-engine business jet applications

Appendix C

Milestones of turbofan engines

Year	Manufacturer	Engine	Notes
1943	Daimler-Benz	DB-007	First running turbofan, bypass ratio: 71 %
1943	Metropolitan-Vickers	Metrovick F.3	The first British turbofan, bypass ratio: ~2.9
1950s	Rolls-Royce	RB.80 Conway	First RR turbofan engine, bypass ratio of about 25 %. Major applications: Boeing 707, Douglas DC-8, Vickers VC10
1958	General Electric	CJ805-23 – military designation TF35	A turbofan derivative of turbojet CJ805-3, powered the Convair 990 airliners
1960s	General Electric	TF39 engine	The first high-bypass turbofan engine (8:1). Powered: Lockheed C-5 Galaxy military transport aircraft.
1960s	Pratt & Whitney	TF30 low-bypass military engine	Originally designed for the subsonic F6D Missileer missile carrier. It was later adapted with an afterburner to be the world's first production of afterburning turbofan to power the F-111 and the F-14A Tomcat
1964	P&W Aircraft	STF200 experimental turbofan	It delivered 140 kN thrust from 2:1 bypass-ratio engine
1967	Rolls-Royce	RB.203 Trent engine	Medium-bypass turbofan engine of around 10,000 lb

(continued)

Year	Manufacturer	Engine	Notes
1969	Rolls-Royce	RB2111	The first three-spool engine, bypass ratio:5–1
1969	Pratt & Whitney	JT9D	The first high-bypass-ratio jet engine to power a wide-body aircraft . It was the company's first high-bypass-ratio turbofan
1970	Honeywell, USA	TFE731	The first geared turbofan engines. Originally designed/built by Garrett AiResearch, later produced by AlliedSignal and currently Honeywell Aerospace
1971	General Electric	CF6	Airbus A300 , Airbus A330 , Boeing 747 , Boeing 767 , McDonnell Douglas DC-10 , MD-11 Lockheed C-5 M Super Galaxy
1974	CFM International	CFM56	Since 1974, it is the most common turbofan engines in the world, (more than 20,000 engines in four major variants). Boeing 737, Airbus A320 and A340
1980	Lycoming Engines/ Honeywell Aerospace	ALF 502	One of the first geared turbofan engines. Powered the British Aerospace 146 and Bombardier Challenger 600. The improved, higher-thrust LF 507 was used on the Avro RJ
1980s	General Electric	GE YF120	A variable cycle bypass ratio for different flight regimes and more efficient at high altitude comparable to traditional low bypass turbofans. Complexity and extra weight are its disadvantages, which may be overcome by using simple pressure driven valves rather than complex mechanical ones
1990	Rolls-Royce	Trent series	A family of high bypass turbofan engines, developed from RB211 with thrust ratings of 240–420 kN. Trent power Airbus A330, A340, and A380, Boeing 777 and 787
1990s	General Electric	GE CF-34 engine	Uses the “soft-wall” approach for fan casing which involves wrapping a thick, high-strength fabric around a thinner aluminum fan casing
1995	General Electric	The GE90 engine	Holds two records; namely, highest BPR (12:1) and highest pressure ratio of 45:1. Used for Boeing 777 series

(continued)

Year	Manufacturer	Engine	Notes
1998	Pratt & Whitney	PW8000 engine	Pratt & Whitney first P&W geared turbofan. It is an upgrade of the existing PW6000 that replaced the fan section with a gearing system and new single-stage fan
2001	General Electric	GE90-115B	The Guinness Book of World Records recognized the engine as the “World’s Most Powerful Commercial Jet Engine” with 123,000-lb thrust
2003	General Electric	GE CF34-8C5	The first application of chevrons (sawtooth patterns on the trailing edges of nozzles) on the Bombardier CRJ900 aircraft for noise reduction
Nov 10, 2005	General Electric	GE90-110B1	GE90-110B1 entered the Guinness World Records when powered a 777-200LR during the world's longest flight (21,601 km) (22 h, 42 min) from Hong Kong to London “the long way”: over the Pacific, the Continental United States, the Atlantic to London
2006	General electric	GEnx	<p>First to use:</p> <p>°Gamma TiAl low pressure turbine blades</p> <p>°Fan case manufactured entirely from composite materials</p> <p>Powers Boeing 787; Dreamliner, B777, B747-8</p>
Feb 2008	Virgin Atlantic/England	Boeing 747-400	Virgin Atlantic flew the very first biofuel test flight between London and Amsterdam, using a 20 % blend of biofuels in one of its engines, the biofuel being Coconut and Babassu oil
July 2008	Pratt and Whitney	PW1000G program for a geared turbofan (GTF)	<p>GTF was renamed the PW1000G, as the new line of “PurePower” engines. PW1000G is:</p> <p>10–15 % more fuel efficient</p> <p>Substantially quieter</p>
Jan 2009	CFM International	CFM56-7B26	Continental Airlines 737-800 ran the first flight of an algae-fueled jet. The flight from Houston’s George Bush Intercontinental Airport completed a circuit over the Gulf of Mexico
25, Mar 2010	General Electric	TF34	USAF Fairchild Republic A-10 Thunderbolt II conducted the first flight of an aircraft with all engines

(continued)

Year	Manufacturer	Engine	Notes
			powered by a biofuel blend. The flight used a 50/50 blend of JP-8 and Camelina -based fuel
Apr 2010	General Electric	F414 turbofan	The Navy tested this biofuel blend Camelina on the fighter jet F/A-18 Super Hornet, aka “Green Hornet.” Results indicated the aircraft performed as expected through its full flight envelope with no degradation of capability
Jun 2011	CFM International	CFM56-7 series	KLM flew Boeing 737-800, the world’s first commercial biofuel flight, carrying 171 passengers from Amsterdam to Paris, using biofuel derived from used cooking oil
Oct 2012	National Research Council, Canada, and Dassault Falcon 20	General Electric CF700 turbofans	First jet to fly on 100 % <i>biofuels</i> that meet petroleum specifications without blending. Fuel was produced from carinata oil supplied by Agrisoma Biosciences
2013	Pratt and Whitney	Pratt & Whitney PW1000G engine	A high-bypass geared turbofan engine selected for the Bombardier CSeries (2015), Airbus A320neo (2015), Mitsubishi Regional Jet (2017), Irkut MS-21 (2017), and Embraer’s second-generation E-Jets (2018)
2016	CFM International	LEAP-X engine	The LEAP engine will be the first commercial engine with CMC “Ceramic Matrix Composites” turbine components, with future plans to extend CMC use throughout the engine hot section

Appendix D

Milestone of rockets

400 BC	Archytas; a Greek lived in Southern Italy used reaction principle in flying wooden pigeon
67AD	<i>Hero</i> , a second Greek who lived in Alexandria, Egypt, invented the rocket principle. His aeolipile machine was working on the reaction principle (discovered later on by Sir I. Newton) and steam power (also discovered later by James Watt)

(continued)

First century	<i>Chinese</i> used a simple form of gunpowder made from saltpeter, sulfur, and AD charcoal dust. They put the gunpowder in bamboo tubes and tossed them in fire mostly for fireworks in religious and other festive celebrations
970 AD	<i>Feng Jishen</i> , a Chinese considered as the real inventor of rockets
1200s	<i>Tatars and Moors</i> used rockets in their invasion to Europe
1232	<i>Chinese</i> repelled the Mongol invaders during the battle of Kai-Keng by a barrage of “arrows of flying fire.” These fire arrows were a simple form of a solid-propellant rocket. A tube, capped at one end, contained gunpowder. The other end was left open and the tube was attached to a long stick. Chinese Wan Hu tried to fly in a rocket propelled chair, but died in the explosion before taking off
1275	<i>Kubali Kahn</i> used rocket in Japanese invasion
1650	<i>Kazimierz Siemienowicz</i> , a Polish artillery expert, published a series of drawings for a staged rocket
1642–1727	<i>Sir Isaac Newton</i> laid the scientific foundations for modern rocketry through his three laws of motion
1700s	<i>Hyder Ali</i> and his son Tipu Sultan, Mysore, India, used rockets against British invasion to India
1806	<i>William Congreve</i> ’s incendiary rocket used black powder, an iron case, and a 16-foot guide stick. The British used Congreve rockets in 1806 to attack Napoleon’s headquarters in France
1807	<i>Congreve</i> directed a rocket attack against Copenhagen; approximately 25,000 rockets were fired
1875–1935	<i>Konstantin Tsiolkovsky</i> , mathematician who developed rocket equation and wrote on multistage rockets, artificial satellites, and space travel
1923	<i>Hermann Oberth</i> , a Romanian, published a book on rocket travel into outer space
1926	<i>Robert Goddard</i> , an American, launched the first liquid-propellant (gasoline and liquid oxygen, LOX) rocket. He was granted 214 patents on liquid fuelled rocket engines. He conducted practical experiments in rocketry. He developed the single and multistage rocket engines for both rocket and jet-assisted take-off (JATO) aircraft in 1945
1930	<i>Wernher von Braun</i> assisted Oberth in his early experiments in testing a liquid-fueled rocket with about 15 pounds of thrust
1942	The V-2 was the world’s first long-range ballistic missile ; Fig. 11.2. The liquid-propellant rocket was developed during the Second World War in Germany as a “vengeance weapon,” designed to attack Allied cities as a form of retaliation for the ever-increasing Allied bomber effort against German cities. The V-2 rocket was also the first man-made object to enter the fringes of space
1957 (Oct. 4)	Soviet Union stunned the world by launching an Earth-orbiting artificial satellite called <i>Sputnik I</i> , the satellite was the first successful entry
1957 (Nov. 3)	Soviets launched satellite <i>Sputnik II</i> carrying a dog named Laika on board
1957 (Jan. 31)	<i>Jupiter-C</i> rocket carried the US satellite Explorer I into space
1961 (Apr. 12)	<i>Yuri Alekseyevich Gagarin</i> (Russian) was a Soviet pilot and cosmonaut . He was the first human to journey into outer space , when his Vostok spacecraft completed an orbit of the Earth

(continued)

1961 (May 5)	<i>Allan Shepard</i> , the first American astronaut to ride to space on, Shepard rode inside a Mercury space capsule on top of a Redstone rocket
1965	NASA's <i>Scout rocket</i> (a four-stage solid rocket booster) carried Explorer 27 scientific satellite
1965 (March)	<i>Virgil I. Grissom</i> and John W. Young rode to orbit inside a Gemini spacecraft mounted at the top of Titan rocket. The spacecraft reached an orbit ranging from 161 to 225 km on
1969 (July 20)	<i>Apollo 11</i> was the spaceflight launched by a Saturn V rocket (111 meter high) from Kennedy Space Center and landed the first humans on the Moon , Americans Neil Armstrong and Buzz Aldrin , on July 20, 1969, at 20:18 UTC. Armstrong became the first to step onto the lunar surface 6 h later on July 21 at 02:56 UTC
1970 (Aug. 17)	Venera-7 (USSR) was launched for Venus, which landed on Dec. 15
1972 (Dec. 7)	Apollo-17, took three men crew for Moon, landed on Dec 11, 1972, had a total stay on Moon of 75 h, and traversed 26 km on lunar surface
1975 (Sep. 5)	A Titan III Centaur rocket carried Voyager 1, the first interplanetary spacecraft to fly
Sep 21, 1984	NASA's rocket Delta lifted the Galaxy-C communication satellite to space
1990 (April 5)	The Pegasus air-launched space booster roars toward orbit following its release from a NASA B-52 aircraft
1992 (Dec. 2)	NASA Astronauts launch into space onboard the Space Shuttle. The Shuttle consists of a winged orbiter that climbs into space as a rocket, orbits Earth as a satellite, and lands on a runway as an airplane
1981–2011	A total of 135 missions from 1981 to 2011 of the <i>Space Shuttle</i> ; a crewed, partially reusable low Earth orbital spacecraft operated by the US National Aeronautics and Space Administration (NASA)

Index

A

Adiabatic efficiency, 410, 412, 637, 823, 826
Advance ratio, 288, 293–301, 304, 305, 313
Advantages and disadvantages of hybrid rocket engines, 980–981
Advantages of rocket staging, 940–941
Aerial cranes, 38, 44
Aerial firefighting-attack, 11–12, 40
Aerial refueling, 27–28, 101, 614
Aerodynamics, viii, 3–5, 49, 50
Aerostats, viii, 3–5, 49, 50
Afterburner, vii, ix, x, 70, 72, 73, 75, 76, 221, 338, 405, 407–410, 413–417, 430–432, 434–437, 439, 440, 446, 447, 464–468, 483, 484, 486, 487, 492, 493, 500, 503, 507, 508, 512, 513, 520–522, 527, 637, 653, 666, 675–677, 700, 995, 996
Aft-fan, 73, 75, 447, 568
Agricultural aircrafts, 10, 50, 207
Agriculture, 9, 37, 39
Airborne reconnaissance, 28–29
Airborne Warning and Control System (AWACS), 26–30, 84
Aircraft propellers, 241, 242, 261–265, 393, 703, 704, 993–994
Aircraft range, 178, 200–204
Altitude, 50, 98, 161, 222, 316, 408, 547, 621, 738, 908
Analogy between turboprop and turbofan engines, x, 552
Angular momentum equation, 103–106
Annular combustion chamber, 62, 656–658
Appendix A, 223, 993–994
Appendix B, 407, 994–996
Appendix C, 446, 996–999

Appendix D, 908–909, 999–1001

Athodyd engines, viii, 315, 386, 403
Autogyro, 5, 31–34, 84
AWACS. *See* Airborne Warning and Control System (AWACS)
Axial flow compressor, 405, 408, 654, 658, 704, 705, 747–818
Axial flow turbine, xi, 839–872, 895, 896
Axial momentum, (or actuator disk) theory, 274–281
Axial speed, 652, 739, 755, 757, 796, 807, 818, 824, 834, 835, 847, 848, 859, 863, 901, 973

B

Bipropellant liquid rocket, 963–964, 977
Blackbird, 28, 71, 154, 161, 481, 487, 509
Blade loading coefficient (or temperature drop coefficient) of turbine, 846
Blade material selection, 808
Bleed, 174, 178, 410, 417, 451, 457, 459, 471, 472, 474, 476, 481, 520, 523, 541, 547, 557, 572, 587, 773, 815, 816, 818, 820, 839, 886, 892
Bomber, 11–12, 21–26, 28, 31, 49, 50, 53, 54, 58, 65, 82, 83, 206, 207, 229, 231, 317, 386, 404, 483, 484, 534, 537, 608, 613, 1000
Bore, 232, 248, 249, 269, 305, 307, 309, 331
Burner, 53, 63, 64, 72, 321, 324, 341, 343–346, 352, 354, 368–370, 372, 386, 389, 395, 399, 408, 410, 417, 422, 431, 487, 493, 500, 501, 519, 526, 580, 583, 645, 653, 655, 656, 658, 666, 670, 676, 969, 970

- Burning rate, 950–959, 977, 987
 Bypass ratio, x, 72, 73, 75, 78, 173, 181, 184,
 185, 190, 191, 194, 215, 217, 446–448,
 454, 457, 459, 464, 465, 490, 498,
 520–524, 552, 565, 572, 584, 587, 595,
 621, 632, 633, 678, 684, 748, 750–751,
 817, 900, 903, 996, 997
- C**
 Can-annular combustor, 660
 Capture area, 623–632, 641, 642
 Cargo aircrafts, 14–15, 20, 27, 532, 591, 621
 Cascade, 282, 598, 707–708, 735–736, 751,
 768, 795, 808–811, 867
 Casing, 73, 225, 445, 634, 654, 655, 657, 658,
 704, 708, 711, 716, 736, 738, 748, 750,
 753, 773, 794, 797, 867, 907, 946, 949,
 972, 973, 997
 Centrifugal bending stress, 764–766
 Characteristic velocity of rocket, 914, 922,
 926, 955
 Chemical rocket engines, 945–946
 Chemistry of combustion, x, 665–667
 Choking point, 745, 833
 Chord length, 283–284, 301, 303
 Civil aircrafts, 3, 9–20, 71, 430, 461, 532,
 592, 603
 Civil helicopters, 37, 50
 Classification of ramjet engines, 337–364
 Classification of turbofan engines, 446–448
 Classification of turbojet engine, 406–407
 Classification of turboprop engines, 532–552
 Classifications based on rotor, 31–44
 Classifications of aircrafts, 1–89
 Classifications of propfans, 567–569
 Classifications of rockets, xi, 912–914
 Coaxial rotors, 35, 36
 Coleopter, 5, 45–46
 Combat Fixed Wing Military Aircrafts, 21
 Combined fuselage and tail installation, 599
 Combined wing and tail installation (three
 engines), 598
 Combustion, 51, 120, 180, 219, 315, 403, 538,
 590, 708, 886, 907
 Combustion chamber, 60, 120, 180, 315, 404,
 538, 590, 708, 886, 907
 Commercial transport, 9, 14–20, 37, 58, 69, 86,
 482–483, 996
 Commuter, 15–17, 60, 83, 531, 532, 577, 599
 Comparisons between turboprop, propfan and
 turbofan, 569–587
 Components of combustion chamber, 658–661
 Composition of a solid propellant, 948–949
 Compressor efficiency, 410, 500, 720, 728,
 743, 797, 822, 833, 886, 893, 894
 Compressor map, 296, 742–746, 752, 813–819,
 886, 887, 890–892, 894
 Conceptual design procedure for axial
 compressor, 794–808
 Continuity equation, 92, 94–96, 99, 126, 147,
 167, 345, 553
 Control volume, viii, 91–95, 97–101, 104,
 105, 107–109, 123, 131, 499, 554–556,
 586, 587, 633, 647, 668, 711, 714, 715,
 915, 916
 Convection turbine cooling, 868–869
 Convergent divergent nozzle, 134, 392, 468,
 496, 677, 678, 680, 682, 684–686, 689,
 699, 920, 945, 981
 Convergent nozzle, 160, 175, 195, 392, 677,
 680, 682, 897, 898
 Cooling, xi, 57, 58, 76, 219, 223–225, 228, 258,
 305, 309, 343, 367, 403, 410, 417, 459,
 571, 590, 655, 658–660, 674, 676, 682,
 692, 867–869, 901, 960, 961, 968, 970,
 971, 980
 Critical point, 137, 209, 212–213
 Cruise, 3, 43, 58, 60, 72, 76, 86, 153, 161,
 162, 165–167, 181, 200, 203, 204, 206,
 210–212, 214, 218, 221, 279, 312, 317,
 318, 331, 361, 404, 408, 410, 441, 454,
 465, 479, 500, 508, 516, 517, 545, 562,
 572, 585, 590, 616–619, 623–625, 627,
 633–635, 670, 697, 912
- D**
 Degree of reaction, 735, 770–773, 777, 778,
 783, 784, 789–791, 799, 804–808, 827,
 829, 831, 832, 834, 835, 846–858, 863,
 864, 895–901
 Design point, 643, 744, 813, 815, 883, 885,
 902, 903
 Diesel cycle, 235, 252, 254–256, 306, 308–310
 Diffuser, 64, 110, 231, 316, 408, 557, 589, 707,
 873, 972
 Diffuser efficiency, 410, 620, 877
 Dimensionless parameters for propellers,
 287–293
 Dimensionless parameters for turbines,
 878–879
 Direction of propeller rotation, 269
 Displacement volume, 232, 242, 248, 249, 310
 Double spool, ix, x, 405–407, 447–461,
 556–557

- Double spool turbofan double spool turboshaft, 558–564
Double spool turbojet, 430–441, 493
Double spool turboprop, 544, 547
Dual-entry impellers, 709
Dual-mode combustion engine (dual ram-scram jet), 376, 386
- E**
Effective exhaust speed of rockets, 917–918
Electric powered aircraft, 78–81
Electric rocket propulsion, 982–990
Electromagnetic rockets, 984–990
Electrostatic rockets, 983
Electro-thermal rockets, 983
Emission, 28, 51, 62–63, 78, 219, 224, 469–471, 570, 660, 674–675
Endurance, viii–ix, 48, 205–206
Energy equation, 106–110, 123, 126, 147, 149, 381, 556, 633, 648, 668, 703, 716–718, 755
Engine performance, viii–x, 178–186, 218
Enhanced takeoff and landing (TOL), 6, 8, 9, 22, 25, 26, 83
Enthalpy, 93, 109, 110, 112, 114, 130, 258, 350, 413, 515, 539, 543, 548, 647, 668, 669, 699, 704, 716, 755–763, 770, 771, 773, 775, 791, 845–846, 858–859, 874–876
Equation of state, 111–114, 121, 126, 147, 151, 711
Equivalent engine power, 545–552
Euler equation, 715, 756, 841–843
Evolution of scramjets, 365–367
Experimental aircraft, 12–13, 30, 56, 227
Exponential design method, 791, 834
External compression intake (inlet), 641–644
- F**
Factors affecting thrust, 174–178
Fan, 5, 91, 163, 220, 315, 403, 531, 590, 703, 839
Fan efficiency, 71–72, 192, 619
FanWing, 4, 5, 47–50
Fighter-fire fighting, 31
Film cooling, 659, 868, 869, 901
Film cooling of turbines, 869
Firefighting aircraft, 11–12
First law analysis of combustion, 668–669
First power design, 833
Fixed wing aircrafts, 4–31
- Flapping wing, viii, 4, 5, 47–48
Flight Mach number, 64, 193, 203, 320, 331, 338, 365, 372, 375–378, 382, 390–393, 396–398, 410, 423, 424, 444, 492, 494, 501, 506, 511, 517, 526, 527, 538, 563, 573, 627–629, 634
Flight speed, 15, 48, 63, 64, 69, 98, 102, 163, 166–175, 180, 181, 184, 191, 193, 195, 208, 215, 217, 218, 221, 280, 289, 294, 296, 303, 311, 313, 315, 323, 334, 337, 338, 341, 342, 345, 351, 357, 365, 378, 385, 386, 404, 408, 422, 424, 426, 428, 429, 454, 455, 478–480, 514, 515, 539, 541, 544, 552, 563, 590, 591, 623, 646, 932
Flow coefficient, 770, 846–848, 852, 854, 870, 871, 878, 879, 895, 896, 898–900
Forward fan, 447–478
Forward fan mixed flow engine, 461–471
Forward fan turbofan, 447, 465–466
Forward fan unmixed double spool configuration, 448–461
Four stroke engine, ix, 223, 225, 232–233, 236, 241, 247, 251, 254
Free power turbine, 532, 541–544, 556, 559, 568, 583, 889, 891–905
Free vortex design, 777, 779, 784, 790, 799, 829, 858–867, 899
Fuel consumption, x, 77, 161, 162, 178, 193–200, 203–205, 208, 209, 211, 212, 215, 216, 219, 221, 240, 244, 245, 249, 251, 315, 318, 322, 324–327, 333–336, 338, 352, 355, 371, 372, 375, 382, 384, 386, 389, 390, 396, 400, 403, 404, 416, 436, 437, 439–443, 445, 446, 454, 464, 465, 475, 478, 486, 495, 501, 508, 514, 518, 523, 527, 528, 546–552, 560, 562, 564, 570, 572, 582, 583, 675, 695
Fuel heating value, 188, 190, 249, 309, 322, 334, 354, 357, 374, 392, 393, 397, 426, 443, 445, 454, 511, 514, 516, 517, 519, 522, 524, 525, 547, 560, 562, 582–585
Fuel-to-air ratio, 99, 149, 157, 173, 174, 179, 191, 194, 215, 351, 354, 355, 357, 364, 372, 374, 377, 391, 393, 396–398, 410, 412, 414, 417, 418, 420, 421, 424, 426, 427, 429, 432, 435, 436, 443, 450, 454, 455, 457, 459, 464, 474, 507, 511, 514, 515, 517, 518, 520, 522, 539, 541, 557, 563, 585, 666, 671, 675
Full-coverage film cooling, 868
Future TBCC engine, 509

G

Gas turbine engine, 70, 161, 403, 553, 590, 659, 672, 675, 748, 885–905
 Glider, 5–6, 26–27, 31, 84
 Gloster aircraft, 264, 404, 536, 994
 Gross thrust, 100, 162, 165–167, 169, 170, 177, 214, 512
 Ground-attack, 21–24, 29, 82, 83
 Gyrodyne, 31–34, 84

H

Head-and tail-wind, 206–209
 Helicopter, 5, 101, 188, 221, 318, 531, 615, 747, 839, 994
 High pressure compressor (HPC), 62, 72, 73, 407, 430–433, 448, 450, 451, 457, 458, 471–473, 476, 522–524, 547, 548, 572, 574, 586, 587, 748, 783, 795, 817, 818, 832
 High pressure turbine (HPT), 62, 72, 73, 431–433, 448, 450–451, 471, 472, 476, 523, 524, 542, 547, 548, 572, 575, 586, 854, 871, 900
 HPA. *See* Human-powered aircraft (HPA)
 HPC. *See* High pressure compressor (HPC)
 HPT. *See* High pressure turbine (HPT)
 Hub, 18, 261, 264, 267, 283, 289, 293, 300, 706, 711, 720, 750, 752, 754, 764–766, 769, 773, 775, 777, 779, 780, 782, 784, 791, 793–799, 807, 808, 821, 823, 828, 829, 833–836, 841, 860, 863, 868, 870
 Human-powered aircraft (HPA), 81–89
 Hybrid fixed/rotary wings, viii, 4, 5, 44–47, 50
 Hybrid rocket engine, 616, 977
 Hydrogen fuel, 362, 366, 382, 500, 509, 966
 Hypersonic engine, 645

I

Ideal ramjet, 331, 354, 357, 358, 390, 392, 393, 397, 398
 Ideal turbojet, 421, 422, 443
 Impeller, 70, 705, 883, 972
 Impingement cooling of turbine, 869
 Impulse-to-weight ratio, rockets, 930
 Impulse turbine, 105, 840, 847, 900, 974
 Inlet guide vanes, 487, 737–738, 760, 767, 812, 818, 824, 829
 In-line piston engines, 57, 227–228
 Intake, 63, 127, 164, 230, 315, 405, 538, 589, 705

Intermeshing rotors, 36–37

Intermittent (or piston) engines, 221–232

Internal compression intake (inlet), 342, 641, 644, 645

Isentropic efficiency, 260, 321, 342, 343, 346, 369, 370, 408, 411, 432, 433, 451, 452, 457, 458, 493, 494, 498, 538, 540, 543, 582, 590, 619–620, 695, 700, 705, 708, 713, 714, 720, 728–733, 736, 739, 823–825, 860, 899, 902, 946

Isentropic relations, 114–116, 135, 136, 145, 682

J

Jet nozzle, 164, 174, 175, 577

L

Launch mode of rockets, 913
 Liquid propellant rocket engines (LRE), 959–976
 Loss coefficients in nozzle and rotor of turbine, 845–846, 877–878, 902
 Low pressure compressor, 62, 72, 76, 407, 430–432, 448–451, 457, 458, 469, 471, 523, 524, 533, 547, 548, 586, 748, 783, 817
 Low pressure turbine (LPT), 62, 72, 73, 407, 430, 431, 433, 434, 438, 446, 448, 449, 451, 457, 459, 463, 464, 468–469, 471–472, 477, 523, 524, 533, 535, 547, 549, 572, 586, 677, 870, 871, 903, 904, 998
LPT. See Low pressure turbine (LPT)
LRE. See Liquid propellant rocket engines (LRE)

M

Mach number, 15, 115, 165, 288, 320, 408, 538, 589, 711, 850, 921
 Manifold, 231, 246, 309, 655, 706, 708, 711, 742, 823
 Maritime, 25, 40, 41, 43, 84, 222, 577
 Maritime patrol, 21, 22, 24–25, 28, 83
 Mass air flow, 175
 Mass ratio (MR), rockets, 929
 Matching between compressor and turbine, 889
 Material of axial compressors, 818–815, 821
 Material of centrifugal compressors, 821
 Mean line flow, 293, 812

- Mean radius, 752, 754, 756, 786, 791, 797, 798, 801, 803, 807–808, 827, 832–834, 852, 854, 895, 896, 898–900
- Medium haul, 15–16, 18–20, 83, 537
- Micro turbojet, ix, 441–445
- Milestones, xi, 2–3, 223, 264, 407, 446, 534–538, 908–909, 993–1001
- Military aircrafts, 6, 8, 20–31, 50, 71, 82–84, 155, 161, 178, 180, 207, 217–218, 221, 230, 328, 406, 407, 417, 419, 432, 461, 464, 484, 590, 591, 604, 609, 622, 679, 813
- Military helicopters, 40, 41
- Mission segment weight fraction, 206
- Mixed compression intakes, 342, 641, 645
- Mixed turbofan, 447, 461, 462, 464–468, 521
- Modified momentum/simple vortex model for propellers, 281–282
- Module matching, 886
- Momentum equation, 92, 97, 99–101, 103–106, 121, 126, 147, 555, 714–716, 775, 858
- Monopropellant liquid rocket, 962–963
- Mono-tilt-rotor rotary wing, 5, 45, 47, 84
- N**
- NASP. *See* National Aerospace Plane (NASP)
- National Aerospace Plane (NASP), 484
- Noise, x, 51, 53, 61, 62, 66–68, 71, 78, 219, 254, 274, 311, 315, 316, 318, 327, 330–331, 337, 404, 445, 461, 469, 471, 472, 486, 523, 565, 566, 568, 570, 571, 589, 590, 594, 595, 598, 601, 679, 747, 998
- Non-combat fixed wing military aircrafts, 26–31
- Normal shock wave, 125–139, 342, 348, 362, 380, 392, 394, 637, 641, 645, 648, 696–698
- NO_x emission, 674
- Nozzle, 25, 97, 315, 393, 405, 538, 589, 767, 839, 907
- Nuclear engine, viii, 51, 53–55, 361, 406, 982
- Nuclear ramjet, 360–362
- Nuclear rocket, 221, 972, 981–983
- Number of propellers coupled to each engine, 269
- Number of stages in rocket, 914
- O**
- Oblique shock wave, viii, 64, 139–144, 146, 160, 342, 343, 348, 391, 497, 643, 648, 649, 697, 698
- Observation, 28, 40, 41, 44, 84
- Off design, x, xi, 132–138, 646, 795, 872, 885, 888–905
- Operations helicopters, 43
- Opposed-type piston engines, 59
- Ornithopter, viii, 5, 47–48
- Otto cycle, 235–253, 258, 306, 308, 309
- Overall efficiency, 178, 189–192, 202, 203, 215, 371, 372, 375, 377, 382, 385–386, 392, 397, 400, 436, 437, 439, 474, 475, 478, 494, 495, 501–512, 518, 522, 526, 736, 930, 932, 933, 985, 988
- P**
- Parallel staging of rockets, 938, 944
- PDE. *See* Pulse detonation engine (PDE)
- Podded intake, 621, 622
- Point of no return, 209–212, 218
- Polytropic efficiency of axial compressor, 797, 798, 828
- Powered rotorcrafts, 31–44
- Power plant installation, x, 590–618
- Prewhirl, x, 710, 711, 737–742, 820–822, 824, 829, 873
- Propellant feed system of LREs, 961–962
- Propellant mass fraction (ζ), rockets, 929–930
- Propeller, 3, 120, 162, 219, 446, 531, 599, 703, 839
- Propeller, blade element considerations, 282–287
- Propeller efficiency, 162, 178, 189, 204, 216, 247, 279, 280, 286, 290, 293–295, 297, 300, 301, 310–313, 582
- Propeller modified momentum/simple vortex model, 281–282
- Propeller power coefficient, 288, 293, 295–297, 300, 301, 305
- Propeller thrust coefficient, 287, 293, 296, 297
- Propfan, viii, ix, x, 52, 55, 59–63, 73, 78, 82, 88, 180, 181, 183, 219–221, 264, 509, 531–587
- Propulsion, 1, 97, 192, 219, 316, 479, 532, 589, 839, 907
- Propulsive efficiency, 178–187, 189–191, 194–196, 199–200, 202, 215, 216, 247, 278–282, 286–289, 292, 357, 371, 372, 375, 382, 385, 392, 398, 400, 421, 436, 437, 439, 478, 501, 512, 514, 515, 518, 521, 525, 531, 532, 569, 570, 572, 577, 582, 584, 587, 695, 748, 930–932
- Puller turboprop, 601
- Pulsating nature of flow parameters in pulsejet engines, 329–330

- Pulse detonation engine (PDE), ix, 68, 316, 330–336, 382, 386
- Pulsejet, viii, ix, 52, 55, 63–68, 82, 219, 220, 315–400
- Pump-fed system, 962, 968–971
- Pumps materials and fabrication processes, 973
- Pusher turboprop, 599
- R**
- Radial inflow turbine, 231, 705, 873–880, 902
- Radial vs. axial turbines, 880–885
- Ram effect, 177–178, 320, 338, 595
- Ramjet engines, ix, 64–65, 75, 148, 173, 219, 315–400, 487, 494, 496, 499, 501, 506–508, 520, 527, 616, 675
- Range factor, 205
- Rayleigh-flow equations, 146–151
- Reciprocating engines, 29, 44, 53, 55, 56, 223, 227–230, 236, 252, 305, 908
- Recommended design values for radial inflow turbines, 879–880
- Regional airliner, 18
- Relative speed, 207, 208, 217, 294, 296, 710, 713, 738, 747, 766, 767, 796, 841
- Remote sensing, 37, 39, 84
- Rocket equation for a parallel multi-stage rocket, 940
- Rocket equation for a series multi-stage rocket, 938–940
- Rocket performance parameters, xi, 914–933
- Rocket propulsion, vii, xi, 221, 365, 907–990
- Rocket pumps, 972–973
- Rolls Royce, xi, 59–61, 66, 70, 74, 76, 78, 182–184, 188, 228–229, 231, 264, 270, 430, 446–448, 465, 471–472, 483, 532, 535, 536, 554, 567, 581, 603, 654–657, 671, 672, 678, 705, 817, 993, 995–997
- Root section, 748–749, 834
- Rotary piston engines, 58, 261
- Rotational speed, 56, 174, 178, 227, 281, 287, 289, 298–300, 308, 311–313, 468, 578, 711, 715, 719, 722, 724, 727, 732–734, 738, 740, 743, 752, 753, 755, 764–767, 770, 773, 782, 784–786, 795, 796, 798–801, 813, 817, 822–832, 834–836, 841, 852–854, 860, 863, 866, 872, 881, 885, 895, 898, 900–902, 969, 974, 976, 987
- Rotorcrafts (rotor-wing aircrafts), 31–44
- Route planning, ix, 209–218
- Russian Tu-95, 406, 537, 554, 603
- S**
- SAR. *See* Search and rescue aircrafts (SAR)
- Scramjet engine, ix, 64, 68, 69, 192, 315–400, 404, 479, 480, 528, 590
- Scroll, x, 706, 708, 709, 711, 742, 873
- Seaplanes, 8, 10, 13–14, 594
- Search and rescue aircrafts (SAR), 13, 42, 43
- Second law of thermodynamics, 92, 110–111
- Series staging of rockets, 938
- SFC. *See* Specific fuel consumption (SFC)
- Shaft-based engines, ix, x, 82, 619, 653, 839
- Shaft power, x, 187–189, 194, 403, 540–541, 545, 553, 557, 582, 974
- Short haul-surveillance, 16, 18–19
- Simplified radial equilibrium equation (SRE), 775–794
- Single entry, 709, 710
- Single main rotor, 33–35
- Single spool, 405–417, 419–421, 430, 432, 441, 447, 464–466, 493, 500, 516, 517, 521, 525, 533, 556–558, 816
- Single spool turboprop, 535, 538–541, 580, 581
- Slip factor, 718–724, 739, 784, 799, 824–827, 829, 830, 832
- Small transport, 16
- Solid propellant rocket engines, 221, 907–909, 946–948, 953, 954, 956, 980, 987, 1000
- So_x emission, 219, 674
- Specific fuel consumption (SFC), x, 162, 178, 193–200, 203, 204, 216, 244, 245, 249, 251, 416, 454, 464–465, 546, 547, 560, 562–564, 582, 583, 695
- Specific impulse, viii, xi, 76, 213–218, 316, 330, 331, 333, 334, 336, 367, 371, 372, 375, 382, 691, 914, 924–929, 942, 944, 945, 948, 955, 956, 959, 963, 966–968, 977, 979, 981, 982, 984, 986–989
- Specific propellant consumption in rockets, 789, 988
- Specific thrust, 163, 181, 190, 191, 215, 322, 331, 336, 354, 355, 371, 372, 375, 376, 382, 384, 392, 396–398, 400, 416, 428, 435, 436, 453, 454, 464, 475, 478, 494, 495, 499, 501, 508, 512, 514, 519, 523, 551, 552, 695, 927
- Spouting velocity of radial turbine, 875–876, 902, 987
- SRE. *See* Simplified radial equilibrium equation (SRE)
- Stage loading, 770, 870, 878, 879, 895, 896
- Stagnation pressure ratio, 352, 393, 395, 396, 619, 742

- Stagnation temperature, 64, 134, 160, 214, 343, 392, 411, 514, 720, 860, 895, 898, 899
 Stall, x, 13, 595, 620, 623, 627, 628, 630, 646, 662, 747, 751, 767–768, 810, 813–816, 818
 Standard atmosphere, 151–160, 176, 390
 Static condition for turboprop, 545, 546
 Stationary modules, vii, x, 408, 589–700
 Steam turbine, 704, 839
 Stoichiometric ratio, 520
 Stresses on rotor blades, 764
 Subsonic, x, 15, 23, 64, 65, 71, 118–120, 122, 125, 127, 132–134, 137–140, 175, 177, 190, 203, 287, 315, 330, 334, 337, 338, 341, 342, 348, 362, 364, 368, 378, 381, 386, 394, 395, 446, 447, 454, 479, 490–491, 496, 497, 531, 572, 577, 590–603, 619, 621–637, 641, 645, 646, 648, 653–658, 680, 682–684, 694, 696–698, 795, 804, 810, 812, 813, 996
 Subsonic combustion chamber, 653–658
 Supercharging and turbocharging engines, 230–232
 Supersonic, 6, 119, 175, 274, 315, 430, 537, 590, 776, 920
 Supersonic aircrafts, x, 65, 120, 139, 175, 481–484, 590, 591, 603–614, 619, 637, 653, 675, 816
 Surge, x, 727, 745–747, 753, 813–820, 833
 Surveillance, 3–4, 26–29, 44, 71, 509
- T**
- Tactics and operations helicopters, 43
 Tactics helicopters, 41, 43, 84
 Tail installation, 488, 533, 598, 599
 Takeoff thrust, 178, 192, 193, 404, 987
 Tandem rotor, 35, 585
 TBCC Engines. *See* Turbine based combined cycle (TBCC) engines
 Terminology for four-stroke engine, 232–233
 Thermal efficiency, ix, 178, 186–188, 190, 192, 193, 215, 224, 238–240, 244, 249, 251, 255–257, 306, 308–310, 322, 336, 371–372, 375, 382, 385, 390, 398, 400, 436, 437, 439, 440, 478, 501, 511, 512, 514, 515, 518, 526, 695, 748, 924, 930, 931
 Thermodynamic analysis of afterburner (Rayleigh Flow), 676–677
 Three-dimensional variations, 759–760
 Thrust coefficient (CF), xi, 287, 293, 295–297, 914, 922–924, 955
 Thrust force, 60, 102, 161, 221, 322, 406, 540, 675, 738, 907
 Thrust of propeller, 219, 221, 261, 265, 276–278, 284–286, 295
 Thrust reverse, x, 102
 Thrust specific fuel consumption (TSFC), x, 162, 193–195, 202, 205–208, 215, 217, 218, 322, 325, 327, 334, 336, 341, 352, 354, 355, 371, 372, 375, 376, 382, 384, 388–390, 392, 393, 396, 400, 416, 436, 437, 439, 440, 443, 454, 455, 475, 478, 486, 494, 495, 499–501, 505, 506, 508, 512–516, 518, 520–524, 527, 546, 580, 695
 Tilt rotor, 45, 46, 532, 581
 Tiltwing, 44–45, 49, 50, 84
 TIT. *See* Turbine inlet temperature (TIT)
 Torque of propeller, 227, 240, 247, 270, 283–287
 Total impulse (I_t), 914, 924, 926, 955, 956, 984, 985, 988
 Trainer, 9–11, 26–28, 41, 60, 83, 84, 207, 441
 Training, 11, 28, 37, 38, 40, 82, 84, 225, 621
 Transonic, 15, 119, 274, 293, 446, 464, 591, 680, 764, 766, 795, 804
 Transpiration cooling, 599, 869
 Transport, vii, 1, 3, 9, 13–20, 27, 31, 37–38, 40, 41, 43, 49, 50, 58, 60, 69, 71, 72, 74, 82–84, 86, 94, 96–97, 104, 107, 161, 173, 178, 180, 207, 264, 330–331, 404, 406, 425–426, 430, 446, 447, 479, 481–483, 500, 531, 532, 537, 554, 577, 578, 582, 586, 590–592, 599, 603, 607, 619, 621, 622, 705, 815, 996
 Transports aircrafts, 15–16
 Transverse rotors, 35
 Triple spool, 446, 474, 475, 523, 533, 577, 694, 748, 903
 TSFC. *See* Thrust specific fuel consumption (TSFC)
 Turbine based combined cycle (TBCC) engines, 76, 479–510
 Turbine-based engines, viii, ix, 82, 338, 365, 403–528, 531, 620, 653, 839
 Turbine cooling techniques, 867–869
 Turbine efficiency, 410, 500, 888, 890, 969, 971, 976, 987
 Turbine inlet temperature (TIT), 174, 178, 414, 426, 428, 492, 500, 514, 521, 524, 525, 527, 539, 543, 560, 562, 582, 583, 585, 839, 867, 888, 890, 892
 Turbine map, 872, 888, 891, 892, 903, 904

Turbofan, 18, 119, 163, 220, 330, 403, 531, 590, 705, 900, 907
 Turbojet, 18, 120, 163, 220, 330, 403, 531, 590, 705, 900, 907
 Turboprop, 16, 154, 162, 219, 446, 531, 590, 705, 886
 Turboprop installation, 599
 Turbo-pump, 839
 Turbo ramjet, viii, ix, x, 55, 63, 74–77, 220, 340, 341, 487, 499
 Turboshaft, ix, x, 35, 37–44, 50, 52, 55, 59, 61, 82, 188, 219, 220, 509, 531–587, 615, 616, 705, 783
 Two-spool turboprop, 533, 541–545, 547, 586
 Two stroke engine, 223, 225, 231, 240, 241, 248, 251, 254
 Types of combustion chamber, 653–658
 Types of missiles, 912–913

U

UAV. *See* Unmanned aerial vehicle (UAV)
 UHB engines. *See* Ultrahigh bypass (UHB) engines
 Ultra-high-bypass (UHBP), 61, 565
 Ultrahigh bypass (UHB) engines, 61
 Unchoked, 162–164, 173, 175, 178, 181, 184, 186, 187, 190, 192, 194, 216, 346, 350, 415, 420–422, 434, 435, 452, 453, 464, 477, 478, 511, 512, 525, 580, 689, 851
 Unchoked nozzle, 173, 186, 187, 190, 192, 420–422, 511, 525
 Unducted fan (UDF) engines, x, 61, 62, 73, 552, 565, 572, 586
 Unmanned aerial vehicle (UAV), ix, 26–29, 40, 41, 44, 56, 84, 86, 225, 227, 316, 318, 331, 441, 479
 Unmixed turbofan, 333, 447, 456, 461, 474, 475, 677, 694

V

Valved pulsejet, 66, 318–319, 327, 329–331
 Valveless pulsejet, 67, 316, 318, 327–328, 337
 Vaned diffuser, 707–708, 714, 736, 737
 Vaneless diffuser, 707, 736–737, 821, 824
 Variable stator vanes (VSV), 817–819
 Velocity triangles, 711–713, 724, 725, 728, 729, 733, 739, 752, 754–757, 761, 762, 767, 773, 774, 779, 782, 784, 786, 787, 791, 793, 799, 801, 820, 821, 823, 827–829, 841, 843, 847, 848, 852, 854, 857, 858, 863, 864, 873–875, 895, 896, 898, 901, 974, 975
 Vertical takeoff and landing (VTOL), 6, 8, 22, 25, 45, 47, 83, 227, 532, 679, 839
 Volute, x, 706, 708, 709, 711, 736, 742, 747, 873, 972, 973
 von Ohain, 70, 404, 408, 705, 750, 994
 V/STOL, 8, 25, 83
 VSV. *See* Variable stator vanes (VSV)
 VTOL. *See* Vertical takeoff and landing (VTOL)
 V-type piston engine, 57, 59, 227–229

W

Wankel engine, ix, 56, 225–227
 Weight, 37, 48, 51, 57, 58, 62, 66, 73, 75, 78, 79, 88, 93, 110, 111, 151, 157, 162, 165, 166, 200, 203, 204, 206, 207, 210, 214, 219, 224, 225, 227, 228, 230, 247, 254, 266, 305, 307, 328, 338, 366, 382, 403, 441, 442, 463, 465, 472, 486, 488, 512, 518, 589–591, 593, 594, 605, 609, 620, 637, 658, 675, 682, 691, 705, 709, 748, 753, 818–819, 902, 908, 920, 930, 936, 940–942, 948, 968, 969, 972, 974, 982, 987, 988, 996, 997
 Whittle, Frank, 70, 223, 404, 408, 654, 705, 750, 994
 Wing installation, 269, 488, 591, 594, 599–602, 608, 612